Vol. 19, No. 2, June, 2020
ISSN (Print): 0972-6268; ISSN (Online) : 2395-3454

Nature Environment & Pollution Technology

A Multidisciplinary, International Journal on Diverse Aspects of Environment

Technoscience Publications
website: www.neptjournal.com

Technoscience Publications
A-504, Bliss Avenue, Balewadi,
Opp. SKP Campus, Pune-411 045
Maharashtra, India

www.neptjournal.com

Nature Environment and Pollution Technology

(An International Quarterly Scientific Research Journal)

Published by : Mrs. T. P. Goel, B-34, Dev Nagar, Tonk Road, Jaipur-302 018 Rajasthan, India

Managing Office : Technoscience Publications, A-504, Bliss Avenue, Balewadi, Pune-411 045, Maharashtra, India

E-mail : contact@neptjournal.com; journalnept@gmail.com

INSTRUCTIONS TO AUTHORS

Scope of the Journal

The Journal publishes original research/review papers covering almost all aspects of environment like monitoring, control and management of air, water, soil and noise pollution; solid waste management; industrial hygiene and occupational health hazards; biomedical aspects of pollution; conservation and management of resources; environmental laws and legal aspects of pollution; toxicology; radiation and recycling etc. Reports of important events, environmental news, environmental highlights and book reviews are also published in the journal.

Format of Manuscript

- The manuscript (*mss*) should be typed in double space leaving wide margins on both the sides.
- First page of mss should contain only the title of the paper, name(s) of author(s) and name and address of Organization(s) where the work has been carried out along with the affiliation of the authors.

Continued on back inner cover...

Nature Environment and Pollution Technology

Vol. 19, No. (2), June, 2020

CONTENTS

The Journal is Currently Abstracted and Indexed in:

International Scientific Indexing (UAE) with Impact Factor 2.236 (2018)

NAAS Rating of the Journal (2019) = 3.85

Scopus®, SJR (0.146) 2018

Index Copernicus (2018) = 135.97

EI Compendex of Elsevier

Indian Science Abstracts, New Delhi, India

Chemical Abstracts, U.S.A.

Pollution Abstracts, U.S.A.

Elsevier Bibliographic Databases

Paryavaran Abstract, New Delhi, India

Zoological Records

Indian Citation Index (ICI)

Scopus CiteScore (2018) = 0.28

Electronic Social and Science Citation Index (ESSCI)

EBSCO: Environment Index™

Ulrich's (Refereed) database

CrossRef (DOI)

DOAJ

Zetoc

Google Scholar

ProQuest, U.K.

J-Gate

Environment Abstract, U.S.A.

British Library

Centre for Research Libraries

WorldCat (OCLC)

JournalSeek

Connect Journals (India)

CSA: Environmental Sciences and Pollution Management

Research Bible (Japan)

Indian Science

Geobase

Elektronische Zeitschriftenbibliothek (EZB)

SHERPA/RoMEO

Directory of Science

CNKI Scholar (China National Knowledge Infrastructure)

Access to Global Online Research in Agriculture (AGORA)

AGRIS (UN-FAO)

Full papers are available on the Journal's Website:
www.neptjournal.com

UDL-EDGE (Malaysia) Products like *i*-Journals, *i*-Focus and *i*-Future

www.neptjournal.com

Nature Environment and Pollution Technology

Nature Environment and Pollution Technology
An International Quarterly Scientific Journal

p-ISSN: 0972-6268
(Print copies up to 2016)
e-ISSN: 2395-3454

Vol. 19 | No. 2 | pp. 421-439 | 2020

Original Research Paper

https://doi.org/10.46488/NEPT.2020.v19i02.001

Open Access Journal

Assessment of Trace and Rare Earth Element Levels in Stream Sediments in Ijero-Ekiti Area, Southwest Nigeria

H. Y. Madukwe*†, O. A. Ibigbami and R. A. Obasi***

*Department of Geology, Ekiti State University, PMB 5363, Ado-Ekiti, Nigeria

**Department of Chemistry, Ekiti State University, PMB 5363, Ado-Ekiti, Nigeria

†Corresponding author: H. Y. Madukwe; henry.madukwe@eksu.edu.ng

Nat. Env. & Poll. Tech.
Website: www.neptjournal.com

Received: 03-06-2019
Accepted: 24-07-2019

Key Words:
Sediments; Trace elements; Rare earth elements; Enrichment factor; Pollution load index

ABSTRACT

The study considered the level, sources and extent of trace and rare earth elements (REE) contamination in Agbangudu stream sediments in Ekiti State, Southwestern Nigeria. The samples were analysed with Laser Ablation Inductively Coupled Plasma Spectrometer (LA-ICP-MS). The trace and rare earth elements' concentration ranged from 0.50 (Mo) to 750 (Ba) and 0.16 (Lu) to 175 (Ce) ppm respectively. The results revealed that the sediments are not that enriched in REEs. The Pollution Load Index (PLI) indicates baseline levels of the metals. The geochemical index (Igeo) of the elements revealed uncontaminated to moderately contaminated, except for Cs and Ta with strongly to extremely contaminated status. The Average Shale Value (AVS) and the Upper Continental Crust (UCC) normalized REE distribution patterns of the sediments. To establish the relationship between the metals, Principal Component Analysis (PCA) and Clusters Analysis (CA) were used as classification techniques. Despite the common occurrences of the elements, their overall patterns were much different as revealed by the cluster analysis.

INTRODUCTION

Sediments are transported and deposited particles or aggregates derived from rocks, soils or biological material (SSSA 2008). Generally, stream sediments are composed of weathering products of basement rocks introduced into streams. Studies of the chemistry of stream sediments have been used in mineral prospecting (Levinson 1974, Rose et al. 1979, Hale & Plant 1994) and environmental studies (Förstner 1983, Howarth & Thornton 1983, Förstner et al. 1991). Most streams in southwestern Nigeria are located on the Basement complex, which lies within the reactivated part of the Pan-African mobile belt between the West African and Congo Cratons (Kennedy 1965). The geochemical compositions of stream sediments reflect the average composition of an entire drainage basin (Halamic et al. 2001, Reimann & Melezhik 2001). According to Grunsky & Sutphin (2009), geochemical studies based on the chemical analysis of active stream sediments are an effective tool with several applications. The expression "rare earth elements" (REEs) does not infer that they are rare in nature; rather, REEs are relatively abundant in the earth. The total contents of REEs exceed 200 ppm in the average crust. Some REEs are even more common than copper or lead in the crust (Castor & James 2006, Chen 2011). REEs are at the lower part of the Periodic Table, which includes 15 lanthanides (from lanthanum to lutetium) and two other elements: scandium and yttrium. These 17 elements form a coherent group with similar chemical properties. Usually, REEs can be divided into three groups by their atomic number and masses - the light rare earth elements (LREE), which comprises of La, Ce, and Pr, the middle rare earth elements (MREE), made up of Nd, Sm, Eu, and Gd, while the heavy rare earth elements (HREE) include those from Tb to Lu (EPA 2012).

Trace and rare earth elements in sediments are derived from both natural (geogenic) and anthropogenic sources. Heavy metals and rare earth elements (REEs) are potentially toxic substances in ecosystems. According to Lin et al. (2008), heavy metals and REEs are added to the hydrological system by natural processes such as rock weathering, volcanic eruption and long-distance atmospheric deposits. In recent times, the chief sources of these elements are due to the human activities: industrialization, agriculture, urban development and waste discharge (Senesi et al. 1999, Ochieng et al. 2007, Chen et al. 2013, Ong et al. 2013, Sofianska & Michailidis 2013, Zhuang et al. 2013). Stream sediments contamination by heavy metals has become a widespread serious problem in many parts of the world (Sofianska & Michailidis 2013). Trace and rare earth element contamination in soils has attracted so much attention because of the hazard it poses to human health (Loska et al. 2004). Rivers,

streams and sediments are contaminated by trace elements such as: As, Fe, Hg, Mn and Pb from artisanal mining activities, and their values have also been found to exceed standard safety levels (Ojo & Oketayo 2006, Nartey et al. 2011). Some metals like Fe, Cu, Co, Mn, Cr and Zn are essential micronutrients, but they can be detrimental to man and other living organisms at higher concentrations (Nurnberg 1982, Kar et al. 2008, Nair et al. 2010). According to Wakida et al. (2008), industrial waste reaching the sea via atmospheric precipitation and dumping of urban and rural waste is mostly responsible for the input of trace elements into the marine and stream environments, which are afterwards incorporated into the sediments. Trace and rare earth elements are serious pollutants because of their toxicity, persistent and non-degradability and thus imparting into the water and debasing its quality in an environment (Tijani et al. 2005). Several studies have shown the harmful effects and health hazards of REEs to human beings, and it has already been proven that long-term exposure of REE dust may cause pneumoconiosis in humans (Hirano & Suzuki 1996).

This work analyses trace and rare earth elements concentration in the Agbangudu stream sediments and pollution indices such as enrichment factor (EF), contamination factor (CF), pollution load index (PLI), degree of contamination (DC) and geochemical index (Igeo).

MATERIALS AND METHODS

Study Area

Ijero-Ekiti is located 42km northwest of Ado-Ekiti, the state capital, and lies between longitudes 5°00'E and 5°07'E, and latitudes 7°46'N and 7°53'N. The Ijero-Ekiti area is underlain by the basement complex rocks of Southwest, Nigeria (Fig. 1). The local geology consists of the migmatite gneiss, quartzite, schist biotite gneiss, calc-gneiss, epidiorite, biotite schist, amphibole schist, granite and pegmatite (Fig. 2). Fig. 3 shows the Ijero area and the sampling points.

The migmatite gneiss occurs within the eastern part covering about two-fifth of the area, biotite gneiss predominantly

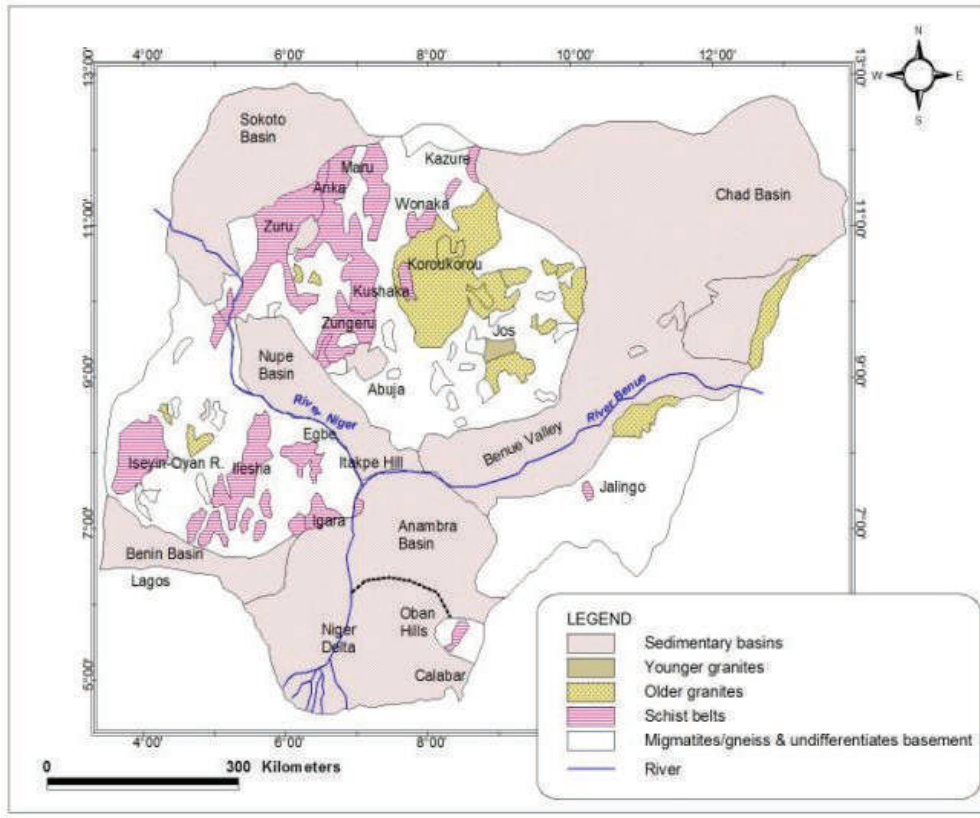

Fig. 1: Geological map of Nigeria showing basement complex, schist belts, and sedimentary terrain (After Akinola et al. 2014).

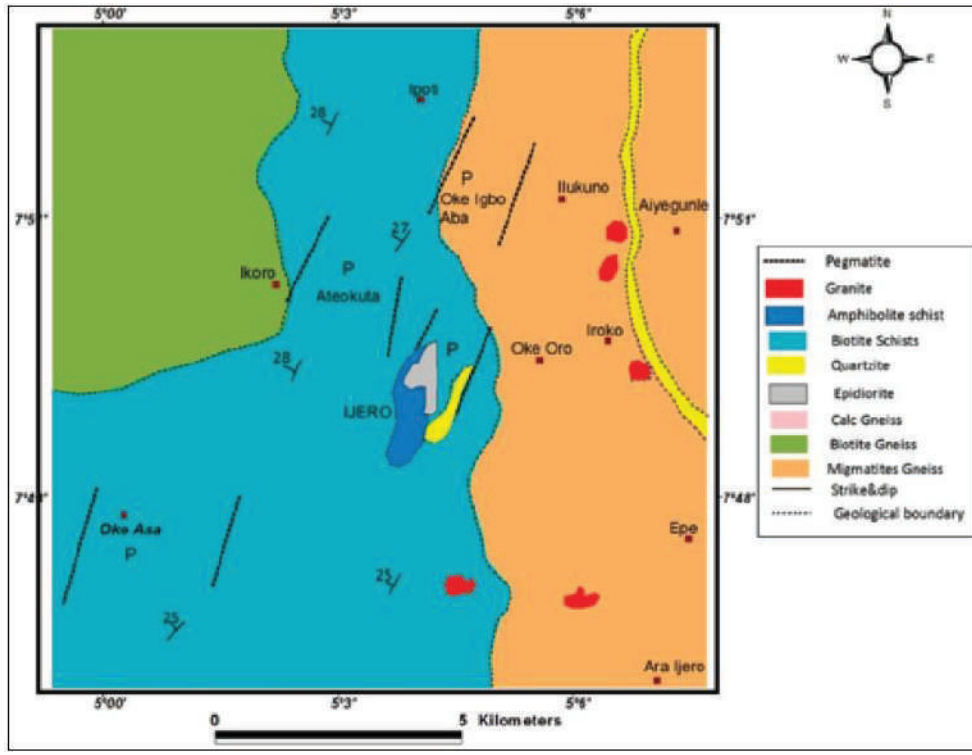

Fig. 2: Geological map of Ijero Ekiti area (After Okunlola & Akinola 2010).

covers the northwest (the gneissic rocks are essentially highly foliated and denuded); calc-gneiss and quartzite occupy a narrow NE-SW strip around Ijero-Ekiti town (Okunlola & Akinola 2010). Epidiorite occurs as the major ultramafic assemblage while amphibole schist and biotite schist occupy the central, low-lying area that is occasionally pulsed with granites and pegmatite intrusions now exposed due to prolonged weathering activities. The pegmatite occurs as very coarse-grained dykes, dykelets and sometimes of extensive dimension (Okunlola & Akinola 2010). Steeply dipping complex pegmatite around Ijero-Ekiti typically consists of an outer medium-grained microcline-albite-quartz-muscovite zone, an intermediate zone comprising coarse-grained microcline-albite-quartz, blocky microcline-quartz, coarse-grained quartz or lepidolite-quartz and finally, a core of coarse-grained muscovite-quartz and quartz (Okunlola 2005). Several workers have worked on the geology, tectonics, etc., of the Nigerian Precambrian Basement complex (Burke & Dewey 1972, Oyawoye 1972, Rahaman 1976, Rahaman & Ocan 1978, Black et al. 1979, Turner 1983, Ajibade et al. 1987, Rahaman 1988).

Sample Pre-treatment

Several samples were initially obtained while 10, which were representative of the stream channels, were eventually selected and analysed. Samples were taken at a depth of 20-25cm and bagged and labelled to avoid mix up. The geographical locations of each sample collected were noted and recorded in the field notebook. The samples were air-dried, pulverized, homogenized, packaged and sent to the laboratory in Stellenbosch University, South Africa for geochemical analysis. The trace and rare elemental data for this work were acquired using Laser Ablation inductively coupled plasma spectrometer (LA-ICP-MS) analyses. LA-ICP-MS is a powerful and sensitive analytical technique for multi-elemental analysis. The laser was used to vaporize the surface of the solid sample, while the vapour, and any particles, were then transported by the carrier gas flow to the ICP-MS.

The analytical results were compiled to form a multi-elemental database using Excel and Past. The statistical analyses, including principal component analysis (PCA) and cluster analysis (CA), were performed using Past statistical software.

RESULTS AND DISCUSSION

Distribution of Trace and Rare Earth Elements

The trace and rare elements composition, average values, background values of the Ijero stream sediments sampled,

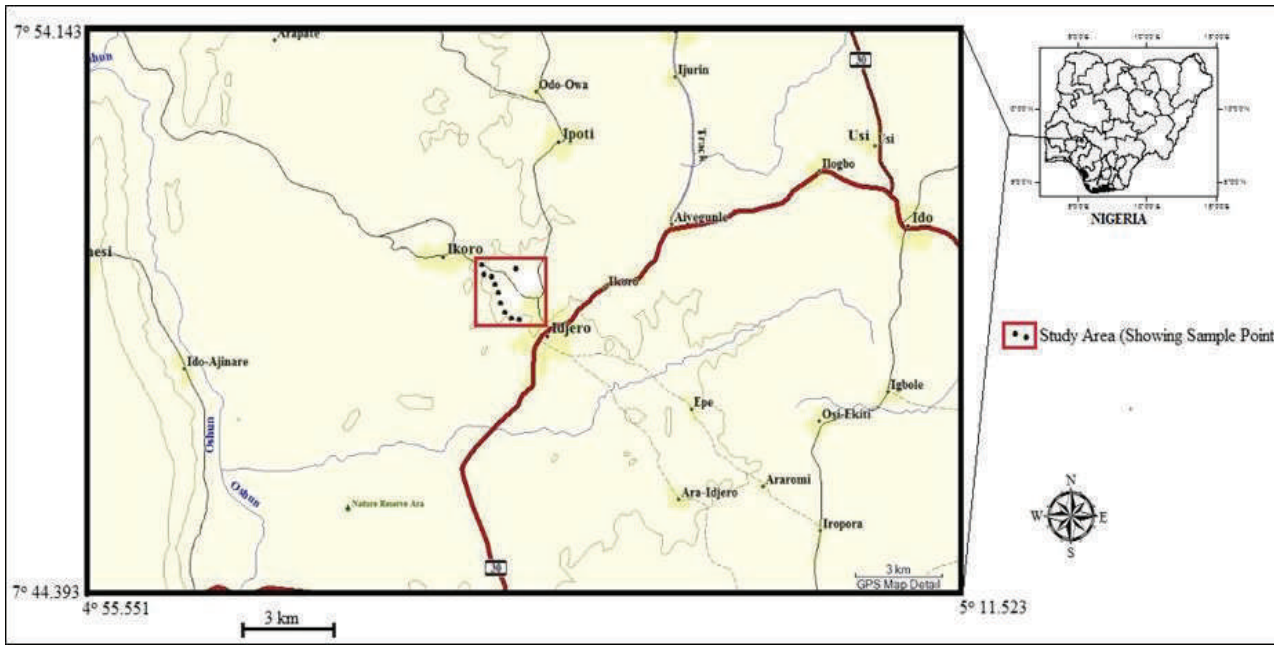

Fig. 3: The study area showing the sampling points.

upper continental crust values and average shale values are presented in Table 1. The background or control sample is the normal abundance of uncontaminated background levels in the stream sediments. These data revealed that the mean values of V, Co, Cu, Zr, Nb, Hf, Th, Mo and REEs: La, Ce, Pr, Nd, Sm, Sc, are below the background values, while Cr, Ni, Zn, Rb, Sr, Cs, Ba and the REEs: Eu, Gd, Tb, Dy, Er, Tm, Yb, Lu, Y, exceeded the background values. These elements with higher concentrations than the background values could become a major cause of concern. Figs. 4 and 5 are bivariate plots comparing trace element concentration and REE concentration of the samples studied with the mean of the upper continental crust and the average shale value respectively. Zn, Rb, Zr, and Nb showed significant enrichment compared to UCC and AVS. For the REEs, the concentrations showed the same pattern with the UCC and AVS. Fig. 6 is an AVS and UCC-normalized trace elements patterns for the stream sediments showing high levels of Nb and Ta, and to a lesser extent Rb, Zn, Cs and Hf. The AVS and UCC-normalized REE patterns for the stream sediments show an almost flat pattern, which might suggest the stream sediments are not that enriched in REEs (Fig. 7).

Enrichment Factor

Enrichment Factor (EF) is a useful pointer in assessing the level of contamination in an environment. According to Hernandez et al. (2003), the enrichment factor is the relative abundance of a chemical element in stream sediment compared to the bedrock. EF evaluates the degree of anthropogenic influence on element load in sediments and differentiates between elements of geogenic or anthropogenic origin (Fagbote & Olanipekun 2010). Enrichment factor values of trace and rare earth elements in the Agbangudu stream sediments are presented in Table 2. It was calculated using the formula originally introduced by Buat-Menard & Chesselet (1979):

$$EF = (C_n/C_{ref})_{sample} / (B_n/B_{ref})_{background} \quad \ldots(1)$$

Where, C_n is the concentration of the examined element in the examined environment; C_{ref} is the concentration of the reference element in the examined environment; B_n is the background value of the examined element, and B_{ref} is the background value of the reference element. The method by Salomons & Forstner (1984) was used, which entails comparing the present-day metal concentrations in sediments with standard earth materials as a normalizer in average shale.

Average shale value (AVS) and control value from Turekian & Wedepohl (1961), UCC: Upper Continental Crust (Taylor & McLennan 1985, 1995)

The global average shale is frequently employed to provide background metal levels; the element's concentration

Table 1: Chemical composition (ppm) of trace and rare earth elements in the stream sediment

Elements	SAMPLE ID										Mean	Control sample	ASV	UCC
	AG-1	AG-2	AG-3	AG-4	AG-5	AG-6	AG-7	AG-8	AG-9	AG-10				
V	85.54	112.76	68.83	69.07	46.87	56.93	62.47	61.52	115.41	53.16	73.26	86.43	130	107
Cr	151.38	211.07	86.39	84.29	54.21	67.57	244.49	58.37	79.47	45.84	108.31	30.04	90	85
Co	16.56	24.74	10.38	12.34	6.91	9.26	24.05	9.43	9.05	5.02	12.77	431.16	19	17
Ni	60.39	85.44	33.96	31.94	18.74	24.6	56.34	18.77	29.31	13.72	37.27	10.24	50	20
Cu	22.06	24.86	16.28	13.73	8.04	18.43	15.9	19.93	32.5	15.54	18.73	19.54	45	25
Zn	146.9	107.94	128.61	94.81	76.3	116.2	113.76	206.61	171.71	242.64	140.53	67.37	95	71
Rb	317.34	292.35	363.46	363.75	449.51	406.48	323.89	253.69	330.87	220.87	332.22	59.17	140	112
Sr	145.58	117.11	67.16	101.1	74.88	72.55	181.55	119.72	36.06	27.41	94.31	75.87	170	350
Zr	468.62	524.06	341.4	386.98	436	440.37	170.08	565.6	407.85	580.99	432.2	5573	160	190
Nb	204.05	112.54	114.32	226.24	132.57	188.13	108.09	292.49	127.68	214.27	172.04	280.5	11	12
Mo	0.77	0.63	0.66	0.59	0.5	0.77	0.75	0.77	1.56	0.52	0.69	1.4	2.6	1.5
Cs	12.85	14.83	17.18	11.42	10.25	11.7	16.05	7.89	18.03	9.15	12.94	0.28	5	4.6
Ba	317.77	343.6	311.66	361.12	281.17	272.79	750.85	368.04	274.87	210.53	349.24	123.43	580	550
Hf	14.84	14.82	10.3	10.81	12.83	12.86	5.04	20.64	11.87	15.89	12.99	26.23	5	5.8
Ta	125.97	32.55	32.2	77.29	45.57	48.67	16.49	49.55	32.97	43.95	50.521	1.02	1	1
Pb	20.22	21.13	26.16	26.99	21.7	25.54	31.53	31.19	22.53	16.61	24.36	15.21	20	17
Th	13.69	13.01	7.18	7.86	11.01	11.2	6.68	48.18	12.82	16.35	14.798	41.69	12	10.7
U	8.03	6.76	7.39	6.64	6.24	11.85	8.52	18.89	9.52	4.7	8.854	4.25	2.7	2.8
La	47.12	53.96	27.82	33.92	40.42	32.97	23.94	82.28	35.18	47.05	42.466	74.11	43	30
Ce	102.19	113.75	58.73	72.96	80.86	72.52	51.68	175.42	63.82	97.55	88.948	163.1	82	64
Pr	11.36	12.55	6.49	7.41	9.25	7.71	5.17	19.69	7.45	11.35	9.843	15.53	9.8	7.1
Nd	42.33	46.32	23.91	26.95	34.41	28.34	19.69	72.53	28.44	42.97	36.589	52.21	33	26
Sm	9.57	9.47	4.95	5.02	7.1	6.37	3.62	16.1	5.85	8.04	7.609	8.07	6.2	4.5
Eu	1.28	1.68	0.83	1.03	1.07	0.94	0.85	1.04	0.92	1.04	1.068	0.68	1.2	0.88
Gd	7.31	7.86	4.4	3.91	5.94	5.63	3.25	12.07	5.17	6.47	6.201	5.7	5.1	3.8
Tb	1.05	1.1	0.76	0.62	1.05	0.95	0.42	1.93	0.97	0.93	0.978	0.64	0.84	0.64
Dy	5.09	6.1	4.37	3.78	6.6	5.06	2.55	7.72	5.91	5.66	5.284	3.27	4.7	3.5
Ho	0.84	1.08	0.89	0.77	1.15	0.83	0.46	0.98	1.05	1.1	0.915	ND	1.11	0.8
Er	2.27	3.39	2.56	2.01	3.03	2.55	1.2	1.99	3	3.02	2.502	1.88	2.5	2.3
Tm	0.32	0.41	0.35	0.31	0.39	0.36	0.17	0.29	0.42	0.41	0.343	0.28	0.44	0.33
Yb	2.03	2.89	2.53	2.2	2.74	2.62	1.11	2.04	3.14	3.03	2.433	2.05	2.8	2.2
Lu	0.32	0.45	0.36	0.3	0.47	0.38	0.16	0.31	0.42	0.43	0.36	0.31	0.42	0.32
Sc	12.42	16.23	10.72	9.42	8.15	9.31	8.69	8.39	14.27	8.07	10.57	13.64	13	13.6
Y	24.09	30.19	24.27	20.84	32.34	26.09	11.87	29.17	30.42	28.94	25.82	24.17	26	22

in average shale obtained from Turekian & Wedepohl (1961) was used. An element can be considered as a reference element if it is of low occurrence variability and present in the environment in trace amounts (Loska et al. 2003). According to Loska et al. (1997), it is also possible to apply an element of geochemical nature, which occurs in significant amounts in the environment but has no interaction or resistance towards an examined element. A reference element is often a conservative one, unchanged by anthropogenic influences; and the most used reference elements include Sc, Mn, Ti, Al, Fe, Zn, etc. (Loska et al. 1997, Mediolla et al. 2008).

Table 2: Enrichment Factor (EF) of trace and rare earth elements in the stream sediments.

Elements	AGU- 1	AGU-2	AGU-3	AGU-4	AGU-5	AGU-6	AGU-7	AGU-8	AGU-9	AGU-10	MEAN
V	0.43	0.76	0.39	0.53	0.45	0.36	0.4	0.22	0.49	0.16	0.42
Cr	1.09	2.07	0.71	0.94	0.75	0.61	2.27	0.3	0.49	0.2	0.94
Co	0.57	1.15	0.4	0.65	0.45	0.4	0.06	0.23	0.26	0.1	0.43
Ni	0.78	1.5	0.5	0.64	0.47	0.4	0.94	0.17	0.33	0.11	0.58
Cu	0.32	0.49	0.27	0.31	0.22	0.34	1.05	0.2	0.4	0.14	0.37
Rb	1.47	1.84	1.92	2.6	4.01	2.37	1.93	0.83	1.31	0.62	1.89
Sr	0.56	0.61	0.29	0.6	0.55	0.35	0.89	0.32	0.12	0.06	0.44
Zr	1.9	2.88	1.58	2.41	3.39	2.25	0.89	1.63	1.41	1.42	1.98
Nb	11.9	8.99	7.66	20.5	14.98	13.9	8.19	12.19	6.41	7.61	11.3
Mo	0.19	0.21	0.19	0.23	0.24	0.24	0.24	0.14	0.33	0.07	0.10
Cs	1.67	2.61	2.55	2.29	2.55	1.91	2.68	0.73	2.00	0.72	1.97
Ba	0.36	0.52	0.4	0.62	0.6	0.39	1.08	0.29	0.26	0.14	0.47
Hf	1.92	2.61	1.52	2.17	3.19	2.10	0.84	1.90	1.31	1.24	1.88
Ta	81.6	28.6	23.8	77.4	56.7	39.8	13.7	22.8	18.2	17.2	38.0
Pb	0.65	0.93	0.97	1.35	1.35	1.04	1.32	0.72	0.62	0.33	0.93
Th	0.74	0.95	0.44	0.66	1.14	0.76	0.46	1.85	0.59	0.53	0.81
U	1.93	2.20	2.02	2.46	2.88	3.59	2.64	3.22	1.95	0.68	2.36
La	1.45	1.29	0.81	1.14	0.91	1.03	1.34	2.17	0.86	1.10	1.21
Ce	1.65	1.43	1.43	0.89	1.28	0.95	1.18	1.52	2.42	0.82	1.36
Pr	1.53	1.32	0.83	1.09	0.91	1.05	1.27	2.28	0.80	1.17	1.22
Nd	1.70	1.44	0.90	1.18	1.01	1.15	1.44	2.49	0.91	1.31	1.35
Sm	2.04	1.57	1.00	1.17	1.11	1.37	1.41	2.94	1.00	1.31	1.49
Eu	1.41	1.44	0.86	1.24	0.86	1.05	1.71	0.98	0.81	0.87	1.12
Gd	1.89	1.58	1.08	1.11	1.12	1.48	1.54	2.68	1.07	1.28	1.48
Tb	1.65	1.35	1.13	1.06	1.21	1.51	1.21	2.60	1.22	1.12	1.41
Dy	1.43	1.33	1.16	1.16	1.36	1.44	1.31	1.86	1.33	1.22	1.36
Er	1.20	1.39	1.28	1.16	1.17	1.36	1.16	0.90	1.27	1.22	1.21
Tm	0.96	0.96	0.99	1.02	0.86	1.09	0.93	0.75	1.01	0.94	0.95
Yb	0.96	1.06	1.13	1.13	0.94	1.25	0.96	0.83	1.19	1.09	1.05
Lu	1.01	1.10	1.07	1.03	1.08	1.21	0.92	0.84	1.06	1.03	1.03
Sc	0.62	1.1	0.62	0.73	0.78	0.59	0.56	0.3	0.61	0.24	0.62
Y	0.60	1.02	0.69	0.80	0.55	0.82	0.38	0.52	0.65	0.44	0.75

Zn is moderately abundant; its natural abundance and sources surpass its anthropogenic source. In this study, the trace elements were normalized to Zn at global average shale value and Ho for the REE. These elements were chosen as the reference elements because there is no known anthropogenic activity either within the vicinity of the sampling locations or in the long-distance which can be traceable as the source of these elements. Five contaminated categories are recognized on the basis of the Enrichment Factor: EF <2 (deficiency to minimal enrichment); EF = 2 to 5 (moderate enrichments); EF = 5-20 (significant enrichment); EF = 20-40 (very high enrichment) and EF > 40, is extremely high enrichment (Sutherland 2000). According to Zhang & Liu (2002), EF values between 0.5 and 1.5 suggests that the element concerned may be derived entirely from crustal materials or natural weathering processes (geogenic). Values greater than 1.5 suggest a significant portion of the element has been supplied from non-natural (anthropogenic) sources. As the

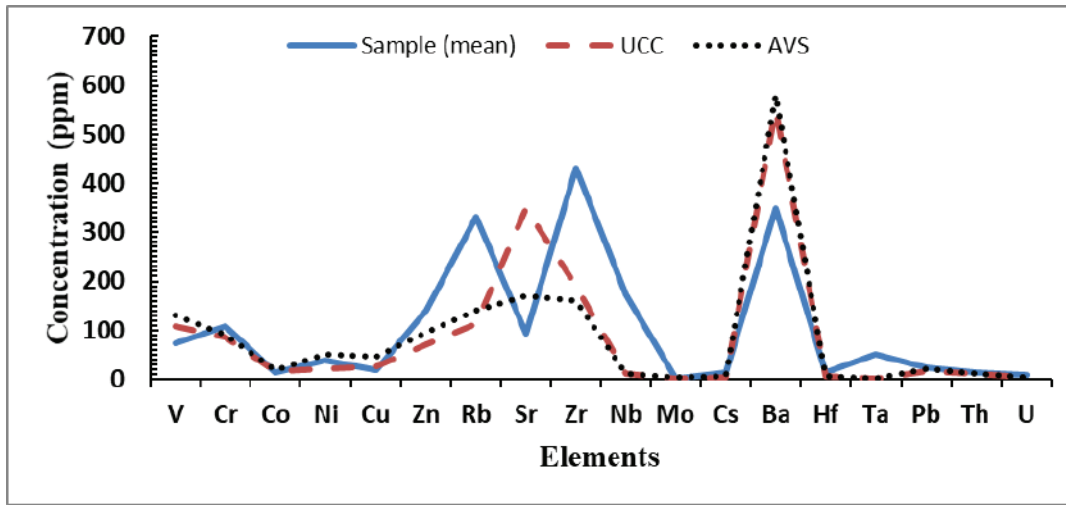

Fig. 4: Trace element concentration comparison between the mean of the samples studied, the upper continental crust and the average shale value.

EF values increase, the contributions of the anthropogenic origin also increase (Sutherland 2000).

The results of the enrichment factors of V, Cr, Co, Ni, Cu, Sr, Mo, Ba, Pb, Th, La, Ce, Pr, Nd, Sm, Eu, Gd, Tb, Mo, Dy, Er, Tm, Yb, Lu Sc, and Y shows that these metals are deficient to minimal enrichment, because EF were < 2. According to Zhang & Liu (2002), they are therefore naturally derived from the stream sediment and geogenic sources resulting from weathering processes in the environment. The average EF values of Rb, Zr, Hf, U and Cs indicated moderate enrichment, because they fall within the range of 2 < EF < 5. Only the EF of Nb has significant enrichment since the EF falls within the range 5 < EF < 20; and Ta has variable EF values from significant enrichment; very high enrichment to extremely high enrichment. Most of the EF values in the sediments were < 2 and 2< EF <5, except the Nb and Ta. According to Sutherland (2000) and Zhang et al. (2007), the metals, therefore, originated from anthropogenic activities.

Contamination Factor (CF) and Degree of Contamination (C_d)

According to Demie (2015), the degree of contamination is aimed at providing a measure of the degree of overall contamination in surface layers of a particular sampling site. CF is calculated for individual elements using the formula proposed by Hakanson (1980): $CF = C_{Element} / C_{Background}$, where $C_{Element}$ is the concentration of elements at the con-

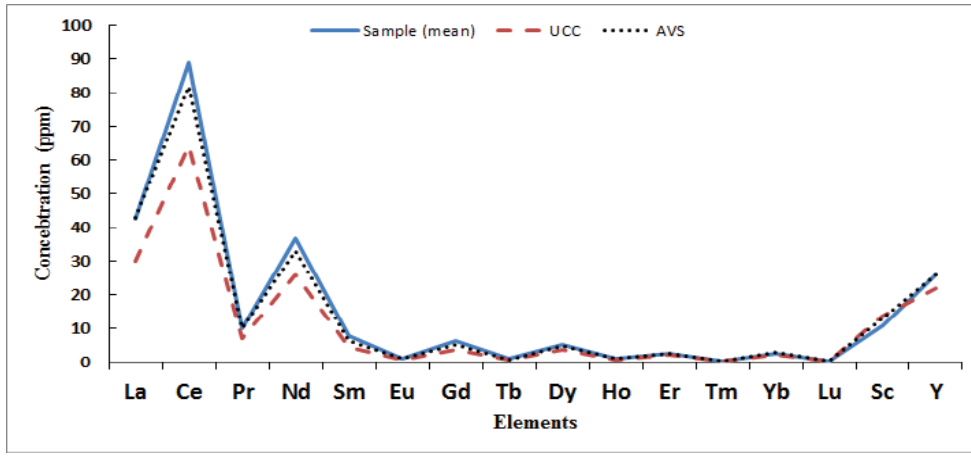

Fig. 5: REE concentration comparison between the mean of the samples studied, the upper continental crust and the average shale value.

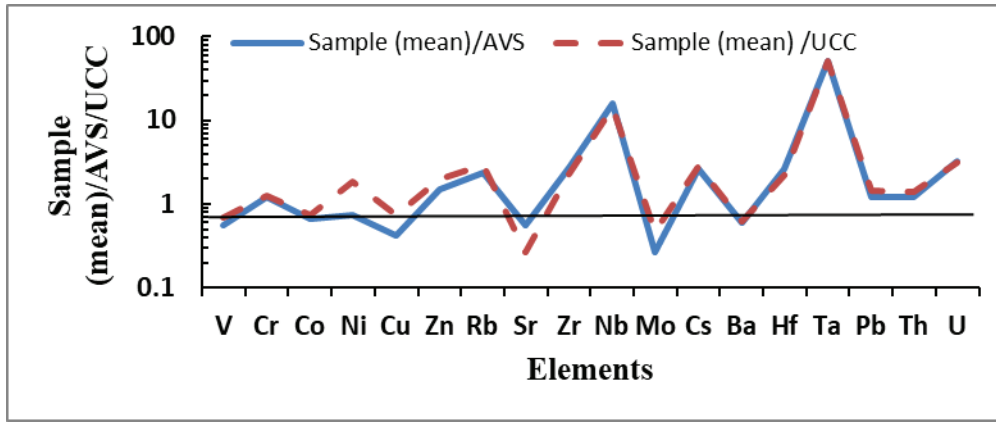

Fig. 6: AVS and UCC-normalized trace elements patterns for the stream sediments investigated.

taminated site and $C_{background}$ is the background value of the same element.

Contamination Factor values of trace and rare earth elements in the Agbangudu stream sediments are presented in Table 3. Hakanson (1980) applied the CF under four categories: CF<1 indicates low contamination; 1<CF<3 indicates moderate contamination; 3<CF<6 indicates considerable contamination; and CF>6 indicates very high contamination. The results revealed that the CF of V, Co, Zr, Nb, Mo, Hf, Th, La, Ce, Pr, Nd, Sm are Scare low; CF<1. The CF of Cu, Zn, Sr, Ba, Pb, U, Eu, Gd, Tb, Dy, Ho, Er, Tm, Yb, Lu and Y all have moderate contamination. The CF of Cr, Ni, and Rb have considerable contamination; all of Cs and Ta locations have very high contamination because they have CF > 6. The high values for Cs and Ta may be due to geogenic and anthropogenic sources.

The degree of contamination (C_d) is the sum of individual contamination factor of the pollutant (Hakanson 1980). This parameter is aimed at providing a measure of the degree of overall contamination in surface layers in particular sampling sites. The degree of contamination (C_d) is computed by the equation by Hakanson (1980):

$$C_d = \sum_{i=1}^{n} Cf^i \quad \text{.....(2)}$$

Where, Cf is the contamination factor of each element; n is the number of elements under investigation. A modified form of the Hakanson (1980) equation proposed by Abrahim & Parker (2008) for the calculation of the overall degree of contamination was utilized in this study and computed by the equation 3:

$$mC_d = \frac{\sum_{i=1}^{n} Cf^i}{n} \quad \text{...(3)}$$

Where, mC_d is modified degree of contamination, n is the number of analysed element and Cf^i is the contamination factor; the mC_d data for the work are presented in Table 4.

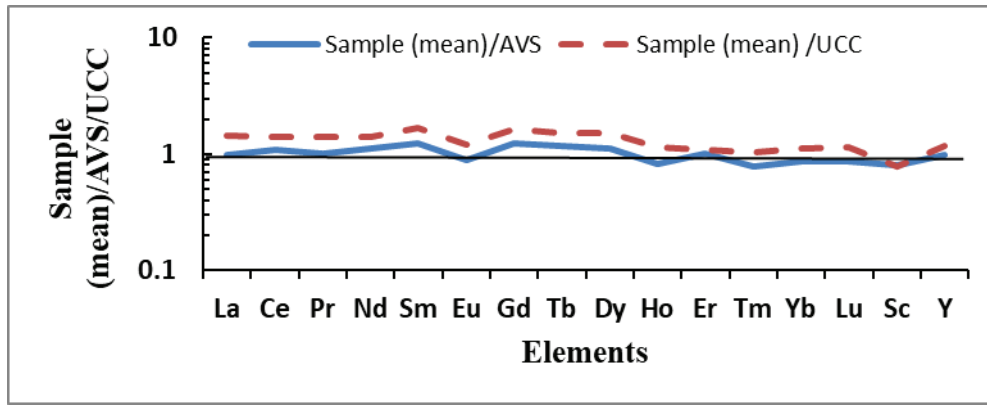

Fig. 7: AVS and UCC-normalized REE patterns for the stream sediments investigated.

Table 3: Contamination factor (CF) of trace and rare earth elements in the stream sediment.

Elements	AGU-1	AGU-2	AGU-3	AGU-4	AGU-5	AGU-6	AGU-7	AGU-8	AGU-9	AGU-10	MEAN
V	0.99	1.31	0.80	0.80	0.54	0.66	0.72	0.71	1.34	0.62	0.85
Cr	5.04	7.03	2.88	2.81	1.81	2.25	8.14	1.94	2.65	1.53	3.61
Co	0.04	0.06	0.02	0.03	0.02	0.02	0.06	0.02	0.02	0.07	0.04
Ni	5.09	8.34	3.32	3.12	1.83	2.40	5.50	1.83	2.86	1.34	3.56
Cu	1.13	1.27	0.83	0.71	0.41	0.94	0.81	1.02	1.66	0.80	0.96
Zn	2.18	1.60	1.91	1.42	1.13	1.73	1.69	3.07	2.55	3.60	2.09
Rb	5.36	4.94	6.14	6.15	7.60	6.87	5.48	4.29	5.59	3.73	5.62
Sr	1.92	1.54	0.89	1.33	0.99	0.96	2.39	1.58	0.48	0.36	1.24
Zr	0.80	0.09	0.06	0.07	0.08	0.08	0.03	0.10	0.07	0.10	0.15
Nb	0.73	0.40	0.41	0.81	0.47	0.67	0.39	1.04	0.46	0.76	0.61
Mo	0.55	0.45	0.47	0.42	0.36	0.55	0.54	0.55	1.11	1.09	0.61
Cs	45.89	52.96	61.36	40.79	36.61	41.79	57.32	28.18	64.39	32.68	46.20
Ba	2.58	2.78	2.53	2.93	2.28	2.21	6.08	2.98	2.23	1.71	2.83
Hf	0.57	0.57	0.39	0.41	0.49	0.49	0.19	0.79	0.45	0.61	0.50
Ta	123.50	31.91	31.57	75.77	44.68	47.72	16.17	48.58	32.32	43.09	49.53
Pb	1.33	1.39	1.72	1.77	1.43	1.68	2.07	2.05	1.48	1.09	1.60
Th	0.33	0.31	0.17	0.19	0.26	0.27	0.16	1.16	0.31	0.39	0.35
U	1.89	1.59	1.74	1.56	1.47	2.79	2.00	4.44	2.24	1.11	2.08
La	0.64	0.73	0.38	0.46	0.55	0.44	0.32	1.11	0.47	0.63	0.57
Ce	0.63	0.70	0.36	0.45	0.50	0.44	0.32	1.08	0.39	0.60	0.55
Pr	0.73	0.81	0.42	0.48	0.60	0.50	0.33	1.27	0.48	0.73	0.63
Nd	0.81	0.89	0.46	0.52	0.66	0.54	0.38	1.39	0.54	0.82	0.70
Sm	1.19	1.17	0.61	0.62	0.88	0.79	0.45	2.00	0.72	1.00	0.94
Eu	1.88	2.47	1.22	1.51	1.57	1.38	1.25	1.53	1.35	1.53	1.57
Gd	1.28	1.38	0.77	0.69	1.04	0.99	0.57	2.12	0.91	1.14	1.09
Tb	1.64	1.72	1.19	0.97	1.64	1.48	0.66	3.02	1.52	1.45	1.53
Dy	1.56	1.87	1.34	1.16	2.02	1.55	0.78	2.36	1.81	1.73	1.62
Ho	0.94	1.21	1.00	0.87	1.29	0.93	0.52	1.10	1.18	1.24	1.03
Er	1.21	1.80	1.36	1.07	1.61	1.36	0.64	1.06	1.60	1.61	1.33
Tm	1.14	1.46	1.25	1.11	1.39	1.29	0.61	1.04	1.50	1.46	1.23
Yb	0.99	1.41	1.23	1.07	1.34	1.28	0.54	1.00	1.53	1.48	1.19
Lu	1.03	1.45	1.16	0.97	1.52	1.23	0.52	1.00	1.35	1.39	1.16
Sc	0.91	1.91	0.79	0.69	0.60	0.68	0.64	0.62	1.05	0.59	0.85
Y	1.00	1.25	1.00	0.86	1.34	1.08	0.49	1.21	1.26	1.20	1.07

Abrahim & Parker (2008) proposed the following classes for the modified degree of contamination: mCd<1.5, nil to very low degree of contamination; 1.5≤mCd<2, low degree of contamination; 2≤mCd<4, moderate degree of contamination; 4≤mCd<8, high degree of contamination; 8≤mCd<16, a very high degree of contamination; 16 ≤ mCd< 32, an extremely high degree of contamination and mCd≥32 means the ultra-high degree of contamination. Results from this study classified the level of the metal as non-contaminated to very low contamination, while Ta and Nb showed a high degree of contamination.

Pollution Load Index (PLI)

The Pollution Load Index (PLI) was developed by Tomlin-

son et al. (1980) to compare pollution levels between sites and propose a necessary line of action. According to Priju & Narayana (2006), PLI represents the number of times by which the element concentrations in the sediments exceeds the background concentration, and gives a summative indication of the overall level of element toxicity at a particular sample site. The PLI was computed based on the method proposed by Tomlinson et al. (1980). The PLI of the area was evaluated by obtaining the n-root from the n-CFs that were obtained for all the elements. This parameter is expressed as:

$$PLI = (CF1 \times CF2 \times CF3 \times .....CFn)1/n \quad \ldots(4)$$

Where, n is the number of elements and CF is the contamination factor, the PLI values are shown in Table 4. According to Tomlinson et al. (1980), a Pollution Load Index (PLI) <1 denote perfection; PLI = 1 present that only baseline levels of pollutants are present and PLI > 1 would indicate deterioration of site quality. The results obtained put the PLI values at approximately 1, which indicates only baseline levels of metals. However, PLI data without Ta and Cs denotes perfection. Likuku et al. (2013) proposed that a PLI value of ≥1 indicates an immediate intervention to ameliorate pollution; 0.5≤PLI<1 suggests that more detailed study is needed to monitor the site, whilst a value of <0.5 indicates that there is no need for drastic rectification measures to be taken.

Geoaccumulation Index (Igeo)

Geoaccumulation index (Igeo) was first introduced by Muller (1969) to compare the present-day heavy metal concentration with the pre-civilized background values. According to Singh et al. (1997), Igeo can be used to quantify the degree of contamination in stream sediments. Afkhami et al. (2013) affirmed that Igeo values can be used effectively and more meaningfully in explicating sediment quality. The Igeo of the elements was calculated by computing the base 2 log of the measured total concentration of the element over its background concentration using this equation:

$$Igeo = \log_2 [Cn/1.5 \times Bn] \quad \ldots(5)$$

Where, Cn is the measured concentration of the stream sample for the element (n), and Bn is the background value of the element (n). The correction factor; 1.5 was used to account for possible variations in background data due to lithogenic effects. Muller (1969) proposed seven descriptive classes for increasing Igeo values: Igeo>5 indicates extremely contaminated; 4<Igeo<5 indicates strongly to extremely contaminated; 3<Igeo<4 indicates strongly contaminated; 2<Igeo<3 indicates moderately to strongly contaminated; 1<Igeo<2 indicates moderately contaminated; 0<Igeo<1 indicates uncontaminated to moderately contaminated; and Igeo = 0 indicates uncontaminated. The geoaccumulation index (Igeo) of the elements in the stream sediments is shown in Table 5. All the elements showed uncontaminated to moderately contaminated, except for Cs and Ta with strongly to extremely contaminated status.

Rare Earth Element

The chondrite normalisation curves (Fig. 8) show enrichment in light rare earth elements (LREE) and depletion of heavy rare earth elements (HREE). The Average Shale Value (AVS) and the Upper Continental Crust (UCC) normalized REE distribution patterns of the stream sediments are given in Figs. 9A and 9B indicating a moderate enrichment in LREE. All the samples show a (La/Yb)n>1, meaning an enrichment in LREE in the stream sediments (Table 6). These observations show that the REEs are mainly derived from intermediate and felsic rocks (McLennan 1989). Flat REE distribution

Table 4: Modified Degree of Contamination (mCd) Pollution Load Index (PLI) of the trace and rare earth elements in the stream sediments.

Sample ID	mCd	PLI	mCd*	PLI*
AGU-1	6.40	1.32	1.42	1.03
AGU-2	4.12	1.40	1.62	1.13
AGU-3	3.88	1.00	1.14	0.79
AGU-4	4.55	1.02	1.12	0.79
AGU-5	3.56	1.03	1.17	0.82
AGU-6	3.82	1.07	1.18	0.85
AGU-7	3.49	0.86	1.33	0.69
AGU-8	3.74	1.43	1.48	1.17
AGU-9	4.11	1.16	1.27	0.93
AGU-10	3.31	1.05	1.08	0.84

mCd* and PLI* = without Ta and Cs values

Table 5: Geoaccumulation Index (Igeo) of trace and rare earth elements in the stream sediment.

Elements	AG-1	AG-2	AG-3	AG-4	AG-5	AG-6	AG-7	AG-8	AG-9	AG-10	Mean
V	-0.60	-0.20	-0.91	-0.91	-1.47	-1.19	-1.05	-1.08	-0.17	-1.29	-0.89
Cr	0.22	2.23	0.94	0.90	0.27	0.58	2.44	0.37	0.82	0.02	0.88
Co	-5.29	-4.71	-5.96	-5.71	-6.55	-6.13	-4.75	-6.10	-6.16	-7.01	-5.84
Ni	1.98	2.48	1.14	1.06	0.29	0.68	1.87	0.29	0.93	-0.16	1.06
Cu	-0.41	-0.24	-0.68	-1.09	-1.87	-0.67	-0.88	-0.56	0.15	-0.92	-0.72
Zn	0.54	0.10	0.35	-0.09	-0.41	0.20	0.17	1.03	0.76	1.26	0.39
Rb	1.84	1.72	2.03	2.04	2.34	2.20	1.87	1.52	1.90	1.32	1.88
Sr	0.36	0.04	-0.76	-0.17	-0.60	-0.65	0.67	0.07	-1.66	-2.05	-0.48
Zr	-4.16	-4.00	-4.61	-4.43	-4.26	-4.25	-5.62	-3.89	-4.36	-3.85	-4.34
Nb	-1.04	-1.90	-1.88	-0.90	-1.67	-1.83	-1.96	-0.52	-1.72	-0.97	-1.44
Mo	-1.45	-1.74	-1.67	-1.83	-2.07	-1.45	-1.49	-1.45	-0.43	-2.01	-1.56
Cs	4.94	5.14	5.35	4.77	4.61	4.80	5.26	4.23	5.42	4.45	4.90
Ba	0.78	0.89	0.75	0.96	0.60	0.56	2.02	0.99	0.57	0.19	0.83
Hf	-1.41	-1.41	-1.93	-1.86	-1.62	-1.61	-2.96	-0.93	-1.73	-1.31	-1.68
Ta	6.36	4.41	4.40	5.66	4.90	4.99	3.43	5.02	4.43	4.84	4.84
Pb	-0.17	-0.11	0.20	0.24	-0.07	0.16	0.47	0.45	-0.02	-0.46	0.07
Th	-2.19	-2.27	-3.12	-2.99	-2.51	-2.48	-3.23	-0.38	-2.29	-1.94	-2.34
U	0.33	0.08	0.21	0.06	-0.03	0.89	0.42	1.57	0.58	-0.44	0.37
La	-1.24	-1.04	-2.00	-1.71	-1.46	-1.75	-2.22	-0.43	-1.66	-1.24	-1.48
Ce	-1.26	-1.11	-2.06	-1.75	-1.60	-1.75	-2.24	-0.48	-1.94	-1.33	-1.55
Pr	-1.04	-0.89	-1.84	-1.65	-1.33	-1.60	-2.17	-0.24	-1.64	-1.04	-1.34
Nd	-0.89	-0.76	-1.71	-1.54	-1.19	-1.47	-1.99	-0.11	-1.46	-0.87	-1.20
Sm	-0.34	-0.35	-1.29	-1.27	-0.77	-0.93	-1.74	0.41	-1.05	-0.59	-0.79
Eu	0.33	0.72	-0.30	0.01	0.07	-0.12	-0.26	0.03	-0.15	0.03	0.04
Gd	-0.23	-0.12	-0.96	-1.13	-0.53	-0.60	-1.40	0.50	-0.73	-0.40	-0.56
Tb	0.13	0.20	-0.34	-0.63	0.13	-0.02	-1.19	1.01	0.01	-0.05	-0.07
Dy	0.05	0.31	-0.17	-0.38	0.43	0.04	-0.94	0.65	0.27	0.21	0.05
Ho	-0.67	-0.31	-0.58	-0.79	-0.22	-0.69	-1.54	-0.45	-0.35	-0.28	-0.59
Er	-0.31	0.27	-0.14	-0.49	0.10	-0.15	-1.23	-0.50	0.09	0.10	-0.23
Tm	-0.39	-0.03	-0.26	-0.44	-0.11	-0.22	-1.30	-0.53	0.00	-0.03	-0.33
Yb	-0.60	-0.09	-0.28	-0.48	-0.17	-0.23	-1.47	-0.59	0.03	-0.02	-0.39
Lu	-0.54	-0.05	-0.37	-0.63	0.02	-0.29	-1.54	-0.58	-0.15	-0.11	-0.42
Sc	-0.72	-0.33	-0.93	-1.12	-1.33	-1.14	-1.24	-1.29	-0.52	-1.34	-1.00
Y	-0.59	-0.26	-0.58	-0.80	-0.16	-0.47	-1.61	-0.31	-0.25	-0.33	-0.54

commonly observed from river sediments is due to the average upper crustal surface composition and source rocks (Sholkovitz 1993). Also, according to Sholkovitz (1993), the mixing and homogenizing effects of sedimentary processes will produce uniform REE pattern which signifies the abundance in the upper continental crust. Enrichment of LREE reflects the intense silicate weathering of crustal materials and a subsequent increase in LREEs in detrital. The LREE/HREE ratios for the stream sediments range from 6.7 to 12.9 with an average of 9.13 (Table 5), which is slightly more than the upper crustal ratio and is equal to average shale ratio. (La/Yb)n ratios range between 7.89 to 28.93 with a mean ratio of 13.22 and that indicates very high erosional rates, which suggests that La was removed from the crustal

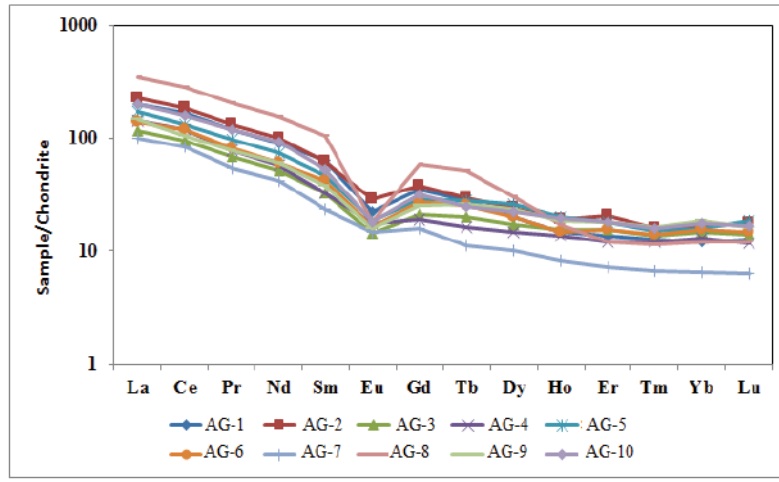

Fig. 8: REE composition of the stream sediments normalized to chondrites based on Taylor & McLennan (1985).

source through the weathering process, then transported and deposited by the streams.

According to McLennan (1988), generally, the La/Yb ratio is found to be very low in sediments rich in coarse size fractions and felsic minerals. Ramesh et al. (2000) opined that physical weathering is predominant in fine-grained sediments, which suggests that REEs fractionation took place in the stream. Y exhibits a moderate positive correlation with the LREEs (0.50), suggesting a partial association with detrital. Variation in Ce anomalies is indicative of terrigenous input, depositional environment and diagenetic conditions (Toyoda et al. 1990). Ce/Ce*>1 and <1 indicates positive (reducing environment) and negative (toxic environment) anomalies, respectively (Toyoda et al. 1990). Ce/Ce* ratio range of 3.14 to 3.70 with a mean ratio of 3.47 suggests minimal terrigenous input in a reducing environment.

All the Eu/Eu* ratios for the stream sediments are <1 (Table 6), implying that the origin of this element (Eu) is rich in feldspar source, contributing to a positive anomaly in the stream. According to Burg et al. (1984) and Gansser et al. (1983), this may also be due to the weathering of granite and granitic gneiss in the source region.

Cluster Analysis

For a more detailed comparison of the analysed metals and oxides in the stream sediments, cluster analysis by Ward (1963) method was performed and a dendrogram illustrating the results were presented in Figs. 10 to 12. This was employed in the study to see a possible association of the elements and to determine the similarities as regards the levels of the analysed metals and oxides. The distance cluster represents the degree of association between the elements and oxides. The lower the values on the distance cluster the more significant the association. Despite the common occurrence of these elements and oxides, their overall patterns were much different as revealed by the

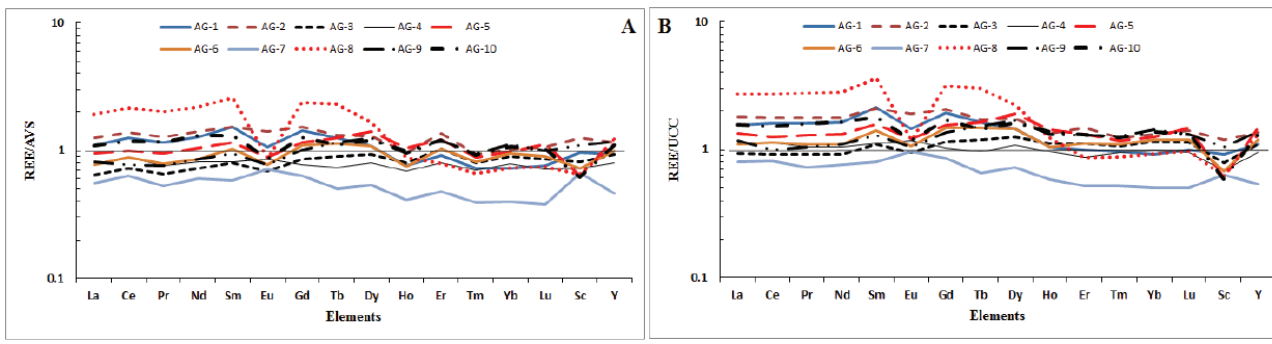

Fig. 9: (A) The average shale value (AVS) and (B) upper continental crust (UCC) normalised REE distribution pattern of the stream sediments.

cluster analysis. In Fig. 10, three distinct clusters can be identified; Cluster 1 contained Y, La, Nd, SiO2 and Ce; indicating a close relationship between La and Nd, while a possible relationship was also exhibited between SiO2 and Ce. This was similar to the enrichment factor of the metals, where the results revealed that the metals were naturally derived and geogenic sources resulting from weathering processes in the sediments. Clusters 2 showed possible interaction between most rare-earth elements and oxides such as CrO_2, MnO, P_2O_5, CaO, TiO_2, Fe_2O_3, K_2O, Na_2O and MgO, while Cluster 3 reflected the strong relationship of Al_2O_3 with Sc, Gd, Dy, Pr and Sm at a particular level. These elements may probably be affected by a similar factor or originate from the same natural parents of the sediments. In Fig. 11, three clusters were also formed. Cluster 1 showed a close relationship between Zr, Rb and Ba. Cluster 2 showed that majority of the trace elements and oxides were found to be closely associated with other elements in natural materials, especially with those that formed a distinct cluster at a distance cluster of below 200, while Cluster 3 showed a close association between Zn, Nb, Cr, Sr, Ta, V and SiO_2. The association may reflect possible

Table 6: Distribution of ΣLREE, Σ HREE, Σ REE, Σ LREE/ Σ HREE and ratios and anomalies of some rare earth elements in the stream sediments.

Sample ID	ΣLREE	ΣHREE	ΣREE	ΣLREE/ΣHREE	La/Yb	La/Sm	Gd/Yb	Eu/Eu*	**Ce/Ce***
AG-1	212.57	20.51	269.59	10.36	16.65	3.18	2.98	0.47	3.51
AG-2	236.05	24.96	307.43	9.46	13.39	3.68	2.25	0.6	3.48
AG-3	121.9	17.05	173.94	7.15	7.89	3.63	1.44	0.54	3.48
AG-4	146.26	14.93	191.45	9.8	11.06	4.36	1.47	0.71	3.66
AG-5	172.04	22.44	234.97	7.67	10.58	3.68	1.79	0.5	3.33
AG-6	147.91	19.32	202.63	7.66	9.03	3.34	1.78	0.48	3.62
AG-7	104.1	10.17	134.83	10.24	15.47	4.27	2.42	0.76	3.7
AG-8	366.02	28.37	431.95	12.9	28.93	3.3	4.89	0.23	3.47
AG-9	140.74	21	206.43	6.7	8.04	3.88	1.36	0.51	3.14
AG-10	206.96	22.09	266.06	9.37	11.14	3.78	1.77	0.44	3.36
MEAN	185.46	20.08	241.93	9.13	13.22	3.71	2.22	0.52	3.47

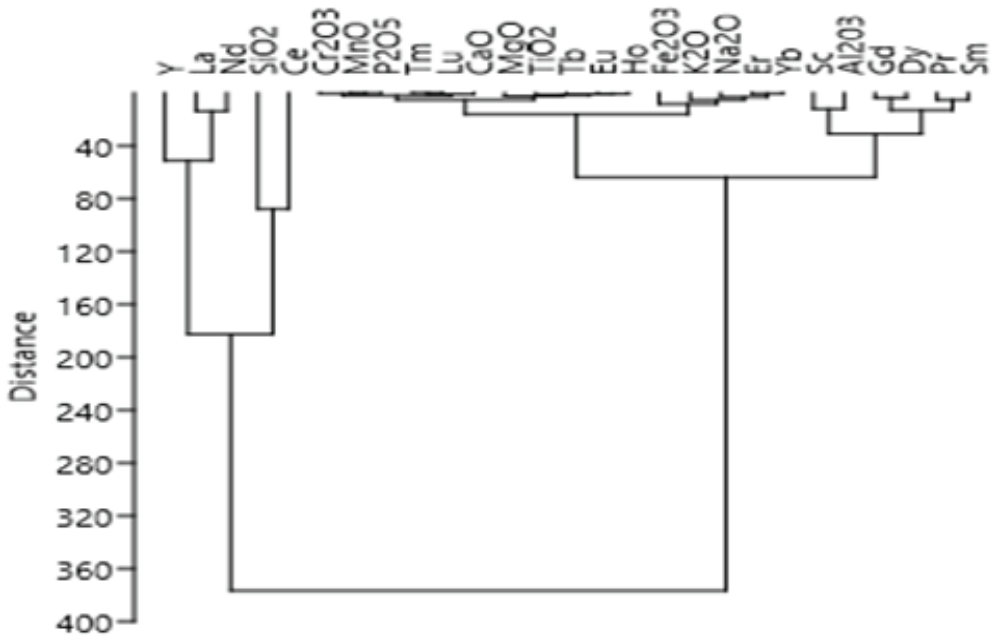

Fig.10: Dendrogram derived from the hierarchical cluster analysis of rare-earth elements and major oxides in the analysed stream sediments.

Table 7: Matrix of the principal analysis loadings of major oxides and trace elements in the stream sediments.

Oxides and elements	PC1	PC2	PC3	PC4	PC5
SiO_2	-0.017	0.011	-0.046	-0.009	-0.04
Al_2O_3	0.005	-0.015	0.01	0.005	0.016
Fe_2O_3	0.004	0.006	0.016	-0.007	0.007
CaO	0.0005	0.0008	0.003	0.004	0.003
MgO	0.002	0.002	0.008	0.004	0.004
MnO	0.0003	0.0004	-0.0002	-0.0001	-0.0003
K_2O	0.002	-0.003	-0.006	0.006	-0.009
Na_2O	0.001	-0.002	-0.001	0.0006	0.002
P_2O_5	0.0006	0.0006	0.0005	0.0003	0.0001
TiO_2	-0.0001	0.002	0.003	-0.002	0.002
Cr_2O_3	-5.70E-38	-3.00E-37	-3.50E-36	7.90E-36	-1,0E-37
V	-0.0008	0.017	0.262	-0.066	0.218
Cr	0.274	0.19	0.607	0.125	0.169
Co	0.025	0.02	0.062	0.027	0.012
Ni	0.053	0.046	0.283	0.096	0.122
Cu	-0.004	0.015	0.046	-0.035	0.064
Zn	-0.127	0.33	-0.179	-0.469	0.189
Rb	0.065	-0.601	-0.105	0.425	-0.225
Sr	0.181	0.188	0.066	0.443	0.127
Zr	-0.552	0.435	0.266	0.318	-0.496
Nb	-0.154	0.325	-0.554	0.39	0.232
Mo	3.70E-05	-0.0002	0.0002	-0.002	0.003
Cs	0.009	-0.012	0.024	-0.027	0.031
Ba	0.732	0.39	-0.207	0.061	-0.339
Hf	-0.017	0.019	-0.0006	0.017	-0.017
Ta	-0.048	0.026	-0.024	0.333	0.613
Pb	0.015	0.006	-0.037	0.013	-0.023
Th	-0.022	0.074	-0.056	0.031	-0.09
U	-0.001	0.015	-0.026	0.015	-0.022

natural parent materials, or inputs of some anthropogenic activities and/or natural geochemical system.

A distance cluster of about 160 was used for trace elements and rare-earth metals analysis (Fig. 12). Cluster 1 showed a close association between Cr, Sr and Ce. Cluster 2 is in three groups, with Ta, La, Ni and Nd in group 1, while the second group contained Cu, Pb, Y and Th and combines with the other group which contain most elements. This suggested that the association between these elements is very significant and further indicates that the elements probably originated from natural materials or natural geochemical system and/or possibly associated with inputs from anthropogenic activities. The clustering of the metals also reaffirms the confirmation of EF results, which shows that the metals are majorly from natural and geogenic sources. A distinct relationship was observed between Zn and Nb, while Rb, Ba and Zr also formed a distinct cluster at about 720 Euclidean distance. Rb and Zr indicated moderate enrichment from the EF, this was also affirmed from the close association of the metals.

Principal Component Analysis

The results of principal component analysis (PCA) of the metals and oxides concentrations in the stream sediments are shown in Tables 7-9. Five principal components were em-

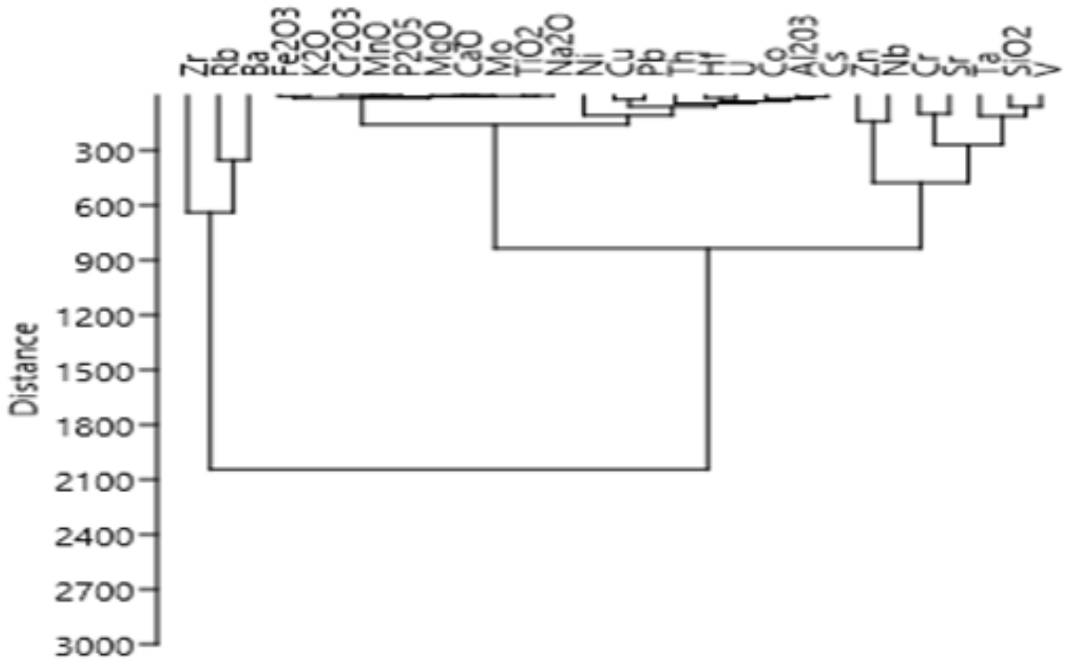

Fig. 11: Dendrogram derived from the hierarchical cluster analysis of trace elements and major oxides in the analysed stream sediments.

Fig. 12: Dendrogram derived from the hierarchical cluster analysis of trace elements and rare-earths in the analysed stream sediments.

ployed, PC1 accounted for 64.5 to 95.9% of the total variance in three interactions. Table 7 showed the factor loadings for major oxides and trace elements. PC1, PC2, PC3, PC4 and PC5 accounted for 65.8%, 18%, 7.32%, 5.6% and 2.10% respectively. Interpretation of PCA patterns factor loadings greater than 0.71 is typically considered excellent, while those less than 0.32 are regarded as very poor (Nowak 1998). Except for Zn, Rb, Sr, Zr, Nb, Ta and Ba, the remaining trace

elements and major oxides were less than 0.32 in the five rotated factors. Factor 2 accounted for 18%, where Zn and Zr were closely associated. Vanadium was found to be associated with Ni and Zr in PC3, while Rb was associated with Sr and Nb in PC4; making up 5.86% of the total variance. The results indicated that the metals are associated with some rock-forming elements, which may have originated from parental materials of the sediments. Factors 2 and 3 association revealed low to moderate contamination of the metals involved as revealed by the contamination factor result.

Table 8 is the factor loadings for the metal oxides and rare-earth elements interactions from PCA. The first component explains 95.9% of the total variance and loads heavily on La, Ce and Nd. The loading pattern of these metals possibly reflects scarcely low contamination level. The second and third component, loaded on Y and (Al_2O_3, La, Dy and Sc), accounting for 1.95% and 1.68% of the total variance. The factors loading for trace and rare-earth elements interaction are shown in Table 9. The principal components that have eigenvalues higher than one were also employed for their interactions. The first component (PC1) explains 64.5% of the total variance and loads heavily on Sr and Ba. The PC2 loads heavily by Zr, Nb and Ba and accounted for 18.9% of the total variance. The third and fourth component PC3 and PC4 account for 7.09% and 5.83% respectively, and loaded by Cr, Rb, Sr and Nb, while the PC5 accounted for 2.3% and loaded by Zr and Ba. The PCA analysis results suggest that the metals that load positively on the same component are likely associated and possibly showed similar sources, distribution pattern

Table 8: Matrix of the principal analysis loadings of major oxides and rare-earth elements in the stream sediments.

Oxides and elements	PC1	PC2	PC3	PC4	PC5
SiO_2	0.052	0.759	-0.322	0.129	-0.057
Al_2O_3	-0.031	-0.226	0.226	-0.542	0.18
Fe_2O_3	-0.001	-0.23	0.077	0.379	0.3
CaO	0.001	-0.039	-0.002	0.004	-0.112
MgO	-9.70E-07	-0.087	-0.004	0.101	-0.165
MnO	0.0001	-0.007	-0.007	0.006	0.016
K_2O	-0.004	-0.005	-0.064	-0.298	0.046
Na_2O	-0.003	-0.018	-0.029	-0.156	-0.068
P_2O_5	0	-0.002	-0.001	-0.004	-0.004
TiO_2	0.005	0.009	0.028	0.143	-0.06
Cr_2O_3	1.43E-35	1.93E-34	-4.32E-03	1.07E-33	-8.72E-33
La	0.385	0.006	0.158	0.0771	0.551
Ce	0.836	-0.135	-0.153	-0.182	-0.396
Pr	0.096	0.019	0.018	0.046	0.045
Nd	0.354	0.086	0.079	0.324	0.343
Sm	0.081	-0.009	0.03	-0.085	0.067
Eu	0.002	-0.014	0.017	0.03	-0.079
Gd	0.057	-0.003	0.051	-0.06	0.04
Tb	0.008	0.005	0.015	-0.038	0.032
Dy	0.026	0.072	0.139	-0.094	0.125
Ho	0.002	0.018	0.025	0.009	-0.008
Er	0.001	0.043	0.094	0.0712	-0.11
Tm	0.0002	0.006	0.011	0.006	-0.011
Yb	0.0007	0.052	0.083	0.052	-0.068
Lu	0.0003	0.008	0.013	0.002	-0.013
Sc	-0.0007	-0.26	0.352	0.455	-0.422
Y	0.065	0.454	0.785	-0.143	-0.141

Table 9: Matrix of the principal analysis loadings of trace and rare-earth elements in the stream sediments.

Elements	PC1	PC2	PC3	PC4	PC5
V	-0.0009	0.014	0.263	-0.059	0.166
Cr	0.27	0.191	0.632	0.041	-0.237
Co	0.024	0.02	0.-065	0.018	-0.018
Ni	0.052	0.047	0.295	0.06	-0.14
Cu	-0.004	0.013	0.039	-0.038	-0.039
Zn	-0.129	0.295	-0.221	-0.479	-0.149
Rb	0.07	0.201	0.101	0.406	-0.17
Sr	0.76	0.201	0.101	0.406	-0.17
Zr	-0.555	0.405	0.311	0.234	0.352
Nb	-0.157	0.315	-0.547	0.379	-0.271
Mo	4.30E-05	-0.0003	-0.0002	-0.002	-0.001
Cs	0.009	-0.012	0.021	-0.027	-0.02
Ba	0.723	0.41	-0.198	0.065	0.311
Hf	-0.017	0.019	0.0008	0.016	0.017
Ta	-0.048	0.026	-0.011	0.296	-0.635
Pb	0.015	0.008	-0.038	0.019	0.033
Th	-0.023	0.074	-0.056	0.036	0.106
U	-0.001	0.016	-0.027	0.019	0.033
La	-0.044	0.112	0.002	0.084	0.132
Ce	-0.089	0.251	0.0007	0.212	0.251
Pr	-0.001	0.028	0.0006	0.021	0.03
Nd	-0.041	0.105	0.003	0.071	0.11
Sm	-0.009	0.023	-2.00E-05	0.02	0.023
Eu	-0.0003	0.0008	0.003	0.001	6.00E-05
Gd	-0.007	0.015	0.002	0.013	0.02
Tb	-0.001	0.002	-0.004	0.002	0.004
Dy	-0.006	0.003	0.002	0.004	0.019
Ho	-0.0009	-0.0002	0.0009	-0.0003	0.002
Er	-0.002	-0.002	0.006	-0.002	0.004
Tm	-0.003	-0.002	0.003	-0.003	0.003
Yb	-0.002	-0.002	0.003	-0.003	0.003
Lu	-0.004	-0.0003	0.0006	-0.0002	0.0007
Sc	-0.0007	-0.0008	0.036	-0.005	-0.015
Y	-0.026	-0.007	0.024	0.0009	0.061

and/or possibly affected by the same factors in the stream sediments.

CONCLUSIONS

This study revealed that the mean values of V, Co, Cu, Zr, Nb, Hf, Th, Mo and REEs: La, Ce, Pr, Nd, Sm, Sc, are below the background values, while Cr, Ni, Zn, Rb, Sr, Cs, Ba and the REEs: Eu, Gd, Tb, Dy, Er, Tm, Yb, Lu, Y, exceeded the background values. The average EF values of Rb, Zr, Hf, U and Cs indicate moderate enrichment, while Nb has significant enrichment. The study also classified the metals as non-contaminated to very low contamination, while Ta and Nb showed a high degree of contamination. The results

showed the PLI values of approximately 1, which indicates only baseline levels of metals. The geoaccumulation index (Igeo) of the elements revealed uncontaminated to moderately contaminated, except for Cs and Ta with strongly to extremely contaminated status. The LREE/HREE ratios for the stream sediments range from 6.7 to 12.9 with an average of 9.13. The (La/Yb)n ratios indicate very high erosional rates, which suggests that La was removed from the crustal source through the weathering process, which was later transported and deposited by the streams.

REFERENCES

Abrahim, G.M.S. and Parker, R.J. 2008. Assessment of heavy metal enrichment factors and the degree of contamination in marine sediments from Tamaki Estuary, Auckland, New Zealand. Environ. Monit. Assess., 136: 227-238.

Afkhami, F., Karbassi, A.R., Nasrabadi, T. and Vosoogh, A. 2013. Impact of oil excavation activities on soil metallic pollution: Case study of an Iran Southern Oil Field. Environ. Earth Sci., 70(3): 1219-1224.

Ajibade, A. C., Woakes, M. and Rahaman, M. A. 1987. Proterozoic crustal development in the Pan- African regime of Nigeria. American Geophysic. J., 259-271.

Akinola, O.O., Okunlola, O.A. and Obasi, R.A. 2014. Compositional characteristics and industrial potential of lateritic clay deposit in Ara-Ijero Ekiti Areas, Southwestern Nigeria. Inter. J. Sci. Tech. Research, 3(3): 278-284.

Black, R., Caby, R., Monssine Pouchkin, A., Bayer, R., Bertrand, J. M., Bourllier, A. M., Fabri, J. and Lesquer, A. 1979. Evidence for late Precambrian plate tectonics in West Africa. Nature, 278: 223-227.

Buat-Menard, P. and Chesselet, R. 1979. Variable influence of the atmospheric flux on the trace metal chemistry of oceanic suspended matter. Earth and Planetary Sci. Letters, 42: 398-411.

Burg, J. P., Brunel, M., Gapais, D., Chen, G. M. and Liu, G. H. 1984. Deformation of the crystalline main central sheet in southern Tibet (China). J. Struc. Geol., 6: 535-542.

Burke, K.C. and Dewey, J.F. 1972. Orogeny in Africa. In: Dessauvagie T.F.J., Whiteman A.J. (eds.), Africa Geology. University of Ibadan Press, Ibadan, pp. 583-608.

Castor, B. and James, B. H. 2006. Rare earth elements. In E. K. Jessica, C. T. Nikhil, M. B. James (eds.), Industrial Minerals and Rocks. Society for Mining, Metallurgy and Exploration, pp. 769-792.

Chen, C., Jia, C.J., Xiong, F. and Lu, Y. 2013. Heavy metal concentrations in soil and agricultural products near an industrial district. J. Environ. Studies, 22: 1357-1362.

Chen, Z. H. 2011. Global rare earth resources and scenarios of future rare earth industry. J. Rare Earths, 29: 1-6.

Demie, G. 2015. Analyzing soil contamination status in garage and auto mechanical workshops of Shashemane City: implication for hazardous waste management. Environ. Systems Resea, 4(15): 1-9.

EPA 2012. Rare Earth Elements: A Review of Production, Processing, Recycling, and Associated Environmental Issues. EPA600/R-12/572.

Fagbote, E.O. and Olanipekun, E. 2010. Speciation of heavy metals in soil of Bitumen deposit impacted area of western Nigeria. European J. Scient. Resear. 47: 265-277.

Förstner, U. 1983. Assessment of metal pollution in rivers and estuaries. In: Thornton, I. (ed.), Applied Environmental Geochemistry, Academic Press, London, pp. 395-423.

Förstner, U., Ahlf, W., Calmano, W. and Kersten, M. 1991. Sediment criteria development. In: Heling, D., Rothe, P., Förstner, U. and Stoffers, P. (eds), Sediments and Environmental Geochemistry. Springer-Verlag, pp. 312-338.

Gansser, A. 1983. Geology of Bhutan Himalayas: Denkenschrift der Schweizerischen Naturforschenden Gesellschaft. Band. 96, Basel, Birkhäuser, pp.181.

Grunsky, E.C., Drew, L.J. and Sutphin, D.M. 2009. Process recognition in multi-element soil and stream-sediment geochemical data. Appl. Geochem., 24: 1602-1616.

Hakanson, L. 1980. An ecological risk index for aquatic pollution control, a sedimentological approach. Water Res., 14: 975-1001.

Halamic, J., Peh, Z., Bukovec, D., Miko, S. and Galovic, L. 2001. A factor model of the relationship between stream sediment geochemistry and adjacent drainage basin lithology, Medvednica Mt. Croatia. Geol. Croat., 54(1): 37-51.

Hale, M. and Plant, J. (eds.), 1994. Drainage Geochemistry, Handbook of Exploration Geochemistry. Amsterdam; New York, Elsevier 6: pp. 3-766.

Hernandez, L., Probst, A., Probst, J.L. and Ulrich, E. 2003. Heavy metal distribution in some French forest soils: Evidence for atmospheric contamination. Sci. Total Environ., 312: 195-219.

Hirano, S. and Suzuki, K.T. 1996. Exposure, metabolism and toxicity of rare earths and related compounds. Environ. Health Perspec., 104: 85-95.

Howarth, R.J. and Thornton, I. 1983. Regional geochemical mapping and its application to environmental studies. In: Thornton, I. (ed.), Applied Environmental Geochemistry. Academic Press, London, pp. 395-423.

Kar, D., Sur, P., Mandal S.K., Saha T. and Kole, R.K. 2008. Assessment of heavy metal pollution in surface water. Int. J. Environ. Sci. Tech., 5: 119-124.

Kennedy, W.Q. 1965. The influence of basement structure on the evolution of coastal (Mesozoic and Tertiary Basin of Africa) In: Salt basins around Africa. London Institute of Petroleum, p. 16.

Levinson, A. A. 1974. Introduction to Exploration Geochemistry. Applied Publ. Co., Calgary, p. 612.

Likuku, A.S., Mmolawa, K.B. and Gaboutloeloe, G.K. 2013. Assessment of heavy metal enrichment and degree of contamination around the copper-nickel mine in the Selebi Phikwe Region, Eastern Botswana. Environ. Ecol. Resear., 1(2): 32-40.

Lin, C., He, M., Zhou, Y., Guo, W. and Yang, Z. 2008. Distribution and contamination assessment of heavy metals in sediment of the second Songhua River, China. Environ. Monitor, Assess., 137: 329-342.

Loska, K., Cebula, J., Pelczar, J., Wiechula, D. and Kwapuli´nski, J. 1997. Use of enrichment, and contamination factors together with geoaccumulation indices to evaluate the content of Cd, Cu, and Ni in the Rybnik Water Reservoir in Poland. Water, Air, and Soil Pollution, 93: 347-365.

Loska, K., Wiechula, D. and Korus, I. 2004. Metal contamination of farming soils affected by industry. Environ. Interna., 30: 159 -165.

Loska, K., Wiechula, D., Barska, B., Cebula E. and Chojnecka A. 2003. Assessment of arsenic enrichment of cultivated soils in Southern Poland. Pol. J. Environ Stud., 12:187- 92.

McLennan, S. M. 1988. Recycling of the continental crust. Pure Appl. Geophys., 128: 683-724.

McLennan, S.M. 1989. Rare earth elements in sedimentary rocks: Influence of provenance and sedimentary processes. Rev. Mineral., 21: 116-200.

Mediolla, L. L., Domingues, M. C. D. and Sandoval, M. R. G. 2008. Environmental assessment of an active tailings pile in the State of Mexico (Central Mexico). Res. J. Environ. Sci., 2(3): 197-208.

Muller, G. 1969. Index of geoaccumulation in sediments of the Rhine river. J. Geol., 2:108-118.

Nair, I.V., Singh, K., Arumugam, M., Gangadhar K. and Clarson, D. 2010. Trace metal quality of Meenachil River at Kottayam, Kerala (India) by principal component analysis. World Appl. Sci. J., 9:1100-1107.

Nartey, V. K., Klake, R. K., Hayford, E. K., Doamekpor, L. K. and Appoh, R. K. 2011. Assessment of mercury pollution in rivers and streams

around artisanal gold mining areas of the Birim North District of Ghana. J. Environ. Protect., 2:1227-1239.

Nowak, B. 1998. Contents and relationship of elements in human hair for non-industrialised population in Poland. Sci. Total Environ., 209(1): 59-68.

Nurnberg, H.W. 1982. Voltametric trace analysis in ecological chemistry of toxic metals. Pure and Appl. Chem., 54(4): 853-878.

Ochieng, E.Z., Lalah, J.O. and Wandiga, S.O. 2007. Analysis of heavy metals in water and surface sediment in five rift valley lakes in Kenya for assessment of recent increase in anthropogenic activities. Bulletin Environ. Contam. Toxicol., 79: 570-576.

Ojo, J. and Oketayo, O. 2006. Trace elements in the food chain- environmental impact of small scale/artisanal gold mining in Ile-Ife 2: Heavy metal contamination of water. Proceedings of an International Symposium on Trace Elements in the Food Chain, Budapest, Hungary, 25-27 May, 201-205.

Okunlola, O. A. and Akinola, O.O. 2010. Petrochemical characteristics of the Precambrian rare metal pegmatite of Oke Asa area, southwestern Nigeria: Implication for Ta-Nb mineralization. RMZ- Materials and Geo environment, 57(4): 525-538.

Okunlola, O.A. 2005. Metallogeny of Ta-Nb mineralization of Precambrian pegmatite of Nigeria. Mineral Wealth, p.137.

Ong, M.C., Menier, D., Shazili, N. and Kamaruzzaman, B.Y. 2013. Geochemical characteristics of heavy metals concentration in sediments of Quiberon bay waters, South Brittany, France. Oriental J. Chem., 29: 39-45.

Oyawoye, M.O. 1972. The basement complex of Nigeria. In: Dessauvagie T.F.J., Whiteman A.J. (eds.) African geology. Ibadan University Press, pp. 66-102.

Priju, C.P. and Narayana, A.C. 2006. Spatial and temporal variability of trace element concentrations in a Tropical Lagoon, Southwest Coast of India: Environmental implications. Proceedings of the 8th International Coastal Symposium, 2: 1053-1057.

Rahaman, M.A. 1976. Review of the basement geology of South-Western Nigeria. In: Kogbe C.A. (ed.) Geology of Nigeria, 2nd (ed.), Elizabethan Publishers, Lagos, pp. 41-58.

Rahaman, M.A. 1988. Recent advances in the study of the basement complex of Nigeria. In: Geological Survey of Nigeria (ed.) Precambrian Geology, Nigeria, pp. 11-43.

Rahaman, M.A. and Ocan, O. 1978. On relationships in the Precambrian Migmatite-gneisses of Nigeria. Nig. J. Min. Geol., 15: 23-32.

Ramesh, R., Ramanathan, A. L., Ramesh, S., Purvaja, R. and Subramanian, V. 2000. Distribution of rare earth elements and heavy metals in the surficial sediments of the Himalayan river system. Geochem. J., 34: 295-319.

Reimann, C. and Melezhik, V. 2001. Metallogenic provinces, geochemical provinces and regional geology-what causes large-scale patterns in low density geochemical maps of the C-horizon of podzols in Arctic Europe. Appl. Geochem., 16: 963-983.

Rose, A.W., Hawkes, M.E. and Webb, J.S. 1979. Geochemistry in Mineral Exploration. 2nd ed., Academic Press, pp. 657.

Salomons, W. and Forstner, U. 1984. Metals in the Hydrocycle. Springer-Verlag Berlin Heidelberg, pp. 352.

Senesi, G.S., Baldassarre, G., Senesi, N. and Radina, B. 1999. Trace element inputs into soils by anthropogenic activities and implications for human health. Chemosphere, 39: 343-377.

Sholkovitz, E.R. 1993. The geochemistry rare earth elements in the amazon river Estuary. Geochem. Cosmochim. Acta., 57: 2181-2190.

Sholkovitz, E.R. 1995. The aquatic chemistry of rare earth elements in rivers and estuaries. Aqua. Geochem., 1: 1-34.

Singh, M., Ansari. A.A., Muller, G. and Singh, I.B. 1997. Heavy metals in freshly deposited sediments of the Gomati river a tributary of the Ganga River: Effects of human activities. Environ. Geol., 29: 246-252.

Sofianska, E. and Michailidis, K. 2013. Environmental impact of a large scale Manganese mining activity in drama district, Macedonia, Northern Greece. 13th SGEM Geoconference on Ecology, Economics, Education and Legislation, June 16-22, 1: 393-400.

SSSA 2008. Glossary of Soil Science Terms. Committee SSGT, Ed., Soil Science Society of America, 92.

Sutherland, R.A. 2000. Bed sediment-associated trace metals in an urban stream, Oahu, Hawaii. Environ. Geol., 39(6): 611-626.

Taylor, S.R. and McLennan, S.M. 1985. The Continental Crust: Its Composition and Evolution. Blackwell, Oxford, p. 312.

Taylor, S.R. and McLennan, S.M. 1995. The geochemical evolution of the continental crust. Rev. Geophys., 33: 241-265.

Tijani, M.N., Onodera, S. and Adeleye, M.A. 2005. Environmental implications of adsorbed and total trace metals concentrations in bottom-sediments of an urban drainage network in a developing country. Materials and Geo Environ., 52(1): 127-130.

Tomlinson, D.L., Wilson, J.G., Harris, C.R. and Jeffney, D.W. 1980. Problems in the assessment of heavy metal levels in estuaries and the formation of a pollution index. Helgol. Wiss. Meeresunters, 33: 566-572.

Toyoda, K., Nakumara, Y. and Masuda, A. 1990. Rare earth elements of pacific pelagic sediments. Geochim. Cosmochim. Acta., 54: 1053-1103.

Turekian, K.K. and Wedepohl, K.H. 1961. Distribution of the elements in some major units of the earth's crust. American Geol. Soc. Bull., 72: 175-182.

Turner, D.G. 1983. Upper Proterozoic schist belts in the Nigerian sector of the Pan-African province of West Africa. Prec. Res., 21: 55-79.

Wakida, F.T.D., Lara-Ruiz, E.J. and Temores, P. 2008. Heavy metals in sediments of the Tecate River, Mexico. Environ. Geol., 54: 637-642.

Ward, J. H., Jr. 1963. Hierarchical grouping to optimize an objective function. J. American Statist. Associa., 58: 236-244.

Zhang, J. and Liu, C.L. 2002. Riverine composition and estuarine geochemistry of particulate metals in China-weathering feature, anthropogenic impact and chemical fluxes. Estuar. Coast. Shelf, 54: 1051-1070.

Zhuang, P., Li, Z., Zou, B., Xia, H. and Wang, G.I. 2013. Heavy metal contamination in soil and soybean near the Daboshan mine, South China. Pedosphere, 23: 298-304.

Nature Environment and Pollution Technology
An International Quarterly Scientific Journal

p-ISSN: 0972-6268
(Print copies up to 2016)
e-ISSN: 2395-3454

Vol. 19 | No. 2 | pp. 441-452 | 2020

Original Research Paper

https://doi.org/10.46488/NEPT.2020.v19i02.002

Open Access Journal

A Study on Pullout Test of Root Subjected to Axial Load

Lun Zhang*, Zhenyao Xia*(**), Wennian Xu*(**), Xiao Hai*, Daxiang Liu*(**), Liming Liu*(***) and Bingqin Zhao*†**

*Key Laboratory of Geological Hazards on Three Gorges Reservoir Area (China Three Gorges University), Ministry of Education, Yichang, 443002, People's Republic of China

**Collaborative Innovation Center for Geo-hazards and Eco-environment in Three Gorges Area of Hubei Province, China Three Gorges University, Yichang, 443002, People's Republic of China

***Engineering Research Center of Eco-environment in Three Gorges Reservoir Region, Ministry of Education, China Three Gorges University, Yichang, 443002, People's Republic of China

†Corresponding author: Bingqin Zhao; bingqinzhao@163.com

Nat. Env. & Poll. Tech.
Website: www.neptjournal.com

Received: 19-07-2019
Accepted: 15-10-2019

Key Words:
Root-soil interface; Pullout test; Pullout force; Soil density; Root diameter

ABSTRACT

Vegetation can enhance the stability of slopes by increasing the shear resistance of the soil. Shear stress applied to the soil matrix is resisted by the pullout strength of the roots via the friction at contact points between the soil and the roots. The effectiveness of root reinforcement depends on interface friction between soil and roots. In this study, tests were carried out on *Indigofera amblyantha* Craib roots, by measuring resistance as they are pulled out of the soil where the soil has varying dry densities. The results reveal three phases in the relationship between the pullout force and the slippage of the roots, i.e. (1) steep rise, (2) steep fall, and (3) gradual decline. In the first phase, the pullout force is increasing sharply and linearly up to a maximum when the slippage is about 10mm. With continued slippage, the required pullout force decreases significantly and nonlinearly in up and down fluctuations. Eventually, the pullout force reaches zero. For soil with a given dry density, the maximum pullout force increases linearly with increasing root diameter, and the correlation coefficient is greater than 0.9. Further, for a root with a given diameter, the maximum pullout force increases with increasing soil dry density. When the root breaks on pulling, it is called tensile failure; when the root is fully pulled out, it is called friction failure. The mode of failure for all roots is friction failure, for soil with dry densities of 1.35 g/cm^3, 1.45 g/cm^3, and 1.55 g/cm^3. For soil with a dry density of 1.65 g/cm^3, and root diameter under 0.716 mm, the observed failure mode is generally tensile; for diameters over 0.716 mm, the failure mode changes to friction; that is, thin roots break, thick roots get pulled out.

INTRODUCTION

Over the past several decades, the rapidly expanding economy has led to a continuous increase in construction projects; this has caused large-scale disturbances in slopes, which require ecological restoration. Vegetation restoration techniques are widely accepted, effective, affordable, and environment-friendly to prevent soil erosion. Vegetation plays an important role in the slope stability by root reinforcement (Gray & Sotir 1996, Simon et al. 2000, Li & Eddleman 2002, Fan & Su 2008, Mickovski et al. 2009, Dazio et al. 2018)). Root systems in the soil change the mechanical properties of the soil consolidation (Mickovski et al. 2010, Yang et al. 2016). Plant roots can hold soil in the steep slopes depending on the advantage of extensive root proliferation and mechanical properties (Schwarz et al. 2010). Additionally, photosynthesis of plants can decrease soil moisture by root, and the matrix suction and mechanical strength were increased (Schwarz et al. 2010). As shown in Equation 1, these different mechanical effects were concentrated on a significant increase in soil cohesion as defined by the Mohr-Coulomb analysis (Genet et al. 2008).

$$\tau_{cr} = c_r + c_s + \sigma \tan(\phi) \quad \ldots(1)$$

τ_{cr} shear stress of the soil;

c_r: additional cohesion (in roots);

c_s : bare soil cohesion;

σ: effective normal stress (in the shear plane);

ϕ: bare soil friction angle.

The effect of root enhancement on the stability of a slope can be directly assessed by the additional shear strength provided by roots in the root-enhanced soil (Gray & Sotir 1996). Gray & Ohashi's (1983) laboratory experiments provide a useful interpretation of soil reinforcement by roots (Abernethy & Rutherfurd 2001). Root-soil is a fibre inclusion (Gray & Barker 2004), and it can be considered as a composite material (Gray & Ohashi, 1983, Abe & Ziemer

1991). Root fibre improves soil shear strength by transferring the shear stress in the soil matrix into the pullout strength of fibre inclusions through friction along with the points of contact between the fibre and the soil (Gray & Barker 2004, Cazzuffi et al. 2014a).

A large number of studies showed that the shear strength increase compared with no root-soil can result from many mechanisms, including pullout or breakage of individual roots (Wu et al. 1979) or composite action (Wu et al. 1988a) rely on root morphology and soil condition (e.g., soil density) (Mickovski et al. 2010, Comino & Marengo 2010). Soil root shear strength, the mechanical reinforcement effect of plant roots on slope stability, has been studied (Wu & Watson 1998). The pullout strength of roots can be measured by *in situ* root tests (Wu et al. 1979, Wu & Watson 1998, Comino & Marengo 2010) and laboratory root tensile tests (Abe & Ziemer 1991, Docker & Hubble 2008, Bischetti et al. 2009, Gray & Barker 2004, Liu et al. 2014). Wu et al. (1988b), Wu & Watson (1998) conducted an *in situ* shear test between the root-soil system and bare soil. The results show that the shear strength of the root-soil composite is higher than that of the bare soil, and the plant roots significantly enhance the cohesion of the soil; further, the stability of the slope is enhanced. The most critical parameters of root systems as soil reinforcement are root density, depth, and pullout strength. These papers provide a substantial introduction to the role of the root system in soil shear strength.

Previous studies involving root tensile tests have concluded that root destruction generally consists of the following processes: (1) root fibres slip, (2) root fibres stretch, and (3) root fibres break (Abe & Ziemer 1991, Gray & Barker 2004, Comino & Marengo 2010). Plant root response depends on plant species and plant growing conditions (Comino & Marengo 2010).

Waldron (1977) and Wu et al. (1979) assumed that the shear force generated in the soil when the soil layer (slope) moves was converted to the pullout force in the roots. Moreover, the shear stress can be decomposed into tangential and normal components, and that the soil friction was not affected, the additional cohesion coefficient ranges from 1.0 to 1.3 (Bischetti et al. 2009). Many researchers believe that the additional cohesion coefficient is a universal value of 1.2 (Waldron 1977, Wu et al. 1979, Wang et al. 2019). In particular, the mechanical characteristics (mean values of root pullout force and root diameter) of plant roots are very important.

From Fig. 1, the slope perspective of geotechnical engineering, the mechanical effect of the roots involves two significant actions: (i) Friction; the roots are resistant to axial tension and compression. When the roots touch and rub against the soil such that they serve as individual anchors, thereby preventing a pullout failure. (ii) Bearing, the roots are resistant to shear forces and bending moments. When the root-soil composite is subjected to external loading, the horizontal shearing force on the soil matrix is transferred into the pullout strength in the root fibre, enhancing the shear strength of the composite (Waldron 1977, Waldron & Dakessian 1981, Wästerlund 1989, Ennos 1989, Abe & Ziemer 1991, Cazzuffi et al. 2014b, Liang 2015). Therefore, plant roots need to strengthen the soil.

Pullout tests are a standard method to determine root pullout force in the laboratory (Shewbridge & Sitar 1996, Mickovski et al. 2005, Devkota et al. 2006, Stokes et al. 2007, Tosi 2007, Burylo et al. 2009).

In the process of ecological restoration, pioneer plant species are most relevant for a local application of these resource-saving, environment-friendly techniques. *Indigofera*

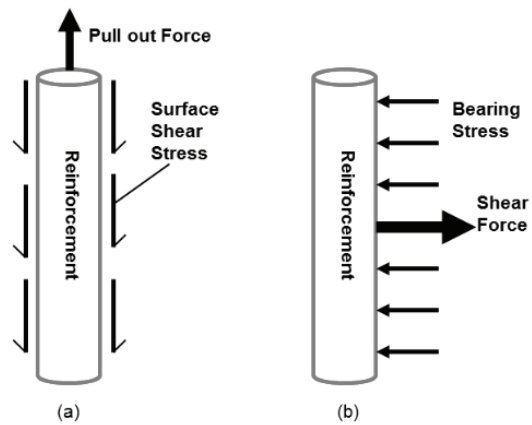

Fig. 1: Mechanism of soil inclusion interaction: The component force of force diagram: (a) Friction; (b) Bearing (Liang 2015).

amblyantha Craib (Fabaceae) is a shrub that is suitable for slope protection, especially because they have rapid growth, well-developed roots, drought resistance, disease resistance, and adaptability to bare soil (Chen et al. 2013, Zhao et al. 2018, Zhang et al. 2018). We selected the root of *Indigofera amblyopia* Craib as a research subject, investigating the root pullout force and its influential factors by pulling out test. Further, we developed a theoretical basis and foundation for root-soil interface friction.

MATERIALS AND METHODS

Study Area

A point at Yichang city in the Three Gorges Reservoir area in China was selected for collection of samples. As shown in Fig. 2, in this study area, the altitude is between 30-2057m; and more than 67.4% of the area is a low mountainous terrain; the climate is humid subtropical monsoon; the annual precipitation is 1100-1200mm; the annual average temperature is 16.9 °C; the average relative humidity is 70-80%; and the annual frost-free period is 340 days. Rainfall is unevenly distributed throughout the season, with the most rainfall in the period between May and September (Tang et al. 2014).

The purple soil developed from the Triassic to Tertiary is the dominant soil type in this study area, accounting for more than 70% of the area (He et al. 2009). It is characterized by low permeability, high hydrophobicity, and natural weathering (Zhang et al. 2016). It has been classified as a Regosols in FAO Taxonomy and Entisols in USDA Taxonomy (Tang et al. 2014). This purple sloping farmland is a vital cultivated land resource in the Three Gorges Reservoir area. It is also the primary source of soil erosion and sedimentation into the Three Gorges Reservoir; it is estimated that the annual soil erosion of the sloping farmland is 3,464-9,452 tons per square kilometre (Wei et al. 2018).

In restoration programs, the plant *Indigofera amblyopia* Craib has been used for slope vegetation protection. It is a deciduous perennial shrub of the genus *Magnolia* in the Leguminosae family and commonly grows at the edges of the forests, roadsides, barren slopes, and on the hillside below 1,200 m. It can hold the soil, improve soil permeability, effectively intercept precipitation, and has a good drought, cold resistance, and strong roots. As desirable vegetation for soil and water conservation and slope protection, *Indigofera amblyopia* Craib can prevent soil erosion, and it can be planted on both sides of a highway or railway slope along with grasses.

Sample Preparation

The purple soil with the experiment is widely distributed in the Three Gorges Reservoir area. The sampling site is located at Longkou Village (31°13’37’’N, 110°41’16”E with a mean altitude of 110 m), Shuitianba Town, Zigui County, Yichang City in the Hubei Province in China. The samples are 0-20 cm, acquired from the surface soil in the middle of the slope, and they were collected in late June 2014. The soil samples were placed indoor and air-dried. Crumbled big clods, decomposed plant roots, residues of dead insects, stones, and other debris were removed. The air-dried soil samples were then sifted through 2 mm standard sieve to be used as standardized soil samples. The sieving method was

Fig. 2: Location of the study area and sampling sites.

used to measure the particle size distribution of the final soil samples. The stoving and cutting ring methods measured the natural water content and dry density of the final soil samples. Further, the pH of the final soil samples was measured using a potentiometer. The basic physical properties of the final purple soil sample are as follows: solid density, 1.33 g/cm^3; natural moisture content, 17.76 %; pH, 6.1; more than 2 mm, 28.49 %; 2-0.5 mm, 26.46 %; 0.5-0.25, 21.75%; 0.25-0.075, 11.89 %; 0.075-0.002, 6.54 %; less than 0.002, 4.87 %. As given in Tables 1 and 2, the range of shear stress is 47.65-85.23 kPa, the purple soil is clay, and liquid index, liquid limit, plastic limit, plasticity limit index are as follows: 0.28-0.74, 13.37-15.75%, 9.77-11.67%, and 3.15-4.33%, respectively (Hua et al. 2008).

In July 2014, we collected 38 well-grown and typical *Indigofera amblyopia* Craib as full plant samples. After collecting the samples, the soil off the plant was cleaned in still water and the plants were let to dry. We then used WinRHIZO to analyse the root diameters statistically. In some studies (Hales et al. 2009, Montagnoli et al. 2012), the root diameter is divided into four categories: very fine (< 0.5 mm), fine (0.5-1 mm), medium (1-2 mm), coarse (>2 mm). Extremely fine roots (0-0.5 mm) have been recognized in some studies; however, they have been questioned due to their rapid turnover (Adhikari et al. 2013). After using WinRHIZO to determine the average diameter of the samples with single roots, all roots were put into sealed bags and stored in a refrigerator. Hence, the pullout test was only performed on the roots with diameters between 0.5-1.0 mm. The root length is 100 mm, and the pullout tests of roots are completed within 24 h.

Pullout Test

Table 1 summarizes the basic parameters of the soil; the natural moisture content of the soil is 17.76%. We used a methodology of restoring the dry soil uniformly to that condition. The water content of the air-dried and screened soil, w_0, was determined. Since the natural water content is 17.76%, the design target moisture content of the soil samples, w_i, for the pullout test was set at 17.76%, and then the soil quantity was calculated. Using equations (2) and (3), the target is calculated under the condition of moisture content w_i, wherein water is added to the soil samples considering moisture content w_{wi} and soil quality, as follows:

$$m_{wi} = \frac{m}{1+0.01w_0} \times 0.01\left(w_i - w_0\right) \quad \ldots(2)$$

$$m_i = \left(1+0.01w_i\right)\rho_d V \quad \ldots(3)$$

Where, m: Soil mass

g: Mass unit

m_{wi} (g): Soil quality of the target water when preparing the soil samples

m(g): Soil quality of the air-dried soil when preparing the soil samples

m_i(g): Soil quality required for sample preparation

w_i(%): Target water content of the soil samples

w_0 (%): Water content of the air-dried soil

ρ_d(%) (g/cm^3): Dry density of the soil

V (cm^3): Volume of the soil

Table 1: Basic physical properties of the soils used in the study.

Soil	Index	Clay (< 0.002 mm) %	Organic matter content %	Natural moisture content %
Purple Soil	Maximum	15.31	1.48	13.76
	Minimum	11.08	1.16	11.08
	Average value	13.18	1.31	12.48
	Sample size	30.00	30.00	30.00

Table 2: Strength properties of the soils used in the study.

Soil	Index	Liquid index	Shear strength kPa	Liquid limit %	Plastic limit %	plasticity index %
Purple Soil	Maximum	0.74	85.23	15.75	11.67	4.33
	Minimum	0.28	47.65	13.37	9.77	3.15
	Average value	0.50	61.91	14.42	10.55	3.86
	Sample size	30.00	30.00	30.00	30	30.00

The soil sample was prepared as follows: (1) Mass m was measured for the air-dried soil sample, and mass m_{wi} was measured by adding water into a measuring cylinder. Then, water with mass m_{wi} was sprayed evenly on the soil sample with mass m. Next, the soil sample and water were mixed well, and the wetted soil sample was placed in a container. The soil sample was then left in the container until it reached the target moisture level at which point it was sealed with a tight cover. The sample was remoulded, and the initial dry density was controlled at ρ_d =1.35g/cm^3. We used equation (2) to calculate the soil mass m_i and prepared the sample of volume V to reach the target moisture content w_i. Then, as preparation for the soil sample to reach the target soil moisture, the soil sample was weighed; the mass of the soil was m_i. The container size of the test was 100×100×20mm. Before the test, the relationship between hitting times and the dry density was determined by the compaction method, and that increasing the hitting times was required for each 0.1g/cm^3 at the same height. When the test is conducted, the dry target density of the test is controlled by hitting times. By the soil mechanics test specification, the sample of pullout test is reconstituted by geotechnical test manual. A 100mm long single root of the *Indigofera amblyatha* Craib was embedded horizontally in the centre of a 100mm × 100mm × 200mm box packed with soil. The root-soil composite material is composed of an *Indigofera amblyatha* Craib single root and the soil.

A modified HANDPI's HP-50 digital tester of pullout force was then used to perform the pullout test on the single root-soil composite. The root protruding from the soil surface was clamped and pulled out of the soil at a constant rate of 10mm/min. During the test, the pullout force and the slippage were continually recorded. The device, HANDPI's HP-50, can record 60 data points per second. If the root in the soil with the initial dry density did not break, the dry density of the soil was increased by 0.1g/cm^3 until the single root pulled out or tensile failure occurred. In the test, the average diameter of the root was chosen between 0.50 and 1.00mm. Tests in which the position of the breakage is near the clamp were regarded as failures. The failure means that the root system is damaged by the clamp or because the root surface is damaged, it is pulled off by the action of the external force, and the value is not the actual test result. Because Zhang et al. (2014) said that when root breaking was caused by stress concentration near the clamp rather than by the pullout force, it is not like a natural break in the soil. The clamp is a fastening device made of a pair of steel blocks according to the diameter of the root. A circle of kraft paper was wrapped around the root system to improve the friction of the clamp and minimize breakage, caused by stress concentration near the clamp. In the test, one end of the root is in the soil, and the other end is in the clamp. Fig. 3 shows a schematic of the pullout test of a single root.

RESULTS

Pullout Tests

The pullout tests were performed on 38 root samples of *Indigofera amblyatha* Craib. Even if the root part is covered with kraft paper, it is easy to pinch the root, which causes the test to fail, and therefore, several trials had to be neglected. The roots of the pull test were pulled out of 38 roots, but only 14 of the 38 roots were properly pulled out or resulted in tensile failure. Table 3 lists the measured maximum pullout

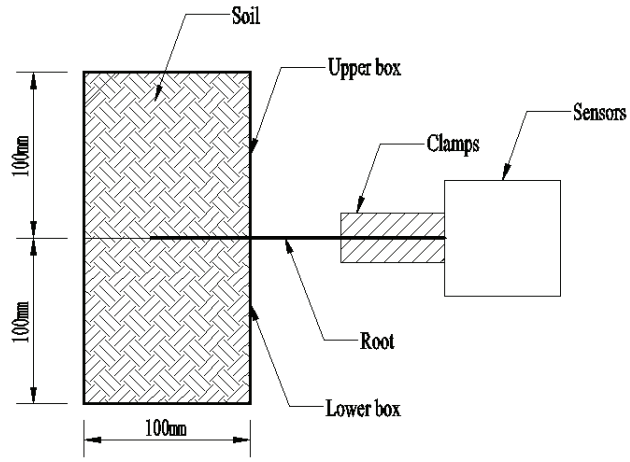

Fig. 3: Schematic plot for the pull-out test of a single root.

force, and maximum pullout strength with the corresponding root diameters.

From Table 3, there are 25 root systems in the table, and the results of two times are completed. The first pullout test has been performed on 38 root samples of *Indigofera amblyatha* Craib, and 14 roots have been pulled out by the device. In the second test, 22 roots pullout tests were completed, and 11 roots pulls were successful. From the two experiments, 25 roots were pulled successfully or experienced tensile failure it can be seen that for roots with an average diameter between 0.50-1.00 mm, the maximum pullout force varies between 4.39N and 13.51N. Further, the maximum pullout force increases with increasing average root diameter, as shown in Fig. 4; this relationship can be described by the power regression curve, which is also shown in Fig. 4.

Table 4 indicates that for the 14 *Indigofera amblyatha* Craib pulled out roots with the average diameter between 0.50-1.00 mm, the maximum pullout strength varies between 12.81 and 25.38 MPa. Further, the maximum pullout strength decreases with increasing average root diameter, as shown in Fig. 4. This relationship can be described by the power regression curve, also shown in Fig. 4.

Relationship Between Pullout Force and Slippage of Roots

Fig. 5 shows the measured pullout force and slippage of single roots of *Indigofera Amblyantha* Craib with diameters between 0.50-1.00 mm in the pullout tests for soils with four dry densities. Fig. 5(a) shows the pullout force and the slippage of the single root for the initial soil dry density $\Delta\rho_d = 1.35g/cm^3$. The results show that the failure mode is friction, and there is no tensile failure. The dry density of the soil was then increased by $\Delta\rho_d = 0.1g/cm^3$ until the dry soil density reached $\Delta\rho_d = 1.65g/cm^3$. The roots with diameters of 0.59

Table 3: Measured maximum pullout force, maximum pullout strength with corresponding root diameters from pullout tests.

N	D1 (mm)	D2 (mm)	D3 (mm)	Average diameter D (mm)	Maximum pullout force (N)	Maximum pullout strength (MPa)
1	0.73	0.52	0.32	0.52	4.40	20.46
2	0.63	0.56	0.43	0.54	4.97	21.70
3	0.42	0.46	0.84	0.57	5.00	19.37
4	0.76	0.48	0.46	0.57	6.40	25.38
5	0.56	0.59	0.61	0.59	5.82	21.51
6	0.66	0.51	0.61	0.59	5.91	21.47
7	0.76	0.50	0.56	0.61	6.47	22.28
8	0.78	0.68	0.43	0.63	5.80	18.61
9	0.84	0.70	0.35	0.63	6.70	21.49
10	0.92	0.62	0.42	0.65	6.90	20.58
11	0.61	0.71	0.65	0.66	7.20	21.26
12	0.48	0.72	0.82	0.67	6.75	19.03
13	0.59	0.61	1.16	0.79	8.46	17.48
14	0.83	0.70	0.81	0.78	8.06	16.87
15	0.88	0.79	0.72	0.80	7.30	14.64
16	0.93	0.76	0.83	0.84	7.82	14.14
17	1.07	0.84	0.61	0.84	8.90	16.06
18	0.75	0.82	0.96	0.84	8.13	14.53
19	0.84	0.89	0.97	0.90	10.59	16.68
20	0.86	0.91	0.94	0.90	11.11	17.34
21	1.01	0.92	0.83	0.92	10.50	15.80
22	0.89	0.92	0.99	0.93	8.87	13.00
23	0.89	0.92	1.03	0.95	9.04	12.81
24	1.10	0.93	0.87	0.97	11.41	15.55
25	1.20	0.91	0.88	1.00	13.51	17.32

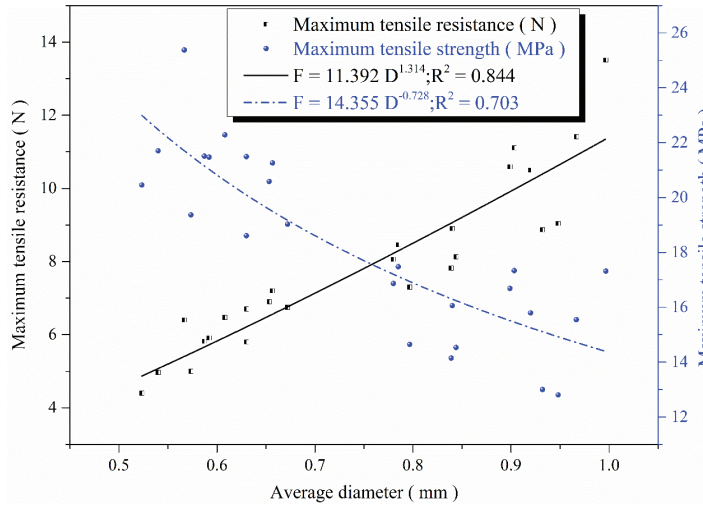

Fig. 4: Relationship between the maximum pullout force, the maximum pullout strength and the average root diameter.

mm and 0.63 mm must be broken, and the larger diameter roots (0.79 mm, 0.90 m, and 0.93 mm) may be completely pulled out or exhibit tensile failure, as shown in Figs. 5(b), 5(c) and 5(d), respectively.

As shown in Fig. 5(d), the change in the single root pullout force with increasing slippage can be divided into three phases, i.e. from A to B, which is the steep rise; from B to C, which is the steep fall; and from C to D, which is the gradual decline. With increasing slippage, the pullout force of the single root is linear upwards and reaches a maximum in the first phase. The pullout force is at its maximum when the slippage is about 10 mm. After reaching the maximum, the pullout force declines rapidly and nonlinearly in the second phase. The pullout force then fluctuates up and down and reaches zero eventually in the third phase. At the beginning of the test when the root is pulled, the slippage is almost zero due to the elastic modulus of the root in the soil. It is assumed that the root-soil complex is a homogeneous specimen. When the root system is pulled or broken by an external force (pullout force), the volume of the specimen is changed (Fig. 1). The root-soil contact surface of the soil particles with the pullout force enhances dislocation and rotation of the root, which is accompanied by the change in the soil volume. This process needs to use an external force to complete, and thus, pullout force rapidly reaches a maximum in the early stage of the test. Then, the pullout process continues, the movement and rearrangement of the soil particles around the roots make the root-soil interface smoother. The friction between the root and the soil particles decreases gradually and then reaches a constant. The drawing force also decreases and eventually reaches zero. These findings are consistent with those in the earlier study (Liu et al. 2012).

From Fig. 5(d), although the single root failure curve of tensile failure mode is similar to that of friction failure, there is a difference. The following two points can be seen from Fig. 5(d). (1) When tensile failure occurs, the pullout force reaches the maximum value; thereafter, the pullout force of the tensile failure decreases sharply and linearly. (2) When the pullout force is close to zero, the corresponding pulling resistance slippage decreases.

De Baets et al. (2008) reported that when the pullout test occurs the root fibre deforms. As shown in Fig. 1, the root fibre is stretched as long as there is enough interfacial friction, confining stress, and anchoring length to lock the fibres and prevent slippage or pullout. As the pullout force increases, the root system will have a tensile failure or be pulled out. The root reinforcement model assumes that the pullout strength of the roots is fully mobilized during failure.

The following two differences cause the tensile failure and the friction damage of the roots:

(1) Roots intersect with soil to improve the bond force between the roots and soil matrix. When tensile failure occurs, the bond force decreases as well as pullout force. (2) When the root system is broken, which is equivalent to the reduction of the effective length of the root system, the force of the root system being pulled out is small, and the root pullout time is shorter.

In the other case, when the root is pulled, the length of the root in contact with the soil decreases. Therefore, the length of the non-extracted root becomes shorter, and the pulling resistance slippage is reduced. Therefore, the slippage decreases more rapidly when the pullout force is close to zero.

Maximum Pullout Force

Fig. 4 shows the maximum pullout force of the root of *Indigofera Amblyantha* Craib with an average root diameter between 0.50-1.00 mm. The maximum pullout force increases significantly with the increasing average diameter of the root. The relationship between the maximum pullout force of the root of *Indigofera amblyantha* Craib and the average root diameter is power growth. Fig. 4 shows the fitted equation to the data.

Effect of Dry Soil Density on the Maximum Pullout Force

Table. 4 shows the relationships between the maximum pullout force and the average root diameter for four dry soil densities. Equations have been fitted to the data, and the smallest correlation coefficient is more significant than 0.9 from Table 4, it can be seen that for each dry soil density, the maximum pullout force of the single root increases with increasing average root diameter. This shows that the larger the root diameter, the larger the contact area between the root and the soil, resulting in more friction at the root-soil interface. Hence, the pullout force of the single root is also larger. For a given root diameter, the maximum pullout force of the single *Indigofera Amblyantha* Craib root increases with the increase of dry soil density. This result is consistent with that obtained from the earlier study (Song et al. 2006). For soil with lower dry density, the soil particles are looser.

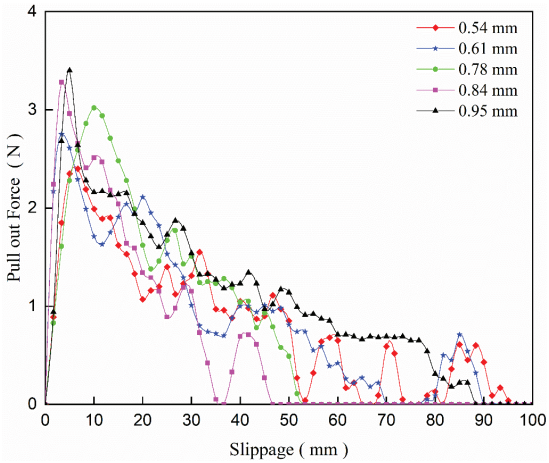

(a) Dry soil densities $\rho_d = 1.35$ g/cm^3

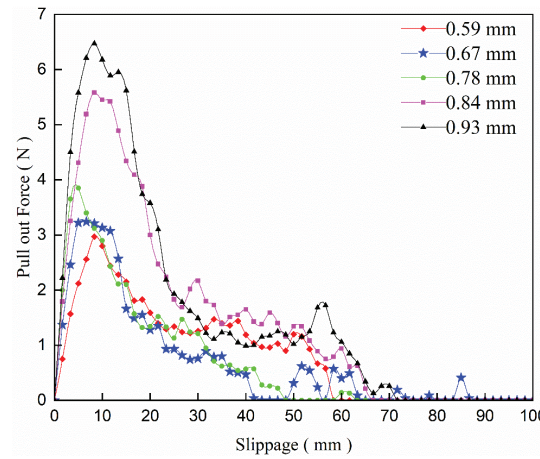

(b) Dry soil densities $\rho_d = 1.45$ g/cm^3

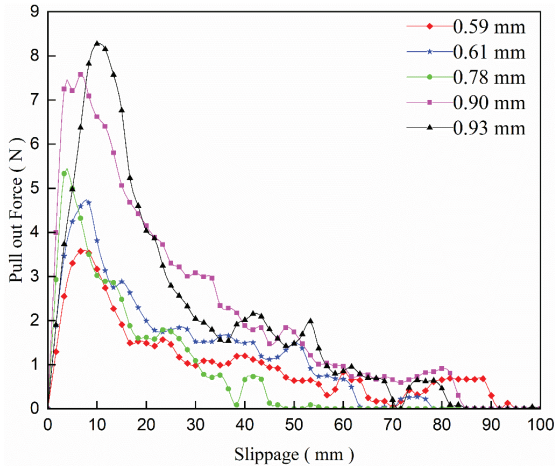

(c) Dry soil densities $\rho_d = 1.55$ g/cm^3

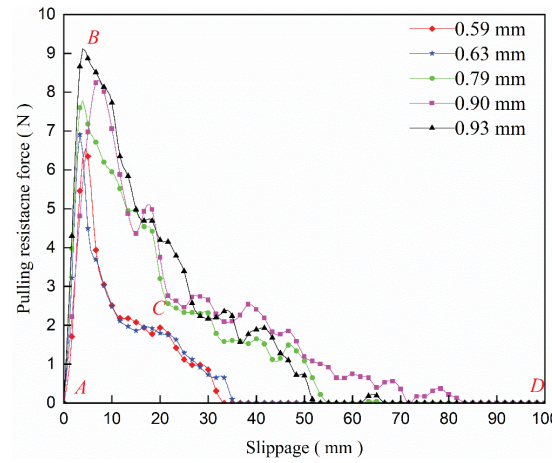

(d) Soil dry density $\rho_d = 1.65$ g/cm^3

Fig. 5: Relationships between pullout force and slippage for four dry soil densities.

Table. 4: Relationships between maximum pullout force and average root diameter for four dry soil densities.

Dry soil densities	Fitting equation	R^2
$\rho_{d\ =\ 1.35g/cm^3}$	$F = 3.572\ D^{0.731}$	0.932
$\rho_{d\ =\ 1.45g/cm^3}$	$F = 6.952\ D^{1.752}$	0.958
$\rho_{d\ =\ 1.55g/cm^3}$	$F = 8.909 D^{1.732}$	0.940
$\rho_{d\ =\ 1.65g/cm^3}$	$F = 9.142\ D^{0.662}$	0.957

Hence, there is less contact between the soil particles and the root surface, resulting in a smaller friction force between the root and the soil. For soil with higher dry density, there is more contact between the soil particles and the root surface, resulting in more friction at the root-soil interface. Hence, the pullout force of the root is larger.

In Fig. 6, the relationships between the maximum pullout force and maximum pullout strength with average root diameter for $\rho_d = 1.65$ g/cm^3 are fitted with power equations, with $R^2 = 0.854$ and 0.959, respectively.

When the dry soil density is $\Delta\rho_d = 1.65 g/cm^3$, the *Indigofera amblyantha* Craib root undergoes a pullout failure. From Fig. 6, the maximum pullout force increases with increasing average root diameter. Further, at the average root diameter of $r = 0.716$ mm, the maximum pullout force equals the maximum pullout strength. This is an indication that $r = 0.716$ mm is a critical diameter of the single root of *Indigofera Amblyantha* Craib in which the pulling resistance failure mode changes from friction to tensile failure. Therefore, for $D < 0.716$ mm, the pullout failure mode is expressed as breaking mode, and for $D > 0.716$ mm, the pullout failure mode of the single root is expressed as friction damage. Hence, the pulling resistance of a plant is greatly dependent on the friction at the root-soil interface (Abe & Ziemer 1991, Anderson & Richards 1987, Leung et al. 2018).

DISCUSSION

Based on measured data from the pullout tests, Fig. 5 shows for the average root diameter between 0.5-1.0 mm and the pullout force increases with increasing average root diameters. After the load peaks, the pullout force decreases as the friction between root and soil lessens owing to the slippage of the roots and because of the decreasing interface area between the root and soil when the root is extracted from the soil. As can be seen from Fig. 5 (d), the pullout force is 0 when the slippage is about 40 mm, and this means that the contact area between the root system and the soil becomes smaller. These results are similar to those in the study of the extraction of sunflower taproot seedlings by Ennos (1989). After the load peaks, it fluctuates significantly, and there are further slippages.

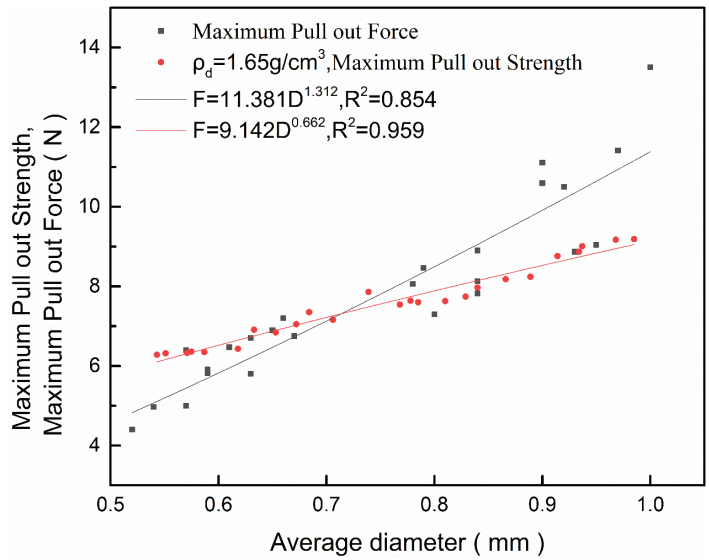

Fig. 6: Relationship between maximum pullout force and maximum pullout strength with average root diameter for $\rho_d = 1.65$ g/cm^3.

Fig. 5(a) shows that for a smaller root diameter, the pullout strength is greater. Further, the pullout strength first increases sharply and reaches a maximum when the slippage is about 10mm. As the test continues, the pullout strength decreases gradually with increasing slippage. The pullout strength eventually reaches zero.

The results of this study show a positive power function correlation between the root diameter and the stress, which is consistent with the results of earlier studies (Stokes et al. 2008, ChunJuan et al. 2011, Zhang et al. 2012, Zhang et al. 2014). The effect of the root diameter on the tensile properties of the root can be explained from the perspective of chemical composition, as follows:

The percentage of cellulose increases with a decreasing percentage of lignin. Therefore, for a larger root diameter, the lignin-cellulose ratio is smaller. As the lignin-cellulose ratio is positively correlated with the pullout strength, the pullout strength decreases with increasing root diameter (Genet et al. 2005, Hales et al. 2009, Lü & Chen 2013, Zhang et al. 2014). Using a power function, earlier studies have confirmed the negative correlation between the root diameter and the pullout strength (Nilaweera & Nutalaya 1999, Bischetti et al. 2005, Genet et al. 2007, ChunJuan et al. 2011). In this study, the results also show that the root pulls out strength decreases with increasing root diameter. However, the effect of the root diameter on the pullout strength is not always significant. This can be explained by the autocorrelation between the pullout strength and the diameter, i.e.

$$\sigma = \frac{F}{S} = \frac{4F}{\pi D^2} \quad \ldots(4)$$

Where σ is the pullout strength of the root, F is the pullout force of the root, S is a cross-sectional area of the root, and D is the diameter of the root. Equation 3 shows that the pullout strength of the root system is opposite to the root diameter (D). It can be seen from Equation 3 that the root diameter (D) is the denominator, which is opposite to the pullout force (F).

CONCLUSIONS

The study was conducted under conditions of the natural water content of soil = 17.76%, soil depth = 50 mm, and embedding root length = 100 mm. The pullout tests were carried out on single roots of *Indigofera amblyantha* Craib by the axial load method. The pullout force of *Indigofera amblyantha* Craib was investigated. The test results showed that:

(1) The relationship between the pullout force and the slippage of *Indigofera amblyantha* Craib roots can be summarized in three phases: (1) steep rise, (2) steep fall, and (3) gradual decline. During the first phase, the pullout force increases sharply and linearly up to a maximum when the slippage is about 10 mm. With the increase in slippage, the pullout force decreases significantly and nonlinearly, with up and down fluctuations. Eventually, the pullout force reaches zero.

(2) For soil with a given dry density, the maximum pullout force increases linearly with increasing root diameter, and the coefficient of correlation is greater than 0.9. This is an indication that the larger the root diameter, the longer is the embedded root length in the soil, and the greater is the friction at the root-soil interface. Hence, the force required to pull out the root is greater.

(3) For a root with a given diameter, the maximum pullout force increases with increasing soil dry density. The mode of pulling resistance failure of all roots is friction failure for soil with dry densities of 1.35 g/cm^3, 1.45 g/cm^3, and 1.55 g/cm^3. For soil with a dry density of 1.65 g/cm^3, the failure mode changes from friction to tensile failure when the root diameter is 0.716 mm (i.e., the pullout failure mode is a tensile failure when the root diameter is smaller than 0.716 mm; it is friction failure when the root diameter is larger than 0.716 mm).

ACKNOWLEDGEMENT

This study was supported by the National Key R&D Program of China (Grant No. 2017YFC0504902-01), the National Natural Science Foundation of the People's Republic of China (Grant No. 51708333, 51678348), the Open Fund of Key Laboratory of Disaster Prevention and Mitigation, Hubei Province (Grant No. 2016KJZ13), and the Natural Science Foundation of Hubei Province (Grant No. 2017ACA189, 2016CFA085). It was also sponsored by the Research Fund for Excellent Dissertation of China Three Gorges University (Grant No.2019BSPY005).

REFERENCES

Abe, K. and Ziemer, R. R. 1991. Effect of tree roots on a shear zone: Modeling reinforced shear stress. Canadian Journal of Forest Research, 21(7): 1012-1019.

Abernethy, B. and Rutherfurd, I. D. J. H. P. 2001. The distribution and strength of riparian tree roots in relation to riverbank reinforcement. Hydrological Processes, 15(1): 63-79.

Adhikari, A. R., Gautam, M. R., Yu, Z., Imada, S. and Acharya, K. 2013. Estimation of root cohesion for desert shrub species in the Lower Colorado riparian ecosystem and its potential for streambank stabilization. Ecological Engineering, 51: 33-44.

Anderson, M. G. and Richards, K. S. 1987. Slope Stability: Geotechnical Engineering and Geomorphology. John Wiley & Sons.

Bischetti, G. B., Chiaradia, E. A., Epis, T. and Morlotti, E. 2009. Root cohesion of forest species in the Italian Alps. Plant and Soil, 324(1-2): 71-89.

Bischetti, G. B., Chiaradia, E. A., Simonato, T., Speziali, B., Vitali, B., Vullo, P. and Zocco, A. 2007. Root strength and root area ratio of forest species in Lombardy (Northern Italy). Plant & Soil, 278(1/2): 11-22.

Burylo, M., Rey, F., Roumet, C., Buisson, E. and Dutoit, T. 2009. Linking plant morphological traits to uprooting resistance in eroded Marlylands (Southern Alps, France). Plant and Soil, 324(1-2): 31.

Cazzuffi, D., Cardile, G. and Gioffrè, D. 2014a. Geosynthetic engineering and vegetation growth in soil reinforcement applications. Transportation Infrastructure Geotechnology, 1(3): 262-300.

Chen, F., Xu, Y., Wang, C. and Mao, J. 2013. Effects of concrete content on seed germination and seedling establishment in vegetation concrete matrix in slope restoration. Ecological Engineering, 58: 99-104.

ChunJuan, L. V., Chen, L. H., Zhou, S., Song, H. C., Gai, X. G., Ji, X. D. and Zhang, X. P. 2011. Root basic mechanical properties of soil reinforcement of *Pinus tabulaeformis*. Journal of Soil & Water Conservation, 25(5): 17-390.

Comino, E. and Marengo, P. 2010. Root pullout strength of three shrub species: *Rosa canina, Cotoneaster dammeri* and *Juniperus horizontalis*: Soil reinforcement estimation by laboratory tests. Catena, 82(3): 227-235.

Dazio, E., Plinio, R., Conedera, M. and Schwarz, M. 2018. Impact of different chestnut coppice managements on root reinforcement and shallow landslide susceptibility. Forest Ecology and Management, 417: 63-76.

De Baets, S., Poesen, J., Reubens, B., Wemans, K., De Baerdemaeker, J. and Muys, B. 2008. Root pullout strength and root distribution of typical Mediterranean plant species and their contribution to soil shear strength. Plant and Soil, 305(1-2): 207-226.

Devkota, B. D., Omura, H., Kubota, T., Paudel, P. and Inoue, S. 2006. Revegetation condition and morphological characteristics of grass species observed in landslide scars, Shintategawa watershed, Fukuoka, Japan. Journal of Applied Sciences, 6(10): 2238-2244.

Docker, B. and Hubble, T. J. G. 2008. Quantifying root-reinforcement of river bank soils by four Australian tree species. Geomorphology, 100(3-4): 401-418.

Ennos, A. R. 1989. The mechanics of anchorage in seedlings of sunflower, *Helianthus annuus* L. New Phytologist, 113(2): 185-192.

Fan, C.C. and Su, C.F. 2008. Role of roots in the shear strength of root-reinforced soils with high moisture content. Ecological Engineering, 33(2): 157-166.

Genet, M., Kokutse, N., Stokes, A., Fourcaud, T., Cai, X., Ji, J. and Mickovski, S. 2008. Root reinforcement in plantations of *Cryptomeria japonica* D. Don: effect of tree age and stand structure on slope stability. Forest Ecology and Management, 256(8): 1517-1526.

Genet, M., Stokes, A., Salin, F. ., Mickovski, S. B., Fourcaud, T., Dumail, J. F. and Van Beek, R. 2005. The influence of cellulose content on pullout strength in tree roots. Plant & Soil, 278(1/2): 1-9.

Gray, D. H. and Barker, D. 2004. Root-soil mechanics and interactions. Riparian Vegetation and Fluvial Geomorphology, 8: 113-123.

Gray, D. H. and Ohashi, H. 1983. Mechanics of Fiber Reinforcement in Sand. Journal of Geotechnical Engineering, 109(3): 335-353.

Gray, D. H. and Sotir, R. B. 1996. Biotechnical and Soil Bioengineering Slope Stabilization: A Practical Guide For Erosion Control. John Wiley & Sons.

Hales, T. C., Ford, C. R., Hwang, T. ., Vose, J. M. and Band, L. E. 2009. Topographic and ecologic controls on root reinforcement. Journal of Geophysical Research Earth Surface, 114(F03013).

He, X., Bao, Y., Nan, H., Xiong, D., Wang, L., Liu, Y. and Zhao, J. 2009. Tillage pedogenesis of purple soils in southwestern China. Journal of Mountain Science, 6(2): 205-210.

Leung, F. T. Y., Yan, W. M., Hau, B. C. H. and Tham, L. G. 2018. Mechanical pullout capacity and root reinforcement of four native tree and shrub species on ecological rehabilitation of roadside slopes in Hong Kong. Journal of Tropical Forest Science, 30(1): 25-38.

Li, M.H. and Eddleman, K. E. 2002. Biotechnical engineering as an alternative to traditional engineering methods: A biotechnical streambank stabilization design approach. Landscape and Urban Planning, 60(4): 225-242.

Liang, T. 2015. Seismic Performance of Vegetated Slopes. Doctoral dissertation, University of Dundee.

Liu, X., Zhao, H., Ji, X. D. and Chen, L. H. 2012. Friction characteristics of root-soil interface of *Pinus tabulaeformis* and *Larix gmelinii* (in Chinese). Tribilogy, 32(6): 550-556.

Liu, Y., Rauch, H. P., Zhang, J., Yang, X. and Gao, J. 2014. Development and soil reinforcement characteristics of five native species planted as cuttings in local area of Beijing. Ecological Engineering, 71: 190-196.

Lü, C. and Chen, L. 2013. Relationship between root tensile mechanical properties and its main chemical components of tipical tree species in North China. Transactions of the Chinese Society of Agricultural Engineering, 29(23): 69-78.

Mickovski, S. B., van Beek, L. H. and Salin, F. 2005. Uprooting of vetiver uprooting resistance of vetiver grass (*Vetiveria zizanioides*). Plant and Soil, 278(1-2): 33-41.

Mickovski, S.B., Bransby, M.F., Bengough, A. G., Davies, M. C. R. and Hallett, P. D. 2010. Resistance of simple plant root systems to uplift loads. Revue Canadienne De Géotechnique, 47(47): 78-95.

Mickovski, S.B., Hallett, P.D., Bransby, M.F., Davies, M. C., Sonnenberg, R. and Bengough, A. G. 2009. Mechanical reinforcement of soil by willow roots: impacts of root properties and root failure mechanism. Soil Science Society of America Journal, 73(4): 1276.

Montagnoli, A., Terzaghi, M., Di Iorio, A., Scippa, G. S. and Chiatante, D. 2012. Fine-root morphological and growth traits in a Turkey-oak stand in relation to seasonal changes in soil moisture in the Southern Apennines, Italy. Ecological Research, 27(6): 1015-1025.

Nilaweera, N.S. and Nutalaya, P. 1999. Role of tree roots in slope stabilisation. Bulletin of Engineering Geology and the Environment, 57(4): 337-342.

Schwarz, M., Cohen, D. and Or, D. 2010. Root-soil mechanical interactions during pullout and failure of root bundles. Journal of Geophysical Research: Earth Surface, 115(F4).

Shewbridge, S. E. and Sitar, N. 1996. Formation of shear zones in reinforced sand. Journal of Geotechnical Engineering, 122(11): 873-885.

Simon, K., Steinemann, A. 2000. Soil bioengineering: Challenges for planning and engineering. Journal of Urban Planning and Development, 126(2): 89-102.

Song, W., Chen, L. and Liu, X. 2006. Experiment on characteristic of interface between root system and soil (in Chinese). Science of Soil and Water Conservation, 4(2): 62-65.

Stokes, A., Lucas, A. and Jouneau, L. 2007. Plant biomechanical strategies in response to frequent disturbance: Uprooting of *Phyllostachys nidularia* (Poaceae) growing on landslide-prone slopes in Sichuan, China. American Journal of Botany, 94(7): 1129-1136.

Stokes, A., Norris, J.E., Van Beek, L.P.H., Bogaard, T., Cammeraat, E., Mickovski, S.B., Jenner, A., Di Iorio, A. and Fourcaud, T. 2008. How vegetation reinforces soil on slopes. In Slope Stability and Erosion Control: Ecotechnological Solutions, pp. 65-118. Springer, Dordrecht.

Tang, Q., Bao, Y., He, X., Zhou, H., Cao, Z., Gao, P., Zhong, R., Hu, Y. and Zhang, X. 2014. Sedimentation and associated trace metal enrichment in the riparian zone of the Three Gorges Reservoir, China. Science of the Total Environment, 479-480: 258-266.

Tosi, M. 2007. Root pullout strength relationships and their slope stability implications of three shrub species in the Northern Apennines (Italy). Geomorphology, 87(4): 268-283.

Waldron, L.J. and Dakessian, S. 1981. Soil reinforcement by roots: calculation of increased soil shear resistance from root properties. Soil Science, 132(6): 427-435.

Waldron, L.J. 1977. The shear resistance of root-permeated homogeneous and stratified soil. Soil Science Society of America Journal, 41(5): 843-849.

Wang, X., Hong, M. M., Huang, Z., Zhao, Y. F., Ou, Y. S., Jia, H. X. and Li, J. 2019. Biomechanical properties of plant root systems and their ability to stabilize slopes in geohazard-prone regions. Soil and Tillage Research, 189: 148-157.

Wästerlund, I. 1989. Strength components in the forest floor restricting maximum tolerable machine forces. Journal of Terramechanics, 26(2): 177-182.

Wei, J., Shi, B., Li, J., Li, S. and He, X. 2018. Shear strength of purple soil bunds under different soil water contents and dry densities: A case study in the Three Gorges Reservoir Area, China. Catena, 166: 124-133.

Wu, T. H. and Watson, A. 1998. *In situ* shear tests of soil blocks with roots. Canadian Geotechnical Journal, 35(4): 579-590.

Wu, T. H., Beal, P. E. and Lan, C. 1988a. *In-situ* shear test of soil-root systems. Journal of Geotechnical Engineering, 114(12): 1376-1394.

Wu, T. H., Iii, M. K. and Swanston, D. N. 1979. Strength of tree roots and landslides on Prince of Wales Island, Alaska. Canadian Geotechnical Journal, 16(1): 19-33.

Wu, T. H., McOmber, R. M., Erb, R. T. and Beal, P. E. 1988b. Study of soil-root interaction. Journal of Geotechnical Engineering, 114(12): 1351-1375.

Yang, Y., Chen, L., Li, N. and Zhang, Q. 2016. Effect of root moisture content and diameter on root tensile properties. PLoS One, 11(3): e0151791.

Zhang, C., Chen, L., Jiang, J. and Zhou, S. 2012. Effects of gauge length and strain rate on the pullout strength of tree roots. Trees, 26(5): 1577-1584.

Zhang, C.B., Chen, L.H. and Jiang, J. 2014. Why fine tree roots are stronger than thicker roots: The role of cellulose and lignin in relation to slope stability. Geomorphology, 206: 196-202.

Zhang, D., Chen, A., Wang, X., Yan, B., Shi, L. and Liu, G. 2016. A quantitative determination of the effect of moisture on purple mudstone decay in Southwestern China. Catena, 139: 28-31.

Zhang, L., Li, M. and Zhao, B. 2018. Experimental study on tensile properties and reinforcement ability of plant roots. Nature Environment and Pollution Technology, 17(3): 729-738.

Zhao, B., Liu, D., Xia, Z., Xu, W., Xia, L., Xia, D. and Zhao, J. 2018. Effect of cement content in vegetation concrete on soil physico-chemical properties. Enzyme Activities and Microbial Biomass, 17(4).

Nature Environment and Pollution Technology
An International Quarterly Scientific Journal

p-ISSN: 0972-6268
(Print copies up to 2016)
e-ISSN: 2395-3454

Vol. 19 | No. 2 | pp. 453-467 | 2020

Original Research Paper

https://doi.org/10.46488/NEPT.2020.v19i02.003

Open Access Journal

Evaluation of Urban Wetland Ecosystem Service Value in Zhuzhou City

Wen Zhan*, Huifeng Cheng† and Shouyun Shen***
*Central South University of Forestry and Technology, Changsha 410004, China
**Changsha Environmental Protection College, Changsha 410018, China
†Corresponding author: Huifeng Cheng; chenghuifeng_cepc@163.com

Nat. Env. & Poll. Tech.
Website: www.neptjournal.com

Received: 15-07-2019
Accepted: 06-10-2019

Key Words:
Zhuzhou city;
Urban wetland;
Double counting;
Ecosystem service value

ABSTRACT

Zhuzhou is an important part of the Changsha-Zhuzhou-Xiangtan city group in southern China. To grasp the economic benefits of urban wetland resources value in Zhuzhou City, strengthen wetland conservation and utilization, and ensure the sustainable development of cities, this paper takes Zhuzhou 2016 wetland remote sensing image interpretation map and multi-source data as the foundation, and build urban wetland ecosystem service evaluation system. Through deduplicate double counting, this paper evaluates the value of urban wetland ecosystem service in Zhuzhou City employing shadow project method, replacement cost method, travel cost method, conditional value method and other economic value evaluation methods. The results indicate: (a) The total value of urban wetland ecosystem services is $1,527,908,900 in 2016. (b) The ultimate value of urban wetland services ranked as follows: water storage regulation value ($539,566,265), climate regulation value ($424,930,361), tourism recreation value ($174,543,328), water supply value ($133,183,901), biological product value ($121,987,952), atmospheric composition regulation value ($92,111,687), soil erosion prevention value ($15,799,608), water purification value ($14,598,298), and aesthetic heritage value ($10,075,346); (c) The value of different types of wetlands ranked as follows: paddy fields ($526,111,672), riverine wetland ($526,111,672), ponds ($329,628,343), reservoirs ($149,275,241), wastewater treatment plant ($207,831/a); (d) The value per unit area of different types of wetlands ranked as follows: reservoirs ($240,919/ha), riverine wetland ($236,627/ha), pond ($145,693/ha), paddy fields ($26,551/ha) and wastewater treatment plant ($17,003/ha). The evaluation results reveal the great contribution of urban wetland system service to the Zhuzhou city with numbers, that not only provides data basis for wetland conservation and management but also provides a reference for the refined evaluation of urban wetland ecosystem service value.

INTRODUCTION

Wetland ecosystem services refer to the direct or indirect contribution of wetland ecosystems to human well-being and benefits (USEPA 2009, TEEB 2010). The study of wetland ecosystem services began in the middle and late 20th century. With the emergence of global environmental issues, this work has gradually become one of the hot topics of concern in ecology and economics. Numerous international organizations, experts and scholars have carried out a lot of research on wetland ecosystem services in terms of concept definition (Costanza et al. 1997, MA 2005, Wallace 2007, Boyd & Banzhaf 2007, Fisher & Kerry 2008, Fisher et al. 2008, Fisher et al. 2009), classification method (Daily 1997, De Groot et al. 2002, Woodward & Wui 2001, Brander et al. 2006, De et al. 2006), evaluation method (Costanza 2008, Adamus et al. 1987, Odum & Nilsson 1996, Turner et al. 2010, Hawkins 2003), and value evaluation (Hoekstra & Hung 2002, Nelson et al. 2009, Musamba et al. 2012, Jiang et al. 2015, De et al. 2012, Sun et al. 2018, Zhao & He 2018). Through many cases, it has fully revealed the multi-faceted ecosystem service functions and values provided by wetlands for human society. Among these wetland case types, natural wetlands outside the urban area are the main targets of ecosystem service value assessment research, while research on urban wetlands is relatively rare.

Wetlands are the birthplace of human "civilization" and are closely related to the beginning and decline of the city. On the one hand, wetlands provide many natural resources and material basis for the urban production and life, which provide a strong guarantee for the urban ecological balance and social development, while on the other hand, under the background of intensified global urbanization, human activities have caused serious disturbance and damage to wetlands, especially the shrinking area and increasing degree of fragmentation of wetlands within the urban area, and their ecosystem services are also affected in many aspects. The evaluation of urban wetland ecosystem service value is a process of quantitative evaluation of multiple service values

of various types of wetlands within the city, which provides scientific data support for comprehensive protection and utilization of wetlands and sustainable development of the city (De et al. 2006).

At present, the economic value evaluation method is the most widely used one in many wetland ecosystem service evaluation methods. It is a quantitative assessment of the monetization of wetland ecosystem services. It not only reflects the impact of human activities on the structure and function of wetland ecosystem (Costanza et al. 2014), but also provides a basis for ecological compensation decision-making (Farley et al. 2010), and improves people's understanding of the importance of wetland ecosystem services (Braat et al. 2012).

Zhuzhou is an old industrial base in southern China. Its natural conditions are superior and its wetland resources are abundant. The Xiangjiang River flows through the city from south to north, dividing the urban area into two sides. In the past, the characteristics of traditional industries dominated by heavy chemical industry have caused huge consumption of natural resources in Zhuzhou City, which has caused a great impact on urban wetlands, serious water pollution, and the shrinking of wetland area and quantity. In the 21st century, Zhuzhou has become an important part of Changsha-Zhuzhou-Tan urban agglomeration, which is a demonstration area of "two-oriented society construction". Its urbanization process is intensifying and the urban area is expanding. Therefore, coordinating urban sustainable development and wetland conservation and utilization has become the focus of government and society. It is urgent to scientifically evaluate the value of wetland ecosystem services in Zhuzhou City, and provide a reference for management decision-makers. Based on the socio-economic environment of Zhuzhou City and the ecological characteristics of wetlands, this paper evaluates the value of urban wetland ecosystem services by various suitable economic value evaluation methods and reveals the wetland ecosystem services to provide urban survival and development with intuitive economic figures.

MATERIALS AND METHODS

Research Area Overview

Zhuzhou located in the east of Hunan province in China, in the west of Luoxiao Mountain Range, Nanling Mountains Range to the tilting area of Jianghan Plain, and the downstream of the Xiangjiang River water system, between the northern latitude 26°03'05"~28°01'07", east longitude 112°57'30"~114°07'15" (Fig. 1). Zhuzhou is a subtropical monsoon humid climate, four seasons, adequate rainfall, and rich in wetland resources. As of 2016, the total area of Zhuzhou (including city and counties) is about 11247.55 km^2, of which the urban area is located in the northwest of Zhuzhou with an area of 853.4k km^2 and a permanent resident population of about 4,016,300. This paper takes 2016 urban area (Zhuzhou City) as the specific research area, covering urban planning area and built-up area.

Classification of Urban Wetland in Zhuzhou City

The concept of urban wetlands does not currently have a scientific definition in a strict sense. The academic community

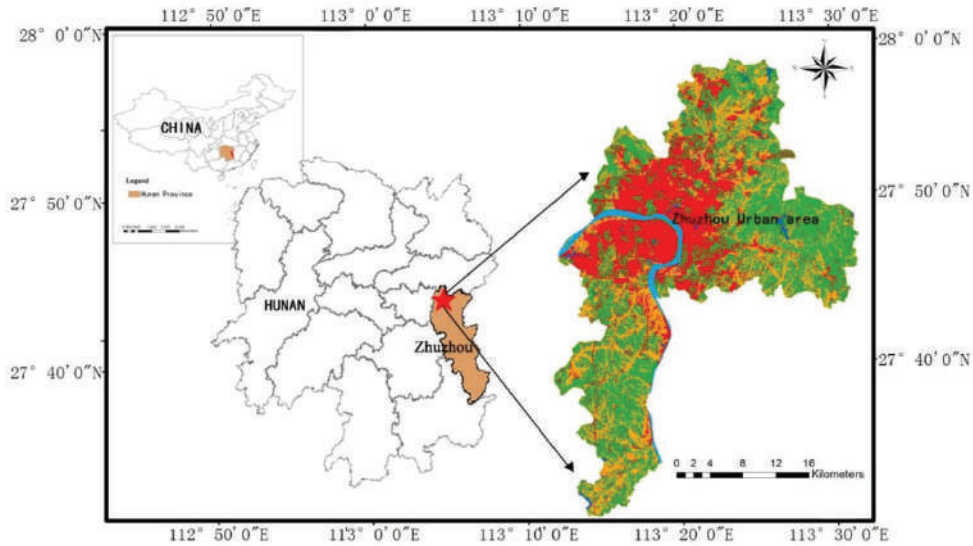

Fig. 1: Location of the study area.

Table 1: Classification of urban wetlands in Zhuzhou City.

Category	Primary type	Secondary type	Description
Urban wetland	Natural wetland	Riverine wetland	Permanent river, including rivers and their tributaries, stream, waterfall seasonal (has seasonal attributes) or intermittent (no obvious seasonal dependence) rivers, streams, floodplains (refers to the flood of flood-waters on both sides of the river)
		Reservoirs (area greater than 8ha)	Reservoir, lake, barrage, water storage area formed by the dyke, park wetland
	Artificial wetland	Pond (area less than 8ha)	Agricultural pond, water storage pond, Aquatic ponds such as fish and shrimp culture and small landscape water bodies
		Paddy fields	Rice fields, lotus, water bamboo fields, etc.
		Wastewater treatment plant	Sewage plant, treatment pool, oxidation pool, etc.

generally believes that urban wetlands refer to coastal and estuary, riverbanks, shallow lakes, water conservation areas, natural and artificial ponds, and wastewater treatment plants within urban areas. An ecosystem with a land-sea transitional nature (Wang & Lv 2007).

Based on the Ramsar Convention and the wetland classification system monitored by China's current wetland survey as the main basis, referring to "China's Land Use Status Classification" (GB/T 21010-2017), and other relevant norms, combined with the actual needs of the study, urban wetlands in Zhuzhou City are divided into natural wetlands and artificial wetlands. The specific classification and description are shown in Table 1.

Research Data Source

Data source and classification: The basic data of this paper mainly includes image data and statistical data. The main contents and sources are given in Table 2.

The Landsat 8 OLI remote sensing image data of Zhuzhou City come from the Geospatial Data Cloud Platform of the Chinese Academy of Sciences Computer Network Information Center (http://www.gscloud.cn); Zhuzhou City Administrative Border (2016), Zhuzhou City wetland Survey plaque data (2010) provided by Zhuzhou municipal forestry bureau; Zhuzhou City Google HD satellite map is downloaded from the internet employing 91 graphic assistant software.

Data interpretation: Based on the analysis software of ENVI5.3, ArcGIS10.4 and ecognition, and the object-oriented information extraction method, this paper finally obtained the classification and distribution of urban wetland in Zhuzhou city in 2016 (Fig. 2) and relevant data (Table 3).

Establishment of Evaluation System for Urban Wetland Ecosystem Service Value in Zhuzhou City

From the perspective of evaluating and managing ecosystems, the Millennium Ecosystem Assessment Classification System divides ecosystem services into four categories: supply services, regulatory services, cultural services and support services (Ma 2005), which is currently the most widely used wetland ecosystem service classification system. However, this classification system confuses the intermediate and ultimate services of wetland ecosystem, leads to double counting of ecosystem services, causes the unclear causal relationship between ecosystem functions and ecosystem services, and reduces the scientificity and applicability of wetland ecosystem services value assessment results (Boyd 2007, Johnston & Russell 2011, Nahlik et al. 2012, Ringold et al. 2013, Keeler et al. 2012, Wong et al. 2015). Therefore, the deduplication double-counting of ecosystem services has become the focus and difficulty of the refined assessment of

Table 2: Sources of data.

Classification	Data	Scope	Type	Time
Image data	Landsat 8 OLI	Row number 123/41	Landsat 8 OLI, 30m	07-23-2016
	Zhuzhou City wetland census spot	Zhuzhou City	Shapefile	2010
	Google Hd satellite maps	Zhuzhou City	TIFF	2016
	Zhuzhou City administrative boundaries	Zhuzhou City	Geodatabase	2016
Statistical data	Zhuzhou statistical yearbook	Zhuzhou City	Electronic document	2016
	Zhuzhou water resources bulletin	Zhuzhou City	Electronic document	2016

Table 3: Urban wetland types and acreage in 2016 in Zhuzhou City.

Urban wetland types	Area (ha)	Proportion (%)
Riverine wetland	2208.9	8.86
Reservoirs	619.6	2.49
Ponds	2262.5	9.08
Paddy fields	19819.9	79.52
Wastewater treatment plant	12.2	0.05
Total	24923.1	100

wetland ecosystem services and the optimal management of wetland ecosystem services (Jiang et al. 2015).

Due to the different scales and research purposes of ecosystems, wetland ecosystem services can exist in multiple classifications (Fisher et al. 2009, Costanza 2008) depending on the specific assessment environment and assessment objectives. Based on the classification of urban wetland in Zhuzhou City, this study takes the millennium ecosystem service classification as the main reference, conducts a comprehensive survey and analysis of Zhuzhou socio-economic environment and urban wetland ecological characteristics, and establishes the urban wetland ecosystem service evaluation system (Table 4) with the direct contribution to human benefits as the only criterion. Urban wetland ecosystem services are divided into ultimate services and intermediate services. The ultimate services include atmospheric composition regulation, climate regulation, water storage regulation, water purification, prevention of soil erosion, biological products, water supply, tourism, and aesthetic heritage. The sum of these services is the total value of the urban wetland ecosystem services in Zhuzhou City. Intermediate services include biodiversity, water conservation, and nutrient cycling, etc. These intermediate services contribute indirectly to human well-being through the ultimate service, and by excluding these intermediate services in the calculation of total value, double counting can be avoided.

CALCULATION PROCESS AND RESULTS

The value of urban wetland ecosystem services is a dynamic variable that changes with time and space. The evaluation process needs to indicate the time and region of its calculation. Based on the relevant basic data of urban wetland, this

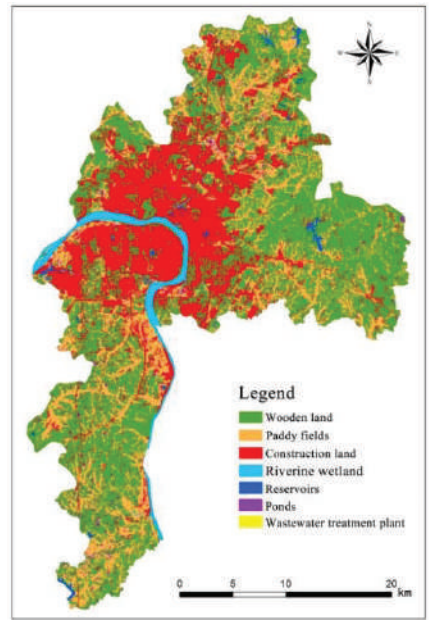

Fig. 2: Urban wetland classification in 2016 in Zhuzhou city.

paper uses Zhuzhou City as the research scope (853.4 km^2) in 2016 and uses the economic value evaluation method to calculate the ultimate service value and intermediate service value of urban wetland (all economic data is converted into 2016 prices based on the GDP deflator).

Final Service Value

Atmospheric composition regulation value: The adjustment value of atmospheric composition of urban wetland in Zhuzhou City mainly includes the value of oxygen release from wetland vegetation, soil carbon sequestration value and negative value of methane emission from paddy fields. It is mainly evaluated by the carbon tax value method and the market value method. The calculation equations are:

$$V_1 = V_C + V_t - V_f \quad \ldots(1)$$

$$V_C = C_1 \times P_1 \quad \ldots(2)$$

$$V_t = C_2 \times P_2 \quad \ldots(3)$$

$$V_f = C_3 \times P_3 \quad \ldots(4)$$

In the equations, V_1 is the value of the atmospheric composition of the wetland; V_c is the total value of oxygen release ($), C_1 is the total amount of oxygen released (t), P_1 is the price of oxygen release ($/t); V_t is the value of carbon sequestration of the soil ($), C_2 is Total carbon (t); P_2 is carbon sequestration price ($/t); V_f is the total methane released in paddy fields (kg), C_3 is the total methane release (t); P_3 is methane price ($/t).

***(a) Wetland carbon sequestration and oxygen release positive benefits*:** *Soil carbon sequestration*: According to the relevant data, the carbon sequestration rate of the lake

Table 4: Assessment system of urban wetland ecosystem services in Zhuzhou city.

First level classification	Second level classification	Third level classification	Evaluation index and parameters	Wetland types included in the calculation	Evaluation method
Ultimate Service Value	regulation service value	Atmospheric composition Adjustment Value	Oxygen release, Carbon fixation, greenhouse gas emissions (Methane dominated)	Riverine wetland, Reservoirs, Pond wetlands, Paddy fields	Carbon tax value method, Industrial Oxygen production method
		Climate Adjustment Value	Temperature changes, humidity changes	Riverine wetland, Reservoirs, Pond wetlands, Paddy fields, Wastewater treatment plant	Shadow project method
		Water Storage Adjustment Value	Water storage, flood control and water yield regulation	Riverine wetland, Reservoirs, Pond	Shadow project method
		Water purification value	Removed quantity of N and P	Riverine wetland, Reservoirs, Pond	Replacement cost method
		Preventing soil erosion value	Reducing land waste, reducing soil fertility Loss	Riverine wetland, Reservoirs, Pond, Paddy fields	Replacement cost method
	Supply service value	Biological products value	Fish, rice, reed, etc.	Riverine wetland, Reservoirs, Pond, Paddy fields	Market value method
		Water supply value	Water consumption	Riverine wetland, Reservoirs	Market value method
	Cultural service value	Tourism recreation value	Travel cost, travel time cost, consumer Surplus	Riverine wetland, Reservoirs, Pond	Travel cost method
		Aesthetic heritage value	Willingness to pay, willingness to accept compensation	Riverine wetland, Reservoirs	Conditional value method
Intermediate Service Value		Biodiversity value	Diversity maintenance, habitat	Riverine wetland, Reservoirs, Pond	Result reference method
		Water conservation value	Surface water storage	River wetland, Reservoirs, Pond	Shadow project method
		Nutrient cycling value	Contents of N, P and K in Soil	Riverine wetland, Reservoirs, Pond, Paddy fields	Shadow price method

wetland is 190.2g/m^2·a (Song et al. 2011), and the soil carbon sequestration rate of the paddy fields is 380.78kg/m^2·a (Han et al. 2008).

Vegetation carbon fixation and oxygen release. Different ecosystems have different carbon fixation and oxygen release standards. In this study, the river wetland takes 0.22kg/m^2·a, and the lake wetland takes 0.15kg/m^2·a (Mei & Zhang 2007). The vegetation coverage index (NDVI) is extracted from the 2016 remote sensing image interpretation map of Zhuzhou City by ArcGIS and ENVI software. After the correlation calculation, the coverage area of non-paddy wetland plants is 2,994ha, which obtained the total carbon and oxygen release of wetland vegetation in Zhuzhou City.

Oxygen-releasing carbon price: According to the industrial oxygen production method, the price of oxygen release in 2016 is \$194.10/t. The carbon sequestration price adopts the carbon tax value method, and the 2016 conversion price is \$483.77/t.

***(b) Negative methane release from rice fields*:** Wetlands are important sources of greenhouse gas emissions such as methane, especially in rice fields where methane emissions are large (Song 2004). The paddy fields of Zhuzhou City (99% of rice fields) accounts for more than 80% of the total urban wetland area. Therefore, the economic value loss caused by methane emissions from rice fields is calculated as the economic value loss of greenhouse gas emissions from wetlands in Zhuzhou City. According to the relevant data, 0.36g/m^2·d is taken as the methane emission rate in the paddy field, and the methane emission in 410 months is taken as the total methane emission. The conversion price of methane in 2016 is \$0.19/kg (Shangguan et al. 1994).

(c) Taking the above data into the relevant equation for calculation, the atmospheric composition regulation value of urban wetland is \$92,111,687/a.

Climate regulation value: The climate regulation value of urban wetland in Zhuzhou City mainly includes temperature regulation and increased air humidity. It is mainly evaluated by the shadow engineering method. The calculation equations are:

$$V_2 = V_Q + V_h \quad \ldots(5)$$

$$V_Q = ET \div ER_{ac} \times P_e \quad \ldots(6)$$

$$V_h = EW \times PC_{ew}/m^3 \times P_e \quad \ldots(7)$$

In the equations, V_2 is the value of climate regulation (\$); V_Q is the value of temperature regulation (\$); ET is the heat absorbed by total evaporation (J); ER_{ac} is the energy efficiency ratio of the air conditioner; V_h is the value of air humidity (\$); EW is the amount of water evaporated (m^3); PC_{ew}/m^3 is the evaporation power consumption per cubic meter; P_e is the electricity price (\$/kWh).

***(a) Temperature regulation value*:** The annual evaporation of Zhuzhou City's waters relative to land is 14.3557×10^6 mm^3, which is selected 2.26×10^6 J/kg as the evaporation heat value of the water body. The energy efficiency ratio of the air conditioner is calculated according to 3.0, and the electricity price is \$0.09/kWh in 2016.

***(b) Increase the value of air humidity*:** The evaporation power consumption per cubic meter of water is converted into water vapour consumption of about 125 kWh as a parameter (Wu et al. 2016). The electricity price is taken at 2016 price of \$0.09/ kWh.

(c) Taking the above data into the relevant equation for calculation, the climate regulation value of urban wetland is \$424,930,361.45/a.

Water storage adjustment value: The water storage adjustment value of urban wetland in Zhuzhou City is mainly reflected in flood control and storage, regulation of water flow and flow rate, adjustment of regional water resources, etc., mainly adopted for evaluation by shadow engineering method and protection cost method. The calculation equation is:

$$V_3 = C \times V_i \quad \ldots(8)$$

In the equation, V_3 is the value of water storage adjustment (\$); C is the total amount of water storage regulation (m^3); V_i is the storage capacity per unit of water storage capacity (\$ /m^3).

According to the 2017 Statistical Yearbook of Zhuzhou City, the total water resources in Zhuzhou City in 2016 is 933 $\times 10^6$ m^3. According to the "2001-2010 China Water Yearbook" data, the conversion cost of the unit storage capacity in 2016 is \$0.58/m^3. Taking the above data into the relevant equation for calculation, the water storage adjustment value of urban wetland is \$539,566,265/a.

Water purification value: The water purification value of urban wetland in Zhuzhou City is mainly reflected in the removal capacity of total nitrogen and total phosphorus in water by the wetland. It is mainly evaluated by the alternative cost method. The calculation equation is:

$$V_4 = N \times S \times V_N + P \times S \times V_P \quad \ldots(9)$$

In the equation, V_4 is the value of purification of wetland water (\$); N is the removal rate of nitrogen per unit area of the wetland; P is the removal rate of phosphorus per unit area of the wetland; S is the area of wetland (m^2); V_N is the treatment cost of nitrogen (\$/kg); V_p is the processing cost of phosphorus (\$/kg).

According to relevant data, the average removal rates

of nitrogen and phosphorus per unit area of wetland are 3.98t/ha and 1.68t/ha, respectively (Jin et al. 2006). The total amount of nitrogen and phosphorus removed from the wetland water body is calculated based on the total area of urban wetland in Zhuzhou City. The conversion and treatment costs of N and P are $0.44/kg and $0.73/kg respectively in 2016. Taking the above data into the relevant equation for calculation, the adjusted water storage value of urban wetland is $14,598,298.19/a.

Preventing soil erosion value: The preventing soil erosion value of urban wetlands in Zhuzhou City is mainly reflected in the reduction of land abandonment and soil fertility loss. It is mainly evaluated by the alternative cost method. The calculation equations are:

$$V_5 = V_{F^1} + V_{F2} \quad \ldots(10)$$

$$V_{F1} = S_t \times V_t \quad \ldots(11)$$

$$S_t = M \div D, \mathrm{M} = \mathrm{P} \times \mathrm{S} \quad \ldots(13)$$

$$V_{F_2} = S_t \times D \times R \times L_i \times V_i \quad \ldots(14)$$

In the equations, V_5 is to prevent the value of soil erosion ($); V_{F1} is to reduce the value of land abandonment ($); V_{F2} is to reduce the value of soil fertility loss ($); S_t is to wasteland area (m^2); V_t is to reduce the cost of land abandonment per unit area ($/ha); M is to reduce the total amount of soil erosion (m^3); D is the average thickness of soil topsoil (m); P is the depth of erosion (m), S wetland area (m^2); D is the average thickness of soil topsoil (m), R is the soil bulk density (g/), L_i is the content of the i-th nutrient element in the soil (kg), V_i is the price of the i-th element fertilizer ($/t).

***(a) Reduce land waste value*:** Referring to relevant data, the average value of grassland erosion depth is 25mm/a (Li et al. 2000), which calculates the total annual soil erosion of urban wetland is 6,277,500m^3 in Zhuzhou City. The average thickness of soil topsoil is 85mm, and the cost of reducing land per unit area is $36.97/ha (Wu et al. 2015). The discounted price in 2016 is $188.38 /ha.

***(b) Reduce the loss of soil fertility*:** In this paper, the values of nitrogen, phosphorus and potassium nutrients are used to measure the value of wetland to reduce the loss of soil fertility. The bulk density of the soil is 1.2g/cm^3; the average content of nutrients in the soil surface is N=1.877g/kg, P=0.49g/kg, K=7.96g/kg (Li et al. 2006). The prices of nitrogen fertilizer, phosphate fertilizer and potash fertilizer in 2016 are $189.17/t, $100.39/t and $265.85/t, respectively.

(c) Taking the above data into the relevant equation for calculation, the soil erosion value of urban wetland is $16,911,762.05/a.

Biological product value: The biological products value of urban wetland in Zhuzhou City is mainly reflected in the value of freshwater animal products and rice. It is calculated based on the fishery output value and rice output value and is mainly evaluated by the market value method. The calculation equation is:

$$V_6 = V_y + V_d \quad \ldots(15)$$

In the equation, V_6 is the value of the biological product ($); V_y is the output value of the fishery ($); V_d is the output value of the rice ($).

According to the 2017 Statistical Yearbook of Zhuzhou City, the total annual fishery output value in 2016 is $27,480,422; the total output value of rice is $94,507,530. Taking the above data into the relevant equation for calculation, the biological products value of urban wetland is $121,987,951/a.

Water supply value: The water supply value of urban wetland in Zhuzhou City is mainly reflected in the value of water supply, including the provision of four types of water use, such as domestic water, industrial water, agricultural water, and public ecological water. It is evaluated by the market value method. The calculation equation is:

$$V_7 = \Sigma A_i \times P_i \quad \ldots(16)$$

In the equation, V_7 is the value of water supply ($); A_i is the amount of water used for the i-th use (m^3); P_i is the market price of water for the i-type ($ /m^3).

According to the 2017 Statistical Yearbook of Zhuzhou City, the total water consumption in 2016 is 67.854×10^6 m^3, of which the domestic water consumption is 71.84×10^6 m^3, the unit price is $0.24/$m^3$, the industrial water consumption is 386.89×10^6 m^3, and the unit price is $0.29/$m^3$; The water and public ecological water use are 140.44×10^6 m^3 and 79.37×10^6 m^3 respectively, and the unit price is $0.02 /$m^3$. Taking the above data into the relevant equation for calculation, the supply value of the urban wetland water source is $133,183,901/a.

Tourism recreation value: The tourism recreation value of urban wetland in Zhuzhou City is mainly reflected in the value of sightseeing and tourism in wetlands, the value of leisure and entertainment, the value of popular science education, and the value of health and fitness. This paper uses the Travel Cost Method (TCM) to evaluate the non-market value evaluation method of tourism resources based on consumer choice theory (Dong et al. 2011), which generally includes two parts: consumer expenditure and consumer surplus. Among them, consumer expenditure includes travel expenses and travel time value. This study passed the questionnaire survey (350 questionnaires are distributed, 334 valid questionnaires are returned, feedback rate is 95.43%) and analysis

is obtained; consumer surplus is passed through consumers. The proportional relationship between the remaining and travel expenses is obtained. The equation for calculating the value of urban wetland tourism recreation is:

$$V_8 = a_1 + a_2 + a_3 \quad \ldots(17)$$

In the equation, V_8 is the value of tourism recreation for urban wetlands in Zhuzhou City; a_1 is expenditure for travel expenses; a_2 is value for travel time; a_3 is for consumer surplus.

***(a) Questionnaire statistics and analysis*:** Local tourist spending behaviour. Table 5 shows that urban wetland in Zhuzhou City are more attractive to surrounding residents, and the average length of recreation is 2 to 3 hours. More than half of the people who spend less than $5 per capita have a lower per capita consumption index.

Foreign tourists' consumption behaviour: It can be seen from Table 6 that the foreign tourists of urban wetland in Zhuzhou City mainly come from neighbouring cities, and there are many forms of self-driving tour; and the number of repeated play in the past three years is relatively low; the average playtime is 2 to 4 hours; the average cost per person is $5 to $15 is the main.

Table 5: Analysis of local tourists' consumption behaviour.

Issue	Options	Select the number of	Proportion (%)
How many kilometres are you from the wetland (park/scenic area)?	Within 3 km	83	28.23
	3-5 km	105	35.71
	5-10 km	84	28.57
	10-15 km	18	6.12
	15-20 km	2	1.02
	More than 20 km	1	0.34
How many times a year do you visit urban wetland (park/scenic area)?	Once	12	4.08
	Twice	21	7.14
	3 times	46	15.65
	4 times	32	11.22
	5 times	27	9.18
	6 to 10 times	64	21.77
	Once and twice a week	46	15.65
	Almost every day	45	15.31
How do you travel to urban wetland (park/scenic area)?	Walk	74	25.17
	Bus	107	36.39
	Self-driving	81	27.55
	A bicycle / battery car / motorcycle	19	6.8
	Taxi	12	4.08
How long did you spend in urban wetland (park/scenic area)?	Less than 1 hour	70	23.81
	2 to 3 hours	176	59.86
	3 to 4 hours	33	11.22
	4 to 5 hours	8	3.06
	6 hours and more	6	2.04
What is the cost of your visit to urban wetland (park/scenic area)?	Less than $5	174	59.18
	$5 to $15	76	25.85
	$15 to $30	29	9.86
	$30 to $45	8	2.72
	$45 to $75	5	1.7
	More than $75	2	0.68

***(b) Travel expenses*:** According to the preliminary questionnaire survey, the average daily travel cost of local tourists is $9.94, and the average daily travel cost of foreign tourists is $21.84. From this, the average daily travel cost of urban wetland in Zhuzhou City is about $12.35/person. In 2016, the total number of tourists in Zhuzhou City is 27.1579 million. The number of wetland tourists is estimated based on 30% of the total number.

***(c) Travel time value*:** Travel time value = number of visitors × total travel time × spent unit time opportunity wage cost. The travel time value is calculated according to the per capita disposable income of the urban population of Zhuzhou City $5546.39 in 2016, and the opportunity cost is calculated according to one-third of the wage cost (Chavas et al. 1989). The monthly working hours of tourists from all sources are 168 hours. The travel time of local tourists is calculated as 0.5 hours; the travel time of non-local tourists is calculated as 2 hours. Recreation time is calculated as 3 hours.

***(d) Consumer surplus*:** According to related research, consumer surplus is generally calculated at 40% of travel expenses (Li 2006).

(e) Taking the above data into the relevant equation for calculation, the tourism recreation value of urban wetland is $174,543,328.31/a.

Aesthetic heritage value: The aesthetic heritage value of urban wetland in Zhuzhou City is mainly reflected in the non-use value of the invisible resources such as culture, history, aesthetic sources and species in the wetland.

In this paper, the Conditional Value Method (CVM) is mainly used for evaluation. The value of urban wetland cultural heritage in Zhuzhou City is calculated by building a hypothetical market to know people's willingness to pay for non-market items (WTP) or to obtain wiliness to accept (WTA) (Zhuang 2006). Its calculation equation is:

$$V_9 = V_{wtp} \times A \quad \ldots(18)$$

Table 6: Analysis of consumption behaviour of foreign tourists.

Issue	options	Select the number of	Proportion /%
How do you come to Zhuzhou City?	Self-driving	16	40
	Automobile	7	17.5
	Ordinary train	7	17.5
	High-speed rail/bullet train	8	20
	Aircraft	2	5
	Other	0	0
In the past three years, have you visited urban Wetland (Park / Scenic spot) in Zhuzhou City?	Once	11	27.5
	Twice	13	32.5
	Three times	9	22.5
	Four times	0	0
	Five times	4	10
	6-10 times	1	2.5
How long do you spend in urban Wetland (Park / Scenic spot) in Zhuzhou City?	10 hours and more	2	5
	Less than 1 hour	5	12.5
	2 to 3 hours	23	57.5
	3 to 4 hours	7	17.5
	4 to 5 hours	2	5
	6 hours and more	3	7.5
How much do you spend on visiting urban Wetland (Park / Scenic spot) in Zhuzhou City?	Less than $5	7	17.5
	$5 to $15	15	37.5
	$15 to $30	8	20
	$30 to $45	6	15
	$45 to $75	2	5
	More than $75	2	5

In the equation, V_9 is for the aesthetic heritage value ($); V_{wtp} is for the WTP value ($); A is the number of permanent residents in Zhuzhou City.

***(a) CV questionnaire design*:** Relevant data are collected through the development of the wetland aesthetic heritage value questionnaire. Using a district survey, East area of Xiangjiang River issued 150 questionnaires and recovered 150 copies (including 4 unqualified questionnaires); West area of Xiangjiang River issued 200 questionnaires and recovered 200 copies (including 12 unqualified questionnaires). Besides, the survey covers all types of people.

***(b) Analysis of survey results*:** To facilitate statistics, 3,674 pieces of valid 334 questionnaires are entered into Excel software to establish a CVM questionnaire database. As given in Table 7, the willingness to pay (WTP) produced two calculation results, one is the WTP average of $18.24, and the other is the WTP median value of $8.10. According to the actual situation, it is known that taking the arithmetic mean to calculate the per capita maximum willingness to pay will produce a higher error. Therefore, this paper obtained the WTP median value of $8.10 through the interpolation method and took it as the calculation standard of the paper's willingness to pay (WTP). Besides, the 2017 Yearbook shows that the resident population of Zhuzhou City is 1.2435 million in 2016.

Taking the above data into the relevant equation for calculation, the aesthetic heritage value of urban wetland is $10,075,300/a.

Intermediate Service Value

Biodiversity value: The biodiversity value of urban wetland in Zhuzhou City is mainly reflected in the important value its rich biodiversity provides for the balance of the regional ecosystem. In this paper, the achievement reference method is adopted, and its calculation equation is as follows:

$$V_{10} = V_c \times A \quad \ldots(19)$$

In the equation, V_{10} is for biodiversity value($); V_c is the value of wetland per hectare biodiversity ($/a); A is calculated urban wetland area (ha);

This paper studies the unit value of wetland biodiversity in the value of China's ecosystem services by Xie et al. (2015), and its 2016 conversion price is $2,892.92/ha·a. Taking the above data into the relevant equation for calculation, the biodiversity value of urban wetland is $1,981.89/a.

Water conservation value: The water conservation value of urban wetland in Zhuzhou City is mainly reflected in the water storage value of the wetland to the surface. This paper adopts the alternative cost method, and its calculation equation is:

$$V_{11} = \Sigma A_i \times D_i \times P_s \quad \ldots(20)$$

In the equation, V_{11} is for the conservation of water source value($); A_i is for each type of wetland area (ha); D_i is for each type of wetland storage depth (m); P_s is storage capacity of storage capacity ($/m^3).

According to the survey on the current situation of urban wetland resources in Zhuzhou City, with reference to the data of Zhuzhou City Water Resources Bulletin in 2017, the average depth of river wetland water storage in Zhuzhou City is 8m, and the average depth of water storage in the water storage area is 4m. The average depth of water is 2m; in 2016,

Table 7: Frequency distribution of sample willingness to pay.

WTP value ($)	Absolute frequency / person	Relative frequency (%)	Frequency of adjustment (%)	Cumulative frequency (%)
5	51	15.3	30.2	46.2
15	45	13.5	26.5	72.7
30	22	6.6	13.0	85.7
45	4	1.2	2.4	88.1
60	0	0	0	88.1
75	6	1.8	3.6	91.7
90	1	0.3	0.6	92.3
120	1	0.3	0.6	92.9
150	3	0.9	1.8	94.7
300	7	2.1	4.1	98.8
300 and above	2	0.6	1.2	100
Refusal to pay	164	49.2		
WTP average	18.24			
WTP median value	8.10			

Table 8: Value of urban wetland ecosystem service in Zhuzhou City.

Primary classification	Secondary classification	Tertiary classification	Value (10^6·a)	Unit value (10^3/ha)	Proportion of total value (%)
Ultimate service value	Adjust service value	Adjustment value of atmospheric composition	92.1117	3.7	6.03
		Climate regulation value	424.9304	17	27.81
		Water storage regulation value	539.5663	21.7	35.31
		Water quality purification value	96.9327	0. 6	0.96
		Value of preventing soil erosion	16.9118	0. 7	1.11
	Supply service value	Biological product value	121.9880	4.9	7.98
		Water supply value	3.2002	5.3	8.72
	Cultural service value	Tourism rest value	26.2866	7	11.42
		Aesthetic heritage value	10.0753	0. 4	0.66
Total			1,527.9089	61.3	100.00
Intermediate service value		Biodiversity value	19.8189	-	11.43
		Water conservation value	142.6964	-	82.33
		Nutritional cycle value	10.8107	-	6.24
Total			173.326	-	100.00

the cost of the unit reservoir is \$0.58/m^3; the area of each type of wetland is shown in Table 3. Taking the above data into the relevant equation for calculation, the water conservation value of urban wetland in Zhuzhou City is \$142,696,482/a.

Nutritional cycle value: The nutritional cycle value of urban wetland is mainly reflected in the value of N, P, K and other nutrients in the utilization, conversion, movement and reuse of ecosystems. In this paper, the shadow price method and the soil bank nutrient retention method are used to evaluate the value. The calculation equation is:

$$V_{12} = S_t \times D \times R \times L_i \times V_i \quad \ldots(21)$$

In the equation, V_{12} is for the nutritional cycle value (\$); S_t is for the wetland area (m^2); D is for the soil topsoil average thickness (m); R is for the soil bulk density (g/cm^3); L_i is for the soil N, P, K nutrient content (kg); V_i is the price of N, P, K fertilizer (\$/t).

In this paper, the average thickness of soil surface layer in Zhuzhou City is calculated according to 85mm (Li et al. 2006), the bulk density of soil is 1.2g/cm^3, and the average content of nutrient elements in soil surface is N=1.877g/kg,

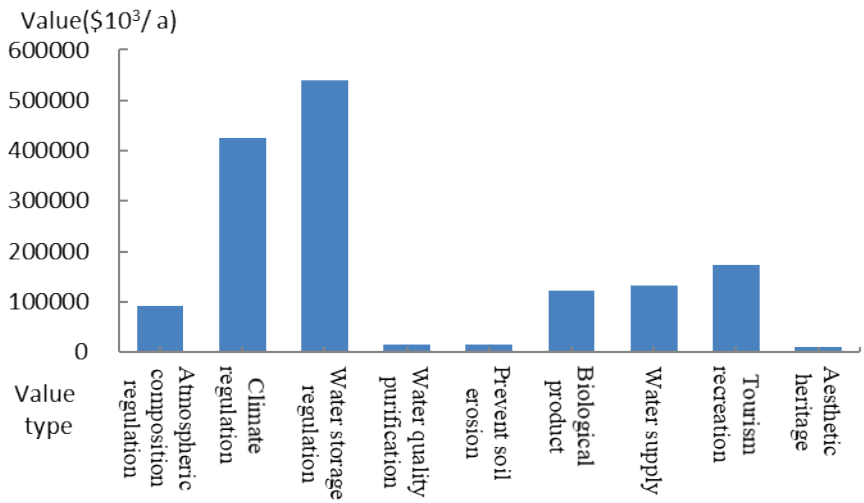

Fig. 3: Histogram of urban wetland value statistics.

P=0.49g/kg, K=7.96g/kg (Dong et al. 2011). The prices of nitrogen fertilizer, phosphate fertilizer and potash fertilizer in 2016 are $189.17/t, $100.39/t and $264.49/t, respectively. Taking the above data into the relevant equation for calculation, the nutritional cycle value of urban wetland is $10,810,707.8/a.

The total value of urban wetland ecosystem service in Zhuzhou City: The total value of urban wetland ecosystem service in Zhuzhou City is the sum of the ultimate service values of wetlands. The calculation equation is:

$$V_s = \Sigma_1^9 V_i \quad \ldots(22)$$

In the equation, V_s is the total value of service for wetlands ($); V_i refers to the value of the i-type value ($) in the ultimate service value.

After calculation, the ultimate service value of urban wetland is $1,527,908,901; the intermediate service value of urban wetland is $173,326,054. The total value of urban wetland ecosystem services in Zhuzhou City in 2016 is $1,527,908,901 (Table 8).

Statistical analysis of urban wetland ecosystem service value in Zhuzhou City: The statistics of the ultimate service value of different urban wetland types in Zhuzhou City are shown in Table 9.

Analysis of the ultimate service values of urban wetland: The ultimate value of the urban wetland ecosystem services in Zhuzhou City is ranked as follows: Water storage regulation value>Climate regulation value>Tourism recreation value >Water supply value>Biological product value>Atmospheric composition regulation value> Preventing soil erosion value>Water purification value>Aesthetic heritage value, as shown in Fig. 3.

Analysis of the value of each type of urban wetland: The value of different types of urban wetland types in Zhuzhou City is as follows: Paddy fields>Riverine wetland>Ponds>Reservoir>Wastewater treatment plant, as shown in Fig. 4.

Analysis of unit area value of each type of urban wetland: The value per unit area of each type of urban wetland in Zhuzhou City is ranked as follows: Reservoirs>Riverine wetland>Pond >Paddy fields>Wastewater treatment plant, as shown in Fig. 5.

DISCUSSION AND CONCLUSIONS

Compared with previous wetland research, this paper focuses on urban wetland ecosystem services, and distinguishes the intermediate service value and ultimate service value of urban wetland ecosystem in the process of constructing service evaluation system, and comprehensively evaluates the direct contribution of the wetland ecosystem of Zhuzhou City to human welfare. From the perspective of the selection of evaluation indicators and methods, the evaluation results of this study are reasonable to some extent, and the value assessment methods are improved compared with the previous ones, providing a reference for the refined evaluation of urban wetland ecosystem service value.

However, part of the economic data has a long time, it has a certain impact on the evaluation results of the paper. Besides, it should be pointed out that deduplicate double-counting not only improves the accuracy and accuracy of ecological service value accounting but also provides a more scientific decision-making basis for urban wetland conservation and management. As a result, the wetland value can be

Table 9: The ultimate service values of different types of urban wetlands in Zhuzhou City.

Value types	Riverine wetland / $10^3	Reservoir / $10^3	ponds / $10^3	Paddy fields /$10^3	Wastewater treatment plant / $10^3	Total value / $10^3
Atmospheric composition regulation	3,059.8	14,325	10,025.3	77,594.2	-	92,111.7
Climate regulation	37,660.9	10,564	38,574.8	337,922.8	207.8	424,930.4
Water storage adjustment	241,412.1	53,647.1	244,507.1	-	-	539,566.3
Water purification	6,334	1,776.7	6,487.7	-	-	14,598.3
Prevent soil erosion	357.7	100.4	366.6	16,087.2	-	16,911.8
Biological product	11,923.3	3,344.5	12,212.6	94,507.5	-	121,988
Water supply	108,968.6	24,215.3	-	-	-	133,183.9
Tourism recreation	104,726	52,363	17,454.3	-	-	174,543.3
Aesthetic heritage	8,243.5	1,831.9	-	-	-	10,075.3
Total value of wetland	522,685.8	149,275.2	329,628.3	526,111.7	207.8	1,527,908.9
Proportion of the total value/%	34.21	9.77	21.57	34.43	0.01	100
Unit value/$10^3/ ha	236.6	240.9	145.7	26.6	17	61.3

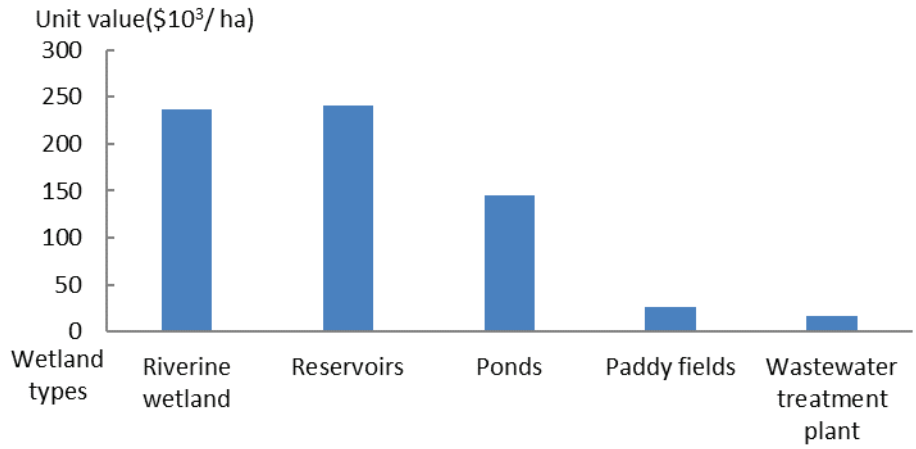

Fig. 4: Total value statistics of urban wetland types.

used to evaluate the results of science into city management decision-making system. For an important direction of urban wetland research and practical application, we need to further grasp the urban wetland ecosystem structure, process, function and service-related mechanism, clear the city spatial flow and transfer characteristic of wetland ecosystem services, clear the ultimate service directly linked with the beneficiaries, adopt more reasonable calculation, establish more scientific and comprehensive wetland ecological service evaluation system, make urban wetland ecosystem service research from the evaluation to the management practice.

Based on 2016, Zhuzhou wetland remote sensing image interpretation map, this paper establishes the urban wetland ecosystem service evaluation system according to the urban wetland classification in Zhuzhou City, combined with the field investigation and relevant basic data, and uses the economic value evaluation method to calculate urban wetland ecology system service value and comprehensive analysis of the evaluation results. The relevant conclusions are as follows:

(a) As of 2016, the total urban wetland area in Zhuzhou City is about 24,923ha, which is divided into five types: riverine wetland, reservoir, ponds, paddy fields, and wastewater treatment plants. The area of paddy fields is the largest, accounting for 19,820ha, accounting for 79.52% of the total urban wetland area. This indicates that as one of the main producing areas of rice in southern China, paddy fields is an important part of urban wetland in Zhuzhou City. It not only provides the city with material products but also plays an outstanding

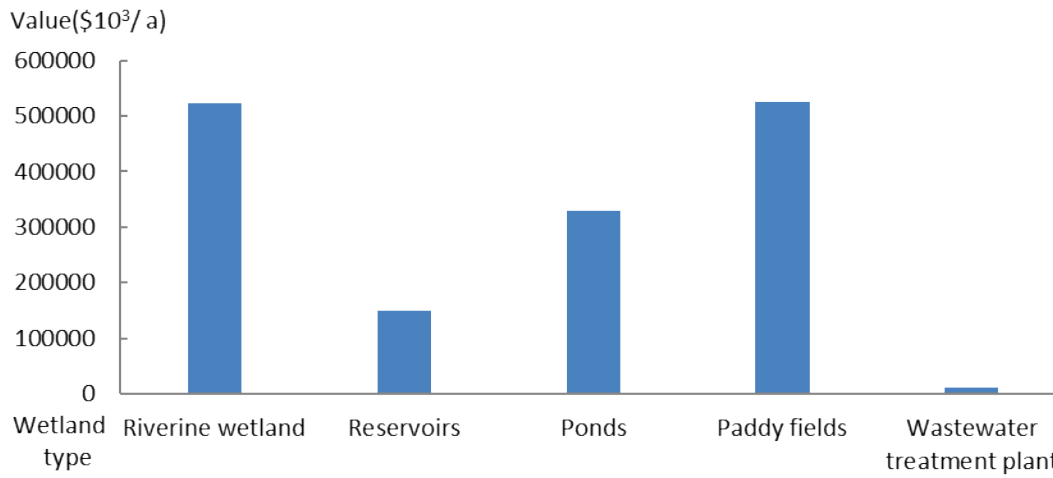

Fig. 5: Unit area value statistics of urban wetland types.

ecological service function. Therefore, it should continue to strengthen protection and management, and illegal occupation, ruin and destruction of paddy fields are strictly prohibited.

(b) In this paper, the urban wetland ecosystem service evaluation system in Zhuzhou City is constructed, and it is divided into ultimate service and intermediate service through deduplicate double counting. The ultimate service incorporates the total value calculation of wetland ecosystem services, while the intermediate services are excluded from the total value, which indirectly contributes to human well-being through the ultimate service. The evaluation index system provides an important direction for distinguishing the intermediate services (functions) and ultimate services of urban wetland ecosystems, and developing dynamic assessment and optimal management of urban wetland ecosystem ultimate services.

(c) In 2016, the total value of urban wetland ecosystem services in Zhuzhou City is about $166,333,305.72, of which the ultimate service value was about $166,333,305.72, the intermediate service value is about $173,326,054.2. The urban wetland unit area ecosystem service value is about $61,310.24/ha; The total value accounts for 8.63% of the total GDP of Zhuzhou City in the same year, which reveals the great contribution of wetland system services to urban development.

(d) The value of water storage regulation and climate regulation the largest among all ecological services of urban wetland in Zhuzhou City, which are about $539,566,265.1/a and $424,930,361.4/a, respectively. The sum of the two values accounts for 63.13% of the total value of urban wetland ecosystem services. This indicates that the urban wetland is the most important source of water vapour and climate regulators in Zhuzhou City, and water storage regulation and climate regulation are the core services provided by the wetlands to the city.

(e) Among all types of urban wetlands in Zhuzhou City, the value of paddy fields and riverine wetland is the highest, which is about $526,111,671.7/a and $522685813.3 /a, respectively. The sum of the two values accounts for 68.64% of the total value of urban wetland ecosystem services. Besides, the reservoir and the riverine wetland have the largest unit value, which is about $240,918.67/ha·a and $236,626.51/ha·a. This indicates that in the wetland conservation work of Zhuzhou City, riverine wetlands, especially the Xiangjiang River (the most important river in the region), should be the primary object, and the conservation of wetlands in reservoir wetland with large water areas should be strengthened, with the focus on guaranteeing their basic ecosystem service functions.

ACKNOWLEDGEMENTS

This research is funded by the Research Foundation of Education Bureau of Hunan Province, China (Grant No. 14B196, 18C1802, XJT2015(291)-186); Key Project of Science and Technology plan of Hunan Province, China (Grant No. 2018NK2052). This study is supported by Hunan Education Department's "12th five-year plan" Key Discipline Funding Project (2011-76); The state forestry administration's 13th five-year key discipline.

REFERENCES

Adamus, P.R., Clairain E.J. and Smith, R.D. 1987. Wetland Evaluation Technique (WET). Volume 2. Methodology. Operational draft. Final report, June 1984-September 1988 (No. PB-89-143028/XAB). Army Engineer Waterways Experiment Station, Vicksburg, MS (USA).

Brander, L.M., Florax, R.J. and Vermaat, J.E. 2006. The empirics of wetland valuation: A comprehensive summary and a meta-analysis of the literature. Environmental and Resource Economics, 33(2): 223-250.

Boyd, J. and Banzhaf, S. 2007. What are ecosystem services? The need for standardized environmental accounting units. Ecological Economics, 63(2): 616-626.

Boyd, J.W. 2007. The end point problem. Resources, 165: 26-28.

Chavas, J.P, Stoll, J. and Sellar, C. 1989. On the commodity value of travel time in recreational activities. Applied Economics, 21: 711~722.

Costanza, R. 2008. Ecosystem services: Multiple classification systems are needed. Biological Conservation, 141(2): 350-352.

Costanza, R., d'Arge, R., de Groot R. 1997. The value of the world's ecosystem services and natural capital. Nature, 387: 253-260.

Costanza, R., Groot, R.D. ,, Sutton, P., van der P.S. and Anderson, S.J. 2014. Changes in the global value of ecosystem services. Glob. Environ. Chang., 26: 152-158.

Daily, G.C. 1997. Nature's Services: Societal Dependence on Natural Ecosystems. Island Press.

De, G.R., Stuip, M., Finlayson, M. and Davidson. 2006. Valuing wetlands: Guidance for valuing the benefits derived from wetland ecosystem services. International Water Management Institute.

De, G.R., Brander L., van der P.S. and Sander. 2012. Global estimates of the value of ecosystems and their services in monetary units. Ecosystem Services, 1(1): 50-61.

De, Groot, R.S., Wilson, M.A. and Boumans, R.M. 2002. A typology for the classification, description and valuation of ecosystem functions, goods and services. Ecological Economics, 41(3): 393-408.

Dong, X.W., Zhang, J. and Zhang, J.H. 2011. Review on several issues of travel cost method in tourist resources valuation. journal of natural resources. Journal of Natural Resources, 26(11): 1983-1997.

Braat, L.C. and De Groot, R., 2012. The ecosystem services agenda: bridging the worlds of natural science and economics, conservation and development, and public and private policy. Ecosystem Services, 1(1): 4-15.

Farley, J., Costanza, R. 2010. Special Section: Payments for ecosystem services: From local to global. Ecol. Econ., 69: 2060-2068.

Fisher, B. and Kerry, T.R. 2008. Ecosystem services: classification for valuation. Biological Conservation, 141(5): 1167-1169.

Fisher, B., Turner, K., Zylstra, M. Brouwer, R. , Groot, R. D. and Farber, S. 2008. Ecosystem services and economic theory: Integration for policy-relevant research. Ecological Applications, 18(8): 2050-67.

Fisher, B., Turner, R.K. and Morling, P. 2009. Defining and classifying ecosystem services for decision making. Ecological Economics, 68(3): 643-653.

Han, B., Wang, X.K., Lu F., Duan X.N. and OuYany Z.Y.. 2008. Soil carbon sequestration and its potential by cropland ecosystems in China. Acta Ecologica Sinica., (02): 612-619.

Hawkins, K. 2003. Economic Valuation of Ecosystem Services. University of Minnesota, 23.

Hoekstra, A.Y. and Hung, P. 2002. Virtual water trade. A quantification of virtual water flows between nations in relation to international crop trade. Value of Water Research Report Series, 11: 166.

Jiang, B., Zhang L. and Ouyang, Z.Y. 2015. Ecosystem services valuation of Qinghai Lake. The Journal of Applied Ecology, 26(10): 3137-3144.

Jin, X.C., Jiang, X., Xu, Y.H. and Wang, Q. 2006. Seasonal variation of dissolved nitrogen and phosphorus in sediments in northeast part of Lake Taihu. China Environmental Science, 26(4): 409-413.

Johnston, R.J. and Russell, M. 2011. An operational structure for clarity in ecosystem service values. Ecological Economics, 70: 2243-2249.

Keeler, B.L., Polasky, S., Brauman, K.A., Johnson, K.A. and Finlay, J.C. 2012. Linking water quality and well-being for improved assessment and valuation of ecosystem services. Proceedings of the National Academy of Sciences of the United States of America, 109: 18619-18624.

Li, C.J., Lu, H.B., Xu J.H. and Wang, Z.C**.** 2000. Problem on calculation of soil and water conservation benefit. Bulletin of Soil and Water Conservation, 3: 29-30.

Li, C.Y., Hua, D.Z., Ren, J. and Li, M.L**.** 2006. The benefit value estimate of anti-erosion of the urban wetland soil of Songbei District of Harbin. Research of Environmental Sciences, 6: 135-138.

Li, J.N. 2006. Studies on the Ecosystem Services of Xixi Wetland, Hangzhou. Chongqing Southwest University, 8: 32-35.

Mei, X.Y. and Zhang, X.F. 2007. Carbon storage and carbon fixation during the succession of natural vegetation in wetland ecosystem on east beach of Chongming Island. Chinese Journal of Applied Ecology, (04): 933-936.

Musamba, E.B., Boon, E.K., Ngaga, Y.M. and Dumulinyi**.** 2012. The recreational value of wetlands: Activities, socio-economic activities and consumers' surplus around Lake Victoria in Musona municipality, Tanzania. Journal of Human Ecology, 37(2): 85-92.

Millennium Ecosystem Assessment (MA) 2005. Ecosystems and Human Well-Being: Wetlands and Water Synthesis. Washington, DC: Island Press.

Nahlik, A.M., Kentula, M.E., Fennessy M.S. and Landers, D. H**.** 2012. Where is the consensus? A proposed foundation for moving ecosystem service concepts into practice. Ecological Economics, 77: 27-35.

Nelson, E., Mendoza, G., Regetz, J.**,** Polasky, J., Chan, K.M.A. and Daily, G.C. 2009. Modeling multiple ecosystem services, biodiversity conservation, commodity production, and trade-offs at landscape scales. Frontiers in Ecology and the Environment, 7(1): 4-11.

Odum, H.T. and Nilsson, P. 1996. Environmental Accounting. Energy and Environmental Decision Making. Wiley New York.

Ringold, P.L., Boyd, J., Landers, D**.** 2013. What data should we collect? A framework for identifying indicators of ecosystem contributions to human well-being. Frontiers in Ecology and the Environment, 11: 98-105.

Shangguan, J.X., Wang, M.X., Shen, R.X., Wang, Y.S., R Wassmann and H.Rennenberg. 1994. The feature of methane emission from a paddy field in the Central China Region. Scientia Atmospherica Sinica, 3: 358-365.

Song, C.C. 2004. Advance in the studies on methane emission from wetlands. Ecology and Environment, (1): 69-73.

Song, H.T., Cui, L.J., Luan, J.W., Duan X.N. and OuYany Z.Y**.** 2011. Wetland function and potential in carbon sequestration. World Forestry Research, 24(06): 6-11.

Sun, B., Lei, Y., Cui, L. Wei, L., Xiaoming, K. and Manyin, Z. 2018. Addressing the modelling precision in evaluating the ecosystem services of coastal wetlands. Sustainability, 10: 1136.

Turner, R.K., Morse, J.S. and Fisher, B. 2010. Ecosystem valuation: A sequential decision support system and quality assessment issues. Annals of the New York Academy of Sciences, 1185: 79-101.

The Economics of Ecosystems and Biodiversity (TEEB) 2010. The Economics of Ecosystems and Biodiversity: Ecological and Economic Foundations. Earthscan, London.

United States Environmental Protection Agency (USEPA) 2009. Valuing the Protection of Ecological Systems and Services. Washington DC: US EPA.

Wallace, K.J. 2007. Classification of ecosystem services: Problems and solutions. Biological Conservation, 139(3): 235-246.

Wang, J.H. and Lv, X.G. 2007. Urban wetland: Its concept, ecological services and protection. Chinese Journal of Ecology, 4: 555-560.

Wong, C.P., Jiang, B., Kinzig, A.P., Lee Kai N and OuYany Z.Y**.** 2015. Linking ecosystem characteristics to final ecosystem services for public policy. Ecology Letters, 18: 108-118.

Woodward, R.T. and Wui, Y.S. 2001. The economic value of wetland services: A meta-analysis. Ecological Economics, 37(2): 257-270.

Wu, H.J., Dan, X.Q., Liu, S.H., Huang, Y. and Shu, Y**.** 2016. Preliminary evaluation of wetland ecosystem services in Hunan province. Wetland Science, 14(06): 781-787.

Wu, T.F., De, X.W., Huang, W.K., Li, C,, Kang, W.X. and Cui, F**.** 2015. Evaluation of forest ecosystem service value in Nan County. Journal of Central South University of Forestry & Technology, 35(10): 109-115.

Xie, G.D., Zhang, C.X., Zhang, C.S., Xiao, Y. and Lu, C.X**.** 2015. The value of ecosystem services in China. Resources Science, 37(09): 1740-1746.

Zhao, M. and He, Z. 2018. Evaluation of the effects of land cover change on ecosystem service values in the upper reaches of the Heihe River Basin, Northwestern China. Sustainability, 10: 4700.

Zhou, B. 2011. Study on the Evaluation Method of the Ecological Service Value of Wild Duck Lake Wetland. Capital Normal University.

Zhuang, D.C. 2006. Evaluation of the no use values of the wetland resources in Dongting Lake Based on CVM. Areal Research and Development, 2: 105-110.

Nature Environment and Pollution Technology
An International Quarterly Scientific Journal

p-ISSN: 0972-6268
(Print copies up to 2016)
e-ISSN: 2395-3454

Vol. 19 | No. 2 | pp. 469-479 | 2020

Original Research Paper

https://doi.org/10.46488/NEPT.2020.v19i02.004

Open Access Journal

CH_4 Emission Flux Model in Rice Growing Season in Cold Region Under Water Saving Irrigation Mode

Lihong Yu and Mengxue Wang†
Department of Agronomy, Heilongjiang Bayi Agricultural University, Daqing, China
†Corresponding author: Mengxue Wang; wangmengxue1978@126.com

Nat. Env. & Poll. Tech.
Website: www.neptjournal.com

Received: 15-07-2019
Accepted: 06-10-2019

Key Words:
Rice paddies;
Methane emission;
Water management;
Empirical models

ABSTRACT

Rice paddies have been identified as major methane (CH_4) source induced by human activities. Water management is an important factor affecting CH_4 emission during the rice growing season, and the water depth in a rice field directly affects the production, oxidation, and transfer. Field experiments on irrigation management are generally conducted under three modes: control irrigation, intermittent irrigation, and long-term flood irrigation. Static opaque chamber gas chromatographic method was adopted in this work for *in situ* observations of CH_4 emission flux in a field in the rice growing season in a cold region of China. Test data from 2016 was adopted to establish the single factor and interaction types of the CH_4 emission flux estimation model for the rice growing season under different water management methods, and the data from 2017 was used for model inspection. The estimation models were based on NO_3-N in soil and soil temperature, 10 cm under the soil surface. All models passed the significance test for significance levels of $P<0.01$. The average forecast error of the model is 13.53-24.78%, and the coefficient of determination R_{adj}^2 is between 0.399-0.675. The calculated values of the model are consistent with the measured values. The model established in this research can be used for estimation of CH_4 emission in the rice growing season in cold regions of China for different water-saving irrigation modes.

INTRODUCTION

Methane (CH_4) is one of the most important greenhouse gases (Sass et al. 2000, Exnerová & Cienciala 2009, Liu et al. 2017) and is the second leading cause of global warming (Zhao et al. 2013). Approximately 50% of the CH_4 in the atmosphere comes from agricultural production, and 20-40% of this total comes from rice production (Scheehle & Kruger 2006). Water management is an important factor affecting CH_4 emission during the rice growing season (Xiong et al. 2007, Hadi et al. 2010, Zschornack et al. 2016), and the water depth in a rice field directly affects the production, oxidation, and transfer rate of CH_4 (Zou et al. 2003). Continuous flooding of the paddy field during the growing season will result in increased CH_4 emissions, while the amount of CH_4 produced will decline when the soil is dry (Towprayoon et al. 2005). Numerous studies have shown that CH_4 emissions from intermittent irrigation and control irrigation are significantly lower than that from long-term flood irrigation (Adhya et al. 2000, Jain et al. 2000, Minamikawa & Sakai 2005), and the rule of seasonal CH_4 emission also differs (Kreye et al. 2007).

The paddy planting area in Heilongjiang province is approximately 6000 hm^2, and it is the largest rice production area in China (Wang & Zhang 2015). It is also an important emission source of CH_4 in China. In recent years, the rice cultivation in Heilongjiang has gradually changed from traditional water storage for flood irrigation to control irrigation and intermittent irrigation modes. Zhu (2012) indicates that water-saving irrigation mode in the rice cultivation area in a cold region affects the seasonal emission flux and accumulative emission flux of CH_4 produced by the rice field, which can effectively reduce the greenhouse effect of CH_4. Therefore, it is of great importance to accurately estimate CH_4 emissions under different irrigation modes.

The most widely used model for estimating CH_4 emissions is CH_4MOD developed by Huang et al. (1998) and DNDC model developed by Li (2001). Many scholars use these two models to estimate and improve their models, and good results have been achieved thus far (Jagadeesh Babu et al. 2006, Xie et al. 2010, Minamikawa et al. 2014, Chun et al. 2016).

The previously researched estimation for rice CH_4 emission may not sufficiently reflect the actual status under multiple water management modes in the cold region of Heilongjiang in northeast China. This research is based on the statistical analysis for field determination of rice CH_4 emission flux in a cold region in China. Multiple empirical models are adopted for analysis, simulation, and verification; single-factor and two-factor interaction empirical models of

environmental factors are established to estimate seasonal rice CH_4 emission flux. The least squares method is adopted for the estimation of parameters and model inspection is performed. The established model can be used for estimation of rice CH_4 emission for different water management modes in rice cultivation areas in cold regions in Heilongjiang and can provide the theoretical basis for establishing emission reduction measures for greenhouse gases.

MATERIALS AND METHODS

General Situation of the Study Area

Rice cultivation experiments were carried out in 2016 and 2017 at the Rice Irrigation Test Station of Heilongjiang (45°63'N, 125°44'E), Qing'an county, Heping town, China. The average annual precipitation here was 500-600 mm, and the annual average temperature was 2-3°C. The hydrothermal growth period of the crops is 156-171 days, and the annual frost-free period is 128 days. The soil belonged to the Lidetun series (loam, mixed, and Albic rice soil), and the pH before the study was neutral (Table 1).

Test Design

To evaluate the effect of different irrigation modes on CH_4 emissions during rice cultivation, three main treatments with different irrigation systems (control irrigation C1, intermittent irrigation C2, and long-term flood irrigation C3) were applied. There were four nitrogenous fertilizer application levels: high (N1) 130 kg/hm^2, medium (N2) 110 kg/hm^2, low (N3) 80 kg/hm^2, and no nitrogenous fertilizer application (N4). A total of 12 treatments (C1N1, C1N2, C1N3, C1N4, C2N1, C2N2, C2N3, C2N4, C3N1, C3N2, C3N3, and C3N4) and three repetitions were adopted for the test.

For long-term flood irrigation, the surface water depth is large; the air temperature in spring in Heilongjiang is low, so flooded soil is favourable to resume growth after rice transplanting. Therefore, large water depths were maintained during the seeding establishment. To reduce ineffective tillering of rice, drainage was performed during the later tillering period. Water levels were not established in the field under control irrigation mode, and the irrigation methods were mainly used to adjust the moisture content of the soil. Under intermittent irrigation mode, the irrigation water is fed to the field in several instalments, and there is no obvious water level in the field. Table 2 summarizes the moisture design for the soil under the different treatment methods.

Test Management

A total of 36 areas were selected for testing, and each area was 100 m^2; the four sides of the areas were protected. To reduce lateral permeation, plastic plates were buried (40 cm underground) along the four sides of each of the areas. Water meters and water gauges were installed for each area to control the irrigation water amount and water depth. Fixed gas sampling points were set in the middle of each area with side dimensions of 4 m and were used for placement of static chambers for CH_4 artificial sampling.

The rice variety used for testing was #5 KENJIAN RICE. Seeding was performed on 15th April 2016, and the planting density was 25 cm, 12 cm and 34 caves/m^2. The rice variety, sprout cultivation, transplant, crop protection, technical measures for pesticide use, and field management conditions were the same for all the areas. Base fertilizer was applied on May 3, the transplant was performed on May 20, striking root fertilizer was applied on May 28, tillering fertilizer was applied on June 15, fertilization for head sprouting was performed on July 9, and rice was harvested on September 20. The rice growth stage is 126 days, period of the seedling establishment was from May 20-May 29, tillering stage was from May 30-July 7, jointing and booting stage was from

Table 1: Chemical properties of the initial soil.

Soil	Values
pH	6.4
Volume- weight (g/cm^3)	1.01
Porosity (%)	61.80
Organic matter (g/kg)	41.4
TN (total nitrogen) (g/kg)	1.08
TP (total phosphorus) (g/kg)	15.23
TK (total potassium) (g/kg)	20.11
Available nitrogen (mg/kg)	154.36
Available phosphorus (mg/kg)	25.33
Available potassium (mg/kg)	25.33

Table 2: Water management mode for different irrigation management methods.

Treatment	Seeding Establishment	Early tillering	Filled tillering	Later tillering	Jointing and booting	Bloom	Grouting	Yellow ripe
Control irrigation	0–30	0.7 θs	0.7 θs	Drainage	0.8 θs	0.8 θs	0.7 θs	Dry set
Intermittent irrigation	0–30	0–40	0–40	Drainage	0–30	0–40	0–40	Dry set
Long-term flood irrigation	0–30	0–40	0–40	Drainage	0–40	0–40	0–40	Dry set

Note: θs is the saturated moisture content of root layer soil. The data before "–" represents the lower limit for moisture control, and the data after "–" represents the upper limit for moisture control. The units of surface water depth: mm.

July 8-July 21, bloom stage was from July 22-August 1, grouting stage was from August 2-August 24, and the yellow ripe stage was from August 25-September 10.

Sample Collection

Field CH_4 samples were collected during the seven stages of main growth (steeping field, tillering, drainage, jointing and booting, bloom, grouting, and yellow ripe) of rice from May to September every year. Besides, samples were obtained for each typical stage, namely, before fertilization, after fertilization, after rain, drainage, high temperature, and high exhaust capacity. The gas samples were collected 19 times during the whole growing period, and 3 samples were collected each time.

Static chamber method was adopted for gas sampling. The static chamber (Harbin Jingwei Glass Machining Co., Ltd.) comprises of 5 mm thick transparent organic glass; the outside of the chamber was sealed by tinfoil for thermal insulation. The chamber height was 60 cm in the rice growth prophase and increased to 110 cm in the late growth stage. Mini fan and digital thermometer probe were installed at the top of the chamber to calibrate the gas mass calculation error caused by temperature rise in the chamber during the sampling process. Gas sampling tube was connected to the side of the chamber and inserted 25 cm inside the chamber. Three-way valves were connected at the end of the gas sampling tube and were connected to the gas sampling bag and injector (60 mL). The collection was performed for durations of 0, 10, 20, and 30 min under each treatment condition; two continuous samplings were performed for each gas sample, and these samples were transferred into the gas sampling bag (120 mL) (Wang & Zhang 2015).

Earth boring auger was used to obtain 0-20 cm fresh soil samples, which were packed into foam insulation boxes together with ice bags to preserve freshness until they were brought to the laboratory for refrigerated storage. The content of nitrate-nitrogen in soil and ammonium nitrogen were determined. When sampling, the water depth and soil temperature of each area at a depth of 10 cm were synchronously determined. The meteorological data were automatically recorded by the DZZ2 automatic meteorological station (Tianjin Meteorological Instrument Factory) of the test station (Fig. 1).

Sample Test

The gas concentration was determined by gas chromatog-

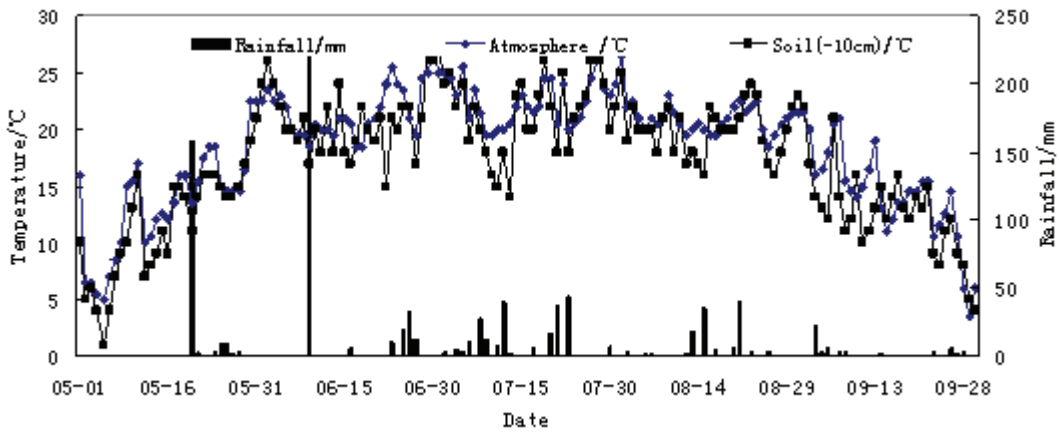

Fig. 1: Changes in atmospheric and soil temperatures and rainfall during rice cultivation in 2016.

raphy GC-17A (Shimadzu) and flame ionization detector (FID); the detection temperature was 300°C, column temperature was 65°C, carrier gas was high purity N_2, and the flow rate was 40 mL/min. The standard gas samples were provided by the National Standard Substance Center.

The colourimetric method was adopted for the determination of nitrate-nitrogen content in the soil. Synchronously, the correspondingly treated soil sample was weighed and dried at 105°C until a constant weight was obtained; the soil moisture content was then determined, to make it convenient for conversion into dry soil mass.

Calculation Method and Data Analysis

Rice CH_4 emission flux is calculated by the following formula (Xiang et al. 2006).

$$F = \rho h \cdot \frac{dc}{dt} \cdot \frac{273}{273+t} \cdot \frac{p}{p_0} \quad \ldots(1)$$

In the formula, F is CH_4 emission flux, $\mu g/(m^2 h)$; ρ is CH_4 density under standard conditions, 0.714 kg/m^3 (Ma et al. 2012); h is the effective height of the chamber (when there is water in the field, it is the height from the water surface to chamber top; when there is no water, it is the chamber height) (0.6 m; 1.1 m). $\frac{dc}{dt}$ is the change rate of CH_4 concentration in the chamber, $\mu L/(m^3 \cdot h)$, t is the average temperature, °C in the sampling chamber, p is pressure in the chamber, Pa; and p_0 is the standard atmospheric pressure, Pa. The area was a plain area, so the atmospheric pressure had a small impact; p was thus deemed to be equal to the standard atmospheric pressure. The gas emission flux was calculated based on the gas sample concentration-time relation curve.

Excel 2003 software was used for conventional graph processing; SPSS 17.0 software was used for statistical analysis to fit the single factor and two-factor interaction models. The significance level was p=0.05, and the extreme significant level was p=0.01. Standards used for model selection were as follows: (1) model–model fitting parameter probability is extremely significant or significantly correlative ($p<0.01$ or $p<0.05$); (2) residual sum of squares (RSS) of the model is small, and F value is large; (3) the coefficient of determination (R_{adj}^2) of the model is relatively high. Two types of models were established in this work to simulate the rice soil CH_4 emission flux in cold regions. The first type was a single factor model based on NO_3-N content in soil and single-factor model based on soil temperature at -10 cm; the other type was an interaction model based on the synergistic effect of the two factors: NO_3-N content in the soil and soil temperature at -10 cm (Table 3). The data for establishing the model was sourced from the test data of 2016, and the data for testing the model was sourced from the test data of 2017.

RESULTS

Data Analysis of CH_4 Emission

In different irrigation modes, the season change of the rice field CH_4 emission ranges from 0.14 $\mu g/(m^2 \cdot h)$ to 53.77 $\mu g/(m^2 h)$. For the whole growing period of rice, the peaks of the CH_4 emission in different irrigation modes all occur at two stages of tillering and field drying: jointing and booting, and the emission is relatively low in the early growth resuming stage to early tillering stage and yellow ripe (Fig. 2).

Establishment of the Model

Single-factor model for CH_4 emission flux based on soil temperature: Temperature is the important environmental factor affecting CH_4 emission of paddy fields; the change of soil temperature causes changes in the activity of methane-producing microorganisms and microorganism causing CH_4 oxidation, the biochemical reaction rate also changes, which affects CH_4 emission. Previous research indicates that temperature has an obvious impact on CH_4 emission (Qin et al. 2006), and points out during a study on double cropping rice in the south area that there is exponential function relation between CH_4 emission flux and the average temperature of 10 cm soil layer. In this research, fitting is performed for the relation between CH_4 emission flux and temperature of the 10 cm deep soil layer by using linear model, logarithmic model, exponential model, and cubic model (Table 4). For the three irrigation modes, the degree of fitting R_{adj}^2 of the three models has a big difference; the adjusted correlation coefficient R_{adj}^2 is between 0.135-0.613. All models passed

Table 3: CH_4 emission flux model based on single and double predictors.

Single predictor	Double predictor
$f=aN^3+bN^2+cN+d$	$f= a N^3+b T^3+c N^2+ dT^2+eN+f T+g$
$f=a\ EXP(b\ N)$	$f=EXP(a+b*N/T)$
$f=aT^3+bT^2+cT+d$	

Note: f, CH_4 emission flux in $\mu g/m^2/h$; N, content of nitrate nitrogen in soil in mg/kg; T,soil temperature at -10 cm in °C; *a, b, c, d, e, f, g:* parameters of the model.

the significance test, and the extremely significant level was reached (P<0.01). Comprehensively considering the parameters of the model, RSS, F value, R_{adj}^2, and significance, the optimal model of all the three irrigation modes was the cubic model; the adjusted correlation coefficient of control irrigation is the largest (R_{adj}^2=0.613), intermittent irrigation is next (R_{adj}^2=0.488), and long-term flood irrigation is the least (R_{adj}^2=0.387).

Single-factor model for CH_4 emission flux based on the content of nitrate-nitrogen in soil: Under the circumstance that soil temperature is not considered, linear model, logarithmic model, exponential model, exponential function model and cubic model are used to simulate the relation between the content of NO_3-N in soil and CH_4 emission flux of paddy field (Tables 5 and 6). The adjusted correlation coefficient R_{adj}^2 of a fitting model of the three irrigation modes is 0.219-0.534, and the correlation reaches the extremely significant level (P<0.01). The parameter sensitivity of power function model of the cultivation mode of long-term flood irrigation reaches the extremely significant level; RSS is the smallest, and F value is the largest, so the optimal model of long-term flood irrigation is the power function model (R_{adj}^2=0.534). Comprehensively considering the parameter sensitivity, RSS, F value, and R_{adj}^2, the optimal model of control irrigation and intermittent irrigation are confirmed as the cubic model (R_{adj}^2=0.467). Through comparison for the optimal model of the three irrigation modes, the probability value of correlation index of long-term flood irrigation is the highest, and it is a little better than that of control irrigation and intermittent irrigation (Tables 5, 6).

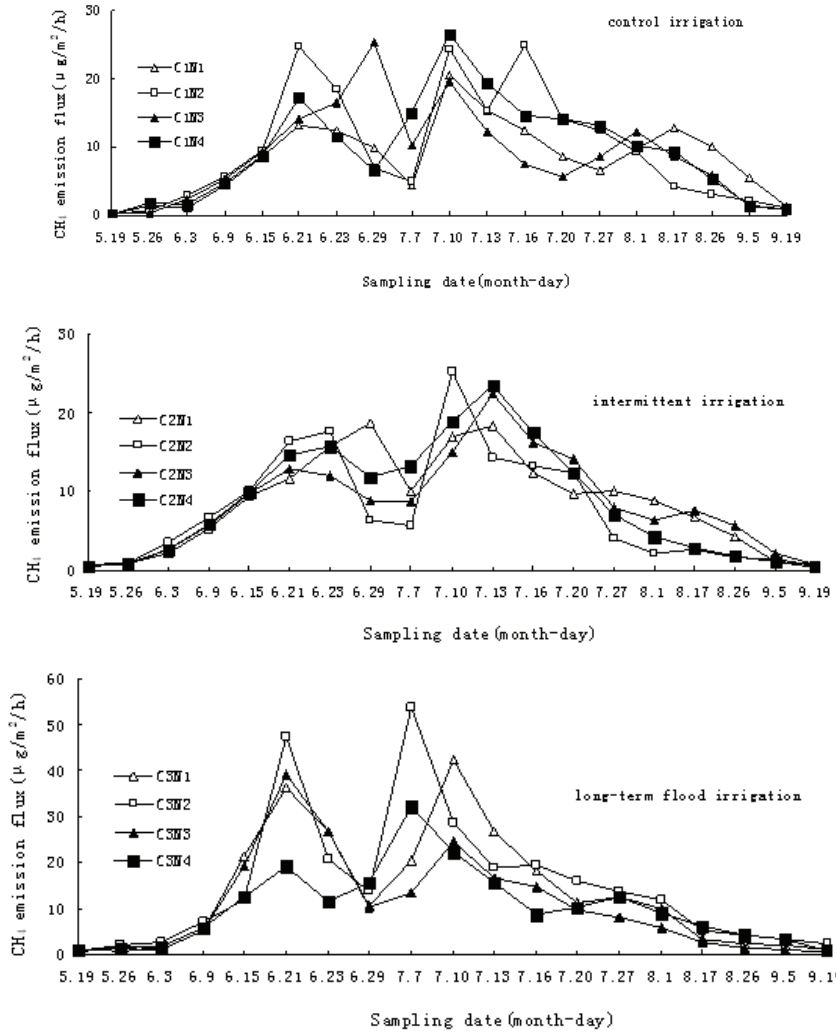

Fig. 2: Seasonal variations of CH_4 emission from rice field for three irrigation models.

The interaction model for CH_4 emission flux based on soil temperature and content of nitrate nitrogen: The proposed model was adopted to fit the relation between soil temperature, the content of nitrate nitrogen, and CH_4 emission flux. The result shows that the degree of fitting of interaction (R_{adj}^2) is higher than that of the single-factor model (Tables 7 and 8). Compared with single-factor models, two-factor models can predict CH_4 emission better; the coefficient of determination R_{adj}^2 is between 0.340-0.715. Soil fertilizer and temperature have a significant impact on CH_4 emission, and all models reach the extremely significant level (P<0.01). Through comprehensive consideration, the optimal model for control irrigation is $f=EXP(a+b\cdot N/T)$, and the explanatory power is 71.5%; the optimal model of intermittent irrigation is $f = aN^3+bT^3+c N^2+ dT^2+eN+fT+g$, and the explanatory power is 53.6%, and the optimal model of long-term flood irrigation is $f =EXP(a+b\cdot N/T)$, and the explanatory power is 57.6%. The degree of fitting of control irrigation is the highest.

Inspection of Model

The experimental data in 2017 was adopted for inspection of the single factor and interaction optimal model of the three irrigation modes (Table 9). Mean prediction error (MPE) and adjusted correlation coefficient R_{adj}^2 are adopted for inspection of prediction accuracy of the model. All models passed the significance inspection and reached an extremely significant level (P<0.01). The mean prediction error of the model is 13.53-24.78%, and the adjusted correlation coefficient R_{adj}^2 is 0.399-0.675. The result shows that the calculated value of the model and measured values are consistent, and the model has good applicability.

$$MPE = \frac{100}{n}\sum_{i=1}^{n}\frac{\left|Y_{iMeasured} - Y_{iCalculated}\right|}{Y_{iMeasured}}$$

DISCUSSION

CH_4 Emission Model Based on Content of Nitrate Nitrogen in Soil and Temperature

In rice cultivation area in the cold region of Heilongjiang, the single factor optimal model for the three irrigation models for CH_4 emission flux based on soil temperature is the cubic model; the optimal model of control irrigation is f=0.152T^3-7.886T^2+132.251T-682.337 (R_{adj}^2=0.613), intermittent irrigation is f=0.035T^3-1.559T^2+22.363T-86.908 (R_{adj}^2=0.488), and long-term flood irrigation is f =0.169T^3-9.345T^2+167.281T-921.248 (R_{adj}^2=0.387). For the single-factor model of CH_4 emission flux based on the content of nitrate nitrogen in the soil, the optimal model of control irrigation and intermittent irrigation is the cubic model: f=1.904N^3-14.267N^2+14.598N+63.470 (R_{adj}^2=0.467) and f=-1.301N^3+15.907N^2-62.968N+101.461 (R_{adj}^2=0.467). The optimal model of long-term flood irrigation is the exponential model: f=363.903 EXP(-0.981 N) (R_{adj}^2=0.534). For interaction model of CH_4 emission flux based on soil temperature and content of nitrate nitrogen in the soil, the optimal model

Table 4: Parameters of soil temperature (-10 cm) based CH_4 emission flux models.

Treatment	Model	Parameter				RSS Parameter	F	R_{adj}^2	Sig
		a	*b*	*c*	*d*				
Control irrigation	f= aT+b	3.047***	-28.504ns			14846.101	10.322	0.257	***
	f=aLn(T)+b	47.819***	-108.947**			15417.700	8.975	0.228	***
	f=aT b	0.001 ns	3.527***			24.807	15.236	0.521	***
	f=aT 3+bT2+cT+d	0.152***	-7.886***	132.251***	-682.337***	140.532	30.339	0.613	***
Intermittent irrigation	f= aT +b	2.790***	-24.759ns			12714.429	14.237	0.329	***
	f=aLn(T+b)	36.923***	-77.521**			14137.505	10.187	0.254	***
	f=aT b	0.019 ns	2.274***			36.807	9.575	0.3393	***
	f=aT3+bT2+cT+d	0.035***	-1.559**	22.363**	-86.908 ns	156.606	14.841	0.488	***
Long-term flood irrigation	f= aT +b	3.403**	-27.336 ns			29828.600	5.789	0.151	***
	f=aLn(T)+b	57.294**	-128.828ns			30368.942	5.223	0.135	***
	f=aT b	0.001***	3.257 ns			36.975	6.688	0.323	***
	f=aT3+bT2+cT+d	0.169***	-9.345***	167.281***	-921.248***	163.841	13.863	0.387	***

Note: Significance: ns, not significant; **, the model or the parameters was significant; ***, the model or the parameters was extreme significant; the same as below.

of control irrigation and long-term flood irrigation is the exponential model: $f=EXP(4.762\text{-}9.302N/T)(R_{adj}^2=0.715)$ and $f=EXP(4.739\text{-}10.564N/T)$ ($R_{adj}^2=0.576$), and the optimal model of intermittent irrigation is cubic model $f=0.189N^3+0.017T^3\text{-}0.693N^2\text{-}0.661N\text{-}7.572T\text{-}0.216$ ($R_{adj}^2=0.536$).

Impact of Water-saving Irrigation Mode on CH_4 Emission

Water management mode in the rice-growing season has an obvious impact on CH_4 emission. During the growth period of rice, the water depth in different growing stages is different, so water management for paddy field affects the seasonal change of CH_4 emission to a large degree. Using the interaction model to predict the seasonal emission of CH_4, the numbers are as follows: control irrigation 257.25 $kg{\cdot}hm^{-2}$; intermittent irrigation 235.25 $kg{\cdot}hm^{-2}$; and long-term flood irrigation 343.75 $kg{\cdot}hm^{-2}$. The total amount of seasonal methane emissions from controlled irrigation and intermittent irrigation respectively decrease by 25.16% and 31.56% compared with that from long-term flooding irrigation. CH_4 emission of paddy field subject to water-saving irrigation mode is lower than that of paddy field subject to long-term flood irrigation.

When Adhya et al. (2000) and Jain et al. (2009) studied CH_4 emissions from paddy fields in India, they found that CH_4 emissions from intermittently irrigated paddy fields decrease by 15% and 22%, respectively, compared with that from continuously flooded paddy fields. Minamikawa & Sakai (2005) found from field experiments that the CH_4 emissions from mid-season drained field and midseason drained-intermittently irrigated paddy fields are 64% and 26% of the CH_4 emissions from flooded paddy fields. From the field experiments, Jiao et al. (2006) found that CH_4 emissions from intermittently irrigated paddy fields decrease by 24.22% compared with that from flooded paddy fields. Towprayoon et al. (2005) found that moisture deficit during rice growth can significantly reduce CH_4 emissions from paddy fields, with the mid-season drainage and the multiple drainages in the course, and the CH_4 emissions from continuously flooded paddy fields respectively reduce by 27% and 35%. Thus, the method of water management has a significant impact on seasonal CH_4 emissions.

The research of Yuan (Yuan et al. 2008) for CH_4 emission effect of paddy field in southern China showed that CH_4 emission of paddy field subject to intermittent irrigation is 46.23% lower than that of paddy field subject to long-term flood irrigation. Peng et al. (2013) obtained the following conclusion according to 5 years' of *in situ* field observation data for paddy areas in southeast China: CH_4 emission of paddy field subject to control irrigation is 83.5% lower than that of paddy field subject to long-term flood irrigation, and the difference reaches the extremely significant level.

Some researchers show that CH_4 emission peak value of paddy field subject to intermittent irrigation mainly occurs in the early stage and middle stage of rice tillering (Yuan et al. 2008), and CH_4 emission peak value of paddy field subject to control irrigation mainly occurs in seeding establishment period-middle stage of tillering (Peng et al. 2013). CH_4 emission peak value of paddy field subject to long-term flood irrigation is relatively lagging. It was found during the research that three emission peak values occur in the tillering stage, jointing and booting stage and bloom stage, and there

Table 5: Parameters of nitrate nitrogen-based CH_4 emission flux models.

Treatment	Model	Parameter			
		a	*b*	*c*	*d*
Control irrigation	f= aN +b	-8.328^{***}	63.605^{***}		
	f=aLn(N)+b	-17.599^{***}	51.754^{**}		
	f=a EXP(b · N)	75.519^{ns}	-3.94^{***}		
	$f=aN^3+bN^2+cN+d$	1.904^{***}	-14.267^{**}	14.598^{**}	63.470^{***}
Intermittent irrigation	f= aN +b	-8.631^{***}	60.931^{**}		
	f=aLn(N)+b	-21.560^{***}	52.308^{**}		
	f=a EXP(b · N)	77.829^{ns}	-0.468^{***}		
	$f=aN^3+bN^2+cN+d$	-1.301^{**}	15.907^{**}	-62.968^{***}	101.461^{***}
Long-term flood irrigation	f= aN +b	-21.233^{***}	104.040^{***}		
	f=aLn(N)+b	-58.376^{***}	100.279^{***}		
	f=a EXP(b N)	363.903^{***}	-0.981^{***}		
	$f=aN^3+bN^2+cN+d$	-2.006^{ns}	21.435^{ns}	-91.560^{ns}	172.668^{ns}

are differences in the change amplitudes of the peak values.

CH_4 formation by paddy field soil includes three processes: generation, oxidation, and emission. CH_4 is produced in an anaerobic environment by methanogens in the soil; most CH_4 is oxidized by methane-oxidizing bacteria, and the remaining CH_4 is emitted into the atmosphere (Lv et al. 2005). Water management influences the generation, oxidation, and emission of CH_4. Methane bacteria are anaerobes; water flooding will cause the reduction of the redox potential of soil; this creates a good soil environment for the generation process of CH_4, finally causing the increase in CH_4 emission. Long-term flood irrigation mode is favourable for the generation and emission of CH_4. Methane-oxidizing bacteria are aerobes; alternation of wetting and drying or soil drying is favourable to gas exchange for increasing the activity, which largely improves the oxidation rate of CH_4 and inhibits the activity of methanogens, reducing the production and emission of CH_4. Therefore, water-saving irrigation mode is significant for relieving the greenhouse effect.

Since the last century, water management practices for rice production in Heilongjiang have begun to change. Before the 1950s, paddy fields were dominated by long-term flooding. Since the 1980s, mid-term soil drying has been widely used as the agricultural management measure to reduce ineffective tillers and improve seed setting rate. With the continuous increase of global greenhouse effects, the reduction of CH_4 emission in paddy fields needs to be solved urgently. In recent years, paddy fields in Heilongjiang have gradually changed from traditional water-filled irrigation to water-saving irrigation modes such as control irrigation and intermittent irrigation (Wang & Zhang 2015). Compared with long-term flooding irrigation, water-saving irrigation technology not only solves the problem of water shortage but also contributes to methane emission control in the paddy field for a win-win strategy.

Uncertainty of Model Simulation

Besides water management, CH_4 emission in paddy planting area in the cold region is also affected by other environmental factors, such as physical and chemical properties of soil, fertilization measures, climatic conditions, variety difference, and cropping system. The rice area in the cold region in Heilongjiang is large; the soil types are diversified, and there are differences in soil pH, redox potential, the content of organic matter, texture, etc. All these will affect CH_4 emission of paddy fields. Some researches show that the heavier the soil, the lower is the CH_4 emission flux (Jiao et al. 2002), there is a negative correlation between the number of methane bacteria and content of clay particles in soils (Neue & Roger 1993). Soil pH mainly affects CH_4 emission from three aspects: decomposition of organic matters in soil, CH_4 production, and CH_4 oxidation (Qin et al. 2006). The research of Wei et al. (2012) indicates that the CH_4 emission increases with the reduction of soil pH; CH_4 emission of acid soil is higher than that of alkaline soil. The impact of soil type on CH_4 emission flux is not considered in this research, so uncertainty exists for the model fitting result.

Fertilization measure is the important factor affecting CH_4 emission of paddy field. In recent years, to protect the environment and realize the sustainable development of agriculture, the fertilization method for paddy field in the cold region in Heilongjiang is changing from traditional

Table 6: Testing results of CH_4 emission flux models based onnitrate content

Treatment	Model	RSS	F	R_{adj}^2	Sig
Control irrigation	f= aN +b	14796.018	10.445	0.259	***
	f=aLn(N)+b	14284.451	8.871	0.285	***
	f=a EXP(b N)	40.448	8.554	0.219	***
	$f=aN^3+bN^2+cN+d$	134.908	11.750	0.467	***
Intermittent irrigation	f= aN +b	12513.424	14.884	0.340	***
	f=aLn(N)+b	10454.825	8.884	0.448	***
	f=a EXP(b N)	36.733	14.923	0.340	***
	$f=aN^3+bN^2+cN+d$	123.399	22.934	0.467	***
Long-term flood irrigation	f= aN +b	21821.874	17.452	0.379	***
	f=aLn(N)+b	21573.832	17.952	0.386	***
	f=a EXP(b N)	25.419	31.985	0.534	***
	$f=aN^3+bN^2+cN+d$	357.328	5.661	0.341	***

application of chemical fertilizer to combined application of inorganic fertilizer, green manure, and animal manure; traditional fertilizer and controlled-release fertilizer are thus used together, and straw mulching is performed. The type, use amount, and application method of fertilizer will affect the emission rules and emission amount of CH_4 of paddy fields. Some researchers show that application of organic fertilizer and straw mulching increase CH_4 emission flux of paddy field (Zhao et al. 2014), and the higher the C/N, the larger is the CH_4 emission (Wu & Ye 1993). CH_4 is mainly generated under the action of methanogens; the applied organic fertilizer makes the nutrient substance of methane-producing microorganisms in soil increase, which causes an increase in CH_4 emission. In this research, only the impact of application amount of nitrogen fertilizer on CH_4 emission flux of paddy field is considered, and the impact of fertilization measure is not considered, which enhances the uncertainty of model fitting.

Heilongjiang province is an important commodity grain production base in China; the paddy planting area involves four accumulated temperature zones, and there are more than 100 varieties. The geographic position is varied, and the climate and the corresponding rice varieties are also different; all these cause the difference in CH_4 emission rules and emission amounts. The following conclusions are obtained by Wei et al. (2012) by the analysis on CH_4 emission data of paddy field (495 groups, 67 observation points): CH_4 emission of single cropping rice area decreases as the increase of latitude and longitude. There is a big difference in CH_4 emission for different rice varieties. More than 50% of unoxidized CH_4 is transferred into the atmosphere after root absorbing via leaves, and the size and activity of roots will affect its absorbing rate (Shao et al. 2011). The metabolic secretions of roots can enhance the activity of CH_4 oxidizing bacteria, which will promote CH_4 oxidation and inhibit its emission (Cao et al. 2000). CH_4 absorbing and inhibition of root system may have different expressions for different varieties, but it enhances the uncertainty for model estimation.

In addition, different test frequencies will also result in uncertainty in model estimation. Data are the basis for model establishment; theoretically, the data determination shall be performed multiple times, so that it is possible to detect the change characteristics of CH_4 emission with time. In this research, static chamber method is adopted to collect CH_4 samples in key growing stages of rice, and 20 repetitions of sample collection were performed in total during the whole growing stage; sampling shall be delayed if sampling cannot be performed due to special weather conditions. Compared with automatic sampling observation systems, some CH_4 emission peak values may be omitted by the static chamber method. Thus, there is still a large uncertainty for model fitting results in this research.

CONCLUSIONS

The interaction model has been designed in this study. Compared with a single factor model, the interaction model further improves the prediction ability. The water-saving irrigation mode changes the characteristics of CH_4 emission flux during the rice-growing season in the cold region; the seasonal CH_4 emission flux models are different under the three irrigation modes. Even if the model structure is the same, the parameters are different. The verification result for the data in 2017 shows that the average forecast error of the interaction model is 13.53%-24.78%; the adjusting correlation coefficient R_{adj}^2 is 0.399-0.675. The calculated value of the model and the measured value show good agreement, thus verifying the applicability of the model.

Table 7: Parameters of CH_4 emission flux models based on soil temperature (-10 cm) and nitrate nitrogen.

Treatment	Model	Parameter						
		a	b	C	d	e	f	g
Control irrigation	$f= a N^3+b T^3+c N^2+ eN+f T+g$	3.070^{***}	0.010^{***}	-29.725^{***}	-	72.922^{***}	-7.314^{**}	61.769^{**}
	f=EXP(a+b*N/T)	4.762^{***}	-9.302^{***}	-	-	-	-	-
	f=aN +bT+c	-7.269^{***}	2.656^{***}	6.074^{ns}	-	-	-	-
Intermittent irrigation	$f= a N^3+b T^3+c N^2+ dT^2+eN+f T+g$	0.189^{***}	0.017^{***}	-0.693^{**}	-0.661^{***}	-7.572^{***}	8.906^{**}	-0.216^{**}
	f=EXP(a+b*N/T)	3.603^{***}	-3.913^{***}	-	-	-	-	-
	f=aN +bT+c	-6.261^{***}	1.987^{***}	13.130^{ns}	-	-	-	-
Long-term flood irrigation	f=EXP(a+b*N/T)	4.739^{***}	-10.564^{***}	-	-	-	-	-
	$f= a N^3+b T^3+c N^2+ eN+f T+g$	0.214^{ns}	0.006^{ns}	-1.886^{ns}	-	-13.522^{ns}	-4.938^{ns}	138.397^{ns}
	f=aN +bT+c	-18.748^{***}	1.196^{ns}	72.169^{ns}	-	-	-	-

Note: - means "none"

Table 8: Testing results of CH_4 emission flux models based on soil temperature (-10 cm) and nitrate nitrogen.

Treatment	Model	RSS	F	R_{adj}^2	Sig
Control irrigation	f= a N^3+b T^3+c N^2+ eN+f T+g	173.353	13.240	0.694	0.000
	f=EXP(a+b*N/T)	14.778	68.575	0.715	0.000
	f(M)=aN +bT+c	10414.216	12.394	0.458	0.000
Intermittent irrigation	f= a N^3+b T^3+c N^2+ eN+f T+g	100.166	15.491	0.536	0.001
	f=EXP(a+b*N/T)	36.230	6.200	0.349	0.001
	f=aN +bT+c	9521.207	13.333	0.477	0.000
Long-term flood irrigation	f=EXP(a+b*N/T)	23.147	37.679	0.576	0.000
	f= a N^3+b T^3+c N^2+ dN+e T+f	112.992	3.782	0.340	0.013
	f=aN +bT+c	21201.933	9.001	0.372	0.001

The climate, soil type, and cropping system of different regions are different; therefore, CH_4 emission has a considerable variation based on time and space. Similar to other empirical models, the proposed CH_4 emission model has no universality. However, for specific climatic features in the rice area in the cold region in Heilongjiang, the model can predict the seasonal emission flux of CH_4 for rice.

In future research, a comprehensive evaluation model for coupling of wetting and drying-physical and chemical properties of soil-agricultural management measures will be established to continually improve the calculation accuracy of CH_4 emission flux.

ACKNOWLEDGEMENTS

This work was supported by the Heilongjiang Bayi Agricultural University cultivate project funding scheme (Project title: "Greenhouse gas Emission Flux Model in Rice Growing Season in Cold Region under Water-Saving Irrigation Mode", XZR2017-2).

REFERENCES

Adhya, T., Kollah, B., Mohanty, S. R., Ramakrishnan, B., Rao, V. R., Sethunathan, N. and Wassmann, R. 2000. Methane emission from rice fields at Cuttack, India. Nutr. Cycl. Agroecosys., 58(1): 95-105.

Cao, Y. Y., Zhu, Q. S., Lang, Y. Z., Yang, J. C., Wang, Z. Q. and Xue, D. Z. 2000. Effect of rice varieties and cultivation approach on methane emission from paddy rice. Jiang Su Agricultural Research, 21(3): 22-27.

Chun, J.A., Shim, K.M., Min, S.H. and Wang, Q. 2016. Methane mitigation for flooded rice paddy systems in South Korea using a process-based model. Paddy and Water Environ., 14: 123-129.

Exnerová, Z. and Cienciala, E. 2009. Greenhouse gas inventory of agriculture in the Czech Republic. Plant Soil Environ., 55: 311-319.

Hadi, A., Inubushi, K. and Yagi, K. 2010. Effect of water management on greenhouse gas emissions and microbial properties of paddy soils in Japan and Indonesia. Paddy Water Environ, 8: 319-324.

Huang, Y., Sass, R. L. and Fisher, F.M. 1998. A semi-empirical model of methane emission from flooded rice paddy soil. Glob. Change Biol., 4: 247-268.

Jagadeesh B. Y., Li, C., Frolking, S., Nayak, D. R. and Adhya, T. K. 2006. Field validation of DNDC model for methane and nitrous oxide emissions from rice-based production systems of India. Nutrient Cycling in Agroecosytems, 74: 157-174.

Jain, M.C., Kumar,S., Wassmann, R., Mitra, S., Singh, S. D., Singh, J. P., Singh. R., Yadav, A. K. and Gupta, S. 2000. Methane emissions from

Table 9: Test results for the optimal model for the three irrigation modes.

Treatment	Optimal model	MPE/%	R_{adj}^2	Sig
Control irrigation	$f=aN^3+bN^2+cN+d$	24.78	0.429	***
	$f=aT^3+bT^2+cT+d$	15.34	0.399	***
	$f=EXP$ (a+b*N/T)	18.52	0.652	***
Intermittent irrigation	$f=aN^3+bN^2+cN+d$	23.11	0.456	***
	$f=aT^3+bT^2+cT+d$	18.43	0.397	***
	f= a N^3+b T^3+c N^2+ dT^2+eN+f T+g	15.24	0.675	***
	f=a EXP(b N)	16.58	0.476	***
Long-term flood irrigation	$f=aT^3+bT^2+cT+d$	20.46	0.416	***
	$f=EXP$(a+b*N/T)	13.53	0.625	***

irrigated rice fields in northern India New Delhi. Nutrient Cycling in Agroecosystems, 58: 75-83.

Jiao, Y., Huang, Y., Zong, L.G., Zhou, Q. S., Sass, R. L. and Fisher, F. M.2002. Methane emission from rice paddy soils as influenced by soil physicochemical properties. Environmental Science, 23(5): 1-7.

Jiao, Z.H., Hou, A., Shi, Y., Huang, G. H., Wang, Y. H. and Chen, X. 2006. Water management influencing methane and nitrous oxide emissions from rice field in relation to redox and microbial community. Commun. Soil Sci. Plant Anal., 37: 1889-1903.

Kreye, C., Dittert, K., Zheng, X. H., Zhang, X., Lin, S., Tao, H. B. and Sattelmacher, B. 2007. Fluxes of methane and nitrous oxide in water-saving rice production in North China. Nutr. Cycl. Agtoecosys., 77: 293-304.

Li, C.S. 2001. Biogeochemical concepts and methodologies. Development of the DNDC mod. Quaternary Sciences, 21: 89-99.

Liu, X., Qi, Z.M., Wang, Q., Ma, Z. W. and Li, L. H. 2017. Effects of biochar addition on CO_2 and CH_4 emissions from a cultivated sandy loam soil during freeze-thaw cycles. Plant Soil Environ., 63: 243-249.

Lv, Z.M., Hang,M., Chen, Z.Y. and Lv, Q. 2005. Contribution of anaerobic oxidation of methane to whole methane oxidation. Environmental Science, 26(4): 13-17.

Minamikawa, K. and Sakai N. 2005. The effect of water management based on soil redox potential on methane emission from two kinds of paddy soils in Japan. Agriculture Ecosystems and Environment, 107: 397-407.

Minamikawa, K., Tamon, F., Itoh, M., Hayano, M., Sudo, S. and Yagi, K. 2014. Potential of prolonged midseason drainage for reducing methane emission from rice paddies in Japan. A long-term simulation using the DNDC-Rice model. Biology and Fertility of Soils, 50: 879-889.

Neue, H.U. and Roger, P.A. 1993. Rice agriculture: factors controlling emissions. In: (Khalil, M.A.K. ed.) Atmospheric Methane Sources, Sinks, and Role in Global Change. New York. Springer-Verlag, pp. 254-298.

Peng, S. Z., He, Y. P., Yang, S. H., Xu, J. Z. and Hou, H. J. 2013. Mitigation of methane emissions from paddy fields under controlled irrigation, Transactions of the Chinese Society of Agricultural Engineering, 29(8): 100-107.

Qin, X. B., Li, Y., Liu, K.Y. and Wan, Y. F. 2006. Methane and nitrous oxide emission from paddy field under different fertilization treatments. Trans. CSAE, 22: 143-148.

Sass, R.L., Fisher, F.M., Jr., Huang, Y. 2000. A process-based model for methane emissions from irrigated rice fields. experimental basis and assumptions. Nutrient Cycling in Agroecosystems, 58: 249-258.

Scheehle, E.A. and Kruger D. 2006. Global anthropogenic methane and nitrous oxide emissions. The Energy Journal, Multi-Greenhouse Gas Mitigation and Climate Policy, 3: 33-34.

Shao, M., Sun, J. and Ruan, G. 2011. Review on greenhouse gases emission and reduction technology in rice fields. Acta Agriculturae Zhejiangensis, 23(1): 181-187.

Towprayoon, S., Smakgahn, K. and Poonkaew, S. 2005. Mitigation of methane and nitrous oxide emissions from drained irrigated rice fields. Chemosphere, 59: 1547-1556.

Wang, M.X. and Zhang, Z.X. 2015. Optimal water-saving irrigation model reducing N_2O emission from rice paddy field in cold region and increasing rice yield. Transactions of the Chinese Society of Agricultural Engineering, 31: 72-79. (In Chinese)

Wei, H., Sun, W. and Hang, Y. 2012. Statistical analysis of methane emission from rice fields in China and the driving factors. Scientia Agricultura Sinica, 45(17): 3531-3540.

Wu, H. and Ye, Z. 1993. Preliminary estimated amount of methane emission in China rice paddy field. China Environmental Science, 13(1): 76-80.

Xie, B.H., Zhou, Z.X., Zheng, X.H., Zhang, W. and Zhu, J. G. 2010. Modeling methane emissions from paddy rice fields under elevated atmospheric carbon dioxide conditions. Advances in Atmospheric Sciences, 27: 100-114.

Xiong, Z.Q., Xing, G.X. and Zhu, Z.L. 2007. Nitrous oxide and methane emissions as affected by water, soil and nitrogen. Pedosphere, 17: 146-155.

Yuan, W. L., Cao, C. G., Cheng, J. P. and Xie, N. N. 2008. CH_4 and N_2O emissions and their GWPs assessment in intermittent irrigation rice paddy field. Scientia Agricultura Sinica, 41(12): 4294-4300.

Zhao, B., Zhang, J., Lv, X., Peng, L. and Padilla, H. 2013. Methane oxidation enhancement of rice roots with stimulus to its shoots. Plant Soil Environ., 59: 143-149.

Zhao, Z., Yue, Y.B., Zhang, Y., Lu, X. X. and Cao, L. K. 2014. Impact of different fertilization practices on greenhouse gas emission from paddy field. Journal of Agro-Environment Science, 33(11): 2273-2278.

Zhu, S.J. 2012. Experiment for water-saving and greenhouse effect of irrigation mode in cold rice area. Haerbin. Northeast Agricultural University, 2012. (In Chinese)

Zou, J. W., Huang, Y., Zong, L. L., Zheng, X. H. and Wang, Y. S. 2003. A field study on CO_2, CH_4 and N_2O emissions from rice paddy and impact factors. Acta Scientiae Circumstantiae, 23: 758-765.

Zschornack, T., Rosa, C. M., Pedroso, G. M.,Marcolin, E., Ferreira da Silva, P. R. and Bayer, C. 2016. mitigation of yield-scaled greenhouse gas emissions in subtropical paddy rice under alternative irrigation systems. Nutrient Cycling in Agroecosystems, 105: 61-73.

Nature Environment and Pollution Technology
An International Quarterly Scientific Journal

p-ISSN: 0972-6268
(Print copies up to 2016)
e-ISSN: 2395-3454

Vol. 19 | No. 2 | pp. 481-492 | 2020

Original Research Paper

https://doi.org/10.46488/NEPT.2020.v19i02.005

Open Access Journal

Machine Learning Model for Revealing the Characteristics of Soil Nutrients and Aboveground Biomass of Northeast Forest, China

Chunyan Wu*, Lifeng Pang, Jun Jiang***†, Miaoying An*** and Yuanjun Yang******

*Research Institute of Forestry, Chinese Academy of Forestry, Beijing 100091, China
**Institute of Forest Resource Information Techniques, Chinese Academy of Forestry, Beijing 100091, China
***Research Center of Forest Management Engineering of State Forestry and Grassland Administration, Beijing Forestry University, Beijing 100083, China
****College of Water Resources and Hydraulic Engineering, Yunnan Agricultural University, Kunming, China
†Corresponding author: Jun Jiang; jiang@bjfu.edu.cn

Nat. Env. & Poll. Tech.
Website: www.neptjournal.com

Received: 29-07-2019
Accepted: 08-10-2019

Key Words:
Mt. Changbai;
Soil properties;
Species diversity;
Aboveground biomass;
Climate change

ABSTRACT

Declining soil quality and climate change may affect species diversity and forest biomass productivity in many temperate regions in the future. Our research objective is to reveal the characteristics of soil nutrients and biomass of forests in Northeast China with climate change. The purpose of this study was to determine the soil physical and chemical properties of mature broad-leaved forest in the cold temperate zone of Mt. Changbai, Jilin Province, by measuring pH, NH^{4+}, organic matter (%), C/N, available phosphorus, alkali-hydrolysable N, rapidly available K, and Cr etc., analysing species diversity characteristics, and estimating aboveground biomass (AGB) of tree species with machine learning models. The results showed that with the increase of soil depth, the soil physical and chemical parameters have a decreasing trend; with the increase of soil depth, the soil nutrient content decreased; the main tree species were the *Acer barbinerve* (6937), *Carpinus cordata* Bl. (6682) and *Acer mandshuricum* Maxim. (5447) etc. The total difference (SOR) showed a similar trend in the four directions and central point; the reference sample size at central point, north, west, south and east direction was 903, 954, 971, 1005 and 1016, respectively; GRNN model was the relatively best model among these models for modelling the aboveground biomass of the trees. Therefore, the diversity of tree species in north-eastern forests was affected by soil nutrients, climate change also has a significant impact on the aboveground biomass of northeast forests, which provides a theoretical basis for the management of northeast forests about soil physical and chemical properties and species diversity.

INTRODUCTION

Global climate change influences the distribution (Wang et al. 2017) and structure of forests (Peñuelas et al. 2016), the stability and balance of ecosystems (Hautier et al. 2015, Kilpeläinen et al. 2017), ecosystem restoration (Deng et al. 2017a, Deng et al. 2017b), the functional composition of trees, and biological accumulation in forests through changes in biodiversity (Van der Sande et al. 2017). The tree mortality induced by global drought and warming reveals the damage to forests caused by climate change (Kennedy et al. 2018). Forest biomass was identified as an important variable by the global climate observing system (GCOS) (Fu et al. 2017) to improve our knowledge of the forest ecosystems (Le Toan et al. 2011). Information about the impact of climate on soil physical and chemical properties can provide valuable insights to promote the natural regeneration of forests, respond to sustainability, and adapt to climate change (Kennedy et al. 2018). Therefore, understanding how the characteristic of soil physical and chemical properties of the forest has become particularly important.

The researchers have determined that soil nutrients play an important role in the soil fertility and environmental condition of plant growth and development (Delgado-Baquerizo et al. 2013, Camenzind et al. 2018). While, seed germination, seedling establishment, growth and reproduction during tree recruitment (Kulmatiski et al. 2008, Collin et al. 2018, Wang et al. 2018), the composition, development, spatial patterns, and geographical distribution of species (Schulz & Glaser 2012, Lu et al. 2017), community biomass and succession, and ecosystem stability are mainly affected by soil nutrients (Andrew et al. 2014, Laliberté et al. 2017). Also, increasing soil nutrient content will increase tree species richness (De Deyn et al. 2004, Cline et al. 2018). Most researches of soil nutrition have focused on the effects of alkaline nitrogen, available phosphorus, available potassium, and water content on plant growth and distribution (Mackay et al. 2017, Netzer

et al. 2017). They have determined that soil nutrient availability of nitrogen, phosphorus, and potassium strongly affect the ecosystem community structure (Sardans et al. 2017, Waldrop et al. 2017). Soil pH value, soluble ion, calcium carbonate content (Carter 1987), different condition of KNO_3 or NH_4NO_3 and soil water content have an impact on germination characteristics, leaf development, photosynthetic pigment content, and seedling photosynthetic efficiency. All of them have a significant correlation with species diversity of the forest (Lal et al. 2017).

Transpiration and reduced rainfall caused by global warming may threaten the vitality of trees, soil nutrient, species diversity and forest biomass. Process-based models have been used to simulate the impacts of climate change on forest biomass (Yousefpour et al. 2018, Kang et al. 2017). However, all of these studies only have different plant characteristics in different climatic regions or populations of a certain place. Although the model method has been developed and created with some new ideas, it is still relatively traditional as a whole (Stegen et al. 2011, Aherne et al. 2012). Besides, climate change is very complex. It is particularly important to explore a fast and efficient model for estimating and predicting precise biomass.

The use of ML models in agricultural industry and forestry has become more popular in classification and discrimination is one of the most important challenges in solving specific non-linear problems in dynamic change systems in the process of model prediction (Soares & Araújo 2016). Artificial neural network (ANN) and support vector machine (SVM) can solve this problem and have been widely used (Ottoy et al. 2017), which can represent the potential organic matter and complex process of climate affecting forest biomass. With the rapid development of machine learning, many advanced data processing technologies have included the combination method of data processing (GMDH), generalized regression neural network (GRNN), adaptive neuro-fuzzy inference system (ANFIS) (Dou & Yang 2017). These methods have been used to identify shell-free rice fungal populations (Chang et al. 2017), predict and map soil organic carbon stocks in landscapes (Were et al. 2015), and accurately predict biomass heating values (Akkaya 2016).

In this study, we used forest tree species data from permanent sample plots to study soil nutrient characteristics and species diversity characteristics and used machine learning-based data processing technology to estimate biomass of trees from forest comprehensive survey data to assess tree species response to climate and soil properties. Specifically, we ask the following questions: (1) what was the soil nutrient characteristics of Mt. Changbai? (2) what was the tree species diversity characteristics? (3) how was the relationship between climate factors and forest biomass?

MATERIALS AND METHODS

Learning Area

The study was conducted in Northeast China along a latitudinal gradient from 42.35° N to 43.57°N. The annual mean temperature in this region ranges between −2.1°C and 2.6°C, and the annual precipitation is between 510 mm and 810 mm. The broad-leaved Korean pine forest, a climax forest of the temperate zone, is characterized by the complex structure and abundant biodiversity. The study sites covered most of the latitudinal range of the broad-leaved Korean pine forest. The plot was near a mature broad-leaved Korean pine forest located in the cold temperate zone of Mt. Changbai, Jilin Province (Fig. 1). The broad-leaved Korean pine forest zone in Mt. Changbai is a typical zonal forest with the greatest number of animal and plant species and the most abundant vegetation on this mountain. It mainly grows at an altitude of 720-1100 m in the areas with a mild climate, heavy rainfall, and dark-brown forest soil. The main tree species include *Abiesholophylla*, *Betulaplatyphylla*, *Carpinuscordata*, *Fraxinusmandshurica*, *Maackiaamurensis, Pinuskoraiensis*, *Populussuriensis*, *Quercusmongolica*, *Tiliaamurensis*, *Ulmus japonica*, and *Ulmuslaciniata* (Hu et al. 2014).

MATERIALS AND METHODS

Sampling plot setting: At the study sites described above, fixed sampling plots of 40 km^2 in size were established in 2015. Both the plots were composed of *Pinus koraiensis* and broad-leaved species such as *Acer* spp., *Fraxinus mandschurica*, and *Tilia* spp. They were divided into 1050 continuous sampling plots of 20 m × 20 m in size, and each of them was further divided into 5 sub-sampling plots of 5 m × 5 m in size in the east, south, west, north direction, and central point of the plot. In each plot, the name of an individual species, diameter at breast height (DBH), tree height, under-branch height, and crown width (east-west crown length, north-south crown length) were identified, measured and mapped for each plant with DBH > 1 cm. The overview of sampling plots is given in Table 1.

Soil data survey: Soil samples at three depths (0-10, 11-20, and 21-30 cm) were randomly collected from three random points using a stainless steel auger at each site. The soil was weighed to 200 g and returned to the laboratory before removing the residual artefacts. The samples were stored under dry, well-ventilated conditions to allow them to dry naturally before they were sieved through a 200-micron mesh, and then

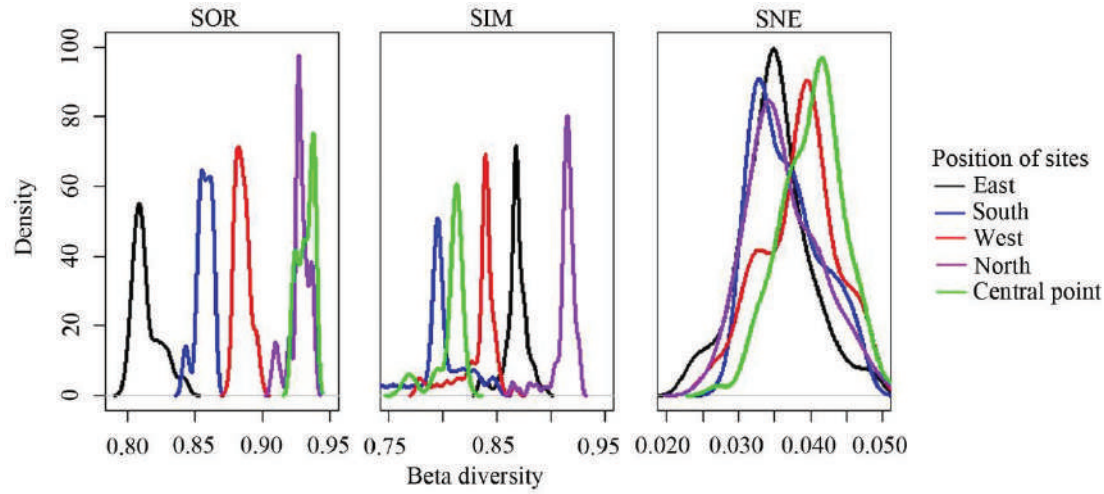

Fig. 1: The sampling plots of the mature broad-leaved forest of Changbai Mountain in Jilin Province.

they were sent to the laboratory for physical and chemical analysis (Pingree & DeLuca 2018).

Climate data: Climate data in tropical China was obtained from the China Meteorological Data Network http://data.cma.cn/data/index/0b9164954813c573.html of the Meteorological Data Center of China Meteorological Administration. Influenced by global climate change, extreme weather (typhoons, tsunami natural disasters) is entering in a more frequent and more normalized trend, which is prone to extreme temperatures and sudden changes in rainfall. Therefore, five bioclimatic variables, average maximum temperature, average minimum temperature, average temperature, relative humidity and precipitation were chosen as independent variables to analyse the changes of biomass (Petus et al. 2018).

Biomass data: In this study, the diameter at breast height (DBH), height (H) and crown width of trees were investigated. One standard tree was selected from each plot for biomass determination. We cut down the tree and measured the fresh weights of the stems, branches, leaves and fruits to determine the water content in the field. The samples were brought to the laboratory and oven-dried at 75°C to a constant weight. The biomass of stems, branches, leaves and fruits was calculated using the dry weight to fresh weight ratio, and the aboveground biomass (AGB) of the tree was obtained by summing all biomass values (Fu et al. 2017). The integral biomass dataset was randomly divided into three groups: training, validation and testing datasets. After several calculations, we found that 735 (70% of 1050 samples) trees for model training, 157 (15%) trees for model validation, and 157 (15%) trees for model testing produced the best results.

Models applications: Using climate variables estimate AGB of trees through machine learning modelling. In this study, the five machine learning algorithms include artificial neural network (ANN), support vector machine (SVM), generalized regression neural network (GRNN), adaptive neuro-fuzzy inference system (ANFIS) and the combination method of data processing (GMDH) (Dou & Yang 2017).

Data Analysis

Beta diversity analysis: Beta diversity measures changes in species composition between locations or communities (Baselga & Orme 2012). Baselga (2012) developed a unified framework for assessing beta diversity that uses the Sørensen or Jaccard indices and their turnover and nesting components to calculate the total differences. We use the Sørensen index:

Table 1: A summary of permanent forest plots in Mt.Changbai.

Forest type	Average elevation (m)	Total basal area (m^2 km^{-2})	Dominant species	Primary vegetation
Primary *Pinuskoraiensis-Tiliaamurensis* mixed forests	779	25.36	*Pinuskoraiensis* *Fraxinusmandshurica* *Tiliaamurensis* *Quercusmongolica*	Broad-leaved *Pinuskoraiensis* forests

Sørensen dissimilarity

$$\beta_{sor} = \frac{b+c}{2a+b+c} \quad \ldots(1)$$

turnover/replacement

$$\beta_{sim} = \frac{\min(b,c)}{a+\min(b,c)} \quad \ldots(2)$$

And nestedness/ richness difference

$$\beta_{sne} = \frac{|b-c|}{2a+b+c} \times \frac{a}{a+\min(b,c)} \quad \ldots(3)$$

Where, β_{sor} is the Sørensen dissimilarity, β_{sim} is the Simpson dissimilarity, β_{size} is the nestedness or richness difference, a is the number of species shared between two cells, b is the number of unique species at the poorest sites, and c is the number of unique species at the richest site.

Rarefaction and extrapolation curves with Hill numbers: Rarefaction and the extrapolation of Hill numbers are used for sampling and estimation in species diversity studies (Chao et al. 2014a). This criterion quantifies and assesses changes in biodiversity, allowing for the differential weighting of rare and abundant species, which is similar to a diversity index, but its meaning is easier to understand. Chao et al. (2014b) applied a uniform approach to sample and individual-based data to estimate the first three Hill numbers for characterizing the diversity of a species assemblage: species richness (q = 0), Shannon entropy index (Shannon diversity, q = 1) and the anti-Simpson concentration (Simpson diversity, q = 2). These proposed estimators are accurate for both sparse and short-range extrapolation.

Sparse and extrapolated curves and Hill numbers were used to compare the plant diversity patterns (Chao et al. 2014a). We estimated plant diversity (species richness and Shannon and Simpson diversity) as the mean of 200 replicates with a 95% confidence interval (Chao et al. 2014b).

Univariate analysis of variance (ANOVA) was used to test significant differences in soil physical and chemical parameters at different position points. All statistical analyses were implemented using R version 3.5.1 (R Development Core Team 2017) and GS+7.0. Beta diversity was analysed by betapart package, and sparse and extrapolated curves were compiled by iNEXT package. Draw numbers and process data using ggplot2 packages (R Development Core Team, 2017).

Data for Model Training and Validation

The input variables for all models are climate variables and diameter at breast-high. The five different ML modelling techniques presented in the previous section have been developed and compared. To achieve accurate and reasonable comparisons of different AGB estimates, all AGB values of trees were modelled using the same input variables (average minimum temperature, average maximum temperature, average temperature, average relative humidity, precipitation) and prediction methods. These input variables and corresponding output variables are normalized to a range between 0 and 1 before training each application model. The toolboxes in the MATLAB software (version 8.2, The MathWorks, Inc., Natick, MA, USA), including the Neural Network Toolbox 8.1 and the Fuzzy Logic Toolbox 2.2.18, were utilized for all models (Li et al. 2014).

Model Evaluation

The data processing performance of the developed model was evaluated based on several statistical data indices, including the coefficient of determination (R^2), Nash-Sutcliffe efficiency (E_{NS}), root mean squared error (RMSE), and mean absolute error (MAE) (Fu et al. 2017). The above statistical indicators are described as follows:

$$R^2 = \left[\frac{\sum_{i=1}^{N} \left(Y_{a,c} - \overline{Y}_a\right)\left(Y_{b,c} - \overline{Y}_b\right)}{\sqrt{\sum_{i=1}^{N} \left(Y_{a,c} - \overline{Y}_a\right)^2 \sum_{i=1}^{N} \left(Y_{b,c} - \overline{Y}_b\right)^2}} \right]^2 \quad \ldots(6)$$

$$RMSE = \sqrt{\sum_{i=1}^{N} \left(Y_{a,c} - Y_{b,c}\right)^2 \Big/ N} \quad \ldots(7)$$

$$E_{NS} = 1 - \sum_{i=1}^{N} (Y_{a,c} - Y_{b,c})^2 \Big/ \sum_{i=1}^{N} (Y_{a,c} - Y_b)^2 \quad (8)$$

$$MAE = \frac{1}{N} \sum_{i=1}^{N} \left|Y_{a,c} - Y_{b,c}\right| \quad \ldots(9)$$

Where, Y_a and Y_b denote the observed and modelled values, respectively; $\overline{Y}_a$ and $\overline{Y}_b$ are the means of the observed and modelled values, respectively; and N is the number of observed values.

RESULTS

Physical and Chemical Properties of Soil

The physical and chemical parameters of soils at Mt. Changbai are different in different soil depths (Table 2). Soil physical and chemical parameters show a decreasing trend with the increase of soil depth. The content of 0-10 cm soil depth was the highest, and 21-30 cm soil depth

was the lowest in the three types of soil depth. The change ranges of pH value were relatively smaller than that of other indicators with the increase of the soil depth, the soil of Mt. Changbai was acidic and neutral in general. The content of NH^{4+} ranged from 0.4 to 0.08. The highest C/N ratio was 13.6. The content of available phosphorus was almost 10 mg kg^{-1} in the 0-10 cm soil layer, and that of the alkali-hydrolysable N was almost 5 mg kg^{-1} in the 21-30 cm soil layer, the rapidly available K was only 2.5 mg kg^{-1} in the 0-10 cm soil layer.

Soil Nutrient Content

Soil nutrients also vary significantly with different locations and soil depths (Table 3). Soil nutrient content decreases as soil depth increases. In the 0-10 cm soil layer of Mt. Changbai, the contents of Cr, Mn, Co, Ni, Cu, Zn and Pb are 45.710, 746, 12.612, 26.531, 13.452, 130.638, 28.711, respectively, while the content of that was decreased sharply in 11-20 cm and the 21-30 cm soil layer.

Species Composition of the Trees

We identified 48 species of trees in the 49684 trees, belonging to 32 genera and 20 families in the Mt. Changbai. Among them, the number of the *Acer barbinerve* (6937), *Carpinus cordata* Bl. (6682), *Acer mandshuricum* Maxim. (5447), *Corylus mandshurica* Maxim. (5387), *Acer mono* Maxim. (4113), *Syringa reticulata* (Blume) H. Hara var. *amurensis* (Rupr.) J. S. Pringle (3026), *Ulmus laciniata* (Trautv.) Mayr. (2813), *Acer ukurunduense* Trautv. et Mey. (2058), *Tilia amurensis* Rupr. (1963), *Acer tegmentosum* Maxim. (1818), *Pinus koraiensis* Sieb. et Zucc. (1339), and *Sorbus alnifolia* (Sieb. et Zucc.) K. Koch (1065) was exceeded 1000 (Fig. 2). The 13 species, such as *Padus racemosa* (Linn.) Gilib., *Juglans mandshurica*, and *Quercus mongolica* Fisch. ex Ledeb, were more than 100 but less than 1000. The 23 species, such as *Betula platyphylla* Suk. and *Fraxinus rhynchophylla* Hance were less than 100.

Changes in the species composition of Mt. Changbai was estimated by beta diversity analysis (Fig. 3). The total difference (SOR) showed a similar trend in the four directions and central point: the greatest difference was the north direction, but with similar values at south direction and west direction, and the lowest difference was on the east direction. The turnover difference (SIM) showed a little different from the SOR in the four directions and central point: the lowest differences were in the south direction. The nesting difference (SNE) was significantly different in the east direction, with the central point being the largest followed by the south direction and the west direction, which were in the middle, and the north direction, which was the smallest.

Diversity Pattern of the Trees

The results showed that the reference sample size (i.e., the number of individual plants) at the central point, north, west, south and east direction was 903, 954, 971, 1005 and 1016, respectively, with Hill numbers q = 0, 1 and 2 curves (Fig. 4). The sample size was close to the complete recovery phase with a base coverage rate of 1.0. The reference sample size was extrapolated to 1746. The corresponding observed species richness (q = 0), Shannon diversity (q = 1) and Simpson diversity (q = 2) showed a consistent trend: gradually increased at the west and south directions but remaining stable

Table 2: Soil physical and chemical parameters (mean ± standard error) for each experimental site.

Forest type	layer	pH	NH^{4+}	Organic matter (%)	NO^{3-}	C/N	Available phosphorus (mg kg^{-1})	Alkali-hydrolysable N (mg kg^{-1})	Rapidly available K (mg kg^{-1})
Changbai Mountain	0-10cm	6.08±0.57a	0.371±0.121a	2.471±0.231a	25.301±2.748b	13.6b	10.514±2.215b	92.813±19.824a	56.763±11.434b
	11-20cm	5.62±0.46b	0.107±0.083b	1.057±0.115b	12.745±1.115b	10.4b	2.451±0.968b	17.836±8.610b	9.632±2.618b
	21-30cm	5.53±0.12bc	0.084±0.021bc	0.685±0.057c	7.163±0.476bc	9.7	1.424±0.043bc	5.725±3.764c	2.451±0.068bc

Note: the compartments with different letters represent the statistical differences of each parameter.

Table 3: Soil nutrient concentration (mg g^{-1} dry soil) at each experimental site (mean ± standard error).

Forest type	Layer	Cr (mg g^{-1})	Mn (mg g^{-1})	Co (mg g^{-1})	Ni (mg g^{-1})	Cu (mg g^{-1})	Zn (mg g^{-1})	Pb (mg g^{-1})
Changbai Mountain	0-10cm	45.710a	746a	12.612a	26.531a	13.452a	130.638b	28.711a
	11-20cm	19.235b	324b	3.752b	11.673b	5.632b	86.452b	17.134b
	21-30cm	6.107b	105bc	1.146bc	4.650c	2.187c	24.951c	4.135c

Note: Compartments with different letters indicate statistical differences in each soil nutrient.

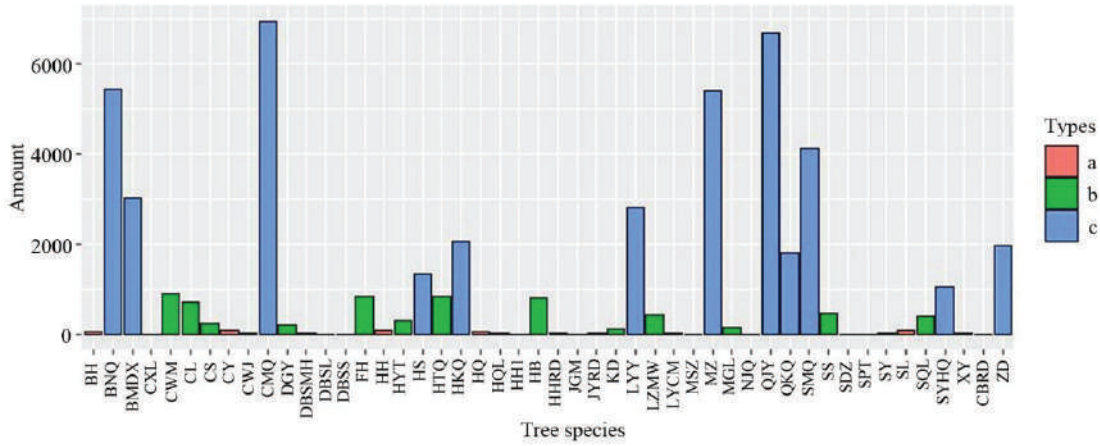

Fig. 2: Summary of species composition of forest trees in study sites.

Note: BH: *Betula platyphylla* Suk.; BNQ: *Acer mandshuricum* Maxim.; BMDX: *Syringa reticulata* (Blume) H. Hara var. *amurensis* (Rupr.) J. S. Pringle; CXL: *Salix koreensis* Anderss.; CWM: *Euonymus phellomana* Loes.; CL: *Padus racemosa* (Linn.) Gilib.; CS: *Abies nephrolepis* (Trautv.ex Maxim) Mazim.; CY: *Ulmus pumila* l.; CWJ: *Acanthopanax senticosus* (Rupr. Maxim.) Harms; CMQ: *Acer barbinerve*; DGY: *Ulmus macrocarpa* Hance; DBSMH: *Philadelphus schrenkii* Rupr.; DBSL: *Rhamnus schneideri* Levl.; DBSS: *Deutzia parviflora* Bge. var. amurensis Regel; FH: *Betula costata* Trautv.; HH: *Betula davurica* Pall.; HYT: *Cerasus maximowiczii* (Rupr.) Kom.; HS: *Pinus koraiensis* Sieb. et Zucc.; HTQ: *Juglans mandshurica*; HKQ: *Acer ukurunduense* Trautv. et Mey.; HQ: *Sorbus pohuashanensis*; HQL: *Fraxinus rhynchophylla* Hance; HH1: *Maackia amurensis* Rupr. et Maxim; HB: *Phellodendron amurense* Rupr.; HHRD: *Lonicera chrysantha* Turcz.; JGM: *Sambucus williamsii* Hance; JYRD: *Lonicera maackii* (Rupr.) Maxim.; KD: *Tilia mandshurica* Rup et Maxim.; LYY: *Ulmus laciniata* (Trautv.) Mayr.; LZMW: *Euonymus verrucosus* Scop.; LYCM: *Aralia elata* (Miq.) Seem.; MSZ: *Crataegus maximowiczii* Schneid.; MZ: *Corylus mandshurica* Maxim.; MGL: *Quercus mongolica* Fisch. ex Ledeb; NJQ: *Acer triflorum*; QJY: *Carpinus cordata* Bl.; QKQ: *Acer tegmentosum* Maxim.; SMQ: *Acer mono* Maxim.; SS: *Abies holophylla* Maxim; SDZ: *Malus baccata* (L.) Borkh.; SPT: *Vitis amurensis* Rupr.; SY: *Populus davidiana* Dode; SL: *Rhamnus davurica* Pall.; SQL: *Fraxinus mandshurica* Rupr.; SYHQ: *Sorbus alnifolia* (Sieb. et Zucc.) K. Koch; XY: *Populus koreana* Rehd.; CBRD: *Lonicera ruprechtiana* Regel; ZD: *Tilia amurensis* Rupr.; a: amount of species less than 100; b: number of species more than 100 but less than 1000, c: the number of species more than 1000.

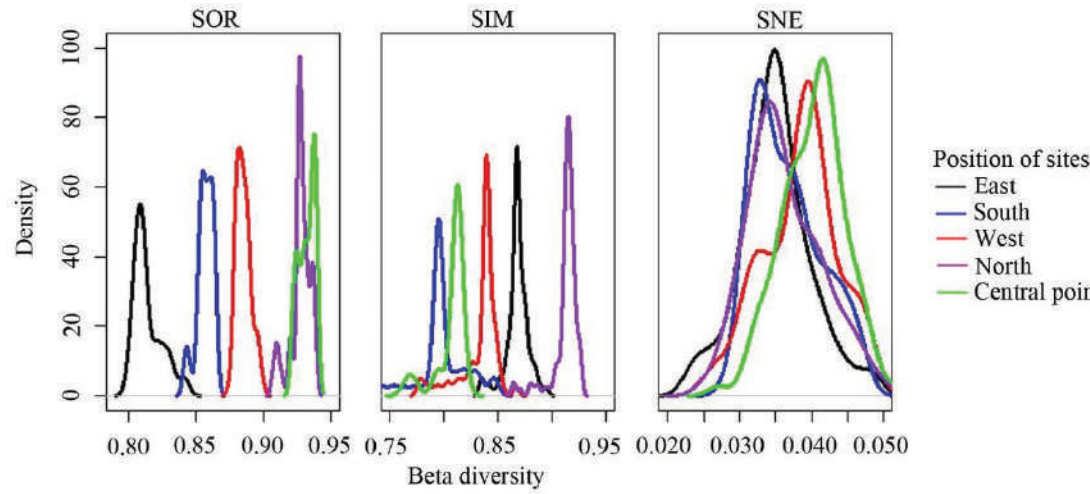

Fig. 3: The beta diversity analysis of the density of the difference in species composition of trees on the forest in study sites.

Note: total dissimilarity (SOR) is divided into conversion difference (SIM) and nesting (SNE) components. Density estimation is performed by using a kernel smoothing method.

at the central point, diversity peaks at the east direction, and then decreased at the north direction.

Modelling Aboveground Biomass

Performance metrics, including R^2, E_{NS}, RMSE and MAE, were used to evaluate the application model in predicting AGB efficiency. The larger the R^2 and E_{NS} values and the smaller RMSE and MAE values, the higher the model efficiency. The results of the estimation were used to predict the training of five data processing methods (ANN, GRNN, ANFIS, SVM and GMDH). The validation and testing times were summarized in Table 4. The table shows the R^2 and E_{NS} size order of model calculation results during training: ANFIS> GRNN> SVM> ANN> GMDH, RMSE and MAE values were in the same order as R^2 and E_{NS}; and verification and testing (The R^2 and E_{NS} order of the model calculation results in the process of validation and testing: GRNN> SVM> ANN> ANFIS> GMDH, RMSE and MAE were in

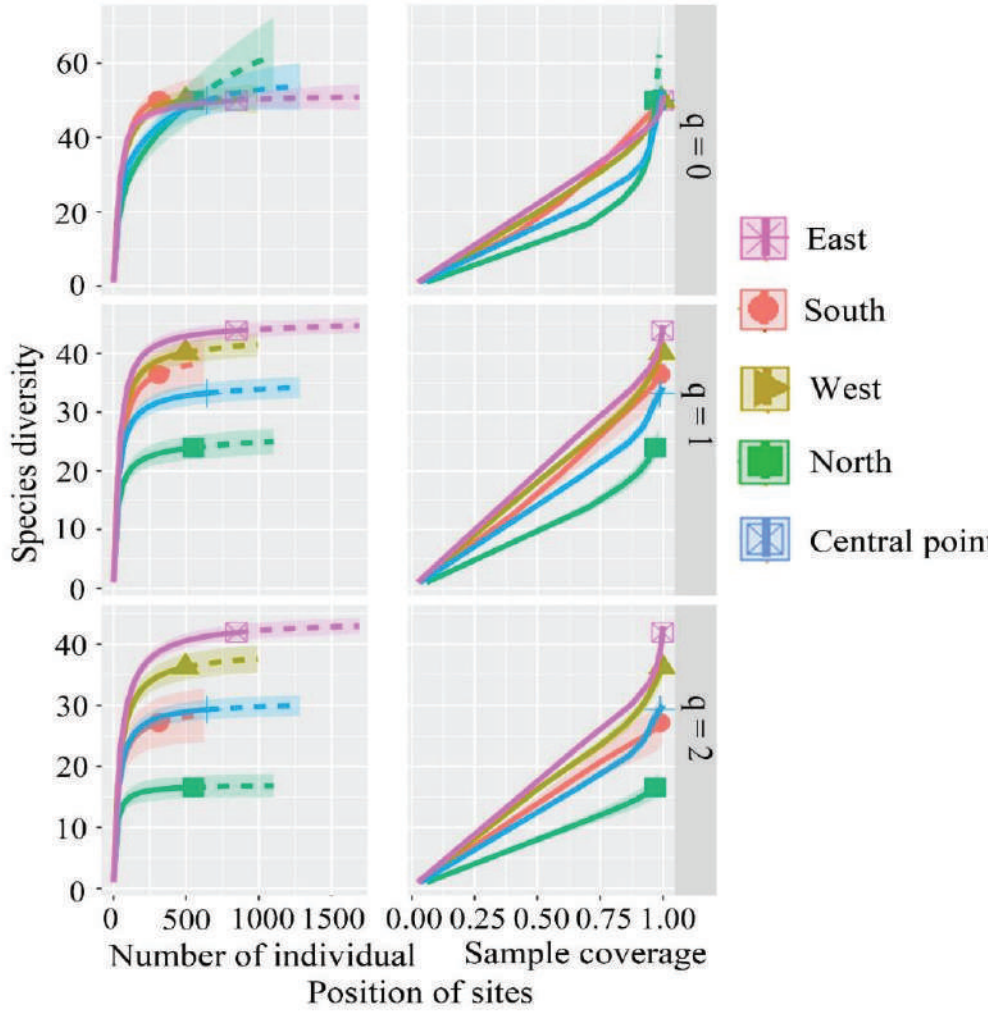

Fig. 4: Individual- and coverage-based rarefaction and extrapolation curves, based on the Hill numbers (q = 0, 1, 2) for the vegetation on Changbai Mountain, Jilin province of China.

Note: the 95% confidence intervals (shaded area) were obtained by bootstrapping (200 copies). Reference samples are denoted by solid dots; the numbers in parentheses are the respective sample size and observed Hill number of each reference sample. In this study, we used the first three Hill numbers to characterize the diversity of a species assemblage based on the individual-based data: species richness (q = 0), the exponential of the Shannon entropy (Shannon diversity, q = 1), and the inverse Simpson concentration (Simpson diversity, q = 2). The proposed estimators are accurate for both rarefaction (solid line) and short-range extrapolation (dashed line, up to double the reference sample size).

the same order as R^2 and E_{NS}).

The AGB using the data model to compare measurements and predictions is shown in Fig. 5 as a scatter plot during the testing. As shown in Fig. 5, the fitted line of GRNN model (slope = 0.937) and SVM model (slope = 0.931) was closer to the ideal line (1:1 line). For the GMDH model, the fitted line (slope = 0.862) was more inconsistent with the ideal-fit line than the other models (ANN model (slope = 0.919), ANFIS model (slope = 0.902)). Besides, none of the estimated values of the GMDH model matches the minimum value around the corresponding observations. Although the applied models have significant AGB prediction performance differences (Table 4), these models provide a similar overall dispersion estimate (Fig. 5). Therefore, the GRNN model was the relatively best model among these models for modelling the AGB of the trees.

DISCUSSION

Soil texture has many effects on forest tree species. Our study shows that there are significant differences in soil physical and chemical properties between different geographical locations and soil depths. This is similar to previous studies by experts. Different authors have demonstrated that soil nutrients are the main factors affecting the composition and structure of forest communities (Valentín-Vargas et al. 2014). Besides, soil texture and topographic factors may change solar incidence angle, slope change, soil organic carbon content, temperature and humidity conditions (Brabcová et

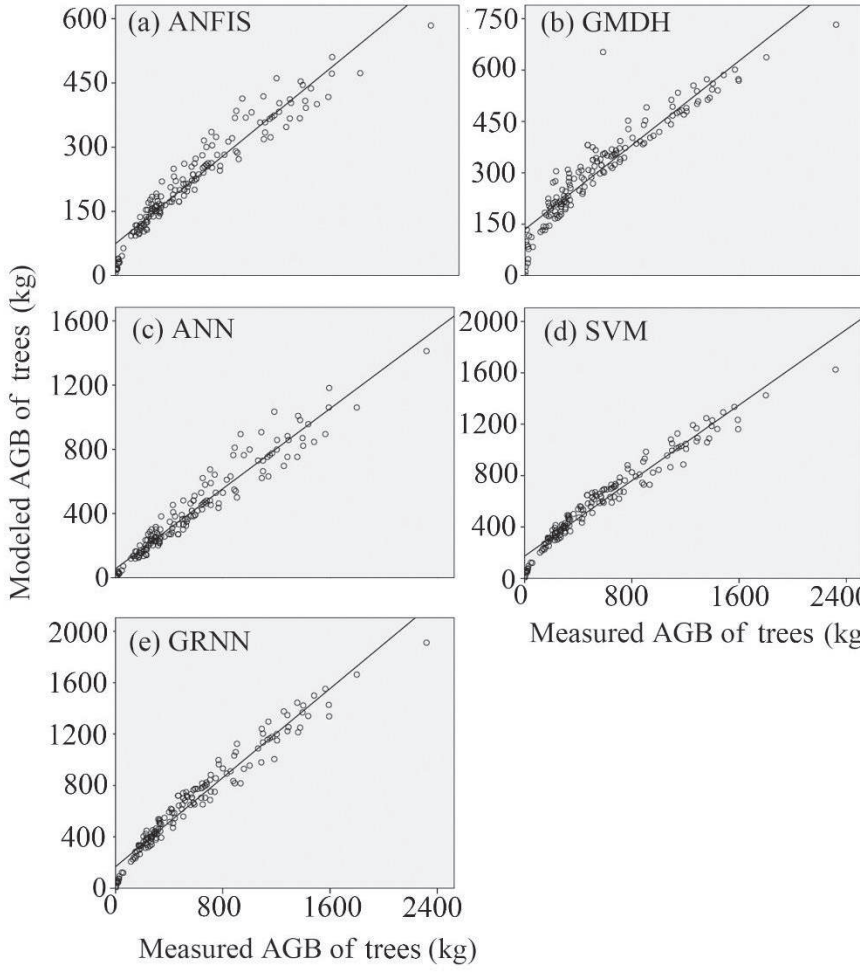

Fig. 5: The AGB measured and predicted by models for the testing period.

Note: (a) ANFIS model; (b) GMDH model; (c) ANN model; (d) SVM model; and (e) GRNN model. AGB is above-ground biomass of trees; ANFIS refer to adaptive neuro-fuzzy inference systems; GMDH refers to group method of data handling; ANN refers to artificial neural network; SVM refers to support vector machine; GRNN refers to generalized regression neural networks.

Table 4: Comparisons of models for AGB for the training, validation and testing periods.

Model	Training				Validation				Testing			
	R^2	E_{NS}	RMSE	MAE	R^2	E_{NS}	RMSE	MAE	R^2	E_{NS}	RMSE	MAE
GMDH	0.8909	0.7912	0.9917	0.6733	0.8142	0.6612	0.9990	0.9564	0.8087	0.6661	0.9293	0.8553
GRNN	0.9273	0.8776	0.6361	0.4022	0.8748	0.7684	0.7512	0.4661	0.8792	0.7858	0.6727	0.4199
ANFIS	0.9331	0.8820	0.5484	0.3580	0.8478	0.7574	0.9130	0.9017	0.8528	0.7720	0.8066	0.7516
SVM	0.9150	0.8773	0.8277	0.4956	0.8747	0.7676	0.9039	0.6198	0.8765	0.7774	0.7742	0.5387
ANN	0.8993	0.8674	0.9127	0.6655	0.8735	0.7656	0.9086	0.8295	0.8757	0.7754	0.7987	0.7217

Note: GMDH refer to group method of data handling; GRNN refer to generalized regression neural networks; ANFIS refer to adaptive neuro-fuzzy inference systems; SVM refer to support vector machine; ANN refer to artificial neural network; R^2 is coefficient of determination; E_{NS} is nash-sutcliffe efficiency; RMSE is mean squared error; MAE is mean absolute error.

al. 2018). The advanced succession of plant communities can significantly change soil water content, soil compactness, improve soil aeration and water holding capacity, and promote the development of soil fertility. The improvement of soil physical properties is also conducive to the process of community species replacement and succession. Soil properties of successive communities were influenced by slope and parent material of sample plots (Zhang et al. 1997). The composition of tree species was also affected by soil properties, such as the C/N ratio, soil organic carbon (Jiang 2016). Different tree species have different soil quality (Yang et al. 2008). The longer the forest age, the higher the soil water content. It shows that tree species are the main factors affecting soil quality. Tree species significantly improve the soil total nitrogen and soil organic matter content (Jiang 2016). Soil texture of parent rock materials and topography is almost the same in each sample plot in the study area, and the differences related to soil properties may be related to the characteristics of vegetation on the ground.

The trend of soil nutrient storage is obvious, and a large quantity of soil nutrients are stored in the surface layer (0-10 cm). Also, there was no significant difference in soil nutrient status between Mt. Changbai, and there was no significant correlation between soil organic matter and nutrients. This result is similar to previous studies, in which different soil nutrient concentrations decrease with increasing soil depth (Berger et al. 2015). In addition, the accumulation of NH_4^+, soil organic matter, NO^{3-}, C/N, available phosphorus and Cr, Mn, Co, Ni, Cu, Zn, Pb were significantly different in different soil depths. The nutrient accumulation in the surface soil layer led to the increase of primary productivity of community plants, while the nutrient in the lower soil layer was significantly less. Vegetation, defoliation, wood debris and dead roots are closely related to soil microorganisms and organic matter.

Due to the low level of soil nutrients and the decline of plant species diversity (Deng et al. 2018), soil nutrient dynamics should be taken into account in any study on the changes of plant species diversity after regional vegetation restoration. Previous studies have shown that changes in species diversity and spatial distribution of most tree species after vegetation restoration are closely related to combinations of multiple factors, including soil nutrients (Pingree & DeLuca 2018). Also, the ratio of soil nutrient supply is a factor that determines the change of plant species diversity in forest communities (Deng et al. 2018). However, functional diversity of nutrient strategies may lead to higher plant species diversity in barren soils (Pingree & DeLuca 2018). Species distribution of tree communities can respond to individual soil nutrients and seasonal drought (Deng et al. 2018). Soil nutrients also play an important role in the nutrient cycle of forest ecosystems and have a great impact on plant species, age and density. The response of soil nutrients to vegetation activities mainly depends on vegetation types, species diversity and restoration activities (Ye et al. 2019). Therefore, soil nutrient supply has an important impact on some important aspects of plant community structure, and soil nutrient has an important impact on plant diversity.

The effects of species diversity on productivity are affected by factors such as resource supply rate (Wang et al. 2008). Total biomass and species richness were negatively correlated. Diversity tended to increase with the increase of soil nutrients (Wang et al. 2008). The topsoil nutrient content of the community was higher than that of deep soil, and the Simpson diversity index of community species was only related to soil potassium (Tan et al. 2017). Therefore, there was a significant correlation between soil nutrients and richness index and diversity index in species diversity.

The results showed that the variables related to temperature, humidity, and precipitation are of great significance in explaining the changes in AGB. Increasing temperatures and new patterns of precipitation due to climate change result in

changes in the morphology, physiology, growth, reproduction, and biology of trees, all of which affect AGB (Stegen et al. 2011). In addition, enhancing the use efficiency of water and light resources could increase forest productivity (Van der Sande et al. 2017). Additionally, water deficiency has the most severe effect on the process of biomass formation (Van der Sande et al. 2017). Climate change is leading to increasing global temperatures and droughts in many areas, which have changed the nutrients in vegetation, AGB and belowground biomass (Peñuelas et al. 2016). Rainfall is highly correlated with the increase in tree stem diameter, which affects the accumulation of AGB, while rainfall together with temperature affects the AGB (Ogaya & Peñuelas 2007).

The AGB values of trees were estimated by the model, which showed that the average value for trees was 90% (Table 4). Therefore, these ML techniques are capable of describing the relationships between climate change and the AGB of trees. These results are similar to previous studies that found that ML-based data processing techniques are effective at modelling and predicting forest biomass (Were et al. 2015, Akkaya 2016). The best model was the ANN, which predicted the AGB with higher accuracy than the allometric equation. The ANFIS-based model is an effective technique for obtaining high-precision predictions of biomass with high heating value (Akkaya 2016). Furthermore, ANN and ANFIS can be used to establish a dynamic behavioural model (Were et al. 2015). Additionally, the models we proposed have achieved higher accuracy in testing compared with the above results. In summary, our current proposed models have great potential for estimating AGB. These models can be considered alternative tools for the traditional AGB models across regional or global scales for different vegetation types.

According to the performance of the various AGB models in this study, no model consistently outperformed the others for all AGB estimates. The GMDH model consistently produced relatively worse simulation results compared with the other models. This result may be partly due to the inherent limitations of the GMDH model, such as the choice of input parameters, multicollinearity and overfitting (Dou & Yang 2017). In addition, the effects of random errors in AGB observations on different time scales (e.g., daily, monthly, and yearly) should be taken into consideration when assessing the differences in predictions (Dou & Yang 2017). Systematic errors can also increase the uncertainty of the AGB estimates. Moreover, AGB is strongly influenced by the complex interactions between photosynthesis and photosynthetic efficiency (Huntingford et al. 2008). The selection of effective driving variables as model inputs could be used to further improve the predictive power of the model, especially for the AGB, and this is of significant importance for future work.

CONCLUSION

Our results show that the diversity of tree species in north-eastern forests is affected by soil nutrients. Also, climate change has a significant impact on the aboveground biomass of forests in northeast China. It shows that the high quality soil in the forest environment is a long-term process. Besides, it is difficult to interpret the field data of forest soil nutrient storage, especially when several factors affect the nutrient cycle. The soil type of Mt. Changbai is dark brown soil, and the climate type is warm and humid. There is a certain relationship between soil nutrient level and climatic conditions: in a hot and humid climate, surface vegetation is abundant, soil humus sources are more natural and fertile. In low temperature or arid climate, surface vegetation is difficult to grow, and soil humus sources are less natural than soil nutrients.

ACKNOWLEDGEMENTS

This study was conducted under the financial supports of The National Key Research and Development Program of China (2017YFC0504106), and the National Natural Science Foundation of China, China (31901306).

REFERENCES

Aherne, J., Posch, M., Forsius, M., Lehtonen, A. and Härkönen, K. 2012. Impacts of forest biomass removal on soil nutrient status under climate change: A catchment-based modelling study for Finland. Biogeochemistry, 107(1-3): 471-488.

Akkaya, E. 2016. ANFIS based prediction model for biomass heating value using proximate analysis components. Fuel, 80: 687-693.

Andrew, K., Anderson-Smith, A., Beard, K.H., Doucette-Riise, S., Mazzacavallo, M., Nolan, N.E., Anderson-Smith, A., Mazzacavallo, M., Ramirez, R.A. and Stevens J.R. 2014. Most soil trophic guilds increase plant growth. A meta-analytical review. Oikos, 123: 1409-1419.

Baselga, A. and Orme, C. 2012. Betapart: An R package for the study of beta diversity. Methods Ecol. Evol., 3: 808-812.

Baselga, A. 2012. The relationship between species replacement, dissimilarity derived from nestedness, and nestedness. Glob. Ecol. Biogeogr., 21: 1223-1232.

Berger, T.W., Duboc, O., Djukic, I., Tatzber, M., Gerbazek, M.H. and Zehetner, F. 2015. Decomposition of beech (*Fagus sylvatica*) and pine (*Pinus nigra*) litter along an alpine elevation gradient: Decay and nutrient release. Geoderma, 251-252: 92-104.

Brabcová, V., Tursová, M. and Baldrian, P. 2018. Nutrient content affects the turnover of fungal biomass in forest topsoil and the composition of associated microbial communities. Soil Biol. Biochem., 118: 187-198.

Camenzind, T., Hättenschwiler, S., Treseder, K.K., Lehmann, A. and Rillig, M.C. 2018. Nutrient limitation of soil microbial processes in tropical forests. Ecol. Monogr., 88: 4-21.

Carter, M.R. 1987. Physical properties of some Prince Edward island soils in relation to their tillage requirement and suitability for direct drilling. Can. J. Soil Sci., 67: 473-487.

Chang, N.B., Bai, K.X. and Chen, C.F. 2017. Integrating multisensor satellite data merging and image reconstruction in support of machine learning for better water quality management. J. Environ. Manag., 201: 227-240.

Chao, A., Chiu, C.H. and Jost, L. 2014a. Unifying species diversity, phylogenetic diversity, functional diversity, and related similarity and differentiation measures through hill numbers. Annu. Rev. Ecol. Evol. Syst., 45: 297-324.

Chao, A., Gotelli, N.J., Hsieh, T.C., Sander, E.L., Ma, K.H., Colwell, R.K. and Ellison, A.M. 2014b. Rarefaction and extrapolation with Hill numbers: A framework for sampling and estimation in species diversity studies. Ecol. Monogr., 84: 45-67.

Cline, L.C., Hobbie, S.E., Madritch, M.D., Buyarski, C.R., Tilman, D. and Cavender-Bares, J.M. 2018. Resource availability underlies the plant-fungal diversity relationship in a grassland ecosystem. Ecology, 99: 204-216.

Collin, A., Messier, C., Kembel, S.W. and Bélanger, N. 2018. Can sugar maple establish into the boreal forest? Insights from seedlings under various canopies in southern Quebec. Ecosphere, 9: 2022-2040.

De Deyn, G.B., Raaijmakers, C.E. and Van Der Putten, W.H. 2004. Plant community development is affected by nutrients and soil biota. J. Ecol., 92: 824-834.

Delgado-Baquerizo, M., Maestre, F.T., Gallardo, A., Bowker, M.A., Wallenstein, M.D., Quero, J.L., Ochoa, V., Gozalo, B., García-Gómez, M., Soliveres, S. and García-Palacios, P. 2013. Decoupling of soil nutrient cycles as a function of aridity in global drylands. Nature, 502: 672-676.

Deng, L., Han, Q.S., Zhang, C., Tang, Z.S. and Shangguan, Z.P. 2017a. Above-ground and below-ground biomass accumulation and carbon sequestration with *Caragana korshinskii* Kom plantation development. Land Degradation & Development, 28: 906-917.

Deng, L., Kim, D.G., Peng, C.H. and Shangguan, Z.P. 2018. Controls of soil and aggregate-associated organic carbon variations following natural vegetation restoration on the Loess Plateau in China. Land Degrad. Dev., 29: 3974-3984.

Deng, L., Liu, S., Kim, D.G., Peng, C., Sweeney, S. and Shangguan, Z 2017b. Past and future carbon sequestration benefits of China's grain for green program. Global Environmental Change-Human and Policy Dimensions, 47: 13-20.

Dou, X.M. and Yang, Y.G. 2017. Modelling and predicting carbon and water fluxes using data-driven techniques in a forest ecosystem. Forests, 8: 498.

Fu, L., Lei, X., Hu, Z., Zeng, W., Tang, S., Marshall, P., Cao, L., Song, X., Yu, L. and Liang, J. 2017. Integrating regional climate change into allometric equations for estimating tree aboveground biomass of Masson pine in China. Annals of Forest Science, 74: 42-57.

Hautier, Y., Tilman, D., Isbell, F., Seabloom, E.W., Borer, E.T. and Reich, P.B. 2015. Anthropogenic environmental changes affect ecosystem stability via biodiversity. Science, 6232: 336-340.

Hu, Y.S., Yao, X.Y. and Liu, Y.H.N. 2014. Stoichiometric traits of plant and soil in different forest succession stages in Changbai Mountain. Chinese J. Applied Ecol., 25(3): 632-638. (In Chinese)

Huntingford, C., Fisher, R.A., Mercado, L., Booth, B.B., Sitch, S., Harris, P.P., Cox, P.M., Jones, C.D., Betts, R.A., Malhi, Y. and Harris, G.R. 2008. Towards quantifying uncertainty in predictions of Amazon "dieback". Philosophical Transactions of the Royal Society B: Biological Sciences, 363: 1857-1864.

Jiang, F. 2016. Spatial heterogeneity of soil organic carbon and total nitrogen in deciduous broad-leaved forest and evergreen broad-leaved forest in central subtropical region. Central South Univer. Forestry Sci. Technol., 5: 132-139. (In Chinese)

Kang, H., Seely, B., Wang, G., Cai, Y., Innes, J., Zheng, D. and Chen P.L. 2017. Simulating the impact of climate change on the growth of Chinese fir plantations in Fujian province, China. New Zealand Journal of Forestry Science, 47(1): 20.

Kennedy, R.E., Ohmann, J., Gregory, M., Roberts, H., Yang, Z., Bell, D.M., Kane, V.H., Joseph Cohen, M.J., Warren, P., Scott, N., Neeti, L., Tara, H., Sam, K., Jonathan, T. M., David, L.P., James, B.J. and Rupert, S. 2018. An empirical, integrated forest biomass monitoring system. Environ. Res. Lett., 13: 25004.

Kilpeläinen, A., Strandman, H., Grönholm, T., Ikonen, V.P., Torssonen, P., Kellomäki, S. and Peltola, H. 2017. Effects of initial age structure of managed Norway spruce forest area on net climate impact of using forest biomass for energy. Bioenergy Research, 10: 499-508.

Kulmatiski, A., Beard, K.H., Stevens, J.R. and Cobbold, S.M. 2008. Plant-soil feedbacks: A meta-analytical review. Eco. Lett., 11: 980-992.

Lal, M.K. and Pandey, R. 2017. Interactive effect of elevated (CO_2) on biomass and carbohydrate partitioning under phosphorus stress. Int. J. Curr. Microbiol. App. Sci., 6: 2966-2977.

Laliberté, B., Wardle, D.A. and Klironomos, J. 2017. Soil fertility shapes belowground food webs across a regional climate gradient. Eco. Lett., 20: 1273-1284.

Le Toan, T., Quegan, S., Davidson, M.W.J., Balzter, H., Paillou, P., Papathanassiou, K., Plummer, S., Rocca, F., Saatchi, S., Shugart, H. and Ulander, L. 2011. The BIOMASS mission: Mapping global forest biomass to better understand the terrestrial carbon cycle. Remote Sensing of Environment, 115: 2850-2860.

Li, H., Leng, W., Zhou, Y.B., Chen, F.D., Xiu, Z.L. and Yang, D.Z. 2014. Evaluation models for soil nutrient based on support vector machine and artificial neural networks. Sci. World J., ID:478569.

Lu, K., Yang, X., Gielen, G., Bolan, N., Ok, Y.S., Niazi, N.K., Xu, S., Yuan, G., Chen, X., Zhang, X. and Liu, D. 2017. Effect of bamboo and rice straw biochars on the mobility and redistribution of heavy metals (Cd, Cu, Pb and Zn) in contaminated soil. J. Environ. Manag., 186: 285-292.

Mackay, J.E., Cavagnaro, T.R., Stöver, D.S.M., Macdonald, L.M., Grønlund, M. and Jakobsen, I. 2017. A key role for arbuscular mycorrhiza in plant acquisition of P from sewage sludge recycled to soil. Soil Biol. Biochem., 115: 11-20.

Netzer, F., Schmid, C., Herschbach, C. and Rennenberg, H. 2017. Phosphorus-nutrition of European beech (*Fagus sylvatica* L) during annual growth depends on tree age and P-availability in the soil. Environ. Experi. Bot., 137: 194-207.

Ogaya, R. and Peñuelas, J. 2007. Tree growth, mortality, and above-ground biomass accumulation in a holm oak forest under a five-year experimental field drought. Plant Ecol., 189: 291-299.

Ottoy, S., De Vos, B., Sindayihebura, A., Hermy, M. and Van Orshoven, J. 2017. Assessing soil organic carbon stocks under current and potential forest cover using digital soil mapping and spatial generalisation. Ecological Indicators, 77: 139-150.

Peñuelas, J., Sardans, J., Filella, I., Estiarte, M., Llusià, J., Ogaya, R., Carnicer, J., Bartrons, M., Rivas-Ubach, A., Grau, O. and Peguero, G. 2016. Assessment of the impacts of climate change on Mediterranean terrestrial ecosytems based on data from field experiments and long-term monitored field gradients in Catalonia. Environmental and Experimental Botany, 152: 49-59.

Petus, C., Devlin, M., da Silva, E.T., Lewis, S., Waterhouse, J., Wenger, A., Bainbridge, Z. and Tracey, D. 2018. Defining wet season water quality target concentrations for ecosystem conservation using empirical light attenuation models: A case study in the Great Barrier Reef (Australia). J. Environ. Manag., 213: 451-466.

Pingree, M.R.A. and DeLuca, T.H. 2018. The influence of fire history on soil nutrients and vegetation cover in mixed severity fire regime forests of the eastern Olympic Peninsula, Washington, USA. Forest. Ecol. Manag., 422: 95-107.

R. Development Core Team 2017. A Language and Environment for Statistical Computing Vienna. R Foundation for Statistical Computing.

Sardans, J., Bartrons, M., Margalef, O., Gargallo-Garriga, A., Janssens, I.A., Ciais, P., Obersteiner, M., Sigurdsson, B.D., Chen, H.Y. and Peñuelas, J. 2017. Plant invasion is associated with higher plant-soil nutrient concentrations in nutrient-poor environments. Glob. Change Biol., 23: 1282-1291.

Schulz, H. and Glaser, B. 2012. Effects of biochar compared to organic and inorganic fertilizers on soil quality and plant growth in a greenhouse experiment. J. Plant Nutrition Soil Sci., 175: 410-422.

Soares, S.G. and Araújo, R. 2016. An adaptive ensemble of on-line extreme learning machines with variable forgetting factor for dynamic system prediction. Neurocomputing, 171: 693-707.

Stegen, J.C., Swenson, N.G., Enquist, B.J., White, E.P., Phillips, O.L., Jørgensen, P.M., Weiser, M.D., Monteagudo Mendoza, A. and Núñez Vargas, P. 2011. Variation in above-ground forest biomass across broad climatic gradients. Global Ecology and Biogeography, 20: 744-754.

Tan, S.D., Yang, Y.T., Chen, B., Wen, L. and Liu, H.B. 2017. Analysis of correlation between soil nutrients and species diversity in typical communities of Dawei Mountain. J. Zhejiang Agricul. Sci., 5: 887-891. (In Chinese)

Valentín-Vargas, A., Root, R.A., Neilson, J.W., Chorover, J. and Maier, R.M. 2014. Environmental factors influencing the structural dynamics of soil microbial communities during assisted phytostabilization of acid-generating mine tailings: A Mesocosm Experiment. Sci. Total Environ., 0: 314-324.

van der Sande, M.T., Peña-Claros, M., Ascarrunz, N., Arets, E.J., Licona, J.C., Toledo, M. and Poorter, L. 2017. Abiotic and biotic drivers of biomass change in a Neotropical forest. J. Ecol., 105: 1223-1234.

Waldrop, M.P., Holloway, J.M., Smith, D.B., Goldhaber, M.B., Drenovsky, R.E., Scow, K.M., Dick, R., Howard, D., Wylie, B. and Grace, J.B. 2017. The interacting roles of climate, soils, and plant production on soil microbial communities at a continental scale. Ecology, 98: 1957-1967.

Wang, C.T., Long, R.J., Cao, G.M., Wang, Q.L., Jing, Z.C. and Shi, J.J. 2008. The relationship between soil nutrients and diversity productivity of different type grasslands in Alpine Meadow. Chinese J. Soil Sci., 39(1): 1-8. (In Chinese)

Wang, J., Sun, Z., Hui, D., Yang, L., Wang, F., Liu, N. and Ren, H. 2018. Responses of seedling performance to altered seasonal precipitation in a secondary tropical forest, southern China. For. Ecol. Manag., 410: 27-34.

Wang, W.J., He, H.S., Thompson, I.I.I.F.R., Fraser, J.S. and Dijak, W.D. 2017. Changes in forest biomass and tree species distribution under climate change in the north-eastern United States. Landscape Ecology, 32: 1399-1413.

Were, K., Bui, D.T., Dick, Ø.B. and Singh, B.R. 2015. A comparative assessment of support vector regression, artificial neural networks, and random forests for predicting and mapping soil organic carbon stocks across an afromontane landscape. Ecol. Indic., 52: 394-403.

Yang, X., Cao, J., Dong, M.X. and Ma, X.J. 2008. Effects of external tree species *Larix japonica* on forest soil quality and bacterial diversity. Chinese J. Applied Ecol., 10: 2109-2116. (In Chinese)

Ye, L.P., Fang, L.C., Shi, Z.H., Deng, L. and Tan, W.F. 2019. Spatio-temporal dynamics of soil moisture driven by 'Grain for Green' program on the Loess Plateau, China. Agr. Ecosyst. Environ., 269: 204-214.

Yousefpour, R., Augustynczik, A.L.D., Reyer, C.P.O., Lasch-Born, P., Suckow, F. and Hanewinkel, M. 2018. Realizing mitigation efficiency of European commercial forests by climate smart forestry. Scientific Reports, 8: 1-11.

Zhang, Q.F., You, W.H. and Song, Y.C. 1997. Influence of plant community succession on soil physical properties in Tiantong Forest Park, Zhejiang Province. J. Plant Resour. and Environ., 6(2): 36-40. (In Chinese)

Nature Environment and Pollution Technology
An International Quarterly Scientific Journal

p-ISSN: 0972-6268
(Print copies up to 2016)
e-ISSN: 2395-3454

Vol. 19 | No. 2 | pp. 493-510 | 2020

Original Research Paper

https://doi.org/10.46488/NEPT.2020.v19i02.006

Open Access Journal

Characterizing the Intensity and Dynamics Change Relationship Between the Land-Use and Landscape Pattern in the Ordos Bojiang Basin

Harrison Odion Ikhumhen*(**)†, Tianxin Li*(**) and Nametso Matomela*(**)

*School of Energy and Environmental Engineering, University of Science and Technology Beijing, 30 Xueyuan Road, Haidian District, 100083, Beijing, China

**Beijing Key Laboratory of Resource-oriented Treatment of Industrial Pollutants, Beijing, 100083, PR China

†Corresponding author: Harrison Odion Ikhumhen; harryspk@yahoo.com

Nat. Env. & Poll. Tech.
Website: www.neptjournal.com

Received: 09-07-2019
Accepted: 19-09-2019

Key Words:
Land Use; Landscape pattern; Transition intensity; Bojiang Lake; Pontius model; Anthropogenic activities

ABSTRACT

This paper seeks to analyse the present and future land-use change transition intensity (using Pontius intensity model) and landscape pattern using landscape metrics to investigate the relationship between the land cover regions, landscape pattern and the changes in the size of Bojiang lake in Ordos basin from 1987-2017. The accelerated changes in each land use region from 1987 and 2017 subsequently led to changes in landscape pattern. The changes experienced within 1987 and 2017 including the future changes indicated that the grassland and sparsely vegetated region increased significantly, dominating the study region which however indicated an increase in anthropogenic activities like agricultural activities in the study region. Based on our observation in this study, the change in each land use region although showed a significant relationship with the change in water region including Bojiang lake, other external factors also contributed to the changes in the size of the lake.

INTRODUCTION

Wetland is referred to a very significant ecological environment and also one of the most important living environments known to man. It is responsible for controlling our ecological environment including plant and animal species with a global area coverage of only 6.2-7.6% of the entire world's land surface (Finlayson 2012, Lehner & Döll 2004). Wetland plays a major role in ensuring the provision of certain ecological services such as ground and freshwater supply, biodiversity, flood and drought mitigation, erosion control and mitigation of water pollution (Bolund & Hunhammar1999, Zedler & Kercher 2005, Ramsar 2007, Alabisky et al. 2011). Within the timeframe of 10 years between 1990 and 2000, about 30% of China's natural wetland has been lost and in the past 50 years, over 50% of wetlands in China have been lost (Guo et al. 1990, Ren et al. 2007, Cyranoski 2009). The driving forces for this decrement experienced in the wetlands are believed to be the changes in climate and increased water extractions from anthropogenic activities. For instance, the continuous drought experienced in the popularly known Yangtze river system and the southwest China's wetland area is believed to possibly result in the decline in the wetland areas in those regions (Cao et al. 2012, Tian et al. 2016). The development of remote sensing technology has been advantageous in ensuring proper evaluation of the ecological health of the environment (Cao 2013). For instance, to monitor wetland changes, the multi-spectral and multi-temporal images (Landsat images) have proven to be quite advantageous because of the possibility to quickly differentiate the Spatio-temporal quality of a landcover region with high accuracy especially in cases of worse climatic conditions such as droughts (Cao et al. 2012) and floods (Hereher 2010, Tian et al. 2016). Land-use change and global processes like climate change, increased population, urbanization, land degradation etc. are interrelated (Kertész et al. 2019). With the continuous growth in population globally (different rates at the different locations in the world) the demand for space, food and infrastructure also increases which requires changes in the land use structure (Szabó et al. 2016). The intensification of the urban growth experienced globally is accompanied by a large increment in the consumption of natural resources, increased habitat fragmentation and ecological disturbance (biodiversity loss) (Foley et al. 2005, Lawler et al. 2014). The establishment of an efficient and effective strategy to manage and conserve the present and future land use is based on adequate knowledge of the land use process (Al-doski et al. 2013, Alo & Pontius 2008).

Shallow assessment of land-use change might not reveal the most significant land-use change dominancy signals which might lead to insufficient management approaches and conservative measures (Pontius et al. 2004). Several studies made use of the land-use transition matrices to compare changes between two different time intervals. The studies however rarely assessed the process behind the change in landscape pattern. The identification of these processes allows us to link the observed land-use transitions to the possible causes (Pontius et al. 2004, Teixeria et al. 2014, Braimoh 2006). Several studies have investigated the relationship between landscape pattern changes and its effect on the ecological process (Dadashpoor 2018, Echeverría et al. 2012, Nagendra et al. 2004, Schröder & Seppelt 2006, Lausch et al. 2015, Tyre et al. 2006), some other have studied just the changes in landscape patterns (Abdullah & Nakagoshi 2006, Cabral & Costa 2017, Frondoni et al. 2011, Hladnik 2005, Kienast et al. 2015, Wan et al. 2015), some scholars also studied the relationship between changes in landscape pattern and driving forces and urbanization growth (Bürgi et al. 2004, Dadashpoor 2018, Aguilera et al. 2011, Chen et al. 2014, Luck & Wu 2002, Reis et al. 2015). However, there are very few studies to analyse the magnitude and intensity of the present and future land-use change and its relationship with the landscape pattern changes and ecological process. In our study, we will be focusing on finding out which land use region are intensively targeted or avoided and analyse the relationship with the degraded wetland from 1987-2017 and also in the next 100 years. We mainly targeted the vegetative regions and the water region to reveal the details of the water reduction and expansion of the vegetative region including the underlying process, dynamic trends and possible driving forces. To the best of our knowledge, this study will be the first to apply the transition intensity approach in the popularly known Ordos Reserve basin whose lake has been going through a series of area reduction.

The following research questions were investigated in this study.

- What are the main LULC types and the transition intensity of the area coverage in the Ordos Catchment from 1987-2017 and the predicted future (2017-2117)?
- What are the changes in landscape pattern and its relationship with the LULC regions?
- What is the influence of the changes in land use and landscape pattern on the changes in the water size?

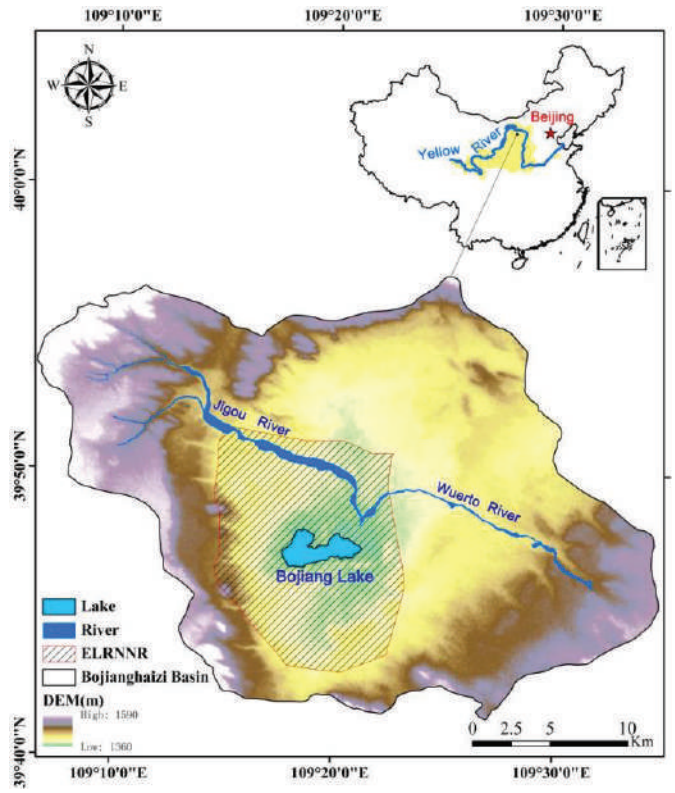

Fig. 1: Regional location of Ordos National Nature Reserve (Kang 2017).

DATA AND METHODOLOGY

Study Area

Ordos National Nature Reserve located in Ordos city of Inner Mongolia Autonomous Region in China is about 45km west of Dongsheng District with an area coverage of 155.66km^2 (situated in latitude 39°41'40'' to 39° 56' 2'' and longitude 109° 6' 30'' to 109° 32' 50''). The reserve is located in the central-southern section of the Bojiang lake basin with a drainage area coverage of about 640 km^2. The annual mean temperature from 1971-2000 of the reserve is approximately 6.16^{0}C. The annual mean precipitation, on the other hand, is approximately 381.2mm in this region, more than half of the precipitation falls between the period of July and August. Bojiang lake is situated in the central basin with Jigou River and Wuertu River flowing through it (Fig. 1). The major vegetation types in this reserve are grasslands and shrubs. According to Liang et al. (2011), Bojiang lake's source of water is the water derived from precipitation and lateral run-off in the closed basin accounting for 22% of the total water recharge from 1996 to 2005. Because of the significance of this wetland to Ordos reserve, more attention should be paid towards its protection which is why it is the only wetland in the semi-arid and arid region of China to be included in the Ramsar list of globally important wetlands. Larus Relictus (Relict Gull) is a species that according to the Convention of International Trade in Endangered Species of Wild Fauna and Flora (CITES) and the Convention on the Conservation of Migratory Species (CMS) is recently in urgent need of protection this makes this nature reserve a very important reserve solely targeted towards the protection of this specie (Liu et al. 2008).

Data

In this research, the remote sensing images for 1987, 1995, 2003, 2010, 2017 were obtained via the United States Geological Survey's (USGS) database (http://earthexplorer.usgs.gov/). The downloaded images were the TM/ETM+ and the OLI with a resolution of 30m which already had some standard pre-processing done by the USGS (https://landsat.usgs.gov/landsat-processing-details) which we considered to be sufficient for the intended analysis in this paper (Mwangi et al. 2017, Phiri & Morgenroth 2017, Young et al. 2017). The images were chosen during the peak vegetation coverage period of summer (August) with minimal cloud coverage. An interval of approximately 8 years was selected as it was considered quite appropriate in tracking the dynamic change in landscape and proper management of the amount of data involved for analysis.

Methodology

Land use classification: In this paper, supervised classification using maximum likelihood algorithm was adopted using the ArcGIS 10.5 software which enabled us to categorize the land cover regions into 5 different categories such as grassland/shrub, highly vegetated, sparsely vegetated, barren soil and water region (Fig. 2 and Table 1). According to Lu & Weng (2007), image classification comprises of several stages such as the selection of a suitable classification method, processing of post-classification images, and accuracy assessment of the map. A geometric image correction was first carried out to reduce the presence of displacement errors, atmospheric calibrations (atmospheric corrections) were also carried out to eliminate the presence of atmospheric effects on each of the image.

A stratified random sampling approach was applied for the assessment of the land use classification accuracy. To measure the extent of landcover accuracy, the Kappa test was applied due to its ability to not only analyse the diagonal elements but all the elements in the land use map confusion matrix (Rosenfield and Fitzpatric-Lins 1986). After the extraction of the land use map using ArcGIS, transfer matrix post-classification change technique was applied to analyse the dynamic changes of the land usage during the period of study.

In this research, the following equation was used;

$$\%\ Land\ Use\ Change = \frac{Area_{i\ Year\ x} - Area_{i\ year\ (x+1)}}{\sum_{i=1}^{n} Area_{i\ year\ x}} \times 100 \quad ...(1)$$

Table 1: Description of the classified regions of the reserve.

Classified Regions	Description of the Classified Region
Grassland/Shrubs	Mixed grasses and trees, shrub plants, agricultural land, aquatic vegetation and wetland vegetation.
Highly Vegetated	Healthy trees, afforested trees, mixed forest,
Sparsely Vegetated	Little to no vegetation land, uncultivated agricultural lands.
Barren Soil	Open soil with no vegetations, lakeshore free of vegetation, road networks, build-up areas.
Water	Lakes

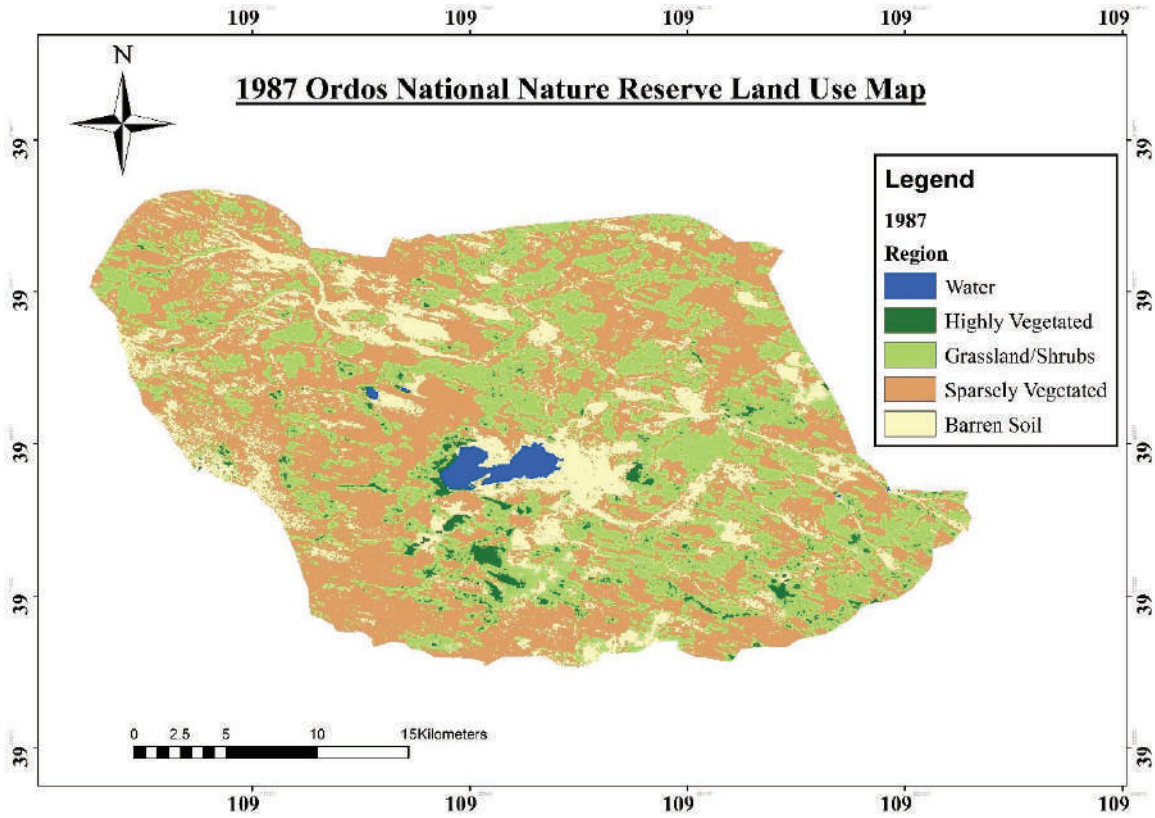

Fig. 2: Land use regions for Ordos catchment in 1987.

$$\%\ Land\ Use\ Coverage = \frac{Area_{i\ Year\ x}}{\sum_{i=1}^{n} Area_{i\ year\ x}} \times 100 \quad \ldots(2)$$

$$Land\ Use\ Area\ Change = Area_{i\ year\ (x+1)} - Area_{i\ year\ x} \quad \ldots(3)$$

Where, $Area_{i\ Year\ x}$ is the land use area *i* at the initial date; while $Area_{i\ Year\ (x+1)}$ is the land-use area *i* in the second period; $\sum_{i=1}^{n} Area_{i\ year\ x}$ is the total land-use area at the initial date.

Land-use transition intensity analysis: To analyse the dynamics of land-use change, intensity and landscape patterns, the land-use transition intensity analysis was performed using the framework of (Aldwaik & Pontius 2012). First, to quantify the land-use change over time, the transitional matrix was applied. A transitional matrix is a two-dimensional table in which land use categories at the earlier time interval are displayed in rows while categories at the later time intervals are displayed in columns (Mallinis et al. 2014, Aldwaik & Pontius 2012). The transitional matrix in this paper was made for each interval (1987-1995, 1995-2003, 2003-2010 and 2010-2017). The method allows us to compute and compare the observed intensities of the changes in land use regions with uniform intensities. For each category gain or loss, the transition level analysis was used to compare the observed intensity of each transition with a hypothetical uniform transition that would occur if there was a uniform distribution of the transition between land use categories. Equations 4 and 5 were used to analyse the transition level analysis from an arbitrary category i to the gaining category n (Aldwaik & Pontius 2012, Pontius et al. 2013) hence identifying which land use category is intensively avoided or targeted by either the loss or gain of a particular category. Equation 4 calculated observed intensity R_{tin} of annual transition category *i* to n for a given time interval. The observed intensity R_{tin} was compared with the uniform intensity W_{tn} calculated in equation 5 if the R_{tin}>W_{tn}, then gain of n is considered to target *i*.

$$R_{tin} = \frac{Size\ of\ annual\ transition\ from\ i\ to\ n\ during\ (Y_t, Y_{t+1})}{size\ of\ i\ at\ t} = \frac{C_{tin}/(Y_{t+1} - Y_t)}{\sum_{j=1}^{J} C_{tij}} 100\% \quad \ldots(4)$$

$$W_{tn} = \frac{size\ of\ annual\ gain\ of\ n\ during\ (Y_t, Y_{t+1})}{size\ of\ not\ n\ at\ t} = \frac{\left[\left(\sum_{i=1}^{I} C_{tin}\right) - C_{tnn}\right]/(Y_{t+1} - Y_t)}{\sum_{j=1}^{J}\left[\left(\sum_{i=1}^{I} C_{tij}\right) - C_{tnj}\right]} 100\% \quad \ldots(5)$$

Where, Y_t = Year at time point t; t = Index for the initial time point of interval (Y_t, Y_{t+1}); i = Index for a category at

an interval's initial time point; j = Index for a category at an interval's final time point; n = Index for the gaining category for the selected transition; C_{tij} = Number of pixels that transition from category i to category j during the interval (Y_t, Y_{t+1}); C_{tin} = Number of pixels that transition from category i to category n during the interval (Y_t, Y_{t+1}); C_{tnn} = Number of pixels that remained category n during the interval (Y_t, Y_{t+1}); J = Number of categories.

Error analysis: To estimate the minimum errors in maps accounting for the difference in two maps from the same extent but different time intervals, (Aldwaik & Pontius 2013) proposed a framework best suited for analysing the error. This error analysis method assesses the strength of the changes identified through the transition intensity analysis. The uniform hypothesis assumes a uniform change intensity with no temporal change in the map. In this analysis, two types of error were estimated (omission and commission error). The commission error indicates that the observed intensity of change > the uniform hypothesized intensity. In the case of omission, the reverse is the case. Both errors are the difference between the observed change and uniform change. Hence, a larger omission and commission error indicates stronger evidence against the null hypothesis of uniform change which also means that there is a great possibility the difference in the maps are not necessarily due to classification errors but rather an actual change in the land use.

$$Commission\ error\ of\ Category\ i\ at\ t = E_{tin}^{R} = \frac{\left(\sum_{i=1}^{J} C_{tij}\right)(Y_{t+1}-Y_t)(R_{tin}-W_{tn})}{100\%-(Y_{t+1}-Y_t)W_{tn}}100\% \quad \ldots(6)$$

$$Commission\ of\ i\ intensity\ at\ t = \frac{E_{tin}^{R}}{C_{tin}}100\% \quad \ldots(7)$$

$$Omission\ error\ of\ Category\ i\ at\ t = O_{tin}^{R} = \frac{\left(\sum_{j=1}^{J} C_{tij}\right)(Y_{t+1}-Y_t)(W_{tn}-R_{tin})}{100\%-(Y_{t+1}-Y_t)W_{tn}}100\% \quad \ldots(8)$$

$$Omission\ of\ category\ i\ intensity\ at\ t = \frac{O_{tin}^{R}}{O_{tin}^{R}+C_{tin}}100\% \quad \ldots(9)$$

Where, E_{tin}^{R}, = number of elements that are observed transitions from category *i* to category *n* during interval [Y_t, Y_{t+1}] but are hypothesized transitions from a non-*i* category to category *n*, O_{tin}^{R} = number of elements that are observed transitions from a non-*i* category to category n during the interval [Y_t, Y_{t+1}] but are hypothesized transitions from a category *i* to category n.

Prediction analysis: In this paper, the prediction analysis was carried through the application of both Markov chain model and Cellular Automata (CA) methods using the CA-Markov model. Both the Markov and CA models are discrete dynamical models of time and status (Liu et al. 2008). The CA possess a powerful ability to simulate spatio-temporal changes of complex spatial systems (Sang et al. 2011), while the Markov model as earlier discusses focus mainly on the simulation and prediction of land cover changes. In this study both the CA and Markov model (CA-Markov model) was applied which is an integrated model that combines the spatial simulation ability of CA and the prediction ability of Markov to analyse and monitor the change evolution of the Ordos Basin. In this paper, based on both models we were able to simulate and predict the changes in the Ordos basin using IDRIS Selva (version 17.02) software under the CA-Markov Model (Eastman 2003).

Spatial pattern estimation: The analysis of the spatial pattern variations of the different regional landscape was used to reveal the dynamic changes on the wetland over time (YuhaiBao et al. 2011). For this study, we estimated the landscape metrics with one of the most popular spatial pattern analysis programs designed specifically for this purpose, FRAGSTAT Software (FRAGSTST 4.2) (Mcgarigal et al. 2000). The FRAGSTAT software offers a diverse choice of landscape metrics and has been greatly applied for the quantification of landscape structure. This approach is mainly used by ecologist and decision-makers in analysing the level of fragmentation of landscape and also to characterize the components of those landscapes. Considering the current situation of the Ordos basin's classification system, to analyse

Table 2: Landscape spatial pattern metrics details.

Metrics	Index	Index Name	Unit
Patch	NP	Number of Patches	n (n≥1)
	PD	Patch Density	n/100Ha
	MPS	Mean Patch Size (Area Mean)	Ha
Edge	TE	Total Edge	m
	ED	Edge Density	m/Ha
Shape	MSI	Mean Shape Index	Ha
Diversity	SHDI	Shannon's Diversity Index	-
	SHEI	Shannon's Evenness Index	-

the landscape pattern of the study site, we selected four metrics shown in Table 2. These metrics comprises of the Patch metrics, shape metrics, edge metrics, and diversity index.

RESULTS

Land Use Change

This study area was aggregated into different land-use regions as shown in Fig. 2. The kappa's coefficient accuracy assessment carried out on the classified images in this study recorded a value between 88 and 99% which indicates a very good agreement among the referenced data and the classified data. The result in Fig. 3 and 4A showed that over the years 1987 to 2017 significant changes occurred in the grassland region and the water region over the year 1987-2017. Within this period, the grassland region emerged the most dominant land cover type covering a total area of 338.75km^2 in 2017 (52.88%) the sparsely vegetated region on the other hand also covered a considerable amount of the area covering 34.89% in 2017. The proportion of the water and the highly vegetated region were the smallest compared to the other land cover regions. However, the water region on the other had experienced a dramatic decline in size from 1.13% to 0.36% during the year 1987-2017.

The upsurge of the grassland region is a clear indication of the increased anthropogenic activities in the region. Based on the examination of the other land use region, in 2017 all other regions except the grassland region showed a reduction in area. The area of the highly vegetated, barren soil and the sparsely vegetated region reduced by 1.73, 10.14, and 34.89% respectively (Fig. 3). The result of the transfer matrix showed that the conversion of all the land-use regions was a two-way conversion with one region changing to another land use region and vice versa.

Prediction analysis: From the 100 years prediction, the result in Fig. 4A and 4B showed that although the grassland region reduced by 5.29% in 2047, it was still observed to be the most dominant region in the study site. while the grassland region reduced slightly in 2047 followed by a continuous increase in the area till 2117, the sparsely vegetated region, on the other hand, showed a slight increase in area from 2017-2047 followed by a continuous decrease in area. The other land cover regions decreased continuously from 2017-2117.

Relationship between Bojiang lake and land-use change: Bojiang lake during the 30 years of study drastically reduced in size losing over 70% of its area to another region. Fig. 3 and 4 showed that while other regions reduced in size the grassland region contrasted in area change. The correlation and regression analysis carried out between Bojiang lake and the land cover regions showed that the changes in grassland region were statistically significant with p-values <0.05 while other regions proved to be not statistically significant. Based on this result of comparison between the change in Bojiang lake and the land cover change, and the effect of the variation

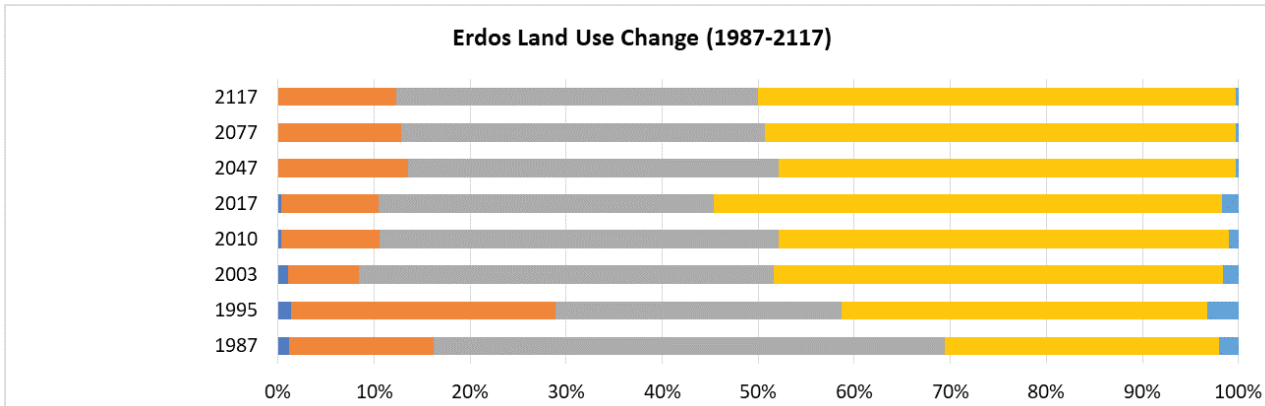

	1987	1995	2003	2010	2017	2047	2077	2117
Water Km2	7.24	8.56	6.55	2.22	2.34	0.27	0.05	0.00
Barren Soil Km2	96.59	176.59	47.24	65.16	64.95	86.14	81.93	78.78
Sparsely Vegetated Km2	341.16	190.79	276.58	266.33	223.48	247.68	242.52	241.27
Grassland/Shrub Km2	182.87	243.54	299.92	300.6	338.75	304.45	313.43	318.29
Highly Vegetated Km2	12.7	21.08	10.28	6.27	11.08	1.89	1.82	1.74

Fig. 3: Ordos Basin's regional area coverage from 1987 to 2117.

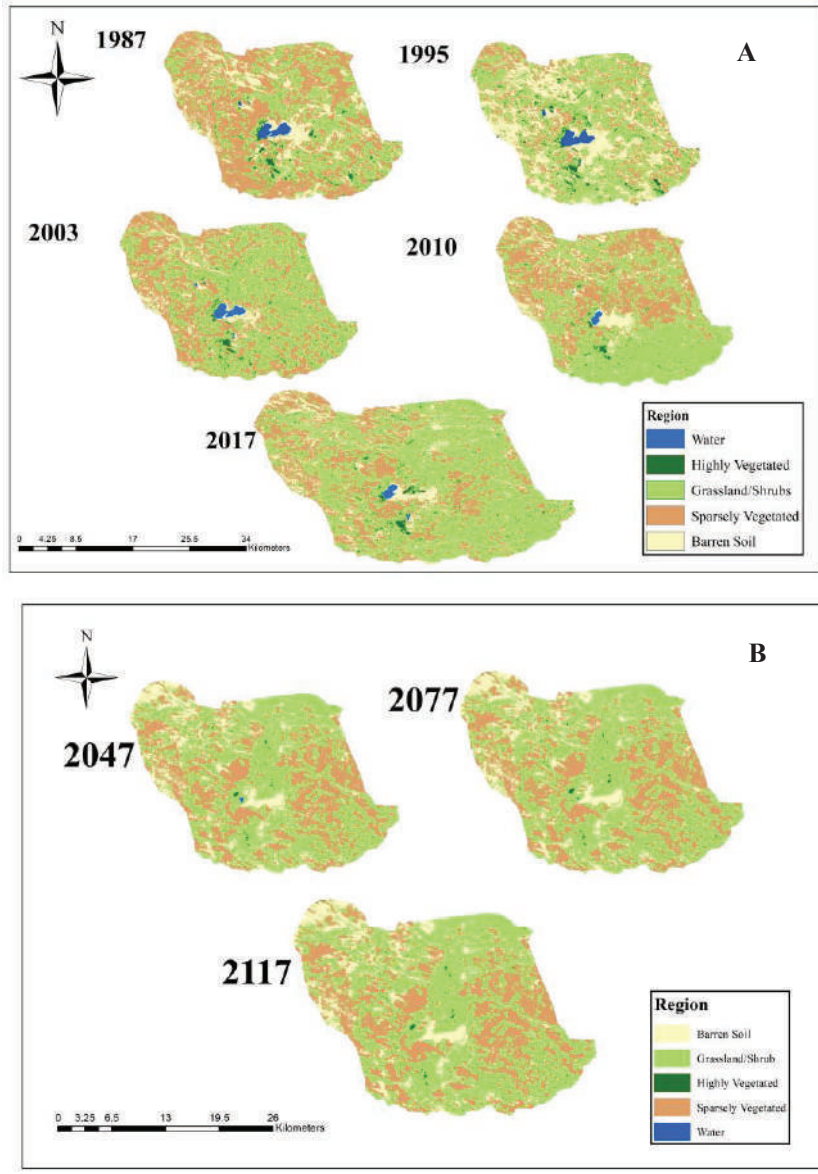

Fig. 4: Ordos Basin land-use change (A) 1987-2017, (B) 2047-2117.

between Bojiang lake and grassland region showed that the continuous increase in grassland region was closely related to the drastic reduction in the lake size.

Landscape pattern analysis: Landscape pattern of Ordos basin were analysed at the landscape and class level through four metrics (shape, patch, edge, and the diversity index). The parameter used were the Patch Density, Area Mean (Mean Patch size (MPS)), Edge Density (ED), Mean Shape Index (MSI), Shannon's diversity index and Shannon's evenness index (SHDI and SHEI). As shown in figure 5A, the result indicated changes in the entire landscape PD, MPS, ED, MSI, SHDI and SHEI from 1987 to 2017. MSI (1.26 to 1.25), MPS (5.6 to 3.7km^2), SHDI (1.1 to 1.02) and SHEI (0.68 to 0.63) showed reduction while the PD (17.8 to 26.7) and ED (104.2 to 129.3) increased hence indicating heterogeneity towards an increased level of fragmentation in the landscape pattern of the Ordos Basin. From the result of the landscape pattern analysis of the 100 years predicted image, we observed that the heterogeneity continued indicating a continued increase in the fragmentation level with the ED (129.3 to 145.9), MPS (3.7 to 7.9), MSI (1.25 to 1.5) increased while, PD (26.7 to 12.6), SHDI (1.02 to 0.99) and SHEI (0.638 to 0.62) reduced.

At the class level shown in Figure 5B, all the regions showed different patterns compared to each other and from the whole pattern of landscape, the grassland and sparsely vegetated region both showed more aggregation over the 3-decade period of study.

Relationship between the landscape pattern change and the land-use change: The land-use changes share a relationship with the changes in the landscape pattern metrics. In Table 3, the coefficient value of each land cover regions represents the intensity of the effect where the consistency or difference in changes between the landscape metrics and the land cover regions are indicated with a positive or negative sign. With the regression analysis proving to be statistically significant having a p-value equal to 0.000 which is <0.05, the comparison of the effect between the land-use regions showed that the change in the sparsely vegetated region proved to possess the highest effect on PD (+5.3) and ED (14.14), this region had the most contrasting effect in the

Table 3: Intensity of land-use change in landscape patterns.

Metrics	Landscape Change	Class level change	P-Value
PD	8.9391	grassland=1.03, sparsely veg=5.3, highly vegetated=1.2, barren soil=1.35, water=-0.014	0.000
ED	25.1631	grassland=37.98, sparsely veg=14.14, highly vegetated=1.89, barren soil=-3.3, water=-0.35	0.000
MPS	-1.873	grassland=3.08, sparsely veg=-8.08, highly vegetated=-0.57, barren soil=-1.01, water=-15.01	0.000
MSI	-0.0124	grassland=-0.09, sparsely veg=0.07, highly vegetated=-0.05, barren soil=-0.018, water=-0.11	0.000

Table 4: Land use transition between vegetative regions (Categories).

Transition to Grassland								
	1987-1995		1995-2003		2003-2010		2010-2017	
	UI=3.05		UI=3.57		UI=4.68		UI=4.92	
Losing Categories	TI	EI	TI	EI	TI	EI	TI	EI
Barren Soil	1.51	**57.19**	1.78	**58.58**	1.71	**72.13**	1.73	**73.82**
Highly Vegetated	(5.06)	52.56	(7.88)	76.51	(8.52)	67.00	(5.56)	17.60
Sparsely Vegetated	(3.46)	15.98	(4.94)	38.80	(5.16)	13.81	(5.73)	21.67
Water	0.00	**99.94**	0.28	**94.23**	0.55	**91.82**	0.10	**98.69**
Transition to Highly Vegetated								
	1987-1995		1995-2003		2003-2010		2010-2017	
	UI=0.28		UI=0.09		UI=0.06		UI=0.16	
Losing Categories	TI	EI	TI	EI	TI	EI	TI	EI
Barren Soil	0.10	**65.75**	0.01	**91.62**	0.02	**60.08**	(0.30)	48.75
Grassland	(0.85)	68.23	(0.20)	57.25	(0.11)	46.34	(0.23)	31.09
Sparsely Vegetated	0.04	**87.61**	0.01	**88.02**	0.01	**81.23**	0.04	**72.38**
Water	0.13	**55.11**	(0.15)	42.56	0.02	**68.40**	0.02	**87.42**
Transition to Sparsely vegetated								
	1987-1995		1995-2003		2003-2010		2010-2017	
	UI=1.82		UI=4.51		UI=4.48		UI=3.15	
Losing Categories	TI	EI	TI	EI	TI	EI	TI	EI
Barren Soil	(1.91)	5.79	(7.79)	65.87	3.64	**25.33**	(3.58)	15.40
Grassland	(1.92)	6.34	2.59	**53.75**	(4.83)	10.55	3.15	**0.17**
Highly Vegetated	0.59	**70.60**	0.82	**87.53**	0.85	**86.23**	0.15	**96.24**
Water	0.00	**99.93**	0.42	**93.82**	0.07	**98.92**	0.03	**99.26**

UI= Uniform intensity (% of other categories, excluding the concerned category); TI= Transition intensity (Parentheses values indicate targeted categories for loss or gain while non-parenthesis indicates the categories was avoided by the change); EI= Error Intensity (Bold values are omission, non-bold values are commission).

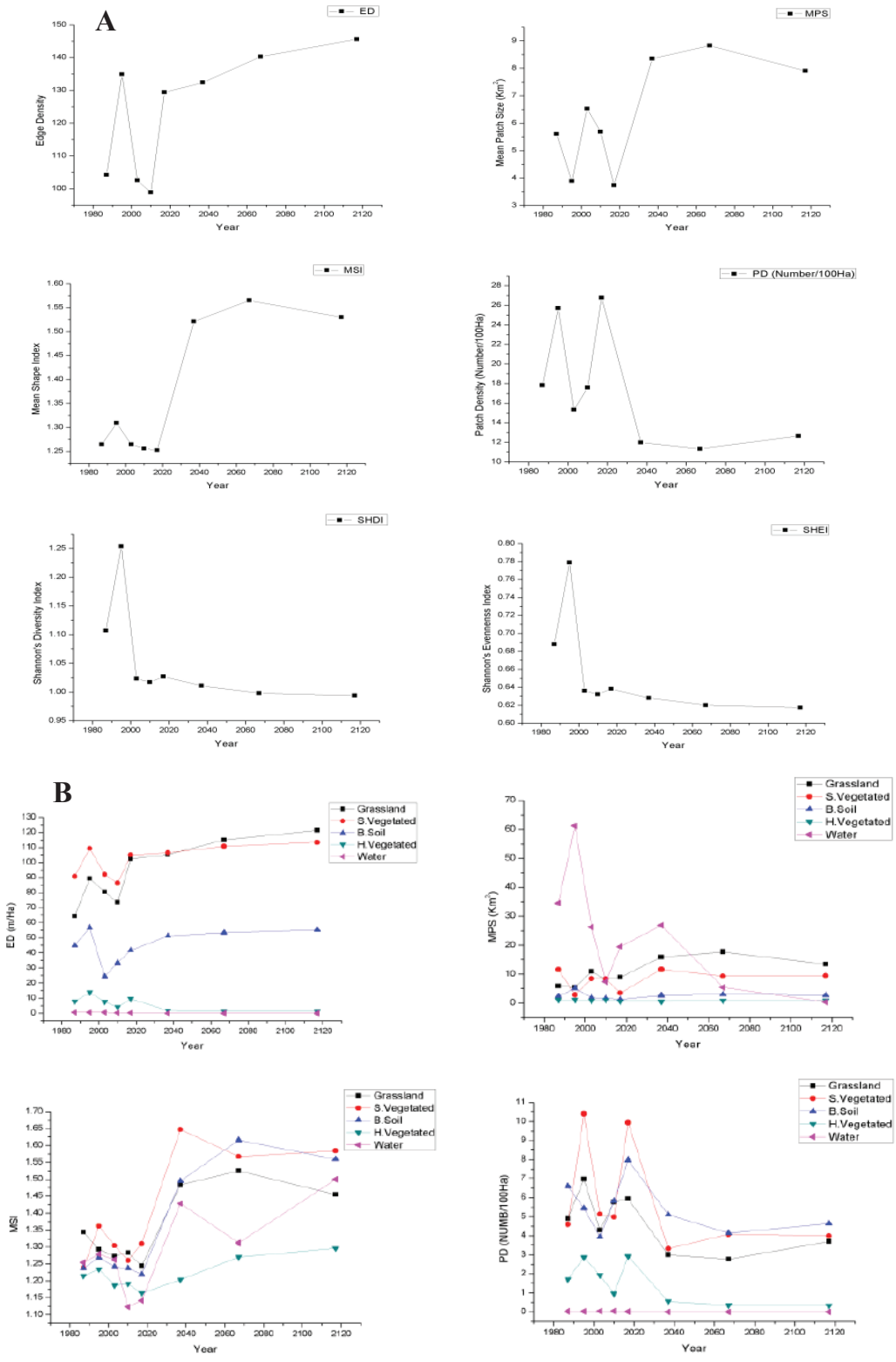

Fig. 5: Landscape pattern change (A) landscape level, (B) class level.

MPS (-8.08). Grassland region, on the other hand, exhibited a significant effect on ED (+37.98) and MPS (+3.08) with its most contrasting effect recorded in MSI (-0.09). The most opposite effect observed was the on water region with its effect on metrics change exhibited in MPS (-15.01) and MSI (-0.11). A regression analysis carried out between Bojiang lake area change and the landscape pattern metrics change proved not to be statistically significant but the reduction in size confirms the opposite effect the water region had on the landscape metrics.

Transition Between Grassland and Vegetated Region

The result of our analysis suggested that the grassland region mainly expanded into the sparsely vegetated and highly vegetated regions all through the study period from 1987-2017 (Table 4). The time intervals (1987-1995, 1995-2003, 2003-2010 and 2010-2017), were categorized based on the changes in the lake area, for instance, the year 1987-1995 was chosen because the lake area increased significantly during this period, from 1995-2003, the lake started reducing gradually, however, during 2003-2010 lost more than half of its area and lastly from 2010-2017, the lake area increased slightly due to the artificial water supply.

During the four intervals, there was an intensive systematic gain of the grassland region from both the sparsely vegetated and highly vegetated region (Fig. 6). An example of this transition is during the second interval (1995-2003) the annual intensity gain of the grassland region from both highly and sparsely vegetated regions were 7.88 and 4.94% respectively of the size of both regions in 1995 (Table 4) compared to the uniform intensity of 3.57% (of the landscape that was not grassland in 1995). This change implies that the grassland region gained from the highly vegetated region over 2 times more than the rate it would be expected to gain uniformly (from all land use categories). The annual intensity is higher for highly vegetated than the sparsely vegetated region in all intervals except the last interval which means the annual intensity of highly vegetated region was higher than the uniform intensity. It was also observed that the highly vegetated region consistently targeted the grassland region in all intervals while the sparsely vegetated region only targeted the grassland region in two intervals (1987-1995 and 2003-2010). Hence indicating that the grassland region may be mainly a transitional land use for both the highly vegetated and sparsely vegetated region.

The error intensity (EI) in Table 4 shows strong evidence that the grassland region gained intensively from both sparsely and highly vegetated regions. Based on the deviations from uniform intensity observed in the study, it implies that there was a real temporal transition between grassland region and the other vegetated regions (sparsely and highly vegetated). An example is the commission error intensity for the transition from grassland to the highly vegetated region during 1995-2003 which was 76.51% (Table 4) this high percentage of error intensity shows strong evidence against the uniform change hypothesis. This error analysis does not provide a threshold of how large an observed intensity's deviation from uniform intensity should be suitable for a real change, this is due to the non-precise nature of the actual map classification error like in the case of our study (Aldwaik & Pontius 2013, Pontius et al. 2013, Enaruvbe & Pontius 2015).

UI= Uniform intensity (% of other categories, excluding the concerned category); TI= Transition intensity (Parentheses values indicate targeted categories for loss or gain while non-parenthesis indicates the categories was avoided by the change); EI= Error Intensity (Bold values are omission, non-bold values are commission).

Transition intensity for predicted image: From the 100-year prediction analysis carried out (2017-2117), it was observed the grassland region intensive gain consistently targeted the highly vegetated. The sparsely vegetated region was only slightly targeted in the first interval. During the three intervals (2017-2047, 2047-2077 and 2077-2117). An example of this transition is during the interval from 2017-2047, the annual intensity gain of the grassland region from the highly vegetated region was 2.27% compared to the uniform intensity of 1.29%. The error intensity (EI) ranging from 52-76.7% in Table 5 at all intervals showed strong evidence that the grassland region gained intensively from the highly vegetated region.

Transition between the vegetated region and the water region: Water region which showed a continuous reduction in size over the cause of this study period (1987-2017), was directly or indirectly influenced by the changes in other land cover region. From the transition analysis results in Table 4, it was observed that the gains in all vegetated region did not target the water region except for the highly vegetated region in one interval (1995-2003) with a transition intensity of 0.15% slightly higher than the uniform intensity of 0.09%. The transition to Barren Soil region on the other hand consistently targeted the water and sparsely vegetated region at 3 intervals (1995-2017). The transition intensity for the water region during 1995-2003 and 2003-2010 was more than 10 times the uniform intensity of each interval. This, however, indicates that although the vegetated region did not directly target the water region in their transition, they, however, had an indirect impact on the change in the water region.

Transition intensity for predicted image: From 2017-2117, the grassland region compared to the other vegetated

regions gained consistently from the water region in all intervals 2017-2047, 2047-2077 and 2077-2117 (Fig. 7). The highly vegetated region, on the other hand, gained a bit from the water region only in the first interval (2017-2047). The annual transition gain of the grassland region during 2017-2117 from water region in all intervals was 2.23, 2.66 and 2.39 compared to the uniform of 1.29, 0.27 and 0.20 respectively. The error intensity, on the other hand, showed strong evidence that the grassland region gained a subsistent amount from the water region with a very high Error index value ranging between 68.57 and 99.59%.

UI= Uniform intensity (% of other categories, excluding the concerned category); TI= Transition intensity (Parentheses values indicate targeted categories for loss or gain while non-parenthesis indicates the categories was avoided by the change); EI= Error Intensity (Bold values are omission, non-bold values are commission).

Land-Use Change Trend Analysis

The land-use changes between 1987 and 2017 were investigated in this paper. The changes in the Ordos basin during the 3-decade duration of study made a significant influence on the land use structure. Significant changes in each land cover region occurred all through the study period with the grassland and sparsely vegetated region occupying a considerable amount of the study region. While the highly vegetated region, barren soil and the sparsely vegetated region were experiencing inconsistency in area change, the grassland

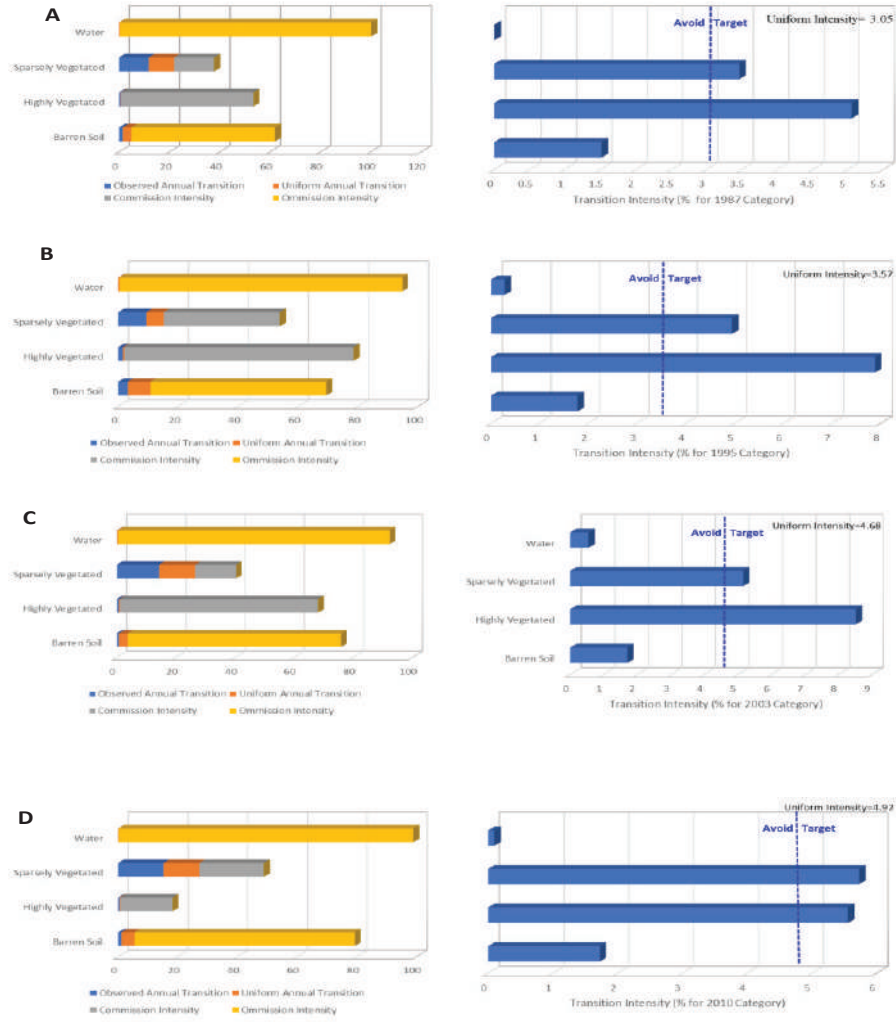

Fig. 6: Transition to grassland (A)1987-1995, (B) 1995-2003, (C) 2003-2010, (D) 2010-2017.

region continuously showed a significant increase in size, the water region, on the other hand, proved otherwise. Most land use categories in the study region underwent swap change though the study period. A swap change depicts changes in land cover regions (loss) occurring in one location while an equal gain in another location (Pontius et al. 2004, Yuan et al. 2016, Zaehringer et al. 2015). The last row of Table 6 reveals that the swap changes from 1995-2017 accounted for more than 50% of the overall land-use change in all three intervals, the same applies to the predicted images 2017-2117 (Table 7). This indicates that land-use change in the Ordos basin was very dynamic during those periods which were followed by a high rate of land use categories relocations. Higher swap change percentage indicates an overall change more than the net change and reveals the significance of detailed analysis of land cover change beyond the net change (Yuan et al. 2016).

From the swap analysis, it was observed that while other regions were experiencing loss in the area the grassland region continued to gain all through the study period in all intervals. For example, for the 1995-2003 interval, while the water and highly vegetated region had a loss rate of (2 and 10km^2/year), the grassland, barren and sparsely vegetated region had a gross gain of (56, 128 and 140km^2/year). The transition matrix also explained that the changes in the regions which reveal that although the grassland region continuously increased in size all through the study, it targeted other land cover regions like the highly vegetated region and sparsely vegetated region during its area change. Based on the analysis of the predicted image (2017-2117), the grassland region also continued to dominate in area coverage occupying about 50% of the total area. This continuous increase in the grassland region and inconsistency in the other regions in-

Table 5: Land use transition between Vegetative Regions (Categories).

Transition to Grassland								
	1987-2017		2017-2047		2047-2077		2077-2117	
	UI=0.57		UI=1.29		UI=0.27		UI=0.20	
Losing Categories	TI	EI	TI	EI	TI	EI	TI	EI
Barren Soil	0.36	**40.22**	(1.37)	9.14	(0.30)	10.51	(0.23)	12.12
Highly Vegetated	(1.56)	76.70	(2.27)	70.36	(0.83)	73.74	(0.39)	52.03
Sparsely Vegetated	(0.58)	3.63	1.22	**9.46**	0.25	**6.64**	0.19	**5.56**
Water	0.03	**95.57**	(2.23)	68.57	(2.66)	97.81	(2.39)	99.59
Transition to Highly Vegetated								
	1987-2017		2017-2047		2047-2077		2077-2117	
	UI=0.05		UI=0.01		UI=0.00		UI=0.00	
Losing Categories	TI	EI	TI	EI	TI	EI	TI	EI
Barren Soil	0.02	**54.10**	0.01	**30.86**	0.00	**48.04**	0.00	**19.57**
Grassland	(0.08)	32.55	(0.01)	27.10	(0.00)	41.51	(0.00)	29.91
Sparsely Vegetated	0.02	**56.40**	0.00	**52.06**	0.00	**70.33**	0.00	**48.47**
Water	0.00	**95.58**	(0.05)	79.67	0.00	**100.00**	0.00	**100.00**
Transition to Sparsely vegetated								
	1987-2017		2017-2047		2047-2077		2077-2117	
	UI=1.57		UI=1.15		UI=0.14		UI=0.13	
Losing Categories	TI	EI	TI	EI	TI	EI	TI	EI
Barren Soil	1.47	**10.94**	0.80	**39.77**	(0.20)	34.14	(0.18)	28.82
Grassland	(1.63)	7.42	(1.24)	10.65	0.12	**14.17**	0.12	**10.02**
Highly Vegetated	0.39	**85.07**	0.67	**51.80**	(0.17)	19.17	0.08	**43.44**
Water	0.00	**99.94**	0.04	**97.41**	0.00	**100.00**	0.00	**100.00**

UI= Uniform intensity (% of other categories, excluding the concerned category); TI= Transition intensity (Parentheses values indicate targeted categories for loss or gain while non-parenthesis indicates the categories was avoided by the change); EI= Error Intensity (Bold values are omission, non-bold values are commission).

dicates an increase in anthropogenic activities in this region.

DISCUSSION

Relationship Between the Land Use change and Spatial Pattern

In recent years, with the development and utilization of coal and oil and gas resources and the continuous development of local economy, the status of its infrastructure has been greatly improved, and road traffic and power facilities have begun to take shape. Agriculture and aquaculture are still the main industries of the people in the region. The industrial industries are mainly petrochemical, chemical, brick, carpet, cement, coal mining, etc. The local residents are mainly engaged in agriculture and aquaculture, and some labourers are engaged in coal mining and oil production. Transportation and other industries. However, the continuous exploitation of coal mines and oil and the rapid development of the agricultural industry not only led to lead to an increase in regional water demand, but it also increased landscape fragmentation. From this study, the landscape pattern and the land-use regions in this study showed a strong relationship. The result from the OLS regression model used to examine the level of accuracy of changes in the landscape metrics and the intensity of the effect each land-use changes has on the landscape pattern showed that the major changes in the landscape pattern had

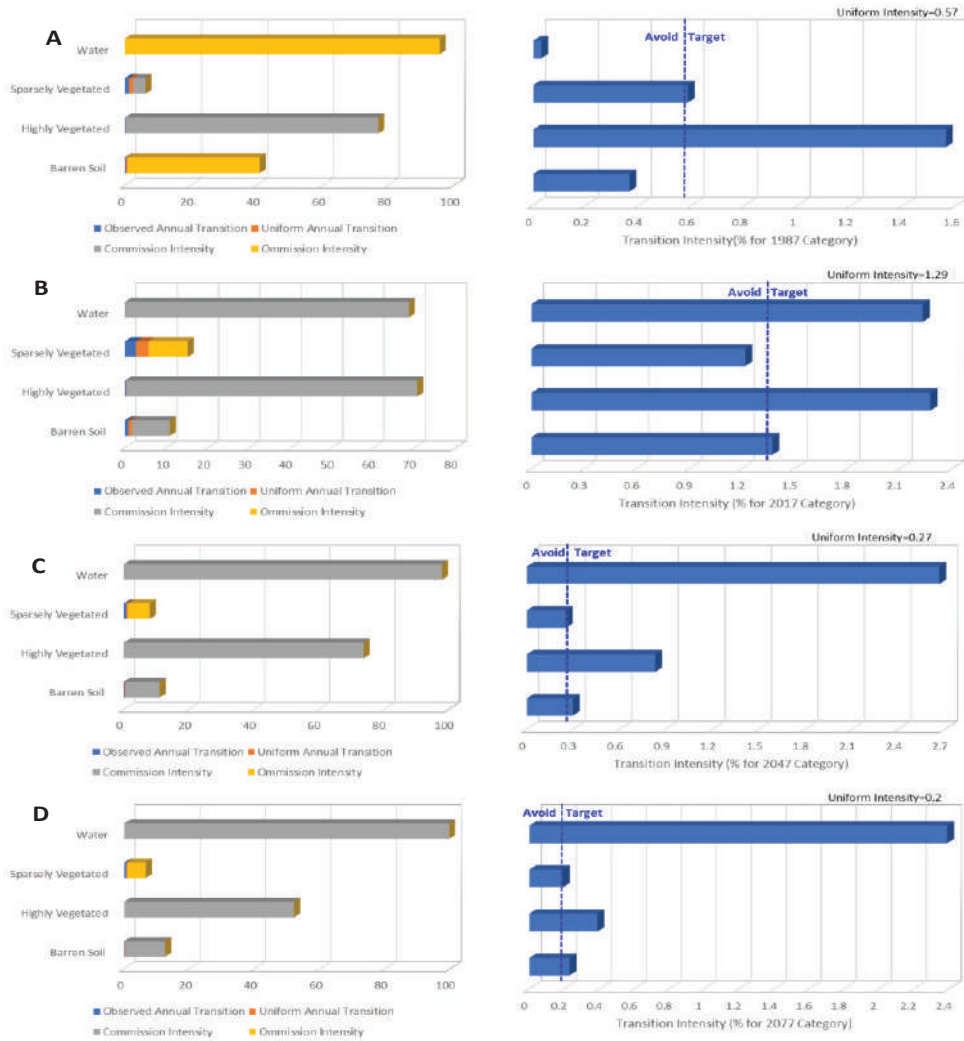

Fig. 7: Transition to grassland (A)1987-2017, (B) 2017-2047, (C) 2047-2077, (D) 2077-2117.

a strong relationship with all four regions (grassland, highly vegetated, sparsely vegetated, and barren soil region) except the water region. Hence the growth experienced in the grassland region which was possibly as a result of the increase in agricultural activities was closely related to the increased heterogeneity and fragmentation of the whole landscape. The result from this study is similar to the result of (Yu & Ng 2006, Hashem Dadashpoor et al. 2019) who believed that in the human landscape, changes in agriculture and garden can lead to fragmentation of the landscape. Several factors can be responsible for the increase in fragmentation an example is increased urbanization, economic development, agriculture and garden land. As of the case of this study, all of the above-mentioned factors are believed to have played a role in the increased fragmentation experienced in the study region.

Effects of Ecological Restoration Measures on the Vegetation Transpiration

Combining the characteristics of land-use change in the basin over the past decade, the impact of ecosystem type conversion was analysed. The Bojiang Lake basin located in the transition zone between grassland and desertified grassland. The vegetation is sparse, grassland is the main ecosystem, followed by cultivated land and forest land (sparsely vegetated and highly vegetated region respectively). Based on the image classification in this study, the basin mainly includes grassland (grassland, meadow, agricultural land, shrub forest etc.), highly vegetated region (mainly the broad forest), water region and the barren soil. Among the major type of ecosystem, the area of grassland, sparsely vegetated, and lake area changed the most mainly due to the implementation of relevant policies such as ecological forest construction in Inner Mongolia Autonomous Region. The Ordos began to implement a ban on grazing, returning farmland to forests and grassland in 2000. With the construction of the project, the area of artificial vegetation in Ordos city increased significantly as we can see in the changes in the grassland region from 182.8 in 1987 to 338.7 in 2017 (Fig. 3). After the enclosure, the vegetation mainly depends on precipitation and soil water growth, and the trees need to be irrigated at the initial stage of planting. After a period of growth, they start to draw groundwater to maintain growth. The local precipitation of around 364 mm cannot fully guarantee the water demand for tree growth, and it is necessary to use groundwater, and the water for ecological construction is increasing sharply. Although the increase of vegetation will play a positive role in preventing soil erosion and protecting the ecological environment, vegetation will have a significant impact on the redistribution of surface water and groundwater through canopy interception and water and will increase water volume due to transpiration. Consumption, thereby reducing the amount of water entering the lake. Vegetation has a significant role in preventing wind, preventing soil erosion and conserving water sources. However, it increases the amount of ecological water consumption in small areas and, to a certain extent, reduces the amount of lake water entering the lake, but the overall impact is very small.

Effect of Population and Urbanization on Lake Reduction

The residents living in the reserve and 18 civil wells were discovered. The survey found that the villagers' daily water and agricultural water are taken from the groundwater, which will have a certain impact on the water volume change of the wetlands in the gull reserve. There have been many large wells built since 2000. These large wells are mostly rectangular, about 100-200 m long, about 30 m wide, with a gentle slope and simple engineering. In recent years, with the development and utilization of coal and oil and gas resources and the continuous development of local economy, the status of its infrastructure has been greatly improved, and road traffic and power facilities have begun to take shape. Agriculture and aquaculture are still the main industries of the people in the region. The industrial industries are mainly

Table 6: Annual land-use change (km^2/year) during the four intervals.

	1987-1995			1995-2003			2003-2010			2010-2017		
Change	Total	Net	Swap (%)	Total	Net	Swap (%)	Total	Net	Swap (%)	Total	Net	Swap (%)
Barren Soil	138	82	40.6	144	-128	11.1	52	16	69.2	52	0.5	99
Grassland	161	62	61.5	170	56	67.1	223	0.4	99.8	196	38	80.6
Highly Vegetated	21	8	61.9	19	-10	47.4	9	-4	55.5	10	4	60
Sparsely Vegetated	240	-153	36.25	242	83	65.7	237	-9	96.2	208	-43	79.3
Water	2	1	50	3	-2	33.3	4	-4	2.03	0	0.2	66.7
Overall Change	281	153	45.6	288	140	51.4	263	17	93.5	233	43	81.5

Total= gross gain + gross loss; Net= gross gain - gross loss; Swap (%) = ((Total - Net)/Total) x 100

Table 7: Annual land-use change (km^2/year) during the four predicted year intervals.

	1987-2017			2017-2047			2047-2077			2077-2117		
Change	Total	Net	Swap (%)	Total	Net	Swap (%)	Total	Net	Swap (%)	Total	Net	Swap (%)
Barren Soil	108.1	31	71.3	106	22	79.2	22	-4	81.8	24	-3	87.4
Grassland	260.2	-159	39	269	-37	86.2	45	9	80	48	5	89.7
Highly Vegetated	17.6	1.9	89.3	12	-8	33.3	1	-0	94	1	-0	92
Sparsely Vegetated	272.7	120	56	263	25	90.5	37	-5	86.5	44	-1	97.7
Water	5.3	4.9	7.5	2	-2.1	3.7	0	-0	0	0	-0	0
Overall Change	331.9	159	52.2	326	47	85.6	52	9	82.7	58	5	91.4

Total= gross gain + gross loss; Net= gross gain - gross loss; Swap (%) = ((Total - Net)/Total) x 100

petrochemical, chemical, coal mining, etc. The local residents are mainly engaged in agriculture and aquaculture, and some of the labour force is engaged in coal mining, oil production and transportation industries. However, the continuous exploitation of coal and oil and the development of the industry will lead to an increase in regional water demand. At the same time, surface subsidence and water-conducting fissures generated by coal mining exploration will affect the protected flow area and runoff direction. Therefore, the coal mining industry enterprises and the sources of agricultural and domestic water are related to the reduction of water in protected areas.

The water consumption of industrial and agricultural waters in the basin has reduced the surface runoff and the groundwater level in the basin through the demand for surface runoff and groundwater resources. However, at present, there are fewer and fewer populations in the Neighbouring Nature Reserve and the surrounding areas. The number of people has increased year by year, and the resident population has declined year by year, accounting for only 21% of the total population (Fig. 8). Therefore, observations from long-term data show that activities such as human production and living activities and industrial and agricultural exploitation in the basin have certain impacts on the water table and lake water volume in the basin. But the long-term impact is small.

Effect of weather conditions: Over the years, climate factors were considered to be the primary driving force for this reduction due to the slight increase in human activities. Research by He et al. (1992), pointed out that a contributing factor to the reduction in the water level in the study site was the sediment-trapping dams built on the rivers after 2000 which intercepted the direct flow of water into the lake including other factors such as increased ecotourism, domestic use of water and so on. All of these coupled with the decrease in precipitation and increased temperature all play a role in the reduction in the water level. Kang Liang's Study (Kang 2017) proved that increased human activities were the main factor for the decrease in the annual streamflow from 2000 to 2013. Although most of the researches ended in 2013, from the observation of this study the water region continued to

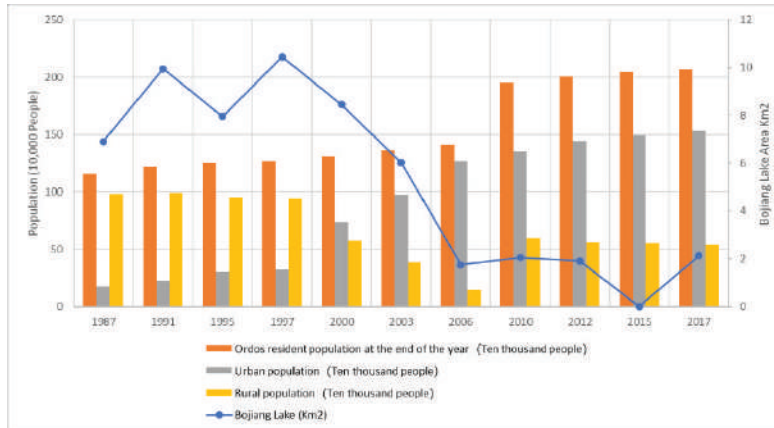

Fig. 8: Ordos city population (overall, rural and urban) Versus Bojiang Lake area.

experience a reduction in area. From this study, a reduction in precipitation coupled with an increase in evaporation rate was a contributing factor to the reduction in water size. For example, in August where the Landsat images used for this analysis was acquired, the weather conditions during that period were dry and hot exhibiting monthly average temperatures above their mean temperature values except for 1987 and 1995, the annual temperature of the study site, however, showed values above its mean annual temperature values all through the study period. The monthly average precipitation in August was all below the mean precipitation value except for 1995 signifying that August was one of the driest periods of the study (Fig. 9).

CONCLUSION

The land-use changes experienced in the Ordos Basin between 1987 and 2017 were attributed to the growth in population and economic development in the region. Based on the assessment of the remote sensing images obtained in 1987, 1995, 2003, 2010 and 2017 the five classified regions (grassland, highly vegetated, sparsely vegetated, barren soil and water region) all regions experienced a significant amount of changes which subsequently led to the changes in landscape patterns.

The land use classification and the transition intensity model were used to analyse the changes in the regions over the past 30 years. The changes experienced in the grassland and sparsely vegetated region were observed to be the greatest in the region and these changes were a clear indication of the increased anthropogenic activities such as agricultural activities in the study region.

The future land-use changes were simulated and predicted using the CA-Markov model, and the landcover map changes from 1987 to 2017. And through this method, the next 30-100 years were predicted and the result shows that grassland and the sparsely vegetated region continued to dominate the study region.

The landscape structural pattern was simulated based on four spatial metrics (patch, shape, diversity and edge metrics) to analyse the fragmentation and heterogeneity level of Ordos basin. The result, however, showed that during the study period the increased population, extensive human activities and urbanization level contributed greatly to the increase in fragmentation and heterogeneity experienced in the region. This effect was reflected in the relationship between the land-use change and the fragmentation level where changes in land use regions except the water region proved to significantly impact the changes in the fragmen-

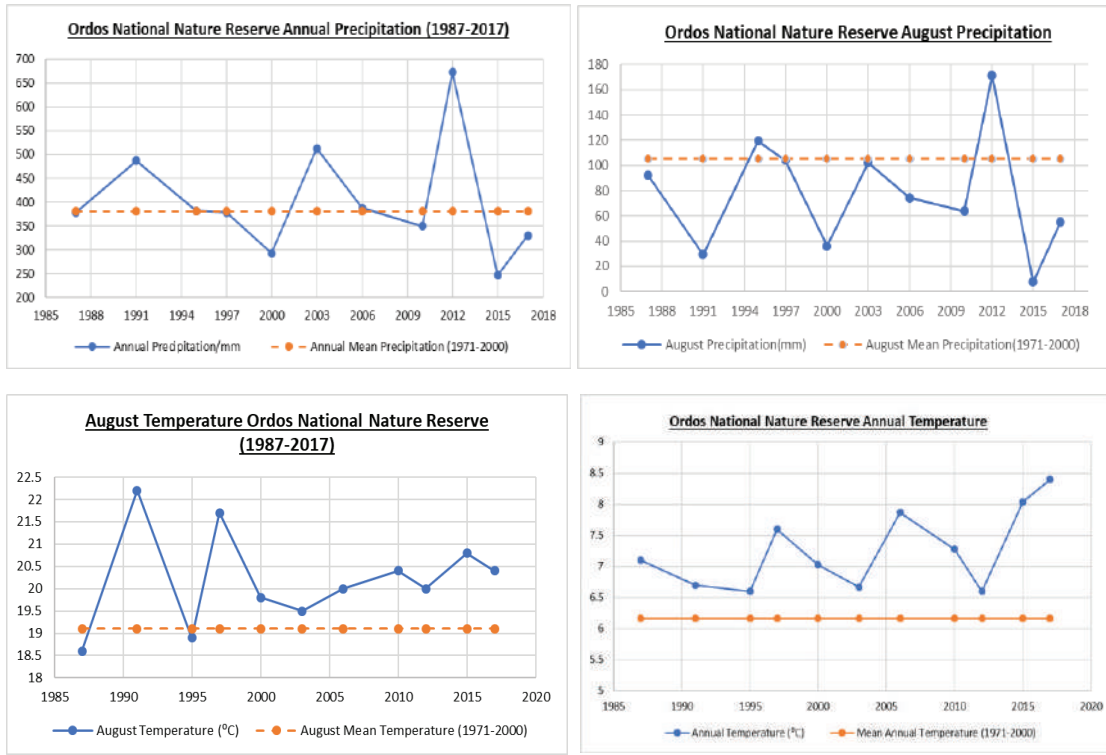

Fig. 9: Weather condition of Ordos national nature reserve.

tation and heterogeneity level of Ordos basin. Between the 3-decade study period and the predicted 100 years, it was observed that while the change in fragmentation level showed no relationship with the change in water level, the changes in each land-use regions were both, directly and indirectly, related to the changes in the water region.

Based on our observation in this study, the change in each land use region although showed a significant relationship with the change in water region including Bojiang lake, other external factors also contributed to the changes in the size of the lake an example is the current climatic conditions, increase in urbanization, extensive human activities such as agricultural and industrial activities all of which were accompanied by an increment in the water consumption which posses a long-term impact on the water level as we can see in the predicted images from 2017-2117. Other contributing factors were poor environmental policy and planning involving the building of trap dams which also blocked the flow of water to the lake, changes in the weather conditions such as increased temperature and decreased precipitation all play a role in the reduction in water level. For effective management of the ecosystem, policymakers should keep in mind that changes in land use also affect the regional climate (Foley et al. 2005). With the increased urbanization and extensive human activities in the study region reflected in the land-use changes, it is suggested that policymakers should emphasize more on the continuous management of the land-use changes and improvement of the ecosystem.

ACKNOWLEDGEMENT

Landsat (http://www.usgs.gov/pubprod/aerial.html#satellite) programme for providing the remote sensing images used for this research. Also, the authors appreciate the support from the Brook Byers Institute for Sustainable Systems, Hightower Chair and the Georgia Research Alliance at Georgia Institute of Technology.

REFERENCES

Abdullah, S.A. and Nakagoshi, N. 2006. Changes in landscape spatial pattern in the highly developing state of Selangor, Peninsular Malaysia. Landsc. Urban Plan., 77 (3): 263-275.

Aguilera, F., Valenzuela, L.M. and Botequilha-Leitão, A. 2011. Landscape metrics in the analysis of urban land use patterns: a case study in a Spanish metropolitan area. Landsc. Urban Plan., 99(3): 226-238.

Al-doski, J., Mansor, S.B. and Shafri, H.Z.M. 2013. Change detection process and techniques. Civ. Environ. Res., 3: 37-45.

Aldwaik, S.Z. and Pontius, R.G. Jr. 2012. Intensity analysis to unify measurements of size and stationarity of land changes by interval, category and transition. Landsc. Urban Plan., 106: 103-114.

Aldwaik, S.Z. and Pontius, R.G. Jr. 2013. Map errors that could account for deviations from a uniform intensity of land change. Int. J. Geogr. Inf. Sci., 27: 1717-1739.

Alo, C.A. and Pontius, R.G. Jr. 2008. Identifying systematic land-cover transitions using remote sensing and GIS: The fate of forests inside and outside protected areas of Southwestern Ghana. Environ. Plan. B Plan. Des., 35: 280-295.

Bolund, P. and Hunhammar, S. 1999. Ecosystem services in urban areas. Ecol. Econ., 29: 293-301.

Braimoh, A.K. 2006. Random and systematic land-cover transitions in northern Ghana. Agric. Ecosyst. Environ., 113: 254-256.

Bürgi, M., Hersperger, A.M. and Schneeberger, N. 2004. Driving forces of landscape change-current and new directions. Landsc. Ecol., 19: 857-868.

Cabral, A.I. and Costa, F.L. 2017. Land cover changes and landscape pattern dynamics in Senegal and Guinea Bissau borderland. Appl. Geogr., 82: 115-128.

Cao, C. 2013. Diagnosis of Environmental Health By Remote Sensing. Beijing: Science Press. Chinese.

Cao, C., Zhao, J., Gong, P., Ma, G., Bao, D., Tian, K., Tian, R., Niu, Z., Zhang, H. and Xu, M. 2012. Wetland changes and droughts in southwestern China. Geomat. Nat. Haz. Risk, 3: 79-95.

Chen, Z., Xu, B. and Devereux, B. 2014. Urban landscape pattern analysis based on 3D landscape models. Appl. Geogr., 55: 82-91.

Cyranoski, D. 2009. Putting China's wetlands on the map. Nature, 458: 134.

Dadashpoor, H., Azizi, P. and Moghadasi, M. 2018. Land use change, urbanization, and change in landscape pattern in a metropolitan area. Science of The Total Environment.

Eastman, J.R. 2003. IDRISI Kilimanjaro: Guide to GIS and Image Processing. Worcester (MA): Clark Labs, Clark University.

Echeverría, C., Newton, A., Nahuelhual, L., Coomes, D. and Rey-Benayas, J.M. 2012. How landscapes change: Integration of spatial patterns and human processes in temperate landscapes of southern Chile. Appl. Geogr., 32 (2): 822-831.

Enaruvbe, G.O. and Pontius, R.G. Jr. 2015. Influence of classification errors on intensity analysis of land changes in Southern Nigeria. Int. J. Remote Sens., 36: 244-261.

Finlayson, M.C. 2012. Forty years of wetland conservation and wise use. Aquat. Conserv., 22: 139-143.

Foley, J.A., DeFries, R., Asner, G.P., Barford, C., Bonan, G., Carpenter, S.R., Chapin, F.S., Coe, M.T., Daily, G.C., Gibbs, H.K. and Helkowski, J.H. 2005. Global consequences of land use. Science, 309 (5734): 570-574.

Frondoni, R., Mollo, B. and Capotorti, G. 2011. A landscape analysis of land cover change in the municipality of Rome (Italy): Spatio-temporal characteristics and ecological implications of land cover transitions from 1954 to 2001. Landsc. Urban Plan., 100: 117-128.

Guo, H., Wu, D. and Zhu, H. 1990. Land restoration in China. Acta Ecol. Sin., 10: 24-26. Chinese.

Halabisky, M., Moskal, L.M. and Hall, S.A. 2011. Object-based classification of semi-arid wetlands. J. Appl. Remote Sens., 5: 053511-053513.

He, F., Zhang, Y., Wu, Y. and Gao, T. 1992. The distribution of the relict gull Larus relictus in Maowusu desert, Inner Mongolia, China. Forktail, 7: 151-154.

Hereher, M.E. 2010. Vulnerability of the Nile Delta to sea level rise: an assessment using remote sensing. Geomat. Nat. Haz. Risk., 1: 315-321.

Hladnik, D. 2005. Spatial structure of disturbed landscapes in Slovenia. Ecol. Eng., 24(1-2): 17-27.

Kang, Liang 2017. Quantifying streamflow variations in ungauged lake basins by integrating remote sensing and water balance modelling: a case study of the Erdos Larus relictus National Nature Reserve, China. Remote Sens., 9: 588.

Kertész, Á., Nagy, L.A. and Balázs, B. 2019. Effect of land use change on ecosystem services in Lake Balaton Catchment. Land Use Policy, 80: 430-438.

Kienast, F., Frick, J., Strien, M.J.V. and Hunziker, M. 2015. The Swiss landscape monitoring program - A comprehensive indicator set to measure landscape change. Ecol. Model., 295: 136-150.

Lausch, A., Blaschke, T., Haase, D., Herzog, F., Syrbe, R.U., Tischendorf, L. and Walz, U. 2015. Understanding and quantifying landscape structure - A review of relevant process characteristics, data models, and landscape metrics. Ecol. Model., 295: 31-41.

Lawler, J.J., Lewis, D.J., Nelson, E., Plantinga, A.J., Polasky, S., Withey, J.C., Helmers, D.P., Martinuzzi, S., Pennington, D. and Radeloff, V.C. 2014. Projected land-use change impacts on ecosystem services in the United States. Proc. Natl. Acad. Sci., 111(20): 7492-7497.

Lehner, B. and Doll, P. 2004. Development and validation of a global database of lakes, reservoirs and wetlands. J. Hydrol., 296: 1-22.

Liang, K., Lou, H. and Cheng, C. 2011. Characteristics of groundwater flow in the Ordos Larus relictus reserve wetland. Resour. Sci., 33(6): 1089-1098 (in Chinese).

Liu, W., Zhang, L., Xing, X., Bao, X., Su, Y., Bai, Z., Ren, Y. and Gao, R. 2008. The relationship between the zoobenthos and Larus relictus' foraging behavior in saline-alkaline wetland of Ordos Plateau. J. Arid Land Resour. Environ., 22: 185-192. Chinese.

Lu, D. and Weng, Q. 2007. A survey of image classification methods and techniques for improving classification performance. International Journal of Remote Sensing, 28: 823-870.

Luck, M. and Wu, J. 2002. A gradient analysis of urban landscape pattern: a case study from the Phoenix metropolitan region, Arizona, USA. Landsc. Ecol., 17(4): 327-339.

Mallinis, G., Koutsias, N. and Arianoutsou, M. 2014. Monitoring land use/land cover transformations from 1945 to 2007 in two peri-urban mountainous areas of Athens metropolitan area, Greece. Sci. Total Environ., 490: 262-278.

McGarigal, K., Cushman, S.A. and Stafford, S. 2000. Multivariate Statistics for Wildlife and Ecology Research. Springer Science & Business Media.

Mwangi, H., Lariu, P., Julich, S., Patil, S., McDonald, M. and Feger, K.H. 2017. Characterizing the intensity and dynamics of land-use change in the Mara River Basin, East Africa. Forests, 9(1): 8.

Nagendra, H., Munroe, D.K. and Southworth, J. 2004. From pattern to process: landscape fragmentation and the analysis of land use/land cover change. Agric. Ecosyst. Environ., 101(2): 111-115.

Phiri, D. and Morgenroth, J. 2017. Developments in landsat land cover classification methods: a review. Remote Sens., 9: 967.

Pontius, R.G. Jr., Gao, Y., Giner, N.M., Kohyama, T., Osaki, M. and Hirose, K. 2013. Design and interpretations of intensity analysis illustrated by land change in Central Kalimantan, Indonesia. Land., 2: 351-369.

Pontius, R.G. Jr., Shusas, E. and McEachern, M. 2004. Detecting important categorical land changes while accounting for persistence. Agric. Ecosyst. Environ., 101: 251-268.

Ramsar 2007. What are wetlands? In: The RAMSAR convention of wetlands information paper no. 1. Available from: http://www.ramsar.org.

Reis, J.P., Silva, E.A. and Pinho, P. 2015. Spatial metrics to study urban patterns in growing and shrinking cities. Urban Geogr., 3638: 1-26.

Ren, H., Shen, W.J., Lu, H.F., Wen, X.Y. and Jian, S.G. 2007. Degraded ecosystems in China: status, causes, and restoration efforts. Landscape and Ecological Engineering, 3: 1-13.

Rosenfield, G.H. and Fitzpatrick-Lins, K. 1986. A coefficient of agreement as a measure of thematic classification accuracy. Photogramm. Eng. Remote Sensing, 52: 223-227.

Sang, L., Zhang, C., Yang, J., Zhu, D. and Yun, W. 2011. Simulation of land use spatial pattern of towns and villages based on CA-Markov model. Math. Comput. Model., 54: 938-943.

Schröder, B. and Seppelt, R. 2006. Analysis of pattern-process interactions based on landscape models-overview, general concepts, and methodological issues. Ecol. Model., 199: 505-516.

Szabó, S., Bertalan, L., Kerekes, Á. and Novák, T.J. 2016. Possibilities of land use change analysis in a mountainous rural area: a methodological approach. Int. J. Geog. Inf. Sci., 30(4): 708-726.

Teixeria, Z., Teixeria, H. and Marques, J.C. 2014. Systematic processes of land use/land cover change to identify driving forces: implications on water quality. Sci. Total Environ., 470-471: 1320-1335.

Tian, R., Cao, C., Peng, L., Ma, G., Bao, D., Guo, J. and Yomwan, P. 2016. The use of HJ-1A/B satellite data to detect changes in the size of wetlands in response into a sudden turn from drought to flood in the middle and lower reaches of the Yangtze River system in China. Geomatics, Natural Hazards and Risk., 7: 287-307.

Tyre, A.J., Tenhumberg, B. and Michael Bull, C. 2006. Identifying landscape-scale patterns from individual scale processes. Ecol. Model., 199: 442-450.

Wan, L., Zhang, Y., Zhang, X., Qi, S. and Na, X. 2015. Comparison of land use/land cover change and landscape patterns in Honghe National Nature Reserve and the surrounding Jiansanjiang. Ecol. Indic., 51: 205-214.

Young, N.E., Anderson, R.S., Chignell, S.M., Vorster, A.G., Lawrence, R. and Evangelista, P.H.A. 2017. Survival guide to Landsat preprocessing. Ecology, 98: 920-932.

Yu, X. and Ng, C. 2006. An integrated evaluation of landscape change using remote sensing and landscape metrics: a case study of Panyu, Guangzhou. Int. J. Remote Sens., 27(6): 1075-1092.

Yuan, Y., Li, B., Gao, X., Liu, H., Xu, L. and Zhou, C.A. 2016. method of characterizing land-cover swap changes in the arid zone of China. Front. Earth Sci., 10: 74-86.

YuhaiBao, SuyaBao and Yinshan 2011. Analysis on temporal and spatial changes of landscape pattern in Dalinor Lake Wetland. Procedia Environ. Sci., 10: 2367-2375.

Zaehringer, J.G., Eckert, S. and Messerli, P. 2015. Revealing regional deforestation dynamics in North-Eastern Madagascar-Insights from multi-temporal land cover change analysis. Land., 4: 454-474.

Zedler, J.B. and Kercher, S. 2005. Wetland resources: status, trends, ecosystem services, and restorability. Annu. Rev. Environ. Resour., 30: 39-74.

Nature Environment and Pollution Technology
An International Quarterly Scientific Journal

p-ISSN: 0972-6268
(Print copies up to 2016)
e-ISSN: 2395-3454

Vol. 19 | No. 2 | pp. 511-520 | 2020

Original Research Paper

https://doi.org/10.46488/NEPT.2020.v19i02.007

Open Access Journal

Hydrolithological Investigation for Near-Surface Aquifers Within Lekki Peninsula, Lagos, Southwestern Nigeria

O. G. Bayowa*, T. A. Adagunodo†, O. A. Olaleye*, A. E. Adeleke*, M. R. Usikalu** and S. A. Akinwumi****
*Department of Earth Sciences, Ladoke Akintola University of Technology, P.M.B. 4000, Ogbomoso, Nigeria
**Department of Physics, Covenant University, P.M.B. 1023, Ota, Nigeria
†Corresponding author: T. A. Adagunodo; theophilus.adagunodo@covenantuniversity.edu.ng

Nat. Env. & Poll. Tech.
Website: www.neptjournal.com

Received: 27-05-2019
Accepted: 22-07-2019

Key Words:
Aquifers; Litho-logs; Vertical electrical sounding (VES); Lekki peninsula; Groundwater

ABSTRACT

This study is aimed at investigating the near-surface aquifers within Lekki Peninsula, Lagos, Southwestern Nigeria. Thirty-one (31) Vertical Electrical Sounding (VES) data were acquired using the Schlumberger array with current electrode spacing, which varies between 1 and 400m. The VES data were quantitatively interpreted, and the final layer parameters obtained were used to generate 2D geoelectric sections. Litho-logs acquired within the Lekki Peninsula were used to correlate the geoelectric sections to understand the nature and depth of groundwater contained in each aquiferous zone. The lithologies delineated in the study area include the topsoil (fill and/or sand) with resistivity value, which varies between 39 and 1535Ωm as well as layer thickness from 0.5 to 5.5m; second layer of wet clay/sandy clay (saturated with brackish water) with resistivity value, which varies between5 and 163Ωm as well as layer thickness from 1.5 to 10m; third layer of clayey sand/sand (saturated with freshwater) with resistivity value, which varies between 10 and 898Ωm as well as layer thickness value from5 to 34m; and fourth layer of clay (saturated with saline water) with resistivity value, which varies between 1 and 9Ωm. Isolated sand bodies (probably unsaturated zone) with resistivity value, which varies from 648 to 3560 Ωm, were delineated beneath VES stations 24, 25, 29 and 30. The study concludes that the topsoil (sand/fill), unsaturated zone (conglomerate), silty mud layer (brackish/freshwater saturated), and sand layer (saline water-saturated) constitute the aquifers and water quality within Lekki Peninsular. The inhabitants of the study area are, therefore, advised to avoid absurd usage of water to reduce the pumping rate and intrusion into the saline water formation.

INTRODUCTION

Water is one of the basic needs of life (Anomohanran 2013, Shishaye & Abdi 2016, Adagunodo et al. 2018a). It is quite abundant on the planet Earth. It is available to man as rain, surface water and groundwater (Adagunodo et al. 2018a), with different uses in domestic, industrial and agricultural settings. However, the availability of potable water with good quality for man's numerous needs is being challenged with pollution and dryness in some locations within Sub Saharan Africa. Therefore, groundwater has been the most preferred resources out of the available sources of water to man. Groundwater is one of the natural resources that are widely distributed in the subsurface, with vital roles in man's life (Kalaivanan et al. 2019). Despite its availability, it is also challenged with pollution (either from geogenic or anthropogenic sources) and inadequate information about the lithologic compositions of the near-surface for groundwater exploitation (Olafisoye et al. 2012, Sunmonu et al. 2012, Adagunodo et al. 2013, Oladejo et al. 2013, Sunmonu et al. 2013, Bayowa et al. 2014a, b, Oladejo et al. 2015, Sunmonu et al. 2015, Sunmonu et al. 2016, Adagunodo 2017a,b, Adagunodo 2018, Adagunodo et al. 2018b, c, Adejumo et al. 2018, Bayowa et al. 2018, Oyeyemi et al. 2018a, b, Sunmonu et al. 2018, Adagunodo et al. 2019a).

Potable water supply in coastal areas of the world has been a major concern due to saltwater intrusion since it constitutes the commonest of all pollutants of freshwater (Demirel 2004 and Batayneh 2006). In Nigeria, coastal communities like Aiyetoro (in Ondo state) and Lekki Peninsula (in Lagos state), are characterized by salty near-surface water, as about 90% of the boreholes drilled so far in these communities have been reported to yield saline-water and 10% known of producing freshwater after drilling become salty few months later (Oteri & Atolagbe 2003). Therefore, understanding the mechanisms of saline-water intrusion is essential for proper management of coastal resources (Ginzburg & Levanon 1987).

To explore these resources for sustainability of life on earth, various geophysical techniques (such as electrical resistivity, electromagnetic, magnetic, seismic refraction,

magnetotelluric and gravity) have been adopted successfully, either solely or as integration with other methods (Anomohanran 2013, 2015). The choice of geophysical method to use is a function of the depth of investigation and the budget for the exercise (Todd 2004). Out of these geophysical techniques that have been found useful in groundwater exploration, the electrical resistivity technique (employing the Schlumberger array) has been the most widely adopted (Imam & Hassan 2019). Its acceptance has been attributed to its simplicity on the field (Sunmonu et al. 2012) and data analysis, which is economical when compared to other geophysical techniques (Anomohanran 2013, Mohamaden & Ehab 2017, Adagunodo et al. 2018a). The geoelectrical technique had been used to map the near-surface characteristics and assess the seawater intrusion in various coastal environments around the globe (Ebraheem et al. 1997, Batayneh 2006, Bauer et al. 2006, Cimino et al. 2008, Adepelumi & Olorunfemi 2000, Kalaivanan et al. 2019). The magnitude of saline water intrusion from the coastal environment to the aquifers had been attributed to the rate of groundwater withdrawal and recharge; hydraulic gradient; and geological composition of that environment (Freeze & Cherry 1979). The present study, therefore, intends to use the geoelectrical technique for hydrolithological investigation of the near-surface aquifers around the Lekki Peninsula in Lagos, Nigeria. The choice for Direct Current (DC) resistivity survey is as a result of its ability to provide a quick synoptic picture of saltwater intrusion in terms of its apparent resistivity contrast of the aquifers.

Location and Geology of the Study Area

The study area is in the south-eastern part of Lagos, it lies between Latitudes 6°25' to 6°28' N and Longitudes 3°24' to 3°30' E (Fig. 1). It is bounded to the north by Lagos and Lekki lagoons, and to the south by the Atlantic Ocean. The area-Lekki and environs constitute part of the extensive barrier-lagoon complex in the coastal margin of Southwestern Nigeria.

This barrier-lagoon system is composed of five physiographic units which are broadly equivalents to sedimentary sub-environments. The units are beaches and barrier islands, channels and creeks, open lagoons, small deltas built into lagoons and swamps bordering the lagoons. The climate of the study area is tropical wet and dry seasons. A bimodal wet season is experienced in Lagos, with the first regime varying from April to July and the second regime from October to November. Two dry seasons are also experienced annually, with the major dry season varying from February to April and minor dry spell varying from August to September. Monthly temperature varies between 20° and 37°C. February to April is the major months with peak records of temperature in the study area. The relative humidity is persistently high and rarely below 70 per cent throughout the year along the Lagos coast.

The regional geology of Nigeria is embedded within the Pan-African mobile belt. This belt is believed to have separated Congo from West Africa Cratons (Adagunodo et al. 2018a, d, e). The separation experienced within this region is as a result of thermotectonic events over the years (Usikalu et al. 2018). The major geological settings in Nigeria are Basement Complex rocks (Adagunodo et al. 2013, 2017a, b, 2018a, 2019b) and Sedimentary Basins (Adagunodo et al. 2018f, g, 2019c). These two geological settings are equally distributed across Nigeria. The study area is underlain by Recent-Oligocene coastal plain sands and alluvium (Benin Formation) of the eastern Dahomey Basin (Fig. 2a). Dahomey six depositional groups are: Abeokuta/ Araromi, Ewekoro, Oshosun, Ilaro, Benin and Alluvium/ Akinbo Formations (Fig. 2b). The general geology, structural settings and stratigraphy of the eastern Dahomey Basin have been discussed in the works of Jones & Hockey (1964). The coastal plain sands are the youngest sedimentary unit in the eastern Dahomey Basin, and consist of series of poorly sorted sands with lenses of black to greyish clays, pebbly sands and sandy-clays deposited under transitional to continental environments (Jones & Hockey 1964). Recent alluvium constituting the deposits of major rivers (Ogun, Osun and Yewa) draining the eastern Dahomey Basin has been incorporated as part of this formation (Adagunodo et al. 2019c). The coastal plain sands are the main aquifer in Lagos coastal areas that are exploited through boreholes for domestic and industrial water supply (Longe et al. 1987).

MATERIALS AND METHODS

Thirty-one Vertical Electrical Survey (VES) stations were occupied with ABEM SAS 1000 Terrameter. The Schlumberger electrode array with current electrode spacing varied between 1 and 400m. The acquired VES data were plotted on bi-log papers, where preliminary partial curve matching analysis was used to produce the parameters of the initial layer (resistivity and thickness of each layer). The final layer's parameters for all the sounding points were obtained usingWinResist1D inversion software. The procedure used in this study for data acquisition, processing and analysis is in line with the geosounding technique for groundwater exploration as documented by Sunmonu et al. (2015). The final interpreted layer parameters were used to generate 2D geoelectric sections. Litho-logs from two boreholes drilled within the Lekki Peninsula area were also acquired to ascertain the subsurface lithologies. The VES results were correlated with the litho-logs to ascertain general near-surface lithology and the quality of the fluid content within the study area.

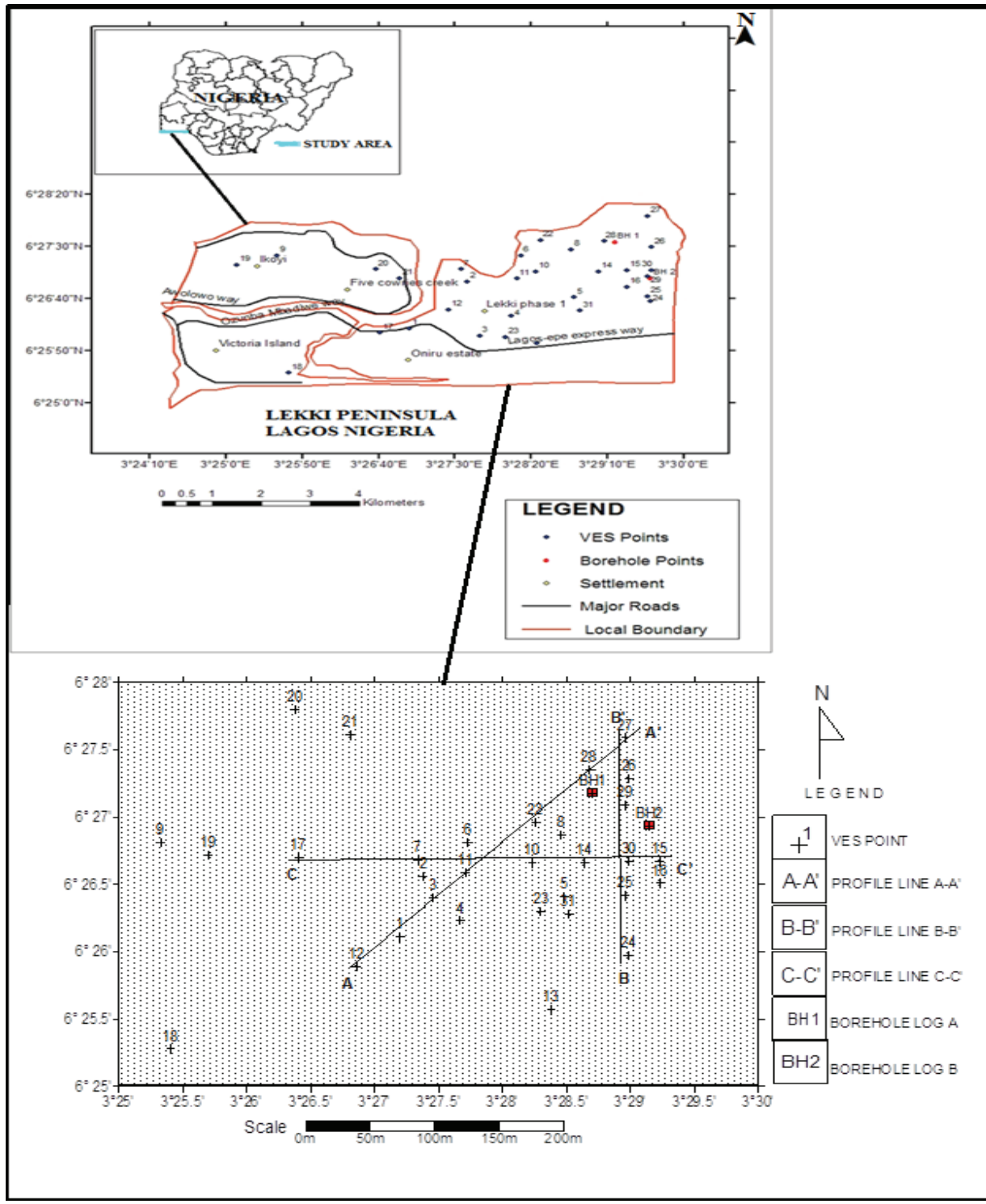

Fig. 1: Base map showing VES points and the borehole locations.

RESULTS AND DISCUSSION

The representative iterative curves as obtained in the study area are presented in Fig. 3. The processed VES layers parameters were used to generate the geoelectric sections. The two borehole logs acquired within the study area were interpreted through qualitative and quantitative approach. To understand the subsurface lithologies for sustainable groundwater exploitation in the study area, the geoelectric sections were correlated with borehole logs (litho-logs). The approach used in this study will enable a better understanding of the hydrodynamic equilibrium of the aquifers around the Lekki Peninsula, Lagos.

The Geoelectric Sections

2D geoelectric sections were generated along the profiles A-A^1, B-B^1 and C-C^1 (Fig. 1) to show the lateral and vertical distribution of resistivities within the volume of the investigated area. The geoelectric sections span through NE-SW, N-S and W-E directions with an approximate length of 600m, 400m and 580m respectively (Figs. 4a-c).

The geoelectric section along the profile A-A^1 (Fig. 4a) relates VES12, 1, 3, 11, 22, 28, and 27. In this section, a maximum of four distinct layers was identified. The topmost layer along this section is characterized by a resistivity value which ranged between 48-1535Ωm with a layer thickness ranging from 0.5-5.5m. This layer generally constitutes the unsaturated zone comprising of sand or fill materials. The second layer beneath this section is a brackish water zone extending southwest of VES12 and dipping beneath VES11 with a later inclination to a more horizontal form beneath VES22, 28 and 27. The lithological composition of this layer constitutes entirely of sand with resistivity value ranging between 14-166Ωm and a layer thickness of 4-23m. The third layer mapped along this section is a zone of silty mud. The hydrodynamics of this layer revealed that brackish water flows at the northeastern flank of the section, while freshwater flows at the southwestern flank. The very steep depression beneath VES11 probably serves as a barrier between the two different water qualities. The depth of the brackish water is between 10-17m with a resistivity value between 12-15Ωm. The freshwater zone thickness ranges between 9-16m with a resistivity value between 75-87Ωm. The fourth layer delineated beneath this section is the infinite layer which is a saline water zone with resistivity value between 1-8Ωm across the section. The thickness of this layer increases along the southwestern trend of the profile (Fig. 4a).

Fig. 4b shows the geoelectric section along the profile B-B^1. This section stretches about 400m in a north-south direction spanning through VES24, 25, 30, 29, 26 and 27. The topmost layer which comprises of sands and fill-materials is only about 2m deep with a range of resistivity value between 62 and 1254Ωm. This layer is considered as the unsaturated zone. The second layer beneath is more of sand formation with differing water quality. At VES24 and 25, it is probably saline water saturated with resistivity value between 2 and 7Ωm, while brackish water is experienced towards the eastern flank of this layer. The zone has a resis-

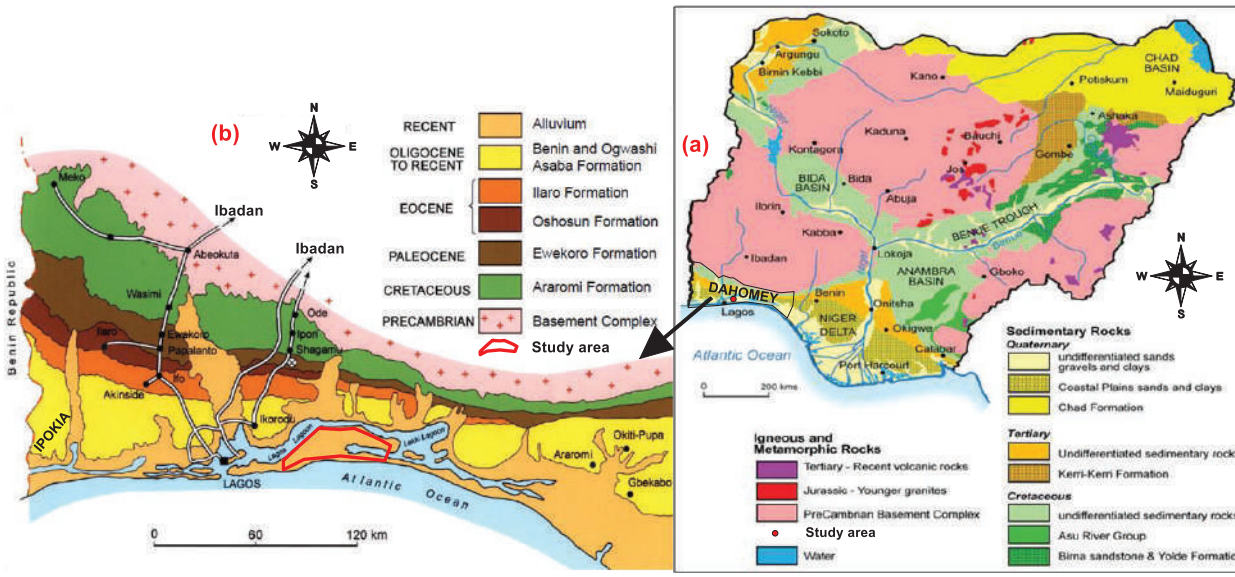

Fig. 2: Geological maps of (a) Nigeria (b) Dahomey Basin revealing the study area [modified from Adagunodo et al. (2018f, 2019c)].

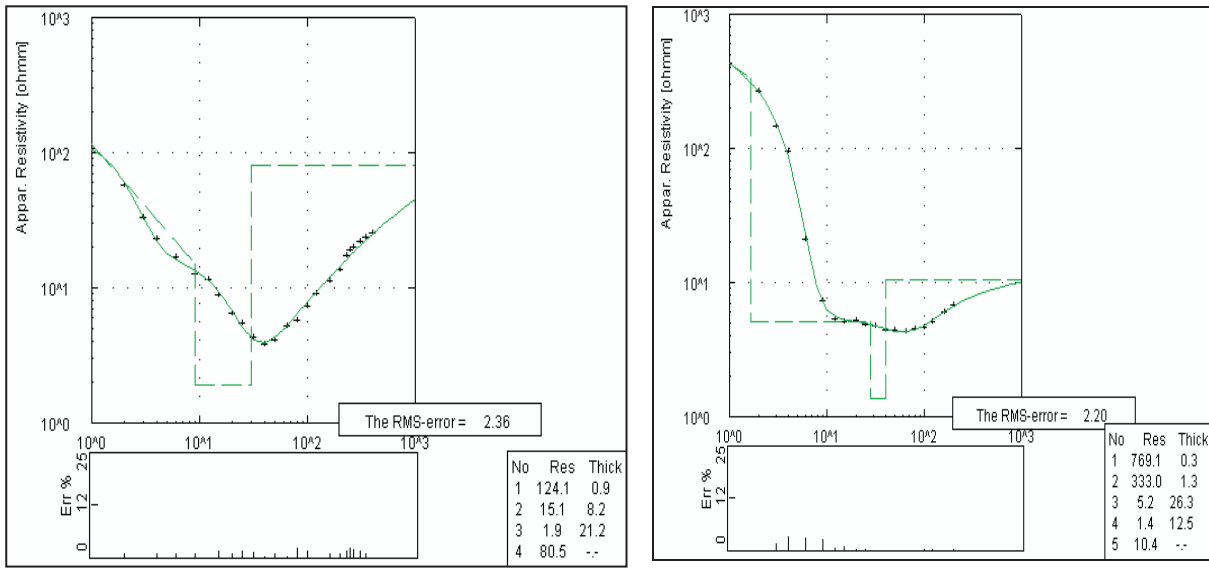

Fig. 3: Selected curve types as obtained in the study area (a) QH curve type (b) QQH curve type.

tivity value between 28 and 74Ωm. This layer has a thickness range between 2-8m and it is directly overlying a silty mud formation with intercalations of conglomerates. This zone could be interpreted as a freshwater aquifer zone, which flows across this profile. The depth range of this aquifer is between 11-42m, with resistivity value between 74-260Ωm. However, conglomerates with resistivity varying between 648 and 3560 Ωm were encountered beneath VES stations 24, 25, 29 and 30 within this layer. The fourth layer in this profile resembles the infinite layer of profile A-A[1].

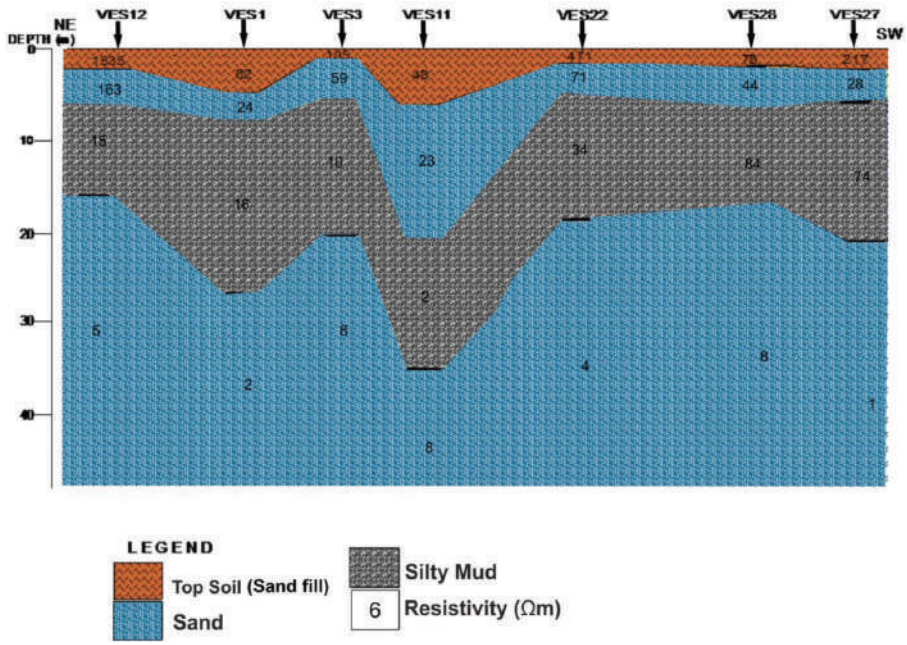

Fig. 4a: Geoelectric section along profile A – A[1].

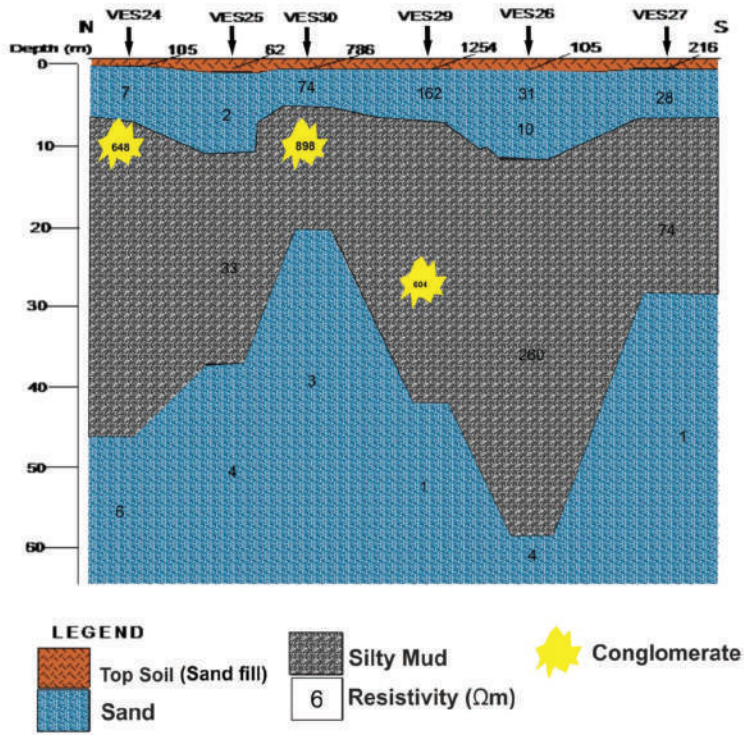

Fig. 4b: Geoelectric section along profile B – B[1].

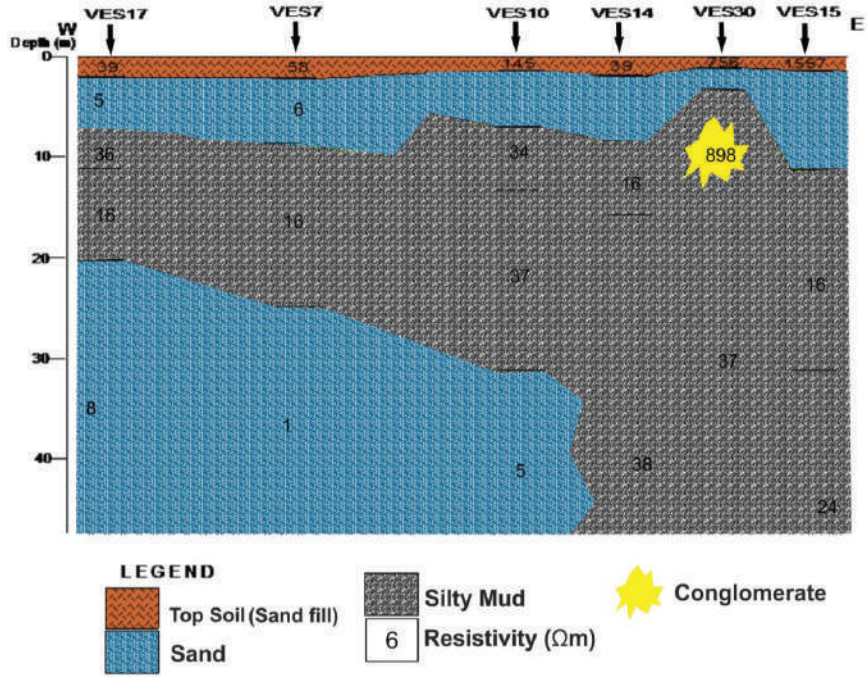

Fig. 4c: Geoelectric section along profile C – C[1].

The geoelectric section along the profile C-C[1] (Fig. 4c) covers about 580m in a west-east direction. This section relates VES17, 7, 10, 14, 30 and 15, which reveals a maximum of four (4) layer sequences. The resistivity value of the first layer ranges between 39 and 780Ωm with the thickness of 0.5-2m. The second layer is interpreted as sand formation, with different hydrodynamic forces. At VES 17 and 7, the water in this zone is probably saline, while beneath VES 10, 14, 30 and 15, the water in this zone could be brackish. Resistivity value along this layer varies between 5 and 81Ωm, with layer thickness of 3 and 10m. The third layer is interpreted as a silty mud zone with isolated conglomerate towards the eastern flank of the profile. This layer could be residing zone for brackish water, with a resistivity value between 16 and 38Ωm. The fourth layer is an infinite layer which could be interpreted as sand formation that is saline water-saturated, with varying resistivity between 1 and 10 Ωm. The fourth layer in the three (3) profiles share the same characteristics, which reveal the mean depth at which saline water could intrude to the aquifer in the Lekki Peninsula.

Borehole Logs

Quantitative and qualitative evaluation of the litho-logs acquired revealed the presence of saline, brackish and freshwater saturated units within the borehole sections (Figs. 5a-b). The lithology of the borehole consists entirely of sand and silty mud, which are typical of the Benin Formation. The borehole log 1 revealed a 5-layer lithology, which varied vertically downward as sand, silty mud, sand, silty mud and sand, with a maximum depth of about 65 m. Borehole log 2 revealed a 4-layer lithology, which varied vertically downward as sand, silty mud, sand and silty mud, with a maximum depth of about 70 m. The zones of freshwater on the two logs correspond to the second layer silty mud, which varied from 18 to 35 m in log 1 (Fig. 5a) and 22 to 38 m in log 2 (Fig. 5b), respectively. As revealed on the logs, the third layer which is composed of sand formation corresponds to the infinite layer (fourth layer) on the geoelectric section, which houses the saline water at this zone.

Integration of VES and Borehole Litho-Logs Results

Figs. 6a-b show the correlation between the VES points and borehole logs. The topmost layer in Fig. 6a has a thickness between 1.2 and 3m and varies in resistivity between 79 Ωm at VES 28 and 478Ωm at VES 22. This layer is underlain by sand formation, with depth varying between 3 and 7m. The third layer correlated with log A is a silty mud formation, with depth varying between 16 and 20 m. The resistivity of this layer varied between 44 and 86Ωm. The range of resistivity value in this layer is an indication of the water saturation (brackish water). The fourth layer correlated is a sand formation, with very low resistivity value of 2-8Ωm. This is an indication of the layer's salinity (that is, saline water formation). Fig. 6b shows log suit B correlation with

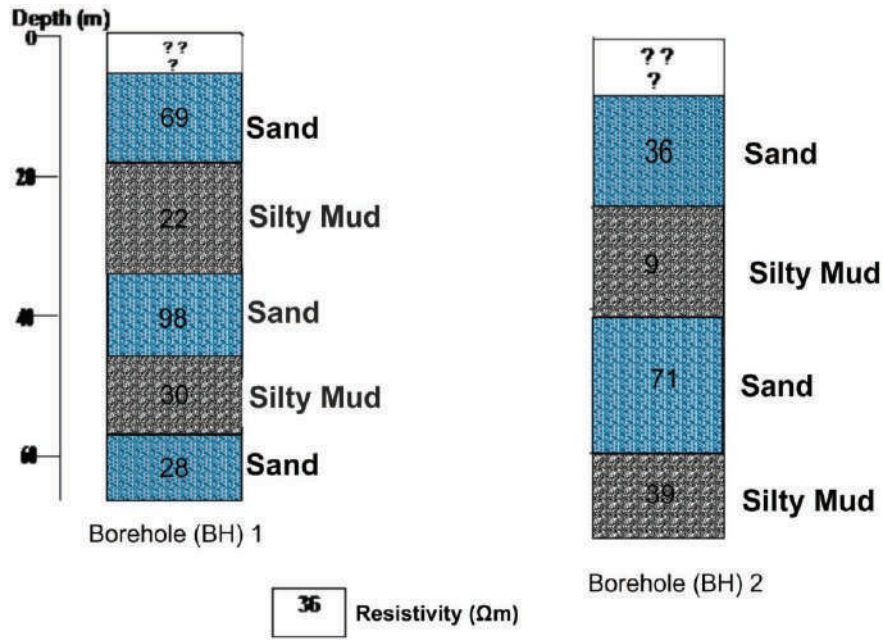

Fig. 5: Borehole Litho logs obtained around Lekki Peninsular (a) Log suit A (b) Log suit B.

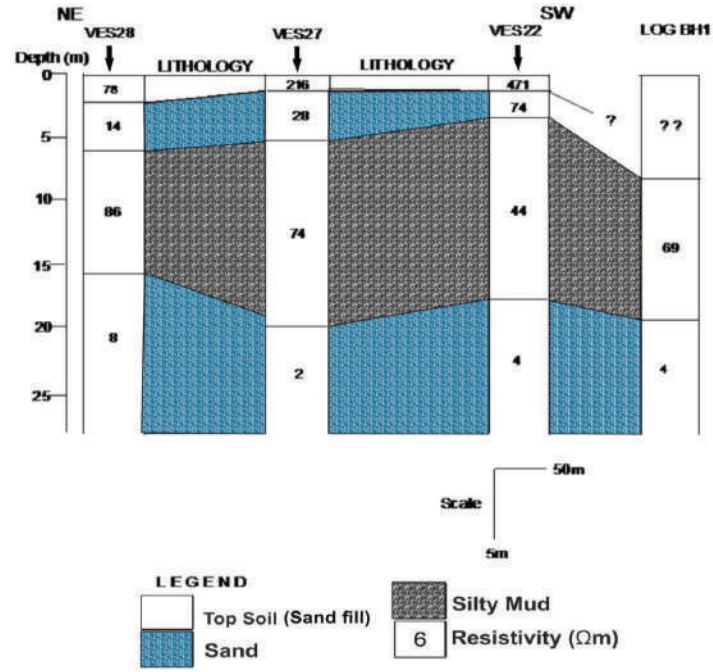

Fig. 6a: Correlation of VES stations with borehole log 1.

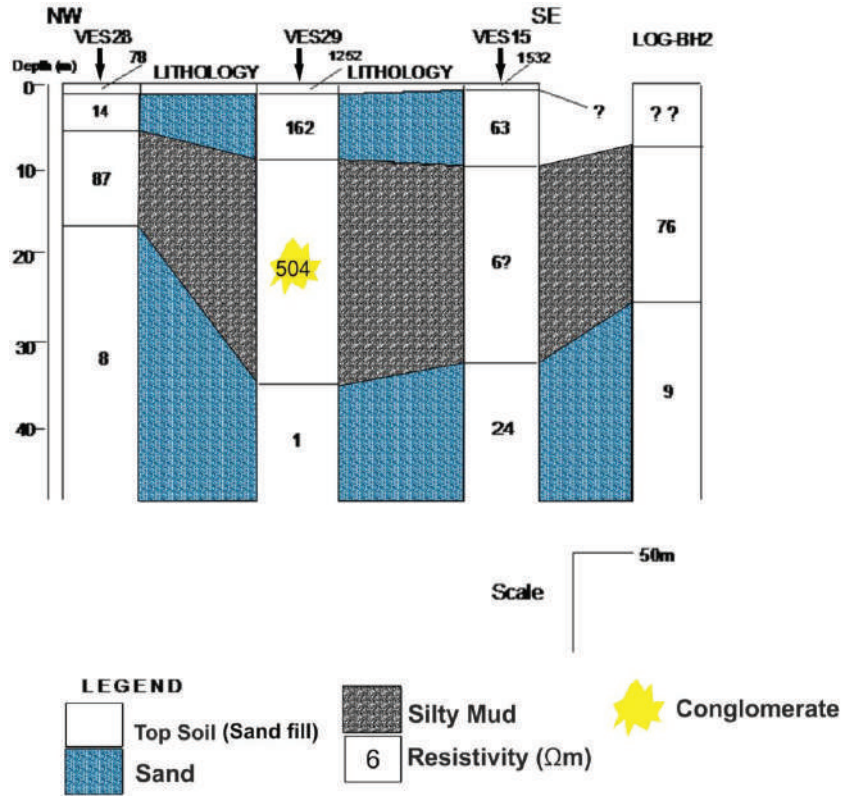

Fig. 6b: Correlation of VES stations with borehole log 2.

VES points 28, 29 and 15. The topmost layer extends to a depth of 1.5m at VES point 28 and thins in the south-east direction towards VES point 15. This layer is characterized by resistivity values between 78 and 1532Ωm. This layer is underlain by sand formation with varying depths between 5 and 9m as well as resistivity value between 14 and 162Ωm. The third layer correlated with the log is silty mud formation with varying depths between 17 and 35 m. The resistivity value in this layer is indicative of freshwater saturated zone. This third layer is underlain by saline water zone with resistivity values ranging between 1 and 9Ωm.

CONCLUSIONS

Hydrolithological investigation of Lekki peninsula area of Lagos, Southwestern Nigeria has been carried out using the surface and borehole litho-logs. The dominant trend of decreasing resistivity value with depth in part of the investigated area indicates an increase in salinity with depth (seawater/lagoon intrusion). Differences in resistivity value within the surveyed area are associated with the various lithologic types, water saturation and groundwater type (saline or freshwater). Distinct zone of saline water intrusion into the freshwater aquifer has been delineated in the near-surface based on resistivity variations. The prominent factor responsible for saline water intrusion observed in the study area is the excessive pumping of groundwater which results to the disturbance in the hydrodynamic equilibrium of the aquifer and the reduction of groundwater gradient allowing saline water to displace freshwater in the aquifer. Along the studied profiles, the upper interface between fresh, brackish and saline waters was encountered at the top 60m as inferred from the borehole log suits. In conclusion, the study area is characterized by the topsoil (sand/fill), conglomerate layer (unsaturated zone), silty mud layer (brackish/freshwater saturated), and sand layer (saline water-saturated). It is recommended that the people living/working within the study area should avoid excessive wastage of water to reduce the pumping rate and intrusion into the saline water formation.

ACKNOWLEDGEMENTS

The authors are indebted to Mr. Abideen of ROWDOT Geological Service for his immense contribution to the success of this study. Our sincere and endless thanks also go to the C.E.O of Groundwater and Geophysical Service Limited and Mr. Jude of Eauxwell Nigeria Limited. We also express our profound gratitude and appreciation to all our colleagues who made the fieldwork realistic. Finally, we acknowledge the support received from Covenant University.

REFERENCES

Adagunodo, T.A., Sunmonu, L.A., Ojoawo, A., Oladejo, O.P. and Olafisoye, E.R. 2013. The hydro geophysical investigation of Oyo state industrial estate Ogbomosho, Southwestern Nigeria using vertical electrical soundings. Research Journal of Applied Sciences, Engineering and Technology, 5(5): 1816-1829.

Adagunodo, T.A. 2017a. Groundwater pollution and control: An overview. In: Anna L. Powell (ed.) Groundwater Contamination: Performance, Limitations and Impacts, 1-135. ISBN: 978-1-153611-017-3; 978-1-53611-003-6, Nova Science Publishers, Inc. pp. 1-12.

Adagunodo T.A. 2017b. Groundwater contamination: performance, effects, limitations and control. In: Anna L. Powell (ed.) Groundwater Contamination: Performance, Limitations and Impacts, 1-135. ISBN: 978-1-153611-017-3; 978-1-53611-003-6, Nova Science Publishers, Inc. Pp. 33-64.

Adagunodo, T.A., Adeniji, A.A., Erinle, A.V., Akinwumi, S.A., Adewoyin, O.O., Joel, E.S. and Kayode, O.T. 2017a. Geophysical Investigation into the integrity of a reclaimed open dumpsite for civil engineering purpose. Interciencia Journal, 42(11): 324-339.

Adagunodo, T.A., Sunmonu, L.A., Adabanija, M.A., Suleiman, E.A. and Odetunmibi, O.A. 2017b. Geoexploration of radioelement's datasets in a flood plain of crystalline bedrock. Data in Brief, 15C: 809-820.

Adagunodo, T.A. 2018. Simple approach to groundwater study for domestic uses in rural area. Journal of Fundamental and Applied Sciences, 10(3): 129-143.

Adagunodo, T.A., Akinloye, M.K., Sunmonu, L.A., Aizebeokhai, A.P., Oyeyemi, K.D. and Abodunrin, F.O. 2018a. Groundwater exploration in Aaba residential area of Akure, Nigeria. Frontiers in Earth Science, 6: 66.

Adagunodo, T.A., Sunmonu, L.A., Oladejo, O.P., Hammed, O.S., Oyeyemi, K.D. and Kayode, O.T. 2018b. Site characterization of Ayetoro housing scheme, Oyo, Nigeria. IOP Conference Series: Earth and Environmental Science, 173: 012031.

Adagunodo, T.A., Sunmonu, L.A., Erinle, A.V., Adabanija, M.A., Oyeyemi, K.D. and Kayode, O.T. 2018c. Investigation into the types of fractures and viable depth to substratum of a housing estate using geophysical techniques. IOP Conference Series: Earth and Environmental Science, 173: 012030.

Adagunodo, T.A., Lüning, S., Adeleke, A.M., Omidiora, J.O., Aizebeokhai, A.P., Oyeyemi, K.D. and Hammed, O.S. 2018d. Evaluation of $0 \leq M \leq 8$ earthquake data sets in African Asian region during 1966-2015. Data in Brief, 17C: 588-603.

Adagunodo, T.A., Sunmonu, L.A. and Emetere, M.E. 2018e. Heavy metals' data in soils for agricultural activities. Data in Brief, 18C: 1847-1855.

Adagunodo, T.A., George, A.I., Ojoawo, I.A., Ojesanmi, K. and Ravisankar, R. 2018f. Radioactivity and radiological hazards from a kaolin mining field in Ifonyintedo, Nigeria. MethodsX, 5C: 362-374.

Adagunodo, T.A., Hammed, O.S., Usikalu, M.R., Ayara, W.A. and Ravisankar, R. 2018g. Data on the radiometric survey over a kaolinitic terrain in Dahomey Basin, Nigeria. Data in Brief, 18C: 814-822.

Adagunodo, T.A., Adejumo, R.O. and Olanrewaju, A.M. 2019a. Geochemical classification of groundwater system in a rural area of Nigeria. In: Chaminé H., Barbieri M., Kisi O., Chen M., Merkel B. (eds) Advances in Sustainable and Environmental Hydrology, Hydrogeology, Hydrochemistry and Water Resources. Advances in Science, Technology & Innovation (IEREK Interdisciplinary Series for Sustainable Development). Springer, Cham.

Adagunodo, T.A., Sunmonu, L.A., Adabanija, M.A., Omeje, M., Odetunmibi, O.A. and Ijeh, V. 2019b. Statistical assessment of radiation exposure risks of farmers in Odo Oba, southwestern Nigeria. Bulletin of the Mineral Research and Exploration, 159: 199-215.

Adagunodo, T.A., Bayowa, O.G., Usikalu, M.R. and Ojoawo, A.I. 2019c.

Radiogenic heat production in the coastal plain sands of Ipokia, Dahomey Basin, Nigeria. MethodsX, 6C: 1608-1616.

Adejumo, R.O., Adagunodo, T.A., Bility, H., Lukman, A.F. and Isibor, P.O. 2018. Physicochemical constituents of groundwater and its quality in crystalline Bedrock, Nigeria. International Journal of Civil Engineering and Technology, 9(8): 887-903.

Adepelumi, A.A. and Olorunfemi, M.O. 2000. Engineering geological and geophysical investigation of the reclaimed Lekki Peninsula, Lagos, Southwestern Nigeria. Bull. Eng. Geol. Environ., 58: 125-132.

Anomohanran, O. 2013. Geophysical investigation of groundwater potential in Ukeleghe, Nigeria. Journal of Applied Sciences, 13(1): 119-125.

Anomohanran, O. 2015. Hydrogeophysical and hydrogeological investigations of groundwater resources in Delta Central, Nigeria. Journal of Taibah University for Science, 9: 57-68.

Batayneh, A.T. 2006. Use of electrical resistivity methods for detecting subsurface fresh and saline water and delineating their interfacial configuration: A case study of the eastern Dead Sea coastal aquifers. Jordan Hydrogeology J., 14(1): 277-1283.

Bauer, P., Supper, R., Zimmermann, S. and Kinzelbach, W. 2006. Geoelectrical imaging of groundwater salinization in the Okavango Delta, Botswana. Journal of Applied Geophysics, 60: 126-141.

Bayowa, O.G., Olorunfemi, M.O., Akinluyi, F.O. and Ademilua, O.L. 2014a. A preliminary assessment of the groundwater potential of Ekiti State, Southwestern Nigeria, using terrain and satellite imagery analyses. Journal of Environmental and Earth Science, 4(18): 33-42.

Bayowa, O.G., Olorunfemi, M.O., Akinluyi, F.O. and Ademilua, O.L. 2014b. Integration of hydrogeophysical and remote sensing data in the assessment of groundwater potential of the basement complex terrain of Ekiti State, Southwestern Nigeria. Ife Journal of Science, 16(3): 353-363.

Bayowa, O.G., Fashola, D.K., Adegoke, A.B., Agesin, A.A. and Oyeniyi, S.A. 2018. Geophysical investigation for groundwater potential around Ladoke Akintola University of Technology campus, Ogbomoso, Southwestern Nigeria. Journal of Earth Science and Climatic Change, 9(8): 2-10.

Cimino, A., Cosentino, C., Oieni, A. and Tranchina, L. 2008. A geophysical and geochemical approach for seawater intrusion assessment in the Acquedolci coastal aquifer (Northern Sicily). Environmental Geology, 55: 1473-1482.

Demirel, Z. 2004. The history and evaluation of saltwater intrusion into a coastal aquifer in Mersin, Turkey. J. Environ. Manage., 70: 275-282.

Ebraheem, A.A.M., Senosy, M.M. and Dahab, K.A 1997. Geoelectrical and hydrogeochemical studies for delineating ground-water contamination due to salt-water intrusion in the Northern part of the Nile Delta, Egypt. Ground Water, 35: 216-222.

Freeze, A.R. and Cherry, J. A. 1979. Groundwater. Prentice Hall Inc., New Jersey.

Ginzburg, A. and Levanon, A. 1976. Determination of a saltwater interface by electric resistivity depth soundings. Hydrogeological Sciences, 21: 561-568.

Imam, A. and Hassan, Q. 2019. Geophysical investigation for groundwater potential of an area in Delhi NCR. Jordan Journal of Civil Engineering, 13(2): 361-376.

Jones, H.A. and Hockey R.D. 1964. Geology of parts of Southwestern Nigeria. Bulletin Geological Survey of Nigeria, 31: 56-77.

Kalaivanan, K., Gurugnanam, B., Suresh, M., Kom, K.P. and Kumaravel, S. 2019. Geoelectrical resistivity investigation for hydrogeology conditions and groundwater potential zone mapping of Kodavanar Sub-basin, southern India. Sustainable Water Resources Management, 1-21.

Longe, E.O., Malomo, S. and Olorunniwo, M.A. 1987. Hydrogeology of Lagos Metropolis. Africa Journal of Earth Sciences, 6(2): 163-174.

Mohamaden, M.I.I. and Ehab, D. 2017. Application of electrical resistivity for groundwater exploration in Wadi Rahaba, Shalateen, Egypt. NRIAG Journal of Astronomy and Geophysics, 6: 201-209.

Olafisoye, E.R., Sunmonu, L.A., Ojoawo, A., Adagunodo, T.A. and Oladejo, O.P. 2012. Application of very low frequency electromagnetic and hydro-physicochemical methods in the investigation of groundwater contamination at Aarada waste disposal site, Ogbomoso, Southwestern Nigeria. Australian Journal of Basic and Applied Sciences, 6(8): 401-409.

Oladejo, O.P., Sunmonu, L.A., Ojoawo, A., Adagunodo, T.A. and Olafisoye, E.R. 2013. Geophysical investigation for groundwater development at Oyo State Housing Estate Ogbomosho, Southwestern Nigeria. Research Journal of Applied Sciences, Engineering and Technology, 5(5): 1811-1815.

Oladejo, O.P., Sunmonu, L.A. and Adagunodo, T.A. 2015. Groundwater prospect in a typical Precambrian basement complex using Karous-Hjelt and Fraser Filtering Techniques. Journal of Industrial Engineering Research, 1(4): 40-49.

Oteri, A.U. and Atolagbe, F.P. 2003. Saltwater intrusion into coastal aquifers in Nigeria the second international conference on saltwater intrusion and coastal aquifers-Monitoring, Modeling, and Management. Mérida, Yucatán, México, March 30-April 2, 2003.

Oyeyemi, K.D., Aizebeokhai, A.P., Ndambuki, J.M., Sanuade, O.A., Olofinnade, O.M., Adagunodo, T.A., Olaojo, A.A. and Adeyemi, G.A. 2018a. Estimation of aquifer hydraulic parameters from surficial geophysical methods: A case study of Ota, Southwestern Nigeria. IOP Conference Series: Earth and Environmental Science, 173: 012028.

Oyeyemi, K.D., Aizebeokhai, A.P., Sanuade, O.A., Ndambuki, J.M., Olofinnade, O.M., Olaojo, A.A. and Adagunodo, T.A. 2018b. The use of geological-based geophysical surveys for groundwater distribution in crystalline basement terrain, SW Nigeria. IOP Conference Series: Earth and Environmental Science, 173: 012029.

Shishaye, H.A. and Abdi, S. 2016. Groundwater exploration for water well site locations using geophysical survey methods. Hydrology Current Research, 7(1): 1-7.

Sunmonu, L.A., Adagunodo, T.A., Olafisoye, E.R. and Oladejo, O.P. 2012. The groundwater potential evaluation at industrial estate Ogbomoso Southwestern Nigeria. RMZ-Materials and Geoenvironment, 59(4): 363-390.

Sunmonu, L.A., Olafisoye, E.R., Adagunodo, T.A. and Alagbe, O.A. 2013. Geophysical and hydro-physicochemical evaluation of hand-dug wells near a dumpsite in Oyo State, Nigeria. Archives of Applied Science Research, 5(6): 29-40.

Sunmonu, L.A., Adagunodo, T.A., Adeniji, A.A., Oladejo, O.P. and Alagbe, O.A. 2015. Geoelectric delineation of aquifer pattern in crystalline bedrock. Open Transactions on Geosciences, 2(1): 1-16.

Sunmonu, L.A., Adagunodo, T.A., Bayowa, O.G. and Erinle, A.V. 2016. Geophysical mapping of the proposed Osun State housing estate, Olupona for subsurface competence and groundwater potential. Journal of Basic and Applied Research, 2(2): 27-47.

Sunmonu, L.A., Adagunodo, T.A., Adeniji, A.A. and Ajani, O.O. 2018. Geoimaging of subsurface fabric in Awgbagba, Southwestern Nigeria using geomagnetic and geoelectrical techniques. Malaysian Journal of Fundamental and Applied Sciences, 14(2): 312-324.

Todd, D.K. 2004. Groundwater Hydrology. 2nd Edition, John Wiley and Sons, New York.

Usikalu, M.R., Oderinde, A., Adagunodo, T.A. and Akinpelu, A. 2018. Radioactivity concentration and dose assessment of soil samples in cement factory and environs in Ogun State, Nigeria. International Journal of Civil Engineering and Technology, 9(9): 1047-1059.

Nature Environment and Pollution Technology
An International Quarterly Scientific Journal

p-ISSN: 0972-6268
(Print copies up to 2016)
e-ISSN: 2395-3454

Vol. 19 | No. 2 | pp. 521-538 | 2020

Original Research Paper

https://doi.org/10.46488/NEPT.2020.v19i02.008

Open Access Journal

Field Performance and Economic Feasibility of Self-Propelled Vertical Conveyor Reaper (VCR) for Harvesting of Rice in West Sikkim and A Technological Strategy for Mitigation of Air Pollution through Crop Residue Burning in India

Abhijit Debnath*†[1] and Narvendra Singh Chauhan*

*Department of Farm Machinery & Power Engineering, College of Agricultural Engineering & Post Harvest Technology (Central Agricultural University, Imphal), Ranipool, Gangtok-737135, Sikkim, India

†Correspondence author: Abhijit Debnath; abhijit1732@gmail.com

[1]Present Address: Department of Civil Engineering, IIT (BHU), Varanasi-221005, Uttar Pradesh, India

Nat. Env. & Poll. Tech.
Website: www.neptjournal.com

Received: 09-08-2019
Accepted: 27-08-2019

Key Words:
Harvesting of rice;
Vertical Conveyor reaper;
Cost efficiency;
Air pollution;
Crop residue

ABSTRACT

Sikkim is a small Indian state located in the Himalayan region with 10.67 thousand hectares under cultivation and rice production of 19.69 thousand tonnes. Mechanized rice harvesting can play a crucial role in reducing grain loss and operational cost. To mechanize rice harvesting in hilly areas, a feasibility study has been undertaken to evaluate the field performance of self-propelled Vertical Conveyor Reaper (VCR) for the harvesting of rice as well as economically in terraces of Daramdin Government farm, Sikkim. In India, out of total 488 MT crop residue, about 24% of it was burnt in agricultural fields during 2017, resulting in emissions of particulate matter (PM2.5), elemental carbon (EC) and organic carbon (OC) and additionally CO_2 equivalent greenhouse gases (CO_2, CH_4, N_2O) were also added to the atmosphere. VCR has been evaluated under the Bureau of Indian Standards (BIS) code in field & laboratory conditions. The pre and post-harvesting field parameters for operating the VCR have been determined. The field capacity and efficiency of VCR were 0.1203 ha/h and 72.03% at 1.52 km/h, compared to 0.0178 ha/h in manual operation. At lower speed and better control, terrace-1 losses were 0.58% less than terrace-2. The harvesting cost/ha calculated considering the field capacity was Rs.1140.59/ha (US$16.44) and Rs. 1368.61/ha (US$19.73) for gear-1 and gear-2 respectively, which leads to considerable savings in time and labour which was 85.2% and 30.8% for the operational cost (gear-1) giving maximum efficiency. Also, instead of manual operation where stubble height remains at 70 mm, VCR harvest the crop at a maximum height of 11-13 mm, which further reduces the crop residue burning in fields and results in mitigation of air pollution. Therefore, in hilly terraces or plane areas where the use of reaper is feasible, its use may be promoted as efficient harvesting and environmental strategy both.

INTRODUCTION

Harvesting of crops is one of the time and labour consuming agricultural operations in peak harvesting season to get maximum return and minimum losses. Mechanical harvesting of all most all cereal crops is a challenging problem in India and tropical countries as India has good potential for increasing production, method of harvesting are still primitive, and farmer use hand sickle for this purpose (Tripathi et al. 2018a, Tripathi et al. 2018b). The agriculture status of Sikkim thus remained highly subsistence-oriented. Major obstacles of the State's agricultural development are the limited area of cultivable land, smaller and fragmented land holdings, difficult hilly terrain, and diverse agro-climatic condition prevailing at short distances, low farm income, declining labour availability for agriculture and allied activities, and lack of adequate supportive infrastructures (FS & ADD 2016). Further, its dependence on traditional methods has made the cost of cultivation very high in Sikkim. Topography and climatic condition of the state are favourable for agriculture and horticulture in the state as different principal crops grown in Sikkim are: wheat, paddy, maize, barley, buckwheat, cardamom, potato, tea, etc. In Sikkim, the cultivation is carried out in two conditions namely in terraces and valleys. The area occupied under rice cultivation and production in 2013-14 was 11040 hectares and 20.18 MT respectively and while from 2012-13 to 2015-16 the production was subsequently decreased from 21.34 MT to 19.69 MT.

It is the fact that crop productivity of any region highly depends on the farm power availability. In Sikkim, most of the field crops are cultivated either in sloping fields or in narrow terraces. The farm mechanization in Sikkim is almost non-existent and mainly depends on human and draft animal. Due to very steep slopes, the terraces are narrow and at times with a vertical interval of nearly 6 to 7 feet. Even scope for the use of conventional power tillers (Rated power 8 to 10

kW; Weight 200 to 400 kg) is limited to a few pockets of West Sikkim. The use of a machine of large size is not feasible due to the narrow and non-uniform width of terraces and the heavy weight of the machine.

Tillage, inter-culture and sowing equipment are specific to the type of land and those designed for plain lands does not necessarily suit to hill agriculture. The soil of Sikkim is mostly rocky and is also prone to landslide. Therefore, there arises a need to tackle these difficulties by carrying out various possible solutions. Despite excellent climatic conditions, abundant rainfall, and fertile soil (high organic content) of the region, the productivity of different crops is much lower as compared to national productivity level. Further, manual harvesting of crop requires considerable labour and time. Harvesting, threshing, and transplanting consume about 70 per cent of the total labour requirement (Kumar et al. 2013). Harvesting operation alone consumes 20 per cent which includes harvesting by sickles and bundle making (Dutt & Prasad 2002). During harvesting season, sufficient labourers are not available, and this leads to delayed harvesting and thus resulting in considerable losses of the crop. Therefore, mechanizing the harvesting, through the introduction of the self-propelled machine is one of the alternatives to tackle the problem, and reduce grain losses due to delayed harvesting and save the duration of harvesting. Where government have adopted and promoted combines for harvesting, but due to large quantity of straw handling after harvesting and disposal of waste products creating environmental pollution by burning in the field to prepare for next season. On the other hand, reaper harvesters are other alternative harvesting equipment.

The present study addresses the relevance of Vertical Conveyor Reaper in the agricultural development of the state. Researchers have analysed for different width of cut and field grain yields and at what width of cut the costs of complete machine are reaping with manual gathering would be equal to those of manual harvesting (Garg et al. 1984, Guruswamy et al. 1996). Reaper performance in relatively high working speed, giving it an overall reaping output of about 0.35 ha/h for 1.6 m wide cut and other three reapers, two were of 1 m cut, and the other was 0.5 m cut (Prasad et al. 1992). The effective field capacity of reaper was 0.43 ha/h using gear combination II with 76% field efficiencies (Nadeem & Gee-Clough 1983). Grain losses in wheat crop harvesting by Sayyed reaper-windrower in two different locations (Malir and Latif farm) were 1.03% and 1.46% at different crop moisture levels, and farm losses in machine and manual harvesting are 41.1 kg/ha and 84.9 kg/ha in case of Malir and Latif farms were 48.0 kg/ha and 139.6 kg/ha respectively (Bukhari et al. 1991). The crop conditions included crop variety, age of the crop, plant height, plant population, straw grain ratio, moisture content and crop yield an also area harvested, operational speed, working width, stubble height achieved and losses (Kathirvel et al. 2009).

Researchers indicated that self-propelled vertical conveyor reaper windrowers are suitable for harvesting crop with low plant population, plant height, crop canopy and low yield levels under rainfed conditions (Alizadeh et al. 2007, Bansal & Sakr 1992, Gill et al. 2018). Three different combined performances in terms of harvesting time, grain losses, fuel consumption, the energy required and total cost were compared and found that field efficiency of 70.5% at speed about 4.0 km/h and grain moisture content of 22% (Badr 2005). The parameters that were used to measure during crop harvesting as follows-(1) speed of travel (2) time losses and effective operating time (3) field efficiencies (4) effective field capacity (5) harvesting loss (6) harvesting cost. Front-mounted NDUAT (Narendra Deva University of Agriculture Technology, Faizabad, India) vertical conveyer reaper was compared with the conventional method regarding field capacity, forward speed and manpower for harvesting in hilly areas. The capacity of the machine at the farm was observed 93% more than the manual harvesting (0.009 ha/h) and saved 35% cost of operation with two times labour (Singh et al. 2007). Improvements and assessment are required due to inherent shortcomings like the drudgery of operation and non-suitability to harvest taller food crops that increase the utility of reaper (Singh et al. 2008). The field capacity of harvesting paddy through VCR was 0.3 ha/h with 73% at speed 3.2 km/h and 5.5 L/ha fuel consumption respectively. Manual harvesting was Rs. 400/ha (US$5.77) costlier than mechanical harvesting (Manjunatha 2009). Performance evaluation of VCR was carried for wheat crop varieties WH 147 and HD 2189 with BIS test code procedure. The header loss, conveying loss, and total machine losses were 0.85 %, 3.1%, and 3.95%, respectively. The cost of the harvesting with the straight-line method was found to be Rs. 677.50 / ha (US$9.77) with field capacity 0.13 ha/h, saving up to 44 per cent cost of harvesting (Kurhekar & Patil 2011). The harvesting for Finger millet (Eleusinecoracona gaertn) in the GKVK (Gandhi Krishi Vignana Kendra), Bangalore with four different commercial reapers viz. Sharchi, Fortune, KAMCO (Kerala Agro Machinery Corporation Ltd., India) and Vinayaka make power tiller reaper attachment was carried out while it is better by using the Shrachi reaper fitted with 24 cutting blades optimized with 90 cm cutting width. The minimum and satisfactory harvesting stubble height of 8-9 cm with negligible shattering losses observed by using Shrachi reaper compared to other reapers. Feasibility study of such equipment is required before their promotion for the harvesting of crops in the hilly region.

Biomass burning is an important source of aerosol and gaseous pollutants in the atmosphere, other than industrial and vehicular emissions having a potential impact on global air quality and climate chemistry (Andreae 1991, Levine et al. 1995, Andreae & Merlet 2001, Yang et al. 2008). Open biomass burning is a global practice to incineration of living and dead vegetation for land clearing and change land-use patterns. According to recent reports, around 730 Tg of biomass is burned annually from both natural and anthropogenic sources in Asia, of which 18% is contributed by India which also includes forest fires, grassland fires, and crop residue burning in agriculture field (Streets et al. 2003a, b). A study by Jain et al. (2014) and Venkataraman et al. (2006) also found that nearly 18-30% of the residue is burned in agricultural fields in India. According to National Policy for Management of Crop Residues (NPMCR) 2014 report, Ministry of Agriculture, Government of India crop residue generated in Sikkim is around 0.15 MT, residue surplus is 0.02 MT, residue burned 0.01 MT. In-situ crop residue burning is practiced not only in India but also worldwide (McCarty et al. 2009, Chen et al. 2017) despite having detrimental effects on air quality and human health. Hence, there is a need to understand pollutants emanated from crop residue burning can also affect properties, materials and human health when they are inhaled, causing respiratory problems (Schwartz 1993, Godish 1997, Mohanraj & Azeez 2004, Thaller et al. 2004, WHO 2004, Pandey et al. 2005).

Air Pollution From Crop Residue Burning

During harvesting periods, open burning of agricultural crop residues leads to emission of a large amount of air pollutants such as particulate matter (PM10, PM2.5, PM1), trace gases [carbon monoxide (CO), ammonia (NH_3), sulphur dioxide (SO_2)], greenhouse gases (GHGs) [carbon dioxide (CO_2), oxides of nitrogen (NOx), methane (CH_4), ozone (O_3)], elemental carbons (EC), organic carbons (OC), along with volatile organic compounds (VOCs) to the atmosphere (Ravindra et al. 2019a, Duan et al. 2004, Lemieux et al. 2004). As many developed countries have banned but it is still a prevailing practice in developing countries to burn the residue due to poor crop residue management (Ravindra et al. 2019a). Also, air quality is significantly affected because of agricultural field burning during the harvest period (Mittal et al. 2009). Witham & Manning (2007) showed that the impact of transport of pollutants during agricultural residue burning on a regional scale of air pollution.

Pollutants emission from crop residue burning and their dispersion varies according to seasons, atmospheric meteorology, and types of agricultural residue which could potentially affect biogeochemical cycles and climate change (Kaskaoutis et al. 2014, Sen et al. 2017, Ramanathan et al. 2005, McNeill 2017). The declining air quality is a great concern due to residue burning in the rural areas which harm human health and the environment, and there is a need to minimize the dispersion of burning emissions in the atmosphere (Awasthi et al. 2011, Ravindra et al. 2016a). Technological improvements in the agricultural sector and the use of modern agricultural practices can minimize the production of crop residue from rice harvesting (Ravindra et al. 2019a).

In the background of the above, the present study has been undertaken to evaluate the field performance and economic feasibility of Self-Propelled VCR (3.64 kW) for the harvesting of rice as well as to corporate a technological strategy to mitigate air pollution by burning paddy crop residues.

STUDY AREA

The present study is covering the Daramdin village located in Himalayan State of Sikkim the north-eastern part of India, covering coordinates of 27.31°N latitude and 88.30°E longitude. Daramdin has an average elevation of 1246 m. The average annual temperature of Sikkim is around 18°C. Fig. 1 depicts the map of CAEPHT, Ranipool and also it includes the area of the Daramdin farm where the performance evaluation of VCR has been undertaken.

MATERIALS AND METHODS

This includes the materials used and methodology followed for evaluating the performance of the commercially available self-propelled vertical conveyer reaper (walking type). The field evaluation of the machine has been undertaken in the laboratories of CAEPHT and Daramdin Government Farm. The details of the machine and other instruments used and methodology adopted is discussed under the following heads.

(a) Brief description of the machine

(b) Instruments used for performance evaluation

(c) Laboratory testing procedure [IS: 11467-1985 (Reaffirmed in 2012)]

(d) Field evaluation procedure [IS: 11467-1985 (Reaffirmed in 2012)]

(e) Cost analysis procedure [IS:9164-1979 (Reaffirmed in 2002)]

(f) Reason and consequences of stubble burning

Brief Description of Self-Propelled Vertical Conveyor Reaper (VCR)

Self-propelled VCR is a commercially available engine operated self-propelled machine (walk-behind type) used for harvesting cereal crops. It consists of crop row divider,

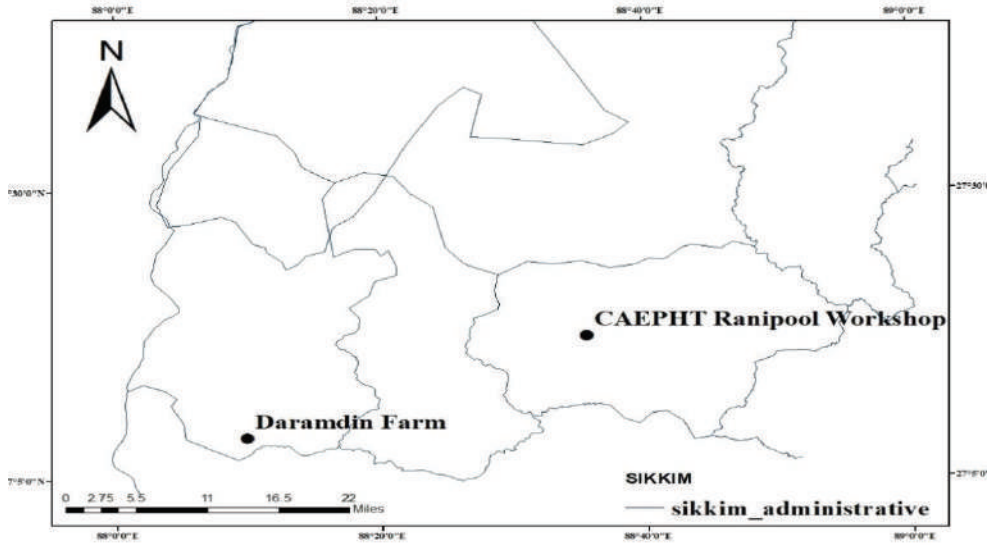

Fig. 1: Laboratory and field evaluation locations in Sikkim.

star wheel, cutter bar, and a pair of lugged conveyor belts and a handle fitted with clutch and brakes, engine, power transmission box, lugged wheels, crop row dividers, conveyor, star wheels, operating controls, and a sturdy frame. The machines cut and convey the crop vertically to one side and windrow the crops on the ground uniformly. Collection of crops for making bundles is done manually. The engine power is transmitted to cutter bar and conveyor chain through chain pulleys. The crop row dividers are provided with star wheels which help in lifting, gathering and guiding the crop towards the cutter bar, where reciprocating action of cutter bar cuts the crop stems. After the crop is cut, it is held in a vertical position during its passage employing pressure springs and star wheel against the vertical frame of the reaper. The vertically-held crop is then delivered one side of the machine by two lugged chain conveyors (one close to the cutter bar and the other at the upper end) and falls on the ground in the form of a fine-windrow perpendicular to the direction of the movement of the machine (El-Sharbasy 2006, Nadeem et al. 2015). It helps in easy collection of crops manually and saves labour for bundling operation.

Instruments and Other Items Used

During laboratory testing for its functionality and performance evaluation of the machine in the field for the harvesting of rice crop, following instruments and other items were used.

1. Measuring scale (1000 mm)
2. Measuring tape (30 m)
3. Tachometer
4. Stopwatch
5. Infra-red moisture meter
6. Hot oven
7. Weighing balance (capacity= 1 kg and 10 kg: LC=0.001 g and 0.5 g)
8. Measuring cylinder for estimation of fuel consumption
9. Sickle
10. Cleaning brushes

Laboratory Testing Procedure

The methodology adopted for both the laboratory testing of the Self-Propelled VCR is as per following test codes:

IS: 11467-1985 (Reaffirmed in 2012): Test Code for Cereal Harvesting Machine (IS: 11467-1985, 2012).

The main component of the self-propelled VCR and specification checking: The machine consists of major components of the machine are prime mover, a steering handle, drive wheel, crop divider, star wheel, conveyor chains, and cutter bar (Fig. 2).

The brief specifications of the VST reaper used for performance evaluation are summarized in Table 1.

Material analysis: The hardness and chemical analysis of critical components, such as knife section (IS: 6025-1982) (IS: 6025-1982, 1999), guard and ledger plate (IS : 6024-1983) (IS:6024-1983, 1999) and knife back (IS : 10378-1982) (IS: 10378-1982, 2001) shall be made and checked as per Bureau of Indian Standards.

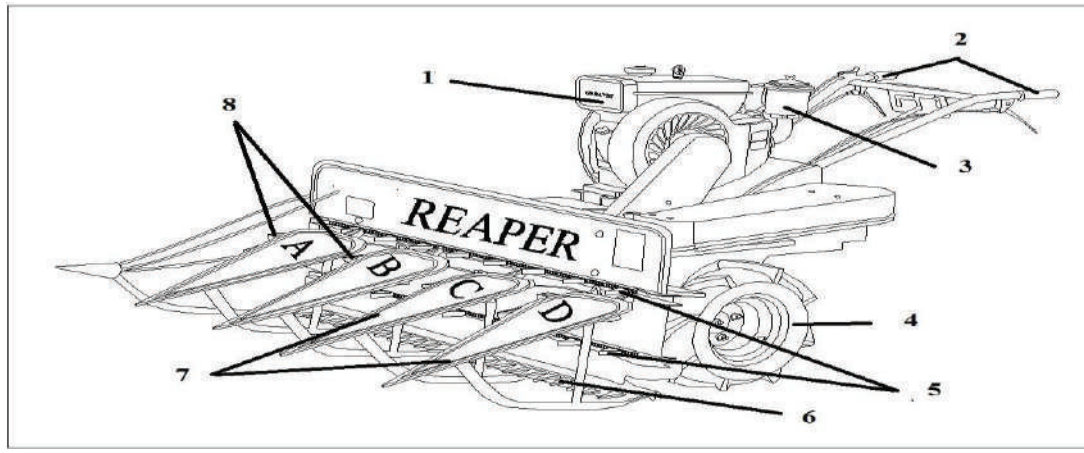

Fig. 2: Schematic diagram of self-propelled VCR showing different components.

1.	Prime mover	2.	Steering handle
3.	Muffler	4.	Drive wheel
5.	Conveyor chain	6.	Cutter bar
7.	Crop divider	8.	Crop guide(star wheel)

Visual observations and adjustments: The machine was thoroughly inspected and lubricated for its bearings, drives and other moving parts and adjustments of forward speed, ground clearance, wheel track, cutting device, marker etc. as per manufacturer's recommendations and Indian standards.

Field Evaluation Procedure [According to IS: 11467-1985 (Reaffirmed in 2012)]

Performance evaluation of vertical conveyor reaper in the field: After completion of the laboratory testing successfully, the machine was operated for normal field conditions for rice crops. The testing was conducted in the Govt. Farm at Daramdin, West Sikkim. Fig. 3 depicts the VST model of Vertical Conveyor Reaper and Fig. 4 shows the harvesting operation in Daramdin farm. As per recommendations of the BIS, following information were recorded.

(a) Field condition: It includes the shape of test field; area of test field; topography of field; type of field; moisture content of soil and frequency of bunds were recorded and reported.

(b) Crop conditions: It includes the name of the crop; the variety of crop; appearance and plant inclination; type of weed present; density of weed; moisture of straw; grain and weeds; crop grain ratio; maturity of the crop (age in days); number of tiller/sq.m; number of grain/ear head were recorded and reported.

(c) Determination of pre-harvest losses: The pre-harvest losses were determined at three places from the area with one-meter length in the direction of travel and width equal to the full width of the cutter bar. All the loose grain and ear heads are picked up manually.

Table 1: Specifications of the self-propelled VCR.

Manufacturer	VST Tiller Tractors Ltd.
Model	VS-4PR
Size of Reaper (mm)(L×W×H)	2200×1520×1100
Total Weight (kg)	210
Maximum power (kW)	4.5
Rated Power (kW)	3.64
No. of Gears	Forward-2, Reverse-1
Availability	Commercially available

Fig. 3: VST model of VCR.

(d) Field operation: The reaper was operated at uniform forward speed with full cutter bar and observations such as cutting width; cutting height; post-harvest losses (cutter bar +conveyance); condition of windrows; forward speed; area covered; fuel consumption, etc. were recorded in the datasheet.

(e) Ease of operations and adjustment: During field test ease of operation, operators' comfort, accessibility of controls and adjustments were noted down and reported.

(f) Defects; breakdowns and repairs: During field operation, the defects observed were noted down and reported. Any breakdown occurred during field test and replacement of any parts/components and repair underwent were noted down and reported.

(g) Labour requirement and cost of operation: Number of workers and man-hour required for side cutting as well as the cost for harvesting were recorded.

As stated earlier the preliminary testing of self-propelled VCR was carried out in the laboratory. Also, the machine was operated at the field of Govt. Farm Daramdin, Sikkim) as the terraces of the farm are wider and thus better suited for operation of VCR. The performance evaluation of the machine for the harvesting of rice was undertaken in two terraces. The side crops of the terrace of about 500 mm width were harvested manually to enable the smooth operation of the reaper and windrowing of harvested crops. Samples of the crop were marked with a square of 1 m side and harvested manually for estimation of various parameters such as grain yield, straw-grain ratio etc. During the field operation of the machine, observations such as the speed of operation, width

Fig. 4: Harvesting operation with VCR on terrace-1.

of operation, time taken to harvest the terrace area and fuel consumption were recorded. Using the above observations, the following parameters were computed for the machine.

(a) Speed of operation (forward speed): To estimate the forward speed of the machine while harvesting, the time taken for covering 10 m was recorded and the speed of travel was calculated.

(b) Time losses and effective duration of operation: Time losses while harvesting crop is the time for adjustments, turning, fuelling, etc. The start and finish time of harvesting in each plot were also noted.

(c) Field capacity: It is the average rate of area harvested. It is two types: (i) Theoretical field capacity and (ii) Actual/ Effective field capacity.

(i) Theoretical field capacity (TFC): Theoretical field capacity is the average rate of area coverage by machine when the machine doing its intended function at the rated speed and width utilized. The theoretical field capacity was calculated by the following equation:

$$TFC = \frac{W \times S}{10} \text{ ha/h} \quad ...(1)$$

Where,

W = Rated width of the implement in meters (m)

S = Speed of travel(km/h)

(ii) Effective field capacity (EFC): Effective field capacity is the actual rate of performance of land or crop processing in a given time, based on total field time. Actual field capacity was the actual average rate of field coverage by the amount of actual time (lost + productive time) consumed in the cutting operation. The effective field capacity was calculated using the following equation:

EFC(ha/h) = [area covered(ha)/time(h)] ...(2)

(d) Field efficiency (FE): Field efficiency is the ratio of effective field capacity to the theoretical field capacity and determined by the following equation

$$FE = \frac{EFC}{TFC} \times 100 \quad ...(3)$$

Where,

TFC = Theoretical Field Efficiency (ha/h)

EFC – Effective Field Efficiency (ha/h)

(e) Harvesting losses: Harvesting losses includes-(i) Uncut losses (ii) Pre-cutting losses, and (iii) Shattering losses.

(i) Un-cutting losses: Un-cutting losses were obtained by collecting un-cutting crop by sickle for each plot area. The total samples were collected and threshed manually, and then the cleaning grains were weighted. The percentage of un-cutting losses was calculated by using the following equation:

$$\text{Un-cutting losses (\%)} = \frac{\text{un – cutting losses / ha}}{\text{total yield / ha}} \times 100 \quad ...(4)$$

(ii) Pre-cutting losses: Pre-cutting losses were obtained by dividing each plot in four parts with the use of a wooden frame of 1m×1m dimensions, all the grains which fell within the frame are collected and weighed, and the mean of the measured values are recorded. The percentage of pre-cutting losses was calculated by using the following equation:

$$\text{Pre-cutting losses (\%)} = \frac{\text{Pre – cutting losses / ha}}{\text{total yield / ha}} \times 100 \quad ...(5)$$

(iii) Shattering losses: Shattering losses were obtained by locating a frame of the square meter on the ground after cutting the crop by machine, and then the grain losses in the frame represent pre-cutting and operating losses together. Then, for indicating the operating losses or shattering losses only, the pre-cutting losses must be subtracted. The percentage of shattering was calculated by using the following equation:

$$\text{Shattering losses (\%)} = \frac{\text{Shattering losses / ha}}{\text{total yield / ha}} \times 100 \quad ...(6)$$

(f) Total grain losses: The percentage of total grain losses was calculated by using the following equation:

Total grain losses (%) = (pre-cutting + un-cutting + shattering) losses ...(7)

(g) Moisture Content of the crop: The moisture content of the grain, straw and soil were measured using oven drying method and an infrared moisture meter. And it is calculated by using the equation.

$$\text{MC (\%Wet basis)} = \frac{\textit{weight of the water content in the product}}{\textit{Total weight of the product sample}} \times 100 \quad ...(8)$$

Where, MC (%Wet basis) = Moisture content of the sample in percentage weight basis.

Cost Analysis Procedure

The total cost of harvesting of Self Propelled VCR is estimated by referring to the Indian Standard Code i.e. IS: 9164-

1979 (Reaffirmed in 2002) [IS: 9164-1979, 2002]. Under these standards, the various cost factors include variable cost and fixed cost.

Fixed costs: (a) Depreciation: This component of cost reflects the reduction in the value of a machine with use (wear) and time (obsolescence). While actual depreciation would depend on the sale price of the machine after its use, based on different computational methods depreciation can be estimated. The following formula based on the straight-line method.

$$D = \frac{P - S}{L} \quad ...(9)$$

Where,

D = depreciation cost

P = purchase price of the machine (Rs/annum)

S = residual value of the machine i.e 5% of the purchase price.

L = useful life of the machine in years

(b) Interest on investment: Annual charges of interest may be calculated by the actual rate of interest payable. If the previous instalment is not available, 12 per cent of the average purchase price may be taken. The following formula shall calculate the average purchase price:

$$A = \frac{P + S}{2} \quad ...(10)$$

Where,

A = average purchase price (Rs)

P = purchase price of the machine (Rs) and

S = residual value of the machine (5% of P)

(c) Insurance and Taxes: Actual amount paid annually for insurance and annual taxes, if any should be charged. If not available, it may be calculated by 2 percent of the average purchase price of the machine per year.

Variable costs: (a) Fuel: Fuel consumption depends on the size of the power unit, load factor, and operating conditions. While the machine is working, the actual oil consumption should be recorded or may be taken from the results obtained at official testing stations. The following formulae can also estimate average fuel consumption:

$$A = 0.15 \times B \quad ...(11)$$

Where,

A = average diesel consumption in L/h,

B = rated power in kW.

(b) Lubricating oil: While the machine is working, the actual oil consumption should be recorded. In case oil consumption data is not available, oil consumption may be taken as 2.5 to 3 per cent of the fuel consumption on a volume basis. The cost of filters, replacement of oil, and other lubricants are included under repairs and maintenance.

(c) Repair and Maintenance: The accumulated repair and maintenance costs (TAR) at any point in a machine's life can be estimated from the following formulae:

For self-propelled machine, reaper,

$$TAR = 0.096\ X^{1.4} \quad ...(12)$$

Where,

TAR = Total Accumulated Repair Cost divided by the purchased price of the machine expressed as a percentage, and

X = 100 times the ratio of the accumulated hours of use to the wear-out life.

(d) Wages and Labour Charges: The wages and labour charges varied from person to person and prevailing rates in the region. The average cost per hour may be computed by dividing the total cost by the number of hours the operator has performed the work.

Total cost per hour: The sum of fixed cost, variable cost per hour gives the total operating cost of the machine for the harvesting of rice in terraces.

Total cost per hectare: The total cost per hectare may be obtained based on the actual field capacity of the machine with the use of the operating cost of the machine and actual field capacity of the machine. The value of harvesting one hectare with VCR may be compared with that of the traditional method of harvesting of rice crop in the region.

Reason and Consequences of Rice Crop Residue Burning

Reasons for stubble burning of rice crop:

(a) Mechanization has tremendously increased due to the Scarcity of labour for manual harvesting and their increasing wage rates.

(b) Due to shortened intervals between multiple cropping and seedbed preparation, urgent clearing of stubble is needed.

(c) To Control weeds, insects, disease sand pest availability of N, P and S in the soil for a shorter time.

(d) Poor storage facilitiesand higher diesel cost in trolley transportation and availability of crop residue market.

Consequences of Rice Crop Residue Burning

(a) Rise of global warming due to the emission of GHGs.

(b) The liberation of soot particles and causing smog in the environment (Lohan et al. 2018).

(c) Emissions of harmful air pollutants cause a serious threat to the health hazards of human, animal, and birds

(Lohan et al. 2018).

(d) Loss of carbon-nitrogen and sulphur present in straw are entirely burnt and lost to the atmosphere burning and deteriorate soil fertility (Lohan et al. 2018).

RESULTS AND DISCUSSION

The performance evaluation results of self- propelled vertical conveyor reaper (VCR) obtained under laboratory and field conditions are discussed in three stages. The functionality of the VCR was tested in the laboratory conditions in the CAEPHT, and then its performance evaluation for harvesting the rice crop was undertaken in the field of Daramdin in November 2013.

Laboratory Test

Under laboratory conditions, the machine was tested for its functionality, and relevant data collected during the laboratory tests were included in this section. The forward speed of the machine was measured in a different gear, and throttle settings of the machine (gear- 1 and gear- 2 with respect to 50% and 75% throttle settings) and the results recorded are summarized in Table 2.

As per the observations, the comfortable speeds for the operation was 1.86 km/h and 2.51 km/h recorded at gear- 1 (50% and 75%) for gear- 2 (50% throttle valve). At the higher speed, the vibration of the machine and the noise produced were higher and inconvenient for the operator to handle it and lower speed would affect the field capacity and thereby result into a higher cost of operation.

Crop Parameters

The details of the crop, on which the performance of the machine was evaluated, are recorded and summarized in Table 3.

The harvesting of rice crop (variety: Panth-12) grown in two terrace plots were 287.66 and 252.86 m^2 areas. The average heights of the crop for terrace 1 and terrace 2 were in the ranges of 850 to 1250 mm and 700 to 900 mm respectively. The age of the crop at the time of harvesting was 110 days. The average number of hills per square meter of terrace-1 and terrace-2 were 45-55 and 40-50 respectively. The average moisture contents of the grain were found to be 16.26% (wet-basis) and 15.71% (wet-basis) for terrace 1 and 2 respectively.

Manual Harvesting

To get the reference data for comparing various parameters for evaluating the performance of the machine, the crop was harvested manually, and relevant data were recorded and summarized in Table 4.

The average weight of the crop grain per square meter was 0.76 kg and 0.73 kg for the terrace 1 and 2 respectively. It is evident from Table 4 that the grain yield of terrace 1 and 2 was 3400 kg/ha and 3000 kg/ha, respectively.

Performance Evaluation of Self-propelled Vertical Conveyer Reaper

Performance evaluation of self-propelled vertical conveyer reaper for the harvesting of rice crop was undertaken at Daramdin Farm (under Department of FSSandAD) Dist. West Sikkim during November 2013. The performance evaluation was undertaken according to the procedure as per BIS codes. During field evaluation procedure, data related to the field, crop, and machine were recorded and summarized in Table 5.

Table 2: Laboratory speed measurement of self-propelled VCR.

Direction of motion	Engine speed (rpm)	Duration (s)	Distance travelled (m)	Speed (km/h)	Average Speed (km/h)
Forward Reverse	Gear 2 and 75% throttle setting	1:44:83 1:50:83	100	3.43 3.25	3.34
	Gear 2 and 50% throttle setting	2:17:79 2:28:91	100	2.61 2.42	2.51
	Gear 2 and 25% throttle setting	3:12:20 3:21:15	100	0.93 0.89	0.91
	Gear 1 and 75% throttle setting	2:20:35 2:25:20	100	2.56 2.47	2.51
	Gear 1 and 50% throttle setting	3:10:21 3:15:57	100	1.89 1.84	1.86
Reverse speed	75% throttle setting	2:46:02 2:64:12	100	2.43 2.27	2.35
	50% throttle setting	3:04:25 3:06:12	100	1.97 1.96	1.97
	25% throttle setting	4:12:21 4:17:70	100	0.71 0.70	0.71

Table 3: Details of crop-related parameters used for harvesting with VCR.

S. No.	Parameters	Observations	
1.	Crop variety	Panth 12 (PD-12)	
2.	Row to row spacing	NA (manual planted)	
3.	Age of the crop at the time of harvesting (days)	110	
4.	Field plots	Observations	
		First terrace	Second terrace
5.	Average plant height (mm)	1020±210	790±100.02
6.	No. of hills/sq. m(No./sq. m)	45-55	40-50
7.	No. of tillers per hill	10-13	9-11
8.	Length of ear head (mm)	225±5.8	203±5.5
9.	No. of grains per ear head (cm)	91±7	55±3
	Moisture content (%wet-basis)		
10.	Straw	65.33±1.32	63.63±1.70
	Grain	16.26±0.81	15.71±1.15

It is evident from Table 5 that effective field capacity of the self-propelled VCR was 0.15 ha/h at an average operating speed of 1.52km/h when the machine was operated in 1st gear. Time taken to harvest rice crop of terrace 1 (Area: 228.61 sq. m) was about 0.19 h and the fuel consumption of the machine was 0.736 L/h. In case of terrace 2, results indicate that in 2nd gear effective field capacity of the machine was 0.117 ha/h at an average speed of 2.189 km/h. Time taken to harvest the rice crop (Area: 202.66 sq. m) was about 0.22 h and the fuel consumption of the machine was 0.545 L/h.

Table 4: Performance data for manual harvesting of rice.

S. No.	Parameters	Terrace 1	Terrace 2
1.	Moisture content (%Wet basis)		
2.	-Straw (Wet basis)	65.33±1.32	63.63±1.70
	-Grains (Wet basis)	16.26±0.81	15.71±1.15
3.	Soil moisture content (%Wet basis)	29.3	27.5
4.	Variety of crop	Panth 12(PD-12)	Panth 12(PD-12)
5.	Maturity of crop (days)	110	110
6.	Area of the terrace (sq. m)	287.66	252.86
7.	Type of weed in the field	*Cyprus* sp. (motha), *Cyanodon dactylum* (durba), *Echinocholo acrrusgalli* (sama grass)	*Cyprus rotendum* sp., *Echinocholoa crrusgalli* (sama grass), *Spilenthus armezera* (kooro)
8.	Stubble height(mm)	70.3±5.7	69±3.6
9.	Plant height (mm)	850-1250	700-900
10.	Length of ear head (mm)	217.6±18.6	203±15.4
11.	No. of grain per ear head	80-110	65-80
12.	No. of hills per sq. m	45-55	40-50
13.	No. of tillers per hill	10-13	9-11
14.	Weight of crop per sq. m (kg)	0.76±0.015	0.73±0.015
15	Mass of grain per sq. m (kg)	0.34±0.02	0.30±0.02
16.	Straw-grain ratio (%)	1.23:1	1.42:1
17.	Grain yield (kg/ha)	3400	3000

The variations in the effective field capacities of the machine were due to variations in the operating speed of the machine. The theoretical field capacity of the machine for terrace-1 and terrace-2 were 0.167 ha/h and 0.241 ha/h respectively. The field efficiency of the machine in terrace 1 (72.03%) was higher than that of terrace-2 mainly because at a lower speed, operator's control on the machine was better and this he could operate the machine in a better manner in terrace 1.

Table 6 gives the data for harvesting losses recorded during the field tests. The measured values of pre-harvest and harvesting losses for 10 m length in the terraces are summarized here. The pre-harvest losses were neglected in the analysis. The losses (viz. shattering loss, cutter bar loss) were calculated by measuring the width of cut of the machine (1.10 m) for 10m length of the forward direction of the machine. The cutter bar loss, conveying loss, and total machine losses were 0.41%, 3.12%, and 3.53% in terrace-1; where 0.44%, 3.67% and 4.11% in terrace-2 respectively.

Cost Analyses

Using the performance data above and referring the Indian Standard IS: 9164-1979 (Reaffirmed in 2002) the operating cost of the machine for the harvesting of rice was estimated. The fixed and variable costs of the machine for harvesting the rice are given in Table 7. Fig. 5 shows the comparison of the cost of harvesting (Rs/ha) for the machine at gear 1 and 2 and that of manual harvesting.

The comparison of fixed and variable cost for gear-1 and gear-2 operation are shown in Fig. 6 and Fig. 7 respectively.

With respect to the purchase price, depreciation, interest, shelter, and insurance, the fixed cost of the machine operated

Table 5: Performance data for machine harvesting of rice.

Sl. No.	Parameters	Observation	
		1st gear/terrace 1	2nd gear /terrace 2
1	No. of operators	1	1
2	Duration of test (h)	0.19	0.22
3	Forward speed (km/h)	1.52	2.189
4	Area (sq. m)	287.66	252.86
5	Area harvested (sq. m)	228.61	202.66
6	Effective Working width (m)	1.10	1.10
7	Stubble height (mm)	15±8	21±3
8	No. of stoppage (times)	1	3
9	Mass of crop per sq. m (kg)	0.754	0.726
10	Mass of grain per sq. m (kg)	0.328	0.288
11	Crop grain ratio	1.29:1	1.52:1
12	Total Grain yield (kg)	94.35	72.82
13	Moisture content (% Wet basis)		
	Grain (% Wet basis)	16.26±0.81	15.71±1.15
	Straw (% Wet basis)	65.55±1.32	63.63±1.70
14	Theoretical field capacity (ha/h)	0.1670	0.241
15	Effective field capacity (ha/h)	0.1203	0.092
16	Field efficiency (%)	72.03	38.50
17	Fuel consumption (L/h)	0.736	0.545
18	Crop handled (kg/h)	941.64	743.29
	Harvesting loss (% total grain yield)		
	Pre-harvest loss (%)	Nil	Nil
19	Conveying loss (%)	3.12	3.67
	Cutter bar loss (%)	0.41	0.44
	Total losses (%)	3.53	4.11

Table 6: Harvesting losses (g) for 10 m of operation.

Sl. No.	terrace	Time taken for 10 m (s)	Width of cut (m)	Height of stubble (mm)	Losses per width of cut × 10 m (g)			Total machine losses for 10m (g)
					Pre-harvest	Cutter bar (Post + Uncut) Loss	Shattering loss in 10 m length	
1	1	23.65	1.10	15	Nil	15	115	130
2	2	16.89	1.10	21	Nil	14	120	134
3	2	16	1.10	23	Nil	12	123	135

in gear-1 was Rs. 48.91/h (US$0.70) which accounts for 13.67% of the operating cost of the machine. The total variable cost of the machine (including fuel, oil and lubricants, repair and maintenance cost and operator charges) was Rs. 88.3/h (US$1.27) which accounts for 24.71% of the machine cost. But the cost will vary according to the fluctuating fuel price and spare and repair rates of the machine parts. Lack of authorized repair shops and suitable after-sale services are also a reason for high repair rate and spare rates. The total cost of the machine was Rs.137.21/h (US$1.98) for gear -1 and Rs.125.91/h (US$1.81) for gear- 2 respectively. The harvesting cost per hectare calculated considering the field capacity was found to be Rs.1140.59/ha (US$16.44) and Rs. 1368.61/ha (US$19.73) for gear-1 and gear-2 respectively. It is observed for harvesting with the gear-1 operation, and it saves the cost, which is more beneficial. The labour requirement for the machine for operating in gear-1 and gear-2 are 8.3 (man-h/ha) and 10.8 (man-h/ha).

Comparison of Harvesting with VCR and Manual Harvesting Methods

The self-propelled VCR was compared with conventional practices and presented in Table 8. It was observed in the field that on an average 56 man-h/ha could harvest rice crop

Table 7: Data related to the cost of rice harvesting with VCR and manual harvesting with a sickle.

Sl. No.	Observations	Harvesting (gear- 1) with VCR	Harvesting (gear- 2) with VCR	Manual harvesting (Sickle)
1	Purchase value (Rs.)	107227	107227	60
2	Machine life (years)	15	15	10
3	Annual use (hours)	300	300	200
4	Salvage value (Rs.)-5%	5361.35	5361.35	3
5	Interest rate (%)	12	12	12
6	Taxes, shelter and insurance (2% of purchase price)	2	2	0
7	Operator's charges, Rs./day (8h)	335	335	235
8	Actual field capacity (ha/h)	0.1203	0.092	0.017857
9	**Fixed cost**			
10	Depreciation (R.s/year	6791.04	6791.04	5.70
11	Interest (Rs./year)	6755.30	6755.30	3.78
12	Shelter and insurance (Rs./year)	1125.88	1125.88	0
13	**Total fixed cost(Rs/h)**	48.91	48.91	0.05
14	**Variable cost**			
	Fuel (Rs./h)	42.68	31.65	0.00
15	Oil and lubricants (Rs./h)	1.06	0.79	0.00
16	Repair and Maintenance (Rs./h)	2.69	2.69	0.00
17	Operator charges (Rs/h)	41.88	41.88	29.38
18	**Total variable cost (Rs./h)**	88.31	77.01	29.38
19	**Total cost (Rs./h)**	137.21	125.91	29.42
20	**Cost of harvesting (Rs./ha)**	1140.59(US$16.44)	1368.61(US$19.73)	1647.67(US$23.75)

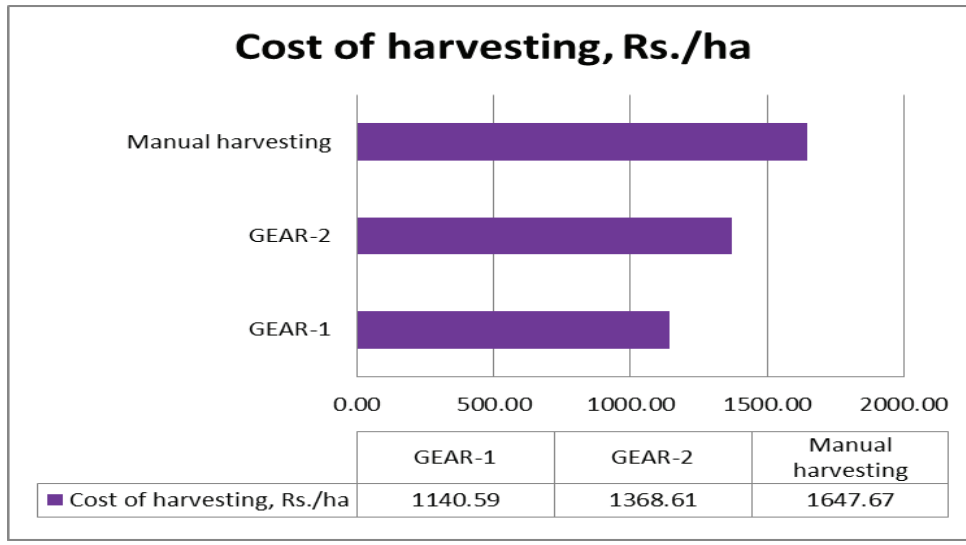

Fig. 5: Bar graph showing the cost of harvesting, (Rs/ha) for the machine (gear-1 and gear-2) and manual harvesting.

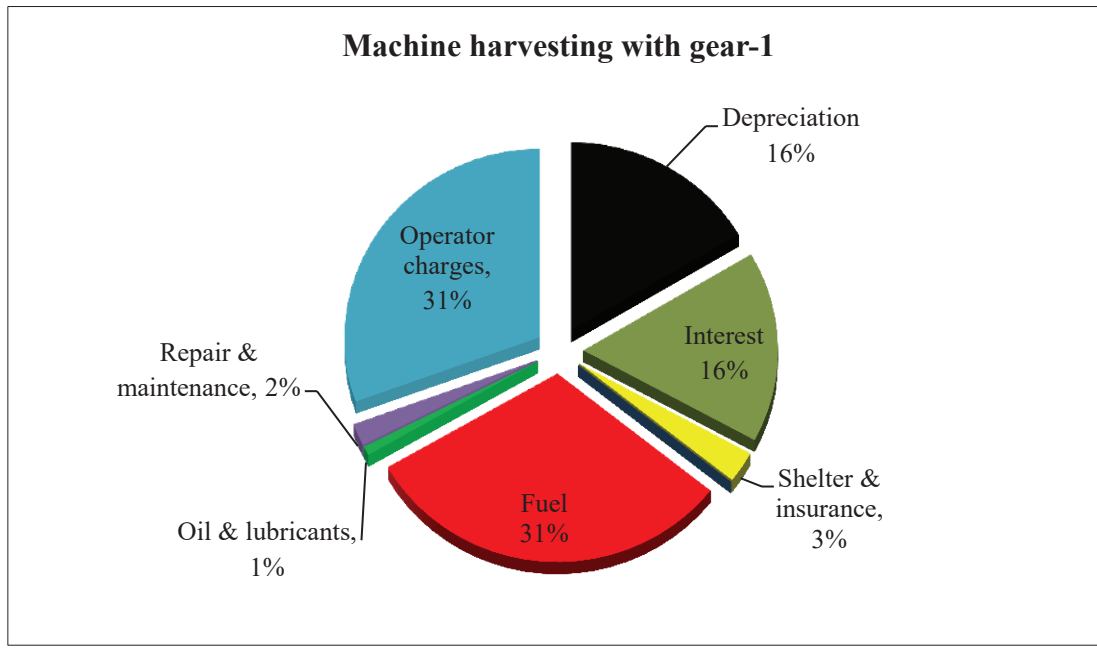

Fig. 6: Comparison of fixed cost and variable cost for gear-1 operation.

manually with the sickle. The use of VCR lead to considerable savings in time and labour was found 85.2% (Gear 1) and 80.6% (Gear 1) higher than that of manual harvesting method and could save 30.8 and 16.9% of the cost of operation in gear-1and gear-2 respectively.

Based on the study it is evident that the use of VCR is certainly helpful in saving time, labour, and cost of the harvesting operation. The lower speed of operation is recommended for better operational control of the machine during the harvesting operation. However, this machine cannot be operated in the terraces having a width less than 4 m.

Total Crop Residue Generation and Amount of Proportion Burnt in Indian Agricultural Fields

The total crop residue generated in India was calculated using Eggleston (2006) guidelines based on annually crop production data acquired from the Department of Agriculture

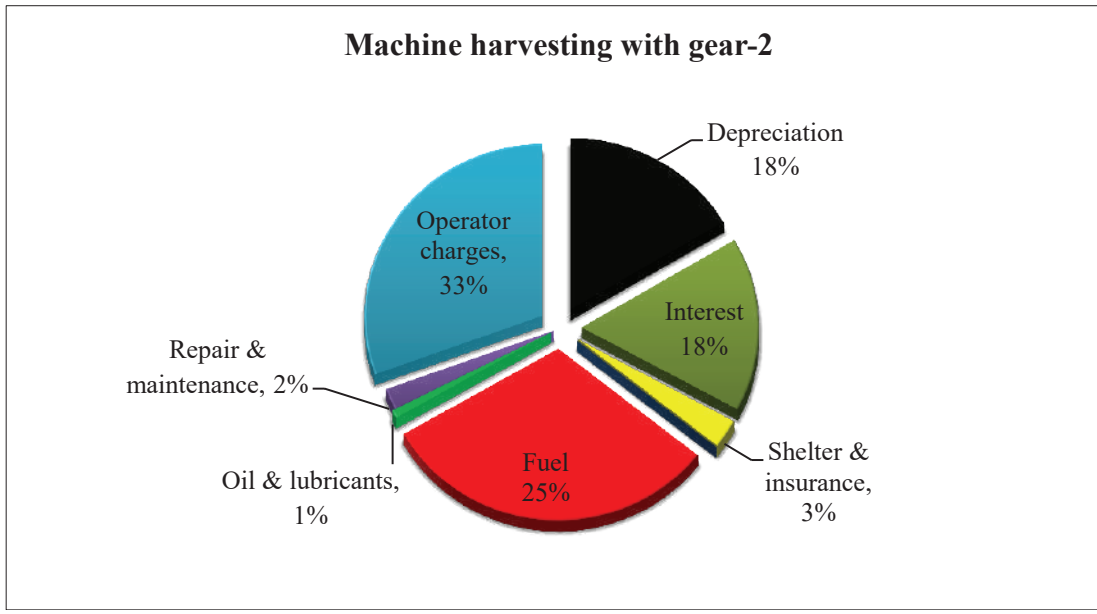

Fig. 7: Comparison of fixed cost and variable cost for gear-2 operation.

(2018) (Ravindra et al. 2019a). Sowing window between the harvesting of Kharif crops, and rabi crops are very short are one of the major causes that farmers prefer to burn residue in agriculture fields (Ravindra et al. 2019a). As can be observed from Table 9, crop production has increased from 476 MT to 618 MT since 2003-04 to 2016-17. Table 10 shows the comparative overview of crop residue burning in India.

Crop Residue Generated by Harvesting with VCR Implement and its Benefits

The plant heights of the crop in terrace 1 and terrace 2 were 850 to 1250 mm and 700 to 900 mm respectively. As per Table 11, the average plant height of paddy crop in terrace 1 and terrace 2 was 1020±210 mm and 790±100.02 mm respectively. But after harvesting with VCR the stubble height in terrace 1 and terrace 2 were 15±8 mm and 21±3 mm respectively, which is 50 mm shorter than manual harvesting in both terraces. The plant height in second terrace slightly higher due to VCR operated at 2nd gear.

VCR harvested crop produces very less amount of stubble which is neither required to burn in the field for sowing next crop. It is because the cutter bar is operated in the field at a height of 1.2 mm. 15-21 mm of average stubble can be easily degraded on the field by in-situ methods, which can lead to enrichment of soil for the next crop. Besides, manual harvesting leaves a gap for cutting of stubbles which needs labour and puts a huge pressure farmer due to increasing wage rates. Also, after cutting no availability of storage facilities and proper market to sell the crop residue.

Harvesting with VCR leaves rare possibilities of burning crop residues by the farmers and subsequently, it reduces the possibility of air pollution and pollutant dispersion in the atmosphere. VCR can be used as a technological solution to reduce biomass burning in paddy fields.

Available Options for Mitigation of After Harvested Crop Residue Burning Pollution

There are various available tech and non-technological based residue burning mitigation options, which will help to reduce air pollution and GHG emissions, but also limit the adverse

Table 8: Performances with VCR for rice harvesting.

Sl. No.	Parameters	Gear-1	Gear- 2
	Labour requirement(man-h/ha)	8.3	10.8
	Total cost of operation (Rs./ha)	1140.59(US$16.44)	1368.61(US$19.73)
	Time and labour Savings (%)	85.2	80.6
	Cost savings (%)	30.8	16.9

Table 9: Annual total crop production, residue generation and residue burnt scenario for all crops in India (Ravindra et al. 2019a).

Year	Crop Production (P) (in MT)	Crop Residue Generated (in MT)	Residue Burnt (in MT)
2003–04	476.79	375.84	89.60
2004–05	464.44	356.27	86.39
2005–06	522.84	383.65	92.56
2006–07	602.98	411.89	97.25
2007–08	615.13	433.02	102.59
2008–09	552.87	422.34	101.07
2009–10	541.49	400.39	96.37
2010–11	626.87	454.02	107.27
2011–12	658.15	480.37	112.86
2012–13	637.06	472.79	111.90
2013–14	658.14	487.82	115.14
2014–15	649.78	468.54	111.02
2015–16	632.26	462.39	110.05
2016–17	618.97	487.71	116.82

Table 10: Comparative overview of crop residue burning estimates for India (Ravindra et al. 2019a).

Year	Crop residue burned (MT)	References
Mid-90s	84	Streets et al. (2003a, b)
2001	116 (58–289)	Venkataraman et al. (2006)
2008-09	98	Jain et al. (2014)
2010	63	Sahai et al. (2011)
2016-17	116	Ravindra et al. (2019a)

Table 11: Manual and VCR harvesting crop residue height.

S. No.	Parameters	Observations	
1.	Crop variety	Panth 12(PD-12)	
2.	Field plots	Observations	
		First terrace	Second terrace
3.	Plant height (mm)	850 -1250	700 - 900
4.	Average plant height (mm)	1020±210	790±100.02
5.	Average Stubble Height (After Harvesting)	*Observations*	
		First terrace	*Second terrace*
6.	Manual Harvesting	70.3±5.7	69±3.6
7.	VCR Harvesting	15±8	21±3

impacts of climate change. Also, these technologies can convert residue into daily usable energy and ameliorated field products.

Crop residues in biomass-based energy generation: Crop residues contain lignocellulosic biomass which meets the needs of production of alternate energy through gasification, bio methanation, and ethanol generation is one of the technological mitigation options for air pollution (Ravindra et al. 2019a, Lohan et al. 2018, Shafie 2016). According to reports, around 500 biomass power and cogeneration plants have been installed in India by the Ministry of New and Renewable Energy which generates 11.5% of the total renewable power supply (Ravindra et al. 2019a, MNRE 2016, Energy statistics 2017). Crop residue can also be used to

produce biofuels as compatible energy for new generating vehicles in an environment-friendly, and cost-effective way.

Biochar and composting: Paddy residue could be used for formulating useful products viz. making compost, organic manure and biochar to improve soil health, soil fertility (Lohan et al. 2018). Uses of vermicompost and biochar in agricultural practices is a sustainable environmental friendly alternative, which could also help to mitigate climate change as it helps in carbon sequestration (Ravindra et al. 2019a).

Promote farm-implements with subsidy: Higher subsidy rate to farmers on farm implements and chemical fertilizers who retain their residue in the field could lead to decrease the crop residue burning pollution (Lohan et al. 2018). Resource conservation technologies (RCTs) based farm machinery such as a Zero-till seed-cum-fertilizer drill, Happy seeder, Straw chopper, Hay rakes, Straw reaper, Super straw management system, Balers and others could provide a better way to control paddy residues for improving soil health, productivity, reducing pollution to achieve sustainable agriculture (Jat et al. 2009, Palma et al. 2014, Lohan et al. 2018).

***In-situ* incorporation:** By retention of crop residues increases soil temperature in winter through reducing upward heat flux and decreases in summer due to shading effect (Pathak et al. 2011, Lohan et al. 2018). Enhanced decomposition transforms combine harvested residues to advance nutrients and also several positive impacts and health attributes such as pH, organic carbon, infiltration rate, higher C: N, and soil alkalinity, hydraulic conductivity, microbial biomass, cation exchange capacity (CEC) and water holding capacity in the soil (Gupta et al. 2004, Gangwar et al. 2006, Kumar et al. 2015, Lohan et al. 2018). Crop residues, particularly from wheat and rice crops, have a wide C:N ratio of 70:1 to 100:1. Moreover, incorporation of residue impacts denitrification rate, an abundance of denitrifier, and N_2O emissions in soil (Shan & Yan 2013) and straw mulching by mechanical means must be promoted (Lohan et al. 2018).

Promotion of hybrid seeds and use of rice straw as livestock feed: The use of hybrid seeds, which has less mature period and producing low residues, can help in sowing within the cropping interval and enforcement of rice-wheat cropping system intensification. However, alternative use of rice straw as livestock feed contains high silica, resulting in low digestibility and nutritive values (Na et al. 2014, Ravindra et al. 2019a).

Education and awareness and promotion: By increasing awareness and education among farmer communities about severe impacts of crop residue burning in fields leads to air pollution and transport of pollutants in the atmosphere and promoting alternative uses of crop residues through different workshops, and training programs at the village and district level.

CONCLUSIONS

The study has been undertaken for the assessing the feasibility and performance of the VCR in laboratory condition and in Daramdin Farm for the harvesting of the rice crop and VCR as a possibility of technological mitigation for after harvesting crop residue burning resulting air pollution. Based on the study, the following conclusions may be drawn:

1. Optimum machine performance was obtained with gear-1 as harvesting at this speed could help to minimize the harvesting losses and maximize the work rate (actual field capacity).
2. The effective field capacity of the VCR for rice harvesting was 0.1203 ha/h and 0.092 ha/h in terrace 1 and 2 compared to 0.0178 ha/h in manual operation.
3. The field efficiency of harvesting operations at operating speeds of 1.52 km/h and 2.19 km/h was found to be 72.03% and 38.50% respectively.
4. The labour requirements for VCR were 8.3 and 10.8 man-h/ha in terrace 1 and 2 as compared to 56 man-h/ha for manual harvesting.
5. The grain losses for VCR harvesting were 3.53% and 4.11% in both the terraces.
6. As the fixed cost is considerable (35.7%), the machine may be promoted for its use on the custom-hire basis to make the venture economically viable.
7. Based on the study, it may be concluded that use of the machine may lead to considerable savings in time (85.2%), labour (80.6%) and cost (30.8%) of harvesting, as compared to manual harvesting methods. Therefore, in terraces where the use of reaper is feasible, its use may be promoted.
8. During the harvesting of paddy crop, the crop stem cuts at an average height of 15-21 mm which leaves shorter residues in the field by this Vertical conveyor reaper.
9. Harvesting paddy with VCR reduces the possibility of air pollution by stubble burning in atmosphere and dispersion of pollutants.
10. The small amount of crop residues left after harvesting enrich the soil for next crop, also further recovery of residue can be used for biocomposting, bioenergy, etc.

ACKNOWLEDGEMENT

The authors are sincerely thankful to Department of Farm Machinery and Power Engineering, College of Agricultural

Engineering and Post Harvest Technology (Central Agricultural University, Imphal), Ranipool, Sikkim, India and Food Security and Agriculture Development Department for cooperation and providing such facilities in Daramdin farm to carryout field evaluation.

REFERENCES

Alizadeh, M.R., Bagheri, I. and Payman, M.H. 2007. Evaluation of a rice reaper used for rapeseed harvesting. American-Eurasian J. Agric. & Environ. Sci., 2: 388-394.

Andreae, M.O. 1991. Biomass burning: Its history, use, and distribution and its impact on environmental quality and global climate. In: Levine, J.S. (Ed.), Global Biomass Burning, Atmospheric, Climatic, and Biospheric Implications. MIT Press, Cambridge, MA, pp. 3-21.

Andreae, M.O. and Merlet, P. 2001. Emission of trace gases and aerosols from biomass burning. Global Biogeochemical Cycles, 15(4): 955-966.

Awasthi, A., Agarwal, R., Mittal, S.K., Singh, N., Singh, K. and Gupta, P.K. 2011. Study of size and mass distribution of particulate matter due to crop residue burning with seasonal variation in rural area of Punjab. India. J. Environ. Monit., 13(4): 1073-1081.

Badr, M.M. 2005. Comparative study between some different combine sizes in respect to unit plot area. M. Sc. Thesis. Agric. Eng. Dept., Faculty of Agric., Zagazig Univ. Egypt.

Bansal, R.K. and Sakr, B. 1992. Development of a vertical conveyor reaper for harvesting chickpeas and lentils in Morocco. American Society of Agricultural and Biological Engineers. 8: 425-428

Bukhari, S., Mughal, A.Q., Baloch, J.M., Malik, R.J. and Mirani, A.N. 1991. Grain losses in wheat harvested by tractor front mounted Reaper windrower. Agricultural Mechanization in Asia, Africa and Latin America, 22: 15-20.

Chen, J., Li, C., Ristovski, Z., Milic, A., Gu, Y., Islam, M.S., Wang, S., Hao, J., Zhang, H., Duan, F., Liu, X., Yu, T. and Cachier, H. 2004. Identification and estimate of biomass burning contribution to the urban aerosol organic carbon concentrations in Beijing. Atmospheric Environment, 38: 1275-1282.

Dutt, P. Prasad, J. 2002. Modification and evaluation of self-propelled reaper for harvesting soybean. Agricultural Mechanization in Asia, Africa and Latin America, 3: 43-46.

Eggleston, H.S., Buendia, L., Miwa, K., Ngara, T. and Tanabe, K. (Eds.) 2006. IPCC Guidelines for National Greenhouse Gas Inventories. National Greenhouse Gas Inventories Programme. IGES, Japan.

El-Sharbasy, M.A. 2006. Construction and manufacture a self-propelled machine suits for cutting some grain crops to minimize losses and maximize efficiency. Misr J. Ag. Eng., 23: 509- 531.

Energy Statistics 2017. Central Statistics Office Ministry Of Statistics And Programme Implementation Government Of India New Delhi http://www.mospi.gov.in/sites/default/files/publication_reports/Energy_Statistics_2017r.pdf.pdf Accessed on 27/07/2018

FS & ADD 2016 Annual Reports. Food Security and Agriculture Development Department, Govt. of Sikkim, India.

Gangwar, K.S., Singh, K.K., Sharma, S.K. and Tomar, O.K. 2006. Alternative tillage and crop residue management in wheat after rice in sandy loam soils of Indo-Gangetic plains. Soil Res., 88: 242-52.

Garg, I. K., Sharma, V.K. and Singh, S. 1984. A power tiller-mounted vertical conveyor reaper-windrower. Agricultural Mechanization in Asia, Africa and Latin America, 15: 41-44.

Gill, N., Dogra, R. and Dogra, B. 2018. Influence of moisture content, particle size, and binder ratio on quality and economics of rice straw briquettes. BioEnergy Research, 11: 54-68.

Godish, T. 1997. Air Quality. Lewis Publishers, Boca Raton, New York, pp. 137-178.

Gupta, P.K., Sahai, S., Singh, N., Dixit, C.K., Singh, D.P. and Sharma, C. 2004. Residue burning in rice-wheat cropping system: causes and implications. Curr. Sci., India, 87(12): 1713-5.

Guruswamy, T., Desai, S.R., Veeranagouda, M. and Barker, R.D. 1996. Performance evaluation of vertical conveyor reaper windrower. Karnataka J. Agric. Sci., 9: 102-105.

IS: 10378-1982(Reaffirmed in 2001). 2001. Specifications for Knife Back for Harvesting Machines. Bureau of India Standards, New Delhi.

IS: 11467-1985(Reaffirmed in 2012). 2012. Test Code for Cereal Harvesting Machines. Bureau of India Standards, New Delhi.

IS: 6024-1983(Reaffirmed in 1999). 1999. Specifications for Guards for Harvesting Machines. Bureau of India Standards, New Delhi.

IS: 6025-1982(Reaffirmed in 1999). 1999. Specifications for Knife Sections for Harvesting Machines. Bureau of India Standards, New Delhi.

IS: 9164-1979(Reaffirmed in 2002). 2002. Guide for estimating cost of farm machinery operation. Bureau of India Standards, New Delhi.

Jain, N., Bhatia, A., Pathak, H., 2014. Emission of air pollutants from crop residue burning in India. Aerosol Air Qual. Res., 14: 422-430

Jat, M.L., Gathala, M.K., Ladha, J.K., Saharawat, Y.S., Jat, A.S., Sharma, V.K., Kumar, V. and Gupta, R.K. 2009. Evaluation of precision land levelling and double zero-till systems in the rice–wheat rotation; water use productivity, profitability and soil physical properties. Soil Res., 105: 112-21.

Kaskaoutis, D.G., Kumar, S., Sharma, D., Singh, R.P., Kharol, S.K., Sharma, M., Singh, A.K., Singh, S., Singh, A. and Singh, D. 2014. Effects of crop residue burning on aerosol properties, plume characteristics, and long-range transport over northern India. J. Geophys. Res. Atmos., 119: 5424-5444.

Kathirvel, K., Jesudas, D.M. and Suthakar, B. 2009. Mechanical harvesting of fodder as influenced by crop, machine and operational parameters. Agricultural Mechanization in Asia, Africa and Latin America, 40: 52-56.

Kumar, P., Kumar, S. and Joshi, L. 2015. Socioeconomic and Environmental Implications of Agricultural Residue Burning: A case study of Punjab, India. Springer Briefs in Environmental Science. pp. 144. ISBN 978-81-322-2014-5

Kumar, S., Singh, M. and Singh, B. R. 2013. Feasibility and economic viability of raised bed planter in western plane zone of Uttar Pradesh, India. Soil and Tillage Research, 128: 37-43.

Kurhekar, S.P. and Patil, S.R. 2011. Performance evaluation of self-propelled walking type vertical conveyor reaper. Internat. J. Proc. & Post Harvest Technol., 2: 29-31.

Lemieux, P.M., Lutes, C.C. and Santoianni, D.A. 2004. Emissions of organic air toxics from open burning: A comprehensive review. Progress in Energy and Combustion Science, 30(1): 1-32

Levine, J.S., Cofer, W.R., Cahoon, D.R. and Winstead, E.L. 1995. Biomass burning: A driver for global change. Environmental Science & Technology, 29(3): 120A-125A.

Lohan, S.K., Jat, H.S., Yadav, A.K., Sidhu, H.S., Jat, M.L., Choudhary, M., Peter, J.K. and Sharma, P. C. 2018. Burning issues of paddy residue management in north-west states of India. Renewable and Sustainable Energy Reviews, 81: 693-706.

Manjunatha, M.V., Reddy, B.G.M., Shashidhar, S.D. and Joshi, V.R. 2009. Field performance evaluation of vertical conveyor paddy reaper. Karnataka J. Agric. Sci., 22: 140-142.

McCarty, J.L., Korontzi, S., Justice, C.O. and Loboda, T. 2009. The spatial and temporal distribution of crop residue burning in the contiguous United States. Sci. Total Environ., 407(21): 5701-5712

McNeill, V.F. 2017. Atmospheric aerosols: clouds, chemistry, and climate. Annual Rev. Chem. Biomol. Eng., 8: 427-444.

Ministry of New and Renewable Energy (MNRE) 2016. http://mnre.gov.in/schemes/gridconnected/ biomass-powercogen/. Accessed on 27/07/2018

Mittal, S.K., Singh, N., Agarwal, R., Awasthi, A. and Gupta, P.K. 2009. Ambient air quality during wheat and rice crop stubble burning episodes in Patiala. Atmospheric Environment, 43(2): 238-244.

Mohanraj, R. and Azeez, P.A. 2004. Health effects of airborne particulate matter and the Indian scenario. Current Science, 87(6): 741-748.

Na, Y.J., Lee, I.H., Park, S.S. and Lee, S.R. 2014. Effects of combination of rice straw with alfalfa pellet on milk productivity and chewing activity in lactating dairy cows. Asian-Australas. J. Anim. Sci., 27: 960-964

Nadeem, A. and Gee-Clough, D. 1983. Field performance evaluation of rice reaper. Agricultural Mechanization in Asia, Africa and Latin America, 14: 35-40.

Nadeem, M., Iqbal, M., Farooque, A., Munir, A., Ahmad, M. and Zaman, Q. 2015. Design and evaluation of self-propelled reaper for harvesting multi crops. ASABE Annual International Meeting, pp. 1-7.

Palma, C., Humberto, B.C., DeClerckc, F., Gaterea, L. and Grace, P. 2014. Conservation agriculture and ecosystem services: an overview. Agr. Ecosyst Environ., 187: 87-105.

Pandey, J.S., Kumar, R. and Devotta, S. 2005. Health risks of NO_2, SPM and SO_2 in Delhi (India). Atmospheric Environment. 39(36): 6868-6874.

Pathak, H., Saharawat, Y.S., Gathala, M. and Ladha, J.K. 2011. Impact of resource-conserving technologies on productivity and greenhouse gas emissions in the rice-wheat system. Greenhouse Gases. Sc. Tech., 1(3): 261-77.

Prasad, J., Devnani, R.S. and Datt, P. 1992. Evaluation of vertical conveyor reaper for harvesting safflower crop. Indian Journal of Agricultural Engineering, 2: 229-233.

Ramanathan, V., Chung, C., Kim, D., Bettge, T., Buja, L., Kiehl, J.T., Washington, W.M., Fu, Q., Sikka, D.R. and Wild, M. 2005. Atmospheric brown clouds: impacts on South Asian climate and hydrological cycle. Proc. Natl. Acad. Sci. Unit. States Am., 102(15): 5326-5333.

Ravindra, K., Sidhu, M.K., Mor, S., John, S. and Pyne, S. 2016a. Air pollution in India: bridging the gap between science and policy. J. Hazardous, Toxic, Radioact. Waste., 20(4): A4015003-10

Ravindra, K., Singh, T. and Mor, S. 2019a. Emissions of air pollutants from primary crop residue burning in India and their mitigation strategies for cleaner emissions. Journal of Cleaner Production, 208: 261-273.

Ravindra, K., Singh, T., Mor, S., Singh, V., Mandal, T. K., Bhatti, M. S., Gahlawat, S.K., Dhankhar, R. and Beig, G. 2019b. Real-time monitoring of air pollutants in seven cities of North India during crop residue burning and their relationship with meteorology and transboundary movement of air. Sci. Total Environ., 690: 717-729.

Sahai, S., Sharma, C., Singh, S.K. and Gupta, P.K. 2011. Assessment of trace gases, carbon and nitrogen emissions from field burning of agricultural residues in India. Nutrient Cycl. Agroecosyst., 89: 143-157.

Schwartz, J. 1993. Particulate air pollution and chronic respiratory disease. Environmental Research, 62(1): 7-13.

Sen, A., Abdelmaksoud, A.S., Nazeer Ahammed, Y., Alghamdi, M.., Banerjee, T., Bhat, M.A., Chatterjee, A., Choudhuri, A.K., Das, T., Dhir, A., Dhyani, P.P., Gadi, R., Ghosh, S., Kumar, K., Khan, A.H., Khoder, M., Maharaj Kumari, K., Kuniyal, J.C.Kumar, M., Lakhani, A., Mahapatra, P.S., Naja, M., Pal, D., Pal, S., Rafiq, M., Romshoo, S.A., Rashid, I., Saikia, P., Shenoy, D.M., Sridhar, V., Verma, N., Vyas, B.M., Saxena, M., Sharma, A., Sharma, S.K. and Mandal, T.K. 2017. Variations in particulate matter over Indo-Gangetic Plains and Indo-Himalayan Range during four field campaigns in winter monsoon and summer monsoon: Role of pollution pathways. Atmos. Environ., 154: 200-224.

Shafie, S.M. 2016. A review on paddy residue based power generation: Energy, environment and economic perspective. Renew. Sustain. Energy Rev., 59: 1089-1100.

Shan, J. and Yan, X. 2013. Effects of crop residue returning on nitrous oxide emissions in agricultural soils. Atmos Environ., 71:170-5.

Singh, L.P., Vagadia, V.R., Jain, K.K. and Menon, A. H. 2008. Evaluation and improvement in design of self-propelled vertical conveyor reaper. Agricultural Mechanization in Asia, Africa and Latin America, 39: 34-38.

Singh, S., Vatsa, D.K. and Verma, M.K. 2007. Feasibility and performance evaluation of power tiller operated reaper in hills of Himachal Pradesh. Agricultural Engineering Today, 31: 6-10.

Streets, D.G., Bond, T.C., Carmichael, G.R., Fernandes, S.D., Fu, Q., He, D., Klimont, Z., Nelson, S.M., Tsai, N.Y., Wang, M.Q., Woo, J.H. and Yarber, K.F. 2003a. An inventory of gaseous and primary aerosol emissions in Asia in the year 2000. J. Geophys. Res. Atmos., 108(D21): 30-1-30-23, 8809

Streets, D.G., Yarber, K.F., Woo, J.H. and Carmichael, G.R. 2003b. Biomass burning in Asia: Annual and seasonal estimates and atmospheric emissions. Global Biogeochem. Cycles, 17(4): 10-1 -10-20, 1099.

Thaller, E., Hollaway, L., Mai, V., Hochman, D., Bharti, B., Brooks, E., Petronella, S. 2004. Air pollution and pulmonary function. Journal of Allergy and Clinical Immunology, 113(2): S65

Tripathi, A., Mishra, B.P., Kumar, M. and Patre, N.K. 2018a. Field Performance of Machine for Harvesting of Wheat and Linseed. Int. J. Pure App. Biosci., 6: 1512-1519.

Tripathi, A., Mishra, B.P., Kumar, M., Thakur, Y.S. and Mahilang, K.K.S. 2018b. Performance evaluation of reaper-cum-binder for harvesting of soybean and rice. Int. J. Curr. Microbiol. App. Sci., 7: 1754-1762.

Venkataraman, C., Habib, G., Kadamba, D., Shrivastava, M., Leon, J.F., Crouzille, B., Boucher, O. and Streets, D.G. 2006. Emissions from open biomass burning in India: integrating the inventory approach with high-resolution moderate resolution imaging spectroradiometer (MODIS) active-fire and land cover data. Global Biogeochem. Cycles, 20(2).

Venkataraman, C., Habib, G., Kadamba, D., Shrivastava, M., Leon, J.F., Crouzille, B., Boucher, O. and Streets, D.G. 2006. Emissions from open biomass burning in India: integrating the inventory approach with high-resolution Moderate Resolution Imaging Spectroradiometer (MODIS) active-fire and land cover data. Global Biogeochem. Cycles 20: 1-12.

WHO (World Health Organization) 2004. Systematic Review of Health Aspects of Air Pollution in Europe. WHO Regional Office for Europe. June, pp. 4-16.

Witham, C., Manning, A. 2007. Impacts of Russian biomass burning on UK air quality. Atmos. Environ., 41(37): 8075-8090.

Yang, S., He, H., Lu, S., Chen, D. and Zhu, J. 2008. Quantification of crop residue burning in the field and its influence on ambient air quality in Suqian, China. Atmospheric Environment, 42(9): 1961-1969.

Nature Environment and Pollution Technology
An International Quarterly Scientific Journal

p-ISSN: 0972-6268
(Print copies up to 2016)
e-ISSN: 2395-3454

Vol. 19 | No. 2 | pp. 539-548 | 2020

Original Research Paper

https://doi.org/10.46488/NEPT.2020.v19i02.009

Open Access Journal

Comparative Assessment of Trace Metal Concentrations and Their Eco-Risk Analysis in Soils of the Vicinity of Roundhill Landfill, Southern Africa

Nyika Joan*† Onyari Ednah*, Megersa Olumana Dinka and Shivani Bhardwaj Mishra*****

*University of South Africa, Department of Civil and Chemical Engineering, University of South Africa [Florida Science Campus], Cnr Christian de Wet Road and Pioneer Avenue, Johannesburg, South Africa

**University of Johannesburg, Department of Civil Engineering Science, University of Johannesburg, APK Campus 2006, Johannesburg, South Africa

***University of South Africa, Nanotechnology and Water Sustainability Unit, University of South Africa [Florida Science Campus], Cnr Christian de Wet Road and Pioneer Avenue, Johannesburg, South Africa

†Corresponding author: Nyika Joan; joashmada2011@gmail.com

Nat. Env. & Poll. Tech.
Website: www.neptjournal.com

Received: 08-07-2019
Accepted: 19-09-2019

Key Words:
Contaminants;
Ecological risk;
Landfill; Soil;
Trace metals

ABSTRACT

Soil is a vital media in transmitting contaminants in the environment. Contamination of soils by trace metals has received much attention due to their associated toxicity, persistence, bioaccumulation and non-biodegradability that is harmful to the ecology. This study assayed the concentrations of trace metals in topsoils of the vicinity of Roundhill landfill using inductively coupled plasma-mass spectrometry (ICP-MS) and X-ray fluorescence (XRF), compared the detection capabilities of the two techniques and determined ecological risks of the contaminants using geographical information system. Soils were collected from nine sampling sites around Roundhill landfill in the Eastern Cape and analysed for five trace metals using the two techniques. Mean concentrations of Cr, Cu, Ni and Zn determined by ICP-MS and XRF were normally distributed ($p<0.05$) from the parametric test while no significant differences between the two datasets were established from the non-parametric test. Under-estimated elemental concentrations determined by XRF were attributed to its high detection limits, matric effects, inter-elemental peak interferences and low sensitivity of the equipment. Correlation values of Cr, Cu and Ni showed a high degree of linearity compared to Pb. Evaluated eco-risk indices revealed low to extremely high ecological risks, posed by assessed trace elements in soils. Cr had the highest potency. Assayed trace metals were ecologically harmful to soils and their origin was linked to landfill leachate pollution.

INTRODUCTION

Soils provide many ecosystem services including vegetation support and modulating the flow of fugitive emissions, heat, nutrients and water (Wang et al. 2012). Besides, they adsorb and attenuate pollutants including trace metal elements. Consequently, trace metal pollution in soils is a growing environmental issue due to their non-biodegradability, bioaccumulation, persistence and toxicity (Zhu et al. 2018). Their entry in the food chain causes harm to organisms, including humans. The sources of these trace elements are either geogenic or anthropogenic-based. In the former, sources include pedogenesis and weathering activities on rocks while in the latter, use of agrochemicals, commercial fertilisers and unscientific disposal of waste, are the main pollution causes (Shokr et al. 2016). The distribution of trace metals in soils is dynamic and influenced by climate, soil parent material and its mobility. The rapid generation of the trace metals due to increased industrialisation and urbanisation activities worldwide and their capacity to become bioavailable and diffuse in other environments once disposed of explains the need to accurately quantify them (Wang et al. 2012, Shokr et al. 2016).

Different analytical techniques in in-situ and at ex-situ conditions have been developed to identify and quantify such pollutants in soils. Most of these assay methods are based on spectroscopy techniques and include X-ray fluorescence (XRF), atomic absorption spectrometry (AAS), inductively coupled plasma (ICP)- atomic emission spectrometry (AES) and ICP- mass spectrometry (ICP-MS) (Towett et al. 2013). ICP-MS/AES is common assay method based on aqua regia digestion to breakdown resistive metals and silicates in soils and have acceptable recovery and sensitivity. However, pre-conditions of sample pre-treatment before analysis that use concentrated acids are considered harsh and induce complex

matrix effects that compromise accurate analysis of trace elements (McComb et al. 2014). Therefore, XRF analysis that is multi-elemental and non-destructive is a growing alternative to aqua-regia-based methods. XRF is dependent on wavelength-dispersive electro-technology, sensitive detectors and sample excitation to assay trace elements in soils and can be carried out intrusively or in-situ (Kilbride et al. 2006). Comparisons of aqua-regia digestion methods and XRF in trace element analysis in existent studies reported close linearity in some studies (Marcos et al. 2011, Towett et al. 2013, Poto et al. 2015) while in others, there were deviations in their sensitivity and detection limits (Kilbride et al. 2006, Radu & Diamond 2009, McComb et al. 2014).

Using these techniques, trace elements can be quantified and their associated ecological risks measured using indices. Eco-risk indices reveal possible contamination in soils and the potency of specific metals to inflict environmental harm (Zhu et al. 2018). Most of the indices are derived from Hakanson's (1980) principle and are practical and quick tools to classify areas based on environmental pollution according to Wang et al. (2012). The distribution of eco-risk can be spatially represented if geographic information systems (GIS) are incorporated. According to Poggio & Vrscaj (2009), GIS tools assess interactions between released trace elements and calculated eco-risk indices with recipient environs based on processes governing contaminant distribution and spatial information on sources. These interactions are interpolations over a georeferenced space and provide a basis for environmental assessment (Wang et al. 2012). In this way, ecological risk indices are diagnostic tools that show pollution pathways. The objectives of this study were to 1) determine contaminant concentrations of topsoils in the Roundhill landfill vicinity using ICP-MS and XRF, 2) compare the detection capabilities of the two techniques and 3) determine ecological risks of the contaminants using GIS.

MATERIALS AND METHODS

Study Area and Sampling

Roundhill landfill is located in Buffalo city municipality of Eastern Cape, South Africa and is situated at latitude 32°53'13.66'S and longitude 27°37'26.20'E (Fig. 1). The facility was commissioned in 2006 and was previously a natural grassland (Dookhi et al. 2015). It receives more than 500 tonnes of general wastes from domestic, healthcare, businesses and building sectors of the vicinity daily. The landfill has a geomembrane liner and a leachate collection system whose effectiveness has been overwhelmed by increased waste disposal at the facility. Consequenlty, waste is inadequately lined and covered while leachate runs off to surroundings posing as a pollution threat (Jewaskiewitz & Dookhi 2017). The climate of the area borders the Mediterranean and humid subtropical climate characterised by an average annual temperature of 21°C, rainfall ranging between 400-100 mm/year and evaporation of 160-170 mm/month. It has clayey soils, low organic matter and low groundwater potential whereby, borehole yields are less than 1 L/s (Chigor et al. 2013).

Sampling was carried out in September 2018 and nine sampling sites around the landfill facility were selected for soil collection including a reference sample (blank) (Fig. 1). At each site, samples were collected using a soil auger and emptied in polyethylene bags for further analysis. In the laboratory, soils were oven-dried and passed through a 2 mm sieve.

ICP-MS Analysis

Analysis of contaminants using ICP-MS began with the digestion of soil samples using the aqua regia EPA method 3015a (USEPA 1998). One gram of each soil sample was placed in a reaction vessel that contained 9 mL nitric acid (65%), 2 mL hydrochloric acid (35%) and 1 mL hydrogen peroxide (30%). The reaction was allowed for 5 min before sealing the reaction vessels and placing it in a rotor for microwave digestion at 180°C for 5.5 min. Samples were then held at the same temperature for 9.5 minutes and allowed to cool after digestion. Particulates in the digestant were removed by sedimentation before collecting it in plastic containers and labelling for ICP-MS analysis. Before this analysis, each sample was diluted 1000 times with 0.1% (v/v) nitric acid prepared using deionised water (milli-Q). ICP-MS Agilent 7500ce containing an octupole reaction system was used in this study that followed the EPA method 6020B (USEPA 2014). Analysis began with configuring the instrument computer using the manufacturer's directions and setting it up using appropriate operating parameters. The instrument was tuned and allowed to equilibrate for 30 minutes before analysis. This was followed by calibration using both internal and external standards containing rhenium and rhodium, respectively. A solution containing 1% nitric acid was used as the blank to flush the ICP-MS system until a steady-state signal was acquired. Samples beyond the linear analysis range were diluted before final analysis. A mixed solution standard was prepared in the blank solution and used to correct background interferences of the equipment from the solvent, air entrainment and plasma gases. Suitable isotopes were selected to eliminate possible isobaric spectral interferences due to ion species with many atoms before analysing the samples. The analysis was done in duplicates for Cr, Cu, Ni, Pb and Zn and their final concentrations were determined using equation 1.

$$\text{Metal concentration (mgkg}^{-1}) = \frac{\text{ICP-MS Reading} \times \text{Digestate volume} \times \text{Dilution Factor}}{\text{Weight of sample digested}} \quad \ldots(1)$$

XRF Analysis

About 10 g of the dried soils were ground in a pulveriser to particles sizes of 75 µm and below. The soils were emptied in crucibles and heated to 950°C for 2 h for loss on ignition (LOI) analysis to remove volatile organics. They were allowed to cool and transferred to aluminium containers for pressing in a semi-automated press. This study used the sequential XRF spectrometer (PW 2404, Phillips, Holland) that uses americium-241 and cadmium-109 isotopes for fluorescence excitation and has a detector made of silicon pin-diode. Before analysis, instrument performance was validated using a blank and two check samples that had high heavy metal levels before making adjustments on the zero level according to EPA method 6200 (USEPA 2016). The samples were placed on carriers that were previously cleaned using acetone and mounted on the equipment cassette for heavy metal analyses in triplicates through direct quantification.

Calculation of Eco-Risk Indices

Four eco-risk indices namely potential ecological risk index (PERI), cumulative risk index (CRI), toxic units (TU) and toxic risk index (TRI) were used to assess the ecological threat of trace metals to soils of the study area. PERI was calculated using equation 2.

$$\text{PERI} = T_r * \frac{C_{obs}}{C_{norm}} \quad \ldots(2)$$

Where, T_r is the toxic response coefficient of a particular metal, C_{obs} is the measured concentration of given trace metal and C_{norm} is the geochemical background levels outlined by the Department of Environmental Affairs (DEA 2013). Toxic response coefficients are predefined values that account for sensitivity and toxic requirement (Pedersen et al. 1998). Elemental values of T_r used to calculate PERI in this study are given in Table 5.

CRI was calculated using equation 3.

$$\text{CRI} = \sum_{i=1}^{n} \text{PERI} \quad \ldots(3)$$

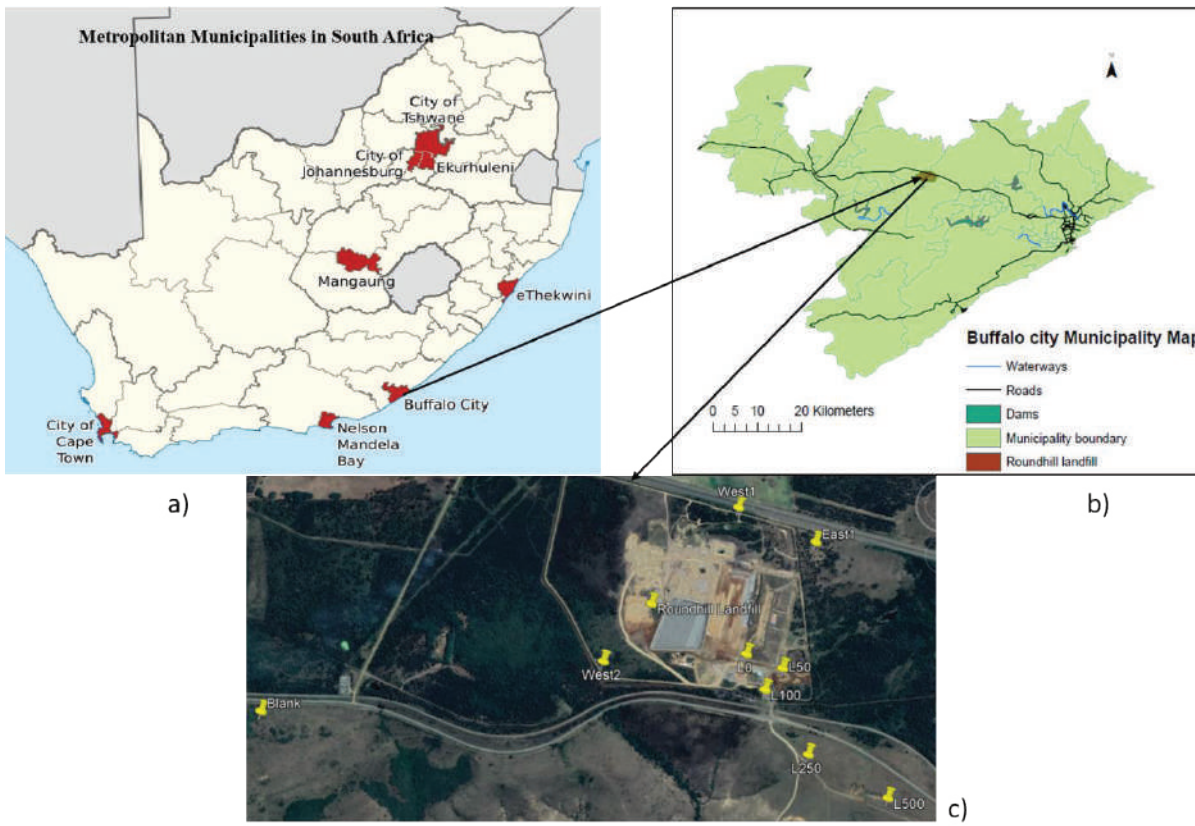

Fig. 1: Map of the study area and the distribution of sampling sites in relation to the landfill site.

Where, n is the number of trace metals assayed and PERI is the potential ecological risk index of each metal.

TUs of individual metals at various sampling sites were calculated as relationships of observed metal concentration at each sampling site to predetermined probable effects level (PEL) as shown in equation 4.

$$TU = \frac{C_{obs}}{PEL} \quad \ldots(4)$$

Where, PEL is the probable effects level of individual metal, which is defined as the lower limit of chemical concentrations, which is affiliated to negative biological effects (Pedersen et al. 1998). PEL values of assayed elements used in this study were as shown in Table 5 and are derived from studies by Pedersen et al. (1998) and Zhu et al. (2018).

TRI assessed the integrated toxic risk using both PEL and threshold effect level (TEL) of heavy metals using equation 5.

$$TRI = \sqrt{\left(C_{obs}/TEL\right)^2 + \left(C_{obs}/PEL\right)^2} \Big/ 2 \quad \ldots(5)$$

Where, TEL is the threshold effects level, which is defined as the upper limit of soil chemical concentration that has no-effect data (Pedersen et al. 1998). TEL values used in this study were as documented by Zhu et al. (2018) and are presented in Table 5. Results of the above indices are categorised as given in Table 1.

Geo-statistical Analysis

The spatial analyst tool of ArcGis 10.3 was used in spatial interpolation of assayed pollutants and calculated indices of various sampling points. Inverse Distance Weighted (IDW) method, which takes a plug point as a core point of determining weighted averages for an entire area within a specified radius was used to represent pollution extent (Yan & Li 2011). The method applied inverse proportioning between known concentrations and was represented using equation 6.

$$Z = \frac{\sum_{i=1}^{n} 1/(Di)^p}{\sum_{i=1}^{n} 1/(Di)^p} Z_i \quad \ldots(6)$$

Where, Z= is the interpolated value, Z_i= the sample value of i which = 1, 2…. n, D = distance and p = distance's power as described by Yan & Li (2011).

Statistical Analysis

Descriptive statistics including the average (avg), standard deviation (SD), kurtosis and skewness of topsoils were applied to explain differences of ICP-MS and XRF elemental concentrations. The t-test assessed significant differences in the means of identified heavy metals for the two methods. The method has been used to compare differences in heavy metal concentrations obtained by XRF and ICP-MS successfully (Ahmed et al. 2012, Maliki et al. 2017). The Kolmogorov-Smirnov (K-S) test, which is an empirical distribution function (EDF) where theoretical and test distribution functions are compared was used in assessing normality or non-normality of the data (Ghasemi & Zahediasi 2012). The method is preferred due to its high sensitivity compared to alternatives such as Shapiro-Wilk test, D'Agostino Pearson omnibus test, Anderson-Darling test and Jarque-Bera test (Oztuna et al. 2006). Mann Whitney U-test, a non-parametric was used to compare if sample means of the two methods were equal. The test was used to complement t-test by show-

Table 1: Criteria to classify calculated ecological risk indices.

Index Method	Values	Ecological risk level	Reference
PERI	≤40	Low	Sun et al. (2015)
	40 < PERI ≤80	Moderate	
	80 < PERI ≤160	High	
	160 < PERI ≤320	Very high	
	>320	Extremely high	
CRI	<150	Low	Zhu et al. (2018)
	150-300	Moderate	
	300-600	Considerable	
	≥600	Disastrous	
TU	<4	Non-toxicity	Gao et al. (2018)
	>6	Acute toxicity	
TRI	<5	No toxic risk	£
	5≤TRI<10	Low risk	
	10≤TRI<15	Moderate toxic risk	
	15≤TRI<20	Considerable toxic risk	
	≥20	Very high toxic risk	

ing differences in the spread for data that did not have normal distribution after the K-S test. To determine the correlation between heavy metal concentrations obtained by the two methods, linear regression analysis was applied. This analysis resulted in a linear model shown in Equation 7 that reduces the square difference between the regression line and the dependent variable (Kilbride et al. 2006).

$$y = mx + c + £ \quad \ldots (7)$$

Whereby, y is XRF concentration, m is the slope, x is the ICP-MS concentration, c is the y-intercept of the regression line and £ is the residual.

Generally, ≥0.7 value of determination coefficient (R^2) represented the significant relationship of concentrations obtained from the two assay methods, while a value of 1.0 depicted an ideal case with no data scattering (Towett et al. 2013). These analyses were done using XLSTAT software at $p < 0.05$ significance level. Regressed data was subjected to a quality analysis using the USEPA (1998) criteria based on their determination coefficients and as shown in Table 2.

RESULTS

Concentration of Contaminants

Statistical comparisons of ICP-MS and XRF for the identified elements were as given in Table 3. Average concentrations of all elements obtained by ICP-MS were higher compared to those of XRF, which revealed under-estimations of the latter. A comparison of SD values of elemental concentrations obtained from the two techniques showed a similar trend of closeness in the variability of values except for Pb. However, a comparison of SD values among identified elements showed a large spread where Cr and Cu had the highest and lowest values, respectively. Skewness, SD and kurtosis values for the two methods had the same tendency whereby values of Cr, Cu, Ni and Zn were nearly similar while those of Pb differed significantly.

Comparison ICP-MS and XRF

Results of K-S test, t-test and Mann Whitney U-test at $P < 0.05$ were as shown in Table 4. K-S results showed normal distribution for all the elements except Pb. The results of the Mann Whitney U-test showed a similar trend where P values of Cr, Cu, Ni and Zn were higher than 0.05 and corresponded to no differences in the two data sets, while Pb had significant differences. The means of the two data sets except Pb were found to be equal from the t-test.

To assess the data quality from the two methods, regression analysis was carried out and R^2 values calculated as shown in Figs. 2 and 3. Determination coefficient values of Cr, Cu and Ni were above 0.8, which indicated that the results of the two methods were statistically similar for the concentrations of these elements. Zn had an R^2 value of 0.7 and concentration levels obtained with the two methods were statistically different, but within the acceptable limit

Table 2: Criteria to categorise regression data quality based on R^2 values (USEPA 1998).

Trace metal	Level of data quality	Statistical requirement	Inference
Cu Cr Ni	Definitive	$R^2 \geq 0.8$	Relationship y=x acceptable
Zn	Quantitative Screening	$R^2=0.7$	Relationship y=mx + c acceptable
Pb	Qualitative screening	$R^2 < 0.7$	No relationship in data sets

Table 3: A comparison of average concentrations, standard deviation, kurtosis and skewness values of top soils obtained by for ICP-MS and XRF.

	Cr	Cu	Ni	Pb	Zn
Avg-ICP ($mgkg^{-1}$)	2197	246.67	535.56	104.96	244.89
Avg-XRF ($mgkg^{-1}$)	2044.56	239.56	497.33	104	175.56
SD-ICP	2159.9	101.77	219.09	84.52	161.23
SD-XRF	2147.98	107.92	205.79	172.03	134.45
Kurt-ICP	8.5	3.38	-0.75	-0.43	7.06
Kurt-XRF	8.56	3.3	-0.62	1.4	7.25
Skew-ICP	2.88	1.89	0.57	1.53	1.58
Skew-XRF	2.9	1.64	0.73	0.52	1.6

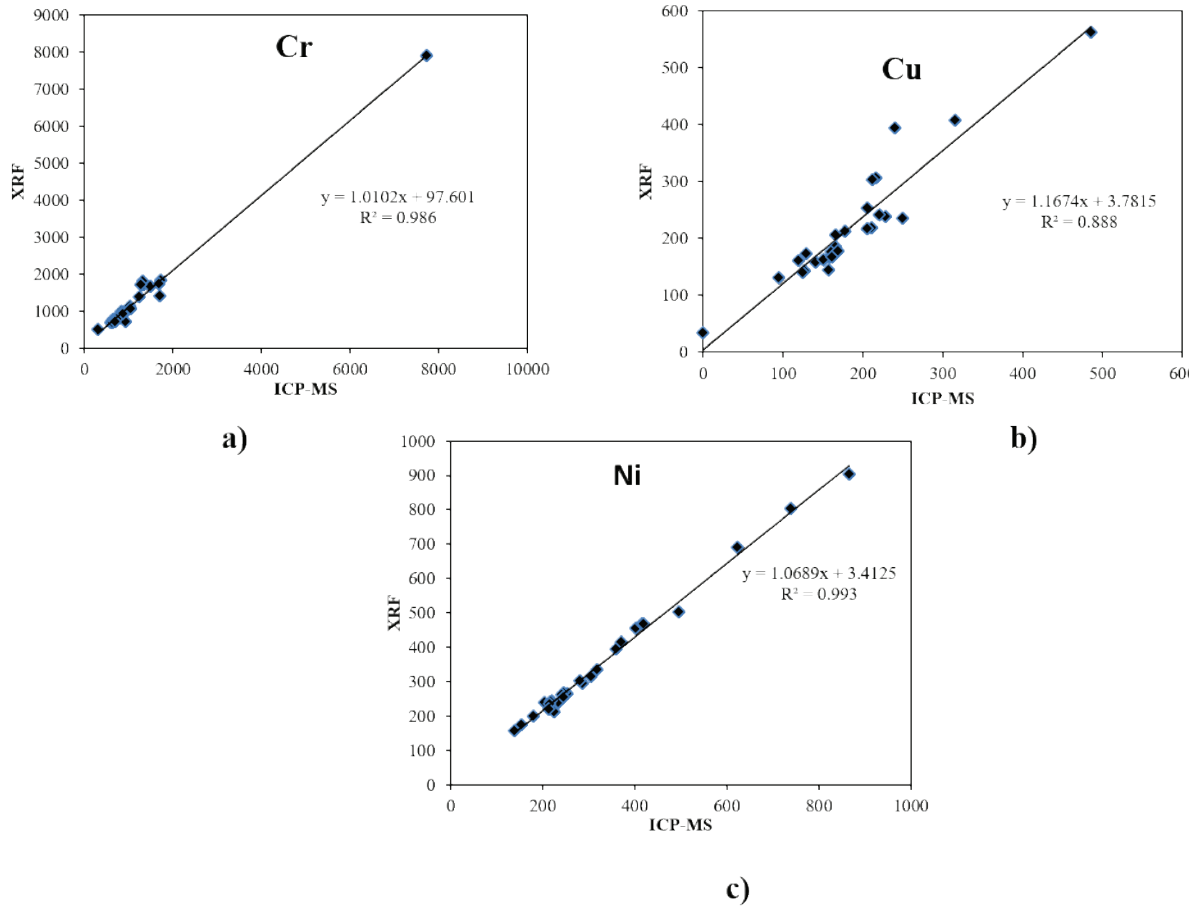

Fig. 2: Regression lines and equations for a) Cr, b) Cu and c) Ni.

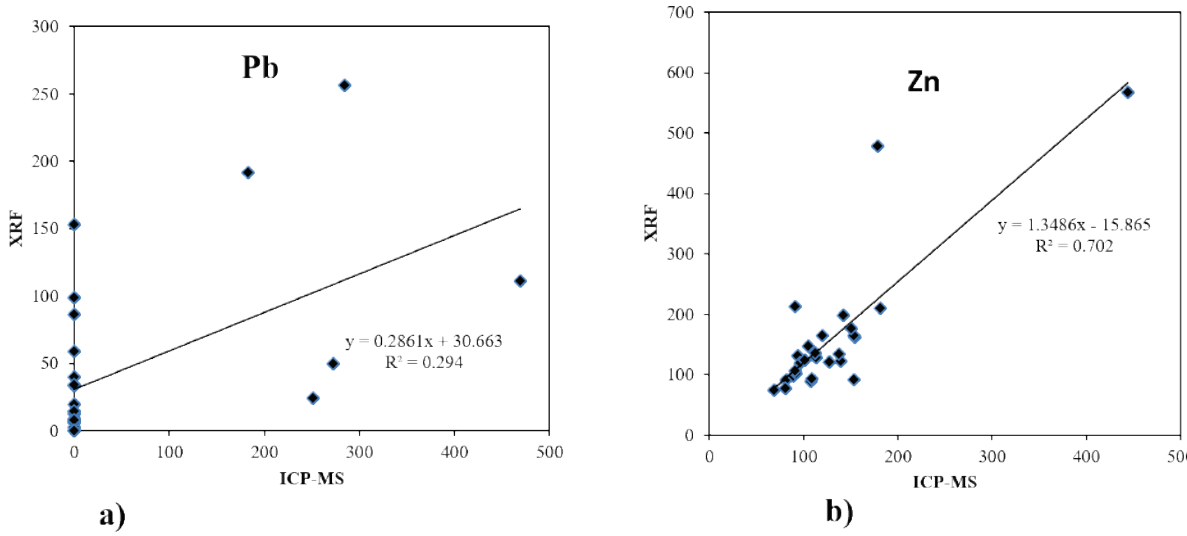

Fig. 3: Regression lines, determination coefficients and regression equations for a) Pb and b) Zn.

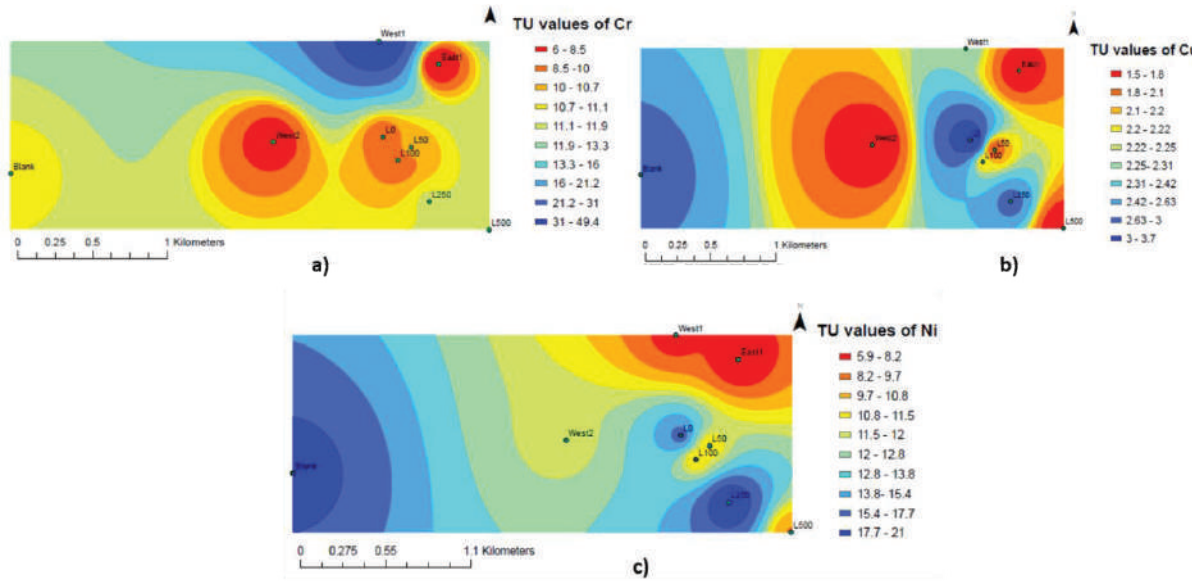

Fig. 4: Toxic Units (TU) of a) Cr, b) Cu and c) Ni.

Table 4: P values for K-S, Mann Whitney U-test and t-test of heavy metals concentrations at 95% significance level.

Variable	K-S test	Mann Whitney U-test	t-test
Cr	0.324	0.254	0.77
Cu	0.518	0.122	0.19
Ni	0.744	0.469	0.6
Pb	<0.0001	0.001	0.02
Zn	0.518	0.250	0.25

(y=mx + c). Pb had R^2 value <0.7 and its concentrations were statistically different. Regression lines of Cr, Cu and Ni showed ideal linear regression models (y=x) of concentrations obtained with the two methods. The regression line of Zn showed a significant and acceptable relationship of data obtained from the two methods, though with some deviations. The regression line of Pb had significant deviations in concentrations of the two methods.

Ecological Risk Indices

The concentrations of trace elements obtained by ICP-MS, which was a superior method compared to XRF were used to calculate ecological risk indices of study area soils. Potential ecological risk indices of trace elements at various sampling sites are given in Table 5. The values of PERI due to Cr were high in all sampling sites and depicted extremely high ecological risk except for the reference sample (Blank) that had a very high risk. PERI values of Cu ranged between 50 and 126, which was classified as moderate to high ecological risk while Ni, Pb and Zn reported low ecological risk and had values <40 with a few exceptions. Cumulative Risk Index (CRI) was calculated as 430.28, which correlated to the considerable ecological risk of the trace elements in sampled soils.

Spatial representation of various toxic units (TU) of assayed heavy metals at various sampling points was as shown in Fig. 4 and 5 (a-b). Toxic units of trace metals decreased in the order of Cr > Ni > Cu > Pb > Zn. Acute risk due to Cr and Ni contamination was evident at all sampling points that had TUs values ≥6. Non-toxicity by Cu, Pb and Zn, however, was reported in all sampling points whose TUs values were <4.

Toxic risk index (TRI) that considers PEL and TEL assessed the risk of trace metals in soils to the ecology of the area and results were spatially distributed as shown in Fig. 5c. TRI ranged between 13 and 113, which represented moderate to very high toxic risk. The highest levels of TRI were found in West 1 sampling site that had the highest concentrations of Cr, which confirmed the high toxicity affiliated with the element.

DISCUSSION

Reproducibility results of XRF and ICP-MS analyses in this study were dependent on the element being quantified, although the former technique underestimated assayed trace elements concentrations. Underestimation was possibly due to differences in equipment sensitivity in the two methods.

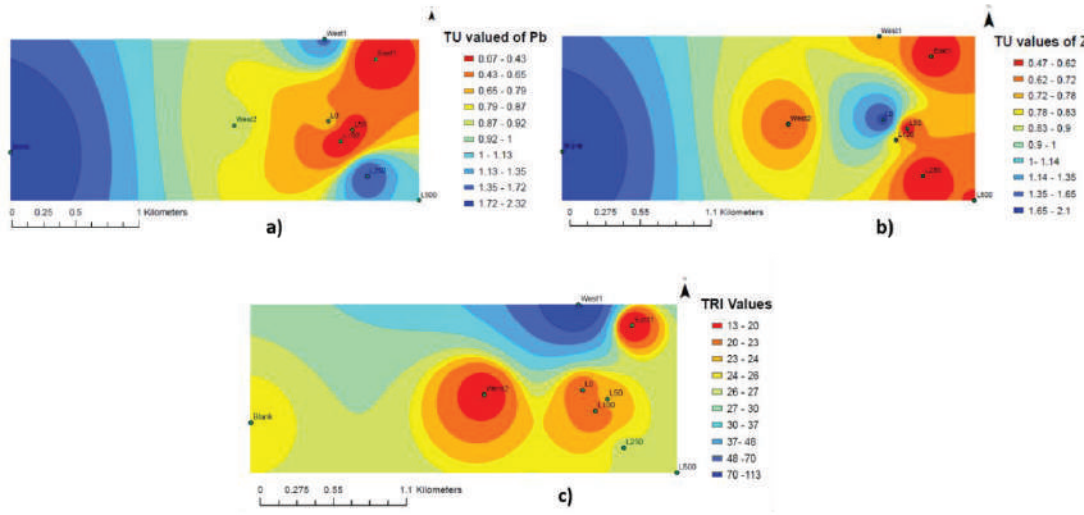

Fig. 5: Toxic units of a) Pb, b) Zn and Toxic Risk index (TRI) values at various sampling sites.

Table 5: Calculated potential ecological risk index (PERI) and cumulative risk index (CRI) values.

	PERI					CRI
	Cr	Cu	Ni	Pb	Zn	
L0	528.31	95.94	17.65	64.00	2.36	430.28
L50	433.54	127.50	15.21	21.53	1.99	
L100	514.46	64.38	10.26	8.38	0.61	
L250	425.85	74.69	10.29	1.83	0.88	
L500	553.85	94.69	19.85	47.85	0.53	
West1	560.92	50.63	9.14	27.80	0.69	
West2	2430.46	79.38	6.90	38.25	0.83	
East1	349.23	50.94	11.05	24.63	0.73	
Blank	287.38	55.63	5.58	1.90	0.56	
Normal concentrations	6.5	16	91	20	240	
T_r	2	5	2	5	1	
PEL	160	110	43	110	270	
TEL	52	19	16	30	120	

XRF has low sensitivity and high detection limits to trace metals in low concentrations while the sensitivity of ICP-MS is high and enhanced by aqua regia digestion (Chen & Ma 2001, Lin 2009). The low sensitivity in XRF explained the differences in skewness and kurtosis results of the two methods, particularly in Pb. These findings disagreed with another comparative study that confirmed no differences in mean concentrations of Pb analysed by XRF and ICP-MS (Merkey et al. 2008). Parametric and non-parametric results of Cr, Cu, Ni and Zn ratified the effectiveness of the two methods and a similar trend was reported in a trace element analysis of soils obtained from Malaysian states (Ahmed et al. 2012) and sub-Saharan Africa (Towett et al. 2013).

Quantitative relationship of Zn and non-relationship of Pb concentrations from regression analysis could be attributable to underestimations of XRF, which is a function of its sensitivity at low concentrations and inter-element interferences (Towett et al. 2013). XRF's detection limits vary from sample to sample based on the anode's X-ray range, the sample composition, the mass of an element, counting time and tube voltage and some of these aspects could have compromised precise concentration measures in this study (Poto et al. 2015). Furthermore, XRF's detection limits differ based on the analyte being assayed, the strength of the excitation source, chemical and physical matrix effects (Makinen et al. 2005). Some of the aspects are difficult to standardize and could have led to the

observed differences. Two studies that reported poor linearity of Pb in comparative XRF and ICP-MS analysis attributed the trend to these XRF equipment flaws (Potts et al. 1995, Kilbride et al. 2006). Under-estimation of concentrations by XRF was attributed to K≥and L≥line inter-elemental line interferences and overlaps, which reduce the equipment's detection intensity of the element (Stonach 2007). These interferences lead to overlapping spectrums that are predominant if assayed samples have arsenic and decrease fluorescence intensity causing underestimation of Pb (USEPA 1998).

ICP-MS was a more sensitive and superior contaminant analysis method over XRF in this study. Other publication agreed with this suggestion and highlighted the advantages of ICP-MS to be lower detection limits, reduced matric effects and no inter-elemental peak overlaps (Ahmed et al. 2012, Towett et al. 2013, McComb et al. 2014). The results differed from those of a study in Maddison, USA, that suggested that XRF had greater sensitivity of both major and trace elements (Herner et al. 2006).

Ecological risk indices showed different potency levels of the assayed elements. Cr had the highest PERI and TU values. The trend could arise due to anthropogenic enrichment of soils of the study area with landfill leachate from wood preservation, metallurgy, varnish, leather and electroplating wastes (Bini et al. 2008). In China, accumulation of Cr in landfill vicinity soils was attributed to the unscientific disposal of solid waste used in industrial processes such as electroplating and the construction industry (Cheng et al. 2014). High values of the indices for Cr compared to other trace elements even in the reference sample could point to its source as lithologic in addition to landfill leachate contamination. A study in urban soils of Beijing reported high PERI values of Cr compared to other elements and attributed it to natural origin from rocks in addition to the accumulation of untreated solid wastes in the area (Wang et al. 2012). CRI results of the current study that showed considerable eco-risk and differed from a study in soils of Yangcaogou region of China, which had CRI levels between 75.07 to 98.61 corresponding to the low ecological risk posed by trace metals (Jiang et al. 2014). However, a great contribution to the CRI was from Cr, which suggested the high potency of the element as reported in another eco-assessment of soils from Caofeidian region of China (Zhu et al. 2018).

Accumulation of consumer and industrial by-products at the landfill could be attributable to acute toxicity by Cr and Ni-based on their TU values. Permenter et al. (2011) attributed the accumulation of Cr and Ni in soils to disposal of stainless steel, chrome pigments, plating and alloy-containing solid waste. This dominance of Cr and Ni toxicity in this study agreed with an eco-risk evaluation study of soils from Bangladesh, where all TU values of sampling sites were >6 (Islam et al. 2015). Soils of the area had moderate to very high toxic risk based on TRI values. The results of this index differed from a related study of Chinese soils that reported a low-risk TRI range of 3.08-8.25 (Zhu et al. 2018).

CONCLUSIONS

Concentrations of Cr, Cu, Ni, Pb and Zn in this study were assayed using ICP-MS and XRF and the results of the former were used to calculate eco-risk indices. Cr had the highest concentration compared to other trace elements. Concentrations determined using XRF for all elements were under-estimated in comparison with ICP-MS, which could be attributed to the low sensitivity, high detection limits and inter-elemental interferences during XRF analysis. These underestimations were reflected in the regression analysis that showed deviations and qualitative relationship in XRF-ICPMS datasets of Pb and Zn, respectively, although Cr, Cu and Ni had ideal relationships. Eco-risk indices showed that Cr had the highest potential ecological risk based on the PERI and TU values and compared to other elements. This trend could arise from landfill leachate generated from wood preservation, metallurgy, varnish, leather and electroplating wastes. Lithologic sources of trace elements were suggested based on the high TU values of Cu, Ni, Pb and Zn in the reference sampling site. Moderate to high toxic risk was deduced from TRI values at various sampling sites. Calculated risk indices and their spatial representation revealed ecological risk from assayed trace elements in soils of Roundhill landfill vicinity, which was possibly linked to leachate pollution.

REFERENCES

Ahmed, A., Abdullah, P., Khalik Wood, A., Hamza, S. and Othman, M. 2012. Determination of some trace metals in marine sediments using ICP-MS and XRF: A comparative study. Oriental Journal of Chemistry, 29: 1-9.

Bini, C., Maleci, L. and Romanin, A. 2008. The chromium issue in soils of the leather tannery district in Italy. Journal of Geochemical Exploration, 96(2-3): 194-202.

Chen, M. and Ma, L. 2001. Comparison of three aqua regia digestion methods for twenty Florida soils. Soil Science Society American Journal, 651: 491-499.

Cheng, H., Zhou, T., Li, Q., Lu, L. and Lin, C. 2014. Anthropogenic chromium emissions in China from 1990-2009. PLoS One, 9(2): e87753.

Chigor V., Sibanda, T. and Okoh. A. 2013. Studies on the bacteriological qualities of the Buffalo River and three water dams along its course in the Eastern Cape province of South Africa. Environmental Science and Pollution Resources 20: 4125-4136.

Department of Environmental Affairs (DEA) 2013. National Environmental Management, Waste Act, 2008. National norms and standards for the remediation of contaminated land and soil quality in the Republic of South Africa. Government Gazette, No. 36447.

Dookhi, N., Jewaskiewitz, S. and Jewaskiewitz, B. 2015. East London regional (Roundhill) waste disposal site-wasting no time on the road

to compliance. Journal of the South African Institution of Civil Engineering, 23(9): 35-42.

Gao, L., Wang, Z., Li, S. and Chen, J. 2018. Bioavailability and toxicity of trace metals (Cd, Cr, Cu, Ni, and Zn) in sediment cores from the Shima River, South China. Chemosphere, 192: 31-42.

Ghasemi, A. and Zahediasi, S. 2012. Normality tests for statistical analysis: A guide for non-statisticians. International Journal of Endocrinology and Metabolism, 10: 486-489.

Hakanson, L. 1980. An ecological risk index for aquatic pollution control: A sedimentological approach. Water Research, 14(8): 975-1001.

Herner, J., Green, P. and Kleeman, M. 2006. Measuring the trace elemental composition of size-resolved airborne particles. Environmental Science and Technology, 40: 1925-1933.

Islam, S., Ahmed, K., Al-Mamun, H. and Masunaga, S. 2015. Potential ecological risk of hazardous elements in different land-use urban soils of Bangladesh. Science of the Total Environment, 512-513: 94-102.

Jiang, X., Lu, W., Zhao, H., Yang, Q. and Yang, Z. 2014. Potential ecological risk assessment and prediction of soil heavy metal pollution around coal gangue dump. Natural Hazards and Earth System Sciences, 14: 1599-1610.

Kilbride, C., Poole, J. and Hutchings, T.R. 2006. A comparison of Cu, Pb, As, Cd, Zn, Fe, Ni and Mn determined by acid extraction/ICP-OES and ex situ field portable X-ray fluorescence analyses. Environmental Pollution, 143: 16-23.

Lin, J. 2009. Performance of the thermo scientific niton XRF analyzer: the effects of particle size, length of analysis, water, organic matter and soil chemistry. Available Online: http://nature.berkeley.edu/classes/es196/projects/2009finalLinJ_2009.pdf [Accessed on 17 March 2018]

Makinen, E., Korhonen, M., Viskari, E., Haapamaki, S., Jarvinen M. and Lu, L. 2005. Comparison of XRF and FAAS methods in analysing CCA contaminated soils. Water, Air and Soil Pollution, 171: 95-110.

Maliki, A., Al-Lami, A., Hussain, H., and Al-Ansari, N. 2017. Comparison between inductively coupled plasma and X-ray fluorescence performance for Pb analysis in environmental soil samples. Environment and Earth Science, 76: 433.

Marcos, D., Jason, P., Humberto, G., Alba, C., Gustavo, C., Alfredo, C., Alberto, D. and Jorge, G. 2011. Comparison of ICP-OES and XRF performance of Pb and As analysis in environmental soil samples from Chihuahua city, Mexico. Physical Review Research International, 1: 29-44.

Mccomb, J., Rogers, C., Han, F. and Tchounwou, P. 2014. Rapid screening of heavy metals and trace elements in environmental samples using portable X-ray fluorescence spectrometer, a comparative study. Water, Air and Soil Pollution, 225: 2169.

Merkey, A., Clark, C., Succop, P. and Roda, S. 2008. Determination of feasibility of using a portable X-ray fluorescence (XRF) analyser in the field for measurement of lead content of sieved soil. Journal of Environmental Health, 70: 24-29.

Oztuna, D., Elhan, A.H. and Tuccar, E. 2006. Investigation of four different normality tests in terms of type 1 error rate and power under different distributions. Turkish Journal of Medical Sciences, 36: 171-176.

Pedersen, F., Bjornestad, E., Andersen, H., Kjolholt, J. and Poll, C. 1998. Characterisation of sediments from Copenhagen Harbour by use of biotests. Water Science and Technology, 37 (6-7): 233-240.

Permenter, M., Lewis, J. and Jackson, D. (2011). Exposure to nickel, chromium, or cadmium causes distinct changes in the gene expression patterns of a rat liver derived cell line. PLoS ONE 6(11): e27730.

Poggio, L. and Vrscaj, B. 2009. A GIS-based human health risk assessment for urban green space planning an example from Grugliasco (Italy). The Science of the Total Environment, 407: e5961-e5970.

Poto, L., Gabrieli, J., Crowhurst, S. and Agostinelli, C. 2015. Cross calibration between XRF and ICP-MS for high spatial resolution analysis of ombrotrophic peat cores for palaeoclimatic studies. Analytical and Bioanalytical Chemistry, 407: 379-384.

Potts, P.J., Webb, P.C., Williams-Thorpe, O. and Kilworth, R. 1995. Analysis of silicate rocks using field portable X-ray Fluorescence instrumentation incorporating a mercury(II) iodide detector: A preliminary assessment of analytical performance. The Analyst, 120: 1273-1278.

Radu, T. and Diamond, D. 2009. Comparison of soil pollution concentrations determined using AAS and portable XRF techniques. Journal of Hazardous Materials, 171: 1168-1171.

Shokr, M., El-Baroudy, A., Fullen, M., El-Beshbeshy, T., Ramadan, A., Halim, A., Guerra, A. and Jorge, M. 2016. Spatial distribution of heavy metals in the middle Nile delta of Egypt. International Soil and Water Conservation Research, 4(4): 293-303.

Stonach, H. 2007. S2 PICOFOX total reflection X-ray fluorescence spectroscopy-working principles. Lab Report. Bruker AXS microanalysis GmbH [Report No. XRF 426].

Sun, Z., Mou, X., Tong, C., Wang, C., Xie, Z., Song, H., Sun, W. and Lv, Y. 2015. Spatial variations and bioaccumulation of heavy metals in intertidal zone of the Yellow River estuary, China. Catena, 126: 43-52.

Towett, E., Shepherd, K., and Cadisch, G. 2013. Quantification of total element concentrations in soils using total X-ray fluorescence spectroscopy (TXRF). Science of Total Environment, 463(4): 374-8.

United States Environmental Protection Agency (USEPA) 1998. Method 3015a, Microwave assisted acid digestion of aqueous samples and extracts. Washington DC: US Environmental Protection Agency.

USEPA 2014. Method 6020B (SW-846): Inductively coupled plasma-mass spectrometry. Revision 2, Washington, DC: US Environmental Protection Agency.

USEPA 2016. SW-846 test method 6200: Field portable X-ray fluorescence spectrometry for the determination of elemental concentrations in soils and sediments. Washington, DC: US Environmental Protection Agency.

Wang, M., Bai, Y., Chen, W., Markert, B., Peng, C. and Ouyang, Z. 2012. A GIS technology based potential eco-risk assessment of metals in urban soils in Beijing, China. Environmental Pollution, 161: 235-242.

Yan, B. and Li, Y. 2011. GIS-based study on spatial variability of groundwater quality in Xianyan city. 2011 International Symposium on Water Resource and Environmental Protection. 20-22 May 2011, IEEE, Xi'an, China.

Zhu, H., Bing, H., Yi, H., Wu, Y. and Sun, Z. 2018. Spatial distribution and contamination assessment of heavy metals in surface sediments of the Caofeidian adjacent sea after the land reclamation, Bohai City. Journal of Chemistry, 1-13.

Nature Environment and Pollution Technology
An International Quarterly Scientific Journal

p-ISSN: 0972-6268
(Print copies up to 2016)
e-ISSN: 2395-3454

Vol. 19 | No. 2 | pp. 549-562 | 2020

Original Research Paper

https://doi.org/10.46488/NEPT.2020.v19i02.010

Open Access Journal

A Review on Emerging Contaminants in Indian Waters and Their Treatment Technologies

Riya Ann Mathew*† and S. Kanmani**
*Department of Civil and Environmental Engineering, University of Houston, Houston, Texas 77204, United States
**Centre for Environmental Studies, Anna University, Chennai-600025, Tamil Nadu, India
†Corresponding author: Riya Ann Mathew; riya.am@gmail.com

Nat. Env. & Poll. Tech.
Website: www.neptjournal.com

Received: 04-09-2019
Accepted: 18-12-2019

Key Words:
Emerging contaminants; Persistent organic pollutants; Ozonation; Photocatalytic degradation

ABSTRACT

Emerging contaminants (ECs) have been detected recently in many water bodies across India. Studies have found the presence of ECs in surface water, groundwater, stormwater, treated wastewater, treated industrial effluent, bottled water and snow from glaciers in Indo-Chinese border which contaminate water bodies. The surface water recharges the groundwater, thereby the ECs make their way to deep water aquifers. The soil also gets contaminated and plants can uptake ECs. These micropollutants can cause adverse ecological and human health effects. Antimicrobial resistance of bacteria to commonly used antibiotics has been observed in India. An exhaustive review of emerging contaminants in Indian waters and their treatment technologies has been carried out. Antibiotic-resistant genes can be easily transferred resulting in a plethora of antimicrobial-resistant bacteria which can cause devastating effects on human health. Conventional biological treatment is not capable of removing ECs completely. Advanced oxidation processes using ozonation and visible light active photocatalyst are a sustainable solution for the removal of most ECs. Hence, it is of utmost importance to monitor the presence of ECs in the water environment and develop treatment technologies for its removal.

INTRODUCTION

United States Geological Survey (USGS) defines an Emerging Contaminant (EC) as any synthetic or naturally occurring chemical or microorganism that is not commonly monitored in the environment but has the potential to enter the environment and cause unknown or suspected adverse ecological and human health effects. Sources of ECs are compounds such as pharmaceuticals and personal care products (PPCPs), contrast media, plasticizers, food additives, wood preservatives, laundry detergents, surfactants, disinfectants, flame retardants, pesticides, natural and synthetic hormones, and a few disinfection by-products (DBPs) (La Farré et al. 2008) that enters through several pathways (Fig. 1). Balakrishnan and Mohan (2016) identified the ECs in stormwater in Chennai. Several aromatic and aliphatic hydrocarbons such as decane, p-xylene, octanol, eicosane etc. were detected in the stormwater. Some of them are used in fuels while others are plasticizers or used as precursors for perfumes and flavouring agents.

Due to its persistent, bioaccumulative and toxic nature, it poses a great risk on the environment and human health. Hence, extensive ecotoxicological studies must be carried out to establish toxicity endpoints. The conventional biological treatment plant is not capable of removing the ECs and requires advanced treatment technologies. This review is intended to present an overview of the presence of ECs in Indian water matrices along with the remediation technologies used for some predominant ECs.

OCCURRENCE OF ECS IN INDIAN WATERS

In India, the contribution of emerging contaminants in aquatic environment comprises of 57% pesticides, 17% pharmaceuticals, 15% surfactants, 7% personal care products and 5% phthalates (Gani & Khazmi 2016). Several studies ascertained the presence of Active pharmaceutical ingredients (API), personal care products (PCP), pesticides, endocrine-disrupting chemicals (EDC) and artificial sweeteners (ASW) in surface water bodies.

Pharmaceuticals

The Delhi-based non-profit Centre for Science and Environment (CSE) reports that 78 percent of the sewage generated in India remains untreated and is discharged in rivers, groundwater or lakes (CSE 2016). This could explain the reason for high levels of API in water matrices.

William et al. (2019) investigated the presence of pharmaceuticals in Ahar River in Udaipur city and found 19 pharmaceuticals including 4 antibiotics. The river originates as a potable water source which gets contaminated as it

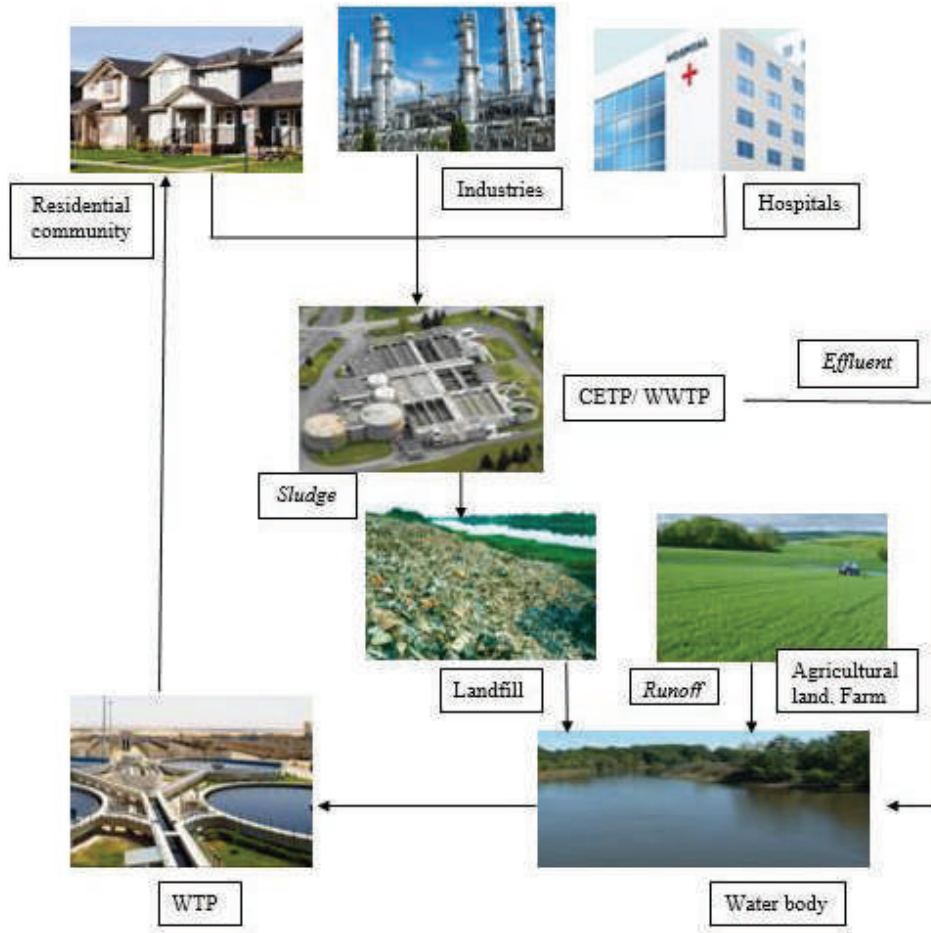

Fig. 1: Pathway for ECs into water environment.

moves through urban areas. It was observed that the concentration of emerging contaminants increased as it passed through densely populated regions indicating the potential discharge of domestic wastewater into the river. Mutiyar & Mittal (2014) studied the occurrence of antibiotics in influent and effluent of STP and Yamuna river in Delhi. Ampicillin concentration in untreated and treated wastewater was 104.2 µg/L and 12.7 µg/L. Fick et al. (2009) found extremely high concentrations of Ciprofloxacin and Cetirizine in the lake water, Isakavagu-Nakkavagu rivers and well water sample from Hyderabad. Lubbert et al. (2017) reported a high concentration of Fluconazole, an antifungal, to be 236,950 µg/L from a sewer in the industrial area apart from several classes of antibiotics. The effluent after preliminary treatment is carried through sewers to the nearby Sewage Treatment Plant (STPs) and treated effluents are finally discharged into the Musi river. The area is home to 30 pharmaceutical drug manufacturers. Similar studies by Larsson et al. (2007) in the water bodies and wells near the pharmaceutical manufacturing industrial zone found the highest reported concentrations of API in the world. Antimicrobial resistance has also been observed in bacteria from this region. Antibiotic resistance caused by sulfamethoxazole (SMX) has been determined in River Ganga and groundwater in Varanasi (Lapworth et al. 2018). Philip et al. (2017) presented a comprehensive review of the presence of antibiotic-resistant genes (ARG) in India.

Ramaswamy et al. (2011) studied the occurrence of carbamazepine (CBZ), antiepileptic in water samples from the Kaveri, Vellar, Tamiraparani rivers and Pichavaram mangrove in Tamil Nadu (TN). This was the first study to report the presence of a pharmaceutical in south Indian rivers. Lapworth et al. (2018) determined the presence of SMX and CBZ in River Ganga. It was interesting to note that the CBZ concentration in River Ganga and groundwater from deep wells at a depth of even 140 meters in Varanasi had a concentration of 0.02 µg/L. Similarly, it was observed that the concentration of CBZ and SMX were much higher in

the groundwater compared to Ganga river water (Sharma et al. 2019). The major reason for the presence of API in groundwater is bank infiltration and the accumulation of API in groundwater due to limited flow as against surface water. Anumol et al. (2016) investigated several pharmaceuticals in the influent and effluent of three wastewater treatment plants (WWTPs) in Chennai and found several API namely CBZ, SMX, naproxen and atenolol in all the effluent samples. Iohexol used as a contrast agent during X-rays was found in high concentrations in the influent and effluent of WWTPs and had very less removal. It was found that the major classes of contributors were X-ray contrast media, pharmaceuticals and stimulant, caffeine. The average concentration of CBZ, SMX and naproxen in the influent of WWTP was 0.92 µg/L. Caffeine presented a high concentration of 65 µg/L in the incoming wastewater. Gemfibrozil, the anti-cholesterol drug was less than 0.1 µg/L. API such as CBZ, SMX, gemfibrozil, caffeine, naproxen, ibuprofen and diclofenac (DCF), Non-Steroidal Anti-inflammatory drug (NSAID), are found to be the chief API in Indian waters. Table 1 represents the details of 42 predominant API found across Indian water bodies.

Personal Care Products

Triclosan and Triclocarban are the commonly used antibacterials in soaps, shampoos, hand sanitizers, etc. The occurrence of triclosan, triclocarban and parabens (preservative in cosmetics), commonly used in personal care products (PCP), in water samples from the Kaveri, Vellar, Tamiraparani rivers and the Pichavaram mangrove in South India (Ramaswamy et al. 2011, Vimalkumar et al. 2018). Triclosan and triclocarban were detected in the influent and effluent of WWTP in Chennai (Anumol et al. 2016).

Table 1: Details of API commonly encountered in Indian waters.

API	Class of drug	Concentration (µg/L)	Location of sampling	Reference
Carbamazepine	Antiepileptic	13.00	Kaveri, TN	Ramaswamy et al. (2011)
		5.14	Tamiraparani, TN	Ramaswamy et al. (2011)
		2.67	Vellar, TN	Ramaswamy et al. (2011)
		6.65	Pichavarom Mangrove, TN	Ramaswamy et al. (2011)
		0.113	Ahar River, Udaipur	William et al. (2019)
		0.09	Groundwater, Varanasi, UP	Lapworth et al. (2018)
		0.02	Groundwater, Ramnagar, UP	Lapworth et al. (2018)
		0.02	River Ganga, UP	Lapworth et al. (2018)
		0.016	Stretch of River Ganga	Sharma et al. (2019)
Fluconazole	Antifungal	236950	Sewer, Patancheru Pashamylaram Industrial area, Hyderabad	Lubbert et al. (2017)
Voriconazole	Antifungal	2500	Sewer, Patancheru Pashamylaram Industrial area, Hyderabad	Lubbert et al. (2017)
Acetaminophen	Analgesic	0.004	Stretch of River Ganga	Sharma et al. (2019)
		0.002	Groundwater near Ganga basin	Sharma et al. (2019)
Atenolol	Beta-blocker	0.001	Stretch of River Ganga	Sharma et al. (2019)
		6.9	Influent, WWTP, Chennai	Anumol et al. (2016)
Ketoprofen	NSAID	0.11	Stretch of River Ganga	Sharma et al. (2019)
		0.023	Groundwater near Ganga basin	Sharma et al. (2019)
Ibuprofen	NSAID	1.89	Ahar River, Udaipur	William et al. (2019)
		0.023	Stretch of River Ganga	Sharma et al. (2019)
		0.049	Groundwater near Ganga basin	Sharma et al. (2019)
Diclofenac	NSAID	0.41	Ahar River, Udaipur	William et al. (2019)
		0.041	Stretch of River Ganga	Sharma et al. (2019)
		0.002	Groundwater near Ganga basin	Sharma et al. (2019)
		5.3	Influent, WWTP, Chennai	Anumol et al. (2016)

Table cont....

...Cont. Table

API	Class of drug	Concentration (µg/L)	Location of sampling	Reference
Naproxen	NSAID	0.24	Ahar River, Udaipur	William et al. (2019)
		0.003	Stretch of River Ganga	Sharma et al. (2019)
		0.002	Groundwater near Ganga basin	Sharma et al. (2019)
Iohexol	X-ray contrast media	9.6	Influent, WWTP, Chennai	Anumol et al. (2016)
		8.7	Effluent, WWTP, Chennai	Anumol et al. (2016)
Caffeine	Cosmetic, Psychoactive drug	37.5	Ahar river, Udaipur	Williams et al. (2019)
		0.743	Stretch of River Ganga	Sharma et al. (2019)
		0.262	Groundwater near Ganga basin	Sharma et al. (2019)
		65	Influent, WWTP, Chennai	Anumol et al. (2016)
		5.4	Effluent, WWTP, Chennai	Anumol et al. (2016)
Hydrochlorothiazide	Diuretics	0.004	Stretch of River Ganga	Sharma et al. (2019)
		0.001	Groundwater near Ganga basin	Sharma et al. (2019)
		0.39	Ahar River, Udaipur	William et al. (2019)
Trimethoprim	Antibiotic	0.05	Ahar River, Udaipur	William et al. (2019)
Azithromycin	Antibiotic	0.99	Ahar River, Udaipur	William et al. (2019)
Moxifloxacin	Antibiotic, fluoroquinolone	694.1	Sewer, Patancheru industrial area	Lubbert et al. (2017)
Linezolid	Antibiotic	37	Sewage storage, Patancheru Kazipally Industrial area, Hyderabad	Lubbert et al. (2017)
Clarithromycin	Antibiotic	27.7	Weir in Musi River, Hyderabad	Lubbert et al. (2017)
		0.05	Ahar River, Udaipur	William et al. (2019)
Levofloxacin	Antibiotic, fluoroquinolone	12.8	Musi River, upstream of Amberpet treatment plant, Hyderabad	Lubbert et al. (2017)
Ciprofloxacin	Antibiotic, fluoroquinolone	14000	Effluent-Patancheru Enviro Tech Ltd. (PETL), Hyderabad	Fick et al. (2009)
		2500	Isakavagu-Nakkavagu River, Hyderabad	Fick et al. (2009)
		6500	Lake, upstream of PETL, Hyderabad	Fick et al. (2009)
		14	Well, near lake, upstream of PETL, Hyderabad	Fick et al. (2009)
		28000-31000	Effluent-CETP, Hyderabad	Larsson et al. (2007)
		0.029	Stretch of River Ganga	Sharma et al. (2019)
		0.005	Groundwater near Ganga basin	Sharma et al. (2019)
Cetirizine	Antihistamine	2100	Effluent- CETP, Hyderabad	Fick et al. (2009)
		1200	Lake, upstream of PETL, Hyderabad	Fick et al. (2009)
Norfloxacin	Antibiotic, fluoroquinolone	25	Effluent-PETL, Hyderabad	Fick et al. (2009)
		520	Lake, upstream of PETL, Hyderabad	Fick et al. (2009)
		390 - 420	Effluent-CETP, Hyderabad	Larsson et al. (2007)
Glibenclamide	Hypoglycemic drug	0.80	Ahar River, Udaipur	William et al. (2019)
Citalopram	Selective serotonin reuptake inhibitor	430	Effluent-PETL, Hyderabad	Fick et al. (2009)
		8	Lake, upstream of PETL, Hyderabad	Fick et al. (2009)

Table cont....

...Cont. Table

API	Class of drug	Concentration (µg/L)	Location of sampling	Reference
Enalapril	Angiotensin-converting enzyme inhibitor	2.2 1	Effluent-PETL, Hyderabad Lake, upstream of PETL, Hyderabad	Fick et al. (2009) Fick et al. (2009)
Enrofloxacin	Antibiotic, fluoroquinolone	210 25	Effluent-CETP, Hyderabad Lake, upstream of PETL, Hyderabad	Fick et al. (2009) Fick et al. (2009)
Metoprolol	Beta-adrenoreceptor antagonist	4 7 0.07	Effluent-PETL, Hyderabad Lake, upstream of PETL, Hyderabad Ahar River, Udaipur	Fick et al. (2009) Fick et al. (2009) William et al. (2019)
Ofloxacin	Antibiotic, fluoroquinolone	55 11 150–160	Effluent-PETL, Hyderabad Lake, upstream of PETL, Hyderabad Effluent-CETP, Hyderabad	Fick et al. (2009) Fick et al. (2009) Larsson et al. (2007)
Terbinafine	Antimycotic	120 15 10.6	Effluent-PETL, Hyderabad Lake, upstream of PETL, Hyderabad Weir in Musi River, downstream of Amberpet treatment plant, Hyderabad	Fick et al. (2009) Fick et al. (2009) Lubbert et al. (2017)
Sulfamethoxazole	Antibiotic	0.82 0.1 0.04 0.02 0.028 0.004	Ahar River, Udaipur River Ganga, UP Groundwater, Varanasi, UP Groundwater, Ramnagar, UP Stretch of River Ganga Groundwater near Ganga basin	William et al. (2019) Lapworth et al. (2018) Lapworth et al. (2018) Lapworth et al. (2018) Sharma et al. (2019) Sharma et al. (2019)
Sulfanilamide	Antibiotic	0.12 0.12	Groundwater, Varanasi, UP Groundwater, Ramnagar, UP	Lapworth et al. (2018) Lapworth et al. (2018)
Ampicillin	Antibiotic, Penicillin	29.1 12.7 13.75	Sewer, Patancheru industrial area Treated wastewater, STP, Delhi Yamuna River, Delhi	Lubbert et al. (2017) Mutiyar & Mittal (2014) Mutiyar & Mittal (2014)
Doxycycline	Antibiotic	14.9	Sewer, Patancheru Pashamylaram Industrial area	Lubbert et al. (2017)
Sparfloxacin	Antibiotic, fluoroquinolone	2.09	Yamuna River, Delhi	Mutiyar & Mittal (2014)
Cefuroxime	Antibiotic	1.7	Yamuna River, Delhi	Mutiyar & Mittal (2014)
Gatifloxacin	Antibiotic, fluoroquinolone	0.48	Yamuna River, Delhi	Mutiyar & Mittal (2014)
Desipramine	Antidepressant	0.075	Ahar River, Udaipur	William et al. (2019)
Tramadol	Analgesic	0.09	Ahar River, Udaipur	William et al. (2019)
Cyclophosphamide	Antineoplastics	0.32	Ahar River, Udaipur	William et al. (2019)
Diltiazem	Calcium channel blocker	0.016	Ahar River, Udaipur	William et al. (2019)
Propranolol	Beta-blocker	0.016	Ahar River, Udaipur	William et al. (2019)
Venlafaxine desmethyl	Antidepressant	1.5	Ahar River, Udaipur	William et al. (2019)
Verapamil	Calcium channel blocker	0.02	Ahar River, Udaipur	William et al. (2019)

Table 2: Details of PCP commonly encountered in Indian waters.

PCPs	Class of PCPs	Concentration (µg/L)	Sampling Location	Reference
Triclosan	Antibacterial	0.04	Kaveri	Ramaswamy et al. (2011)
		0.14	Tamiraparani	Ramaswamy et al. (2011)
		0.009	Vellar	Ramaswamy et al. (2011)
		0.02	Pichavarom Mangrove	Ramaswamy et al. (2011)
		0.005	Stretch of River Ganga	Sharma et al. (2019)
		0.01	Groundwater near Ganga basin	Sharma et al. (2019)
Triclocarban	A[[ntibacterial	1.12	Kaveri	Vimalkumar et al. (2018)
		0.17	Tamiraparani	Vimalkumar et al. (2018)
		0.10	Vellar	Vimalkumar et al. (2018)
		0.003	Stretch of River Ganga	Sharma et al. (2019)
		0.002	Groundwater near Ganga basin	Sharma et al. (2019)
UV-9	BUVSs	0.027	Kaveri	Vimalkumar et al. (2018)
		0.028	Tamiraparani	Vimalkumar et al. (2018)
		0.004	Vellar	Vimalkumar et al. (2018)
UV-329	BUVSs	0.03	Kaveri	Vimalkumar et al. (2018)
		0.03	Tamiraparani	Vimalkumar et al. (2018)
		0.016	Vellar	Vimalkumar et al. (2018)
DEET	Mosquito repellant	0.39	Ahar river, Udaipur	Williams et al. (2019)
		0.022	Stretch of River Ganga	Sharma et al. (2019)
		0.015	Groundwater near Ganga basin	Sharma et al. (2019)
Benzotriazole	UV stabilisers	0.526	Ahar river, Udaipur	Williams et al. (2019)

DEET used in mosquito repellents has been detected in Ahar River, Udaipur (William et al. 2019). This indicates the contamination of river water by domestic wastewater. It was found that the concentration of PCP increased with an increase in population density. The presence of benzotriazole ultraviolet stabilizers (BUVSs) which are used extensively in personal care products such as soaps, shampoos, sunscreen lotions, shaving creams etc. has been detected in the three major rivers in south India - Kaveri, Tamiraparani and Vellar (Vimalkumar et al. 2018). Among the BUVSs, UV-329 and UV-9 were predominant. Benzotriazole has also been reported to be present in Ahar River (William et al. 2019). Table 2 shows PCPs commonly encountered in Indian water bodies.

Perfluorinated Compounds

Recent studies have reported the presence of perfluorinated compounds (PFCs) in groundwater, surface water, drinking water, snow and precipitation water. Of the PFCs reported, short-chain (C<5) PFCs were predominant. PFOS is one of the prominent PFCs present in Ganga river and groundwater samples from Varanasi and Ramnagar besides PFDA and PFNA. The highest concentration reported in the groundwater and River Ganga were 0.033 µg/L and 0.025 µg/L respectively. Interestingly, the PFAS concentration in groundwater in Varanasi was much higher than in river Ganga (Lapworth et al. 2018). It indicates the contamination of ECs in water through the recharge pathway and its mobility through the substrata. Yeung et al. (2009) studied the occurrence of PFCs in surface water bodies in several cities in India including the stretch of River Ganga. High concentrations of PFCs were reported in Chennai followed by Allahabad, Varanasi, Patna and Kanpur. Generally, the PFOS was dominant over PFOA while PFOA was predominant in Chennai. 23.1 ng/L of PFOA was found in Cooum River, Chennai. The concentration of PFOS was 3.91 ng/L and 12 ng/L in Cooum River and untreated sewage respectively. High concentrations of PFOS were reported at Ganges-Yamuna confluence, Allahabad. Sharma et al. (2016) studied the PFAS contamination in river Ganges and groundwater samples from the river basin. The river water had the highest concentration for PFHxA (4.7 ng/L) and PFBS (10.2 ng/L) among PFCAs and PFSAs. In groundwater, PFBA (9.2 ng/L) and PFBS (4.9 ng/L) had the highest concentrations among PFCAs and PFSAs respectively. The daily PFAS exposure was below the safety threshold for oral non-cancer risk for all age groups. The contamination trend in river water and groundwater are similar indicating that the aquifer is recharged by the river.

Sunantha & Vasudevan (2016) investigated the PFOA and PFOS in Velachery Lake, Porur Lake, Chitlapakkam Lake, Pallavaram Lake, Korattur Lake, Ambattur Lake (Chennai), Cauvery River (Erode), and Noyyal River (Tiruppur). PFOA was high in the range 4 to 93 ng/L and PFOS varied from 3 to 29 ng/L. Kwok et al. (2010) studied the occurrence

of PFCs in precipitation samples from several countries including India. PFAS concentration was found to be 0.04 ng/L in samples from Patna. Perfluoro-n-pentanoic acid (PFPeA) accounted for more than 25% of PFCs. Wang et al. (2019) reported the highest PFAS concentration in surface snow sample from glaciers in west China to be 3.97 ng/L. The two predominant atmospheric circulation patterns over western China are Westerly winds and the Indian monsoon, 70 % being contributed by Indian monsoon, indicating the presence of PFC in the atmosphere. The previous studies have reported the presence of short-chain PFAS and other PFC in the Indian water environment.

Endocrine Disrupting Chemicals

Endocrine Disrupting Chemicals (EDCs) have received wide attention recently due to its ability to disrupt the endocrine system of humans, special vulnerable groups include pregnant mothers, children and elderly. The occurrence of phthalates, polychlorinated biphenyls (PCBs), plasticizers and perchlorate have been reported in several studies. Phthalate intake has been estimated by analysing phthalate concentration in urine samples in India, the second highest concentration (389 ng/mL) was found (Guo et al. 2011). PCBs have been reported to affect the reproductive system. Chakraborty et al. (2016) determined the total PCBs in River Hooghly and River Brahmaputra at concentrations of 0.233 µg/L and 0.161 µg/L respectively. PCBs can make their way into the environment through leaching from open dumpsites, poorly managed landfills and improperly discarded electronic waste. William et al. (2019) found six steroid hormones in Ahar river, Udaipur such as estrone, 17αestradiol, 17αestradiol, androsterone, dihydrotestosterone, testosterone. The concentration of estrone and androsterone were 1.55 µg/L and 0.15 µg/L respectively. In addition, bisphenol A, plasticizer, was also found at a concentration of 0.3 µg/L.

Yamazaki et al. (2015) studied the presence of Bisphenol A and bisphenol (BP) analogues including BPS and BPF in surface water samples from Japan, China, Korea and India. In India, the highest BPA concentrations found in Buckingham and Cooum were 1.39 µg/L and 0.423 µg/L respectively. The highest BPS concentrations were 1.08 µg/L and 6.84 µg/L in the Buckingham canal and Adyar river respectively which was higher than in other countries. BP was not detected in Puzhal lake. Selvaraj et al. (2014a) analysed Kaveri, Vellar and Tamaraparani river waters for octylphenol (OP), nonylphenol (NP), and bisphenol A (BPA) and the concentrations of OP, NP and BPA ranged from ND (not detected) to 16.3 ng/L, ND to 2200 ng/L, and 2.8 to 136 ng/L respectively. High concentrations were observed in the Kaveri river. NP was much higher than BPA followed by OP. Srivastava et al. (2010) reported a high concentration of phthalic acid esters (PAE), plasticizer, in the sediments of Gomti river and the mean concentrations of DMP, DEP, DBP, DEHP and DOP were 10.54, 4.57, 10.41, 31.61 and 5.16 µg/kg respectively. DEHP was the most frequently detected PAE. Such high concentration in the sediments from Gomti river indicates the high contaminant load of PAE in the river, which deposit on sediments due to their hydrophobicity. Selvaraj et al. (2014b) studied the presence of phthalates in the stretch of Kaveri river and found the highest concentration of DMP, DEP, DBP, BBP, DEHP and DOP as 94, 520, 372, 145, 822 and 85 ng/L. DEHP and DEP accounted for 57% and 22% of phthalates. The high concentration was observed in Bhavani town sampling location at the confluence of Bhavani and Noyyal rivers. The concentration of phthalates in the sediments of the Kaveri river was lower than the Gomti river.

Das et al. (2014) measured 15 phthalates in drinking water from Jawaharlal Nehru University and the Okhla industrial area. The sum concentration of all phthalates was found to be 0.39 and 3.804 µg/L. DEHP was the most predominant phthalate and the estimated total daily intake level was 70 mg/kg/d. Phthalates such as DEP, DBP, BBP and DEHP have been reported in the three wastewater treatment plants. The highest mean concentration of DEP, DBP and DEHP was 7, 14 and 19 µg/L in summer. The main removal process of phthalates is biotransformation (Gani & Kazmi 2016). Phthalates have also been reported to be present in bottled water at a maximum total phthalate concentration of 7.82 µg/L. Similar to previous studies the highest phthalate contributor was DEHP. The phthalate concentration was found to increase with an increase in shelf life (Selvaraj et al. 2016).

Perchlorate is used extensively in fireworks, matches, arms and ammunition industries. It also finds its application in lubricating oils, aluminium refining, paint and rubber manufacturing, leather tanning, paper and pulp processing (used in bleaching powder) and as a dye mordant. Sodium hypochlorite used as a disinfectant in chlorination during water and wastewater treatment has been identified as a source of perchlorate contamination (USEPA 2007). It can interfere with iodine transport, thereby reducing thyroid production (Fisher & McLanahan 2008). It can cause haemolytic anaemia, delayed development, affect pregnant women, foetus and children (Pearce et al. 2007). The USEPA drinking water standard for perchlorate is 15 µg/L. Nadaraja et al. (2015) analysed surface and groundwater samples from 27 locations in Kerala. Perchlorate was detected in 58% of groundwater samples and the highest concentration was 7270 µg/L. All the surface water sample analysed were reported to be contaminated with perchlorate and the highest observed concentration was 355 µg/L, while all the five bottled drink-

Table 3: Details of the pesticide concentration in Indian waters.

Pesticides	Concentration (µg/L)	Location	Reference
HCH	4.403	Surface water, Dibrugarh, ASM	Mishra & Sharma (2011)
	5.168	Groundwater, Dibrugarh, ASM	Mishra & Sharma (2011)
	4.911	Surface water, Nagaon, ASM	Mishra & Sharma (2011)
	5.574	Groundwater, Nagaon, ASM	Mishra & Sharma (2011)
	1.95	Unnao district, Madya Pradesh	Singh et al. (2007)
	0.022	River Brahmaputra	Chakraborty et al. (2016)
	0.114	River Hooghly	Chakraborty et al. (2016)
DDT	5.402	Surface water, Dibrugarh, ASM	Mishra & Sharma (2011)
	6.549	Groundwater, Dibrugarh, ASM	Mishra & Sharma (2011)
	6.121	Surface water, Nagaon, ASM	Mishra & Sharma (2011)
	6.904	Groundwater, Nagaon, ASM	Mishra & Sharma (2011)
	0.23	Unnao district, MP	Singh et al. (2007)
	0.225	River Brahmaputra	Chakraborty et al. (2016)
	0.026	River Hooghly	Chakraborty et al. (2016)
Total OCP	3.72	Unnao district, MP	Singh et al. (2007)
	0.245	River Brahmaputra	Chakraborty et al. (2016)
	0.154	River Hooghly	Chakraborty et al. (2016)
Endosulfan	0.13	Unnao district, MP	Singh et al. (2007)
	0.053	River Brahmaputra	Chakraborty et al. (2016)
	0.01	River Hooghly	Chakraborty et al. (2016)
Endrin	0.01	Unnao district, MP	Singh et al. (2007)
Aldrin	1.88	Unnao district, MP	Singh et al. (2007)
	0.019	River Brahmaputra	Chakraborty et al. (2016)
	0.009	River Hooghly	Chakraborty et al. (2016)
Chlorpyrifos	0.004	River Ganga, UP	Lapworth et al. (2018)
	0.004	Groundwater, Ramnagar, UP	Lapworth et al. (2018)
	0.003	Groundwater, Varanasi, UP	Lapworth et al. (2018)
Phenoxyacetic acid	0.7	River Ganga, UP	Lapworth et al. (2018)
	0.05	Groundwater, Ramnagar, UP	Lapworth et al. (2018)
	0.2	Groundwater, Varanasi, UP	Lapworth et al. (2018)
Diuron	0.04	River Ganga, Uttar Pradesh	Lapworth et al. (2018)
Atrazine	0.03	River Ganga, Uttar Pradesh	Lapworth et al. (2018)
Heptachlor	0.01	River Brahmaputra	Chakraborty et al. (2016)
	0.026	River Hooghly	Chakraborty et al. (2016)

ing water was free of perchlorate. Raj & Muruganandam (2014) found very high perchlorate concentration of 93,500 µg/L in the real industrial effluent sample from Vellore, Tamil Nadu. The mean perchlorate concentrations in drinking water, groundwater, surface water and effluent water were 126, 831, 1110 and 15754 µg/L respectively. Isobe et al. (2013) studied the perchlorate contamination in Sivakasi and Madurai, which accounts for 90% of the global production of fireworks. The high concentration of 7690 µg/L, 30 µg/L and 0.39 µg/L were reported for groundwater, surface water and drinking water respectively. Firework industries are the source of perchlorate in water.

Pesticides

Lapworth et al. (2018) determined the concentration of pesticides such as Chlorpyrifos, phenoxy acetic acid, diuron and atrazine in Ganga river, groundwater samples in shallow and deep abstraction wells from Varanasi and Ramnagar, Uttar Pradesh (UP). The high concentration of phenoxy acetic acid was observed. Chakraborty et al. (2016) analysed the presence of organochlorine pesticides (OCPs) such as HCH, DDT, endosulfan, heptachlor and aldrin in river Hooghly (RH) and river Brahmaputra (RB). It was found that in RH, HCH was predominant while in RB, DDT was more predom-

inant. Studies have also found organochlorine pesticide residues in water samples from Unnao district, Madya Pradesh (MP) and Dibrugarh and Nagaon, Assam (ASM) (Singh et al. 2007, Mishra & Sharma 2011) (Table 3).

Artificial Sweeteners

Several studies have established the presence of Artificial Sweeteners (ASWs) in Indian water matrices. ASWs such as sucralose are widely used in India in food and beverages. The sucralose concentration in river Ganga was reported as 0.05 µg/L. Besides, the groundwater in Varanasi and Ramnagar were also found to be contaminated with sucralose even at a depth greater than 140 meters (Lapworth et al. 2018). The contribution of ASWs in three WWTPs in Chennai, India was in the range 9.7% to 17.1%, unlike USA WWTPs which accounted for 49.8%. The removal of artificial sweeteners in WWTP was low where Hydraulic Retention Time (HRT) was less while additional removal was observed with increase in HRT. The removal might be due to physical adsorption and flocculation process. The highest sucralose concentrations in the influent and effluent of WWTPs were 1.9 µg/L and 1.87 µg/L indicating very low removal. The concentration of acesulfame was found as 0.89 µg/L in the influent of WWTPs (Anumol et al. 2016). Sharma et al. (2019) investigated the presence of ASWs in river Ganga and groundwater in the vicinity. Saccharine was found at 0.085 µg/L and sucralose had 100% detection frequency in River Ganga and groundwater at concentrations of 0.023 µg/L and 0.024 µg/L respectively. The concentration in the river water and groundwater were nearly equal. It could be due to the high mobility and load of sucralose which accumulates in the aquifer. Acesulfame and cyclamate were also detected in the river and groundwater. From the previous studies, it can be inferred that sucralose, saccharin and acesulfame are predominant ASWs. Fig. 2 shows the prime ECs observed in Indian water.

REGULATORY STANDARDS

To ascertain the risk of ECs, toxicity endpoints are required. Hence, extensive toxicological studies need to be carried out. There is a paucity of regulatory standards on various classes of ECs. In many countries, there are no proper regulations on ECs due to shortage of toxicological data. In India, the drinking water standards include the regulatory standards for only a few pesticides in the Indian Standards (IS 10500). The water treatment plants and WWTPs are not monitored for the presence of ECs. World Health Organisation (WHO) has published extensive regulatory standards for several classes of ECs. The European Union (EU) Water Framework Directive has listed 45 priority compounds with environmental quality standard to be adhered in aquatic environments. The United States Environmental Protection Agency (USEPA), under the Safe Drinking Water Act regulates the ECs listed on the Contaminant Candidate List (CCL) which have been detected in the public water system and has not yet been regulated. The USEPA regulates at least five contaminants from the CCL every five years. It is also required to issue a new list of not more than 30 unregulated contaminants to be monitored by public water systems every five years. CCL 4

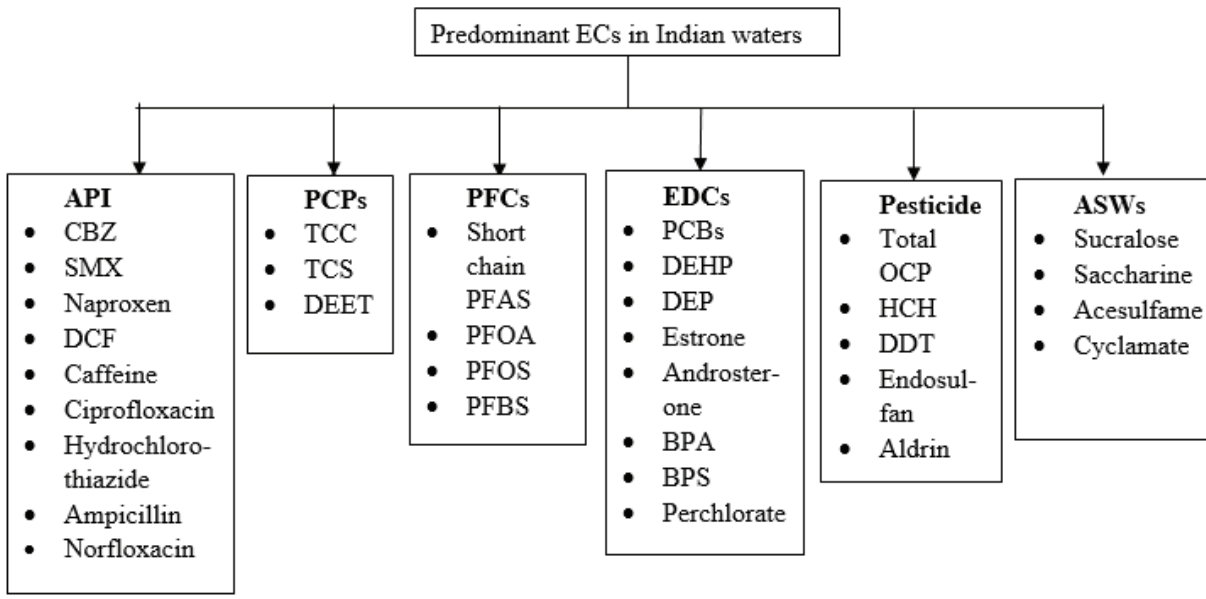

Fig. 2: Predominant ECs from different classes found in the Indian water environment.

Table 4: Regulation of ECs as per WHO, USEPA, EU and IS 10500 (µg/L).

ECs	WHO	USEPA	EU	IS 10500
Pesticides				
DBCP	1	0.2		
2,4-D	30	70		30
Chlordane	0.2	2		
Lindane	2	0.2		2
Chloropyrifos	30	10	0.1	30
DDT	1		0.025	1
Mecoprop	10			
Pentachlorophenol	9	1	1	
Endrin	0.6	2	0.01	
Alachlor	20	2	0.7	
Terbuthylazine	7			
Other Chemicals				
Perchlorate	70	15		
Toluene	700	1000		
1, 4-Dioxane	50			
Benzo (a) pyrene	0.7	0.2	0.1	0.1
Styrene	20	100		
Tetrachloroethene	40			
Vinyl chloride	0.3	2		
Xylenes	500	10,000		
Trichloroethene	20			
Polychlorinated Biphenyls		0.5		0.5
PFOA/ PFOS		0.07	36	
Dichloromethane	20		20	
Pharmaceuticals				
Edetic acid	600			
Disinfection By-products				
Bromate	10			
Bromodichloromethane	60			60
Bromoform	100	80		100
Chlorate	700			
Dibromoacetonitrile	70			
Dibromochloromethane	100	80		100
Dichloroacetonitrile	20			
Dichloroacetate	50	60		
Chloroform	300	80		200
N-Nitrosodimethylamine	0.1			
Trichloroacetate	200			
2,4,6-Trichlorophenol	200			

is the latest list which includes 97 chemicals or chemical groups and 12 microbial contaminants. Table 4 shows the regulation of ECs by WHO, USEPA, EU and IS 10500 (µg/L). The regulation on ECs is critical as it is important in monitoring and mitigating the ill effects of ECs on human health and the environment.

TREATMENT TECHNOLOGIES

Improvement in lifestyle, urbanisation, agricultural and industrial practises has resulted in an increase in the load of ECs into the water environment. The control of ECs is possible through the incorporation of efficient and cost-effective treatment technologies for the removal of ECs. Previous studies employing adsorption, biological treatment and advanced oxidation processes (AOPs) for the abatement of some priority ECs are discussed.

Adsorption

Adsorption of ECs onto the adsorbents is a way to separate the ECs from the water matrix while it presents no significant treatment and reusability of adsorbents is a challenge. Several studies have investigated the various adsorbents for the adsorption of ECs (Sophia & Lima 2017). The commonly employed adsorbent is activated carbon. Sharipova et al. (2016) studied the adsorption of triclosan using activated carbon sorbents. The adsorption capacity is 85 mg/g. Mestre et al. (2014) studied the adsorption of ibuprofen, paracetamol, acetylsalicylic acid, clofibric acid, caffeine and iopamidol using activated carbon from industrial pre-treated cork. Ibuprofen had high sorption capacity of 174.4 mg/g. Removal efficiencies were between 40 and 90%. Salman (2014) studied the use of activated carbon from palm oil fronds as adsorbents for the adsorption of Pesticides - Bentazon, Carbofuran, 2,4-Dichlorophenoxyacetic acid (2,4-D), the removal percentages were 8.2, 1.3 and 9.2% respectively. Suriyanon et al. (2013) studied the adsorption of two pharmaceuticals DCF, NSAID, and CBZ, antiepileptic using silica-based porous material and powdered activated carbon. Low sorption capacities of 31.93 µg/g (DCF) and 27.59 µg/g (CBZ) were reported. Rodríguez-Liébana et al. (2016) studied the adsorption of fungicides, Metalaxyl and Fludioxonil, using natural clay as adsorbent. It was found that Metalaxyl had a high adsorption capacity of 284±4 µg/g, while Fludioxonil had an adsorption capacity of 176±1 µg/g. Han et al. (2012) studied the adsorption of bisphenol-A on lignin from black liquor of paper mill industry. The adsorption capacity observed was 237.07 mg/g. Rajapaksha et al. (2014) studied the adsorption of sulfamethazine on tea waste biochar. The sorption capacity determined was quite low (33.81 mg/g).

Biological Treatment

Biological treatment using constructed wetlands and activated sludge processes have been evaluated by several studies. Ramprasad & Philip (2015) studied the removal of surfactants and personal care products such as sodium dodecyl sulphate (SDS), propylene glycol (PG) and trimethylamine (TMA) from greywater using a hybrid constructed wetland (HYCW). The pilot-scale HYCW system planted with *Phragmites australis* was fed continuously with greywater at a flow rate of 2.5 cu.m/day. It was found that HYCW was capable of removing SDS (94-98%), PG (95-98%) and TMA (95-99%). Kruglova et al. (2014) studied the biodegradation of ibuprofen, DCF and CBZ using nitrifying bacteria activated in sequential batch reactors at 12^0 with the initial concentration of pharmaceuticals as 20±10 µg/L and solids retention time was 10-12 days. It was found that ibuprofen and DCF were biologically degraded while carbamazepine was not biodegraded. Tiwari et al. (2014) studied the biotransformation of chlorpyrifos (CPF), organophosphate insecticide, in aqueous medium under 15 days aerobic and 60 days anaerobic batch experiments. At the end of the batch experiments, 2.78 ± 0.11 mM of CPF was degraded by 82% aerobic and 66% anaerobic aqueous environments.

Advanced Oxidation Processes

AOPs are a promising technique in the degradation of ECs such as pesticides and API. Glaze et al. (1995) are one of the early studies for the removal of 1,2-dibromo-3-chloropropane (DBCP), pesticide using H_2O_2/UV. DBCP is spiked at 0.3 mg/L in distilled water, initial concentration of H_2O_2 was 1.8mg/L and 3.3 mg/L, pH 8-8.2 and UV lamp (254 nm) was used. It was observed that nitrate and bicarbonate/carbonate alkalinity have a detrimental effect on the rate of oxidation of DBCP, the former due to UV shielding and the latter due to hydroxyl radical scavenging. Carbonate Alkalinity (C_T) 0.1 mM and reaction time 19 minutes resulted in 95% removal. Though the H_2O_2/UV system is powerful in oxidising by the generation of hydroxyl radical, residual H_2O_2 increased chlorine demand. It can be quenched by treatment using Granular Activated Carbon (GAC). Smaller size GAC would be more effective (Huang et al. 2018). Studies have been carried on the effectiveness of AOPs in wastewater and drinking water treatment. Ternes et al. (2003) investigated the ozonation in the removal of pharmaceuticals, contrast media and musk fragrance from effluents of a German municipal WWTP. By applying 10-15 mg/L ozone for contact time 18 minutes, all the pharmaceuticals were completely removed. For effective degradation, the ozone concentration should be equal to the dissolved organic carbon value. Asha & Kumar (2015) investigated sulfamethoxazole (SMX) removal from the poultry

wastewater using a continuous-mode membrane-photocatalytic slurry reactor. SMX concentration in poultry wastewater varied from 0 to 2.3 mg/L. The optimized condition for complete SMX removal was 125 minutes of hydraulic retention time and GAC-TiO_2 catalyst dosage 529.3 mg/L.

Few studies have reported the use of Tungsten Trioxide (WO_3) as a visible light photocatalyst. It can provide sustainable solutions in water treatment due to its low cost, low toxicity, ease of availability and visible light activity owing to its low band gap. Nishimoto et al. (2010) studied the degradation of phenol under different combinations such as O_2/vis/WO_3, O_3/dark/WO_3, O_3/vis, O_3/ vis/WO_3 and O_3/dark systems. The study was carried out at ozone dose of 0.45 g/hr, xenon lamp of wavelength > 420nm, 0.6 g of WO_3 and 250 mL of phenol solution (200 ppm). It was found that O_3/vis/WO_3 system removed about 100% TOC after 120 min of treatment and the removal rate of phenol within 40 min was similar to O_3/dark/WO_3, O_3/vis and O_3/dark systems. Rey et al. (2014) investigated photocatalytic ozonation using 0.25 g of composite catalyst TiO_2 and WO_3 (4%) for the removal of ibuprofen, metoprolol and caffeine. The study was carried at an ozone concentration of 10 mg/L and ozone flow rate of 0.34 litres per minute (lpm) by spiking 4 mg/L ECs, the irradiation time of 2 hours and absorbance at the upper visible region (300-350 nm). It was observed that TiO_2-WO_3 had higher efficiency than TiO_2 alone. Ozonation alone was equally effective. The parent ECs were completely removed in 40 mins and 64% TOC removal was achieved in 2 hours. Zhu et al. (2018) studied the degradation of SMX, a veterinary drug, using visible light WO_3-CNT photocatalyst. The light source was solar simulator 300 W Xe Arc lamp. The concentrations of SMX and WO_3 were 10 mg/L and 0.5 g/L respectively. WO_3 has a lower band gap of 2.4-2.8 eV. It was observed that bare WO_3 shows light absorption around 450 nm and incorporation of CNT shifts the wavelength to the visible range. Compared to pure WO_3, all three WO_3-CNT composites showed enhanced photocatalytic activity.

Several studies have shown that integration of ozone and photocatalysis as in case of photocatalytic ozonation can enhance the removal efficiency. Rivas et al. (2012) studied the removal of nine pharmaceuticals using TiO_2 photocatalytic ozonation and in different combination. The study was carried out at an airflow rate of 0.5 lpm, initial concentration of ECs at 10 mg/L, TiO_2 dose of 0.25g/L and UV (313 nm) as the light source. It was found that TOC removal after 120 minutes was 95% for TiO_2 photocatalytic ozonation (PCO), 85% for UV and ozone, 60% for UV and TiO_2, 25% for photolytic (UV) and 30% for ozonation. PCO had the highest removal rate. The higher dose of TiO_2 causes shielding of UV rays.

Garc´ıa-Araya et al. (2010) investigated TiO_2 PCO and its combinations for DCF, NSAID, at ozone concentration of 10 mg/L, initial DCF concentration of 10^{-4} mol/L and TiO_2 concentration of 1.5 g/L. It was found that TOC removal was 50% and 80% for O_3 and TiO_2 photocatalytic systems. O_3 achieves complete removal in less than 7 mins (5% TOC removal). The O_3/UV-A/TiO_2, pH 7, removed DCF (90-95% in 10 mins) and TOC (90% in 15 min).

Rajeswari & Kanmani (2009) studied the TiO_2 PCO of carbaryl pesticide. Optimum values for maximum degradation were 40 mg/L of carbaryl (500 mL) at pH 6 with 0.28 g/h of ozone and 1 g/L of TiO_2. The mineralization rate constant in the photocatalytic ozonation process was 0.09/min while the sum of the mineralization rate constant of photocatalysis and ozonation was only 0.05/min. 92% COD reduction and 76.5% TOC removal were achieved in 180 min. The BOD_5/COD ratio was increased to 0.38.

CONCLUSION

The past studies have established the presence of ECs such as API, PCP, ASW, pesticides and EDC across the Indian water environment. It was observed that certain ECs are predominant and ubiquitous. It includes carbamazepine, sulfamethoxazole, caffeine, triclosan, triclocarban, perchlorate, sucralose and organochlorine pesticides. The regions near the bulk drug manufacturing hub in Hyderabad was found to contain high levels of antibiotics, API and ARG. Several studies have shown ECs in surface water, groundwater, drinking water, treated wastewater from STP and CETP. EDCs such as plasticisers, PCB, steroid hormones were found in water. DEHP was the commonly observed phthalate. ECs can cause harmful impacts on aquatic, terrestrial wildlife, vegetation and human communities. It can persist, bioaccumulate and impart toxicity. Several reports show that biological treatment and adsorption imparts low removal of ECs. Advanced oxidation processes using visible light-driven photocatalytic ozonation is found very effective for the removal of most ECs except PFCs which can be easily removed by electrochemical methods. Hence, the review concludes that incorporation of AOPs in STP, CETP and WTP will aid in the removal of ECs.

REFERENCES

Anumol, T., Vijayanandan, A., Parka, M., Philip, L. and Snyder S.A. 2016. Occurrence and fate of emerging trace organic chemicals in wastewater plants in Chennai, India. Environment International, 92-93: 33-42.

Asha, R.C., Yadav, M.S.P. and Kumar, M. 2018. Sulfamethoxazole removal in membrane photocatalytic reactor system-experimentation and modelling. Environmental Technology, 40(13): 1697-1704.

Balakrishnan, P. and Mohan, S. 2016. Emerging Contaminants in Stormwater, Proceedings of National Conference on Energy and Environment, IIT Madras and CODISSIA.

CSE 2016. Question Raised in Lok Sabha on Management of Sewage. India

Environment Portal 1029 Knowledge for Change, Centre for Science and Environment.

Das M. T., Ghosh P. and Thakur I. S. 2014. Intake estimates of phthalate esters for South Delhi population based on exposure media assessment. Environ Pollut., 189:118-25.

Fick, J., Soderstrom, H., Lindberg, R. H., Phan, C., Tysklind, M. and Larsson D.G.J. 2009. Contamination of surface, ground, and drinking water from pharmaceutical production. Environmental Toxicology and Chemistry, 28(12): 2522-2527.

Fisher, J. and McLanahan, E. 2008. Evidence for perchlorate altering thyroid function. Toxicol. Lett., 180(S182).

Gani, K.M. and Kazmi, A.A. 2016. Contamination of emerging contaminants in Indian aquatic sources: first overview of the situation. J. Hazard. Toxic Radioact. Waste, 04016026: 1-12.

Garc´ıa-Araya, J. F., Beltr´an, F. J. and Aguinaco, A. 2010. Diclofenac removal from water by ozone and photolytic TiO_2 catalysed processes. J. Chem. Technol. Biotechnol., 85: 798-804.

Glaze, W.H., Lay, Y. and Kang, J. 1995. Advanced oxidation processes. a kinetic model for the oxidation of 1,2-dibromo-3-chloropropane in water by the combination of hydrogen peroxide and UV radiation. Industrial & Engineering Chemistry Research, 34(7): 2314-2323.

Guo Y., Alomirah H., Cho H. S., Minh T. B., Mohd M. A., Nakata H. and Kannan K. 2011. Occurrence of phthalate metabolites in human urine from several Asian countries. Environmental Science & Technology, 45(7): 3138-3144.

Han, W., Luo, L. and Zhang, S. 2012. Adsorption of bisphenol A on lignin: Effects of solution chemistry. Int. J. Environ. Sci. Technol., 9: 543-548.

Huang, Y., Nie, Z., Wang, C., Li, Y., Xu, M. and Hofmann, R. 2018. Quenching H_2O_2 residuals after UV/H_2O_2 oxidation using GAC in drinking water treatment. Environ. Sci.: Water Res. Technol., 4(10): 1662-1670.

Isobe, T., Ogawa, S.P., Sugimoto, R., Ramu, K., Sudaryanto, A., Malarvannan, G., Devanathan, G., Ramaswamy, B.R., Munuswamy, N., Ganesh, D.S. and Sivakumar, J. 2013. Perchlorate contamination of groundwater from fireworks manufacturing area in South India. Environmental Monitoring and Assessment, 185(7): 5627-5637.

Kruglova, A., Ahlgren, P., Korhonen, N., Rantanen, P., Mikola, A. and Vahala, R. 2014. Biodegradation of ibuprofen, diclofenac and carbamazepine in nitrifying activated sludge under 12 °C temperature conditions. Sci. Total Environ., 499: 394-401.

Kwok, K.Y., Taniyasu, S., Yeung, L.W., Murphy, M.B., Lam, P.K., Horii, Y., Kannan, K., Petrick, G., Sinha, R.K. and Yamashita, N. 2010. Flux of perfluorinated chemicals through wet deposition in Japan, the United States, and several other countries. Environ Sci Technol., 44: 7043–7049.

La Farré M., Pérez S., Kantiani L. and Barcelo D. 2008. Fate and toxicity of emerging pollutants, their metabolites and transformation products in the aquatic environment. TrAC Trends in Analytical Chemistry, 27: 991-1007.

Lapworth, D. J., Das, P., Shaw, A., Mukherjee, A., Civil, W., Petersen, J.O., Gooddy, D.C., Wakefield, O., Finlayson, A., Krishan, G, Sengupta, P. and MacDonald, A.M 2018. Deep urban groundwater vulnerability in India revealed through the use of emerging organic contaminants and residence time tracers. Environmental Pollution, 240: 938-949.

Larsson, D.G.J., de Pedro, C. and Paxeus, N. 2007. Effluent from drug manufactures contains extremely high levels of pharmaceuticals. J. Hazard. Mater., 148: 751-755.

Lubbert, C., Baars, C., Dayakar, A., Lippmann, N., Rodloff, A.C., Kinzig, M. and Sorgel, F. 2017. Environmental pollution with antimicrobial agents from bulk drug manufacturing industries in Hyderabad, South India, is associated with dissemination of extended-spectrum beta-lactamase and carbapenemase-producing pathogens. Infection, 45(4): 479-491.

Mestre, A.S., Pires, R.A., Aroso, I., Fernandes, E.M., Pinto, M.L., Reis, R.L., Andrade, M.A., Pires, J., Silva, S.P. and Carvalho, A. P. 2014. Activated carbons prepared from industrial pre-treated cork: sustainable adsorbents for pharmaceutical compounds removal. Chem. Eng. J., 253: 408-417.

Mishra, K. and Sharma, R.C. 2011. Contamination of aquatic system by chlorinated pesticides and their spatial distribution over North-East India. Toxicol. Environ. Health. Sci., 3(3): 144-155.

Mutiyar, P. K. and Mittal, A. K. 2014. Occurrences and fate of selected human antibiotics in influents and effluents of sewage treatment plant and effluent-receiving river Yamuna in Delhi (India). Environ. Monit. Assess., 186: 541-557.

Nishimoto, S., Mano, T., Kameshima, Y. and Miyake, M. 2010. Photocatalytic water treatment over WO_3 under visible light irradiation combined with ozonation. Chemical Physics Letters, 500: 86-89.

Nadaraja, A. V., Puthiyaveettil, P. G. and Bhaskaran, K. 2015. Surveillance of perchlorate in groundwater, surface water and bottled water in Kerala, India. Journal of Environmental Health Science & Engineering, 13(56): 1-6.

Chakraborty, P., Zhang, G., Li, J., Sivakumar, A. and Jones, K. C. 2016. Occurrence and sources of selected organochlorine pesticides in the soil of seven major Indian cities: Assessment of air-soil exchange. Environmental Pollution, 204: 74-80.

Pearce, E.N., Leung, A.M., Blount, B.C., Bazrafshan, H.R., Pino, X. He, S., Valentin-Blasini, L. and Braverman L.E. 2007 Breast milk iodine and perchlorate concentrations in lactating Boston-area women. J. Clin. Endocrinol. Metab., 92: 1673-1677.

Philip, J.M., Aravind, U.K. and Aravindakumar, C.T. 2017. Emerging contaminants in Indian environmental matrices - A review. Chemosphere, 190: 307-326.

USEPA 2007. Drinking Water: Regulatory Determinations Regarding Contaminants on the Second Drinking Water Contaminant Candidate List–Preliminary Determinations. Federal Register, 72 FR 24016.

Raj, J.R.A. and Muruganandam, L. 2014. Occurrence of perchlorate in drinking, surface, ground and effluent water from various parts of South India. International Journal of Innovations in Engineering and Technology, 4(4): 1-7.

Rajapaksha, A. U., Vithanage, M., Zhang, M., Ahmad, M., Mohan, D., Chang, S.X. and Ok, Y. S. 2014. Pyrolysis condition affected sulfamethazine sorption by tea waste biochars. Bioresour. Technol., 66: 303-308.

Rajeswari, R. and Kanmani, S. 2009. A study on synergistic effect of photocatalytic ozonation for carbaryl degradation. Desalination, 242: 277-285.

Ramaswamy, B. R., Shanmugam, G., Velua, G., Rengarajan, B. and Larsson, D.G. J. 2011. GC-MS analysis and ecotoxicological risk assessment of triclosan, carbamazepine and parabens in Indian rivers. Journal of Hazardous Material, 186: 1586-1593.

Ramprasad, C. and Philip, L. 2015. Occurrence, fate and removal of emerging contaminants in a hybrid constructed wetland treating greywater. Discovery, 41(188): 59-66.

Rey, A., García-Muñoz, P., Hernández-Alonso, M.D., Mena, E., García-Rodríguez, S. and Beltrán, F. J. 2014. WO_3-TiO_2 based catalysts for the simulated solar radiation assisted photocatalytic ozonation of emerging contaminants in a municipal wastewater treatment plant effluent. Applied Catalysis B: Environmental, 154-155: 274-284.

Rivas, F.J, Beltrán, F.J. and Encinas, A. 2012 Removal of emergent contaminants: Integration of ozone and photocatalysis. Journal of Environmental Management, 100: 10-15.

Rodríguez-Liébana, J. A., López-Galindo, A., de Cisneros, C.J., Gálvez, A., Rozalén, M., Sánchez-Espejo, R., Caballero, E. and Peña, A. 2016. Adsorption/desorption of fungicides in natural clays from Southeastern Spain. Appl. Clay Sci., 132-133: 402-411.

Salman, J.M. 2014. Optimization of preparation conditions for activated carbon from palm oil fronds using response surface methodology on removal of pesticides from aqueous solution. Arab. J. Chem, 7: 101-108.

Selvaraj, K.K., Shanmugama, G., Sampath, S., Larsson, D.G.J. and Ramaswamy, B.R. 2014a. GC-MS determination of bisphenol A and

alkylphenol ethoxylates in river water from India and their ecotoxicological risk assessment. Ecotoxicology and Environmental Safety, 99: 13-20.

Selvaraj, K.K., Sundaramoorthy, G., Ravichandran, P.K., Girijan, G.K., Sampath, S. and Ramaswamy, B.R. 2014b. Phthalate esters in water and sediments of the Kaveri River, India: Environmental levels and ecotoxicological evaluations. Environ. Geochem. Health, 37(1): 83-96.

Selvaraj, K.K., Mubarakali, H., Rathinam, M., Harikumar, L., Sampath, S., Shanmugam, G. and Ramaswamy, B.R. 2016. Cumulative exposure and dietary risk assessment of phthalates in bottled water and bovine milk samples: A preliminary case study in Tamil Nadu, India. Human and Ecological Risk Assessment, 22(5): 1166-1182.

Sharipova, A. A., Aidarova, S. B., Bekturganova, N. E., Tleuova, A., Schenderlein, M., Lygina, O., Lyubchik, S. and Miller, R. 2016. Triclosan as model system for the adsorption on recycled adsorbent materials. Colloids Surf. A: Physicochem. Eng., 505: 193-196.

Sharma, B.M., Bharat, G.K., Tayal, S., Larssen, T., Becanova, J., Karaskova, P., Whitehead, P.G., Futter, M.N., Butterfield, D. and Nizzetto L. 2016. Perfluoroalkyl substances (PFAS) in river and ground/drinking water of the Ganges river basin: emissions and implications for human exposure. Environ. Pollut., 208: 704-713.

Sharma, B.M., Bečanová, J., Scheringer, M., Sharma, A., Bharat, G.K., Whitehead, P.G., Klánová, J. and Nizzetto, L. 2019. Health and ecological risk assessment of emerging contaminants (pharmaceuticals, personal care products, and artificial sweeteners) in surface and groundwater (drinking water) in the Ganges River Basin, India. Science of the Total Environment, 646: 1459–1467.

Singh, K. P., Amrita, M. and Sarita S. 2007 Persistent organochlorine pesticide residues in soil and surface water of Northern Indo-Gangetic Alluvial Plains. Environmental Monitoring and Assessment, 125: 147-55.

Sophia, A.C. and Lima, E.C. 2017. Removal of emerging contaminants from the environment by adsorption. Ecotoxicology and Environmental Safety, 150: 1-17.

Srivastava A., Sharma V. P., Tripathi R., Kumar R., Patel D. K. and Mathur P. K. 2010. Occurrence of phthalic acid esters in Gomti River Sediment, India Environ. Monit. Assess., 169(1-4):397-406.

Sunantha, G. and Vasudevan, N. 2016. Assessment of perfluorooctanoic acid and perfluorooctane sulfonate in surface water - Tamil Nadu, India. Mar. Pollut. Bull., 109: 612-618.

Suriyanon, N., Punyapalakul, P. and Ngamcharussrivichai, C. 2013. Mechanistic study of diclofenac and carbamazepine adsorption on functionalized silica-based porous materials. Chem. Eng. J., 214: 208-218.

Ternes, T.A., Stüber, J., Herrmann, N., McDowell, D., Ried, A., Kampmann, M. and Teiser, B. 2003, Ozonation: A tool for removal of pharmaceuticals, contrast media and musk fragrances from wastewater. Water Research, 37(8): 1976-1982.

Tiwari, M. K. and Guha, S. 2014. Kinetics of biotransformation of chlorpyrifos in aqueous and soil slurry environments. Water Research, 51: 73-85.

Vimalkumar, K., Arun, E., Krishna-Kumar, S., Poopal, R.K., Nikhil, N.P., Subramanian, A. and Babu-Rajendran, R. 2018. Occurrence of triclocarban and benzotriazole ultraviolet stabilizers in water, sediment, and fish from Indian rivers. Science of The Total Environment, 625: 1351-1360.

Wang, X., Chen, M., Gong, P. and Wang, C. 2019. Perfluorinated alkyl substances in snow as an atmospheric tracer for tracking the interactions between westerly winds and the Indian Monsoon over western China. Environ Int., 124: 294-301.

Williams, M., Kookana, R.S., Mehta, A., Yadav, S.K., Tailor, B.L. and Maheshwari, B. 2019. Emerging contaminants in a river receiving untreated wastewater from an Indian urban centre. Science of the Total Environment, 647: 1256-1265.

Yamazaki E., Nobuyoshi Y., Sachi T., James L., Paul L., Hyo-Bang M., Yunsun J., Kannan P., Achyuthan H., Munuswamy N. and Kannan, K. 2015 Bisphenol A and other bisphenol analogues including BPS and BPF in surface water samples from Japan, China, Korea and India. Ecotoxicology and Environmental Safety, 122: 565-572.

Yeung, L.W., Yamashita, N., Taniyasu, S., Lam, P.K., Sinha, R.K., Borole, D.V. and Kannan, K. 2009. A survey of perfluorinated compounds in surface water and biota including dolphins from the Ganges river and in other waterbodies in India. Chemosphere, 76: 55-62.

Zhu, W., Liu, J., Yu, S., Zhou, Y. and Yan X. 2016. Ag loaded WO_3 nanoplates for efficient photocatalytic degradation of sulphanilamide and their bactericidal effect under visible light irradiation. Journal of Hazardous Materials, 318: 407-416.

Nature Environment and Pollution Technology
An International Quarterly Scientific Journal

p-ISSN: 0972-6268
(Print copies up to 2016)
e-ISSN: 2395-3454

Vol. 19 | No. 2 | pp. 563-570 | 2020

Original Research Paper

https://doi.org/10.46488/NEPT.2020.v19i02.011

Open Access Journal

Adsorption of Azo Dye Malachite Green onto Rice Wine Lees: Kinetic and Adsorption Isotherms

Qian Wang, Liping Liang†, Gangliang Tian, Qiaole Mao and Xu Meng
School of Civil Engineering, College of Life Science, College of Textile and Garment, Shaoxing University, Shaoxing, 312000, P.R.China
†Corresponding author: Liping Liang; liangliping0702@163.com

Nat. Env. & Poll. Tech.
Website: www.neptjournal.com

Received: 31-07-2019
Accepted: 18-09-2019

Key Words:
Malachite green;
Rice wine lees;
Adsorption;
Kinetic study;
Isotherm model

ABSTRACT

The adsorption of malachite green in aqueous solution onto rice wine lees was carried out in detail. The effects of different rice wine lees dosage, solution pH and initial concentration on the adsorption of malachite green by rice wine lees were studied. The experimental results showed that the removal rate of malachite green increases with the increasing dosage of rice wine lees. When the dosage of rice wine lees is 5 g/L, the removal rate within 30 min is 96.22%. At the same time, the removal rate increases as the pH of the solution increases, and the removal rate is higher in an alkaline environment. The kinetic study was performed by the pseudo-first-order and the pseudo-second-order reactions. According to the experimental data, the pseudo-second-order kinetic model better described the adsorption of dye onto rice wine lees, it implies that the predominant process is chemisorption. Besides, the adsorption isotherms were studied by Langmuir model, Freundlich and Temkin isotherm models. The results indicated that the adsorption followed the Langmuir model and the maximum adsorption capacity was 21.505 mg/g. The dye malachite green adsorption onto rice wine lees was monolayer adsorption.

INTRODUCTION

With the development of light industry, especially the rise of the textile industry, textile dyes have become the main source of polluted water, of which azo dyes are the most common (Lark & Lark 1979, Shindy 2012). And it is the most widely used synthetic dye in textile and garment printing and dyeing process. Malachite green (MG), as one of the azo dyes, is often used in the dyeing and printing of a variety of natural and synthetic fibres, as well as in the colouring of paints, plastics, rubber and so on (Culp et al. 1999). Not only that, but MG is also a good biocide widely used in aquaculture (Hoffman et al. 1974). However, it has been banned in several countries due to its harmful effects on the immune system, reproductive system, genotoxicity and carcinogenicity of mammals and other animals (Cha et al. 2001, Fernandes et al. 1991). Also, the potential harm of MG to the human body cannot be ignored. Stammati et al. (2005) found that malachite green plays a role as a tumour promoter in the human body. Expect these, the discharge of MG containing sewage would colour the running water and affect the beauty of the river environment. Therefore, dye sewage must be treated innocuously before discharge.

At present, the main treatment methods of printing and dyeing waste water are the electrochemical method, flocculation method, membrane separation method and adsorption method (Purohit et al. 2014). Among these methods, adsorption is considered to be a relatively effective method for removing dyes and controlling BOD. However, the high cost of industrial adsorbents makes the adsorption process more expensive. Therefore, it is of great significance to find cheap and effective adsorbents instead of industrial adsorbents (Tahir et al. 2017). Due to the characteristics of low cost, recyclable and easy to obtain of agricultural waste, some researchers used peanut shell (Liu et al. 2018), straw (Robinson et al. 2002), orange peel (do Nascimento et al. 2014), peanut (do Nascimento et al. 2014), garlic waste (Hameed & Ahmad 2010), rice husk (Forss et al. 2013) and other agricultural waste residues to adsorb waste water, and successfully achieve the purpose of adsorption. Otherwise, some researchers have used steel industry residue successfully removing the treat basic violet 3 dye from aqueous solutions (Amaral et al. 2016). However, the use of rice wine lees to treat dye waste water has rarely been reported at home and abroad.

As we all know, Shaoxing is not only a strong textile city but also the birthplace of rice wine. With the development of the textile industry and the rice wine manufacturing industry, a large amount of dye sewage and rice wine lees will be produced every year, which harms the environment. Baoe et al. (2009) successfully adsorbed two kinds of azo dyes, Reactive Black

31 and Reactive Blue 49, in certain conditions by using beer grains. Xiaolian et al. (2016) used distillers' grain to absorb Congo red and malachite green. The same as the by-product liqueur produced in the wine-making process, if the rice wine lees can be used for the adsorption of azo dyes, it will greatly promote the ecological environment and energy conservation of Shaoxing. In the previous experiments, we found that the main components of rice wine lees were similar to those of raw materials. After fermentation and saccharification, the starch content was significantly reduced, while the proportion of crude protein, crude fibre, crude fat and ash in the rice wine lees is higher. Besides, there was microbial flora in the rice wine grains, including yeast, mould, bacteria, etc. (Xie et al. 2013), which was also a kind of good adsorbent.

In order to further explore the decolourization effect of rice wine lees on azo dyes, malachite green was selected as the object of investigation. And the effects of the pH value of malachite green dye, initial malachite green concentration and the dosage of rice wine lees on the adsorption performance were investigated. The adsorption and removal mechanism of rice wine lees on the malachite green in sewage was discussed by fitting the isothermal adsorption equation and kinetic equation, which may provide a new idea for the treatment of azo dye sewage by rice wine lees.

MATERIALS AND METHODS

Pre-Treatments of the Adsorbents

The rice wine lees used in this experiment was the slag produced during the brewing process of rice wine. A certain amount of rice wine lees was taken in the container, firstly, rinsed with distilled water until the water flow was colourless, and then rinsed again with distilled water 3-4 times. Secondly, the rice wine lees was wrapped with gauze and squeezed to out the water. Then a clean tin foil was put on the tray and spread the previously treated lees. Thirdly, it was put in an oven for drying, during the period, and turned over every 5-6 hours to make it much drier. Finally, it was pulverized using a crusher.

Dye Solution Preparation

The dye solution (1 g/L) was prepared by adding 0.5 g malachite green to 500 mL ultra-pure water. The original solution was diluted to 3 mg/L, 5 mg/L, 7 mg/L and 10 mg/L respectively by dilution method as the experiment concentration.

Adsorption Experiment

The adsorption experiments were carried out in 500 mL jar at 25°C in a constant temperature shock water bath pot. The process variables, rice wine lees dosage (1~5 g/L), pH (5~10) and initial MG dye concentration (10~50 mg/L) were investigated. The pH of the medium was adjusted by 0.01 M NaOH/HCl. And to study the individual effect parameters, one variable was kept varying, while other parameters were kept constant. The residual concentration of MG dye was determined by the spectrophotometry at absorbance 618 nm.

Experimental Data Analysis

A standard curve of absorbance-MG concentration was plotted based on the measured absorbance of MG, and the equation was obtained as follows: $y = 0.1325x + 0.0275$, $R^2 = 0.9998$. Due to the high corresponding correlation coefficients (R^2) of 0.9998, there was a good linear relationship between absorbance and concentration, which indicated that the equilibrium concentration of MG was more accurate. And then the amount of adsorption could be calculated by equation 1.

$$q_e = \frac{(C_0 - C_e)V}{W} \quad \ldots(1)$$

Where, q_e is the equilibrium concentration of MG (mg/L); C_0 and C_e are the initial and equilibrium concentration of MG (mg/L), respectively. V is the volume of MG solution (L) and W is the weight of used rice wine lees (g).

RESULTS AND DISCUSSION

The Influence of Rice Wine Lees Dosage on Removal Efficiency of MG

The adsorption effect of rice wine lees dosage on the malachite green was investigated, and the results are given in Fig. 1. It can be seen that the adsorption capacity of MG increased with the increasing of rice wine lees dosage. When the adsorbent dosage was 1 g/L and 2 g/L, and reaction time was 20 min, the removal rates of malachite green were 44.24% and 57.94%, respectively, as the dosage increased to 3 g/L and 5 g/L, the removal rate increased to 68.67% and 81.36%. This attributed to the increase of adsorption surface area and adsorption functional groups. Based on previous research, in general, the adsorbate removal rate and adsorption capacity of adsorbents always increase with the increase of effective active sites (Fraga et al. 2018).

The Effect of Initial pH on Removal Efficiency of MG

The difference in adsorption of dyes in different pH ranges is related to the surface charge properties of the rice wine lees and the charge properties of the dye after dissociation. Therefore, the effect of initial pH on the removal efficiency of MG by rice wine lees was investigated, and the results are shown in Fig. 2. The removal efficiency of malachite green

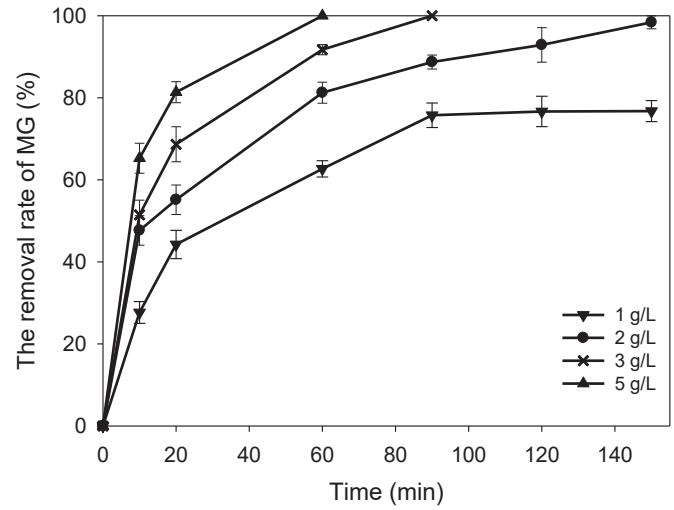

Fig. 1: Effect of different rice wine lees dosage on the removal of malachite green. (C_0=10 mg/L, pH=5.5, t=25)

increased when the pH increased from 5 to 10. When pH value was 5.00 and 7.00, after 20 min reaction, the removal rate of malachite green was 51.21% and 64.51%, respectively. As the pH reached 10, the removal rate of malachite green increased to 86.43%. This may be explained by the fact that MG is a kind of a cationic dye and in the acidic conditions, MG has the same charge as H^+, H_3O^+. The three compete with each other for the adsorption sites on the rice wine lees, resulting in a lower adsorption rate of MG. Contrary to acidic conditions, with the increase of pH, the competitive effect of H_3O^+ or H^+ is weakened, the negative charge functional groups are exposed, the electrostatic attraction between dye cations and adsorbents is produced (Shroff & Vaidya 2011). At this time, the surface of the rice wine lees has a negative charge, which is favourable for adsorbing the positive charge malachite green.

The Effect of Initial Concentration on Removal Efficiency of MG

The effect of initial concentration on the removal efficiency of malachite green by rice wine lees is shown in Fig. 3. The removal efficiency of the MG gradually decreased with the

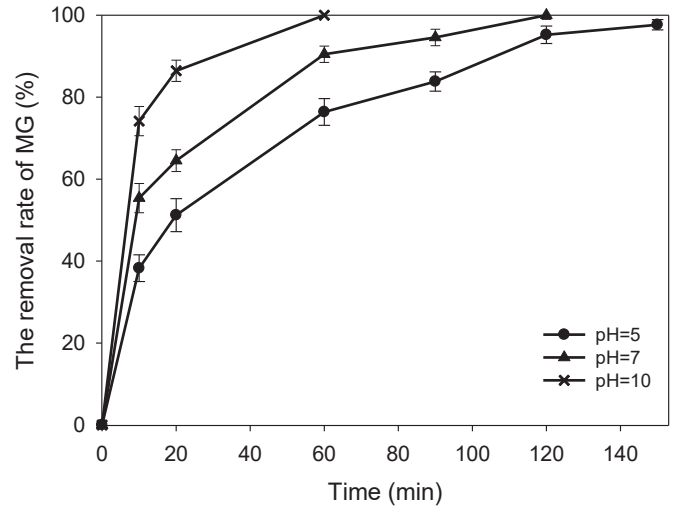

Fig. 2: Effect of different initial pH on the removal of malachite green.

(C_0=10 mg/L, dosage=1 g/L, t=25°C).

increase of the initial concentration of MG under the condition of the same pH value (pH=5) and the same dosage of the rice wine lees (5 g/L). When the initial concentration of MG was 20 mg/L, the removal rate was 93.13% after 24 hours of reaction, and the removal rate decreased to 89.87% and 84.07%, respectively as the initial concentration increased to 30 mg/L and 40 mg/L respectively. When the initial concentration of malachite green increased to 50 mg/L, the removal rate was only 76.42%. This is because when the amount of the adsorbent is constant, the adsorption sites are constant. There are sufficient adsorption sites to bind the MG when the initial concentration of the dye is low, so the adsorption efficiency is high. Therefore, it can be seen that the adsorption depends on the initial concentration, and the effective binding sites are saturated at a very high initial concentration. For the effective binding sites, the competition between ions will intensify and the adsorption will slow down (Manzoor et al. 2013).

Adsorption Isotherms

The adsorption isotherm is a curve, which refers to the relationship between the concentration of solute molecules in the two phases when the adsorption of solute molecules on the interface of the two phases reaches equilibrium at a certain temperature. At a certain temperature, the concentration relationship between the separated substances in the liquid phase and the solid phase can be expressed by the adsorption equation. Therefore, the relationship between adsorbates and adsorbents, the adsorption effect and maximum adsorption capacity of adsorbents can be understood by adsorption isotherms, which is helpful to understand the adsorption mechanism. The Langmuir adsorption model assumes that the surface of the adsorbents is uniform and the energy of each adsorption centre is the same, and in the certain conditions, the adsorption rate is equal to the desorption rate, then the adsorption equilibrium is reached (Nadeem et al. 2016, Ullah et al. 2013). The linear form of Langmuir adsorption isotherm is given in equation 1.

$$\frac{C_e}{q_e} = \frac{1}{K_L q_m} + \frac{C_e}{q_m} \quad \ldots(1)$$

Where, q_e is equilibrium adsorption capacity and q_m is limit adsorption capacity (mg/g), C_e is equilibrium concentration (mg/L) and K_L is Langmuir adsorption equilibrium constant.

The Freundlich isotherm model can be used to describe the adsorption on the non-uniform surface or to describe the multi-layer adsorption. The linear form of the Freundlich isotherm model is given in equation 2.

$$Lnq_e = LnK_F + \frac{1}{n} LnC_e \quad \ldots(2)$$

Where, q_e is the amount of solute adsorbed per unit weight of adsorbent (mg/g), C_e represents the equilibrium concentration of dye in solution (mg/L), and K_F, n are Freundlich constant.

Temkin considered the effects of some indirect adsorbate/adsorbent interactions and suggested that because of these interactions the heat of adsorption of all the molecules in the layer would decrease linearly with coverage. The linear

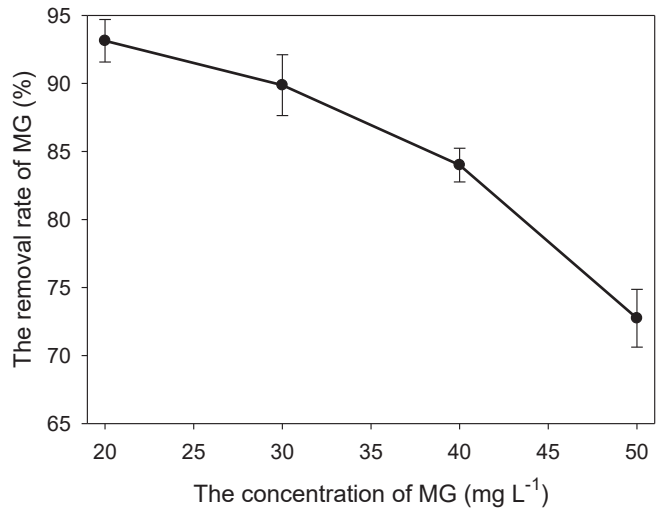

Fig. 3: Removal rate of malachite green at different initial concentrations for 24 hours. (pH=5, dosage=5 g/L, t=25°C).

equation of the Temkin isotherm model is given in equation 3.

$$q_e = \frac{RT}{b_T} LnA_T + (\frac{RT}{b_T}) LnC_e \quad \ldots(3)$$

Where, q_e is the amount of solute adsorbed per unit weight of adsorbent (mg/g), C_e is the equilibrium concentration of GM (mg/L), R, A, T and b are the Temkin constants. The experimental data were simulated by these adsorption models, and the results are shown in Table 1 and Fig. 4. Compared with the R^2 of Langmuir, Freundlich and Tempkin isotherm model, the R^2 of Langmuir is the largest, so the Langmuir monolayer adsorption model can better explain the equilibrium adsorption data of MG dye. The fitted linear equation is y =0.0792x+0.0465. And the maximum adsorption capacity was 21.505 mg/g.

Adsorption Kinetics

The adsorption data of different rice wine lees dosage were subjected to pseudo-first-order and pseudo-second-order kinetic models and the intraparticle diffusion model. The linear form of pseudo-first-order kinetics is given in equation 4.

$$Ln(q_e - q_t) = Lnq_e - k_f t \quad \ldots(4)$$

Where, q_e is the adsorption efficiency (at equilibrium) (mg/g), q_t is the adsorption at time t (mg/g), and $k_f$is the rate constant of pseudo-first-order.

The linear form of pseudo-second-order kinetic model is given in equation 5.

$$\frac{t}{q_t} = \frac{1}{k_s q_e^{\ 2}} + \frac{1}{q_e} t \quad \ldots(5)$$

Where, $q_e$represents the equilibrium adsorption capacity (mg/g), $q_t$represents the adsorption capacity when the time is t (mg/g), and k_s represents the second order adsorption rate constant.

The specific results are given in Table 2 and Fig. 5. According to Table 2, it was obvious that there was a good relationship between t/q_t and t with high R^2 of 0.9923, 0.998, 0.9997. Therefore, the pseudo-second-order kinetic model is more suitable for describing the adsorption of MG by rice wine lees. And the reaction is mainly chemical adsorption.

The linear form of the intraparticle diffusion model is given in Equation 6.

$$q_t = k_{id} t^{1/2} + C \quad \ldots(6)$$

Where, C is the constant of the boundary layer and the thickness. K_{id} is the internal diffusivity constant. If the line between q_t and $t^{1/2}$ through the origin, the internal diffusion is controlled by a single factor (otherwise, the adsorption process may involve multiple mechanisms) (Debrassi et al. 2012).

The fitting results are shown in Fig. 5. The adsorption data of the three kinds of rice wine lees dosages showed that q_t and $t^{1/2}$ had a good linear relationship with high R^2 and the line did not pass through the origin, which indicated that multiple mechanisms may be involved in the adsorption of MG by rice wine lees, and the adsorption was mainly based on chemisorption.

CONCLUSIONS

In this study, the adsorption properties of MG by rice wine lees were studied. The experimental results showed that MG can be adsorbed by rice wine lees, as the dosage is increased, the adsorption rate is faster. And it decreases with the increase in dye concentration. At the same time, the adsorption capacity is the largest when the pH reaches to 10. Kinetic

Table 1: Adsorption results of malachite green by rice wine lees.

Langmuir isotherm equation			Freundlich isotherm equation			Temkin isotherm equation		
R^2	q_m	k	R^2	k	n	R^2	A	B
0.9946	21.505	0.5871	0.9786	2.58597	3.0294	0.9168	2.225	10.415

Table 2: Adsorption kinetics and intra-particle diffusion model constant and correlation of malachite green by rice wine lees.

Rice wine lees (g/L)	q_e	pseudo-first-order kinetic model		pseudo-second-order kinetic model		intraparticle diffusion model	
		R^2	K_1	R^2	K_2	R^2	K_{id}
1	7.4117	0.9287	0.0237	0.9923	0.1142	0.9435	0.6204
2	4.747	0.9194	0.0125	0.998	0.193	0.9156	0.3326
3	2.9131	0.9857	0.027	0.9997	0.2885	0.9515	0.3832

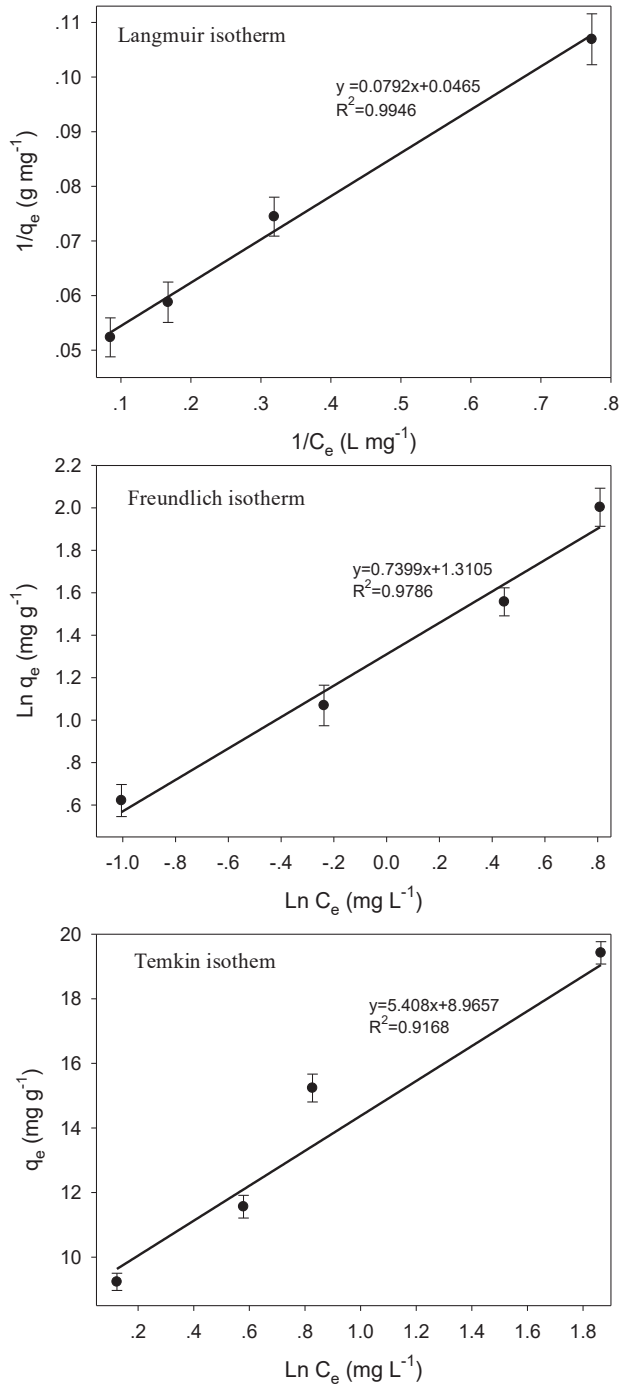

Fig. 4: Three adsorption isotherms for adsorption of malachite green by rice wine lees.

studies showed that the adsorption process of rice wine lees on malachite green accords with the pseudo-second-order kinetic equation. The experimental data were fitted using three theoretical adsorption models, Langmuir, Freundlich and Temkin. The results showed that the Langmuir adsorption equation can better describe the adsorption of dyes by rice wine lees. The saturated adsorption capacity of malachite green was 21.505 mg/g which was calculated by the

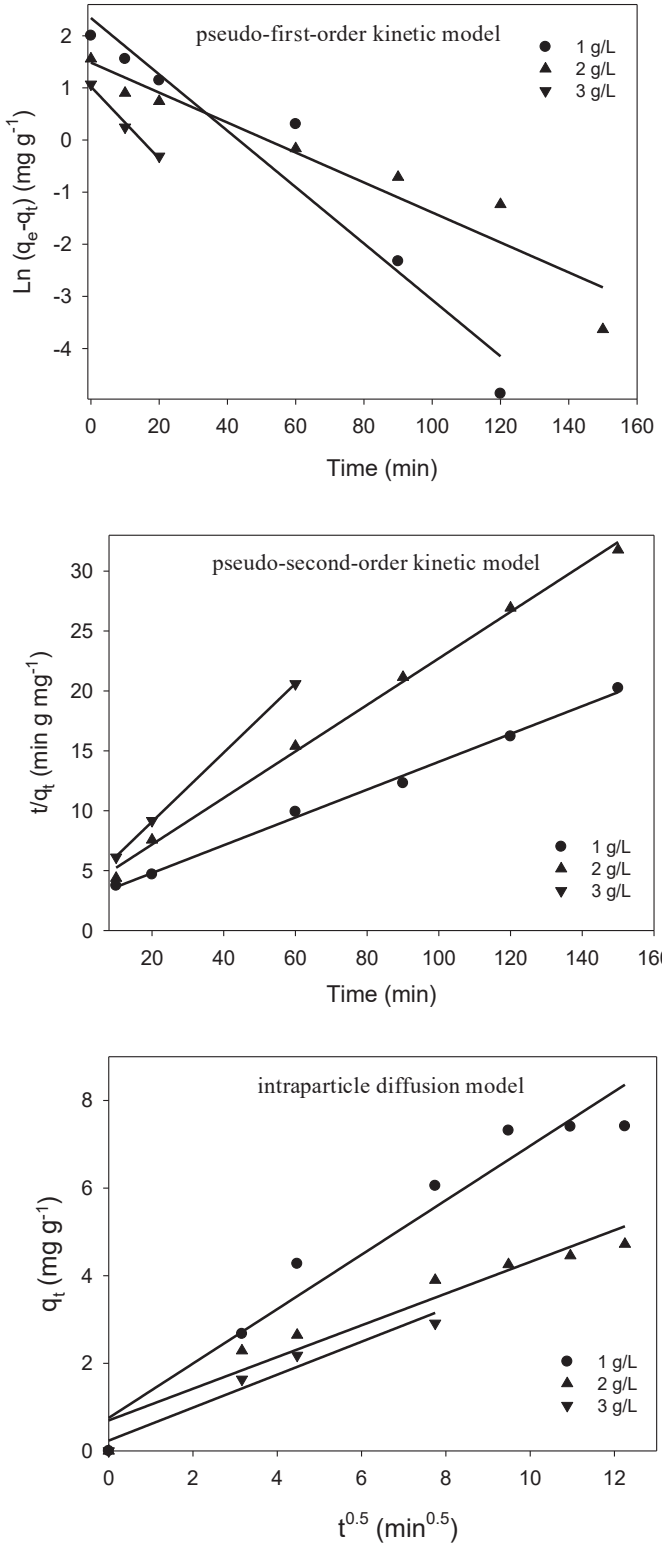

Fig. 5: Pseudo-first-order, pseudo-second-order plots and intraparticle diffusion model plots for MG adsorption on rice wine lees.

Langmuir equation. As a kind of brewing material, rice wine lees is a kind of "waste" for enterprises, if it can be used as a new type of adsorbent, it can provide a new way to treat dye-containing waste water and save energy.

ACKNOWLEDGEMENTS

The authors gratefully acknowledge the financial support of the National Natural Science Foundation of China (Grant No. 41807468), Zhejiang Provincial Natural Science Foundation of China (Grant No. LY18E080018), Shaoxing Public Welfare Project (Grant No. 2017B70042), National Innovation and Entrepreneurship Training Program for College Students (Grant No. 201810349008), and University Students' Science and Technology Innovation Program of Zhejiang Province (Young Talents Program) (Grant No. 2018R432004)

REFERENCES

Amaral, C. N. R. , Feiteira, F. N. , Cruz, R. C. , Vinícius O. Cravo, Cassella, R. J. and Pacheco, W. F. 2016. Removal of basic violet 3 dye from aqueous media using a steel industry residue as solid phase. J. Environ. Chem. Eng., 4(4): 4184-4193.

Baoe, W., Jieping, L., and Ruguang, L. 2009. Adsorption of reactive dyes by beer grains. Environ. Sci. Manag., 5.

Cha, C. J., Doerge, D. R. and Cerniglia, C. E. 2001. Biotransformation of malachite green by the fungus *Cunninghamella elegans*. J. Appl. Environ. Microbiol., 67(9): 4358-4360.

Culp, S. J., Blankenship, L. R., Kusewitt, D. F., Doerge, D. R., Mulligan, L. T. and Beland, F. A. 1999. Toxicity and metabolism of malachite green and leucomalachite green during short-term feeding to fischer 344 rats and b6c3f1 mice. Chem. Biol. Interact., 122(3): 153-170.

Debrassi, A., Corrêa, A. F., Baccarin, T., Nedelko, N., Ślawska-Waniewska, A., Sobczak, K., Dłużewski, P., Greneche, J. and Rodriguesa, C. A. 2012. Removal of cationic dyes from aqueous solutions using n -benzyl- o -carboxymethylchitosan magnetic nanoparticles. Chem. Eng. J., 183(1): 284-293.

do Nascimento, G. E., Duarte, M. M., Campos, N. F., Da, R.O. and Da, S.V. 2014. Adsorption of azo dyes using peanut hull and orange peel: a comparative study. Environ. Technol., 35(11): 1436-1453.

Fernandes, C., Lalitha, V.S. and Rao, K.V. 1991. Enhancing effect of malachite green on the development of hepatic pre-neoplastic lesions induced by n-nitrosodiethylamine in rats. Carcinogenesis, 12(5): 839.

Forss, J., Pinhassi, J., Lindh, M. and Welander, U. 2013. Microbial diversity in a continuous system based on rice husks for biodegradation of the azo dyes reactive red 2 and reactive black 5. Bioresour. Technol., 130(2): 681-688.

Fraga, T.J.M., Carvalho, M.N., Fraga, D.M.D.S.M., da Silva, M.D.C.L., Ferreira, J.M. and da Motta Sobrinho, M.A., 2020. Treated residue from aluminium lamination as adsorbent of toxic reactive dyes – A kinetic, equilibrium and thermodynamic study. Environmental Technology, 41(6): 669-681.

Hameed, B. H. and Ahmad, A. A. 2010. Batch adsorption of methylene blue from aqueous solution by garlic peel, an agricultural waste biomass. J. Hazard Mater., 164(2-3): 870-875.

Hoffman, G. L., Meyer, F. P. and Landolt, J. C. 1974. Parasites of freshwater fishes: A review of their control and treatment. Bioscience, 24(8): 211-211.

Lark, K. G. and Lark, C. A. 1979. Reca-dependent DNA replication in the absence of protein synthesis: characteristics of a dominant lethal replication mutation, dnat, and requirement for reca+ function. Cold Spring Harb. Symp. Quant. Biol., 43 Pt 1(1): 537.

Liu, J., Wang, Z., Li, H., Hu, C., Raymer, P. and Huang, Q. 2018. Effect of solid state fermentation of peanut shell on its dye adsorption performance. Bioresour. Technol., 47(4): 307-314.

Manzoor, Q., Nadeem, R., Iqbal, M., Saeed, R. and Ansari, T. M. 2013. Organic acids pretreatment effect on rosa bourbonia phyto-biomass for removal of Pb(ii) and Cu(ii) from aqueous media. Bioresource Technol., 132: 446-452.

Nadeem, R., Manzoor, Q., Iqbal, M. and Nisar, J. 2015. Biosorption of Pb(ii) onto immobilized and native *Mangifera indica* waste biomass. J. Ind. Eng. Chem., S1226086X15005791.

Purohit, P. S. and Somasundaran, P. 2014. Modification of surface properties of cellulosic substrates by quaternized silicone emulsions. J. Colloid. Interface. Sci., 426: 235-240.

Robinson, T., Chandran, B. and Nigam, P. 2002. Effect of pretreatments of three waste residues, wheat straw, corncobs and barley husks on dye adsorption. Bioresource Technol., 85(2): 119-124.

Shindy, H. A. 2012. Multi choice questions and their answers in colour, dyes and pigments chemistry: A review paper. Mini-Reviews in Organic Chemistry, 9(4): 361-373.

Shroff, K. A. and Vaidya, V. K. 2011. Kinetics and equilibrium studies on biosorption of nickel from aqueous solution by dead fungal biomass of mucor hiemalis. Chem. Eng. J., 171(3): 1234-1245.

Stammati, A., Nebbia, C., Angelis, I. D., Albo, A. G., Carletti, M. and Rebecchi, C. **et al.** 2005. Effects of malachite green (mg) and its major metabolite, leucomalachite green (lmg), in two human cell lines. Toxicology. In Vitro, 19(7): 0-858.

Tahir, N., Bhatti, H. N., Iqbal, M. and Noreen, S. 2017. Biopolymers composites with peanut hull waste biomass and application for crystal violet adsorption. Int. J. Biol. Macromol., 94: 210-220.

Ullah, I., Nadeem, R., Iqbal, M. and Manzoor, Q. 2013. Biosorption of chromium onto native and immobilized sugarcane bagasse waste biomass. Ecol. Eng., 60: 99-107.

Xie, G., Wang, L., Gao, Q., Yu, W., Hong, X., Zhao, L. and Zou, H. 2013. Microbial community structure in fermentation process of Shaoxing rice wine by illumina-based metagenomic sequencing. J. Sci. Food. Agric., 93(12): 3121-3125.

Zhu, X.L., Liu, Z.H., Yang, X., Sun, Y.S., Zhang, Q.L. and Zhang, L.Q. 2016. Adsorption mechanism of distillers' grain to congo red and malachite green. New Chem. Mater., 44(2): 207-209-213.

Nature Environment and Pollution Technology
An International Quarterly Scientific Journal

p-ISSN: 0972-6268
(Print copies up to 2016)
e-ISSN: 2395-3454

Vol. 19 | No. 2 | pp. 571-576 | 2020

Original Research Paper

https://doi.org/10.46488/NEPT.2020.v19i02.012

Open Access Journal

Government's Control Countermeasures Against Environmental Pollution by Introducing Third-Party Constraints

Yanmin Zhao
School of Management, Wuhan University of Technology, Wuhan 430070, China; zymwhut@163.com

Nat. Env. & Poll. Tech.
Website: www.neptjournal.com

Received: 22-02-2020
Accepted: 15-04-2020

Key Words:
Third-Party constraints;
Environmental pollution;
Game analysis;
Government governance

ABSTRACT

With the rapid development of China's economy, environmental pollution becomes increasingly serious in recent years. The environmental governance model of "who pollutes, who governs" is that polluters handle pollutants following relevant laws and regulations under government supervision. Practice shows that this governance model has little effect. The pressure of social groups plays an important role in promoting compliance with laws and regulations and reducing corporate emissions. To improve the government's control of environmental pollution, third-party organizations as binding parties, mainly referring to the public, civil organizations, and the news media were introduced; a game model with government, sewage companies, and third-party organizations as participants was built. The results show that countermeasures against government environmental pollution are constrained third parties and effectively restrict the environmental pollution behaviour of sewage companies. This scenario alleviates the problem of information asymmetry between government and enterprises, reduces the cost of government supervision, and helps strengthen the governance of environmental pollution issues.

INTRODUCTION

With the rapid development of China's economy, environmental pollution becomes increasingly serious in recent years. Environmental pollution directly damages, negatively impacts the ecosystem and indirectly harms the ecosystem and the society. This indirect harm is greater and more difficult to eliminate than direct harm. The environmental impact derived from environmental pollution is lagging, and it is often difficult to detect or anticipate when pollution occurs. However, its occurrence means that environmental pollution has developed to a serious degree. The most direct and most easily felt effect of environmental pollution is the reduction of the quality of the human environment as well as the quality of human life, physical health, and production activities.

The "who pollutes, who governs" environmental governance model is that the polluters handle pollutants by relevant laws and regulations under government supervision. Practice shows that this type of governance has little effect. Pargal et al. (1996) proposed that pressure from social groups plays an important role in promoting compliance with laws and regulations and reducing corporate emissions. This study introduces third-party organizations as binding parties, mainly referring to the public, civil organizations, and the news media. It features a game model for participants to determine effective ways to restrict the behaviour of polluting enterprises and proposes government environmental pollution control measures under the constraints of third parties. It not only provides a theoretical basis for the government's environmental pollution treatment, but it also has reference value for the research and implementation of government governance countermeasures in other fields such as education and medical care.

PAST STUDIES

Many scholars used game theory to study environmental pollution. Mäler et al. (1998) first applied game theory to the study of acid pollution in trans-administrative regions in Europe. He built models for up to 27 countries as participants and found that "unilateral payment" is the premise of cooperation among countries. Frisvold et al. (2000) used game theory to analyse the policy of the US–Mexico border water treatment project. Dungumaro et al. (2003) discussed the positive role and significance of public participation mechanism in environmental protection. Akihiko (2009) established a game model of the pollution behaviour of international duopoly countries in third countries. After a comparative analysis of two environmental policy tools, namely, emission tax and command-and-control regulation, he suggested that tough emissions policies increase the competitiveness of foreign companies. Besides, he pointed out that certain game strategies deviate the effects of environmental policies in third countries from their social optimal levels, and the games around emission taxes have a serious impact on the pollution situation and social welfare on levels of third countries. Kamwa (2012) believed that local governments have a

great deal of enthusiasm to ignore environmental regulations and attract foreign investment by relaxing supervision of environmental issues in their jurisdictions, tax incentives, financial subsidies and other means, which ultimately worsen regional environmental quality. Hottenrott et al. (2015) believed that environmental protection policies based on fiscal decentralization incentivize enterprises to adopt advanced environmental protection technologies. The innovation of environmental protection technologies, in turn, reduces the costs of environmental damage and produces a crowding effect. Chinese scholars performed research in this area relatively late, mainly after 2000. Han et al. (2001) early on studied the prisoner's dilemma of pollution control in China's enterprises and explained the cause of the "tragedy of the commons" of environmental public goods use without government supervision from the perspective of game theory. Zhao et al. (2003) pointed out that information advantage and the absence of other constraints or incentives urge polluting enterprises and local governments to provide incomplete information to their superiors. Zhao et al. (2006) studied the regulatory game between the government and enterprises and believed that, in this game, the cost of pollution control of the company is positively related to the probability of government regulation; the probability of corporate pollution is positively related to the government's regulatory costs, and the impact on government reputation is negatively related to government fines for companies. From the perspective of game theory, Zang, et al. (2010) studied the issue of government environmental policymaking based on information mismatch. Li (2011) used the central and different local governments as participants to establish an "inter-government game" model of water pollution across administrative regions. Through analysis, the Nash equilibrium of the game of voluntary supply of public goods in the river basin was less than the optimal supply of Pareto conclusion. Based on statistical and econometric methods, game theory, and environmental economic theory, Wang (2013) comprehensively and thoroughly analysed the issues related to environmental pollution control and economic development. He discussed many questions about conspiracy issues in the regulation of "emissions tax" and the auctioneers of emission rights. Dong (2016) combined game theory and holistic governance theory to study the inter-governmental relations of urban agglomerations in China and explored strategies and methods for promoting coordinated governance of inter-governmental games in China's urban agglomerations. Yuan (2016) comprehensively applied modern economic research methods, such as public finance theory, fiscal decentralization theory, and game theory. He also used substantial statistical data to support and discuss the mismatch between the fiscal power and the power of local governments in environmental governance.

In summary, previous studies reveal the interactive relationship between the government and related entities like sewage companies and how the government takes countermeasures to control environmental pollution. However, in environmental pollution governance, the starting point of interest between polluting enterprises and the government is different. Hence, asymmetric information is widespread in the actual governance process. Therefore, the current study introduces third-party organizations as binding parties as well as constructs a game model with government, sewage enterprises, and third-party organizations as participants to effectively restrict the behaviour of sewage enterprises. This study also proposes government environmental pollution control measures under the constraints of third parties. Mobilizing third parties such as the public, non-governmental organizations, and the news media to assist government departments in monitoring the state of corporate emissions eases the problem of information asymmetry between the government and enterprises, reduces the cost of government supervision, and helps strengthen the governance of environmental pollution issues.

METHODS

Research Hypothesis

This study introduces a third-party organization as a binding party. However, in the pursuit of maximizing their respective interests, rent-seeking behaviour may occur between third-party organizations and sewage companies, conspiring to deceive government regulators to reduce pollution control costs and avoid economic punishment. With the government, sewage companies and third-party organizations as participants in environmental pollution incidents, a game model of environmental trilateral participation is constructed. The following are the main assumptions of this study. First, game participants are rational decision-makers. The government aims to maximize the overall social benefits, and third-party organizations and sewage companies aim to maximize their interests. Second, all three parties in the game of environmental pollution control introduced by the third party have a full understanding of the game structure and its own benefits and points, that is, a complete information static game. Third, the variables in the model are all greater than 0.

The variables are set as follows:

(1) p is the probability that a sewage company will rent-seeking a third-party organization, and 1-p is the probability that a sewage company will not rent-seeking a third-party organization.

(2) q is the probability that a third-party organization will receive the rent-seeking business of a sewage company.

(3) r is the probability that the government department will supervise, and 1-r is the probability that the government department will not supervise.

(4) C is the cost when the polluting enterprise discharges pollutants according to the standard; μC is the income ($0<\mu<1$) obtained by the polluting enterprise from rent-seeking to a third-party organization. (1-μC) is the cost of rent-seeking and the gains from the third-party organization's acceptance of the rent-seeking enterprise. $\lambda\mu C$ is the penalty received by the sewage-seeking enterprise when its rent-seeking behaviour is discovered. λ is a penalty factor, $\lambda>1$.

(5) L is the penalty for the third organization receiving the sewage-seeking enterprise when rent-seeking is found.

(6) M is the loss caused by the government department's failure to monitor rent-seeking behaviour between sewage companies and third-party organizations.

(7) N is the cost of government supervision;

(8) θ is the supervisory capacity of the government department. Considering its asymmetric information, finding and not discovering rent-seeking behaviour between sewage companies and third-party organizations have two results, $0<\theta<1$.

Based on the above hypothesis, the following section establishes and analyses a game model in which the government, sewage companies, and third-party organizations participate.

Game Income

Let the probability of a rent-seeking behaviour between a sewage company and a third-party organization be s, then $s = 1 - (1 - p) \times (1 - q)$, and the probability of a rent-seeking behaviour between a sewage company and a third-party organization is $1 - s$. You can get the following benefits:

(1) When the sewage-seeking enterprise conducts rent-seeking behaviour with a third-party organization, consider the government's supervisory capacity θ. When rent-seeking behaviour is found, then the benefits of the sewage-emitting enterprise, the third-party organization, and the government are as follows: $(1 - \lambda)\mu C$, $(1 - \mu)C - L$, $L + \lambda\mu C - N - M$. When no rent-seeking behaviour is found, the three parties' returns are as follows: μC, $(1 - \mu)C$, $-N - M$. If the government does not participate in the supervision, then the sewage company, the benefits of the tripartite organization, and the government are as follows: μC, $(1 - \mu)C$, $-M$.

(2) When polluting enterprises and third-party organizations do not conduct rent-seeking behaviours and if the government participates in supervision, then the revenues of the polluting enterprises, third-party organizations, and government are as follows: 0, 0, $-N$. If the government does not participate in supervision, all three parties' returns are 0.

Based on the above analysis, the game return matrix with the participation of sewage companies, third-party organizations, and the government can be obtained, as shown in Table 1.

Model Solving

According to Table 1, given the value of s, the expected returns from government participation in supervision and non-regulation are as follows:

$$E_1 = (L + \lambda\mu C - M - N)\theta s + (-M - N)(1 - \theta)s + (-N)\theta(1 - s) + (-N)(1 - \theta)(1 - s) \quad \ldots(1)$$

$$E_2 = (-M)s + 0 \times (1 - s) \quad \ldots(2)$$

When the expected return from government participation in supervision and the expected return from non-regulation are equal, a game equilibrium state can be reached, that is, $E_1 = E_2$. Then

$$s^* = \frac{N}{\theta\left(L + \lambda\mu C\right)} \quad \ldots(3)$$

At this time, s^* is the Nash equilibrium solution of the rent-seeking behaviour of the sanitary sewage company and the third-party organization.

Table 1: Game income matrix with the participants.

Sewage companies and third-party organizations	Government		
	Participate in supervision (r)		Not involved in supervision (1-r)
	Discover rent-seeking behaviour (θ)	No rent-seeking behaviour discovery (1-θ)	
Rent-seeking (s)	$(1 - \lambda)\,\mu C$, $(1 - \mu)\,C - L$, $L + \lambda\mu C - N - M$	μC, $(1 - \mu)C$, $-N - M$	μC, $(1 - \mu)C$, $-M$
No rent-seeking (1-s)	0, 0, $-N$	0, 0, $-N$	0, 0, 0

According to Table 1, given the r, the expected returns from government participation in supervision and non-regulation are as follows:

$$E_1 = [(1-\lambda)\mu C]\theta r + \mu C(1-q)r + \mu C(1-r) \quad \ldots(4)$$

$$E_2 = 0 \quad \ldots(5)$$

When the expected return from sewage-seeking enterprises is equal to the expected return from non-rent-seeking behaviour, a game equilibrium state can be reached, that is $E_1 = E_2$. Then

$$r^* = \frac{1}{\theta\lambda} \quad \ldots(6)$$

According to Table 1, given r, the expected returns of third-party organizations accepting rent-seeking and rejecting rent-seeking behaviour are as follows:

$$E_1 = [(1-\mu)C - L]\theta r + (1-\mu)C\,(1-\theta)r + (1-\mu)C(1-r) \quad \ldots(7)$$

$$E_2 = 0 \quad \ldots(8)$$

When the expected return from rent-seeking behaviour by a third-party organization is similar to the expected return from rejecting rent-seeking, a game equilibrium state is reached, that is, $E_1 = E_2$. Then

$$r^* = \frac{(1-\mu)C}{\theta L} \quad \ldots(9)$$

In summary, in the case of determining the rent-seeking behaviour of polluting enterprises and third-party organizations and government participation in supervision, the Nash equilibrium solution of the three-party game can be divided into the following cases:

(1) Sewage companies and third-party organizations conduct rent-seeking behaviour with probability $\frac{N}{\theta(L+\lambda\mu C)}$, and the government participates in supervision with probability $\frac{1}{\theta\lambda}$.

(2) Pollution-discharging enterprises and third-party organizations conduct rent-seeking behaviour with probability $\frac{N}{\theta(L+\lambda\mu C)}$, and the government participates in supervision with probability $\frac{(1-\mu)C}{\theta L}$.

RESULT ANALYSIS

Influencing Factors of Rent-Seeking Behaviour Between Sewage Companies and Third-Party Organizations

Formula (3) shows that s^* is an increasing function of N. The cost of government participation in supervision increases with N, decreasing the government's enthusiasm for participation, which increases the probability of sewage companies and third-party organizations to conduct rent-seeking. Meanwhile, s^* is a decreasing function of $\lambda\mu C$, L, θ. The government's penalties for sewage-seeking enterprises and third-party organizations participating in rent-seeking increase with $\lambda\mu C$ and L. These reduce the probability of rent-seeking companies and third-party organizations to conduct rent-seeking. The increase in regulatory capacity also reduces the probability of rent-seeking by polluting companies and third-party organizations.

$\lambda\mu C$ is the government's penalties for polluting enterprises that conduct rent-seeking behaviour, which is mainly controlled by λ. Therefore, reducing the rent-seeking behaviour of polluting enterprises and third-party organizations, that is, reducing s^*, can reduce the government's regulatory cost N, improve the government's regulatory capacity θ, and increase penalties λ and L.

Influencing Factors of the Efficiency of Government Participation in Supervision

Formula (6) shows that the government takes polluting enterprises as the main regulatory object at this time, and r^* is the decreasing function of θ and λ. Therefore, we should start from the supervision efficiency and reduce the supervision probability r^* to improve the supervision efficiency. Therefore, government supervision efficiency is an increasing function of θ and λ. The government's regulatory capacity and the punishment of polluting enterprises that conduct rent-seeking behaviour increase with θ and λ. Hence, the efficiency of government participation in supervision increases.

As shown in Formula (9), the government regards third-party organizations as the main regulatory object, where r^* is an increasing function of $(1-\mu)C$ and a decreasing function of θ and L. Besides, the higher the probability of government participation in supervision, the greater the cost of supervision is. Therefore, we should reduce the supervision probability r^* to improve supervision efficiency. Therefore, the government's supervision efficiency is a reduction function of $(1-\mu)C$, which is the increasing function of θ and L. The cost of sewage-seeking companies' rent-seeking to third-party organizations and the benefits of third-party organizations' acceptance of rent-seeking increase with $(1-\mu)C$. Thus, the efficiency of government participation in supervision is reduced. The government's regulatory capacity and the punishment of third-party organizations increase with parameters θ and L. Hence, the efficiency of government participation in supervision increases. Therefore, reducing the probability r^* of government participation in

supervision and improving supervision efficiency can reduce the cost of sewage-seeking companies' rent-seeking to third-party organizations and the benefits $(1-\mu)C$ obtained by the third-party organizations that accept sewage-seeking companies' rent-seeking. Thus, the supervision capacity coefficient θ and the punishment L of third-party organizations that accept the rent-seeking enterprises of pollutant discharge enterprises must be increased.

PRACTICAL COUNTERMEASURES

The above analysis results show that the government can reduce the probability of rent-seeking behaviour of polluting enterprises and third-party organizations in the process of polluting by formulating effective environmental pollution control measures and protecting the lives and health of the people.

Reduce Regulatory Costs and Improve Regulatory Capacity

The probability of a sewage-seeking enterprise's rent-seeking behaviour is directly proportional to the cost of government supervision and inversely proportional to the ability to supervise it. Therefore, the government should reduce the cost of supervision and improve its supervision capacity. It should also streamline its supervision institutions and curb the trend of further expansion of supervision institutions and the increase in the number of supervisors. Furthermore, the government should establish a lean unit-wide regulatory agency, uniformly formulate unit-wide regulatory rules and guidelines, give full play to the role of synergy, and transform each into time-consuming discrete supervision to cooperate with a coordinated and orderly integrated supervision. Implement a comprehensive and sustainable monitoring process to form a closed supervision system.

Increase Punishment and Reduce Pollution Emissions

The probability of a sewage-seeking enterprise's rent-seeking behaviour is inversely proportional to the penalties of the sewage-seeking enterprise and the third-party organization. Therefore, the government should increase penalties for polluting enterprises and third-party organizations that conduct rent-seeking behaviours. Once pollutant discharge enterprises find rent-seeking behaviour, they should immediately request rectification within a time limit or directly withdraw from the market and impose a large fine. Hence, they feel that the gain from rent-seeking behaviour is less than fine. Third-party organizations should formulate sound laws and regulations to regulate their behaviour, vigorously exert their restrictive role, promote the compliance of pollutant discharge enterprises with relevant laws and regulations, and reduce corporate emissions.

Develop Incentives to Encourage Pollution Control

In addition to the above penalties, the government can also develop incentives to reduce the probability of environmental pollution incidents. Pollution-discharging enterprises with lower-than-standard emissions and strictly monitored third-party organizations are given certain incentives to continue to treat pollution at high standards. Increase investment in environmental protection, support and guide capable environmental service organizations to participate in environmental pollution treatment, and grant subsidies and incentives to eligible third-party organization projects.

CONCLUSION

The environmental governance model of "who pollutes, who governs" is that polluters handle pollutants by relevant laws and regulations under government supervision. Practice shows that this governance model has little effect. This study introduces third-party organizations as binding parties, mainly referring to the public, civil organizations, and the news media. A game model with government, sewage companies, and third-party organizations as participants was built. The conclusions are obtained that the countermeasures against government environmental pollution under the constraints of third parties effectively restrict the behaviour of sewage companies. This study only uses the static game model, and the dynamic game analysis among the government, sewage companies and third-party organizations is the future research direction

REFERENCES

Akihiko, Y. 2009. Global environment and dynamic games of environment policy in an international duopoly. Journal of Economics, 97(2): 121-140.

Dong. S.J. 2016. Research on the overall governance of inter-government games in urban agglomerations. Changsha: Doctoral Dissertation of Hunan University, China.

Dungumaro, W. and Madulu, F. 2003. Public participation in integrate water resources management: The case of Tanzania. Physics and Chemistry of the Earth, 28: 1009-1014.

Frisvold, B. and Caswell, F. 2000. Transboundary water management game-theoretic lessons for projects on the US-Mexico border. Agricultural Economics, 24: 101-111.

Han, G.F. and Ma, N.X. 2001. A game analysis of inefficiency of environmental protection. Ecological Economy, 6: 19-22.

Hottenrott, H. and Rexhäuser, S. 2015. Policy-induced environmental technology and inventive efforts: Is there a crowding out?. Industry and Innovation, 22(5): 375-401.

Kamwa, E. 2012. Tax competition and determination of the quality of public goods. Journal of Applied Microbiology, 112(1): 90-98.

Li, S. 2011. Research on inter-government game of water pollution across administrative regions. Changsha: Doctoral Dissertation of Hunan University, China.

Mäler, K.G. and De Zeeuw, A. 1998. The acid rain differential game. Environmental and Resource Economics, 12(2): 167-184.

Pargal. S. and Wheeler, D. 1996. Informal regulation of industrial pollution in developing countries: Evidence from Indonesia. Journal of Political Economy, 104(6): 1314-1327.

Wang, B. 2013. Game study on environmental pollution control and regulation. Beijing: Doctoral Dissertation of Capital University of Economics and Business, China.

Yuan, H.P. 2016. Research on local government's environmental pollution control under fiscal decentralization. Beijing: Doctoral Dissertation of Capital University of Economics and Business, China.

Zang, C.Q., Liu, Y. and Wang, L. 2010. The design of the policies of the environmental regulation under the condition of information asymmetry: Based on the perspective of game theory. Finance & Economics, 5: 63-69.

Zhao, H.M. and Sun, M.Q. 2006. Game analysis of environmental pollution control in Yangtze River Delta. Environment and Sustainable Development, 5: 36-38.

Zhao, L.J. and Li, H.Z. 2003. Study on countermeasures for transboundary water pollution dissension of the river valley. China Population, Resources and Environment, 6: 52-57.

Nature Environment and Pollution Technology
An International Quarterly Scientific Journal

p-ISSN: 0972-6268
(Print copies up to 2016)
e-ISSN: 2395-3454

Vol. 19 | No. 2 | pp. 577-586 | 2020

Original Research Paper

https://doi.org/10.46488/NEPT.2020.v19i02.013

Open Access Journal

Comparison of Binding and Interaction Studies of Metal Ions/Surfactant with Protein by Various Physical Methods

Shveta Acharya and Arun Kumar Sharma*†
Department of Chemistry, Govt. College, Kota-324010, Rajasthan, India
*Department of Chemistry, Govt. P.G. College, Jhalawar-326001, Rajasthan, India
†Corresponding author: Arun Kumar Sharma; sharmaarun423@gmail.com

Nat. Env. & Poll. Tech.
Website: www.neptjournal.com

Received: 21-07-2019
Accepted: 29-08-2019

Key Words:
Surfactants; Metal ions; Albumin; Viscosity; Diffusion current; Egg-protein; Scatchard plots; Equilibrium dialysis

ABSTRACT

The metal ions play a vital role in a large number of widely differing biological processes. Some of these processes are quite specific in their metal ion requirements. In that only certain metal ions, in specific oxidation states, can fulfil the necessary catalytic or structural requirement, while other processes are much less specific. In this paper, the interactions between triethanolamine, lauryl sulphate and albumin molecules have been reported. The pH and diffusion current measurements on the binding of copper and mercury ions with albumin have been discussed. The effect of physico-chemical factors on the interaction between divalent metal ions and albumin has been carried out. Physico-chemical studies on the binding of Hg(II) and Cu (II) with albumin have been discussed.

INTRODUCTION

The term biopolymer includes a variety of macromolecules including proteins, carbohydrates, nucleic acids, etc., for example, proteins are widely distributed in cells of plants, vertebrates, invertebrates, and microorganisms. They have a variety of functions. The fertilizine, a protein, present at the surface of ova is responsible for reproduction. Some of them act as hormones, enzymes and as inhibitors. In almost every field of biology, biopolymers find remarkable applications. The uses of these proteins as lubricants, carriers, and structural proteins, etc. are well known (Arora et al. 1983a).

The interactions between acidic and basic macromolecules in the living systems in the presence of micromolecule ions form the basis of the formation of biofluids and these combinations have been included under the trophic phase equilibria in systems of interacting polyelectrolytes. It has been assumed that the coacervation mixing process represents the primary ordering process by which mixtures of randomly formed pre biologic polymers were condensed into preprotoplasmic assemblies. Such studies on complex coacervation have thrown light on the development of living systems via interactions between the random polymers produced in the atmosphere of the earth (Harris 1984). The interactions between proteins and a variety of bio-acceptable compound/ion have been carried out for several reasons. The most significant of these is to find out the effect of any particular compound for any specific system among the various bioactive compounds. The metal ions play a vital role in a large number of widely differing biological processes. Some of these processes are quite specific in their metal ion requirements. In that only certain metal ions, in specific oxidation states, can fulfil the necessary catalytic or structural requirement, while other processes are much less specific. It is possible to replace one metal ion by another, although the activity may be reduced. Metals like Mg, Mn, Fe, Co, Cu, Mo and Zn are important catalysts of a variety of enzyme reactions such as group transfer, redox or hydrolytic processes. Some protein system is involved in strong and controlling the concentration of the metal ion and then in transporting it to the appropriate sites of the enzyme (Dudev et al. 2003). Many of them are used in maintaining the structure and controlling the function of the cell wall. Not only the common metals but even the lanthanide that finds usage as a nuclear magnetic resonance shift probe in biological systems. The physiological pH is limited to 7.0-7.5 while these lanthanide ions are reported not to be precipitated even up to pH 8.43, thus it is feasible to say that in this sense they are even superior then

the well-known biologically active ferric and chromic ions (Harding 2004). These ions are reported to form complexes with adenosine monophosphate. The role of uranyl ions in enzymatic systems has recently been reported by several workers (Acharya & Sharma 2018a).

MATERIALS AND METHODS

Characterization of Metal Protein Complex

Many complexities arise in the investigation of proteins, which are ascribed to factors like uncertainty in molecular weights and variation in chemical behaviour depending on the nature, origin, purity and their great sensitivity to denaturation. A large number of physico-chemical methods, viz. ultracentrifugation, ultrafiltration, magnetic susceptibility, light scattering solubility, precipitation, migration in electric field polarography, spectrophotometry, equilibrium dialysis, electrophoretic mobility, pH displacements, electron paramagenetic resonance (EPR), optical rotatory dispersion (ORD), circular dichroism (CD), Mossbauer spectroscopy, etc. have been used in ascertaining the mode of binding and also in achieving greater success in quantitative aspects of metal protein problem. Besides these techniques, the chemical testing of metalloenzyme and aproenzyme for the presence of specific groups has been of great value (Lu et al. 2008).

Detergent-Protein Interaction

The interaction of synthetic detergents to proteins has been studied for several reasons. Depending on the nature of the protein, association or dissociation complexation, denaturation, precipitation, etc. may occur. These have also been used to expose groups in proteins normally unavailable to specific reagents. In many cases, they are used for isolation of protein. SDS has also been used for the extraction of transforming DNA. Several workers have also shown protein precipitated by anionic detergent does not show any change in its viscosity after its recovery from the detergent protein complex (Frassinetti et al. 2006). Among anionic detergents used, the interaction of SDS with proteins, besides including anti-parallel sheet conformation. The survey of the existing literature revealed that the binding of molybdenum, vanadium, zinc, cadmium, copper, nickel and cobalt is lacking to egg albumin, similarly, no binding studies of molybdenum copper and mercury are made with nucleic acid and those of anionic surfactants with albumin (Keilin & Mann 1940). Investigations on the aspects of these binding problems were planned and their binding constants have been determined using suitable physico-chemical methods (Zheng et al. 2008).

pH Measurement

These were carried out with a digital Systronics pH meter using a wide range glass electrode. The instrument was calibrated against 0.05M potassium hydrogen phthalate (pH 4.0) and 0.05M sodium borate (pH 9.20) for acidic and alkaline ranges, respectively.

Diffusion Current Measurements

These measurements were carried out on a Toshniwal polarograph Model Cl 02A in conjunction with an Osaw galvanometer in the external circuit. An H-shaped polarographic cell as recommended by Tanford was used. Nitrogen, purified by passing through a solution of chromous chloride and alkaline pyrogallol, was passed through the solution for producing an inert atmosphere. Triply distilled mercury was used for the D.M.E. The cell was immersed in water thermostat maintained at 25 ± 0.1°C. The capillary used had a flow rate of about 2.2 mg/s with a drop time of 3.5 s. Since the capillary characteristics *(m, t)* have a marked effect on diffusion current, which is directly proportional to ($m^{2/3}$, $t^{1/6}$), these factors were therefore controlled carefully throughout these experiments (Acharya & Sharma 2018b).

RESULTS AND DISCUSSION

Binding Sites of Surfactant with Albumin

In the binding of anionic surfactant to albumin, it has been observed that in each case of the mode of combination of the triethanolamine lauryl sulphate (TEALS) ions to albumin, change in three distinct patterns of the free concentrations of surfactant is progressively raised. The patterns of linking have been roughly demarcated by dividing the logarithmic plots into three areas A, B and C to understand the mechanism of TEALS albumin combination at different stages (Fig. 1). In going from acetylated albumin, formylated albumin to esterified albumin the region 'A' goes on lengthening in area followed by vanishing the vertical shape. Similarly, the logarithmic plots, in case of albumin at varying temperatures, indicated a nature like those of protein derivatives i.e. resin 'A' increasing, B decreasing and 'C' assuming vertical, identifying with the raising temperature. The variation in the pattern of the length of different zones is indicative of the elimination of some intermediates is surfactant albumin interaction, thus the effect of temperature on binding isotherms appears to follow the same course so the protein charge. Further, the relative position and highly vertical shape of the isotherms in case of higher temperature and esterified protein indicates some structural changes in surfactant and protein or both proportion of albumin to surfactant. The plot or Υ vs

log free surfactant concentration followed a linear course. The linearity of plots is in favour of more or less statistical distribution as the surfactant on the entire available albumin molecule in this region. The binding data in the statistical region were determined by the application of Scatchard equation in the form (Lyons et al. 2006):

$$\Upsilon / D_F = K_n - K_r \quad \ldots(1)$$

Υ and D_F have their usual meaning and K is the average apparent association constant for binding at each site and n is the average maximal number of binding sites on macromolecule with the same association constant K. The effect of temperature is highly interesting as is evident from the values of n and K. The hyperbolic character of plots increases with rising temperatures. The linearity of region 'A' continues to increase, region 'B' decreasing and the nature of region 'C' becoming more and more vertical with Υ/D_F axis. The elevated temperature thus vanishes the transition state of unfolding in region 'B' and causes its rapid unfolding as shown by the plots in region 'C'. The increasing values of binding sites(n) in the statistical region and increasing values of surfactant moles bound per mole of albumin (Υ) in region 'C' suggest that conformational variations in the albumin molecule exposed more and more positive and apolar groups for linkage with the TEALS ions (Acharya & Sharma 2018c).

Thermodynamic Studies

The intrinsic constant (log K) at all the reaction temperature appears to be almost the same. This is indicative of a single type of site reacting with the TEALS molecule in the statistical zone. The occurrence of the different number of sites (n) is therefore not responsible for enhanced linkage, which is probably due to the increased availability of the same type of sites. The increasing value of n as the temperature rises at pH 7.40 is indicative of this. The thermodynamic constant viz. free energy ($\Delta G°$) enthalpy ($\Delta H°$) and entropy ($\Delta S°$) also revealed the uniformity of log K and the involvement of a single type of site in TEALS – albumin combination. The free linkage energy is mostly due to changes in entropy, the apparent enthalpy contribution being small and sometimes close to zero. The entropy changes are in the range of 7.8 to 1.9 cal/mole within which the entropy values of the TEALS albumin reaction lie (Harding 1999).

From the data as unmodified and modified proteins, one can see the difference in the ionic and hydrophobic linkage of the straight-line region (A) decrease from EA, A, FA and AA as well as the following sequence EA>A>FA>AA. (Fig. 2) This indicates that the larger the positive charge, the greater is the surfactant linkage. The higher linkage with EA is because there is no electrostatic repulsion between surfactant anions and the protein because extension protected the carboxyl groups so that the negative charge which effected the surfactant linkage line region (Tank et al. 2018). On the other hand, formylation extracts albumin positive charge, thereby resulting in a decreased surfactant linkage. However, in the higher linkage, in all cases the nature of linkage remained unaffected, hence these linking parameters show that hydrophobic linkage is much more significant in surfactant-protein linking (Joshi 2018).

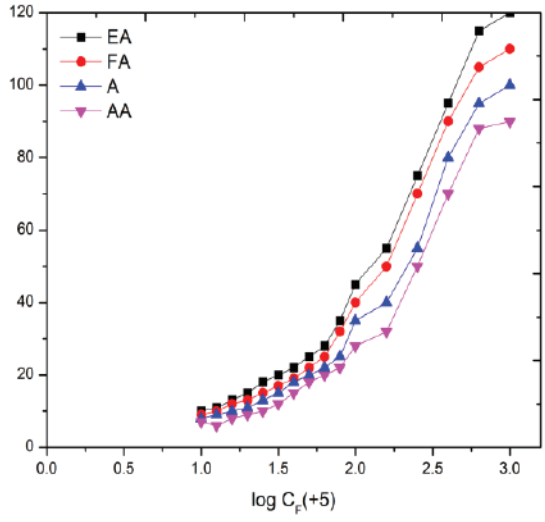

Fig. 1: Logarithmic plots for TEALS albumin and its derivatives at pH= 7.40

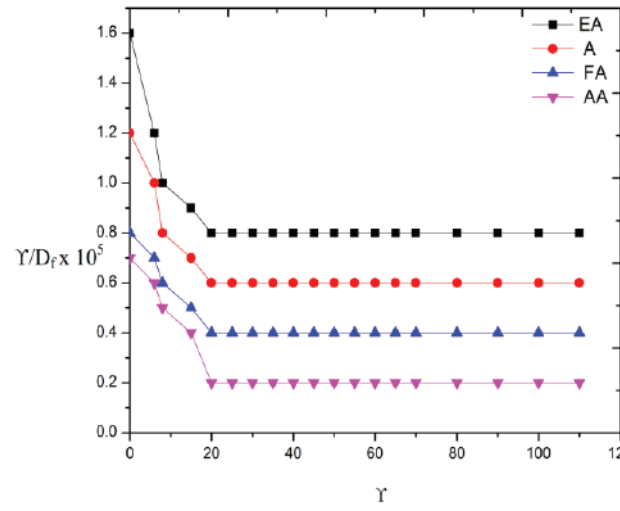

Fig. 2: Scatchard plots of albumin and its derivative for the linkage of TEALS at pH=7.4, T= 25 °C

pH Metric Studies

The pH titration of 0.05 percent albumin in the absence and presence of 2.0×10^{-3} m Hg^{++} and Cu^{++} ions has also been observed (Fig. 3). The titration curve of albumin alone lies above the similar curve of mercury-albumin mixtures throughout the whole pH range. The decrease in pH by the addition of albumin to mercury ion solution indicates that hydrogen is displaced by mercury ions from reactive sites of albumin. This shift of titration curve towards a more acidic side of the functional groups is indicative of an interaction between mercury ions and the albumin. The pH titration of copper is analogous with the mercury curve. The pH displacements are larger in copper-albumin than in mercury-albumin (Kumar et al. 2018).

The polarographic measurements on the mercury-albumin system revealed that the presence of increasing amounts of albumin decreased the diffusion current of mercury ions. Assuming that the decrease in diffusion current in metal ion is solely due to complex formation between metal and protein. The mercury and copper ions also give a reversible polarogram. The strength of the respective linkage may be compared by knowledge of formation constants and thermodynamic parameters. The formation constant (log K) for mercury-albumin was computed from classical Scatchard's equation. These were found out to be 1.16, 2.69 and 3.38 for mercury-carboxyl, mercury-imidazole and mercury-amino linkage respectively, the free energy change for the different linkages were found to be 1.619, 3.755 and 4.718 Kcal/mole. The comparison of log K and free energy values of different linkage justified a stronger combination with amino groups and weakest for carboxyl groups (Kumar et al. 2018).

The addition of albumin to mercury ions solution caused a decrease in its current height, which continuously decreased with increasing concentration of protein and finally become more or less constant. This decrease in the current height could not be due to viscosity changes and absorption on the mercury drops since the studies were made in a higher pH range. The result of the mercury-albumin system may be explained as similar to that of copper-albumin (Hawker et al. 2018).

Diffusion Current Result

The diffusion current of 0.833 molar buffered copper sulphate solution was depressed by the addition of 0.5 percent albumin. This depression was continuous by increasing the albumin concentration and it ultimately becomes constant at an extremely higher concentration of albumin in a similar way. When 0.1 percent albumin was added to varying amounts of copper solution the diffusion current was depressed in proportions of the copper ion solution (Sharma et al. 2018). The linking result can be calculated by taking diffusion current ratio of metal alone and when albumin is present in the mixtures.

For the study of pH displacement from ligand by the added metal cations albumin (A) alone and in the presence of 2.0 × 10.3 M cobalt chloride, nickel chloride and manganese chloride, it was titrated against 0.10 M hydrochloric acid and 0.10 M potassium hydroxide, respectively. Nickel and manganese did not show any binding with the carboxyl groups from the nature of titration curves. It is because the drifts of titration curves above protein are indicative of the adsorption of hydrogen ions (Stern et al. 2007). It appears that these metal ions formed insoluble complexes with

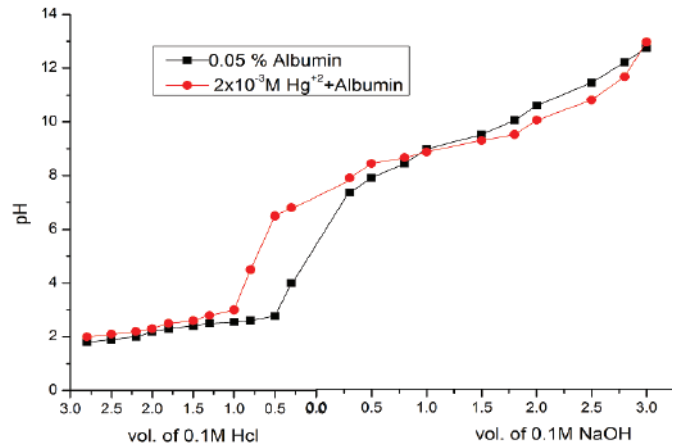

Fig. 3: Titration curve of albumin in the absence and presence of mercury ions.

albumin in lower pH range and the precipitate adsorbs the added hydrogen ions (Stewart et al. 2003). However, in the alkaline range, both nickel and manganese displaced protons from imidazole and ammonium groups of albumins. This cobalt-manganese and nickel ions get co-ordinated with nitrogen atoms with histidyl and lysyl amino acid residues as protein (Harding 2000).

Transmittance Measurements

The absorption spectra of nickel and manganese show maxima at 675 and 775 nm respectively (Fig. 4). The presence of 0.15 to 0.08 percent albumin does not alter the position of maxima, but the absorbance of nickel-albumin mixture is increased. This increase in the absence of the addition of albumin is an indication of interaction between Ni(II) and reactive groups on albumin molecule (Acharya & Sharma 2018d). However, the addition of 0.75 to 1.5 percent albumin at pH 5.0 caused a shift in maxima i.e. it changed from 675 to 600. Such a characteristic shift is due to the chelation of nickel ions with carboxyl groups as protein. The increase in the absorbance by the addition of albumin provides enough qualitative evidence for the linking of cobalt ions by the protein. The addition of gradually increasing amounts of the protein brings about a much marked increase in absorbance so that in the presence of 1.8 percent albumin, the absorbance increases from 0.012 to 0.024. The fact was further supported by the results on mixtures having a fixed amount of albumin and cobalt chloride at different pH values when the absorbance was found in increasing order, since in the pH range 3.25 to 5.30 the carboxylic groups lose their protons. Hence, due to rising pH more carboxylic groups lose their protons and more carboxyl become ionised for linking with the cobalt ions (Drabovich et al. 2013).

The metal oxide colloidal micelles are positively charged and therefore combination with anionic albumin may be affected either through mutual adsorption or through purely chemical forces where the metal ions form the inner part of the double layer, make themselves available for reaction with the reactive sites of the albumin molecule. The titration curves of albumin metal oxide solution lie above the corresponding curves of the solution and for KOH in all the cases, binding occurred above pH 10.50 where all the carboxyl and phenolic groups are anionic while the imidazole and amino groups are fully deprotonated. The extent with which solution alkali or electrolyte may be assumed as a qualitative measure of the extent of metal albumin linking. In general, the complexes are formed through chelation to carboxyl and co-ordination with the nitrogen of imidazole and amino groups of albumins (Van 2013).

Viscometric Results

The viscosity data on the binding also favoured interaction of anionic albumin with metal oxide solution. The progressive addition of metal oxide solution to a fixed amount of albumin caused regularly increased viscosity, providing valuable information about the mutual interaction of hydrophobic and hydrophilic solution. From viscosity solution concentration curves, it is evident that a sharp inflexion occurred in each curve which represented a new slate of aggregation in the colloidal system. It might be concluded that it was due to the formation of absolutely positive charge complexes (Fig. 5) (Acharya & Sharma 2019a-c).

In the case of pH-metry, no binding of nickel ions is indicated with carboxyl groups, while spectrophotometry showed the linking of nickel ions with carboxylate residues

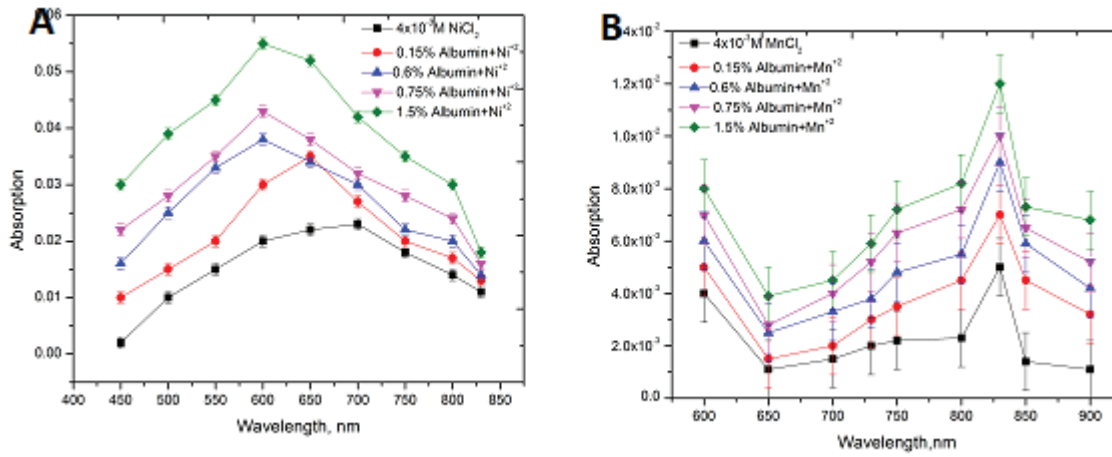

Fig. 4: Absorption spectra 4×10^{-3} M Ni^{+2} (A) Mn^{+2} (B), at different amounts of albumin at pH=5.0.

of albumin. The pH metric as well as viscometric data provided sufficient evidence about the linking of cobalt, nickel and manganese ions with the nitrogen groups of albumins. From the nature and height of curves in the three cases, it may be concluded that nickel ions bound strongly (Fig. 6), while the cobalt ions bound weakly in 10.0 mL, 0.3 percent albumin solution of different pH as the protein (Espósito & Najjar 2002). The pH values of the above mixtures were recorded immediately after mixing and after 24 hours. These measurements at pH 5.35, 9.85 and 11.50 were carried out at 25°C and 40°C respectively.

In the study of binding Cu ions to albumin was calculated by carrying out direct and reserve titrations. The inflexion in the transmittance versus concentration curves indicates the point where the formation of the insoluble complex is incomplete. Furthermore, if this point does not indicate the completion of the formation of the insoluble complex, then with the addition of more Cu would be an even larger

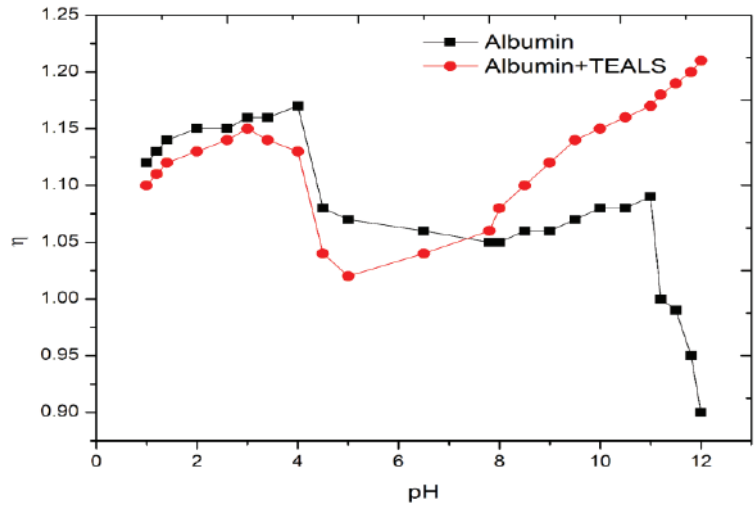

Fig. 5: Relative viscosity v/s pH plots for albumin TEALS system.

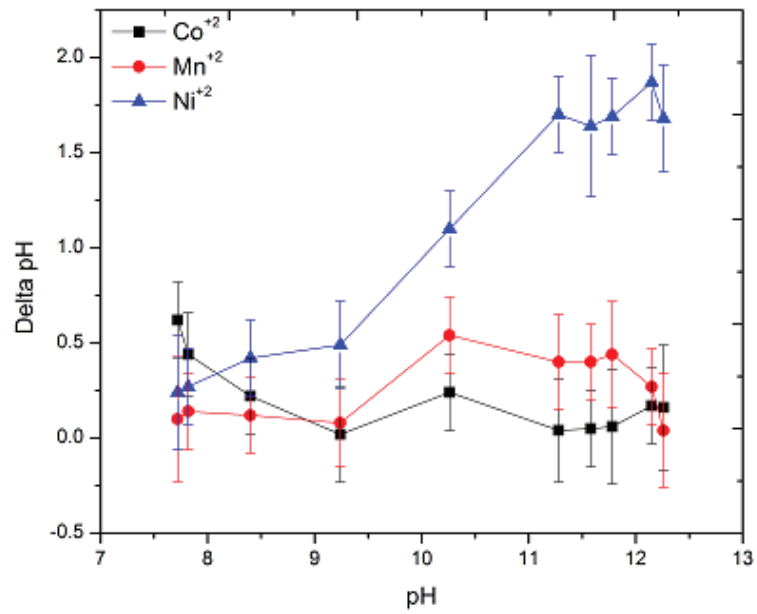

Fig. 6: ΔpH v/s pH plotted against varying concentrations of metal ions showing binding with albumin.

decrease in the percentage transmittance. From the break in the curves, the number of moles of copper bound per mole of protein was found using the relationship $V_M = C_B/P$, where, P is the mortality of protein and C_B the mortality of copper bound at the inflexion point. The anion or cation of Cu interact with albumin at different fixed pH values was studied between 5.35 to 11.50. At all pH values, the pH of protein was found to decrease by the addition of Cu of the same pH value. This decrease in pH was attributed to the preferential binding of Cu ions to the reactive sites of the protein. In such a case, negative pH (pH protein-pH protein + Cu) indicates cation binding while a positive pH (pH protein + Cu - protein) is indicative of anion binding (Acharya & Sharma 2020a).

In the present investigation, the negative pH values showed that Cu binds in the form of the cation. In low pH there was the perception, hence no significant changes in pH occurred. However, above the isoelectric point of the protein, a regular small decrease in pH was observed. This has been assumed to the binding of Cu to the protein. The amount of ligand-bound per mole of albumin (10^5g) was calculated by the method of Scatchard & Black (1957) from which the value of bound (C_B) and free (C_F) molar concentration of Cu was determined from the known molar concentration of albumin ($0.72x10^{-2}$ M). The binding was found to be sigmoidal at pH values 5.35, 7.50 and 9.50, since saturation is attained at higher free Cu concentration. The Cu_M values at the saturation limit correspond to the maximum number of binding sites occupied by ligand molecules on the protein molecule. At pH 9.85 and 11.50, the Cu_M rises linearly as the free ligand increased. This type of sigmoidal and linear binding isotherms is indicative of more than one class of sites and a single set of sites involved in the binding process.

The Cu binding by albumin is observed to be modified by pH and temperature. The number of binding sites decreases with rising pH and temperature but log K remains nearly constant. The importance of constant values of log K, almost independent of pH and temperature, is that only a single primary class of sites is reacting and the appearance of their different number is therefore not responsible for decreased binding which may then be due to decreased availability of the same class of sites owing to irreversible effects in the protein structure. The free energy (ΔG°) enthalpy (ΔH°) and entropy (ΔS°) changes of the interaction were calculated using standard methods (Barnett et al. 2013). The positive entropy (ΔS°) probably indicates that water of hydration is released both from the polar sites of protein and tetrahedral oxo copper species and that the configuration of the polypeptide is changing to a random coil as the complex formation occurs (Table-1). The higher values of entropy and enthalpy change at pH 9.85 possibly indicates that all the above-mentioned factors may be involved at this pH.

The experimental results showed that Cu interaction depends upon the pH of the system. The anion is first attracted to the positive centres on the protein surface by Coulombic forces and when it is sufficiently near, water molecules are removed, making the lone electron pair on nitrogen available for co-ordination with the copper atom of copper ions. The shift of the titration curve of Cu-albumin complex towards higher pH may perhaps be in line with the type of binding because H^+ reacts with $CuSO_4$ ion which in turn is removed as a water molecule on reacting with albumin. In the lower pH range, the complex may be formed through coordination and hydrogen bonding with protonated nitrogen and undissociated carboxyl groups of albumins. However, in the higher pH range, the decreased binding can be explained based on the following facts.

1. The number of –OH groups in the polyacid decreased and as a result, the number of linkages also progressively decreased with the decreasing metal oxide.
2. Protein becomes either swollen or unfolded when the net negative charge increases. As the pH increases and the charge becomes more negative, electrostatic repulsion causes an even greater opening of the protein until a

Table 1: Binding constants of albumin – Cu (II) system by pH displacement method.

pH	n	log k	ΔG^0 (Kcal/mole)	ΔS^0 (cal $mole^{-1}$ deg^{-1})	ΔH^0 (Kcal/mole)
25°C					
5.34	11	3.95	-5415	+5.0	
7.50	9	3.78	-5.182	-	
9.50	8	3.61	-4.949	-	
9.85	7	3.60	-4.835	+14.0	
11.50	3	3.60	-4.835	+8.6	
40°C					
5.34	9	3.81	-5.486	+4.7	+4.000
9.85	6	3.58	-5.155	+14.6	-0.572
11.50	2	3.52	-5.068	+6.0	-2.266

maximum is reached, as predicted by the diminished Cu binding results.

3. The progressive deprotonation of the nitrogen atoms would result in a smaller number of positive loci, therefore, resulting in a decreased binding.
4. Protein becomes swollen or unfolded when the net negative charge increases. As the pH increases and the charge becomes more negative, and the electrostatic repulsion causes an even greater opening up of the protein until a maximum is reached as predicted by the diminished anion binding results.

The polarographic behaviour of mercuric chloride ion is interesting because the polarograms in lower potential range possess a small maximum. The addition of even a smaller amount of albumin suppressed the maxima as well as decreased the current height. The abstraction of maxima from polarograms by the presence of albumin is a direct indication of the combination between albumin and mercury (Hg) ions. Furthermore, the addition of more and more amounts of albumin caused a progressive decrease in the current height. This reduction in current height may be due to successive removal of Hg ions from the systemic increasing amounts of albumin which react with more and more Hg, which is a cause of the depression in the current height of axometal ion.

The polarographic data viz. Hgm and Hgf can be analysed in many ways. For qualitative representation, these are plotted in the form of logarithmic plots i.e. Hgm is plotted against log free equilibrium concentration of Hg ions. These isotherms at 25°C indicate the extent of binding increases progressively as the log free concentration rises and ultimately assumes S-shape. This indicates the saturation of binding sites in both cases i.e. at and 0.5 percent albumin concentrations. The binding data were also explained in terms by a protein, the first bound ion tends to reduce the affinity of the protein for the second oncoming ion because of the electrostatic factor in protein the binding constants n (binging sites) and K (association constant) may be calculated by equation (1).

Where, K is the average apparent association constant for the binding at each site and n is the average maximum number of binding sites on protein with the same association constant K. If all the protein sites are equivalent and independent, a plot of Hgm/HgF as a function of Hgm would reveal a linear nature such that the intercept on the Hgm/HgF axis is Knx, as Hgm approaches zero as a limit. And the intercept on the Hg m axis is n as Hgm/HgF approaches zero as a limit deviation from linearity may occur when linking takes place at more than one set of sites with different values of the association constant (Fig 7). The contribution of the electrostatic factors may also produce deviation from the linear nature of the plot. A linear relationship is found to exist between Hgm/HgF and Hgm at both the albumin concentrations, which is an indication of the involvement of only one class of sites that are equivalent and independent (Sendzik et al. 2017). A slight curvature in the lower limit of Scatchard plot may be due to change in the structure of interacting mercury species as its nature of concentration depended on the binding sites for 0.5 and 0.2 percent albumin were found to be 33 and 50, respectively. While the association constant for the single site being 303 and 140 respectively, corresponding to the

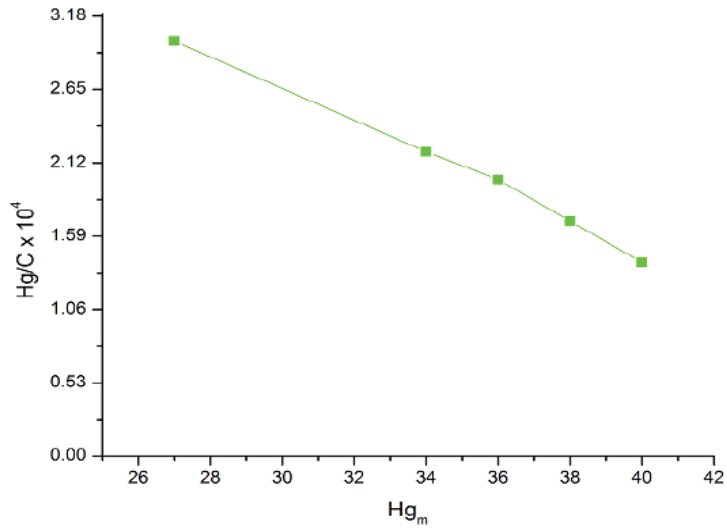

Fig. 7: A plot between Hgm v/s Hgm/C × 10^4 of albumin with Hg at pH = 7.50, T = 30°C, μ = 0.15.

log K value of 2.481 and 2.146 respectively. The free energy changes of the combining sites are found to be only 4.6458 and 4.1852 Kcal/mole.

The difference in the number of binding sites (n) association constant K (log) and free energy at two-protein concentration revealed that the protein molecule possesses different structural organizations in its dilute and concentrated solution. This is a reflection of the availability of different ligand binding sites is less than the total of 53 cationic groups on albumin molecule, but the increased Hgm at pH 9.5 than at 7.50 creates some ambiguity of the mercury ions binding sites. Furthermore, at pH 7.50 the 15 imidazolium would be unprotonated i.e. out of the 53 cationic groups only 38 groups remained protonated. On the other hand, at pH 9.50 both imidazolium and ammonium groups get deprotonated and thus only 24 albumin groups remain protonated (Arora et al. 1983b). As Hg binding is found more at pH 9.50 than at 7.50, hence the ionized carboxyl and phenolic groups have participated in interaction with oxo-mercury (Hg) albumin linkage. The albumin constrains carboxyl group and mercury is known to bind with phenolic oxygens of the metal-binding sites of human serum. Thus, in the case of albumin, the anionic carboxyl and phenolic groups are bound to oxo-mercury rather than the nitrogen-containing groups.

CONCLUSION

Based on the results of the experiments which were conducted to examine the interaction between anionic surfactant/metal ions and protein by measuring the various parameters of the solutions, it is concluded that the interaction of surfactant and protein gives an idea of fundamental understanding of the structure of surfactant-protein complex and the practical applications in every field.

ACKNOWLEDGMENTS

The authors pay their sincere gratitude to UGC for financial assistance as TRF and Principal, Govt. College Kota and S.P.C. Govt. College Ajmer, Rajasthan (India) for providing necessary research facilities to accomplish this study.

REFERENCES

Acharya, S. and Sharma, A.K. 2018a. Interaction Studies of Metals and Surfactant with Protein. ISBN 978-613-8-38751-0, LAP LAMBERT Academic Publisher Germany.

Acharya, S. and Sharma, A.K. 2018b. Binding studies of metal ions and dyes with biopolymers "ISBN 978-613-8-38659-9" LAP LAMBERT Academic Publisher Germany.

Acharya, S. and Sharma, A.K. 2018d. The thermodynamic and pH metric studies on the binding of Hg+2 and Mo+2 with RNA by polarographic and spectrometric techniques Current Phys. Chem., 8(3): 186-193.

Acharya, S. and Sharma, A.K. 2019a. The thermodynamic and binding studies of Hg^{+2} ions with egg protein by polarographic and pH metric techniques. Z. Phy. Chem., 233(8): 1073-1090

Acharya, S. and Sharma, A.K. 2019b. The thermodynamic and pH metric binding studies of Cu^{+2} ions with egg protein by Spectrometric and diffusion current techniques. Z. Phy. Chem. (In Press).

Acharya, S. and Sharma, A.K. 2019c. the binding and viscometric studies of Ni^{+2}, Co^{+2} and Mn^{+2} ions with protein by spectrometric and pH metric techniques. Current Phys. Chem., 9(2): 151-162.

Acharya, S. and Sharma, A.K. 2020a. spectrometric, thermodynamic, pH metric and viscometric studies on the binding of TEALS as surfactant with albumin as biopolymer. Current Phys. Chem., 10(1): 47-64.

Arora, J.P.S., Singh, R.P., Soam, S., Singh, S.P. and Kumar, R. 1983a. Binding of oxovanadium(V) anion to bovine serum albumin, human serum albumin and bovine pancreatic trypsin. Bioelectrochem, Bioererg., 10: 289-300.

Arora, J.P.S., Singh, R.P., Soam, S., Singh, S.P. and Kumar, R. 1983b. The interaction between bovine serum albumin and the molybdate ions. Bioelectrochem. Bioenerg., 10: 441-450.

Barnett, J. P., Blindauer, C. A., Kassaar, O., Khazaipoul, S., Martin, E. M., Sadler, P. J. and Stewart, A.J. 2013. Allosteric Modulation of zinc speciation by fatty acids. Biochimica et Biophysica Acta (BBA) - General Subjects, 1830(12): 5456-5464.

Drabovich, A.P., Pavlou, M.P., Batruch, I. and Diamandis, E.P. 2013. Proteomic and mass spectrometry technologies for biomarker discovery. In: Proteomic and metabolomic approaches to biomarker discovery, Issaq, H.J., and Veenstra, T.D., Eds. Elsevier: London, UK, p. 18-39.

Dudev, T., Dudev, M. and Lim, C. 2003. First-second shell interactions in metal binding sites in proteins: A PDB survey and DFT/CDM calculations. J. Am. Chem. Soc., 125: 3168-3180.

Espósito, B. P. and Najjar, R. 2002. Interactions of antitumoral platinum-group metallodrugs with albumin. Coord. Chem. Rev., 232(1): 137-149.

Frassinetti, S., Bronzetti, G. L., Caltavuturo, L., Cini, M. and Croce, C. D. 2006. The role of zinc in life: A review. JEP(T), 25(3): 597-610.

Harding, M.M. 1999. The geometry of metal-ligand interactions relevant to proteins. Acta Crystallogr. D. Biol. Crystallogr., 55: 1432-1443.

Harding, M.M. 2000. The geometry of metal-ligand interactions relevant to proteins. II. Angles at the metal atom, additional weak metal-donor interactions. Acta Crystallogr. D. Biol. Crystallogr., 56: 857-867.

Harding, M.M. 2004. The architecture of metal coordination groups in proteins. Acta Crystallogr. D. Biol. Crystallogr., 60: 849-859.

Harris, W.R. 1984. Carrano C.J. Binding of vanadate to human serum transferrin. J. Inorg. Biochem., 22: 201-218.

Hawker, R.R., Haines, R.S. and Harper, J.B. 2018. Predicting solvent effects in ionic liquids: Extension of a nucleophilic aromatic substitution reaction on a benzene to a pyridine. J. Phys. Org. Chem., 31: e3730.

Joshi, T. 2018. Interaction of bile salts with Cetylpyridinium chloride: Surface tension and viscosity measurements. Curr. Phys. Chem., 8: 86-94.

Keilin, D. and Mann, T. 1940. Carbonic anhydrase. purification and nature of the enzyme. Biochem. J., 34(8-9): 1163-1176.

Kumar, D. and Rub, M. A. 2018. Interaction of ninhydrin with chromium-glycylglycine complex in the presence of dimeric gemini surfactants. J. Mol. Liquids, 250: 329-334.

Kumar, D., Azum, N., Rub, M. A. and Asiri, A. 2018. Aggregation behaviour of sodium salt of ibuprofen with conventional and gemini surfactant. J. Mol. Liquids, 262: 86-96.

Lu, J., Stewart, A. J., Sadler, P. J., Pinheiro, T. J. T. and Blindauer, C. A. 2008. Albumin as a zinc carrier: properties of its high-affinity zinc-binding site. Biochem. Soc. Trans., 36(6): 1317-1321.

Lyons, T.J. and Eide D.J. 2006. Transport and storage of metal ions in biology. In: Biological Inorganic Chemistry: Structure and Reactivity (ed. Bertini, I., Gray, H., Stiefel, E. and Valentine, J.S.), pp. 57-78.

Scatchard, G., Coleman, J.S. and Shen, A.L. 1957. Physical chemistry of protein solutions. vii. The binding of some small anions to serum albumin. J. Am. Chem., Soc., 79: 12-20.

Sendzik, M., Pushie, M. J., Stefaniak, E. and Haas, K.L. 2017. The structure and affinity of Cu(i) bound to human serum albumin. Inorg. Chem., 56(24): 15057-15065.

Sharma, A.K. Acharya, S. 2018c. The interaction and thermodynamic studies on the binding of congo red dye with collagen protein by polarographic and equilibrium dialysis techniques. Z. Phys. Chem., 233(5), 691-701.

Sharma, A.K. and Acharya, S. 2018. The Interaction and thermodynamic studies on the binding of congo red dye with collagen protein by polarographic and equilibrium dialysis techniques. Z. Phys. Chem., 233(5): 691-701.

Stern, B. R., Solioz, M., Krewski, D., Aggett, P., Aw, T.C., Baker, S., Crump, K., Dourson, M., Haber, L., Hertzberg, R., Keen, C., Meek, B., Rudenko, L., Schoeny, R., Slob, W. and Starr, T. 2007. Copper and human health: biochemistry, genetics, and strategies for modeling dose-response relationships. J. Toxicol. Environ. Health, Part B, 10(3): 157-222.

Stewart, A. J., Blindauer, C. A., Berezenko, S., Sleep, D. and Sadler, P.J. 2003. Interdomain zinc site on human albumin. PNAS, 100(7): 3701-3706.

Tank, P., Sharma, R. and Sharma, A.K. 2018. Micellar features and various interactions of copper soap complexes derived from edible mustard oil in benzene at 303.15 K. Curr. Phys. Chem., 8: 46-57.

Van, Q.N. 2013. Current NMR strategies for biomarker discovery. In: Proteomic and Metabolomic Approaches to Biomarker Discovery, Issaq, H.J., and Veenstra, T.D., Eds. Elsevier: London, UK, pp. 88-119.

Zheng, H., Chruszcz, M., Lasota, P., Lebioda L. and Minor W. 2008. Data mining of metal ion environments present in protein structures. J. Inorg. Biochem., 102: 1765-1776.

Nature Environment and Pollution Technology
An International Quarterly Scientific Journal

p-ISSN: 0972-6268
(Print copies up to 2016)
e-ISSN: 2395-3454

Vol. 19 | No. 2 | pp. 587-601 | 2020

Original Research Paper

https://doi.org/10.46488/NEPT.2020.v19i02.014

Open Access Journal

The Measurement and Influencing Factors of Agricultural Carbon Emissions in China's Western Taiwan Straits Economic Zone

Yihui Chen*(**)(***)† and Minjie Li***

*Anxi College of Tea Science, Fujian Agriculture and Forestry University, Fuzhou 350002, China
**Anxi Cooperative Innovation Centre of Modern Agricultural Industrial Park, Quanzhou 362406, China
***School of Economics and Management, Fuzhou University, Fuzhou 350116, China
†Corresponding author: Yihui Chen; chenyihui@fafu.edu.cn

Nat. Env. & Poll. Tech.
Website: www.neptjournal.com

Received: 01-07-2019
Accepted: 19-09-2019

Key Words:
Agricultural carbon emissions;
WTS economic zone;
OWA aggregation operator;
GTWR

ABSTRACT

Carbon emissions in agricultural production activities have become an important source of accelerating climate warming. At present, low-carbon agriculture is not only an important means to mitigate climate warming, but also a necessary process of transformation from traditional agriculture to modern agriculture. Therefore, to achieve the sustainable development of agriculture in China's Western Taiwan Straits Economic Zone (WTS Economic Zone), the governments should vigorously promote the upgrading and realize the development of low-carbon agriculture. By adopting the latest emission coefficients and the ordered weighted averaging (OWA) aggregation operator, this paper selected agricultural land use, rice paddies, crop production, livestock manure storage and livestock enteric fermentation as the five carbon emission sources, and measured agricultural carbon emissions in the WTS Economic Zone from 2010 to 2017. Thus, from the time perspective, the average agricultural carbon emissions in the WTS Economic Zone showed a fluctuating downward trend, from 762.64 × 10^3 tonnes in 2010 to 710.02 × 10^3 tonnes in 2017. From the spatial perspective, total agricultural carbon emissions among regions are quite different. To further clarify the factors affecting agricultural carbon emissions in the WTS Economic Zone, by applying the geographically and temporally weighted regression (GTWR) model, this paper selected the research and development intensity, the added value of agriculture, the proportion of agricultural labour force, the overall level of urbanization, per capita disposable income of rural residents and per capita arable land areas as the influencing factors, and then measured the direction and degree of the influences on agricultural carbon emissions in different temporal-spatial backgrounds. The results showed that the added value of agriculture, the proportion of agricultural labour force and per capita arable land areas had positive influences on agricultural carbon emissions, while the research and development intensity, the overall level of urbanization and per capita disposable income of rural residents had negative impacts. Although agricultural carbon emissions in the WTS Economic Zone have decreased in recent years, further measures can be taken to effectively reduce agricultural carbon emissions, and ultimately promote the development of low-carbon agriculture according to the results of this study.

INTRODUCTION

Since the 21st century, global warming has attracted widespread attention, and carbon emissions are considered to be the leading cause of global warming, even threatening the survival of mankind. Although carbon emissions are mainly caused by the industrial and the service sector, carbon emissions from the agricultural sector cannot be underestimated. According to the statistics, agricultural activities are responsible for approximate 24% of total anthropogenic carbon emissions and increasing at a fast speed approximate 1% per annum (Lamb et al. 2016, Pellerin et al. 2017). That is, agriculture has brought about problems such as energy consumption and environmental pollution while feeding all human beings. As one of the largest agricultural developing countries on earth, China has a vast territory and a wide range of agricultural regions. Since the adoption of reforms and opening-up policy from 1978, China's agriculture has developed rapidly and became an important aspect to promote social progress and economic development. However, carbon emissions from the agricultural sector should not be neglected. It should be noted that the annual average carbon emissions from agriculture in China increased by 3.15% from 2010 to 2017, accounting for about 17% of the total carbon emissions (Nayak et al. 2015, Wang et al. 2014). Thus, carbon emissions in the agricultural sector in China need to be further considered and effectively controlled. To reduce agricultural carbon emission, estimating agricultural carbon emissions reasonably and accurately, and clarifying

the influencing factors of agricultural carbon are of great significance for formulating reasonable agricultural emission reduction measures.

Fujian is the main part of China's Western Taiwan Straits Economic Zone (WTS Economic Zone). The WTS Economic Zone also includes southwestern Zhejiang, northeastern Guangdong and western Jiangxi. The total land area of the WTS Economic Zone is about 296,800 km^2, the vast majority of which are mountainous and hilly landforms. For instance, Fujian has a total land area of 123,800 km^2, but the mountainous and hilly areas account for more than 80% of the total. Furthermore, per capita land and per capita arable land area in Fujian are both less than half of the national per capita. Hence, to promote the agricultural economic development, a large number of chemical fertilizers, pesticides and plastic sheeting were used in the agricultural practice, resulting in large amounts of carbon emissions, which seriously restricted agricultural sustainable development. Moreover, per capita agricultural carbon emissions in the WTS Economic Zone were higher than the national per capita agricultural carbon emissions as early as 2005. Therefore, in the future, while ensuring agricultural production and farmers' incomes, reducing agricultural carbon emissions is a huge challenge for agriculture in the WTS Economic Zone. Based on the above background, this study systematically calculated agricultural carbon emissions of 20 prefecture-level cities in the WTS Economic Zone from 2010 to 2017, analysed their spatial and temporal characteristics, measured the influencing factors based on geographically and temporally weighted regression (GTWR), and then put forward the countermeasures of agricultural carbon emission reduction combining the influencing factors and regional status.

Compared with the existing literature, the innovative work of this research mainly manifests in the following three aspects. First, based on the data of 20 prefecture-level cities in the WTS Economic Zone, this research measured agricultural carbon emissions by adopting the latest emissions coefficients released by Intergovernmental Panel on Climate Change (IPCC) in 2006 and World Resources Institute (WRI) in 2015, to realize the more scientific and accurate calculation of agricultural carbon emissions. Second, in the comprehensive evaluation of agricultural carbon emissions, previous literature often neglected the weight of the specific index in different periods and only treated it equally, which lead to a large deviation in the final results of the evaluation model. Compared with previous researches, this paper used the ordered weighted averaging (OWA) aggregation operator to determine the weights of years. Thus, the weighted average of agricultural carbon emissions combining time weights and annual emission quantity was adopted to evaluate agricultural carbon emissions comprehensively. Third, because of the huge disparities in production conditions and resource endowments, the level of agricultural economic development, agricultural structure and agricultural production mode show large differences among cities, which lead to significant differences in agricultural carbon emissions in both temporal and spatial distributions. That is, the traditional spatial econometric models will not meet the research requirements any more. This research employed GTWR to analyse the spatial heterogeneity, direction, and degree of the impact of influencing factors on agricultural carbon emissions. On a whole, this paper remeasured agricultural carbon emissions and used OWA aggregation operator to calculate the time weights. Then, by using the GTWR model, this paper analysed the spatiotemporal heterogeneity of the influences of the research and development intensity, the added value of agriculture, the proportion of agricultural labour force, the overall level of urbanization, per capita disposable income of rural residents and the per capita arable land area on agricultural carbon emissions, aiming to provide a reference for the governments of the WTS Economic Zone and other regions to formulate agricultural emission reduction policies.

PAST STUDIES

Measurement of Carbon Emissions in the Agricultural Sector

At present, many existing studies have focused on the evaluation of agricultural carbon emissions. Among them, most studies used the simple summation method and emission coefficients recommended by IPCC Guidelines for National Greenhouse Gas Inventories in 2006 to measure carbon emissions in the agricultural sector (Richards et al. 2016, Tubiello et al. 2013, Peter et al. 2016). For instance, according to the IPCC guidelines, Han et al. (2018) measured the carbon emissions in the agricultural sector in China from 1997 to 2015, Zhang et al. (2019) estimated the agricultural carbon emissions in China's main grain-producing areas during the period from 1996 to 2015, and Tian et al. (2016) estimated carbon emissions from agricultural production in Hunan Province in China during the period from 1995 to 2010. However, the IPCC guidelines neglected soil emissions during the agricultural land-use change in its agricultural inventory (Bell et al. 2014). Besides, carbon emission coefficients released in 2006 is no longer suitable for the current emission situation. That is, different methods applied to estimate carbon emissions may give different results. Therefore, scholars have proposed some novel methods to measure carbon emissions in the agricultural sector. Bell et al. (2014) compared the new approach adopted by the Scottish Government with the IPCC guidelines and national communications. Also, a

novel solution was proposed whereby local governments can measure their carbon emissions independently (Paweł et al. 2018). Yue et al. (2017) estimated the carbon footprint of a range of 6 livestock and 26 crop products, and significant differences between carbon footprints were found across different management patterns and farm scales.

Influencing Factors of Carbon Emissions in the Agricultural Sector

Carbon emissions in the agricultural sector are influenced by many factors from different aspects. For instance, 1 % increase in agricultural economic growth will give rise to a proportional increase in agricultural carbon dioxide emission by 17% (Appiah et al. 2018). The marked changes in the structure of different livestock sectors caused the changes in carbon emission inventories and their spatial distribution (Wei et al. 2017). Besides, agricultural technology (Ismael et al. 2018), land use area per capita (Zhao et al. 2018), agricultural land utilization (Lu et al. 2018), conversion of agricultural fields (Sarauer & Coleman 2018, West & Marland 2003), agricultural income (Zafeiriou et al. 2018) and agricultural populations (Cui et al. 2018) all affect agricultural carbon emissions.

There are abundant research results on the methods of investigating the relationship between agricultural carbon emissions and their influencing factors. The autoregressive distributed lag model (Zafeiriou et al. 2018), the multivariate model (Tian et al. 2016, Cui et al. 2018), the Granger causality test (Khan et al. 2018, Zaman et al. 2012) and the vector error correction models (Mourao & Martinho 2017), the logarithmic mean Divisia index (Xiong et al. 2016a) and the variance decomposition (Ismael et al. 2018) were applied to explore the relationship between agricultural carbon emissions and their influencing factors. In addition, other scholars have applied other novel methods such as the denitrification-decomposition model (Yadav & Wang 2017) and spatial econometric model (Ye et al. 2016) were adopted to explore the relationship between agricultural carbon emissions and their influencing factors.

MATERIALS AND METHODS

Study Area

There are mainly 20 prefecture-level cities in the WTS Economic Zone, including 9 in Fujian, 3 in Zhejiang, 4 in Jiangxi and 4 in Guangdong. On the whole, the WTS Economic Zone is located approximately between the longitude 114°E and 121°E, and between the latitude 22°N and 30°N. Also, the WTS Economic Zone, which borders the Yangtze River Delta in the north and the Pearl River Delta in the south, is an important part of China's coastal economic zone and plays an important role in the layout of China's regional economic development. According to the raw data released in the provincial and municipal statistical yearbooks, the added value of agriculture has reached 421.62 billion Chinese Yuan in 2017, accounting for a proportion of 7.83% of the regional gross product. Additionally, per capita disposable income of rural residents has reached 11,686 Chinese Yuan, which has been increasing every year since 1990. However, the proportion of workers participated in the agricultural sector in the labour force has reached 27.98% by 2017. The increased agricultural growth often comes at the expense of environmental interests in China (Han et al. 2018). That is, at present, in the process of agricultural production in the WTS Economic Zone, which is dominated by pesticides, fertilizers and plastic film, not only high energy consumption and low efficiency are common, but also accompanied by a large amount of carbon emissions, affecting the sustainable development of agriculture. However, there are few researches on carbon emissions in the agricultural sector in the WTS Economic Zone, which leads to some shortcomings in the formulation of agricultural policies to control carbon emissions. The geographical location of the WTS Economic Zone is shown in Fig. 1.

Selection of Measurement Indicators

Because the sources of agricultural carbon emissions are complex and diverse (Zhang et al. 2019), it is necessary to distinguish the sources effectively when measuring carbon emissions. Carbon emissions from the agricultural sector mainly come from greenhouse gas emissions. That means the measurement of carbon emissions in agriculture is transformed into the measurement of greenhouse gas emissions. Then, through conversion coefficients between greenhouse gases and standard carbon, the agricultural carbon emission can be finally obtained. On the whole, the greenhouse gas emissions mainly consist of three types at present: carbon dioxide (CO_2), methane (CH_4) and nitrous oxide (N_2O). According to the data released in the IPCC Fifth Assessment Report in 2006, the greenhouse effect caused by 1 tonne of CO_2 is approximately equivalent to that produced by 0.2727 tonnes of standard carbon. Similarly, 1 tonne of CH_4 approximately emits 6.8182 tonnes of standard carbon and 1 tonne of N_2O approximately emits 81.2727 tonnes of standard carbon.

In the agriculture, there are four major sources of carbon emissions which can also be considered as the source of greenhouse gas emissions: rice paddies and crop production, agricultural land use, livestock breeding and energy consumption in agricultural production, respectively (Cui

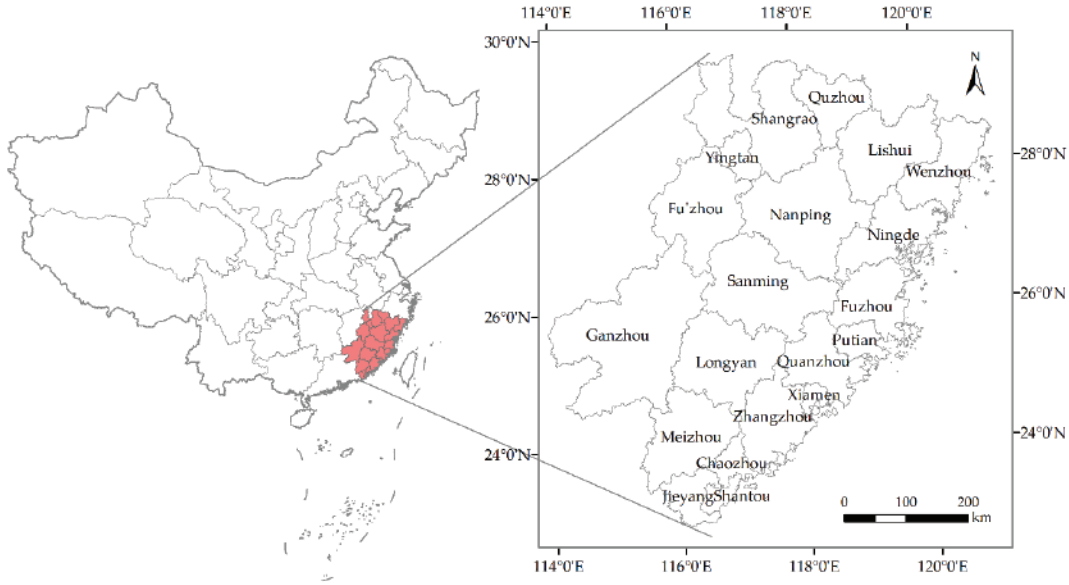

Fig. 1: The geographical location of the WTS Economic Zone.

Table 1: Carbon emission sources and coefficients in agricultural sector.

Sources	Detailed sources (units)	Greenhouse Gases			References
		CO_2	CH_4	N_2O	
agricultural land use	pesticide (kg/kg)	18.09	n/a	n/a	IPCC
	chemical fertilizer (kg/kg)	3.28	n/a	n/a	IPCC
	plastic sheeting (kg/kg)	19.00	n/a	n/a	IPCC
	diesel (kg/kg)	3.17	n/a	n/a	IPCC
	tillage (kg/km^2)	1146.31	n/a	n/a	IPCC
	irrigation (kg/ha)	977.19	n/a	n/a	IPCC
rice paddies	early rice (kg/ha)	n/a	77.39	n/a	IPCC
	late rice (kg/ha)	n/a	525.95	n/a	IPCC
	in-season rice (kg/ha)	n/a	434.66	n/a	IPCC
crop production	paddy rice (kg/ha)	n/a	n/a	0.24	IPCC
	winter wheat (kg/ha)	n/a	n/a	2.05	IPCC
	soybean (kg/ha)	n/a	n/a	0.77	IPCC
	vegetable (kg/ha)	n/a	n/a	4.21	IPCC
	maize (kg/ha)	n/a	n/a	2.53	IPCC
	other dry crops (kg/ha)	n/a	n/a	0.95	IPCC
manure storage (livestock)	dairy (kg/head/year)	n/a	8.33	2.07	WRI
	non-dairy (kg/head/year)	n/a	3.31	0.85	WRI
	goat (kg/head/year)	n/a	0.28	0.11	WRI
	pig (kg/head/year)	n/a	5.08	0.18	WRI
	poultry (kg/head/year)	n/a	0.02	0.01	WRI
	rabbit (kg/head/year)	n/a	0.08	0.02	IPCC
enteric fermentation (livestock)	dairy (kg/head/year)	n/a	89.3	n/a	WRI
	non-dairy (kg/head/year)	n/a	67.9	n/a	WRI
	goat (kg/head/year)	n/a	9.4	n/a	WRI
	pig (kg/head/year)	n/a	1	n/a	WRI
	poultry (kg/head/year)	n/a	n/a	n/a	WRI
	rabbit (kg/head/year)	n/a	0.25	n/a	IPCC

Note: IPCC (Eggleston et al. 2006); WRI (Jiang et al. 2015).

et al. 2018). However, the first three sources of carbon emissions contribute most to agricultural carbon emissions (Johnson et al.2007). Thus, for the convenience of calculation, the carbon emissions from energy consumption in the agricultural sector are negligible. Therefore, agricultural carbon emissions mainly consist of three parts: (1) the CO_2 emissions caused by the agricultural land use; (2) the CH_4 emissions produced from rice paddies and livestock breeding; (3) the N_2O emissions triggered by the crop production and the livestock breeding. Additionally, animals which are not raised and crops which are not planted are negligible. All agricultural carbon emission sources and their corresponding coefficients in the WTS Economic Zone are listed in Table 1.

Based on the existing researches about the carbon emission equation (Xiong et al. 2016a), the total carbon emissions equation in the agricultural sector can be constructed as follows:

$$E = \sum_{i=1}^{n} E_i = \sum_{i=1}^{n} T_i \cdot \mu_i \quad \ldots(1)$$

Where, E represents the total carbon emissions in the agricultural sector; E_i represents the carbon emission of the specific source i, μ_i represents the carbon emission coefficient of the specific source i, and T_i denotes the amount of the specific source i. For the convenience of analysis, it is necessary to convert CO_2, CH_4 and N_2O to the standard carbon based on the conversion coefficient mentioned above.

Selection of Influencing Factors

Research and development intensity (RDI): The investment of research and development (R&D) contributes to the progress and development of the nation's science and technology. Besides, the measurement of R&D investment largely depends on the intensity of R&D, that is, the proportion of R&D to GDP. Thus, to control agricultural carbon emissions, it is necessary and effective for the government and relevant departments to increase the R&D investment intensity (Han et al. 2018, Xiong et al. 2016b). Furthermore, the R&D investment can effectively promote the progress of agricultural technology with more environmentally friendly, enhance the low-carbon scientific and technological content of agricultural products and services, and then reduce the resulting carbon emissions in the agricultural sector. Therefore, the intensity of research and development is applied and noted as RDI to explorer the influence of science and technology on agricultural carbon emissions. However, the agricultural technological investment may take some time to have a significant impact on agricultural carbon emissions, that is, there is a certain time lag effect. Therefore, this paper calculates the influence of RDI, 1-order-lag RDI and 2-order-lag RDI on agricultural carbon emissions, to determine the optimal time lag for the influence of RDI.

Proportion of agricultural labour force (ALF): As a social development factor, the labour force in the agricultural sector can impact carbon emissions from the crop industry, so as to the agricultural carbon emissions. It is worth noting that with the increase of urbanization, ALF continues to decline, and has reached a very low level, such as 2% in Jordan in 2014 (Ismael et al. 2018), 1.4% in the UK in 2010 and less than 1% in 2016 (Zafeiriou et al. 2018). Because of the absolute demand for natural resources and energies from mankind, there is a strong positive correlation between agricultural population and carbon emissions. Furthermore, the reduction of agricultural labour force shows that the demand for the labour force in agriculture is continually decreasing. Thus, agriculture has begun to improve the production technology through technological progress and other means. Therefore, the surplus labour has migrated from the farmland to other non-agricultural sectors of the national economy.

Added value of agriculture (AVA): The gross output values of farming, forestry, animal husbandry and fishery production were used to measure the agricultural economic growth which was generally proven to promote carbon emissions. Also, the standardized output value of farming, the agricultural added value growth (Xiong et al. 2016b) and per capita gross domestic product (Appiah et al. 2018) were also applied as a proxy of agricultural economic growth. The use of the added value of agriculture as economic growth reflects not only the volume of agricultural economic growth but also the speed of agricultural economic development. That is, the added value of agriculture is a combination of absolute growth and relative growth. Therefore, as an important indicator of agricultural economic growth, the added value of agriculture is applied and noted as AVA to explorer the impact of agricultural economic growth on agricultural carbon emissions.

Overall level of urbanization (OLU): There exists a correlation between the urbanization and the proportion of agricultural labour force. That is, as progress increases in urbanization, a large number of agricultural labour force migrate from agriculture to non-agricultural industries. Therefore, the improvement of urbanization level also means that the quality and agricultural technological skills of agricultural labours continuously improve. Thus, the overall level of urbanization noted as OLU reduces the carbon emissions in the agricultural sector. The urbanization is also increasing land competition between agricultural production and urban expansion. However, Hossain showed that there did not exist a long-term relationship between the level of urbanization and the carbon dioxide emission (Hossain 2011). In a word, most researchers

approved that the level of urbanization has a decisive influence on agricultural carbon emissions.

Per capita disposable income of rural residents (DIR): There exists bidirectional causality between real income and carbon emissions. As a proxy of economic growth, per capita disposable income of rural residents, marked as DIR, reflects, in particular, the extent of agricultural economic development. The success of economic development in China comes at the cost of over-exploitation of national resources and a tremendous influence on the environment (Tao et al. 2017). Therefore, the mode for giving up the income growth of rural residents to promote carbon emissions reduction in the agricultural sector will not be implemented in China. That is to say, at this stage, the increase of DIR may lead to an increase in carbon emissions. It should be noted that with the increasing demand for green products, farmers with higher incomes can also promote the consumption of low-carbon products through their buying preferences.

Per capita arable land area (ALA): Agricultural land use and land-use change are two of the important factors impacting agricultural carbon emissions. However, it is difficult to estimate the change in agricultural land use in reality. Thus, agricultural land use, especially the per capita arable land area noted as ALA, has become an important factor related to agricultural carbon emissions to be considered. Because agricultural land use is an important source of agricultural carbon emissions, the reduction of the arable land area means that the agricultural land that can generate carbon emissions is also decreasing. In addition, the change of per capita arable land area will also affect the use of chemical fertilizers, pesticides and plastic sheeting, and then affect agricultural carbon emissions. Furthermore, because of the soil erosion and the like (Cui et al. 2018), and the contaminated farmland, carbon emissions from agricultural land use has been changed.

Research Methodologies

Ordered weighted averaging aggregation operator: The thought of OWA aggregation operator is to determine the corresponding weights according to the decision data itself. Since the introduction of OWA aggregation operator by Yager (1988), researchers have considered and improved the fairness of this weighting method. In this paper, an improved method based on OWA aggregation operator weighting thought proposed by Xu (2005) was applied to determine the time weights, i.e., a smooth and continuous normal distribution density function method. Thus, the problem of weighting specific indicators in different periods, which was ignored in the previous researches of the comprehensive evaluation of agricultural carbon emissions, is solved. When considering the time weights, the fairness of OWA aggregation operator is more scientific and reasonable than that of the traditional arithmetic average. The specific steps of OWA aggregation operator can be listed as follows:

(1) Assuming that there are m regions and n years; in addition, E_{ij} denotes the total carbon emissions in the agricultural sector in the specific region i in the specific year j. Firstly, summing up the specific value of E_{ij} in each year, then the average value can be obtained as follows:

$$\bar{E}_j = \frac{1}{m}\sum_{i=1}^{m} E_{ij} \quad \ldots(2)$$

(2) Then, assuming that the initial weight of total carbon emissions in the specific year is $1/n$, and the average value and standard deviation of E_{ij} are obtained as follows:

$$\bar{E} = \frac{1}{n}\sum_{j=1}^{n} \bar{E}_j \quad \ldots(3)$$

$$\sigma = \sqrt{\frac{\sum_{j=1}^{n}(\bar{E}_j - \bar{E})^2}{n}} \quad \ldots(4)$$

(3) Thirdly, standardizing the total carbon emissions employing the average value and standard deviation mentioned above, and the calculation equation can be obtained as follows:

$$\beta_j = \frac{\bar{E}_j - \bar{E}}{\sigma} \quad \ldots(5)$$

(4) Then, using the commonly accepted standard normal distribution density function, then the corresponding values of α_j under the different β_j can be obtained as follows:

$$\alpha_j = \varphi(\beta_j) = \frac{1}{\sqrt{2\pi}} e^{-\frac{\beta_j^2}{2}} \quad \ldots(6)$$

(5) Finally, normalizing the obtained value of α_j to calculate the time weights by using the formula as follows:

$$\omega_j = \frac{\alpha_j}{\sum_{j=1}^{n}\alpha_j} \quad \ldots(7)$$

Geographical and temporal weighted regression: The application of traditional linear regression model has a large deviation due to the neglect of spatial factors. Thus, the application of a novel method, the geographically weighted regression model (GWR), solves some of the above problems in the previous researches (Brunsdon et al. 1996). Based on adding the geographical location into the regression coefficient, and the estimation of regression coefficient functions,

the GWR model can overcome the spatial heterogeneity among geographic units and break through the limitation of the constant coefficient model. However, GWR can only regress the cross-sectional data. That is, GWR model only embeds geographic location parameters into the model, and then forms a model with spatial characteristics, without considering the temporal characteristics of the actual problem (Li et al. 2019). Thus, as an extension of the weighted regression model of spatial geography, GTWR, is used to analyse the spatial and temporal chrematistics by incorporating the temporal and spatial characteristics of data into the regression model for analysis. GTWR remains the advantage of a high fitting degree of a local regression model compared with GWR. The general model of GTWR can be constructed as follows (Li et al. 2019):

$$y_i = \beta_0(u_i, v_i, t_i) + \sum_{k=1}^{d} \beta_k(u_i, v_i, t_i) x_{ik} + \varepsilon_i \quad \ldots(8)$$

Where, y_i represents the observations of the total carbon emissions in the agricultural sector, and x_{ik} is the influencing factors at the specific observation point (u_i, v_i, t_i). β_0 is the coefficient of the constant. (u_i, v_i, t_i) represents the longitude and latitude coordinates u_i and v_i, and the observation time point t_i of the observation point. $\beta_k(u_i, v_i, t_i)$ denotes the unknown parameter at the specific observation point (u_i, v_i, t_i), and is the arbitrary function of (u_i, v_i, t_i). In addition, ε_i is an independent and identically distributed error term and is usually assumed to obey the $N(0,\sigma^2)$ distribution. Besides, the parameters are estimated by the local weighted least squares method. That is, for a given specific observation point, the observation values near the point are given larger weights, while the observation values far from the point are given smaller weights. By minimizing the weighted sum of squares between the observed values and the fitted values, the estimated values of the parameters can be obtained.

RESULTS

Data Sources

Various sources of carbon emissions in the agricultural sector are chosen to measure total carbon emissions. Therefore, the carbon emissions from agricultural land use, rice and crop growth process and livestock breeding, as well as their carbon emission coefficients are selected in this study. Among them, the emission coefficients mainly come from the coefficients released by WRI in 2015 and IPCC in 2006. Furthermore, the raw data on the amount of carbon emission sources in the agricultural sector of the provinces from 2010 to 2017 comes from the provincial statistical yearbooks and prefectural-level cities statistical yearbooks. This study does not deal with the original data in any other way. In the end, we obtain the raw data covering 20 prefectural-level cities for 8 years, totalling 160 samples.

Measurement of Agricultural Carbon Emissions

Time variation of agricultural carbon emissions: The total agricultural carbon emissions calculated based on the carbon emission coefficients are shown in Table 2. As seen in Table 2, the average agricultural carbon emissions in the WTS Economic Zone showed a fluctuating downward trend, from 762.64×10^3 tonnes in 2010 to 710.02×10^3 tonnes in 2017, with an average annual growth rate of -0.86%. In addition, the time-variation process of average agricultural carbon emissions showed four-stage characteristics of "rise-fall-rise-fall". More concretely, agricultural carbon emissions reached the maximum value of 774.98×10^3 tonnes in 2013 and reached the minimum value of 710.02×10^3 tonnes in 2017. Furthermore, agricultural carbon emissions in which has always been in a downward trend from 2010 to 2017 occur in Putian, Wenzhou and Lishui. Agricultural carbon emissions in Fu'zhou and Ganzhou from 2010 to 2017 present a pattern of "N" shape. By contrast, that of in Fuzhou, Zhangzhou, Nanping, Longyan, Ningde, Quzhou and Shangrao from 2010 to 2017 show an evolutionary trend of the inverse "V" shape, while that of in Xiamen and Quanzhou is "V" shape. In addition, agricultural carbon emissions in Shantou, Jieyang, Chaozhou and Meizhou have a changing pattern of "M" shape, while that of in Sanming and Yingtan have fluctuated. Although some progress has been made during the period in agricultural sustainable development in Fujian, it is still an arduous task at present.

Spatial variation of agricultural carbon emissions: To fully consider the time dimension and ensure that the carbon emissions of different cities can be comprehensively compared, average agricultural carbon emissions calculated based on OWA aggregation operator are listed in the last column of Table 2. That is, these values are calculated by weighting the year first, and then multiplying the carbon emissions of each year and then summing them up. The weights of each year calculated based on OWA aggregation operator are listed in the last row of Table 2. As seen in Table 2, the top five prefecture-level cities of agricultural carbon emissions are Ganzhou, Shangrao, Fu'zhou, Zhangzhou and Nanping, accounting for 51.38% of the total agricultural carbon emissions in the WTS Economic Zone. By contrast, the last five prefecture-level cities of agricultural carbon emissions are Xiamen, Chaozhou, Putian, Shantou and Meizhou, accounting for only 8.51% of total agricultural carbon emissions in the WTS Economic Zone. Among them, the average agricultural carbon emission in Ganzhou is 2122.42×10^3 tonnes,

Table 2: Average agricultural carbon emissions (AACE) in WTS Economic Zone (units: 10^3 tonnes carbon).

Cities	2010	2011	2012	2013	2014	2015	2016	2017	*AACE*
Chaozhou	258.85	287.51	278.66	264.75	259.94	259.62	259.67	247.07	265.91
Fu'zhou	1497.02	1506.76	1508.06	1492.76	1489.49	1477.22	1502.76	1512.78	1495.55
Fuzhou	748.13	761.97	754.29	748.75	741.54	728.36	658.57	645.79	734.16
Ganzhou	2074.76	2089.12	2099.13	2129.65	2139.46	2168.17	2144.4	2157.54	2122.42
Jieyang	409.29	410.64	408.86	402.16	404.92	403.14	398.48	384.35	405.13
Lishui	375.31	368.07	365.53	364	345.4	337.62	318.43	310.56	352.43
Longyan	844.88	847.72	844.65	844.59	835.18	769.2	716.58	715.98	813.5
Meizhou	337.62	340.1	347.05	346.25	343.05	350.68	348.22	336.39	344.4
Nanping	1053.41	1065.75	1065.76	1299.81	1088.8	1086.94	1145.93	933.96	1099.56
Ningde	513.09	515.18	511.42	505.39	497.19	489.83	478.49	474.64	500.88
Putian	328.08	322.95	311.75	299.66	278.62	278.43	267.48	228.45	296.14
Quanzhou	705.85	691.92	677.6	663.43	640.98	633.5	628.09	655.61	662.42
Quzhou	552.27	574.68	578.98	553.93	479.65	443.69	422.27	414.03	509.81
Sanming	914.94	921.81	907.74	906.69	901.55	903.8	770.21	779.9	891.01
Shangrao	1847.69	1870.82	1880.33	1913.7	1914.66	1919.65	1902.57	1890.62	1892.82
Shantou	279.48	304.96	309.37	307.77	311.55	312.75	312.92	288.5	304.85
Wenzhou	857.63	841.71	837.06	812.57	777.19	760.31	750.61	723.04	802.49
Xiamen	87.28	86.33	86.19	82.6	66	62.09	61.48	63.72	75.04
Yingtan	391.39	388.04	390.67	395.45	394.15	396.71	397.2	393.49	393.35
Zhangzhou	1175.91	1181.57	1181.36	1165.64	1155.07	1143.35	1131.38	1043.93	1159.13
Average	762.64	768.88	767.22	774.98	753.22	746.25	730.79	710.02	n/a
Weights (%)	15.67	12.76	13.60	9.56	17.97	17.38	10.75	2.31	n/a

which is equivalent to 28.28 times of that of in Xiamen, 75.04×10^3 tonnes, which is the smallest. It can be found that the total agricultural carbon emissions among regions are quite different.

Time variation of the structure of agricultural carbon emission sources: The compositions and sources of agricultural carbon emission vary from year to year, as shown in Table 3. Among them, agricultural carbon emissions from rice paddies accounted for the largest proportion, accounting for 42.82% in 2013. By contrast, agricultural carbon emissions from crop production accounted for the smallest proportion, accounting for only 3.73% in 2012. Besides, from the perspective of greenhouse gases, the proportion of CH_4 emitted by the five main carbon emission sources was the highest, which can up to 58.94%, and the proportion of N_2O emitted was the smallest, which can down to 9.32%.

Table 3: The proportion of sources of agricultural carbon emissions in WTS Economic Zone (units: %).

Sources	2010	2011	2012	2013	2014	2015	2016	2017
Agricultural land use	31.69	32.08	32.26	31.92	33.03	33.51	34.11	33.88
Rice paddies	42.75	42.14	41.92	42.82	41.90	42.10	41.72	42.77
Crop production	3.76	3.79	3.73	3.77	3.93	4.02	3.92	3.80
Livestock: manure storage	13.04	13.39	13.50	13.04	12.61	11.97	12.22	11.84
Livestock: enteric fermentation	8.76	8.60	8.59	8.45	8.53	8.40	8.03	7.71
CO_2	31.69	32.08	32.26	31.92	33.03	33.51	34.11	33.88
CH_4	58.94	58.31	58.15	58.61	57.44	57.02	56.41	56.80
N_2O	9.37	9.61	9.59	9.47	9.53	9.47	9.48	9.32

Influencing Factors on Agricultural Carbon Emissions

The descriptive statistics of all selected variables used in GTWR model, including total carbon emissions and its influencing factors, are shown in Table 4. The standard deviations of some variables reflect that there exist great differences among the cities, that is, the deviation trend is noticeable. For instance, the maximum of ALF is 178.23 times of the minimum, while that of AVA, AACE and RDI reach 35.63, 35.27 and 33.31 times of the minimum respectively. Besides, the concentration trends of DIR, ALF and OLU are more obvious than the dispersion trends. Therefore, the maximum values of DIR and OLU are only 6.02 and 2.40 times of the minimum respectively. It should be noted that to overcome the defect of heteroskedasticity, the original data used in GTWR are applied in the logarithmic form without changing the nature and correlation of original data. Thus, the coefficients of the GTWR model in this paper measure the elasticity of dependent variables to the independent variable, that is, the percentage of the dependent variable change when the independent variable changes by 1%.

This paper applied the GTWR model to measure the direction and degree of factors' influences on agricultural carbon emissions. The descriptive statistics of regression coefficients in the GTWR model are shown in Table 5. As seen in Table 5, the regression coefficient estimation of GTWR model calculated by ArcGIS 10.4.1 shows great heterogeneity of total carbon emissions in the agricultural sector among cities in geographically and temporal attributes. Thus, the GTWR model is suitable for estimating the regression coefficients because of the obvious spatial and temporal non-stationary characteristics of agricultural carbon emissions. Besides, the goodness of fit of the GTWR model is also much better than other models, such as the GWR model and the Ordinary Least Square (OLS). For instance, the value of R^2 of the GTWR model is as high as 0.9957 which is very close to 1, while that of the GWR model and the OLS model only reach 0.9929 and 0.8303 respectively. The estimated regression coefficients reflect the influencing direction and degree of each selected factor on agricultural carbon emissions in different cities in each year. Furthermore, the optimal bandwidth used in GTWR model is determined based on the spatial-temporal weight function of the Gauss function method and the cross-validation. The geographical distribution of regression coefficients of each influencing factor in 2010, 2014 and 2017 are shown in Fig. 2 respectively.

The influence of RDI on agricultural carbon emissions: Considering that the influence of RDI on agricultural carbon emissions may have a time lag period, this paper examines the effects of RDI, 1-order-lag RDI and 2-order-lag RDI on agricultural carbon emissions. The results show that the regression coefficients of RDI and 2-order-lag RDI are not statistically significant, and the regression coefficients of 1-order-leg RDI are significantly negative at the level of 1%.

Table 4: The descriptive statistics of raw data of variables used in the GTWR model.

Variables	Units	Mean	SD	Minimum	Q_1	Median	Q_3	Maximum
AACE	10^3 tonnes	751.75	544.56	61.48	345.61	603.53	930.92	2168.17
RDI	%	1.06	0.91	0.13	0.59	0.76	1.14	4.33
ALF	%	30.31	11.21	0.26	27.08	32.92	38.37	46.34
AVA	10^8 CNY	112.73	63.23	9.69	70.34	101.60	144.23	345.22
OLU	%	55.96	11.09	37.20	48.45	53.55	63.15	89.10
DIR	10^3 CNY	11.60	3.85	4.18	8.84	11.38	13.88	25.15
ALA	ha / person	0.04	0.02	0.01	0.03	0.04	0.06	0.09

Table 5: The descriptive statistics of the estimated results of regression coefficients in the GTWR model.

Variables	Mean	Minimum	Q_1	Median	Q_3	Maximum	SE	t	p-value
Intercept	6.1626	-37.0190	-0.5719	7.1805	12.8774	43.8987	179.024	5.508	0.000
LNRDI	-0.4353	-4.7932	-0.8848	-0.2211	-0.1746	4.2874	16.208	-4.297	0.000
LNALF	0.0241	-0.5754	-0.0467	0.0115	0.0791	0.6831	2.528	1.765	0.081
LNAVA	0.7532	-0.0293	0.2959	0.7100	1.1292	2.0646	6.608	18.249	0.000
LNOLU	-0.6123	-2.7852	-0.9478	-0.3873	-0.1537	0.9413	9.136	-10.728	0.000
LNDIR	-0.4224	-5.5209	-1.3634	-0.5564	0.7064	5.4261	22.112	-3.057	0.003
LNALA	0.2268	-2.5617	-0.2484	0.0888	0.9536	3.0768	13.296	2.728	0.007

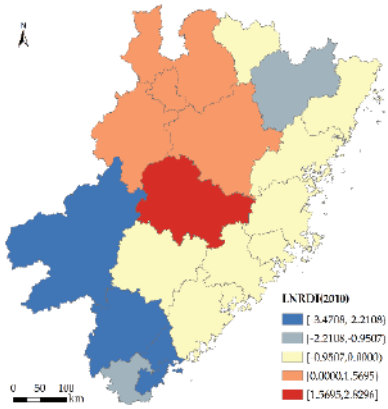

(**a**)-2010

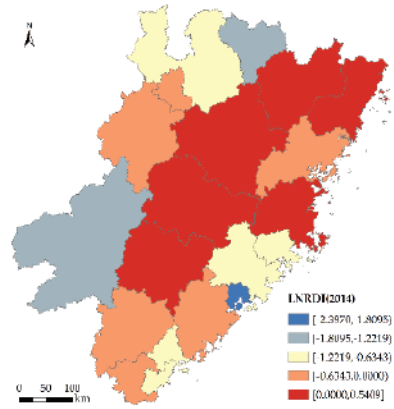

(**a**)-2014

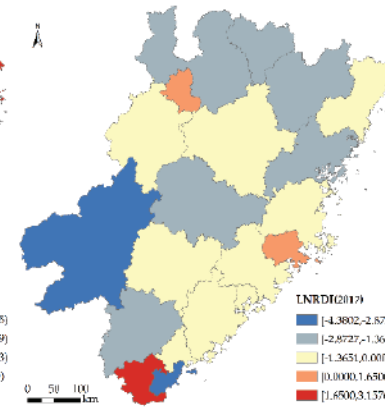

(**a**)-2017

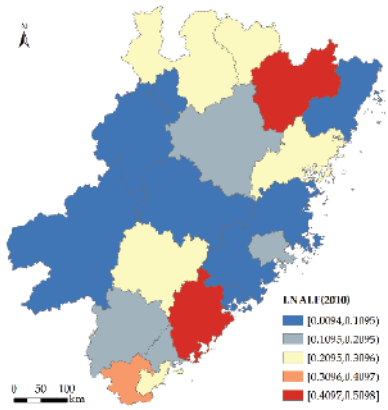

(**b**)-2010

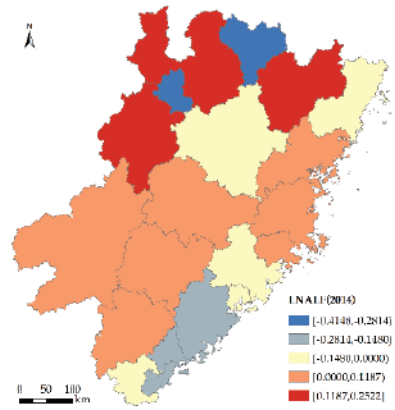

(**b**)-2014

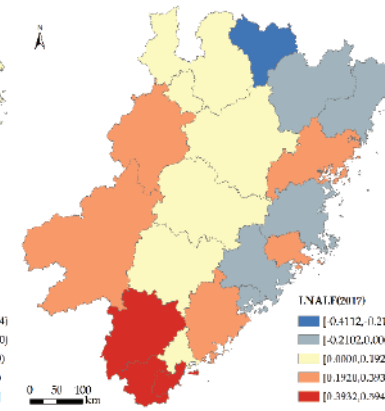

(**b**)-2017

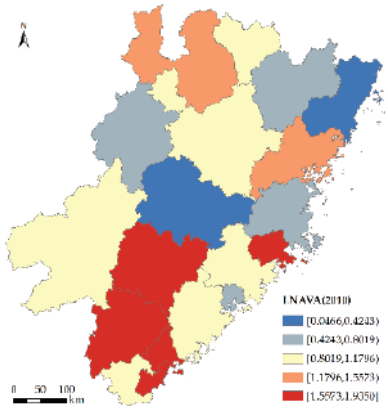

(**c**)-2010

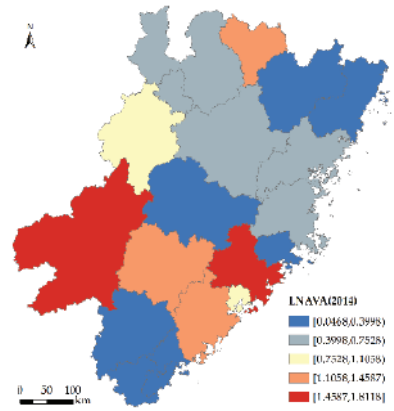

(**c**)-2014

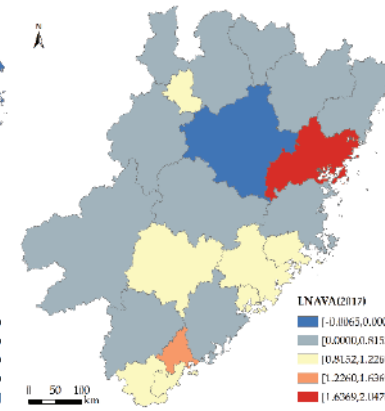

(**c**)-2017

Fig. cont....

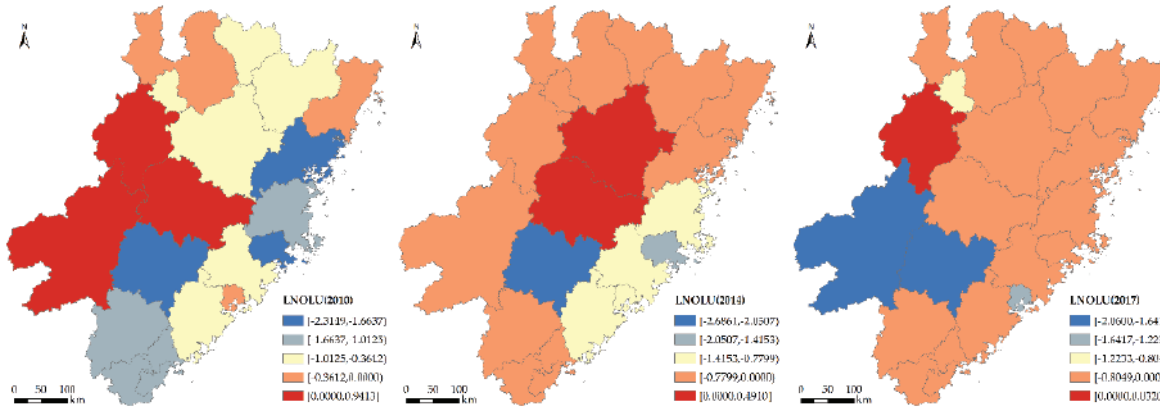

(**d**)-2010 (**d**)-2014 (**d**)-2017

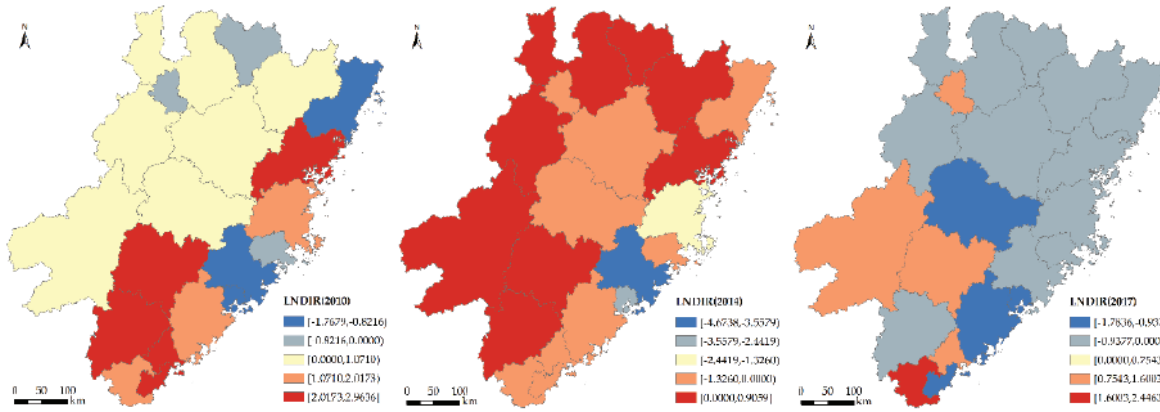

(**e**)-2010 (**e**)-2014 (**e**)-2017

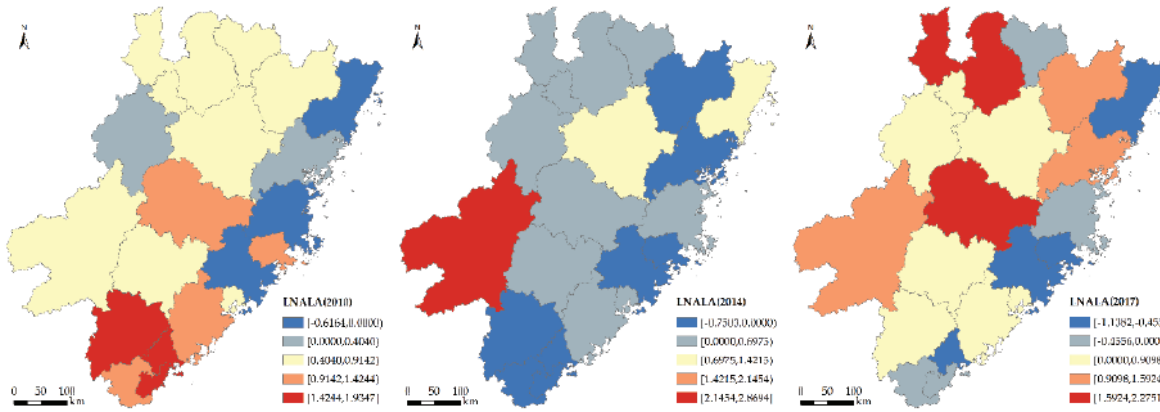

(**f**)-2010 (**f**)-2014 (**f**)-2017

Fig. 2: Spatial distribution of regression coefficients in 2010, 2014 and 2017.

Therefore, the RDI selected in this paper is the 1-order-lag RDI. As shown in Table 5, the impact of 1-order-lag RDI on agricultural carbon emissions is mainly negative, which is in good agreement with the expectations. That is, when RDI increase by 1%, the agricultural carbon emissions will decrease by 0.4353% on average in the opposite direction. Specifically, as shown in Fig. 2(a). from the time perspective, in 2010, the RDI of Fu'zhou, Nanping, Sanming, Shangrao and Yingtan promoted agricultural carbon emissions while that of only in Jieyang, Putian and Yingtan promoted agricultural carbon emissions in 2017. In addition, RDI in other cities in each year has effectively restrained agricultural carbon emissions. Besides, from the spatial perspective, in 2010, RDI of Ganzhou and Chaozhou had great influences on agricultural carbon emissions while that of in 2014 were Quzhou and Ganzhou, and that of in 2017 were Ganzhou and Shantou. The southern cities are relatively advanced in agricultural science and technology compared with those in the northern cities. Thus, governments and enterprises can invest heavily in research and development, and effectively control agricultural carbon emissions through technological improvements.

The influence of ALF on agricultural carbon emissions: The results in Table 5 and Fig. 2(b) showed that ALF had a significant positive impact on agricultural carbon emissions at a significant level of 10%. That is, when ALF increase by 1%, agricultural carbon emissions will increase by 0.0241% on average in the same direction. In 2010, ALF in all 20 prefecture-level cities promoted agricultural carbon emissions. However, in 2014 and 2017, ALF in some cities, such as Xiamen, Quzhou, Fuzhou and Quanzhou, reduced agricultural carbon emissions. One possible explanation is that in the process of the rapid development of agricultural modernization, these above cities have trained and introduced agricultural technicians and technological professionals, improved the level of agricultural science and technology, and thus reduced agricultural carbon emissions. From the spatial perspective, ALF in cities such as Fu'zhou, Zhangzhou, Yingtan and Jieyang accounts for about 40% of the total labour force, which has a great impact on agricultural carbon emissions. By contrast, ALF in Xiamen, Fuzhou and Quanzhou only accounts for about 20% of the total labour force, which has little impact on agricultural carbon emissions. The conclusion may be mainly due to the different orientation and role of different cities in regional development. For instance, some cities mainly develop agriculture to provide agricultural products and services for the surrounding cities while others develop services and manufacturing.

The influence of AVA on agricultural carbon emissions: As seen in Table 5, AVA mainly promotes the average increases of carbon emissions in the agricultural sector by 0.7532% when AVA increases by 1%. As shown in Fig. 2(c), the positive effect of AVA on agricultural carbon emissions in most cities is obvious. One explanation might simply be that the success of the rapid growth of agriculture at the cost of over-exploitation of natural resources and tremendous impact on the environment, especially in Longyan, Quanzhou and Ningde. However, the negative correlation between AVA and total agricultural carbon emissions will become the trend in the future. For instance, AVA showed a negative influence on agricultural carbon emissions in Nanping in 2017. As the main grain producing area in Fujian, Nanping realizes the organic production of agricultural products, the effective control of land use, and the wide application of the Internet of Things in agriculture. Therefore, it is an effective way for governments and enterprises to increase the added value of agriculture to achieve agricultural sustainable development through the improvement and promotion of agricultural technologies.

The influence of OLU on agricultural carbon emissions: The urbanization level is often accompanied by a large number of infrastructure investment, the industrial transfer and agglomeration, and the population migration which has an impact on energy consumption and agricultural carbon emissions. As shown in Table 5, the negative impact of OLU on agricultural carbon emissions is significant in most of the cities. That is, when OLU increase by 1%, the agricultural carbon emissions will decrease by 0.6123% on average in the opposite direction. The positive influence of OLU on agricultural carbon emissions only existed in Fu'zhou, Ganzhou and Sanming in 2010, narrowing to 2 cities including Nanping and Sanming in 2014 and narrowing to 1 city only including Fu'zhou in 2017. As a whole, the overall level of urbanization of southern cities is higher than that of northern cities, that is, the industrial structure, the environmental regulation and the technical level of southern cities of the WTS Economic Zone are better than that of northern cities. Therefore, northern cities should pay more attention to coordinating the relationship between urbanization and agricultural modernization, then realize the synchronous development of agricultural modernization and the transformation of agricultural production organizations.

The influence of DIR on agricultural carbon emissions: On the whole, as shown in Table 5 and Fig. 2(e), DIR has a negative influence on agricultural carbon emissions. When DIR changes by 1%, the average change of agricultural carbon emissions is 0.4224% in the opposite direction. In 2010, DIR in 6 cities curbed agricultural carbon emissions, expanding to 12 cities in 2014 and 15 cities in 2017. From the perspective of spatial distribution, the regression coeffi-

cients of DIR in Putian, Quanzhou, Wenzhou and Xiamen were all negative in 2010, 2014 and 2017 while that of in Ganzhou and Longyan were positive. However, other cities have experienced a transformation process of positive-negative influence. The increase of DIR could have promoted the choice of green agricultural products and prompted agricultural producers to reduce chemical fertilizers and pesticides to realize sustainable development. Therefore, the rural residents' rational consumption concept including moderate consumption and green consumption needs to be guided, cultivated and strengthened by governments and enterprises.

The influence of ALA on agricultural carbon emissions: Combining the results of Table 5 and Fig. 2(f), ALA mainly promotes the average increases of carbon emissions in the agricultural sector by 0.2268% when ALA increases by 1%. From the original data, although the per capita arable land area of cities has little difference, the impact of ALA on agricultural carbon emissions has obvious spatial and temporal differences. On the whole, the positive influence of ALA on agricultural carbon emissions mainly exists in the western cities, especially in Ganzhou and Shangrao. By contrast, Quzhou, Lishui and Wenzhou which located in the northern part became the cities that arable land area exists a negative impact on agricultural carbon emissions. The results further prove that the agricultural development of many cities is at the expense of environmental interests, that is, increasing arable land means increasing agricultural carbon emissions. Therefore, enhancing the capability of deep soil to store the carbons and scientifically changing the way of land cultivation are effective ways to reduce carbon emissions and ultimately achieve sustainable development.

DISCUSSION AND CONCLUSIONS

This paper remeasured the total agricultural carbon emissions based on the emission coefficients and OWA aggregation operator in the WTS Economic Zone during the period from 2010 to 2017. Moreover, the GTWR model was applied to empirically test the influencing factors on agricultural carbon emissions. By and large, the main findings could be listed as follows. First, from the temporal dimension, although total agricultural carbon emissions in most cities showed a downward trend in the WTS Economic Zone. Second, from the spatial dimension, Fu'zhou, Shangrao and Ganzhou have relatively large agricultural carbon emissions, while Xiamen, Chaozhou and Putian have relatively small agricultural carbon emissions. Finally, the empirical results of the GTWR model indicated that the influences on agricultural carbon emissions had the characteristics of geospatial nonstationarity. Based on the above results, this paper puts forward constructive suggestions on the development of low-carbon agriculture and reduction of agricultural carbon emissions in the WTS Economic Zone.

(1) Low-carbon agriculture is based on science and technology, so to reduce agricultural carbon emissions, it is necessary to strengthen innovative research in agricultural science and technology. Although the total amount of investment in agricultural science and technology in the cities of the WTS Economic Zone has increased, the intensity of investment is still insufficient. For instance, although China's agricultural science and technology investment accounted for 2.14% of GDP in 2017, Fujian's agricultural science and technology investment accounted for only 0.96% of GDP. Therefore, in the process of constructing the WTS Economic Zone, the governments need to continuously increase investment in agricultural science and technology, support basic and frontier agricultural scientific research, and accelerate the popularization and application of agricultural technology achievements, e.g., reduce agricultural carbon emissions by promoting intermittent irrigation in paddy fields and improving livestock collection and storage technology. Moreover, organic agriculture may present a positive role in mitigating the environmental burden.

(2) The agricultural industry structure needs to be adjusted and optimized to vigorously develop modern agriculture and ecological agriculture, and finally improve the multifunction of agricultural production. Under the circumstances of ensuring food security, the planting industry is an important breakthrough in reducing agricultural carbon emissions. The interrelated main bodies need to optimize the planting structure, reduce the crop cultivation with large energy consumption and chemical input, and actively adopt new varieties with low carbon, high yield and stress resistance. Besides, combining the advantages of resources in different cities, governments and enterprises should vigorously cultivate characteristic agriculture and take the road of agricultural modernization. Besides, the development of urban agriculture is of great significance to the reduction of agricultural carbon emissions.

(3) The government should effectively control the process of urbanization, improve the basic quality of agricultural personnel, and deepen the concept of green consumption. The governments should strengthen the training of rural residents' skills and environmental awareness of modern agriculture, then train a group of practical talents with both knowledge and quality to meet the needs of modern low-carbon agriculture construction. Furthermore, in the process of urbanization, the governments should increase the investment of infrastructure, and provide necessary conditions for the realization

of agricultural scale and industrialization. Thus, the governments should correctly handle the nurturing relationship between industry and agriculture, actively implement the strategy of urban-rural integration, and ultimately realize the coordinated development of urbanization and agricultural modernization.

(4) As a regional concept, the WTS Economic Zone aims to highlight the overall regional advantages through resource integration and mutual exchanges and links. Therefore, in the process of developing low-carbon agriculture and reducing agricultural carbon emissions, exchanges and integration are indispensable. For 20 prefecture-level cities in the WTS Economic Zone, agricultural cooperation and linkages can be strengthened in terms of variety, technology and processing. Besides, the WTS Economic Zone can take advantage of the geographical advantages of Taiwan Province, introduce advanced planting technology and new agricultural varieties, learn new agricultural management mode, to effectively reduce agricultural carbon emissions.

ACKNOWLEDGEMENTS

This research was funded by The Ministry of Agriculture and Rural Affairs: The Construction of Anxi Modern Agricultural Industrial Park (Grant No. KMD18003A) and The Social Science Planning Project of Fujian Province (Grant No. FJ2018C045) in China.

REFERENCES

Appiah, K., Du, J.G. and Poku, J. 2018. Causal relationship between agricultural production and carbon dioxide emissions in selected emerging economies. Environmental Science and Pollution Research, 25: 24764-24777.

Bell, M.J., Cloy, J.M. and Rees, R.M. 2014. The true extent of agriculture's contribution to national greenhouse gas emissions. Environmental Science & Policy, 39: 1-12.

Brunsdon, C., Fotheringham, A.S. and Charlton, M.E. 1996. Geographically weighted regression: A method for exploring spatial nonstationarity. Geographical Analysis, 28(4): 281-298.

Cui, H., Zhao, T. and Shi, H. 2018. STIRPAT-based driving factor decomposition analysis of agricultural carbon emissions in Hebei, China. Polish Journal of Environmental Studies, 27(4): 1449-1461.

Eggleston, S., Buendia, L., Miwa, K., Ngara, T. and Tanabe, K. 2006. 2006. IPCC guidelines for national greenhouse gas inventories (Vol. 4). Hayama, Japan: Institute for Global Environmental Strategies.

Han, H.B., Zhong, Z.Q., Guo, Y., Xi, F. and Liu, S.L. 2018. Coupling and decoupling effects of agricultural carbon emissions in China and their driving factors. Environmental Science and Pollution Research, 25: 25280-25293.

Hossain, M.S. 2011. Panel estimation for CO_2 emissions, energy consumption, economic growth, trade openness and urbanization of newly industrialized countries. Energy Policy, 39(11): 6991-6999.

Ismael, M., Srouji, F. and Boutabba, M.A. 2018. Agricultural technologies and carbon emissions: Evidence from Jordanian economy. Environmental Science and Pollution Research, 25(11): 10867-10877.

Jiang, X., Fang, W., Zhuang, G., Bai, W., Zhu, S., Lu, L. and Feng, J. 2015. Greenhouse gas accounting tool for Chinese cities (Version 2.0). World Resources Institute.

Johnson, M.F., Franzluebbers, A.J., Weyers, S.L. and Reicosky, D.C. 2007. Agricultural opportunities to mitigate greenhouse gas emissions. Environmental Pollution, 150(1): 107-124.

Khan, M.T.I., Ali, Q. and Ashfaq, M. 2018. The nexus between greenhouse gas emission, electricity production, renewable energy and agriculture in Pakistan. Renewable Energy, 118: 437-451.

Lamb, A., Green, R., Bateman, I., Broadmeadow, M. and Balmford, A. 2016. The potential for land sparing to offset greenhouse gas emissions from agriculture. Nature Climate Change, 6(5): 488-492.

Li, M., Wang, J. and Chen, Y. 2019. Evaluation and influencing factors of sustainable development capability of agriculture in countries along the Belt and Road Route. Sustainability, 11(7): 2004.

Lu, X., Kuang, B., Li, J., Han, J. and Zhang, Z. 2018. Dynamic evolution of regional discrepancies in carbon emissions from agricultural land utilization: Evidence from Chinese provincial data. Sustainability, 10(2): 552.

Mourao, P.R. and Domingues Martinho, Vítor. 2017. Erratum to: Portuguese agriculture and the evolution of greenhouse gas emissions—can vegetables control livestock emissions? Environmental Science and Pollution Research, 24: 16107-16119.

Paweł, Wiśniewski and Kistowski, M. 2018. Assessment of greenhouse gas emissions from agricultural sources in order to plan for needs of low carbon economy at local level in Poland. Geografisk Tidsskrift-Danish Journal of Geography, 118(2): 123-136.

Pellerin, S., Bamière, Laure, Angers, D., Béline, Fabrice, Benoit, M. and Butault, J.P. 2017. Identifying cost-competitive greenhouse gas mitigation potential of French agriculture. Environmental Science & Policy, 77: 130-139.

Peter, C., Fiore, A., Hagemann, U., Nendel, C. and Xiloyannis, C. 2016. Improving the accounting of field emissions in the carbon footprint of agricultural products: A comparison of default IPCC methods with readily available medium-effort modeling approaches. The International Journal of Life Cycle Assessment, 21(6): 791-805.

Richards, M., Metzel, R., Chirinda, N., Ly, P., Nyamadzawo, G. and Duong Vu, Q. 2016. Limits of agricultural greenhouse gas calculators to predict soil N_2O and CH_4 fluxes in tropical agriculture. Scientific Reports, 6(1).

Sarauer, J.L. and Coleman, M.D. 2018. Converting conventional agriculture to poplar bioenergy crops: Soil greenhouse gas flux. Scandinavian Journal of Forest Research, 33(8): 781-792.

Tao, F., Zhang, H., Hu, J. and Xia, X.H. 2017. Dynamics of green productivity growth for major Chinese urban agglomerations. Applied Energy, 196: 170-179.

Tian, J.X., Yang, H.L., Xiang, P.A., Liu, D.W. and Li, L. 2016. Drivers of agricultural carbon emissions in Hunan province, China. Environmental Earth Sciences, 75(2): 121.

Tubiello, F.N., Salvatore, M., Rossi, S., Ferrara, A., Fitton, N. and Smith, P. 2013. The FAOSTAT database of greenhouse gas emissions from agriculture. Environmental Research Letters, 8(1).

Wang, W., Koslowski, F., Nayak, D.R., Smith, P., Saetnan, E. and Ju, X. 2014. Greenhouse gas mitigation in Chinese agriculture: Distinguishing technical and economic potentials. Global Environmental Change, 26: 53-62.

Wei, S., Bai, Z.H., Chadwick, D., Hou, Y., Qin, W. and Zhao, Z.Q. 2017. Greenhouse gas and ammonia emissions and mitigation options from livestock production in peri-urban agriculture. Journal of Cleaner Production, 178: 515-525.

West, T.O. and Marland, G. 2003. Net carbon flux from agriculture: carbon emissions, carbon sequestration, crop yield, and land-use change. Biogeochemistry, 63(1): 73-83.

Xiong, C., Yang, D. and Huo, J. 2016a. Spatial-temporal characteristics and LMDI-based impact factor decomposition of agricultural carbon

emissions in Hotan Prefecture, China. Sustainability, 8(3): 262.

Xiong, C., Yang, D., Huo, J. and Zhao, Y. 2016b. The relationship between agricultural carbon emissions and agricultural economic growth and policy recommendations of a low-carbon agriculture economy. Polish Journal of Environmental Studies, 25(5): 2187-2195.

Xu, Z. 2005. An overview of methods for determining OWA weights: research articles. International Journal of Intelligent Systems, 20(8): 843-865.

Yadav, D. and Wang, J. 2017. Modelling carbon dioxide emissions from agricultural soils in Canada. Environmental Pollution, 230: 1040-1049.

Yager, R.R. 1988. On ordered weighted averaging aggregation operations in multicriteria decision making. IEEE Trans. Systems Man Cybernet, 18(1): 80-87.

Ye, R., Espe, M.B., Linquist, B., Parikh, S.J., Doane, T.A. and Horwath, W.R. 2016. A soil carbon proxy to predict CH_4 and N_2O emissions from rewetted agricultural peatlands. Agriculture, Ecosystems & Environment, 220: 64-75.

Yue, Q., Xu, X., Hillier, J., Cheng, K. and Pan, G. 2017. Mitigating greenhouse gas emissions in agriculture: From farm production to food consumption. Journal of Cleaner Production, 149: 1011-1019.

Zafeiriou, E., Mallidis, I., Galanopoulos, K. and Arabatzis, G. 2018. Greenhouse gas emissions and economic performance in EU agriculture: An empirical study in a non-linear framework. Sustainability, 10(11): 3837.

Zaman, K., Khan, M.M., Ahmad, M. and Khilji, B.A. 2012. The relationship between agricultural technologies and carbon emissions in Pakistan: Peril and promise. Economic Modelling, 29(5): 1632-1639.

Zhang, L., Pang, J., Chen, X. and Lu Z. 2019. Carbon emissions, energy consumption and economic growth: Evidence from the agricultural sector of China's main grain-producing areas. Science of the Total Environment, 665: 1017-1025.

Zhao, R., Liu, Y., Tian, M., Ding, M., Cao, L., Zhang, Z. and Yao, L. 2018. Impacts of water and land resources exploitation on agricultural carbon emissions: The water-land-energy-carbon nexus. Land Use Policy, 72: 480-492.

Nature Environment and Pollution Technology
An International Quarterly Scientific Journal

p-ISSN: 0972-6268
(Print copies up to 2016)
e-ISSN: 2395-3454

Vol. 19 | No. 2 | pp. 603-610 | 2020

Original Research Paper

https://doi.org/10.46488/NEPT.2020.v19i02.015

Open Access Journal

Capital Allocation Efficiency Evaluation of Energy Conservation and Environmental Protection Enterprises in the Yangtze River Delta of China

Hongjun Xiong
School of Business, Shanghai Dianji University, Shanghai 201306, China; jackson0306@163.com

Nat. Env. & Poll. Tech.
Website: www.neptjournal.com

Received: 20-02-2020
Accepted: 10-04-2020

Key Words:
Energy conservation;
Environmental protection;
Capital allocation efficiency;
Yangtze river delta

ABSTRACT

Various measures are implemented to promote the construction of China's ecology. These measures aim to accelerate the green transformation of the economy and promote the rapid development of energy conservation and environmental protection industry under the promotion of relevant policies. Consequently, the numbers of enterprises and the market scale have shown explosive growth. However, energy conservation and environmental protection enterprises are faced with lack of technological innovation, shortage of capital, and high cost. Effective measures must optimize the efficiency of capital allocation. To evaluate the capital allocation efficiency of energy conservation and environmental protection enterprises, 26 listed companies of energy conservation and environmental protection in the Yangtze River Delta of China were selected as samples. Monetary capital, accounts receivable, inventory, fixed assets, and construction in progress were used as input scalars. Net profit, undistributed profit, and surplus reserve were used as output variables. The Data Envelopment Analysis (DEA) model was used for analysis. Results show that capital allocation efficiency of 11 sample companies is DEA-effective. Power, heat, gas, water production, and supply industry rank first with the real estate industry divided by industry. Shanghai ranks first in the regional division. Specific improvement strategies are proposed for non-DEA effective sample enterprises.

INTRODUCTION

The energy conservation and environmental protection industry provide technical basis and equipment support for energy conservation, circular economic development, and environmental protection. Among the specific industries included are energy conservation, resource recycling, and environmental protection equipment, which are involved in conservation, energy-saving products and services (Wang 2017). The 13th Five-Year Plan for the development of energy conservation and environmental protection industry proposes to develop energy conservation and environmental protection industry and strengthen the prevention and control of air, water, soil, and other pollution. At the same time, by 2020, energy conservation and environmental protection industry will become a pillar of the national economy.

In 2018, China's environmental protection and energy conservation support reached 635.3 billion yuan, with a year-on-year increase of 13%. The proportion of financial expenditure of the environmental protection industry in the GDP has increased as well. In the same year, the proportion of financial expenditure of the environmental protection industry in GDP was 0.7%. In recent years, China's energy conservation and environmental protection industry has grown rapidly, with the total output value increasing from approximately 3 trillion yuan in 2012 to 5.8 trillion yuan in 2017 and breaking through 7 trillion yuan in 2018. This growth was driven by the acceleration of ecological civilization construction, establishment and implementation of demonstration pilot projects in multiple circular economy fields, and improvement of public awareness of energy conservation and environmental protection. With the continuous increase of policies and regulations, such as environmental protection tax and emission permit system, the market space of China's energy conservation and environmental protection industry will continue to expand in the future (Peng et al. 2017, Bravo-Macias et al. 2019). Hence, the output value of energy conservation and environmental protection industry is expected to exceed 10 trillion yuan in 2020. However, the development of energy conservation and environmental protection industry depends on the forced promotion of policies (Xiong et al. 2010, Xiong et al. 2020). Driven by the policy, the potential demand for energy conservation and environmental protection will become a huge market space, which can attract the convergence of various capitals and enterprises and stimulate new employment demand. The development of energy conservation and environmental protection to a certain scale can realize the win-win of social and economic benefits.

From the perspective of industrial structure, the further expansion of industrial-scale can result in the large proportion for energy-saving and environmental protection equipment manufacturing industry. Furthermore, the proportion of the energy-saving and environmental protection service industry can further increase. With the acceleration of the market-oriented process, new modes and formats are rapidly emerging in the energy-saving and environmental protection industry. These trends continue the improvement of industrial scale and technology level. At the same time, the government continues to issue policies that promote enterprises to increase capital investment and subsequently form a diversified financing pattern (Sun 2018). However, problems such as unreasonable structure, irregular market, low industrial concentration, weak technological innovation ability (Yan et al. 2019), fund shortage and imperfect service system must be solved. The energy conservation and environmental protection industry is a heavy asset industry with large investment and long cycle. However, many small and medium-sized energy conservation and environmental protection enterprises in China lack financing capacity and serious capital shortage (Hao et al. 2018). According to the Development Research Center of the State Council, the corresponding investment demand for green development in China from 2015 to 2020 is approximately 2.9 trillion yuan per year. The proportion of government investment only accounts for 10%–15%, which is more than 80% of the funds needed to be solved by social capital. Thus, the financing demand for green development is in great shortage. Therefore, the efficiency of capital allocation of the energy conservation and environmental protection industry is worth exploring. The input is capital, whereas output comprises the indicators of operating results and equity. The source of capital includes equity capital and debt capital, and assets are the external form of expression. Assets come in various kinds. Different input combinations determine different output forms and output quantities. In the Yangtze River Delta region of China, economic development is fast. Environmental protection measures are increasing daily and environmental protection industrial policies are constantly issued. Studying the capital allocation efficiency of energy-saving and environmental protection enterprises in this region is significant.

The rest of this study is arranged as follows. Section 1 presents the design of research model, construction of the data envelopment analysis (DEA) model, selection of samples and indicators, and the extraction of data. Section 2 is the empirical analysis, which focuses on the DEA analysis results from the overall, industry, and regional situations, and puts forward the improvement strategy of capital allocation efficiency for energy-saving and environmental protection enterprises. Section 3 concludes this study.

METHODS

Modelling

In 1978, Charles and Cooper established an efficiency evaluation method known as the data envelopment analysis (DEA). DEA is a quantitative analysis method that aims to evaluate the effectiveness of comparable similar evaluation objects by using a linear programming method using multiple inputs and output indicators. The first DEA model proposed by Charles, Cooper, and Rhodes is the C2R model, which analyses and evaluates the effectiveness of decision-making units. The second DEA model is called the BC2 model, which was proposed by Banker, Charles, and Cooper in 1984. As an extension of the C2R model, the BC2 model measures the comprehensive efficiency of multiple inputs and output decision-making units under the assumption of variable returns to scale and distinguishes comprehensive efficiency into pure technical and scale efficiency. When choosing the BC2 model for efficiency evaluation, an input- or output-oriented model can be used (Yu et al. 2016). This study fully considers the limited input of energy-saving and environmental protection enterprise resources and tests the output of energy-saving and environmental protection enterprises under a given capital input. Hence, the output-oriented BC2 model is selected.

The basic principle of BC^2 model is that if given n DMUs, each DMU_j ($j = 1, 2 \ldots n$) uses p inputs, namely X_{ij} ($i = 1, 2 \ldots p$), and produces q outputs, namely Y_{kj} ($k = 1, 2 \ldots q$). The relative efficiency value of m DMUs can be obtained from the following models:

$$\begin{cases} Max\ h_m = \dfrac{\sum_{k=1}^{q} u_k Y_{km} - U_0}{\sum_{i=1}^{p} v_i X_{im}} \\ s.t.\ \ \dfrac{\sum_{k=1}^{q} u_k Y_{kj}}{\sum_{i=1}^{p} v_i X_{ij}} \le 1, j = 1, 2, \ldots, n \end{cases} \quad \ldots(1)$$

In formula (1), u_k and v_i are weight coefficients for measuring output input, with the relation u_k, $v_i \ge \varepsilon \ge 0$. Generally, the larger h_m is, the more output can be obtained when the input of the m decision unit is certain. Therefore, the maximum value of h_m can be examined by trying to change as many weight coefficients as possible, which can lead to judging whether the m^{th} decision-making unit is relatively optimal in the decision-making unit. According to the linear programming technique, we can obtain the optimal solution h_m^* of the equation. If the optimal solution $h_m^*=1$, then the decision unit DMU_m is DEA-efficient.

Variables

According to the component stocks of "beautiful China," we reduced the sample range and considered the following factors when screening. The first is selecting the samples from the Yangtze River Delta of China, which included listed companies in Zhejiang, Jiangsu, and Anhui Provinces, and Shanghai. The second is considering that the number of samples is equal to or exceeds the total number of input and output indicators twice, according to the requirements of the DEA model for samples and indicators. In this study, 26 listed companies of artificial intelligence in China are selected as samples, that is, the decision unit (DMU) in the model.

Referring to the research on capital input and output of the home appliance industry (Xu et al. 2017), we considered the characteristics of energy conservation and environmental protection industry. Thus, we selected monetary fund (X_1), account receivable (X_2), inventory (X_3), fixed assets (X_4), and construction in progress (X_5) as capital input variables of energy conservation and environmental protection enterprises. We selected net profit (Y_1), undistributed profit (Y_2), and surplus reserve (Y_3) as capital output variable of energy conservation and environmental protection enterprises, as shown in Table 1 below:

Data Source

Variable data comes from the Wind Database. Monetary capital, accounts receivable, inventory, fixed assets, and construction in progress are presented from the opening and closing balance of corresponding subjects of sample balance sheets in 2017 and 2018. Net profit, undistributed profit, and surplus reserve come from the opening and closing balance of corresponding subjects of sample balance sheets in 2017 and 2018. Table 2 presents variable data after calculation. We adjusted the variable from the negative value to 0 in the empirical analysis.

RESULTS

Capital Allocation Efficiency Analysis

The original data of input and output variables of 26 skilled environmental protection enterprises in the Yangtze River Delta of China were imported into the DEAP2.1 software, and the parameters of the guidance file were set. The decision-making unit was 26, time was 1 year, the number of output indicators was 3, the number of input indicators was 5, and output leading type was 1 = OUTPUT ORIENTATED, 1 = VRS, 0 = DEA (MULTI-STAGE).

Overall Results

Based on the BC^2 model, the operation results of the DEA of business efficiency of enterprises in the Yangtze River Delta are shown in Table 3. The average comprehensive efficiency of capital allocation and the pure technical and scale efficiency of 26 energy-saving and environmental protection enterprises in the Yangtze River Delta are 0.709, 0.739, and 0.95, respectively. At the same time, the results showed that the DEA of 11 sample enterprises is effective, having accounted for 42.308%.

In comprehensive efficiency, 11 enterprises, such as Weifu Group, Cec Environmental Protection, and Weiming Environmental Protection, are DEA-effective, with a value of 1. Comprehensive efficiency of *St Feida is only 0.096, and the comprehensive efficiency of 11 sample enterprises is lower than the average level, indicating that the capital allocation efficiency of energy-saving and environmental protection enterprises in the Yangtze River Delta is different.

In pure technical efficiency, 11 sample enterprises are below the average level, with a minimum value of 0.097 (*ST Feida). However, although Jiaao's environmental protection has reached 1, its scale efficiency is insufficient, resulting in a comprehensive efficiency of less than 1.

Table 1: Capital input and output variables of energy conservation and environmental protection enterprises.

Variable type	Variable name	Computing method
Input variables	Monetary fund (X_1)	(Initial balance + Ending balance) / 2
	Account receivable (X_2)	
	Inventory (X_3)	
	Fixed assets (X_4)	
	Construction in progress (X_5)	
Output variables	Net profit (Y_1)	
	Undistributed profit (Y_2)	
	Surplus reserves (Y_3)	

In scale efficiency, only six sample enterprises are below the average level, with a minimum value of 0.639 (Anhui Construction Engineering Group). The scale efficiencies of Skyray Instrument, Chuangyuan Technology, and Guozhen Environmental Protection Technology are 0.999, 0.997, and 0.994, respectively, which are close to 1. The pure technical efficiency indicates that comprehensive efficiency is not high.

Table 2: Original data of capital input and output of energy conservation and environmental protection enterprises in the Yangtze River Delta of China (Unit: 100 Million Yuan).

Serial number	Code	Securities abbreviation	Input variables					Output variables		
			X_1	X_2	X_3	X_4	X_5	Y_1	Y_2	Y_3
DMU1	000551	Chuangyuan Technology	8.364	5.410	9.534	8.249	0.968	1.455	5.828	1.514
DMU2	000581	Weifu Group	28.675	19.577	14.385	26.461	1.334	25.568	104.043	5.101
DMU3	000925	UniTTEC	8.950	14.096	4.271	3.389	1.759	0.744	-0.933	0.159
DMU4	002015	GCL Energy Technology	0.557	0.363	1.370	0.660	0.000	0.073	-11.268	0.180
DMU5	002479	Fuchunjiang Environmental Thermoelectric	5.897	2.529	1.307	29.265	1.310	2.921	9.381	1.556
DMU6	002499	*ST Kelin	1.224	6.424	0.057	2.018	0.018	-2.505	-0.938	0.247
DMU7	002645	Huahong Technology	3.845	1.850	5.916	3.927	0.111	1.415	4.136	0.445
DMU8	300090	Shengyun Environment Protection Group	8.194	11.888	9.092	6.892	5.523	-22.230	-14.956	1.066
DMU9	300165	Skyray Instrument	4.946	2.935	3.680	2.035	0.070	0.825	3.292	0.563
DMU10	300172	Cec Environmental Protection	1.157	4.343	1.882	1.185	3.741	1.248	5.576	0.632
DMU11	300190	Welle Environmental Group	10.631	9.833	11.798	4.973	2.335	1.956	5.528	0.501
DMU12	300203	Focused Photonics	10.814	17.030	12.833	4.819	0.889	5.850	18.294	1.681
DMU13	300262	Safbon Water Service	5.139	4.046	5.916	1.596	0.196	1.224	5.675	0.495
DMU14	300266	Xingyuan Environment Technology	6.209	14.155	43.119	3.890	0.138	-4.554	1.297	0.414
DMU15	300272	Canature Health Technology Group	1.258	1.501	1.375	4.630	2.527	1.801	2.582	0.676
DMU16	300385	Xuelang Environmental Technology	2.139	4.934	4.389	3.439	0.027	0.571	3.512	0.495
DMU17	300388	Guozhen Environment Protection Technology	9.317	8.623	5.824	2.233	7.376	2.593	8.093	0.618
DMU18	300495	Misho Ecology & Landscape	13.978	18.192	14.752	0.736	0.028	3.354	9.547	0.610
DMU19	600475	Huaguang Boiler	16.298	25.320	14.429	19.210	4.096	4.702	36.155	2.274
DMU20	600481	Shuangliang Eco-energy Systems	12.393	7.484	4.179	4.788	0.341	1.748	1.811	3.484
DMU21	600502	Anhui Construction Engineering Group	86.058	168.370	256.454	30.805	0.536	8.007	27.037	3.924
DMU22	600526	*ST Feida	9.004	12.557	24.798	9.993	2.429	-3.127	-1.536	0.353
DMU23	600649	Chengtou Holding	53.396	0.502	208.799	0.198	0.000	14.683	120.883	22.518
DMU24	601199	Jiangnan Water	9.926	1.798	0.353	19.691	5.019	2.191	11.353	1.664
DMU25	603568	Weiming Environment Protection	8.636	3.015	0.900	1.070	7.855	6.225	15.636	1.459
DMU26	603822	Jiaao Enprotech Stock	2.900	0.423	2.561	2.919	1.461	0.543	3.335	0.401
Average			12.689	14.123	25.538	7.657	1.926	2.203	14.360	2.040
Maximum			86.058	168.370	256.454	30.805	7.855	25.568	120.883	22.518
Minimum			0.557	0.363	0.057	0.198	0.000	-22.230	-14.956	0.159

Table 3: Overall results of capital allocation efficiency of energy conservation and environmental protection enterprises in the Yangtze River delta of China.

DMU	Comprehensive efficiency	Pure technical efficiency	Scale efficiency	Increase or decrease of returns to scale	DMU	Comprehensive efficiency	Pure technical efficiency	Scale efficiency	Increase or decrease of returns to scale
DMU1	0.586	0.588	0.997	irs	DMU14	0.156	0.159	0.982	irs
DMU2	1	1	1	-	DMU15	1	1	1	-
DMU3	0.157	0.170	0.922	irs	DMU16	0.821	0.892	0.921	irs
DMU4	1	1	1	-	DMU17	0.397	0.399	0.994	drs
DMU5	1	1	1	-	DMU18	1	1	1	-
DMU6	1	1	1	-	DMU19	0.620	0.642	0.967	drs
DMU7	0.571	0.614	0.930	irs	DMU20	1	1	1	-
DMU8	0.356	0.398	0.895	drs	DMU21	0.268	0.419	0.639	drs
DMU9	0.716	0.716	0.999	drs	DMU22	0.096	0.097	0.982	drs
DMU10	1	1	1	-	DMU23	1	1	1	-
DMU11	0.281	0.290	0.967	irs	DMU24	1	1	1	-
DMU12	0.943	0.983	0.959	irs	DMU25	1	1	1	-
DMU13	0.607	0.847	0.717	irs	DMU26	0.863	1	0.863	irs

According to the increase and decrease of returns to scale, 11 DEA-effective sample enterprises show the same returns to scale, nine sample enterprises show the same returns to scale. Hence, 76.923% of sample enterprises show the same returns to scale. Only six sample enterprises show decreasing returns to scale, accounting for 23.077% of the total sample enterprises. This result is closely related to the state-issued relevant policies that aim to strengthen environmental protection and encourage the development of environmental protection enterprises. Many energy-saving and environmental protection enterprises, under the incentive of preferential policies, increase capital investment, promote the continuous growth of market scale, and seize market share with the rapid growth of enterprise scale.

Results by industry: Table 4 shows the average values of comprehensive, purely technical, and scale efficiencies of the capital allocation efficiency of enterprises in different industries: power, heat, gas, and water production and supply industry (1), real estate industry (1) > manufacturing industry (0.671) > water conservancy, environment, and public facilities management industry (0.634) > construction industry (0.268). Among the 13 manufacturing enterprises, five enterprises have increasing returns to scale, and three enterprises have unchanged returns to scale. Among the seven

Table 4: Results of capital allocation efficiency of energy conservation and environmental protection enterprises in the Yangtze River Delta of China by Industry.

Industry	Type	Comprehensive efficiency	Pure technical efficiency	Scale efficiency
Manufacturing industry	Average	0.671	0.700	0.957
	Minimum	0.096	0.097	0.863
Water conservancy, environment and public facilities management	Average	0.634	0.671	0.951
	Minimum	0.156	0.159	0.717
Power, heat, gas and water production and supply industry	Average	1	1	1
	Minimum	1	1	1
Real estate industry	Average	1	1	1
	Minimum	1	1	1
Construction industry	Average	0.268	0.419	0.639
	Minimum	0.268	0.419	0.639

Table 5: Results of capital allocation efficiency of energy conservation and environmental protection enterprises in the Yangtze River delta of China by region.

Region	Type	Comprehensive efficiency	Pure technical efficiency	Scale efficiency
Jiangsu	Average	0.815	0.826	0.983
	Minimum	0.281	0.290	0.921
Zhejiang	Average	0.602	0.630	0.958
	Minimum	0.096	0.097	0.863
Shanghai	Average	0.869	0.949	0.906
	Minimum	0.607	0.847	0.717
Anhui	Average	0.340	0.405	0.843
	Minimum	0.268	0.398	0.639

water conservancy, environment, and public facility management enterprises, three enterprises show increasing returns to scale, and only one enterprise indicates decreasing returns to scale. The capital allocation efficiency of power, heat, gas, and water production and supply enterprises is DEA-effective, and the returns to scale remain unchanged. Only one real estate enterprise and its capital allocation efficiency is DEA-efficient, and the returns to scale remain unchanged. The number of construction enterprises is 1, and the returns to scale decrease. Power, heat, gas, and water production and supply enterprises belong to government monopoly enterprises that have strong capital investment and stable market. However, the construction industry has high technical standards, increased requirements, slow technological innovation, and long capital return cycle. The manufacturing industry has many kinds, a large number of enterprises, and a variety of products. Several enterprises actively invest in capital, accelerate the research and development of energy conservation and environmental protection technology, and quickly seize the market. Other enterprises may maintain the status quo or change the original business scope, resulting in overall scale decline.

Results by region: According to Table 5, the average values of comprehensive, purely technical, and scale efficiencies of enterprise capital allocation in different regions are Shanghai (0.869) > Jiangsu (0.815) > Zhejiang (0.602) > Anhui (0.340). Among the 13 enterprises in Zhejiang Province, four enterprises are with increasing returns to scale, seven enterprises with unchanged returns to scale, and only two enterprises are with decreasing returns to scale. Among the seven enterprises in Zhejiang Province, four enterprises have increasing returns to scale, and only one enterprise with decreasing returns to scale. Among the three enterprises in Shanghai, two enterprises are with unchanged returns to scale, and one enterprise with increasing returns to scale. It shows that decreasing returns to scale of the three enterprises in Anhui Province. Shanghai has good location advantages and financial and human resources. It has also issued a series of measures to encourage the development of energy-saving and environmental protection enterprises. However, due to the relatively poor geographical environment, lack of high-level talents, and technological innovation, the overall efficiency of the capital allocation of energy-saving and environmental protection enterprises is low. Jiangsu and Zhejiang Provinces are strong economic provinces and have strong capital, human resources, and technical support. Consequently, the energy-saving and environmental protection enterprises in those provinces have high capital allocation efficiency and show rapid growth.

Improvement Strategy of Capital Allocation Efficiency

Table 6 shows the many improvements in the input and output variables of non-DEA effective energy conservation and environmental protection enterprises in the Yangtze River Delta. Taking *ST Feida as an example, its capital allocation efficiency projection points on the production front are (0, 0, 3.591) and (9.004, 2.451, 24.798, 4.169, 1.862), whereas its initial input and output are (9.004, 12.557, 24.798, 9.993, 2.429) and (−3.127, −1.536, 0.353), respectively. As the negative output is adjusted to 0 in DEA analysis, *ST Feida should adjust its net profit by 3127 million RMB, the undistributed profit of 153.6 million RMB, and surplus reserve of 323.8 million RMB. When DEA is effective, *ST Feida can reduce the accounts receivable of 1.0106 billion RMB, fixed assets of 580.1 million RMB, and construction in progress of 56.7 million RMB. The many accounts receivable and fixed assets in *ST Feida lead to the high capital occupation. Poor performance leads to continuous losses of the enterprise. Thus, launching relevant preferential strategies, recovering accounts receivable, promoting inventory sales, and speeding up the turnover of fixed assets are necessary. For example, the investment of Anhui Construction Engineering Group is (86.058168.370256.454, 30.805, 0.536). The first four inputs are the highest level in the industry, but the

Table 6: Improvement strategy for capital allocation efficiency of energy conservation and environmental protection enterprises in the Yangtze River Delta of China.

DMU	Comprehensive efficiency	Improvement strategy							
		Output variables			Input variables				
		Y_1	Y_2	Y_3	X_1	X_2	X_3	X_4	X_5
DMU1	0.586	2.798	9.914	2.568	8.360	4.108	9.530	8.250	0.970
DMU2	1	25.568	104.043	5.101	28.675	19.577	14.385	26.461	1.334
DMU3	0.157	4.351	0	1.000	6.770	5.091	4.270	3.390	1.760
DMU4	1	0.073	0	0.180	0.557	0.363	1.370	0.660	0
DMU5	1	2.921	9.381	1.556	5.897	2.529	1.307	29.265	1.310
DMU6	1	0	0	0.247	1.224	6.424	0.057	2.018	0.018
DMU7	0.571	2.296	10.119	0.943	3.643	1.850	5.920	2.646	0.110
DMU8	0.356	0	0	2.691	8.190	4.332	9.090	4.570	1.404
DMU9	0.716	1.145	4.677	0.782	2.884	2.584	3.680	2.030	0.070
DMU10	1	1.248	5.576	0.632	1.157	4.343	1.882	1.185	3.741
DMU11	0.281	6.750	26.295	2.119	10.630	6.276	11.800	4.970	2.340
DMU12	0.943	5.951	23.893	1.819	10.810	8.419	12.830	4.820	0.890
DMU13	0.607	1.773	6.692	0.654	4.418	4.050	5.920	1.600	0.200
DMU14	0.156	0	12.979	2.580	6.210	0.438	23.398	0.831	0.140
DMU15	1	1.801	2.582	0.676	1.258	1.501	1.375	4.630	2.527
DMU16	0.821	0.837	3.936	0.585	1.889	0.795	4.390	1.236	0.030
DMU17	0.397	6.522	20.264	1.922	9.320	3.918	5.820	2.230	6.782
DMU18	1	3.354	9.547	0.610	13.978	18.192	14.752	0.736	0.028
DMU19	0.62	13.351	56.325	3.537	16.300	11.614	14.430	13.373	2.376
DMU20	1	1.748	1.811	3.484	12.393	7.484	4.179	4.788	0.341
DMU21	0.268	19.102	114.043	15.447	43.363	8.247	129.867	10.862	0.536
DMU22	0.096	0	0	3.591	9.004	2.451	24.798	4.169	1.862
DMU23	1	14.683	120.883	22.518	53.396	0.502	208.799	0.198	0.000
DMU24	1	2.191	11.353	1.664	9.926	1.798	0.353	19.691	5.019
DMU25	1	6.225	15.636	1.459	8.636	3.015	0.900	1.070	7.855
DMU26	0.863	0.543	3.335	0.401	2.900	0.423	2.561	2.919	1.461

output is not high. According to the improvement strategy, the projection point of capital allocation efficiency on the production front is (19.102, 114.043, 15.447) and (43.363, 8.247129.867, 10.862, 0.536). The comprehensive efficiency of the salary cost allocation of Anhui construction is only 0.268, and the scale efficiency is the lowest (0.639) of the sample enterprises. These figures show that the returns on the scale are decreasing, that is, enterprises do not give full play to the scale effect, as many investments cause great waste and consume most of the profits. Therefore, enterprises should increase output and adjust net profit of 1.109 billion yuan, the undistributed profit of 9.106 billion yuan, and surplus reserve of 1.152 billion yuan. In addition, enterprises should consider reducing diversified operation, centralizing advantages, and improving profit point. Besides, according to the results of Jiaao Enprotech Stock, although pure technical efficiency reaches 1, its scale efficiency is insufficient at only 0.863, which increases the scale reward. Hence, its scale must be expanded, and its scale advantage should be given full play.

CONCLUSION

Through the analysis of the capital allocation efficiency of energy-saving and environmental protection enterprises in the Yangtze River Delta of China, this study mainly draws the following conclusions. First, the comprehensive efficiency of

the capital allocation of energy-saving and environmental protection enterprises is high at an average value of 0.709. The scale efficiency is 0.951. Overall, 42.308% of sample enterprises realize DEA efficiency, which shows that the capital utilization efficiency and income of energy-saving and environmental protection enterprises are good. Second, the comprehensive efficiency of the capital allocation of energy-saving and environmental protection enterprises is different, as the highest is 1, and the minimum is 0.096. Hence, huge differences are observed at the development level and in the strength among enterprises, and the market competition is intense. Third, differences are found in the average value of comprehensive efficiency among different industries, including power, heat, gas, and water production and supply industry (1), real estate industry (1), manufacturing industry (0.671), water conservancy, environment and public facilities management industry (0.634), and construction industry (0.268); Fourth, differences are observed in comprehensive efficiency among different regions, such as Shanghai (0.869), Jiangsu (0.815), Zhejiang (0.602), and Anhui (0.340). Fifth, more than two-thirds of the sample enterprises show constant or increasing scale. Hence, capital is not only in the stage of increasing in energy-saving and environmental protection enterprises but also forms scale effect, realizes effective integration of resources, and improves comprehensive income. Sixth, from the perspective of monetary capital, accounts receivable, and fixed assets, the average values are 1268.9, 1413.3, and 765.7 million RMB, respectively. The fixed assets are at a low level, whereas accounts receivable are too many. Hence, attention should be paid to prevent the risk of bad debts of accounts receivable. In addition, the average value of inventory is 2553.8 million RMB, which is at a high level. Hence, a necessary program is to speed up inventory turnover and prevent inventory depreciation.

ACKNOWLEDGEMENT

The study was supported by Grant from the Development Center of Shanghai Municipal People's Government (2019-U-A02).

REFERENCES

Bravo-Macias, C., Sarmentero-Bon, I., Rodriguez-Sanchez, Y. and Gomez-Figueroa, O. 2019. Evaluation of organizational competencies through performance indicators. DYNA, 94(5): 490.

Hao, W.B., Li, S.G., Lei, Y.X., Song, Z.J. and Dong, J.C. 2018. Study on efficiency evaluation of energy conservation and environmental protection industry in China. Science and Technology for Development, 14(4): 223-231.

Peng, H., He, Z.C., Wu, Y. and Deng, Y. 2017. Research on composition and cultivation of modern energy conservation and environmental protection industry. Mining Research and Development, 37(3): 112-120.

Sun, Y. 2018. Development status and policy recommendations of energy conservation and environmental protection industry. China Energy, 40(12): 23-24.

Wang, Z.K. 2017. Definition and scope of energy conservation and environmental protection industry. China Strategic Emerging Industry, (12): 45-46.

Xiong, Z., Wang, P.J. and Zhao, Y. 2020. Re-innovation from failure, institutional environmental differences, and firm performance: Evidence from China. Amfiteatru Economic, 22(53): 197-219.

Xiong, Z.D. and Lin, X. 2010. Financial support efficiency of listed companies in energy conservation and environmental protection industry and its influencing factors. Economic Management, (11): 26-33.

Xu, F.J. and Dai, F. 2017. Capital allocation efficiency evaluation of household appliance enterprises based on DEA model. Journal of Finance and Accounting, (8), 44-48.

Yan, J.Z. and Qi, N.N. 2019. Research on performance evaluation of China's strategic emerging industries - taking energy conservation and environmental protection industries as an example. Journal of Henan University of Engineering (Social Science Edition), 34(1): 13-18.

Yu, Y.B., Du, Y.C. and Gao, Y. 2016. Evaluation of the operation efficiency of listed companies in LED lighting industry of China based on DEA model. Light & Engineering, 24(3): 161-165.

Nature Environment and Pollution Technology
An International Quarterly Scientific Journal

p-ISSN: 0972-6268
(Print copies up to 2016)
e-ISSN: 2395-3454

Vol. 19 | No. 2 | pp. 611-625 | 2020

Original Research Paper

https://doi.org/10.46488/NEPT.2020.v19i02.016

Open Access Journal

Potential of Urban Wetlands for Ecotourism Development- A Case of Deepor Beel, Guwahati

Pratiksha Baruah
Deptt. of Planning, School of Planning and Architecture, Vijayawada, Andhra Pradesh, India; pratikshabaruah@yahoo.com

Nat. Env. & Poll. Tech.
Website: www.neptjournal.com

Received: 11-08-2019
Accepted: 18-09-2019

Key Words:
Anthropogenic activities; Biodiversity; Economy; Ecotourism; Local community; Wetland

ABSTRACT

Wetlands are amongst the most productive ecosystems of the Earth. The system includes diverse features in terms of components, functions and attributes. Wetland ecosystems are essential to human well-being (Finlayson et al. 2005). A substantial body of evidence demonstrates that wetlands can deliver a great variety of benefits to human society (Ghermandi et al. 2010). Up to 87% of the global wetland resource has been lost since 1700. The planet is losing wetlands three times faster than natural forests. Tourism is one of the significant tools to enhance and support environmental conservation. According to UNWTO, sustainable tourism means putting the principles of sustainable development, set out at the Rio Earth Summit in 1992, into practice in tourism. Deepor Beel is a permanent freshwater lake and the only Ramsar site in Assam which is experiencing adverse human activities; filling of wetlands for habitation purpose, cutting the sides of wetlands, pollution, fishing and killing of migratory birds. Degradation of water quality, sedimentation in the lake surface, deforestation activities in and around the Beel area has increased the importance of conservation and restoration of the Beel. Presently, Deepor Beel is a degrading Beel, facing threats due to urban encroachment and its illegal uses. Therefore, the research questions for this study are- (i) What are the causes and effects of deterioration of the wetland ecosystem? (ii) How to manage the wetland ecosystem through ecotourism development? The study aims to conserve urban wetlands to enhance eco-tourism and have a balanced urban development of Guwahati. To understand the potentiality of eco-tourism in Deepor Beel in Guwahati, the objectives are to understand the importance of urban wetland ecosystem and its present status, to assess the development initiatives in terms of tourism development by government and private sectors in Guwahati, to analyse the socio-economic and governance aspects of the wetland management and tourism in Guwahati and finally to suggest strategies or measures to enhance ecotourism-based wetland development. Primary and secondary data are used in the study through field study and secondary data collection from various organisations. Ecotourism opportunity spectrum is an analysis done to understand the suitability of the wetland for ecotourism development. To understand the anthropogenic impacts of human activity, water quality index, spatial pattern analysis, species diversity index, correlation analysis, carrying capacity analysis, Kuppuswamy's socio-economic scale, Karl Pearson correlation, vulnerable economic index, WTP-Demand Curve, SWOT analysis and Pralong's method is used to derive the potentiality of the wetland for ecotourism. Tools like Arc GIS, SPSS, MS Excel, Google Sketch Up and Google Earth have been used for the various analyses of the study. The study would find its application in the field of ecotourism development at the state level which would contribute to the growth of GDP to the nation. The initiatives were taken under ecotourism that incorporates policies and strategies at the organizational level, spatial planning, local community level that would also benefit the local community by generating employment as well as conserving the richness of the biodiversity of the lake. The findings and proposals of the study can be a helpful strategy to develop an appropriate policy for tourism to be beneficial to both the economic benefits of the state and empowerment of the local people.

INTRODUCTION

A wetland is a place where the land is covered by water, either salt, fresh or somewhere in between. Marshes and ponds, the edge of a lake or ocean, the delta at the mouth of a river, low-lying areas that frequently flood - all of these are wetlands. The destruction of wetlands is a concern because they are some of the most productive habitats on the planet. The Millennium Ecosystem Assessment (MEA) is a major assessment of the human impact on the environment, called for by the United Nations Secretary-General Kofi Annan in 2000, launched in 2001 and published in 2005 that popularized the term ecosystem services, the benefits gained by humans from ecosystems. Ramsar COP 11 delegates met in the morning and adopted resolutions on tourism, recreation and wetlands; wetlands and energy issues; principles for the planning and management of urban and peri-urban wetlands.

Up to 87% of the global wetland resource has been lost since 1700. The planet is losing wetlands three times faster than natural forests. Wetland loss may be defined as "the loss of wetland area, due to conversion of wetland to non-wetland

areas as a result of human activity" and wetland degradation is "the impairment of wetland functions as a result of human activity". About 50% of the world's wetlands have been lost in the last century, primarily through drainage for agriculture, urban development and water system regulations. According to the survey conducted by Wildlife Institute of India, 70 to 80 per cent of freshwater marshes and lakes in the Gangetic flood plains have been lost during the last 50 years. As a matter of fact, during the last century, 50 per cent of India's wetlands have been lost. The mangrove area of the country has been reduced from 7 lakh hectares in 1987 to 4.53 lakh hectares in 1995. About 32 per cent of the wetlands in India has been lost primarily through hunting and associated disturbances, 22 per cent due to human settlements, 19 per cent due to fishing and 23 per cent through drainage from agriculture. Removal of vegetation in the catchment leading to soil erosion and siltation contributes to about 15 per cent loss of wetlands. Pollution from the industries contributes to about 20 per cent loss of wetlands.

According to World Travel and Tourism Council (WTTC) tourism generates 11% of global GDP, employs 200 million people, and transports nearly 700 million international travellers per year (Eco-tourism or Eco-exploitation?, n.d.)). Of the 2,263 Ramsar Sites in the database as of March 2017, 1,660 (73%) are reported to provide ecosystem services related to tourism and recreation. Ecotourism developed in India in 1970s and 1980s. Ecotourism was globally identified as a means of achieving twin goals of biodiversity conservation and sustainable development. As per World Travel and Tourism Council (WTTC), India's tourism sector ranks 7th in the world in terms of its total contribution to the country's GDP- 6.23% and 6.23% to the 8.78% of the total employment in India (2016). According to the Central Statistical Organisation (CSO) Enterprise, Ministry of Tourism, Government of India, tourism has the highest contribution to generating employment compared to different economic sectors in the country. There is a rising decadal trend in tourist visits in India, both domestic and foreign from 2006-2016.

The Need of the Study

Urbanization has turned into a reason for most environmental issues globally and therefore, has turned into a global significance. The study area, i.e. the Deepor Beel Wetland is located in Guwahati, in the state of Assam, India. The city of Guwahati is the gateway to North-Eastern India as well as an important centre for economic, social, educational, commercial and transportation activities, it has experienced rapid urban growth resulting into various environmental problems. Changing urban landscape with an increase in population growth and more demand for land is creating significant pressure on the natural land cover of Guwahati. Deepor Beel, the lone Ramsar site in the Brahmaputra valley has been facing immense pressure in the form of drastic changes of adjoining land covers and eco-sensitive areas due to rapid urbanization in the city. The rapid growth of the city population and land cost increase has resulted in the encroachment of the Deepor Beel. Northern and eastern parts of the Beel have been occupied by the private as well as the government organizations. Encroachment problem and land-use change have changed the spatial pattern of Deepor Beel water area. Blocked natural drainage pattern and the water level imbalance in the Beel is also a cause of encroachment around the wetland. Waste disposal from industries, factories and surrounding areas are also among the major causes of degradation to the wetland. In tourism point of view, Guwahati has a high potential for tourism according to Assam Science Technology and Environment Council. Ecotourism is slowly but surely becoming a trend in the state. Guwahati endowed with splendid natural beauty, an abode of rich floral and faunal biodiversity, the treasure of plants, shrubs and herbs of medicinal value, unique ecosystems, wetlands, their grandeur and awe-inspiring beauty are the sources of perennial attraction.

Research Framework

Presently, Deepor Beel is a degrading Beel, facing threats due to urban encroachment and its illegal uses. Therefore, the research questions for this study are-

(i) What are the causes and effects of deterioration of the wetland ecosystem?
(ii) How to manage the wetland ecosystem through ecotourism development?

The basic elements of sustainable development- equity, economic sustainability and ecological sustainability represent the primary objectives of balanced urban development. Thus, the purpose of the study is to apply the elements of sustainability to the tourism industry in Guwahati. The study aims to conserve urban wetlands to enhance eco-tourism and have a balanced urban development of Guwahati.

To understand the potentiality of eco-tourism in Deepor Beel in Guwahati, the objectives are-

Objective 1: To understand the importance of urban wetland ecosystem and its present status.

Objective 2: To assess the development initiatives in terms of tourism development by government and private sectors in Guwahati.

Objective 3: To analyse the socio-economic and governance aspects of the wetland management and tourism in Guwahati.

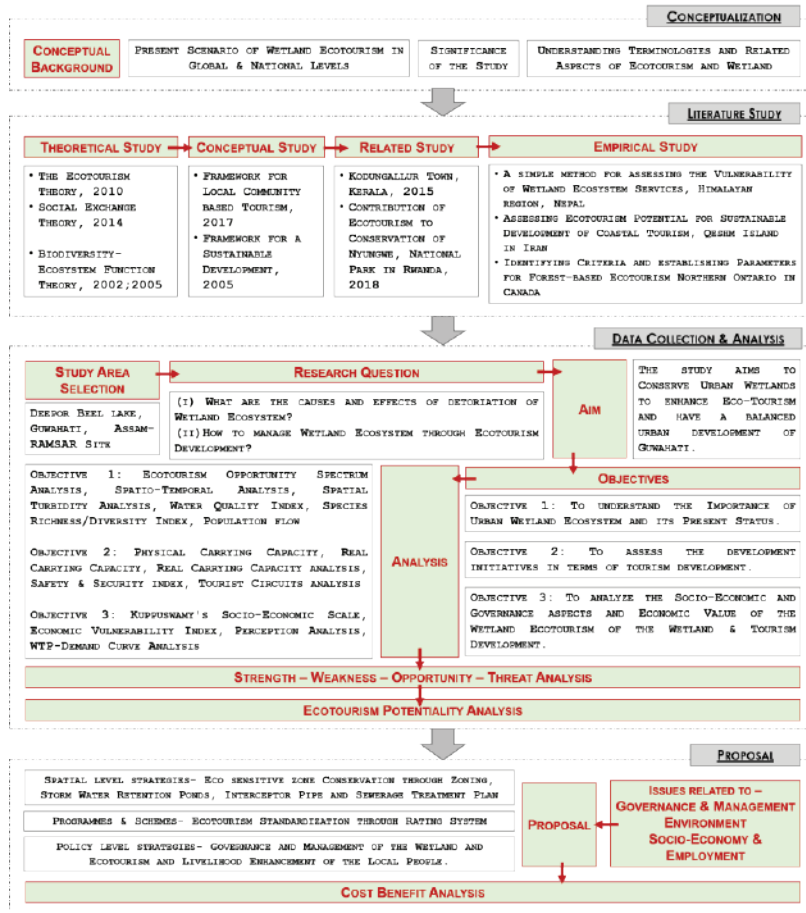

Fig. 1: Methodology.

Objective 4: To suggest strategies or measures to enhance ecotourism-based wetland development.

The methodology of the research is shown in the Fig. 1.

Profile of the Study Area

'Beel', in Assamese, means a wetland or a waterbody with diverse flora and fauna. Deepor Beel is a natural, permanent wetland, located towards the southwest of Guwahati and is considered as an important riverine wetland in the Brahmaputra valley of Assam. Deepor Beel is the only Ramsar site in Assam and among the third Ramsar site of the northeastern region of India. Deepor Beel is designated as "Wetlands of International Importance" under the Ramsar Convention on Wetlands, 1971 and was declared as Ramsar site in 2002.

The Deepor Beel lake is located about 18 km southwest of Guwahati city between 90°36'39" E and 91°41'25" E longitude and 26°05'26" N and 26°9'26" N latitude and 55 m above the mean sea level, considered as one of the largest and prominent flood-plain lakes in the Brahmaputra valley in Jalukbari Mouza of Guwahati sub-division under Kamrup (Metropolitan) district. The Beel and its adjacent villages fall under Azara revenue circle of Kamrup-metro district. The national highway 37 (NH-37) is located in the northern side of the Beel and touches its periphery at different places like Dharapur, Azara etc. The Deepor Beel falls within the jurisdiction of the Guwahati Metropolitan Development Authority within the Kamrup District, Assam. The location of the Deepor Beel has been shown in Fig. 2.

The study area has been delineated to 5 km buffer from the Deepor Beel lake. The study area includes a total of 18 villages within the Azara Revenue Circle under the Jalukbari Mouza- (1) Garal, (2) Mirjapur, (3) Azara, (4) Barjhar, (5) Maj-Jalukbari, (6) Gatangarh, (7) Dakshin Jalukbari, (8) Uttar Jalukbari, (9) Paschim Jalukbari, (10) Dehangarigaon, (11) Teteli, (12) Kachharigarigaon, (13) Dharapur, (14) Pub-Gaon, (15) Paschim Baragaon, (16) Kahikuchi, (17) Mikirapara Chakardai and (18) Jugipara.

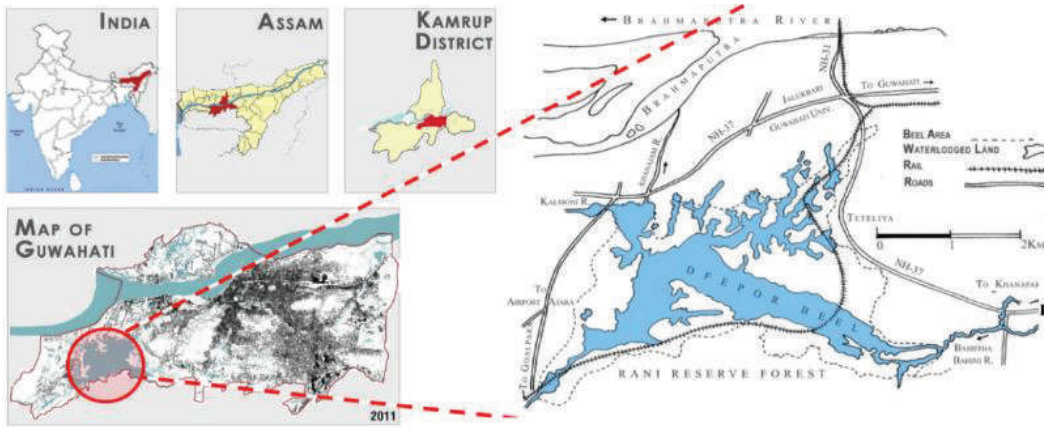

Fig. 2: Location of Deepor Beel lake.

ANALYSIS

The Importance of Urban Wetland Ecosystem and its Present Status

To understand the potential of ecotourism of the wetland, Ecotourism Opportunity Spectrum (ECOS) has been used based on past researches, experts' opinion and primary survey; of the factors - Normalized Differential Vegetation Index (NDVI), Land Surface Temperature (LST), Contour, Rarity; in terms of tourists' spots, proximity to solid waste landfill sites, proximity, proximity to modes of communication. The total ECOS score obtained is 22 in total weightage of 24. According to the factored points, there is a strong potentiality of tourism in the Deepor Beel wetland.

There is an increase in built-up land use within the study area which is encroaching over the wetland area causing a reduction in the wetland area as shown in Table 1. There is a reduction in inland water (wetland area), cropland, fallow land and vegetation area due to built-up in the study area.

The calculation of the Water Quality Index (WQI) has been done using the weighted arithmetic water quality index, originally proposed by (Horton 1965) and developed by (Brown et al. 1970). Table 2 shows the location of the sampling sites.

Table 1: Change in land use.

	Area (sq. km.)		Change (in %)
Parameters	2008	2018	2008-2018
Crop Land	12.19	10.11	17.06
Fallow Land	10.88	9.19	15.53
Inland Water	16.92	11.54	31.79
Built Up	16.14	31.28	-93.9
Vegetation	24.73	21.17	14,39

Table 2: Location of the sampling sites.

Sampling Site	G.P.S Point	
Site 1	26°07'05.2" N	91°39'02.8"E
Site 2	26°06'45.2"N	91°40'14.5"E
Site 3	26°08'01.1"N	91°37'40.1"E
Site 4	26°07'38.9"N	91°38'28.1"E
Site 6	26°07'21.9"N	91°39'02.8"E

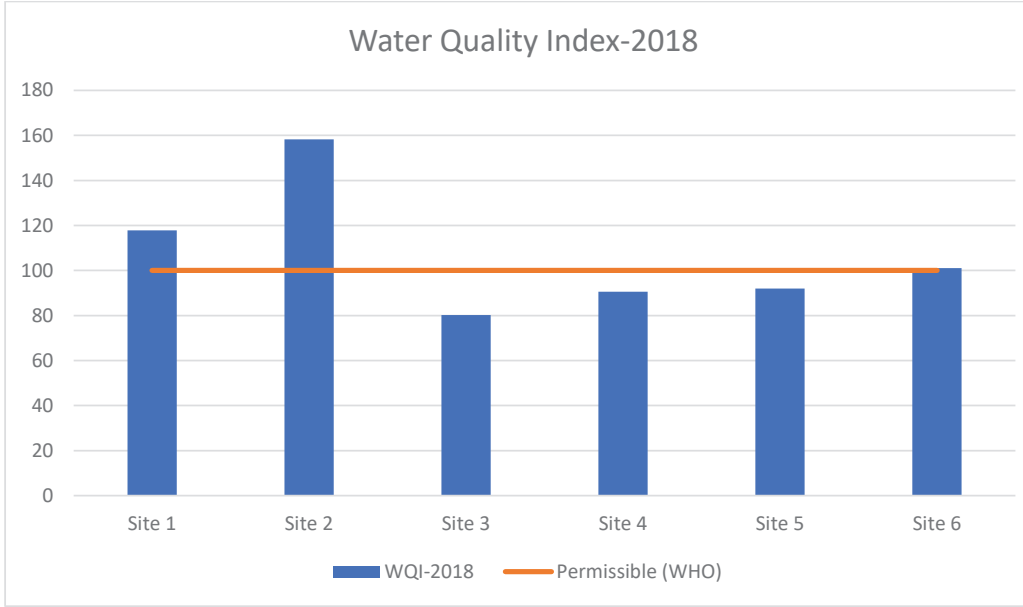

Fig. 3: Water Quality Index- 2018.

Comparing 2008 and 2018 water quality, the amount of non-satisfactory limits of parameters are temperature, total dissolved solids, turbidity and total hardness. The weighted arithmetic water quality index (WQIA) is in the following form: $WQIA = \Sigma_0^n wi \Sigma_0^n qi$,, where, n = the number of variables or parameters, wi = relative weight of the i^{th} parameter, qi = water quality rating of the i^{th} parameter. The permissible range of Water Quality Index for Drinking Water (as per WHO, World Health Organization) is below 100 (Fig. 3).

There is a significant decrease of birds count from the year 2008 to 2018 by 47.30% of species population of above 1000-12000 and a decrease of 39.6% of species population of above 500-900 as shown in Fig. 4 and Fig. 5 respectively.

Fish yield (in MT) has declined from 2015 to 2018 in the Deepor Beel. Fish growth rates are directly affected due to suspended matter. Increased turbidity is a form of pollution and it has consequences for nutrient supply, transport of dissolved organic materials, macrophytes, periphyton, and

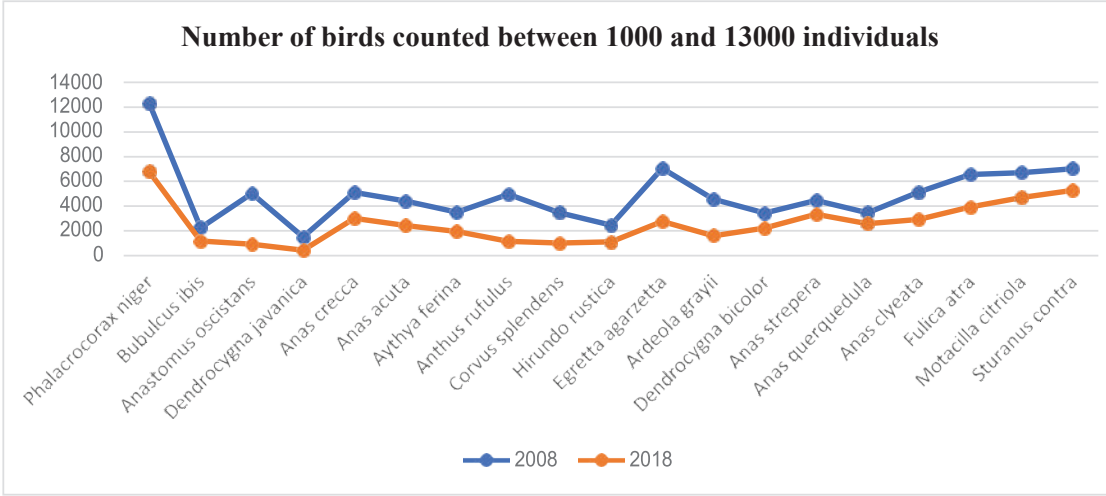

Fig. 4: Species count between 1000-13000 individuals.

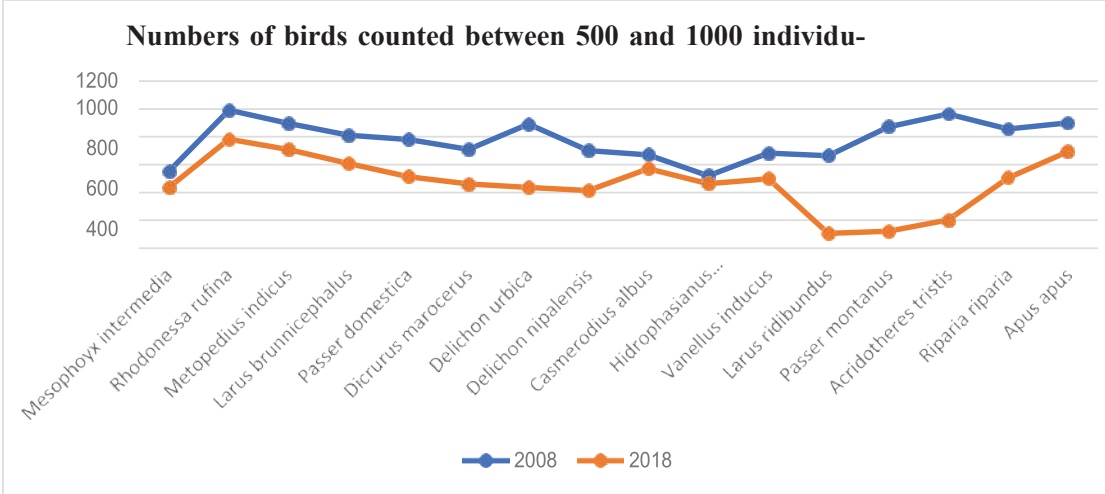

Fig. 5: Species count between 500-1000 individuals.

utilization. Applying Karl Pearson Correlation, the value of R, Pearson's Correlation is -0.8608. This is a strong negative correlation, which means that with increasing turbidity level, there is a decreasing fishing yield. The p-value is 0.00616. The result is significant at $p<0.05$ (Fig. 6).

The untreated wastewater was finding its way from Basistha and Dead Bharalu into Deepor Beel and was deteriorating the condition of the Beel. The original channel of Bharalu bifurcates into two rivulets- One of the rivulets known as the Basistha River flows towards Deepor Beel. Total wastewater generation is 44 MLD from the Basistha River and 25 MLD for Bharalu river. According to the State Pollution Control Board, the Bharalu and Bahini rivers pass through 11 numbers of municipal wards of the GMC area.

Development Initiatives of Tourism by Government and Private Sectors in Guwahati

Presently there are total 10 tourism agencies and operators within the city namely (1) Kamakshi Tours, (2) Sarothi Tourism, (2) Luit Tours and travels, (3) River Tours, (4) Assam on Wheels, (5) Ride & Climb, (6) Tourism NE, (7) Barapani Boats, (8) My Voyage Tours & Travels, (9) Zero-Valley Tourism and (10) Grand Eastern Holidays. Out of the total agencies, there are only 3 who are including Deepor Beel lake in their daily tour.

There are 5 tourism circuits in the state namely:

Circuit 1: Guwahati- Nameri- Kaziranga- Dirag-Tawang- Tezpur- Bomdila- Guwahati;

Circuit 2: Cherrapunjee- Shillong- Mawlynong;

Circuit 3: Guwahati- Hajo- Sualkuchi- Manas- Dhubri- Guwahati;

Circuit 4: Dibrugarh- Saikhowa- Dehing- Patkai- Dibrugarh;

Circuit 5: Jorhat- Kaziranga- Majuli- Sivasagar- Jorhat

Out of all the tourism circuits in the state, only Circuit 3 is including the Deepor Beel lake within the tour.

Guwahati tourist spots included in the tourism circuits are categorized into pilgrimage tourism circuit, cultural tourism circuit, wildlife tourism circuit and leisure tourism circuit. The tourist spots included in the circuits are: -

Pilgrimage Circuit 1: Kamakhya temple- Umananda Temple- Basistha;

Cultural Circuit 2: NE Tribal Museum & Cultural Centre- Sankardeva Kalakshetra- State Museum;

Wildlife Circuit 3: Deepor Beel lake- Amchang Wildlife Sanctuary- Nehru Park;

Leisure Circuit 4: Accoland amusement park- Northbrook Gate- Brahmaputra River cruise;

Out of all the tourism circuits in the state, only the Wildlife tourism circuit includes the Deepor Beel lake within the tour.

Current tourist inflow to the Deepor Beel Wetland (2018-19) is 305095 and 836 per day. If the tourist inflow is projected to 5 years, the projected tourist inflow according to geometric population growth calculation is 411835.17.

Physical Carrying Capacity, $PCC - A \times V/a \times Rf$; where, A = available area for public use; V/a = one visitor / M2; Rf

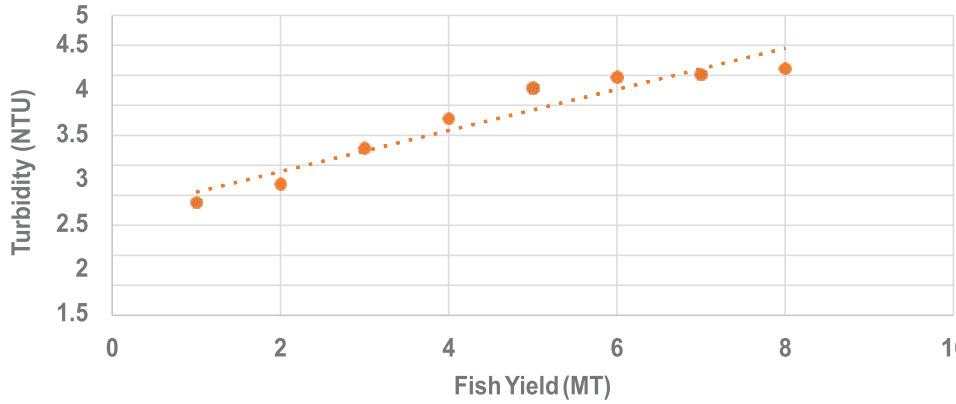

Fig. 6: Karl Pearson's coefficient.

= rotation factor (number of visits per day). There can be accommodated the projected population of tourist visitors per day to the Deepor Beel lake recreational area for ecotourism at 42660 tourists per day according to the physical carrying capacity.

Real carrying capacity, $RCC - Cf_1 \times Cf_2 \ldots Cfn$; where, Cf is a corrective factor expressed as a percentage. As the corrective factors are "site-specific", and are expressed in percentage as:

$Cf - M1/Mt \times 100$; where, Cf = corrective factor; M1 = limiting magnitude of the variable; Mt = total magnitude of the variable. Considering the corrective factors as excessive rainfall and disturbance to wildlife, there can be accommodated the projected population of tourist visitors per day to the Deepor Beel Lake Recreational Area for Ecotourism at 42463 Tourists per Day according to the Real Carrying capacity.

Governance and Socio-Economic Aspects of the Wetland Management and Tourism

The study area delineates a total of 18 villages which falls under the jurisdiction of the Guwahati Metropolitan Development Authority under the Kamrup Metropolitan District. The study area of 18 villages falls under the Azara revenue circle. There is an issue of overlapping of responsibilities at the same time lack of coordination and civic involvement in terms of the Deepor Beel lake management. There are active authorities like the Revenue Department that looks after the livelihood of the villages within the Azara Revenue circle in the study area and the Assam Forest Department who is the management authority of the Wetland.

The Assam Fisheries Department is the functional authority but is inactive because of which illegal fishing is taking place in the wetland. The Aaranyak and Eco-Concepts are the two Non-Governmental Organisations who researched the wetland in relation to conservation of biodiversity in the wetland.

Based on the socio-economic survey done on 800 households (respondents) out of 7127 households in the study area, the socio-economic status is determined using the Kuppuswamy's socioeconomic status scale, (Table 3) (Kishore et al. 2015).

Comparing self-employed weavers is 88%, to weavers working under merchant is 12% and a negligible percentage of weavers working in cooperative societies. Merchants get more wages while the self-employed get lesser wages as 45.9% of weavers worked in domestic production. Weavers working under merchants got an average monthly income of Rs. 200-600, while self-employed got 600-1000. The region has more than 50% of idle looms as almost half of the weavers worked in domestic production and therefore, there is low productivity. There is a lack of commercial production due to which the share of handloom income to the total household income is below 5% while average share of handloom income to the total household income in India is 30.2%.

Analytical Hierarchical Process (AHP) has been used as a tool to assess the six important parameters of ecotourism based on perception analysis as shown in Table 4. As high as 67% of the visitors were very satisfied with their experiences in visiting the wetland and about 21% were somewhat satisfied. However, 3% were not sure about the concept of ecotourism and its need. Only 1% of the visitors were very dissatisfied and 5% were quite satisfied with their experience. The major reasons for the dissatisfaction of the visitors were poor amenities and security concerns.

Willingness to pay is the Maximum Price at which the buyer would buy a good. Because the demand curve shows

Table 3: Kuppuswamy's socioeconomic status scale.

Kuppuswamy's Socio-economic Status Scale		Class	
Socio-Economic Class	Upper (i)	26-29	15.65- Lower Middle
	Upper Middle (ii)	21-25	
	Lower Middle (iii)	15-20	
	Upper Lower (iv)	10-15	
	Lower (v)	<10	

the maximum amount buyers are willing to pay for a given market quantity, the price given by the demand curve represents the willingness to pay of the marginal buyer. Consumer surplus is defined as the difference between the total amount that consumers are willing and able to pay for a good or service (indicated by the demand curve) and the total amount that they do pay (i.e. the market price). There is a maximum quantity demanded and consumer surplus at Rs. 50 as entry fee to the wetland as shown in Table 5.

Visitors were also asked to rate the components that need to be given importance for ecotourism development. Also, how likely the tourists are willing to use the activities/facilities if developed and their willingness to pay for the same.

Ecotourism Potential Analysis

The SWOT analysis categorizes and uses the scoring of the elements of importance applying Flavel and Williams' (Peacock, 1998) weighted quantifiable and measurable scoring methodology. The SWOT matrix is shown in Table 6.

The required data has been gathered through questionnaire and field study of the stakeholders at various levels and by applying Pralong's method, ecotourism potential of the Deepor Beel lake is evaluated. A tourism scale (scientific, aesthetic, economic and cultural attractiveness) has been developed based on the potentiality study. Tourism Scale = 5.45 which means there is an average potentiality of ecotourism in the Deepor Beel Lake.

PROPOSALS

The objective of the Proposal is to suggest Strategies to enhance ecotourism for wetland development. The Proposals, therefore, aims at Socio-Economic improvement, generation of Funds for the conservation of wetland and Environmental conservation in terms of policy level strategies, spatial ecotourism plan and organizational services.

Socio-Economic Improvement: Introducing Co-operative Societies of Artisans

Introducing Co-operative Societies of Artisans as an autonomous association of persons united voluntarily through a jointly owned and democratically controlled enterprise could result in socio-economic improvement in the study area. By providing 2 looms per household would provide profitability by 51% of the household income among the villages from

Table 4: AHP ranking- 6A's tourists' perception analysis.

Range	Rank			
1-12.0	1	Very Bad		
12.5-25	2	Bad		
25.5-37.0	3	Good		
37.5-50	4	Very Good		
Indicator			Rank	
Attraction		43.2	4	Very Good
Accessibility		42.5	4	Very Good
Amenities		12.5	2	Bad
Alertness		40	4	Very Good
Accord		46.25	4	Very Good
Attendance		30	3	Good

Table 5: Willingness to pay.

Price (P)	Quantity Demanded (Visitors Number)	Consumer Surplus (WTP-P)
50	95	10805
100	66	6125
150	65	2675
200	36	-775
250	39	-4225
300	18	-7675

the revenue generated per loom. Profitability from the loom is shown in Table 7.

Environmental Conservation: Ecotourism Circuits

The Deepor-Beel lake should be added with more Circuits to increase the revenue to the wetland community. The proposed Ecotourism Circuit may have the Deepor Beel Lake and it's Handloom Village added to the existing Cultural Ecotourism Circuit, Leisure Circuit and a new One Day Transit Tour. The proposed Ecotourism Circuits that includes the Deepor Beel and its Handloom Village are as shown in Table 8 and the map is as shown in Fig. 7.

Environmental Conservation: Conservation Zone

The conservation of the Deepor Beel lake is intended to bring people close to nature. Preservation of the diverse habitat of birds with the strategy to preserve the livelihood of the dependent community is the vision towards conservation proposals for Deepor Beel. The zoning has been done ensuring the conservation and preservation of the natural habitat and divided into 3 parts (Fig. 8)- the core area as ecologically protected Aquatic Eco-System, water conservation zone; A riparian corridor along the lake on all sides acts as a protective buffer and to arrest any further encroachment towards the water boundary.

Activities like eco-parks (biophilic), bird watching, forest camps, boardwalks along the forest wilderness and nature watches, picnic area, are conceived in these nature reserve areas. In the southern side, between the road and the railway line, botanical garden and children play area is proposed which will enhance the greenery of the shoreline of the lake and generate economy as well as employ some of the locals. Active recreation areas such as picnic spots and parks are proposed on the southern side of the lake. And crafts' and Fishermen village is proposed near the Beel area specially the Azara, Kahikuchi and Mirjapur. Convention Centre is proposed on the opposite side of that road. The conceptual view of the proposed eco-tourism development is as shown in Fig. 9.

The proposed riparian corridor of native trees species will further result in carbon sequestration capturing and storing atmospheric carbon dioxide. It is one method of reducing the amount of carbon dioxide. The Riparian Zone is divided into 3 zones as it is evidenced that total biomass carbon

Table 6: SWOT Matrix

Strength	Weakness
S1: Site Suitable for Ecotourism S2: Funding for Conservation & Maintenance S3: RAMSAR Site of International Importance S4: Traditional Villages actively engage in Handloom Sector S5: Increasing Tourists Inflow, High Carrying Capacity and Tourists actively take interest in Handloom sector of local people.	W1: Local Community lacking awareness of the importance of ecotourism W2: Lack of National awareness and Source of Information W3: Water Contamination due to Sewerage Disposal W4: Tourist Circuits not including the Wetland W5: Clash of overlapping Responsibilities among the Authorities.
Opportunity	**Threat**
O1: Masterplan 2025- GMDA focusing on Deepor Beel Wetland Tourism O2: Tourists Willing to Pay for Recreation O3: Local Community ready to engage in Handloom Village O4: Area available for Nature-Based Development & Afforestation O5: High Fish Culture Potential	T1: Increasing Built Up area due to Urbanization in the Eco sensitive Zone T2: Political Conflicts effects the Administration T3: Proposed Solid Waste Landfill site within the Wetland Area in the Proposed Masterplan-2025 T4: Weal national perception on Ecotourism and among the various Experts stakeholders T5: Located in Zone V-Highest Seismic Zone in India.

Table 7: Profitability calculation.

Revenue	Unit	Amount
Total no. of Households to be engaged	In Nos.	82354.2
Total Fixed Cost (TFC)	In Rs.	200
Total Variable Cost (TVC)	In Rs.	1800
Average Fixed Cost	In Rs.	200
Average Variable Cost	In Rs.	900
Gross Return (GR)	In Rs.	5000
Gross Margin = GR-TVC	In Rs.	3200
Gross Cost of Industry	In Rs.	2000
Net Return	In Rs.	3000
Average Return	In Rs.	1500
Per Loom Profit	In Rs.	1500
Profitability	In Rs.	4100

Table 8: Ecotourism circuits.

Circuits
Circuit 1: Cultural Ecotourism Circuit Engaging the tourists with the region's culture, specifically the lifestyle of the people in those geographical areas, the history of those people, their art, architecture, religion and elements that helped shape their way of life.
Circuit 2: Leisure Ecotourism Circuit Providing leisure travel to tourists with an educational and adventurous experience visiting complex and fascinating ecosystems and their associated cultures and traditions.
Circuit 3: Education Ecotourism Circuit It includes pursuing education, carrying out research activities and knowledge acquisition.
Circuit 4: One Day Transit Tour Taking to the most important Tourism spots in the city which will increase the frequency of tourists to the sites.

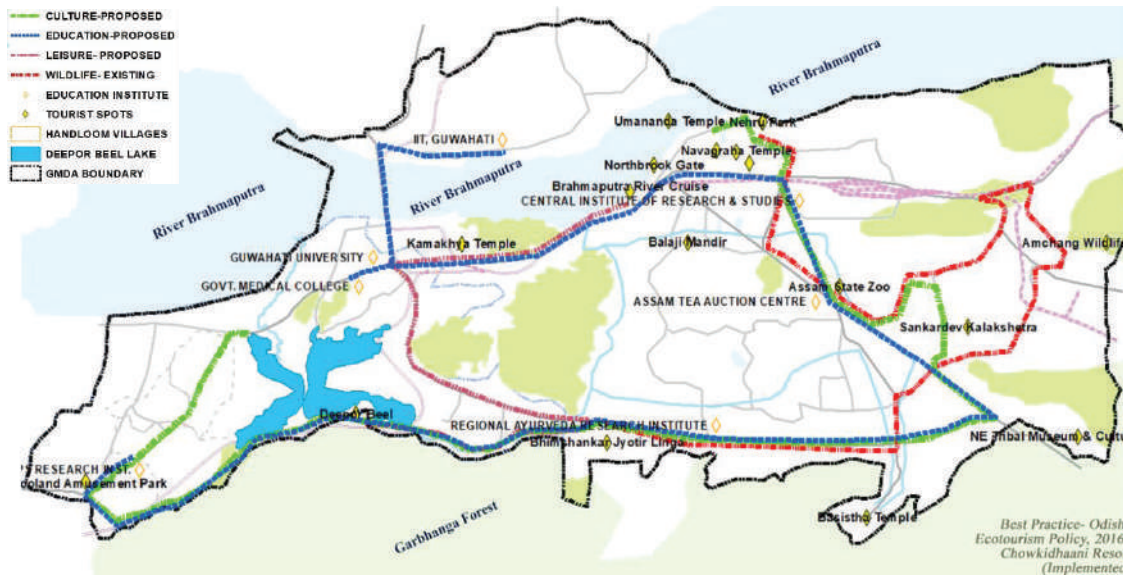

Fig. 7: Proposed tourism circuits.

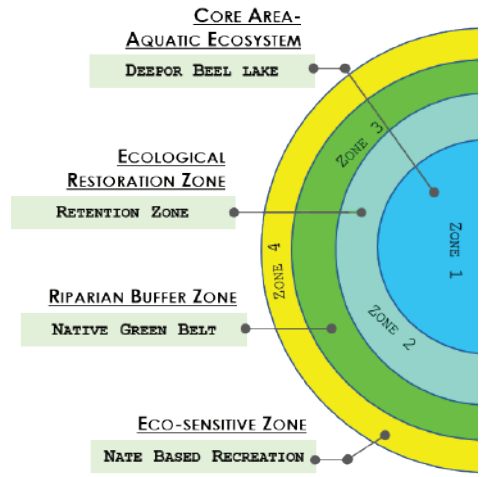

Fig. 8: Zoning of the study area.

content varies in shrubs, trees and herbs in native vegetation as shown in Fig. 10.

The amount of biomass present in the native vegetation was estimated by destructive analysis as shown in Table 9. Three native species of shrub species, herb species and tree species have been selected for biomass sampling. The biometrical parameters like height, basal diameter and root length of the uprooted plants and trees were taken.

Environmental Conservation: Floating Islands

Creating Floating Islands with indigenous Plant Species can attract more migratory and resident Water Bird Species to the Lake. Creating habitat for water birds and another aquatic biodiversity as well as improving water quality in agricultural landscapes. Due to the shrinkage of the wetland, there is a decreasing habitat for the waterbird species. These islands can act as ideal nesting grounds for animals and birds seeking safer areas as they are anchored away from the shore to help protect from predators. The map showing the potential location of the floating islands and the conceptual sketch of the floating island is as shown in Fig. 11.

Environmental Conservation: Interceptor Sewerage Treatment Plant

There is continuous damage to the Deepor Beel lake's ecosystem, due to alleged unregulated flow of sewage at the Dispur

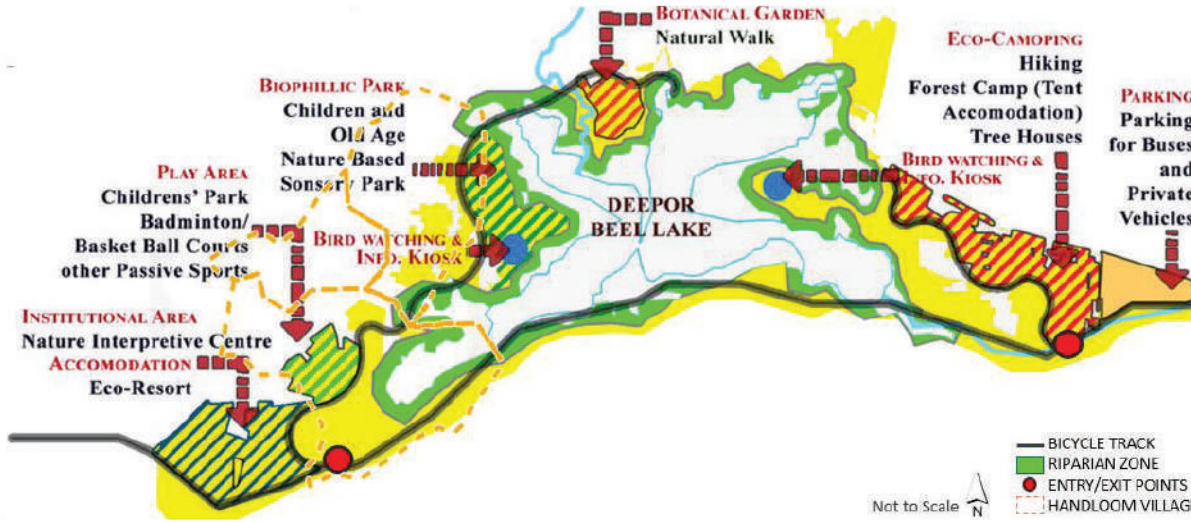

Fig. 9: Conceptual view of the proposed Ecotourism Development

Sub-Basin which leads to deterioration of the wetlands' water quality due to seepage of such leachate through the Bharalu river. The collection of the existing sewage and stormwater drains in interceptor pipes would run parallel to the length of Bharalu Riversides and would be conveyed to the proposed site of the 35 MLD STPs near the Deepor Beel Wetland. The estimation of the capacity of the proposed STP and the estimated cost is as shown in Table 10 and Table 11 respectively.

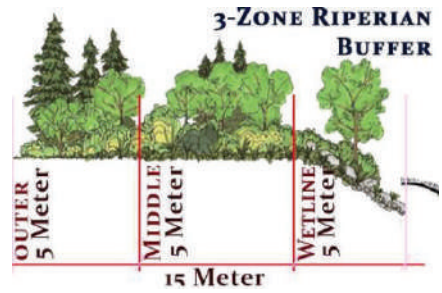

Fig. 10: Riparian buffer zoning.

Table 9: Carbon sequestration of the riparian buffer- destructive method.

Details					
Total Area of the Riparian Buffer Zone	0.375 Sq. Kms. (Area)	Width= 0.15 Kms; Perimeter= 24 Kms; No. of Zones- 3			
Native Species	Tree	Acacia leucophloea			
	Shrub	Cassia auriculate			
	Herb	Abutilon indicum			
Calculating Biomass Carbon Storage (kg/ha)- Capacity using Destructive Method					
Tree= 532.32	Shrub= 487.85	Herb= 189.19			
Total Carbon Sequestration		**1209.36 kg/ha**			
Carbon Storage		45351 Kg			
	Leaf	**Branch**	**Stem**	**Root**	**Total**
Acacia leophloea	35.95	125.05	251.04	120.28	532.32
Cassia auriculate	53.18	134.14	181.35	119.18	487.85
Abutilon indicum	16.85		44.01		189.19

Table 10: Estimation of STP capacity.

Calculation of per Capita Sewage Generation	Demand (lpcd)
Net per capita water demand	135
Add 10% for ICI demand @ 10%	13.5
Add ground water infiltration @ 5%	6.75
Sub-Total	155
Considering 80% for sewage generation	124
Projection for Total Waste Water Generation for Bharalu Catchment Area	
Wards	Ward No. 24,42,43,44,45,46, 47, 48, 49, 50, 51, 52, 53, 54, 55, 56, 57, 58
Total Projected Population 2020	3,97,166
Total Projected Population 2035	43, 073
Sewerage Contribution	125 lpcd
Sewage Generation 2020	25
Sewage Generation 2035	33
Proposed STP	35 MLD

Considering the watershed of the wetland and the greater flow in the city, the location of the proposed STP is as shown in Fig. 12.

Cost-Benefit Analysis

The cost of the Project has been estimated based on the current value of the infrastructures in Guwahati (collected from Dora Beel Ecotourism Project, NGO, Assam) as shown in Table 12. The yearly operating cost of the Project has been estimated based on GMDA estimate for Deepor Beel considering approx. cost for Site Maintenance, Running Expenses/ Utilities, Marketing & Stationary, Wages to Permanent Employee and Misc. Expenses which has been included in the Initial Capital Cost.

Total initial investment for the Ecotourism Project has been estimated as Rs. 551.51 Lakhs. Conservation Surplus

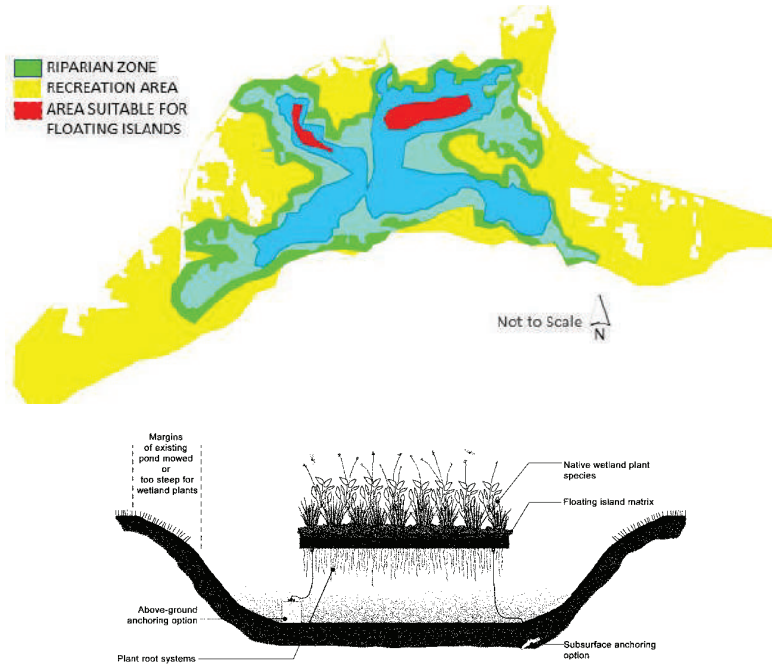

Fig. 11: Proposed floating islands

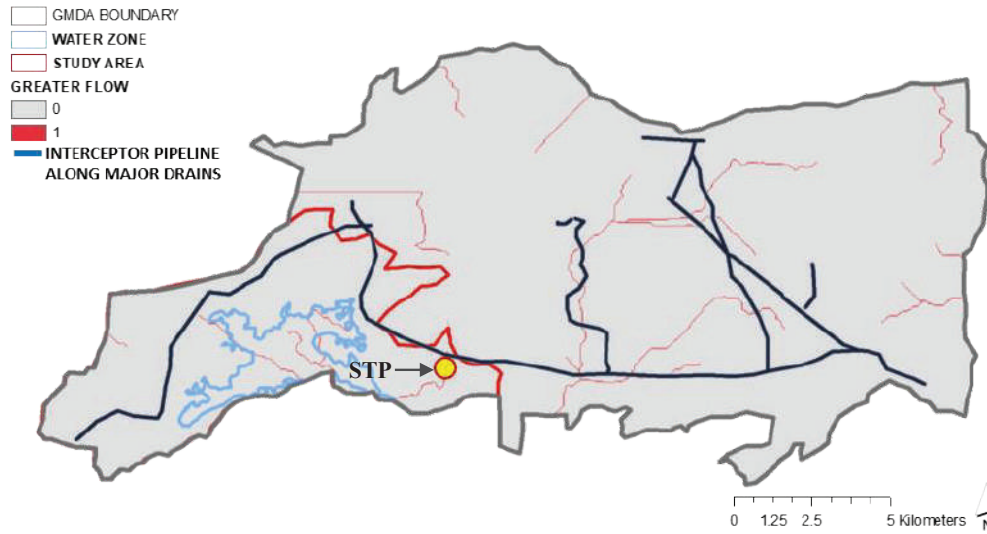

Fig. 12: Map showing the proposed Interceptor pipelines and the STP

Table 11: Cost estimation of the proposed STP.

Calculation of per Capita Sewage Generation	Demand (lpcd)
Net per capita water demand	135
Add 10% for ICI demand @ 10%	13.5
Add ground water infiltration @ 5%	6.75
Sub-Total	155
Considering 80% for sewage generation	124
Total Projected Population 2020	3,97,166
Total Projected Population 2035	43, 073
Sewerage Contribution	125 lpcd
Sewage Generation 2020	25
Sewage Generation 2035	33
Proposed STP	35 MLD

Table 12: Total cost.

Particulars/ Activities/ Facilities	Amount (in Lakhs)
Total Yearly Operating Cost of Project	**6.75**
Total Initial Capital Cost of the Project (operative expenses for 05 years)	**551.51**

Table 13: Total benefit.

		Revenue Generated
Benefits to Economy	Tourists visiting the Wetland-41,1835 Tourists.	Recreation- Rs. 102958750
Social Benefit	20 skilled and semi-skilled personnel with appx 12.5 L Wages per annum based on Infrastructure Facilities	Rs. 6250000
Opportunity Cost	Handloom Industry (Weaving)	Rs. 590400
Total Benefit Revenue Generated		**Rs. 1097.99 Lakhs**

Rs. 540250 is the Benefit to the Environment for maintenance of the Ecosystem. The project benefits to Economy, Society and Opportunity Cost as shown in Table 13.

The calculated Cost-Benefit Ratio is 1:2.

CONCLUSION

The paper focuses on bringing out the importance of ecotourism for the conservation of urban wetland by which the wetland may contribute to the growth and development of the city. The analysis on the present status of the Deepor Beel carried out identifies issues in increasing encroachment of the wetland, deterioration of water quality and reduction in biodiversity. Further, assessment of the tourism infrastructure development establishes that there is a moderate development of physical infrastructure within the study area and that more than 30 times the projected tourists in 5 years may be accommodated in the study area with respect to physical and real carrying capacity. The governance assessment showed that there is a lack of coordination and civic involvement. The local community in the study area has a lower-middle-class socio-economic status and there is very low productivity of weaving. Analysis of the economic value of the wetland strengthens the necessity of wetland conservation through ecotourism. Based on the analysis, it is found that there is a potential of the wetland area for ecotourism. Various proposals have been established for the management of the wetland through ecotourism which would result in economic prosperity, environmental sustainability and empowerment of local communities. The cost-benefit analysis shows a ratio of 1:2 that says that the ecotourism development would add to benefit to the economy, society and environment.

ACKNOWLEDGEMENT

The publication of the research was carried out towards partial fulfilment of the requirements of the award of Master of

Planning at the Department of Planning, School of Planning and Architecture, Vijayawada. The author wishes to thank supervisor and coordinator, Dr. Abdul Razak Mohammad, Professor, Department of Planning, for his simplified valuable guidance, motivations and encouragement.

The author also appreciates the support and cooperation received during data collection from the Guwahati Metropolitan Development Authority, Assam Pollution Control Board, Aaranyak NGO, Tourism Directorate of Assam, the local people in the villages around the Deepor Beel wetland and other authorities if missed any. The author would also like to thank the experts who were involved in the various perception analysis for the research and the participants in the survey, who have willingly shared their precious time during the process of interviewing.

REFERENCES

Brown, R. M., McClelland, N. I., Deininger, R. A. and Tozer, R. G. 1970. A water quality index-do we dare? Water Sewage Works, 117(10): 339-343.

Finlayson, M., Cruz, R.D., Davidson, N., Alder, J., Cork, S., de Groot, R.S., Lévêque, C., Milton, G.R., Peterson, G., Pritchard, D. and Ratner, B.D. 2005. Millennium Ecosystem Assessment: Ecosystems and Human Well-being: Wetlands and Water Synthesis. Island Press.

Eco-tourism or Eco-exploitation? (n.d.). Retrieved 2019, from https://sites.google.com/site/globalecotourism1/

Ghermandi, A., van den Bergh, J. C., Brander, V. M., Groot, H. L. and Nunes, P. A. 2010. Values of natural and human-made wetlands: A meta-analysis. Water Resources Research, 46(12).

Horton, R. 1965. An index number system for rating water quality. Journal of the Water Pollution Control Federation, 37(3): 300-306.

Kishore, J., Kohli, C. and Kumar, N. 2015. Kuppuswamy's socioeconomic scale-update for July 2015. International Journal of Preventive, Curative and Community Medicine, 26-28.

Peacock, R. Flavel, Ron and Williams, Joe 1998.Strategic Management. A Practical Approach. Small Enterprise Research, 6(1): 73-74.

Nature Environment and Pollution Technology
An International Quarterly Scientific Journal

p-ISSN: 0972-6268
(Print copies up to 2016)
e-ISSN: 2395-3454

Vol. 19 | No. 2 | pp. 627-636 | 2020

Original Research Paper

https://doi.org/10.46488/NEPT.2020.v19i02.017

Open Access Journal

Preparation and Adsorption Properties of Polyacrylamide/Graphene Oxide Composite Aerogel

Yanyan Dong*, Wendan Wu*, Liping Liang*, Shuqi Tao* and Xu Meng*(**)†
N*College of Textile and Garment, College of Life Science, Shaoxing University, Shaoxing, 312000, China
**Key Laboratory of Clean Dyeing and Finishing Technology of Zhejiang Province, Shaoxing University, Shaoxing, 312000, China
†Corresponding author: Xu Meng; xumeng@usx.edu.cn

Nat. Env. & Poll. Tech.
Website: www.neptjournal.com

Received: 13-07-2019
Accepted: 05-10-2019

Key Words:
Polymer;
Composite material;
Adsorption;
Aerogel

ABSTRACT

Graphene oxide (GO) and acrylamide (AM) were polymerized and cross-linked to form a composite aerogel. The microscopic properties and thermal stability of the composite aerogel were characterized by infrared spectroscopy, thermogravimetric instrument and scanning electron microscopy. The adsorption properties of the composite aerogel were tested. The effects of temperature, GO/AM ratios, pH values, feed amounts, dye liquor concentrations and times on the adsorption properties of composite aerogels were investigated. The results showed that under the same experimental conditions, the more the aerogel dosage and the longer the adsorption time, the better the adsorption performance of the composite aerogel on the active yellow dye liquor; the temperature had little effect on the adsorption of the dye liquor. The gel had the greatest adsorption effect under acidic conditions. The pH was 0.99, the dosage was 0.25g, the concentration of the dye solution was 40mg/L, and the adsorption rate reached 65.51% after adsorption for 24 hours.

INTRODUCTION

With the rapid development of textile printing and dyeing industry, large quantities of industrial wastewater which contain dyes are discharged into the water (Ali et al. 2012, Liu et al. 2017). Adsorption is a simple and low-cost method, especially suitable for printing and dyeing wastewater treatment. The key to adsorption method is to find adsorbent with low price, simple preparation and good adsorption effect (Fei et al. 2016, Mahdavinia et al. 2014).

Aerogels are composed of polymer molecules or nanoparticles that cluster together (Buerkle et al. 2009). The main component of aerogels is gas, and the periphery of them is made up of cross-linked three-dimensional network solid structures. These properties of aerogels make them to have excellent physical performance, such as porous, low-density, excellent adsorption, good light transmittance, large specific surface area and especially low thermal conductivity (Gaharwar et al. 2011, Sorour et al. 2013, Nanda et al. 2012).

GO is the oxidation derivative of graphene, the chemical structure of GO is roughly, and a lot of oxygen-containing active groups attach in the two-dimensional plane of GO (Akhavan et al. 2011). These reactive groups can not only make the GO have good hydrophilicity, also provide the surface functionalization of GO with many active sites (Heidarizad et al. 2016). Due to the good dispersion of GO in the water, it is difficult to achieve effective separation after adsorption through centrifugation and filtration. In practical applications, it is general that modify magnetic nanoparticles on the surface of GO or implement the solid-phase extraction of GO-based materials by immobilization. Normally, the immobilization or surface modification processes will occupy or consume some functional sites on the surface of GO, reducing the role position of target molecules in adsorption, which affect GO adsorption properties.

PAM is mainly used in flocculation, precipitation, sludge dewatering, and sewage treatment of industrial wastewater. The molecular chain of PAM contains some polar groups, which can cross-link the particles through suspended solid particles in the adsorption solution or form larger flocculates through neutralization (Pal et al. 2018, Shettigar et al. 2018, Ou et al. 2017). These accelerate the sedimentation of particles, which has an obvious effect of accelerating solution clarification.

This work based on huge application value of PAM and GO in sewage treatment, composite modified GO and PAM innovatively and prepared the polyacrylamide/GO composite aerogel. In this experiment, the adsorption properties of composite aerogel were investigated. The influencing factors on the adsorption process were explored, such as the ratio of GO/AM in the composite, pH, temperature, time, inventory and concentration of dye solution.

MATERIALS AND METHODS

Chemicals and Equipment: All the chemicals and equipment were procured from standard and reputed companies.

Preparation of graphene oxide: The desired amount of grapheme (2 g) was added to a 500 mL three-necked flask containing 46 mL of concentrated sulfuric acid in an ice water bath. The suspension was stirred by a magnetic stirrer for 15 min, and 6 g of $KMnO_4$ was added as slowly as possible to the solution. The temperature of the solution was strictly controlled below 20°C during the addition. After the addition, the mixture was stirred by mechanical stirring for 2 h and then kept at 35°C for 30 minutes. The solution was diluted by 92 mL of DI water. After 15 minutes, a dose of 280 g of DI water was further added to the solution for further dilution and then 20 mL H_2O_2 with a concentration of 30 % was added. The reaction continued until the solution turned bright yellow. After filtration, the solid product was washed with hydrochloric acid with a concentration of 30%. The pH of the solid product was maintained at 7.0 by washing with DI water. The product was dried to constant weight with a vacuum freeze dryer and ground into suitable fine particles to obtain a final product.

Preparation of GO/AM composite aerogel: 2 g of acrylamide, 0.01 g of azobisisobutyronitrile and 50 g of absolute ethanol were added into a 250 mL three-necked flask. Then the mixture was shaken and slightly heated to completely dissolve the acrylamide. And then 1 mL of diethylene glycol dimethacrylate and 0.05 g of anhydrous sodium carbonate was sequentially added to the vessel. The desired amount of graphene oxide (0.01 g) was weighed and put into 50 g of absolute ethanol. After the graphene oxide was sufficiently dispersed in absolute ethanol by ultrasonic vibration, it was added to the three-necked flask. Then, the mixture was mechanically stirred at 70°C and reacted with condensed water for three hours to obtain a solid-liquid mixture, which was subjected to vacuum filtration, and the obtained solid which was frozen in a refrigerator for 12 h was dried to constant weight by a vacuum freeze dryer. The dried solid was ground to obtain a polyacrylamide/graphene oxide composite aerogel.

Drawing of the reactive yellow standard curve: 0.5 g of reactive yellow was added into a beaker containing 50 mL of DI water, stirred well with a glass rod. Then the solution in beaker was poured into a volumetric flask (500 mL). Then solution which was made by washing the beaker multiple times with DI water was poured into the volumetric flask. The DI water was added to the volumetric flask to near the marked line and then was slowly added to the marked line with a plastic dropper. The reactive yellow stock solution with a concentration of 1000 mg/L was prepared by shaking the solution well.

0.5 mL of the reactive yellow stock solution was accurately measured added into 49.5 mL of DI water to obtain a reactive yellow solution at the concentration of 10 mg/L. The other solutions of different concentrations (20 mg/L, 30 mg/L, 40 mg/L, 50 mg/L, 60 mg/L, 70 mg/L) was prepared according to the same method.

The absorbance of the reactive yellow solution from 10 mg/L to 70 mg/L was measured by UV-Vis spectrophotometer. The relationship between absorbance and concentration was calculated by a computer. The results are given in Table 1 and Fig. 1, respectively.

Adsorption performance of GO/AM composite aerogel: 11 mL stock solution was added to 1089 mL DI water to prepare reactive yellow solution at the concentration of 10 mg/L. After thoroughly stirring, 10 mL of the solution was taken to measure the absorbance. Then 200 mL of reactive yellow solution (10 mg/L) was added into 250 mL Erlenmeyer flask, added with 0.40 g of composite aerogels with different GO/AM ratios, then sealed and placed in a gas bath thermostat for adsorption at 25°C and 110 rpm for 24 hours. Then, the supernatant was filtered with a filter to measure the absorbance, and the adsorption after adsorbing was obtained according to the standard curve. The aerogel with the best adsorption performance was obtained according to the before and after comparison.

The adsorption was measured using the aerogel of best GO/AM ratio at different pH to get the best pH for adsorption. Then the same method was used to obtain the optimal adsorption temperature and the adsorption performance in different adsorbent dosages and different solution concentrations.

RESULTS AND DISCUSSION

FTIR spectroscopy analysis: The infrared spectroscopy spectra of GO/AM composite aerogel before and after adsorption were investigated. As shown in Fig. 2, a relatively broad absorption peak appeared around 3381 cm^{-1}, indicating that a red-shift of intermolecular or intramolecular hydrogen

Table 1: Data source of the standard curve.

Concentration (mg/L)	10	20	30	40	50	60	70
Absorbance	0.149	0.305	0.492	0.66	0.828	0.981	1.112

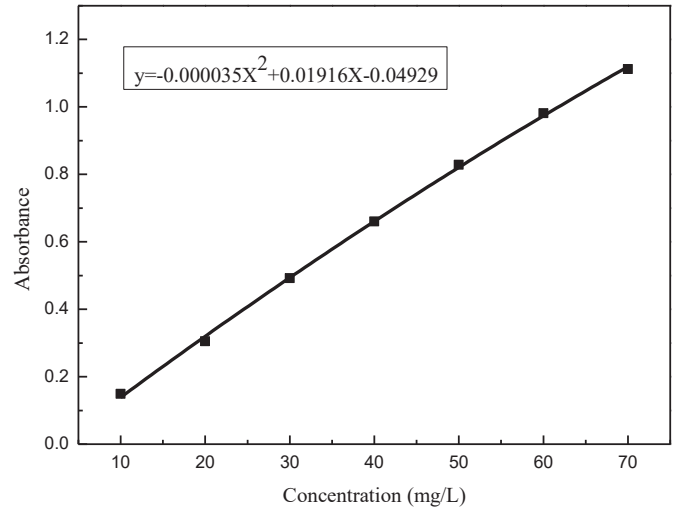

Fig.1: Standard curve of the reactive yellow.

bond occurred. The peak appeared at about 3176 cm^{-1} indicated that a stretching vibration of the N-H bond occurred. The peak appeared at about 1645 cm^{-1} which was assigned to the C=C vibration on the aromatic ring of the graphene oxide sheet. The absorption peak appeared at 1596 cm^{-1} and 1494 cm^{-1} could likely be assigned to the skeleton vibration of the aromatic ring. The characteristic absorption peak of C-O-C was 1132 cm^{-1}. According to the absorption peak, the GO/AM complex aerogel was formed successfully.

Analysis of SEM morphology: Typical scanning electron microscopic (SEM) images of GO/AM composite aerogels at different multiples before and after adsorption were shown in Fig. 3. By observing and comparing the SEM images at the same multiples, it could be seen that there were many pores on the surface of the composite aerogel before adsorption. These pores appeared because the ice had sublimated during the freeze-drying process, and the pores on the composite aerogel were advantageous to adsorb the dye. The pores on the aerogel after adsorption were greatly reduced because the aerogel adsorbed a large number of dye particles which blocked the pores in the composite aerogel.

Thermogravimetric analysis: The curve a indicated the

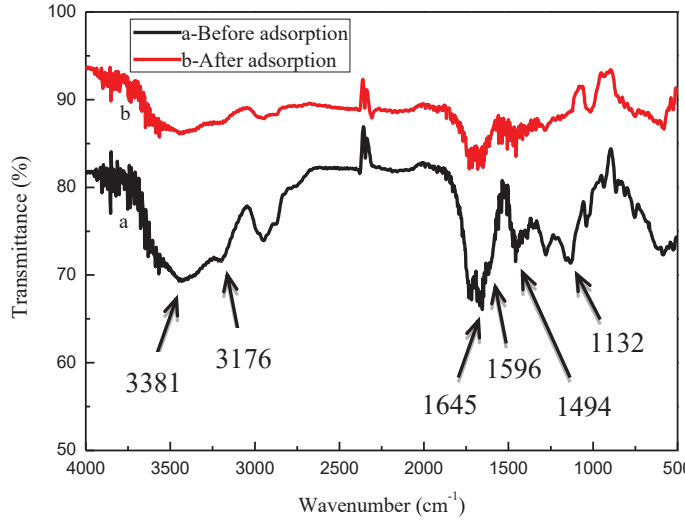

Fig. 2: Infrared spectroscopy before and after adsorption of composite aerogel.

thermogravimetric curve before the adsorption of the 4.5 % GO/AM composite aerogel, and the curve b indicated the thermogravimetric curve after the adsorption of the active yellow dye solution by the 4.5 % GO/AM composite aerogel. According to Fig. 4, the weight loss before 180°C was assigned to the decomposition of a part of oxygen-containing functional groups and small molecular substances in the aerogel. The weight loss from about 180°C to 326°C corresponded to the decomposition of the remaining oxygen-containing functional groups. The weight loss from 326°C to 410°C was mainly due to the process of deamination of adjacent amide groups and formation of acyldiamine. The weight loss above 410°C is the process of dehydrogenation and carbon dioxide formation. The comparison of the two curves showed that the thermal stability of the adsorbed material was slightly increased because the composite aerogel adsorbed a certain amount of reactive yellow, and the thermal stability of the reactive yellow was higher than that of the

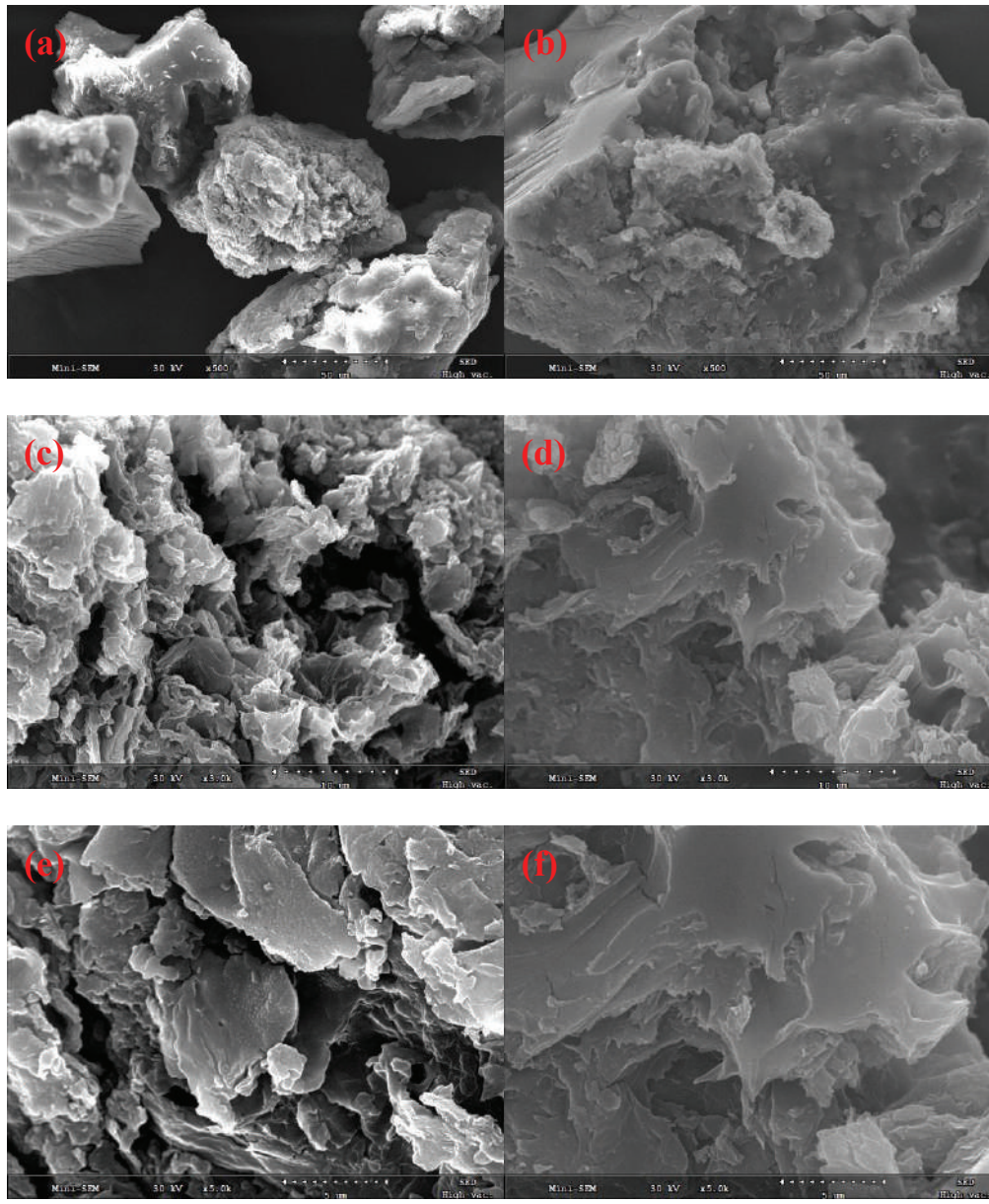

Fig. 3: a. before adsorption (500 times); b. after adsorption (500 times); c. before adsorption (3000 times); d. after adsorption (3000 times); e. before adsorption (5000 times); f. after adsorption (5000 times).

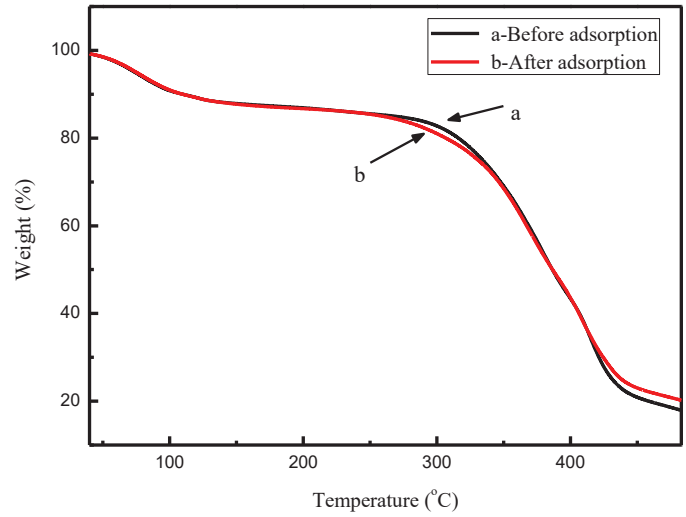

Fig. 4: Thermogravimetric diagram before and after adsorption of composite aerogel.

GO/AM composite aerogel, which caused the enhancement of the thermal stability.

Adsorption isotherm: Fig. 5 was the adsorption isotherm of the 0.5 % GO/AM composite aerogel. As shown in Fig. 5, as the concentration of the reactive yellow dye solution, increased from 20 mg/L to 60 mg/L, the equilibrium adsorption amount of the composite aerogel increased. This was because of the initial concentration of the dye solution increased, the number of molecules of the reactive yellow dye increased too, and the diffusion driving force increased as well so that the adsorption between the composite aerogel and the reactive yellow dye was more sufficient.

Adsorption equilibrium model: Equations such as Freundlich and Langmuir could usually be used to express the adsorption equilibrium of dyes in aqueous solutions. By fitting the equations of Freundlich and Langmuir in the adsorption test data of the composite aerogel on the reactive yellow dye solution, it was found that the adsorption of the reactive yellow by the composite aerogel was suitable for fitting with the Freundlich equation. Assuming that the adsorption reaction occurred on the surface of the inhomogeneous medium, the Freundlich equation could be expressed

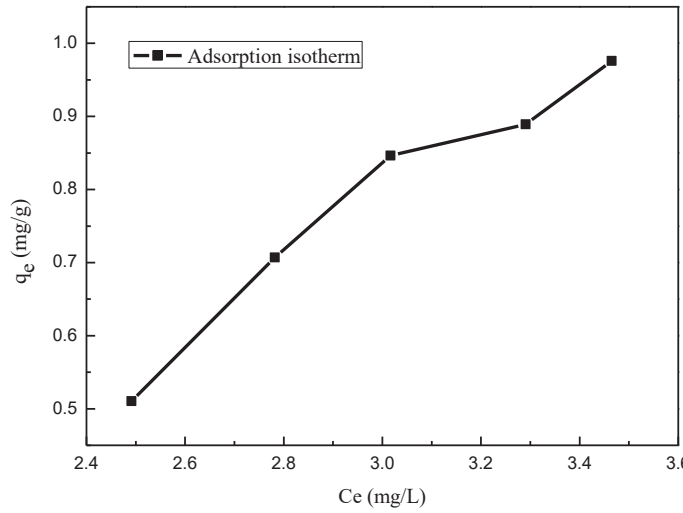

Fig. 5: Adsorption isotherm.

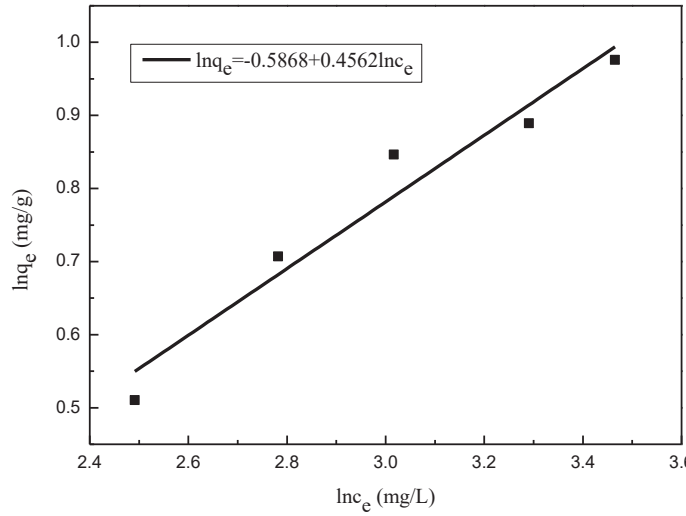

Fig. 6: Freundlich isotherm fitting line.

as $\ln q_e = \ln qF + (1/n) \ln C_e$, where the q_e (mg/g) is the equilibrium adsorption capacity, the kF (L/mg) is the constant of adsorption capacity, the 1/n is an empirical parameter, related to the adsorption density, the C_e is the equilibrium concentration of the solution, and the values of 1/n and kF can be calculated from the linear relationship between $\ln q_e$ and $\ln C_e$. The fitting curve is presented in Fig. 6, and the value of R^2 is 0.9519, which indicated that the adsorption reaction of reactive aerogel on reactive yellow occurred on the surface of the composite aerogel.

Effect of different ratios of GO/AM composite aerogel on adsorption effects: As shown from the picture in Fig. 7, from left to right is the dye solution before adsorption (1) and the dye solution after adsorption [(2) 0.5 % GO/AM, (3) 1.5 % GO/AM, (4) 2.5 % GO/AM, (5) 3.5 % GO/AM, (6) 4.5 % GO/AM].

The adsorption parameters from left to right were the solution before adsorption and after adsorption (0.5 %, 1.5 %, 2.5 %, 3.5 %, 4.5 % GO: AM mass ratio). The time of adsorption was 24 h, the adsorption temperature was 25°C, and the adsorption pH was 1.5. The amount of aerogel feed was 0.3 g, and the reactive yellow dye solution concentration

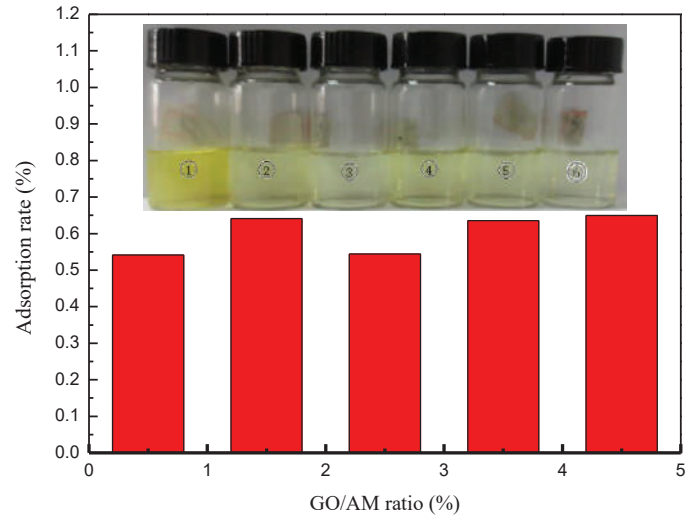

Fig. 7: Adsorption rate of reactive yellow dye by different ratios of GO/AM.

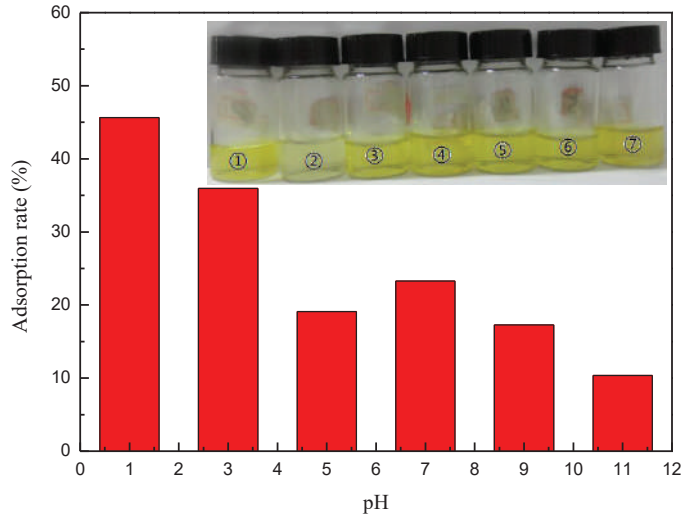

Fig. 8: Column chart of adsorption rate of different pH.

was 20 mg/L. It can be seen from Fig. 7 that the adsorption effect of aerogel tends to increase with the increasing of GO. It is because that GO contains a large number of active groups containing oxygen. And the amount of active site increases with the increasing of GO content what result in the enhancement of adsorption performance.

Effect of different pH of GO/AM composite aerogel on adsorption effects: As shown from the picture in Fig. 8, from left to right, are solution before and after adsorption with different pH ((1) pH=1, (3) pH=3, (4) pH=5, (5) pH=7, (6) pH=9, (7) pH=11). The adsorption parameters were GO: AM mass ratio with 4.5 %, the time of adsorption of 24 hours, and the adsorption temperature of 25°C. The aerogel dosage was 0.15 g, and the concentration of reactive yellow dye was 20 mg/L. It can be seen from Fig. 8 that the GO/AM composite aerogel has the best adsorption effect under acidic conditions, the feed amount is 0.15 g, and the adsorption rate can reach 45.64 %.

GO/AM composite aerogel adsorption effect with different feeding amount: The pictures in Fig. 9 from left to

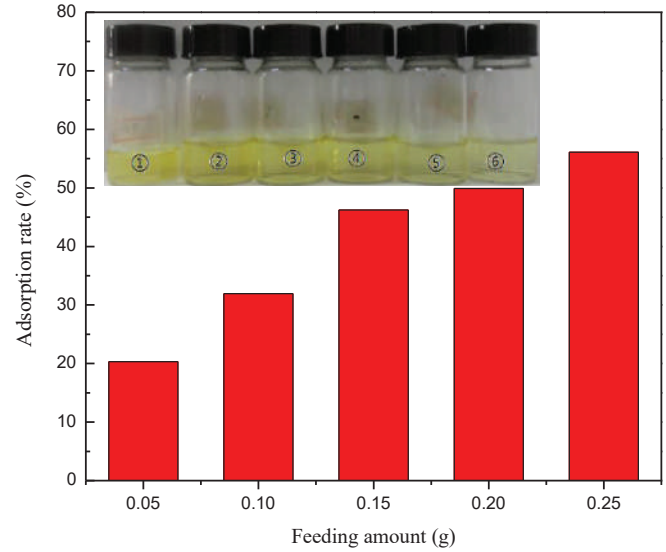

Fig. 9: Column chart of adsorption rate of different feed rates.

right were solution before adsorption (1) and the solution of different feeds [(2) 0.05 g, (3) 0.10 g, (4) 0.15 g, (5) 0.20 g, (6) 0.25g] after adsorption. Adsorption parameters: The aerogel charge amount was 0.05 g, 0.10 g, 0.15 g, 0.20 g, 0.25 g, and the GO: AM mass ratio was 4.5 %.The adsorption time was 24 hours, the adsorption temperature was 25°C, the adsorption pH was 1.9, and the concentration of the reactive yellow dye solution was 20 mg/L.

According to Fig. 9, as the composite aerogel dosage increased from 0.05 g to 0.25 g, the adsorption rate of the adsorbent to the reactive yellow dye solution increased from 20.33 % to 56.10 %. This is because of the amount of adsorbent increased, the adsorbent provided more active sites and functional groups, making the adsorption reaction more sufficient, thereby increasing the adsorption rate of the aerogel to the reactive yellow dye solution.

Adsorption effect of different concentrations of dye solution: In Fig. 10, the pictures from left to right were the concentration of the reactive yellow dye solution before and after adsorption [(1) 20 mg/L, (2) 30 mg/L, (3) 40 mg/L, (4) 50 mg/L, (5) 60 mg/L]. Adsorption parameters: The concentrations of reactive yellow dye solution were 20 mg/L, 30 mg/L, 40 mg/L, 50 mg/L and 60 mg/L. The GO: AM mass ratio was 4.5 %, the adsorption time was 24 hours, the adsorption temperature was 25°C, the adsorption pH was 1.9, and the feed amount was 0.25 g. Fig. 10 and Fig. 11 show that when the concentration of the dye solution is between 20 mg/L and 60 mg/L, the concentration of the dye solution has little effect on the adsorption rate.

Adsorption effect at different temperatures: In Fig. 12, the pictures from left to right were the solution before adsorption and after adsorption [(2) 10 °C, (3) 20 °C, (4) 30 °C, (5) 40 °C, (6) 50 °C]. Adsorption parameters: adsorption temperatures were 10 °C, 20 °C, 30 °C, 40 °C and 50 °C, GO: AM mass ratio was 4.5 %, adsorption time was 24 hours, adsorption temperature was 25 °C, adsorption pH was 1.75, feed amount was 0.15 g.

It can be seen from Fig. 12 that there is almost no difference in the adsorption effect of aerogel at 10°C, 20°C, 30°C, 40°C, and 50°C, indicating that the temperature has little effect on the adsorption of GO/AM composite aerogel.
Adsorption effect at different times: In Fig. 13, the pictures from left to right, the adsorption effects were as follows: adsorption for 0 h, 3 h, 6 h, 9 h, 12 h, and 24 h. Adsorption parameters: from left to right, adsorption for (1) 0 h, (2) 3 h, (3) 6 h, (4) 9 h, (5) 12 h, (6) 24 h. The adsorption temperature

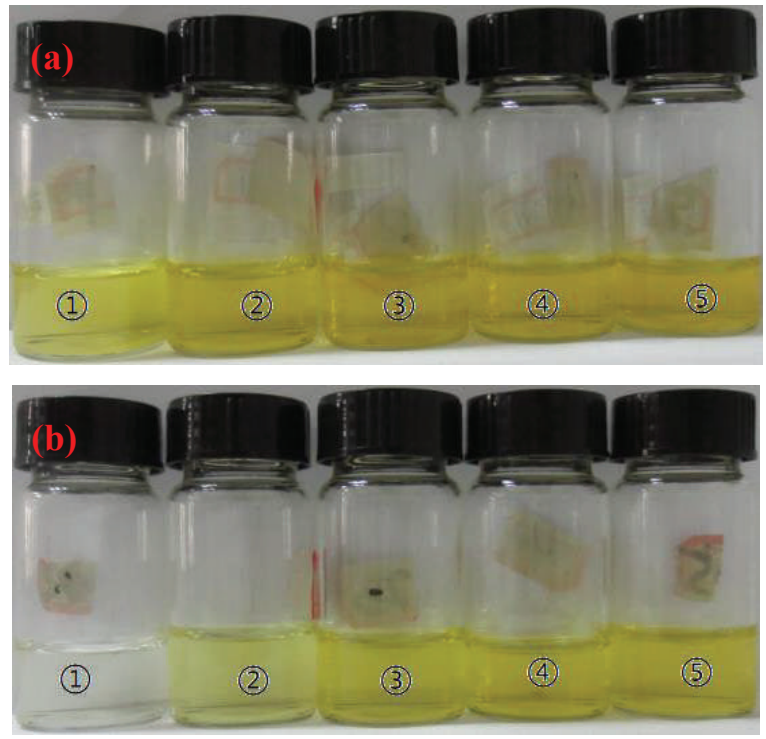

Fig.10: Different concentrations of dye solution before (a) and after (b) adsorption.

was 25°C, adsorption was pH = 0.99, feed amount was 0.25 g and the concentration of reactive yellow dye solution was 40 mg/L.

It can be seen from Fig. 13, the adsorption amount of the reactive yellow dye solution by the GO/AM composite increases with time, but the increasing rate of the adsorption amount decreases with time gradually increases. The reason is that there are a large number of active sites and functional groups on the composite aerogel. At the beginning of adsorption, these active sites and functional groups participate in the adsorption reaction of the reactive yellow dye solution, so that the adsorption rate at the beginning of adsorption is faster. As the reaction proceeds, the active sites and functional groups on the composite aerogel are gradually consumed. Therefore, the adsorption amount will continue to increase, but the adsorption rate will gradually decrease.

CONCLUSION

The polymerization and crosslinking process of acrylamide are used to combine GO and AM to form a composite aerogel, which combined the polyacrylamide and graphene oxide. The prepared composite aerogel has many pores and exhib-

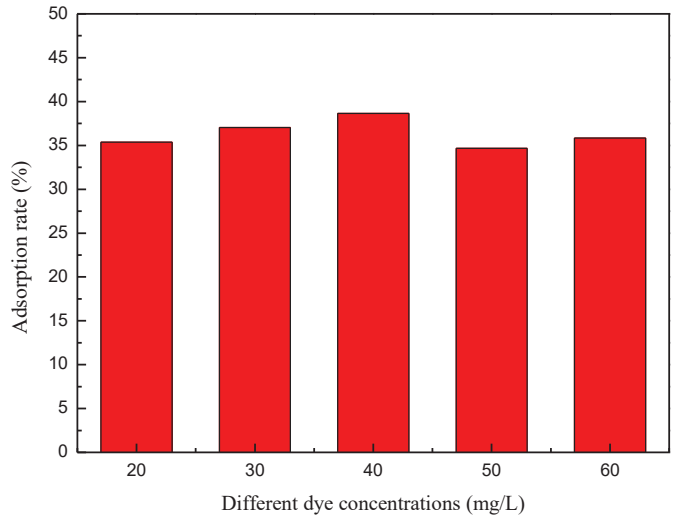

Fig. 11: Adsorption rate of different dye liquor concentrations.

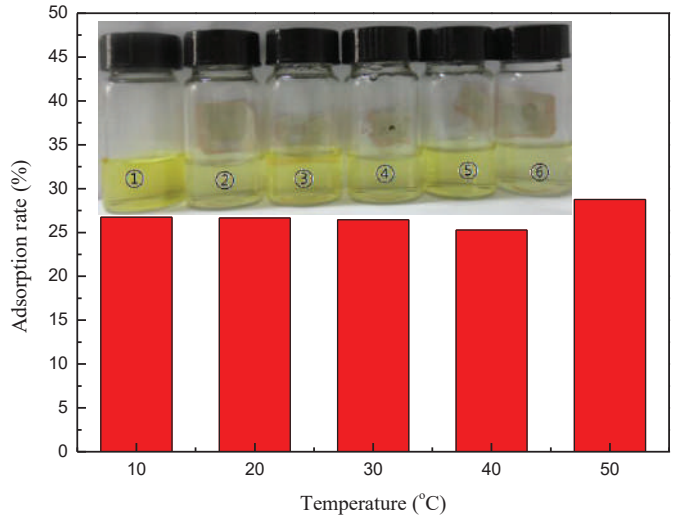

Fig. 12: Column chart of different temperature adsorption rates.

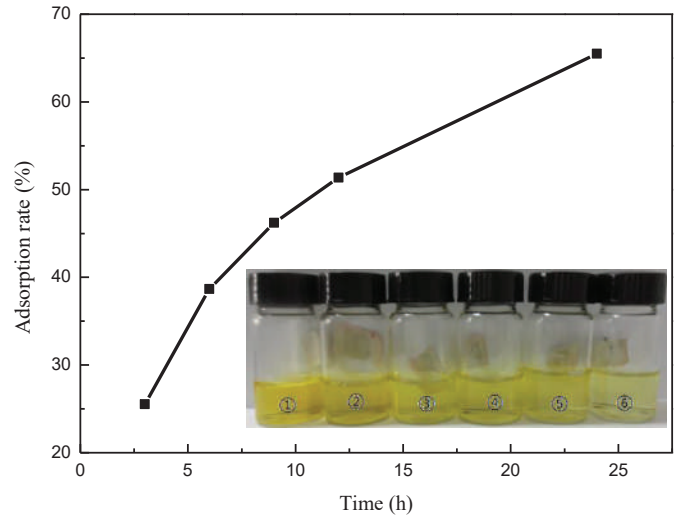

Fig. 13: Adsorption rate at different times.

its excellent adsorption performance to the reactive yellow dye solution. Through the adsorption experiment and the analysis of the adsorption results, it is concluded that 4.5% GO/AM (mass ratio) has the best adsorption performance for the reactive yellow dye solution. The optimum adsorption temperature is 50 °C, and the pH is 1. The adsorption effect is enhanced as the aerogel feed increased.

ACKNOWLEDGEMENT

The authors gratefully acknowledge the financial support of the National Natural Science Foundation of China (Grant No. 51703130), Zhejiang Provincial Natural Science Foundation of China (Grant No. LY18E080018), Shaoxing Public Welfare Project (Grant No. 2017B70042), and the International Science and Technology Cooperation Project of Shaoxing University (Grant No. 2019LGGH1004).

REFERENCES

Akhavan, O. 2011. Photocatalytic reduction of graphene oxides hybridized by ZnO nanoparticles in ethanol. Carbon, 49: 11-18.

Ali, I. 2012. New generation adsorbents for water treatment. Chemical Reviews, 112: 5073-5091.

Buerkle, L.E., Li, Z., Jamieson, A.M. and Rowan, S.J. 2009. Tailoring the properties of guanosine-based supramolecular hydrogels. Langmuir, 25: 8833-8840.

Fei, P., Wang, Q., Zhong, M. and Su, B. 2016. Preparation and adsorption properties of enhanced magnetic zinc ferrite-reduced graphene oxide nanocomposites via a facile one-pot solvothermal method. Journal of Alloys and Compounds, 685: 411-417.

Gaharwar, A.K., Dammu, S.A., Canter, J.M., Wu, C.J. and Schmidt, G. 2011. Highly extensible, tough, and elastomeric nanocomposite hydrogels from poly(ethylene glycol) and hydroxyapatite nanoparticles. Biomacromolecules, 12: 1641-1650.

Heidarizad, M. and Şengör, S.S. 2016. Synthesis of graphene oxide/magnesium oxide nanocomposites with high-rate adsorption of methylene blue. Journal of Molecular Liquids, 224: 607-617.

Liu, C., Liu, H., Xu, A., Tang, K., Huang, Y. and Lu, C. 2017. In situ reduced and assembled three-dimensional graphene aerogel for efficient dye removal. Journal of Alloys and Compounds, 714: 522-529.

Mahdavinia, G.R., Iravani, S., Zoroufi, S. and Hosseinzadeh, H. 2014. Magnetic and K+-cross -linkedkappa-carrageenan nanocomposite beads and adsorption of crystal violet. Iranian Polymer Journal, 23: 335-344.

Nanda, J. and Banerjee, A. 2012. ŞAmino acid containing proteolitically stable dipeptide based hydrogels: encapsulation and sustained release of some important biomolecules at physiological pH and temperature. Soft Matter, 8: 3380-3386.

Ou, K., Dong, X., Qin, C., Ji, X. and He, J. 2017. Properties and toughening mechanisms of PVA/PAM double-network hydrogels prepared by freeze-thawing and anneal-swelling. Materials Science and Engineering: C, 77: 1017-1026.

Pal, P., Pandey, J.P. and Sen, G. 2018. Synthesis and study of hydrolyzed polyacrylamide grafted polyvinyl pyrrolidone (Hyd.PVP-g-PAM) as flocculant for removal of nanoparticles from aqueous system. Materials Science and Engineering: B, 236-237: 32-42.

Shettigar, R.R., Misra, N.M. and Patel, K. 2018. CTAB grafted PAM gel and its application in drilling fluid. Journal of Petroleum Science and Engineering, 160: 129-135.

Sorour, M., El-Sayed, M., Moneem, N.A.E., Talaat, H.A., Shalaan, H. and Marsafy, S.E. 2013. Characterization of hydrogel synthesized from natural polysaccharides blend grafted acrylamide using microwave (MW) and ultraviolet (UV) techniques. Starch-Stärke, 65: 172-178.

Nature Environment and Pollution Technology
An International Quarterly Scientific Journal

p-ISSN: 0972-6268
(Print copies up to 2016)
e-ISSN: 2395-3454

Vol. 19 | No. 2 | pp. 637-650 | 2020

Original Research Paper

https://doi.org/10.46488/NEPT.2020.v19i02.018

Open Access Journal

Analysis of Water Balance Components and Parameter Uncertainties Based on SWAT Model with CMADS Data and SUFI-2 Algorithm in Huangbaihe River Catchment, China

Huijuan Bo*(**), Xiaohua Dong*(**)†, Zhonghua Li*, Gebrehiwet Reta*(**), Lu li*(**) and Chong Wei*(**)**
*China Three Gorges University, College of Hydraulic and Environmental Engineering, Yichang, 443002, China
**Hubei Provincial Collaborative Innovation Center for Water Security, Wuhan, 430070, China
***Comprehensive Law Enforcement Bureau for Protection of Water Resources in the Huangbaihe River Basin, Yichang, Hubei, 443005, China
†Corresponding author: Xiaohua Dong; bohuijuan027@126.com

Nat. Env. & Poll. Tech.
Website: www.neptjournal.com

Received: 05-08-2019
Accepted: 07-11-2019

Key Words:
SWAT model; Streamflow; SUFI-2 algorithm; Parameter uncertainty analysis; Water balance components

ABSTRACT

The Huangbaihe River is the primary water source for Yichang city. Large-scale phosphate mining activities in the Huangbaihe River Catchment area could change the proportion of streamflow components; therefore, an accurate simulation of streamflow and its components is vital to enable effective water resource management and protection. In this study, the Soil and Water Assessment Tool (SWAT) model with input data from China Meteorological Assimilation Driving Datasets (CMADS) and the traditional gaging station was applied to simulate hydrological processes in the upper reaches of the Huangbaihe River Catchment area. The constructed model was calibrated and validated using observed streamflow on a monthly scale. Parameter sensitivity and uncertainty analysis were conducted using the Sequential Uncertainty Fitting (SUFI-2) algorithm, and the strengths of calibration and uncertainty analysis were evaluated by applying the p-factor (proportion of measurements covered by the 95PPU) and r-factor (mean thickness of 95PPU band separated using the standard deviation of measurements). The results show that the SWAT model with the two kinds of data source proficiently simulated streamflow records compared with only one data from traditional gauging stations in both the calibration and validation periods at the whole outlet. For the calibration (2009-2012) and validation (2013-2016) periods, the statistical indexes are all good at the Xuanmiaoguan gaging station and the whole outlet. Furthermore, spatiotemporal changes in overland runoff and lateral flow were strongly consistent with precipitation, and significant differences in the contribution from hydrological elements to the water balance were observed between high and low-flow years.

INTRODUCTION

Global problems associated with water quantity and quality (such as floods and droughts, water quality deterioration, and eutrophication) are attracting increasing scientific, political, and public attention. The hydrological cycle and processes are complex within a region or watershed, and they are affected by both natural and human-related phenomena, such as heterogeneous soil characteristics, variations in land use and cover, climate change, and other factors (Mou et al. 2015, Dey & Mishra 2017, Wu et al. 2017). To enable effective water resource management within a region, it is necessary to study the water balance and the various hydrological elements (Dhami et al. 2018, Shawul et al. 2013). Hydrological models are effective tools that have been employed in recent years to provide a visual representation of hydrological processes and accurate flow simulations, particularly when assessing the impacts that land-use change and climate variability have on hydrological cycles and water balance components (Dong et al. 2015).

The SWAT model is a commonly used semi-distributed model (Arnold et al. 1998) that has been applied to predict the hydrological cycle within basins and to quantify nutrient migration, transformation, and large quantities of load within watersheds (Nie et al. 2011, Gan et al. 2015, Abbaspour et al. 2015, Abubakari et al. 2017). However, calibrating the model is challenging, and analysing uncertainties is the focus of much hydrological model research (Uniyal et al. 2015, Song et al. 2015). There are four main sources of uncertainty associated with the model: the model structure, the parameters, input data, and the operational model. In this respect, the uncertainty of the model structure mainly originates from over-simplifying hydrological processes in the natural world (Zhao et al. 2018); model input uncertainty relates to limitations in data representation and observational errors within the studied watershed; uncertainty with respect to the operational model

originates from human errors; and parameter uncertainty is associated with the large numbers of parameters and equifinality in the model. Of these uncertainties, model input should relate to an area in space and time, and parameter uncertainties can be minimized through an appropriate calibration method. Various techniques have been applied to analyse these uncertainties, including the Markov chain Monte Carlo (MCMC) method (Yang et al. 2008), parameter solution (ParaSol) (Wu & Chen 2015), SUFI-2 (Abbaspour et al. 2015, Narsimlu et al. 2015) and generalized likelihood uncertainty estimation (GLUE) (Gong et al. 2011).

Currently, numerous studies are focusing on model input and parameter uncertainty issues in SWAT models (Yatheendadas et al. 2008, Zhang et al. 2009, Li et al. 2010, Yang et al. 2018). For regions that have scarce observational data, input data have been developed using satellites that provide data on different spatiotemporal scales (Thiemig et al. 2013, Serrat et al. 2016, Tramblay et al. 2016). Accordingly, CMADS data (from 2008 to 2016) provided by the China Institute of Water Resources and Hydropower Research (IWHR) (Liu et al. 2018) have been applied in certain areas and can produce a better runoff simulation for incorporation into the SWAT model (Meng et al. 2017, Li et al. 2019).

The Huangbaihe River is a first-order tributary of the Yangtze River and the primary water source of Yichang City. However, there have been reductions in water quantity and quality in recent years within the Huangbaihe River Catchment in relation to intense climate variations and human interaction. Hence, it is extremely important to make an accurate prediction of streamflow to enable proficient water resource management. Although CMADS data have been applied in many basins in China where traditional weather stations are scarce, to the best of the author's knowledge, they have not been applied in the Huangbaihe River Basin. For example, the study of Wan et al. 2018 used traditional weather data to simulate streamflow in the Huangbaihe River Basin but the simulation accuracy in the upper reservoir watershed was inadequate.

Therefore, meteorological data from CMADS and traditional weather stations were both employed as SWAT model inputs in this study, enabling the prediction of streamflow in the upper reaches of the Huangbaihe River Catchment. Parameter sensitivity and uncertainty analyses and model calibration and validation were conducted by applying the SUFI-2 algorithm, and water balance components were then investigated based on the simulation outputs. Furthermore, spatiotemporal changes in hydrological components were identified, and the relationships between water balance components and precipitation were finally determined.

MATERIALS AND METHODS

Site Description

The studied catchment area is located within the east branch of Huangbaihe River that lies between 110°04′ and 111°30′ E longitude and 30°42′ and 31°29′ N latitude (Fig. 1).

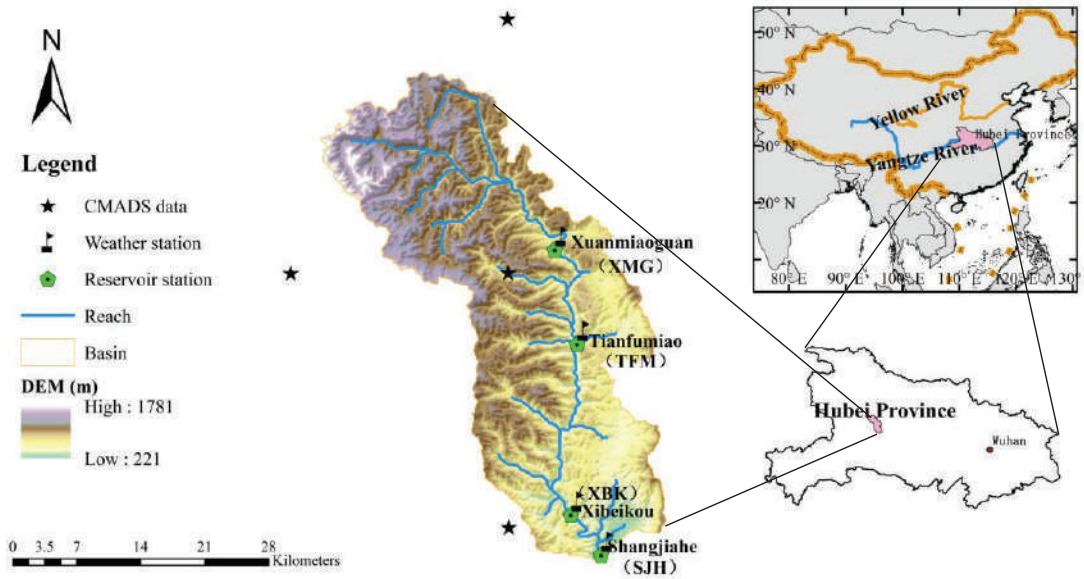

Fig. 1: Digital Elevation Model (DEM), rivers, and locations of discharge observation stations in Huangbaihe River Catchment.

The elevation ranges from 221 m above sea level (a.s.l.) at the outlet to 1781 m a.s.l. at the headstream and the area measures 937.97 km^2. The angles of slopes in most areas of the catchment are larger than 25°, and the average slope has an angle of 19.73°. The climate lies within the humid subtropical monsoon region, and mean annual precipitation and temperature are 1101 mm and 16.9°C respectively. The rainy season can extend from May to October, and there is heavy rainfall during summer.

The main land use types are forestry and agriculture, and these occupy percentage land areas of 81.4% and 15.3%, respectively. Other land cover types are urban (1.9%) and water (1.3%). Bare land is rare and is primarily distributed in mountainous areas, where large-scale phosphate mining activities are conducted. The main soil types are Lithosols and Chromic Cambisols (I-Bc-2c) and Orthic Acrisols (Ao13-3bc), which cover 48.6% and 42.6%, respectively. Other soil types are Calcic Cambisols (Bk42-2b) and Lithosols and Eutric Cambisols (I-Be-2c).

The following four dams were constructed from upstream to downstream in the study area in 2005, 1978, 1991, and 1971, respectively: Xuanmiaoguan (hereafter referred to as XMG), Tianfumiao (TFM), Xibeikou (XBK), and Shangjiahe (SJH). Over the past 40 years, the study catchment has experienced industrialization and rapid economic growth, which has resulted in serious soil erosion and nutrient loss.

Input Data

The Shangjiahe (SJH) reservoir dam was chosen as the outlet for the catchment, which is determined by the limitation of data accessibility. To derive the SWAT model, spatial and temporal data of soil characteristics, land use, and topography were acquired, and a DEM map was employed. To calibrate the model, hydrological and meteorological data were applied. The datasets are summarized in Table 1.

Spatial data: A DEM map (Fig. 1) of the study catchment was obtained from the Geospatial Data Cloud website (http://srtm.csi.cgiar.org/). The map has a spatial resolution of 3 arc-seconds (approximately 90 m), and it was used to derive the river network, sub-catchments divisions, and slope reclassifications.

The land cover/land use data map was obtained from 2015 LANDSAT data and downloaded from http://www.gscloud.cn/sources/. It was then reclassified using supervised image classification, and five classes of land use data were determined: agricultural field (AGRL), forest (FRST), bare land (BARR), urban (URBN), and water (WATR) (Fig. 2).

The soil types were initialized by applying the FAO-UNESCO Digital Soil Map of the World (DSMW) (http://www.fao.org/geonetwork), where soil information provided by the DSMW has a resolution of 5 km. Four soil classes were identified in the study catchment (Fig. 2), and the corresponding lookup table was subsequently manually generated.

Streamflow data and meteorological elements: Monthly streamflow data and a subset of precipitation datasets were collected from the Huangbaihe Catchment Authority, and a further precipitation dataset subset was obtained from CMADS version 1.1 (http://westdc.westgis.ac.cn/). Other meteorological elements were generated using SWAT's weather generator (WGEN). The data employed to construct WGEN was obtained from the National Centres for Atmospheric Prediction (NCEP). Weather stations w3231134 and w3261138 were included to calculate statistical parameters of the study catchment for WGEN (https://globalweather.tamu.edu/).

Description and Application of SWAT Model

The SWAT is a watershed-scale, continuous-time, and semi-distributed hydrological model that incorporates meteorological elements, soil characteristics, land cover/use, and management practices to predict streamflow, sediments, nutrient loading, pesticide transport, and so on (Arnold et al. 1998). It enables the simulation of spatial details by dividing the whole watershed into a series of sub-watersheds. Each sub-watershed then comprises hydrologic response units (HRUs) that represent homogenous soil properties, land cover, and slopes. Surface runoff, soil water, nutrient cycles, sediment, and crop yields are calculated within each

Table 1: Input data for model and their sources.

Data type	Spatial Resolution/Time period	Source
DEM	90 m	Geospatial Data Cloud website (http://srtm.csi.cgiar.org/)
Land use	30 m	2015 LANDSAT data (http://www.gscloud.cn/sources/)
Soil	5 km	FAO-UNESCO Digital Soil Map of the World (DSMW) (http://www.fao.org/geonetwork)
Precipitation	28 km for CMADS data and 2009-2016 for observations	CMADS version 1.1 (http://westdc.westgis.ac.cn/) and gauging station for Huangbaihe Catchment Authority
Streamflow	2009-2016	Gauging station for Huangbaihe Catchment Authority

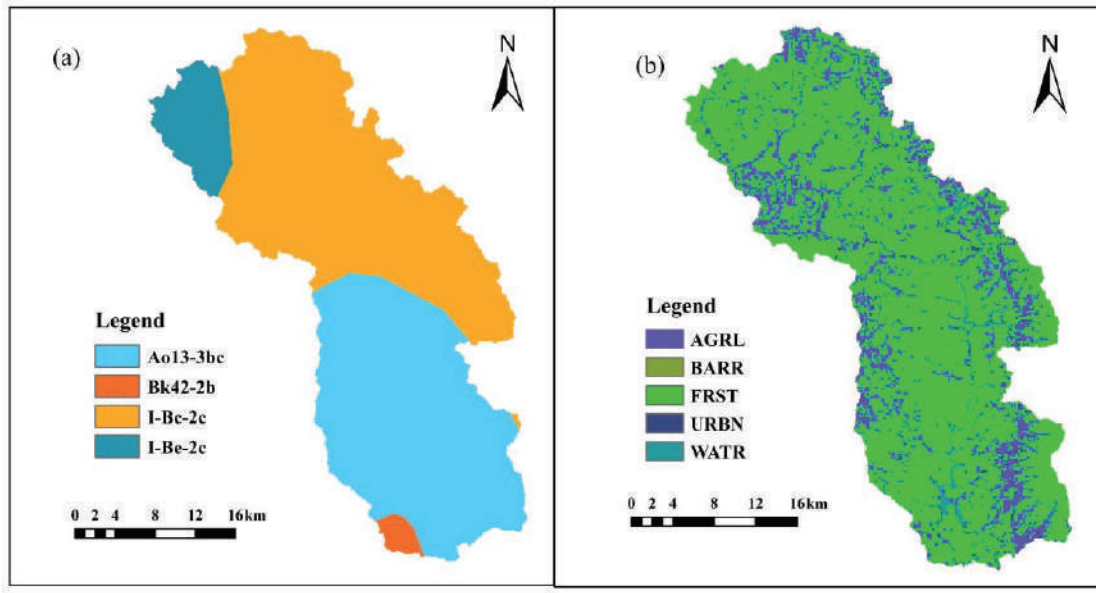

Fig. 2: (a) Soil data; (b) Land-use data

HRU (i.e., the smallest element), and they are subsequently lumped to the sub-catchment using the weighted mean method and finally routed into river systems. Four water storage types are assumed: surface runoff, soil water, and shallow and deep aquifers. The SWAT model assumes that shallow groundwater runs into the river channel as base flow or returns to the soil by evaporation, whereas flow in deep aquifers leaves the watershed system. Details of the SWAT model are provided by Neitsch et al. (2011) and can also be obtained from http://swatmodel.tamu.edu.

In this study, the following calculation methods were employed: the SCS curve number method for overland flow; kinematic storage routing for lateral flow (which creates a shallow aquifer and thus return flow); the Penman-Monteith method for potential evapotranspiration; and the variable storage routing method for channel routing. The Huangbaihe River Catchment was delineated by the interface of SWAT2012 using the 90-m DEM. The boundary of the study catchment was delineated by applying a threshold area of 1400 ha to ensure that the extracted river networks were consistent with the topographic map. Furthermore, a total of 27 sub-catchments were delineated for the SWAT model, and maps of soil and land cover were clipped at the catchment boundary. All layers were projected in the "WGS_1984_UTM_Zone_49N" coordinate system. Soil and land use types were linked using lookup tables, space databases, and attribute databases. Through reclassifying the soil layers and types, land cover/use, and slope classes, the sub-catchment layer was overlaid on the HRU layer. The threshold levels for soil, land use, and slope class percentages were provided for the SWAT model and were used to define the HRUs. In this study, a threshold percentage (10%) was adopted for all databases, and 202 HRUs were finally established in the SWAT model.

Model Calibration, Validation and Uncertainty Analysis

Model calibration of the SWAT model is challenging, and two techniques can be employed in calibration: a manual (trial-and-error) method and an auto-calibration method. However, a parameter sensitivity and identifiability analysis should first be conducted before model calibration. Parameter sensitivity is analysed to determine which parameters significantly influence the model simulation results, and parameter sensitivity varies between catchments; therefore, it has been suggested that it is necessary to conduct a sensitivity analysis in every catchment (Cibin et al. 2010).

The SWAT Calibration Uncertainty Procedure (SWAT-CUP) program (Abbaspour 2015) was adopted in this study. SWAT-CUP is a useful tool that facilitates parameter sensitivity analysis, model calibration and validation procedure by different optimization methods. It can also be used to conduct an uncertainty analysis of the model's operation results. Of these methods, we chose the SUFI-2 algorithm (Yang et al. 2008), because it has been extensively used to analyse parameter sensitivities and all uncertainty sources can be considered (Wu & Chen 2015), including uncertainties related to input data, model structure, and a large number

of parameters. Uncertainty is quantified based on 95% prediction uncertainty (95PPU) band. Two statistics are used to evaluate the strength of the uncertainty analysis, the p-factor (proportion of measurements covered by the 95PPU) and the r-factor (mean thickness of the 95PPU band separated using the standard deviation of measurements). In general, when the value of the p-factor is equal to 1 and the r-factor is equal to 0, the simulation results are considered to have an exact match with the observed data (Abbaspour et al. 2015). It is therefore desirable to achieve a balance between the p- and r-factors, as a large p-factor can raise the value of the r-factor. Details about SUFI-2 and other approaches are given in the work of Abbaspour (2015).

Based on data availability, the model was calibrated for streamflow on a monthly time scale for the period 2009-2012 after a one-year warm-up (2008), which was conducted to enable the parameters to reach an equilibrium state. In general, the length of the warm-up period is determined by the watershed properties and the length of available data. For model validation, four years from 2013 to 2016 were employed. Streamflow data for the whole outlet (sub-catchment 27) of the study catchment area were calculated by applying the water balance method, and streamflow data were thus restored to a natural condition without considering the dams that have been constructed. To check the accuracy of model prediction, streamflow data at an additional upstream station (sub-catchment 9) were also used to calibrate and validate the model. NSE was selected as the objective function, as it can reflect the overall model fit (Nash & Sutcliffe 1970). The original parameter ranges were determined by referring to previous literature relating to similar or close basins, and also by using recommendations from the SWAT manuals, which are guided through an understanding of the given watershed hydrological cycle (Liu et al. 2016, Stehr et al. 2010). The best parameter sets were employed in each iteration, and new ranges were then suggested based on an evaluation of the model. It is of note that some of the suggested ranges were outside of physically meaningful ranges, and they were thus manually adjusted to ensure that they did not exceed maximum/minimum absolute range values (Me et al. 2015).

Performance Evaluation

Both graphical and statistical approaches should be applied to assess model performance (Nyeko 2015). Only using the performance metrics can be misleading and produce unrealistic simulations; hence, a visual inspection of the differences between the hydrographs of simulated and observed data was conducted in this study (Daggupati et al. 2015). Graphical methods, such as streamflow hydrographs, can enable a visual and direct comparison of observed and simulated datasets, and enable trends in variations of flow magnitude and timing to be detected. In addition to using the graphical approach, the agreement between simulated and observed data was also evaluated based on statistical indicators, including the Nash-Sutcliffe efficiency coefficient (NSE), RMSE-observations standard deviation ratio (RSR) and percentage bias (PBIAS).

A positive NSE indicates that the measured data have a positive correlation with simulated data; in contrast, a negative NSE reflects a negative correlation,

$$NSE = 1 - \frac{\sum_{i=1}^{n}(O_i - S_i)^2}{\sum_{i=1}^{n}(O_i - \overline{O})^2} . \quad \ldots(1)$$

The RSR, shown in Eq. (2), has the advantages of providing a scaling factor and error criteria statistics, and these statistics can be used with different constituents (Singh et al. 2005),

$$RSR = \frac{RMSE}{STDEV} = \frac{\sqrt{\sum_{i=1}^{n}\left(O_i - S_i\right)^2}}{\sqrt{\sum_{i=1}^{n}\left(O_i - \overline{O}\right)^2}} . \quad \ldots(2)$$

The PBIAS index determines the average trend between simulations and their corresponding observations (Gupta et al. 1999), as shown in Eq. (3),

$$PBIAS = \frac{\sum_{i=1}^{n}\left(O_i - S_i\right)}{\sum_{i=1}^{n} O_i} \times 100 \quad \ldots(3)$$

Where, O_i and S_i are measurements and simulations, respectively, and $\overline{O}$ is the average of the observations. A positive (negative) index reflects that the bias is underestimated (overestimated).

The performance of the model was divided into four categories with respect to flow simulation on a monthly time scale following the research of Moriasi et al. (2007).

RESULTS AND DISCUSSION

Sensitivity Analysis

A sensitivity analysis of two outlets of the studied catchment was conducted, where 26 parameters relating to streamflow were used to identify sensitive parameters on a monthly scale (including the curve number (CN2) and parameters of soil properties and topography). The relative changes of the distributed parameters, which are different in every HRU or sub-catchment, were assessed using the Latin hypercube method. The *t*-test was applied in the SWAT-CUP program to determine relatively significant parameters with two statistics

(the *t*-stat and *p*-value). The parameters with larger *t*-stat values and smaller *p*-values were determined as being sensitive parameters. These two statistics, the sensitivity ranking, initial parameter ranges, final parameter uncertainty ranges, and the best simulated estimate of monthly streamflow are summarized in Table 2. Only sensitivity parameters ranked from 1 to 15 are listed in Table 2.

The results indicate that parameters associated with surface runoff generation (CN2 and CANMX), the evapotranspiration parameter (ESCO), and soil characteristics (including SOL_Z, SOL_BD, and SOL_AWC) are highly sensitive to the objective function (NSE). Therefore, it can be concluded that both overland flow and sub-surface water significantly affect the streamflow simulation results. The final ranges of the 15 significant parameters can be well applied in model calibration and validation with respect to the two outlets on a monthly time scale.

Model Calibration and Validation

Many studies have demonstrated that the results of the SWAT model are generally better when using a monthly rather than a daily step (Shen et al. 2010, Jang et al. 2018, Uniyal et al. 2015). Therefore, in this study, monthly streamflow data from January 2009 to December 2016 were adopted to calibrate and validate the SWAT model. Model input parameters were selected carefully for the calibration period (with their respective uncertainty ranges), and the selected parameters were then applied to calibrate the model using the SUFI-2 algorithm. In this study, the NSE was the objective function with a threshold value of 0.5, and parameters were identified using ranges rather than specific values; the calibrated model can also be used to validate the model using the same parameter ranges. Furthermore, calibration in a single site was not sufficient to the large catchment area, due to the parameters are distributed and heterogeneous. Consequently, multi-site calibrations were better than single-site calibration for the distributed hydrological model.

Observations and simulations for the calibration periods 2009-2012 and the validation period 2013–2016 at the XMG gauging station (the outlet of sub-catchment 9) and the whole out are graphically displayed in the top and bottom of Fig. 3 and Fig. 4, respectively. From the figures, the simulated monthly streamflow trends for both periods are close to those of measurements, and peak flow timings are usually well-simulated. Furthermore, the streamflow characteristics of the studied catchment are similar to those of most watersheds with the same climate; for example, streamflow is higher (lower) in the wet (dry) season. However, the peak flow values are underestimated (overestimated) in 2010 and 2014 (2009 and 2011). It is speculated that this relates to an over- (under-) estimation of precipitation.

The results of statistical indicators for observations and simulations on a monthly scale at the two stations in both the calibration and validation periods are compared in Table

Table 2: Sensitivity, best values, and final optimal parameter uncertainty ranges for streamflow simulation on a monthly scale using SUFI-2

Parameters	Ranking value	*t*-stat	*p*-value	Initial parameter ranges	Best estimate	Final parameter uncertainty ranges
r_CN2.mgt	1	36.25	0	-0.5~0.5	0.05	-0.01~0.11
v_CANMX.hru	2	-30.32	0	0~100	1.04	0.79~5.29
r_SOL_Z.sol	3	-9.66	0	-0.5~0.5	-0.03	-1.18~0.11
r_SOL_BD.sol	4	8.29	0	-0.5~0.5	0.61	0.36~0.8
v_ESCO.hru	5	8.03	0	0.01~1	0.22	0.13~0.3
r_SOL_AWC.sol	6	-7.1	0	-0.5~0.5	-0.68	-0.85~-0.56
v_ALPHA_BF.gw	7	6.36	0	0.01~1	0.42	0.41~0.56
v_RCHRG_DP.gw	8	5.37	0	0.01~1	0.35	0.27~0.42
r_HRU_SLP.hru	9	4.32	0	-0.5~0.5	-0.15	-0.39~-0.05
v_SLSUBBSN.hru	10	-4.28	0	-0.5~0.5	0.33	0.21~0.46
r_SOL_K.sol	11	4.25	0	-0.5~0.5	0.16	0.03~0.2
v_EPCO.hru	12	-3.96	0	0.01~1	0.65	0.59~0.92
v_GWQMN.gw	13	-3.23	0.001	0.0~1000	345.4	190.39~357.24
v_CH_K2.rte	14	-2.55	0.01	0.0~100	4.73	0.39~10.19
v_GW_REVAP.gw	15	-1.66	0.09	0.02~0.2	0.15	0.14~0.17

Note: v: initial parameter value is replaced by an active value; r: initial value is changed by multiplying (1+ a given value) (Abbaspour et al. 2007).

3 and Table 4, respectively. For the XMG gaging station, the NSE, RSR, and PBIAS were 0.81, 0.44, and 2.69 for the calibration period, respectively, and 0.87, 0.35 and 0.7 for the validation period, respectively. For the whole outlet, the NSE, RSR, and PBIAS are 0.91, 0.3, and 4.8 for the calibration period, respectively, and 0.94, 0.24, and -1.53 for the validation period, respectively. These results show that the simulations of both periods are quite good (Moriasi et al. 2007). However, in general, simulated stream flows are all underestimated in both the calibration and validation periods (i.e., PBIAS of 2.69 and 0.7, respectively,) for the XMG gaging station, and simulated streamflow is underestimated (i.e., PBIAS of 4.8) in the calibration period but overestimated in the validation period (PBIAS of -1.53) at the whole outlet. Compared with the results from the study of Wan et al. (2018), the values of statistical indexes are all better. Therefore, using the SWAT model with inputs from a regular gauging station and CMADS data can provide reliable results for the studied catchment. Furthermore, the calibrated SWAT model can be applied in further research,

Table 3: Evaluation indicators of SWAT performance at the XMG gaging station.

Statistics	Calibration period (2009-2012)		Validation period (2013-2016)		Wan et al. (2018)	
	Measured	Simulated	Measured	Simulated	Measured	Simulated
Mean (m^3/s)	4.62	4.50	4.91	4.87		
Median (m^3/s)	2.87	3.87	3.56	3.8		
Standard deviation (m^3/s)	3.43	3.13	3.72	3.46		
Minimum (m^3/s)	1.62	1.24	1.61	0.96		
Maximum (m^3/s)	14.46	16.37	18.23	14.16		
NSE	0.81		0.87		0.64	0.86
RSR	0.44		0.35		0.59	0.37
PBIAS	2.69		0.70		-5.5	11.9
p-factor	0.81		0.83		0.78	0.80
r-factor	0.65		0.72		1.04	0.81

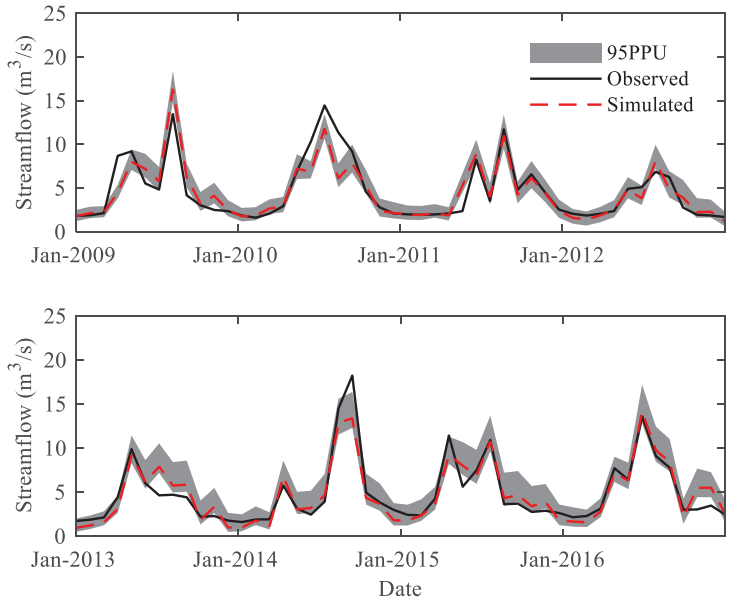

Fig. 3: Observation and simulation at monthly scale for the XMG gaging station in the calibration period of 2009-2012 (top) and the validation period of 2013-2016 (bottom).

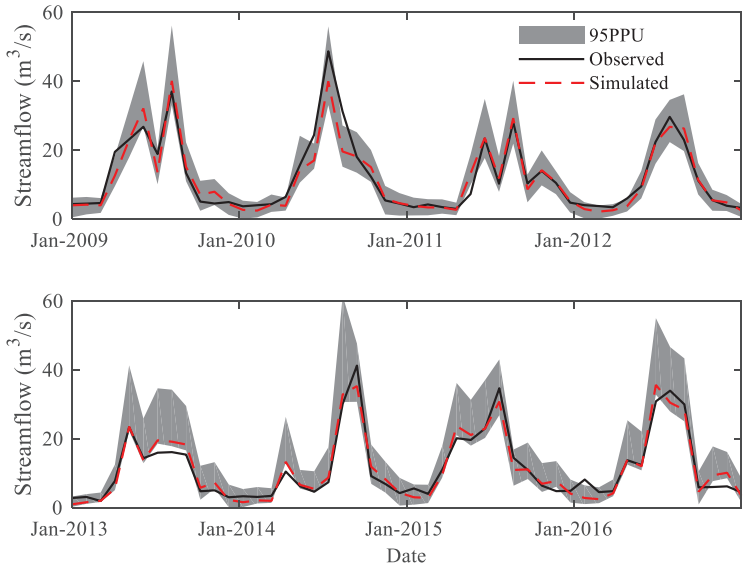

Fig. 4: Observations and simulations on a monthly scale at the whole outlet for calibration period of 2009-2012 (top) and the validation period of 2013-2016 (bottom).

such as that relating to water balance analysis and water quality evaluation.

Uncertainty Analysis

The p-factor was 0.94 for the calibration period for the whole outlet, which indicates that 94% of the measured streamflow data were bracketed by the 95PPU band. In addition, the r-factor was 0.84 (Table 4). For the validation period, 85% of the measured data were bracketed by the 95PPU band (p-factor = 0.85), and the r-factor was 1.05. Based on previous research (Abbaspour et al. 2015, Schuol et al. 2008), when the p-factor is larger than 0.75 and the simultaneous r-factor is less than 1.5, the uncertainty of streamflow simulation results is considered to be acceptable. Therefore, it can be deduced that the SUFI-2 algorithm is capable of successfully capturing measured streamflow for both the calibration and validation periods. However, a careful examination of uncertainty analysis results shows that peak flow in 2010 is missing from the 95PPU band, which could be the result of limitations in the SWAT model and associated uncertainties. Therefore, surface runoff generation and groundwater recharge are important in study catchment. The parameters relating to

Table 4: Evaluation indicators of SWAT performance at the whole outlet.

Statistics	Calibration period (2009-2012)		Validation period (2013-2016)	
	Measured	Simulated	Measured	Simulated
Mean (m^3/s)	12.36	11.76	11.74	11.74
Median (m^3/s)	6.83	8.26	7.13	8.48
Standard deviation (m^3/s)	10.69	10.1	10.02	10.08
Minimum (m^3/s)	2.93	2.14	1.91	0.96
Maximum (m^3/s)	48.7	40.11	41.23	35.63
NSE	0.91		0.94	
RSR	0.30		0.24	
PBIAS	4.80		-1.53	
p-factor	0.94		0.85	
r-factor	0.84		1.05	

groundwater recharge and overland flow generation are vital hydrological processes. Besides, correlations between parameters were also evaluated, and all values were found to be less than 0.001. Parameter correlations are therefore weak and should be neglected.

Water Balance Components

Water balance is the foundation and driving force used in watershed analysis when employing the SWAT model. The objective of calibration is to ensure that simulation results are close to the measurements. In this respect, the SWAT model was re-run using the optimal parameters for the entire period (2009–2016) and water-balance components were then identified for the output files. The mean annual contributions of the water balance are listed in Table 5.

The results show that mean annual precipitation was 1003.8 mm from 2009 to 2016, which comprises mean annual rainfall (980.3 mm) and mean annual snowfall (23.5 mm), and the mean annual actual evapotranspiration comprised 57.03% of this total (572.5 mm). Therefore, evapotranspiration was the main form of water loss, which is related to the fact that the predominant land use type is forestry (accounting for 81.41% of all land use types) (Fig. 2 b). Furthermore, the mean temperature was 16.9°C, also indicating the larger evapotranspiration. Water yield is streamflow generated at the whole catchment outlet and comprises overland flow, lateral soil flow, and shallow groundwater (baseflow). Water yield was 370.46 mm, which is equal to the total water yield of 396.78 mm minus that of deep groundwater (26.32 mm) because the SWAT model assumes that water entered the deep aquifer flowing out of the catchment (Arnold et al. 1993). Overland flow, lateral subsurface runoff, and baseflow contribute 47.02 mm (approximately 12.69% of the total water yield), 201.48 mm (54.42%), and 121.48mm (32.79%), respectively. The proportion of overland flow is high compared to that of other watersheds with a similar percentage of forest cover. This is mainly due to the soil properties within the catchment, where the predominant soil horizon type is C (91.2%) and the remainder is D (8.8%). This indicates a lower infiltration rate with the greater generation of surface runoff (Neitsch et al. 2011). Furthermore, the average slope is 19.73°, which indicates that lateral subsurface runoff is easily generated and perched water flows out. However, there is less groundwater, and this may be related to the amount of water that gushes from the phosphate mining sites. In addition, the proportion of base flow to total runoff is approximately 30% using the baseflow separation method, which was downloaded from SWAT website (https://swat.tamu.edu/software/). Therefore, the simulation results are reasonable.

The spatial distributions of average annual precipitation, actual evapotranspiration, and each hydrological component (overland runoff, lateral flow, and groundwater) and their contributions to precipitation across the sub-catchments are shown in Fig. 5. The middle of the study catchment receives a greater volume of precipitation. These results indicate that ET rises with a decline in elevation, which is due to the temperature increase at lower altitudes. Besides, the comparison between the spatial distribution of land use (Fig. 2) and ET (Fig. 5) shows that ET is higher in the sub-catchments that have larger river portion (reservoirs). The distribution of the contribution from the overland flow and lateral flow to runoff is consistent with the spatial distribution of precipitation. Furthermore, the distribution of lateral subsurface runoff was also consistent with the variation of elevation. As the

Table 5: Average annual values of hydrological components (in mm/year).

Components	Value (mm/year)
Rainfall (PRECIP)	980.3
Snowfall	23.5
Surface runoff (SURQ)	47.02
Lateral soil flow (LATQ)	201.96
shallow groundwater (GWQ)	121.48
Deep groundwater	26.32
Total aquifer recharge	154.56
Deep aquifer recharge	26.68
REVAP	42.19
Total water yield	396.78
Actual evapotranspiration (AET)	572.5
Potential evapotranspiration	1169.5

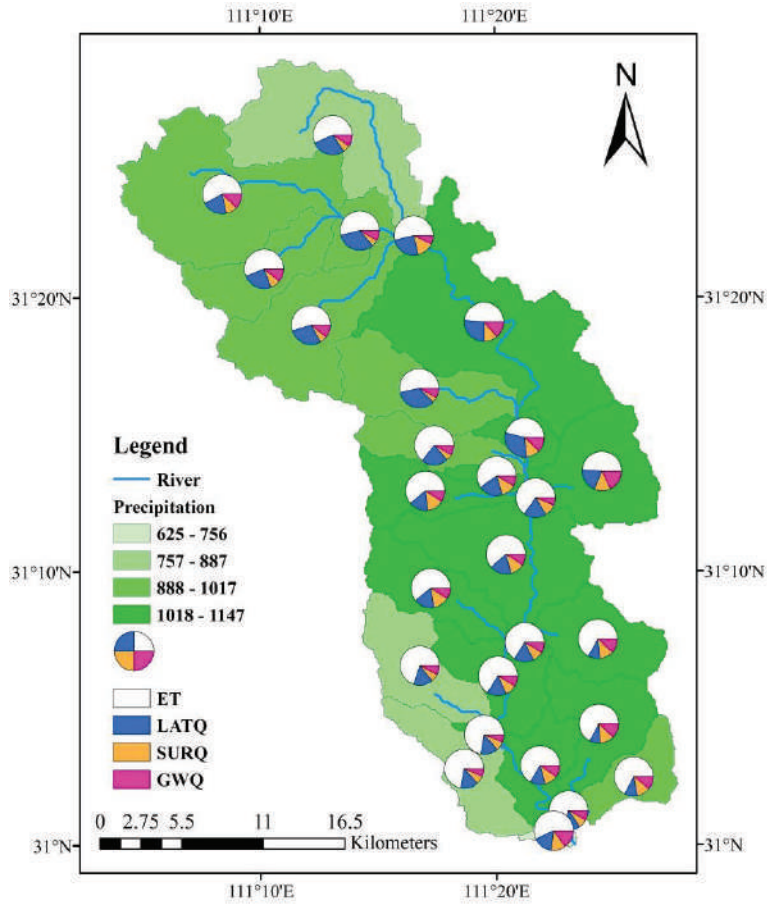

Fig. 5: Spatial distribution of average annual precipitation, actual evapotranspiration, and total water yield.

elevation declined, the contribution of lateral flow decreased. However, the distribution of groundwater contribution was less significant with the distribution of precipitation.

The mean annual contribution values of water balance components from 2009 to 2016 are presented in Fig. 6. It is worthy of note that the annual changes in water yield values (including overland flow, lateral flow, and baseflow) are consistent with annual variations in precipitation. However, the variation in the contribution from overland runoff is contrary to that of precipitation in 2012. Subsequent analysis shows that this relates to the temporal distribution of internal precipitation. In early 2012, the initial soil water content was higher because of excessive rainfall. Therefore, when precipitation continued, a larger amount of surface runoff was generated. However, the annual variation in ET was not significant during the whole period, and the change rate in mean annual ET was approximately -0.6%.

Monthly values were also computed for the water balance components and are shown in Fig. 7, where it is evident that changes in ET, which is an important source of water loss, were seasonal. ET was reduced in winter and higher in summer. Seasonal changes in overland flow, lateral sub-surface runoff, and groundwater agree with variations in rainfall. The results show that approximately 62.8% of precipitation occurred during four months from May to August, and the water yield in this period occupied approximately 60.7% of the annual runoff volume. Furthermore, there was a significant difference in the contribution of hydrological components between the dry and wet seasons. The percentage of overland runoff to precipitation ranged from 0 to 22.26% on a monthly step, and a clear difference is identified between wet and dry seasons. Groundwater lags behind precipitation, which is a reality in the natural condition.

The relationships between individual water balance components and monthly precipitation were analysed, and the results are presented in Fig. 8. Further, R^2 was also calculated to show the significance of correlation relationships. The results show that surface runoff and lateral subsurface flow were significantly influenced by precipitation. The

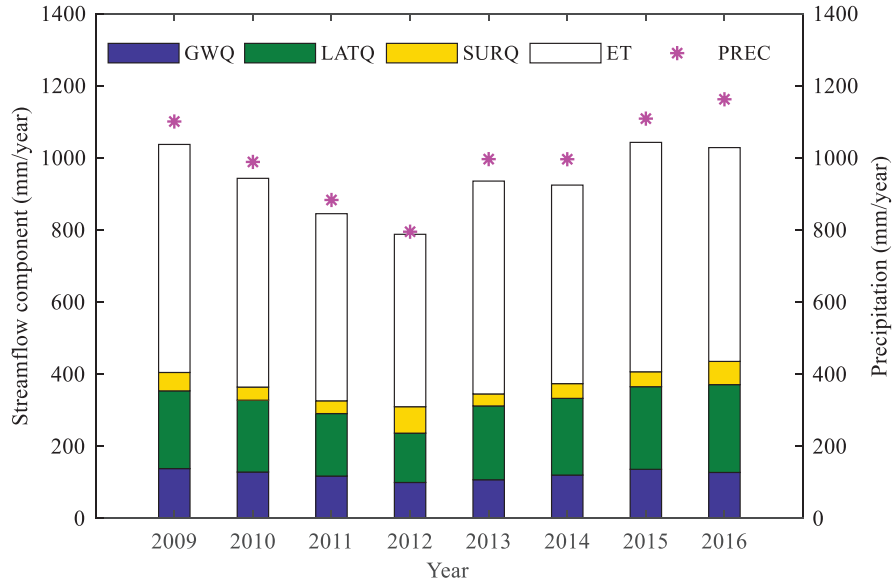

Fig. 6: Mean annual values of water balance components from 2009 to 2016.

curvilinear relationships with R^2 were 0.6 for overland flow and precipitation, 0.93 for lateral subsurface runoff and precipitation, and 0.86 for ET and precipitation. Significant indicators were all less than 0.001, which indicates a significant correlation and implies that intense precipitation can quickly increase overland flow and interflow, thus causing flooding and water pollution. However, there was only a slight increase in groundwater, and this is considered to be because the soil thickness ranges from 2–10 m in the study catchment (Wang et al. 2016); therefore, groundwater is stable and is less influenced by precipitation. In addition, changes in baseflow are intensively affected by phosphate

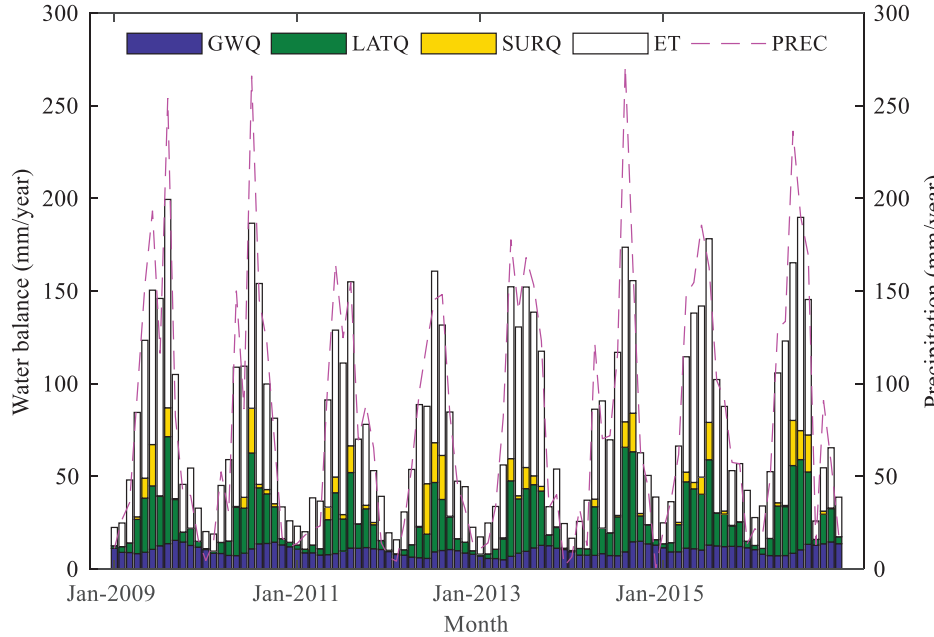

Fig. 7: Monthly values of hydrological components.

mining activities, and this weakens the correlation between groundwater and precipitation.

CONCLUSIONS

In this study, two sources of meteorological data, the CMADS data and observations obtained from four gauging stations, were applied to drive the SWAT model in the upper reaches of the Huangbaihe River Catchment. Furthermore, the model was calibrated and validated at multi-sites simultaneously. The results show that the constructed SWAT model successfully simulates monthly streamflow compared with input only from traditional gauging stations. The main results are provided as follows:

(1) A sensitivity analysis of the monthly streamflow simulation shows that CN2, CANMX, and SOL_Z are the most sensitive parameters but the correlation between these parameters is weak. The p- and r-factor values were acceptable for both the calibration and validation periods, which indicates that the parameters have low uncertainty. Furthermore, the model performed quite well when simulating streamflow on a monthly scale in both the graphical and statistical indexes.

(2) Based on the model output files, mean annual actual evapotranspiration was 572.5 mm, which accounts for approximately 57.03% of mean annual precipitation (1003.8 mm). In addition, mean annual streamflow for the whole outlet of the catchment was 370.46 mm. Furthermore, lateral sub-surface flow contributed to approximately 54.53% of runoff, surface runoff contributed approximately 12.69%, and groundwater baseflow contributed the remaining 32.79%, which is acceptable compared with the result of base-flow separation method (30%).

(3) The spatial distributions of overland flow and lateral subsurface flow are consistent with the precipitation distribution. The highest ET is distributed in areas where the river occupies a larger area, and where there is more agricultural land cover. ET was stable during the entire period (2009–2016). Based on regression results, apart from groundwater, the surface runoff, lateral flow and ET were significantly related to precipitation.

It is considered that the water balance component results obtained here can be used in water environment protection and sustainable utilization of the Huangbaihe River Catchment.

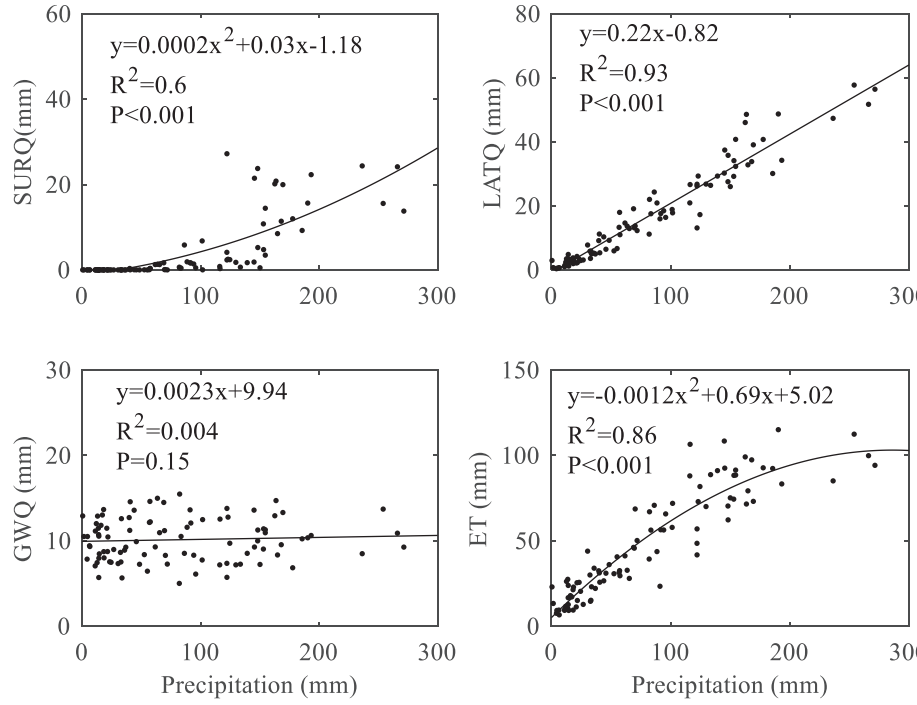

Fig. 8: Relationship between water balance components and precipitation on a monthly time scale (a) overland flow (SURQ) and precipitation; (b) lateral soil flow (LATQ) and precipitation; (c) groundwater (GWQ) and precipitation; (d) evapotranspiration (ET) and precipitation.

ACKNOWLEDGEMENTS

We thank the Protection of Water Resources in the Huangbaihe River Basin for providing the runoff and precipitation data. And this paper was supported by the Natural Science Foundation of China (40701024, 41101511, 51409152), the Non-profit Industry Financial Program of Ministry of Water Resources of China (No. 201301066), the PhD Thesis Foundation of China Three Gorges University (2018BSPY003), and the Hubei Provincial Collaborative Innovation Center for Water Security.

REFERENCES

Abbaspour, K. C. 2015. SWAT-CUP: SWAT Calibration and Uncertainty Programs - A User Manual Eawag, Dübendorf.

Abbaspour, K. C., Rouholahenjad, E., Vaghefi, S., Srinivasan, R., Yang, H. and Klve, B. 2015. A continental-scale hydrology and water quality model for Europe: Calibration and uncertainty of a high-resolution large-scale SWAT model. Journal of Hydrology, 524: 733-752.

Abbaspour, K. C., Yang, J., Maxomov, I., Siber, R., Bonger, K., Mieleitner, J., Zobrist, J. and Srinivasan, R. 2007. Modelling hydrology and water quality in the pre-alpine/alpine Thur watershed using SWAT. Journal of Hydrology, 333: 413-430.

Abubakari, S., Dong, X. H., Su, B., Hu, X. N., Liu, J., Li, Y. H., Peng, T., Ma, H. B., Wang, K. and Xu, S. J. 2017. Modelling the Spatial Variation of Hydrology in Volta River Basin of West Africa under Climate Change. Nature Environment and Pollution Technology, 16(4): 1095-1105.

Arnold, J. G., Allen, P. M. and Bernhardt, G. 1993. A comprehensive surface-groundwater flow model. Journal of Hydrology, 142: 47-69.

Arnold, J. G., Srinivasan, R., Muttiah, R. S. and Williams, J. R. 1998. Large area hydrologic modeling and assessment-Part I: Model development. Journal of the American Water Resources Association, 34: 73-89.

Cibin, R., Sudheer, K. P. and Chaubey, I. 2010. Sensitivity and identifiability of stream flow generation parameters of the SWAT model. Hydrological Processes, 24: 1133-1148.

Daggupati, P., Yen, H., White, M. J., Srinicasan, R., Arnold, J. G., Keitzer, C. S. and Sowa, S. P. 2015. Impact of model development, calibration and validation decisions on hydrological simulations in West Lake Erie Basin. Hydrological Processes, 29: 5307-5320.

Dey, P. and Mishra, A. 2017. Separating the impacts of climate change and human activities on streamflow: A review of methodologies and critical assumptions. Journal of Hydrology, 548.

Dhami, B., Himanshu, S. K., Pandey, A. and Gautam, A. K. 2018. Evaluation of the SWAT model for water balance study of a mountainous snowfed river basin of Nepal. Environmental Earth Sciences, 77: 20.

Dong, W., Cui, B., Liu, Z. and Zhang, K. 2015. Relative effects of human activities and climate change on the river runoff in an arid basin in northwest China. Hydrological Processes, 28: 4854-4864.

Gan, R., Luo, Y., Zuo, Q. and Sun, L. 2015. Effects of projected climate change on the glacier and runoff generation in the Naryn River Basin, Central Asia. Journal of Hydrology, 523: 240-251.

Gong, Y., Shen, Z., Hong, Q., Liu, R. and Liao, Q. 2011. Parameter uncertainty analysis in watershed total phosphorus modeling using the GLUE methodology. Agriculture, Ecosystems and Environment, 142: 246-255.

Gupta, H. V., Sorooshian, S. and Yapo, P. O. 1999. Status of automatic calibration for hydrologic models: Comparison with multilevel expert calibration. Journal of Hydrologic Engineering, 4: 135-143.

Jang, W. S., Engel, B. and Ryu, J. 2018. Efficient flow calibration method for accurate estimation of baseflow using a watershed scale hydrological model (SWAT). Ecological Engineering, 125: 50-67.

Li, Y., Wang, Y., Zheng, J. and Yang, M. 2019. Investigating Spatial and Temporal Variation of Hydrological Processes in Western China Driven by CMADS. Water, 11: 435.

Li, Z., Shao, Q., Xu, Z. and Cai, X. 2010. Analysis of parameter uncertainty in semi-distributed hydrological models using bootstrap method: A case study of SWAT model applied to Yingluoxia watershed in northwest China. Journal of Hydrology, 385: 76-83.

Liu, J., Shang, D., Liu, S. and Ding, Y. 2018. Evaluation and hydrological simulation of CMADS and CFSR reanalysis datasets in the Qinghai-Tibet plateau. Water, 10: 513.

Liu, R., Xu, F., Zhang, P., Yu, W. and Men, C. 2016. Identifying non-point source critical source areas based on multi-factors at a basin scale with SWAT. Journal of Hydrology, 533: 379-388.

Me, W., Abell, J. M. and Hamilton, D. P. 2015. Effects of hydrologic conditions on SWAT model performance and parameter sensitivity for a small, mixed land use catchment in New Zealand. Hydrology and Earth System Sciences, 19: 4127-4147.

Meng, X., Hao, W., Meng, X. and Hao, W. 2017. Significance of the China meteorological assimilation driving datasets for the SWAT model (CMADS) of East Asia. Water, 9: 765.

Moriasi, D. N., Arnold, J. G., Liew, M. W. V., Bingner, R. L., Harmel, R. D. and Veith, T. L. 2007. Model evaluation guidelines for systematic quantification of accuracy in watershed simulations. Transactions of the Asabe, 50: 885-900.

Mou, L. T., Ibrahim, A. L., Yusop, Z., Zheng, D. and Ling, L. 2015. Impacts of land-use and climate variability on hydrological components in the Johor River basin, Malaysia. International Association of Scientific Hydrology Bulletin, 60: 17.

Narsimlu, B., Gosain, A. K., Chahar, B. R., Singh, S. K. and Srivastava, P. K. 2015. SWAT Model Calibration and uncertainty analysis for streamflow prediction in the Kunwari River Basin, India, using sequential uncertainty fitting. Environmental Processes, 2: 79-95.

Nash, J. E. and Sutcliffe, J. V. 1970. River flow forecasting through conceptual models part I - A discussion of principles. Journal of Hydrology, 10: 282-290.

Neitsch, S. L., Arnold, J. G., Kiniry, J. R. and Williams, J. R. 2011. Soil and water assessment tool theoretical documentation version 2009. Texas Water Resources Institute Technical Report 406.

Nie, W., Yuan, Y., Kepner, W., Nash, M. S., Jackson, M. and Erickson, C. 2011. Assessing impacts of Landuse and Landcover changes on hydrology for the upper San Pedro watershed. Journal of Hydrology, 407: 105-114.

Nyeko, M. 2015. Hydrologic Modelling of Data Scarce Basin with SWAT Model: Capabilities and Limitations. Water Resources Management, 29: 81-94.

Schuol, J., Abbaspour, K. C., Srinivasan, R. and Yang, H. 2008. Estimation of freshwater availability in the West African sub-continent using the SWAT hydrologic model. Journal of Hydrology, 352: 30-49.

Serrat, A., Merino, M., Valdes, J. and Durcik, M. 2016. Evaluation of the performance of three satellite precipitation products over Africa. Remote Sensing, 8: 836.

Shawul, A. A., Alamirew, T. and Dinka, M. O. 2013. Calibration and validation of SWAT model and estimation of water balance components of Shaya mountainous watershed, Southeastern Ethiopia. Hydrol. Earth Syst. Sci. Discuss., 2013: 13955-13978.

Shen, Z. Y., Hong, Q., Yu, H. and Niu, J. F. 2010. Parameter uncertainty analysis of non-point source pollution from different land use types. Science of the Total Environment, 408: 1971-1978.

Singh, J., Knapp, H. V., Arnold, J. G. and Demissie, M. 2005. Hydrological modeling of the Iroquois River Watershed using HSPF and SWAT. Journal of the American Water Resources Association, 41: 343-360.

Song, X. M., Zhang, J. Y., Zhan, C. S., Xuan, Y. Q., Ye, M. and Xu, C. G. 2015. Global sensitivity analysis in hydrological modeling: Review of

concepts, methods, theoretical framework, and applications. Journal of Hydrology, 523: 739-757.

Stehr, A., Aguayo, M., Link, O., Parra, O., Romero, F. and Alcayaga, H. 2010. Modelling the hydrologic response of a mesoscale Andean watershed to changes in land use patterns for environmental planning. Hydrology and Earth System Sciences Discussions, 14: 1963-1977.

Thiemig, V., Rojas, R., Zambrano, B. M. and Roo, A. D. 2013. Hydrological evaluation of satellite-based rainfall estimates over the Volta and Baro-Akobo Basin. Journal of Hydrology, 499: 324-338.

Tramblay, Y., Thiemig, V., Dezetter, A. and Hanigh, L. 2016. Evaluation of satellite-based rainfall products for hydrological modelling in Morocco. International Association of Scientific Hydrology Bulletin, 61: 2509-2519.

Uniyal, B., Jha, M. K. and Verma, A. K. 2015. Parameter identification and uncertainty analysis for simulating streamflow in a river basin of eastern India. Hydrological Processes, 29: 3744-3766.

Wan, H., Dong, X., Peng, T., Liu, J., Yu, D., Bo, H. and Chen, L. 2018. Application of the SWAT model into the runoff simulation based on SUFI-2 algorithm in the east branch of Huangbai river basin. China Rural Water and Hydropower, 12: 94-100.

Wang, K., Lin, Z. and Zhang, R. 2016. Impact of phosphate mining and separation of mined materials on the hydrology and water environment of the Huangbai River basin, China. Science of the Total Environment, 543: 347.

Wu, H. and Chen, B. 2015. Evaluating uncertainty estimates in distributed hydrological modeling for the Wenjing River watershed in China by GLUE, SUFI-2, and Para Sol methods. Ecological Engineering, 76: 110-121.

Wu, L., Wang, S., Bai, X., Luo, W., Tian, Y., Zeng, C., Luo, G. and He, S. 2017. Quantitative assessment of the impacts of climate change and human activities on runoff change in a typical karst watershed, SW China. Science of the Total Environment, 601-602: 1449.

Yang, C., Jing, Z., Yang, M., Lei, X. and Qu, J. 2018. Application of SWAT Model with CMADS data to estimate hydrological elements and parameter uncertainty based on SUFI-2 algorithm in the Lijiang river basin, China. Water, 10: 742.

Yang, J., Reichert, P., Abbaspour, K. C., Xia, J. and Yang, H. 2008. Comparing uncertainty analysis techniques for a SWAT application to the Chaohe Basin in China. Journal of Hydrology, 358: 1-23.

Yatheendadas, S., Wagener, T., Gupta, H., Unkrich, C., Goodrich, D., Schaffner, M. and Anne, S. 2008. Understanding uncertainty in distributed flash flood forecasting for semiarid regions. Water Resource Research, 44: W05S19.

Zhang, X., Srinivasan, R. and Bosch, D. 2009. Calibration and uncertainty analysis of the SWAT model using genetic algorithms and Bayesian model averaging. Journal of Hydrology, 374: 307-317.

Zhao, F., Wu, Y., Qiu, L., Sun, Y., Sun, L., Li, Q., Niu, J. and Wang, G. 2018. Parameter uncertainty analysis of the SWAT model in a mountain-loess transitional watershed on the Chinese Loess Plateau. Water, 10.

Nature Environment and Pollution Technology
An International Quarterly Scientific Journal

p-ISSN: 0972-6268
(Print copies up to 2016)
e-ISSN: 2395-3454

Vol. 19 | No. 2 | pp. 651-662 | 2020

Original Research Paper

https://doi.org/10.46488/NEPT.2020.v19i02.019

Open Access Journal

Solar Photocatalytic Degradation of Organic Contaminants in Landfill Leachate Using TiO_2 Nanoparticles by RSM and ANN

Naveen N. Desai*(**), Veena S. Soraganvi*† and Vijay Kumar Madabhavi*

*Department of Civil Engineering, Basaveshwar Engineering College Bagalkot-587102, Karnataka, India

**Department of Civil Engineering, B.L.D.E.A's V.P. Dr. P.G. Halakatti College of Engineering & Technology, Vijayapur-586103, Karnataka, India

†Corresponding author: Veena S. Soraganvi; veena.snv@gmail.com

Nat. Env. & Poll. Tech.
Website: www.neptjournal.com

Received: 23-07-2019
Accepted: 29-08-2019

Key Words:
Artificial neural network; Chemical oxygen demand; Compound parabolic collector; Response surface methodology; TiO_2 nanomaterial

ABSTRACT

In the present study, artificial neural network (ANN) and response surface methodology (RSM) models were used to investigate the heterogeneous photocatalysis performance in removal of chemical oxygen demand (COD) from landfill leachate using compound parabolic collector. Effect of the three parameters, i.e. pH, catalyst dosage and irradiation time were studied for COD removal efficiency and these parameters are optimized by the RSM. The optimum values of pH 5, the dosage of 0.75 g/L and irradiation time of 100 minutes is capable to remove 32.19% of COD from the leachate. A good agreement is shown by the analysis of variance for the regression coefficient R^2 for predicted value (0.92268) and adjusted value (0.9776). The proposed RSM and ANN model R^2 values were found to be 0.9882 and 0.9974 respectively, which confirms the ideality of RSM and ANN. The results also confirm that the input and output data from RSM could be appropriate to build the ANN model. Further BOD_5/COD ratio is studied for the biodegradability of leachate and it was found that increase of biodegradability value from 0.17 to 0.47 was at pH 3, catalyst dosage of 1 g/L and irradiation time of 150 minutes.

INTRODUCTION

It is observed that the countries having high Gross Domestic Product (GDP) are generating more MSW compared to the developing and underdeveloped countries (Shekdar 2009). Municipal Solid Waste Management (MSWM) is now becoming an important segment, because of increased population, environmental degradation caused by pollution, emerging newer technologies, rapid urbanization and public importance towards hygiene and sanitation (Joshi & Ahmed 2016). Most of the developing countries including India have adopted landfilling as the final disposal method for their MSW, because of proven technology, cost-effectiveness, easy to implement and operate. Unavoidable pollutants produced from the landfill are methane gas and leachate.

Leachate is highly hazardous, consisting of high organic pollutants, salts, ammonia and toxic heavy metals. The organic pollutants studied for leachate globally are for Chemical Oxygen Demand (COD), Total Organic Carbon (TOC), five-day Biochemical Oxygen Demand (BOD_5), and Dissolve Organic Carbon (DOC). Other two indicator ratios are BOD_5/COD and COD/TOC (Deng 2009, Renou et al. 2008, Abu-Daabes et al. 2013). Available conventional treatment methods, for treating these parameters are not feasible in the present days, because of continuous hardening of the discharge standards in many countries and new pollutants emerging from the industrial processes where conventional methods fail to treat these pollutants (Gehrke & Somborn-schulz 2015, Renou et al. 2008). The treatment using nanotechnology is gaining importance due to its efficiency, significant reduction in treatment time and combining this technology with conventional treatment will offer new technology opportunity in liquid waste treatment (Saleh & Gupta 2012, Gehrke & Somborn-schulz 2015).

Nanotechnology is found useful in wastewater treatment by adsorption, membrane process, advanced oxidation process and disinfection (Qu et al. 2013, Gehrke & Somborn-schulz 2015). The last 10 years of research papers (2001 to 2011) show that the researchers are more interested in the field of biological process and Advanced Oxidation Process (AOP) for treating the leachate (Silva et al. 2013). Heterogeneous photocatalysis is an AOP over the surface of a semiconductor-based photocatalyst. Semiconductor metal oxides are used as a photocatalyst, because of light-absorbing capacity, the favourable combination of electronic structure, charge transport characteristics and excited state lifestyles (Thiruvenkatachari et al. 2008). Semiconductor nanomaterials such as TiO_2, α-Fe_2O_3, ZnO, WO_3, CdS, SnO_2 etc.

are used in the process of heterogeneous photocatalysis. Titanium dioxide (TiO_2) is a widely used semiconductor nanomaterial, because of its nontoxicity, cost-effectiveness, high chemical stability during the reaction with acidic and basic compounds, and has high oxidizing power (Spasiano et al. 2015).

Photocatalysis process depends upon different factors such as catalyst dosage, pH, contact time, temperature and light intensity (Julkapli & Bagheri 2018). The Central Composite Design (CCD) and Response Surface Methodology (RSM) are systematic tools, which provide an optimum number of experiments, mathematical and statistical techniques for understanding the effects of different factors and their interactions at the response and helps in optimizing the process (Varank et al. 2016, Ghaedi et al. 2015, Garba & Rahim 2014).

ANN is a technique used for solving nonlinear systems when there is more than one parameter interaction involved in the process. One of the advantages of ANN is that, it does not require previous information on the interactions of process variables for handling simulation of the complicated systems. ANN has achieved more popularity in water and wastewater treatment studies (Garg et al. 2017, Sabonian & Behnajady 2015, Aghaeinejad-Meybodi et al. 2015).

Photocatalysis is carried out in photoreactors to absorb maximum solar radiation which helps in performing the photochemical reaction. Compound Parabolic Collectors (CPC) are more efficient than that of the parabolic and non-concentrating collectors, because of the high amount of sunlight absorption, no solar trackers required, small place to install and can be used in cloudy days also. (Thiruvenkatachari et al. 2008, Spasiano et al. 2015).

In recent days, many researchers have studied the removal of organic contaminants such as COD, BOD_5, TOC and DOC from the leachate and wastewater using TiO_2, with UV lamps as the light source and few studies show using natural sunlight. Jia et al. (2011) used UV mercury-vapour lamp and TiO_2 nanomaterial for the removal of COD, DOC and colour from the landfill leachate. Their study shows that, at pH 4 and dosage of 2 g/L, the removal efficiency of COD, DOC and colour was 60, 72 and 97% respectively. El-mekkawi et al. (2016) investigated the percentage of COD removal in six different substrates by ten different synthesized and commercial TiO_2 samples. They have considered the initial COD concentration as 30 mg/L and volume taken was 100 mL for their study. They have carried out their experimental procedure at pH 3 and TiO_2 dosage of 0.5 g/L. Results of the study revealed that, TiO_2 of Degussa P25 found to be more efficient in removal of COD from all the substrates in exposure dose of ≤ 9.36 mWH/cm^2.

With the best of our knowledge, the study based on RSM and ANN is not reported for the COD removal from landfill leachate using photoreactor in natural sunlight. Therefore, in the present study TiO_2/H_2O_2/sunlight are used for the treatment of COD, BOD_5 and BOD_5/COD using CPC (photoreactor). The RSM, CCD and ANN techniques are used for modelling and optimizing the influencing parameters on COD. The BOD_5 and BOD_5/COD ratio are studied for the improvement in biodegradability of the leachate.

MATERIALS AND METHODS

Collection and Characterisation of Leachate

Leachate sample is collected from the "Turmuri sanitary landfill" Belgaum, Karnataka. The existing capacity of Integrated Municipal Solid Waste (IMSW) facility is 100 tonnes per day (TPD) and it is proposed to expand up to 450 TPD. The total landfill area is of 26.7 hectares, which includes compost processing facility, material recovery, refuse-derived fuel and sanitary landfill. The aerobic composting method was adopted at the site (Windrow Compost Method) (Ramky Enviro Engineers Ltd. n.d.). Leachate sample was collected from the leachate collection tank of landfill site in a plastic container and stored at below 4°C until use. The initial physicochemical characteristics are analysed and summarised in Table 1.

Experimental Study

In the present study the raw leachate is diluted to 1:25 dilution with tap water. Photocatalytic TiO_2 is procured from Sisco Research Laboratories Pvt. Ltd (SRL)-India, which is Anatase and has a specific surface area of 326 m^2/g with an average particle size of 7 nm. Hydrogen peroxide (H_2O_2) reagent (30% w/v) is used to trap the photo-induced electron and further it acts as an oxygen source to improve the mineralisation. 1 M nitric acid and sodium hydroxide were used for pH adjustment in the process.

All the photocatalysis experiments were conducted during the summer, the solar irradiance found during April and May months are 2212 kWh/m^2 and 2303 kWh/m^2 respectively. Photocatalysis process is carried out in CPC, wherein CPC profile is prepared in AutoCAD software by taking two halves of the parabola with closely located focal points and their axes inclined to each other (Tanveer & Tezcanli 2013, Strauss et al. 2018). The half acceptance angle (θ_c) is 15.8° for the constructed CPC. The CPC height, width of receiver and width of the absorber are 417.5, 360 and 100 mm respectively. The aluminium foil is used on the reflective surface to collect maximum photons from the sun.

Table 1: Physicochemical characteristics of raw leachate.

Parameters	Range value
Temperature (°C)	31
pH	8.06
Electrical Conductivity (μS/cm)	15880
Total Dissolved Solids (mg/L)	8099
Total Suspended Solids (mg/L)	400
COD (mg/L)	6418
BOD_5 (mg/L)	1106
BOD_5/COD	0.17
Chloride (mg/L)	2345
Sulphates (mg/L)	350
Nitrate (mg/L)	1496
Sodium (mg/L)	80
Potassium (mg/L)	1720
Alkalinity (mg/L as $CaCO_3$)	1800
Lead (mg/L)	0.0091
Cadmium (mg/L)	0.0014
Chromium (mg/L)	0.0777
Copper (mg/L)	0.0267
Zinc (mg/L)	0.0528
Iron (mg/L)	3.0290

The transparent borosilicate glass tube of capacity one litre is mounted on CPC as shown in Fig. 1. The glass tube is having an internal diameter of 6 cm and a length of 38 cm. The end of the glass tube is fitted with rubber bush and pipes are connected to it. The collection tank of capacity 1.5 litres is built with glass. The connectors, motor parts and recirculating pipes in contact with the leachate were of PVC material. The diluted leachate, 2 mL of hydrogen peroxide and TiO_2 are added in suspension, which is then magnetically stirred for 30 minutes in dark to attain adsorption and desorption equilibrium between the leachate and TiO_2. After the dark adsorption whole solution was taken into the CPC reactor for the photocatalysis experiment and recirculated through the glass cylinder with the aid of a low rpm water pump. During all the runs a uniform flow rate of 1000 mL/minute was maintained.

After the treatment, the solution was filtered through 0.45 μm membrane filter paper. The COD (Open reflux method) and BOD_5 tests were conducted as per the standard methods (APHA 1999). The pH was measured with a Systronics Make 361.

Central Composite Design (CCD)

The DESIGN EXPERT 11 (Stat-Ease Inc., Minneapolis, MN, USA) software was used to study the individual and synergetic effects of three factors: pH, dosage and irradiation time on the reduction of COD and biodegradability of the leachate. CCD is performed with 2^n factorial runs (n=3), the number of runs is obtained by the equation $2^n + 2n + n_c$, which provides 2^n factorial points are in 8 numbers and axial (2n) and centre (n_c) points as 6 each in numbers with a total of 20 runs. The factors are coded as +1 and -1 for high and low values. The range of high and low variables was decided based on the literature and are provided in Table 2. The response values obtained from the CCD and percentage removal of COD against each experiment is shown in Table 3. Rotatability value of α=1.687 is obtained by Eq. (1). The value of α depends on the number of factors in the factorial portion of the design (Garba & Rahim 2014, Ghaedi et al. 2015, Amini et al. 2008).

$$\alpha = N_p^{1/4} \quad \ldots(1)$$

Where $N_p = 2^n$ is the number of points, n is the number of factors.

The quadratic equation model is used to optimize and predict the response Y against the three independent factors, which can be expressed according to Eq. (2) (Ghafari et al. 2009, Varank et al. 2016).

$$Y = \beta_0 + \sum_{i=1}^{k} \beta_i X_i + \sum_{i=1}^{K} \beta_{ii} X_i^2 + \sum_{i \le j}^{k} \sum_{j}^{k} \beta_{ij} X_i X_j + \cdots + \varepsilon \quad \ldots(2)$$

Where Y is the predicted response; X_i and X_j are the variables (independent factors), and β_0 is the constant coefficient, β_i, β_{ii} and β_{ij} are the coefficients for the linear, quadratic, and interaction effect respectively, k signifies the number of independent variables and ε is the random error.

Artificial Neural Network (ANN)

In the present study sigmoid transfer function with a back propagation structure is used in the ANN modelling, which consists of a total of three layers of input, hidden and output layers as shown in Fig. 2. All calculations were done with MATLAB®2013 to develop the ANN model. Input variables examined for the neural network are pH, dosage and irradiation time. The output value is the percentage of COD removal from the leachate. The sigmoid transfer function is commonly used transfer function for the input and hidden layers because of its differentiability. ANN will provide input-output mapping with nonparametric statistical inference, adaptive and fault-tolerant. The ANN output is expressed by Eq. (3).

$$P(w) = f[x_1, x_2, \ldots x_n, w] \quad \ldots(3)$$

Where, $P(w)$ is the expected output of the multilayer neural network. The hyperbolic tangent function is given by

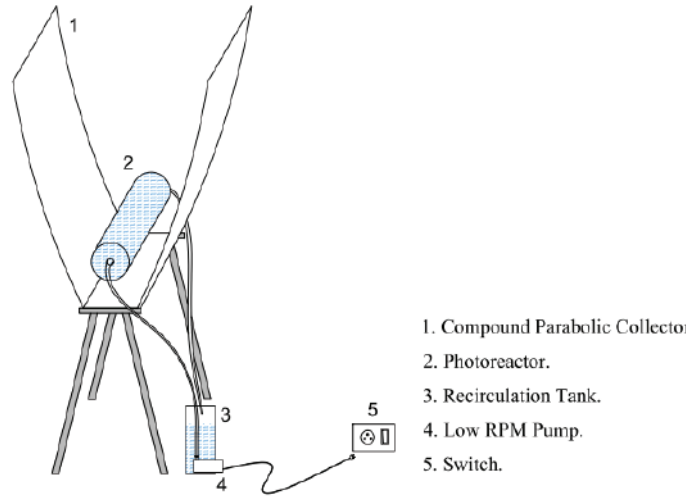

Fig. 1: Compound parabolic collector (CPC) schematic diagram.

Eq. (4) and it is used as the activation function for the hidden layer. Whereas, linear activation function specified in Eq. (5) will be employed for the output layer.

$$\phi(v)\ tanh(v)_{tanh} \quad \ldots(4)$$

$$\phi_{lin}(v) = v \quad \ldots(5)$$

Where, v is the net input of the neuron, further, w is the weight factor vector which need to recognize throughout the course of action of training and $x_1, x_2, \ldots x_n$ characterize the system inputs. The weights w are estimated by minimizing the cost function $\xi(w)$ which is given in Eq. (6)

$$\xi(w) = \frac{1}{2N}\sum \varepsilon(w)^2 + \frac{1}{N} w^T D w \quad \ldots(6)$$

Where, $\varepsilon(w) = y - \hat{y}(w)$ and D is the weight decay matrix and calculation of D is given by Eq. (7).

$$D = \beta[I]_{m\times m} \quad \ldots(7)$$

Where, β is the weight decay term and I is the identity matrix. To get a better overview, data on network points are separated arbitrarily into three subsets consisting of 70%, 15% and 15% of data. The first subsets are employed for training while the other two subsets are employed for validation and cross-validation (Simon 2014, Liang et al. 2002).

RESULTS AND DISCUSSION

Statistical Analysis

A quadratic polynomial RSM was used to analyse the experimental results found by CCD. Based on the experimental design results, the regression equations with coded variables established for the photocatalysis processes is presented in Eq. (8). The coded equation will help in finding the relative effect of the factors by comparing the factor coefficients.

% COD removal by photocatalysis process =

$$30.77 - 11.14X_1 + 8.43X_2 + 3.87X_3 - 0.45X_1X_2 - 1.95X_1X_3 - 3.26X_2X_3 + 2.78X_1^2 - 2.70X_2^2 - 1.52X_3^2 \quad \ldots(8)$$

The positive and negative signs before the expressions indicate the synergistic and antagonistic influence of the respective variables. The presence of a single variable in a term shows a unifactor influence; two variables indicate a double factor influence and a second-order term of variable occurrence indicate the quadratic influence.

In mandate to evaluate the individual interface and quadratic effects of the variables influencing on the percentage removal of COD, analysis of variance (ANOVA) is carried out. ANOVA validated the importance and adequacy of the models. The superiority of polynomial model suitability

Table 2: Experimental factors and levels in the central composite design.

Factors	Levels			Star Point α=2	
	Low	Central	High	$-\alpha$	$+\alpha$
(X_1) pH	3	5	7	1.634	8.363
(X_2) Dosage (g/L)	0.5	0.75	1	0.329	1.170
(X_3) Irradiation time (min)	50	100	150	15.910	184.09

Table 3: Data statistics of model variable.

Std	Run	X_1: pH	X_2: Dosage g/L	X_3: Irradiation time Minutes	COD % Removal
6	1	7.00	0.50	150.00	15.88
19	2	5.00	0.75	100.00	32.19
9	3	2.00	0.75	100.00	57.97
5	4	3.00	0.50	150.00	39.92
4	5	7.00	1.00	50.00	26.82
16	6	5.00	0.75	100.00	29.89
20	7	5.00	0.75	100.00	28.75
7	8	3.00	1.00	150.00	53.16
14	9	5.00	0.75	184.00	32.12
3	10	3.00	1.00	50.00	44.86
15	11	5.00	0.75	100.00	32.19
17	12	5.00	0.75	100.00	29.89
12	13	5.00	1.17	100.00	37.85
18	14	5.00	0.75	100.00	31.34
13	15	5.00	0.75	16	22.86
10	16	8.00	0.75	100.00	21.35
11	17	5.00	0.33	100.00	10.45
8	18	7.00	1.00	150.00	24.13
2	19	7.00	0.50	50.00	2.35
1	20	3.00	0.50	50.00	21.78

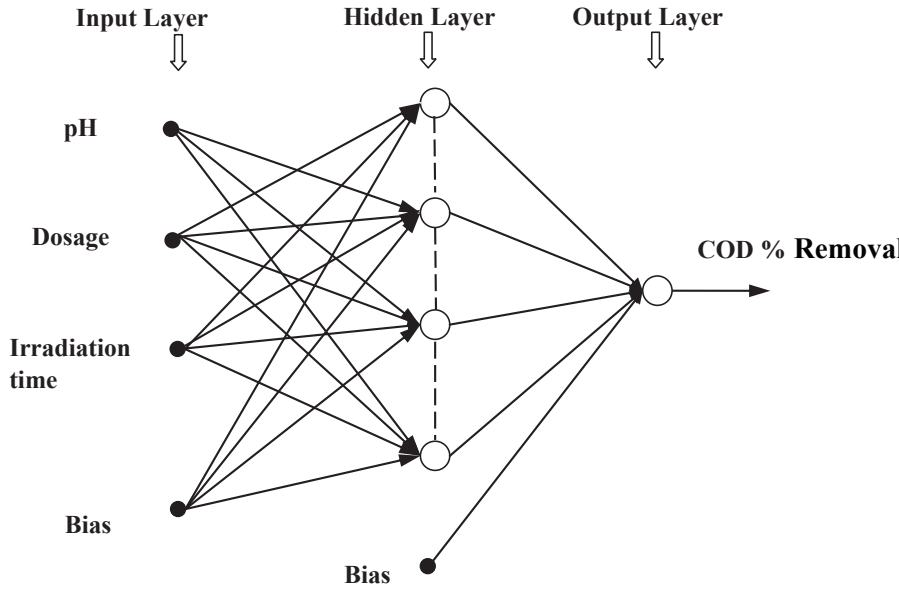

Fig. 2: Artificial neural network.

is studied in terms of coefficient of determination R^2 and model terms are assessed by p-value and F-value (Varank et al. 2016).

For the COD removal, whether the model is significant or insignificant is studied by the relationship between predicted and actual data as shown in Fig 3. The R^2 value predicted for the COD is 0.9268 and is in reasonable agreement with the adjusted R^2 value of 0.9776; the difference is less than 0.2. To check the model significance, further, it is verified in terms of F-value, P-value and adequate precision.

Therefore, the sum of squares and mean square of each factor, F-values as well as P-values are shown in Table 4 for the percentage of COD removal. In Table 4, dividing the sum of the squares of each of the various sources, the model and the error variance by the respective degrees of freedom gives the mean square values. The model terms with values of P less than 0.05 are considered significant. With respect to COD percentage removal, the Model F-value of 2.90 suggests that the Lack of Fit is not significant compared to the pure error. There is a 13.35% chance for a lack of Fit F-value, this could happen due to noise. Non-significant lack of fit is suggested to be good.

P-values less than 0.05 indicate model terms are significant. In this case X_1, X_2, X_3, X_1X_3, X_2X_3, X_1^2, X_2^2, X_3^2 are significant model terms. X_1X_2 are not significant as values greater than 0.05 indicate the model terms are not significant.

The adequate precision ratio should be more than 4 for a significant model. In the present study, COD has an adequate precision ratio of 37.53. From the statistical results attained, it was observed that the COD model (Eq. 8) was adequate to predict the COD removal within the applied range of variables.

ANN Modelling

To develop a suitable model for ANN requires large data. However, if the data of input and output are statistically significant by the ANOVA in RSM it could be appropriate to build the ANN model (Sarve et al. 2015). Different topologies of ANN with the number of hidden neurons varying from 2 to 10 are trained in the present study. The topology which provides minimum mean square error (MSE) is chosen as the best topology to predict the parameter of COD reduction. The MSE corresponding to the best architecture (number of

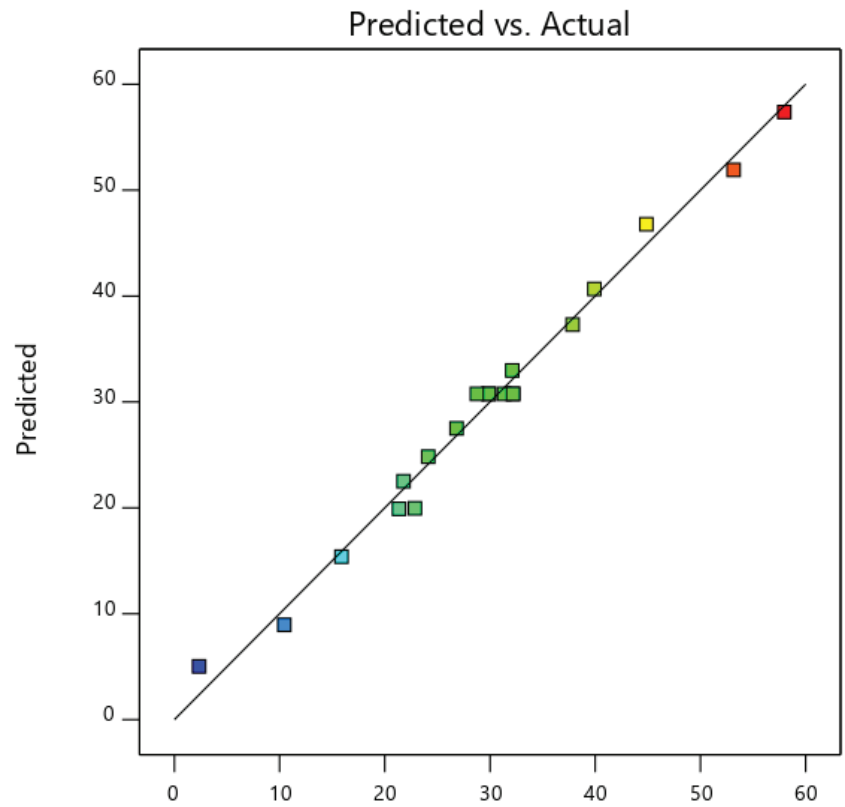

Fig. 3: Relationship between predicted and experimental data for COD removal.

Table 4: The ANOVA for response surface quadratic model of COD removal by photocatalysis.

Source	Sum of Squares	Degree of Freedom	Mean Square	F-value	p-value	Remarks
COD Model	3261.27	9	362.36	93.18	< 0.0001	significant
X_1-pH	1694.59	1	1694.59	435.76	< 0.0001	significant
X_2-Dosage	970.42	1	970.42	249.54	< 0.0001	significant
X_3-Irrdiation time	204.55	1	204.55	52.60	< 0.0001	significant
$X_1 X_2$	1.62	1	1.62	0.4166	0.5332	Not significant
$X_1 X_3$	30.42	1	30.42	7.82	0.0189	significant
$X_2 X_3$	84.89	1	84.89	21.83	0.0009	significant
X_1^2	111.71	1	111.71	28.73	0.0003	significant
X_2^2	105.01	1	105.01	27.00	0.0004	significant
X_3^2	33.23	1	33.23	8.55	0.0152	significant
Residual	38.89	10	3.89			
Lack of Fit	28.92	5	5.78	2.90	0.1335	Not significant

hidden neurons) for parameter prediction is given in Table 5 and also shown in Fig. 4. The best architectures found (Table 5) is 3_8H_1 with MSE validation of 0.0235 which is used for predicting of COD removal.

The accuracy of the developed model is evaluated by regression analysis. The criterion used for measuring the model accuracy in regression analysis is correlation coefficient R^2. The correlation coefficient measures the strength of the relationship between estimated and measured variables and it can be expressed by Eq. (9).

$$R^2 = \left(\frac{N\sum X_{meas} X_{est} - \sum X_{meas} \sum X_{est}}{\sqrt{\left[N\sum X_{meas}{}^2 - \left(\sum X_{meas}\right)^2 \right]\left[N\sum X_{est}{}^2 - \left(\sum X_{est}\right)^2 \right]}} \right) \quad \ldots(9)$$

Where, N, X_{mesa}, and X_{est} are the number of operating points in a data set, measured variable and estimated variable respectively. The value of R^2 represents the correlation coefficient of determination. The R^2 ranges between -1 and +1. R^2 value close to +1 indicates a stronger positive linear relationship, while R^2 value close to -1 indicates a stronger negative linear relationship. Further, the comparison of measured and estimated COD is done for all the data sets of points.

The coefficient of determination (R^2) for COD is depicted in Fig. 5 and it is concluded that the developed model allows the accurate prediction of COD as it is having a coefficient of determination of 0.9974.

Effect of Independent Factors on COD Removal and Optimisation of Process

Effect of pH on COD removal: The percentage removal of COD is studied with the independent factors by the RSM in the form of 3-dimensional charts as shown in Fig. 6. It is observed from Fig. 6(a), that the set of optimum values of pH 5, a dosage of 0.75 g/L and irradiation time of 100 minutes are capable to remove 32.19% of COD from the leachate. To study the effect of various individual parameters on COD removal, the ramp diagrams are used. In ramp diagrams, two optimized parameters are kept as constant and the other one is varied to obtain maximum and minimum values.

To understand the effect of pH on COD reduction, the value of pH is fixed at 3 and 7 as shown in ramp diagrams in

Table 5: Results of the ANN model to predict COD reduction.

S. No.	Input Parameters	Output Parameter	Architecture	MSE (Validation)
	pH, Dosage, Irradiation time	COD	3_2H_1	0.1372
	pH, Dosage, Irradiation time	COD	3_4H_1	0.1263
	pH, Dosage, Irradiation time	COD	3_6H_1	0.0362
	pH, Dosage, Irradiation time	COD	3_8H_1	0.0235
	pH, Dosage, Irradiation time	COD	3_10H_1	0.0471

Figs. 7(a) and 7(b) respectively. The results obtained from the ramp diagrams indicate that at pH 3 (COD removal 44.69%) the removal efficiency of COD is higher than at pH 7 (COD removal 22.41%) for the dosage of 0.75 g/L and irradiation time of 100 minutes. Many researchers have reported that the maximum COD removal can be achieved in acidic pH (Pekakis et al. 2006, Iqbal et al. 2017), and pH plays a very important role in photocatalysis solution, which provides greater influence on the mechanism of OH radicals production and point of zero charge (pH_{zpc}) of TiO_2 nanomaterial. The pH_{zpc} for TiO_2 is 6.5 when pH value is lower than pH_{zpc} the TiO_2 surface becomes positively charged and attracts anionic pollutants. If pH is greater than 6.5 then surface gets charged negatively and attracts cationic pollutants. It is assumed that the pollutants whose exact composition is not known are negatively charged species, therefore their photodegradation process would be favoured at acidic condition rather than of neutral or alkaline conditions (Fotiadis et al. 2007, Pekakis et al. 2006, Julkapli & Bagheri 2018).

Effect of catalyst dosage on COD removal: Figs. 6(b), 8(a) and 8(b) show the effect of catalyst dosage on COD removal. Which indicate that, as the dosage increases, the percentage removal of COD also increases. In the ramp diagram 8(a) and 8(b) the highest dosage of 1 g/L and minimum dosage of 0.5 g/L is fixed at the pH 5 and irradiation time 100 minutes. The ramp diagram clearly shows that, at 1 g/L (COD removal 36.49%) catalyst dosage is efficient compared to 0.5 g/L (COD removal 19.63%). The dosage plays an important role in the photocatalysis process as an increase in the concentration of nanoparticles in the area of illumination helps in improved availability of catalyst sites for the adsorption. Further, it helps in generation of reactive free radicals and their interaction. It is also reported that the application of excessive dosage above the saturation level can reduce the light absorption coefficient due to the shielding effect, which in turn reduce the efficiency of the pollutant reduction. It is also necessary to note that, the dosage of catalyst depends on the initial concentration of the pollutant and operating conditions of the reactor (Julkapli & Bagheri 2018, Manassah 2011).

Effect of irradiation time on COD removal: Fig. 6(c), 9(a) and 9(b) demonstrate the change in the percentage of COD removal with respect to the graph and ramp diagram. These indicate that, as the time increases, the removal efficiency of COD increases. In Fig. 9(a) and 9(b) maximum (150 minutes) and minimum (50 minutes) irradiation time were considered, and COD removal efficiency is calculated as 33.11% and 25.37% respectively for the pH 5 and dosage of 0.75 g/L. Extended irradiation time helps in speeding up mixing and dispersion of adsorbent into the solution, COD from the leachate will biodegrade faster in initial stages and further increase of time may not help in removal of COD, because COD removal amount is fixed by the refractory compounds and by-products produced during the longer reaction time of photocatalyst (Sahar et al. 2018, Mokhtarani et al. 2016).

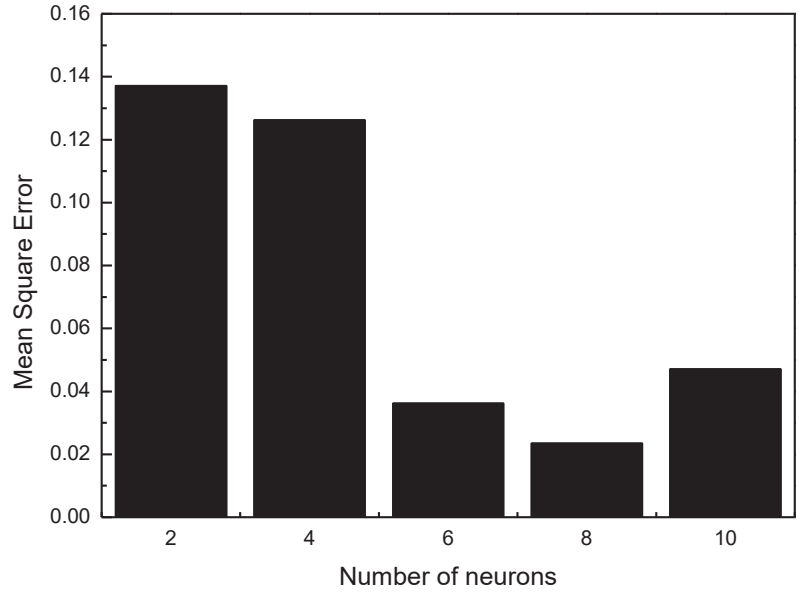

Fig. 4: Effect of the number of hidden neurons on the performance of the neural network.

Biodegradability Study of Leachate

BOD_5/COD ratio has been commonly used to indicate the biodegradability of the waste. This ratio helps in coupling biological treatment with chemical treatment. It is suggested that the BOD_5/COD ratio should be more than 0.4 for biological treatment. If it is in the range of 0.3 to 0.4, it indicates the partial biodegradability of waste (Jia et al. 2011, Khattab et al. 2012). The biodegradability study was carried out for each run and is shown in Fig. 10 with respect to pH, catalyst dosage and irradiation time. The results indicate that there will be a considerable increase of BOD_5 fraction with initial and final irradiation time. At the initial stage of 0-100 minutes, BOD_5 fraction was increased due to the active changes in structures and chemical properties of the refractory materials and due to the presence of original organic matter. The catalyst dosage plays a crucial role in the increase of BOD_5 fraction, because of reduction in organic by-products residual in the treated medium and to the upswing of decarboxylation rate. The pH of the medium was studied with biodegradability and it is seen that at acidic pH the BOD_5/COD is more. The results of Wiszniowski et al. (2006) indicated that at pH 7.2 BOD_5/COD, percentage removal is less compared to the pH 4. In the present study, the BOD_5/COD ratio was 0.17 and it was found to be increased up to 0.47 at pH 3, catalyst dosage of 1 g/L and irradiation time of 150 minutes. The optimum BOD_5/COD ratio of 0.35 can be attained by a pH of 5, dosage 0.75 g/L and irradiation time of 100 minutes.

CONCLUSION

Performance of TiO_2 was studied with CCD based on RSM and ANN models for the COD removal from the landfill leachate using photoreactor in natural sunlight. The constructed photoreactor was found to be efficient in capturing solar photons from sunlight, and maximum removal of COD at pH 2 and pH 3 was found to be 57.97% and 53.16% respectively with dosage of 1.0g/L and irradiation time of 150 min. The favourable condition for COD removal from leachate is an acidic phase and the same is reported by other authors also. Further results indicate that the other two parameters, catalyst dosage and irradiation time, also influence the COD removal. In the present study, optimum parameters were obtained as pH 5, the dosage of 0.75 g/L and irradiation time of 100 minutes for COD removal of 32.19%. The ANOVA results of p values less than 0.05 indicate that the models are significant, F-value of 2.90 and the adequate precision ratio of 37.53 from statistical results confirm that the COD model is adequate to predict the COD removal within the applied range of variables. The ramp diagrams are shown to help in varying weights or importance of the parameters to check the percentage removal of COD. The ANN model R^2 value, found to be 0.9974, indicates that the model has been trained perfectly for the input and output data of CCD based RSM. In ANN, best architecture found is 3_8H_1 with MSE validation of 0.0235 which is used for predicting of COD removal.

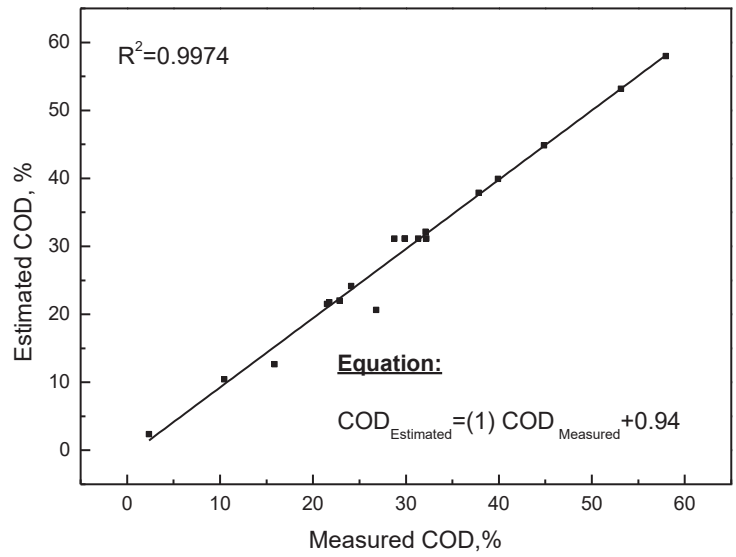

Fig. 5: Measured and estimated COD.

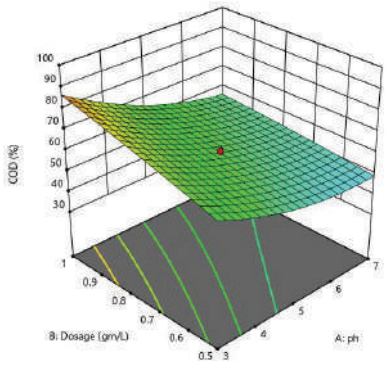

Fig. 6(a): Effect of pH and Dosage on removal of COD.

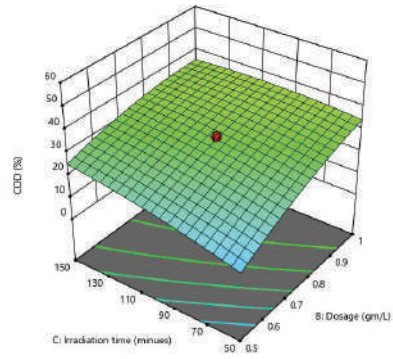

Fig. 6(b): Effect of Dosage and Irradiation time on removal of COD.

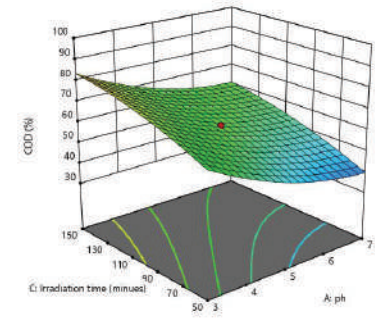

Fig. 6(c): Effect of pH and Irradiation time on removal of COD.

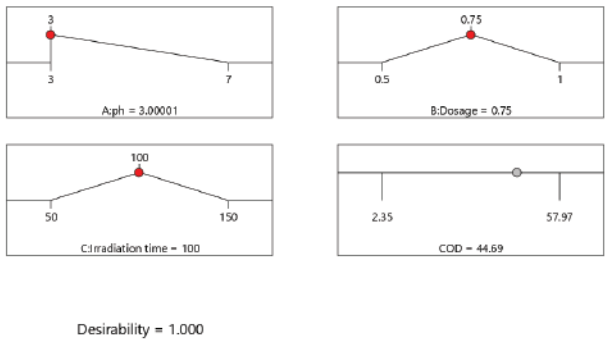

Fig. 7(a): Effect of 3 pH on removal of COD.

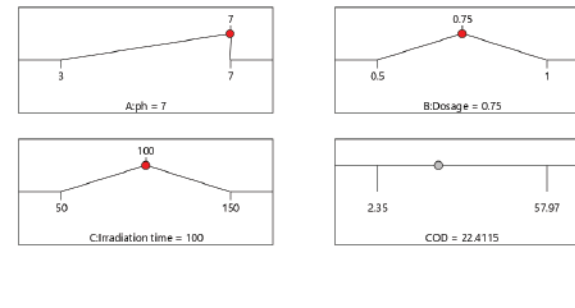

Fig. 7(b): Effect of 7 pH on removal of COD.

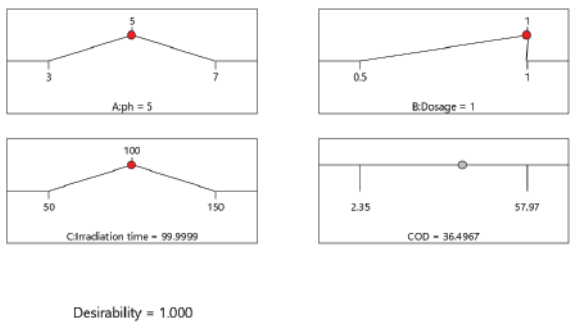

Fig. 8(a): Effect of 1 g/L catalyst dosage on removal of COD.

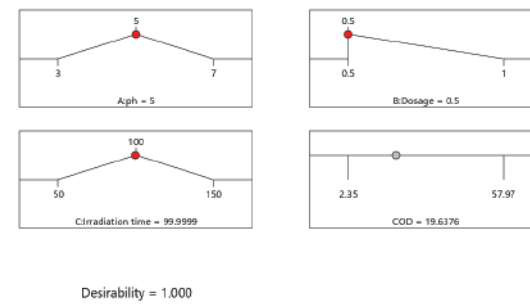

Fig. 8(b): Effect of 0.5 g/L catalyst dosage on removal of COD.

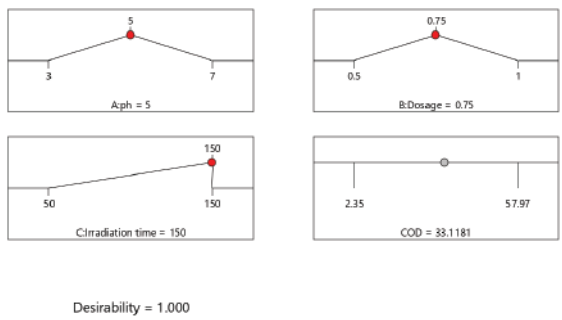

Fig. 9(a): Effect of 150 minutes irradiation time on removal of COD.

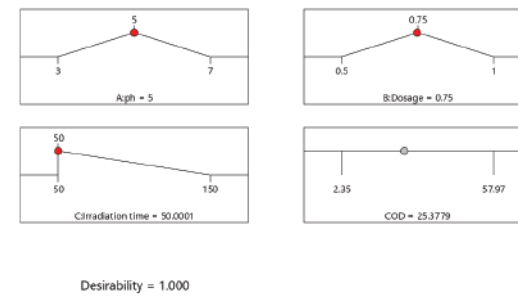

Fig. 9(b): Effect of 50 minutes irradiation time on removal of COD.

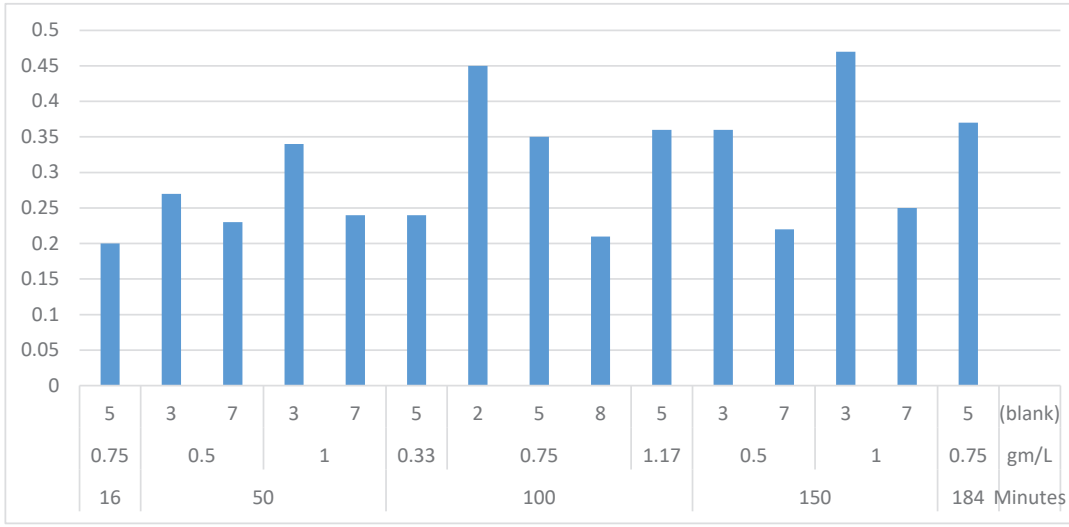

Fig. 10: BOD_5/COD ratio during the photocatalytic process.

REFERENCES

Abu-Daabes, Malyuba, Hani Abu, Qdais and Hatem, Alsyouri 2013. Assessment of heavy metals and organics in municipal solid waste leachates from landfills with different ages in Jordan. Journal of Environmental Protection, 4: 344-52.

Aghaeinejad-Meybodi, A., Ebadi, A., Shafiei S., Khataee, A.R. and Rostampour, M. 2015. Modeling and optimization of antidepressant drug fluoxetine removal in aqueous media by ozone/H_2O_2 process: comparison of central composite design and artificial neural network approaches. Journal of the Taiwan Institute of Chemical Engineers, 48: 40-48.

Amini, Malihe, Habibollah Younesi, Nader Bahramifar, Ali Akbar, Zinatizadeh Lorestani, Farshid Ghorbani, Ali Daneshi, and Mazyar Sharifzadeh 2008. Application of response surface methodology for optimization of lead biosorption in an aqueous solution by *Aspergillus niger*. Journal of Hazardous Materials, 154: 694-702.

APHA 1999. Standard Methods for the Examination of Water and Wastewater. Prepared and Published Jointly by the American Public Health Association, American Water Works Association, Water Pollution Control Federation, Joint Editorial Board, Michael J. Taras, Arnold, 2671.

Deng, Yang 2009. Advanced oxidation processes (AOPs) for reduction of organic pollutants in landfill leachate: a review. International Journal of Environment and Waste Management, 4(3-4): 366-384.

El-mekkawi, Doaa M., Norhan Nady, Nourelhoda A. Abdelwahab, and Walied A. A. Mohamed 2016. Flexible bench-scale recirculating flow CPC photoreactor for solar photocatalytic degradation of methylene blue using removable TiO_2 immobilized on PET sheets, International Journal of Photoenergy, 9270499 [CrossRef].

Fotiadis, Christos, Nikolaos, P. Xekoukoulotakis and Dionissios, Mantzavinos 2007. Photocatalytic treatment of wastewater from cottonseed processing: effect of operating conditions, aerobic biodegradability and ecotoxicity. Catalysis Today, 124(3-4): 247-53.

Garba, Zaharaddeen N. and Afidah Abdul Rahim 2014. Process optimization of $K_2C_2O_4$-activated carbon from *Prosopis africana* seed hulls using response surface methodology. Journal of Analytical and Applied Pyrolysis, 107: 306-12.

Garg, Alok, Vikas K. Sangal and Pramod, K. Bajpai 2017. Photocatalytic treatment of binary mixture of dyes using UV/TiO2 process: calibration, modeling, optimization and mineralization study. International Journal of Chemical Reactor Engineering, 15(2).

Gehrke, Ilka and Annette Somborn-schulz 2015. Innovations in nanotechnology for water treatment. Nanotechnology, Science and Applications, 8: 1-17.

Ghaedi, M., Hajati, S., Zaree, M., Shajaripour, Y., Asfaram, A. and Purkait, M.K. 2015. Removal of methyl orange by multiwall carbon nanotube accelerated by ultrasound devise: optimized experimental design. Advanced Powder Technology, 26(4): 1087-93.

Ghafari, Shahin, Hamidi Abdul Aziz, Mohamed Hasnain Isa and Ali Akbar Zinatizadeh 2009. Application of response surface methodology (RSM) to optimize coagulation-flocculation treatment of leachate using poly-aluminum chloride (PAC) and alum. Journal of Hazardous Materials, 163(2-3): 650-56.

Iqbal, Munawar, Jan Nisar, Muhammad Adil, Mazhar Abbas, Muhammad Riaz, M. Asif Tahir, Muhammad Younus and Muhammad Shahid 2017. Mutagenicity and cytotoxicity evaluation of photo-catalytically treated petroleum refinery wastewater using an array of bioassays. Chemosphere, 168: 590-98.

Jia, Chenzhong, Yanxin Wang, Caixiang Zhang and Qiaoyan Qin 2011. UV-TiO_2 photocatalytic degradation of landfill leachate. Water, Air & Soil Pollution, 217(1-4): 375-385.

Joshi, Rajkumar and Sirajuddin Ahmed 2016. Status and challenges of municipal solid waste management in India : A review. Cogent Environmental Science, 28(1): 1-18.

Julkapli, Nurhidayatullaili Muhd and Samira Bagheri 2018. Applications of titania as a heterogeneous catalyst for degradation of landfill leachates. In: Nanocatalysts in Environmental Applications, pp. 51-67, Springer, Cham.

Khattab, Ibrahim A., Montaser Y. Ghaly, Lars Österlund, Mohamed E.M. Ali, Joseph Y. Farah, Fatama M. Zaher and Mohamed I. Badawy 2012. Photocatalytic degradation of azo dye reactive red 15 over synthesized titanium and zinc oxides photocatalysts: a comparative study. Desalination and Water Treatment, 48(1-3): 120-29.

Liang, Jin, Nikiforuk, P.N. and Gupta, M.M. 2002. Neural networks for modelling and control of discrete-time nonlinear systems. In: Proceedings of IEEE International Conference on Systems, Man and Cybernetics, 2: 1122-1127.

Manassah, J. 2011. Treatment of highly polluted paper mill waste water by solar photocatalytic oxidation with synthesized nano TiO_2. Proceedings of the International Conference on Green Technology and Environmental Conservation, GTEC-2011, 168(1): 356-361.

Mokhtarani, Nader, Saeid Khodabakhshi and Bita Ayati 2016. Optimization of photocatalytic post-treatment of composting leachate using UV/TiO_2. Desalination and Water Treatment, 57(47): 22232-22243.

Pekakis, Pantelis A, Nikolaos, P. Xekoukoulotakis and Dionissios Mantzavinos Ã. 2006. Treatment of textile dyehouse wastewater by TiO_2 photocatalysis. Water Research, 40(6): 1276-1286.

Qu, Xiaolei, Pedro, J. J. Alvarez and Qilin, Li. 2013. Applications of nanotechnology in water and wastewater treatment. Water Research, 47(12): 3931-46.

Ramky Enviro Engineers Ltd. n.d. Prefeasibility Report For Expansion of Integrated Municipal Solid Waste Vengurla Road, Turmuri Village, Belgaum District, Karnataka, No. 19.

Renou, S., Givaudan, J.G., Poulain, S., Dirassouyan, F. and Moulin, P. 2008. Landfill leachate treatment: Review and opportunity. Journal of Hazardous Materials, 150(3): 468-493.

Sabonian, Maryam and Mohammad, A. Behnajady 2015. Artificial neural network modeling of Cr(VI) photocatalytic reduction with TiO_2-P25 nanoparticles using the results obtained from response surface methodology optimization. Desalination and Water Treatment, 56(11): 2906-2016.

Sahar, A., Ali, S., Hussain, T., Jahan, N. and Zia, M.A. 2018. Efficient optimization and mineralization of UV absorbers: A comparative investigation with Fenton and UV/H_2O_2. Open Chemistry, 16(1): 702-708.

Saleh, T.A. and Gupta, V.K. 2012. Column with CNT/magnesium oxide composite for lead (II) removal from water. Environmental Science and Pollution Research, 19(4): 1224-1228.

Sarve, A., Sonawane, S.S. and Varma, M.N. 2015. Ultrasound assisted biodiesel production from sesame (*Sesamum indicum* L.) oil using barium hydroxide as a heterogeneous catalyst: Comparative assessment of prediction abilities between response surface methodology (RSM) and artificial neural network (ANN). Ultrasonics Sonochemistry, 26: 218-228.

Shekdar, Ashok V. 2009. Sustainable solid waste management : An integrated approach for Asian countries. Waste Management, 29(4): 1438-48.

Silva, T.F., Silva, M.E.F., Cunha-Queda, A.C., Fonseca, A., Saraiva, I., Sousa, M.A., Gonçalves, C., Alpendurada, M.F., Boaventura, R.A. and Vilar, V.J. 2013. Multistage treatment system for raw leachate from sanitary landfill combining biological nitrification–denitrification/solar photo-Fenton/biological processes, at a scale close to industrial-biodegradability enhancement and evolution profile of trace pollutants. Water Research, 47(16): 6167-6186.

Simon, Haykin 2014. Neural Networks and Learning Machines. Third Edition, ArXiv Preprint.

Spasiano, D., Marotta, R., Malato, S., Fernandez-Ibanez, P. and Di Somma, I. 2015. Solar photocatalysis: Materials, reactors, some commercial, and pre-industrialized applications. A comprehensive approach. Applied Catalysis B: Environmental, 170: 90-123.

Strauss, A., Reyneke, B., Waso, M. and Khan, W. 2018. Compound parabolic collector solar disinfection system for the treatment of harvested rainwater. Environmental Science: Water Research & Technology, 4(7): 976-991.

Tanveer, Muhammad and Gokce Tezcanli 2013. Solar assisted photo degradation of wastewater by compound parabolic collectors: Review of design and operational parameters. Renewable and Sustainable Energy Reviews, 24: 534-43.

Thiruvenkatachari, R., Vigneswaran, S. and Moon, I.S. 2008. A review on UV/TiO_2 photocatalytic oxidation process (Journal Review). Korean Journal of Chemical Engineering, 25(1): 64-72.

Varank, Gamze, Senem Yazici Guvenc, Gokhan Gurbuz and Guleda Onkal Engin 2016. Statistical optimization of process parameters for tannery wastewater treatment by electrocoagulation and electro-Fenton techniques. Desalination and Water Treatment, 57(53): 25460-25473.

Wiszniowski, J., Robert, D., Surmacz-Gorska, J., Miksch, K. and Weber, J.V. 2006. Leachate detoxification by combination of biological and TiO_2-photocatalytic processes. Water Science and Technology, 53(3): 181-190.

Nature Environment and Pollution Technology
An International Quarterly Scientific Journal

p-ISSN: 0972-6268
(Print copies up to 2016)
e-ISSN: 2395-3454

Vol. 19 | No. 2 | pp. 663-668 | 2020

Original Research Paper

https://doi.org/10.46488/NEPT.2020.v19i02.020

Open Access Journal

Ecological Compensation Mechanism of Ambient Air Quality: A Case Study of Hubei Province, China

Ming Zhong* and Long Wang(**)†
*Academic Affairs Office, Wuhan University of Technology, Wuhan, 430070, China
**School of Safety Science and Emergency Management, Wuhan University of Technology, Wuhan 430070, China
†Corresponding author: Long Wang; zmwl@whut.edu.cn

Nat. Env. & Poll. Tech.
Website: www.neptjournal.com

Received: 20-02-2020
Accepted: 15-04-2020

Key Words:
Ambient air quality;
Ecological compensation;
Compensation mechanism

ABSTRACT

Given the increase in energy consumption and the advancement of urbanization, the expected level for the prevention and control of air pollution has not been achieved, and urban air quality has deteriorated significantly. Environmental air ecological compensation has become an important method to control air pollution to realize sustainable economic and societal development. The object, method, and standard for compensation were discussed based on the case study of the environmental air ecological compensation mechanism in the Hubei Province of China. Results show that the compensation mechanism solves the negative externality of the environment caused by the fuzzy air property rights to a certain extent. Besides, the mechanism addresses the dilemma caused by the fragmented management of the local government to the collective action and promotes the transformation from the traditional pollution control mode of the regulated enterprises to the governance mode to strengthen government regulation.

INTRODUCTION

Environmental air has the characteristics of public goods, and its property rights cannot be defined. The strong fluidity of air expands the external spill over range of pollution, often across multiple administrative areas. Changes in air pollution in different cities in a region show significant synchronicity, and severe pollution weather usually occurs successively in one day. At the same time, the improvement in air quality due to the protection of air by a local government has a strong spill over effect, providing incentives for other governments to free-ride (Mao et al. 2020). Given the cross-regional nature of air pollution, a single local government may have difficulty implementing effective measures to control air pollution, which requires all governments within the scope of pollution to take collective actions and cooperate to control air pollution. However, an interest game between local governments exists under the externality of air pollution and governance and the principle of environmental protection localization. Every rational local government tends to take inaction or passive governance, and collaborative governance encounters a situation in which two local governments might not cooperate, although collaborative governance will be of their mutual interests (Wang 2014). Therefore, air pollution prevention and control strategy should be formulated. The institutional design, organizational function, and implementation of cross-regional governance should be innovated. Also, the compensation mechanism of interest driving and interest coordination of cross-regional governance of air pollution should be improved. Governments that contribute to the protection of air should be compensated and governments with the free-rider problem and passive governance need to be punished. Therefore, local governments are encouraged to take responsibility for protecting their air ecological environment and actively control air pollution.

Ecological compensation is a kind of institutional arrangement that considers the law as the premise, and market, economy, and policy as the means to promote the occurrence of compensation activities, coordinate people's interests, and mobilize and motivate people to protect the ecological environment actively (Yu et al. 2016). In this study, the ecological compensation of ambient air quality is defined as an institutional arrangement to regulate the interest relationship of various interested subjects of an air ecological environment by using the market, economy, and policy to reduce air pollution and protect the air ecological environment. This process includes not only charging the air polluter but also compensating the victims who suffer from loss caused by air pollution. The beneficiaries apply the corresponding compensation to the cost of protecting the air ecological environment. Much ecological compensation in the field of air protection is practiced in China. For example, Hubei province implemented the *Interim Measures for Ecological Compensation of Ambient Air Quality* in 2015. From 2015 to 2018, the annual average concentrations of major air pol-

lutants, such as sulphur dioxide (SO_2), inhalable particulate matter (PM_{10}), and fine particulate matter ($PM_{2.5}$), in the region has a decreasingly yearly trend (Fig. 1). The results show the environmental air quality of Hubei Province has been improving continuously, and the effect of ecological compensation incentive mechanisms for environmental air quality is obvious.

An in-depth study on the ecological compensation mechanism for protecting air quality in Hubei Province, China should be conducted to implement better a green ecological development strategy and promote the construction of ecological civilization and sustainable economic and societal development. The main ideas, policy framework, and compensation methods of the ecological compensation mechanism should also be analysed. Further studies should be conducted to provide reference and enlightenment to improve this mechanism of protecting air quality in relevant areas.

STATE OF ART

Ecological compensation refers to the payments for ecosystem/environmental services (PES), specifically to the voluntary transaction behaviour of conditional payments made by users of environmental services to environmental service providers for providing certain natural resource services (Wunder 2015). PES is a transparent system based on the beneficiary payment principle (rather than polluter payment) and certain natural resource management rules require the environmental services traded to be clear and measurable. In recent years, PES has become an increasingly important tool for resource and environmental management. As an important endogenous incentive and constraint mechanism, PES has become the core content of cross-border environmental pollution control (Kolinjivadi et al. 2014).

Tran et al. (2016) considered the implementation of the forest environmental service project in Dabei District, Heping Province in Vietnam as an example to reveal how the PES project can help achieve the goals of the central government. The results showed that because of the incomplete design at the central level and the lack of strategic management, proving whether the project improved the level of ecosystem services and forest management is difficult. Ingram et al. (2014) analysed four cases in Guatemala, Cambodia, and Tanzania, and summarized the general experience and lessons on the use of PES to protect the biodiversity and support poverty reduction in rural areas of tropical developing countries. Grima et al. (2016) analysed 40 PES cases in Latin America and provided concepts for decision-makers to design future PES projects with a high probability of success. Leimona et al. (2015) made an empirical observation of the emerging PES mechanism in Asia by analysing case studies in Indonesia, the Philippines, and Nepal. The results showed equity and efficiency should be achieved simultaneously in the design and implementation of sustainable programs, especially in developing countries. Guo (2016) analysed the interprovincial air ecological compensation mechanism in Shandong Province from the perspectives of background, thinking, and policy framework. The author believed promoting this interprovincial air ecological compensation model is necessary for China. Shi et al. (2017) proposed the ecological compensation model for ambient air quality based on regional integration by analysing the practice of ecological compensation for ambient air quality in Shandong, Hubei, Henan, and other provinces. This model solved to some extent the dilemma caused by the fragmentation management model of a local government to the collective action. Liu (2015) proposed the implementation of the market-oriented ecological compensation model for environmental air pollution in Beijing, Tianjin, and Hebei, emphasizing the role of

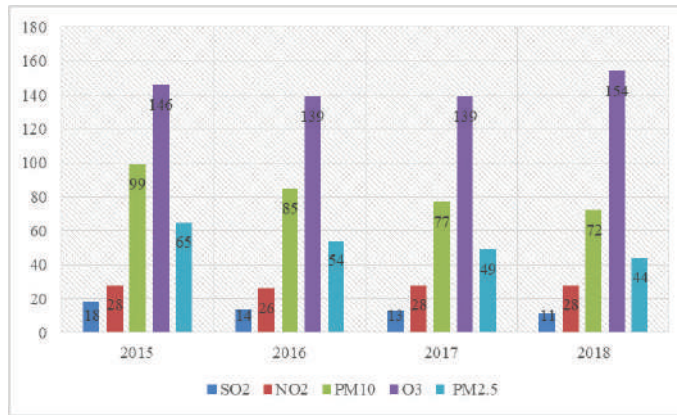

Fig. 1: Variation in the annual average concentration (μg/m^3) of the main air pollutants in Hubei Province, China (2015-2018).

the market in the optimal allocation of clean environmental air quality resources.

Ecological compensation can be divided into two categories. First, this process is dominated by the government, which pays for the ecological environment service through the purchase expenditure and the main purchase funds are financed by the government. The main forms of compensation include the establishment of the ecological fund, direct compensation, or transfer payment, such as the "Land Reclamation Plan" in the United States and the "Ecological Value-Added Tax" in Brazil (Yang et al. 2020). Second, the market-oriented type, that is, the introduction of market competition mechanism, is within the scope of ecological environment protection, elucidating the property rights. Thus, the protectors and consumers of the environment and resources can buy and sell in the free and open trading market, in which the quantification and standardization of the ecological environment are essential (He et al. 2019).

METHODOS

A detailed investigation of the compensation mechanism of ambient air quality in Hubei Province was performed using the method of text investigation to explore the actual scheme of ecological compensation for ambient air quality in Hubei Province of China. The investigation contents include the basic situation of compensation for ambient air quality, methods and modes of ecological compensation for ambient air quality, and the benefits of environmental quality improvement. We also heeded the opinions of experts and relevant management departments on the problems in the implementation of ecological compensation for ambient air quality. Finally, we obtained a clear understanding of the overall situation of the ecological compensation mechanism for ambient air quality in Hubei Province.

RESULT ANALYSIS AND DISCUSSION

Subject of Ecological Compensation

The pursuit of cost and income equality is the basic condition and important driving force for local governments to actively participate in the treatment of environmental air pollution. The ecological compensation system of ambient air quality is an effective way to realize the win-win scenario of economic development and environmental protection in a short period. According to the basic concept of "who pollutes, who governs, who benefits, who pays," the subject of ecological compensation for environmental air quality should be the consumer who destroys the environmental air quality. The object to be compensated should be the subject whose benefit of ambient air quality has been damaged or the actor who protects the ambient air quality and improves the ambient air quality. The object of environmental air quality protection is environmental interest. Environmental air quality pollution involves three kinds of interest subjects, namely, the government (pollution control subject), public (public interest subject), and polluter (pollution discharge subject). According to the principal-agent theory, the government collects fees from the polluters to control environmental air pollution to protect the public's "healthy breathing right." At present, the ecological compensation of ambient air quality in Hubei Province is focused mainly on charging the polluter, emphasizing the incentive and restriction to the subject of pollution control, and less on the incentive, restriction, and interest coordination to the subject of pollution control (local governments) at all levels. Therefore, the leading role of the government should give a full role in the prevention and control of environmental air pollution. To some extent, how to play a positive and active role of the government determines the performance of environmental air quality management, regardless of how the responsibility of environmental air pollution or the responsibility of environmental air quality protection is pursued. In the actual operation of ecological compensation for environmental air quality, based on a clear definition of property rights, local governments are usually mainly responsible for environmental air pollution control. These governments are supplemented by high-level governments, which constitute the regional ecological compensation mechanism.

Mode of Ecological Compensation

Ecological compensation of ambient air quality should not only determine the subject of compensation responsibility but also formulate compensation methods. In general, ecological compensation of ambient air quality includes direct and indirect compensation. Among these compensation mechanisms, direct compensation is provided mainly by the government departments to the compensated areas with certain funds or physical objects, such as government financial transfer payment, special compensation funds, and production equipment compensation, which can better save transaction costs and improve the regional ambient air quality in the short term. At present, financial transfer payment and special compensation funds are used increasingly in the ecological compensation of ambient air quality because of their advantages of special funds and institutional management. Indirect compensation is when the government gives certain financial and tax policy preferences, environmental protection technology, and scientific and technological personnel support to the compensated area. Indirect compensation emphasizes the pulling effect of the development of the green industry in

the compensated area on the beneficiary area and reduces the financial burden of the government. Although direct and indirect compensations have their distinct advantages, the enthusiasm of direct compensation in mobilizing enterprises and the public to participate in ecological construction is limited, and the government's sufficient financial payment capacity and the limitation in the overall institutional environment should be considered. The difficulty of indirect compensation lies not only in the challenge in identifying the eco-environmental protection industry but also in the prevention of the regional ecological deprivation caused by the transfer of pollution industries. The ecological compensation of ambient air quality not only needs to improve the ambient air quality in the short term but also a long-term regional sustainable development model. Therefore, the dual role of direct and indirect compensations should be strengthened to better promote the improvement of ambient air quality. The majority of the ecological compensation methods for ambient air quality in Hubei Province involves direct compensation. Hence, indirect compensation methods should be further optimized to promote the continuous improvement of ambient air quality.

The policy framework of the air ecological compensation mechanism in Hubei Province is shown in Fig. 2. The framework mainly includes the withholding and compensation system of an air ecological compensation fund, an innovative air monitoring management system, and improved performance assessment. Among these parameters, the withholding and compensation system of air ecological compensation fund is the core content, which not only stipulates the way of withholding and compensation but also specifies the scope of use of funds. These processes further strengthen the legal responsibility and obligation of local governments to protect air ecology.

Using the withholding and compensation system of an air ecological compensation fund, Hubei Province has detected accurately the changes in the various pollutant concentrations in the air of each city. The Environmental Protection Department calculated the amount to be withheld and compensated every quarter. For cities with deteriorating air quality, the provincial Environmental Protection Leading Group reports the withholding amount to the Provincial Department of Finance. The Provincial Department of Finance then withholds directly from the city's financial account and issues a written notice of withholding to the city. For cities with improved air quality, the Provincial Department of Finance issues compensation to the municipal finance and publishes the withholding and compensation amount and ranking of each city in the brief on Hubei's environmental protection and the official website of the Hubei Environmental Protection Department. Following the practice of the provincial government, cities at all levels have formulated a withholding and compensation system of air ecological compensation in each region, but knowing how the compensation standard is determined is the key to implement air ecological compensation. Given the regional differences, the year-on-year changes of ambient air quality of each place can be considered reasonably as the starting point for the calculation.

Standard of Ecological Compensation

At present, three main methods are used in determining the payment standard of ecological compensation. The first method is based on the cost assessment method, including the opportunity cost method and the conservation cost method. The second technique is based on the income evaluation method, including the ecosystem services value method and the market value method. The third method is based on the payment ability evaluation method, which includes the contingent valuation method and the payment ability method (Wei et al. 2019).

The standard of ecological compensation is the key and most difficult point of establishing an ecological compensation mechanism. However, when implementing compensation, distinguishing between the natural value of ambient air quality and added value of ecological construction is difficult. In practice, the most widely used method is the

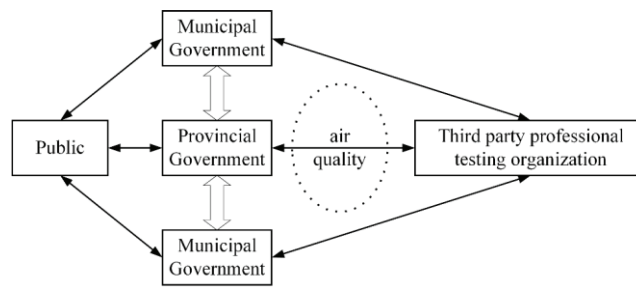

Fig. 2: Policy framework of air ecological compensation mechanism in Hubei Province.

willingness negotiation method between the payer and the compensated party. This method can be used in designing the ecological compensation standard of ambient air quality through the willingness of the payer and the payee. In the actual operation, the game between the payer and the compensation party often leads difficulties in determining the compensation standard. Thus, this method requires high-level coordination agencies to play a positive role in promotion and adjudication. In selecting the true and accurate cost accounting indicators and methods, the ecological value of ambient air quality and the enthusiasm of local governments to improve ambient air quality and the government's financial expenditure capacity should all be considered. Fair and effective compensation standards should also be established.

The assessment indicators of ecological compensation for ambient air quality are PM_{10} and $PM_{2.5}$. PM_{10} and $PM_{2.5}$ are assessed by the city (prefecture). PM_{10} and $PM_{2.5}$ of counties (districts) were assessed from 2017. The assessment data adopt the automatic monitoring data of ambient air quality confirmed by an audit. The ecological compensation fund for ambient air quality is calculated according to Equations (1) – (3).

Calculation of ecological compensation fund for city (prefecture) ambient air quality:

$$M_1 = (A_{last\ year} - A_{this\ year}) \times m_1 \times k + (B_{last\ year} - B_{this\ year}) \times m_1 \times k. \quad \ldots(1)$$

Calculation of ecological compensation fund for county (district) ambient air quality:

Calculation method in 2017:

$$M_2 = (A_{last\ year} - A_{this\ year}) \times m_2 \times k. \quad \ldots(2)$$

Calculation method in 2018 and later:

$$M_2 = (A_{last\ year} - A_{this\ year}) \times m_2 \times k + (B_{last\ year} - B_{this\ year}) \times m_2 \times k, \quad \ldots(3)$$

Where,

M_1 and M_2 are ecological compensation funds for ambient air quality (unit: ten thousand RMB);

m_1 and m_2 are the ecological compensation fund coefficients of ambient air quality [unit: ten thousand RMB/(μg/m^3)];

$A_{last\ year}$ represents the average concentration of PM_{10} in the previous year (unit: μg/m^3);

$A_{this\ year}$ refers to the average concentration of PM_{10} in the present year (unit: μg/m^3);

$B_{last\ year}$ represents the average concentration of $PM_{2.5}$ in the previous year (unit: μg/m^3);

$B_{this\ year}$ is the average concentration of $PM_{2.5}$ in the present year (unit: μg/m^3); and

k is the weather change coefficient, with a value between 0.5 – 1.

If the annual average concentrations of PM_{10} and $PM_{2.5}$ reach the secondary standard of the Ambient Air Quality Standard (GB3095-2012) for two consecutive years, the capital coefficient m_1 of the city (prefecture) is 80 and the capital coefficient m_2 of the county (district) is 40.

If the annual average concentrations of PM_{10} and $PM_{2.5}$ meet the secondary standard of the Ambient Air Quality Standard (GB3095-2012), the calculation result is negative according to the above method. The ecological compensation fund for ambient air quality will not be withheld. If the annual average concentrations of PM_{10} and $PM_{2.5}$ fail to meet the secondary standard of the Ambient Air Quality Standard (GB3095-2012), the calculation result is positive following the above method, but the assessment index fails to meet the annual goal. Thus, the ecological compensation fund for ambient air quality will not be awarded and will be implemented from 2019.

CONCLUSION

An ecological compensation system of environmental air quality that can address serious environmental air quality problems should be established with the government as the leading force and the fiscal policy of allocating public resources as the main tool. This system can enhance the enthusiasm of the region to maintain the ecological environment. Based on the regional integration of the environmental air quality ecological compensation system in Hubei Province of China, the basic starting point is to solve the problems in the regional environmental air quality, focusing on promoting the solution of the external problems of environmental air pollution. According to the characteristics of publicity, mobility, and externality of environmental air pollution, a fair and reasonable responsibility-sharing, and regional unified planning and accountability should be established to truly improve the ecological compensation system to protect the environmental air quality.

REFERENCES

Grima, N., Singh, S.J., Smetschka, B. and Ringhofer, L. 2016. Payment for ecosystem services (PES) in Latin America: Analysing the performance of 40 case studies. Ecosystem Services, 17: 24-32.

Guo, G. J. 2016. Research on intergovernmental air ecological compensation mechanism in context of cross-border governance in air pollution: Based on case of Shandong province's intergovernmental air ecological compensation practice. Resource Development & Market, 32(7): 832-837.

He, J., Wan, Y., Tang, Z., Zhu, X. and Wen, C. 2019. A developed framework for the multi-district ecological compensation standards integrating

ecosystem service zoning in an urban area in China. Sustainability, 11(18): 4876.

Ingram, J. C., Wilkie, D., Clements, T., McNab, R.B., Nelson, F., Baur, E.H., Sachedinae, H.T., Peterson, D.D. and Foley, C.A.H. 2014. Evidence of payments for ecosystem services as a mechanism for supporting biodiversity conservation and rural livelihoods. Ecosystem Services, 7: 10-21.

Kolinjivadi, V., Adamowski, J. and Kosoy, N. 2014. Recasting payments for ecosystem services (PES) in water resource management: A novel institutional approach. Ecosystem Services, 10: 144-154.

Leimona, B., Van Noordwijk, M., De Groot, R. and Leemans, R. 2015. Fairly efficient, efficiently fair: Lessons from designing and testing payment schemes for ecosystem services in Asia. Ecosystem Services, 12: 16-28.

Liu, W. 2015. Establishment of market-oriented ecological compensation model for air pollution in Beijing-Tianjin-Hebei. Modernization of Management, 35(2): 64-65.

Mao, B., Ao, C., Wang, J., Sun, B. and Xu, L. 2020. Does regret matter in public choices for air quality improvement policies? A comparison of regret-based and utility-based discrete choice modelling. Journal of Cleaner Production, 120052.

Shi, H. J. and Guang, X. 2017. Study on the Ecological Compensation System of the Atmospheric environment Based on the Regional Integration. Environment and Sustainable Development, 42(3): 27-30.

Tran, T.T.H., Zeller, M. and Suhardiman, D. 2016. Payments for ecosystem services in Hoa Binh province, Vietnam: An institutional analysis. Ecosystem Services, 22: 83-93.

Wang, W.Q. 2014. Cross regional cooperative treatment of air pollution: Taking Beijing as an example. Journal of Public Management, 1: 60-69.

Wei, W.X. and Wang, Y. H. 2019. A study on the payment standards for environmental services in air pollution governance of Beijing-Tianjin-Hebei. Journal of Finance and Economics, 45(4): 96-110.

Wunder, S. 2015. Revisiting the concept of payments for environmental services. Ecological Economics, 117: 234-243.

Yang, Y., Yao, C. and Xu, D. 2020. Ecological compensation standards of national scenic spots in western China: A case study of Taibai Mountain. Tourism Management, 76: 103950.

Yu, B., Xu, L. and Yang, Z. 2016. Ecological compensation for inundated habitats in hydropower developments based on carbon stock balance. Journal of Cleaner Production, 114: 334-342.

Nature Environment and Pollution Technology
An International Quarterly Scientific Journal

p-ISSN: 0972-6268
(Print copies up to 2016)
e-ISSN: 2395-3454

Vol. 19 | No. 2 | pp. 669-675 | 2020

Original Research Paper

https://doi.org/10.46488/NEPT.2020.v19i02.021

Open Access Journal

Comparison Study of Various Cellulose Acetylation Methods from its IR Spectra and Morphological Pattern of Cellulose Acetate as a Biomass Valorisation

Roni Maryana*†, Muslih Anwar, Andri Suwanto**, Siti Uswatun Hasanah*** and Eka Fitriana*****

*Research Center for Chemistry, Indonesian Institute of Sciences, Building 452, Kawasan PUSPIPTEK, Serpong Tangerang Selatan, Banten, Indonesia

**Research Division for Natural Products Technology, Indonesian Institute of Sciences, Jl. Yogya Wonosari, Gading, Playen, Gunungkidul, Yogyakarta, Indonesia

***Department of Chemistry, Semarang State University, Gedung D6 Lantai 2, Kampus FMIPA UNNES, Sekaran, Gunungpati, Semarang, Jawa Tengah, Indonesia

†Corresponding author: Roni Maryana; roni_yogya@yahoo.co.id

Nat. Env. & Poll. Tech.
Website: www.neptjournal.com

Received: 18-07-2019
Accepted: 05-10-2019

Key Words:
Cellulose acetate; Cellulose; Catalyst; Trichloroacetate; Acetylation

ABSTRACT

Recently substitution of fossil fuel-based polymer by natural polymer sources has been studied. Cellulose acetate that can be produced from the cellulose of biomass waste is an environmentally friendly and important polymer with many applications. This study was undertaken to determine the most suitable and effective method in the cellulose acetate (CA) production. Moreover, the role of catalyst and usefulness of trichloroacetate and I_2 catalyst has been studied. As many as 12 methods of acetylation for CA synthesis has been carried out, and the results have been compared. The peak height ratio of infrared (IR) spectra of acetyl groups was studied to determine the formation of CA. The result showed that the activation step resulted in higher IR spectra peak than the direct synthesis method. An important result of this study was shown when trichloroacetate catalyst combined with H_2SO_4 resulted in significantly higher IR spectra than the conventional method. Interestingly, I_2 catalyst resulted in better IR spectra peak than H_2SO_4 did, even the activation step was not performed. It showed that the addition of trichloroacetate and I_2 in the CA synthesis with acetic anhydride as an acetylating agent was better than conventional CA acetylation method. Furthermore, I_2 *catalyst showed the best result among other methods and will be the promising pathway to produce CA. Scanning electron microscopy* (*SEM*) analysis showed that the diameter of cellulose fibre was decreased and fracture surface occurred after the synthesis reaction.

INTRODUCTION

Indonesia, as well as other regions near the equator, generally have abundant biomass sources. Palm oil is one of the widely planted plants in Indonesia. Based on the statistics of Indonesia in 2018, the plantation area for oil palm is 14.3 million ha (Statistics Indonesia 2018). During processing, biomass waste such as oil palm empty fruit bunch, oil palm trunk and kernel were produced. Other potential agricultural waste biomass such as sugarcane bagasse, rice straw, forest and wood residue is also available in huge quantity. Cellulose is a major compound of biomass, besides lignin and hemicellulose. Biomass utilization for producing fuels such as bioethanol and dissolving pulp from cellulose; and chemical products such as xylitol from hemicellulose, sodium lignosulphonate and vanillin from derivatization of lignin has been reported (Judiawan 2019, Messaoudi 2019, Maryana 2017, Pramudono 2018). Another study reported the production of ethanol, lignin, and carbon source for fungal culture from lignocellulosic materials (Smichi 2018). Enzyme production such as cellulase, xylanase, and ligninolytic that utilized agricultural biomass from biomass waste has also been studied (Namasivayam 2014, Rajwar 2016).

The cellulose-derivatives study has also gained high intention in the recent year since the lignocellulosic biomass could be a raw material for a valuable chemical and widely apply in industry. Cellulose acetate, the most important esters of cellulose, has wide application such as thermoplastics, textile industry, food packaging, film coating, reverse osmosis, and gas separation (Warth 1997, Reddy & Yang 2005, Gemili 2008, Kumar 2015, Duarte 2006, Najafi 2018).

Introducing acetyl functional group to the cellulose has been known as efficient derivatization of cellulose, one of them is cellulose acetate production. Many methods have been developed to produce cellulose acetate. In general, cellulose acetate is produced from the reaction of cellulose with acetic anhydride in acetic acid condition by using H_2SO_4 as

catalyst (Hummel 2004). Several studies have been reported to modify this conventional method. It has reported the addition of $NaHSO_4$ as a catalyst to reduce H_2SO_4 amount and to make the temperature of acetylation reaction becoming lower (Djuned 2014). Meanwhile, a study by using strong organo-halogen acid, trifluoroacetic acid, as a catalyst has also been studied (Morgan 1951). Morgan reported that trifluoroacetic acid catalyst would prevent derivative products formed during the acetylation of cellulose that could bound acid sulfate groups if the sulfuric acid catalyst is used. Another study used I_2 as a catalyst in a heterogeneous medium in the presence of acetic anhydride. Iodine catalyst mechanism reaction was proposed and is presented in Fig. 1 (Das 2014). Iodine is currently studied extensively as a catalyst because of its economic factor, convenience and environmentally friendly. Meanwhile, trichloroacetate, the catalyst in this study, has been known as powerful organic acid with pKa1 0.66 compared with acetic acid pKa1 4.756 and similar to trifluoroacetate pKa1 0.52 (Lide 2004). Morgan (1951) reported that in the case of trifluoroacetate, the cellulose esters prepared by using this catalyst, will not need special washing because of the complete removal of catalyst. Moreover, it will not combine with alcohol in the presence of other carboxylic acids (Morgan 1951). Meanwhile, iodine has been known to react to form a complex with amylose and cellulose (Wang 1999). Therefore, this complex reaction could improve solubility of cellulose in the acetylation process. The previous study reported that acetylation of alcohol by acetic anhydride was promoted by iodine (Phukan 2004).

This study was carried out to determine the most suitable and effective method in the cellulose acetate (CA) synthesis. Moreover, the role of catalyst and usefulness of trichloroacetate and I_2 catalyst will be studied and be compared to the catalyst that is used in the conventional method synthesis. We focused on the role of catalyst and usefulness of trichloroacetate and I_2 in the cellulose acetate (CA) synthesis. The effective methods among available and modified methods will be important for cellulose acetate production from biomass. Furthermore, we reported the new several catalyst combinations such as $H_2SO_4/CCl_3COOH/NaHSO_4$ and H_2SO_4/CCl_3COOH in the cellulose esterification.

MATERIALS AND METHODS

Materials

The commercial pure cellulose C6228 fibres were obtained from Merck and cellulose acetate with average Mn ~ 30,000 by GPC was obtained from Aldrich chemistry. The reagents used for the acetylation were acetic anhydride from ajax chemicals; Acetic acid (glacial) 100% from Merck; Trichloroacetic acid from Merck; Iodine from Merck; Sulfuric acid 95-97% from Merck; Sodium thiosulfate pentahydrate from Merck and Sodium hydrogen sulfate monohydrate from Merck.

Methods

The cellulose acetates were prepared by using twelve different methods. The experimental design with 12 methods is presented in Table 1, and the methods from 1 to 12 were named A to L, respectively. The acetylation procedures were categorized as three steps, activation; acetylation; and hydration. Method A and B (conventional method with activation step); method C (conventional method without activation); method D, E, F, G (using I_2 catalyst); method H (using H_2SO_4 and $NaHSO_4$ catalyst); J, K, L (catalyst combination including trichloroacetate).

Material characterization: Functional groups of cellulose and cellulose acetate were studied by using Fourier Transmission Infrared Spectroscopy. The samples were blended with KBr and followed by compressing this mixture in the sample disc and analysed with the transmission wavenumber range 4000 to 400 cm^{-1}. Meanwhile, the surfaces of the samples were analysed by using Scanning Electron Microscope (SEM), with SE 5 kV 2000x to 2500x magnification.

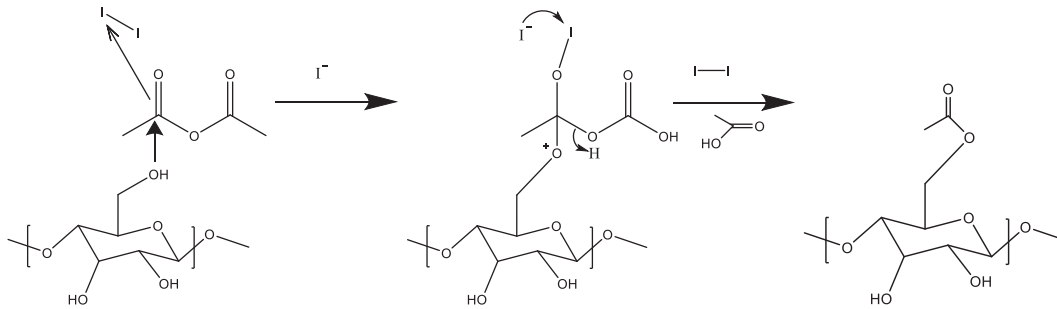

Fig. 1: Mechanism of cellulose acetate production by using iodine catalyst.

RESULTS AND DISCUSSION

Currently, the utilization of infrared spectroscopy is considered as one of the most important techniques. It was well known that infrared techniques provide fast, low-cost analysis, besides the non-destructive method with promising results (Xu 2013). Chemically, hundreds of glucose molecules linked by a glycosidic bond to form cellulose (Zugenmaier 2001). Meanwhile, FTIR is an efficient method to study hydrogen-bonding in the crystalline and amorphous structure of cellulose (Kondo 1996). Therefore, IR spectroscopy is a suitable method for studying CA characteristics, especially to observe the ester and hydroxyl group absorption. These functional groups are referred to CA formation in the synthesis of CA from cellulose.

The cellulose acetylation methods that were carried out in this study can be divided into three major steps (i) activation; (ii) acetylation; and (iii) hydration. Fig. 2 shows the IR spectra of twelve acetylated samples that were further compared to the IR spectra of cellulose and cellulose acetate. The peak height 1728-1743 cm^{-1}, an indication of C=O stretching of carbonyl ester band, as compared to the adsorbed water band at 1635-1651 cm^{-1} (Das 2014) and the height ratio was determined based on this comparison.

It was observed from Fig. 2 that the major change of stretching band of acetylated samples was at 1728-1743 cm^{-1} and 1635-1651 cm^{-1}. Cellulose fibre has no peak at 1728-1743 cm^{-1} because it has no carbonyl ester group. Meanwhile, pure cellulose acetate showed the highest peak among acetylated cellulose samples. Sample methods A and B were previously treated with CH_3COOH and H_2SO_4 at 40°C for 3h as activation step before acetylation step. Activation step aims to open hydrogen bond in the hydroxyl functional group to make the acetylation process with acetic anhydride easier. The difference in sample method A and B was in the acetylation step, ratio $(CH_3CO)_2O : H_2SO_4$ was 2 and 10 for sample A and B, respectively. Meanwhile, sample code C was acetylated without activation step. The results in Table 2 showed that the IR peak ratio for sample A (0.51) is higher than the peak of sample B (0.22). This phenomenon can be explained by the quantity of H_2SO_4 catalyst, for sample method A, sulfuric acid was 2.5 mL, and this was more than for the sample B (1 mL). This result supports many of the previous studies that the catalyst is important for the conventional acetylation method. In the case of method B, the sulfuric acid was not enough to catalyse the reaction. Regarding method C, the sample showed no peak at all. In this case, it has no peak because besides no activation step, the

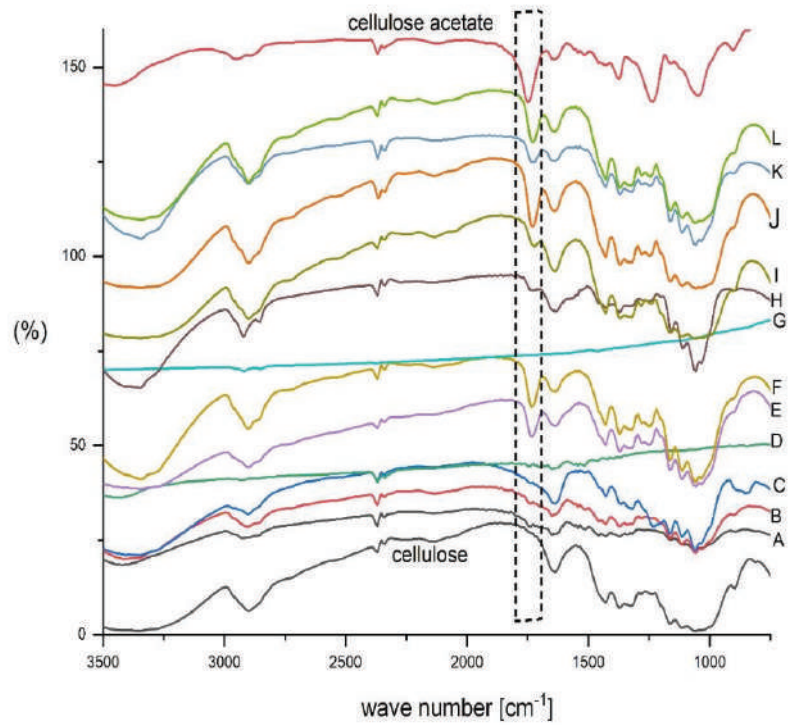

Fig. 2: Comparison of IR spectra of cellulose, acetylated cellulose with sample code A-L and cellulose acetate.

Table 1: Experimental design of twelve methods of cellulose acetate synthesis.

Sample code	Sample weight (g)	Activation		Acetylation		Hydration/further treatment	
A	2	CH_3COOH 3M, 50mL H_2SO_4 98%, 2.5mL	reflux 40°C, 3h	$(CH_3CO)_2O$ 5mL H_2SO_4 98% 2.5mL	reflux 40°C, 8h		
B	2	CH_3COOH 3M, 50mL H_2SO_4 98%, 2.5mL	reflux 40°C, 3h	$(CH_3CO)_2O$ 10mL H_2SO_4 98% 1mL	reflux 40°C, 8h		
C	1			$(CH_3CO)_2O$ 2.9mL CH_3COOH 2.9mL H_2SO_4 98% 0.29mL	7°C, 1h	CH_3COOH 0.4mL H_2SO_4 98% 0.4mL	Aging 15h
D	1			$(CH_3CO)_2O$ 50mL, I_2 1.5g	reflux 80°C, 5h	$Na_2S_2O_3$ 5 H_2O 25 mL C_2H_5OH 150 mL Filter and wash Residue is dissolved Filtrate is evaporated	room temp. stirrer 1 h ethanol 75% and aquadest CH_2Cl_2
E, F, G	1			$(CH_3CO)_2O$ 50mL, I_2 1.5g	reflux 120°C, 5h	$Na_2S_2O_3$ 5 H_2O 25 mL C_2H_5OH 150 mL Filter and wash Residue is dissolved Filtrate, Residue (E) Residue is bleached (F) Filtrate is evaporated (G)	room temp. stirrer 1 h ethanol 75% and aquadest CH_2Cl_2 50 ml H_2O_2 5%, 70°C, 5h
H, I	5	CH_3COOH 90mL	stirrer 1h at room temperature	$(CH_3CO)_2O$ 25mL H_2SO_4 98% 0.125mL $NaHSO_4$ 0.19g	stirrer 30 min. at room temp. Aging for 3h	CH_3COONa 0.125g in 10 ml CH_3COOH Aquadest 1L to form solid phase Filtrate was evaporated (H) Residue (I)	stirrer 15 min. at room temp.
J, K, L	5	CH_3COOH 90mL H_2SO_4 98% 0.125mL CCl_3COOH 0.22g (J) CH_3COOH 90mL H_2SO_4 98% 0.125mL CCl_3COOH 0.22g $NaHSO_4$ 0.19g (K) CH_3COOH 90mL H_2SO_4 98% 0.125mL NaHSO4 0.19g (L)	stirrer 1h at 40°C	$(CH_3CO)_2O$ 20mL	stirrer 30 min. at 40°C; Aging for 4h, 40°C	CH_3COONa 0.125g in 10 mL CH_3COOH Aquadest 1L to form solid phase Filtrate was evaporated Residue	stirrer 15 min. at 40°C

acetylation condition, temperature and time were decreased to 7°C and 1 h compared to 40°C for 8 h in the method A and B. The result confirmed the importance of activation step and suitable acetylation condition.

Samples with method D, E, F, G were acetylated without activation step. However, the iodine catalyst was used in the acetylation reaction. Sample method D was acetylated at 80°C for 5 h. The difference in the sample method E, F, G is the acetylation temperature; for these three samples, acetylation conditions were at 120°C for 5 h. From Fig. 2 and Table 2, it can be seen that the peak height ratio for method D at 80°C (0.49) was lower than those of method E and F at 120°C (1.75 and 2.01 for sample E and F). Meanwhile, sample G has no peak because this was the side product of method E and F. Regarding differences, E and F methods were bleached by H_2O_2 10%. Method E was the unbleached sample, and F was the bleached one. In case of the sample with method G, after adding sodium thiosulphate and transferring the mixture to the beaker containing ethanol, the product was filtered and the residue becoming sample E and filtrate was sample G. It can be observed that there was no cellulose acetate in the filtrate.

Method H and I were similar to the conventional method. However, the activation step was carried out by using acetic acid and mixing for one hour in the room temperature. Additionally, in the acetylation step, sodium bisulphate, together with sulfuric acid was used as a catalyst. It was observed that both showed adsorption peak around 1730 cm^{-1}, the peak height ratio was 0.27 for H and 0.40 for I. These results were lower than those of conventional method with activation step, A and B. The activation step for H and I was only by adding CH_3COOH. Meanwhile, in the case of A and B, the CH_3COOH and H_2SO_4 were added and mixed at 40°C for 3 hours. It seems that the activation condition gave significant influence, even sodium bisulphate was added in the acetylation step.

Method J, K, L were modified method of H and I. For the J method, the new combination of catalyst CH_3COOH, H_2SO_4, and CCl_3COOH were applied. Meanwhile, for the K method, also the new catalyst combination CH_3COOH, H_2SO_4, CCl_3COOH, and $NaHSO_4$ was studied. Furthermore, for sample code L, a new combination of catalyst CH_3COOH, H_2SO_4, and $NaHSO_4$ in the activation step was applied. It was observed that peak heights of J, K, L method were much better than those of H and I. For J method, the peak ratio was 1.94 and the better than those of K method (1.43) and L method (1.74). We can study the effect CCl_3COOH catalyst by comparing method J and method L. It was observed that method by using trichloroacetate was the best among all conventional methods. We can conclude that CCl_3COOH as powerful organic acid showing a significant role in the cellulose acetate formation.

However, interestingly, we found that iodine catalyst, method F, showed better peak height ratio than the conventional method by adding trichloroacetate, J method. Therefore, we confirm that method with using iodine catalyst is the best method and a promising catalyst in the cellulose acetate production.

Table 2: Peak height ratio of the carbonyl functional group to the adsorbed water band.

No	Method name	Peak Height (Δ %T)		Ratio 1735/1651
		1728-1743 cm^{-1}	1635 -1651 cm^{-1}	
1	A	1.41	2.79	0.51
2	B	0.87	3.98	0.22
3	C	0.00	7.16	0.00
4	D	0.60	1.22	0.49
5	E	7.90	4.52	1.75
6	F	9.90	4.78	2.07
7	G	-	-	-
8	H	1.64	6.08	0.27
9	I	3.26	8.08	0.40
10	J	12.64	6.53	1.94
11	K	4.66	3.25	1.43
12	L	9.40	5.40	1.74
13	Cellulose Acetate	14.28	3.08	4.64
14	Cellulose	0.00	8.70	0.00

Besides, changes in the stretching band of C=O carbonyl, it was observed that the O-H spectrum from alcohol functional group at 3300-3400 cm^{-1} is decreased.

Cellulose Acetate Morphologies

Surface structure of cellulose, acetylated cellulose and cellulose acetate commercial was studied. Fig. 3 shows the diameter of pure cellulose, method F and method J. Method F and J were the best methods of this study. It was observed that the diameter fibre of cellulose method F and J decreased compared to the pure cellulose. The pure cellulose diameter ranges from 26 to 29.9μm. Meanwhile, acetylated cellulose

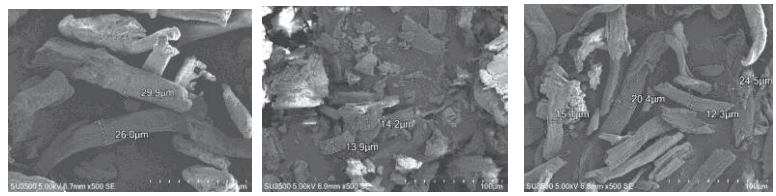

(a) (b) (c)

Fig. 3: SEM micrograph for commercial cellulose (a), acetylated cellulose method F (b) and acetylated cellulose method J (c).

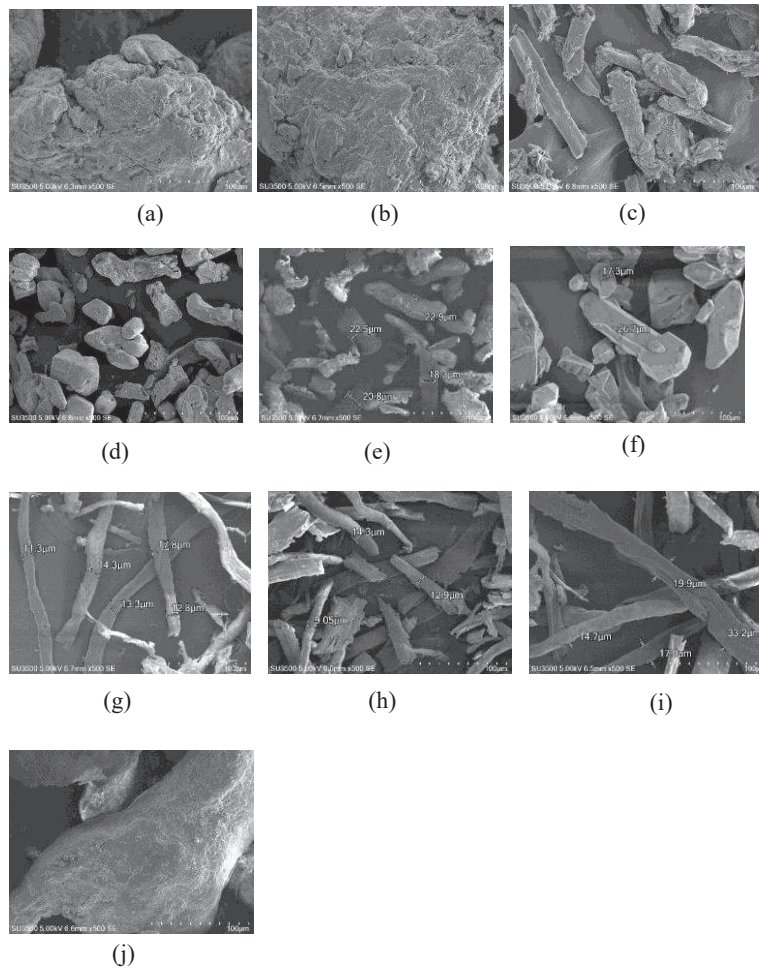

(a) (b) (c)

(d) (e) (f)

(g) (h) (i)

(j)

Fig. 4: SEM micrograph for acetylated cellulose A method (a), B method (b), C method (c), D method (d), E method (e), G method (f), I method (g), K method (h), L method (i) and cellulose acetate commercial (j).

ranges from 13.9 to 14.2μm for F method and 12.3 to 25.5 μm for the J method. There was a modification in cellulose surface structure following esterification.

Meanwhile, other cellulose acetate resulted from other methods showed varying diameter and is presented in Fig. 4. Based on Fig. 4, it showed that acetylation process influence the surface structure of cellulose fibre.

CONCLUSIONS

This study confirmed that the activation step in the synthesis of cellulose acetate is important. Meanwhile, the addition of trichloroacetate catalyst resulted in better peak ratio than that of catalyst in the conventional methods. Therefore, the addition of strong organic acid will improve the acetylation process. The important finding of this study is that iodine catalyst showed superior effect than that of all the catalysts and it is a promising catalyst agent in the production of cellulose acetate in the future.

ACKNOWLEDGEMENT

The authors acknowledge the Ministry of Research, Technology, and Higher Education of The Republic of Indonesia for the research grant Incentive Research National Innovation System Batch I, 2019.

REFERENCES

Das, A.M., Ali, A.A. and Hazarika, M.P. 2014. Synthesis and characterization of cellulose acetate from rice husk: Eco-friendly condition. Carbohydrate Polymers, 112: 342-349.

Djuned, F.M., Asad, M., Ibrahim, M.N.M. and Daud, W.R.W. 2014. Synthesis and characterization of cellulose acetate from TCF oil palm empty fruit bunch pulp. Bioresources, 9(3): 4710-4721.

Duarte, A.P., Cidade, M.T. and Bordado, J.C. 2006. Cellulose acetate reverse osmosis membranes: Optimization of the composition. J. Appl. Polym. Sci., 100: 4052-4058.

Xu, F., Yu, J., Tesso, T., Dowell, F. and Wang, D. 2013. Qualitative and quantitative analysis of lignocellulosic biomass using infrared techniques: A mini-review. Applied Energy, 104: 801-809.

Gemili, S., Yemenicio-lu, A. and Altinkaya, S. 2007. Development of cellulose acetate based antimicrobial food packaging materials for controlled release of lysozyme. Journal of Food Engineering, 90(4): 453-462.

Hummel, A. 2004. Acetate manufacturing process and technology, 3.2 industrial process. Macromolecular Symposia, 208(1): 61-79.

Judiawan, W., Sudiyani, Y. and Nurnasari, E. 2019. Conversion of hemicellulose from kenaf core fibre to xylose through dilute sulfuric acid hydrolysis. Indonesian Journal of Applied Chemistry, 21(1): 14-22.

Kondo, T. and Sawatari, C.A. 1996. Fourier transform infra-red spectroscopic analysis of the character of hydrogen bonds in amorphous cellulose. Polymer, 37: 393-9.

Kumar, V.K., Kumar, K.K., Kishore, P.V. and Sushma, S. 2015. Investigation of the impact of cellulose acetate coating on the release pattern of freely soluble drug: metoprolol succinate. Res. J. Pharm, 6(4): 249-255.

Lide, David R. 2003. Handbook of Chemistry and Physics. 84th edition. CRC Press LLC

Maryana, R., Nakagawa-Izumi, A., Kajiyama, M. and Ohi, H. 2017. Environment-friendly non-sulfur cooking and total chlorine-free bleaching for preparation of sugarcane bagasse cellulose. Journal of Fiber Science and Technology, 73(8): 182-191.

Messaoudi, Y., Smichi, N., Bouachir, F. and Mohamed Gargouri, M. 2019. Fractionation and biotransformation of lignocelluloses-based wastes for bioethanol, xylose and vanillin production. Waste Biomass Valor., 10: 357-367.

Morgan, P.W. 1951. Trifluoroacetic acid as an esterification catalyst. Industrial and Engineering Chemistry, 43(11): 2575-2577.

Najafi, M., Sadeghi, M., Bolverdi, A., Chenar, M. and Pakizeh, M. 2018. Gas permeation properties of cellulose acetate/silica nanocomposite membrane. Adv. Polym. Technol., 37: 2043-2052.

Namasivayam, S.K.R., Babu, M. and Bharani, R.S.A. 2014. Evaluation of lignocellulosic agro wastes for the enhanced production of extracellular cellulase and xylanase by *Trichoderma harzianum*. Nature Environment and Pollution Technology. 11(1): 47-52.

Phukan, P. 2004. Iodine as an extremely powerful catalyst for the acetylation of alcohols under solvent-free conditions. Tetrahedron Letters, 45: 4785-4787.

Pramudono, B., Aji, H.A., Priyanto, S., Kusworo, T.J., Suherman, Untoro, E. and Ratu, P. 2018. Utilization of biomass waste of pulp and paper industry for production of sodium lignosulphonate (SLS). Nature Environment and Pollution Technology. 17(4): 1299-1303.

Rajwar, D., Joshi, S. and Rai, J.P.N. 2016. Ligninolytic enzymes production and decolorization potential of native fungi isolated from pulp and paper mill sludge. Nature Environment and Pollution Technology. 15(4): 1241-1248.

Reddy, N. and Yang, Y. 2005. Biofibers from agricultural byproducts for industrial applications. Trends in Biotechnology, 23(1): 22-27.

Statistics Indonesia 2018. https://www.bps.go.id/dynamictable/2015/09/04/838/luas-tanaman-perkebunan-menurut-propinsi-dan-jenis-tanaman-indonesia-000-ha-2011-2018-.html

Smichi, N., Messaoudi, Y. and Gargouri, M. 2018. Lignocellulosic biomass fractionation: Production ethanol, lignin and carbon source for fungal culture. Waste Biomass Valor, 7: 1549-1554.

Warth, H., Mülhaupt, R. and Schätzle, J. 1997. Thermoplastic cellulose acetate and cellulose acetate compounds prepared by reactive processing. J. Appl. Polym. Sci., 64: 213-242.

Wang, Y. and Easteal, A.J. 1999. Interaction between iodine and ethyl cellulose, J. Appl. Poly., 71(8): 1303-1314.

Zugenmaier, P. 2001. Conformation and packing of various crystalline cellulose fibres. Prog. Polym. Sci., 26: 1341-417.

Nature Environment and Pollution Technology
An International Quarterly Scientific Journal

p-ISSN: 0972-6268
(Print copies up to 2016)
e-ISSN: 2395-3454

Vol. 19 | No. 2 | pp. 677-685 | 2020

Original Research Paper

https://doi.org/10.46488/NEPT.2020.v19i02.022

Open Access Journal

Lithium Induced Toxicity Profile of Oxygen Consumption, Haematological Parameters and Biochemical Profiles of *Channa punctatus* and *Oreochromis niloticus*

S. ThangaMalathi and V.Anuradha†
Department of Biochemistry, Mohamed Sathak College of Arts and Science, Sholinganallur, Chennai-600119, Tamilnadu, India
†Corresponding author: V. Anuradha; vanuradha.2003@gmail.com

Nat. Env. & Poll. Tech.
Website: www.neptjournal.com
Received: 16-08-2019
Accepted: 18-09-2019

Key Words:
Lithium; *Channa punctatus*; *Oreochromis niloticus*; Oxygen consumption; Haematological indices; Biochemical profiles

ABSTRACT

Freshwaters are highly vulnerable to pollution since they act as immediate sinks for the consequences of human activity always associated with the danger of accidental discharges. Heavy metals constitute a core group of aquatic pollutants and additional concentrations of these metals accumulate in the aquatic ecosystems as a result of land-based activities. Fish mostly tend to bioaccumulate heavy metals, and humans can be at great risk, sometimes even lethal, through contamination of the food chain. An attempt has been made in the present investigation to determine the acute toxicity of lithium and its toxicological effects on survival, physiological, haematological and biochemical parameters of the widely consumed spotted sneak head *Channa punctatus* and Nile Tilapia *Oreochromis niloticus*. Short-term acute toxicity tests were performed by exposing the test species to different concentrations of lithium chloride. The results showed that the normal respiratory activity of the fish was significantly affected and there was a depression in the metabolic rate at the end of 24, 48, 72 and 96h exposure. Appreciable decline changes occur in haematological parameters and biochemical profiles of the fish. This study reflects the extent of the toxic effects of lithium and the metal-induced cumulative deleterious effects at various functional levels in the widely consumed freshwater fish, *Channa punctatus* and *Oreochromis niloticus.*

INTRODUCTION

Aquatic pollution has become a global problem in recent years. Extensive industrialization has measurably influenced the quality of water lakes, ponds and rivers all over the world. Heavy metals are recognized as one of the most hazardous environmental pollutants and toxic to many organisms. The natural aquatic systems may extensively contaminate with heavy metals released from domestic, industrial and other man-made activities (Vutukuru 2003). Heavy metal contamination may have devastating effects on the ecological balance of the recipient environment and a diversity of aquatic organisms (Ashraj 2005). Among animal species, fishes are inhabitants that cannot escape from the detrimental effects of these pollutants. Heavy metals at high concentrations can cause hazardous effects to metabolic, physiological and biochemical systems of fishes (Heath 1987). Fishes are widely used to evaluate the health of aquatic ecosystems because the pollutants build up in the food chain and are responsible for adverse effects and death in the aquatic ecosystems. Fish respond sensitivity to an increased concentration of contaminants (metals, organic pollutants) in water. The accumulation levels of metals in organs and tissues of fish depend upon taxonomic belonging of fish species, age patterns, their physical-biochemical characteristics and chemical status of the environment they live. Biochemical profiles in fish and other aquatic organisms under heavy metal stress serves as an important bio-indicators in the monitoring of aquatic environment (Ambrose et al. 1994, Vutukuru et al. 2000, Sornaraj et al. 1995, Abbasi et al. 1995, Kszos et al. 2003 and Smithberg & Dixit 1982). Blood chemistry indices including enzymes, nutrients, metabolites, waste products and inorganic ions have been used to detect cellular damage and measure the responses to metals (O'Neil et al. 1998 and Congleton & La Voie 2001). The present study aims to investigate the responses of serum biochemical parameters, including haematological indices, enzymes, ions (Na^+, K^+ and Cl^-) and oxygen consumption in *C. punctatus* and *O. niloticus* exposed to lithium metal. Lithium is the lightest metal, in its elemental form, and is highly reactive as a pure element. Because of its reactivity, Li does not occur naturally as a pure element. It occurs instead in stable minerals and salts. It is the 27th most abundant element in nature. Lithium is widely used in ceramics, glass and aluminium production and has some applications for synthetic rubber, pharmaceuticals, chemical manufacturing, lubricants, batteries and

nuclear reactor coolant and air treatment (Kszos et al. 2003). Since 2007, the most important and the fastest growing area of lithium consumption is the lithium-containing batteries. These are extensively used in small electronic devices like cellular phones, cameras, watches, signal devices as well as laptops. Lithium batteries are increasingly substituting other batteries, so their consumption is constantly expanding (Lenntech 2007). Knowledge of acute toxicity of a xenobiotic often can be very helpful in predicting and preventing acute damage to aquatic life in receiving waters as well as in regulating aquatic toxic waste discharges (Scrosati & Garche 2010). Because of this, short-term acute toxicity tests were performed on *Channa punctatus* and *Oreochromis niloticus*for 96h to determine the LC_{50} value to elucidate the acute effects of lithium on the survival, oxygen consumption, haematological parameters (Hb, MCHC, MCV, WBC, HCT and MCH), enzymes (SGOT, SGPT, ACP and ALP) and some biochemical constituents (total protein, triglyceride, cholesterol, phospholipid, free fatty acid and carbohydrate) of the fishes.

MATERIALS AND METHODS

Determination of LC_{50}: Laboratory bioassays were conducted to determine the 24hr, 48hr, 72hr and 96hrs LC_{50} values for *C.punctatus* and *O.niloticus* exposed to lithium chloride. The experimental design and calculations for the acute toxicity procedures were followed as given by Finney (1971).

Acute toxicity tests: The freshwater healthy fish, *Channa punctatus* and *Oreochromis niloticus* of the weight (2 ± 0.84g and 1.5 ± 0.53g) and length (15.67 ± 3.14cm and 16 ± 2cm) were selected for the toxicity tests and samples were collected from Pothur (Thirumullaivoyal) Chennai. Healthy fishes were then transferred to glass aquaria containing unchlorinated groundwater before they were used for experiments. The fishes were acclimated in the laboratory condition for 30days. The feeding and maintenance of the fish and the physico-chemical characteristics of the water used for acclimation, controls and experiments are followed as per the report given earlier (Lenntech 2007). Short-term tests of acute toxicity for 96h were performed on the fish following renewal bioassay. Only fishes which were healthy and showed active movements were used for the tests. The desired concentration of lithium chloride anhydrous (SRL pure, Maharashtra, India) was prepared by adding aliquots of 1% stock solution in double-distilled water. The toxicant solution in the test chambers was replaced with a fresh solution of the same concentration every 24hours. Renewal bioassays were using following concentrations of lithium chloride viz., 80mg/L, to 300mg/L which resulted in mortality of the fish within the range of 5 to 95%. Ten fishes (both species) were tested at each concentration and the loading was at the recommended level (Sastry & Sunitha 1984). Controls (both species) without toxicants were also run simultaneously. The behaviour and condition of the fishes were noted every 24h up to 96h. Between the experiments, the test chambers (15-litre capacity) were carefully washed to eliminate residual metal adsorption to the walls. No differentiation was made between sexes.

Statistical analyses: The experiments were repeated thrice and only the arithmetic mean of the three experiments at each concentration was taken to express the results. Probit analysis a log dose against (mortality) was performed adopting standard protocol (Finney 1953).

Oxygen consumption: Since respiratory distress is one of the important manifestations of acute heavy metal toxicity and is known to produce physiological imbalance, *Channa punctatus* and *Oreochromis niloticus* were exposed to lithium duration of the period 96hr. In the present study, the respiration rate of the same fish was measured from 24h to 96h with a 24h interval. At the end of 24h exposure, each fish was transferred from the test chamber (5l capacity) to respiratory chamber of 1-litre capacity, which is also numbered in accordance with the test chamber. The fish were allowed to stabilize for five minutes and then the experiment was run for a period of 1h. Only one fish was introduced into each aquarium and a thick layer of coconut oil was spread on the surface (care was taken to avoid trapping air bubbles) of the fish medium to prevent the contact of the medium to the atmosphere and to prevent the fish from reaching the atmospheric air. After the experiment, the fishes were replaced in their test chambers. The same procedure repeated for 48h, 72h and 96h. Any dead fish during the experiment was removed and the test repeated to get the response of at least three fishes. Controls were also run simultaneously to obtain information on the oxygen consumption of the fish in the normal state. Respiratory measurements were made by the method adopted by Fitch (APHA, AWWA, WPCP 1998) and the dissolved oxygen was estimated adopting Winkler's method. All the rate of oxygen consumption per gram weight of the fish per hour was calculated and the values were expressed as mL O_2/gm/hour. The respiratory measurements were made in diffused daylight and the time of the experiment was kept constant (11.00am to 3.00pm) to avoid the effect of time of day on the respiration of the fish. The temperature and pH during experiments were 26.15°C ± 0.59°C and 7.4 ± 0.21, respectively.

Haematological studies: Twenty fishes (in both the species, *Channa punctatus* and *Oreochromis niloticus*) were used in this investigation. The fish were maintained in the aquaria

Table 1: Standard methods for the haematological analysis.

Parameters	Methods	References
RBC count (10^6/mm³)	Haemocytometrically with Neubauer chamber	Davidson et al. (1969)
Hb (g%)	Cyanmethaemoglobin method	Drabkins (2010)
WBC count (10^3/mm³)	Neubauer counting chamber	Donald & Bonford (1963)
HCT (%)	Haematocrit method	Schalm et al. (1975)

at room temperature 27±2°C. The fish were introduced into 10-litre capacity containers of water containing specific heavy metal lithium. After the recovery period, all such treated fishes were separated from the experimental containers and blood samples were collected from five experimental individuals from each group at each time with an interval of 24hrs during the experiment. Fish was collected and gently wiped with a dry cloth to remove water. Caudal peduncle was cut with a sharp blade and the blood was collected in small vials (anticoagulated with 0.02mL of 10% EDTA). All the haematological analysis was performed using standard techniques mentioned in Table 1.

Determination of mean corpuscular volume (MCV): MCV indicates the average size of the blood cell in a given sample of blood. MCV was calculated by the following formula and expressed as femtoliter (fL)

$$\text{MCV} = \text{Haematocrit (\%)} \times 10/\text{RBC count} \quad \ldots(1)$$

Determination of mean corpuscular haemoglobin (MCH): MCH represents the average content of the Hb in each red blood cell. MCH is influenced by the Hb concentration and the number of RBC. MCH was calculated by the following formula and expressed in pictogram (pg).

$$\text{MCH} = \text{Haemoglobin (g/dl)} \times 10/\text{RBC count} \quad \ldots(2)$$

Determination of mean corpuscular haemoglobin concentration (MCHC): MCHC reflects the average concentration of the haemoglobin in the red blood cells in the blood. MCHC was obtained by the following formula and expressed in terms of gram percentage (g%).

$$\text{MCHC} = \text{haemoglobin (g/dl)} \times 100/\text{Hb(\%)} \quad \ldots(3)$$

Collection of blood and tissues for the assay: Blood samples were collected in small vials by heart puncture using plastic disposable syringes fitted with prechilled and heparinized 26gauge needle. The blood sample was centrifuged at 10000 rpm for 20minutes to separate the serum. Simultaneously liver and tissue were excised and homogenized in ice-cold 0.25M sucrose buffer, pH 7.4. The homogenate was centrifuged at 5000rpm for 15minutes at 4°C. The tissue supernatant, as well as serum, was further used for measurement of following biochemical parameters.

Biochemical studies: The activities of SGPT (ALT), SGOT (AST), ALP and ACP and the concentration of total protein, phospholipid, free fatty acid, triglyceride, carbohydrate and cholesterol, and ions (Na^+, K^+, Cl^-) in the serum and tissues were calculated by using the methods shown in Table 2.

SGPT and SGOT activities were measured by using the method of Bergmeyer et al (1985); King and Armstrong method for ALP activity; Tenniswood et al. (1976), for ACP activity; Tietz & Logan (1987), for the electrolytes (Na^+, K^+, Cl^-).

RESULTS AND DISCUSSION

Survival: The concentration of lithium chloride tested (*Channa punctatus* and *Oreochromis niloticus*) in the present study were 80mg/L (Li as 0.29mg/L and 0.22mg/L), 100mg/L (Li as 0.32mg/L and 0.42mg/L), 120mg/L (Li as 0.53mg/L and 0.44mg/L) and 150mg/L (Li as 0.61mg/L and 0.13mg/L).The mortality ranged from 10% to 95% and increased with a corresponding increase in the toxicant con-

Table 2: Biochemical studies.

Parameters	Methods
Estimation of carbohydrate	GOD - POD method
Estimation of cholesterol	Zak's method
Estimation of triglyceride	Foster & Dunn's method
Estimation of free fatty acid	Hron & Menahan method
Estimation of protein	Lowry's method
Estimation of phospholipid	Folch method

Table 3: Changes in the oxygen uptake of *Channa punctatus* and *Oreochromis niloticus* at following an exposure period of lithium (O_2 mL/g/hr).

Period of exposure	Control X ± SD		Experiment X ± SD	
	Channa punctatus	*Oreochromis niloticus*	*Channa punctatus*	*Oreochromis niloticus*
24h	3.98 ± 0.16	3.52 ± 0.36	3.31 ± 0.14	2.48 ± 0.27
48h			2.50 ± 0.35	2.03 ± 0.08
72h			1.94 ± 0.08	1.41 ± 0.29
96h			2.00 ± 0.44	0.85 ± 0.12

Values are mean ± SD, – or + indicate percent decrease or increase over control.

centration and also duration of the exposure demonstrating both time and concentration dependent responses.

Behavioural Manifestations

The behaviour and condition of the fishes in both the control and test solution were noted every 24h up to 96h. The fishes showed a marked change in their behaviour when exposed to different concentrations of the test solution. Behavioural manifestations of acute toxicity like copious secretion of mucus, loss of scales, discolouration, surfacing and darting movements were observed in *Channa punctatus* and *Oreochromis niloticus* exposed to higher concentrations of lithium chloride viz., 80mg/L to 150mg/L from 24h to 96h. The reaction and survival of aquatic animals depend on not only the biological state of the animals and physico-chemical characteristics of water, but also on kind, toxicity, type and time of exposure to the toxicant. Behavioural manifestations of acute toxicity of chromium in *Labeo rohita* was more or less similar to those reported in other fishes (Mukherjee 1988). Fishes may be attributed to the fact that metal-induced changes in physiology and survival of aquatic organisms under metallic stress are complicated because such changes differ from metal to metal, species to species and from one experimental condition to another. The exact causes of death due to heavy metal poisoning are multiple and depend mainly on time-concentration combinations. However, there is no clear-cut explanation on the exact mode of action of different metals causing the mortality in aquatic animals.

Oxygen consumption: The mean metabolic rates of the control and exposed fishes at the end of 24h, 48h, 72h and 96h along with the percent decrease from control are given (Table 3). It is clear from the results that the metabolic rate of *Channa punctatus* and *Oreochromis niloticus* exposed to lithium decreased from control with the exposure period 24h to 96h. The action of heavy metals on the respiratory function of fishes appears to be diversified. Alterations in the cellular components isa cause of depression in the respiratory activity of fishes exposed to acute metallic stress has been suggested (Pondey et al. 1963). Inhibition of the respiratory enzymes in fishes exposed to heavy metals was also reported (Lowry et al. 1951).

A perusal of the available information reveals that heavy metal-induced alterations in the respiratory function of fishes differ not only from metal to metal but also the sites of action. The decrease in the oxygen consumption of *Channa punctatus* and *Oreochromis niloticus* exposed to lithium indicates the onset of acute hypoxia under metallic stress. Further, the fact that the drop in metabolic rate of the fish as a protective measure to ensure that there is a low intake of the toxic substance also cannot be ruled out. Gills are vital respiratory and osmoregulatory organs and cellular damage induced by the metal might impair the respiratory function of the fish by reducing the respiratory surface area (Taylor et al. 1985). These findings suggest decreased respiratory surface area can also account for the drop in the metabolic rate of the fish.

Haematological studies: The present study reveals that the *Channa punctatus* and *Oreochromis niloticus* exposed to lithium exhibited a significant increase in their RBC, Hb, HCT, MCH, MCV, MCHC and WBC compared to control are given in Table 4 and Table 5. The reason for increased haematological values indicates macrocytic type of anaemia. The previous study shows that high level of RBC was recorded in *L. calcarifer* followed by *C. chanes*. The high erythrocyte number was associated with fast movement, predaceous nature and high activity (Rambhaskar & Srinvasa Rao 1986). The elevated RBC counts and Hb concentrations were recorded in lithium exposed *C. punctatus* and *O. niloticus*. This elevated level is responsible for the high metabolic demand. The increased level of RBC indicates oxygen demand in the tropical region to meet the higher oxygen requirement at high metabolic rates (Engel & Davis 1964). Hb value in the present study shows that 19.25±0.30 (96hr, *C. punctatus*) and 19.52 ± 0.32 (96hr, *O. niloticus)* respectively. RBC & Hb concentrations tend to increase with length and age of the fishes (Das 1965). Blaxhall & Daisley (1973), have reported the possibility of using HCT as a tool in the aquaculture and fishery management for checking the anaemic condition. HCT value in the present study was

within the range 35.33 ± 3.05 (96hr, *C. punctatus*) and 22.34 ± 1.53 (72hr, *O. niloticus*) respectively; fish HCT values were usually between 20% and35% and rarely attain greater than 50% (Clark et al. 1976). Besides, high leukocyte values depend on stress factors resulted in regulatory effects of toxic substances on the immune system. High RBC count perhaps lessens the requirement for a large number of WBC (Xiaoyun et al. 2009). From the results (Table 4 & 5) shows that the increased amount of MCV, MCH and MCHC observed in *C. punctatus* and *O. niloticus* indicates the microcytic anaemia. This study indicates that changes in haematological parameters in fish serves as an effective tool in the diagnosis of the extent of environmental pollution and also the abiotic fish diseases. Increased in total WBC count in the present study was a result of direct stimulation for its defence from diseases due to the presence of heavy metals. Increase in WBC count as in the present study was also reported by Murugesen & Haniffa (1985), in heavy metal treated fish blood, suggesting induction of some pathology and also might be due to the effect of metal toxicants on bone marrow. Leucocytosis has been considered to be an adaptation to meet stressful conditions by aquatic species.

Haematological parameters are very important parameters for the evaluation of fish physiological status under metabolic stress. From the results, (Table 4 & Table 5) clearly shows that the changes in blood indices and their peculiarities depend on the concentration of heavy metals and duration of exposure of fish to them. In the present study, the anaemia could be probably due to structural alterations of heme leading to disturbed haemoglobin synthesis and also the inhibitory effect of lithium on the enzyme system in the synthesis of haemoglobin cannot be ruled out as suggested in earlier studies (Vincent et al. 1996).

Biochemical studies: The carbohydrate, phospholipid, total protein, cholesterol, triglyceride and free fatty acid levels in liver, muscle and blood of control fish and exposed fish of *Channa punctatus* and *Oreochromis niloticus* to the 96hr concentration of Lithium are represented in Table 6. It is clear from the results that there is an appropriate decline in different biochemical constituents of the fish under lithium stress.

The ranges of biochemical parameters vary from species to species and can be influenced by many biotic and abiotic factors such as water, temperature, seasonal pattern, food age and sex of the fish (Jawad et al. 2004). In the present investigation increased level of biochemical profiles (Carbohydrate, Protein, Phospholipid, Triglyceride, Free fatty acid and Cholesterol) increased in the liver and muscle tissues compared to the blood sample in *C.Punctatus* and

Table 4: Haematological parameters of *Channa punctatus* on exposure to Lithium.

Parameters	Normal	24	48	72	96
RBC (10^6/mm³)	4.08 ± 0.49	8.82 ± 0.27	8.54 ± 0.21	9.10 ± 0.11	8.99 ± 0.24
Hb (g%)	10.78±0.54	14.62 ± 1.02	16.71 ± 1.18	18.93 ± 0.25	19.25 ± 0.30
WBC (10^3/mm³)	5.18±0.17	5.09 ± 0.09	5.56 ± 0.51	6.23 ± 0.66	7.28 ± 0.51
HCT (%)	19.2±1.66	26 ± 2	30.33 ± 3.05	32.67 ± 3.00	35.33 ± 3.05
MCV (fL)	168.66±0.98	183.28 ± 4.86	184.04 ± 1.85	189.57 ± 0.99	193.66 ± 5.48
MCH (pg)	46.3±1.97	66.03 ± 1.92	63.42 ± 4.11	70.28 ± 1.06	71.29 ± 0.86
MCHC (g%)	7.14±0.59	9.99 ± 0.10	11.2 ± 0.25	12.67 ± 0.49	14.83 ± 0.38

Values are mean ± SD, – or + indicate percent decrease or increase over control.

Table 5: Haematological parameters of *Oreochromis niloticus* on exposure to Lithium.

Parameters	Normal	24	48	72	96
RBC (10^6/mm³)	4.84±0.13	6.78 ± 0.22	7.98 ± 0.14	8.52 ± 0.35	8.39 ± 0.27
Hb (g%)	10.3±0.17	18.59 ± 0.54	18.29 ± 0.58	19.09 ± 0.10	19.52 ± 0.32
WBC (10^3/mm³)	6.13±0.25	6.49 ± 0.45	7.51 ± 0.30	7.68 ± 0.50	8.45 ± 0.05
HCT (%)	15.23±0.49	21.67 ± 1.53	19.67 ± 2.08	22.34 ± 1.53	21.00 ± 1.00
MCV (fL)	195.29±4.09	200.67 ± 0.48	210.43 ± 0.58	216.73 ± 2.34	222.34 ± 2.30
MCH (pg)	33.11±0.96	63.91 ± 2.18	68.7 ± 2.08	70.25 ± 0.98	76.11 ± 3.15
MCHC (g%)	19.10±2.03	21.78 ± 1.44	25.42 ± 0.93	27.33 ± 1.08	25.55 ± 3.10

Values are mean ± SD, – or + indicate percent decrease or increase over control.

O.Niloticus. An increased level of carbohydrate and protein level was recorded in *C.punctatus* and *O.niloticus*, this may be caused due to an increased depletion of liver glycogen (Ojolick et al. 1995). The increased protein concentration can be caused by structural liver alterations (Kavadias et al. 2004). Carbohydrate concentration increased significantly in Li exposed fish when compared to control group (Table 6). Alterations in the glucose level might be related to renal injury, liver damage, and lack of nutrition (Canli 1995). Increased level of total protein concentration in *Channa punctatus* and *Oreochromis niloticus* indicates liver damage, reduced absorption and protein loss. Increased level of triglyceride recorded (muscle>liver>blood) in both the species compared to control. Canli (1995), showed that serum triglyceride levels in *C.carpio* exposed to Ga increased considerably compared to the control. Triglyceride concentration is important to evaluate lipid metabolism and higher levels may occur with nephritic syndrome and glycogen storage impairment. Triglyceride functions primarily in providing cellular energy and can be used as an indicator of nutritional status. Increased level of cholesterol concentration in metal exposed fish compared to control fish. The concentration of cholesterol, an essential structural component of membranes and the precursor of all steroid hormones, may increase due to the liver and kidney failure causing the release of cholesterol into the blood. Elevation of phospholipid and free fatty acid

Table 6: Levels of biochemical parameters in blood, liver and tissue of *Channa punctatus* and *Oreochromis niloticus* on exposed to Lithium (mg/dL).

Parameters		Channa punctatus			Oreochromis niloticus		
		Blood	Liver	Tissue	Blood	Liver	Tissue
Total Protein	Normal	7.78 ± 0.55	7.35 ± 0.54	8.73 ± 0.55	9.59 ± 0.41	10.35 ± 0.36	11.32 ± 0.51
	Treated	13.52 ± 0.53	19.08 ± 0.51	20.70 ± 1.20	28.76 ± 0.81	27.73 ± 0.86	27.88 ± 1.43
Carbohydrate	Normal	66.81 ± 0.99	71.31 ± 2.58	74.24 ± 4.23	84.18 ± 1.74	89.05 ± 1.00	94.12 ± 5.20
	Treated	97.39 ± 3.10	125.88 ± 2.75	134.1 ± 6.76	142.17 ± 3.09	159.18 ± 6.43	153.93 ± 5.36
Phospholipids	Normal	3.07 ± 0.25	2.73 ± 0.21	2.03 ± 0.05	7.27 ± 0.47	8.10 ± 0.56	7.24 ± 0.60
	Treated	3.5 ± 0.36	4.13 ± 0.65	5.16 ± 1.10	9 ± 0.7	11.56 ± 0.58	12.2 ± 1.25
Free Fatty Acids	Normal	52.19 ± 0.93	51.57 ± 0.54	49.08 ± 0.92	62.76 ± 0.52	65.88 ± 0.77	68.75 ± 0.57
	Treated	49.05 ± 0.96	60.33 ± 0.66	61.35 ± 1.65	56.86 ± 1.74	64 ± 2.01	70.99 ± 1.05
Triglycerides	Normal	16.34 ± 1.46	18.69 ± 0.46	19.91 ± 0.13	27.39 ± 2.05	32.21 ± 1.59	33.80 ± 2.53
	Treated	30.54 ± 0.78	30.76 ± 1.07	31.64 ± 1.59	41.51 ±0.62	47.21 ±0.55	56.05 ± 4.73
Cholesterol	Normal	213.07 ± 3.52	229.76 ± 10.49	211.62 ± 9.44	182.66 ± 1.84	179.38 ± 1.44	189.10 ± 9.55
	Treated	154.96 ± 4.51	159.88 ± 10.10	167.31 ± 5.10	219.30 ± 5.99	222.18 ± 3.38	266.10 ± 37.38

Values are mean ± SD, – or + indicate percent decrease or increase over control.

Table 7: Levels of enzyme parameters in blood, liver and tissue of *Channa punctatus* and *Oreochromis niloticus* exposed to Lithium (IU/L).

Parameters		Channa punctatus			Oreochromis niloticus		
		Blood	Liver	Tissue	Blood	Liver	Tissue
SGPT	Normal	30.17 ± 1.01	29.57 ± 1.13	28.65 ± 1.00	28.67 ± 0.59	29.4 ± 0.4	30.33 ± 0.76
	Treated	29.93 ± 0.07	36.55 ± 5.64	21.09 ± 0.92	36.03 ± 0.38	48.66 ± 0.72	40.04 ± 1.24
SGOT	Normal	18.04 ± 0.91	19.11 ± 0.13	18.74 ± 0.86	15.46 ± 0.58	16.43 ± 1.11	16.12 ± 0.91
	Treated	11.86 ± 1.40	10.54 ± 1.02	10.12 ± 1.13	18.43 ± 1.04	21.85 ± 1.74	22 ± 1.69
ACP	Normal	31.21 ± 0.60	31.67 ± 0.67	30.67 ± 1.45	36.09 ± 0.55	34.50 ± 1.53	33.38 ± 0.62
	Treated	52.55 ± 1.05	54.9 ± 1.78	66.88 ± 0.95	45.45 ± 1.37	58.90 ± 1.01	53.46 ± 3.43
ALP	Normal	99.14 ± 1.00	106.14 ± 5.32	98.43 ± 1.44	113.13 ± 2.79	117.70 ± 5.01	106.74 ± 5.03
	Treated	145.16 ± 12.26	142.24 ± 12.35	148.73 ± 13.60	165.83 ± 6.84	155.75 ± 2.57	131.51 ± 3.02

Values are mean ± SD, – or + indicate percent decrease or increase over control; SGPT – Serum glutamate pyruvate transaminase; SGOT – Serum glutamate oxaloacetate transaminase; ALP – Alkaline phosphatase; ACP – Acid phosphatase

Table 8: Levels of biochemical parameters in blood, liver and tissue of *Channa punctatus* and *Oreochromis niloticus* exposed to lithium (mmol/L).

Parameters		Channa punctatus			Oreochromis niloticus		
		Blood	Liver	Tissue	Blood	Liver	Tissue
Na	Normal	74.77 ± 4.17	45.71 ± 2.13	22.07 ± 1.65	81.01 ± 1.89	56.66 ± 3.39	45.07 ± 2.74
	Treated	60.79 ± 1.45	110.23 ± 1.95	41.39 ± 2.17	94.78 ± 4.49	63.78 ± 1.52	103.01 ± 2.32
K	Normal	6.4 ± 0.48	5.63 ± 0.73	4.64 ± 0.47	2.46 ± 0.52	1.72 ± 0.56	0.74 ± 0.51
	Treated	8.86 ± 0.08	7.54 ± 0.62	6.73 ± 0.45	3.72 ± 0.24	3.28 ± 0.16	2.65 ± 0.42
Cl	Normal	92.28 ± 6.01	82.46 ± 2.50	64.47 ± 2.09	103.60 ± 3.38	94.64 ± 4.61	98.11 ± 1.80
	Treated	105.53 ± 2.08	80.79 ± 1.40	87.67 ± 1.40	103.01 ± 2.32	116.59 ± 5.29	117.58 ± 2.16

Values are mean ± SD, – or + indicate percent decrease or increase over control.

(96hr-both species) in the present study may be attributed to the prevention of tissue damages in the fish. Similarly, Swelium (2006), also reported an increased level of phospholipids in *Oreochromis niloticus* exposed to the pesticide. In the present study, the elevated level of phospholipid and free fatty acid shows that utilization of lipid for meeting the energy demand under the metal stress.

Transaminases like SGOT and SGPT play a significant role in protein and amino acid metabolism and they may release into the plasma following tissue damage and dysfunction. Increased level of SGOT and SGPT amount shows that damage of tissues and impairment of fish metabolism. Zikic et al. (2001), showed the increased level of AST & ALT in Cd-exposed fish *Carassius auratusgibeli*o; the author indicated that liberation of these transaminases into the circulation might occur due to damage of the liver, kidney, heart and other tissues in the state of stress influenced by metals. Acid phosphatases are enzymes concerned with the biosynthesis of fibrous proteins and mucopolysaccharides or they may serve as regulators of intracellular phosphatase concentration (Gutman 1959). They are also hydrolytic enzymes which play an active part in the dissolution of the body's dead cells; stimulation or inhibition of these enzymes will thus result in metabolic disturbances (Sanisa et al. 1982). In the present investigation Table 7 shows that the increased level of acid phosphatase level in all the tissues show in both *C. punctatus* and *O. niloticus* species. The elevated level in the acid phosphatase activity in the tissues of metal exposed fish indicates that, disruption of the lysosomal membrane, cytotoxic action and alteration in the membrane stability. Alkaline phosphatase exposed in treated fish compared to control (Table 7). In the previous study, increased ALP activity in the serum and gill in *Cyprinus carpio* exposed to Cu (Singh & Reddy, 1990). Increased level ALP observed in both (*C. punctatus* and *O. niloticus*) species compared to control fish. The elevated level of metal exposure causes structural changes in the fish.

Table 8, shows that alteration of ion levels occurred in Li-exposed fish when compared to the control group. Increased level in the order of *C. punctatus* (liver>blood>tissue) and *O. niloticus* (tissue>blood>liver) in sodium. Increased level of potassium in the order of *C. punctatus* (blood>liver>tissue) and *O.niloticus* (blood>liver>tissue). Increased level of chlorine in the order of *C. punctatus* (blood>tissue>liver) and *O. niloticus* (tissue>liver>blood). Cerqueira & Fernandas (2002) also showed that there was a significant decrease in plasma Na and Cl levels and an increase in K level in the serum of *Prochilodus scrofa* following acute Cu exposure, indicating gill tissue damage of fish. Alterations in ion levels reflected with an inhibition in the activity of bronchial Na, K and disruption of ionoregulatory systems. Due to exposure of lithium, it leads to failure of Na and Cl regulatory mechanisms. Electrolyte levels are one of the significant biomarkers in ecotoxicology because their levels can be altered sensitively due to reduced bronchial ion extrusion, reduced intestinal fluid absorption and changes in the morphological structure of cells.

SUMMARY

Blood glucose or carbohydrate is a sensitive tool and reliable indicator of pollutants causing environmental stress in fish. Lithium toxicity possibly associated with changes in liver carbohydrate metabolism which causes activation of liver glycogenolysis and glycolysis as well as increased levels of plasma glucose and lactate. Increased level of total protein, triglyceride, phospholipid, cholesterol (increased in lithium exposed *Channa punctatus* and decreased in lithium exposed *Oreochromis niloticus*) and free fatty acid in *C.Punctatus* and *O. niloticus* exposed to lithium. Lipids are an important fuel reserve of aquatic organisms during stress. The depletion in tissue proteins of *C. punctatus* and *O. niloticus* may be due to impaired protein synthesis under metallic stress or due to their utilization in the formation of mucoproteins, which are eliminated in the form of mucous. Further, direct or indirect

utilization of proteins and lipids for energy needs was also reported (Janardhana Reddy et al. 1998). Also, the utilization of proteins in cell repair and organization as causes of their depletion in the tissues cannot be ruled out. Cholesterol and phospholipids are generally considered to be structural or functional lipid being incorporated to a large extent in the membrane structure of the cell and subcellular organelles. Cholesterol concentrations in the serum of metal - exposed fish generally increased when compared to that of the control fish in *Channa punctatus*. The concentration of cholesterol, an essential structural component of membranes and the precursor of all steroid hormones, may increase due to the liver and kidney failure causing the release of cholesterol into the blood. Heavy metals are known to have hazardous effects on cell structure, especially on the membranes. Therefore, increases in cholesterol may be a good indication of environmental stress. Triglyceride concentration is important to evaluate lipid metabolism and higher levels may occur with nephritic syndrome and glycogen storage impairment. Triglyceride functions primarily in providing cellular energy and can be used as an indicator of nutritional status. Enzymes are sensitive tools to analyse the environmental stress indicator. Transaminases like SGOT and SGPT play a significant role in protein and amino acid metabolism and they may release into the plasma following tissue damage and dysfunction. Alkaline phosphatase is a polyfunctional enzyme that acts as transphosphorylase at alkaline pH and plays an important role in the mineralisation of the skeleton of aquatic animals and in membrane transport activities. ACP is a lysosomal enzyme that hydrolysis organic phosphates at an acid pH. Changes in ALP and ACP activity also could be as a result of physiological and functional alterations in metal exposed fish. Lithium assumed as an ion regulatory toxicant. Water ions K and Na play a protective role against Li. Serum ion levels are one of the significant biomarkers in eco-toxicology because their levels can be altered sensitively due to reduced bronchial ion extrusion, reduced intestinal fluid absorption, and changes in the morphological structure of cells. The present study showed that lithium-induced alterations at the biochemical level, more pronounced changes occurring at the end of 96h and thus it is time-dependent.

CONCLUSION

Acute exposure of lithium proved to be highly toxic to *Channa punctatus* and *Oreochromis niloticus* and induced cumulative deleterious effects at various vital functional sites like metabolic rate, haematological indices and biochemical profiles. Though significant changes are observed both at the end of 24h and 96h exposure periods, these changes are more pronounced at the end of 96h suggestive of time-dependent toxicity. The metal-induced decrease in the total protein content could affect the enzyme-mediated bio-defence mechanisms of the fish, which pose a serious threat to human beings by secondary poisoning through the food chain. Haematological and biochemical parameters are valuable tools for monitoring fish health, confirming maturation and monitoring any changes in the quality of water and related soil. The ranges of normal values of the key biochemical parameters are still undefined for different species in different aquaculture conditions. The results of this present investigation indicate the knowledge about lithium toxicity in aquatic ecosystems and also show that haematological and biochemical profiles are sensitive tools to analyse the toxicity studies and significant to show the awareness of the pollution in pisciculture and aquatic environments.

REFERENCES

Abbasi, S.S., Kunahmed, T., Nipaney, P. C. and Soni, R. 1995. Influence of the acidity on chromium toxicity- a study with the teleost, *Nuria danricus* as model.Poll. Res., 14(3): 317-323.

Ambrose, T., Cyril Arun Kumar, L., Vincent, S. and Roselyn Lambert 1994. Biochemical responses of *Cyprinus carpiocommunis* to toxicity of tanneryeffluent. J. Ecobiol. 6(3): 213-216.

APHA, AWWA and WPCP 1998. Standard methods for the examination of Water and Wastewater. 20th ed.American Public Health Association, Washington,DC.

Ashraj, W 2005. Accumulation of heavy metals in kidney and heart tissues of *Epinephelusmicrodon* fish from the Arabian Gulf. Environ. Monit. Assess., 101 (1-3): 311-316.

Bergmeyer, H.U., Horder, M. and Rej, R. 1985. International federation of clinical chemistry (IFCC) scientific committee. J Clin Chem Clin Biochem 24: 481-495.

Blaxhall, P.C. and Daisley, K.W. 1973. Routine haematological methods for use with fish blood. J. fish biolo 5:771-781.

Canli, M. 1995. Effects of mercury, chromium and nickel on some blood parameters in the carp *Cyprinus carpio*. Turkish journal of zoology 19: 305-311.

Cerqueira, C.C.C. and Fernandes, M.N. 2002. Gill tissue recovery after copper exposure and blood parameters responses in the tropical fish *Prochilodus scrofa*. Ecotoxicol Environ saf 52: 83-91.

Clark, S., Whitemore, D.H. and McMahon, R.F. 1976. Consideration of blood parameters of large mouth bass, *Micropterus salmoides*, J.Fish. Biol 14:147-154.

Congleton, J.L. and La Voie, W.J. 2001. Comparison of blood chemistry values of samples collected from juvenile *Chinook* salmon by three methods. J Aquat Health 13: 168-172.

Davidson, I., Henry, J.B. and Todd-Sanford 1969. Clinical diagnosis by laboratory methods, edn, 14, p1165.

Das, B.C. 1965. Age related trends in the blood chemistry and haematology of the Indian carp *Catlacatla*. Geronotologia 10:47-64.

Donald, H. and Bonford Hutchinson, 1963. Clinical methods 14th edition. London. Pp145.

Drabkins , 2010. Practical haematology, 18:90.

Engel, D.M. and Davis, E.M. 1964. Relationship between activity and blood composition in certain marine teleosts, *copei* 3:586-587.

Finney, D.J. 1953. Probit analysis 2nd edition. CambridgeUniversity press, Cambridge England.

Finney, D.J. 1971. Probit analysis 2nd edition. Cambridge University Press, Cambridge England.

Fitch, D.D. 1975. Oxygen consumption in the Prosobranch snail, Viviparous contectoides (*Mollusca:Gastropoda*) - Effects of weight and activity. Comp. Biochem. Physio.l,51A,815-820.

Folch, J., Lees, M. and Sloane-Stanley, G.H. 1957. A simple method for the isolation and purification of total lipids from animal tissues. J.Biol. Chem, 226, 497 – 509.

Foster, L.B. and Dunn, R.T. 1973. Stable reagents for determination of serum of serum triglycerides by colorimetric Hantzsch condensation method. Clin. Chem. 19: 338 – 340.

Gutmann, A.B. 1959. Serum alkaline phosphatase activity in diseases of skeletal and hepatobiliary system. American Journal of medicine. 27:pp875.

Heath, A.G. 1987. Water pollution and fish physiology. CRC, Boca, Raton, FL, USA, pp245.

Hron, W.T. and Menahan, L.A. 1981. A sensitive method for the determination of free fatty acids in plasma. J. Lipid Res. 22: 371 – 381.

Janardhana Reddy, S., Kalarani, V., Tharakanadha, B., Reddy, D.C. and Ramamurthi, R. 1998. Changes in energy metabolism of the fish, *Labeo rohita* in relation to prolonged lead exposure and recovery. J.Ecotoxicol. Environ. Monit.,8 (1): 43-53.

Jawad, L.A., Al-Mukhtal, M.A. and Ahmed, H.K. 2004. The relationship between haematocrit and some biological parameters of the Indian shed, *Tenualosailisha* (family Clupidae) Animbiodivers, conservation 27:478-483.

Kavadias, S., Castritsi-Catharibs, J. and Dessyprie, A. 2004. Annual cycles of growth rate, feeding rate, food conversion, plasma glucose and plasma lipids in the population of *Europian seabass* (*Dicentrarchuslabrax*) farmed J.Appl.Ichthyol 19:29-34.

King, E.J and Armstrong, A.R. 1934. Cannada medical association journal. 31, 376.

Kszos, L.A. Beauchamp, J.J. and Stewer, A.J. 2003. Toxicity of lithium to three freshwater organisms and the antagonistic effect of sodium ecotoxicol 12: 427-437.

Lenntech, 2007. Lithium and water. Reaction mechanisms, environmental impact and health effects.

Lowry, O.H., Rosebrough, N.J., Lewis Farr, A. and Randall, R. 1951. Protein measurement with Folin Phenol Reagent. J. Biol. Chem.193, 265-275.

Mukherjee, K.L. 1988. Medical Laboratory Technology. A procedure manual for routine diagnostics tests, Vol I., Tata-McGraw- Hill, New Delhi, pp. 48.

Murugesen, A.G. and Haniffa, M.A. 1985. Effect of textile mill effluent on haematological changes of the obligatory air breathing fish *Anabas Testudineus*. Proc. Nat. symp. Asses. Env. Pollut. Pp121-128.

Ojolick, E.J. Cusack, R. Benfey, T.J. and Kerr, S.R. 1995. Survival and growth of all female diploid and triploid *Claris macrocephalus*. Fish genetics biotro special pub 52:79-86.

O'Neil, M.D. Wesp, H.M. Mensinger, A.F. and Hanlon, R.T. 1998. Initial baseline blood chemistry of the oyster toadfish, *Opsanus tau*. Biol Bull 195: 228-229.

Pondey, S. V., Khan, A.P. and Subramanyam, T.A.V. 1963. Micro determination of lipids and serum fatty acids. Analyst. Biochem., 6(5): 120-125.

Rambhaskar, B. and Srinivasa Rao, K. 1986. Comparative haematology of ten species of marine fish from Visakhapatnam coast. J fish boil 30:59-66.

Sanisa, P.K., Bedi, R. and Soci, C.I. 1982. Effects of vegetable oil factory effluent on the levels of phosphatises and dehydrogenases in the liver and kidney of the freshwater teleost, *Channa punctatus* (Bloch). Environmental Pollution Sci., 4(28): 245-253.

Sastry, K.V. and Sunitha, K. 1984. Chronic toxic effects of chromium in *Channa punctatus*: Biochemical studies. J. Environ. Biol.,5(1): 53-56.

Scrosati, B. and Garche, J. 2010. Lithium batteries: status, prospects and future. J Power Sources 195; 2419-2430.

Schalm, O.W., Jain, N.C. and Carrol, E.J. 1975. Veterinary haematology, 3rd ed., Lea and Febiger, Philadelphia.

Singh, H.S. and Reddy, T.V. 1990. Effect of copper sulfate on haematology, blood chemistry, and hepatosomatic index of an Indian catfish, *Heteropneustes fossillis* (Bloch), and its recovery. Eco-toxicol environ saf 20:30-35.

Smithberg, M. and Dixit, P.K. 1982. Teratogenic effects of lithium in mice Teratology 26: 239- 246.

Sornaraj, R., Baskaran, P. and Thanalakshmi, S. 1995. Effects of heavy metals on some physiological responses of air breathing fish, *Channa punctatus*(Bloch). Environmental Ecology 13(1):202-207.

Swelium, M.A. 2006. Effect of sub-lethal toxicity of some pesticides on growth parameters, haematological properties and total production of *Nile tilapia* and water quality of ponds. Aquacult. Rese., 37: 1079-1089.

Taylor, D. Maddock, B.G. and Mance, G. 1985. The acute toxicity of nine "grey-list' metals (Arsenic, Boron, Chromium, Copper, Lead, Nickel, Tin, Vanadium and Zinc) to two marine fish species, *Limandalimandaand Chelonlabrosus*. Aquatic. Toxicol.7,136-144.

Tenniswood, M., Bird , C.E. and Clark A.T. 1976. Canadian journal of biochemistry., 54: p350.

Tietz, N.W. and Logan, N.M 1987. Fundamentals of clinical chemistry. WB Saunders, Philadelphia, PA, USA.

Vincent, S., Ambrose, T., Cyril Arun Kumar, L. and Selvanayagan, M. 1996. Heavy metal cadmium influenced anaemia in *Catlacatla*. J. Environ. Biol.,17(1): 81-84.

Vutukuru, Srinivas, S. and Balaparmeswara, Rao M. 2000. Impact of hexavalent chromium on survival of the frewshwater fish, *Sarotherodonmossambicus*. J.Aqua. Biol., Vol. 15 (1 and 2): 71-73.

Vutukuru, S.S. 2003. Chromium induced alterations in some biochemical profiles of the Indian major carp, *Labeorohita* (Hamilton). Bull. Environ. Contam.Toxicol. 70, 118-123.

Winkler, L.W. 1888. Die Bestimmung des in Wasser gelosten Sauerstoffen Berichte der Deutschen Chemischen Gesellschaft. 21: 2843 – 2855.

Xiaoyun, Z., Mingyun, L., Khalid, A. and Weinmin, W. 2009. Comparative of haematology and serum biochemistry of cultured and wild *Dojoloach Misgurnusanguilicadatus*. Fish physiolbiochem 35:435-441.

Zak, B. and Ressler, N. 1955. Methodology in determination of cholesterol: A review. American Journal of Clinical Pathology, 25(4_ts): 433-446.

Zikic, R.V. Stajn, S. Pavlovic, Z. Ognjanovic, B.I. and Saicic, Z.S. 2001. Activities of superoxide dismutase and catalase in erythrocyte and plasma transaminases of *goldfish*, exposed to cadmium. Physiol res 50:105-111.

Nature Environment and Pollution Technology
An International Quarterly Scientific Journal

p-ISSN: 0972-6268
(Print copies up to 2016)
e-ISSN: 2395-3454

Vol. 19 | No. 2 | pp. 687-694 | 2020

Original Research Paper

https://doi.org/10.46488/NEPT.2020.v19i02.023

Open Access Journal

Effective Utilization of Fly Ash for Vermicompost Production by Employing *Eisenia fetida*

Selvakumar Muniraj*, Logeswari Ravi, Harisankar Ganesh**, Murugavel Sethuraman* and Vasanthy Muthunarayanan*†**

*Water and Solid Waste Processing Lab, Department of Environmental Biotechnology, School of Environmental Sciences, Bharathidasan University, Tiruchirappalli-620024, Tamilnadu, India

**Department of Biotechnology, Sri Ganesh College of Arts and Science, Ammapet, Salem-636014, Tamilnadu, India

†Corresponding author: Vasanthy Muthunarayanan; vasanthy@bdu.ac.in

Nat. Env. & Poll. Tech.
Website: www.neptjournal.com

Received: 16-08-2019
Accepted: 18-09-2019

Key Words:
Fly ash; *Eisenia fetida*; Enzyme activity; Antioxidant assay

ABSTRACT

Thermal Power plants cater the energy needs in many of the countries across the globe, but they indeed pose health hazard to the atmosphere by the release of pollutants such as fly ash, particulate matter, dust, smoke-laden with gaseous pollutants etc., As it is mandatory to meet the energy demand of the increasing population, it is also important to manage the waste produced as the result of these industries. Though there exist various methodologies to manage the waste, vermicomposting is one of the cost-effective and simple techniques available to manage many of the solid waste emanated from different industries. Hence, this study was made to manage the fly ash waste by vermicomposting technique after the addition of carbon substrate namely, the cow dung in different rations such as 1:1, 1:4, 4:1, 2:3 and 3:2. The organism selected for the research was *Eisenia fetida*. The number of days for the process was about 60 days. The physico-chemical changes were monitored throughout the study period at regular intervals. The bacterial strains were isolated from the end product, namely the vermicast or vermicompost. Their enzyme activity was also checked and the end product was characterized using FTIR and XRD. Of the different proportions, 1:4 was found to be a suitable proportion in terms of the parameters checked.

INTRODUCTION

Excessive growth of population leads to rapid urbanization and industrialization which increases the demand for electricity throughout the world. In most of the developing countries, power has been observed as an important tool of growth (Usmani et al. 2017). The power generating facilities results in the production of fly-ash, which contains 0.01 to 100 mm particles mimicking glass (Davison et al. 1974). In fly ash trace amount of oxides, hydroxides, carbonates, silicates, and sulphates of calcium, iron, aluminium, and other metals are present (Adriano et al. 1980). During the 20th century, the production of fly ash in India was about 95 million tons and it has reached up to 112 million tons during 2005-2006. In 2009-2010 fly ash production of the country reached 180 million tons (Chattopadhyay & Bhattacharya 2010). For the year of 2011-12, the electricity generated was about 985 terawatt hours (TWh) (SEPSI 2000). During the electricity generation, combustion of powdered coal leads to the production of fly ash, one of the most abundant waste materials. As per MOEF (2007) at the end of the 11th 5-year plan, about 150-170 million tons of fly ash was expected to be generated per year.

Fly ash is reported to be present in the atmosphere for a reasonable time and is reported to cause varied health effects (T.E.R.I. 1998). It poses a threat to the environment too. It blocks natural drainage and reduces the pH, potability of water and makes it turbid. Fly ash further affects the process of photosynthesis and damages the plants too (Gupta et al. 2005). In the coming years, the disposal of fly ash would be a challenging task. Though the accepted disposal methods include dumping the fly ash in settling ponds, stockpiling, and in landfills, such disposal methodologies have their limitations too. The disposed fly ash in landfills contaminates the soil, groundwater and surface water (Pandey et al. 2009).

In India, the fly ash generated is being used massively for the construction purposes, which includes the production of bricks and cement and it is also being used for the formation of embankments too. Further, it is utilised for the land reclamation by filling the low-lying areas and for the reclamation of wasteland too. It is also being utilised for mine filling too.

Solid waste management is a problem which needs immediate attention as far as Indian cities are concerned. (Karthika et al. 2014). It was reported that vermicomposting would be a feasible, low-cost and an eco-friendly technique

for organic waste management (Logsdson 1994). It has been demonstrated by several workers regarding the ability of the earthworms to decompose the organic wastes including animal wastes, crop residues, sewage sludge and industrial refuse (Edwards 1998). Some of the earthworm species are identified as heavy metal tolerant species. They were found to detoxify the municipal solid waste including industrial sludge through the process of vermicomposting (Saxena et al. 1998). Vermicomposting is capable of handling fly ash from very low to high quantities. It is a process with significant advantages such as low-cost and comparatively simple. Hence it could be practised in both small scale and large scale too. The vermicast was found to contribute many nutrients to the soil facilitating the plant growth (Abbasi & Ramasamy 1999, Ismail 1997).

Based on the review made regarding the fly ash disposal, we attempted in this study to convert the fly ash as organic fertilizer by vermicomposting which benefits the environment. The present study was made to estimate various physicochemical parameters from the initial till final vermicompost (0^{th} day to 60^{th} day) samples. Further, the vermicompost was characterised using FTIR and XRD and the antioxidant enzymes of the earthworm were determined. The study also includes the isolation of the bacterial strains and to perform the enzyme assays for amylase, protease, lipase and cellulase.

MATERIALS AND METHODS

Waste collection: The fly ash waste was obtained from Neyveli, Tamil Nadu, India. The carbon substrate namely cow dung was obtained near Bharathidasan University, Tiruchirappalli from a farm. The proportion of waste subjected to vermicomposting is listed in the Table1.

Physicochemical characterization of the vermicompost: The vermicompost samples from different ratios such as 1:1, 1:4, 4:1, 3:2 and 2:3 were drawn on initial, 15^{th}, 30^{th}, 45^{th} and 60^{th} day. The physico-chemical characters such as pH, electrical conductivity (EC), total organic carbon (TOC), total organic matter (TOM), total phosphorus (TP) and total potassium (TK) of the samples were analysed (Tandon 2009).

Microbial study: Serial dilutions of 1 g of the sample up to 10^{-3} to 10^{-7} dilution were made and plated on nutrient agar to enumerate the bacterial colonies (Yasir et al. 2009). Further from the isolated bacterial colonies, genomic DNA was isolated using DNA extraction mini kit (Real Biotech Corporation, Chennai). The universal primers (27 F 5′-AGAGTTTGATCMTGGC TCAG-3′ and 1492R 5′-TAC GGYTACCTTGTTAC GACTT-3′) were used for PCR amplification (Vivas et al. 2009).

Enzyme assay: The activity of SOD refers to measure the tendency to inhibit the pyrogallol oxidation in an alkaline environment. The method utilized was of Giannopolitis & Ries (1977) with slight modification. The catalase function was estimated as per Song et al. (2009). The activity of GPX was assayed as per Gunzler & Flohe (1985). The activity of GST was assayed according to the method of Saint Denis et al. (1998). The quantification of protein was done as per Bradford (1976).

Fourier transform infrared (FTIR): About 10 mg of dried end sample along with 500 mg of (KBr) was pelletized for 5 min with a hydraulic press and the resultant spectrum was recorded employing PerkinElmer Spectrum Version 10.03.09 (Zainab et al. 2009).

RESULTS AND DISCUSSION

Physico-chemical characteristics of fly ash waste: The vermicompost was prepared from the mixture containing cow dung, different quantities of fly ash waste, along with the earthworm population. The vermicompost was analysed for the parameters such as pH, EC, alkalinity, TOC, TOM, phosphorous and potassium. The values are presented in Fig. 1.

In the current scenario, waste management is a prime necessity. Agricultural soils lack nutrients due to the increased usage on fertilisers, pesticides thereby losing the native organisms and fertility. On the other hand, various nutritive wastes are improperly disposed and they are wasted. It is reported by (Bhide et al. 1994) that about 700 million tons of organic wastes are either landfilled or burnt. Instead, such wastes could be effectively managed by vermicomposting in-

Table 1: Waste subjected to vermicomposting.

S.No	Samples	Ratio of the sample	Wt. of the sample (g)
1	Fly Ash + Cow Dung	1:1	250 + 250 (500g)
2	Fly Ash + Cow Dung	1:4	100 + 400 (500g)
3	Fly Ash + Cow Dung	4 :1	400 + 100 (500g)
4	Fly Ash + Cow Dung	2:3	200 + 300 (500g)
5	Fly Ash + Cow Dung	3:2	300 + 200 (500g)

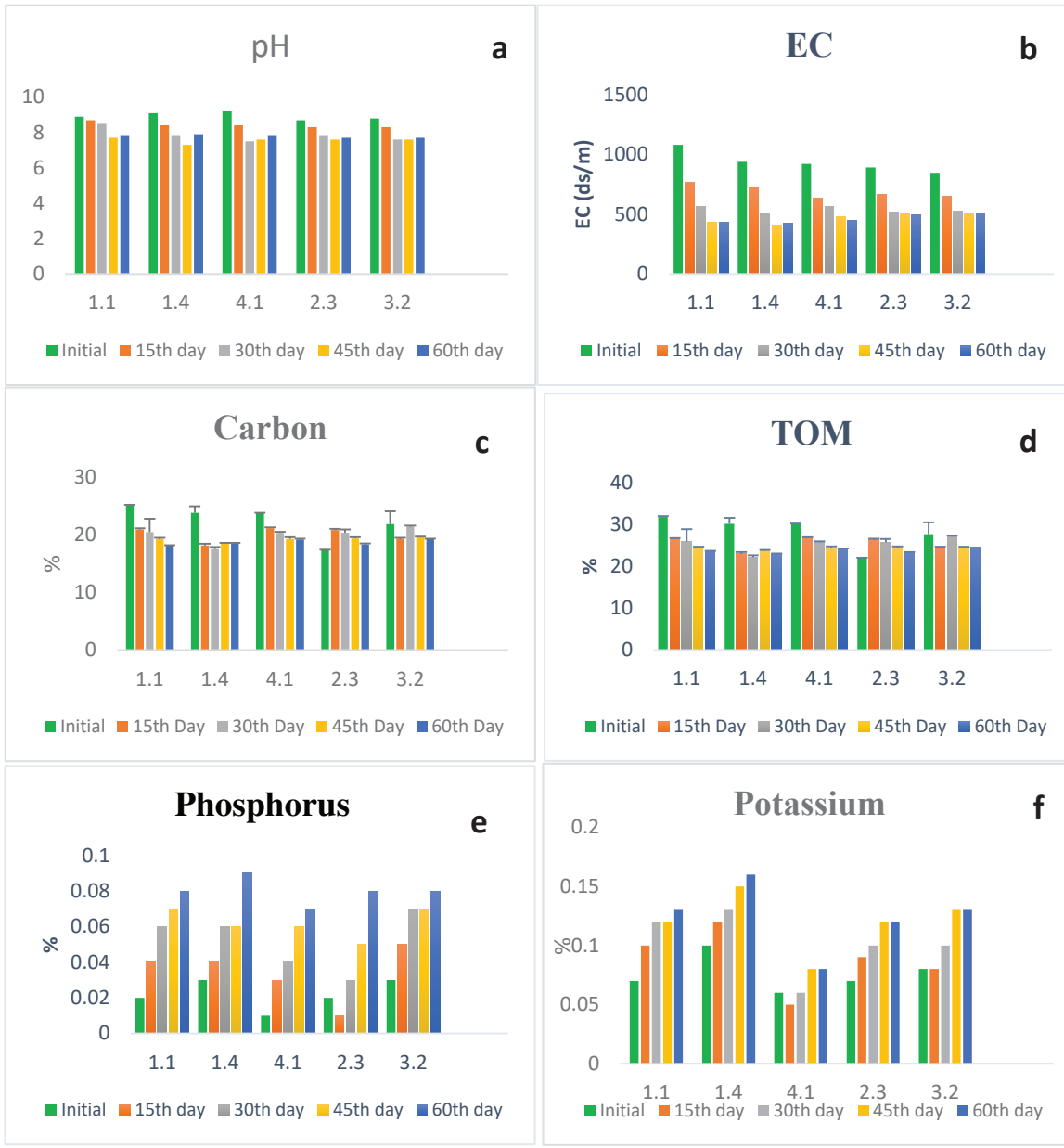

Fig. 1: (a–f) Physico-chemical properties fly ash waste vermicompost.

volving both earthworms and microbes efficiently. However, composting and vermicomposting differs significantly due to the pronounced activity of the earthworms (Gandhi et al. 1997). Hence this work includes the management of fly ash by vermicomposting. The entire process of vermicomposting of ash waste was carried out with the addition of cow dung and earthworm. The process was performed for 60 days. During the process, the variations in the physicochemical parameters were observed.

pH is an important parameter which is used to find the suitability of the vermicompost as manure. Hogg et al. (2002) have reported that the pH of about 6.0-8.5 would be suitable for promoting plant growth in most of the soils. Following the experiments, it was clear that the pH was reduced compared to the initial value, which may be due to the fulvic and humic acids produced during the vermicomposting process. Similar results were reported by Atiyeh et al. (2002). The EC values have decreased significantly in final vermicompost as follows

in different ratios of wastes: in 1:1 ratio, the reduction was by 60%, in 1:4 by 55%, in 4:1 by 51%, in 2:3 ratio it was by 44% and in 3:2 ratio the reduction was about 40.6%. The decrease in EC could be attributed to the volatilisation of ammonia accompanied by the precipitation of certain salts in the dissolved state produced including ammonium salts in the final product (Singh et al. 2016). Lim et al. (2012) have noticed a remarkable decrease in the electrical conductivity of vermicompost produced from the sludge of the beverage industry.

During the decomposition of the waste by earthworms, the total organic carbon undergoes a reduction as per Pattnaik & Reddy (2010). Similar result was observed in this study during the decomposition of fly ash too. In this study, Fig. 1c shows that the TOC has highly reduced during the vermicomposting, the percentage of reductions in TOC was around 5-23.5 in all the treatments. The reduction was higher in the ratio 1:4, which was about 26%. Such loss of carbon in the form of carbon dioxide results in an increase in the nitrogen production (Crawford 1983) which could be attributed to the earthworm and microbial respiration. This study too showed a reduction of 26% in 1:4 ratio vermicomposting, which may be attributed to the presence of consortia of microbes Fig. 1d.

During the vermicomposting process, the total phosphorus content in the feed mixture got significantly increased. Data showed in Fig. 1e revealed that the percentage of total phosphorus got increased by 15-18% in all the treatments. The increase was higher in 1:4 (19 %) vermicompost for fly ash waste. The increase in the total phosphorus may be due to the presence and function of the earthworms and phosphate solubilizing microbes during the processing of the wastes which includes the mineralization of phosphorus (Ravindran et al. 2008). Similar report was reported by Satchell & Martin (1984). They stated that both earthworms and microbes could attribute the increase in total phosphorus. Similar trend has been reported earlier by Rajesh Banu et al. (2008). Along with an increase in the phosphorus content, a mild increase in the potassium was also noticed (08-13%) in all the treatments. The increase was higher in 1:4 (16%) vermicompost for fly ash waste (Fig. 1f). The increase in potassium is normally attributed to the acid-producing gut microbes of the earthworm as per Suthar (2006). However, Kaushik & Garg (2004) has interpreted that the increase in potassium may be due to the draining of water from the feed mixture. As a result of vermicomposting MSW, Kaviraj & Sharma (2003) reported an increase (10%) of total potassium by *Eisenia fetida* and by *Lampito mauritii* (5%) and it was attributed to the presence of microflora.

Isolation of genomic DNA and 16s rRNA: The isolated bacterial strains were subjected to genomic DNA isolation and PCR and the amplification results are shown in Figs. 2a and b.

Bacterial enzyme activity: The isolated bacterial strains were subjected to enzyme activity such as protease, amylase, cellulase and lipase and the results are as shown in Fig. 3.

Enzyme assay: The medium used for the enzyme assay includes starch agar medium, skim milk agar medium, LB tributyrene and Czapek mineral salt agar for amylase, protease, lipase and cellulose respectively. The plates were observed for the zone of clearance called halo. The appearance of clear halos around the bacterial strains confirmed

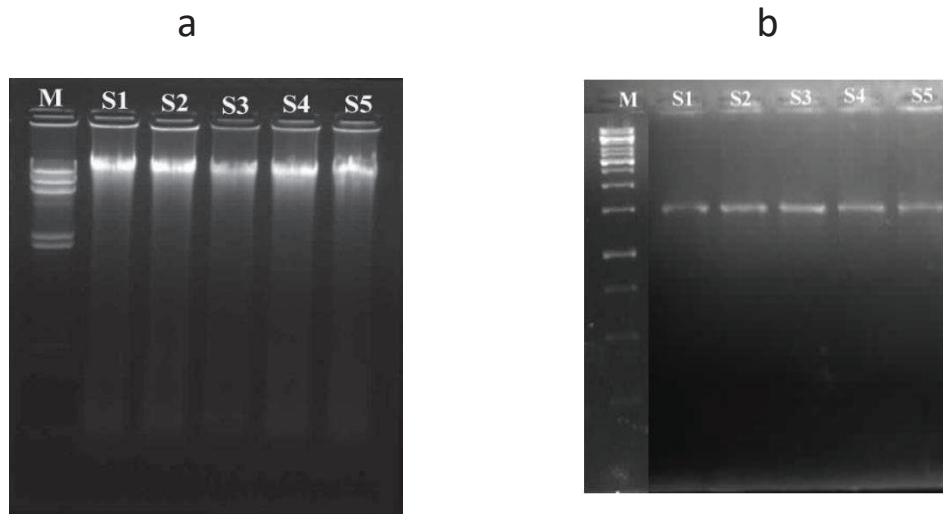

Fig. 2: a. Genomic DNA and b. PCR profile.

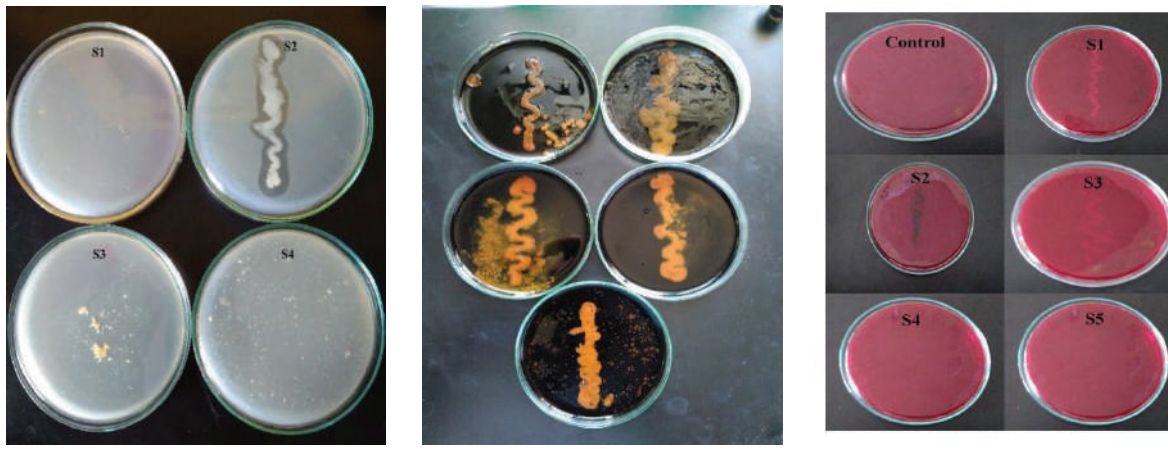

Fig. 3: Isolation of a- Protease, b- Amylase and c- Cellulase producing bacteria from fly ash vermicompost.

Table 2: Enzyme assay.

Enzymes	Strain 1	Strain 2	Strain 3	Strain 4	Strain 5
Amylase	+	+	+	+	+
Cellulase	+	+	+	-	-
Lipase	-	-	-	-	-
Protease	-	+	-	-	-

the respective enzyme production of the strains (Figs. 3 a, b, c and Table 2).

Antioxidative assay: The antioxidative assays such as Glutathione Peroxidase (GPx), Glutathione S-Transferase (GST), Super Oxide Dismutase (SOD) and Catalase (CAT) were performed for the earthworm samples. The results are represented in Fig. 4.

The biochemical responses of *E. fetida* during vermicomposting of the waste containing fly ash and butte sheet are shown in Fig. 4. There was an increase noticed in CAT and SOD activities and a reduction was noticed in the GST after 60 days. No significant change was noticed for GPx. However, oxidative stress was noticed in the earthworm which may be due to the continuous consumption of fly ash resulting in higher ROS production along with the subduing of the natural antioxidant enzymes (Nel et al. 2006). The authors have reported that during such process, subcellular injuries (protein denaturation, membrane damage, DNA damage, etc.) may occur. But the enzymes were reported to protect cells against the effects of ROS (Sharma et al. 2012). However, increased SOD and CAT activity may be related to the toxicity of fly ash.

Reports exist to prove that SOD catalyses the superoxide anion dismutation and the cells are protected by the elimination of H_2O_2 due to the presence of Catalase (Saint-Denis et al. 1998). Similarly, the reduction in CAT and SOD activity might be attributed to the SOD inactivation by singlet oxygen, hydrogen peroxide and peroxyl radicals (Fatima et al. 2007, Sandrini et al. 2008). Similarly, reduction in SOD and CAT was reported by Fatima et al. (2007) in the ASDI-exposed group representing a common cascade of events and Ribera et al. (2001) reported CAT reduction in the earthworm (*E. fetida*) exposed to carbaryl, an insecticide.

The hypothesis framed is that the fly ash degradation has posed stress to the earthworms thereby damaging the cells and its DNA. Similarly, the variation noticed in the enzyme activities were in accordance with the reports of Honda et al. (2000).

FTIR analysis for vermicompost: The vermicompost prepared were subjected to FTIR analysis and the results are shown in Fig. 5.

FTIR analysis provides the details about the functional groups present which thereby informs us of the degree of waste stabilization (Ravindran et al. 2008). FTIR spectra of the

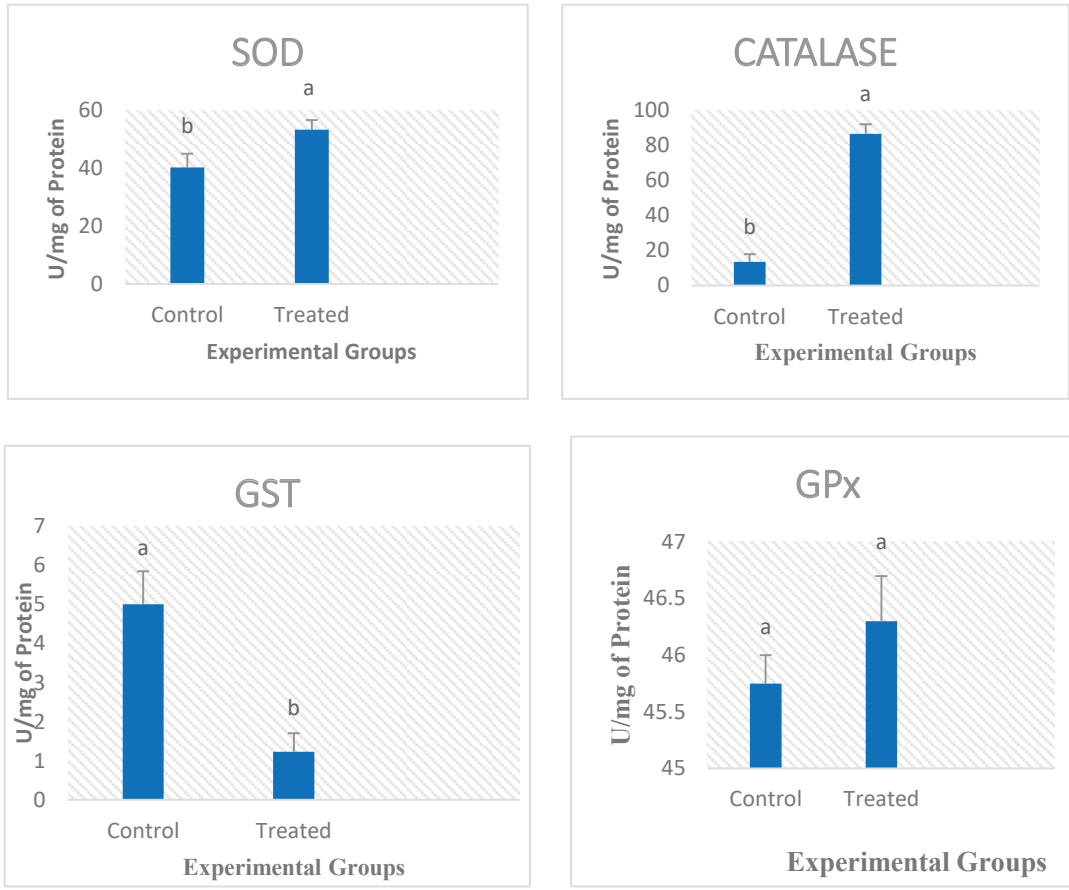

Fig. 4: Biochemical responses SOD, CAT, GST and GPx activity of *Eisenia fetida* utilized for vermicomposting of Fly ash waste. Values were expressed as mean ± SD (N=6). Bar with different alphabets are significantly different from each other and with same alphabets have insignificant changes (P<0.05).

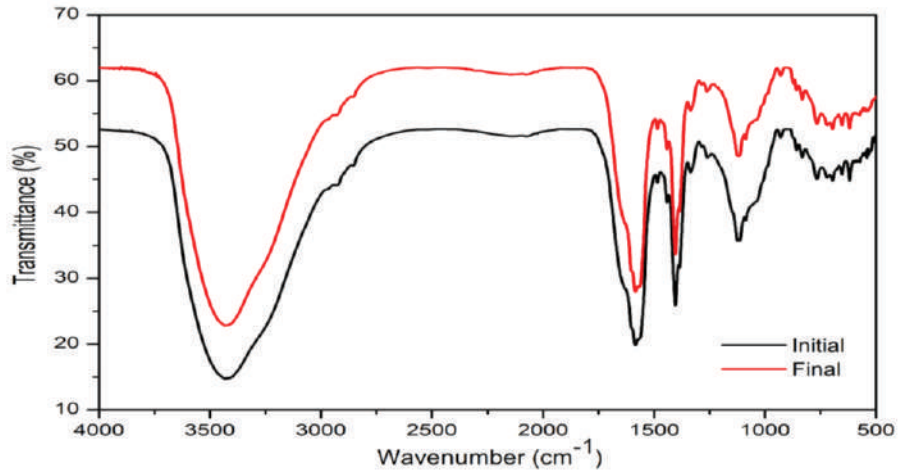

Fig. 5: FTIR pattern of the initial and final vermicompost.

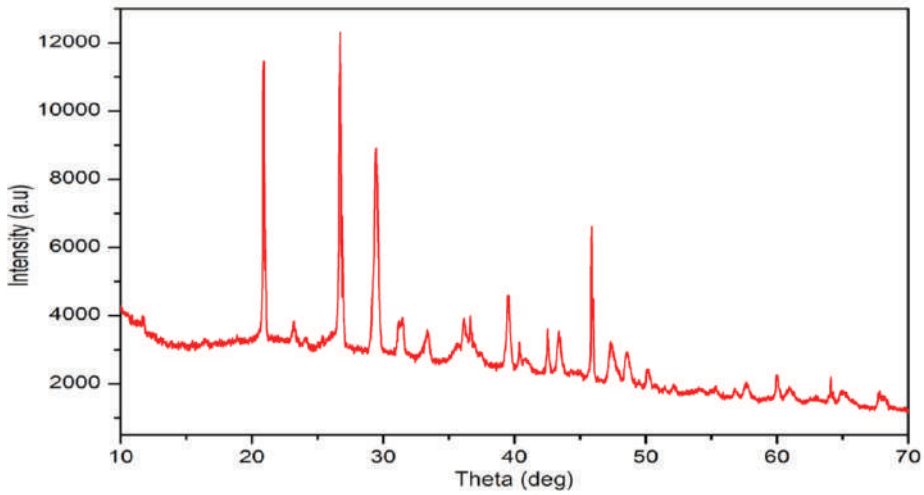

Fig. 6: XRD pattern of the vermicompost.

initial and final stage of ash waste vermicompost samples are shown in Fig. 5. By comparing the initial and final stage there is a strong hydrogen bond due to -OH stretch was observed at 3431.78 cm^{-1}. The band at 1123.67 cm^{-1} and 1117.69 cm^{-1} absorbed for lignin were also observed. While comparing the initial and final stage of vermicompost produced there is a slight reduction observed in the previously discussed band. This proves the partial mineralization of cellulosic material.

Hence the result confirms the reduction of aromatic structure, polypeptides and polysaccharides in the vermicompost prepared using ash waste.

X-ray diffraction analysis: The vermicompost prepared was subjected to XRD analysis and the results are shown in Fig. 6.

The crystallographic nature of the vermicompost prepared was studied using X-Ray Diffractometer (Mohan et al. 2009), Fig. 6. The XRD results indicate that the Quartz peak at 60.9 θ, Mullite peak at 40 θ and Magnetite peak at 31 θ present in the fly ash waste.

CONCLUSION

The waste selected for the study namely fly ash was degraded when it was subjected for vermicomposting along with cow dung in different ratios. The EC, TOM, TOC content has decreased when compared with the initial values. The amount of phosphorus and potassium has increased in the final vermicompost, 1:4 (fly ash + cow dung). Hence, this study confirms the possibility of converting fly ash waste into manure utilizing earthworms and microorganisms.

The role of bacterial species is also highlighted in terms of their enzyme activity and the Genomic DNA helps to identify the bacterial community in the vermicompost which could be utilized for further research. Also, the FTIR results show that the reduction of both aliphatic and aromatic structures in the vermicompost which is associated with extensive organic matter mineralization and from the XRD analysis, Quartz, Mullite, Magnetite waste types of fly ash was identified. It is also understood as in the stress environment, reactive oxygen species (ROS) get potentially increased which could result in changes in the antioxidant enzymes like Catalyses (CAT), Superoxide dismutase (SOD), Glutathione peroxide (GPX) and Glutathione S transferase (GST). The increase and decreased level of ROS can produce oxidative damage to macromolecules such as proteins and nucleic acid due to the stress produced by the presence of foreign material during waste degradation.

ACKNOWLEDGEMENTS

The authors are grateful and would like to thank the Department of Science and Technology (DST), MoEFCC and UGC, Government of India, New Delhi, for the financial support and encouragement. They also acknowledge the DST-FIST, DST-PURSE, UGC – SAP and MHRD-RUSA for providing the instrumentation facilities in the department.

REFERENCES

Abbasi, S.A. and Ramasamy, E.V. 1999. Biotechnological Methods of Pollution Control. Orient Longman (Universities Press India Ltd.), Hyderabad. 168 pp.

Adriano, D.C., Page, A.L., Elseewi, A.A., Chang, A.C. and Straugham, I. 1980. Utilization and disposal of fly-ash and coal residues in terrestrial ecosystem: A review. Journal of Environmental Quality, 9: 333-344.

Atiyeh, R., Lee, S., Edwards, C.A., Arancon, N.Q. and Metger, J.D. 2002. The influence of humic acid derived from earthworm processed organic wastes on plant growth. Bioresource Technology, 84: 7-14.

Bradford, M.M. 1976. A rapid and sensitive method for the quantitation of microgram quantities of protein utilizing the principle of protein-dye binding. Anal Biochem., 72: 248-254.

Bhide, S.V., Azuine, M.A., Lahiri, M. and Telang, N.T. 1994. Chemoprevention of mammary tumor virus-induced and chemical carcinogen-induced rodent mammary tumors by natural plant products. Breast Cancer Research and Treatment, 30(3): 233-42.

Chattopadhyay, G.N. and Bhattacharya, S.S. 2010. Use of coal ash in agriculture. In: Proceedings of Coal Ash Utilization, pp. 36.

Crawford, J.H. 1983. Review of composting. Process Biochem., 18: 14-15.

Davison, R.L., Natusch, D.F.S., Wallace, J.R. and Evans, C.A. 1974. Trace elements in flyash: Dependence of concentration on particle size. Environmental Science and Technology, 8: 1107-1113.

Edwards, C.A. 1998. The use of earthworms in the breakdown and management of organic wastes. In: Edwards, C.A. (Ed.), Earthworm Ecology. CRC Press, The Netherlands, pp. 327-354.

Fatima, M., Mandiki, S.N.M., Douxfils, J., Silvestre, F., Coppe, P. and Kestemont, P. 2007. Combined effects of herbicides on biomarkers reflecting immune-endocrine interactions in goldfish immune and antioxidant effects. Aquat. Toxicol., 81: 159-167.

Gandhi, M., Sangwan, V., Kapoor, K.K. and Dilbaghi, N. 1997. Composting of household wastes with and without earthworms. Environment and Ecology, 15(2): 432-434.

Giannopolitis, C.N. and Reis, S.K. 1997. Superoxide dismutase I. Occurrence in higher plants. Plant Physiol., 59: 309-314.

Gunzler, W. and Flohe-Clairborne, A. 1985. Glutathione peroxidase. In: Green-Wald, R.A., Ed., Handbook of Methods for Oxygen Radical Research, CRC Press, Boca Raton, pp. 285-290.

Gupta, K.S., Anamika Tewari., Richa Srivastava, R.C., Murthy, R.C. and Saurabh Chandra 2005. Potential of *Eisenia fetida* for sustainable and efficient vermicomposting of fly ash. Water, Air, and Soil Pollution, 163: 293-302.

Hogg, E., Eavoino, V., Caimi, F., Amlinger, W., Devliegher, W. and Brinton Antler, S. 2002. Comparison of compost standards within the EU, North America and Australia. The Waste and Resources Action Programme (WARP).

Honda, M., Yamada, Y., Tomonaga, M., Ichinose, H. and Kamihira, S. 2000. Correlation of urinary 8-hydroxy-2-de-oxyguanosine (8-OHdG), a biomarker of oxidative DNA damage, and clinical features of hematological disorders: a pilot study. Leuk. Res., 24: 461-468.

Ismail, S.A. 1997. Vermicology: The Biology of Earthworms, Orient Longmans, Hyderabad, pp. 92.

Karthika, A., Seetha Devi, G., Vasanthy, M., Swabna, V., Susila, S. and Vivekanadhan, M. 2014. Potentiality of *Eisenia fetida* to degrade disposable paper cup waste- An eco-friendly solution to solid waste pollution. Environmental Science and Pollution Research, 22(4): 2868-7286.

Kaushik, P. and Garg, V.K. 2004. Dynamics of biological and chemical parameters during vermicomposting of solid textile mill sludge mixed with cow dung and agricultural residues. Bioresour. Technol., 94: 203-209.

Kaviraj and Sharma, S. 2003. Municipal solid waste management through vermicomposting employing exotic and local species of earthworms. Biores. Technol., 90: 169-173.

Lim, S.L., Wu, T.Y., Sim, E.Y.S., Lim, P.N. and Clarke, C. 2012. Biotransformation of rice husk into organic fertilizer through vermicomposting. Ecological Engineering, 41: 60-64.

Logsdson, G. 1994. Worldwide progress in vermicomposting. Biocycle, 35: 63-65.

Ministry of Environment and Forests, (MOEF) Notification, 3rd April 2007. Fly Ash Notification 2007. Ministry of Environment and Forests, New Delhi.

Mohan, S. and Gandhimathi, R. 2009. Removal of heavy metal ions from municipal solid waste leachate using coal fly ash as an adsorbent. Journal of Hazardous Materials, 169: 351-359.

Nel, A., Xia, T., Madler, L. and Li, N. 2006. Toxic potential of materials at the nanolevel. Science, 311: 622-627.

Pandey, V. C., Abhilash, P.C. and Singh, Nandita 2009. The Indian perspective of utilizing fly ash in phytoremediation, phytomanagement and biomass production. Journal of Environmental Management, 90: 2943-2958.

Pattnaik, S. and Reddy, M.V. 2010. Assessment of municipal solid waste management in Puducherry (Pondicherry) India. Resources, Conservation and Recycling, 54: 512-520.

Rajesh Banu, J., Lcktae Yeom., Esakkiraj., Naresh Kumar., Young Woo Lee. and Vallinayagam, S. 2008. Feasibility of vermicomposting in biostabilization of biomanagement of sago-sludge using an earthworm sludge from a distillery industry, *Lampito mauritii*. J. Environ. Biol., 29(5): 753-757.

Ravindran, B., Dinesh, S.L., John, K. and Sekaran, G. 2008. Vermicomposting of solid waste generated from leather industries using epigeic earthworm *Eisenia fetida*. Appl. Biochem. Biotechnol., 151: 480-488.

Ribera, I., Doledec, S., Downie, I.S. and Foster, G.N. 2001. Effect of land disturbance and stress on species traits of ground beetle assemblages. Ecology, 82(4):1112-29.

Saint-Denis, M., Labrot, F., Narbonne, J.F. and Ribera, D. 1998. Glutathione, glutathione related enzymes, and catalase in the earthworm *Eisenia fetida* Andrei. Arch. Environ. Contam. Toxicol., 35: 602-614.

Sandrini, J.Z., Lima, J.V., Regoli, F., Fattorini, D., Notti, A., Marins, L.F. and Monserrat, J.M. 2008. Antioxidant responses in the nereidid *Laeonereis acuta* (Annelida, Polychaeta) after cadmium exposure. Ecotoxicol. Environ. Saf., 70: 115-120.

Satchell, J.E. and Martin, K. 1984. Phosphate activity in earthworm's faeces. Soil Biology and Biochemistry, 16(2): 191-194.

Saxena, M., Chauhan, A. and Ashokan, P. 1998. Fly ash vermicomposting from non-ecofriendly organic wastes. Pollut. Res., 17: 5-11.

Singh, S., Sartaj, A. B., Jaswinder Singh, Rajinder Kaur and Adarsh, P. V. 2016. Vermistabilization of thermal power plant fly ash using *Eisenia fetida.* Jr. of Industrial Pollution Control, 32(2): 554-561.

Sixteenth electric power survey of India (SEPSI), 2000. Part V, Long Term Forecast up to 2016-17 (Public Utilities). Central Electricity Authority Ministry of Power, Government of India, New Delhi.

Song, Y., Zhu, L.S., Wang, J., Wang, J.H., Liu, W. and Xie, H. 2009. DNA damage and effects on antioxidative enzymes in earthworm (*Eisenia fetida*) induced by atrazine. Soil Biology & Biochemistry, 41: 905-909.

Sharma, P., Jha, A.B., Dubey, R.S. and Pessarakli, M. 2012. Reactive oxygen species, oxidative damage, and antioxidative defense mechanism in plants under stressful conditions. Journal of botany, 1-26.

Suthar, S. 2007. Production of vermifertilizer from guar gum industrial wastes by using composting earthworm *Perionyx sansibaricus* (Perrier). The Environmentalist, 27: 329-335.

T.E.R.I. 1998. Reclaiming ash pond by means of mycorrhizal-organo-biofertilizer. Quarterly reports submitted to fly ash mission, TIFAC, DST, Tata Energy Research Institute, New Delhi, India.

Tandon, H.L.S. 2009. Methods of Analysis of Soils, Plants, Waters. Fertilisers and Organic Manures. Fertilizer Development and Construction Organisation, New Delhi, India.

Usmani, Z., Kumar, V. and Mritunjay, S.K. 2017. Vermicomposting of coal fly ash using epigeic and epi-endogeic earthworm species: Nutrient dynamics and metal remediation. RSC Adv, 7: 4876-4890.

Vivas, A., Moreno, B., Garcia, S. and Rodriquez, B.E. 2009. Assessing the impact of composting and vermicomposting on bacterial community size and structure and microbial functional diversity of an olive-mill waste. Bioresour. Technol., 100: 1319-1326.

Yasir, M., Aslam, Z., Kim, S.W., Lee, SW., Jeon, C.O. and Chung, Y.R. 2009. Bacterial community composition and chitinase gene diversity of vermicompost with antifungal activity. Bioresour. Technol., 100(19): 4396-4403.

Zainab, D., Valeria, D., Maria, R.P., Mohamed, H. and Aaziz, O. 2009. Study of the biodegradation and transformation of olive-mill residues during composting using FTIR spectroscopy and differential scanning calorimetry. J. Hazar. Mater., 164: 1281-1285.

Nature Environment and Pollution Technology
An International Quarterly Scientific Journal

p-ISSN: 0972-6268
(Print copies up to 2016)
e-ISSN: 2395-3454

Vol. 19 | No. 2 | pp. 695-701 | 2020

Original Research Paper

https://doi.org/10.46488/NEPT.2020.v19i02.024

Open Access Journal

Changes in Enzyme Activity and Bacterial Succession During Sewage Sludge Composting

Chuang Ma*, Hui-jia Jin*, Bin Hu*, Nan Liu*, Ke Zhang*, Ji-hong Zhao and Hong-zhong Zhang**†**

*Zhengzhou University of Light Industry, Zhengzhou 450001, PR China

**Collaborative Innovation Center of Environmental Pollution Control and Ecological Restoration, Henan Province, Zhengzhou 450001, PR China

†Corresponding author: Hong-zhong Zhang (E-mail: Chuang Ma; machuang819@qq.com)

Nat. Env. & Poll. Tech.
Website: www.neptjournal.com

Received: 24-07-2019
Accepted: 08-10-2019

Key Words:
Bacteria;
Composting;
Correlation;
Enzyme activity;
Sewage sludge

ABSTRACT

To study the variations in microorganisms and enzyme activity during sewage sludge composting, the dynamic changes in temperature, enzyme activity and microorganism composition were studied by co-composting municipal sludge and corn straw. The results show that the pile underwent mesophilic, thermophilic, and cooling phases and that the high-temperature duration (≥ 50 °C) had reached 5 days, which meets harmlessness requirements. During the composting process, the protease, arylsulfatase (ARS) and cellulase content increased gradually; urease content first decreased and then increased rapidly; and peroxidase (POD) content first increased and then decreased. *Ureibacillus*, *Bacillus*, *Pseudomonas*, *Flavobacterium* and *Sporosarcina* were the dominant bacteria during sludge composting. Microorganisms played different roles at different stages of the composting. *Ureibacillus* and *Bacillus* were the dominant strains in the mesophilic and thermophilic phases, respectively, and *Pseudomonas* and *Flavobacterium* were the dominant strains in the cooling phase. *Sporosarcina* mainly played a role later in the thermophilic and cooling phases. The effect of different bacteria on enzyme activity varied; *Pseudomonas* played a clear role in promoting the production of urease while *Bacillus* had a clear inhibitory effect on the production of urease. *Ureibacillus* inhibited the production of ARS, POD, protease and cellulase. By studying the changes in microbial and enzymatic activities at different stages of sludge composting, it is possible to thoroughly explore the nature of the latter and provide a reference for optimizing composting processes.

INTRODUCTION

Sewage sludge is a by-product of municipal wastewater treatment plants that is rich in organic matter, nitrogen, phosphorus and other nutrients, and qualified sludge compost is a high-quality soil amendment (Ma et al. 2018). Composting is the process of converting organic waste into stable humus through microbial activities, which are largely influenced by C/N, moisture content, temperature, pH and ventilation conditions (Du et al. 2019). In composting, microorganisms are the main players in various organic metabolic activities, but their main function is the biochemical decomposition of degradable organic matter through enzymatic action (Langarica-Fuentes et al. 2014). Bacteria are the main microbial population that decompose organic matter and produce heat during composting. Their diversity and abundance directly affect the composting process (Vieira et al. 2019). Microorganisms promote the mineralization and decomposition of organic matter by secreting extracellular enzymes (Geisseler et al. 2008, Becarelli et al. 2019). For example, degradable organic matter (starch and sugars) and refractory organic matter (cellulose and lignin) are gradually mineralized and decomposed under the action of various specific enzymes, but the activities of these enzymes are closely related to the composition of bacterial communities. Composting cannot occur without the work of a series of specific functional enzymes such as protease, urease, and peroxidase (POD) (Krajewska et al. 2009, Du et al. 2018). Cellulase plays a major role in the degradation of cellulose to glucose and POD is related to lignin degradation. Both enzymes contribute to the degradation of organic matter and the carbon cycle (He et al. 2013). Protease and urease are involved in the nitrogen cycle during composting processes, while arylsulfatase (ARS) is involved in the sulphur cycle (Zeng et al. 2010). The sulphur cycle is closely related to the main odorous substances (NH_3 and H_2S) produced during composting. Enzyme activities are also closely related to microbial composition and activity in the different stages of composting. Microbial composition analysis during mesophilic, thermophilic, and cooling phases can help us understand the nature of composting more thoroughly.

Little attention has been paid, to date, to the dynamic changes in the functional enzymes in aerobic sludge com-

posting, and the relationship between the composition and structure of bacteria and functional enzyme activity at different stages of fermentation (Krajewska et al. 2009, He et al. 2013). Therefore, temperature and enzyme content analysis of different fermentation stages in sludge composting, and modern high-throughput sequencing methods, can be used to obtain a thorough understanding of the changes in enzyme activity and bacterial community structure. This can lead to a comprehensive understanding of the evolution of microbial communities and the degradation of organic matter during the composting process.

MATERIALS AND METHODS

Composting Material and Technology

Dewatered sludge was collected from a domestic sewage treatment plant in Zhengzhou City. The water content was 80.8% and the volatile organic compound (VOC) content was 54.8%. Corn straw was used as the auxiliary material. The particle size was 1-2 cm, the moisture content was 9.27%, and the VOC content was 87.27%.

The dewatered sludge and corn straw were evenly mixed in a 3:1 weight ratio and then fermented by static stacking and high-temperature aerobic composting. The VOC content was 80.31% and the heap bulk density was 570.46 kg·m^3.

The fermentation reactor was 1.2 m high and 0.6 m in diameter. There was a ventilation system at the bottom of the fermentation reactor. Forced ventilation was controlled by an automatic blower. The ventilation interval was 12-15 min and the duration of the blast (regulated and controlled by a computer according to the fermentation temperature feedback) was 1-3 min.

Sampling and Analysis Method

Based on the composting temperature, 1 kg of compost (from 30 cm under the surface layer of the compost body) was sampled in a sealed bag during the mesophilic phase (days 1 and 3), thermophilic phase (days 5 and 7), and cooling phase (day 10) and then taken to the laboratory for analysis. The temperature of the sludge fermentation process was monitored automatically with a temperature probe. Protease content was determined by ninhydrin colourimetry, urease activity was determined by sodium phenol-sodium hypochlorite colourimetry (Nannipieri et al. 2002), and ARS content was determined by sodium hydroxide-calcium chloride colourimetry (Tabatabai et al. 1970). POD content was determined by pyrogallol colourimetry and cellulase content was determined by 3,5-Dinitrosalicylic acid colourimetry.

The compost samples were sent to Shanghai Meiji Biomedical Technology Co., Ltd. for high-throughput sequencing. Microbial DNA was extracted with a soil FastDNA Spin Kit (MPBio) method. The DNA was purified and determined using a NanoDrop 2000 ultraviolet-visible spectrophotometer (Thermo Scientific, Wilmington, USA). The v3-v4 hypervariable region of the 16S rRNA gene was amplified with primers 338F (ACTCCTGGGAGGCGAGCGAG) and 806R (GGACTACHVGGTWTCTAAT).

Statistical Analysis

SPSS (V 19.0) was used for statistical analysis, the Duncan method was used for multiple comparisons, and Origin 9.0 was used to draw charts.

RESULTS AND DISCUSSION

Dynamic Change of Temperature During Sewage

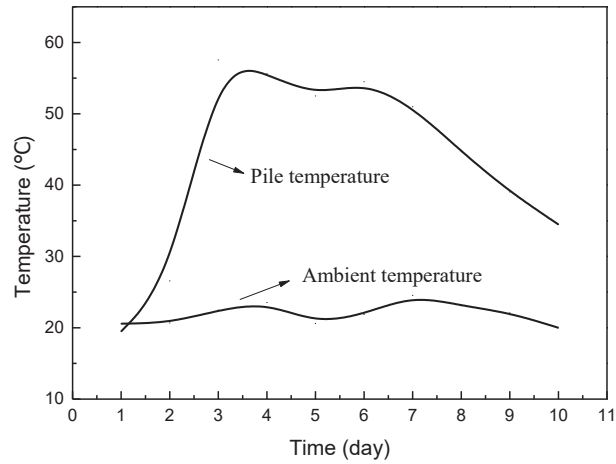

Fig. 1: Changes in pile temperature during composting.

Sludge Composting

During aerobic composting of sewage sludge, microorganisms (through enzymatic action) decompose organic matter and heat is released (He et al. 2013). The composting temperature is thus influenced by microbial activity and material oxidation. The decomposition of organic matter is accompanied by the rise and fall of composting temperature so that the composting material can be matured and harmless. As illustrated in Fig. 1, the ambient temperature fluctuated around 20°C throughout the composting process and the sludge and straw composting process lasted for 10 days. The heap experienced mesophilic (day 1-3), thermophilic (day 4-7) and cooling (day 8-10) phases. The reactor temperature began to rise on day 1 and reached its highest temperature of 57.6°C on day 3, with a heating rate of 12.7°C/day. The thermophilic phase (temperature>50°C) duration of the compost was approximately 5 days, which meets the hygienic index of composting and effectively kills pathogenic bacteria and weed seeds in the compost (Zeng et al. 2010).

Dynamic Changes of Enzyme Activities in Sludge Composting Process

Corn straw, which can be classified as microbial refractory organic matter, has high cellulose content, a complex structure, and is difficult to degrade (Vieira et al. 2019). It is usually degraded by POD and polyphenol oxidase. As illustrated in Fig. 2(a), POD activity increased gradually and then decreased significantly ($P<0.05$) during composting. POD content was significantly higher during the high-temperature phase than in the heating and cooling periods, reaching a maximum value of 192.50 μmol/h.g on day 7. The higher POD levels were due to the high population and activity of microorganisms during the high-temperature period, which thus meant that more POD was produced to promote the degradation of cellulose, lignin, and other refractory organic matter.

Hydrolytic enzymes are key enzymes in organic mineralization during composting (Du et al. 2019). Their activity can be used to characterize the degradation efficiency of organic matter (Krajewska et al. 2009). Protease and urease are closely related to the nitrogen cycle in composting and are important functional enzymes. During sludge composting, protease activity increased gradually (Fig. 2(b)), and reached a maximum of 3.25 mg/g on day 10. The urease content first decreased and then increased, and reached a maximum of 1.90 mg/g at the end of composting (Fig. 2(c)). The urease content in the cooling phase was significantly higher than in the mesophilic and thermophilic phases, while the urease content was significantly higher in the mesophilic phase than in the thermophilic phase ($P < 0.05$).

Cellulose-decomposing bacteria degrade corn straw cellulose by secreting cellulase. During sludge composting, the cellulase content increased gradually ($P < 0.05$) and reached a maximum of 335.79 μg/g*min at the end of composting (Fig. 2(d)). This is consistent with the conclusion that cellulase activity increased gradually during the composting of chicken, pig, and cow manure. This finding is also consistent with the fact that cellulose is a relatively refractory organic matter and that its degradation occurs mainly in the middle and late stages of composting (Becarelli et al. 2019). ARS is mainly involved in the conversion of organic sulphur to SO_4^{2-} (Toledo et al. 2018). As illustrated in Fig. 2(e), the ARS activity increased steadily and continuously. The ARS activity during the cooling phase (days 7-10) was significantly higher ($P < 0.05$) than during the mesophilic and thermophilic phases. This may be due to the gradual release of organic sulphur from straw with the degradation of cellulose and other refractory organic matter (Toledo et al. 2018).

Dynamic Changes of Microbial Composition in Sludge Composting Process

Coverage reflects whether the sequencing results represent the true situation of microorganisms in the samples. Here, the mesophilic, thermophilic and cooling phases reached 0.9956, 0.9956 and 0.9973, respectively (Table 1), which indicated that the sequencing results were highly representative (Ye et al. 2017). Bacterial composition varied during sludge composting, and the richness and diversity of the bacterial community are different at different fermentation stages (Table 1). Sobs, Ace and Chao are all indicators of microbial community richness (Ke et al. 2018). From Table 1, we can see that Sobs, Ace and Chao decreased, respectively, from 573, 655.40 and 651.54 in the mesophilic phase (day 3) to 407, 531.21 and 535.82 in the thermophilic phase (day 5), and then to 325, 379.08 and 374.91 in the cooling phase (day 10). Shannon is an index reflecting microbial community diversity (Huang et al. 2013), which decreased from 3.62 in the mesophilic phase (day 3) to 3.47 in the thermophilic phase (day 5) and then to 2.97 in the cooling phase (day 10) (Table 1). This indicated that the richness and diversity of the microbial community decreased with composting. This may be due to the abundant degradable organic matter such as sugars in the raw material during the early stage of composting, which resulted in higher bacteria richness in the mesophilic phase compared to the thermophilic and cooling phases.

The dominant bacteria in the composting process were *Ureibacillus*, *Bacillus*, *Pseudomonas*, *Flavobacterium* and *Sporosarcina* (Fig. 3). The proportion of *Ureibacillus* in the bacterial community decreased with time. The proportion of *Ureibacillus* decreased rapidly from 37.9% in the mesophilic

phase to 3.82% in the thermophilic phase, and then to 0.48% in the cooling phase. The proportion of *Ureibacillus* in the mesophilic phase was significantly higher than in the thermophilic and cooling phases. This indicates that it was the dominant bacteria in the mesophilic phase and played a major role during this stage of composting (Vieira et al. 2019). The proportion of *Bacillus* in the community first increased and then decreased. The proportion of *Bacillus* increased rapidly from 11.50% in the mesophilic phase to 31.58% in the thermophilic phase and then decreased rapidly to 1.66% in the cooling phase. The proportion of *Bacillus* in the thermophilic phase was the largest; significantly higher than in the mesophilic and cooling phases. This indicated that *Bacillus* was the dominant bacteria in the thermophilic phase and played a major role in this composting phase. *Pseudomonas* increased from an extremely low proportion of the bacterial community in the mesophilic and thermophilic phases to 36.69% in the cooling phase, which indicated that *Pseudomonas* played a major role in the cooling phase of the composting process and was the dominant bacteria during this period. The proportion of *Sporosarcina* in the bacterial community increased rapidly during the composting process, from 0% in the mesophilic phase to 3.88% and 9.81% in the thermophilic and cooling phases, respectively, which indicated that *Sporosarcina* played a role in the thermophilic and cooling phases of the composting process (Du et al. 2019).

Correlation between Dominant Bacteria and Functional Enzyme Activity in Sludge Composting Process

The Heatmap diagram clearly shows the relationship between functional enzyme activity and functional microorganisms. As illustrated in Fig. 4, urease was positively correlated with *Pseudomonas* (r=1, P=0), indicating that *Pseudomonas* played a significant role in promoting the production of urease (Vieira et al. 2019). There was a significant negative correlation between urease and *Bacillus* (r=-1, p=0), indicating that *Bacillus* had a significant inhibitory effect on urease production, which is consistent with the minimum urease activity in the thermophilic phase and the maximum urease activity in the cooling phase (Fig. 2). There was a significant

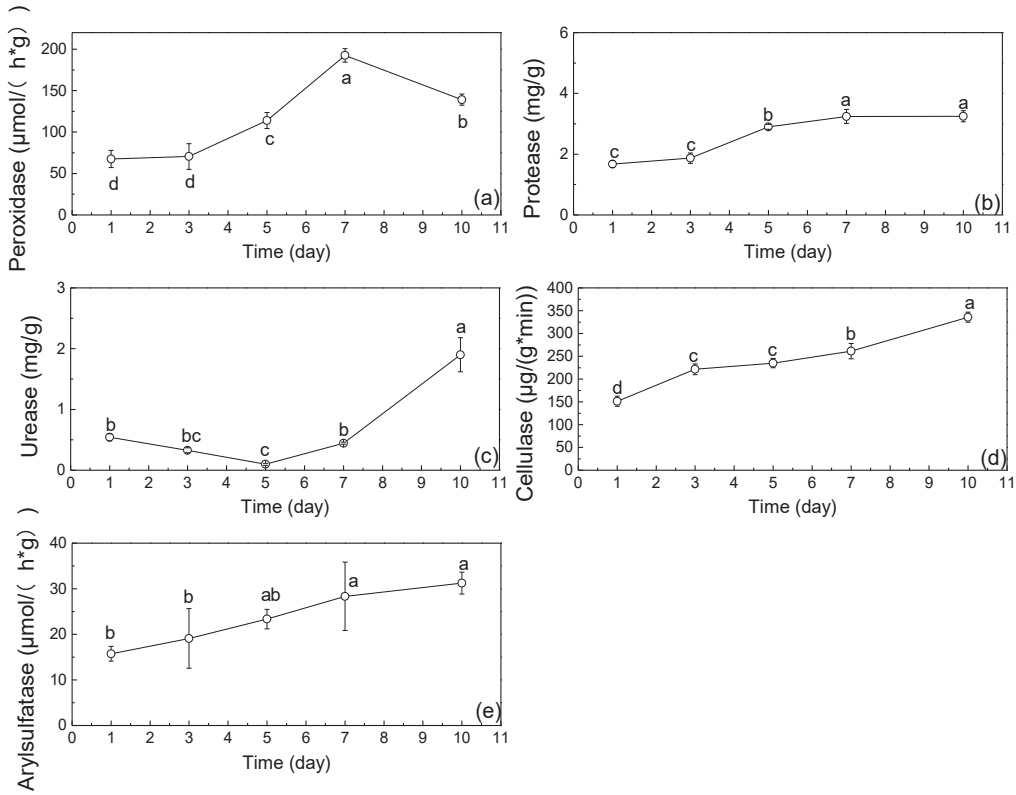

Fig. 2: Evolution of enzyme activities of different piles during composting.
Note: Different letters indicate significant difference at P < 0.05 among different samples.

negative correlation between ARS and *Ureibacillus* (r=-1, p=0). This indicates that *Ureibacillus* had a significant inhibitory effect on ARS production. ARS is an important enzyme involved in the sulphur cycle of composting materials. It can be inferred that *Ureibacillus* can inhibit the degradation of organic sulphur during the heating period. There was a significant negative correlation between POD and *Ureibacillus* (r=-1, p=0), indicating that *Ureibacillus* had a significant inhibitory effect on POD production. This finding was the most consistent with POD activity in the later thermophilic phase (Du et al. 2019). There was a significant negative correlation between protease and *Ureibacillus* (r=-1, p=0), indicating that *Ureibacillus* had a significant inhibitory effect on protease production. This was also consistent with the maximum activity of protease during the cooling phase. There was a significant negative correlation between cellulase and *Ureibacillus* (r=-1, p=0), indicating that *Ureibacillus* had a significant inhibitory effect on cellulase production. This was also consistent with the fact that cellulose is a relatively refractory organic

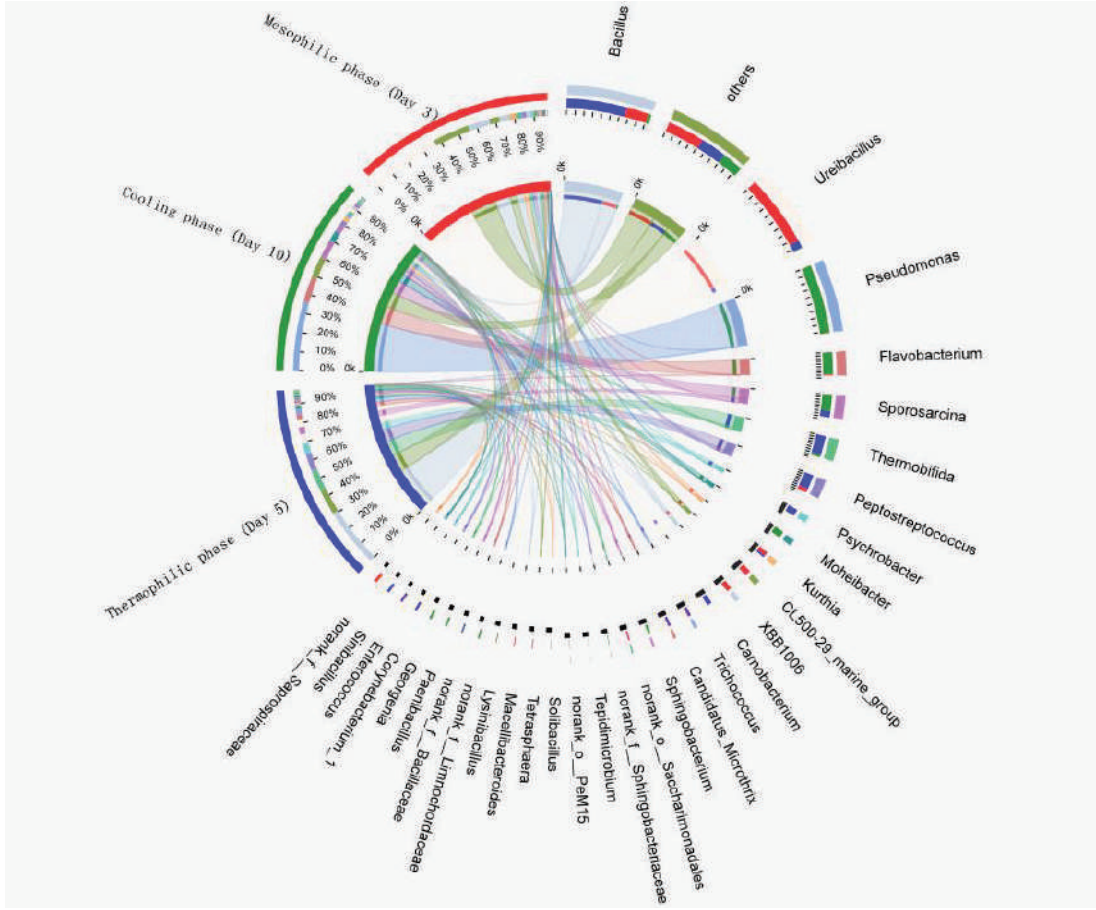

Fig. 3: Distribution of bacterial community compositions at different composting stages.

Table 1: Bacterial diversity indices during sewage sludge composting.

Fermentation stage	Sobs	Shannon	Ace	Chao	Coverage
Mesophilic phase (Day 3)	573	3.62	655.40	651.54	0.9956
Thermophilic phase (Day 5)	407	3.46	531.21	535.82	0.9956
Cooling phase (Day 10)	325	2.97	379.08	374.91	0.9973

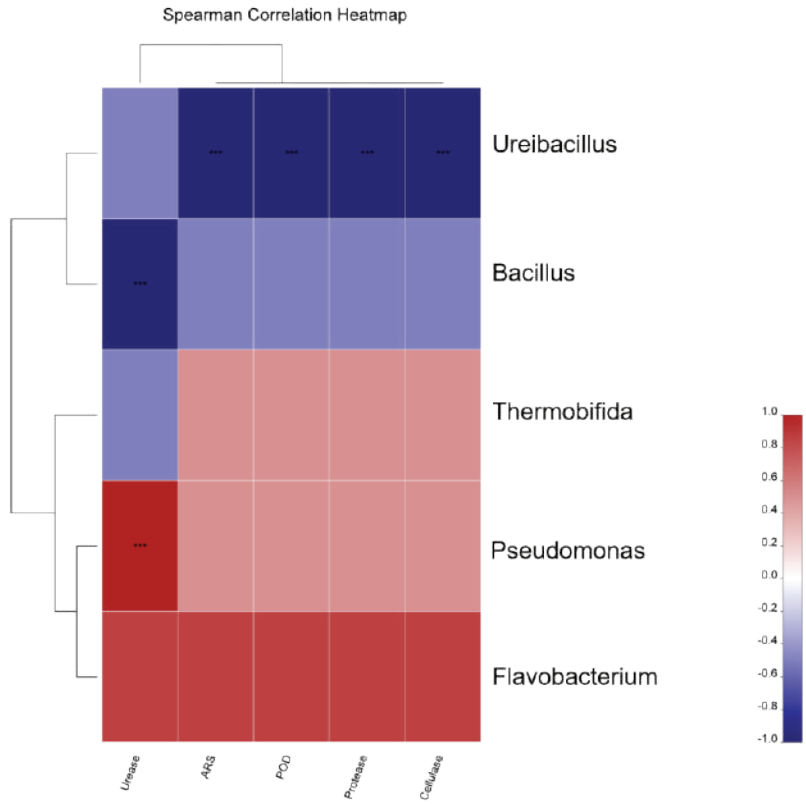

Fig. 4: Correlation between enzyme activity and bacteria in sludge composting process.

matter, and its degradation process mainly occurs in the late stage of composting (Becarelli et al. 2019).

CONCLUSION

The composting of corn straw and sludge experienced mesophilic, thermophilic and cooling phases, and the thermophilic duration (temperature >50°C) reached 5 days, which meets the harmlessness requirement. During the composting process, protease, ARS and cellulase increased gradually, urease content first decreased and then increased rapidly, and POD activity first increased and then decreased. *Ureibacillus*, *Bacillus*, *Pseudomonas, Flavobacterium* and *Sporosarcina* were the dominant bacteria in the sludge composting process. Microorganisms played different roles in different fermentation stages. Among them, *Ureibacillus* was the dominant bacteria in the mesophilic phase, and *Bacillus* was the dominant bacteria in the thermophilic phase. *Pseudomonas* and *Flavobacterium* were the dominant bacteria in the cooling phase, while *Sporosarcina* also mainly occurred and played a role in the cooling phase. Different bacteria have different effects on different enzymes in sludge composting. *Pseudomonas* can promote urease, while *Bacillus* can inhibit urease. *Ureibacillus* had a clear inhibitory effect on ARS, POD, protease and cellulase.

ACKNOWLEDGEMENTS

This research was financially supported by the National Natural Science Foundation of China (No.41501527), and the Zhengzhou University of Light Industry (Grant No. 2013BSJJ022).

REFERENCES

Becarelli, S., Chicca, I., Siracusa, G., La China, S., Gentini, A., Lorenzi, R., Munz, G., Petroni, G., Levin, D.B. and Di Gregorio, S. 2019. Hydrocarbonoclastic Ascomycetes to enhance co-composting of total petroleum hydrocarbon (TPH) contaminated dredged sediments and lignocellulosic matrices. New Biotechnology, 50: 27-36.

Du, J.J., Zhang, Y.Y., Qu, M.X., Yin, Y.T., Fan, K., Hu, B., Zhang, H.Z., Wei, M.B. and Ma, C. 2018. Effects of biochar on the microbial activity and community structure during sewage sludge composting. Bioresource Technology, 272: 171-179.

Geisseler, D. and Horwath, W. R. 2008. Regulation of extracellular protease activity in soil in response to different sources and concentrations of nitrogen and carbon. Soil Biology & Biochemistry, 40(12): 3040-3048.

He, Y., Xie, K., Xu, P., Huang, X., Gu, W., Zhang, F. and Tang, S. 2013. Evolution of microbial community diversity and enzymatic activity during composting. Research in Microbiology, 164(2): 189-198.

Huang, K., Li, F., Wei, Y., Chen, X. and Fu, X. 2013. Changes of bacterial and fungal community compositions during vermicomposting of vegetable wastes by *Eisenia foetida*. Bioresource Technology, 150(4): 235-241.

Ke, W., Hailong, M., Zhe, W. and Yu, T. 2018. Succession of organics metabolic function of bacterial community in swine manure composting. Journal of Hazardous Materials, 360: 471-480.

Krajewska, Barbara. 2009. Ureases I. Functional, catalytic and kinetic properties: A review. Journal of Molecular Catalysis B Enzymatic, 59(1): 9-21.

Langarica-fuentes, A., Handley, P.S., Houlden, A., Fox, G. and Robson, G.D. 2014. An investigation of the biodiversity of thermophilic and thermotolerant fungal species in composts using culture-based and molecular techniques. Fungal Ecology, 11: 132-144.

Ma, C., Liu, F.Y., Wei, M.B., Du, J.J., Liu, N. and Zhang, H.Z. 2018. Effects of initial moisture content on phenanthrene degradation behavior during sludge composting. Nature Environment and Pollution Technology, 17(4): 1167-1173.

Nannipieri, P., Kandeler, E., Ruggiero, P., Burns, R.G. and Dick, R.P. 2002. Enzyme activities and microbiological and biochemical processes in soil. In: Enzymes in the Environment. Marcel Dekker, New York, pp. 1-33.

Tabatabai, M. and Bremner, J. 1970. Arylsulfatase activity of soils. Soil Science Society of America Journal, 34(2): 225- 229.

Toledo, M., Gutiérrez, M.C., Siles, J. A. and Martín, M.A. 2018. Full-scale composting of sewage sludge and market waste: Stability monitoring and odor dispersion modeling. Environmental Research, 167: 739-750.

Vieira, F. R., Pecchia, J. A., Segato, F. and Polikarpov, I. 2019. Exploring oyster mushroom (Pleurotus ostreatus) substrate preparation by varying phase I composting time: changes in bacterial communities and physicochemical composition of biomass impacting mushroom yields. Journal of Applied Microbiology, 126: 931-944.

Ye, J., Joseph, S.D., Ji, M., Nielsen, S., Mitchell, D.R.G., Donne, S., Horvat, J., Wang, J., Munroe, P. and Thomas, T. 2017. Chemolithotrophic processes in the bacterial communities on the surface of mineral-enriched biochars. The ISME Journal, 11(5): 1087-1101.

Zeng, G.M., Yu, M., Chen, Y.N., Huang, D.L., Zhang, J.C., Huang, H.L., Jiang, R.Q. and Yu, Z. 2010. Effects of inoculation with *Phanerochaete chrysosporium* at various time points on enzyme activities during agricultural waste composting. Bioresource Technology, 2101(1): 222-227.

Nature Environment and Pollution Technology
An International Quarterly Scientific Journal

p-ISSN: 0972-6268
(Print copies up to 2016)
e-ISSN: 2395-3454

Vol. 19 | No. 2 | pp. 703-710 | 2020

Original Research Paper

https://doi.org/10.46488/NEPT.2020.v19i02.025

Open Access Journal

Effects of Soybean Stover-Derived Biochar on Microbial Community and Structure in Loess Soil

Baowei Zhao†, Alexandar J. Niebuhr, Yude Lv and Khamhak Douangdalangsy
School of Environmental and Municipal Engineering, Lanzhou Jiaotong University, Lanzhou 730070, Gansu, P. R. China
†Corresponding author: Baowei Zhao; zhbw2001@sina.com

Nat. Env. & Poll. Tech.
Website: www.neptjournal.com

Received: 15-07-2019
Accepted: 06-10-2019

Key Words:
Biochar;
Soil microbial community;
Lysobacter; Loess soil;
Soybean stover

ABSTRACT

Soil microorganisms play a crucial role in nutrient availability and overall soil health. However, the effects that biochar has on soil microbial communities are not well understood. This study analysed the effects of biochar pyrolysis temperature and application rate on the soil microbial community of loess. Two biochars derived from soybean stover were produced at 300 and 600°C (BC300 and BC600, respectively) and were applied to loess at the rates of 1, 3, and 5% (w/w). After fifteen weeks of incubation, soil microbial analysis was performed using 16S rDNA amplicon sequencing technology. All of the BC300 and BC600 treated soils were shown to have an increase in the relative abundance of *Gemmatimonadetes* and a decrease in *Actinobacteria* and *Chloroflexi*. *Proteobacteria* also showed a significant increase in the majority of the biochar treated soils. Biochar led to a shift in the soil microbial community and caused a significant increase in the relative abundance of bacteria from the genus *Lysobacter*. Based on the results of this study, soybean stover-derived biochar should be considered as a potential soil amendment for improving the health of loess or other soils in semi-arid climates.

INTRODUCTION

The use of biochar, a carbon-rich material which results from the pyrolysis of biomass (Lehmann & Joesph 2009), has gained much attention due to its potential benefits as a soil amendment.

Biochar has been shown to alter both the physical and chemical properties of soil (Verheijen et al. 2010). In doing so, biochar has the potential to increase land fertility by increasing soil pH (Prasad et al. 2018), water and nutrient retention (Verheijen et al. 2010), and soil organic matter (Han et al. 2016, Khadem & Raiesi 2017). A growing number of studies also suggest that biochar can increase soil microbial biomass (Fox et al. 2014, Yao et al. 2017, Zhu et al. 2017a) and bacterial community network complexity (Zhou et al. 2018). However, there is still a lack of evidence for this and the interaction between biochar and soil microbial activity is not well understood (Zhu et al. 2017b). Some have also noted that by merely altering the physicochemical properties of soil, biochar can, therefore, indirectly cause shifts in the microbial community (Anderson et al. 2011). With this in mind, appropriate biochar pyrolysis temperatures and application rates need to be determined to provide sustainable and positive effects based on soil type, as well as other site-specific factors.

This study aimed to better understand the effects biochar has on soil microorganisms and how pyrolysis temperature and application rate influence these changes. The hypothesis was that the soils treated with soybean stover-derived biochar would cause an increase in soil microbial diversity due to its large surface area and potentially suitable habitat.

MATERIALS AND METHODS

Soil Sampling and Analysis

The loess used in this study was collected from the top 20 cm of a soybean field in the town of Santan (Jingyuan County) in China's Gansu Province. After the soil was collected, it was air-dried and passed through a 0.43 mm sieve.

pH value was measured, first, by weighing 20 g of sample and adding 50 mL of deionized water. Then, the sample was placed in a mechanical shaker for 30 min at 250 rpm. The sample was filtered and the pH value was measured using a PHS-3C pH meter from INESA Scientific Instrument Co., Ltd. EC was measured following the same process as pH except for 10 g of sample was used instead of 20 g. EC was then measured using a DDS-11A conductivity meter from Hangzhou Aolilon Instrument Co., Ltd. Finally, SOM was tested using potassium dichromate oxidation according to the methods described by Chen & Lu (2012).

The initial pH, electrical conductivity (EC), and soil organic matter (SOM) were 8.08, 0.251mS.cm^{-1}, and 3.1%, respectively.

Biochar Production and Characterization

The soybean (*Glycine max*) stover that was used for biochar production was collected from a field in the town of Santan (Jingyuan County) in China's Gansu Province. After being collected, the stover was washed to remove impurities, air-dried, and ground to pass through a 0.43 mm sieve. Biochar was then produced by placing the soybean stover biomass in a covered crucible and heating it in a muffle furnace (SX2, Shanghai Jiazhan Instrument Equipment Co., Ltd.) at 300°C and 600°C for 6 and 4 h, respectively.

C, H, N, and S content was determined using a combustion analyser (Vario Microcube, Elementar, Germany) and the BET surface area of both biochars was determined with a TriStar II surface area analyser (Micromeritics). SEM images were taken with a JSM-5600LV scanning electron microscope to compare the structures of BC300 and BC600. Ash content was tested by adding 1.0 g of biochar to a pre-weighed 30 mL crucible. The crucible was then heated in a muffle furnace until it reached 650°C ± 20°C. After cooling, the final weight of the ash and crucible was recorded and the ash content of BC300 and BC600 was calculated by the difference in the final weight and the pre-weighed crucible.

Pyrolysis temperature had a slight effect on the biochar's elemental composition, ash content, and pH. The chemical characterization and properties of the 300°C and 600°C biochar (BC300 and BC600) are shown in Table 1. BC600 had a slightly higher carbon content, ash content, and pH when compared with BC300. Scanning electron microscopy (SEM) images were used to compare the structure of BC300 and BC600 (Fig. 1). BC600 had a relatively large BET surface area as 13.84 $m^2 \cdot g^{-1}$, while BC300's surface area was only 2.00 $m^2 \cdot g^{-1}$. However, it is unclear why BC600 did not have an even larger surface area. A soybean stover-derived biochar with a much higher surface area (420.33 $m^2 \cdot g^{-1}$ with a pyrolysis temperature of 700°C) was reported by Ahmad et al. (2016a). Other studies (Windeatt et al. 2014, Khadem & Raiesi 2017) also saw higher BET surface areas (from 88.4 to 222.5 $m^2 \cdot g^{-1}$) with various types of biochars pyrolyzed at 600°C. Nevertheless, the higher surface area of BC600 still, in theory, makes it a more suitable habitat for soil microbiota.

Experimental Design

BC300 and BC600 were added to 100 g of loess at the rates of 1, 3, and 5% (w/w), with the control containing no biochar. These samples will be referred to as BC300-1, BC300-3, BC300-5, BC600-1, BC600-3, and BC600-5. Three replicates of each treatment were incubated for fifteen weeks at 25±1°C. After fifteen weeks, the methods outlined as following were used to analyse changes and shifts in soil microbial community of each treatment group.

DNA Extraction, Sequencing and PCR Amplification

Microbial analysis was conducted using a 16S rDNA amplicon sequencing technology based on the IonS5TM XL sequencing platform. The genomic DNA of the sample was extracted using a CTAB extraction protocol, and then the purity and concentration of the DNA were detected by agarose gel electrophoresis. The appropriate amount of sample DNA was taken in a centrifuge tube and the sample was diluted to 1 $ng \cdot \mu L^{-1}$ with sterile water. Phusion® High-Fidelity PCR Master Mix with GC Buffer (New England Biolabs) was used to perform all of the polymerase chain reactions (PCR).

PCR products were detected using a 2% agarose gel and electrophoresis. The samples were mixed according to the concentration of the PCR products. After thorough mixing, the PCR products were purified by electrophoresis using a 1×TAE concentration of 2% agarose gel. The products

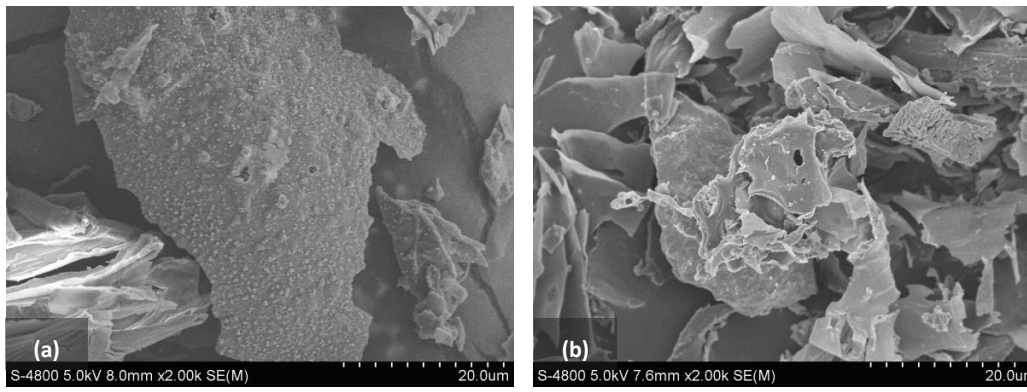

Fig. 1: SEM images at 20.0 μm of BC300 and BC600 (a and b, respectively).

were then purified using a GeneJET™ Gel Extraction Kit (Thermo Scientific).

Sequencing libraries were generated using Ion Plus Fragment Library Kit 48 rxns (Thermo Scientific) following the manufacturer's recommendations. The quality of the library was evaluated on the Qubit@ 2.0 Fluorometer (Thermo Scientific). Finally, the library was sequenced on an Ion S5™ XL platform and 400 bp/600 bp single-end reads were generated.

Data Processing

Quality filtering on the raw reads was performed under specific filtering conditions to obtain the high-quality clean reads according to the command-line tool Cutadapt (Martin 2011). The reads were then compared with the Silva database project (Quast et al. 2013). UCHIME (Edgar et al. 2013) was used to detect and remove chimaera sequences (Haas et al. 2011). Clean reads were then finally obtained.

Sequence analysis was performed by UPARSE (version 7.0.1001) (Edgar et al. 2013) and sequences with ≥97% similarity were assigned to the same operational taxonomic units (OTUs).

Statistical Analysis

QIIME (version 1.7.0) was used for statistical analysis for this study. Bacterial community richness was identified using the Chao1 estimator and abundance-based coverage estimator (ACE). Shannon and Simpson's indices were used to identify bacterial community diversity. Nonmetric multidimensional scaling (nMDS) (Kruskal 1964) was used to determine the variance in and overall effect on the bacterial community due to the addition of biochar. Linear discriminant analysis (LDA) effect size (LEfSe) (Segata et al. 2011) was also utilized to further analyse the metagenomic data.

RESULTS AND DISCUSSION

The Effects of Biochar on Microbial Structure and Bacterial Diversity

Variance in bacteria phyla distributions showed that the application of biochar did cause a shift in the microbial community of loess (Fig. 2). The majority of the control (81.9%), BC300 treatments (83.4% to 86.9%), and BC600 treatments (85.6% to 87.1%) were all mainly associated with five different bacteria phyla (*Proteobacteria*, *Gemmatimonadetes*, *Actinobacteria*, *Bacteroidetes*, and *Chloroflexi*). This trend in soil bacterial community is similar to studies conducted by Ahmad et al. (2016b) and Kolton et al. (2011). However, the results of this study were less pronounced. Every treatment, except for BC300-1, showed an increase in the relative abundance of *Proteobacteria* from the control (27.3%) with BC300-5 and BC600-5 being the highest at 34.2% and 35.2%, respectively. The relative abundance of *Gemmatimonadetes* increased significantly in all biochar

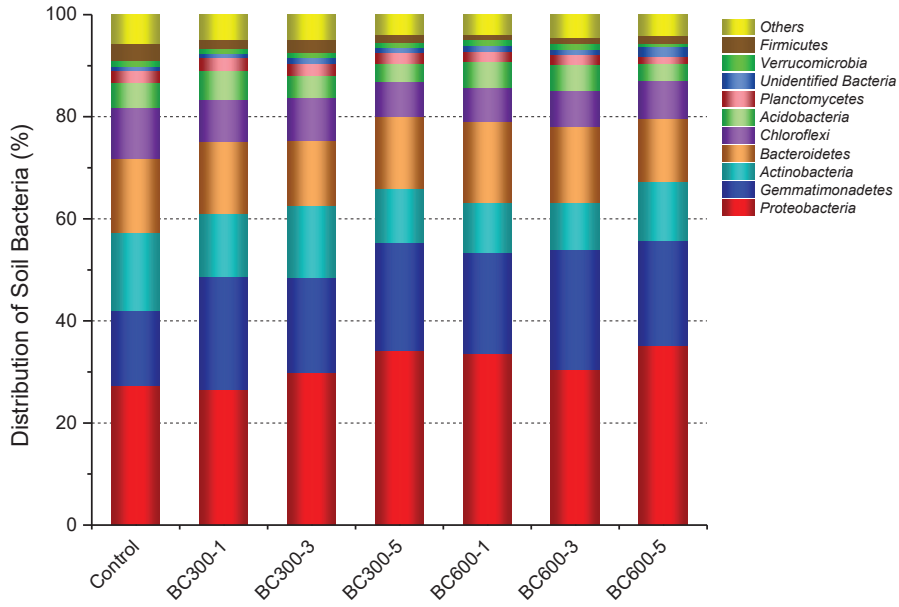

Fig. 2: Distribution of soil bacteria phyla from soils treated with BC300 and BC600.

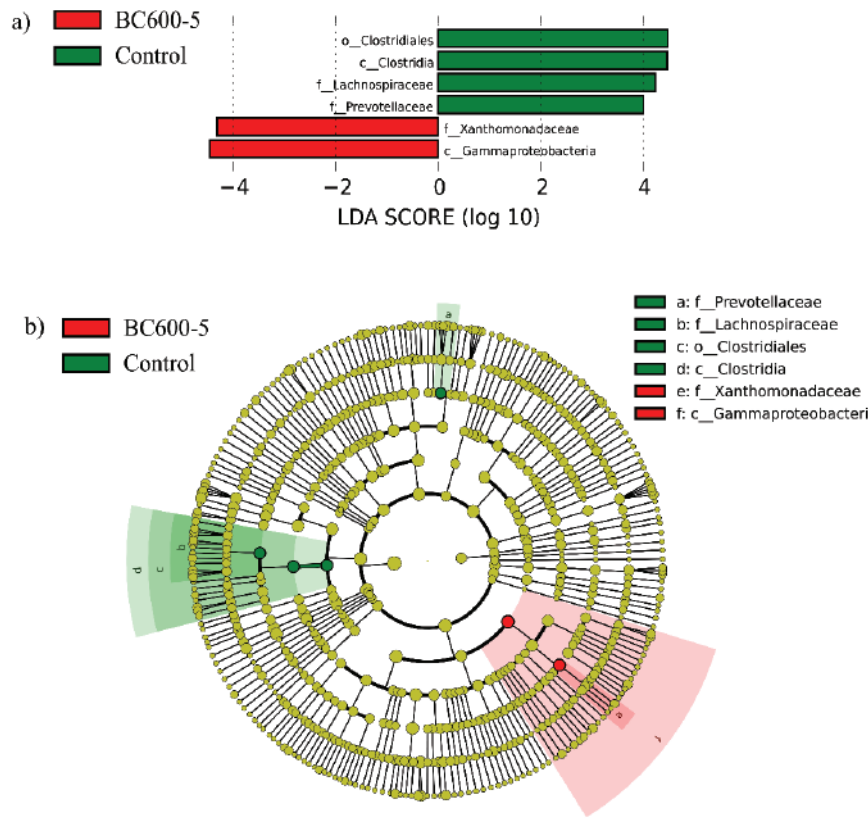

Fig. 3: LEfSe comparison between the control and BC600-5: (a) Effect size of class variations with LDA scores greater than 4, (b) Cladogram of phylogenic distributions based on class.

treatments where BC300-1 and BC600-3 were the most notably different than the control (14.6%) at 22.0% and 23.6%, respectively. *Actinobacteria* and *Chloroflexi* both saw small reductions in relative abundance with the addition of biochar whereas *Bacteroidetes* and *Acidobacteria* saw little to no change. Ahmad et al. (2016b) also reported a similar decrease in *Chloroflexi* and increase in *Proteobacteria* with the addition of soybean and peanut stover-derived biochars. The study conducted by Kolton et al. (2011), on the other hand, saw a significant decrease in *Proteobacteria* and a significant increase in *Bacteroidetes* with the addition of citrus wood biochar. These variances in results are most likely due to different types of biomass, pyrolysis temperatures, and soil types.

The total observed species, diversity indices, richness estimators, and Good's coverage values are shown in Table 2. BC300-3 had the highest number of observed species at 2,767 ± 196 with the control and BC600-3 slightly lower at 2,728 ± 466 and 2,723 ± 132, respectively. The Good's coverage values (0.991-0.996) were all very high indicating the number of sequencing reads was sufficient in covering the full diversity of the samples. The Shannon and Simpson diversity indices showed that BC300-3 had the highest bacterial diversity and that the rest of the biochar treatments were either slightly higher or similar to the control. BC600-5 was shown to have the highest bacterial richness based on Chao1 and ACE richness indices. The bacterial richness of the other treatments were either slightly lower or similar to the control.

Shifts in Microbial Community Based on LEfSe Analysis

LEfSe was used to further analyse the impact of biochar on soil microbial community. The first comparison made was between BC600-5 and the control. The results showed that BC600-5 and the control's variations occurred between not only different classes of bacteria, but different phyla of bacteria (*Proteobacteria*, *Bacteroidetes* and *Firmicutes*,

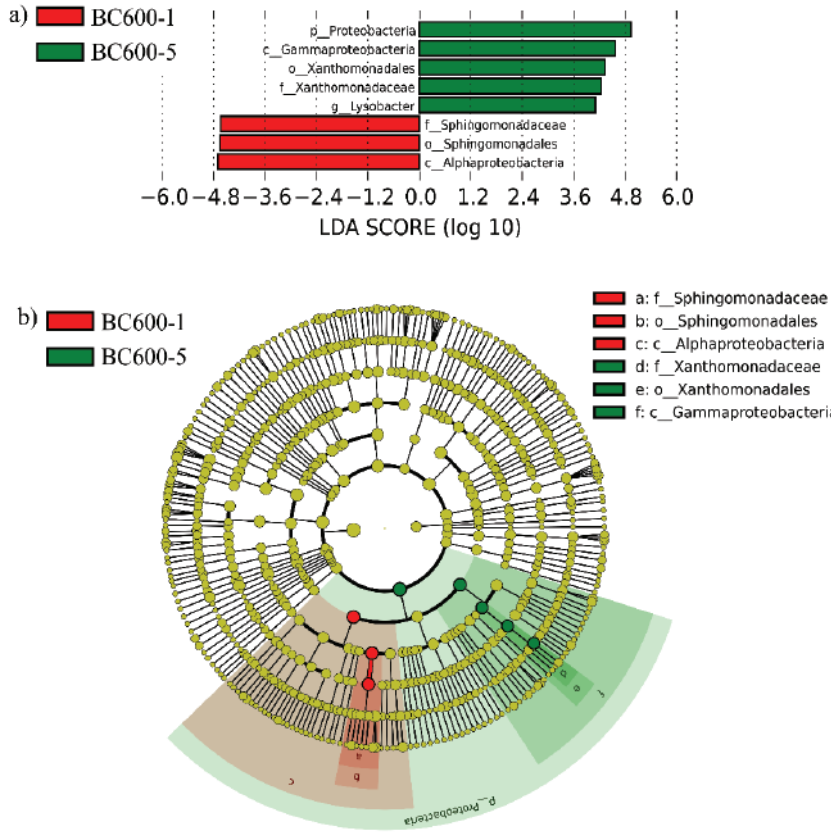

Fig. 4: LEfSe comparison between the BC600-1 and BC600-5: (a) Effect size of class variations with LDA scores greater than 4, (b) Cladogram of phylogenic distributions based on class.

respectively). This again shows that application of biochar, specifically BC600 in this case, led to a shift in the structure of the microbial community. The variations between these two samples can be seen in Fig. 3. The rings in the cladograms (Figs. 3b and 4b) from inside out represent phylogenic level from phylum to species.

The second comparison was made between B600-1 and BC600-5. This was done to compare the variance between two biochar groups when different application rates were used. The variations between these two samples, which are shown in Fig. 4, are from two different classes stemming from the phylum *Proteobacteria*. BC600-1 was associated with bacteria from the class *Alphaproteobacteria* and order *Sphingomonadales*, whereas BC600-5 was associated with bacteria from the class *Gammaproteobacteria* and order *Xanthomonadales*. BC600-5 had the highest relative abundance of bacteria from the genus *Lysobacter* (the relative abundance of each sample can be seen in Fig. 5), which proves significant for a variety of reasons. First, bacteria from the genus *Lysobacter* have been shown to suppress damping-off disease (Islam et al. 2005); a disease which affects a variety of crops including soybeans (Zitnick-Anderson et al. 2014). Second, research has also proven bacteria from this genus can be used as a means of biological control against various soybean fungal diseases (Nian 2015). Third, *Lysobacter* has been found in soybean cyst nematodes and could be used as a potential biocontrol agent against such cysts (Nour et al. 2003). BC300-5 (cladogram not shown) also showed similar

Table 1: Physical and chemical characterization of BC300 and BC600.

	Elemental Composition (%)							
	C	H	S	N	O	Ash (%)	pH	BET Surface Area ($m^2 \cdot g^{-1}$)
BC300	66.43	3.51	0.53	1.58	14.46	13.5	7.87	2.00
BC600	74.23	1.59	0.58	1.46	6.64	15.5	8.42	13.84

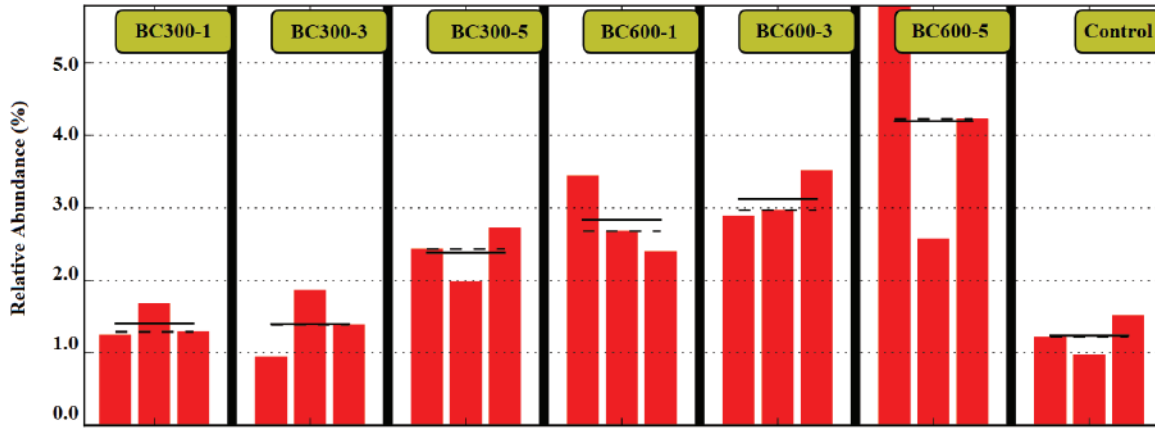

Fig. 5: Relative abundance of bacteria from the genus *Lysobacter* (LEfSe biomarkers).

variations from the control with differences stemming from the class *Proteobacteria*.

The fact that BC600-5 and the control had more variance than BC600-1 and BC600-5 shows that the microbial communities of biochar amended soils were more similar in structure. This also supports the idea that biochar can significantly influence the structure of microbial communities in loess.

Nonmetric Multidimensional Scaling (nMDS) Analysis

nMDS analysis, based on OTU level, showed that biochar addition did cause a statistically significant change in the bacterial community, especially when considering pyrolysis temperature. BC300-1 and BC300-3 were more like the control whereas the other treatments showed more variance. When BC300 and BC600 were added at 5%, there also appeared to be more variance than with 1% and 3% amendments. The nMDS plot grouped by the various biochar treatments can be seen in Fig. 6.

CONCLUSIONS

The results of this study showed that soybean stover-derived biochar caused shifts in the soil microbial community of loess and in some samples led to higher bacterial diversity and richness. Based on LEfSe analysis, BC600 was shown to provide the most suitable habitat for bacteria from the genus *Lysobacter*. The higher BET surface area and pH of BC600 most likely led to changes seen in microbial structure and the increase in the relative abundance of *Lysobacter*.

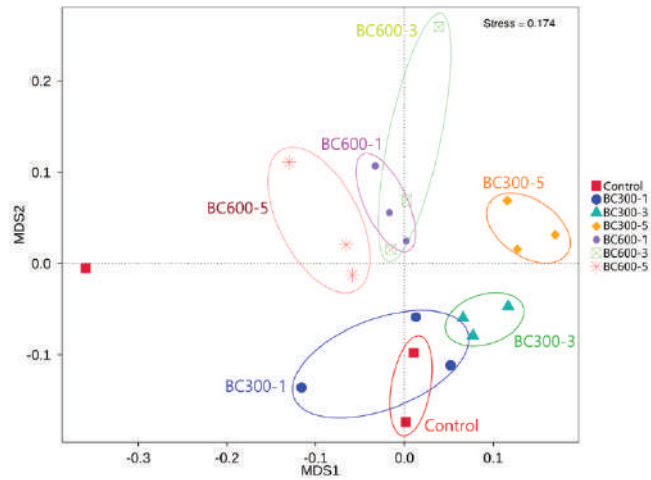

Fig. 6: nMDS plot based on OTU level from soils treated with BC300 and BC600.

Table 2: Summary of sequencing data from soils treated with BC300 and BC600.

	Observed Species	Diversity Index		Richness Estimator		Good's Coverage
		Shannon	Simpson	Chao1	ACE	
Control	2728 ± 466	8.921 ± 1.294	0.983 ± 0.024	2914.12 ± 451.85	2919.43 ± 446.70	0.995 ± 0
BC300-1	2670 ± 135	9.206 ± 0.533	0.992 ± 0.008	2857.47 ± 130.16	2858.73 ± 123.73	0.995 ± 0.001
BC300-3	2767 ± 196	9.529 ± 0.199	0.996 ± 0.001	2954.89 ± 182.25	2955.65 ± 188.26	0.995 ± 0
BC300-5	2562 ± 120	9.29 ± 0.024	0.996 ± 0	2760.80 ± 140.28	2760.87 ± 151.27	0.995 ± 0.001
BC600-1	2667 ± 131	9.103 ± 0.246	0.995 ± 0.001	2881.97 ± 114.87	2891.95 ± 121.17	0.995 ± 0.001
BC600-3	2723 ± 132	9.254 ± 0.042	0.995 ± 0.001	2906.38 ± 153.33	2913.67 ± 144.29	0.995 ± 0.001
BC600-5	2670 ± 267	9.125 ± 0.355	0.995 ± 0.002	3370.22 ± 1077.31	2962.14 ± 401.58	0.994 ± 0.003

Soybean stover-derived biochar should be considered as a soil amendment due to its positive effect on the microbial community in loess.

ACKNOWLEDGEMENT

This work was financially supported by the National Natural Science Foundation of China (51766008, 21467013, 21167007).

REFERENCES

Ahmad, M., Ok, Y. S., Rajapaksha, A. U., Lim, J. E., Kim B-Y., Ahn, J-H., Lee, Y. H., Al-Wabel, M., Lee, S-E. and Lee, S. S. 2016a. Lead and copper immobilization in a shooting range soil using soybean stover- and pine needle-derived biochars: Chemical, microbial and spectroscopic assessments. J. Hazard. Mater., 301(1): 179-186.

Ahmad, M., Ok, Y. S., Kim, B., Ahn, J-H., Lee, Y. H., Zhang, M., Moon, D. H., Al-Wabel, M. I. and Lee, S. S. 2016b. Impact of soybean stover- and pine needle-derived biochars on Pb and As mobility, microbial community, and carbon stability in a contaminated agricultural soil. J. Environ. Manage., 166(1): 131-139.

Anderson, C. R., Condron, L. M., Clough, T. J., Fiers, M., Stewart, A., Hill, R. A. and Sherlock, R. R. 2011. Biochar induced soil microbial community change : Implications for biogeochemical cycling of carbon, nitrogen and phosphorus. Pedobiologia-Int. J. Soil Biol., 54(5-6): 309-320.

Chen, D. and Lu, J. 2012. Low-temperature external-heat potassium dichromate oxidation-photo-colorimetric method for determination of organic carbon in dewatering sludge. Yunnan Chem Technol., (1): 39-42, 50.

Edgar, R. C. 2013. UPARSE: Highly accurate OTU sequences from microbial amplicon reads. Nat. Methods, 10(10): 996-998.

Edgar, R. C., Haas, B. J., Clemente, J. C., Quince, C. and Knight, R. 2011. UCHIME improves sensitivity and speed of chimera detection. Bioinformatics, 27(16): 2194-2200.

Fox, A., Kwapinski, W., Griffiths, B. S. and Schmalenberger, A. 2014. The role of sulfur- and phosphorus-mobilizing bacteria in biochar-induced growth promotion of Lolium perenne. FEMS Microbiol. Ecol., 90(1): 78-91.

Haas, B. J., Gevers, D., Earl, A. M., Feldgarden, M., Ward, D. V., Giannoukos, G., Ciulla, D., Tabbaa, D., Highlander, S. K., Sodergren, E., Methé, B. and DeSantis, T. Z. 2011. Chimeric 16S rRNA sequence formation and detection in Sanger and 454-pyrosequenced PCR amplicons. Genome Res., 21(3): 494-504.

Han, F., Ren, L. and Zhang, X. C. 2016. Effect of biochar on the soil nutrients about different grasslands in the Loess Plateau. Catena, 137: 554-562.

Islam, M. T., Hashidoko, Y., Deora, A., Ito, T. and Tahara, S. 2005. Suppression of damping-off disease in host plants by the rhizoplane bacterium Lysobacter sp. strain SB-K88 is linked to plant colonization and antibiosis against soilborne peronosporomycetes. Appl. Environ. Microbiol., 71(7): 3786-3796.

Khadem, A. and Raiesi, F. 2017. Responses of microbial performance and community to corn biochar in calcareous sandy and clayey soils. Appl. Soil Ecol., 114(1): 16-27.

Kolton, M., Harel, Y. M., Pasternak, Z., Graber, E. R., Elad, Y. and Cytryn, E. 2011. Impact of biochar application to soil on the root-associated bacterial community structure of fully developed greenhouse pepper plants. Appl. Environ. Microbiol., 77(14): 4924-4930.

Kruskal, J. B. 1964. Nonmetric multidimensional scaling: A numerical method. Psychometrika, 29(2): 115-129.

Lehmann, J. and Joseph, S. 2009. Biochar for Environmental Management: An Introduction. Earthscan.

Martin, M. 2011. Cutadapt removes adapter sequences from high-throughput sequencing reads. EMBnet. J., 17(1): 10-12.

Nian J. 2015. Evaluation of Lysobacter Enzymogenes C3 for Control of Soybean Fungal Diseases. University of Illinois at Urbana-Champaign.

Nour, M. S., Lawrence, J. R., Zhu, H., Swerhone, G. D. W., Welsh, M., Welacky, T. W. and Topp, E. 2003. Bacteria associated with cysts of the soybean cyst nematode (Heterodera glycines). Appl. Environ. Microbiol., 69(1): 607-615.

Prasad, M., Tzortzakis, N. and McDaniel, N. 2018. Chemical characterization of biochar and assessment of the nutrient dynamics by means of preliminary plant growth tests. J. Environ. Manage., 216: 89-95.

Quast, C., Pruesse, E., Yilmaz P, Gerken, J., Schweer, T., Yarza, P., Peplies, J. and Glöckner, F. O. 2013. The SILVA ribosomal RNA gene database project: Improved data processing and web-based tools. Nucleic Acids Res., 41(D1): D590-D596.

Segata N, Izard J, Waldron L, Gevers, D., Miropolsky, L., Garrett, W. S. and Huttenhower, C. 2011. Metagenomic biomarker discovery and explanation. Genome Biol., 12(6): R60.

Verheijen, F., Jeffery, S., Bastos, A. C., Velde, M. van der and Diafas, I. 2010. Biochar Application to Soils - A Critical Scientific Review of Effects on Soil Properties, Processes and Functions. European Commission.

Windeatt, J. H., Ross, A. B., Williams, P. T., Forster, P. M., Nahil, M. A. and Singh, S. 2014. Characteristics of biochars from crop residues: Potential for carbon sequestration and soil amendment. J. Environ. Manage., 146(1): 189-197.

Yao, Q., Liu, J., Yu, Z, Li, Y., Jin, J., Liu, X. and Wang, G. 2017. Changes of bacterial community compositions after three years of biochar application in a black soil of northeast China. Appl. Soil Ecol., 113(1): 11-21.

Zhou, Z., Gao. T., Zhu, Q., Yan, T., Li, D., Xue, J. and Wu, Y. 2019. Increases

in bacterial community network complexity induced by biochar-based fertilizer amendments to karst calcareous soil. Geoderma, 337: 691-700.
Zhu, L., Xiao, Q., Cheng, H., Shi, B., Shen, Y. and Li, S. 2017a. Seasonal dynamics of soil microbial activity after biochar addition in a dryland maize field in North-Western China. Ecol. Eng., 104(1): 141-149.
Zhu, L., Xiao, Q., Shen, Y. and Li, S. 2017b. Microbial functional diversity responses to 2 years since biochar application in silt-loam soils on the Loess Plateau. Ecotoxicol. Environ. Saf., 144: 578-584.
Zitnick-Anderson, K., Markell, S. and Nelson, Jr. B. 2014. Pythium Damping-off of Soybean. North Dakota State University.

Nature Environment and Pollution Technology
An International Quarterly Scientific Journal

p-ISSN: 0972-6268
(Print copies up to 2016)
e-ISSN: 2395-3454

Vol. 19 | No. 2 | pp. 711-719 | 2020

Original Research Paper

https://doi.org/10.46488/NEPT.2020.v19i02.026

Open Access Journal

Caffeine Residue in Terengganu River Basins in Malaysia: Distribution and Risk Assessment

Wan Mohd Afiq Wan Mohd Khalik*(**)†, Saw Hong Loh*, Haslina Albani*, Siti Aisyah Syazwani Alias* and Khaeriah Ulfah Rahman*

*Faculty of Science and Marine Environment, Universiti Malaysia Terengganu, 21030, Kuala Nerus, Malaysia
**Centre for Water Research and Analysis, Faculty of Science and Technology, Universiti Kebangsaan Malaysia, 43600, Bangi, Malaysia
†Corresponding author: Wan Mohd Afiq Wan Mohd Khalik; wan.afiq@umt.edu.my

Nat. Env. & Poll. Tech.
Website: www.neptjournal.com

Received: 09-06-2019
Accepted: 30-08-2019

Key Words:
Emerging contaminant;
Stimulant drug;
Risk quotient;
Pharmaceutical residue

ABSTRACT

The occurrence of caffeine residue in Malaysian waters was successfully studied. The micropollutant abundance was recorded for three selected main rivers namely Terengganu, Ibai and Setiu which are located in Terengganu, Peninsular Malaysia. Surface water samples were taken twice in September and November 2018 from 15 sampling stations. Caffeine residue was determined using the solid phase extraction technique followed by a final analysis using a high performance liquid chromatography-UV detector. Measured concentration levels ranged from 384 to 426 ng/L for both datasets obtained from the two sampling surveys. The ecological risk assessment was calculated to be at low risk ranging from RQ 0.075 to 0.085, while the risk quotients (RQ) of human health risk was recorded below than 0.20 for three life-stage categories. The MaxRI values fall under class II which means that there is a risk of sublethal effects to aquatic organisms.

INTRODUCTION

Caffeine is classified as a non-prescription stimulant and psychoactive substance. The global average consumption of caffeine is estimated to be in the range of 80 to 400 mg per person per day. Humans excrete approximately 0.5 to 10% of unchanged caffeine through urine and faeces (Edward et al. 2015). The main sources of caffeine in environmental waters are primarily anthropogenic and are often detected in wastewater. Caffeine has high solubility (13.5 $g.L^{-1}$) but negligible volatility in water. It has gained attention since its presence in environmental waters is ubiquitous, human-related, source-specific and released in significant quantities. Caffeine has thus become suitable as a chemical marker for river and groundwater pollution; this fact has been well-documented in past literature (Buerge et al. 2003, Ferreira 2005, Wu et al. 2008, Yang et al. 2017). Caffeine has a half-life of 30 days in natural environments and up to 100 days in estuarine waters (Cantwell et al. 2016).

The possibility of chronic or acute toxicity in aquatic organisms due to long-term exposure to pharmaceutically active compounds, including caffeine has become of great concern. The risk quotient (RQ) is a mathematical approach to express the ecological risk of a stressor in the environment at low-level concentrations (Ramaswamy et al. 2011, Guzel et al. 2018). In terms of risk to human health, the quotient value is associated with the level of human exposure to contaminated water. The calculation may express the posed threat of a single or a mixture of contaminants. The interpolated data is then scaled into a numerical range; the common rule is RQ> 1 which signifies the high potential of environmental risk.

To calculate the ecological risk or human health risk from contaminants like caffeine, the baseline data are designated as latent information. However, there is limited documentation on the distribution and risk assessment of caffeine reported in Malaysian rivers. Only two previous studies have performed a risk assessment in west Peninsular Malaysia, namely the Lui River and Selangor River (Praveena et al. 2018) and the Klang River (Subari et al. 2017). To date, no scientific document on pharmaceutical residue has been reported for the east coast of Peninsular Malaysia. Indeed, this research work takes the initiative to report the existence of pharmaceutical residue in Terengganu rivers by using caffeine as the subject of study. As caffeine may pose ecotoxicological and human health risks, the RQ analysis was performed to assess the potential environmental risk on both aquatic organisms living underwater and humans who use these rivers as their source of drinking water.

MATERIALS AND METHODS

Chemical

Highly pure caffeine was purchased from Sigma-Aldrich in

St Louis. The standard solution was dissolved in methanol solution to construct a series of working solutions. Liquid chromatography grade solvents (acetone, methanol, methyl tert-butyl ether) were used for sample preparation and analysis.

Study Area

This study chose to focus on Terengganu, one of the states located in Peninsular Malaysia. Terengganu is located in the east coast region and is adjacent to Kelantan and Pahang on its northern and southern sides, respectively. The Terengganu River and Ibai River are situated in Kuala Terengganu (Laila et al. 2018). Both rivers flow through Terengganu's main capital where many major developments close to the coastal zone are located. Domestic industries and human settlements are the major activities located close to the Terengganu and Ibai Rivers (Suratman et al. 2015). Meanwhile, the Setiu River is situated in Setiu which is a district in the northern part of Terengganu. It is considered as a rural area; thus, water from the river plays a significant role in the livelihood of the population as their source of water for daily use, aquaculture and agriculture (Zaideen et al. 2017).

Sampling Activity

Water samples were taken twice in September and November 2018. Fifteen sampling stations were designated as locations to study the anthropogenic impact of the nearby riverine systems. The coordinates for each station were taken using a handheld GPS and tabulated in Table 1 and Fig. 1, respectively. 1-L grab surface water samples were taken using high-density polyethylene (HDPE) bottles. Separate water samples were also collected in 500-mL quantities for physicochemical water analysis (ammoniacal-nitrogen, biochemical oxygen demand, and suspended solids). The rinsed bottles were submerged below the water surface and filled up to full capacity before immediately capped underwater and kept in a cooler until ready for analysis. In-situ parameters namely pH, dissolved oxygen, temperature, salinity and conductivity were recorded using a YSI 660 hydrolab multiparameter.

Laboratory Analysis

Caffeine residue was extracted using the solid phase extraction technique, Oasis HLB cartridge 500 mg 6 cc (Waters, Milford). The procedure for caffeine analysis was adapted from the researchers' previous method (Al-Qaim et al. 2017). Samples were pre-filtered using a GF/C glass microfiber filter 0.7-µm (Whatman, Buckinghamshire) to remove the suspended matter. The cartridges were conditioned with 2-mL methyl tert-butyl ether, 2-mL methanol and 2-mL deionised water, respectively. 250-mL water samples were loaded continuously at a controlled flow rate of 2.0 $mL.min^{-1}$ using the vacuum system. The cartridges were later washed using 2-mL deionised water. The enrich sample was extracted

Table 1: The coordinates of sampling location in Terengganu rivers, Malaysia.

River	Station Code	Latitude (N)	Longitude (E)
Ibai	S1-Ibai	5°17'03.3"	103°10'13.5"
	S2-Ibai	5°16'43.9"	103°10'06.0"
	S3-Ibai	5°16'38.0"	103°09'20.6"
	S4-Ibai	5°16'11.4"	103°08'59.4"
	S5-Ibai	5°16'49.3"	103°08'31.2"
Setiu	S1-Setiu	5°38'26.6"	102°46'32.6"
	S2-Setiu	5°36'50.2"	102°48'22.1"
	S3-Setiu	5°36'14.9"	102°48'52.8"
	S4-Setiu	5°35'14.1"	102°46'42.3"
	S5-Setiu	5°34'45.2"	102°46'09.8"
Terengganu	S1-Terengganu	5°19'22.8"	103°07'27.4"
	S2-Terengganu	5°19'24.4"	103°06'58.6"
	S3-Terengganu	5°19'26.5"	103°05'58.8"
	S4-Terengganu	5°17'55.3"	103°05'14.6"
	S5-Terengganu	5°17'15.9"	103°05'40.6"

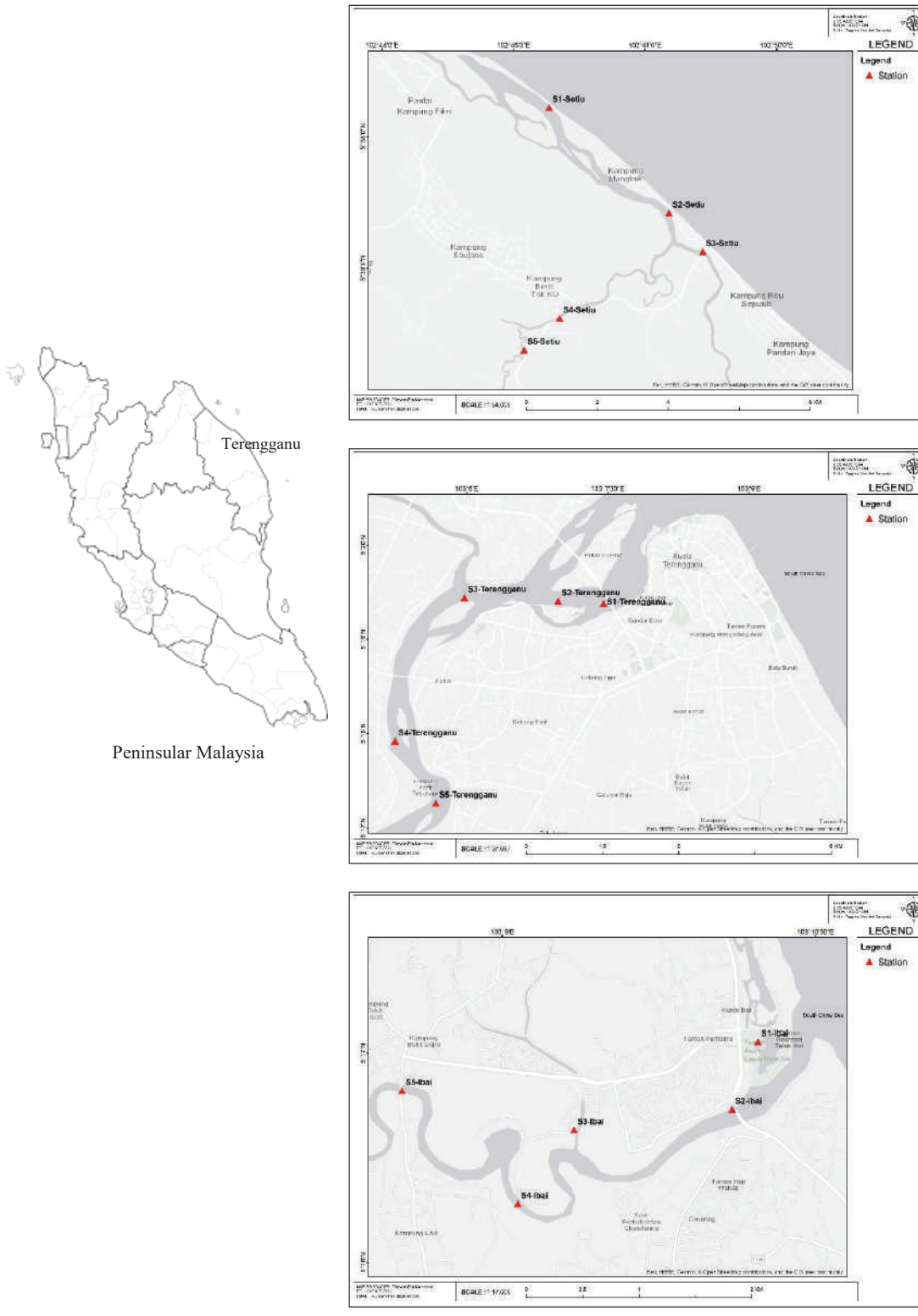

Fig. 1: The map of sampling stations located in Terengganu, Malaysia.

from the sorbent using 2-mL methyl tert-butyl ether, 2-mL acetone and 3-mL methanol, respectively. Later, the solution was concentrated in a vacuum concentrator till a final volume of 1-mL was obtained.

Before chromatographic analysis, the sample extracts were filtered through a 0.45-µm nylon syringe filter. The final extracts were analysed using a High Performance Liquid Chromatography-UV detector (Shimadzu, Kyoto) equipped with an Apollo C_{18} (250 mm × 4.6 mm, 5 µm) GraceTM column. The mobile phase composition is methanol and deionised water at a ratio of 65:35 in the isocratic mode. The flow rate was controlled at 1.5 mL.min^{-1}. The wavelength for caffeine compound was set at 273 nm. The retention time for caffeine was achieved at 3.0 minutes with a total runtime of 4 minutes. The injection loop of the sample was 20-µL for every injection. Quantitative analyses were performed using external calibration standards. The calibration graph was constructed using concentration levels ranging from 0.1 ng.mL^{-1} – 1 µg.mL^{-1} (r^2=0.996). The instrument detection limit was 0.014 ng.mL^{-1}.

The identification of caffeine in river waters was also conducted using gas chromatography-mass spectrometry. One sample from each river was used as representative of the total samples. The settings selected for the gas chromatography are as follows: injection temperature and detector at 250 and 220°C respectively; oven programme maintained at 200°C for 1.5 minutes, then ramped at 30°C/minutes to 275°C, column flow was 1 mL min^{-1}; retention time and run time analysis are 7.24 and 13.4 minutes, respectively; and mass range was scanned from 50 to 300 m/z. The extracted mass chromatogram of caffeine was 194 m/z as elucidated from the NIST11 library.

The level of ammoniacal nitrogen was determined using the 4500-NH_3 phenate method, while the final analysis was carried out using a Carry 50 UV-Vis spectrophotometer (Varian, Palo Alto). The peak spectra were recorded at 640 nm and the scan rate was controlled at 10 nm s^{-1}. The ammonia reacted with phenol to form indophenol in the presence of an alkali and an oxidising agent. Sodium nitroprusside served as a catalyst. The total suspended solids were calculated using the gravimetric method. The 500-mL water samples were filtered through a 0.7 µm glass fibre filter (Whatman, Buckinghamshire). The filter was dried at 102°C till a constant weight was obtained. The weight difference between the dry filter after filtering and the clean filter was expressed as the weight of the suspended solids.

Statistical Analysis

Statistical analyses were conducted using Minitab Version 17.0 (Minitab Inc., Pennsylvania) to identify the significant differences and relationship between caffeine and water quality. In this work, the hierarchal cluster analysis was implemented using Ward's hierarchical agglomerative method of clustering and Euclidean distance measure to analyse the relationship between caffeine and water quality of the studied rivers.

The risk quotient (RQ) was used to assess the ecological risk of caffeine in the selected Terengganu rivers. The equation is expressed as follows:

$$RQ_{MEC} = \frac{MEC}{PNEC} \quad \ldots(1)$$

Where, *MEC* is the measured environmental concentration and *PNEC* is the predicted no-effect concentration. The lowest *PNEC* value for caffeine in water was obtained from literature, 5000 ng.L^{-1} (He et al. 2018). The RQ measure was scaled as follows: > 1.0 (high), 0.1-1.0 (medium), and 0.01-0.1 (low).

For human health, the risk assessment was calculated as the worst-case scenario if the water was used as a source of drinking water. The formula used is expressed as Equation 2 below:

$$RQ = \frac{MC}{DWEL} \quad \ldots(2)$$

Where, *MC* is defined as the maximum measured concentration and *DWEL* is the age-dependent drinking water equivalent level. *DWEL* was estimated for three age categories using the formula expressed below:

$$DWEL = \frac{ADI\ X\ BW}{DWI\ X\ AB\ X\ FOE} \quad \ldots(3)$$

Where, *ADI* is the average daily intake (µg/kg/day). The value for ADI of caffeine (150) was adopted from literature. *BW* is the median body weight (kg) of the age-specific groups. *DWI* is the daily drinking water intake (L/day) of the age-specific groups. *AB* is the gastrointestinal absorption rate, which was assumed to be 1, while *FOE* is the frequency of exposure which was put as 365 days (Sharma et al. 2018). The method reporting limit was calculated at 21.20 µg.L^{-1}.

The risk index was calculated using Equation 4 as expressed below:

$$[\sum_{i=1}^{n}(Toxj,k \div MECj,k)i]\text{x } 0.1 \quad \ldots(4)$$

Where, *i* is defined as selected pharmaceutically active compounds, *j* is sampling site, *k* is sampling date, and *Tox j,k* is acute toxicity for pharmaceutically active compounds (Fernández et al. 2010). In this case, the compound refers to the measured total concentration of caffeine.

Table 2: Physico-chemical data of water quality recorded in Terengganu rivers.

Parameter	Terengganu River		Ibai River		Setiu River	
	Range	Mean	Range	Mean	Range	Mean
Water pH	6.23-6.90	6.58±0.22	6.01-7.53	6.83±0.50	4.04-7.89	5.79±1.07
Water temperature	19.50-29.40	25.47±4.28	22.70-29.20	26.10±3.15	28.60-29.80	29.81±0.50
Dissolved oxygen	6.55-8.19	7.31±0.59	1.90-7.12	5.11±1.50	5.20-7.06	6.56±0.54
Suspended solids	12.01-84.40	46.12±22.28	16.80-70.80	39.84±19.25	18.00-54.80	39.44±13.09
Biochemical oxygen demand	1.84-5.04	3.14±1.02	3.65-5.59	4.76±0.86	4.85-7.01	6.41±0.71
Ammoniacal nitrogen	0.01-0.20	0.07±0.06	0.03-0.16	0.06±0.03	0.02-0.16	0.05±0.04

Unit expressed as $mg.L^{-1}$ except for temperature (°C)

RESULTS AND DISCUSSION

Water Chemistry

The pH values of the river waters were recorded to have acidic characteristics. This fact is not only recorded in this study, but the trend has been well-documented in past literature for all rivers studied. For example, studies conducted by Suratman et al. (2015) and Laila et al. (2018) recorded pH values of less than 7 with mean values of 6.37 and 6.62 for Terengganu River and Ibai River, respectively. The level of dissolved oxygen content in upstream locations was found to be higher compared to downstream areas. It is believed that the anthropogenic input from development works in downstream areas have caused this situation. The Terengganu river revealed higher organic content present in comparison to the Ibai River and Setiu River. This pattern has been predicted on the back of the high level of urbanisation in this area which has caused more pollutants to be introduced into the river basin. In line with this finding, the biochemical oxygen demand recorded in a past study was below 5 $mg.L^{-1}$ for the Ibai River as documented by Suratman et al. (2005) in a field survey conducted from August to December 2003.

Suspended solids were recorded highest for the Terengganu river, followed by the Ibai and Setiu Rivers (Table 2). A similar pattern was observed for ammonia concentration during the period of study. No drastic input into the Terengganu river basin was recorded; this result is in line with the low concentrations recorded in past literature with a mean value of 0.065±0.038 $mg.L^{-1}$ (Suratman et al. 2015). This goes similarly with ammonia concentration where 0.04 to 0.24 $mg.L^{-1}$ recorded in 2011 by Zaideen et al. (2017) for the Terengganu River. In the researchers' study, the ammonia concentration was measured to be in the range of 0.01 to 0.20 $mg.L^{-1}$. A similar finding of 0.01 to 3.4 $mg.L^{-1}$ was reported by Laila et al. (2018) for the Ibai River.

Concentration Levels of Caffeine

Caffeine was detected in all 30 (100%) samples collected during the period of study. The concentration levels of caffeine in Terengganu ranged from 384-406 $ng.L^{-1}$ and 404-422

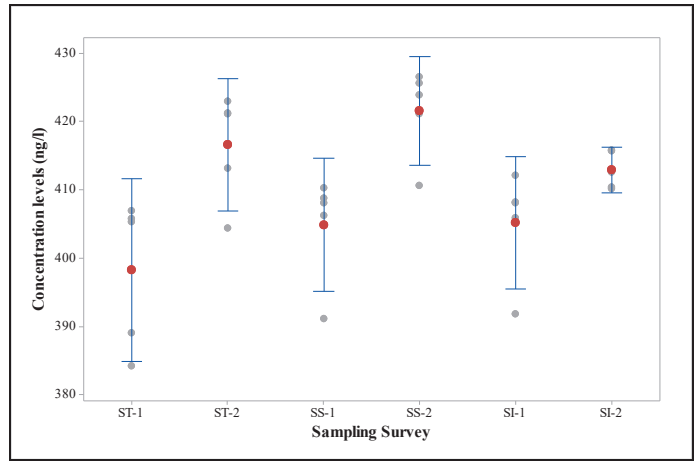

Fig. 2: Concentration range of caffeine residue found in rivers water. Red colour represents the median concentration.

ng.L^{-1} for the first and second sampling surveys, respectively. Caffeine levels were found in the Setiu River to range from 391-410 ng.L^{-1} and 410-426 ng.L^{-1} for both sampling surveys. Meanwhile, the concentration of caffeine in the Ibai River was recorded to be in the range of 391-412 ng.L^{-1} and 410-415 ng.L^{-1} for both sampling surveys (Fig. 2). The t-test revealed that the concentration levels found between the two surveys were significantly different, $p<0.05$. This gave the idea that the anthropogenic input introduced into the riverine system has dynamic variations. Past studies by Al-Qaim et al. (2014) and Al-Qaim et al. (2015) mentioned that caffeine is one of the studied analytes with the highest concentration in Malaysia. However, the concentration of caffeine found in the Terengganu river was much lower than rivers situated in Negeri Sembilan (1644 ng.L^{-1}) and Selangor (351 ng.L^{-1}). The continuous inflow of human domestic waste into the river has led to higher concentration levels, especially in areas with a high density of human settlements.

Based on the cluster analysis, the samples were grouped into two clusters at $(D_{link}/D_{max}) \times 100 < 0.90$. The formation of cluster SI-2 is believed to be due to a small range of concentration levels recorded during the second sampling programme (Fig. 3). The Ibai River basin is smaller than the other two rivers, thus it was believed that its dilution factor is weaker and thus, its concentration levels are rigid at a small range of variation. It can be observed that the concentration levels of caffeine residue vary for the other riverine systems (Fig. 2). The rain had occurred a day before the first sampling, thus it is believed that the river water was relatively diluted when the samples were taken. For the Setiu River, the similarity between both sampling surveys is high; this is believed to be due to the existence of the main source of contaminants which is human settlements which remained constant during the sampling event; additionally, no drastic new input had occurred.

Risk Assessment

An assessment of the RQs on the surface waters of the three rivers was conducted. The RQ values were calculated from the acute and chronic toxicity data for two trophic levels, namely *Daphnia magna* and *Pseudokirchneriella subcapitata*. The RQ values recorded ranged from 0.075 to 0.085 (Fig. 4). The findings revealed that the quality of surface waters has been affected by the emergence of caffeine; however, the risk of contamination had remained low. Hence, the contaminant has a minor influence on the ecological environment.

Despite its high frequency of detection in these river waters, caffeine has proven in past studies to only pose a low risk to the surrounding environment. For instance, a preliminary risk assessment on Brazilian surface waters revealed that the ecological risk remained low even with the high levels of detection in 175 samples (Sodre et al. 2018). The low risk status was also recorded for urban rivers in China. Although high concentration levels were recorded at 66-8571 ng.L^{-1}, the RQ value calculated at 0.02 was far below the moderate risk level (Zhou et al. 2016). Low ecological risk of caffeine in the range of < 0.01 to 0.07 in the Tama River and its tributaries was also recorded. The study had used this level to determine its toxicity value toward an alga species, *Pseudokirchneriella subcapitata* (Mano & Okamoto 2016). In contrary, a high ecological risk of caffeine was measured in the Sinos River basin, Brazil where 5 out of 34 samples indicated RQ > 1 toward the same species used in this study (Peteffi et al. 2018). Meanwhile, the medium risk

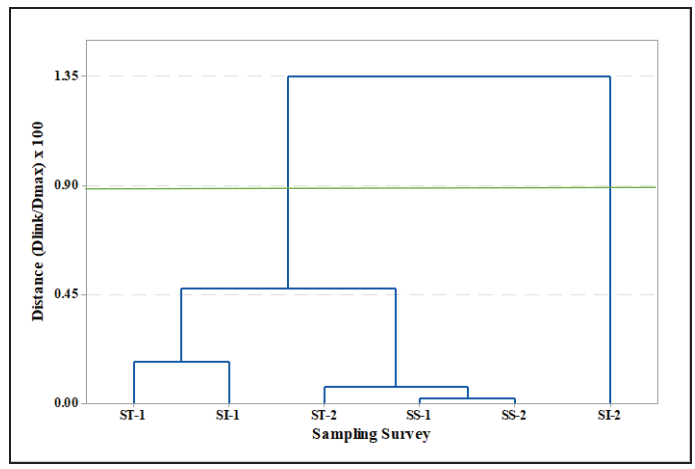

Fig. 3: Dendrogram of clustering the temporal similarities.

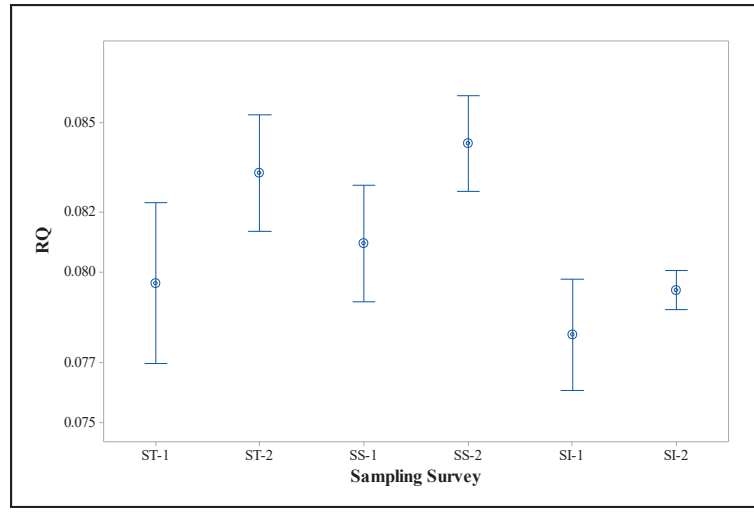

Fig. 4: Risk quotient of ecological assessment based on caffeine concentrations.

was reported in a study carried out by Komori et al. (2013) which dealt with environmental samples from rivers in Japan. The RQs calculated for caffeine present in the Terengganu rivers are not much different from other studies which also suggested a low chance of ecological impact for many pharmaceuticals based on acute toxicity tests. However, it is important to note that assessment of pharmaceutical residue using single compounds does not explain the real situation of environmental water health.

For human health risks, the RQs ranged from 0.19 to 0.20 for infants, 0.102 to 0.105 for children, and 0.093 to 0.097 for adults (Fig. 5). The DWEL values were calculated to be at 2120.53 $\mu g.L^{-1}$ (infant), 4007.05 $\mu g.L^{-1}$ (children), and 4398.3 $\mu g.L^{-1}$ (adult), respectively. In the present findings, the calculated RQ value of ≤0.2 is considered to unlikely pose a risk to human health through water consumption. The RQ level for infants was at least 2.0 times greater than the RQ levels for adults. Similar patterns were reported in the literature, although the RQ values had varied depending on the concentration levels of caffeine (de Jesus Gaffney et al. 2015). Yang et al. (2017) found that infant exposure was recorded to be four times higher compared to adults; this was linked to infants' lower body weight. Although the finding of this study showed that the concentration levels posed no appreciable concern to human health, it, however, had only taken into account a single contaminant. Therefore, the water

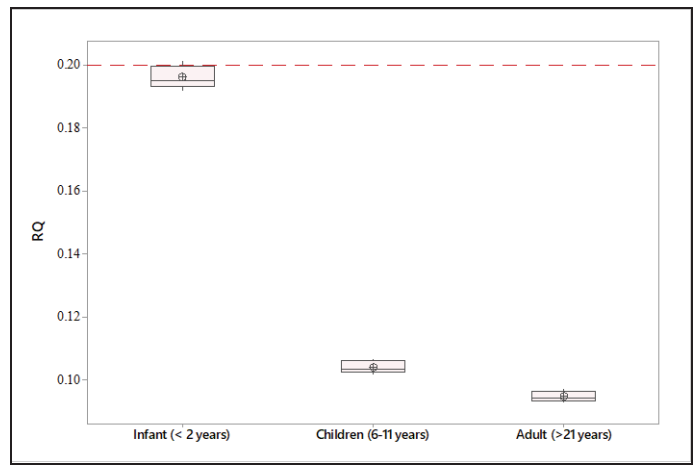

Fig. 5: Risk quotient of caffeine concentrations toward three life stages.

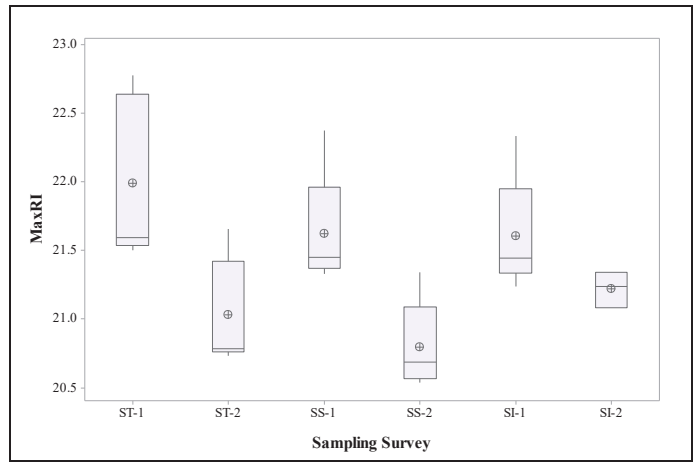

Fig. 6: MaxRI values of caffeine contamination in three Terengganu riverine systems.

quality as affected by contaminants is expected to be higher when pharmaceutical residues as a mixture are taken into consideration. Additional risks may be exhibited due to the presence of transformation products.

All sampling sites recorded MaxRI values (21.08-22.33) which fall under class II or the risk of sublethal effects to aquatic organisms (classified as ranging from 10<MaxRI<100) (Fig. 6). It is noteworthy to highlight here that the risk levels have the potential to increase when more input is introduced into the river system. Continuous discharge from anthropogenic sources into environmental waters will constantly replenish contaminant levels regardless of the amount of degraded caffeine, therefore creating a dynamic equilibrium. The results for the caffeine risk potential were lower than the one obtained in previous research conducted on the Henares-Jarama-Tajo river in Spain which recorded a MaxRI <10 (Fernández et al. 2010). However, a similar class to this research study results was reported by Letić et al. (2015) for the Danube River in Serbia. MaxRI values reported by authors ranged from 20.27-71.66.

CONCLUSION

This is the first scientific study that provides an estimation of both health and ecological risks associated with caffeine abundance in the river waters of Malaysia. The assessment on the ecological impact revealed that the emergence of caffeine residue in river waters have yet to cause acute toxicity towards aquatic organisms. In the case of river water used for human consumption, it has also proven unlikely to pose a risk on human health. The three rivers were grouped under class II for the maximum risk index. Although the occurrence of a single contaminant has been successfully evaluated, the real situation must take into account the presence of other pharmaceutical residues as a mixture of compounds. The present findings provide a good baseline data for further studies on contaminants of emerging concern since caffeine is frequently detected in Malaysian environmental waters.

ACKNOWLEDGEMENTS

The authors would like to thank Universiti Malaysia Terengganu for its financial support for the study under the analytical and environmental chemistry programme.

REFERENCES

Al-Qaim, F. F., Abdullah, M. P., Othman, M. R., Latip, J. and Afiq, W. 2014. A validation method development for simultaneous LC-ESI-TOF/MS analysis of some pharmaceuticals in Tangkas river-Malaysia. J. Brazil Chem. Soc., 25(2): 271-281.

Al-Qaim, F. F., Abdullah, M. P., Othman, M. R., Mussa, Z. H., Zakaria, Z., Latip, J. and Afiq, W. M. 2015. Investigation of the environmental transport of human pharmaceuticals to surface water: A case study of persistence of pharmaceuticals in effluent of sewage treatment plants and hospitals in Malaysia. J. Brazil Chem. Soc., 26(6): 1124-1135.

Al-Qaim, F. F., Jusof, S. H., Abdullah, M. P., Mussa, Z. H., Tahrim, N. A., Khalik, W. M. A. W. M. and Othman, M.R. 2017. Determination of caffeine in surface water using solid phase extraction and high performance liquid chromatography. Malays. J. Anal. Sci., 21(1): 95-104.

Buerge, I. J., Poiger, T, Müller, M. D. and Buser, H. R. 2003. Caffeine, an anthropogenic marker for wastewater contamination of surface waters. Environ. Sci. Tech., 37: 691-700.

Cantwell, M. G, Katz, D. R, Sullivan, J. C, Borci, T. and Chen, R. F 2016. Caffeine in Boston Harbor past and present, assessing its utility as a tracer of wastewater contamination in an urban estuary. Mar. Pollut. Bull., 108: 321-324.

de Jesus Gaffney, V., Almeida, C. M., Rodrigues, A., Ferreira, E., Benoliel, M. J. and Cardoso, V. V. 2015. Occurrence of pharmaceuticals in a water supply system and related human health risk assessment. Water Res., 72: 199-208.

Edwards, Q. A., Sergei, M. Kulikov and Leah D. Garner-O'Neale 2015. Caffeine in surface and wastewaters in Barbados, West Indies. SpringerPlus, 4.1: 57.

Fernández, C., González-Doncel, M., Pro, J., Carbonell, G. and Tarazona, J. V. 2010. Occurrence of pharmaceutically active compounds in surface waters of the Henares-Jarama-Tajo river system (Madrid, Spain) and a potential risk characterization. Sci. Total Environ., 408(3): 543-551.

Ferreira, A. P. 2005. Caffeine as an environmental indicator for assessing urban aquatic ecosystems. Cad Saúde Pública., 21: 1884-1892.

Guzel, E.Y., Cevik, F. and Daglioglu, N. 2018. Determination of pharmaceutical active compounds in Ceyhan River, Turkey: Seasonal, spatial variations and environmental risk assessment. Hum. Ecol. Risk Assess., 1-16.

He, K., Echigo, S., Asada, Y. and Itoh, S. 2018. Determination of caffeine and its metabolites in wastewater treatment plants using solid-phase extraction and liquid chromatography-tandem mass spectrometry. Anal. Sci., 34(3): 349-354.

Komori, K., Suzuki, Y., Minamiyama, M. and Harada, A. 2013. Occurrence of selected pharmaceuticals in river water in Japan and assessment of their environmental risk. Environ. Monit. Assess., 185: 4529-4536.

Laila, O. M. A, Gasim, M. B., Toriman, M. E. and Hassa, M. A. A. 2018. The assessment of physico-chemical and biological water quality characteristics of the Ibai River between wet and dry seasons, Kuala Terengganu, Malaysia. J. Fundam. Appl. Sci., 10: 396-411.

Letić, N. N. G., Milanović, M. L., Milić, N. B., Miloradov, M. B. V., Radonić, J. R., Mihajlović, I. J. and Sekulić, M. M. T. 2015. Determination of emerging substances in the Danube and potential risk evaluation. CLEAN Soil Air Water, 43(5): 731-738.

Mano, H. and Okamoto, S. 2016. Preliminary ecological risk assessment of 10 PPCPs and their contributions to the toxicity of concentrated surface water on an algal species in the middle basin of Tama River. J. Water Environ. Tech., 14: 423-436.

Peteffi, G.P, Fleck, J.D., Kael, I.M., Rosa, D.C., Antunes, M.V. and Linden, R. 2018. Ecotoxicological risk assessment due to the presence of bisphenol A and caffeine in surface waters in the Sinos River Basin-Rio Grande do Sul-Brazil. Brazil J. Bio., 712-721.

Praveena, S.M, Shaifuddin, S.N.M, Sukiman, S., Nasir, F.A.M, Hanafi, Z., Kamarudin, N. and Aris A.Z. 2018. Pharmaceuticals residues in selected tropical surface water bodies from Selangor (Malaysia): Occurrence and potential risk assessments. Sci. Total Environ., 642: 230-240.

Ramaswamy, B.R., Shanmugam, G., Velu, G., Rengarajan, B. and Larsson, D. J 2011. GC-MS analysis and ecotoxicological risk assessment of triclosan, carbamazepine and parabens in Indian rivers. J. Hazard. Mater., 186: 1586-1593.

Sharma, B.M., Bečanová, J., Scheringer, M., Sharma, A., Bharat, G.K., Whitehead, P.G. and Nizzetto, L. 2019. Health and ecological risk assessment of emerging contaminants (pharmaceuticals, personal care products, and artificial sweeteners) in surface and groundwater (drinking water) in the Ganges River Basin, India. Sci. Total Environ., 646: 1459-1467.

Sodre, F. F., Santana, J. S., Sampaio, T. R. and Brandão, C. 2018. Seasonal and spatial distribution of caffeine, atrazine, atenolol and DEET in surface and drinking waters from the Brazilian Federal District. J. Brazil Chem. Soc., 29(9): 1854-1865.

Subari, S. N. M, Osman, R. and Saim, N. 2017. Occurrence, source apportionment and environmental risk assessment of pharmaceuticals in Klang River, Malaysia. Pertanika J. Sci. Technol., 25: 119-128.

Suratman, S., Ali, A. and Lo, T. T. 2005. Determination of water quality index at Ibai River basin, Terengganu. Sains. Malays., 34: 55-59.

Suratman, S., Sailan, M. M, Hee, Y. Y, Bedurus, E. A. and Latif, M. T. 2015. A preliminary study of water quality index in Terengganu River basin, Malaysia. Sains. Malays., 44: 67-73.

Wu, J., Yue, J., Hu, R., Yang, Z. and Zhang L. 2008. Use of caffeine and human pharmaceutical compounds to identify sewage contamination. World Acad. Sci. Eng. Technol., 44: 438-442.

Yang, Y. Y., Toor, G. S., Wilson, P. C. and Williams, C. F. 2017. Micropollutants in groundwater from septic systems: Transformations, transport mechanisms, and human health risk assessment. Water Res., 123: 258-267.

Zaideen, I. M. M., Suratman, S. and Tahir, N. M. 2017. The evaluation of spatial variation of water quality in Sungai Setiu Basin, Terengganu. Sains. Malays., 46: 1513-1520.

Zhou, H., Ying, T., Wang, X. and Liu, J. 2016. Occurrence and preliminarily environmental risk assessment of selected pharmaceuticals in the urban rivers, China. Sci. Rep., 6: 34928.

Nature Environment and Pollution Technology
An International Quarterly Scientific Journal

p-ISSN: 0972-6268
(Print copies up to 2016)
e-ISSN: 2395-3454

Vol. 19 | No. 2 | pp. 721-728 | 2020

Original Research Paper

https://doi.org/10.46488/NEPT.2020.v19i02.027

Open Access Journal

Estimation of Environmental Damages of Cement Building and Environmental Benefits of Prefabricated Building: A Case Study Based on a Residential Project in Henan Province, China

Chen Nan† and Zhang Jie
Department of Architectural Engineering, Jiyuan Vocational and Technical College, Jiyuan 459000, China
†Corresponding author: Chen Nan; jynancy86@126.com

Nat. Env. & Poll. Tech.
Website: www.neptjournal.com

Received: 22-02-2020
Accepted: 24-04-2020

Key Words:
Cement building;
Environmental damage;
Prefabricated building;
Environmental benefit;

ABSTRACT

Traditional cement building generates abundant construction wastes during construction and waste transportation. Thus, it incurs high building resource consumption, low building efficiency, and frequent occurrence of safety accidents, which result in relatively low utilization ratio of building resources and relatively serious environmental pollution pressure. A prefabricated building can save building materials and energies and decrease construction waste emission; it is also an essential choice when the construction industry develops to a high level in a country. A case study based on a residential project in Henan Province, China was carried out. Firstly, studies concerning the environmental benefits of prefabricated building in foreign developed countries were reviewed. Second, the types of environmental damage from cement building were summarized. Third, an evaluation index system of environmental benefits of the prefabricated building was established. Finally, environmental benefit scores in the case study were calculated using the fuzzy comprehensive evaluation method based on the analytic hierarchy process. Results demonstrated that prefabricated building is extensively applied in Europe. Traditional cement buildings bring various types of environmental pollution, including water, solid waste, and dust pollutions and vegetation damage. In a case study, the environmental benefits of the prefabricated building are assessed at a good level close to excellent. Environmental benefits of the prefabricated building can be improved by encouraging real estate developers to adopt prefabricated building. In this manner, the installation efficiency of mechanical devices and construction efficiency can be increased, and the construction safety of projects can be improved. Research conclusions can provide references not only for the government to formulate policies in favour of prefabricated building development and measures for reducing environmental pollutions but also for the construction industry to enrich benefit evaluation systems for prefabricated building projects. This study is highly important in the realization of green sustainable development in the construction industry.

INTRODUCTION

Recently, the construction industry has achieved considerable progress as a response to the rapid development of China's real estate industry. China has begun to explore building industrialization since the 1950s, which brought China's building industrialization into a new fast development stage. Disadvantages of traditional cast-in-place construction mode, such as high energy consumption, heavy pollution, low efficiency, and low quality, become increasingly prominent. Particularly, cement dust during construction activities is produced by human activities. The dust particles move with airflow under the influence of human activities and finally become tiny particles that are easy to be inhaled by humans. These tiny particles cause a series of diseases (e.g., pneumoconiosis) and even threaten human life once they infect the lungs. Moreover, a considerable amount of dust in the atmosphere will be produced by human activities or machine operation during construction; this phenomenon increases dust concentration and lowers air quality. Particularly, dust concentration has severely exceeded the limit in the metropolis. Dust can affect the growth of surrounding plants and the physical health of human beings because it contains a large amount of heavy metals and other compounds, which easily generate toxic substances after a reaction. Developing prefabricated building is conducive for the promotion of the formation of an emerging industry and deep integration of the construction industry with industrial construction, information, logistics, and modern service industries. This approach has a positive effect on developing a new economy and new energy and promoting economic growth by driving social investment.

Henan is a province in Central China with a large population. As shown in Fig. 1, the permanent resident population increased from 94.87 million in 2009 to 96.05 million in 2018. Moreover, the urbanization process in Henan Province accelerated due to population aggregation. The total output

of the construction industry increased from 359.649 billion yuan in 2009 to 1136.052 billion yuan in 2018, showing an annual growth rate of as high as 24%. This result fully reflects the large pressure of the construction industry over the environmental pollution in Henan Province. However, the disadvantages of traditional construction mode in Henan Province became increasingly prominent due to the excessive energy and resource consumption by the construction industry, serious ecological environmental damage, backward production management mode, and low technological level of first-line operators. Therefore, the development of prefabricated building in China is facilitated considerably by assuring transformation and updating of the construction industry, thereby developing the guidance role of the government, offering enterprises certain preferential subsidy policies, and motivating enterprises to change their traditional construction modes. Demonstration bases of the prefabricated building have been constructed in the major cities of Henan Province to promote the local development of the prefabricated building. Promoting construction industrialization can lower the consumption of building resources and energy effectively, increase economic benefits, decrease wet operation and construction noises in the construction site, and improve heat-insulating performance compared with cast-in-site construction. In sum, the prefabricated building can save energy sources and decrease environmental pollution significantly.

PAST STUDIES

Environmental pollution caused by traditional cement building has attracted global concerns. A prefabricated building that can decrease environmental pollution effectively is a mainstream development trend of the global construction industry. After World War II, many houses were ruined. In this background, prefabricated buildings were developed and became an important development opportunity for its unique production characteristics, such as the short construction period and high construction speed. Prefabricated buildings have caused a series of housing industrialization tides. At present, the increasingly mature prefabricated building technology in Europe is attributed to the continuous studies of many scholars. With respect to environmental pollution caused by traditional cement building, Morledge et al. reported that the construction industry has the highest pollution frequency among industries, accounting for 22% of confirmed water pollution events of the industry. Finally, the author proposed some measures on how to relieve the adverse impact of the construction industry on the environment (Morledge et al. 2001). Yang et al. analysed China's control standards for solid waste pollution caused by cement products and pointed out that solid waste pollution caused by cement building was one source of solid waste pollution (Yang et al. 2011). Wu et al. indicated that the large-scale

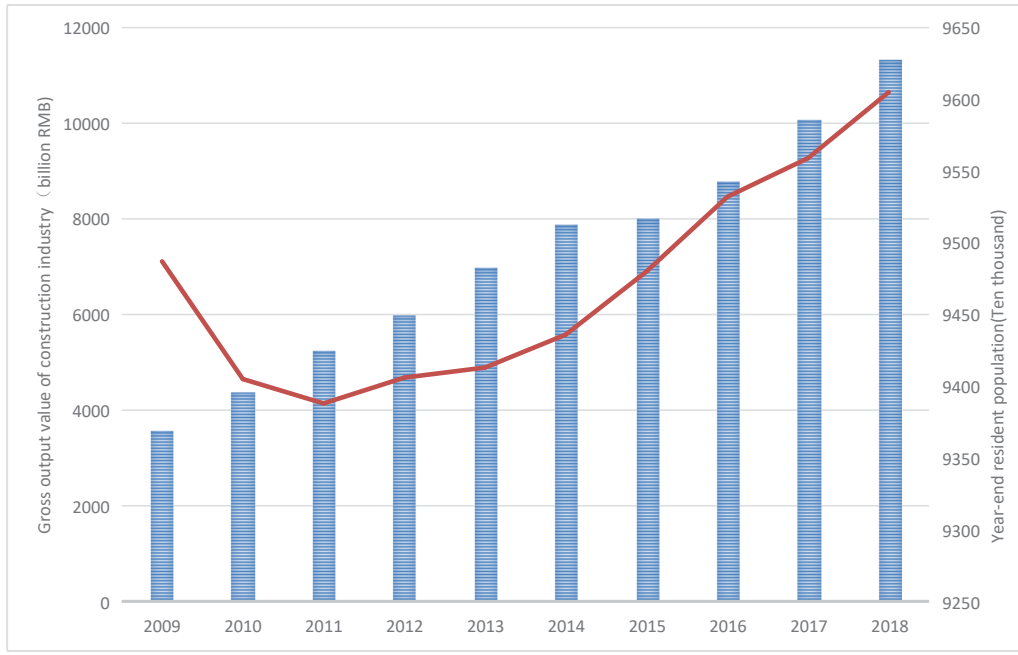

Fig. 1: Permanent resident population and total output of the construction industry at end of a year in Henan Province during 2009–2018. (Data source: China Statistics Database: http://data.stats.gov.cn).

construction of cement buildings is a result of the accelerating urbanization process in China, which has brought considerable dust emissions. Based on the investigations on the current dust control status of China's construction industry, the authors determined the main source of construction dust and finally proposed measures to control construction dust pollution (Wu et al. 2016). Wang et al. investigated the differences in the environmental effects of prefabricated plates, composite plates, and cement pouring construction during their life cycles and analyzed the influence of building life on construction environmental pollutant emissions. The authors found that abundant buildings are dismantled during China's urbanization process, which shortens the average life of buildings and wastes a considerable amount of energies and resources (Wang et al. 2018). Tam et al. analyzed and studied the reduction of construction wastes of four prefabricated buildings compared with those of traditional cast-in-site buildings and proposed the environmental benefits of prefabricated buildings in terms of energy-saving and emission reduction. The authors concluded that the construction waste production and the template quantity of prefabricated buildings are approximately 55% and 80% lower than those of traditional cast-in-site construction, respectively (Tam et al. 2005). Jaillon et al. believed that the standard design of prefabricated buildings not only can increase production efficiency of product parts effectively but also has advantages of energy-saving, emission reduction, and relieving environmental pollutions. Therefore, they suggested the promotion and application of prefabricated buildings on a large scale (Jaillon et al. 2009). Pons et al. studied the influence of school construction on the environment based on the industrialization technology in Catalonia, Spain. They found that using prefabricated buildings could decrease resource consumption, waste production, and environmental pollutions (Pons et al. 2011). Silva et al. constructed a three-dimensional model for the module reconstruction of the external walls of existing prefabricated buildings and analyzed its cost efficiency (Silva et al. 2013). Lehmann reported that the promotion of low-carbonization construction of prefabricated buildings can decrease greenhouse gas emissions of building materials. The author suggested that the government should reduce taxis for the use of renewable energy houses and offer fiscal subsidies to real estate developers who meet certain conditions (Lehmann 2013). Mao et al. discussed the differences between prefabricated and traditional construction modes in greenhouse gas emission and confirmed that the former has significant environmental benefits on greenhouse gas emission (Mao et al. 2013). In the theoretical background of the full life cycle, Lu discussed the potential of prefabricated building technology in waste reduction in the construction and transnational transportation industries. The results showed that prefabrication in a factory environment can decrease wastes more than traditional cast-in-site construction does (Lu 2013). Bonamente et al. investigated the prefabricated building department in Italy. They analyzed the carbon and energy footprints of prefabricated components in preproduction, in-production, assembly, use, and dismantling stages. They also discussed the influence types of prefabricated buildings on the environment and finally proposed corresponding suggestions to decrease environmental impact (Bonamente et al. 2014). Dong et al. performed a case study based on a private house in Hong Kong to compare the carbon emissions of prefabricated technology and traditional cast-in-site construction technology. Based on their results, they strongly suggested the adoption of prefabricated concrete during construction, which can decrease the carbon emission of the construction industry (Dong et al. 2015). Jeong et al. evaluated the differences between new prefabricated columns and traditional concrete columns in terms of productivity, cost, and CO_2 emission through a case study. They concluded that the former increased productivity by 42.5% and saved costs by 1.32%. Moreover, the new fabricated column is a reliable substitute for traditional concrete columns (Jeong et al. 2017). On the basis of the aforementioned studies, traditional cement buildings may cause considerable environmental pollution in construction and building recycling, whereas prefabricated buildings can decrease the consumption of construction resources and energies and increase economic benefits. However, existing studies on prefabricated building mainly focus on design, construction technology, cost control, and economic benefits. Only few studies on environmental benefits of the prefabricated building have been reported. Thus, in the present work, a case study based on a residential project community in Henan Province was performed. Weights of major evaluation indexes were determined by analytic hierarchy process (AHP), and environmental benefits of the prefabricated building project were calculated using a fuzzy comprehensive evaluation method. Some specific improvement suggestions were proposed based on the evaluation results.

ENVIRONMENTAL DAMAGE CAUSED BY CEMENT BUILDING

Water Pollution

Traditional cement building in cities inevitably produces sewage and industrial slurry during construction. Many construction units lack essential environmental protection consciousness and pursue economic benefits blindly by discharging slurry and sewage directly rather than after purification. As a result, sewage in the construction site containing industrial raw materials, cement mortar, sundries, and dust

is discharged to surrounding sewers of the construction site directly, causing serious pollution to surrounding water areas. In the long run, the sub drainage systems in cities will be blocked by these sundries and slurries, which will decrease drainage and flooding prevention capacities significantly. Some construction projects will even affect the underground water level in cities during the construction of the foundation.

Solid Waste Pollution

Generally, cement building projects will surely produce a considerable amount of solid wastes, such as graves and slags during construction, which often brings a great challenge in disposal. Such solid wastes generally have no value of recycling and incur high processing costs. Many construction projects directly pour these solid wastes in open areas in suburbs or landfilled directly to save processing cost, which will cause relatively serious soil pollution in local areas and occupy spaces for processing other household wastes.

Dust Pollution

Dust pollution, which is produced in the construction sites of cement buildings, mainly comes from the transportation of materials. Handling of raw materials and earthwork in the site can cause dust pollution. Dust pollution can also be generated when construction workers are paving pipeline network and transporting materials, such as cement and lime. If dust concentration becomes thick during construction, then a considerable amount of dust will be lifted into the air when vehicles drive quickly. Waste gases, which are produced during construction, generally come from construction materials, such as paints or other decoration materials. These materials will generate some harmful gases in special environments and places with a large population. The physical health of individuals is exposed to serious damage.

Vegetation Damage

Road network in Chinese cities is expanding, accompanied by endless emergence of high-rise residential building projects and business district construction projects. All of these require plentiful cement pouring tasks. During land development, cement building projects ignore water and soil protection in the construction field. Many construction sites do not comply with the regulation of setting retaining walls and revetment. Many land development regions become idle after smoothing and exposure to air and may thus suffer serious water and soil losses after being scoured by rainstorms. In the long run, it will cause serious mud accumulation in the river, reservoir sedimentation, and gradual failure of the drainage system in urban areas.

BRIEF INTRODUCTION OF THE MODEL AND INDEX SYSTEM

Brief Introduction of the Model (AHP-based Fuzzy Comprehensive Evaluation)

(1) Determination of weights of indexes (AHP method): The AHP is a multicriteria decision method that combines qualitative and quantitative analyses. It divides evaluation indexes into several layers and quantizes qualitative understanding of people through certain scales. On this basis, qualitative and quantitative analyses are performed. Weights of evaluation indexes can be gained through AHP, as shown as follows:

$$W = [w_1, w_2, \cdots, w_n], \quad \ldots(1)$$

Where, w_n refers to the weights of the nth index calculated by the AHP.

(2) Construction of comment set: The set of experts' comments for the comprehensive evaluation of prefabricated building project is set up and defined as

$$V = \{v_1, v_2, \cdots, v_n\}, \quad \ldots(2)$$

where v_n is the evaluation grade of the project, which generally includes excellent, good, moderate, poor, and very poor. For the convenience of calculation, the common method in most associated studies is used in defining the five grade levels of excellent, good, moderate, poor, and very poor, which are equivalent to 95, 85, 75, 65, and 55, respectively. Next, the evaluation factor set is determined again, as shown as follows:

$$U = \{u_1, u_2, \cdots, u_n\}, \quad \ldots(3)$$

where u_i is the i^{th} influencing factor of the evaluated object.

***(3) Construction of a membership matrix for project evaluation*:** Subsequently, technicians of the studying prefabricated building project were invited to score the index system, obtaining a membership matrix (B).

***(4) Final scores*:** Finally, the final scores are calculated through weighted averaging of scores in accordance with the comment set. The final scores are defined as C, as shown as follows:

$$C = W * B * [95, 85, 75, 65, 55]^T. \quad \ldots(4)$$

Index System

Fabricated buildings decrease environmental resource wastes and energy consumption effectively because of their capacity to overcome the disadvantages of traditional construction mode to some extent. This study selected five representative indexes on the basis of the influence of fabricated building construction on the environment (Table 1).

CASE STUDY

The study area lies in Zhenzhou City, Henan Province. It covers a construction land area of 45,230 m^2, and the planning built-up area is approximately 130,000 m^2, which includes 12 floors. The area can meet the needs of 2,310 replacement households. This project adopted prefabricated building technology and, all prefabricated parts were all manufactured and supplied by a construction company in Zhenzhou City, Henan Province.

Determination of Weight Indexes

According to the AHP model for environmental benefit evaluation of the study project, a questionnaire survey was filled out by 10 members of the project team using 1-9 scale criteria.

On the basis of the judgment matrix in Table 2, the eigenvector and maximum eigenvalue of the judgment matrix are calculated by the most common square root method in the AHP model. They were applied to check whether judgment matrixes meet the consistency requirement (Table 3).

Table 3 shows that all judgment matrixes meet the consistency test.

Membership Matrix

Ten members of the project team were invited again to score the environmental benefit indexes of the project. Table 4 lists the results.

On the basis of the scores in Table 4, the membership matrix is gained as follows:

$$B=\begin{bmatrix}0.3 & 0.6 & 0.1 & 0 & 0\\ 0.6 & 0.3 & 0.1 & 0 & 0\\ 0.8 & 0.1 & 0.1 & 0 & 0\\ 0.5 & 0.3 & 0.2 & 0 & 0\\ 0.1 & 0.2 & 0.5 & 0.2 & 0\end{bmatrix}$$

Final Scores

On the basis of Eq. (3), the final scores are calculated as follows:

$$C=[0.246,0.158,0.39,0.130,0.076]*\begin{bmatrix}0.3 & 0.6 & 0.1 & 0 & 0\\ 0.6 & 0.3 & 0.1 & 0 & 0\\ 0.8 & 0.1 & 0.1 & 0 & 0\\ 0.5 & 0.3 & 0.2 & 0 & 0\\ 0.1 & 0.2 & 0.5 & 0.2 & 0\end{bmatrix}*[95,85,75,65,55]^T$$

The final scores of the environmental benefit are C=88.794. Table 5 shows the relations between environmental benefit scores and evaluation levels are shown in Table 5.

C=88.794 indicates that the environmental benefit of prefabricated building is at a good level and it is close to the excellent level. Thus, the prefabricated building project in this case study achieved "good" environmental benefits, which indicates that it presented good environmental benefits. Therefore, the prefabricated building technology was proven to save resources and energies significantly, as well as decrease production of construction wastes and dust emission. Furthermore, with the reduction of wet operation quantities, noises from the use of mechanical devices were decreased, and the living environmental quality for surrounding residents was improved significantly. The studied prefabricated building realized the goal of "water-saving, land saving, energy saving, material saving and environmental protection" through standard design and unique characteristics. The unique energy-saving design was made according to the functions of the building. In the design stage, the prefabricated building's demands for construction site were decreased significantly because most parts were prefabricated in factories. In the construction stage, the installation of prefabricated parts could increase the utilization of water resources significantly compared with that in traditional cast-in-site mode. In the use stage, the prefabricated building could increase the utilization of parts and saving materials through unique standard design and energy design. In the

Table 1: Evaluation index system of the environmental benefits of prefabricated buildings.

Indexes	Explanation
Resource consumption (w_1)	House construction has great resource consumption. Resource consumption is an indispensable index in the evaluation of environmental benefits.
Energy consumption (w_2)	House energy consumption mainly refers to daily energy consumption needed for heating, air conditioning, and illumination of the house.
Solid waste emission (w_3)	Solid wastes mainly refer to those that are produced during construction and dismantling stages of houses.
Dust emission (w_4)	Dust emission refers to the sum of various dust types produced during house construction.
Noise pollution (w_5)	During house construction, noises mainly come from frequent uses of large-size mechanical devices.

Table 2: Judgment matrix of environmental benefits.

	w_1	w_2	w_3	w_4	w_5
w_1	1	3	1	1	2
w_2	1/3	1	1/3	2	3
w_3	1	3	1	4	5
w_4	1	½	¼	1	2
w_5	1/2	1/3	1/5	1/2	1

dismantling stage, the prefabricated building had prominent environmental protection performance compared with the traditional cast-in-site mode. For example, the safety of building dismantling was increased, and a high recycling rate of parts was achieved.

POLICY SUGGESTIONS

Encouraging Real Estate Developers to Adopt Prefabricated Buildings to Decrease Overall Environmental Pollution

The government sectors shall offer preferential taxes to real estate developers who adopt prefabricated building mode to relieve their financial pressure from economic cost. Direct economic expenditures of real estate developers for prefabricated building can be compensated by using various forms of tax preference policies, such that real estate developers are more willing to adopt prefabricated building mode. The increasing prefabricated building projects in the market is the fundamental source of promoting the expansion of market demands. Only expanding the scales of prefabricated component demands can further promote the development of part manufacturers, installation professionals, and construction enterprises. In the early industrial development stage, subsidies can be provided to real estate developers through various ways, such as exemption from tax, tax reduction, or tax reimbursement, which can effectively promote the development of prefabricated buildings.

Increasing Installation Efficiency of Mechanical Devices and Decreasing Noise Pollution and Dust Emission

At present, few installation devices support prefabricated buildings, and most prefabricated parts are installed using basic hoisting devices. This situation not only leads to low installation efficiency but also significantly intensifies noise pollution during installation compared with that in foreign countries. Hence, providing professional installation services can solve the low assembly efficiency of mechanical devices directly, thereby decreasing unnecessary noise pollution problems caused by the low efficiency of devices. Prefabricated part manufacturers are encouraged to expand their business scope and provide house assembly services while meeting prefabricated part manufacturing demands of real estate developers. Through the training of installation skills of operators, a group of technicians who are skilled in the installation of mechanical devices can be trained. As a result, resource waste caused by damage of prefabricated parts during the use stage of installation devices can be decreased. Moreover, these technicians can increase installation efficiency and decrease noise pollutions during installation.

Increasing Construction Productivity and Reducing Environmental Influencing Period of Projects

Prefabricated buildings can also affect the daily life of surrounding residents during construction to some extent. During construction, noises, dust, solid waste, and road blocking all bring great inconveniences to normal life and rests of residents. Such influence is related to time. Therefore, construction productivity can increase social benefits significantly. Increasing construction productivity can shorten the construction period, relieve the effects of construction activities on surrounding residents, increase the quality performance of house products, and meet the diversified demands of residents. In prefabricated buildings, residents can make appropriate reconstruction of houses according to personnel demands. Moreover, early planning design provides diversified house types that can meet the living demands of different groups. Prefabricated buildings claim relatively low costs for repairing or maintenance and long maintenance period because of the abundant use of prefabricated parts. In addition, a maintenance property team is set

Table 3: Eigenvector and maximum eigenvalue of judgment matrixes.

Eigenvector W	λ_{max}	CI
(0.246, 0.158, 0.390, 0.130, 0.076)	5.371	0.082

Table 4: Statistics on scores of environmental benefit evaluation indexes.

Indexes	Evaluation results				
	Excellent	Good	Moderate	Poor	Very poor
Resource consumption (w_1)	3	6	1	0	0
Energy consumption (w_2)	6	3	1	0	0
Solid waste emission (w_3)	8	1	1	0	0
Dust emission (w_4)	5	3	2	0	0
Noise pollution (w_5)	1	2	5	2	0

up for the community to make common plans for existing problems, choose the most reasonable maintenance schemes, and settle disputes over house maintenance.

Increasing Construction Safety of Project and Decreasing the Adverse Effects of Construction Activities on the Environment

In comparison with traditional construction, prefabricated building projects involve few construction workers, which can decrease the number of injury accidents and adverse social impacts dramatically. The adverse impacts of high injuries and deaths in the traditional construction mode on the society can be changed by improving construction safety. Prefabricated buildings produce a good demonstration effect in the inner heart of surrounding residents and increase social benefits. On this basis, this study suggests to (1) increase construction safety, set up strict construction safety norms, and regularly examine the implementation progress to realize civilized construction and safety construction; (2) construct a weekly safety summary system to point out attentions and remind construction workers to be always alert to prevent accidents strictly; and (3) increase training to construction workers to improve their technological skills and decrease safety accidents caused by inadequate technological abilities.

CONCLUSIONS

China's urbanization achieves outstanding progress because of its rapid economic development, which drives the continuous expansion of the construction industry in China. The traditional cast-in-site mode still takes the dominant role in China's construction industry. This traditional mode is characterized by great resource consumption, low construction efficiency, frequent occurrence of safety events, and serious environmental pollution. Prefabricated buildings balance the contradiction between economic development and environmental protection and meets the demands for green development. Thus, such buildings are an essential choice for green sustainable development of the construction industry. This work performs a case study based on a residential project in Henan Province. Here, the types of environmental damage caused by cement building are summarized, and environmental benefit scores are calculated by an AHP-based fuzzy comprehensive evaluation method. The results indicate that water pollution, solid waste pollution, dust pollution, and vegetation damage are four major pollution types caused by traditional cement building. In this case study, the environmental benefits of the prefabricated building are at a good level and close to the excellent level. Finally, some suggestions are proposed, including encouraging real estate developers to adopt prefabricated buildings, increasing installation efficiency of mechanical devices, increasing construction productivity, and improving the construction safety of projects. Further studies on increasing environmental benefit evaluation accuracy based on further refined classification, calculating environmental benefits of the prefabricated building by combining multiple evaluation methods, and enriching the comprehensive evaluation systems of full-process environmental benefits of the prefabricated building should be conducted.

REFERENCES

Bonamente, E., Merico, M. C., Rinaldi, S., Pignatta, G., Pisello, A., Cotana, F. and Nicolini A. 2014. Environmental impact of industrial prefabricated buildings: carbon and energy footprint analysis based on an LCA approach. Energy Procedia, 61: 2841-2844.

Dong, Y. H., Jaillon, L., Chu, P. and Poon, C. 2015. Comparing carbon emissions of precast and cast-in-situ construction methods–A case study of high-rise private building. Construction and Building Materials, 99: 39-53.

Table 5: Evaluation results and definition of the five grade levels.

Levels	Excellent	Good	Moderate	Poor	Very poor
Scores	[90,)	[80, 90)	[70, 80)	[60, 70)	[0, 60)

Jeong, J., Hong, T., Ji, C., Kim, J., Lee, M., Jeong, K. and Lee, S. 2017. An integrated evaluation of productivity, cost and CO2 emission between prefabricated and conventional columns. Journal of Cleaner Production, 142: 2393-2406.

Jaillon, L. and Poon, C. S. 2009. The evolution of prefabricated residential building systems in Hong Kong: A review of the public and the private sector. Automation in Construction, 18(3): 239-248.

Lehmann, S. 2013. Low carbon construction systems using prefabricated engineered solid wood panels for urban infill to significantly reduce greenhouse gas emissions. Sustainable Cities and Society, 6: 57-67.

Lu, W. and Yuan, H. 2013. Investigating waste reduction potential in the upstream processes of offshore prefabrication construction. Renewable and Sustainable Energy Reviews, 28: 804-811.

Mao, C., Shen, Q., Shen, L. and Tang, L. 2013. Comparative study of greenhouse gas emissions between off-site prefabrication and conventional construction methods: Two case studies of residential projects. Energy and Buildings, 66: 165-176.

Morledge, R. and Jackson, F. 2001. Reducing environmental pollution caused by construction plant. Environmental Management and Health, 12(2):191-206.

Tam, C. M., Tam, V. W. Y., Chan, J. K. W. and Ng, W. C. Y. 2005. Use of prefabrication to minimize construction waste-a case study approach. International Journal of Construction Management, 5(1): 91-101.

Pons, O. and Wadel, G. 2011. Environmental impacts of prefabricated school buildings in Catalonia. Habitat International, 35(4): 553-563.

Silva, P. C. P., Almeida, M., Bragança, L. and Mesquita, V. 2013. Development of prefabricated retrofit module towards nearly zero energy buildings. Energy and Buildings, 56: 115-125.

Wang, J., Zhang, Y. and Wang, Y. 2018. Environmental impacts of short building lifespans in China considering time value. Journal of Cleaner Production, 203: 696-707.

Wu, Z., Zhang, X. and Wu, M. 2016. Mitigating construction dust pollution: State of the art and the way forward. Journal of Cleaner Production, 112: 1658-1666.

Yang, Y., Huang, Q., Yang, Y., Huang, Z. and Wang, Q. 2011. Formulation of criteria for pollution control on cement products produced from solid wastes in China. Journal of Environmental Management, 92(8): 1931-1937.

Nature Environment and Pollution Technology
An International Quarterly Scientific Journal

p-ISSN: 0972-6268
(Print copies up to 2016)
e-ISSN: 2395-3454

Vol. 19 | No. 2 | pp. 729-737 | 2020

Original Research Paper

https://doi.org/10.46488/NEPT.2020.v19i02.028

Open Access Journal

Application of Recycled Coarse Aggregate in Steel Tubular Members

Gajalakshmi Pandulu†, Revathy Jayaseelan and Mohana Priya
Department of Civil Engineering, B. S. Abdur Rahman Crescent Institute of Science & Technology, Chennai, Tamil Nadu, India
†Corresponding author: Gajalakshmi Pandulu; gajalakshmi@crescent.education

Nat. Env. & Poll. Tech.
Website: www.neptjournal.com

Received: 18-07-2019
Accepted: 29-08-2019

Key Words:
Demolition waste; Recycled coarse aggregate; Concrete filled steel tubes; Taguchi approach

ABSTRACT

Recycled aggregate from the demolition of buildings provides a sustainable solution in reducing the space required for dumping demolished waste as landfill and also reduces the consumption of natural aggregate. A percentage of recycled coarse aggregate can be used in structural members which can be economical and environmentally useful. This experimental study consists of three phases. In Phase I, an attempt was made to use Recycled Coarse Aggregate (RCA) in place of Natural Coarse Aggregate(NCA) in concrete. Experimental results of concrete for various combinations of RCA with NCA wereanalysed numerically for the optimum value using Taguchi's method. In Phase II, the confirmation study was conducted to study the strength and durability characteristics of concrete made with the optimized value of recycled aggregate. In Phase III, the application of optimized recycled coarse aggregate concrete was done by conducting a study on the load-carrying capacity of recycled coarse aggregate concrete-filled steel tube members. The results revealed that there is a marginal increase in load-carrying capacity of recycled coarse aggregate concrete-filled steel tube members than natural coarse aggregate concrete-filled steel tube members. This application proves to be eco-friendly and environmentally sustainable by using the demolished concrete in the structural member.

INTRODUCTION

Concrete is a man-made product which consists of large chunks of cement, coarse and fine aggregate mixed with water and/or admixture. Concrete is the most widely used construction material across the world in all types of construction. In a concrete mixture, aggregate occupies the major part. In conventional construction, coarse aggregate from quarries and sand from river beds play a vital role. The availability of these natural sources is decreasing at a larger scale due to overconsumption and increased development in the field of construction (Tiwari 2015, Chakradhara Rao 2011). The supply of the aggregates has emerged as a major problem in many cities across India. For this purpose, recycling of demolition waste is gaining importance (Matias 2013, Vieira 2016). Also,beams cast with RCA rather experienced greater deflections under a service load and smaller cracking moments (Ganesh 2014). The recycled coarse aggregate can be used only after reducing it to the normal size and standards. While universally accepting the need to promote the use of RCA in the wider application, it must be remembered that the aggregate for the concrete application must adhere to the requirements set in the relevant specification for its intended use (Kazuhisa 2014, Alexandre Bogas 2014). The effect of recycled aggregate must be assessed and worked out for the optimum percentage to produce a concrete of good quality.

In the case of composite construction, the concrete and steel are coupled in such a manner that the advantages of both the materials are utilized effectively in composite members. Concrete-filled steel tubular (CFT) members have evolved to become popular structural members used in buildings, bridges etc., due to their outstanding structural performance characteristics such as high strength, high ductility, savings in formwork, smaller cross-section over reinforced concrete structures and high fire resistance over the steel structures (Gajalakshmi 2011). RCA filled stainless steel tube stub columns and beams under short-term loadings exhibit stable load versus deformation responses and the performance of core RAC was usually enhanced to the appreciable extent due to the confinement of the outer stainless steel tube (Wang 2015, YouFu 2006, Youfu 2013). The variation in compressive strength for the columns filled with RCA is noticeable (Vivian 2016, Kou 2012). In this study, an attempt is made to study the performance of CFT members filled concrete prepared by partially replacing NCA with RCA. This application renders to maintain a sustainable environment.

MATERIALS AND METHODS

Phase I - Experimental Study on Materials

In Phase I, an experimental study was conducted on testing of material properties, development of mix design for M25

and M35 grade concrete and testing of hardened properties such as compressive and split tensile strength. The optimum value of RCA has been found out by Taguchi's approach by using these experimental results in Phase I.

Material properties: The physical properties of natural coarse aggregate and recycled coarse aggregate are compared and are given in Table 1. The cement of grade OPC 53 is used for testing. The concrete mix was designed for the cube compressive strength of 25MPa and 35MPa at 28 days with mix ratios of 1:1.37:2.6 @ 0.45 w/c ratio and 1:1.8:2.7 @ 0.5 w/c ratio respectively with 12.5mm (max)size of natural and recycled coarse aggregate and 2.36mm (max) size fine aggregate based on ACI committee 211.1.1991 recommendations. From the concrete mixes, cubes and cylinders were cast for various percentages of recycled coarse aggregate (RCA) (40%, 60%, 80%, and 100%) with and without admixture (modified polycarboxylic ether) and were tested to obtain the optimum percentage of RCA using Taguchi method.

Taguchi's approach- Analysis of results of compressive and tensile strength: Taguchi (1986) (Ganesan, 2011) developed a method based on orthogonal array for designing experiments to investigate how different factors affect the response especially the mean and variance. Taguchi has coupled design of experiments with optimization of control factors to ensure the best optimal results. He also introduced the concept of signal to noise ratio (S/N), where the signal is the mean response and noise is variation due to uncontrolled factors. The signal to noise ratio is nothing but log functions of desired response and also serve as an objective function for optimization in experimental data analysis. Taguchi has tabulated 18 basic orthogonal arrays called 'Standard Orthogonal Array'. The process of fitting an orthogonal array to a specific experimental study has been made easy by employing one of the standard orthogonal arrays. The average S/N ratio for each factor and levels were calculated. Keeping in mind the objective of the experiment, viz., maximization or minimization of the performance measure, the best level for each factor can be selected and as per Taguchi's approach S/N ratio is given by-

$$\text{S/N ratio} = -10 \log \left[\frac{1}{N}\sum Y_i^2\right]$$

where N is the number of experiments and Y_i is the mean of all the experiments.

Analysis of Results Using the Taguchi Approach

Based on Taguchi method, the suitable array for the compressive test results selected for the analysis is 4^2 (L8), where 4 represents the factors and 2 represents the levels which are shown in Table 2 with four factors as percentage replacement of natural coarse aggregate with recycled coarse aggregate (A1-40%, A2-60%, A3-80% and A4-100%) and two levels of different grades (C1-M25 and C2-M35) and admixtures (B1-0% and B2-0.6%). The S/N ratios were calculated for both compressive strength and tensile strength as shown in

Table 1: Physical properties of Aggregates.

Physical properties	Water absorption (%)	Specific gravity
NCA	1.48	2.68
RCA	5.8	2.2
Fine Aggregate (Zone II)	-	2.65

Table 2: Array table.

	C1		C2	
	B1	B2	B1	B2
A1	33.35	40.4	38.66	45.42
A2	34.51	38.73	38.27	43.37
A3	29.24	34.78	35.36	38.97
A4	28.80	29.07	30.76	33.16

Table 3: S/N ratio of compressive strength of cube.

% of Replacement	% of Admixture	Compressive strength results (N/mm^2)		S/N ratio	
		M25	M35	M25	M35
0	0	24.4	35.16	27.75	30.92
0	0.6	27.42	40.13	28.76	32.06
40	0	33.35	38.66	30.46	31.75
40	0.6	40.4	45.42	32.12	33.14
60	0	31.57	38.27	31.66	31.66
60	0.6	38.73	43.37	31.76	32.14
80	0	29.24	35.36	29.32	30.97
80	0.6	34.78	38.97	30.83	31.81
100	0	28.8	30.76	29.19	29.75
100	0.6	29.07	33.16	29.27	30.41

Tables 3 and 4. The 40% replacement of RCA for NCA has shown improved strength in both compressive and split tensile strength. Hence the optimum value of RCA mixed with NCA is 40% and 0.6% admixture which in turn is applied in the casting and testing of structural members. These members, which were cast for this optimum value,were compared with the control member of M35 grade with 0% RCA and 0.6% admixture.

RESULTS AND DISCUSSION

Phase II - (Confirmation Test)

In Phase II, the confirmation test has been done by studying the strength and durability performance of M25 and M35 grade concrete made with the optimum percentage of RCA and admixture determined by Taguchi's approach.

Strength Performance

From the Figs. 1 and 2, maximum strength was obtained for the grade M35 with 40% replacement of natural aggregate with recycled concrete aggregate and 0.6% of admixture. It is observed to be an 11% increase when compared with conventional concrete cubes. From the split tensile strength test results, maximum strength was obtained for the grade M35 with 40% replacement of natural aggregate with recycled concrete aggregate and 0.6% of admixture. It was observed

Table 4: S/N ratio of the tensile strength of cylinder.

% of Replacement	% of Admixture	Tensile strength results (N/mm^2)		S/N ratio	
		M25	M35	M25	M35
0	0	2.70	2.99	8.63	9.513
0	0.6	2.82	3.05	9.00	9.69
40	0	2.85	2.99	9.09	9.513
40	0.6	2.96	3.19	9.43	10.08
60	0	2.72	2.81	8.69	8.97
60	0.6	2.80	2.91	8.94	9.28
80	0	2.70	2.64	8.63	8.43
80	0.6	2.85	2.82	9.09	9.00
100	0	2.56	2.84	8.16	9.07
100	0.6	2.71	2.99	8.63	9.51

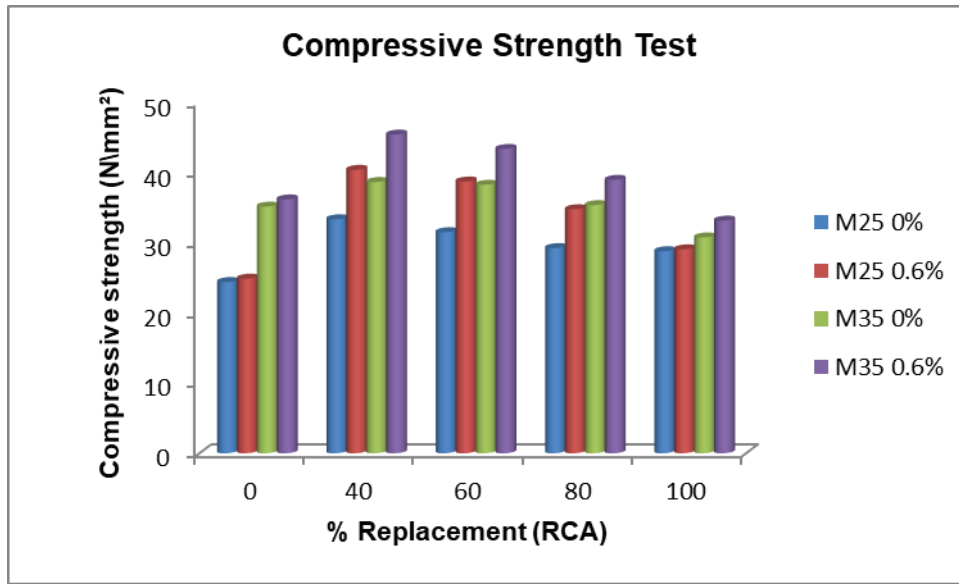

Fig. 1: Compressive strength test results.

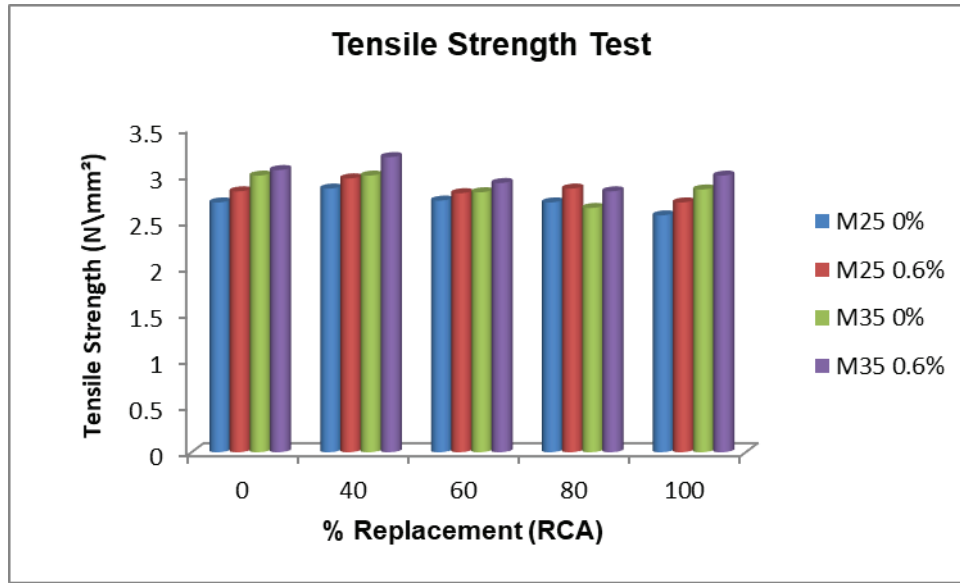

Fig. 2: Tensile strength Test results.

to be a 7.2% increase when compared with the conventional concrete cylinders.

Durability Performance (Confirmation Test)

Rapid chloride penetration: The Rapid Chloride Penetration Test (RCPT) is conducted using the cells and the values are recorded for 6 hours at 30 minutes interval with NaOH and NaCl on either side of the cell for the specimen of 100mm diameter and 50mm height. The specimen is kept in the testing apparatus where one end of the specimen is exposed to sodium chloride and the other end is exposed to sodium hydroxide.A constant potential voltage of 60 V was applied across the specimens.The current across the specimen was measured every 30 minutes for the complete 6-hour test. The total charge passing through the specimen was calculated in coulombs.Higher the value, higher is the permeability. The chloride ion penetrations are measure in terms of the current passed through the specimen. The current passage will be more if the resistance offered by the specimen is less. Based on the test results given in Fig. 3, the chloride penetrating rate is "Moderate" as per ASTM C1202for all grades of concrete with natural coarse aggregate and recycled concrete aggregate.

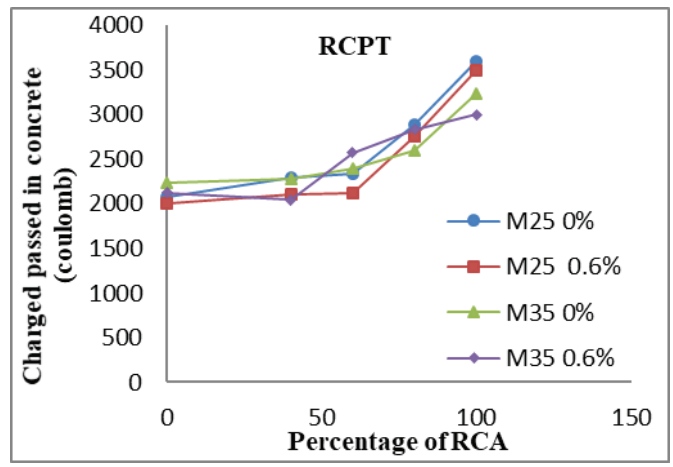

Fig. 3: RCPT test results.

Sorptivity: Sorptivity test is done to measure thecapillary rise absorption rate of concrete. The cylindrical specimen of diameter 100mm was cut into pieces of thickness 50mm. These specimens were kept in an oven at 100° Celsius for 24 hours. Waterproofing coating needs to be done on the sides of the specimen. Dry weight has to be taken and the specimen is dumped in water for 30 minutes with 5mm above the specimen surface. The wet weight of the specimen was measured. From Figs. 4 and 5, RCA 40% in M25 grade of concrete shows about 33% and 33.5% higher sorptivity values without and with admixture respectively. Similarly, in case of M35, it was found to be 33.2% and 33.7% higher sorptivity value than RCA 0%. But still, RCA 40% satisfies the same range requirements as 0% RCA. Old mortar in RCA increases the sorptivity of the concrete. Sorptivity values increase with the increase of RCA in new concrete.

Correlation evaluation of the results: The correlation expression is developed between the ratio of the compressive strength of concrete with recycled aggregate and percentage of replacement of recycled concrete is shown in Fig. 6. The value of the regression coefficient (R2) and its corresponding linear equation are presented in Fig. 8. The R^2 coefficient is 0.98, which is greater than 0.85 (Montgomery & Peck 2015) exhibiting a remarkable correlation between the chosen parameters. The correlation expression can be adopted in the mix design of concrete made with recycled concrete.

Phase III - (Application of RCA in Steel Tube Members)

The main objective of this work is to utilize the construction and demolitionconcrete waste from which coarse aggregate is extracted for the use of the manufacturing concrete. The

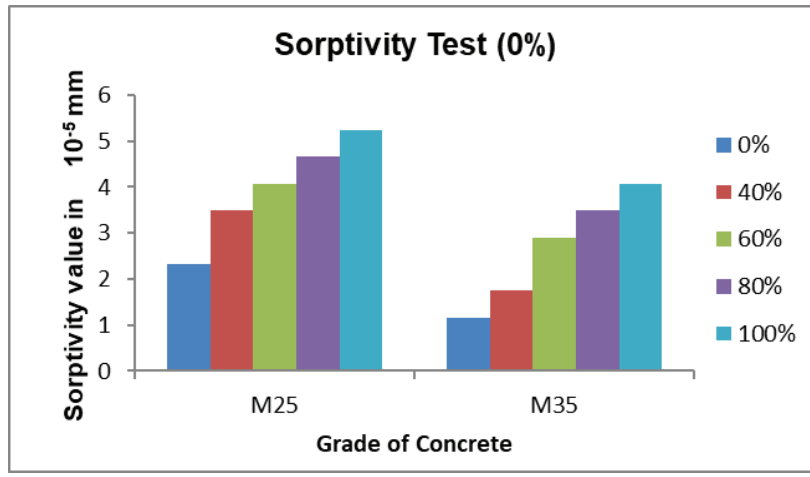

Fig. 4: Sorptivity test results for specimen without admixture.

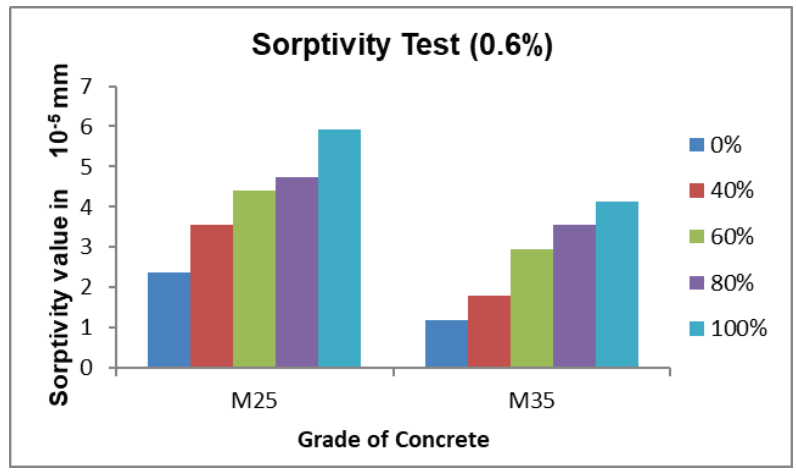

Fig. 5: Sorptivity test results for the specimen with admixture.

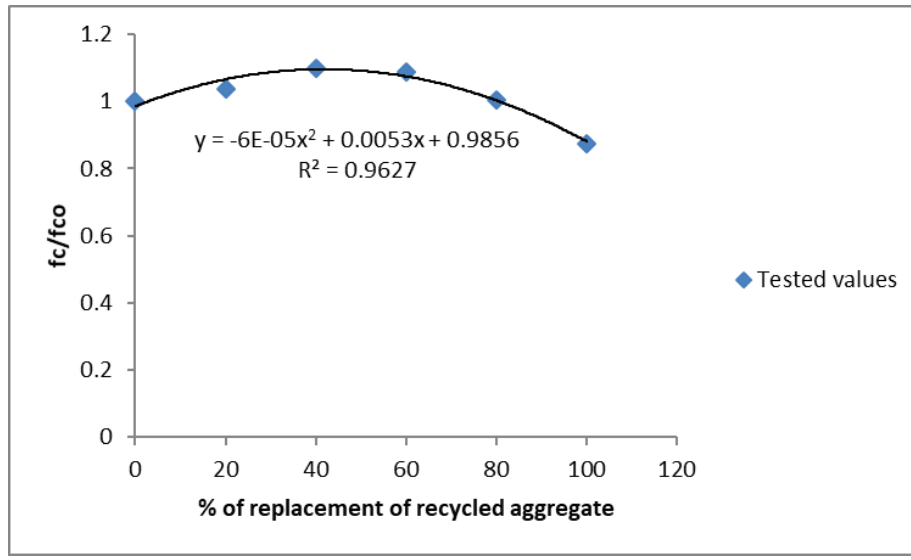

Fig. 6: Correlation evaluation of the results.

optimum percentage of recycled coarse aggregate is obtained from the results of compressive strength and tensile strength tests conducted. The durability of the concrete specimens for the various percentages of RCA in different grades of concrete is observed. In phase III, the experimental program consists of tests on CFT circular columns of diameter 114mm and rectangular columns of cross-section 98x48mm, both members of length 500mm with the thickness of the steel tube being 2.5mm.The CFT circular and rectangular sections of diameter to thickness ratio of 45.6 and 39.2 respectively. The first part consists of testing of recycled coarse aggregate filled rectangular and circular sections of columns under axial loading. The second part consists of testing of recycled coarse aggregate concrete-filled rectangular beams under two-point loading with simply supported condition. The cross-sections of the beams were 98x48mm and the length 1m. The specimens tested are observed for the maximum load-carrying capacity, axial shortening, strain in column and beam, deflection in beams and failure modes. The specimen labels are given in Table 5.

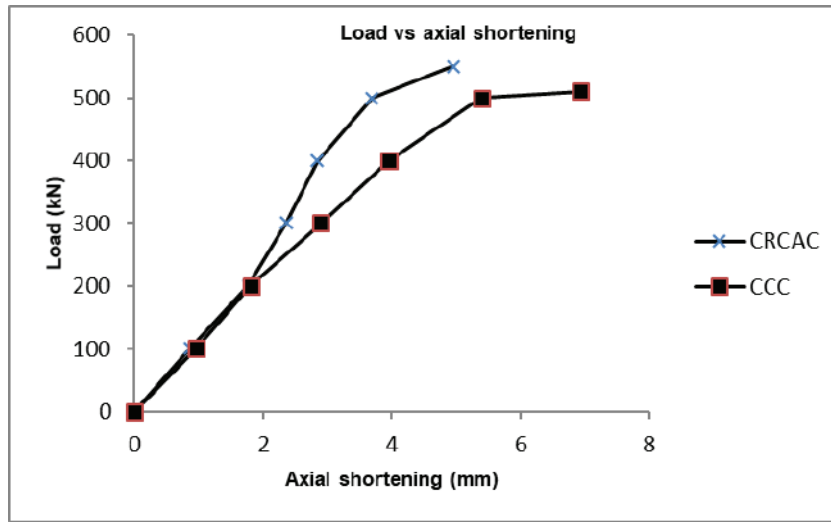

Fig. 7: Load vs axial shortening in the circular column.

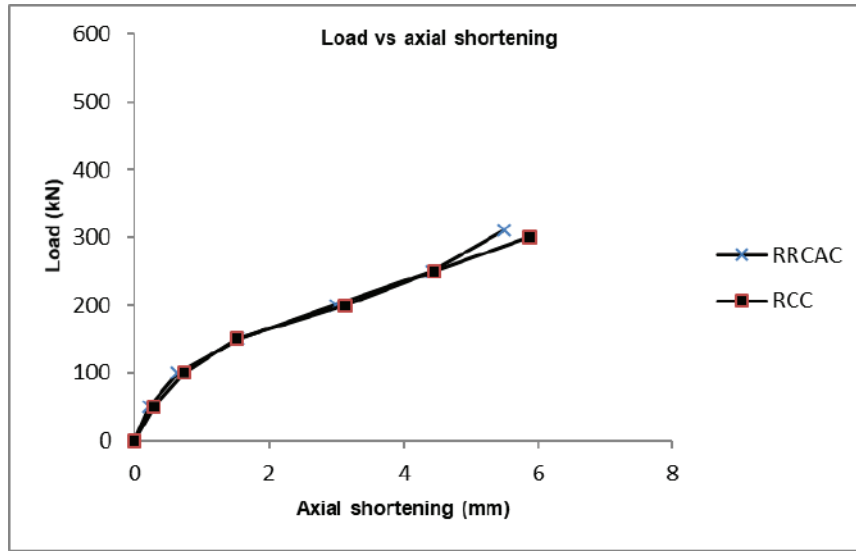

Fig. 8: Load vs axial shortening in rectangular column.

Failure modes and behaviour of RCA concrete-filled steel columns: The test specimens behaved in a ductile manner and testing proceeded in a smooth and controlled fashion. Typical failure modes ofconcretefilled with normal concrete and recycled coarse aggregate concrete were local buckling in columnare shown in Fig. 9. The columns were tested and the crushing of concrete inside the filled tube was heard when 70% of the load was applied to CCC and 80% of the load was applied to CRCAC. Similarly, in the case of rectangular columns,the crushing of concrete was observed at 75% of the load in RCC and 70% of the load in RRCAC. The buckling in columns occurred at 120mm from bottom in both CCC and CRCAC, whereas the buckling occurred at 90mm from the top in RCC and 110mm from the top in RRCAC. Typical failure modes of columns are shown in Fig. 9. On testing control and RCA concrete in filled columns, the ultimate load carrying capacity of CRCAC was found to be 558kN which is 7.2% increase than CCC. The axial shortening of CRCAC and CCC was found to be 6.9mm and 4.9mm respectively. Similarly, the ultimate load carrying capacity of RRCAC was found to be 308kN which is 7.2% lower than RCC and their corresponding axial shortening was found to be 5.5mm and 5.8mm respectively. The load vs axial shortening of the columns are given in Fig. 7 and Fig. 8. The load carrying capacity of CRCAC has shown 7.2% increase in comparison with CCC and RRCAC has shown 3.45% decrease with RCC. Considering the overall ultimate load carrying capacity, CRCAC has shown an increase of 44.8% than RRCAC. Similarly, CCC has a 37.8% increase than RCC which shows that circular columns have higher load carrying capacity than rectangular sections in both control and recycled coarse aggregate concrete infilled column.

Failure modes and behaviour of RCA concrete-filled steel beams: The failure modes of concrete filled with normal concrete and recycled coarse aggregate concrete was bending in beams. The concrete in filled steel beams exhibited bending at the centre with maximum load transferring at the loading points as shown in Fig. 11. When the load was applied, the bottom face of the steel tube exhibited an elongation allowing the beam to bend completely at the ultimate load. RRCAB exhibited a deflection measuring 60mm, 8.3% greater than RCB. The bending increased with increase in load upto 70% which is shown in Fig. 10

Table 5: Specimen label for columns and beam.

Specification	Specimen label for Column		Specimen label for beam
	Circular	Rectangular	Rectangular
Control specimen	CCC	RCC	RCB
Recycled aggregate specimen	CRCAC	RRCAC	RRCAB

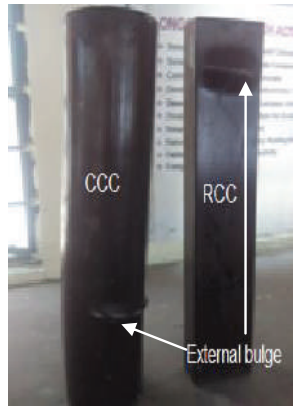

Fig. 9 (a): External buckling in control columns.

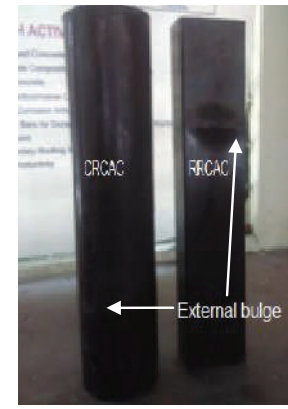

Fig. 9 (b): External buckling in RCA concrete-filled columns.

CONCLUSIONS

Based on the experimental work done, the following conclusions were drawn.

Taguchi method used to analysea wide range of values was employed to analyse the compressive and split tensile strengths to obtain the optimum percentage as 40% of RCA to be replaced for NCA.

It is observed that as per ASTM C1202, the chloride penetration rate is moderate for 40% RCA in concrete for all grades of concrete.

The correlation expression developed between compressive strength and percentage replacement of recycled aggregate in concrete and correlation expression exhibits a remarkable correlation between the chosen parameters.

RCA filled circular columns exhibit higher load-carrying capacity than rectangular sections in both normal and recycled aggregate concrete in filled column.

In the case of beams, the load-carrying capacity of RCA filled beams increased upto 3.62% and can be used in construction sites.

Use of recycled coarse aggregate in the concrete mixture is found to have sufficient strength properties close to that of natural coarse aggregate. This would enable many construction companies and developers to effectively use

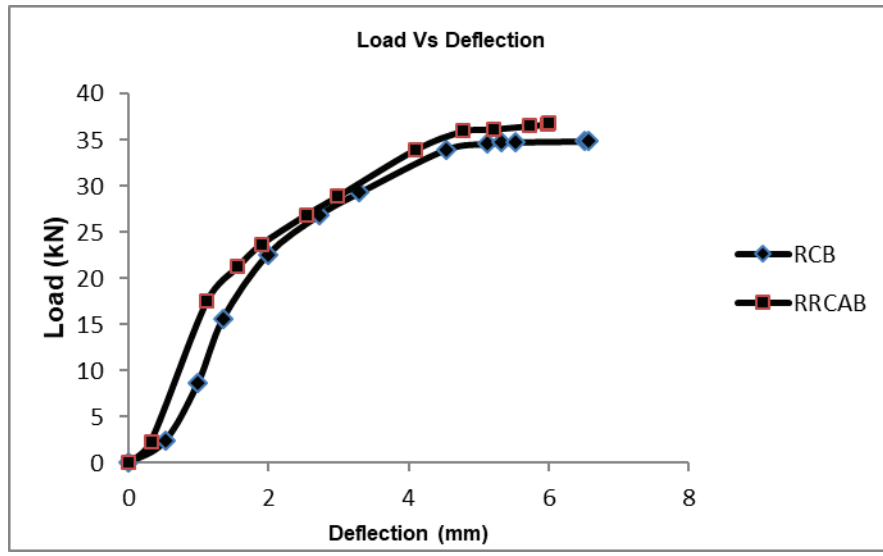

Fig. 10: Load vs deflection curve for beams.

Fig. 11: Failure pattern of beams.

the construction and demolition concrete waste thereby reducing itsimpact as landfills and provide an eco-friendly and sustainable environment.

REFERENCES

Alexandre Bogas J. and J. de Brito, J. 2014. Long-term behaviour of concrete produced with recycled lightweight expanded clay aggregate concrete. Construction and Building Materials, 65: 470.

Chakradhara, Rao, Bhattacharyya, S.K. and Barai, S.V. 2011. Influence of field recycled coarse aggregate on properties of concrete. Materials and Structures, 44: 205.

Gajalakshmi, P., Jane Helena, H. and Srinivasa Raghavan, R. 2011. Experimental investigation on the Behaviour of concrete-filled steel columns. Asian Journal of Civil Engineering, 2: 691.

Ganesan, 2011. Experiments using Taguchi's Approach. Research Methodology for Engineers. MJP Publishers.

Ganesh, S. and Gajalakshmi, P. 2014. Recycled aggregate concrete for structural applications: A Review. International Journal of Earth Sciences and Engineering, 7: 959.

Kazuhisa, Yoda and Akira,Shintani 2014. Building application of recycled aggregate concrete for upper-ground structural elements. Journal of Construction and Building Materials, 67: 379.

Kou, S.C. and Poon, C.S. 2012.Enhancing the durability properties of concrete prepared with coarse recycled aggregate.Construction and Building Materials, 35: 69.

Matias, D., de Brito, J., Rosa, A. and Pedro, D. 2013. Mechanical properties of concrete produced with recycled coarse aggregates-influence of the use of superplasticizers. Constr. Build. Mater., 44: 101.

Montgomery, D. C., and Peck, E. A. 2015. "Introduction to linear regression analysis". 5th Edn., Wiley, New York.

Taguchi G. 1986. Orthogonal Arrays and Linear Graphs. American Supplier Institute, Inc; Dearborn, MI.

Tiwari, Akansha 2015. Recycled concrete aggregate. International Research Journal of Engineering and Technology, 02: 2395.

Vieira, T., Alves, A., Brito, J., de Correia, J.R. and Silva, R.V. 2016. Durability-related performance of concrete containing fine recycled aggregates from crushed bricks and sanitary ware. Mater. Des., 90: 767.

Vivian, W., Tam, Y., Wang Zhi-Bin and Zhong Tao, 2014. Behaviour of recycled aggregate concretefilled stainless steel stub columns. Materials and Structures, 47: 293.

Wagih, A.M., El-Karmoty, H.Z., Ebid, M. and Okba, S.H. 2013. Recycled construction and demolition concrete waste as aggregate for structural concrete. Housing and Building National Research Center, 9(3): 193-200.

Wang,Yuyin, Chen,Jie and Geng, Yue 2015. Testing and analysis of axially loaded normal-strength recycled aggregate concrete filled steel tubular stub columns. Eng. Struct.,86: 192.

Yang,Youfu and Han,Linhai 2006. Compressive and flexural behaviour of recycled aggregate concrete filled steel tubes (RACFST) under short-term loadings. Steel Compos. Struct.,6: 257.

Yang,Youfu and Ma, Guoliang 2013. Experimental behaviour of recycled aggregate concrete filled stainless steel tube stub columns and beams. Thin Walled Struct., 66: 62.

Nature Environment and Pollution Technology
An International Quarterly Scientific Journal

p-ISSN: 0972-6268
(Print copies up to 2016)
e-ISSN: 2395-3454

Vol. 19 | No. 2 | pp. 739-745 | 2020

Original Research Paper

https://doi.org/10.46488/NEPT.2020.v19i02.029

Open Access Journal

Effects of Hydropower Reservoir Withdrawal Temperature on Generation and Dissipation of Supersaturated TDG

Lei Tang*, Ran Li *†, Ben R. Hodges, Jingjie Feng* and Jingying Lu***

*State Key Laboratory of Hydraulics and Mountain River Engineering, Sichuan University, 24 south Section 1 Ring Road No.1 ChengDu, SiChuan 610065 P.R.China

**Department of Civil, Architectural and Environmental Engineering, University of Texas at Austin, USA

†Corresponding author: Ran Li; liran@scu.edu.cn

Nat. Env. & Poll. Tech.
Website: www.neptjournal.com

Received: 29-07-2019
Accepted: 08-10-2019

Key Words:
Hydropower;
Total dissolved gas;
Supersaturation;
Hydropower station

ABSTRACT

One of the challenges for hydropower dam operation is the occurrence of supersaturated total dissolved gas (TDG) levels that can cause gas bubble disease in downstream fish. Supersaturated TDG is generated when water discharged from a dam entrains air and temporarily encounters higher pressures (e.g. in a plunge pool) where TDG saturation occurs at a higher gas concentration, allowing a greater mass of gas to enter into solution than would otherwise occur at ambient pressures. As the water moves downstream into regions of essentially hydrostatic pressure, the gas concentration of saturation will drop, as a result, the mass of dissolved gas (which may not have substantially changed) will now be at supersaturated conditions. The overall problem arises because the generation of supersaturated TDG at the dam occurs faster than the dissipation of supersaturated TDG in the downstream reach. Because both generation and dissipation of TDG are functions of water temperature, there is an opportunity to affect the TDG process through selective withdrawal structures at a reservoir. Using a combination of field observations, and hydrodynamic modelling, we analysed the dependence of the water temperature difference on TDG generation from different-elevation release structures of high-dam reservoirs. By using of the dissipation model coupled with TDG and temperature, the evolution of supersaturated TDG from different withdrawal structures was simulated and compared in a natural river reach. It showed that warmer withdrawals result in reduced generation of TDG and enhanced dissipation of TDG.

INTRODUCTION

Water temperature is an amazing controlling factor that affects water quality and aquatic system in many aspects, such as the activity of microorganisms, the mass transfer of dissolved gas, and the suitability of habitats for aquatic organisms. The increasing number of dam constructions and operations are causing distinct spatial and temporal changes in the water temperature (Deng et al. 2011). Temperature stratification is one of the dominant characteristics of large and deep reservoirs. According to the literature (Deng 2003), the temperature difference between the surface and the bottom layer in a reservoir may reach as high as 17°C. To reduce the negative effects on aquatic organisms, various mitigation measures, such as stoplog intake and eco-regulation strategies, have been implemented (Deng et al. 2011, Chen et al. 2016). The temperature-related responses have aroused more public concern, among which is the response of supersaturated total dissolved gas (TDG) to temperature changes.

TDG supersaturation (TDGS) is an adverse impact caused by spill discharge from reservoirs, which is widely understood to cause bubble disease and thereby increase fish mortality (Weitkamp et al. 2003, Liang et al. 2013, Xue et al. 2019). Many studies have been performed on the evolution of TDGS and its mitigation strategies (Politano et al. 2012, Urban et al. 2008, Yingzhu et al. 2018). Li et al. (2009) proposed that two processes are involved in the TDGS problem of large dams. The first process is the generation process of TDGS, in which excessive air is dissolved under high pressure. The second consequent process is the dissipation process, in which the supersaturated TDG dissipates from water in the downstream river. Shen (2014) conducted experiments to explore the effect of water temperature on supersaturated TDG dissipation in static and turbulent conditions. Ou (2016) carried out experiments in both a straight flume and a converted flume to study the relationship between the dissipation coefficient and temperature in flowing water. However, before the present work, no investigation has provided insight into the quantitative response of TDGS to the water temperature stratification related to the reservoir operation. Determining the relationship between TDGS and water temperature variation is not only a practical but also a theoretical challenge for improving high dam operations.

With respect to the two processes of TDGS, both air dissolution and degasification are closely related to the water temperature. Herein, the paper will describe the response of TDG supersaturation to water temperature changes in each process.

RESPONSE OF SUPERSATURATED TDG GENERATION TO TEMPERATURE CHANGES

The generation extent of TDGS is closely related to the air solubility at a specific pressure and temperature in a plunge pool. Therefore, we first examine the air solubility dependence on temperature and then discuss the effect of water temperature regulation on the generation of supersaturated TDG.

Air Solubility in Terms of Temperature

It is well understood that the solubility of dissolved gas decreases as the temperature is increased under specific pressure and salinity (Colt 1984). The air solubilities of oxygen, nitrogen, and carbon dioxide, in units of mg/L, as a function of temperature are presented in Fig. 1. The data indicate that the air solubility varies with the change in temperature. For example, the solubility of oxygen at barometric pressure is 14.6 mg/L, 9.1 mg/L, and 6.4 mg/L at 0°C, 20°C, and 40°C, respectively. The total dissolved gas concentration at barometric pressure is 39.6 mg/L, 25.1 mg/L, and 18.0 mg/L at 0°C, 20°C, and 40°C, respectively. The percentage of dissolved gas saturation level is defined as the ratio of the actual gas concentration to its solubility at a specific temperature. The gas concentration (in mg/L) is expected to be different, even if the per cent TDGS level under different water temperature conditions is equal.

Effect of Water Temperature Regulation on the Generation of TDGS

In engineering practice, discharges from different elevations of a reservoir usually exhibit different temperatures. Herein, we consider two typical reservoirs as examples to analyse the contribution of the water temperature difference to TDG generation.

Pubugou reservoir in Daduhe River: The Pubugou hydropower station is located at the middle of the Daduhe River. The maximum height of the dam is 186 m, and the backwater length is 72 km. The authors conducted field observations on the water temperature and the TDG from 2012 to 2013. Fig. 2 illustrates the distribution of water temperature in the Pubugou reservoir in August. The water temperature is vertically stratified obviously.

The open spillway and the bottom spillway tunnel are the main release structures of the Pubugou hydropower station, for which the crest elevations are 833 m and 795 m, respectively. According to the observed results of the water temperature in 2012, the temperatures corresponding to the inlet of the open spillway and the bottom spillway tunnel are 21.4°C and 17.3°C, respectively. The temperature difference is approximately 4.1°C.

A TDG supersaturation level of 127% was observed during the discharge of the bottom spillway tunnel, with a flow rate of 2195 m^3/s. As the flow rate of 2195 m^3/s didn't occur during the operation practice of the open spillway, the TDG level under the same discharge rate was failed to obtain. To compare the sole temperature effect on TDGS, it is reasonable to assume that the open spillway exhibits the

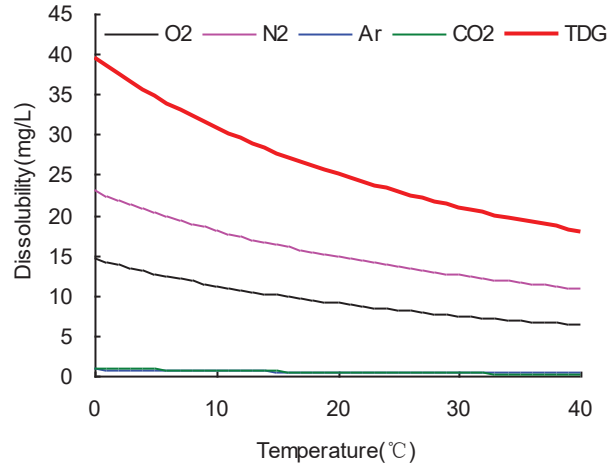

Fig. 1: Solubility of the air compositions and the total dissolved gas versus temperature.

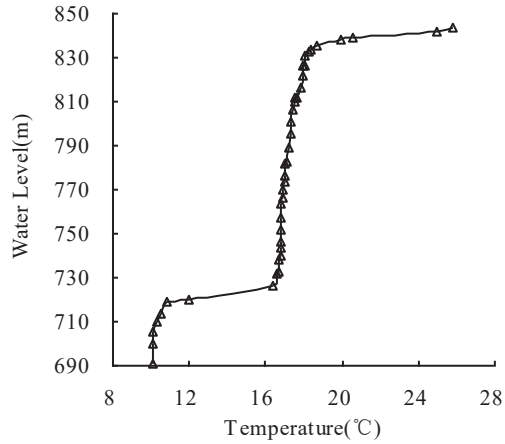

Fig. 2: Observed vertical temperature 1400-m of upstream the dam in the Pubugou Reservoir (Mid-August, 2012).

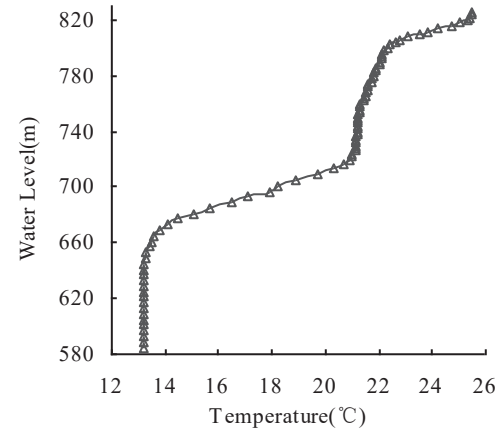

Fig. 3: Predicted vertical temperature upstream of the dam in the Baihetan Reservoir (Mid-September, Dry year).

same TDG level, 127%, with the bottom spillway tunnel. Hence the TDG concentration in mg/L can be obtained by multiplying the TDG solubility at the corresponding temperature by the TDG level of 127%. According to Fig. 1, the TDG solubility at 21.4°C is 24.4 mg/L and that at 17.3°C is 26.4 mg/L. Thus, the TDG concentrations in mg/L of the open spillway and the bottom spillway tunnel are determined to be 31.0 mg/L and 33.5 mg/L, respectively. The absolute TDG difference is 2.5 mg/L, which is equivalent to 8.1% of the TDG quantity of the open spillway. The reason for the difference is the TDG solubility difference caused by the temperature difference. According to previous studies, a higher level of TDG generation causes a larger adverse impact on TDG (Li et al. 2013). Therefore, with respect to TDG generation, discharge from the open spillway is more advisable than that from the spillway tunnel.

Baihetan reservoir in Jinshajiang River: The Baihetan hydropower station is a high-dam hydropower station currently under construction on the Jinshajiang River. The maximum height of the dam will be 289 m and the backwater length will be 182 km. Six surface orifices and seven bottom orifices will be included on the on-dam release structures for flood discharge, and the crest elevations will be 810 m and 714 m, respectively. The predicted temperature distributions in the reservoir for different typical years were obtained by the use of a laterally averaged numerical simulation model (SKLH 2013). Fig. 3 depicts the temperature distribution in the reservoir in September of a dry year. The predicted water temperature corresponding to the depths of the surface orifices and the bottom orifices are 24.8°C and 20.8°C, respectively.

According to Fig. 1, at barometric pressure, the air dissolubility at 24.8°C and 20.8°C is 22.93 mg/L and 24.67 mg/L, respectively. The difference in TDG concentration is 1.74 mg/L, and the relative difference is approximately 7.6%. According to the predicted results of TDG supersaturation caused by the release structures (SKLH 2008), the percentage level of TDG supersaturation at the exit of the plunge pool will be as high as 140% when the dam discharges. Assuming that the supersaturation value of 140% is valid for both the surface-orifice discharge and the bottom-orifice discharge,

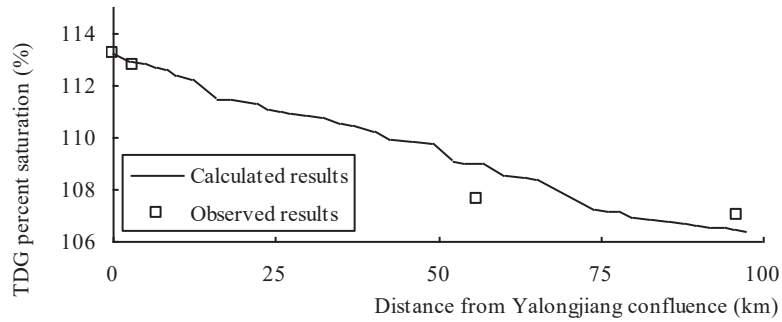

Fig. 4: Comparison of the TDG level between the calculated and observed results in the Jinshajiang River.

the equivalent TDG contents at 24.8°C (surface orifice) and 20.8°C (bottom orifice) are 32.10 mg/L and 34.54 mg/L, respectively. The difference of the TDG concentrations for the surface-orifice discharge and the bottom-orifice discharge is as high as 2.45 mg/L due to the temperature difference, which is equivalent to 7.6% of the TDG level at the surface orifice. For this reason, discharge from the surface orifices is more advisable than that from the bottom-orifices.

RESPONSE OF THE SUPERSATURATED TDG DISSIPATION PROCESS TO TEMPERATURE CHANGES

During the transport of the TDG-supersaturated discharge flow downstream, the water temperature changes as it travels due to the effects of solar radiation and heat transfer with air. In response to the change in water temperature, the gas solubility and the dissipation rate of supersaturated TDG changes, consequently resulting in different dissipation processes of the TDG.

Using the discharge flow from the Baihetan hydropower station as an example, a 1-D model was employed to simulate the dissipation process of TDGS at different temperature conditions.

Prediction Model

The model couples hydrodynamics, temperature and TDG. The governing equations are as follows:

Continuity equation:

$$\frac{\partial A}{\partial t}+\frac{\partial Q}{\partial x}=L_q \qquad \ldots(1)$$

Momentum equation:

$$\frac{\partial Q}{\partial t}+\frac{\partial}{\partial x}\left(\frac{\alpha Q^2}{A}\right)+gA\left(\frac{\partial Z}{\partial x}+S_f\right)+L_q\frac{Q}{A}=0 \qquad \ldots(2)$$

Temperature equation:

$$\frac{\partial (QT)}{\partial x}=\frac{\partial}{\partial x}\left(AD_L\frac{\partial T}{\partial x}\right)+\frac{b\varphi_n}{\rho C_p} \qquad \ldots(3)$$

TDG equation:

$$\frac{\partial (AC)}{\partial t}+\frac{\partial (QC)}{\partial x}=\frac{\partial}{\partial x}\left(AD_L\frac{\partial C}{\partial x}\right)-K_T(C-C_{s(T)}) \qquad \ldots(4)$$

In the above equations, x = the longitudinal distance (m). t = time (s^{-1}). T = Temperature (°C). Q = the flow rate (m^3/s). A = the area of the cross-section (m^2). D_L= the turbulent diffusivity (m^2/s). ρ = the water density (kg/m^3). C_p = the specific heat of water [J/(kg·°C)], b = the width of the cross-section (m). φ_n = the heat flux between water and air (W/m^2). C = the TDG concentration in mg/L. $C_{s(T)}$ = the TDG solubility capacity in mg/L with respect to the local temperature T. K_T = the first-order transfer rate coefficient with respect to the local temperature T (1/s).

φ_n is estimated according to the meteorological data from the weather stations in Qiaojia in the Yunnan province and Huize in the Sichuan province.

In previous studies, degasification was modelled using first-order kinetics for the TDG concentration (USACE 2005). Liu (2013) conducted a series of TDG dissipation experiments at different water temperatures and developed the relationship of the TDG dissipation coefficient versus water temperature that is described as follows:

$$K_T=K_{20}\times 1.062^{(T-20)} \qquad \ldots(5)$$

Where, K_{20} in equation (5) can be determined by the observed values analogically or can be determined according to the following equation derived by Feng et al. (2014):

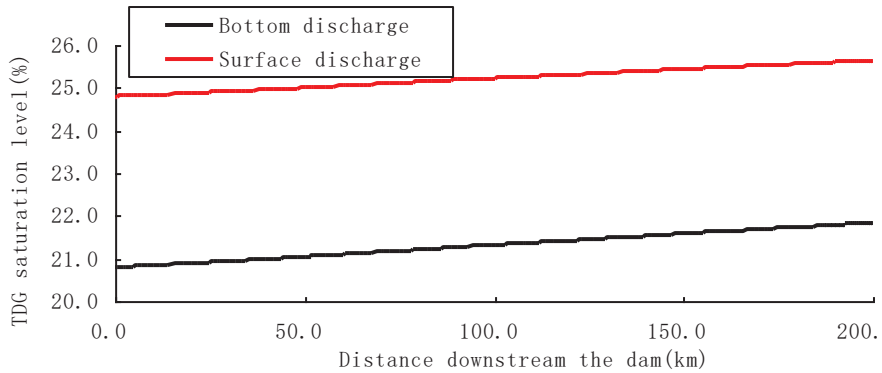

Fig. 5: Evolution of the temperature in the Jinshajiang River downstream of the Baihetan Dam.

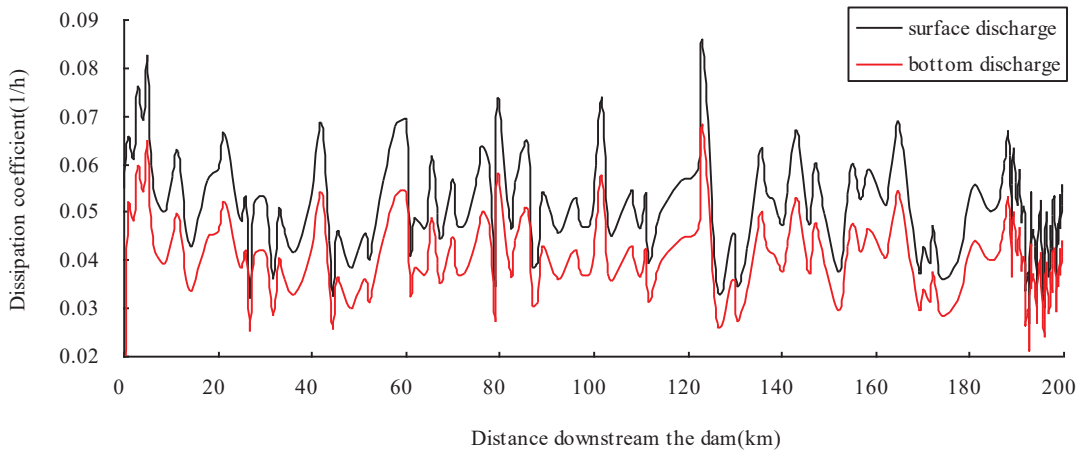

Fig. 6: TDG dissipation coefficient of the Jinshajiang River downstream of the Baihetan Dam.

$$K_{20} = 3600\phi \frac{u_*}{R}\left(\frac{H}{R}\right)^{2.02} Fr^{1.73} \quad \ldots(6)$$

According to equation (5), the TDG dissipation coefficient will increase to 1.4 times the original value when the water temperature rises 5°C and 1.8 times the original value when the water temperature rises 10°C, resulting in very different dissipation states of the supersaturated TDG.

Model Verification

A field observation on the dissipation of supersaturated TDG was conducted by Sichuan University on the river reach from the confluence of the Yalongjiang River and the Jinshajiang River to Longjie ferry. The observed reach is approximately 100 km. The observed results were used to verify the model as depicted in Fig. 4.

Case Description

Using the discharge of the Baihetan hydropower station as an example, the morphological data were employed to simulate the dissipation process of TDGS at different temperature conditions. The simulation cases and the boundary conditions are listed in Table 1.

RESULTS AND DISCUSSIONS

Fig. 5 shows that the water temperature increases slowly along the river reach. The temperature increment within 200 km is 0.8°C for the bottom discharge and 0.97°C for the surface discharge. The temperature increase along the river reach is very small due to the large flow rate and the high water depth. This result indicates that the impact of the temperature difference from different release structures continues for a very long distance from the dam.

As a function of velocity and water depth, the TDG dissipation coefficient of the Jinshajiang River downstream of the Baihetan Dam was calculated according to equation (6), as derived by Feng et al. (2014), and the results are shown in Fig. 6. The coefficient values fluctuate in the range of 0.03 h^{-1}~0.09 h^{-1} for the surface discharge and 0.02 h^{-1}~0.07 h^{-1} for the bottom discharge. The maximum difference of the coefficients of the two discharges is 0.018 h^{-1} at the section 123-km downstream of the dam.

The evolution of the TDG per cent saturation level for each discharge case is presented in Fig. 7. The dissipation process of TDG from the surface discharge is significantly faster than that of the bottom discharge. The percentage of the TDG saturation level of the surface discharge decreases

Table 1: Simulation cases and boundary conditions of the Baihetan hydropower station.

Case No.	Discharge Structure	Discharge temperature (°C)	TDG level in per cent (%)	TDG level (mg/L)
1	Surface orifice	24.8	140	32.10
2	Bottom orifice	20.8	140	34.54

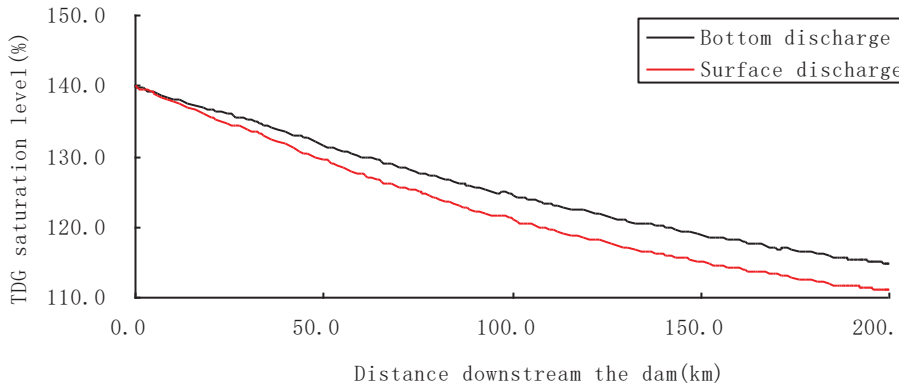

Fig. 7: Evolution of the TDG saturation level in the Jinshajiang River downstream of the Baihetan Dam.

27.9% within 200 km, whereas that of the bottom discharge decreases 24.0% within 200 km. The maximum difference of the TDG level at 200-km downstream of the dam is 3.9%, which is equivalent to 16% of the TDG dissipation of the bottom discharge.

The water temperature is a governing factor in both TDG generation and dissipation. Spills from different elevations result in different generation and dissipation processes of TDG. With respect to TDGS, the use of release structures at the surface is recommended to discharge floods due to the higher temperature near the surface of the reservoir. This result demonstrates that TDGS can be mitigated further by exploring temperature-based operational regulations.

CONCLUSIONS

The development of hydropower stations and reservoirs causes distinct spatial and temporal changes in water temperature. For high dam hydropower stations, the release structures are designed to be at different elevations. Due to the temperature stratification for large and deep reservoirs, the spill from different release structures may exhibit different water temperatures. This temperature difference can not only result in different TDG generation levels but can also affect the dissipation rate and per cent saturation level in terms of dissolubility.

According to the temperature stratification results of the Pubugou and Baihetan reservoirs, the water temperature difference from different release structures was approximately 4°C. The relative difference of the TDG generation from the different release structures of the Pubugou and Baihetan reservoirs was analysed to be approximately 7.6% and 8.1%, respectively, due to the temperature difference.

By using the discharge of the Baihetan high dam as an example, the dissipation processes of supersaturated TDG from different release structures at different water temperatures were simulated employing a proposed numerical model. Two different dissipation processes of TDG were obtained. The difference of the TDG per cent saturation levels at 200-km downstream of the dam is 3.9%, which is equivalent to 16% of the TDG decrement of the bottom discharge. This result demonstrates that water temperature plays an important role in the TDG dissolubility, both in the dissipation rate and the per cent saturation level. The response of TDG to water temperature changes implies that water temperature changes should be taken into account in the study of the TDG supersaturation problem of high dam discharges.

Discharges from different elevations exhibit different TDG generation and dissipation processes. With respect to TDG supersaturation, the use of release structures at higher elevations is recommended for discharge due to the elevated temperature near the surface of the reservoir. This recommendation implies that the temperature-based operational regulation is an effective approach to minimize the effect of TDG supersaturation.

ACKNOWLEDGEMENTS

The research was supported by the National Key R&D Program of China (Grant No. 2016YFC0401710) and the Open Fund of the State Key Laboratory of Hydraulics and Mountain River Engineering, Sichuan University (SKHL1702).

REFERENCES

Chen, D., Chen, Q., Leon, A. S. and Li, R. 2016. A genetic algorithm parallel strategy for optimizing the operation of reservoir with multiple eco-environmental objectives. Water Resources Management, 30(7): 2127-2142.

Colt, J. 1984. Computation of dissolved gas concentration in water as a function a temperature, salinity and pressure. American Fisheries Society Special Publication, No 14. Bethesda, USA.

Deng, Y. 2003. Study on the Water Temperature Prediction Model for the Huge and Deep Reservoir (in Chinese). PhD Thesis of Sichuan University. Chengdu.

Deng, Y., Tuo, Y., Li, J., Li, K. and Li, R. 2011. Spatial-temporal effects of temperature control device of stoplog intake for Jinping I hydropower station. Science China Technological Sciences, 54(1): 83-88.

Feng, J.J., Li, R. and Ma, Q. 2014. Experimental and field study on dissipation coefficient of supersaturated total dissolved gas. Journal of Central South University, 21(5): 1995-2003.

Li, R., Hodges, B.R., Yong, X.D. and Feng, J.J. 2013. Comparison of supersaturated total dissolved gas dissipation with dissolved oxygen dissipation and reaeration. Journal of Environmental Engineering, ASCE, 139(3): 385-390

Li, R., Li, J., Li, K. F., Deng, Y. and Feng, J.J. 2009. Prediction for supersaturated total dissolved gas in high-dam hydropower projects. Science in China, 52(12): 3661-3667.

Liang, R.F., Li, B., Li, K.F. and Tuo, Y.C. 2013. Effect of total dissolved gas supersaturated water on early life of David's schizothoracin (*Schizothorax davidi*). Journal of Zhejiang University-Science B (Biomedicine & Biotechnology), 14(7): 632-639.

Liu, S.Y. 2013. Temperature Impact on Supersaturated Total Dissolved Gas Generation and Dissipation (in Chinese). Master Thesis of Sichuan University. Chengdu:

Ou, Y. M., Li, R., Hodges, B. R., Feng, J. J. and Pu, C.X. 2016. Impact of temperature on the dissipation process of supersaturated total dissolved gas in flowing water. Fresenius Environ. Bull., 25: 1927-1934.

Politano, M., Amado, A. A., Bickford, S., Murauskas, J. and Hay, D. 2012. Evaluation of operational strategies to minimize gas supersaturation downstream of a dam. Computers and Fluids, 68: 168-185.

Shen, X., Liu, S.Y., Li, R. and Ou Y.M. 2014. Experimental study on the impact of temperature on the dissipation process of supersaturated total dissolved gas. Journal of Environmental Science, 26(9): 1874-1878.

State Key Laboratory of Hydraulics and Mountain River Engineering (SKLH) 2008. Evaluation of the Total Dissolver Gas Supersaturation Impact of Baihetan Hydropower Station on Jinshajiang River. Chengdu, China.

State Key Laboratory of Hydraulics and Mountain River Engineering (SKLH) 2013. Evaluation of the Water Environmental Impact of Baihetan Hydropower Station on Jinshajiang River. Chengdu, China.

Urban, A.L., Gulliver, J.S. and Johnson, D.W., 2008. Modeling total dissolved gas concentration downstream of spillways. Journal of Hydraulic Engineering, 134(5): 550-561.

US Army Corps of Engineers (USACE) 2005. Technical analysis of TDG processes. US Army Corps of Engineers -Northwest Division, Environmental Resources and Fish Planning offices.

Weitkamp, D.E., Sullivan, R.D., Swant, T. and DosSantos, J. 2003. Gas bubble disease in resident fish of the lower Clark Fork River. Transactions of the American Fisheries Society, 132(5): 865-876.

Xue, S., Wang, Y., Liang, R., Li, K. and Li, R. 2019. Effects of total dissolved gas supersaturation in fish of different sizes and species. International Journal of Environmental Research and Public Health, 16.(13): 2444.

Yingzhu, M., Hang, W., Jingjie, F. and Ran, L. 2018. Using the characteristics of river confluence to reduce the negative impact of supersaturated total dissolved gas (TDG). Nature Environment and Pollution Technology, 17(3): 845-852.

Nature Environment and Pollution Technology
An International Quarterly Scientific Journal

p-ISSN: 0972-6268
(Print copies up to 2016)
e-ISSN: 2395-3454

Vol. 19 | No. 2 | pp. 747-753 | 2020

Original Research Paper

https://doi.org/10.46488/NEPT.2020.v19i02.030

Open Access Journal

Prototype of Eco-Friendly Indoor Air Purifier to Reduce Concentrations of CO_2, SO_2 and NO_2

Saisantosh Vamshi Harsha Madiraju*†, P.V.S. Gopi Raghunadh and K. Ravi Kumar****

*Department of Civil and Environmental Engineering, University of Toledo, Toledo, Ohio-43606, USA

**Department of Civil Engineering, VNR Vignana Jyothi Institute of Engineering & Technology, Hyderabad-500090, Telangana, India

†Corresponding author: Saisantosh Vamshi Harsha Madiraju

Nat. Env. & Poll. Tech.
Website: www.neptjournal.com

Received: 29-08-2019
Accepted: 09-10-2019

Key Words:
Adsorption;
Prototype;
Indoor air;
Plant extractions;
Design;
Suction

ABSTRACT

Urbanization and industrialization lead to the increased usage of fossil fuels for running various types of automobiles and industries in developing countries. The rapid growth of automobiles usage in major cities causes air pollution and its direct impact on public health. This impact is alarming the worsening of the health of urban dwellers. But this impact can be reduced by breathing the filtered air. Filtering of air can be done in multiple ways. Among all, filters prepared from natural materials have become popular. In this study, an attempt has been made to find the novel approach to reduce the pollutants' level in the air by preparing prototype indoor air purifier which is designed, fabricated and tested with eco-friendly materials and adsorbents prepared from plant extractions. The three pollutants considered were CO_2, SO_2, and NO_2. Activated carbon was used as an adsorbent for CO_2 and NO_2 removal, whereas Neem bark, Mango bark, Orange peel powder and Neem leaf powder were used for SO_2 removal. The prototype was designed for Hyderabad city, Telangana State of India and tested at houses of five different locations (Balanagar, Jeedimetla, Zoo Park, MGBS and JNTU) which are major traffic intersections in the city. The level of pollution before and after the installation of the instrument was measured for three months (January, February, March) and analysed. Results indicate the improvement of air quality after filtration.

INTRODUCTION

In the urbanized world, lifestyle is automated and dependency on automobiles is increasing enormously. The sudden lifestyle change resulted in increasing automobiles decade after decade. This massive shift is damaging the ambient air quality which is impacting the millions of urban dwellers (Kura et al. 2013, Gurjar & Nagpure 2015). Next to industrial and power plants, the gigantic automobile growth rate of two, three and four-wheelers, passenger buses and multi-axle trucks, etc. are burning fossil fuel leading to permanent damage to air and atmosphere. The problem is aggravating in developing countries like India. The economic growth and industrialization are the two fundamental factors producing regional pockets of heavy pollutants especially, in metro-cities which have seen a rapid rise in the fleet of vehicles in the last decade (CMIE 1998, Garg et al. 2001).

The causes of rapid growth of automobile increase include but not limited to (i) increasing human dependency on the automobiles, transport of commercial goods etc., (ii) marketing tactics include lot of attractive finances availability even for common man to buy a vehicle according to one's interest and (iii) the frequent old vehicle exchange offers from suppliers exhilarating the existing users to go for new vehicles etc.

Increase in the number of vehicles producing large amounts of pollution into the air which leads to multiple impacts. Impact on human health is quite alarming news nowadays (Gurjar & Nagpure 2015, Jain & Khare 2009). UNEP (2010) reports that urban air pollution is linked to about 1 million premature deaths and 1 million pre-native deaths each year. It is believed that diesel vehicle fumes can cause cancer than petrol vehicles in India. Diesel vehicles also have high risk in causing non-cancerous effects like allergy, asthma and other respiratory problems (Bhandarkar 2013). According to Vannan Kandi Vijayan et al. (2015), the recent data on the amount of exposure to indoor and outdoor air pollution further revealed a strong reason for cardiovascular diseases, such as strokes and ischemic heart disease.

The main pollutants such as CO_2, SO_2 and NO_2 present in the air cause health problems. Carbon dioxide is emitted when carbon compounds go through combustion. Nitrogen dioxide is the main source of nitrate aerosols. This is mainly

released during heating, power generation and engines in vehicles and ships. It causes severe respiratory problems, lowering the immune system, especially in children. It is also responsible for the formation of surface-level ozone, toxic nitrates, etc. Sulphur dioxide is released when any organic matter is burned. Sulphur dioxide causes several diseases like asthma, inflammation of respiratory organs, chronic bronchitis, etc.

Reducing the concentration of these pollutants is very much important for healthy living in the urbanized world. To breathe air free from pollutants, there is a need to purify surrounding air using an air purifier. The British Thoracic Society on Asthma Management recommended the use of air filters for removal of the pet and other allergens (Vannan Kandi Vijayan et al. 2015). USEPA (2009) recommends the usage of gas-phase air filters to remove gaseous pollutants by using a material called a sorbent, such as activated carbon to adsorb pollutants. Reshma et al. (2017) have presented the review of literature discussing the importance of using the ornamental plants, weedy trees, and green space as natural filters of air pollution reduces respiratory illness mortality rates and reducing visits to the hospitals. Many species of ornamental shrubs and herbaceous landscape plants have been identified for phytoremediation to improve indoor and outdoor air quality. The research on the removal of air pollutants using natural materials and natural methods is scanty in the literature.

The objective of the present study is to reduce the pollutants' level in the air by preparing a physical prototype indoor air purifier which is designed, fabricated and tested with eco-friendly materials and adsorbents prepared from plant extractions. Selection of the natural materials is inspired by the culture and customs in the age-old traditions of India, in which Neem tree, Tulasi and *Ficus religiosa* considered as holy plants and Mango leaves. These age-old practices inspired us to test these plant materials concerning air purification. The physical model developed with these plant materials works on the principle of adsorption and suction of pollutants. The three pollutants considered were CO_2, SO_2 and NO_2. Activated carbon was used as an adsorbent for CO_2 and NO_2 removal, whereas Neem bark, Mango bark, Orange peel powder and Neem leaf powder were used for SO_2 removal. The adsorbents were considered in four different sizes. The sizes were considered in such a way that the parameters can be distinguished.

For the case study, the Hyderabad, metropolitan city of Telangana State, India was selected which is witnessing the rapid growth of the number of two-wheelers and four-wheelers in the past two decades due to over-population and migration from rural to urban areas. According to Sood (2012), both the two-wheelers and four-wheelers together contributing more than 80 per cent of the vehicle population in Hyderabad city. Sarath & Rakesh (2009) investigated using the data, the contribution of various pollutants in Hyderabad City. Overall, the transport sector is expected to contribute particulate matter (PM) direct emission of about 50%, PM indirect emission of 30%, and high contributions to ozone and CO along the main activity corridors. Considering the importance of reducing the air pollution at a major junction of the city, the prototype is tested at houses of five different locations such as Balanagar, Jeedimetla, Zoo Park, Mahatma Gandhi Bus Station (MGBS) and Jawaharlal Nehru Technological University (JNTU), Kukatpally which are major traffic intersections in the city. The level of pollution before and after the installation of the instrument was measured for three months (January, February and March) and analysed.

MATERIALS AND METHODS

The major components of the air purifier were made of eco-friendly materials. The body of the purifier was made up of a wood called Novopan. It was designed in a cuboidal shaped box with four inlets and one outlet. This prototype works on the principle of adsorption and suction. The workflow is shown in Fig. 1.

The four exits consist of filters made of jute, a strong durable natural fibre. It has properties like UV protection, heat insulation, sound insulation, anti-static properties, high tensile strength, low extensibility, and low thermal conduction, carbon dioxide neutral and also naturally decomposable. It can be recycled once and also bio-degradable. It is an eco-friendly and low-cost fibre extracted from the plant's stem. Artificial polymer filters were also prepared to test the efficiency and compared with natural filters. The exhaust fan with properties of Volts 230 AC: 50Hz 1Phase, 2800Rpm, Sweep of 150 mm was inserted on the fifth side. The adsorbents were prepared from plant extractions of neem bark powder, mango bark powder, neem leaf powder, orange peel powder and also activated carbon. The adsorbing media based on the pollutants are categorized in Table 1.

The compartments are made in the filters with an ascending of size towards the outlet fan. These compartments are filled with four different sizes of adsorbents as mentioned in Table 2.

Fabrication

Novopan wood material was used for the body of the air purifier. Cuboid shaped box with five side openings was designed to place the filters at the four sides for inlet purpose and one for insertion of a suction fan of 2800rpm speed. Filters were made with both natural and artificial fibres to

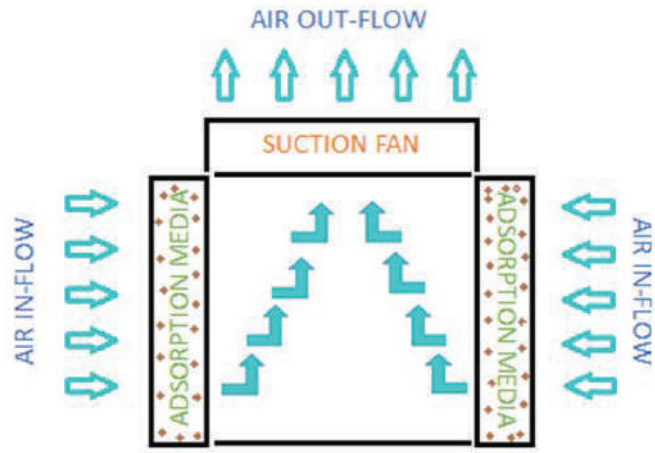

Fig. 1: Workflow of prototype air purifier.

compare the efficiency between them. Natural fibre as jute and artificial fibre as polymer were used. Filters were divided into three horizontal compartments to the adsorbing material in increasing order as the suction pressure varies with the distance from the fan. Adsorption material was inserted in the filters. The male part of Velcro was attached to the four openings of inlet and female to the filters (both natural and artificial). A suction fan was attached to the body of the purifier at the opening provided for the insertion. It was fixed tightly in such a way that the body does not vibrate while it works. Filters were attached to the purifier and measured the concentrations of pollutants at inlet and outlet. The values were tabulated. The procedure of measuring concentrations of pollutants with varying sizes of absorbing materials was repeated and the filters with natural and artificial fibres were interchanged.

Table 1: Adsorbent allotment to pollutants.

Pollutants	Adsorbing Media
CO_2	Activated carbon
NO_2	Activated carbon
SO2	Neem bark powder
	Mango bark powder
	Neem leaf powder
	Orange peel powder

Table 2: The adsorbents used in filters and their sizes.

Adsorbents Used	Sizes
Neem bark powder	>1.18 mm, 1.18-2.36 mm, 2.36-4.75 mm, >4.75 mm
Mango bark powder	>1.18 mm, 1.18-2.36 mm, 2.36-4.75 mm, >4.75 mm
Neem leaf powder	<300 microns, 300-425 microns, 425-600 microns, >600 microns
Orange peel powder	>1.18 mm, 1.18-2.36 mm, 2.36-4.75 mm, >4.75 mm
Activated carbon for carbon dioxide	>1.18 mm, 1.18-2.36 mm, 2.36-4.75 mm, >4.75 mm
Activated carbon for nitrogen dioxide	>1.18 mm, 1.18-2.36 mm, 2.36-4.75 mm, >4.75 mm

The Experiment

The prototype prepared was installed in the houses in the selected locations. Then the concentrations of pollutants were measured before installation and after installation at the air outlet of the purifier. The SO_2 and NO_2 values were measured with the respiratory dust sampler followed by spectrophotometer, and carbon dioxide by CO_2 analyser. A similar number of experiments were conducted with varying the size of adsorbents and also all the five adsorbents. The experiment was conducted for the three months of January, February and March in the year 2016. Then the sampling recordings were analysed after conducting an on-site experiment with respiratory dust sampler. The concentrations of SO_2, NO_2 and CO_2 were calculated in the laboratory.

Sampling and Analysis of SO_2

The Modified West and Geake method was used for the measurement of sulphur dioxide in the air. The concentration of sulphur dioxide (µg/m³) was calculated using the calibration graph. The SO_2 concentration was calculated using equation 1 and equation 2.

$$C = \frac{(V1-V2) \times N \times K}{V} \quad ...(1)$$

Where,
C = Sulphite concentration (mg/mL)
V1 = Volume of thiosulfate for blank (mL)
V2 = Volume of thiosulfate for sample (mL)
N = Normality of thiosulfate
K = 32000 (Milli-equivalent weight SO_2/µg)
V = Volume of standard sulphite solution (mL)

$$C\ (S0_2\ \mu g/m^3) = (As\text{-}Ab) \times CF \times (Vs/Va) \times Vt \quad ...(2)$$

Where,
C (SO_2) = Concentration of sulphur dioxide (µg/m^3)
As = Absorbance of sample
Ab = Absorbance of the reagent blank
CF = Calibration factor
Va = Volume of air sampled (m^3)
Vs = Volume of sample (mL)
Vt = Volume of aliquot taken for analysis (mL)

Sampling and Analysis of NO_2

Modified Jacobs and Hochheiser method was used for the measurement of nitrogen dioxide in the air. The concentration of nitrogen dioxide (µg/m³) was measured using the calibration graph. The concentration of NO_2 was calculated using equation 3.

$$C\ (NO_2\ \mu g/m^3) = (As\text{-}Ab) \times CF \times (Vs/Va) \times Vt \times 0.82 \quad ...(3)$$

Where,
C (NO_2) = Concentration of nitrogen dioxide (µg/m^3)
As = Absorbance of sample
Ab = Absorbance of the reagent blank
CF = Calibration factor
Va = Volume of air sampled (m^3)
Vs = Volume of sample (mL)
Vt = Volume of aliquot taken for analysis (mL)
0.82 = Sampling efficiency

Sampling and Analysis of CO_2

Handheld carbon dioxide analyser of the model 1205B gas analyser was used. This accurately measures the concentration of carbon dioxide in a duct. It has a two-line LCD to display the concentrations of carbon dioxide before installation and at the outlet of the purifier after installation with a sampling probe. 225 sets of readings can be stored simultaneously measuring the concentrations at intervals from 1 to 10 minutes. The readings were recorded with varying adsorbent sizes. The maximum limits for the recordings were at temperatures 32°F to 104°F, relative humidity limits of 10 to 90 % with 1 ppm resolution.

RESULTS AND DISCUSSION

The final concentration of the pollutants was measured after installation of this prototype at five major locations in the city to estimate the maximum efficiency of adsorbents under practical working conditions. The initial and final mean concentrations of the pollutants in the three months from January to March with varying sizes of adsorbents are shown in Fig. 2 to Fig. 17.

Change of adsorbent size indirectly means the change of surface area. The pattern observed is the increase in surface area increases the rate of adsorption through which maximum efficiencies are achieved. Particles with the size less than 1.18 mm have greater efficiency than the particles with the size greater than 4.75 mm irrespective of the absorbents used in this research. These four natural adsorbents were used only for sulphur dioxide removal. Among them, neem leaf powder has the least efficiency and mango bark powder has the highest efficiency. But in the case of carbon dioxide and nitrogen dioxide, activated carbon was found to be more efficient. The eco-friendly components used in fabrication have high stability factors towards the environment. The purifier is portable and can easily fit in windows. This helped us in performing the experiments at different locations.

All the laboratory experiments mentioned in this study were carried out at room temperature (25 ± 5°C) at 1 atm pressure. All the instruments (respiratory dust sampler, CO_2 gas analyser, spectrophotometer) used in this research were

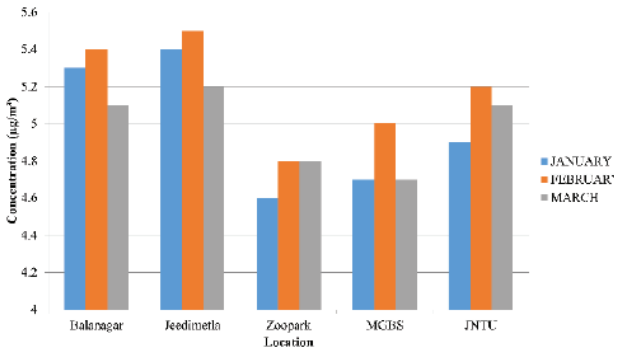

Fig. 2: Initial readings of SO_2 in selected areas.

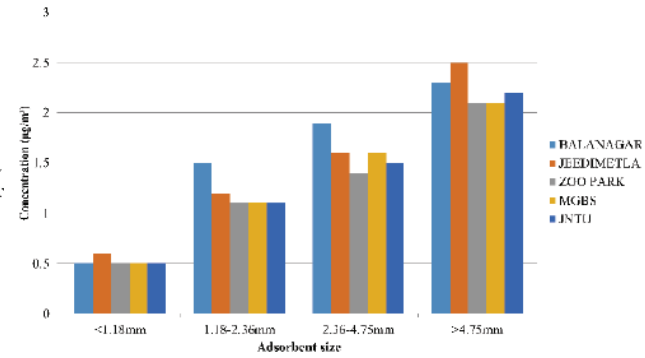

Fig. 3: Concentrations of SO_2 at the outlet of purifier using neem bark powder.

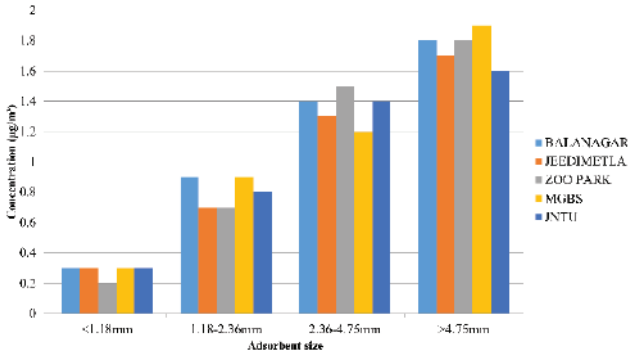

Fig. 4: Concentrations of SO_2 at the outlet of purifier using mango bark.

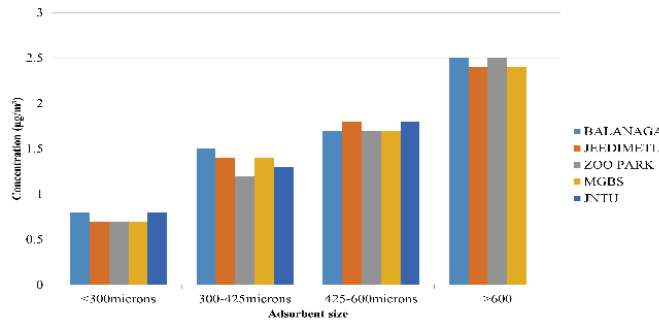

Fig. 5: Concentrations of SO_2 at the outlet of purifier using neem leaf powder.

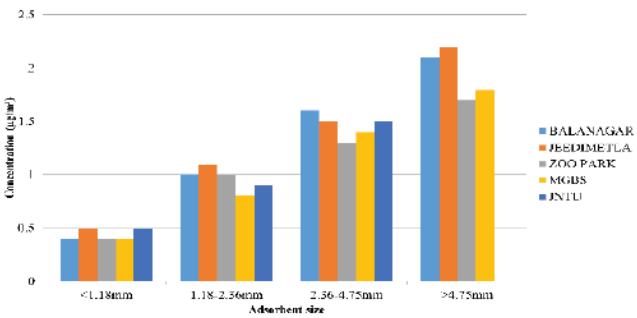

Fig. 6: Concentrations of SO_2 at the outlet of purifier using orange peel powder.

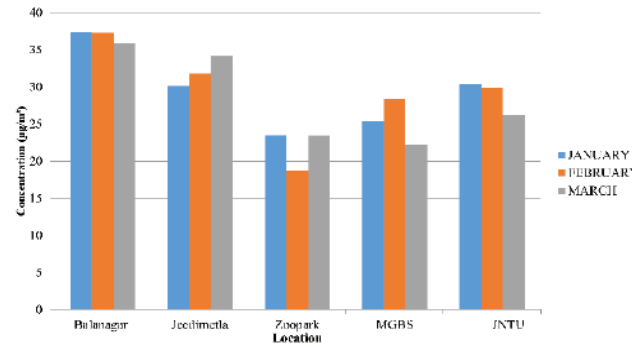

Fig. 7: Initial readings of NO_2 at selected locations.

calibrated for respective readings. All the materials used for fabricating the prototype were eco-friendly. No chemicals or any hazardous substances were used in this prototype. The adsorbents used in the study, after they reach the saturation point, can be disposed off through incineration.

CONCLUSIONS

In the present study, five different locations were selected (i) Balanagar (Industrialized area), (ii) Jeedimetla (Industrial and residential area), (iii) MGBS (Main bus station), (iv) JNTU (High population density) and (v) Zoo park area (Tourist place) in Hyderabad city.

- The reading of SO_2 was measured in three months (January, February and March) in Balanagar, Jeedimetla, Zoo-park, JNTU, MGBS, and results are 5.3, 5.4, 5.1 µg/m^3 in Balanagar; 5.4, 5.5, 5.2 µg/m^3 in Jeedimetla,

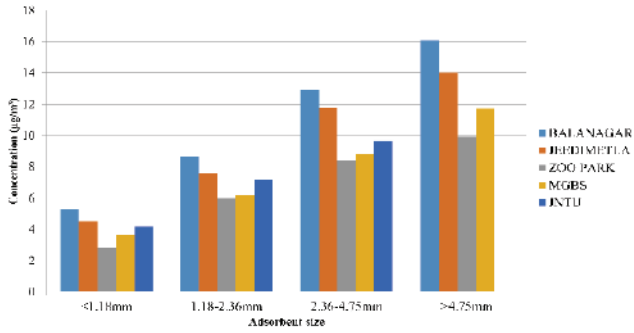

Fig. 8: Concentrations of NO_2 at the outlet of the purifier.

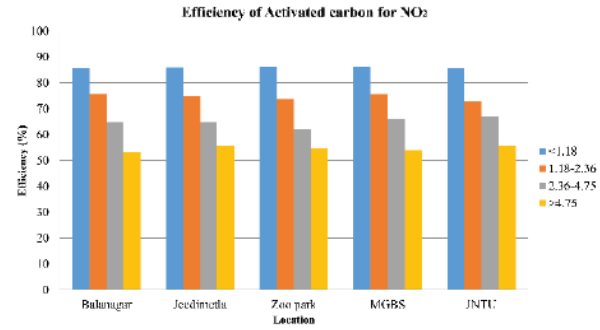

Fig. 9: The efficiency of activated carbon for NO_2.

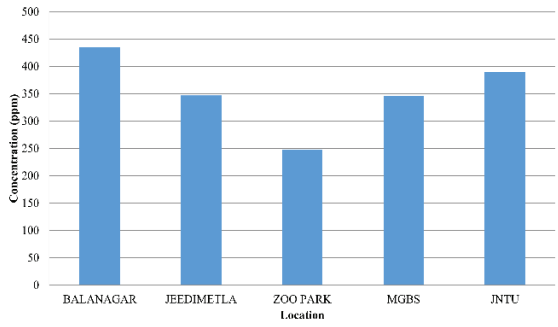

Fig. 10: Initial concentrations of CO_2 at various locations.

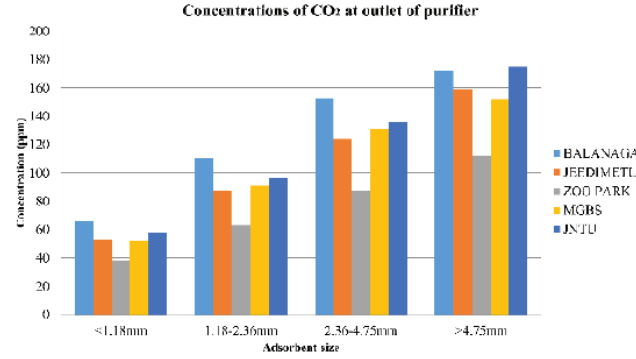

Fig. 11: Concentrations of CO_2 at the outlet of the purifier.

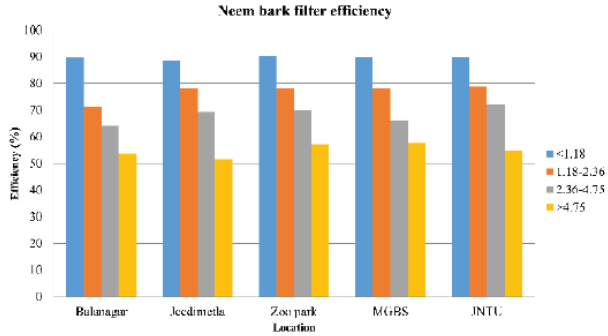

Fig. 12: The efficiency of neem bark filter.

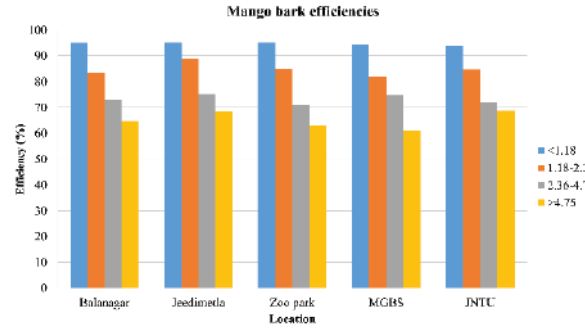

Fig. 13: The efficiency of mango bark.

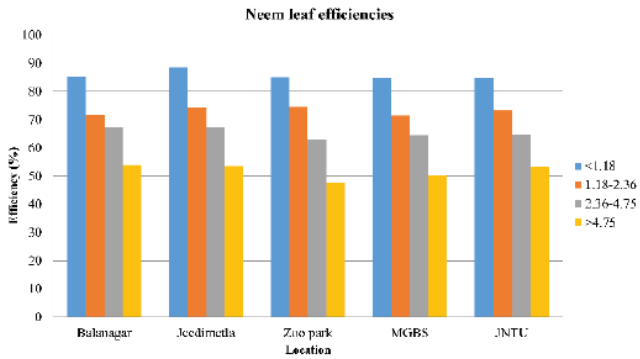

Fig. 14: The efficiency of neem leaf powder.

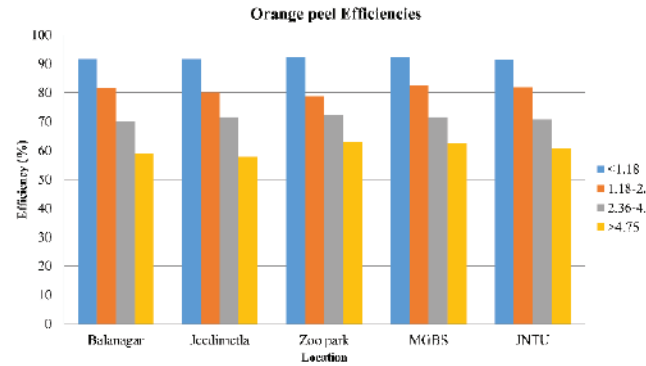

Fig. 15: The efficiency of orange peel powder.

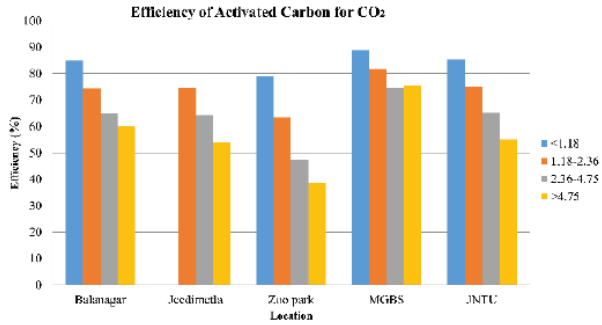

Fig. 16: The efficiency of activated carbon for CO_2.

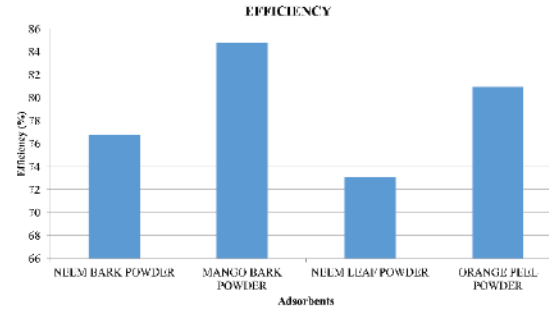

Fig. 17: The overall efficiency of the adsorbing materials.

4.6, 4.8, 4.8 µg/m^3 in Zoo park area, 4.7, 5, 4.7 µg/m^3 in MGBS and 4.9, 5.2, 5.1 µg/m^3 in JNTU.

- The adsorbents used were neem bark powder, mango bark powder, neem leaf powder, orange peel powder of sizes 1.18 mm, 1.18-2.36 mm, 2.36-4.75 mm, and >4.75 mm.
- In the study, it was identified that mango bark powder adsorbs more SO_2 as compared to other materials.
- As the size of adsorbents increases, the adsorption capacity decreases.
- It was observed that activated carbon is more efficient for NO_2 as compared to other materials.
- It was observed that activated carbon is quite efficient in the removal of CO_2.

For the present study, only a few materials were considered for the adsorption of CO_2, SO_2 and NO_2 for indoor purpose. But it is possible to use other materials or a combination of materials for multi pollutants and to even operate at outdoors by changing the functionality of the purifier.

ACKNOWLEDGEMENT

We would like to express our thanks to the Department of Civil Engineering, VNR VJIET Hyderabad, India and Environmental & Biotechnical Engineering Section, JNTU, Hyderabad for helping us in the experimentation. The technical assistance provided by the technical staff is gratefully acknowledged.

REFERENCES

Bhandarkar, Shivaji 2013. Vehicular pollution, their effect on human health and mitigation measures. Vehicle Engineering (VE), 1(2): 33-40.

CMIE 1998. Infrastructure. Center for Monitoring Indian Economy, Mumbai.

Elsom, D.M. and Loughurst, J.W.S. 2004. Local and Regional Aspects of Air Quality Management: An Overview, Regional and Local Aspects of Air Quality Management, 1st ed. In: D. M. Elsom & J. S. M. Longhurst (Eds.), Southampton, UK: WIT, pp. 1-13.

Garg, Amit, Shukla, P.R., Bhattacharya, Sumana and Dadhwal, V.K. 2001. Sub-region (district) and sector level SO_2 and NOx emissions from India: Assessment of inventories and mitigation flexibility. Atmospheric Environment, 35/4: 703-713.

Gurjar, Bhola R. and Nagpure, Ajay S. 2015. Indian megacities as localities of environmental vulnerability from air quality perspective. Journal of Smart Cities, 1(1): 15-30.

Jain, Suresh and Khare, Mukesh 2009. Urban air quality in megacities: A case study of Delhi city using vulnerability analysis. Environmental Monitoring and Assessment, 136: 257-265.

Kura, Bhaskar, Verma, Suruchi, Ajdari, Elena and Iyer, Amrita 2013. Growing public health concerns from poor urban air quality: Strategies for sustainable urban living. Computational Water, Energy and Environmental Engineering, 2: 1-9.

Reshma, V.S., Prashant Kumar and G.S. Chaitra 2017. Significant role of ornamental plants as air purifiers-A Review. International Journal of Current Microbiology and Applied Sciences, 6(8): 2591-2606.

Sarath, K.G. and Rakesh, A. 2009. Contribution of vehicular activity to air pollution in Hyderabad, India: Measurements, chemistry and analysis. Indian Journal of Air Pollution Control, IX(1): 37-46.

Sood, Pranav Raghav 2012. Air Pollution through vehicular emission in urban India and preventive measures. International Conference on Environment, Energy and Biotechnology, IPCBEE, 33: 45-49.

UNEP 2010. Urban Air Quality. United Nations Environment Programme, Urban Environment Unit - http://www.unep.org/urban_environment/issues/urban_air .asp.

USEPA 2009. Residential Air Cleaners. EPA 402-F-09-002. www.epa.gov/iaq.

Vannan Kandi Vijayan 2105. Enhancing indoor air quality-The air filter advantage. Lung India, 32(5): 473-479.

Nature Environment and Pollution Technology
An International Quarterly Scientific Journal

p-ISSN: 0972-6268
(Print copies up to 2016)
e-ISSN: 2395-3454

Vol. 19 | No. 2 | pp. 755-760 | 2020

Original Research Paper

https://doi.org/10.46488/NEPT.2020.v19i02.031

Open Access Journal

Removal of Cadmium in Aqueous Solution by Sulfidated Nanoscale Zero-Valent Iron

Weiyun Yang*, Ruolin Qin, Rui Qin**, Linli Zhang** and Muqing Qiu**†**

*Pharmaceutics and Materials Engineering School, Jinhua Polytechnic, Haitang West Street 888, Jinhua, 321007, P.R. China

**College of Life Science, Shaoxing University, Shaoxing, 312000, P.R. China

†Corresponding author: Muqing Qiu; qiumuqing@126.com

Nat. Env. & Poll. Tech.
Website: www.neptjournal.com

Received: 01-07-2019
Accepted: 30-08-2019

Key Words:
Cadmium removal;
Zero-valent iron;
Sulfidated nanoscale iron;
Aqueous solution

ABSTRACT

Due to mining, industrial wastewater discharge and agricultural fertilization and other human activities, heavy metal cadmium pollution in water bodies has become increasingly prominent. In this study, the sulfidated nanoscale zero-valent iron was prepared by the method of liquid-phase reduction. The removal behaviour of Cd(II) ion in aqueous solution and the effect of pH in solution on its removal rate were investigated. The synthesized materials before and after the adsorption reaction were characterized by scanning electron microscopy, X-ray diffraction and Zeta potential tester. The removal mechanism of Cd(II) ion in solution was explored in details. The results showed that the S-nZVI particles present a polymeric sheet. They contained Fe^0, Fe_3O_4 and FeS. The removal rate of Cd(II) ion by the S-nZVI particles is higher than the nZVI particles. The reaction mechanism for S-nZVI particles to remove Cd(II) ion is that Cd(II) ion replaces Fe in FeS and then combines with S to form stable CdS compound. S has a significant effect on the oxidation process of iron.

INTRODUCTION

The heavy metal cadmium is a non-essential element of the human body. It mainly comes from the discharge of industrial wastewater such as mining, electroplating, batteries, smelting and dyes (Su et al. 2015). At present, the presence of heavy metal of cadmium can be detected in the environment (Lv et al. 2018). Compared with other heavy metals, cadmium has higher fluidity and is easily absorbed by plants. Additionally, it also can be enriched in the human body through the food chain, thus causing serious harm to human health (Qiu et al. 2018). Nowadays, the treatment techniques for removing cadmium from water mainly include adsorption, precipitation, ion exchange, membrane separation and so on (Zhang et al. 2014, Soleymanzadeh et al. 2015). Among these methods, the adsorption method mainly uses some chemical and biological adsorbents, such as activated carbon, hydrogel, carbon nanotubes, bagasse and so on. Precipitants commonly used in precipitation methods are sulphides, hydroxides and iron oxides (Gil-Díaz et al. 2017, Hu et al. 2017). These treatment techniques limit their large-scale applications due to cost or treatment efficiency issues. Therefore, there is an urgent need to develop more treatment methods for cadmium removal efficiency, low cost, and environmental friendliness.

Nano zero-valent iron (nZVI) is widely used in the pollution control of groundwater and soil heavy metals due to its high reactivity (Li et al. 2016, Zhu et al. 2019). The nZVI particles have a unique core-shell structure in which the core is Fe(0) and the shell is FeOOH based iron oxide. In the processing of reaction with heavy metals, the nucleus acts as an effective electron donor to reduce the nZVI particles (Vaidotas et al. 2018). The shell provides adsorption points for the removal of heavy metals, and the core has a special complimentary effect with the shell (Li et al. 2017a). However, the removal efficiency of nZVI particles for heavy metal cadmium ion in solution close to its oxidation-reduction potential is low and unstable (Li et al. 2017b, Meghdad et al. 2019).

In recent years, many researchers have found that sulfidated nZVI particles can further increase its reactivity and selectivity, depending on the type and amount of sulfidated agent, the synthesis method and the target contaminant (Soleymanzadeh et al. 2015, Janja et al. 2018). The commonly used sulfidated agents for the preparation of sulfidated nZVI particles are sodium sulphide, sodium dithionite and sodium thiosulfate (Kong et al. 2016). In the study of the synthesis method, the synthesis according to the sulfidated agent is added before and after the formation of nZVI can be divided into a one-step method and a two-step method. Han & Yan (2016) studied the effects of different sulfidated agents and synthetic methods on the degradation of triethylene compounds. The results showed that the effect of the degradation rate of triethylene was independent of the

sulfidated agent and the synthesis method, but was related to the ratio of S/Fe. The S-nZVI particles were synthesized with a two-step process using Na_2S as a sulfided agent and removed the $^{99}TcO_4^-$ ion in solution. The experimental results showed that $^{99}TcO_4^-$ was reduced to TcO_2 and fixed to the surface (Fan et al. 2013).

In this research, the main objective is 1) the S-nZVI particles were prepared by the method of liquid-phase reduction; 2) the adsorption of Cd(II) by the S-nZVI particles was tested; 3) The synthesized materials before and after the adsorption reaction were characterized by scanning electron microscopy, X-ray diffraction and Zeta potential tester; 4) The removal mechanism of Cd(II) ion in solution was explored.

MATERIALS AND METHODS

Preparation of S-nZVI

The S-nZVI was prepared by the method of liquid-phase reduction and a two-step method. 1 L 0.25 mol/L $NaBH_4$ solution was gradually added to a beaker containing 1 L 0.045 mol/L $FeCl_3$ solution. The solution was stirred by an electric stirring bar at the speed of 600 r/min, and the stirring operation was continued for 15 min after completion of the mixture reaction. The mixture was filtered through a Buchner funnel. The collected solid particles were rinsed 3 times with deionized water and then washed once with absolute ethanol. The nZVI particles were obtained. Ten g of nZVI particles

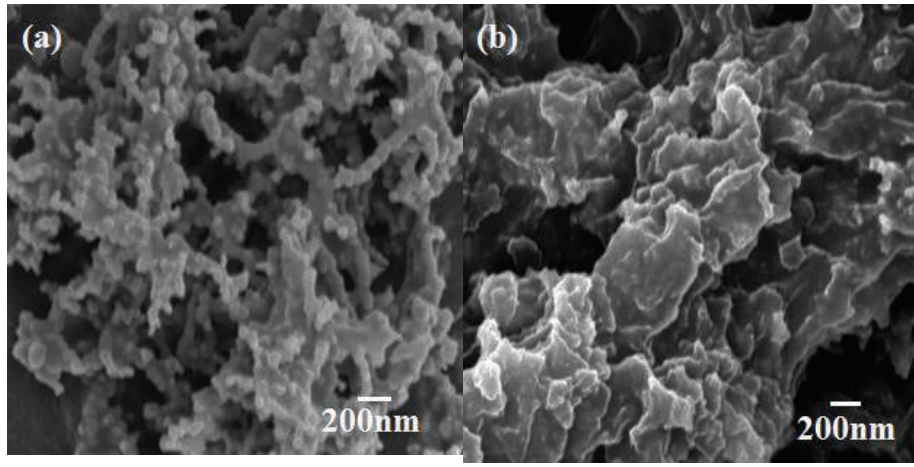

Fig. 1: SEM images of nZVI and S-nZVI [(a) nZVI particles and (b) S-nZVI particles].

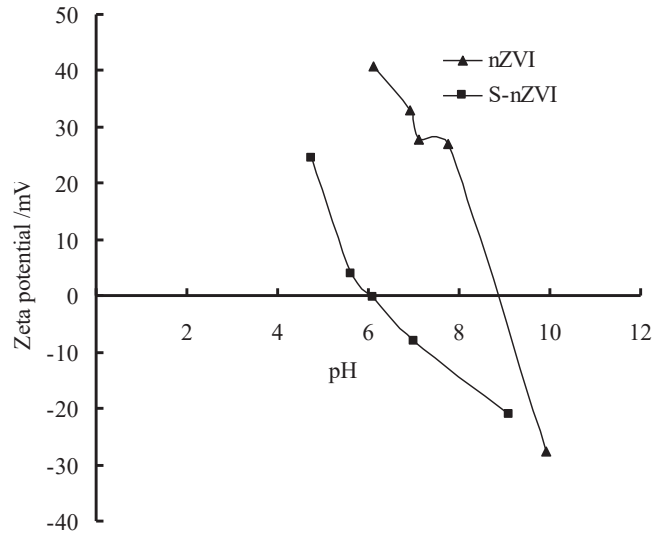

Fig. 2: The zeta potential of nZVI particles and S-nZVI particles as a function of pH.

were weighed into a 250 mL beaker containing 150 mL 215 g/L Na_2S solution and then shaken for 15 min at the speed of 600 r/min. Then, the S-nZVI particles were obtained for the experiment.

Characterization of S-nZVI

The morphology of S-nZVI particles was observed with SEM (JEOL 6500F, Japan). The XRD analysis was conducted in a D/Max-IIIA Powder X-ray Diffractometer (Rigaku Corp., Japan). The Zeta-potential was determined by Zeta potential tester (DT-1202, U.S.A.).

Adsorption Experiment

Adsorption experiments were conducted in a set of 250 mL Erlenmeyer flasks containing 0.1 g the S-nZVI and 100 mL of 200 mg/L Cd (II) ion solutions. The initial pH was adjusted to 4.0 with 1 mol/L HCl. The flasks were placed in a shaker at a constant temperature of 298 K and 200 rpm. The samples were filtered and analysed.

Analytical Methods

The concentration of cadmium ions was analysed by atomic absorption spectrophotometry. The amount of adsorbed Cd (II) ion q_t (mg/g) at different times, was calculated as follows:

$$Q = \frac{C_0 - C_t}{C_0} \times 100\% \quad \ldots(1)$$

Where, C_0 and C_t (mg/L) are the initial and equilibrium concentrations of Cd(II) ion in solution respectively. Q is the degradation rate of Cd(II) ion.

Statistical Analyses of Data

All the experiments were repeated in duplicate and the data of results were the mean and the standard deviation (SD). The value of the SD was calculated by Excel Software. All error estimates given in the text and error bars in figures are the standard deviation of means (mean ± SD). All statistical significances were noted at α=0.05 unless otherwise stated.

RESULTS AND DISCUSSION

Characterization of S-nZVI

The SEM images of the synthetic nZVI and S-nZVI are shown in Fig. 1. As can be seen from Fig. 1(a), the surface of synthetic nZVI particles exhibited a chain shape. After sulfidation, the surface of the S-nZVI particles exhibits a polymeric sheet structure (Fig. 2(b)).

Fig. 2 is a graph showing the zeta potential of nZVI particles and S-nZVI particles as a function of pH. It can be seen from Fig. 2 that as the pH increases, the zeta potential gradually changes from a positive value to a negative value. The zeta potential of nZVI particles and S-nZVI particles are 8.91 and 5.95.

The results of XRD in Fig. 3 showed that the synthetic nZVI particles have characteristic peaks at 2θ=44.6°, 64.9, 64.9° and 82.3°.

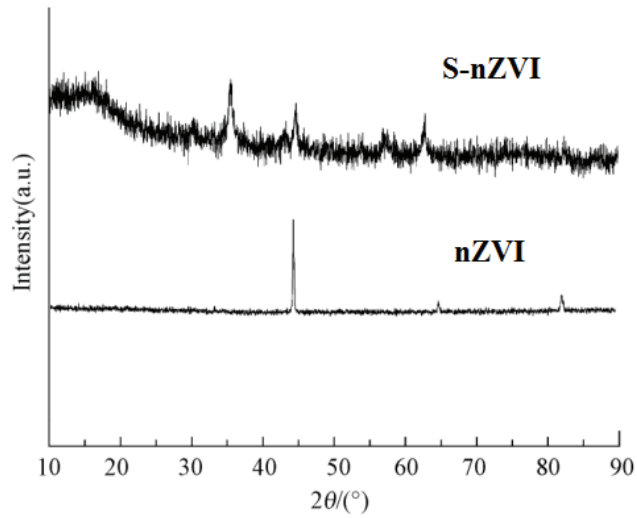

Fig. 3: XRD of nZVI particles and S-nZVI particles.

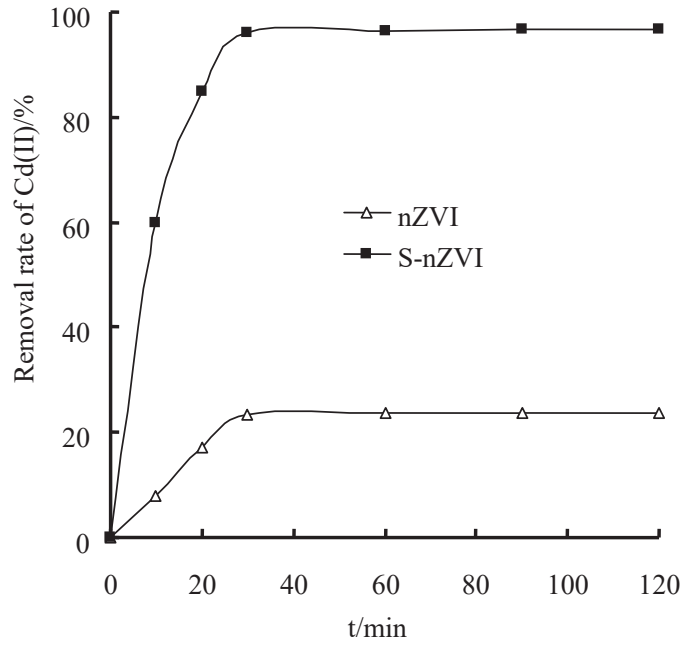

Fig. 4: Removal rate of Cd(II) ion by the nZVI particles and the S-nZVI particles.

This peak is the characteristic peak of $\alpha - Fe^0$. It also indicates that the synthetic nZVI particles are mainly present in the form of $\alpha - Fe^0$. There is no characteristic peak of iron oxide found in the synthetic nZVI particles. It may be the reason that the synthetic nZVI particles have low iron oxide content or a poor crystallinity and exist in an amorphous state (Sikder et al. 2014).

The synthetic S-nZVI particles detected a broad $\alpha - Fe^0$ peak at 2θ=44.6°. It indicates that the crystallinity of $\alpha - Fe^0$ becomes low after the sulfidation treatment.

Besides, characteristic peaks of Fe_3O_4 and FeS were also detected. It indicates that the nZVI particles are loaded with S (Li et al. 2018).

Removal of Cadmium

Fig. 4 shows the removal rate of Cd(II) ion by the nZVI particles and the S-nZVI particles. As shown in Fig. 4, in the first 30 minutes, the removal rates of Cd(II) ion by the

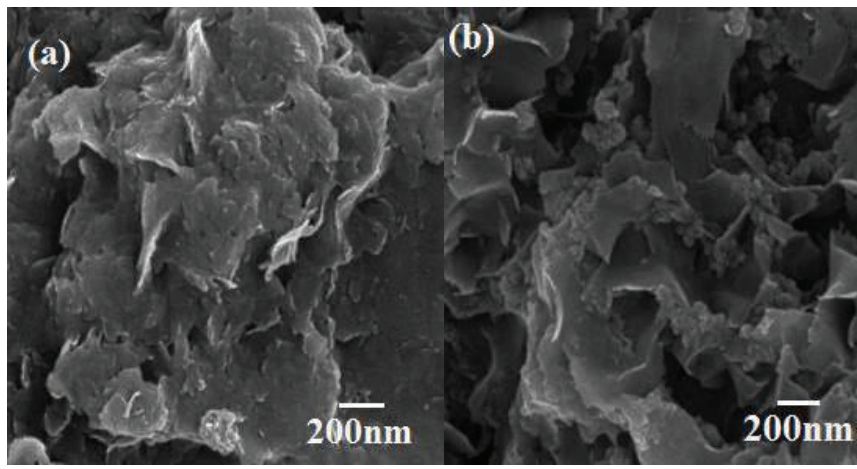

Fig. 5: SEM images of nZVI particles and S-nZVI particles after the reaction.

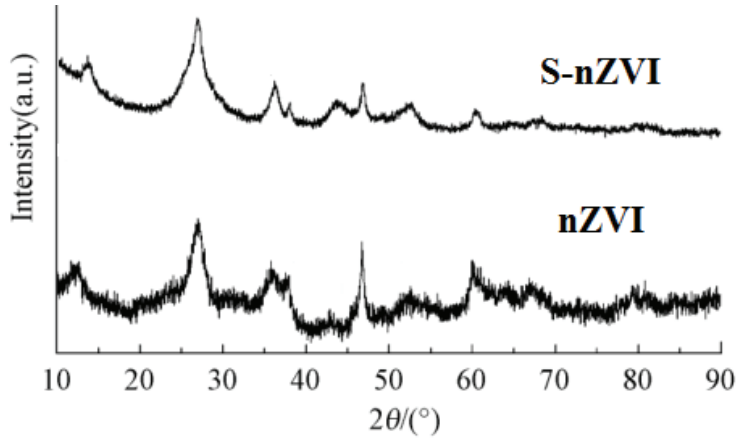

Fig. 6: XRD of nZVI particles and S-nZVI particles after the reaction.

nZVI particles and the S-nZVI particles are increasing. At 30 minutes, the removal rate of Cd(II) ion reached its maximum. Subsequently, the removal rate of Cd(II) ion increases very little. Additionally, the removal rate of Cd(II) ion by the S-nZVI particles is higher than the nZVI particles. The removal rate of Cd(II) ion by the S-nZVI particles reaches 96.1% at 30min.

Reaction Mechanism of Cadmium Removal

Fig. 5 is SEM images of the nZVI particles and S-nZVI particles after the reaction. As can be seen from the figure that the surface of the nZVI particles and S-nZVI particles is oxidized to a shape of a random sheet after reaction with Cd(II) ion in solution. The XRD of nZVI particles and S-nZVI particles after the reaction with Cd(II) ion is shown in Fig. 6.

It can be seen from Fig. 6 that there are strong γ–$FeO(OH)$ characteristic peaks in the nZVI particles and S-nZVI particles after the reaction with Cd(II) ion in solution. The FeS characteristic peak disappeared and a CdS characteristic peak was detected. This indicates that Cd(II) ion will react with Fe in FeS compound to generate CdS. Additionally, the weak S^0 characteristic peaks were also detected. This may be due to the action of FeS in the reaction and the residual O_2 in the solution (Crane et al. 2018, Holmes & Crundwell 2013 and Xia et al. 2010). After the reaction of nZVI with Cd(II) ion, the iron oxidation product in the material is mainly γ–$FeO(OH)$. For S-nZVI, the iron oxidation product in the material is mainly γ–$FeO(OH)$ and $\alpha - Fe_2O_3$. This indicates that S has a significant effect on the oxidation process of iron (Hardiljeet et al. 2011, Xue et al. 2018).

CONCLUSIONS

(1) The S-nZVI particles were prepared by the method of liquid-phase reduction and a two-step method. The S-nZVI particles present a polymeric sheet. They contain Fe^0, Fe_3O_4 and FeS.

(2) The removal rate of Cd(II) ion by the S-nZVI particles is higher than the nZVI particles.

(3) The reaction mechanism for S-nZVI particles to remove of Cd(II) ion is that Cd(II) ion replaces Fe in FeS and then combines with S to form stable CdS compound. S has a significant effect on the oxidation process of iron.

ACKNOWLEDGEMENTS

This study was financially supported by the Project of Science and Technology Plan in Zhejiang Province (LGF19C030001 and LGF20C030001) and the Project of Science and Technology Plan in Shaoxing City (2017B70058).

REFERENCES

Crane, R.A. and Sapsford, D.J. 2018. Selective formation of copper nanoparticles from acid mine drainage using nanoscale zerovalent iron particles. J. Hazard. Mater., 347: 252-265.

Fan, D., Anitori, P.R., Tebo, B.M., Tratnyek, P.G., Pacheco, J.S.L., Kukkadapu, R.K., Mark, H., Engelhard, M., Bowden, E. and Libor, K. 2013. Reductive sequestration of pertechnetate ($^{99}TcO_4^-$) by nano zerovalent iron (nZVI) transformed by abiotic sulfide. Environ. Sci. Technol., 47: 5302-5310.

Gil-Díaz, M., Pinilla, P., Alonso, J. and Lobo, M.C. 2017. Viability of a nanoremediation process in single or multi-metal(loid) contaminated soils. J. Hazard. Mater., 321: 812-819.

Han, Y.L. and Yan, W.L. 2016. Dechlorination of trichloroethene by zero-valent iron nanoparticles: reactivity enhancement through sulfidation treatment. Environ. Sci. Technol., 50: 12992-13001.

Hardiljeet, K.B., Meera, J. and Denis, M.O. 2011. Kinetics and thermodynamics of cadmium ion removal by adsorption onto nano zerovalent iron particles. J. Hazard. Mater., 186: 458-465.

Holmes, P.R. and Crundwell, F.K. 2013. Polysulfides do not cause passivation: Result from the dissolution of pyrite and implications for other sulfide minerals. Hydrometallurgy, 139: 101-110.

Hu, B.W., Chen, G.H., Jin, C.G., Hu, J., Huang, C.C., Sheng, J., Sheng, G.D., Ma, J.Y. and Huang, Y.Y. 2017. Macroscopic and spectroscopic studies of the enhanced scavenging of Cr(VI) and Se(VI) from water by titanate nanotube anchorednanoscale zero-valent iron. J. Hazard. Mater., 336: 214-221.

Janja, V., Primož, O., Radmila, M., Ana, M. and Ščančar, J. 2018. Investigation of the behaviour of zero-valent iron nanoparticles and their interactions with Cd^{2+} in wastewater by single particle ICP-MS. Sci. Total Environ., 634: 1259-1268.

Kong, X.K., Han, Z.T., Zhang, W., Song, L. and Li, H. 2016. Synthesis of zeolite-supported microscale zero-valent iron for the removal of Cr^{6+} and Cd^{2+} from aqueous solution. J. Environ. Manage., 169: 84-90.

Li, B., Yang, L., Wang, C.Q., Zhang, Q.P., Liu, Q.C. and Li, Y.D. 2017a. Adsorption of Cd(II) from aqueous solutions by rape straw biochar derived from different modification processes. Chemosphere, 175: 332-340.

Li, J., Chen, C.L., Zhu, K.R. and Wang, X.K. 2016. Nanoscale zero-valent iron particles modified on reduced graphene oxides using a plasma technique for Cd(II) removal. J. Taiwan Inst. Chem. Eng., 59: 389-394.

Li, S.L., Wang, W., Liang, F. and Zhang, W.X. 2017b. Heavy metal removal using nanoscale zero-valent iron (nZVI): Theory and application. J. Hazard. Mater., 322: 163-171.

Li, Z.T., Wang, L., Meng, J., Liu, X.M., Xu, J.M., Wang, F. and Brookes, P. 2018. Zeolite-supported nanoscale zero-valent iron: New findings on simultaneous adsorption of Cd(II), Pb(II), and As(III) in aqueous solution and soil. J. Hazard. Mater., 344: 1-11.

Lv, D., Zhou, X.X., Zhou, J.S., Liu, Y.L., Li, Y.Z., Yang, K.L., Lou, Z.M., Shams, A.B., Wu, D.L. and Xu, X.H. 2018. Design and characterization of sulfide-modified nanoscale zerovalent iron for cadmium(II) removal from aqueous solutions. Appl. Sur. Sci., 442: 114-123.

Meghdad, P., Sajad, M., Mohsen, S., Wang, X.K. and Negin, F. 2019. A new composite of nano zero-valent iron encapsulated in carbon dots for oxidative removal of bio-refractory antibiotics from water. J. Clean. Prod., 209: 1523-1532.

Qiu, M.Q., Wang, M., Zhao, Q.Z., Hu, B.W. and Zhu, Y.L. 2018. XANES and EXAFS investigation of uranium incorporation on nZVI in the presence of phosphate. Chemosphere, 201: 764-771.

Sikder, M.T., Tanaka, S., Saito, T. and Kurasaki, M. 2014. Application of zerovalent iron impregnated chitosan-caboxymethyl-αcyclodextrin composite beads as arsenic sorbent. J. Environ. Chem. Eng., 2: 370-376.

Soleymanzadeh, M., Arshadi, M., Salvacion, J.W.L. and SalimiVahid, F. 2015. A new and effective nanobiocomposite for sequestration of Cd(II) ions: Nanoscale zerovalent iron supported on sineguelas seed waste. Chem. Eng. Res. Design, 93: 696-709.

Su, Y.M., Adeyemi, S.A., Arturo, A.K., Huang, Y.X., Dai, C.M., Zhou, X.F. and Zhang, Y.L. 2015. Magnetic sulfide-modified nanoscale zerovalent iron (S-nZVI) for dissolved metal ion removal. Water Res., 74: 47-57.

Vaidotas, D., Saulius, V. and Vaidotas, V. 2018. Batch removal of Cd(II), Cu(II), Ni(II), and Pb(II) ions using stabilized zero-valent iron nanoparticles. Energy Procedia, 147: 214-219.

Xia, J.L., Yang, Y., He, H., Zhao, X.J., Liang, C.L., Zheng, L., Ma, C.Y., Zhao, Y.D., Nie, Z.Y. and Qiu, G.Z. 2010. Surface analysis of sulfur speciation on pyrite bioleached by extreme thermophile *Acidianus manzaensis* using Raman and XANES spectroscopy. Hydrometallurge, 100: 129-135.

Xue, W.J., Huang, D.L., Zeng, G.M., Wan, J., Zhang, C., Xu, R., Cheng, M. and Deng, R. 2018. Nanoscale zero-valent iron coated with rhamnolipid as an effective stabilizer for immobilization of Cd and Pb in river sediments. J. Hazard. Mater., 341: 381-389.

Zhang, Y.L., Li, Y.T., Dai, C.M., Zhou, X.F. and Zhang, W.X. 2014. Sequestration of Cd(II) with nanoscale zero-valent iron (nZVI): Characterization and test in a two-stage system. Chem. Eng. J., 244: 218-226.

Zhu, L., Tong, L.H., Zhao, N., Li, J. and Lv, Y.Z. 2019. Coupling interaction between porous biochar and nano zero valent iron/nano α-hydroxyl iron oxide improves the remediation efficiency of cadmium in aqueous solution. Chemosphere, 219: 493-503.

Nature Environment and Pollution Technology
An International Quarterly Scientific Journal

p-ISSN: 0972-6268
(Print copies up to 2016)
e-ISSN: 2395-3454

Vol. 19 | No. 2 | pp. 761-766 | 2020

Original Research Paper

https://doi.org/10.46488/NEPT.2020.v19i02.032

Open Access Journal

Influence of Tannery Effluents on Morphological Characters of *Ipomoea pes-caprae* (L.) Sweet and *Clerodendron inerme* (L.) Gaertn.

A. Venkatesan
Department of Botany, Annamalai University, Annamalainagar-608 002, Tamilnadu, India; venkatesan2k@yahoo.com

Nat. Env. & Poll. Tech.
Website: www.neptjournal.com

Received: 16-07-2019
Accepted: 29-08-2019

Key Words:
Tannery effluent;
Halophytes;
Ipomoea pes-caprae;
Clerodendron inerme

ABSTRACT

Tannery industry is common in many parts of the world, which is polluting groundwater ecosystems and producing major heavy metals and sodium chloride. The present study is aimed at some morphological characters in phytoremediation of heavy metals and ions from tannery effluents by using halophytic species such as *Ipomoea pes-caprae* and *Clerodendron inerme*. The morphological characters were analysed at an interval of 30, 60, 90 and 120 days. The results indicated that all the morphological characters were increased with an increasing concentration of tannery effluents and no injury symptoms in growth condition. It may be concluded that these halophytic species are potentially suitable for phytoremediation of heavy metals from the tannery effluent contaminated soils, which will reclaim the soil for further use as crop cultivation or crop improvement.

INTRODUCTION

Soil and water pollution by toxic heavy metals is a major environmental concern worldwide. Heavy metals are extremely toxic and present in our immediate environment. Irrespective of the origin of the metals in soils, excessive levels of many metals can result in the quality degradation, crop yield reduction, and poor quality of agricultural products (Long et al. 2002). Naturally occurring heavy metals have a great adsorption capacity in soil and are thus not readily available for living organisms. The bonding energy between heavy metals and soil is very high compared to that with anthropogenic sources. Heavy metals from anthropogenic source typically have a high bioavailability due to their soluble and mobile relative forms (Dixit et al. 2015).

Bioremediation is a process that uses microorganisms on their enzymes to promote degradation and/or removal of contaminants from the environment (Perpetuo et al. 2011). One of these strategies, biostimulation, involves promoting the growth of microorganisms at the contaminated site in order to introduce pH-correction substances, nutrients surfactants and oxygen. Another strategy, bioaugmentation or bioaddition is the addition of microbial populations indigenous alien or genetically modified organisms in places where there is an insufficient of indigenous microorganisms with ecophysiologically characteristics compatible with the habitat conditions that are conducive for the promotion of bioremediation (Li & Li 2011).

Generally, the majority of plants used for environmental restoration are typical glycophyte species. Nevertheless, metal phytoremediation by halophytes plants receives only little attention. Recently, it has been reported that halophytes species would be better adapted to cope up with environmental constraints, including heavy metals (Ghanya et al. 2007). A great deal of recent studies strongly indicates that halophytic plants could be more suitable for heavy metal extraction mainly from saline soils than glycophytes (Milic et al. 2012). The objective of the present study is to analyse the influence of different concentrations of tannery effluent on *Ipomoea pes-caprae* and *Clerodendron inerme* to characterize the morphological parameters for phytoremediation of tannery effluent contaminated soils.

MATERIALS AND METHODS

Ipomoea pes-caprae and *Clerodendron inerme* seedlings were collected from salt marsh area of Pichavaram, Cuddalore district, Tamilnadu, India. The seedlings were selected for the characterization and screening for phytoremediation of heavy metals and salts from tannery effluents with special reference to morphological studies. The experimental site was located at Annamalai University, Tamil Nadu, India.

Experimental Design

The experiment was conducted in an open air area with natural light, temperature and humidity. Red soil and sand (3:1 ratio) free from pebbles and stones was filled in polythene bags.

The seedlings from the selected species of similar size were transplanted from the nursery bed and planted at the polythene bags. Two experiments comprised of the three

sets of treatments with five replicates were conducted and the average values were reported. Plants were watered every 2-3 days once, depending on the evaporative demand. The plants were harvested at intervals of 30, 60, 90 and 120 days after the treatment for further study. Physical and chemical characteristics of the tannery effluent soil were determined before planting and harvesting of halophytes. The control plants were treated without the effluent with only tap water. The various concentrations of 30, 60 and 90% of the tannery effluent was prepared and treated with 250 mL for 4 times with a gap of 7 days interval. During each and every sampling day, samples were collected, washed thoroughly with tap water followed by distilled water. The shoot length, root length (cm plant^{-1}), fresh and dry weight (g plant^{-1}) number of leaves and total leaf area (cm^2 plant^{-1}) were calculated at monthly intervals. Five samples were collected from each concentration and used for studying the morphological characteristics.

Shoot Length and Root Length

The plant height was recorded by measuring the height of the plant from the surface of the soil to the tip of the plant. Root length was recorded by measuring the length of the surface soil to the tip of the root. This was recorded on 30, 60, 90 and 120 days after the treatment and expressed in cm plant^{-1}.

Fresh and Dry Weight

For the estimation of fresh weight of the leaf, stem and root portions were separated and weighed. They were dried in a hot air oven at 80°C for 24 hours. The fresh and dry weight was taken by using an electronic balance.

Total Number of Leaves

The total number of leaves per plant was counted immediately after harvesting the plant samples.

Total Leaf Area

The leaf area was calculated by measuring the length and breadth of the leaf and multiplying it by a correlation factor derived from the method of Kalra & Dhiman (1977).

Statistical Analysis

The experimental data were subjected statistically by the technique of analysis of the variance and standard deviation (Suedector & Cochran 1967).

RESULTS AND DISCUSSION

In the present investigation, observations on morphological characteristics such as shoot and root length, fresh and dry weight, number of leaves and total leaf area were determined after 30, 60, 90 and 120 days of *Ipomoea pes-caprae* and *Clerodendron inerme* treated with tannery effluent. The maximum accumulation of shoot and root length of both the species increased up to 90% on all the sampling days when compared to control (Figs. 1 and 2). The maximum

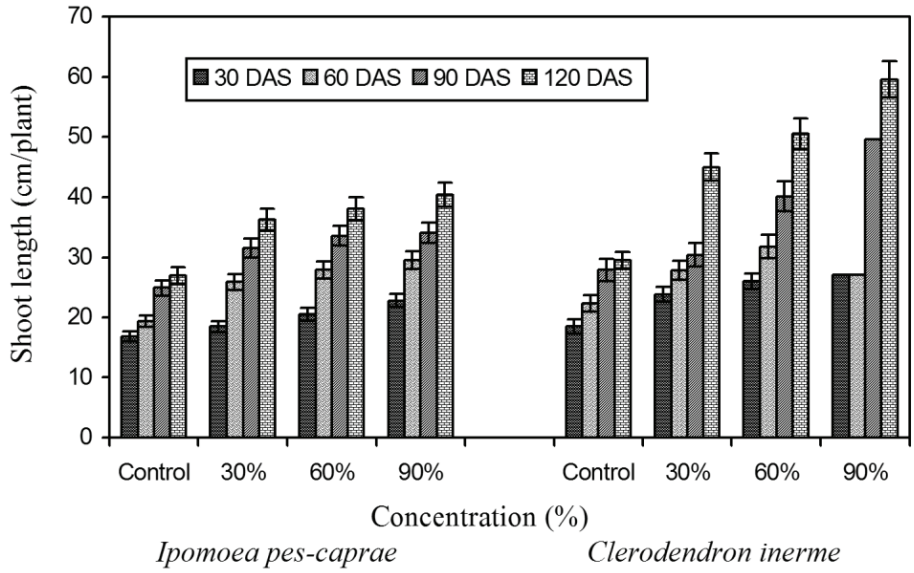

Fig. 1: Effect of different concentrations of tannery effluent on shoot length of *Ipomoea pes-caprae* and *Clerodendron inerme.*

percentage of shoot and root length observed in *Ipomoea pes-caprae* (170.3% and 142.8%) and *Clerodendron inerme* (183% and 173%) respectively higher when compared to control of 120th days after treatment.

The fresh and dry weight of *Ipomoea pes-caprae* and *Clerodendron inerme* plants treated with tannery effluent are presented in Figs. 3 and 4. The maximum percentage of shoot and root fresh weight and dry weight observed in *Ipomoea pes-caprae* (283% and 223%) and *Clerodendron inerme* (427% and 250%) respectively were higher when compared to control on 120th day after the treatment. The similar findings were observed in the other morphological parameters such as number of leaves and total leaf area, which also increased up to 90% tannery effluent when compared

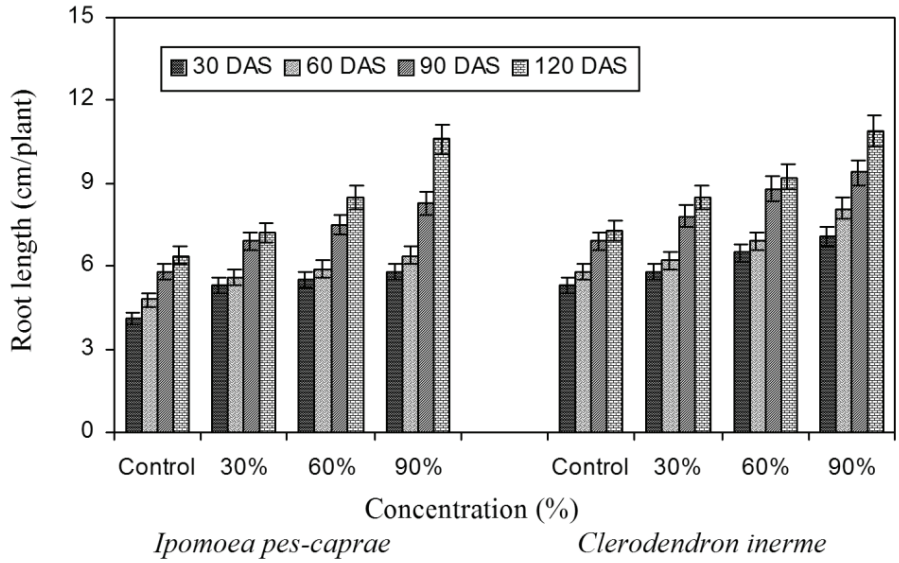

Fig. 2: Effect of different concentrations of tannery effluent on root length of *Ipomoea pes-caprae* and *Clerodendron inerme.*

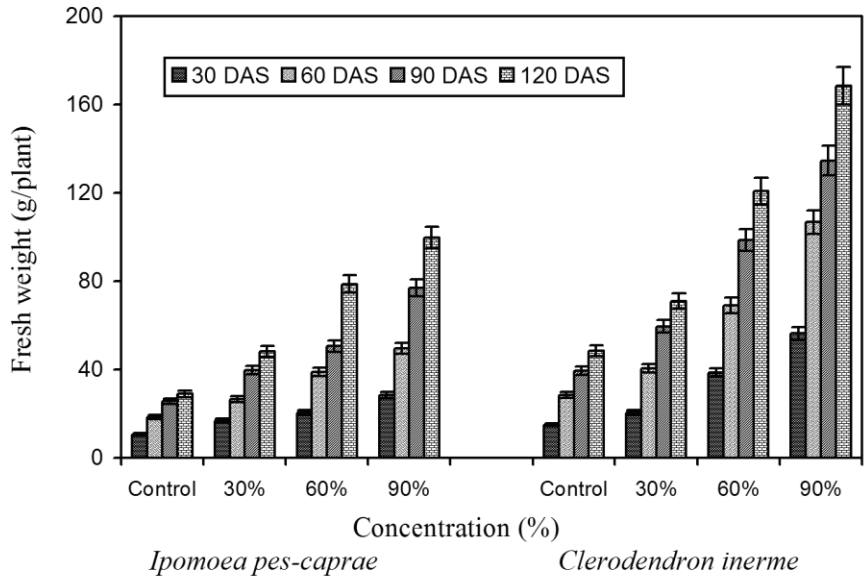

Fig. 3: Effect of different concentrations of tannery effluent fresh weight of *Ipomoea pes-caprae* and *Clerodendron inerme.*

to control on 120 day after the treatment. The maximum percentage increased in the number of leaves (121.05% and 443%) in *Ipomoea pes-caprae* and (400% and 504%) in *Clerodendron inerme*, respectively higher when compared to control on 120th day after treatment (Figs. 5 and 6).

The ability to tolerate both Cd^{2+} and Pb^{2+} accumulation in the shoot without deleterious effects on growth suggest as efficient protection of the cellular biochemical machinery against free metal ions (Cd^{2+} and Pb^{2+}) and could be of critical interest for phytomanagement of polluted areas which are frequently contaminated with several heavy metals (Eid & Eisa 2010). The effect of artificial pollution with 25 $mg.kg^{-1}$ soil of multiple Zn, Cu and Ni on *Sporobolus virginicus* and *Spartina petens* grown for 8 weeks. They reported that no growth inhibition of shoot biomass was observed.

The reduction in fresh and dry weight due to heavy metal

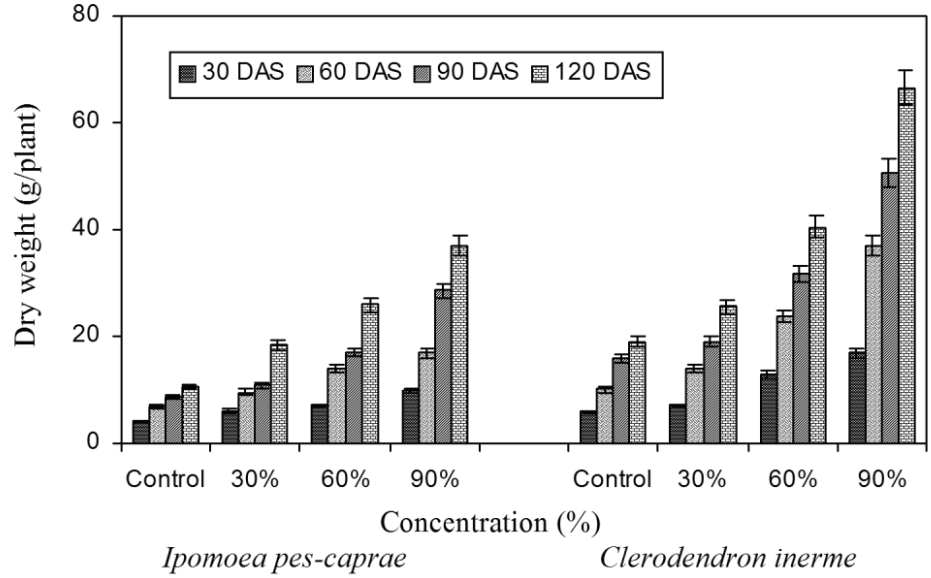

Fig. 4: Effect of different concentrations of tannery effluent dry weight of *Ipomoea pes-caprae* and *Clerodendron inerme.*

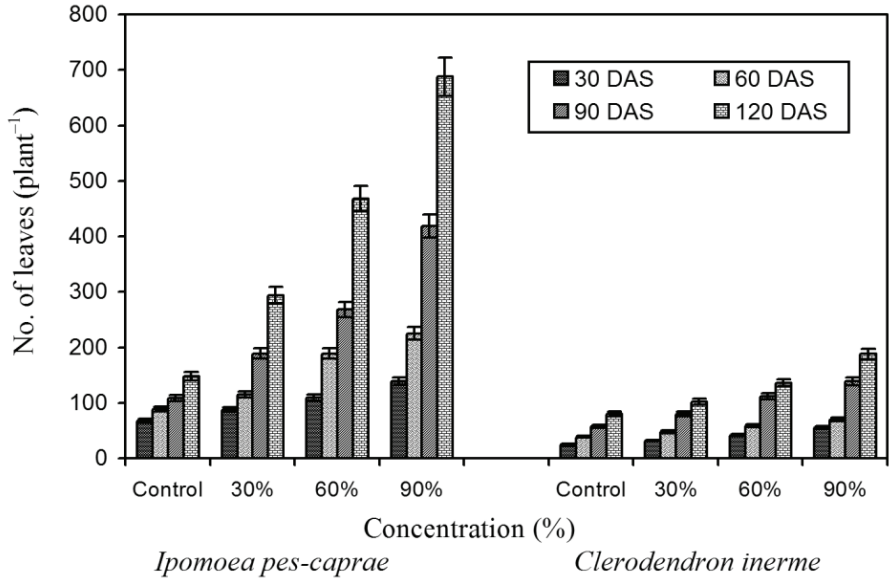

Fig. 5: Effect of different concentrations of tannery effluent total number of leaves of *Ipomoea pes-caprae* and *Clerodendron inerme.*

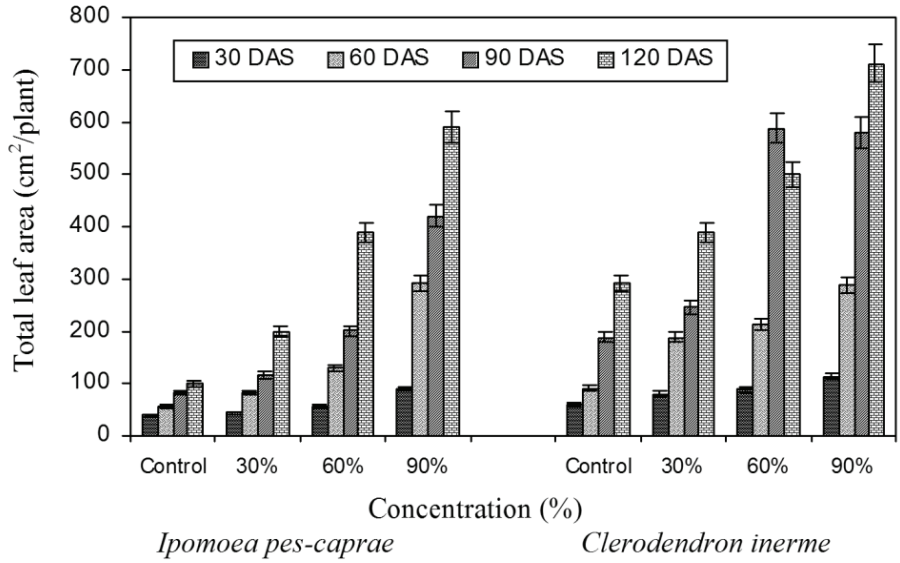

Fig. 6: Effect of different concentrations of tannery effluent total leaf area of *Ipomoea pes-caprae* and *Clerodendron inerme.*

treatment may be attributed to the decrease in metabolic rate and reduced transport from the cotyledons and at the same time it may also be due to the higher rate of leakage in the membrane permeability (Chitra 2017). Increase in fresh and dry weight was observed in the species of halophytes cultivated in tannery effluent treated soil. This is in accordance with the studies with several species showing that the NaCl stimulated the root and shoot growth of *Suaeda altissima* (Meychick et al. 2013) and *Suaeda fruticosa* (Ajmal Khan et al. 2000).

Duarte et al. (2012) identified the most abundant salt marsh halophytic species *Halimione portulacoides*, considered as suitable for Cr(VI) phytoremediation process by phytoextraction. The growth of *Spartina alterniflora*, a salt marsh halophyte was not inhibited under Cu stress (50, 200, 800 $mg.kg^{-1}$) with no chlorotic and brown points on leaves and could be considered to be a promising candidate for phytoremedaition of copper contaminated areas (Chai et al. 2014). In the present study, the plants cultivated in tannery effluent and salt treated soil stimulated the leaf production and increased the number of leaves throughout the study period when compared to control plants. Along with increase in the leaf number there was increase in leaf area. The increase in leaf area might be due to increase in the volume of mesophyll cells with the increase in the water content of the leaves and greater accumulation of heavy metals in the mesophyll tissue with consequent increase in the leaf thickness.

REFERENCES

Ajmal Khan, M., Ungar, V. and Showalter, M. 2000. Effects of salinity on growth, water relations and ion accumulation of the subtropical perennial halophyte, *Suaeda fruticosa* (L.) Forsk. J. Arid Environ., 45: 73-84.

Chai, M., Shi, F., Li, R., Qiu, G., Liu, F. and Liu, L. 2014. Growth and physiological responses to copper stress in a halophyte *Spartina alterniflora* (Poaceae). Acta Physiol. Plant., 36: 745-754.

Chitra, K. 2017. Effect of copper on germination and seedlings growth of radish (*Raphanus sativum* L.). J. Environ. Sci., 11(4): 1-2.

Dixit, R., Malaviya, D., Pandiyan, K., Singh, U.B., Sahu, A., Shukla, R., Singh, B.P., Rai, J.P., Sharma, P.K. and Lade, H. 2015. Bioremediation of heavy metals from soil and aquatic environment – An overview of principles and criteria of fundamental processes. Sustainability, 7: 2189-2212.

Duarte, B., Silva, V. and Cacador, I. 2012. Hexavalent chromium reduction, uptake and oxidative biomarkers in *Halimione portulacoides*. Ecotoxicol. Environ. Safety, 82: 1-7.

Eid, M.A. and Eisa, S.S. 2010. The use of some halophytic plants to reduce Zn, Cu and Ni in soil. Aus. J. Basic Appl. Sci., 4(7): 1590-1596.

Ghnaya, T., Nouairi, I., Slama, I., Messedi, D., Grignon, C., Abdelly, C. and Ghorbel, M.H. 2007. Cadmium effects on growth and mineral nutrition of two halophytes: *Sesuvium portulacastrum* and *Mesembryanthemum crystallinum*. J. Plant. Physiol., 162: 1133-1140.

Kalra, G.S. and Dhiman, S.D. 1977. Determination of leaf area of wheat plants by a rapid method. J. Ind. Bot. Soc., 56: 261-264.

Li, Y. and Li, B. 2011. Study on fungi-bacteria consortium bioremediation of petroleum contaminated mangrove sediments amended with mixed biosurfactants. Adv. Mat. Res., 183(1): 1163-1167.

Long, X.X., Yang, X.E. and Ni, E.Z. 2002. Current status and perspective on phytoremediation of heavy metals polluted soils. J. Appl. Ecol., 13: 757-762.

Manousaki, E. and Kalogerakis, N. 2011. Halophytes- An emerging trend in phytoremediation. Int. J. Phytoremed., 13(10): 959-969.

Meychik, N.R., Nikolaeva, I.Y. and Yermakov, I.P. 2013. Physiological response of halophyte (*Suaeda altissima* (L.) Pall.) and glycophyte (*Spinacia oleracea* L.) to salinity. Am. J. Plant Sci., 4: 427-435.

Milic, D., Lukovic, J., Ninkov, J., Zeremski-Skoric, T., Zoric, L., Vasin, J. and Milic, S. 2012. Heavy metal content in halophytic plants from inland and maritima saline areas. Cent. Eur. J. Biol., 7: 307-317.

Perpetuo, E.A., Souza, C.B. and Nascimento, C.A.O. 2011. Engineering Bacteria Bioremediation. CEPEMA, Univeristy of Sao Paulo, Brazil, ISBN: 978-953-307-268-5, p. 646.

Suedector, G.W. and Cochran, W.G. 1967. Statistical Methods. Iowa State University Press, Ames, IA.

Nature Environment and Pollution Technology
An International Quarterly Scientific Journal

p-ISSN: 0972-6268
(Print copies up to 2016)
e-ISSN: 2395-3454

Vol. 19 | No. 2 | pp. 767-773 | 2020

Original Research Paper

https://doi.org/10.46488/NEPT.2020.v19i02.033

Open Access Journal

Regularities and Characterization of Arsenic Adsorption by Sediment in the Presence of Coexisting Ions

Song Gang-fu*, E. Zheng-yang*, Li Hai-hua*†, Hua Yong-peng, Yan Shao-feng**, Li Gui-liang*** and Zhang Zan-ping*****

*Faculty of Environmental & Municipal Engineering, North China University of Water Resources and Electric Power, Zhengzhou 450011, China

**Henan Academy of Environmental Protection Sciences, Zhengzhou 450046, China

***No. 4 Institute of Geological & Mineral Resources Survey of Henan, Zhengzhou 450046, China

†Corresponding author: Li Hai-hua; lihaihua918@163.com

Nat. Env. & Poll. Tech.
Website: www.neptjournal.com

Received: 15-07-2019
Accepted: 06-10-2019

Key Words:
Sediment; Arsenic; Adsorption; Kinetics; Surface characterization; Coexisting ions

ABSTRACT

To reveal the regularity of arsenic adsorption of sediment, this study explores the law of arsenic adsorption by sediment when Fe^{3+} and Mn^{2+} coexist. The experimental results fit the first-order kinetic model and the second-order kinetic model. The surface physicochemical properties of sediment particles were analysed by scanning electron microscopy (SEM), nitrogen adsorption-desorption isotherm and fractal dimension. Characterization of surface area and pore distribution were measured by the BET equation and BJH equation. The results illustrate that the adsorption of arsenic by sediment shows the phenomenon of rapid adsorption in the early stage, slow adsorption in the middle stage and finally adsorption equilibrium. In the presence of coexisting ions, the BET specific surface area was as high as 20.14m^2/g, the pore volume as 0.047826cm^3/g, the surface pore volume as 43.25cm^3, and the surface fractal dimension Ds as the largest.

INTRODUCTION

Arsenic, which is a kind of metalloid, is similar to the heavy metal because the toxicity of arsenic ions in aqueous solution is very high (Chwirka 2000, Li 2017). In particular, arsenic is classified as a type of pollutant because its toxicity to humans and its migration and transformation in the environment are similar to heavy metals (Bissen 2003, He & Charlet 2013). As a natural adsorbent, sediment has a large specific surface area and effectively reduces the concentration of heavy metals in water by adsorption (Wang & Hu 2006, Withers & Jarvie 2008, He 2005, Wang et al. 2006). For example, Jia et al. (2010) found that fine particles of sediment with a large specific surface area have a strong adsorption capacity. Huang et al. (1995) showed that the larger the sediment particle size, the smaller the adsorption rate. Zhao et al. (2003) found that the sediment in the middle reaches of the Yellow River has a strong adsorption capacity for Cu^{2+}.

In the natural environment, the adsorption of arsenic in sediment occurs through competition or complexation under the coexistence of multiple ions (Ma 2017, Ma et al. 2015, Ghurye et al. 2004, Bhowmick et al. 2014, Kleinert et al. 2011). Yellow River Water Resources Bulletin (China Water Resources Bulletin 2009-2017) shows that in the cross-section of Huayuankou Zhengzhou, iron and manganese often exceeded from 2009 to 2017. Based on the high content of Fe^{3+} and Mn^{2+} in the Yellow River water source of Zhengzhou City, the sediment particles were taken as the research object to study the change of arsenic adsorption and surface characteristics of sediment in the presence of Fe^{3+} and Mn^{2+}. The study result can provide a theoretical basis and technical support for arsenic treatment and prevention of high Fe^{3+} and Mn^{2+} water sources.

MATERIALS AND METHODS

Experimental Materials

The experimental material was sediment taken from shallow water near the bank of the Yellow River at Huayuankou Madu village. The dried sand was crushed by a Pulveriser for 2 to 3 minutes and sieved through 325 mesh sample sieves to obtain 0.0375 to 0.088 mm size sediment. The sand was soaked in deionized water, washed with $NH_2OH{\cdot}HCl$ and H_2O_2 in turn, baked at 60°C for 24 hours and then cooled to room temperature in a desiccator.

Experimental Procedure

Firstly, 0.6g of clean sand, 30mL of deionized water and 0.3mL of arsenic standard solution at a concentration of 0.01mg/mL were put into a conical flask. Then 0.15mL of iron standard solution or manganese standard solution at a concentration of 0.1mg/mL was added to make the solution with the sediment at a concentration of 20kg/m^3, the initial arsenic at a concentration of 0.1mg/L, and the coexistence of ion at a concentration of 0.5mg/L. After being oscillated in the constant temperature oscillator (speed 120r/min, temperature 20°C), the solution was allowed to stand, be filtered and dried. The sampling time points were 5, 10, 15, 30, 60, 90, 120, 180, 240, 360, 480, 600, 1440min.

Determination Methods

Atomic fluorescence spectrophotometer (Model 8220) was used to determine the concentration of arsenic(III). Arsenic(III) (GSB 04-1714-2004) was purchased from the market. Quantification of arsenic(III) was based upon the calibration curves of standard solutions of arsenic(III) ion. The equation of calibration curve was y = 44.3678 x - 31.0218, and the detection limit of arsenic(III) was 0.01 mg·L^{-1}. The correlation coefficients were approximately 0.9997.

Adsorption Kinetic Model

The first-order kinetic model: The first-order kinetic model is the kinetic equation of the relationship between the reaction rate and the concentration of the reactant in the system. It can be expressed as:

$$\frac{dq}{dt} = k_1(q_e - q_t) \quad \ldots(1)$$

The second-order kinetic model: The second-order kinetic model is used to describe the adsorption process of divalent metal ions, assuming the adsorption is proportional to the amount of adsorption site on the adsorbent. It can be expressed as

$$\frac{dq_t}{dt} = k_2(q_e - q_t)^2 \quad \ldots(2)$$

Characterization

The microscopic morphology of sediment particles was observed by Japan JSM-7001F field emission scanning electron microscope. The pore structure of the sample was measured by Japan BELSORP-Mini II specific surface area and porosity analyser. Nitrogen was used as the adsorption medium at a temperature of 77 K. The measured pore size of sediment particles ranged from 0 to 100 nm. Samples were degassed at 300°C for 12 hours before testing. The total specific surface area of sediment particles was calculated by the BET method. The pore volume of sediment particles was calculated by the BET equation and BJH equation respectively.

RESULTS AND DISCUSSION

Study on Arsenic Adsorption by Sediment

Curve of arsenic adsorption by sediment: Adsorption of arsenic by sediment is a dynamic equilibrium process. According to the experimental procedure, in the presence of Fe^{3+} and Mn^{2+}, the adsorption rate of arsenic by sediment and the adsorption amount of sediment per unit time changed with time and the changing law is shown in Fig. 1.

From Fig. 1, it can be seen that the sediment adsorption is characterized by rapid adsorption in the early stage, slow adsorption in the middle stage, and finally adsorption equilibrium. On the whole, the adsorption rate of arsenic by sediment and the adsorption capacity of sediment show the same trend. Taking the analysis of arsenic adsorption rate as an example, when there was no Fe^{3+} and Mn^{2+}, at 5 to 10min, the arsenic adsorption rate curve was not obvi-

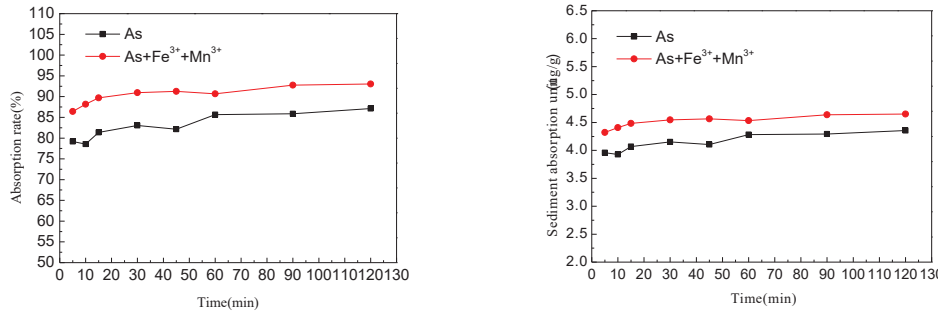

Fig. 1: Sediment adsorption curves.

ous with time. The reason for this phenomenon is that the water-sand system is not well mixed. Just at the time when the adsorption reaction begins, the desorption also begins. The adsorption-resolution rate is inconsistent, which does not reach the dynamic stability, so the changes of arsenic adsorption rate are not stable. After adding Fe^{3+}, Mn^{2+}, the coexistence of two kinds of ions effectively counteracted the mutual interference, showing the phenomenon that the overall adsorption rate continuously increases. Subsequently, the arsenic adsorption rate increased significantly with the increase of time. After 60 min, the arsenic adsorption rate changed little or no change over time, reaching the equilibrium of adsorption. Adsorption rate of arsenic by sediment ranged from 86.44% to 93.03% after adding Fe^{3+} and Mn^{2+}. However, when there was only arsenic, the adsorption rate ranged from 79.137% to 87.109%, indicating that the presence of coexisting ions promotes the adsorption of arsenic by sediment.

Sediment arsenic adsorption kinetic model fitting: The first-order kinetics and the second-order kinetics were used to fit the data of arsenic adsorption by sediment. The fitting parameters are shown in Table 1 and the fitting model images are shown in Fig. 2.

Fig. 2 shows that the second-order kinetic equation can better describe the process of arsenic adsorption by sediment, which was a good linear correlation. From Table 1, it can be seen that the correlation coefficient R^2 of the second-order kinetic model reached 0.996 to 0.998. From the difference between the equilibrium adsorption quantity and the equilibrium adsorption quantity obtained from the experiment, the data of the second-order kinetics fitting differed by 0.02μg/g

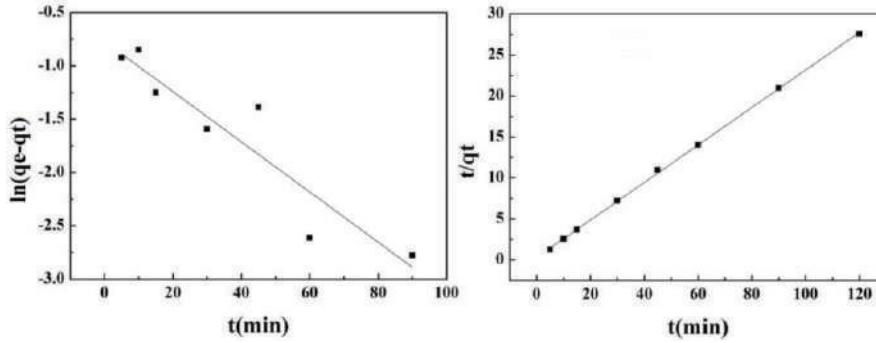

(a) Kinetic model fitting of arsenic adsorption by sediment alone

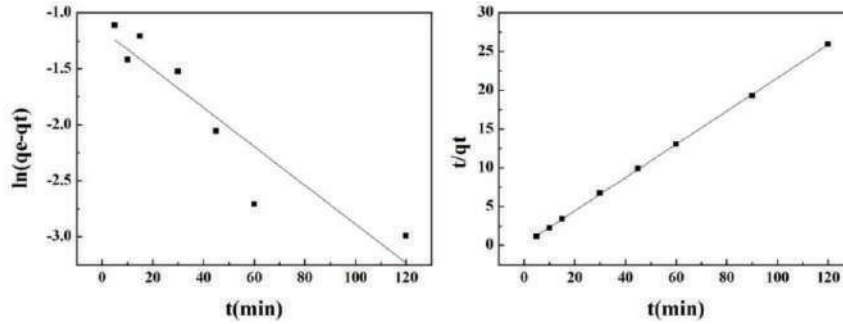

(b) Kinetic Model Fitting of Arsenic Adsorption by Sediment in the Presence of Fe^{3+}, Mn^{2+}

Fig. 2: The kinetic model fitting curves.

Table 1: The kinetic model parameters.

Conditions	The first-order kinetics				The second-order kinetics			
	k_1	q_e	q_e*	R^2	k_2	q_e	q_e*	R^2
As	0.0236	0.4628	4.3555	0.8506	0.1665	4.3760	4.3555	0.9996
As+Mn^{2+}+Fe^{3+}	0.0173	0.3156	4.6709	0.8460	0.2632	4.6666	4.6709	0.9998

Table 2: Specific surface area, pore volume and average pore diameter of sediment particles.

Sample	BET specific surface area/m^2/g	BJH the total pore volume/cm^3/g	The average pore diameter/nm
Clean sand	11.52	0.043017	14.938
Sand sample with As	15.28	0.045787	13.074
Sand sample with As + Fe^{3+} + Mn^{2+}	20.14	0.047826	11.295

and -0.0043μg/g respectively, and the data of the first-order kinetic fitting varied greatly. This shows that under the laboratory conditions, the second-order kinetic equation is more suitable for describing the process of arsenic adsorption by sediment. The second-order kinetics assumes that the adsorption rate is governed by the chemical adsorption mechanism that involves electron-sharing or electron transfer between the adsorbent and the adsorbate. It indicates the presence of chemisorption in the process of arsenic adsorption by sediment, which is consistent with the chemical adsorption of Cu on sediment in the existing literature (Chen 2008). It indicates that arsenic has properties of heavy metals in the environment.

Surface Characteristics of Sediment after Arsenic Adsorption

Surface morphology changes of sediment samples before and after arsenic adsorption: As shown in Fig. 3, the appearance of the clean sand before and after the adsorption of arsenic significantly changed. When there was only arsenic, the surface porosity of sediment particles decreased due to the adsorption of arsenic, and the flow of water exerted different forces on the sediment so that the surface structure changed and became smoother. When Fe^{3+} and Mn^{2+} coexist, the three ions were adsorbed on the sediment surface, and migrated and transformed under the effect of water flow to form flaky and striped structures that adhered to the particle surface.

Adsorption isotherm of sediment sample: According to the difference of molecular adsorption in pores with different sizes, IUPAC (Arami-Niya et al. 2011, Yang et al. 2007) classifies adsorbed pores into three types: macropores with pore width> 50 nm, mesopores with pore width from 2 to 50 nm and micropores with pore width<2 nm. Fig. 4 shows the adsorption-desorption isotherms of nitrogen on sediment particles.

As what can be seen from Fig. 4, the sediment adsorption isotherms belonged to the multi-layer adsorption model of porous media, and the pore structure was close to the slit-shaped pores of the parallel walls. As for the volume of the unit mass of particles after nitrogen adsorption when the condition was near the saturated vapour pressure, cleaning sand was 37.45cm^3, the arsenic-containing solution was 39.87cm^3, and solution with As, Fe^{3+}, Mn^{2+} was 43.25cm^3. This shows that when the ions of Fe^{3+}, Mn^{2+} are coexisting, the surface pore volume of the sediment sample after adsorption is the largest one. The specific surface area, pore volume and other pore structure parameters calculated by the BET and BJH equations are given in Table 2. It can be seen that BET and BJH in the sand sample containing As + Fe^{3+} + Mn^{2+} were larger than those in the sand sample only containing arsenic, indicating that the presence of Fe^{3+}, Mn^{2+} has a greater impact on the pore structure of sediment particles.

Fractal dimension: According to the classical FHH model method, the fitted curve of the fractal dimension and the

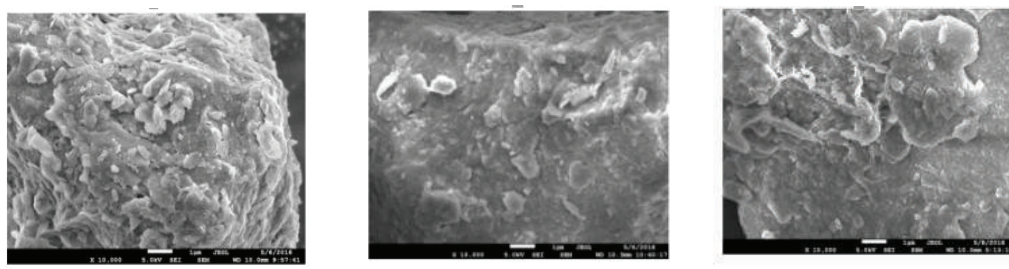

Particle a (×10000) Particle b (×10000) Particle c (×10000)

(a: clean sand; b: arsenic adsorption by sediment alone; c: arsenic adsorption by sediment in the presence of coexisting ions)

Fig. 3: SEM images of sediment particle surface under different states.

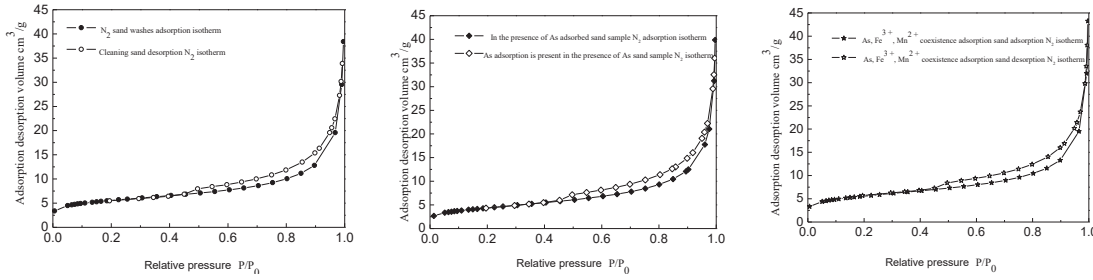

Fig 4: Adsorption-desorption isotherms.

surface fractal dimension of the clean sand sample and the adsorbed sample were calculated by the least square fitting method, as shown in Table 3 and Figs. 5 to 7.

The surface fractal dimension of sediment particles was between 2 to 3, with the minimum number of clean sand and the maximum number of the sample with As, Fe^{3+} and Mn^{2+}. This is because the fractal dimension is the macroscopic displaying of the surface roughness and self-similarity of sediment particles and the slight change of microstructure does not change the fractal dimension of the surface, indicating that the presence of Fe^{3+} and Mn^{2+} has a significant effect on the microstructure of sediment particles.

CONCLUSIONS

This paper focuses on the analysis of the changes of arsenic adsorption and its surface characteristics of sediment in the presence of $Fe^{3+}$and Mn^{2+}. The experimental results show that:

(1) The adsorption of arsenic by sediment is a dynamic equilibrium process, which shows the phenomenon of rapid adsorption in the early stage, slow adsorption in the middle stage, and finally adsorption equilibrium.

(2) Arsenic has properties of heavy metals in the environment. The adsorption of arsenic by sediment has the

Table 3: Surface fractal dimension of sediment particles (R^2>0.98).

Sample	FHH the equation of adsorption X>0.35	FHH the equation of adsorption 0.7320<X<0.9826	FHH the equation of adsorption X>0.35
Clean sand	2.588	2.579	2.601
Sand sample with As	2.637	2.624	2.646
Sand sample with As + Fe^{3+} + Mn^{2+}	2.672	2.659	2.674

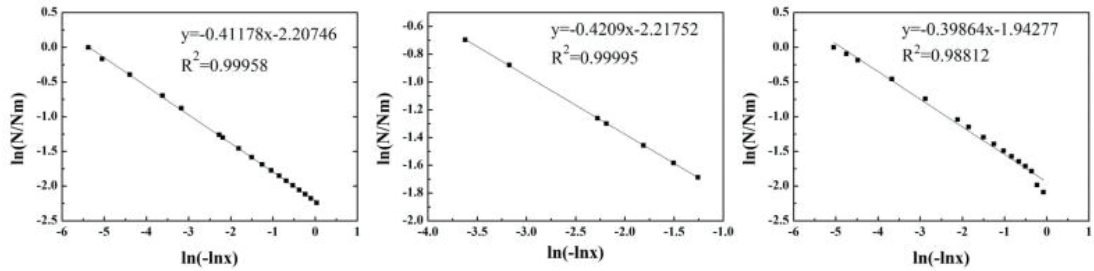

(a) (b) (c)

Fig. 5: Surface fractal dimension fitting curves of clean sand particles.

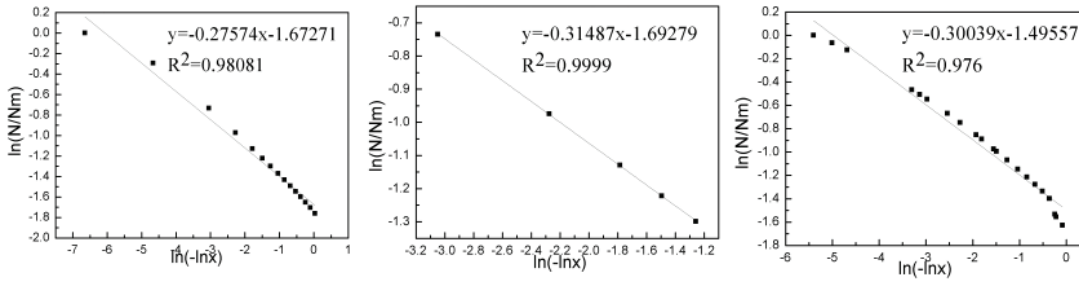

(a) (b) (c)

Fig. 6: Surface fractal dimension fitting curves of sediment particles after adsorption equilibrium with arsenic alone in lateral seepage.

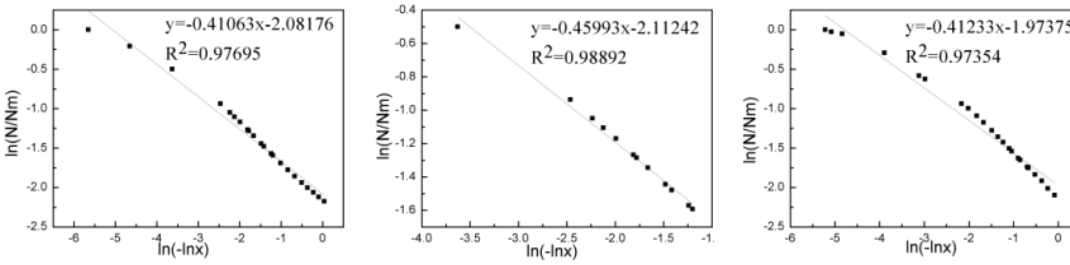

(a) (b) (c)

Fig. 7: Surface fractal dimension fitting curves of the sediment particles after adsorption equilibrium with the coexistent of arsenic, iron and manganese in lateral seepage.

(a) x>0.35; (b) 0.7320<x<0.9826; (c)x>0.35

function of chemisorption and the second-order kinetic equation is more suitable for describing the adsorption of arsenic.

(3) In the presence of coexisting ions, the BET specific surface area was as high as 20.14m^2/g, the pore volume was 0.047826cm^3/g, the surface pore volume of sand sample which was the largest was 43.25cm^3, and the surface fractal dimension Ds of arsenic adsorbed by sediment was the largest.

(4) The fractal dimension of sediment particles is the same as that of its specific surface area and pore volume. It can be used to characterize the surface roughness of sediment particles, i.e., micropore content.

REFERENCES

Arami-Niya, A., Daud, W. M. A. W. and Mjalli, F. S. 2011. Comparative study of the textural characteristics of oil palm shell activated carbon produced by chemical and physical activation for methane adsorption. Chemical Engineering Research and Design, 89(6): 657- 664.

Bhowmick, S., Chakraborty, S., Mondal, P., Van Renterghem, W., Van den Berghe, S., Roman-Ross, G., Chatterjee, D. and Iglesias, M. 2014. Montmorillonite-supported nano-scale zero-valent iron for removal of arsenic from aqueous solution: kinetics and mechanism. Chem. Eng. J., 243: 14-23.

Bissen, M. and Frimmel, F. H. 2003. Arsenic-A review. Part I: occurrence, toxicity, speciation, mobility. Clean-Soil, Air, Water, 31(1): 9-18.

Chen, Z.H. 2008. Sediment Adsorption Heavy Metal Copper Ion Surface Morphology and Structural Characteristics. Tsinghua University.

Chwirka, J.D., Thomson, B.M. and Stomp, III J.M. 2000. Removing arsenic from groundwater. American Water Works Association Journal, 92(3): 79.

Ghurye, G., Clifford, D. and Tripp, A. 2004. Iron coagulation and direct microfiltration to remove arsenic from groundwater. J. Am. Water Works Assoc., 96(4): 143-152.

He, J. and Charlet, L. 2013. A review of arsenic presence in China drinking water. Journal of Hydrology, 492(10): 79-88.

He, Y. 2005. Water and Sediment Process and the Role of the Ecological Environment of the River. Wuhan University.

Huang, S.L., Wan, Z.H. and Wang, L.X. 1995. Static test on sediment desorption of heavy metal pollutants with different particle size. Research and Progress of Hydrodynamics (Series A), 2: 204-13.

Jia, X.F., Ying, Y.M., Li, Y. and Wang, L.C. 2010 Study on the interaction between sediment and heavy metal pollutants in the Yellow River. Yellow River, 8: 50.

Kleinert, S., Muehe, E.M., Posth, N.R., Dippon, U., Daus, B. and Kappler, A. 2011. Biogenic Fe(III) minerals lower the efficiency of iron-mineral-based commercial filter systems for arsenic removal. Environmental Science & Technology, 45(17): 7533-7541.

Li, H.H., Yan, W.F., Liang, Q., Zheng-yang, E. and Ge, K.J. 2017. Effect of initial arsenic concentration on sediment adsorption of arsenic. Nature Environment and Pollution Technology, 16(2): 627-632.

Ma, J., Guo, H.M. and Lei, M. 2017. Disparity of adsorbed arsenic species and fractions on the soil and soil colloids. Procedia Earth and Planetary Science, 17: 642-645.

Ma, J., Guo, H., Lei, M., Zhou, X., Li, F., Yu, T., Wei, R., Zhang, H., Zhang, X. and Wu, Y. 2015. Arsenic adsorption and its fractions on aquifer sediment: effect of pH, arsenic species, and iron /manganese minerals. Water, Air & Soil Pollution, 226(8): 260.

Ministry of water resources. China Water Resources Bulletin. Beijing: Ministry of water resources, 2009-2017.

Wang, G.Q. and Hu, C.H. 2006. Sediment Research Progress. China Water Power Press, Beijing, pp. 392-413.

Wang, S., Jin, X., Bu, Q., Zhou, X. and Wu, F. 2006. Effects of particle size, organic matter and ionic strength on the phosphate sorption in different trophic lake sediments. Journal of Hazardous Materials, 128(2/3): 95-105.

Withers, P.J.A. and Jarvie, H.P. 2008. Delivery and cycling of phosphorus in rivers: are view. Science of the Total Environment, 400(1/2/3): 379-395.

Yang, H., Yan, R., Chen, H., Lee, D.H. and Zheng, C. 2007. Characteristics of hemicellulose, cellulose and lignin pyrolysis. Fuel, 86(12-13): 1781-1788.

Zhao, R., Ni, J.R., Sun, W.L. and Zhang L. 2003. Studies on the adsorption and desorption of copper ions by sediment in the middle Yellow River. Acta Scientiae Circumstantiae, 4: 441.

Nature Environment and Pollution Technology
An International Quarterly Scientific Journal

p-ISSN: 0972-6268
(Print copies up to 2016)
e-ISSN: 2395-3454

Vol. 19 | No. 2 | pp. 775-782 | 2020

Original Research Paper

https://doi.org/10.46488/NEPT.2020.v19i02.034

Open Access Journal

Effect of Crop Protective Agents on Seed Germination and Seedling Emergence in Chilli (*Capsicum annum L.*) - An *In-vitro* Study

Pilla Venkateswara Rao†*, Namuduri Srinivas and AVVS Swamy*****

*Associate Scientist, Research Department, ITC, Agri-Business Division, Rajahmundry-533 102, India

** Department of Environmental Studies, GITAM Institute of Science, Rushikonda, Visakhapatnam-530 045, A.P., India

***Department of Environmental Sciences, Acharya Nagarjuna University, Nagarjunanagar, Guntur-522 510, India

†Corresponding Author: Pilla Venkateswara Rao; pvrao268@gmail.com

Nat. Env. & Poll. Tech.
Website: www.neptjournal.com

Received: 08-08-2019
Accepted: 29-08-2019

Key Words:
Chilli; Ethion; Triazophos; Flubendiamide; Emamectin Benzoate; Tebuconazole; Trifloxystrobin; Seed spoilage

ABSTRACT

Crop protective agents (CPAs) are prime requisite for protecting crops from pests and diseases. CPAs are used at different stages of the crop from the seed sowing to harvesting. Seeds are treated with different fungicides as a prophylactic measure against pre-emergence diseases and during seed germination stage different protective agents are applied to safeguard young seedlings from pests. To find out the effect of crop protective agents on seed germination and seedling growth in chilli (*Capsicum annum* L.) an *in-vitro* study was conducted using Ethion (1.25, 2.5, 3.75 and 5.0mL/L), Triazophos (0.625, 1.25, 1.875 and 2.5mL/L), Flubendiamide (0.15, 0.3, 0.45 and 0.6mL/L), Emamectin Benzoate (0.2, 0.4, 0.6 and 0.8 g/L) and Tebuconazole + Trifloxystrobin (0.625, 1.25, 1.875 and 2.5 g/L) against control (distilled water). Correlation study revealed that seedling growth was positively affected by Flubendiamide (r = 0.287), neutral by Emamectin Benzoate (r = 0.012), while retarded growth was observed in Ethion (r = -0.584), Trizophos (r = -0.473) and Tebuconazole+ Trifloxystrobin (r = -0.331) chemicals compared to control. From the statistical analysis, it was found that chilli seed germination was not affected at the tested concentration levels of crop protective agents. Seedling shoot length was significantly (P = 0.05) reduced in Tebuconazole + Trifloxystrobin (1.763cm) and Ethion (3.175cm) compared to control (5.088cm). Seedling shoot length was not significantly affected by Emamectin Benzoate and Triazophos, while it was significantly increased in Flubendiamide@0.45mL/L (5.88cm) compared to control (5.088cm). Seedlings in Flubendiamide and Emamectin Benzoate produced significantly (P=0.05) longer roots of 7.488cm and 7.688cm respectively, while seedlings in Ethion, Tebuconazole + Trifloxystrobin and Triazophos produced shorter roots (4.00, 4.45 and 4.6cm respectively) compared to control (6.363cm). Rotten seed per cent on 15th day was significantly (P=0.05) lower in Tebuconazole + Trifloxystrobin and Triazophos (5.61 and 11.73%) compared to control (22.45%).

INTRODUCTION

Crop protective agents are a prime requisite for the protection of crop from pests and diseases. To safeguard the seed and emerging seedlings from diseases and insects, seeds are treated with protective agents. Once the seedlings emerge and grow, they need to be protected by applying protective agents. To find out the effect of crop protective agents on seed germination and initial seedling growth at different concentrations, this experiment was initiated using commonly used protective agents from zero concentration to double the recommended dose on chilli (*Capsicum annum* L.).

In chilli crop, the decline in seed germination per cent was observed with the seed-borne fungi viz. *Aspergillus flavus, Colletotrichum capsici, Curvularia lunata, Fusarium moniliforme* and *Rhizopus stolonifer* were associated with seed during germination (Alam et al. 2014).

Influence of pesticides on seedling emergence and growth have been reported earlier. To protect the maize crop from diseases during germination a study on Tebuconazole encapsulation on Maize seed was done and which resulted in growth promotion, whereas emergence was inhibited at higher concentrations (Yang et al. 2014). From another experiment done with two fungicides, Bavistin and Deltan in chilli (*Capsicum annuum* L. var. x235) showed both seed germination and seedling survival were affected with an increase in concentration (Prakash et al. 1988).

The study conducted on tomato seed germination with different chemicals (emamectin benzoate, alpha-cypermethrin, lambda-cyhalothrin and imidacloprid) revealed that seed germination was decreased by the pesticides and this effect was more prominent at early stages of exposure (Shakirullah et al. 2016). Another study revealed that exposure of tender tissue to ethion showed genotoxic effects on mitotic divisions (Lamsal et al. 2010).

The preliminary investigative survey in a village Koonavaram near Rajamahendravaram with the farmers, gave some insights to shortlist the chemicals and identify the knowledge gap farmers have in selecting and using the crop protective agents.

The shortlisted crop protective agents cover different groups of commonly used pesticides namely Organophosphorous (Ethion and Triazophos), Ryanoid (Flubendiamide) and Avermectin (Emamectin Benzoate) and fungicides covering azole and strobilurin group (Tebuconazole + Trifloxystrobin) (Table 1).

MATERIALS AND METHODS

To find out the seed germination and emerged seedling growth in relation to crop protective agents at different concentration on chilli (*Capsicum annum* L.) an *in-vitro* study was conducted with Ethion (1.25, 2.5, 3.75 and 5.0 mL/L), Triazophos (0.625, 1.25, 1.875 and 2.5 mL/L), Flubendiamide (0.15, 0.3, 0.45 and 0.6 mL/L), Emamectin Benzoate (0.2, 0.4, 0.6 and 0.8 g/L) and Tebuconazole + Trifloxystrobin (0.625, 1.25, 1.875 and 2.5 g/L) against control (distilled water). Experiment was conducted in ITC, ABD, Research Department, Rajamahendravaram.

Chilli seeds were sown following the top of paper method (Rao et al. 2006) using grade 181 filter paper from Whatman, each Petri plate was sown with 49 seeds, replicated 4 times. Germination chamber was used for germination of the chilli seeds. An ambient temperature of 25°C was maintained during the experimental period. During the germination period, 12 hours light and 12 hours dark were maintained. Everyday morning and evening Petri plates were provided with moisture according to the treatment concentrations.

Germination papers were kept in Petri plates moist with crop protective agent's spiked solution of 0 % (distilled water), 50% of RSD (Recommended Spray Dose), 100% RSD, and 150% RSD and 200 % RSD as shown in Table 2. Crop protective agents namely Ethion, Triazophos, Flubendiamide, Emamectin benzoate and Tebuconazole + Trifloxystrobin.

Seed germination count was taken on 4^{th}, 10^{th} and final count on 15^{th} day. Seedling length (shoot and root length) was noted on 15^{th} day. From the germination count, germination per cent was calculated. On final count along with the germinated seeds, spoiled (fungal infested) seed count was also taken in all the Petri plates. From the spoiled seed

Table 1: Recommended spray dose for the shortlisted crop protective agents.

Active Ingredient	Crop Protective Agent type	Group	Recommended Spray Dose (RSD)
Ethion	Insecticide	Organophosphorus	2.5 mL/L
Triazophos	Insecticide	Organophosphorus	1.25 mL/L
Tebuconazole & Trifloxystrobin	Fungicide	Azole & Strobilurin	1.25 g/L
Flubendiamide	Insecticide	Ryanoid	0.3 mL/L
Emamectin Benzoate	Insecticide	Avermectin	0.4 g/L

Table 2: Different concentrations of shortlisted crop protective agents (From 0 concentration to double the recommended dose on the crop.

Control (Distilled Water)	50% of RSD	100% of RSD	150% of RSD	200% of RSD
		Triazophos		
0	0.625mL/L	1.25mL/L	1.875mL/L	2.5mL/L
		Flubendiamide		
0	0.15mL/L	0.3mL/L	0.45mL/L	0.6mL/L
		Emamectin Benzoate		
0	0.2g/L	0.4g/L	0.6g/L	0.8g/L
		Tebuconazole+Trifloxystrobin		
0	0.625g/L	1.25 g/L	1.875g/L	2.5g/L
		Ethion		
0	1.25mL/L	2.5mL/L	3.75mL/L	5mL/L

count, spoiled seed per cent was calculated. The data were subjected to statistical analysis.

RESULTS AND DISCUSSION

Seed Germination

Chilli seed (*Capsicum annum* L.) germination percent in Table 3 was recorded during final count using Petri plates (*in-vitro*) in all the crop protective agents at different concentrations. The following concentrations were used, Ethion (1.25, 2.5, 3.75 and 5.0 mL/L), Triazophos (0.625, 1.25, 1.875 and 2.5 mL/L), Flubendiamide (0.15, 0.3, 0.45 and 0.6 mL/L), Emamectin Benzoate (0.2, 0.4, 0.6 and 0.8 g/L) and Tebuconazole & Trifloxystrobin (0.625, 1.25, 1.875 and 2.5 g/L) against control (distilled water).

Though the germination per cent in Ethion 83.16 to 87.76 %, Triazophos 80.10 to 87.76 %, Flubendiamide 81.12 to 88.78%, Emamectin Benzoate 84.69 to 90.31 % and Tebuconazole & Trifloxystrobin 79.59 to 82.65 % showed a range compared to control 84.69 % which is statistically nonsignificant (P=0.05). Shakirullah et al. (2016) reported that seed germination was decreased with the early stage of exposure to the pesticide. Whereas in another study Triazophos reduced the germination of wheat seeds (Khanday et al. 2014). Tebuconazole inhibited seed germination in wheat (Gao et al. 2000)

Spoiled Seed Count

While taking final seed germination per cent total spoiled seed count per Petri plate was recorded in Table 4. From the spoiled seed data, it is evident that there is a significant reduction of spoiled seed in Flubendiamide (200% of RSD) which is 11.73% compared to control 22.45%, and all the concentration of Tebuconazole + Trifloxystrobin combination showed a significant reduction of 5.10 to 6.63% to 22.45% over control. All the other crop protective agents namely Ethion, Flubendiamide, and Emamectin Benzoate didn't show any significant reduction in spoiled seed compared to control @ 0.05 level of significance. Powdery mildew fungi are very effectively controlled by Trifloxystrobin (Moshe 2000).

Correlation of Seedling Length with Crop Protective Agents

From the correlation studies (Table 5) using the seedling length, it is evident that crop protective agents Triazophos (-0.473), Tebuconazole & Trifloxystrobin (-0.331) and Ethion (-0.584) were negatively correlated, whereas Flubendiamide

Table 3: Germination count on 15th day.

	Ethion	Triazophos	Flubendiamide	Emamectin Benzoate	Tebuconazole & Trifloxystrobin
Control (0% of RSD)	84.69	84.69	84.69	84.69	84.69
50% of RSD	87.76	87.76	85.71	87.24	79.59
100% of RSD	82.14	85.71	82.65	90.31	78.06
150% of RSD	87.24	80.10	81.12	85.20	81.12
200% of RSD	83.16	80.10	88.78	84.69	82.65
S Em ±	2.28	2.35	2.68	1.84	2.93
CD (P=0.05)	N S	N S	N S	N S	N S
CV (%)	5.36	5.62	6.34	4.26	7.22

Table 4: Spoiled seed per cent on 15th day.

	Ethion	Triazophos	Flubendiamide	Emamectin Benzoate	Tebuconazole + Trifloxystrobin
Control (0% of RSD)	22.45	22.45	22.45	22.45	22.45
50% of RSD	15.31	24.49	23.47	16.33	5.10
100% of RSD	19.90	20.92	17.35	17.86	5.10
150% of RSD	12.76	19.39	17.35	20.92	6.63
200% of RSD	17.86	11.73	20.41	14.80	5.61
S Em ±	2.45	2.28	2.36	2.50	1.29
CD (P=0.05)	N.S	6.87	N.S	N.S	3.88
CV (%)	27.79	23.01	23.39	27.02	28.69

(0.287) and Emamectin Benzoate (0.012) showed positive correlation between seedling length and crop protective agents. Shoot length was positively correlated with Flubendiamide (0.224) and negatively correlated with Triazophos (-0.250), Emamectin Benzoate (-0.076), Tebuconazole & Trifloxystrobin (-0.768) and Ethion (-0.698). While root length was positively correlated with Flubendiamide (0.265) and Emamectin Benzoate (0.012), and negatively correlated with Triazophos (-0.448), Tebuconazole & Trifloxystrobin (-0.331) and Ethion (-0.417). Seedling length, shoot length and root length data was made a scatter in Figs. 1 and 2.

Effect of Crop Protective Agents on Seedling Length

Ethion: From the statistical analysis, effect of ethion on seedling growth (Table 6), the seedling length was found to be significantly (P=0.05) lower in Ethion 3.75mL/L and 5.0mL/L concentrations (9.8cm and 7.175cm) compared to control (11.450cm). Shoot length was lower in all Ethion concentrations 1.25mL/L (4.500cm), 2.5mL/L (3.800cm), 3.75mL/L (3.513cm) and 5mL/L (3.175cm) compared to control (5.088cm). While root length was significantly lower in Ethion concentration 5mL/L (4.00cm) compared to control (6.363cm). Griffiths et al. (1970) reported that seedlings were not damaged by ethion treatment.

Tebuconazole + Trifloxystrobin

Statistical analysis of seedling length, shoot length and root length in Tebuconazole + Trifloxystrobin (Table 7) combination chemical showed significant reduction in shoot length in all the concentrations 0.625g/L (2.738cm), 1.25g/L (2.413), 1.875g/L (2.425) and 2.5g/L (1.763) compared to control (5.088cm). Root length was significantly reduced at concentration of 2.5g/L (4.450cm) compared to control (6.363cm). While total seedling length was lower in all the concentrations of Tebuconazole + Trifloxystrobin 0.625g/L (9.475cm), 1.25g/L (8.513), 1.875 g/L (8.275) and 2.5g/L (6.213) compared to control (11.450cm).

Tebuconazole + Trifloxystrobin at 2.5g/L showed significantly lower shoot, root and seedling total length (1.763cm, 4.450cm and 6.213cm) when compared among the concentrations of 0.625g/L, 1.25g/L, 1.875g/L and 2.5g/L. A similar trend was observed in wheat by Xuehong et al. (2000) where Tebuconazole inhibited seedling growth.

Emamectin benzoate: From the statistical analysis of shoot, root and seedling total length in different concentrations of Emamectin Benzoate (Table 8) root length was found to be significantly increased in 0.2g/L (7.688cm), 0.4g/L (7.463cm), and 0.6g/L (7.438cm) compared to control (6.363cm). While in shoot length and total seedling length

Table 5: Correlation of crop protective agents on seedling length (shoot and root length).

	Correlation coefficient (r)		
	Shoot	Root	Total
Triazophos	-0.250	-0.448	-0.473
Flubendiamide	0.224	0.265	0.287
Emamectin Benzoate	-0.076	0.012	0.012
Tebuconazole & Trifloxystrobin	-0.768	-0.331	-0.331
Ethion	-0.698	-0.417	-0.584

Table 6: Effect of Ethion concentration on seedling length (shoot, root and total length).

	Shoot length (cm)	Root Length (cm)	Total Length (cm)
Control	5.088	6.363	11.450
Ethion (1.25mL/L)	4.500	7.300	11.800
Ethion (2.5mL/L)	3.800	6.650	10.450
Ethion (3.75mL/L)	3.513	6.288	9.800
Ethion (5mL/L)	3.175	4.000	7.175
S Em ±	0.102	0.379	0.414
CD (P=0.05)	0.308	1.142	1.249
CV (%)	5.091	12.381	8.172

there was no significant change in length. A similar trend was observed in tomato crop where Emamectin Benzoate reduced the growth when applied in higher concentration than the recommended dose, but at lower doses had some stimulatory effects on growth (Shakirullah et al. 2016)

Flubendiamide: Statistical analysis revealed that there was a significant increase in seedling length in Flubendiamide (Table 9) at 0.3mL/L (13.188cm) and 0.45mL/L (13.225) compared to control (11.450cm). Shoot length was significantly increased in 0.3mL/L (5.888cm) and 0.45mL/L (5.738cm) compared to shoot length in control (5.088cm). While root length was significantly increased in 0.45mL/L (7.488cm) compared to control (6.363cm). Similar observation that Flubendiamid stimulated growth in rice seedlings was observed by Deng et al. (2011).

Triazophos: From the statistical analysis no significant change in shoot length was noticed compared to different concentrations of Triazophos (Table 10). Root length was

Table 7: Effect of Tebuconazole + Trifloxystrobin concentration on seedling length (shoot, root and total length).

Treatment	Shoot length (cm)	Root Length (cm)	Total Length (cm)
Control	5.088	6.363	11.450
Tebuconazole + Trifloxystrobin (0.625 g/L)	2.738	6.738	9.475
Tebuconazole + Trifloxystrobin (1.25 g/L)	2.413	6.100	8.513
Tebuconazole + Trifloxystrobin (1.875 g/L)	2.425	5.850	8.275
Tebuconazole + Trifloxystrobin (2.5 g/L)	1.763	4.450	6.213
S Em ±	0.116	0.322	0.397
CD (P=0.05)	0.351	0.970	1.196
CV (%)	8.072	10.911	9.028

Table 8: Effect of Emamectin Benzoate concentration on seedling length (shoot, root and total length).

Treatment	Shoot length (cm)	Root Length (cm)	Total Length (cm)
Control	5.088	6.363	11.450
Emamectin Benzoate (0.2g/L)	4.538	7.688	12.225
Emamectin Benzoate (0.4g/L)	5.000	7.463	12.463
Emamectin Benzoate (0.6g/L)	4.963	7.438	12.400
Emamectin Benzoate (0.8g/L)	4.650	6.563	11.213
S Em ±	0.178	0.329	0.415
CD (P=0.05)	N.S	0.993	N.S
CV (%)	7.358	9.272	6.950

Table 9: Effect of Flubendiamide concentration on seedling length (shoot, root and total length).

Treatment	Shoot length (cm)	Root Length (cm)	Total Length (cm)
Control	5.088	6.363	11.450
Flubendiamide (0.15mL/L)	5.375	6.338	11.713
Flubendiamide (0.3mL/L)	5.888	7.300	13.188
Flubendiamide (0.45mL/L)	5.738	7.488	13.225
Flubendiamide (0.6mL/L)	5.525	7.138	12.663
S Em ±	0.181	0.327	0.414
CD (P=0.05)	0.547	0.986	1.250
CV (%)	6.568	9.445	6.660

Table 10: Effect of Triazophos concentration on seedling length (shoot, root and total length).

Treatment	Shoot length (cm)	Root Length (cm)	Total Length (cm)
Control	5.088	6.363	11.450
Triazophos (0.625mL/L)	4.450	6.450	10.900
Triazophos (1.25mL/L)	4.650	5.200	9.850
Triazophos (1.875mL/L)	4.650	5.150	9.800
Triazophos (2.5mL/L)	4.350	4.600	8.950
S Em ±	0.17	0.245	0.276
CD (P=0.05)	N.S	0.738	0.833
CV (%)	7.17	8.817	5.425

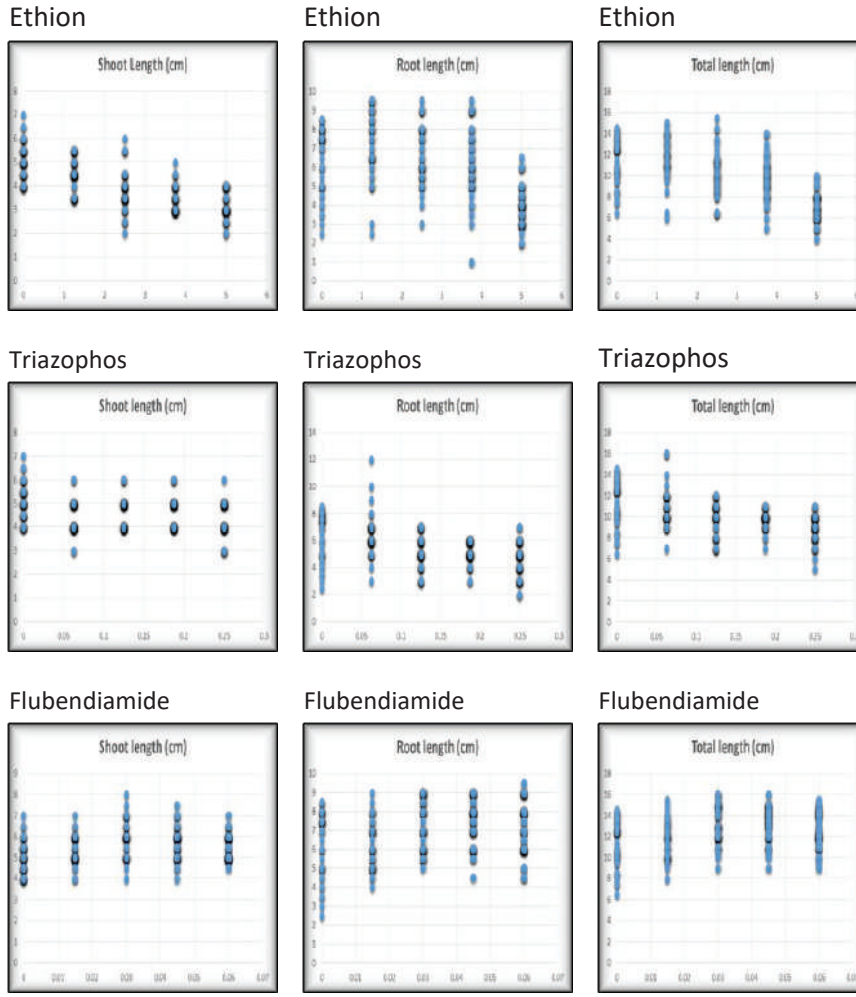

Fig. 1: Scatter of seedling growth (shoot, root and total length) in relation to crop protective agents and at different concentrations (Ethion, Triazophos and Flubendiamide).

significantly reduced in 1.2mL/L (5.2cm), 1.875mL/L (5.150cm) and 2.5mL/L (4.6cm) compared to control (6.363cm). while total seedling length was significantly reduced in 1.25mL/L (9.85cm), 1.875mL/L (9.8cm) and 2.5mL/L (8.95) compared to control (11.450cm). A similar trend was observed, the residual content of Triazophos

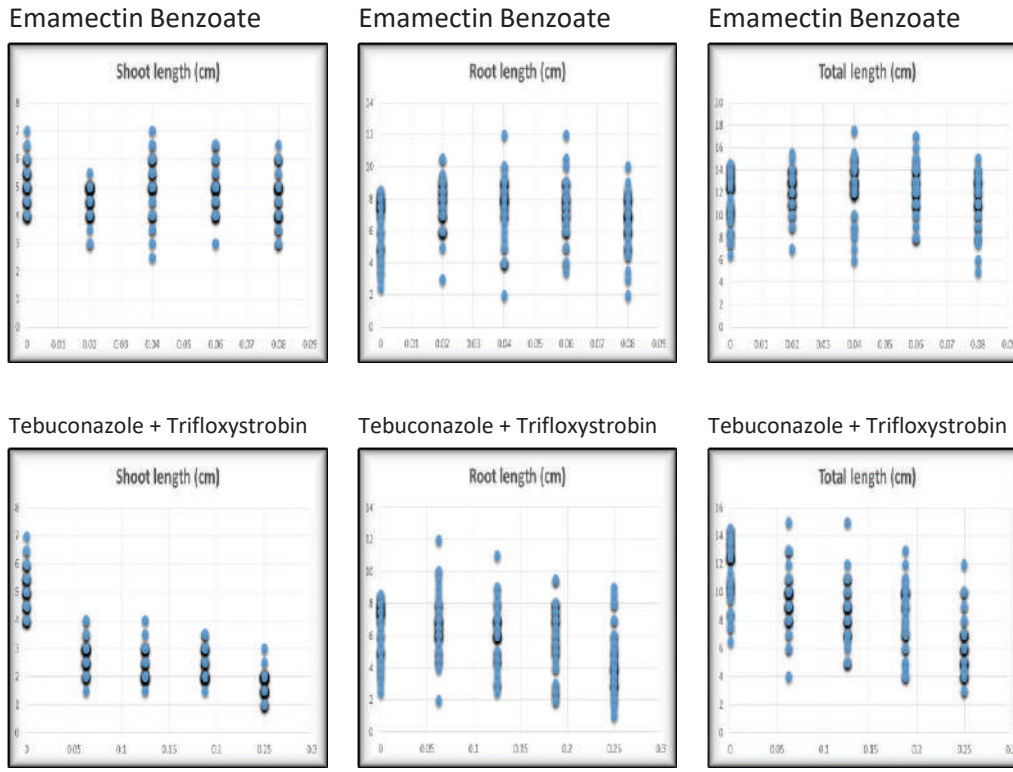

Fig. 2: Scatter of seedling growth (shoot, root and total length) in relation to crop protective agents and at different concentrations (Emamectin Benzoate and Tebuconazole + Trifloxystrobin).

reduced the seedling growth in wheat crop (Khanday et al. 2014).

CONCLUSION

From the study, it is evident that there is no variance in germination count among the treatments with crop protective agents (Ethion, Tebuconazole + Trifloxystrobin, Emamectin Benzoate, Flubendiamde and Triazophos at all the concentrations compared to control (distilled water).

Seedling growth was positively correlated to treatment with Flubendiamide and Emamectin Benzoate while, negatively correlated to Ethion, Triazophos and Tebuconazole+Trifloxystrobin combination. Shoot growth was slower in Tebuconazole + Trifloxystrobin, Ethion, Triazophos and Emamectin Benzoate and Flubendiamide enhanced growth was observed compared to control. While root length was found to increase in Emamectin Benzoate and Flubendiamide, the values showed a reduction in Ethion, Tebuconazole+ Trifloxystrobin and Triazophos treatments compared with control.

Crop protective agent Tebuconazole + Trifloxystrobin combination was very effective in protecting against chilli seed spoilage till 15 days and Triazophos at higher concentration reduced seed spoilage compared with Emamectin Benzoate, Flubendiamide and control though there was a negative correlation with respect to seedling growth.

ACKNOWLEDGEMENT

The authors are thankful to the Head, Research Department, ITC, ABD, Rajahmundry, for providing necessary research facilities to carry out these studies.

REFERENCES

Alam, M.Z., Hamim, I., Ali, M.A. and Ashrafuzzaman, M. 2014. Effect of seed treatment on seedling health of chilli. Journal of Environmental Science and Natural Resources, 7: 1.

Deng, Li'nan, Li Baotong, Xu Yueming, Shi Qinghua and Pan Xiaohua 2011. Efficacy of two flubendiamide ready-mixture insecticides on *Stenchaetothrips biformis* and the growth of direct-seeding rice by seed dressing. Chinese Agricultural Science Bulletin, 12.

Gao, RenJun, Den, Chun Yan, Wu, XueHong and Li, JinYu 2000. Effects of seed coating treatments with triadimenol and tebuconazole on the

growth and development of wheat seedling. Acta Phytophylacica Sinica, 27(4): 359-363.

Griffiths, D.C., Scott, G. C., Maskell, F.E., Mathias, P.L. and Roberts, P. F. 1970. The effects of known amounts of γBHC and organophosphorus seed dressings on growth of wheat seedlings and attack by larvae of wheat bulb fly (*Leptohylemyia coarctata* (Fall.). Plant Pathology, 19(3): 111-118.

Khanday, Arshid Ahmad, Dwivedi, H.S. and Dwivedi, P. 2014. Residual impact of Triazophos on the germination of wheat (*Triticum aestivum* L.) Var. Lok-1. Advances in Life Science and Technology, 21.

Lamsal, K., Ghimire, B.K., Sharma, P., Ghimiray, A.K., Kim, S.W., Yu, C.Y., Chung, I.M., Lee, Y.S., Kim, J.S. and Shakya, S.R. 2010. Genotoxicity evaluation of the insecticide ethion in root of *Allium cepa L.* African Journal of Biotechnology, 9: 27.

Moshe, Reuveni 2000. Efficacy of trifloxystrobin (Flint), a new strobilurin fungicide, in controlling powdery mildews on apple, mango and nectarine, and rust on prune trees. Crop Protection, 19(5): 335-341.

Prakash, N.S., Lakshmi, N. and Harini, I. 1988. Effects of fungicides "Bavistin" and "Deltan" on chilli (*Capsicum annuum* L.). Cytological Effects of Agricultural Chemicals II, 53(4): 709-715.

Rao, N.K., Hanson, J., Dulloo, M.E., Ghosh, K. and Nowell, A., 2006. Manual of Seed Handling in Genebanks (No. 8). Bioversity International.

Shakirullah, K. Shakir, Kanwal, M., Murad, W., ur Rehman, Z., ur Rehman, S., Daud, M.K. and Azizullah, A. 2016. Effect of some commonly used pesticides on seed germination, biomass production and photosynthetic pigments in tomato (*Lycopersicon esculentum*). Ecotoxicology, 25(2): 329-341.

Xuehong, G.R.D.C.W. and Jinyu, L. 2000. Effects of seed coating treatments with Triadimenol and Tebuconazole on the growth and development of wheat seedling. Journal of Plant Protection, 4.

Yang, D., Wang, N., Yan, X., Shi, J., Zhang, M., Wang, Z. and Yuan, H. 2014. Microencapsulation of seed-coating tebuconazole and its effects on physiology and biochemistry of maize seedlings. Colloids and Surfaces B: Biointerfaces, 114: 241-246.

Nature Environment and Pollution Technology
An International Quarterly Scientific Journal

p-ISSN: 0972-6268
(Print copies up to 2016)
e-ISSN: 2395-3454

Vol. 19 | No. 2 | pp. 783-790 | 2020

Original Research Paper

https://doi.org/10.46488/NEPT.2020.v19i02.035

Open Access Journal

Heavy Metal Contamination and Human Health Risk Associated with Sediment of Ganges River (Northwestern Bangladesh)

Md. Abu Sayed Jewel*, Md. Ayenuddin Haque*†, Ruhul Amin, Jakia Hasan***, LubnaAlam****, Subrata Mondal***** and Sharif Ahmed********

*Department of Fisheries, University of Rajshahi, Rajshahi, Bangladesh
**Bangladesh Council of Scientific and Industrial Research (BCSIR), Rajshahi, Bangladesh
***Bangladesh Fisheries Research Institute (BFRI), Marine Fisheries & Technology Station, Cox's Bazar-4700, Bangladesh
****Institute for Environment and Development (LESTARI), National University of Malaysia, Bangi, Malaysia
*****Department of Fisheries and Marine Bioscience, Jessore University of Science and Technology, Bangladesh
******Marine Fisheries Academy, Fish Harbour, Isanagore, Chittagong-4000, Bangladesh
†Corresponding author: Md. Ayenuddin Haque; ayenuddin41@gmail.com

Nat. Env. & Poll. Tech.
Website: www.neptjournal.com

Received: 15-03-2019
Accepted: 30-05-2019

Key Words:
Heavy metals;
Sediments;
Human health risk;
Ganges river

ABSTRACT

Metal contamination of sediment of Ganges River (Northwestern Bangladesh) and its possible health risk to the local people were evaluated at four different sites during three seasons (summer, monsoon, winter) in the year 2016. Followed by wet digestion, the samples were analysed by Flame Atomic Absorption Spectrophotometer. Mean concentration of Cr, Pb, Ni, Cd, Mn, As, Cu and Zn were 9.31, 6.43, 0.19, 1.90, 61.66, 0.65, 9.33 and 16.14 mg/kg, respectively. According to metal indices (contamination factor, contamination degree and pollution load index), the sediment was low to moderately contaminated with the studied metals, while human health risk assessment indicated unacceptable risk (hazard index (HI) values > 1) for non-carcinogenic adverse health effect. Therefore, the sediment of the river was not contaminated enough to prevail high risk on ecological health of river and to pose health risk on local people, but regular practice of discharging contaminants can somehow worsen the river quality in the coming years.

INTRODUCTION

Sediment is an essential and dynamic part of the river basin, with the variation of habitats and environment (Morillo et al. 2004). Sediments are regarded as ultimate sink and indicator of changes in water column as well as the influence of anthropogenic activities in air and watersheds environment (Emad et al. 2012). In the aquatic environment, sediments have been widely used as environmental indicators for the assessment of metal pollution in the natural water (Islam et al. 2015). In the hydrological cycle, less than 0.1% of the metals are dissolved in the water and more than 99.9% are stored in sediments and soils (Pradit et al. 2010). Indiscriminate use of heavy metal-containing fertilizers and pesticides in agricultural fields are major sources of heavy metals in river ecosystem (Reza & Singh 2010). The entry of municipal, industrial and agricultural waste into the environment is another way of environment pollution by human interferences (Shanbehzadeh et al. 2014). Therefore, the investigation of heavy metals in sediments can be used to assess the anthropogenic and industrial impacts and risks posed by waste discharged on the riverine ecosystems (Yi et al. 2011, Saleem et al. 2015).

Nowadays, pollutants from Rajshahi City pose a serious threat to the ecosystem and biodiversity of Ganges river (Northwestern Bangladesh). This river plays a vital role as an important freshwater resource of Bangladesh. Water of Padma river is used for different purposes such as bathing, irrigation, navigation, fisheries and recreation. But nowadays, surface water quality of Ganges River (Northwestern Bangladesh) is being poorer day by day because of the discharge of untreated drainage water from the city that is continuously polluting the aquatic ecosystem of the river. All the polluted and contaminated waters of the drainage network are being discharged into the river directly through the major outlets and round the clock. Besides, the people residing along the river bank are throwing their clinical and household wastes either to the connecting drains or into the river regularly that polluted the river. The flow of the river is also decreasing after the construction of the Farakka Barrage in the West Bengal (India) region that also significantly reduces the maximum flow of water in this part of the river in Bangladesh.

The population of many natural fish species has been reported to reduce from this river considerably due to the consequences of natural causes such as climate change,

siltation and manmade anthropogenic activities. Such activities, therefore, lead to aquatic pollution and loss of natural habitat for spawning and growth of fish species (Bhuiyan et al. 2008, Hassan et al. 2015). Despite the existing problem of reducing fish population from Ganges River (Northwestern Bangladesh), the data regarding the pollution status and its effect on ecology and human health are still lacking and gotten less attention from the local authorities and researchers. Therefore, the purpose of the present study was to characterize the pollution status of the Ganges River (Northwestern Bangladesh) by analysing the concentration of heavy metals in the surface sediment and the evaluation of health risk to the local people living along the river bank.

MATERIALS AND METHODS

Selection of Study Locations

The present study was conducted at T-dam, Padma garden, I-dam and Talaimari point covering most part of the Rajshahi City Corporation area along the bank of the Ganges River (Northwestern Bangladesh). Samplings were done on three respective seasons namely summer, monsoon and winter in the year 2016. Location of sampling sites and their description are given in Table 1 and Fig. 1.

Sampling Technique and Preparation of Sample

Surface sediments from the studied sites were collected using hand driven stainless steel corers, following a simple random and judgmental sampling technique. The sediments were collected up to a depth of 10 cm from the surface layer. In the laboratory, the collected samples were oven dried at 40°C for 48 h; passed through a 1 mm plastic sieve to remove plant materials, debris and gravel-sized materials; and then sieved through a nylon sieve (aperture 125 µm). All the necessary precautions and care were taken during drying, sieving, grinding and storage of sediment samples to avoid any kind of contamination. Wet digestion of the samples was

Table 1: Sampling station, sampling code and observation.

Sampling station	Sampling code	Coordinates	Observations
T-dam	Site-1	Latitude: N-24°21'42.41" Longitude: E-88°34'31.18"	Discharge of effluent from some household garbage, no human activities except recreational activities.
Padma garden	Site-2	Latitude: N-24°21'42.30" Longitude: E-88°35'52.44"	Direct discharges of effluent from vegetable markets and slaughter discharges; discharge from household septic tanks, more human activities as recreational site.
I-dam	Site-3	Latitude: N-24°21'34.95" Longitude: E-88°36'39.92"	Direct discharges of effluent from household septic tanks, more human activities as recreational site.
Talaimari point	Site-4	Latitude: N-24°21'29.30" Longitude: E-88°37'30.55"	No human activities and no source of discharge into the river

Fig. 1: Location of study sites. Map modified from Google Earth-2017.

conducted in freshly prepared aqua regia (1:3 HNO_3: HCl) on a block digester.

Metal Analysis

The determination of heavy metals (Cr, Pb, Ni, Cd, Mn, As, Cu and Zn) concentration in the sediment samples was carried out by Flame Atomic Absorption Spectrometer (Shimadzu, AA-6800) in the central lab of University of Rajshahi, Rajshahi, Bangladesh.

Assessment of Sediment Contamination

To assess the sediment contamination status, contamination factor (*CF*) together with degree of contamination (C_d) and pollution load index (*PLI*) were used. *CF* was calculated according to Tomlinson et al. (1980). In this study standard pre-industrial reference level (mg/kg) proposed by Hakanson (1980) and Turekian & Wedepohl (1961) were considered as background concentration of the studied metals. Methods of calculation and classification criteria of the studied indices with references are presented in Table 2.

Risk Assessment on Human Health to Contaminated Sediments

Three major pathways are generally considered in human health risk assessment: ingestion, dermal contact and respiration. This study focused on the dermal contact of sediment as it may come into human contact through various household activities such as bathing, washing and recreational activities. The following equation was applied in calculating the exposure through this pathway (USEPA 1989, 2004, Rovira et al. 2011, Iqbal et al. 2013).

$$EXP_{derm} = \frac{\text{Cm} \times \text{CF} \times \text{SA} \times \text{AF} \times \text{ABS} \times \text{EF} \times \text{ED}}{\text{BW} \times \text{AT}} \quad \ldots(1)$$

Where, EXP_{derm} is the dermal uptake; *Cm* represents the measured concentration of the metals in sediment; *CF* represents the unit conversion factor (10^{-6} kg/mg); *SA* is the exposed skin surface area (5700 cm^2); *AF* represents the adherence factors from sediment to skin (0.07 $mg.cm^{-2}$); *ABS* is the dermal absorption from sediment (0.001); *EF* is the exposure frequency (350 days/years); *ED* represents the exposure duration (30 years); *BW* is the body weight (70 kg) and *AT* represents the average days (10,950 days).

Hazard quotients (*HQ*) were used to assess the non-carcinogenic health risks from the exposure to heavy metals in sediment according to USEPA (2004) health risk assessment guidelines. The following equations were adopted to evaluate *HQs* for the two exposure pathways:

$$HQ_{derm} = \frac{EXP_{derm}}{\text{RfD}_0} \quad \ldots(2)$$

$$HI = \sum_{i=1}^{n} HQ_{derm} \quad \ldots(3)$$

Where, *HI* is Hazard index, HQ_{derm} is hazard quotient via dermal contact under the respective exposure amount; RfD_0 is the reference dose for the resulting hazardous health effect caused by contaminants. The reference dose via dermal contact is typically hypothesized to be identical to the reference dose via dermal contact for heavy metals in sediment (Iqbal et al. 2013). HI is less than 1.0 indicative of highly unlikely significant toxic interactions, while HI greater than 1.0 refers to a concern for potential non-cancer health effect (Enuneku et al. 2018). In the present study, risk assessment on human health was conducted only for studied seasons and not for study sites. Assessment of risk due to Mn was also not evaluated due to lack of information on RfD_0 of this metal.

Table 2: Sediment contamination indices and their classification system.

Index	Equation	Classification	References
CF	$CF = \frac{C_{Metals}}{C_{Background}}$	*CF*< 1 (low *CF*) 1 ≤ *CF*< 3 (Moderate *CF*) 3 ≤ *CF*< 6 (Considerable *CF*) *CF* ≤ 6 (High *CF*)	Tomlinson et al. (1980)
Cd	$C_d = \sum_{i=1}^{n} CF$	*Cd*< 8 (Low *Cd*) 8 ≤ *Cd*< 16 (Moderate *Cd*) 16 ≤ *Cd*< 32 (Considerable *Cd*) *Cd* ≤ 32 (Very high *Cd*)	Mortuza & Al-Misned (2017)
PLI	$PLI = (CF_1 \times CF_2 \times CF_3 \times \ldots\ldots \times CF_n)^{1/n}$	*PLI* = 1 (baseline levels of pollutants present) *PLI*> 1 (progressive deterioration of site)	Tomlinson et al. (1980)

Note: *CF* = Contamination factor; *Cd* = Contamination degree; *PLI* = Pollution load index

Statistical Analysis

The data was analysed using Statistical Package for Social Science (SPSS software Version 20.0). The means and standard deviations of the heavy metal concentrations in sediment were calculated. The cluster analysis was also performed using standard method as Squared Euclidean Distance and Ward's linkage method to evaluate common possible sources of the studied metals.

RESULTS AND DISCUSSION

Concentration of Heavy Metals in Sediment

Seasonal distribution of heavy metals at different sites in the sediment of Ganges River (Northwestern Bangladesh) is shown in Fig. 2. In general, metal concentration was higher during summer season followed by winter and monsoon season. During summer, concentrations of Cr, Pb, Ni, Mn and Zn were the highest at Site-2, whereas the maximum concentration of Cd, As and Cu were observed during winter season. All the metals showed their lowest concentrations during monsoon season. The summer and winter maxima of heavy metals might be due to declining in water level and flow, which cause rapid sedimentation from municipal and domestic wastes (enriched with these metals). The results were in accordance with the findings of Pandey & Singh (2017), Kumar et al. (2013) and Dey et al. (2015), where they also observed that low water flow was responsible for the accumulation of higher concentrations of metals during dry months. The result also showed that big drains that located at Site-2 emptying their contents loaded with a huge amount of garbage of the city people, which were responsible for higher concentration of metals in that study site.

Mean concentration of Cr, Pb, Ni, Cd, Mn, As, Cu and Zn were 9.31, 6.43, 0.19, 1.90, 61.66, 0.65, 9.33 and 16.14 mg/kg, respectively (Table 3). Present data indicated that Mn accumulation in the sediment of Ganges River (Northwestern Bangladesh) was the highest, as it is one of the commonly found elements in the lithosphere. However, the steel industries might also be responsible for some extent to increase Mn in the sediment of Ganges River (Northwestern Bangladesh) during the present study (Sehgal et al. 2012). Zn and Cu were the second most abundant metals in the sediment of the river, whereas As and Ni were found in less amount. Higher concentration of Zn and Cu indicated their anthropogenic origin in the study sites as there were no big industries in Rajshahi City which could produce these metals. Among the metals studied, the concentration of Cr, As and Cu were within the range, while other metals such as Pb, Ni, Mn and Zn were below the range reported by Jolly et al. (2013). Concentrations of Cr, Pb, Ni, Mn, As, Cu and Zn were below the findings of Datta & Subramanian (1998), Hassan et al. (2015), Ali et al. (2016), Mohiuddin et al. (2015) and Pandey & Singh (2017), which is also an indication of the comparatively lower metal pollution of the river during the present study.

Risk Assessment Due to Contamination with Heavy Metals

In the present study, the contamination factor, degree of contamination and *PLI* were used to determine the contamination status of the sediment of Ganges River (Northwestern Bangladesh) (Table 4). Based on the mean values of *CF*, sediments were found enriched with metals in the order of: Cd >Pb> Cu > Zn > Cr >Mn> As > Ni. However, mean *CF* values of Cd (1.790) exceed the reference value 1, indicating the contamination of sediment by Cd. The mean value of C_d of Ganges River (Northwestern Bangladesh) was calculated as 2.839, which was also an indication of lower contamination of the sediment (Mortuza & Al-misned 2017). The *PLI* represents the number of time by which the metal content exceeds the background concentration and gives a summative indication of the overall level of heavy metal toxicity in a sample (Mohiuddin et al. 2010, Barakat et al. 2012). In

Table 3: Descriptive statistics of heavy metals in sediment (mg/kg) of Ganges River (Northwestern Bangladesh).

Metals	Minimum	Maximum	Mean±SD
Cr	1.71	23.64	9.31±7.50
Pb	1.85	15.26	6.43±4.43
Ni	0.01	0.54	0.19±0.18
Cd	0.16	3.77	1.90±1.15
Mn	26.96	110.52	61.66±27.87
As	0.07	1.30	0.65±0.52
Cu	0.01	22.41	9.33±9.22
Zn	0.03	43.26	16.14±16.01

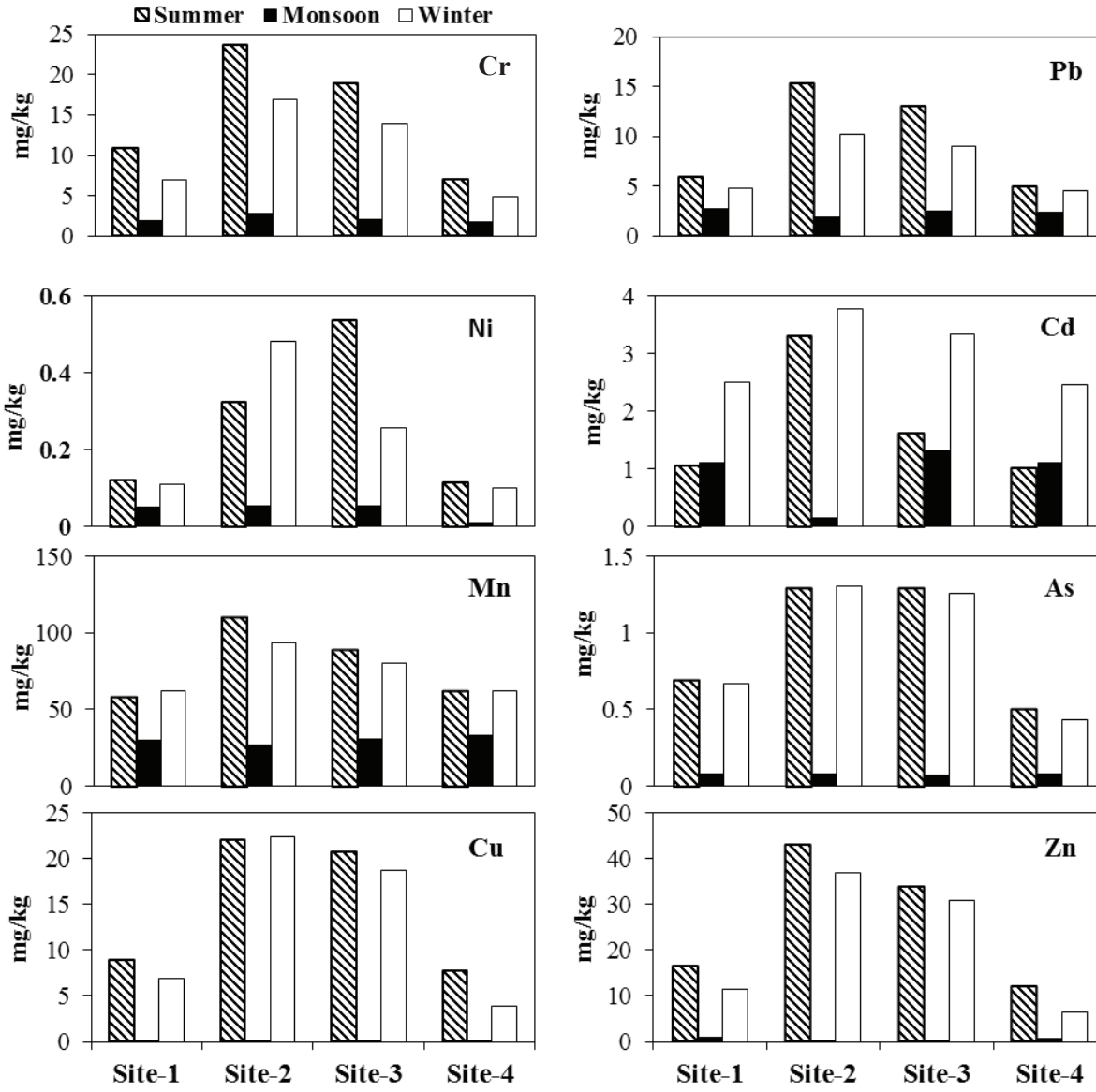

Fig. 2: Mean concentrations of heavy metals (mg/kg) in sediment of Ganges River (Northwestern Bangladesh) at different sites and seasons during the study period.

the present study, the mean value of *PLI* was 0.100 which was lower than the reference value of 1. Therefore, it was confirmed that the sediment of the river was not polluted in terms of *PLI* value (Tomlinson et al. 1980). However, during the study period, the highest *PLI* value was recorded during summer season at Site-2 (0.231), which might be due to the lower water level and the discharge of untreated pollutants.

The resulting dendrogram contains two distinct clusters (Fig. 3). Cr, Pb, Ni, Cd, As, Cu and Zn formed the cluster "A", which indicates their similar source of origin and similar behaviour and mostly come from anthropogenic sources. Mn formed distinct cluster "B" on its own which indicated completely different behaviour and origin from the metals of cluster "A" and it might come from lithogenic sources. Differences in the metal content of parent rock materials are likely the main reason for different clustering of the studied metals in the present study. Therefore, the discharging of sewage and municipal wastewater were the main source of the contamination of heavy metal in Ganges River (Northwestern Bangladesh).

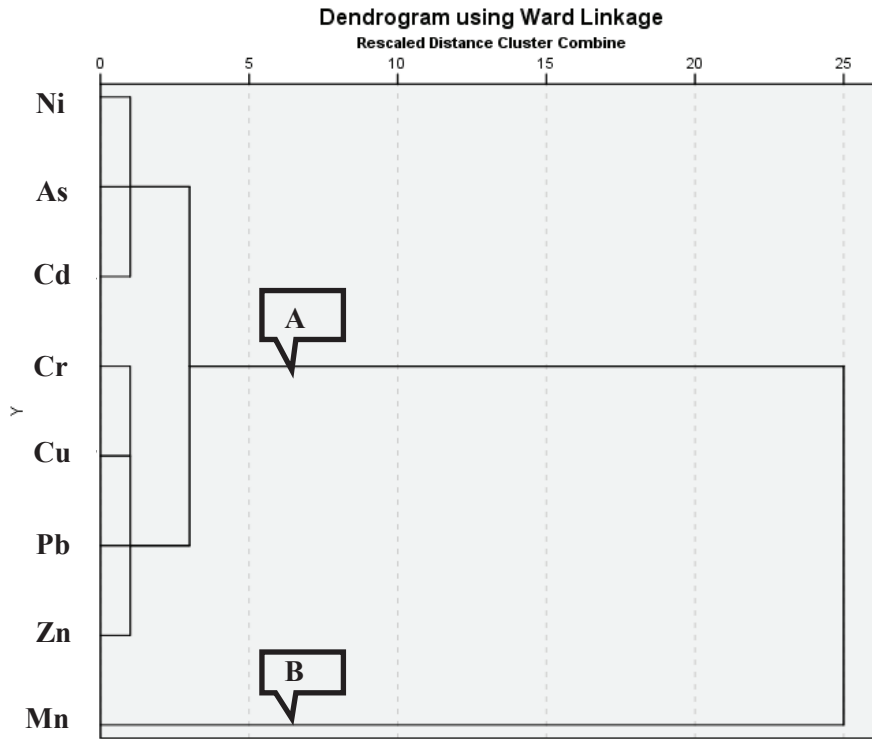

Fig. 3: Dendrogram of cluster analysis amongst metals in Ganges River (Northwestern Bangladesh) sediment.

Risk Assessment on Human Health

Table 5 shows the estimated average exposure value, non-carcinogenic *HQs* and *HI* of the sediment during summer, monsoon and winter of Ganges River (Northwestern Bangladesh). The *HQ* value was in order of Cr > As >Pb> Cd > Cu > Zn > Ni during summer, Cd > Cr >Pb> As > Ni > Cu > Zn during monsoon, and Cr > As > Cd >Pb> Cu > Zn > Ni during winter season. The *HI* for dermal contact of sediment was 7.24×10^{-5}, 1.41×10^{-5} and 6.60×10^{-5} during

Table 4: Contamination factor (CF) and pollution load index (PLI) of sediment of Ganges River (Northwestern Bangladesh) at different seasons and sites during the study period.

Seasons	Locations	Cr	Pb	Ni	Cd	Mn	As	Cu	Zn	C_d	*PLI*
Summer	Site-1	0.121	0.294	0.002	1.060	0.062	0.047	0.223	0.176	1.986	0.097
	Site-2	0.263	0.763	0.005	3.324	0.116	0.086	0.553	0.455	5.565	0.231
	Site-3	0.211	0.648	0.008	1.632	0.094	0.086	0.519	0.358	3.556	0.201
	Site-4	0.077	0.248	0.002	1.021	0.066	0.034	0.197	0.128	1.773	0.081
Monsoon	Site-1	0.021	0.139	0.001	1.102	0.031	0.005	0.000	0.009	1.309	0.014
	Site-2	0.031	0.092	0.001	0.163	0.028	0.005	0.003	0.001	0.325	0.011
	Site-3	0.023	0.128	0.000	1.326	0.032	0.000	0.003	0.000	1.518	0.001
	Site-4	0.019	0.122	0.000	1.102	0.035	0.005	0.000	0.008	1.291	0.011
Winter	Site-1	0.077	0.238	0.002	2.513	0.065	0.045	0.174	0.121	3.235	0.091
	Site-2	0.188	0.512	0.007	3.770	0.099	0.087	0.560	0.388	5.611	0.216
	Site-3	0.155	0.449	0.004	3.330	0.084	0.084	0.468	0.325	4.898	0.176
	Site-4	0.054	0.227	0.001	2.463	0.065	0.029	0.097	0.068	3.005	0.070
Mean		0.103	0.322	0.003	1.790	0.065	0.043	0.233	0.170	2.839	0.100

Table 5: Health risk posed by the contaminated sediment of Ganges River (Northwestern Bangladesh) during summer, monsoon and winter seasons.

Metals	RfD_0	Summer		Monsoon		Winter	
		Exposure assessment	Non-carcinogenic risk	Exposure assessment	Non-carcino-genic risk	Exposure assessment	Non-carcinogenic risk
		EXP_{derm}	HQ_{derm}	EXP_{derm}	HQ_{derm}	EXP_{derm}	HQ_{derm}
Cr	3.00×10^{-3}	8.25×10^{-8}	2.75×10^{-5}	1.16×10^{-8}	3.87×10^{-6}	5.85×10^{-8}	1.95×10^{-5}
Pb	3.50×10^{-3}	5.34×10^{-8}	1.53×10^{-5}	1.32×10^{-8}	3.77×10^{-6}	3.90×10^{-8}	1.11×10^{-5}
Ni	1.10×10^{-2}	1.51×10^{-9}	1.37×10^{-7}	2.30×10^{-10}	2.09×10^{-8}	1.30×10^{-9}	1.18×10^{-7}
Cd	1.00×10^{-3}	9.61×10^{-9}	9.61×10^{-6}	5.04×10^{-9}	5.04×10^{-6}	1.65×10^{-8}	1.65×10^{-5}
As	3.00×10^{-4}	5.19×10^{-9}	1.73×10^{-5}	4.21×10^{-10}	1.40×10^{-6}	4.99×10^{-9}	1.66×10^{-5}
Cu	4.00×10^{-2}	8.15×10^{-8}	2.04×10^{-6}	3.50×10^{-10}	8.75×10^{-9}	7.10×10^{-8}	1.78×10^{-6}
Zn	3.00×10^{-1}	1.45×10^{-7}	4.83×10^{-7}	2.37×10^{-9}	7.90×10^{-9}	1.17×10^{-7}	3.90×10^{-7}
HI_{derm}			7.24×10^{-8}		1.41×10^{-5}		6.60×10^{-5}

Note: EXP_{derm} = Exposure *via* dermal contact, HQ_{derm} = Hazard quotients *via* dermal contact, HI_{derm} = Hazard index *via* dermal contact.

summer, winter and monsoon season, respectively. The non-carcinogenic health risk posed by dermal contact of contaminated sediment was found lower during the present study. According to Lim et al. (2008), $HI > 1$ indicates an unacceptable risk of non-carcinogenic effects on health, while $HI < 1$ indicates an acceptable level of risk. Therefore, metal content of the sediment of the river was supposed not to have any carcinogenic effects on human health.

CONCLUSIONS

It can be concluded that the present pollution status of Ganges River (Northwestern Bangladesh) was not worse enough to prevail high risk on ecological health of river and to pose health risk on local people, but if the current trend of pollution is likely to continue, at least in the future, the river quality will get worse enough in the coming years, especially in the summer season. In such a situation, implementation of suitable management plan along with proper sewage treatment network, maintenance of enough dilution flow and other watershed management approaches should be in practice to control the metal pollution of this river ecosystem.

REFERENCES

Ali, M.M., Ali, M.L., Islam, M.S., Rahman, M.Z. 2016. Preliminary assessment of heavy metals in water and sediment of Karnaphuli River, Bangladesh. Environ. Nanotechnol. Monit. Manag., 5: 27-35.

Barakat, A., Baghdadi, M.E. and Mellal, J. 2012. Assessment of heavy metal in surface sediments of Day River at Beni Mellal region, Morocco Region, Morocco. Res. J. Environ. Earth Sci., 4: 797-806.

Bhuiyan, S.S., Joadder, M.A.R. and Bhuiyan, A.S. 2008. Occurrence of fishes and non-fin fishes of the river Padma near Rajshahi, Bangladesh. Uni. J. Zool., 27: 99-100.

Datta, D.K. and Subramanian, V. 1998. Distribution and fractionation of heavy metals in the surface sediments of the Ganges-Brahmaputra-Meghna river system in the Bengal basin. Environ. Geol., 36(1-2): 93-101.

Dey, S., Das, J. and Manchur, M.A. 2015. Studies on heavy metal pollution of Karnafully River, Chittagong, Bangladesh. IOSR J. Environ. Sci. Toxicol. Food Tech., 9: 79-83.

Emad, A., Salah, M., Zaidan, T.A. and Al-Rawi, A.S. 2012. Assessment of heavy metals pollution in the sediments of Euphrates River, Iraq. J. Water Res. Protec., 4: 1009-1023.

Enuneku, A., Omoruyi, O., Tongo, I., Ogbomida, E., Ogbeide, O. and Ezemony, L. 2018. Evaluating the potential health risks of heavy metal pollution in sediment and selected benthic fauna of Benin River, Southern Nigeria. App. Water Sci., 8: 224.

Hakanson, L. 1980. An ecological risk index for aquatic pollution-control-A sedimentological approach. Water Res.,14: 975-1001.

Hassan, M., Mirza, A.T.M., Rahman, T., Saha, B. and Kamal, A.K.I. 2015. Status of heavy metals in water and sediment of the Meghna River, Bangladesh. Am. J. Environ. Sci., 11: 427-439.

Iqbal, J., Tirmizi, S.A. and Shah, M.H. 2013. Statistical apportionment and risk assessment of selected metal in sediments from Rawal Lake (Pakistan). Environ. Monit. Assess., 185: 729-743.

Islam, M.S., Ahmed, M.K., Raknuzzaman, M., Habibullah-Al-Mamun, M. and Islam, M.K. 2015. Heavy metal pollution in surface water and sediment: A preliminary assessment of an urban river in a developing country. Ecol. Indic., 48: 282-291.

Jolly, Y.N., Akter, J.S., Kabir, A.I. and Akbar, S. 2013. Trace elements contamination in the river Padma. Bangladesh J. Phys., 13: 95-102.

Kumar, R.N., Solanki, R. and Kumar, J.N. 2013. Seasonal variation in heavy metal contamination in water and sediments of river Sabarmati and Kharicut canal at Ahmedabad, Gujrat. Environ. Monit. Assess., 185: 359-368.

Lim, H.S., Lee, J.S., Chon, H.T. and Sager, M. 2008. Heavy metal contamination and health risk assessment in the vicinity of the abandoned Songcheon Au-Ag mine in Korea. J. Geochem. Explor., 96: 223-230.

Mohiuddin, K.M., Zakir, H.M., Otomo, K., Sharmin, S. and Shikazono, N. 2010. Geochemical distribution of trace metal pollutants in water and sediments of downstream of an Urban River. Int. J. Environ. Sci. Tech., 7: 17-28.

Morillo, J., Usero, J. and Gracia, I. 2004. Heavy metal distribution in marine sediments from the southwest coast of Spain. Chemosphere, 55: 431-442.

Mortuza, M. and Al-Misned, F.A. 2017. Environmental contamination and assessment of heavy metals in water, sediments and shrimp of Red Sea Coast of Jizan, Saudi Arabia. J. Aqua. Pollut. Toxicol., 1: 5.

Pandey, J. and Singh, R. 2017. Heavy metals in sediments of Ganga River: Up- and downstream urban influences. Appl. Water Sci., 7: 1669-1678.

Pradit, S., Wattayakorn, G., Angsupanich, S., Baeyens, W. and Leermakers, M. 2010. Distribution of trace elements in sediments and biota of Songkhla Lake, Southern Thailand. Water Air Soil Pollut., 206(1): 155-74.

Reza, R. and Singh, G. 2010. Heavy metal contamination and its indexing approach for river water. Int. J. Environ. Sci. Tech., 7(4): 785-792.

Rovira, J., Mari, M., Schuhmavher, M., Nadal, M. and Domingo, J.L. 2011. Monitoring environmental pollutants in the vicinity of a cement plant: a temporal study. Arch. Environ. Contam. Toxicol., 60: 372-384.

Saleem, M., Iqbal, J. and Shah, M.H. 2015. Geochemical speciation, anthropogenic contamination, risk assessment and source identification of selected metals in fresh water sediments- A case study from Manglalake, Pakistan. Environ. Nanotech. Monit. Manag., 4: 27-36.

Sehgal, M., Garg, A. Suresh, R. and Dagar, P. 2012. Heavy metal contamination in the Delhi segment of Yamuna basin. Environ. Monit. Assess., 184: 1181-1196.

Shanbehzadeh, S., Dastjerdi, M.V., Hassanzadeh, A. and Kiyanizadeh, T. 2014. Heavy metals in water and sediment: A case study of Tembi River. J. Environ. Public Health, Article ID 858720, 5.

Tomlinson, D.L., Wilson, J.G., Harris, C.R. and Jeffrey, D.W. 1980. Problems in the assessments of heavy-metal levels in estuaries and formation of a pollution index. Helgolander Meeresunters, 33: 566.

Turekian, K.K. and Wedepohl, K.H.1961. Distribution of the elements in some major units of the earth's crust. Geol. Soci. Am. Bull., 72: 175-192.

USEPA 1989. Sediment Classification Methods Compendium. Draft Final Report, United States Environmental Protection Agency, Watershed Protection Division, USA.

USEPA 2004. Risk Assessment Guidance for Superfund. Volume I: Human Health Evaluation Manual (Part E). EPA/540/R/99/005 OSWER 9285.7-02EP PB99-963312.

Yi, Y., Yang, Z. and Zhang, S. 2011. Ecological risk assessment of heavy metals in sediment and human health risk assessment of heavy metals in fishes in the middle and lower reaches of the Yangtze river basin. Environ. Pollut., 159: 2575-2585.

Nature Environment and Pollution Technology
An International Quarterly Scientific Journal

p-ISSN: 0972-6268
(Print copies up to 2016)
e-ISSN: 2395-3454

Vol. 19 | No. 2 | pp. 791-797 | 2020

Original Research Paper

https://doi.org/10.46488/NEPT.2020.v19i02.036

Open Access Journal

Carbon Emission Efficiency in the Construction Industry and Its Carbon Emission Control Measures: A Case Study of Henan Province, China

Qing jing Shi and Chun Bai†
Department of Architecture and Civil Engineering, Shang Qiu University, Shang Qiu 476000, China
†Corresponding author: Chun Bai; ansysbc@163.com

Nat. Env. & Poll. Tech.
Website: www.neptjournal.com

Received: 25-02-2020
Accepted: 18-04-2020

Key Words:
Construction industry;
Carbon emission efficiency;
Environmental pollution

ABSTRACT

With the rapid development of urbanization, the Chinese construction industry has generated a large quantity of carbon emission and brought about challenges to sustainable development while making enormous contributions to national economic development. Thus, this industry is the key field of energy conservation and emission reduction. Facilitating sustainable development of the construction industry and scientifically and reasonably evaluating the carbon emission efficiency of the construction industry will be important for effectively controlling carbon emission and boosting the sustainable development of the construction industry. Carbon emission was added into the total-factor productivity model of the traditional construction industry as an environmental factor in this study, and a total-factor evaluation model for the carbon emission efficiency of the construction industry was constructed. Henan Province was taken as an example, and empirical analysis was conducted to determine the differences of Henan construction industry in the period of 2012-2018 in the aspect of carbon emission efficiency. Results showed that the total-factor carbon emission efficiency of Henan construction industry in the period of 2012–2018 was 1.084%, which indicated a certain increase in the total-factor emission efficiency of Henan construction industry over the 7 years. The overall resource utilization efficiency of Henan construction industry was improved by 0.84% due to the joint actions of elevated technological progress (by 0.35%) and improved technical efficiency (by 0.47%). Average pure technical efficiency was slightly reduced by 0.03%, which indicated that building scale was the driving force for improving the total-factor efficiency of the construction industry. The study results can provide systematic and comprehensive carbon emission information in the construction industry for policy making. Therefore, the carbon emission status of the construction industry in one province can be mastered from a provincial level to clarify responsibilities, facilitate coordinated development, and boost the efficiency and equity of emission reduction in the construction industry. This way will be important for finally realizing the goals of energy conservation, emission reduction, and low-carbon development.

INTRODUCTION

The rapid growth of China's economy in the past nearly 40 years has stimulated massive energy consumption and ever-growing carbon emission. China is a developing country with an enormous population base and a country with the greatest energy consumption and the highest carbon emission. Therefore, with the high-speed development of urbanization, the Chinese construction industry is consuming a large quantity of resources and energy, generating massive carbon emission, and posing challenges to sustainable development while making great contributions to national economic development. Therefore, this industry shoulders heavy reasonability for carbon emission reduction. Chinese buildings belong to buildings with high energy consumption and enormous every-saving potential, and the energy conservation and transformation of buildings should be given close attention. Different from developed countries, China is faced with the rapid growth of energy consumption and carbon emission of the construction industry induced by large-scale construction projects in the current urbanization progress in addition to enormous energy consumption and carbon emission in the daily operation of buildings. Thus, the construction industry is important to the overall consumption of natural resources and carbon emission. The scale of the Chinese construction industry, which is an industry with the most concentrated energy consumption and carbon emission, accounts for half of the global construction industry. Cement and steel materials used in buildings occupy approximately half of global consumption. Thus, the energy conservation and emission reduction of the construction industry are imperative and especially important to understand and analyze the energy consumption and carbon emission in the total industrial chain of the Chinese construction industry using the idea of the life cycle.

Henan Province, China is a province undergoing typical severe environmental pollution induced by the construction industry. Fig. 1 shows that the house construction area in Henan construction industry was 245,960,000 m^2 in 2009, but this figure rapidly rose to 637,890,000 m^2 up to 2018 with the rapid population growth and economic development, and the annual average growth rate reached as high as 17.7%. This situation has fully verified the rapid growth of energy consumption and carbon emission triggered by large-scale construction projects in the construction industry during the urbanization progress in Henan Province. In recent years, Henan construction industry has still presented high energy consumption and severe environmental pollution. Henan Province was taken as an example in this study to measure carbon emission efficiency of its construction industry and its measures for minimization of environmental pollution to perfect the evaluation of pollutant discharge in the construction industry and finally reach the effect of environmental improvement by implementing the concepts of sustainable development and green buildings.

PAST STUDIES

Among abundant studies on carbon emission of the construction industry, most have concentrated on carbon emission in the construction product life cycle, calculation of total carbon emission in the construction industry, and carbon emission factor and activity level of the construction industry. Carbon emission efficiency is a current environmental problem and a major research topic. Carbon emission, which is the most significant environmental impact, is usually used to characterize the degree of environmental impact, and carbon emission efficiency in the construction industry is also an important content in current environmental pollution of the construction industry. Works related to the carbon emission of the construction industry are discussed as follows. Suzuki et al. used the classified input-output table of basic Japanese departments to quantify carbon emissions generated by all kinds of house buildings (Suzuki et al. 1995). Mielnik et al. proposed the "carbonization index," which was extensively applied to studies on carbon emission in the construction industry as a useful index used to evaluate evolution patterns of climatic changes in industrialized and developing countries (Mielnik et al. 1999). Acquaye et al. calculated energy and greenhouse gas emission intensities of Irish construction sector and subsector, estimated their contributions to nationwide emission in Ireland and analyzed the influence of the construction industry on carbon emission (Acquaye et al. 2010). Chang et al. constructed an input-output life cycle assessment model of the construction industry based on the economic benchmarks of China in 2002, 2005, and 2007. The results showed that the embodied energy of Chinese construction projects accounted for 25%-30% of the total energy consumption, the emission of embodied SO_2 was controlled, and the emission intensity of embodied NOx and CO_2 was reduced (Chang et al. 2011). Zuo et al. considered that China was one of the countries with the largest energy consumption and carbon emission in the world, held a semi-structured interview with people occupied in the construction industry and determined the influencing factors of the construction industry to realize low carbonization. The results indicated that market demand, material selection, knowledge of facility manager, and governmental support and leadership were critical influencing factors of the low-carbon development of the construction industry (Zuo et al. 2012). Jeong et al. quantified CO_2 emissions generated by primary building materials, which were consumed in the construction process of six apartments with different sizes in Korea. The results were of certain reference value to the sustainable design of residential complexes and could serve

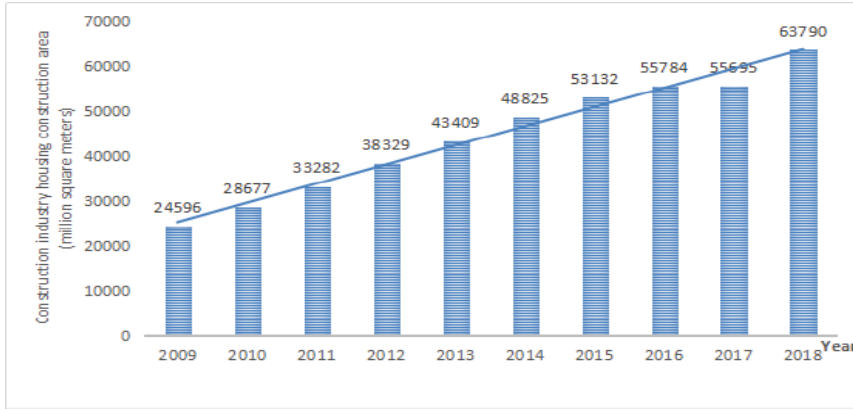

Fig. 1: House construction areas (ten thousand square meters) in Henan construction industry in the period of 2009-2018.

as technical measures for CO_2 emission reduction in the construction industry (Jeong et al. 2012). Li et al. analyzed the influence of embodied carbon of residential buildings in China, evaluated the influence of concrete carbon by taking three types of residential buildings in China as an example, and introduced concrete carbon emission measures for the construction industry (Li et al. 2014). Onat et al. quantified carbon footprints of American houses and commercial buildings and calculated carbon emissions in construction, use, and disposal phases in the base year 2002. The results showed that the emission was the highest in the use phase of the construction industry and accounted for 91% of the total emission in the total life cycle phase of American buildings (Onat et al. 2014). Feng et al. used panel data of 30 provinces in the period of 2004-2011 to conduct an empirical study of the total-factor energy efficiency of the interprovincial construction industry in China. The results indicated that the construction industries in different provinces had evident differences in energy efficiency and CO_2 emission, and scale of the construction industry, population density, liquidity of building materials, and urbanization rate were important influencing factors of interprovincial CO_2 emission differences (Feng et al. 2014). Xue et al. used the DEA (Data Envelopment Analysis)-based Malmquist productivity index (MPI) to conduct an empirical study on the changes in energy consumption and productivity of the construction industries in 26 provinces in China in the period of 2004-2009. The findings showed that the construction industries in northeast, west, central, and east regions in China had different energy conservation conditions, and carbon accounting could help decision-makers improve sustainable development strategies for the Chinese construction industry (Xue et al. 2015). Hong et al. used a multi-regional input-output model to investigate the energy consumption status in the Chinese construction industry. The results showed that the total coal consumption of the construction industry, which is a typical demand-driven industry, was 793,740,000 tons in 2007 and accounted for 29.6% of the total energy consumption in China. This study provided a basis for formulating and implementing policies used to reduce energy use and reduce carbon emission in the construction industry (Hong et al. 2016). Lu et al. evaluated the effectiveness of emission policies of Chinese buildings and calculated carbon emissions of the Chinese construction industry from 1994 to 2012. The results showed that the annual average emission of the Chinese construction industry grew by 6.9% between 1994 and 2012, and "consumption of building materials" had the greatest contribution to the growth of total carbon emission. This study provided a new scientific basis for carbon emission in the Chinese construction industry (Lu et al. 2016). Zhang et al. used the data of the construction industries in 30 provinces in Mainland China from 2005 to 2016 to conduct an empirical study of their carbon emission efficiency. The results manifested that effective popularization of low-carbon construction technologies and market-oriented reform of state-owned construction enterprises must be conducted to improve the development level of the Chinese construction industry (Zhang et al. 2019). The existing studies show that international incentive policies and control standards for accounting method of building carbon emission and low-carbon building development are quite mature and complete. By contrast, Chinese low-carbon buildings have a late start, and related supporting systems, such as financial and tax incentive policies and evaluation criteria specific to evaluation market of low-carbon buildings, are still incomplete. Most works on the evaluation system of low-carbon buildings are qualitative, while quantitative studies are insufficient, which radically restricts the construction and implementation of the evaluation system of Chinese low-carbon buildings. A few scholars have explored the complete carbon emission of the overall Chinese construction industry, but the emission condition and features of the construction industry in one province remain unclear. Thus, understanding and analysing the current carbon emission status and the tendency of the Chinese construction industry are important. Therefore, Henan Province, China, was taken as an example in this study. By calculating the overall carbon emission efficiency of Henan construction industry and establishing the evaluation framework for its carbon emission efficiency, the differences among various cities in carbon emission efficiency of the construction industry and the historical variation trends of carbon emission efficiency in various regions were compared. The coordinated development conditions between the construction industry and environmental carbon emission reduction in these regions were also analyzed. The contributing factors of the improvement in efficiency level were identified as well.

MODEL INTRODUCTION AND DATA DESCRIPTION

Introduction of DEA-Malmquist Model

Charnes et al. (1978) proposed the DEA-CCR (Charnes, Cooper, Rhodes) model at the earliest. Its principle is that the input or output of decision-making units (DMUs) is kept unchanged, and relatively effective production frontier is determined using statistical data through mathematical programming method. This model as a method of constructing nonparametric frontier can clearly define comparison benchmarks without the need to hypothesize the measurement function or requiring any preset condition. This

method evaluates the relative effectiveness of each DMU by comparing the degree of deviation after projecting DMUs onto the frontier. It has been gradually applied to evaluate production performance.

Given *n* DMUs with each DMU having m input variables and s output variables, the input and output variables of the j(th) DMU are defined as follows:

$$\begin{aligned} &X_j = (x_{1j}, x_{2j}, \quad, x_{mj})^T \rangle 0 \\ &Y_j = (y_{1j}, y_{2j}, \quad, y_{mj})^T \rangle 0 \\ &j = 1,2,3, \quad, n \end{aligned} \qquad \ldots(1)$$

A solution, as shown in Formula (2), is established by programming.

$$s.t. \begin{cases} \theta \sum_{nj=1}^{n} \lambda_j x_{ij} + s^- = \theta x_0, i = 1, 2, 3m \\ \sum_{j=1} \lambda_j y_{ij} - s^+ = y_0, i = 1,2,3, \quad, s \\ s^-, s^+, \lambda_j \geq 0, j = 1,2,3, \quad, n \end{cases} \qquad \ldots(2)$$

Where, x_{ij} and y_{ij} are the input and output variables of DMU, respectively; x_0 and y_0 are the target input and output values, respectively; θ is a parametric variable; s^- and s^+ are the slack variables of input and output, respectively; λ_j is the weight coefficient of each input and output variables. DEA-CCR model assumes constant returns to scale (CRS) of DMU. Banker et al. (1992) made some improvements based on this model because of the difficulty in realizing the above-mentioned assumption. Under variable returns to scale (VRS), constraint condition $\sum \lambda_j = 1$ is added, and DEA-BCC model is obtained.

DEA-Malmquist model generates a production possibility set S_t for all feasible inputs and outputs in the period *t*, and the distance function of production possibility set in period D^t is defined as:

$$D^t(x_0^t, y_0^t) = \inf(\theta \left| (x_0^t, y_0^t / \theta) \right. \qquad \ldots(3)$$

The calculation method of Malmquist performance change index (MPCI) is shown in Formula (4).

$$MPCI_t^{t+1} = \left(\frac{D_{CRS}^t(x_0^{t+1}, y_0^{t+1})}{D_{CRS}^t(x_0^t, y_0^t)} \bullet \frac{D_{CRS}^{t+1}(x_0^{t+1}, y_0^{t+1})}{D_{CRS}^{t+1}(x_0^t, y_0^t)}\right)^{1/2} \qquad \ldots(4)$$

MPCI can be decomposed into pure technical efficiency change index (PTECI), scale efficiency change index (SECI), and technological change index (TCI) to present more valuable analytical information, as shown in Formula (5).

$$MPCI_t^{t+1} = PTECI_t^{t+1} \times SECI_t^{t+1} \times TCI_t^{t+1} \qquad \ldots(5)$$

Where $PTECI_t^{t+1} = \frac{D_{VRS}^{t+1}(x_0^{t+1}, y_0^{t+1})}{D_{VRS}^t(x_0^t, y_0^t)}$,

$SECI_t^{t+1} = \frac{D_{CRS}^{t+1}(x_0^{t+1}, y_0^{t+1}) / D_{VRS}^{t+1}(x_0^{t+1}, y_0^{t+1})}{D_{CRS}^{t+1}(x_0^t, y_0^t) / D_{VRS}^{t+1}(x_0^t, y_0^t)}$, and

$TCI_t^{t+1} = \left(\frac{D_{CRS}^t(x_0^{t+1}, y_0^{t+1})}{D_{CRS}^{t+1}(x_0^{t+1}, y_0^{t+1})} \bullet \frac{D_{CRS}^t(x_0^t, y_0^t)}{D_{CRS}^{t+1}(x_0^t, y_0^t)}\right)^{1/2}$. CRS and VRS denote constant returns to scale and variable returns to scale.

Data Description

Most studies on the total-factor production efficiency of the construction industry have investigated from two aspects: input and output. The existing works have neglected unexpected environmental output while considering production factors. CO_2 emission obtained through the process analysis method was taken as an input index, namely, environmental input, to investigate the total-factor emission efficiency of the construction industry in each prefecture-level city in Henan Province.

Environmental input: Total carbon emission environment variable of the construction industry was selected as the input index. On the one hand, environmental impact can be regarded as a price of economic development; on the other hand, carbon emission permit is gradually commercialized, is equivalent to the cost to be paid by enterprises during their production process, and can influence production as a production factor. Here, carbon emission, which is an unexpected environmental output, was turned into an input variable.

Labour input: The construction industry is a labour-intensive industry. The development degree and competitiveness of this industry rely on labour quantity and quality to a great extent. Here, the annual average number of people directly occupied in production and management was selected as labour input index.

Capital input: Expanding the extension for reproduction is the main development pattern of Henan construction industry, where capital input is an important driving force for the economic growth of the construction industry. The fixed asset was used as capital input index in this study, the average value of fixed assets at the end of the last year and those at the end of the year was taken as the annual input value of fixed assets, and the values were uniformly converted into the constant price in 2012 using GDP (Gross Domestic Product) deflator to eliminate the influence of price change factor.

The input of construction machinery equipment: Henan construction industry relies on the artificial or semi-artificial operation to a great extent. The improvement of construction mechanization level can facilitate the production efficiency of the construction industry, the total power of construction machinery equipment of the construction industry in each region can represent its input level of

construction machinery equipment, and the annual index value is the average value of total power of construction machinery equipment at the end of the last year and that at the end of the year.

Output index: For consistency of evaluation scope, the total output value of the constant price of the construction industry in each prefecture-level city in Henan Province was taken as input index in this study.

The above-mentioned used total output value, construction area, completion area, average number of people directly occupied in production and management, fixed assets and total power of construction machinery equipment of the construction industry in each province over the years were all derived from China Statistical Yearbook of Construction over the years. Total output value was converted into the constant price in 2012 using annual GDP deflator in the construction industry. All data in this study were related data of 17 prefecture-level cities in Henan Province from 2012 to 2018.

RESULT ANALYSIS

Panel data of 17 prefecture-level cities in Henan Province in the period of 2012–2018, as given in Table 1, were calculated via Deap2.1 software package.

Table 1 shows that the total-factor carbon emission efficiency of Henan construction industry in the period of 2012-2018 was 1.084, which was greater than 1. This finding indicated that the total-factor carbon emission efficiency of Henan construction industry was elevated to a certain degree during the 7 years. The Malmquist index decomposition results showed that the mean values of technical efficiency and technological progress were 1.047 and 1.035, respectively. This result implied that the overall resource utilization efficiency of Henan construction industry was improved by 0.84% due to the joint actions of elevated technological progress (by 0.35%) and improved technical efficiency (by 0.47%). Various regions in Henan Province promoted the movement of production frontier by enhancing technological innovation and elevating the overall production level in the construction industry to realize optimal allocation of production factors brought by progress of the construction industry and improve the efficiency. In the construction industry of each region, the previous production pattern of "emphasized quantity while neglecting quality" was gradually changed. Moreover, technological innovation would become a critical factor in enhancing industrial competitiveness. The average value of pure technical efficiency of Henan construction industry was slightly reduced by 0.03%, and the change in pure technical efficiency reflected whether the construction industry in each city in Henan Province could effectively use production technology to maximize the output. The construction industries in most regions failed to rapidly keep up with innovation to improve R&D quality because of low carbon emission efficiency due to ineffective overall production organization strategy and poor management ability of Henan construction industry. This situation, from another aspect, explained Henan Province had a space for continuous improvement in optimizing management mode of the construction industry, popularizing energy conservation and emission reduction technology, and rapidly following the industrial development. The average value of scale efficiency was improved by 0.51%, which was very obvious. This finding fully certified that Henan construction industry realized scale growth between 2012 and 2018. Scale efficiency reflected that Henan construction industry was at a proper investment scale, which manifested that the construction industries in most regions of Henan Province kept a slow growth trend, and effective scale expansion was the driving force for improving their total-factor efficiency.

CARBON EMISSION REDUCTION MEASURES OF THE CONSTRUCTION INDUSTRY

Advocating Application of Low-Carbon Energy in Buildings and Lengthening Service Life of Buildings

The energy structure in the use phase of most buildings in

Table 1: Total-factor carbon emission efficiency of Henan construction industry in the period of 2012-2018.

Year	Technical efficiency	Technological progress	Pure technical efficiency	Scale efficiency	Total-factor productivity
2012-2013	0.867	0.986	1.002	0.865	0.855
2013-2014	0.967	0.865	0.987	0.980	0.836
2014-2015	1.034	1.023	0.934	1.107	1.058
2015-2016	1.024	1.086	1.092	0.938	1.112
2016-2017	1.176	1.154	0.953	1.234	1.357
2017-2018	1.214	1.098	1.012	1.200	1.333
Average value	1.047	1.035	0.997	1.051	1.084

Henan Province now mainly concentrates on electric energy. The carbon emission factor of electric energy is far higher than those of other energy sources, and the carbon emission in the use phase is far higher than those in other phases. On the one hand, the carbon emission of electric energy is high because electric energy belongs to the secondary energy source, and a certain energy loss will be generated in the transformation or processing process of primary energy sources. On the other hand, coal and fuel oil are energy sources with high carbon emission given that the current electric energy has an extreme dependence on them. Therefore, the energy structure of public buildings should be changed, low-emission clean energies, such as solar energy, wind energy, and ocean energy should be energetically developed, and high-efficiency, clean, and low-carbon power supply technology and power supply system should be popularized to reduce the carbon emission factor of electric energy and reduce carbon emission in the use phase. Transformation and reinforcement measures should be taken to lengthen the structural lifetime of buildings, improve their use functions and functional quality, and lengthen their service life to promote their sustainable development.

Conducting Reasonable and Scientific Building Construction and Reducing Carbon Emission in the Building Construction Link

By scientifically formulating construction organization and dismantling schemes, materials and personnel transportation can be reduced within the scientific and feasible scope and the operations in the construction process can be simplified. Energy-saving construction machinery equipment should be selected as far as possible to realize optimization of use efficiency of machinery and reduce carbon emission in the construction process. Two defects exist in night-time construction, namely, low construction efficiency and demand for a large quantity of temporary lighting. These defects will not only consume massive electricity but also increase construction-induced carbon emission. Therefore, actual construction technological characteristics should be combined to reasonably arrange construction and demolition time, shorten night-time operation hours, and reduce carbon emission. The specific demolition process should be clarified when the construction method is determined. Reasonable demolition equipment should be confirmed. The use of cranes and equipment that may damage the buildings should be reduced to decrease carbon emission in the demolition phase. The government should perfect low-carbon technical indexes and requirements of demolition engineering and reduce carbon emission in building demolition under the constraints of compulsory standards.

Strengthening the Propaganda of Low-Carbon Use of Buildings and Encouraging Low-Carbon Construction Projects

We need to comprehensively popularize the concepts of energy conservation, emission reduction, and low carbon from two angles, namely, professionalism and territoriality, for popularizing the carbon trading-based economic evaluation model for carbon emission of public buildings. Universal education among the public should be generalized. The government and construction industry should propagandize the calculation of potential benefits of low-carbon public buildings by formulating policies and implementing standards, media publicity, and compulsory education to ensure that the public can be aware of the existence of the potential benefits. This way provides the market basis for low-carbon public buildings. Professional education in the building field should be reinforced. The government can create a good environment and conditions for energy conservation and emission reduction market by promoting policies and guiding the market. Meanwhile, real estate enterprises have advantages in capital, technology, and talent. Advantages of the two can be combined to push a series of low-carbon public building products recognized by the market at various pilot areas, create a thick atmosphere of carbon trading, and publicize economic benefits of low-carbon public buildings. In this way, investors can be aware of the real values of low-carbon public buildings. Their enthusiasm for developing low-carbon buildings will be motivated to enhance their decision-making tendency toward investing in low-carbon public buildings.

Stimulating Related Interest Subjects to Participate in Emission Reduction and Reinforcing Technological Innovation of the Construction Industry

The government should exert its role of policy promotion and guiding, stimulate interesting interest subjects involved in the development of low-carbon public buildings, and fully motivate related subjects' initiative in participating in low-carbon development of public buildings. Moreover, the government should give subsidies to electric energy saved by public buildings with good energy operation and management, stimulate investors to enter the low-carbon field of public buildings, encourage related subjects to be occupied in development of new-type energy, emission reduction technology, equipment, and products in the form of scientific research funds, reduce the development cost of enterprises' low-carbon technologies, and provide financial support and subsidies, such as loans, for subjects using and popularizing low-carbon technologies. The subjects should do heat insulation work of building envelopes and improve the efficiency

of heating, HVAC (Heating, Ventilation and Air Conditioning), and lighting equipment and system and create a natural ecological environment for buildings. They should also popularize building sun-shading technology, solar water heater technology, and passive solar house technology. They should manage natural ventilation and natural lighting very well and advocate roof greening as well. Furthermore, they should continuously perfect energy-saving industrial structure of buildings, promote comprehensive upgrading of various energy-saving construction industries, and gradually form a complete range of modernized energy-saving construction industry system with advanced technologies and standard management.

CONCLUSION

Construction products manufactured by construction activities, which are basic human behaviours of nature remaking, are the main consumers of resources and energy sources and also main dischargers causing environmental pollution. The pressure imposed by the construction industry on resources and the environment is increasing daily. With accelerated China's urbanization progress, the energy consumption and carbon emission of the building field are increasing, and reducing environmental pollution of the construction industry while ensuring its sustainable development is especially critical. Improving the total-factor carbon emission efficiency of the construction industry is a primary measure. This study constructed a carbon emission efficiency model that took carbon emission as an environmental factor and calculated carbon emission efficiency of Henan construction industry in the period of 2012-2018. The study results indicated that the total-factor carbon emission efficiency of Henan construction industry was 1.084 from 2012 to 2018, and the elevated 0.84% part was derived from 0.35% elevation of technological progress and 0.47% improvement of technical efficiency. The average value of pure technical efficiency was slightly reduced by 0.03%, while that of scale efficiency was elevated by 0.51%. The carbon emission efficiency of the construction industry could be improved by advocating the use of low-carbon energy sources in buildings, reasonably and scientifically organizing building construction, reinforcing propaganda of low-carbon use of buildings, and motivating related interest subjects to participate in the emission reduction of the construction industry to reduce environmental pollution caused by the construction industry. In-depth research is suggested from the aspects of perfecting life cycle assessment method for carbon emission calculation of the construction industry, analysing the influence paths of associated industries on carbon emission of the construction industry, deeply probing into the environmental impact of the construction industry and its structure, and comprehensively considering all kinds of environmental impacts of the construction industry.

ACKNOWLEDGEMENT

This work was supported by the Key Scientific Research Projects of Colleges and Universities in He nan Province (18A560019, 20B560013).

REFERENCES

Acquaye, A.A. and Duffy, A.P. 2010. Input-output analysis of Irish construction sector greenhouse gas emissions. Building and Environment, 45(3): 784-791.

Banker, R.D. and Thrall, R.M. 1992. Estimation of returns to scale using data envelopment analysis. European Journal of Operational Research, 62(1): 74-84.

Charnes, A., Cooper, W.W. and Rhodes, E. 1978. Measuring the efficiency of decision making units. European Journal of Operational Research, 2(6): 429-444.

Chang, Y., Ries, R.J. and Wang, Y. 2011. The quantification of the embodied impacts of construction projects on energy, environment, and society based on I–O LCA. Energy Policy, 39(10): 6321-6330.

Feng, B., Wang, X. and Liu, B. 2014. Provincial variation in energy efficiency across China's construction industry with carbon emission considered. Resources Science, 36(6): 1256-1266.

Hong, J., Shen, G.Q., Guo, S., Xue, F. and Zheng, W. 2016. Energy use embodied in China' s construction industry: a multi-regional input-output analysis. Renewable and Sustainable Energy Reviews, 53: 1303-1312.

Jeong, Y.S., Lee, S.E. and Huh, J.H. 2012. Estimation of CO_2 emission of apartment buildings due to major construction materials in the Republic of Korea. Energy and Buildings, 49: 437-442.

Li, X., Yang, F., Zhu, Y. and Gao, Y. 2014. An assessment framework for analysing the embodied carbon impacts of residential buildings in China. Energy and Buildings, 85: 400-409.

Lu, Y., Cui, P. and Li, D. 2016. Carbon emissions and policies in China's building and construction industry: evidence from 1994 to 2012. Building and Environment, 95: 94-103.

Mielnik, O. and Goldemberg, J. 1999. Communication The evolution of the "carbonization index" in developing countries. Energy Policy, 27(5): 307-308.

Onat, N.C., Kucukvar, M. and Tatari, O. 2014. Scope-based carbon footprint analysis of US residential and commercial buildings: An input-output hybrid life cycle assessment approach. Building and Environment, 72: 53-62.

Suzuki, M., Oka, T. and Okada, K. 1995. The estimation of energy consumption and CO_2 emission due to housing construction in Japan. Energy and Buildings, 22(2): 165-169.

Xue, X., Wu, H., Zhang, X., Dai, J. and Su, C. 2015. Measuring energy consumption efficiency of the construction industry: the case of China. Journal of Cleaner Production, 107: 509-515.

Zuo, J., Read, B., Pullen, S. and Shi, Q. 2012. Achieving carbon neutrality in commercial building developments–Perceptions of the construction industry. Habitat International, 36(2): 278-286.

Zhang, P., Jia, G., Mou, Q., Song, M., He, C. and Xu, Q. 2019. Carbon productivity convergence club and its initial conditions: China's construction industry. Chinese Journal of Population Resources and Environment, 17(1): 12-24.

Nature Environment and Pollution Technology
An International Quarterly Scientific Journal

p-ISSN: 0972-6268
(Print copies up to 2016)
e-ISSN: 2395-3454

Vol. 19 | No. 2 | pp. 799-807 | 2020

Original Research Paper

https://doi.org/10.46488/NEPT.2020.v19i02.037

Open Access Journal

Inhibition of Mild Steel Corrosion in Hydrochloric Acid Solution by Leaves of *Ziziphus jujuba*

Rakesh Kumar Dubey*†, Nitin Gupta, S. M. Nafees** and Kalpana S.****
*Govt. College, Gangapur city-322201, Sawai Madhopur, Rajasthan, India
** Govt. College Kota-324001, Rajasthan, India
†Corresponding author: Rakesh Kumar Dubey; rakeshdubeygangapurcity@gmail.com

Nat. Env. & Poll. Tech.
Website: www.neptjournal.com

Received: 19-08-2019
Accepted: 18-09-2019

Key Words:
Ziziphus jujuba leaves;
Corrosion;
Langmuir isotherm;
Weight loss method

ABSTRACT

Weight loss method was used to assess the inhibition of mild steel corrosion in 1M HCl solution with aqueous extract of *Ziziphus jujuba* leaves at 303 to 333K temperatures. It was found that *Ziziphus jujuba* leaves extract retarded the dissolution of mild steel in 1M HCl solution. The inhibition efficiency increases with a rise in the concentration of extract and decreased with increase in temperature. Maximum 88.54% inhibition efficiency was observed at 303 K and 8% (v/v) composition of the extract. Adsorption of extract at mild steel surface follows Langmuir adsorption isotherm. Values of Gibbs free energy, variation in inhibition energy with temperature and with activation energy values trend proposed the physisorption. Negative values of Gibbs energy propose the spontaneous process of inhibition process in the extract at studied temperatures.

INTRODUCTION

Steel is widely used alloy in transportation, mechanical and petrochemical industries. However, it suffers from a major problem of corrosion. Corrosion is the degradation of metals and their alloys by an electrochemical reaction and environment. The introduction of corrosion inhibitors is the best way to prevent metallic corrosion, which can save the great economic loss. Most of the corrosion inhibitors are synthetic chemicals which are expansive and hazardous to the environment. Due to the toxicity of chemical corrosion inhibitors, there has been a rise in thrust for the search for green corrosion inhibitors (Al-Sehaibani 2000).

This has provoked the researchers to search for new eco-friendly, low cost, easily available effective corrosion inhibitors to foster green environment and for the sustainability of living beings. Plant products are organic in nature, and contain certain photochemicals including tannins, flavonoids, saponins, amino acids, alkaloids, and pigments which can be extracted by simple and less expensive procedures. Extracts from different parts of the plants have been widely reported as effective and good metal corrosion inhibitors in various corrosive environments.

Literature survey also reveals that various plant extracts have been used as corrosion inhibitors for protection of different metals and their alloys in the last few decades. Extract of fenugreek seeds and leaves (Noor 2008), essential oils of *Mentha spicata, Lavandula multifida, Pulicaria mauritanica* (Znini 2012) *Azadirachta indica* (Sharma 2010), extract of *Ananas comosus* L. (Ekanem et al. 2010), *Embilica officinalis* (Saratha et al. 2010), *Garcinacola* and *Cola nitida* (Eddy 2010), *Nerium olender* leaves, *Calotropis procera*, *Ziziphus jujba,* etc. In the continuity of above corrosion inhibition studies, the present work has been chosen which indicate studies of corrosion prevention properties of aqueous extract of leaves of *Ziziphus jujuba* L. for mild steel in 1 M HCl solution.

MATERIALS AND METHODS

Preparation of the extract: The leaves of *Ziziphus jujuba* plant were taken, washed and air-dried for 6-7 days, crushed and ground mechanically. 20 g of ground leaves were heated in 200 mL distilled water for one hour using air condenser at 70°C-80°C. This extract was left overnight and then filtered and made up to 200 mL with distilled water for the experiment.

Selection of the steel specimens: Rectangular mild steel specimens of 5 cm length and 1 cm diameter were taken and abraded with a series of emery papers, degreased with acetone, washed with distilled water, dried and constant weight was recorded by electronic balance.

Solution preparation: 1M HCl solution was prepared by 37% HCl using distilled water. The employed concentration

range of aqueous extract of *Ziziphus jujuba* leaves (AEZJL) was 1% to 8% (v/v).

Gravimetric measurement: Gravimetric method is a widely used method because of its reliability and simplicity in corrosion inhibition experiments. For each experiment 100 mL test solution was taken in 250 mL beaker and a rectangular specimen was immersed in it with plastic thread for one hour.

The experiments were carried out at different temperatures 303, 313, 323 to 333 K in a thermostatic water bath. After one-hour specimens were removed, washed with distilled water, acetone dried and abraded with series of emery papers and then weighed up to constant weight.

RESULTS AND DISCUSSION

Corrosion rates: Corrosion rates were calculated by the following equation (1) (Behpour et al. 2011, Umoren et al. 2016).

$$CR\ (g\ cm^{-2}min^{-1}) = (W_1\text{-}W_2/At) \quad \ldots(1)$$

Where, CR is corrosion rate, W_1 is weight loss of mild steel specimen without inhibitor and W_2 is weight loss of mild steel specimen with inhibitor, A is the area of MS specimen and t is immersion time. Table 1 shows that corrosion rates of mild steel decrease with increase in the concentration of *Ziziphus jujuba* leaves inhibitor at all studied temperatures. This could be subjected to the adsorption of the phyto-constituents of inhibitor molecules with the increase in the concentration of inhibitor. The corrosion rate obeys Arrhenius type reaction, as it increases with the rise in temperature (Noor 2007).

Inhibition efficiency: From the obtained corrosion rates, inhibition efficiencies were calculated by using equation (2) (Behpour et al. 2011, Umoren et al. 2016).

$$IE\% = \frac{CR_{blank} - CR_{inh}}{CR_{blank}} \times 100 \quad \ldots(2)$$

Where, CR_{blank} is the corrosion rate in the absence of inhibitor and CR_{inh} is the corrosion rate in the presence of inhibitor. Mild steel corrosion rates in 1 M HCl solution with *Ziziphus jujuba* leaves are given in Table 1. Data in Table 2 and Fig. 1 show that % IE increase with the rise in extract concentration, which is an indication of an increase in the number of components of extract adsorbed on mild steel surface, which block the active sites of metal from acid attack and protect the metallic corrosion (Obi-Egbedi et al. 2012). Further, the decrease in % IE with the rise in temperature suggests electrostatic interaction (physical adsorption) of the extract molecules on the mild steel surface. This further indicates desorption of adsorbed inhibitor species at higher temperatures and metal dissolution takes place (Yadav et al. 2014). 88.54% inhibition efficiency is observed at 8% (v/v) concentration of inhibitor.

Table 1: Mild steel corrosion rates in 1 M HCl solution in the absence and presence of different concentrations of *Ziziphus jujuba* leaves at different temperatures.

C_{inh} in (v/v)%	CR × 10^{-3} (g cm^{-2} min^{-1})			
	303 K	313 K	323 K	333 K
0	0.96	1.53	2.19	2.76
1	0.73	1.14	2.03	2.64
2	0.57	0.87	1.94	2.59
3	0.39	0.73	1.83	2.53
5	0.27	0.57	1.74	2.47
8	0.11	0.39	1.58	2.38

Table 2: Inhibition efficiencies of *Ziziphus jujuba* leaves at different concentrations and temperatures in solutions of 1M HCl.

C_{inh} in (v/v)%	IE (%)			
	303 K	313 K	323 K	333 K
1	23.96	25.49	7.31	4.35
2	40.63	43.14	11.42	6.16
3	59.38	52.29	16.44	8.33
5	71.88	62.75	20.55	10.51
8	88.54	74.51	27.85	13.77

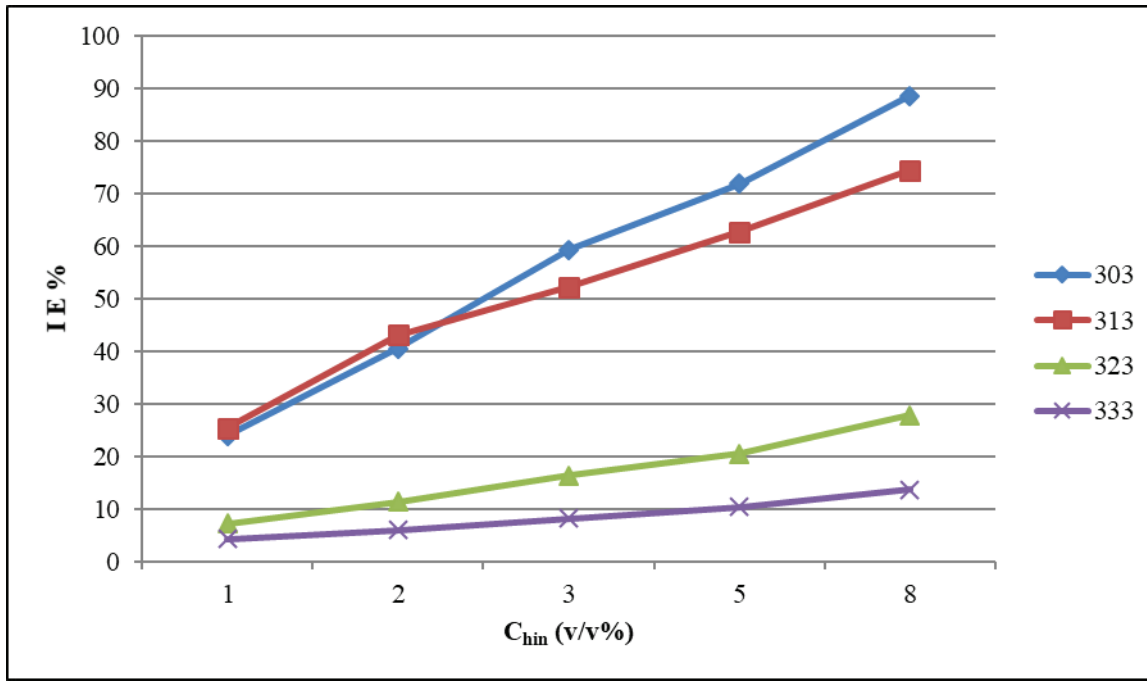

Fig. 1: Variation in % IE for mild steel corrosion in 1M HCl at different concentration of *Ziziphus jujuba* leaves at different temperatures.

Kinetic parameters: Assuming that corrosion rates of steel specimens against the concentration of inhibitor obey kinetic relationship as equation (3) (Noor 2007, Khamis 1990).

$$\log CR = \log K + B \log C_{inh} \quad \ldots(3)$$

Where, K is rate constant and equal to CR when inhibitor concentration is unity. B is reaction constant which is the measure of inhibitor effectiveness and C_{inh} is the concentration v/v % (mL/100 mL) of *Ziziphus jujuba* leaves. Fig. 2 represents the plot between log CR and log C_{inh} values at different studied temperatures. B and K were calculated by the slope and intercept of straight lines obtained in Fig. 2. The obtained results are summarized in Table 3 which can be discussed as follows (Noor 2007). Negative values of B indicate that the corrosion rate is inversely proportional to the concentration of inhibitor. In other words, the corrosion rates decrease with increase in the concentration of inhibitor species.

The high negative values of B reflect the good inhibitive property of inhibitor. The high negative value of B was observed as a steep slope in the graph (Fig. 2). Value of B is high at lower temperatures, indicating that inhibitive species are more effective at comparatively lower temperatures. The increase in K values with increase in temperature, indicating the increase in corrosion rates with temperatures.

Thermodynamic and activation parameters: Thermodynamic and activation parameters like apparent activation energy E_{act}, enthalpy of activation ΔH^*, and the entropy of activation ΔS^* were calculated for the steel dissolution process. Activation energies E_{act} were calculated by following Arrhenius equation (4) (Umoren et al. 2016, Yadav et al. 2014)

$$\log CR = \log A - \frac{Eact}{2.303RT}) \quad \ldots(4)$$

Where, A is Arrhenius pre-exponential factor, E_{act} is the activation energy, R is the universal gas constant, T is the absolute temperature. The slope of log CR vs 1/T in Fig. 3 gives the values of activation energies at studied concentrations. Table 3 represents the calculated data of activation energies. The values of activation energies in the presence of inhibitor were found higher than in uninhibited solution. This indicates the formation of a higher energy barrier in corrosion reaction by inhibitor molecules. The increase in E_{act} for corrosion process in inhibitor solution further interpreted as physical adsorption of inhibitor species on mild steel surface (Popova et al. 2003). Besides this, according to Damaskin (1971), the value of activation energy lesser than 80kJ/mol and even smaller than 5kJ/mol represents physical adsorption. This assertion supports the experimental results obtained in the present study. The values of enthalpy of activation ΔH^* and entropy of activation ΔS^* were calculated by following the transition state as in equation (5) (Umoren et al. 2016, Yadav et al. 2014).

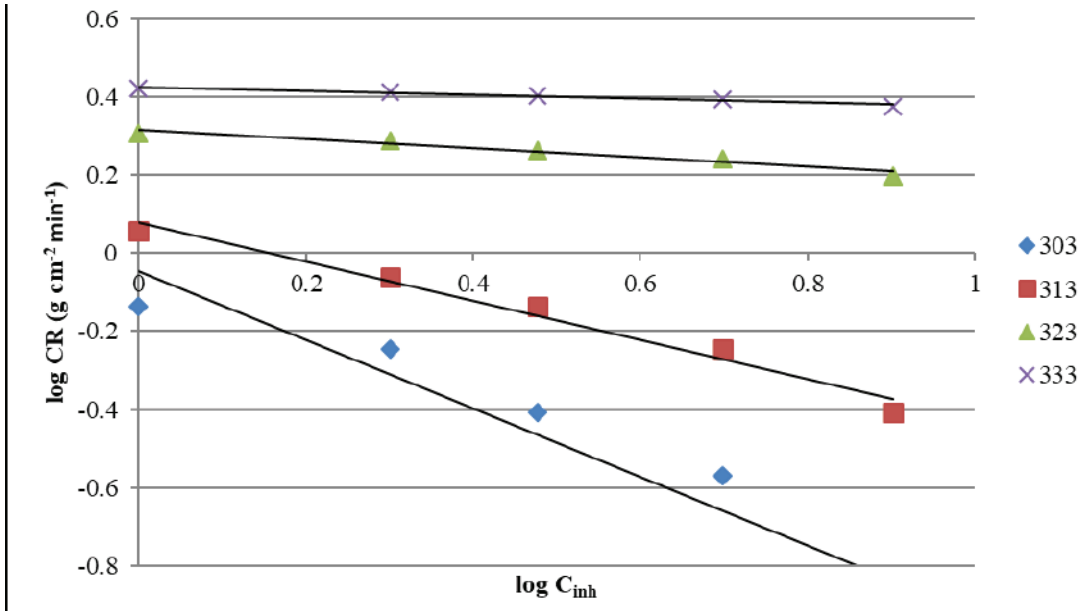

Fig. 2: Variation in log CR with log C_{inh} for mild steel corrosion in 1M HCl in the presence of different concentrations of *Ziziphus jujuba* leaves at different temperatures.

Table 3: Kinetic parameters for mild steel corrosion in 1M HCL solution with *Ziziphus jujuba* leaves.

Temperature (K)	Kinetic Parameters	
	B	K × 10^{-3} (g cm^{-2} min^{-1})
303 K	-0.049	2.660725
313 K	-0.118	2.06538
323 K	-0.502	1.202264
333 K	-0.876	1.111732

$$\log_{(CR/T)} = [\log_{(R/Nh)} + (\Delta S^*/2.303R - (\Delta H^*/2.303RT)] \quad \ldots(5)$$

Where, h is Planck's constant, N is Avogadro number, R is the gas constant. A plot of log (CR/T) vs 1/T gave a straight line with the slope of (-ΔH*/2.303R) and intercept of [(log R/Nh) +(ΔS*/2.303 R)] from which the values of Δ H* and ΔS* were calculated (Fig. 4). These values are tabulated in Table 4. Values of ΔH* were found positive. Positive values indicate endothermic nature of steel dissolution process (Yadav et al. 2014, Behpour et al. 2011) Endothermic process further indicates that mild steel dissolution reduces at lower temperatures and increases with increase in temperature. Negative values of ΔS* are indicative of the formation of an activated complex in the rate-determining step, which represents association rather than dissociation step, meaning the decrease in disorder takes place on going from reactants to activated complex. (Gomma & Wahdan 1995). It is also observed from data in Table 4 that E_{act} and ΔH* vary in the same manner. Values of both E_{act} and ΔH* increase with the increase in the concentration of inhibitor, suggesting that energy barrier increases with increase in inhibitor concentration. This means that corrosion reaction will further be pushed to surface sites that are characterized by progressively higher values of E_{act} as the concentration of inhibitor becomes greater (Solmaz et al. 2008).

The values of activation energy were found larger than corresponding values of enthalpy of activation, indicate the involvement of a gaseous reaction, simply hydrogen evolution in the corrosion process, associated with a decrease in total reaction volume (Noor 2007).

Adsorption isotherm and Gibbs energy: The nature of adsorption can be explained by understanding the process at metal/electrolyte interface. Further, to understand the nature of adsorption, obtained surface coverage θwere fitted in different adsorption isotherms. Langmuir adsorption isotherm was the best fit. The mathematical expressions for Langmuir

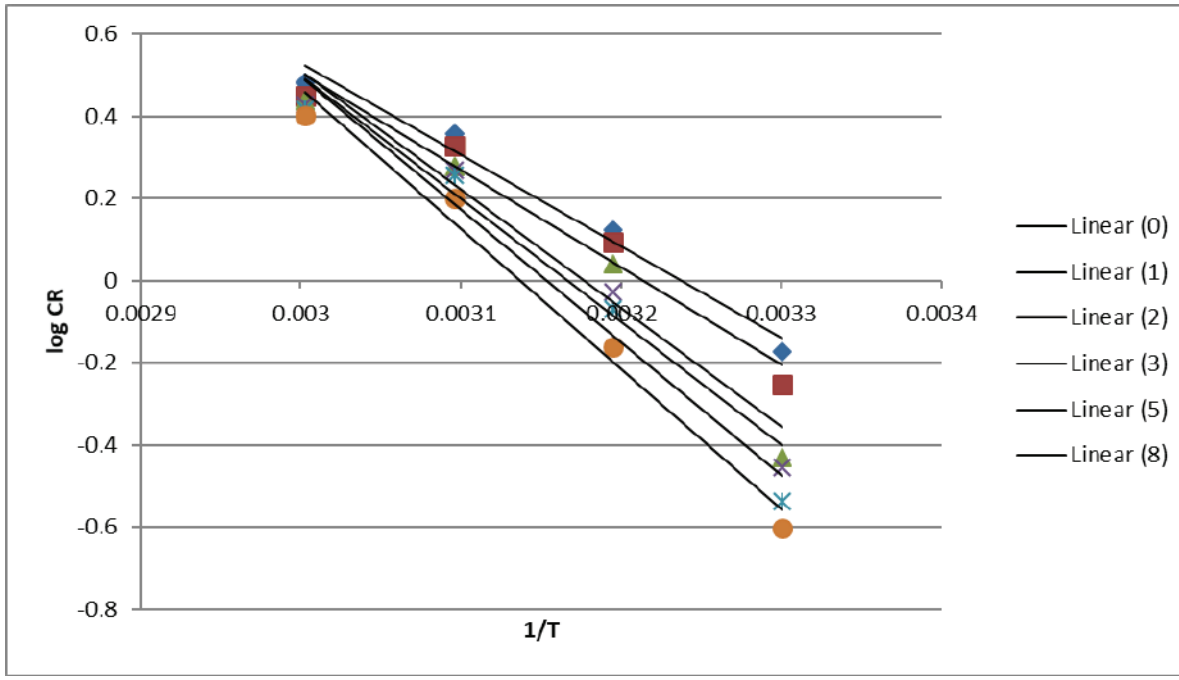

Fig. 3: Arrhenius plots for mild steel corrosion in 1M HCl in the absence and presence of the different concentrations of *Ziziphus jujuba* leaves.

Table 4: Activation and thermodynamic parameters for mild steel corrosion in 1 M HCl solution with *Ziziphus jujuba* leaves.

C_{inh} in (v/v)%	E_{act} (kJ/mol)	ΔH^* (kJ/mol)	ΔS^* (J/mol/K)
0.0	29.68	27.12	-200.82
1.0	37.26	34.76	-179.88
2.0	44.86	42.36	-175.67
3.0	54.89	52.42	-162.88
5.0	65.23	62.77	-149.57
8.0	89.51	87.08	-117.92

adsorption isotherm can be expressed by the equation (6) (Fragoza-Mar et al. 2012, Quartarone et al. 2012, Vasudha et al. 2013).

$$\frac{C}{\theta} = \frac{1}{Kads} + C_{inh} \quad \ldots(6)$$

Rearranging the above equation (6) we get

$$\frac{\theta}{1-\theta} = K_{ads}\, C_{inh} \quad \ldots(7)$$

$$\mathrm{Log}\left(\frac{\theta}{1-\theta}\right) = \log K_{ads} + \log C_{inh} \quad \ldots(8)$$

Where, K_{ads} is the equilibrium constant of adsorption, θ is the surface coverage, (1-θ) is the uncovered surface, C_{inh} is the concentration of inhibitor. Values of K_{ads} were calculated from the intercept of Langmuir adsorption isotherm drawn according to the equation (8) between log (θ /1-θ) and log C_{inh} (Fig. 5). The value of K_{ads} obtained from Langmuir adsorption isotherm is related to Gibbs energy according to the equation (9) (Noor 2007).

$$K_{ads} = 1/C_{H2O} \exp^{(-\Delta G/RT)} \quad \ldots(9)$$

It can be written as:

$$\Delta G_{ads} = -2.303\ RT\ \mathrm{Log}\ (K_{ads}.\ CH_2O) \quad \ldots(10)$$

Where, CH_2O is the concentration of water in (mL/L) at metal/solution interface, R is the universal gas constant and T is the absolute temperature. The values of ΔG_{ads} were tabulated in Table 5. Obtained values of Gibbs energy were

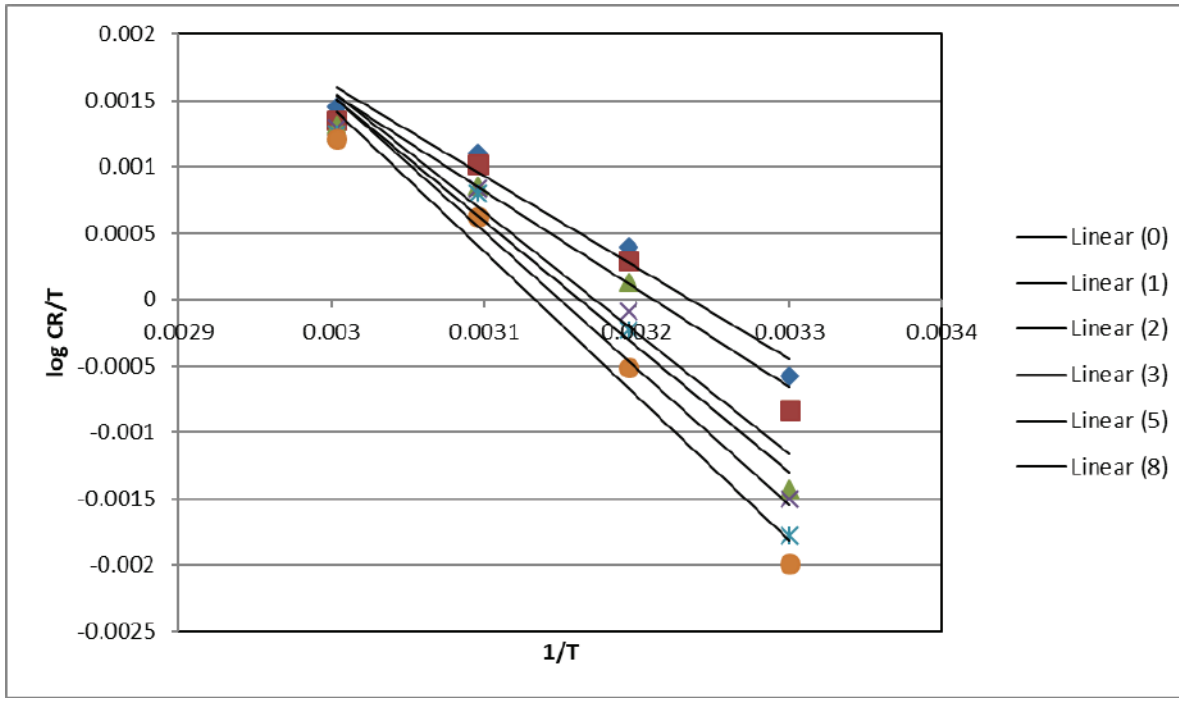

Fig. 4: Transition-state plots for mild steel corrosion in 1M HCl in the absence and presence of the different concentrations of *Ziziphus jujuba* leaves.

plotted against temperature as per the basic equation (11) (El-Awady et al. 1992).

$$\Delta G_{ads} = \Delta H_{ads} - T \Delta S_{ads} \quad \ldots(11)$$

The intercept of the graph between ΔG_{ads} vs T in Fig. 6 gives the value of ΔH_{ads} and by putting the value of intercept in equation (11) values of ΔS_{ads} were obtained. These obtained adsorption parameters, i.e. Gibbs free energy of adsorption (ΔG_{ads}), enthalpy of adsorption (ΔH_{ads}) and entropy of adsorption (ΔS_{ads}) are listed in Table 5. ΔG_{ads} values have been found negative at all studied temperatures indicating spontaneous adsorption process of inhibitor molecules on the metal surface (Behpour 2011). Generally, values of ΔG_{ads} up to -20 KJ/mol are consistent with electrostatic interactions (physical adsorption) between charged molecules and charged metal surface and values up to -40 KJ/mol or higher involve charge sharing or transfer from inhibitor molecules to metal surface to form the coordinate type of bond (chemical adsorption) (Bouklah et al. 2006). The obtained values of ΔG_{ads} were found less than -20kJ/mol indicated physical adsorption of inhibitor molecules. It has been observed that adsorption of negatively charged species is facilitated due to the positively charged metal. But positively charged species can also be adsorbed and protect the positively charged metal surface acting with a negatively charged intermediate such as acid anions, adsorbed on the metal surface (Popova et al. 2003). Values of ΔH_{ads} have been found negative indicating the exothermic adsorption process (Li et al. 2010, Li et al. 2009), which further indicates lower % IE at higher temperatures, due to desorption of inhibitor molecules. The exothermic process is attributed to either physical or chemical adsorption or the mixture of both (Bentiss et al. 2005). In the exothermic process, values of ΔH_{ads} predict physisorption or chemisorption. For physisorption, the values of ΔH_{ads} are lower than 40kJ/mol, while for chemisorption it approaches to 100kJ/mol (Benabdellah et al. 2007) Values of ΔH_{ads} in Table 5 indicate physisorption. Negative values of ΔS_{ads} indicate a decrease in entropy of adsorption process.

This behaviour can be explained as follows: Before the adsorption of inhibitor molecules on to mild steel surface, they might freely move in bulk solution (inhibitor molecules were chaotic). But with the process of adsorption, inhibitor molecules were orderly adsorbed on to the steel surface, as a result, decrease in entropy is observed (Li et al. 2010) A more interesting behaviour is observed in Table 5 that negative ΔH_{ads} value is accompanied with negative ΔS_{ads} value. This further agrees that when the adsorption is an exothermic process, it must be accompanied by a decrease in the entropy change and vice versa (Obi-Egbedi et al. 2012). The obtained positive values of ΔS_{ads} are the algebraic sum of the

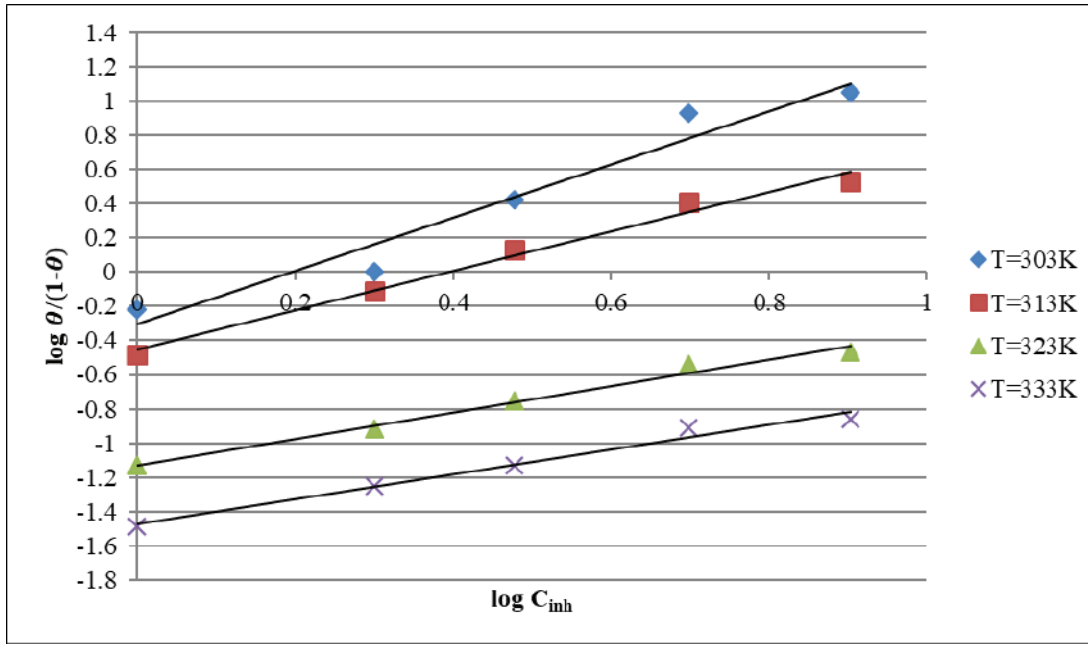

Fig. 5: Langmuir adsorption isotherms of *Ziziphus jujuba* leaves on mild steel surface in 1M HCl at different temperatures.

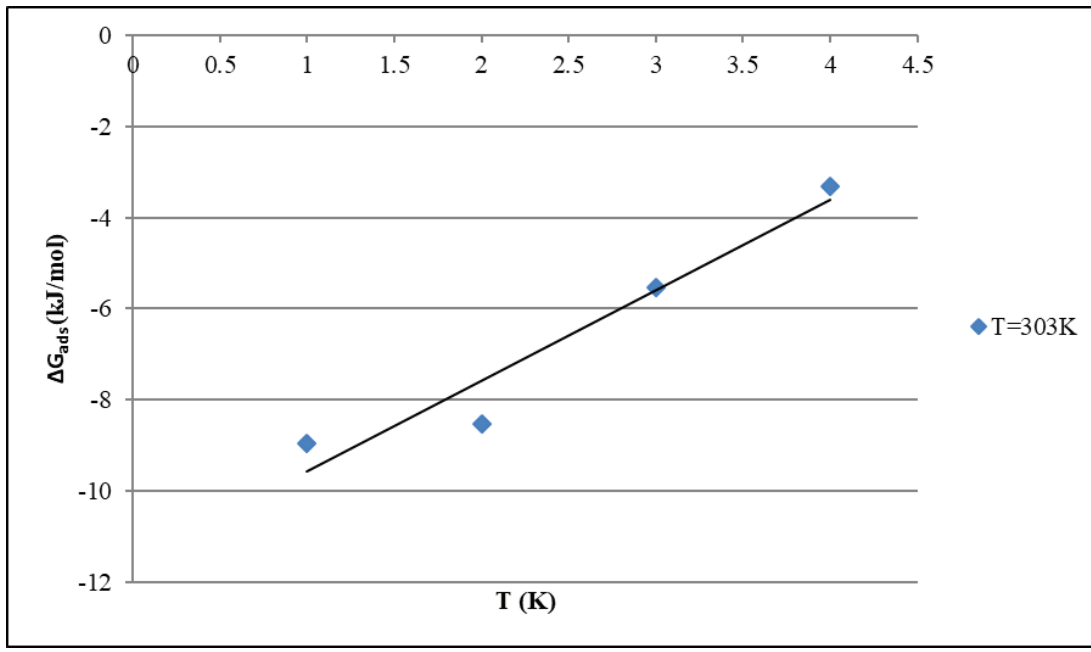

Fig. 6: The Variation of ΔG_{ads} (kJ/mol) with T (K) for mild steel corrosion in 1M HCl solution with *Ziziphus jujuba* leaves.

Table 5: Adsorption parameters for mild steel corrosion in 1 M HCl solution with *Ziziphus jujuba* leaves.

Temperature (K)	ΔG_{ads} (kJ/mol)	ΔH_{ads} (kJ/mol)	ΔS_{ads} (J/mol/K)
303 K	-8.96765	-69.94	-201.229
313 K	-8.52646		-196.209
323 K	-5.52726		-199.42
333 K	-3.32651		-200.041

adsorption of organic molecules and the desorption of water molecules (Li et al. 2009, Kumar et al. 2004). Therefore, the positive values of entropy of adsorption are the result of the substitution process, which can be attributed to the rise in the solvent entropy and more positive water desorption entropy (Badiea & Mohana 2009).

CONCLUSIONS

1. The results showed that *Ziziphus jujuba* leaves are good corrosion inhibitor for mild steel in 1M HCl solution under as permitted conditions denoted.
2. Corrosion rates increase with the increase in temperature and decrease with increase in inhibitor concentration.
3. Inhibition efficiencies increases at lower temperature suggest the physisorption process of inhibitor on the mild steel surface.
4. Apparent activation energy increases with increase in inhibitor concentrations also suggests physisorption.
5. Enthalpy of adsorption comes out to be negative and lower than 40kJ/mol, which shows exothermic and physical adsorption process of inhibitor.
6. The values of Gibbs free energies calculated were negative showing spontaneity of corrosion inhibition process of mild steel in 1 M HCl in *Ziziphus jujuba* leaves.

ACKNOWLEDGEMENT

The authors are thankful to the Head of Chemistry Department and Principal, Government College, Kota for providing necessary laboratory facilities.

REFERENCES

Al-Sehaibani, H. 2000. Evaluation of extracts of henna leaves as environmentally friendly corrosion inhibitors for metals. Materialwissenschaft und Werkstofftechnik: Materials Science and Engineering Technology, 31(12), pp.1060-1063.

Badiea, A.M. and Mohana, K.N. 2009. Effect of temperature and fluid velocity on corrosion mechanism of low carbon steel in presence of 2-hydrazino-4,7-dimethylbenzothiazole in industrial water medium. Corrosion Science, 51: 2231-2241.

Behpour, M., Ghoreishi, S.M., Khayatkashani, M. and Soltani, N. 2011. The effect of two oleo gum resin exudate from Ferula assafoetida and Dorema ammoniacum on mild steel corrosion in acidic media. Corrosion Science, 53: 2489-2501.

Benabdellah, M., Touzani, R., Dafali, A., Hammouti, B. and El Kadiri, S. 2007. Ruthenium-ligand complex, an efficient inhibitor of steel corrosion in H3PO4 media. Materials Letters, 61: 1197-1204.

Bentiss, F., Lebrini, M. and Lagrenée, M. 2005. Thermodynamic characterization of metal dissolution and inhibitor adsorption processes in mild steel/2,5-bis(n-thienyl)-1,3,4- thiadiazoles/hydrochloric acid system. Corrosion Science, 47: 2915-2931.

Bouklah, M., Benchat, N., Hammouti, B., Aouniti, A. and Kertit, S. 2006. Thermodynamic characterization of steel corrosion and inhibitor adsorption of pyridazine compounds in 0.5 M H2SO4. Materials Letters, 60(15): 1901-1905.

Damaskin, B.B. 1971. Adsorption of Organic Compounds on Electrodes, Plenum Press, New York, 221.

Eddy, N.O. 2010. Adsorption and inhibitive properties of ethanol extract of *Garcinia kola* and *Cola nitida* for the corrosion of mild steel in H_2SO_4. Pigment and Resin Technology, 39: 348-354.

Ekanem, U.F., Umoren, S.A., Udousoro, I.I. and Udoh, A.P. 2010. Inhibition of mild steel corrosion in HCl using pineapple leaves (*Ananas comosus* L.) extract. J. Mater. Sci., 45: 5558-5566.

El-Awady, A.A., Abd-El-Nabey, B.A. and Aziz, S.G. 1992. Kinetic-thermodynamic and adsorption isotherms analysis for the inhibition of acid corrosion of steel by cyclic and open chain amines. Journal of Electrochemical Society, 139(8): 2149-2154.

Fragoza-Mar, L., Olivares-Xometl, O., Domínguez-Aguilar, M.A., Flores, E.A., Arellanes- Lozada P. and Jiménez-Cruz F. 2012. Corrosion inhibitor activity of 1,3-diketone malonates for mild steel in aqueous hydrochloric acid solution. Corrosion Science, 61: 171-184.

Gomma, G.K. and Wahdan, M.H. 1995. Schiff bases as corrosion inhibitors for aluminium in hydrochloric acid solution. Materials Chemistry and Physics, 39(3): 209-213.

Khamis, E. 1990. The effect of temperature on the acidic dissolution of steel in the presence of inhibitors. Corrosion (NACE), 46(6): 476-484.

Kumar, E. T., Vishwanathan, S. and Udayabhanu, G. 2004. Synergistic effects of formaldehyde and alcoholic extract of plant leaves for protection of N80 steel in 15% HCl. Corrosion Engineering Science Technology, 39: 327-332.

Li, X., Deng, S. and Fu, H. 2010. Adsorption and inhibition effect of vanillin on cold rolled steel in 3.0 M H_3PO_4. Progress in Organic Coatings, 67(4): 420-426.

Li, X., Deng, S., Fu, H. and Mu, G. 2009. Inhibition effect of 6-benzylaminopurine on the corrosion of cold rolled steel in H_2SO_4 solution, Corrosion Science, 51: 620-634.

Noor, E.A. 2007. Temperature effects on the corrosion inhibition of mild steel in acidic solutions by aqueous extract of fenugreek leaves. International Journal of Electrochemical Science, 2: 996- 1017.

Noor, E.A. 2008. Comparative study on the corrosion inhibition of mild steel by aqueous extract of fenugreek seeds and leaves in acidic solutions. Journal of Engineering and Applied Sciences, 3(1): 23-30.

Obi-Egbedi, N.O., Obot I.B. and Umoren, S.A. 2012. Spondias mombin L. as a green corrosion inhibitor for aluminium in sulphuric acid: Correlation between inhibitive effect and electronic properties of extracts

major constituents using density functional theory. Arabian Journal of Chemistry, 5: 361-373.

Popova, A., Sokolova, E., Raicheva, S. and Christov, M. 2003. AC and DC study of the temperature effect on mild steel corrosion in acid media in the presence of benzimidazole derivatives. Corrosion Science, 45(1): 33-58.

Quartarone, G., Ronchin, L., Vavasori, A., Tortato, C. and Bonaldo, L. 2012. Inhibitive action of gramine towards corrosion of mild steel in deaerated 1.0 M hydrochloric acid solutions. Corrosion Science, 64: 82-89.

Saratha, R. and Vasudha, V.G. 2010. *Emblica officinalis* (Indian Gooseberry) leaves extract as corrosion inhibitor for mild steel in 1 N HCl medium. European Journal of Chemistry, 7: 677-684.

Sharma, R.K., Mudhoo, A., Jain, G. and Sharma, J. 2010. Corrosion inhibition and adsorption properties of *Azadirachta indica* mature leaves extract as green inhibitor for mild steel in HNO_3. Green Chemistry Letters and Reviews, 3: 7-15.

Solmaz, R., Kardas, G., Culha, M., Yazıcı, B. and Erbil, M. 2008. Investigation of adsorption and inhibitive effect of 2-mercaptothiazoline on corrosion of mild steel in hydrochloric acid media. Electrochimica Acta, 53(20): 5941-5952.

Umoren, S.A., Eduok, U.M., Solomon, M.M. and Udoh, A.P. 2016. Corrosion inhibition by leaves and stem extracts of *Sida acuta* for mild steel in 1 M H_2SO_4 solutions investigated by chemical and spectroscopic techniques. Arabian Journal of Chemistry, 9: S209-S224.

Vasudha, V.G. and Shanmuga Priya, K. 2013. *Polyalthia longifolia* as a corrosion inhibitor for mild steel in HCl solution. Research Journal of Chemical Sciences, 3(1): 21-26.

Yadav, M., Sushil Kumar, Bahadur, I. and Ramjugernath, D. 2014. Corrosion inhibitive effect of synthesized thiourea derivatives on mild steel in a 15% HCl solution. International Journal of Electrochemical Science, 9: 6529-6550.

Znini, M., Paolini, J., Majidi, L., Desjobert, J.M., Costa, J., Lahhit, N. and Bouyanzer, A. 2012. Evaluation of the inhibitive effect of essential oil of *Lavandula multifida* L. on the corrosion behaviour of C38 steel in 0.5 M H_2SO_4 medium. Research on Chemical Intermediates, 38(2): 669-683.

Nature Environment and Pollution Technology
An International Quarterly Scientific Journal

p-ISSN: 0972-6268
(Print copies up to 2016)
e-ISSN: 2395-3454

Vol. 19 | No. 2 | pp. 809-813 | 2020

Original Research Paper

https://doi.org/10.46488/NEPT.2020.v19i02.038

Open Access Journal

Growth and Removal of Nitrogen and Phosphorus by a Macroalgae *Cladophora glomerata* Under Different Nitrate Concentrations

Aulia Ulfah Farahdiba*, Euis Nurul Hidayah*†, Gina Aprilliana Asmar* and Yadanar Win Myint**

*Department of Environmental Engineering, University of Pembangunan Nasional Veteran Jawa Timur, Surabaya, Indonesia

**Nanotechnology Research Department, Department of Research and Innovation Yangon, Ministry of Education, Myanmar

†Corresponding author: Euis Nurul Hidayah; euisnh@gmail.com

Nat. Env. & Poll. Tech.
Website: www.neptjournal.com

Received: 18-07-2019
Accepted: 05-10-2019

Key Words:
Macroalgae;
Cladophora glomerata;
Nitrate; Phosphate;
Kinetics

ABSTRACT

Effectiveness of macroalgae was investigated for enhancing wastewater treatment processes. Bioremediation using macroalgae could remove nitrate and phosphate contaminants in the water where algae assimilate nitrogen and phosphorus and convert them to biomass. This study evaluates the effects of high nitrate concentration on the kinetics of cell growth during nitrate and phosphate removal by a macroalga *Cladophora glomerata*. The algal growth and nitrate removal from media containing initial nitrate concentrations of 5mg/L to 400 mg/L were monitored in batch growth, whereas control media has no additional nitrate. Light exposure was kept for 12 and 20 hours. The purpose of this research was to find out the effect of various nitrate concentrations on nitrate and phosphate removal with macroalgal growth. Maximum growth kinetic reaches μ=0.075/day in 20 hours light exposure with 100 mg/L initial nitrate concentration. Nitrate and phosphate reach about 90% removal rates on the fifth day. Nitrate concentration was not significantly affected by biomass growth (Pearson correlation: 0.295). But, phosphate concentration has a moderate correlation with macroalgae biomass (Pearson correlation: 0.533).

INTRODUCTION

In recent years, microalgae and macroalgae have been used in many environmental applications. Bioremediation using algal technology is believed to be a promising alternative technology. Several macroalgae have been suggested for the treatment of wastewaters with high nitrogen concentration (Cole et al. 2016, Ge & Champagne 2017). Moreover, previous studies have shown that *Cladophora glomerata* has significant potential of bioremediation for wastewater treatment (Whitton 1970b).

Nitrogen in biogeological cycles produces compounds with different oxidation states like nitrate, nitrite, ammonium, organic nitrogen including amino acids, urea and proteins that are available to phytoplankton. Furthermore, high nitrate concentration will enhance the possibility of eutrophication. According to a study conducted by Lee et al. (2015), the nutrients with the complement of substrates greatly affected the optimization of macroalgae growth. Furthermore, if nutrient concentration is in excess in the water, macroalgal growth will be inhibited (Han et al. 2016).

Recently, *C. glomerata* became the most prodigal algae in the water streams. Eutrophication, caused by high nutrient content, will have a high influence of *C. glomerata* biomass with the optimal growth conditions of 0.07 mg/L phosphorous (P), 0.6 mg/L nitrate-nitrogen (NO_3-N) and 0.2 mg/L ammonium nitrogen (NH_4-N) (Whitton 1970a).

Algae can use nitrate (NO_3^-), nitrite (NO_2^-) or ammonium (NH_4^+) as a nitrogen source. Nitrate (NO_3^-) is the main form of nitrogen in natural waters as well as a major nutrient for plant growth and algae (Putra & Farahdiba 2018). The main sources of nitrogen in the water are nitrate and ammonium ions.

Phosphate is a form of phosphorus that can be used by plants. Phosphorus is also an essential nutrient for higher plants and algae and becomes a limiting factor for plants and algae (Selvaratnam et al. 2015). Orthophosphate (PO_4^{3-}) is an inorganic phosphorus source which is important for algal growth and can be produced by various forms of phosphorus-containing organic matter (Han et al. 2016). Macroalgal growth will also be affected by the duration of light exposure. Furthermore, among many environmental conditions, it was hypothesized that the macroalgae-bacteria system would respond to different photoperiod conditions in terms of an increase or decrease in the algal population and nitrogen concentration (Lee et al. 2015).

Therefore, controlling the concentration of nitrate in water resources light exposure is required. Currently, there is limited data available on the toxicity of high concentration of nitrate and its influence on macroalgal biomass with N and P removal. In this study, the effects of high nitrate concentration and nitrate as the nitrogen source for the growth of *Cladophora glomerata* and nitrate and phosphate removal in the growth media have been investigated.

MATERIALS AND METHODS

The experiment was conducted at the Research Laboratory, Environmental Engineering UPNV. The study took place from the beginning of February to the end of May 2019, from the preparation stage to the analysis results. USEPA (1996) was followed to find nitrate concentration within the range finding test (RFT). Nitrate concentration used in this study was 100-1000mg/L. This preliminary study found that the critical macroalgae could live in nitrate concentration of 100-400 mg/L (Farahdiba et al. 2019). When nitrate concentration was higher than 400mg/L, macroalgae became withered and yellow immediately.

Batch scale experiment was conducted with 300 mL of laundry wastewater sample in a glass jar within 5 days with 5 different nitrate concentrations. Each reactor was spiked with macroalgae *C. glomerata* to remove high nitrate and phosphate concentration. This research was conducted for 5 days with additional light from a LED lamp of 20 watts (or 3600 lux) for 12 and 20 hours illumination. Nitrate and phosphate were determined according to Standard Methods (González-Camejo et al. 2018).

Nitrate concentration used from RFT test was 0-400 mg/L. Macroalgae spiked with the water laden with 5 different concentrations: a) 5 mg/L (control reactor, without additional nitrate); b) 100 mg/L; c) 200 mg/L; d) 300 mg/L, and e) 400 mg/L.

Initial macroalgae biomass was measured as the average of 10 samples weighing from fresh algal sample to dry weight of macroalgae biomass at 105°C for 4 hours (Horwitz & Chemists 2000). The preliminary test was to determine the initial macroalgae biomass value obtained from drying 10 macroalgae samples with the same weight. The dry weight results of the 10 macroalgae samples were averaged and the initial biomass yield was 1332.9 mg/L (Ge & Champagne 2017). This data becomes the baseline of the algae biomass within sampling on the day.

In this study, the calculated specific growth rate μ/day in the exponential phase of algal growth was measured by using Eq. 1 (Issarapayup et al. 2009, Zhu et al. 2013).

$$\mu(/\text{day}) = \ln(N_2 - N_1)/(t_2 - t_1) \quad \ldots(1)$$

where N1 and N2 are defined as dry biomass (mg/L) at time t_1 and t_2, respectively.

The biomass productivity (P) was calculated according to the formula given in Eq. 2.

$$P\left(\frac{mg}{l}.day\right) = (DW_i - DW_0)/(t_i - t_0) \quad \ldots(2)$$

Where, DWi and DW0 are dry biomass (mg/L) at time t_i and t_0 (initial time), respectively.

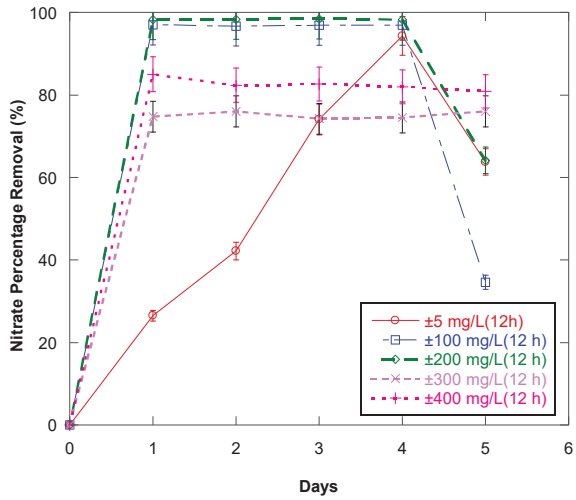

Fig. 1: Nitrate removal with 12h light exposure by macroalgae under five nitrate concentration levels within five days.

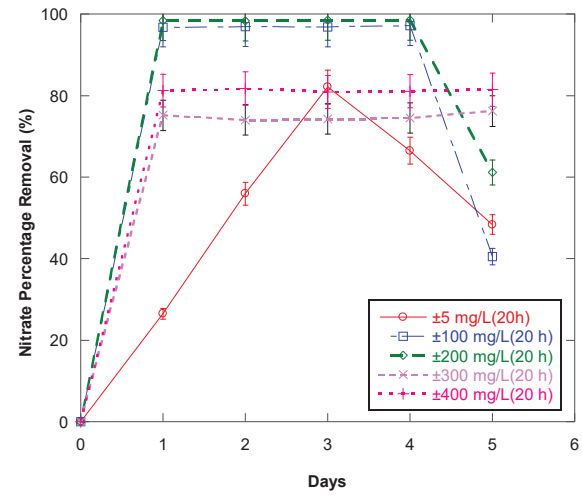

Fig. 2: Nitrate removal with 24h light exposure by macroalgae under five nitrate concentration levels within five days.

Data analysis was performed with EXCEL (Microsoft Office Enterprise 2010) and Minitab 2016 for Windows and correlation was determined wherever applicable.

RESULT AND DISCUSSION

Effect of Nitrate Concentration and Light Exposure on Nitrate Removal

Fig. 1 shows that the nitrate dramatically decreased within 5 days in all the experiments. Furthermore, the removal in the treatment with an initial nitrate concentration of 5 mg/L (control) was slowed down as compared to other nitrate concentrations. However, the control reactor has a different downward trend. Other reactors showed an increase slightly from day 1 to 4 and a reduction on the fifth day.

In the first day's observation, the maximum nitrate reduction was 98.26% with the initial nitrate concentration of 200mg/L. When the test came to the fourth day, 94.32%, 96.89%, 98.21%, 74.53% and 81.97% were accordingly removed from 5, 100, 200, 300 and 400 mg/L nitrate cultures. Nitrate in 0, 100 and 200 mg/L increased on the first day and dropped on the fifth day; while in 300 and 400 mg/L, it increased on the first day and stabilized until the end of the experiment.

Nitrate removal efficiency in 20-hour irradiation reactor could be seen in Fig. 2, which has a similar trend with 12 hours of exposure. Moreover, in 5 mg/L nitrate concentration with 20 hours, the faster removal efficiency was reached than the 12 hours exposure (on the third day); while in the following days it reduced significantly.

In the four days of observation, the maximum nitrate reduction of 98.18%, 98.51%, 74.26%, and 81.07% was accordingly removed from 100, 200, 300 and 400 mg/L.

The significantly high removal efficiency of nitrate was achieved among all the treatments (Figs. 1 and 2). Based on Fig. 1 and Fig. 2, the nitrate level in the test reactor is sufficient to reach a very high removal efficiency in nitrate on days 1 to 4 and decreases on the last day. Whereas, in the control reactor it gradually increases from days 1 to 4 and began to fall on the fifth day. Increased level of nitrate reduction is because the algae have well adapted to the day and night period. This has increased the dissolved organic carbon in water through active photosynthesis which is strongly correlated with the bacterial system (Kouzuma & Watanabe 2015, Lee et al. 2015, Unnithan et al. 2014). Throughout the experiment, pH condition is in the normal range, which indicates that nitrification and denitrification were not the main processes responsible for nitrogen removal. Since the mean pH in the reactor was less than 8.5, ammonia volatilization through the surface might have been limited (Derabe-Maobe 2014).

In addition, increased nitrate concentration could be caused by the release of cellular nutrients by microalgae. Macroalgae lysis during the death phase can also increase nitrates (Ma et al. 2014).

The average nutrient removal rates were not significantly different among the two photoperiod conditions during the experiment as the 12 or 20 hours time exposure could be partially attributed to the high adaptability of algae in controlling carbon assimilation and respiration (Ma et al. 2014).

Effect of Nitrate Concentration and Light Exposure Variation on Phosphate Removal

The phosphate removal with 12 hours light exposure in this study was measured and shown in Fig. 3. On the first day until fourth day phosphate reduction was relatively stable. Four days were assumed to be the optimum time for macroalgae to remove phosphate. On the last day of the main study (day 5), it was found that the percentage of phosphate reduction began to decline, the condition was considered to be the point or time of saturation of macroalgae in remaking phosphate.

Furthermore, this trend is similar to the 20 hours trend. The phosphate removal is not significantly directly affected by light illumination. From the two irradiation periods, it can be seen that the highest per cent reduction is achieved by macroalgae on the fourth day, which is considered as the optimum macroalgae time in absorbing phosphate.

Table 1: Growth parameters of macroalgae under five nitrate concentrations and light exposure in 5 days.

Initial nitrate concentration (mg/L nitrate)	Specific growth rate μ (/day)		Biomass increase (mg/L)		Biomass productivity (mg/L.day)	
	12 h	24h	12 h	24h	12 h	24h
5 (Control)	0.009	0.014	61.433	96.767	18.937	30.912
100	0.056	0.075	431.433	604.767	44.321	60.888
200	0.035	0.0262	259.766	186.767	35.165	36.679
300	0.027	0.0261	194.767	185.433	31.176	31.570
400	0.011	0.0264	77.767	187.767	20.558	29.547

The four days observation on both the hours' exposure, showed that the maximum phosphate reduction of 92.72%, 92.82%, 92.72%, 92.57%, 92.77% was accordingly achieved from 5, 100, 200, 300 and 400 mg/L of nitrate concentration.

Reduced phosphate levels in microalgae media are caused by the use of phosphate as a nutrient for microbial growth (Fig. 3). Phosphate functions are energy metabolism, protein synthesis, regulation of starch and starch production, formation of proteins, carbohydrates, cell structures and cell membrane stabilizers (Grover & Mar 2008). Decreasing in phosphate levels is due to the increasing number of macroalgae which increases the requirement for phosphate (Tang et al. 2016).

The efficiency of the resulting phosphate reduction varies depending on the composition of the media and environmental conditions such as initial nutrient concentration, irradiation time, and the ratio of nitrate:phosphate, light or dark. Moreover, the process of decreasing of pollutants in wastewater using aquatic plants is a collaboration between plants and microbes associated with these plants (Lee et al. 2015).

Macroalgae Growth Kinetics

Table 1 shows the growth kinetics and biomass productivity in this experiment with 12 hours and 20 hours of light exposure. Biomass testing can be used as a reference to determine the growth of macroalgae by dry weight biomass. Macroalgae growth can be observed by determining the growth phase which is divided into four phases which include the lag, exponential, stationary and lysis (Zhu et al. 2013, Cahyonugroho et al. 2020). The results in Fig. 4 show the macroalgae growth obtained from the five different nitrate concentrations. All reactors have increased biomass growth on the first day. The results of biomass growth in the reactor with 20:4 irradiation were found to have similar trends. Furthermore, the specific growth rate in 12 and 24 hours has a high correlation, with the Pearson correlation coefficient of 0.879.

The macroalgae, cultivated in the media with the nitrate concentration of 5, 100, 200, 300 and 400 mg/L had an exponential stage and then fluctuate in the stationary phase with 12 to 20 hours light exposure (Fig. 4).

Statistical analysis was conducted to determine the correlation between biomass concentration and N, P concentrations using Pearson correlation value. Biomass is greatly affected by phosphate concentration (Pearson value: 0.533 in 12 and 20 hour). Nevertheless, nitrate concentration has a lower correlation value (0.295 in 12 and 20 hour).

However, the exponential growth in the culture with all the reactors lasted for one to two days, following a predicted lag phase, which lasted for about 4 days. In five days, algal cells reduce in all the nitrate concentrations; in order with similar trends with a lower removal efficiency of N and P. It was predicted that on the fifth day, macroalgae would be in the stationary-lysis stage. In this study, the lack of a visible lysis phase was because the cultivation period was short. Research by Taziki et al. (2016) showed that the completed algal life stage would appear after about 12 days. However, the algal life stage is dependent on the algal species, nutrient and environmental condition.

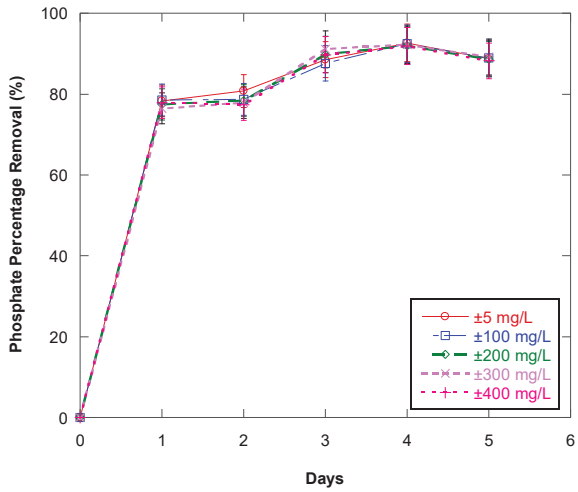

Fig. 3: Phosphate removal with 12h and 20h light exposure by macroalgae under five nitrate concentration levels in five days.

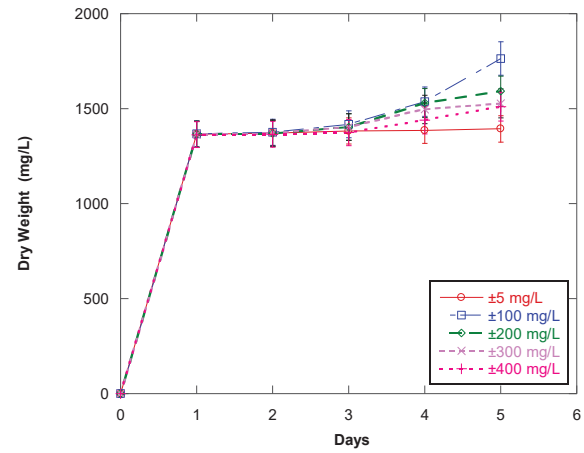

Fig. 4: Growth curves for macroalgae (*Cladophora glomerata)* grown under five nitrate concentration levels in five days.

The specific growth rate (μ) of macroalgae in 5, 100, 200, 300 and 400 mg/L nitrate concentration was 0.024, 0.075, 0.0262, 0.0261 and 0.0264 day/L respectively. The final biomass productivity increase significantly at 100 mg/L which was the highest, reaching to 60.88 mg/L.day, while the culture in 5 and 400 mg/L nitrate showed the lowest biomass increase (30 and 29 mg/L.day, respectively). The biomass productivity in this study was lower than that in the research by Zhu et al. (2013).

CONCLUSION

The macroalgae *Cladophora glomerata* has high removal efficiency to reduce nitrate and phosphate concentration in high nitrate concentration, but macroalgae biomass was not directly influenced by nitrate concentration. Moreover, the reactor has low growth kinetics and biomass productivity. This is probably the complication in the algae reactor because of various factors which affect the macroalgae performance to remove contaminants in the water.

ACKNOWLEDGEMENT

This study was a part of funding supported by grants from Directorate of Research and Community Service, Directorate General of Research Development, Ministry of Research Technology and Higher Education of Indonesia. This research was carried out under contract No. 201/SP2H/LT/DRPM/2019.

REFERENCES

Cahyonugroho, O.H., Yuniawati, D.D. and Hidayah, E.N. 2020. Kinetics of *Chlorella* sp. growth models in reducing CO_2 emission. Rasayan Journal of Chemistry, 12(4): 2306-2310.

Cole, A. J., Neveux, N., Whelan, A., Morton, J., Vis, M., de Nys, R. and Paul, N. A. 2016. Adding value to the treatment of municipal wastewater through the intensive production of freshwater macroalgae. Algal Research, 20: 100-109.

Derabe-Maobe, H. 2014. High Rate Algal Pond for Greywater Treatment in Arid and Semi-Arid Areas. Hokkaido University.

Farahdiba, A.U., Hidayah, E.N. and Asmar, G. A. 2019. Utilization of *Cladophora glomerata* for organic substance removal in laundry wastewater with artificial light exposure. Journal BIOTA, 5(2).

Ge, S. and Champagne, P. 2017. Cultivation of the marine macroalgae *Chaetomorpha linum* in municipal wastewater for nutrient recovery and biomass production. Environmental Science and Technology, 51(6): 3558-3566.

González-Camejo, J., Barat, R., Pachés, M., Murgui, M., Seco, A. and Ferrer, J. 2018. Wastewater nutrient removal in a mixed microalgae-bacteria culture: Effect of light and temperature on the microalgae-bacteria competition. Environmental Technology (United Kingdom), 39(4): 503-515.

Grover, J.P. and Mar, N. 2008. phosphorus-dependent growth kinetics of 11 species of freshwater algae phosphorus-dependent growth lunatics of 11 species of freshwater algae. Limnology, 34(2): 341-348.

Han, L., Xu, B., Qi, F. and Chen, Z. 2016. Effect of nitrogen/phosphorus concentration on algal organic matter generation of the diatom *Nitzschia palea*: Total indicators and spectroscopic characterization. Journal of Environmental Sciences (China), 47: 130-142.

Horwitz, W. 2000. Official Methods of Analysis of AOAC. Association of Official Analytical Chemists, Washington, DC.

Issarapayup, K., Powtongsook, S. and Pavasant, P. 2009. Flat panel airlift photobioreactors for cultivation of vegetative cells of microalga *Haematococcus pluvialis*. Journal of Biotechnology, 142(3-4): 227-232.

Kouzuma, A. and Watanabe, K. 2015. Exploring the potential of algae/bacteria interactions. Current Opinion in Biotechnology, 33: 125-129.

Lee, C. S., Lee, S. A., Ko, S. R., Oh, H. M. and Ahn, C. Y. 2015. Effects of photoperiod on nutrient removal, biomass production, and algal-bacterial population dynamics in lab-scale photobioreactors treating municipal wastewater. Water Research, 68: 680-691.

Ma, X., Zhou, W., Fu, Z., Cheng, Y., Min, M., Liu, Y. and Ruan, R. 2014. Effect of wastewater-borne bacteria on algal growth and nutrients removal in wastewater-based algae cultivation system. Bioresource Technology, 167: 8-13.

Putra, A.H. and Farahdiba, A.U. 2018. Performance of algae reactor for nutrient and organic compound removal. In: International Conference on Science and Technology (ICST 2018) (pp. 119-125), Atlantis Press.

Selvaratnam, T., Pegallapati, A., Montelya, F., Rodriguez, G., Nirmalakhandan, N., Lammers, P.J. and van Voorhies, W. 2015. Feasibility of algal systems for sustainable wastewater treatment. Renewable Energy, 82: 71-76.

Tang, C.C., Zuo, W., Tian, Y., Sun, N., Wang, Z. W. and Zhang, J. 2016. Effect of aeration rate on performance and stability of algal-bacterial symbiosis system to treat domestic wastewater in sequencing batch reactors. Bioresource Technology, 222: 156-164.

Taziki, M., Ahmadzadeh, H. and A. Murry, M. 2016. Growth of *Chlorella vulgaris* in high concentrations of nitrate and nitrite for wastewater treatment. Current Biotechnology, 4(4): 441-447.

Unnithan, V. V., Unc, A. and Smith, G.B. 2014. Mini-review: A priori considerations for bacteria-algae interactions in algal biofuel systems receiving municipal wastewaters. Algal Research, 4(1): 35-40.

USEPA 1996. Ecological Effects Test Guidelines Aquatic Plant Toxicity Test Using *Lemna* spp., Tiers I and II. Environmental Protection, (January).

Whitton, B. A. 1970a. Biology of *Cladophora* in freshwaters. Water Research, 4(7): 457-476.

Whitton, B. A. 1970b. Review Paper: Biology of Cladophora. Water Research, 4: 457-476.

Zhu, L., Wang, Z., Shu, Q., Takala, J., Hiltunen, E., Feng, P. and Yuan, Z. 2013. Nutrient removal and biodiesel production by integration of freshwater algae cultivation with piggery wastewater treatment. Water Research, 47(13): 4294-4302.

Nature Environment and Pollution Technology
An International Quarterly Scientific Journal

p-ISSN: 0972-6268
(Print copies up to 2016)
e-ISSN: 2395-3454

Vol. 19 | No. 2 | pp. 815-823 | 2020

Original Research Paper

https://doi.org/10.46488/NEPT.2020.v19i02.039

Open Access Journal

Studies on Decomposition of Banana Leaf and Mixture of Cattle Dung and Urine by Thermophilic Coprophilous Fungi

Ajmera Shanthipriya*†, Sana Shanawaz* and Sivadevuni Girisham**

*†Department of Microbiology, Palamuru University, Mahabubnagar-509001, Telangana, India

**Department of Microbiology, Kakatiya University, Warangal-506009, Telangana, India

†Corresponding author: Ajmera Shanthipriya; sreeja.poorvi@gmail.com

Nat. Env. & Poll. Tech.
Website: www.neptjournal.com

Received: 01-09-2019
Accepted: 18-09-2019

Key Words:
Banana leaf; Cattle dung; Thermophilic coprophilous fungi; Soil fertility

ABSTRACT

In this study, the microbial population responsible for decomposition of banana leaf with dung and urine of cattle (cow and sheep used here) was isolated, identified, and their incidence calculated. During this study, significant changes were observed in different physio-chemical properties (temperature, pH, moisture content, humidity, ash content, total organic carbon, total nitrogen content, phosphorus) of decomposing material which focuses particularly on the role of thermophilic coprophilous fungi in reducing the time for decomposition. It also gives a clear demonstration of various effects of different environmental conditions on the microbial population during the process of decomposition. The decomposition product thus obtained was found to be rich in organic phosphorous and nitrogen, raising our hopes for a successful implementation of it in daily agricultural practices.

INTRODUCTION

Dung has an ecological community of microorganisms which supports the growth of thermophilic coprophilous fungi mainly because of its higher nitrogen content, pH and moisture content when compared with other substrates utilized by fungi (Webster 1970). Microbial changes during the decomposition of leaves have been reported by Hankin et al (1975), Sofia Duarte et al. (2009) and Manoharachary et al. (2014). Thermophilic coprophilous fungi are believed to contribute significantly to the rate of decomposition (Ross & Harris 1983, Richardson 2002, Masunga et al. 2006). Generally, decomposition involves both mesophilic and thermophilic microorganisms. The optimal temperature range for thermophilic coprophilous fungi for growth and sporulation is 40-50°C. Temperature, oxygen, C/N ratio and moisture are important factors which affect composting (Waksman & Cordon 1939). The composition of plant residues changes during decomposition. The final products of their decomposition include carbon dioxide, water, energy, microbial biomass, inorganic nutrients and re-synthesized organic carbon compounds such as humus, phenolics, celluloses, hemicelluloses and lignin. Under aerobic conditions, microbial decomposition results in a release of CO_2. Under anaerobic or oxygen-limited conditions, anaerobic decomposers produce organic acids (Liu et al. 2006, Jianru 2013).

In the succession of dung, urine and banana leaf residues with thermophilic coprophilous fungi, the temperature increased continuously up to 36°C-50°C. This group of fungi grows above 20°C-60°C (Rosenberg et al. 1972, Vijay & Pathak (2014). In previous reports, the authors were concerned about the composition and dynamics of the microflora during the decomposition of different wastes like garbage and plant material, organic wastes (Beffa et al. 1996, Atkinson et al. 1997, Donkova et al. 2008 & Ghaudhry et al. 2013) and animal manure on vermicomposting of mixed leaves litter (Viji & Neelanarayanan 2015).

The populations of thermophilic and mesophilic microorganisms have been identified during decomposition. Monitoring of the microbial succession is very important in the effective management of the decomposition process as microbes play a key role in the process and the appearance of some microorganisms reflect the quality of maturing compost. Decomposition of organic matter by microbial activity is beneficial to mankind (Manoharachary et al. 2014).

Decomposition of fresh plant materials by microbes releases additional nitrogen and converts organic nitrogen to available forms. The pattern and timing of mineralization depend on the quality of residue, C/N ratio, temperature, moisture content and method of incorporation (Swift et al. 1979). Ammonification occurs when organic matter is broken down into simpler amino compounds. Nitrogen is released in the form of ammonia through enzymatic digestion of bacteria and fungi, and then is dissolved in the soil solution as ammonium (NH_4^+). Plants can use NH_4^+, although most nitrogen uptake is in the nitrate (NO_3^-) form.

MATERIALS AND METHODS

Yeast extract, starch agar-agar and all other chemicals were purchased from HiMedia Laboratories Pvt Ltd., Mumbai, India. Cow dung and urine, sheep dung and urine and banana leaves were collected from Warangal, Telangana, India.

The decomposition of banana leaves by thermophilic fungi was studied by the method suggested by Joshi & Thakre (1992). Banana leaves were chopped with the help of a chopping machine making its length to 5-6 cm. Five kg of leafy biomass was well soaked in water and placed under the direct sunshade of a tree and laboratory conditions for degradation. Replicate sets were employed and repeated twice. The banana leaf material was subjected to the following treatments:

Banana leaf (5 kg) with water (1000 mL) was taken as control and banana leaf (3kg) + cow dung (2kg) + urine (1000mL) and banana leaf (3kg) + sheep dung (2kg) + urine (1000 mL) as experimental sets. The observation was made for 6 months. The decomposing leaf material was analysed for its association of thermophilic fungi at monthly intervals. Simultaneously, physico-chemical changes in decomposed leaf were also analysed. The presence of thermophilic fungi was analysed by serial dilution and paired plate method (Cooney & Emerson 1964) using the medium composition of starch, 30g; yeast extract, 5.0g; $MgSO_4.7H_2O$, 0.5 g; K_2HPO_4, 1.0g; agar-agar, 20g, and distilled water 1000mL. The isolated strains were identified based on the morphological characters (Mouchacca 1997).

Temperature: Temperature of the decomposing leaf in pits was determined at the time of analysis for the thermophilic fungi. The thermometer was inserted into the decomposing material by removing the upper layer of the pit and temperature was recorded in °C.

pH: Ten grams of the decomposing leaf litter was taken and cut into small pieces in 100 mL of distilled water and shaken for 30 minutes. The pH of the decomposing leaf litter suspension was determined with the help of Elico pH meter.

Moisture: 100 grams of the decomposing leaf of banana was dried at 105°C for 48 hours followed by cooling in desiccators and weighed to a constant weight and moisture was expressed in percentage of weight loss.

Humidity: Relative humidity (RH) is the ratio of the partial pressure of water vapour to the equilibrium vapour pressure of water at a given temperature. It depends on temperature and the pressure of the system of interest.

Ash content: Total ash content of decomposing banana leaf was estimated by the method suggested by Ward & Johnston (1962). Two grams of the oven-dried sieved sample of decomposing leaf material was weighed into porcelain crucible and kept in a muffle furnace at 558°C for 2 hours and weighed to a constant weight after cooling the sample in a desiccator and expressed in mg.

Organic carbon (titration method): Estimation of organic carbon was made by Walkley-Black titration method. 0.1 mL of sieved sample was taken in 500mL Erlenmeyer flask add 20mL of 1N potassium dichromate and stirred and 20mL of concentrated H_2SO_4 was added and stirred (Bailey et al. 1992). Above mixture was allowed to stand for 30 minutes followed by addition of 200mL of distilled water and 10mL orthophosphoric acid. Before titration with ferrous ammonium sulphate, 1mL of diphenylamine was added and titration was done till the colour changed blue to green.

Total nitrogen: Colorimetric method of Wolf (1947) improvised by Ward & Johnson (1962) was employed for estimating the total amount of nitrogen in decomposing banana leaf material. One hundred grams of leaf material was digested in a Kjeldahl flask and a yellow colour was developed with Nessler's solution whose intensity was measured at 480 nm with the help of a colorimeter. The amount of nitrogen was calculated from the standard curve. The total protein nitrogen was also calculated by multiplying the total nitrogen with a factor of 6.3.

RESULTS AND DISCUSSION

Succession of the Fungi on Cow Dung

The succession of thermotolerant and thermophilic coprophilous fungi in the decomposing mixture of cow dung and urine with banana leaf (CDUB), and banana leaf (BL) without dung were studied and their incidence, frequency and abundance results were recorded (Table 1). It reveals that the incidence of different fungi in decomposing CDUB and BL varied with the progress of decomposition. Among all, 13 species belonging to 9 genera of fungi were involved in decomposing CDUB & BL. *M. pulchuella* followed by *H. insolens* and *S. thermophilum* were dominant in decomposing CDUB. *A. nidulans* was active at early stages of decomposition but disappeared completely as their population increased later.

The least incidence % was recorded with *Torulla thermophila*, *Cheatomium v. coprophiles* followed by *A. nidulans*. Rest of the species were found to be intermediate in their incidence, while *M. pulchuella* was recorded with the highest frequency followed by *R. arrhizus*, *R. pusillus* and *S. thermophilum*, all of them similar in the percentage of frequency, with differing incidence. *M. pulchuella* was recorded with the highest abundance followed by *Acremonium thermophilum* and *S. thermophilum.*

Table 1: Incidence, frequency and abundance of thermophilic coprophilous fungi in decomposing of CDUB and BL.

	Incidence												Frequency %		Abundance %	
	Feb		March		April		May		June		July					
Name of the fungi	CDUB	BL	CDUB	BL	CDUB	BL	CDUB	BL	CDUB	BL	CDUB	BL	CDUB	BL	CDUB	BL
Acremonium thermophilum	_	_	_	_	25.4	_	_	_	46.1	_	_	_	33. 0	_	13. 0	_
Aspergillus fumigates	_	17.5	_	_	_	23.9	_	_	_	_	_	_	_	33. 0	_	6.3
A. flavus	_	6.5	_	_	_	_	_	_	_	7.1	_	_	33. 0	33. 0	4. 0	8.8
A. nidulans	5.6	_	_	29.3	16.4	_	_	28.1	_	_	_	_	_	33. 0	_	2. 0
Cheatomium thermophile	_	_		_	_	_	23.7	_		_	15.6	_	33. 0	_	7.1	_
Cheatomium v. coprophile	_		11. 0	_	_		_		5.7	_	_		33. 0	_	3. 0	_
Humicola grisea	22.2	_	_	_	_	_	_	_	_	_	_	_	33. 0	_	8.6	_
H. insolens	18.5	_	_	_	_	54.9	41.7	_	_	_	25.6	_	33. 0	17. 0	10.9	8.4
H. fuscoatra	_	39.2	_	_	_	_	_	_	_	_	_	_	_	16.6	_	6. 0
Malbranchea cinnamomea	_	_	_	_	_	_	_	_	19. 0	_	_	_	16. 0	_	3.4	_
M. pulchuella	11. 0	_	42. 0	20.3	50.1	_	_	30.4	14.1	_	_	_	66. 6	_	21.3	_
Rhizomucor arrizhus	_	_	7.6	_	_	_	19.8	_	_	_	7.3	_	50. 0	33.3	10.1	7.7
R. podiformis	_	_	_	30. 0	_	_	_	_	_	_	_	28.2	_	33. 0	_	8.9
R. pusillus	_	_	15.3	_	_	21.6	_	_	15.2	_	_	_	50. 0	16.6	6.8	1.6
Scytalidium thermophilum	31.3	_	19. 0	_	_	_	17.3	_	_	_	28.5	_	50. 0	_	12.2	_
Sporotrichum thermophilum	_	_	_	_	_	_	_	_	_	_		10.6		16.6	_	_
Thermomyces lanuginosus	_	_	_	16.7	8.8	25.1	_	_	_	62	24.2	56.3	33. 0	67. 0	6. 0	24.6
Torulla thermophila	12. 0	15.7	5.1	7.2	_	_	_	2.3	_	_	_	10.5	_	66.6	_	5.4
Sterile mycelium	_	23.1	_	_	_	4.8	_	41.6	_	32.6	_	_	_	50. 0	_	15.7

CDUB = Cow dung, urine and banana leaf, BL = Banana leaf

The BL decomposing sample supported 11 fungal species representing 7 genera and their incidence, frequency and abundance were calculated and given in Table 1. In the initial days of incubation (May-June), the BL decomposing sample supported *H. fuscoatra, R. rhizopodiformis*, *A. nidulans, M. pulchuella, A. fumigatus, Thermomyces lanuginosus*, *Torulla thermophila* and *A. flavus* in a descending order. The highest incidence was recorded with *Thermomyces lanuginosus* followed by *H. insolence.* The least incidence was recorded with *A. flavus, Torulla thermophila* and *Sporotrichum thermopilum.* Rest of the species were recorded intermediate in their incidence. *Thermomyces lanuginosus* and *Torulla thermophila* were recorded with the highest frequency followed by *A. nidulans, A. fumigates, A. flavus* and *R. rhizopodiformis* which are similar in the percentage of frequency while differing in their incidence. The highest abundance was recorded again with *Thermomyces lanuginosus* followed by *R. rhizopodiformis* and *A. nidulans.* When compared with CDUB, the important thermophilic fungi such as *Cheatomium thermophilum, C.v. coprophile, H. gresia, M. cinnamomea, R. arrhizus* and *S. thermophilum* did not participate and thermotolerant fungi such as *A. thermophilum* was not found in BL decomposing sample.

The analysis of physico-chemical changes in the decomposing of the two samples (CDUB & BL) is presented in Table 2.

The pH of the decomposing CDUB sample changed with the observation period. Generally, the dung of herbivores will be of neutral pH (7.0). The changes were observed to increase up to 8.5 and a final pH of 7.3 was recorded at the end of the experiment. In the decomposing sample of banana leaf, pH was found to be fluctuating from 6.5 to 7.5 and later recorded as 7.0. These changes must be due to the involvement of different thermophilic coprophilous fungi (Fig. 1). The role of temperature plays is crucial in the process of decomposition. During the decomposition of CDUB sample, the temperature recorded in the range of 32°C to 50°C due to the presence of thermophilic fungi, while 36°C to 43°C was recorded during six months of BL decomposition period (Fig. 2).

During the decomposition of BL and CDUB, the ash and moisture content showed a gradual decrease in both the samples comparatively, the ash and moisture content was high in BL than CDUB at the end of the experiment, displaying utilization of substances by thermophilic fungi in CDUB sample.

A gradual change is observed in the percentage of humidity of BL and CDUB samples. As expected, the phosphorus content was also highest in CDUB (65 µg) than BL (55 µg) because of the percentage of rich nutritious dung. The organic carbon % was higher in decomposing sample BL (6.8%) than CDUB (6.5%) sample.

Succession on Sheep Dung

The succession of thermotolerant and thermophilic copro-

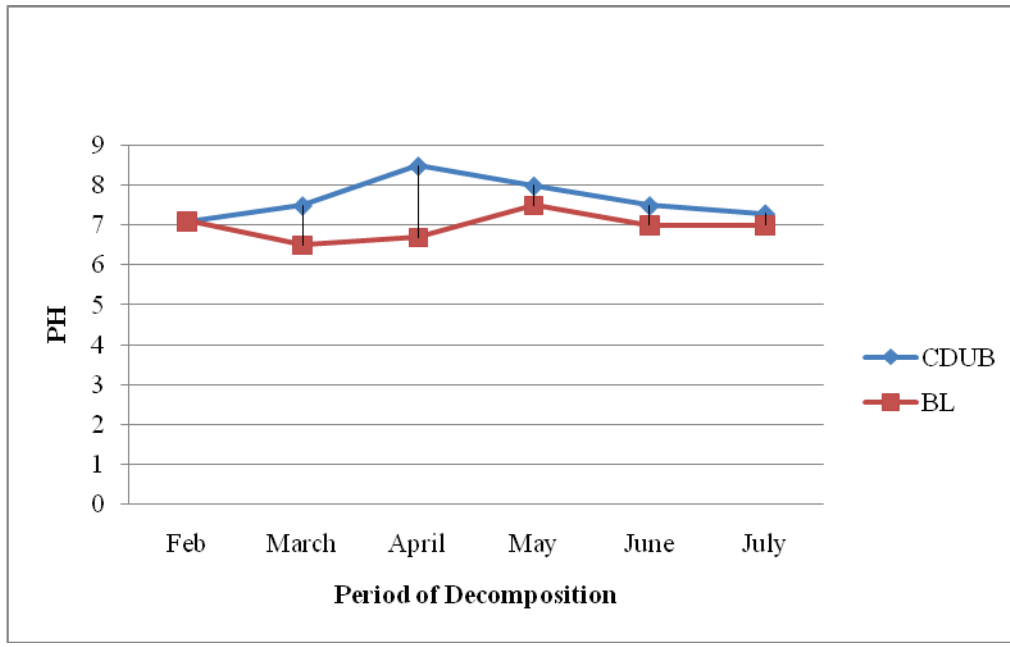

Fig. 1: pH changes during the CDUB and BL decomposition.

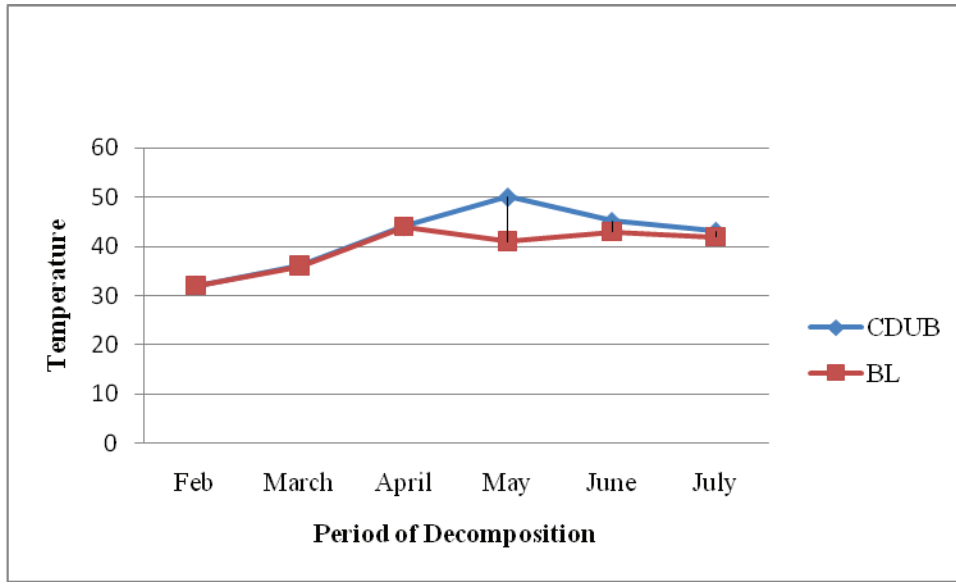

Fig. 2: Temperature changes during the decomposition of CDUB and BL.

Table 2: Physico-chemical changes in the decomposing mixture of cow dung, urine and banana leaf and banana leaf alone.

	Feb		March		April		May		June		July	
Month	CDUB	BL	CDUB	BL	CDUB	BL	CDUB	BL	CDUB	BL	CDUB	BL
Ash content (g)	0.26	0.29	0.24	0.25	0.21	0.24	0.19	0.23	0.18	0.23	0.17	0.2
Moisture (%)	88	89	80	83	80.4	80	70	76	69	65	58	60
Humidity (%)	73	75	83	81	98	99	93	80	80	78	70	75
Nitrogen (µg)	45	40	46	45	60	45	65	55	58	50	50	40
Organic carbon (%)	13.4	12.4	25.8	19.7	10.3	17.2	7.8	16.3	6.7	12	6.5	6.8
Phosphorus (µg)	70	60	65	60	80	65	65	61	60	70	65	55

philous fungi in in decomposing mixture of sheep dung and urine with banana leaf (SDUB), and banana leaf without dung (BL) sample were studied and their incidence, frequency and abundance are presented in Table 3. It reveals that the incidence of different fungi in decomposing SDUB and BL varied with the progress of decomposition. Among all the organisms studied, only 19 species representing 11 genera of fungi were involved in decomposing SDUB and BL. As the process progressed for SDUB decomposition, *H. fuscoatra* was recorded with the highest % of incidence followed by *C. thermophile, M. cinnamomea, Scytalidium thermophilum* and *Thermomyces lanuginosus* in a decreasing order. *A. nidulans, H. insolens* and *Torulla thermophila* showed their activity at initial stages only and later disappeared. *A. terreus*, *R. arrizhus* and *Sporotrichum thermophilum* occurred only in the second month of decomposition. The dynamics of *C. thermophile* may be in occurrence with temperature. The highest % of the incidence of *H. fuscoatra* was recorded at 5th month of the decomposition period. *M. albomyces* was recorded with a moderate percentage of incidence, while *H. lanuginosus* was detected only at the end of the decomposition period. *Sporotrichum thermophilum* was recorded with least incidence followed by *A. terreus* in SDUB decomposing sample. *Cheatomium thermophilum, R. pusillus, M. cinnamomea* and *M. pulchuella* were present in decreasing order.

During banana leaf (BL) decomposition incidence of important thermophilic fungi like *A. terreus, C. thermophilum, H. grisea, M. cinnamomea, M. pulchuella, Myriococcum albomyces*, *S. thermophilum, T. duponti* and *R. arrhizus,* was not observed as in SDUB decomposition sample. Whereas

A. fumigatus, *A. flavus* and *R. podiformis* were not recorded during the decomposition of SDUB but observed during decomposition of BL.

The highest % of incidence was recorded with *Thermomyces lanuginosus* followed by *H. insolens, H. fuscoatra, M. pulchuella* and *R. podiformis* in a decreasing order. *A. flavus* was recorded with least incidence, while others with moderate incidence.

The highest % of frequency was recorded with *T. lanuginosus* followed by *T. thermophila*. *Sporotrichum thermopilum* was recorded with least incidence followed by A. terreus in SDUB decomposing sample. *C. thermophile* was again recorded with the highest % of abundance followed by *R. pusillus*, *M. cinnamomea* and *M. pulchuella* in a decreasing order.

During Banana leaf BL decomposition, the incidence of important thermophilic fungi like *A. terreus*, *C. thermophilum*, *H. grisea*, *M.cinnamomea*, *Myriococcum albomyces*, *S. thermophilum*, *T. duponti* and *R. arrhizus* was not observed as in SDUB decomposing sample. Whereas *A. fumigatus*, *A. flavus* and *R. podiformis* were not recorded during decomposition of SDUB, but observed during decomposition of BL. The highest % of incidence was recorded with *Thermomyces lanuginosus* followed by *H. insolens*, *H. fuscoatra*, *M. pulchuella* and *R. podiformis* in decreasing order. *A. flavus* was recorded with least incidence, while others with moderate incidence.

The highest per cent of frequency was recorded with *T. lanuginosus* followed by *T. thermophila* and sterile mycelium.

If we compared both SDUB and BL decomposing samples, important thermophilic fungi like *C. thermophile*, *M. cinnamomea*, *R. arrizhus* and *S. thermophilum* were absent in BL decomposing sample.

The physico-chemical analysis of decomposing sample SDUB and BL were analysed and presented in Table 4.

Initially, the pH of SDUB sample was recorded as 7.2 and as the process progressed it varied between pH 7.2 to 8.0 and a final pH of 7.5 was recorded at the end of the decomposition period. During the decomposition period of banana leaf (BL), the pH ranged from 7.2 to 8.0 and the final pH was observed at 7.5 during decomposition of SDUB. The pH values varied from 7.1 to 7.5 and finally, a neutral pH (7.0) was recorded (Fig. 3). The temperature has a crucial role to play in the process of decomposition. During the decomposition of SDUB sample, the temperature recorded was in the range of 37°C to 51°C due to the presence of thermophilic fungi, while it was observed between 36°C to 42°C during the six months of BL decomposition period (Fig. 4).

The ash and moisture content gradually decreased during the process of decomposition of SDUB and BL. Comparing both the samples, the ash content and moisture of BL were relatively higher than in SDUB sample which shows more utilization by thermophilic fungi in SDUB sample. Humidity was gradually higher in the middle of the decomposition period (99%) and later decreased to 75% and 76% in BL and SDUB samples respectively.

The total nitrogen and phosphorus contents were increased in SDUB samples and decreased in BL. The organic carbon percentage was higher in BL (6.2%) than in SDUB

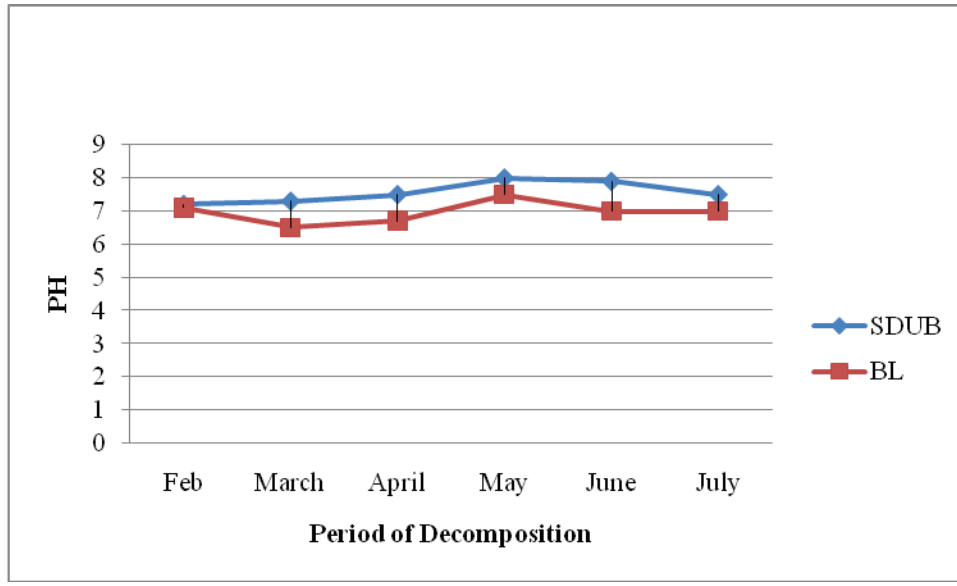

Fig. 3: pH changes during the decomposition of SDUB and BL.

Table 3: Incidence, frequency and abundance of thermophilic coprophilous fungi in decomposing in the mixture of SDUB and BL.

	Incidence %															
	May		June		July		Aug		Sep		Oct		Frequency %		Abundance %	
Name of the fungi	SDUB	BL		BL		BL	SDUB	BL	SDUB	BL	SDUB	BL	SDUB	BL	SDUB	BL
Aspergillus fumigates	_	17.5	_	_	_	23.9	_	_	_	_	_	_	_	33. 0	_	6.3
A. flavus	_	6.5	_	_	_	_	_	_	_	7.1	_	_	_	33. 0	_	8.8
A. nidulans	15.4	_	_	29.3	_	_	_	28.1	_	_	_	_	16.6	33. 0	2.56	2. 0
A. terreus	_	_	13.7	_	_	_	_	_	_	_	_	_	16.6	_	2.27	_
Cheatomium thermophile	_	_	40.5	_	9.6	_	37.2	_	_	_	_	_	50	_	14.5	_
Humicola grisea	_	_	_	_	13.3	_	_	_	17. 0	_	_	_	33.3	_	4.8	_
H. insolens	21.3	_	_	_	_	54.9	_	_		_	_	_	16.6	17. 0	3.54	8.4
H. fuscoatra	_	39.2	_	_	_	_	_	_	42.8	_	_	_	16.6	16.6	7.1	6. 0
Malbranchea cinnamomea	30.1	_	_	_	_	_	29.6	_	_	_	33.2	_	33	_	10.5	_
M. pulchuella	_	_	21.5	20.3	_	_	_	30.4	_	_	_	_	33	_	8.5	_
Myriococcum albomyces	10. 0	_	_	_	14.2	_	_	_	_	_	_	_	33	_	4. 0	_
Rhizomucor arrizhus	_	_	14	_	_	_	_	_	_	_	_	_	17	33.3	2.27	7.7
R. podiformis	_	_	_	30. 0		_		_		_		28	_	33. 0	_	8.9
R. pusillus	_	_	_	_	21.6	21.6	_	_	25.4	_	23.5	_	50	16.6	11.7	1.6
Scytalidium thermophilum	13.9	_	_	_	32. 0	_	_	_	_	_	_	_	33	_	5.36	_
Sporotrichum thermophilum	_	_	11. 0	_	_	_	_	_	_	_	_		16.6	16.6	1.8	_
Talaromyces duponti	_	_	_	_	9.3	_	20	_	_	_	_	_	33.3	_	4.7	_
Thermomyces lanuginosus	_	_	_	16.7	_	25.1	_	_	16.5	62. 0	27.1		33.3	67. 0	7.3	24.6
Torulla thermophila	9.2	15.7	_	7.2	_	_	_	2.3	_		16.6		16.6	66.6	4.2	5.4

SDUB = Mixture of Sheep dung, BL = Banana leaf

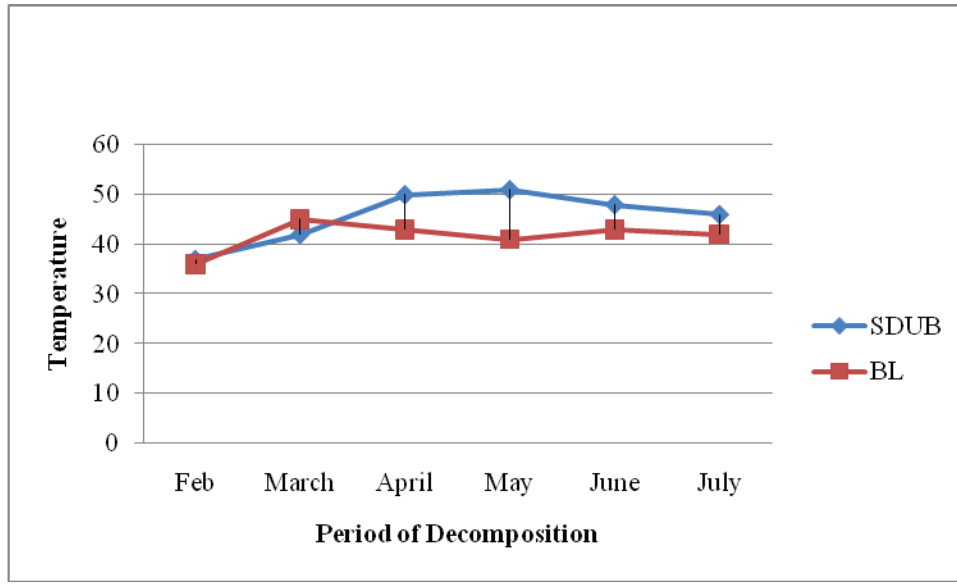

Fig. 4: Temperature changes during the decomposition of SDUB and BL.

Table 4: Physico-chemical changes in the decomposing mixture of sheep dung, urine and banana leaf and banana leaf alone.

Month	Feb		March		April		May		June		July	
	SDUB	BL	SDUB	BL	SDUB	BL	SDUB	BL	SDUB	BL	SDUB	BL
Ash content (g)	0.27	0.29	0.23	0.25	0.21	0.24	0.22	0.23	0.19	0.23	0.18	0.21
Moisture (%)	74	89	80	83	76	80	65	76	56.4	65	54	60
Humidity (%)	74	75	80	81	99	99	85	80	81	78	76	75
Nitrogen (µg)	50	40	45	45	59	45	63	55	60	50	55	40
Organic carbon (%)	12.4	12.4	19.8	19.7	22.7	17.2	14.6	16.3	9.4	12	6.2	6.8
Phosphorus (µg)	65	60	70	60	75	65	71	61	65	70	61	55

(6.8%) whereas phosphorus content was higher in SDUB (61 µg) than BL (55 µg) decomposing sample.

CONCLUSIONS

During this study, significant changes were observed in different physio-chemical properties of decomposing material which focuses particularly on the role of thermophilic coprophilous fungi in reducing the time for decomposition. It also gives a clear demonstration of various effects of different environmental conditions on the microbial population during the process of decomposition. The decomposition product thus obtained was found to be rich in organic phosphorus and nitrogen, raising the hopes for a successful implementation of it in daily agricultural practices.

ACKNOWLEDGEMENT

Authors are thankful to the Head, Department of Microbiology, Kakatiya University and Palamuru University for providing the necessary facilities.

REFERENCES

Atkinson, R.B., Zipper, C., Daniels, W.L. and Cairns, J. Jr 1997. Constructing wetlands during reclamation to improve wildlife habitat. Reclamation Guidelines for Surface Mined Land in Southwestern Virginia. Powell River Project-Virginia Cooperative Extension Publication, 460-129.

Bailey, S.W. and Hornbeck, J.W. 1992. Lithologic composition and rock weathering potential of forested, glacial-till soils. Res. Pap. NE-662. U.S. For. Serv., Northeastern For. Exp. Stn., Radnor, PA.

Beffa, T., Blanc, M., Lyon, P. F., Vogt, G., Marchiani, M., Fischer, J.L. and M. Arango, 1996. Isolation of Thermus strains from hot composts (60 to 80 degrees C). Appl. Environ. Microbiol., 62: 1723-1727.

Cooney, D.C. and Emerson, R. 1964. Thermophilic fungus: An Account of their Biology, Activities, and Classification. W.H. Freeman and Co., San Francisco, pp. 1-188.

Donkova, R., Stoichkova, M. and Slavov, D. 2008. Dynamic of microbial population during composting of organic wastes. International Confer-

ence- Potential for Simple Technology Solutions in Organic Manure Management, Albena, Bulgaria, pp. 409-413.

Ghaudhry, A., Chaudhry, N., Naeem, M.A., Jilani, G., Razzaq, A., Dong-Mei Zhang, Azeem, M. and Ahmed, M. 2013. Influence of composting and poultry litter storage methods on mineralization and nutrient dynamics. The Journal of Animal and Plant Sciences, 23: 500-506.

Hankin, L., Poincelot, R.P. and Anagnostakis, S.L. 1975. Microorganisms from composting leaves: Ability to produce extracellular degradative enzymes. Microbial Ecology, 2(4): 296-308.

Sofia, Duarte, Claudia Pascoal and Fernanda Cassio 2009. Functional stability of stream dwelling microbial decomposers exposed to copper and zinc stress. Freshwater Biology, 54: 1683-1691

Jianru, Shi 2013. Decomposition and Nutrient Release of Different Cover Crops in Organic Farm Systems. Dissertations & Theses in Natural Resources, 6.

Joshi, P. and Thakre, R.P. 1991. Composting of leafy biomass into farm manure. Proceedings of the seventh international conference on solid waste management and secondary materials. 3B: Philadelphia PA, USA.

Liu, P., Huang, J., Han, X., Sun, O.J. and Zhou, Z. 2006. Differential responses of litter decomposition to increased soil nutrients and water between two contrasting grassland plant species of Inner Mongolia, China. Applied Soil Ecology, 34: 266-275.

Manoharachary, C., Kunwar, I.K. and Rajithasri Kavaka, A.B. 2014. Advances in applied mycology and fungal biotechnology. KAVAKA, 43: 79-92.

Masunga, G., Andresen, S., Taylor, J.E. and Dhillion, S.S. 2006. Elephant dung decomposition and coprophilous fungi in two habitats of semi-arid Botswana. Mycology Research, 110(10): 1214-1226.

Mouchacca, J. 1997. Thermophilic fungi: Biodiversity and taxonomic status. Cryptogamie Mycologie, 18: 19-69.

Richardson, M. J. 2002. The coprophilous succession. Fungal Diversity, 10: 101-111.

Ross, R.C. and Harris, P.J. 1983. The significance of thermophilic fungi in mushroom compost preparation. Sci. Hortic. (AMST), 20: 61-70.

Rosenberg, S.L. 1975. Temperature and pH optima for 23 species of thermophilic and thermotolerant fungi. Canandian J. Microbiol., 21: 1535-1540.

Swift, M.J., Heal, O.W. and Anderson, J.M. 1979. Decomposition in Terrestrial Ecosystems. Univ. of California Press.

Vijay, B. and Pathak A. 2014. Exploitation of thermophilic fungi in compost production for white button mushroom (*Agaricus bisporus*) cultivation-A Review. In: Proceedings of the 8th International Conference on Mushroom Biology and Mushroom Products (ICMBMP8), pp. 19-22.

Viji, J. and Neelanarayanan, P. 2015. Effect of different animal manure on vermicomposting of mixed leaves litter by utilizing an exotic earthworm. International Journal of Advanced Research, 3(7): 1360-1376.

Waksman, S.A. and Cordon, T.C. 1939. Thermophilic decomposition of plant residues in composts by pure and mixed cultures of micro-organismsms. Soil Sci., 47: 217-224.

Ward, G.M. and Johnston, F.B. 1962. Chemical Methods of Plant Analysis. Publ. Research Branch., Canada Dept. Agric., Ottawa

Webster, J. 1970. Presidential Address. Coprophilous Fungi. Transactions of the British Myco1ogical Society, 54: 161-180.

Wolf, B. 1947. Determination of nitrate, nitrite and ammonium nitrogen. Rapid photometric determination in soil and plant extracts. Industr. Engg. Chem., (Anal., ed.), 16: 446.

Nature Environment and Pollution Technology
An International Quarterly Scientific Journal

p-ISSN: 0972-6268
(Print copies up to 2016)
e-ISSN: 2395-3454

Vol. 19 | No. 2 | pp. 825-830 | 2020

Original Research Paper

https://doi.org/10.46488/NEPT.2020.v19i02.040

Open Access Journal

Synthesis of Molecularly Imprinting Polymers for the Removal of Xylenol Orange from Water

Showkat Ahmad Bhawani*†, Nur Anati Bazilah Daud*, Salma Bakhtiar*, Rachel Marcela Roland* and Mohamad Nasir Mohamad Ibrahim**

*Faculty of Resource Science and Technology, Universiti Malaysia Sarawak (UNIMAS), Kota Samarahan, Sarawak, 94300, Malaysia

**School of Chemical Sciences, Universiti Sains Malaysia, Pulau Pinang, 11800, Malaysia

†Corresponding author: Showkat Ahmad Bhawani; sabhawani@gmail.com

Nat. Env. & Poll. Tech.
Website: www.neptjournal.com

Received: 01-08-2019
Accepted: 07-11-2019

Key Words:
Molecularly imprinted polymers; Microemulsion; Xylenol orange

ABSTRACT

The molecularly imprinted polymers (MIPs) were prepared by using the non-covalent approach. In the polymerization process, xylenol orange was used as a template (T), acrylic acid as a functional monomer (M), divinylbenzene as a cross-linker (CL) and 2,2'-azobisisobutyronitrile (AIBN) as an initiator and microemulsion as a solvent. The synthesized polymers were characterized by using FTIR and SEM micrograph. The batch binding analysis was used to evaluate the rebinding efficiency of imprinted polymers. The highest rebinding efficiency was obtained from the MIP-R2 (0.1:0.6:2, T:M:CL). The selected MIP-R2 was used for the removal of xylenol orange from the water sample and have shown removal efficiency of about 80%.

INTRODUCTION

The molecularly imprinting technology was first introduced by Wulff & Sarhan (1972) and was expanded by Mosbach and coworkers in 1980s (Andersson et al. 1984). This technology enables us to synthesize the materials with highly specific receptor sites towards the target molecules. MIPs are categorized as highly cross-linked polymers and can bind target compounds with high specificity. They are synthesized in the presence of the target molecule which acts as a template (Lok & Son 2009). MIPs have been attributed several advantages such as high selectivity and affinity, high stability and the ease of preparation (Piletsky et al. 2006). They can also be used repeatedly without loss of activity with high mechanical strength and are durable to harsh chemical media, heat and pressure as compared to biological receptors (Lavignac et al. 2004). Svenson and Nicholas (Svenson & Nicholls 2001), have proved that polymers are thermally resilient and can retain their chemical affinity.

The most important condition to produce MIP network with high potential recognition sites is that there must be a good interaction between monomer and template. Based on the nature of pre-polymerization interactions between the template and monomer, there are two strategies employed for MIP technology. Self-assembling approach (Arshady & Mosbach 1981), similar to the biological recognition systems where non-covalent forces like hydrogen bonds, Van der Waals forces, ion or hydrophobic interaction and metal coordination were used. The most frequent approach for the preparation of MIPs is self-assembling. This is due to the simplicity of complex formation and dissociation and the flexibility where available functional monomers can interact with almost any type of templates.

MIPs have been successfully applied in various fields such as in chiral separation, solid-phase extraction, biomimetic sensor, and controlled release devices of several drugs (Caro et al. 2006). It has been used widely for the detection and treatment of water pollutants even at very low concentrations (Schreibera et al. 2009). Molecularly imprinted materials can also be used in combination with the catalyst to form novel composite adsorbent or catalyst systems.

Xylenol orange, [3,3-bis-N, N, bis-(carboxymethyl) aminomethyl-o-cresolsulfonephthalein] is used for the determination of many metal ions because it is an excellent complexometric indicator and potentiometric reagent. The effluents discharged from xylenol orange manufacturing industries and laboratories pollute water bodies. In this way, the presence of xylenol orange in the water bodies further attracts heavy metals and causes various health problems to both humans and aquatic animals. Therefore, removal of xylenol orange from the water is very important to safe-

guard the aquatic as well as terrestrial life. The presence of dyes in water bodies interferes with the absorption of light and in other words colour is the prominent contaminant in the water. In this regard, molecular imprinting polymers are promising materials for the removal of pollutants from environmental water.

MATERIALS AND METHODS

Chemicals and reagents: The following chemicals were used in this study: Xylenol orange ($C_{31}H_{32}N_2O_{13}S$) was purchased from Acros Organics USA, 2,2'-azobis (isobutyronitrile) (AIBN) was purchased from R&M Marketing Company (Essex, United Kingdom), cetyltrimethylammonium bromide (CTAB) from R&M Chemicals, hexane from HmbG Chemical (Hamburg, Germany), butanol from R&M Chemical, acrylic acid (AA) from Sigma-Aldrich, divinylbenzene (DVB) from Merck Schuchardt OHG (Hohenbrunn, Germany), acetic acid from Avantor Performance Materials Incorporated (Center Valley, Pennsylvania), acetone from HmbG Chemical and methanol from R&M Marketing Company.

Equipment: Fourier transformed infrared (FTIR) spectrometer (Nicolet iS10), Scanning Electron Microscopy (SEM) (JEOL JSM-6390LA), Ultraviolet-Visible (UV-Vis) spectrophotometer (V-630) and (SP-830 plus), sonicator bath (2510 Branson), shaker (Multi Shaker NB-101MT), hot plate.

Preparation of microemulsion: In this study, water in oil microemulsion was used as a solvent for the synthesis of the polymer. The microemulsion was prepared by mixing 8 grams of CTAB powder, 10 gram of distilled water, 160 mL of hexane and 25 mL of butanol in a conical flask. The solution mixture was sonicated for about 20 minutes.

Preparation of MIP and NIP: The MIPs of xylenol orange were prepared by using the non-covalent approach. The composition of the two different MIPs is given in Table 1. Initially, xylenol orange was dissolved in microemulsion followed by the addition of acrylic acid, divinylbenzene and AIBN. The reaction mixture was sonicated for 15 min followed by the purging with nitrogen gas for 15 min to remove traces of oxygen. Finally, the conical flask was sealed tightly and kept in the water bath for 6 hours. Initially, the temperature was maintained at 55°C for the first three hours and then the temperature was increased up to 60°C and kept constant for the next three hours. The synthesized polymers were filtered and washed with methanol. The same procedure was repeated for the preparation of non-imprinted polymer without the template.

The template was removed from the polymer matrix by washing with methanol/acetic acid solution (10: 1, v/v, methanol and acetic acid) several times. The removal of the xylenol orange was monitored by the disappearance of xylenol orange band at 588 nm in UV-vis spectra.

Characterization: Scanning electron microscope (SEM) was used to observe the surface morphology of the polymer particles. Before the SEM analysis, the dried specimen was coated under vacuum with a thin layer of gold (Lian & Wang 2012).

FTIR was used to observe the functional groups present in the polymer matrix in the range of 4000-400 cm^{-1} by using KBr pellet.

Batch binding assay: Batch adsorption experiment was performed to evaluate the binding efficiency of imprinted polymers (Komiyama et al. 2003). A 10 ppm solution was prepared from the stock solution of xylenol orange. A series of three flasks were used for three different polymers (MIP1, MIP2 and NIP). In three different flasks containing 10 ppm of 75 mL solution, 50 mg of polymers (MIP1, MIP2 and NIP) were added. After that, all the flasks were kept on the shaker and then samples were collected after different time intervals (0, 30, 60, 90, 120, 150, 210, and 270 min). The absorbance of each extracted solution was determined by the UV spectrometry. The degree of extraction of xylenol orange was calculated using the following equation (1):

$$Extraction\ (\%) = \frac{C\ (initial) - C\ (final)}{C\ (initial)}\ x\ 100 \qquad \ldots(1)$$

Where C (initial) and C (final) are the concentrations of xylenol orange before and after extraction in the solution, respectively.

Selectivity Study

Selectivity study of MIP and NIP towards xylenol oranges dye was studied by comparing the uptake behaviour of MIP and NIP towards xylenol orange and a competitive malachite

Table 1: Composition of polymers.

Polymers	Xylenol Orange (mmol)	AA (mmol)	DVB (mmol)
MIP 1	0.1	0.4	2.0
MIP 2	0.1	0.6	2.0
NIP	0.0	0.6	2.0

green dye. The solutions of both the dyes were mixed and analysed for both MIP and NIP. The batch binding procedure was followed up to a contact time of 60 min. The extraction efficiency of MIP and NIP were calculated by using the following equations.

$$Kd = [(Ci - Cf)/ Cf \times M] \times V \quad \ldots(2)$$

Where,

kd = the distribution coefficient

Ci = the initial volume of solution

Cf = final volume of the solutions,

Where, V and M are the volume of the solution and mass of MIP or NIP used respectively.

The selectivity coefficient (kXO-MG) was calculated by using Eq. 3 as follows:

$$ksel\ XO - MG = KdXO/ Kd, MG \quad \ldots(3)$$

Where, KdXO and KdMG are the distribution coefficient of xylenol orange and malachite green, respectively.

Relative selectivity coefficients, K′ can be calculated by using Eq. 4.

$$K' = kselMIP/ kselNIP \quad \ldots(4)$$

Where, kselMIP and kselNIP are the selectivity coefficients of imprinted polymers and non- imprinted polymers, respectively

Removal of Xylenol Orange from Spiked Water Sample

The water sample was collected from the river. The sample water was filtered and centrifuged to remove suspended materials. After that 40 mL of water was spiked with 40mL of 20 ppm of xylenol orange solution. The final concentration obtained after spiking was 10 ppm. The selected MIP was used for the removal of Xylenol orange from lake water and the same procedure was followed as adopted in the batch binding process. The absorbance of free xylenol orange was observed by the UV-vis spectrophotometry. The degree of removal of xylenol orange from the water sample was calculated by using equation 1.

RESULTS AND DISCUSSION

The molecularly imprinted polymers for xylenol orange were prepared in microemulsion by free radical polymerization method. The microemulsion can solubilize both hydrophilic and hydrophobic compounds as compared to other organic solvents. Microemulsions are isotropic and thermodynamically stable mixture of oil, water, surfactant and usually with a co-surfactant (Shinoda & Lindman 1987).

Infrared Spectroscopy

The IR spectra for MIPs (Ratio 1 and 2) and NIP are shown in Fig. 1, and exhibited similar characteristic peaks. These

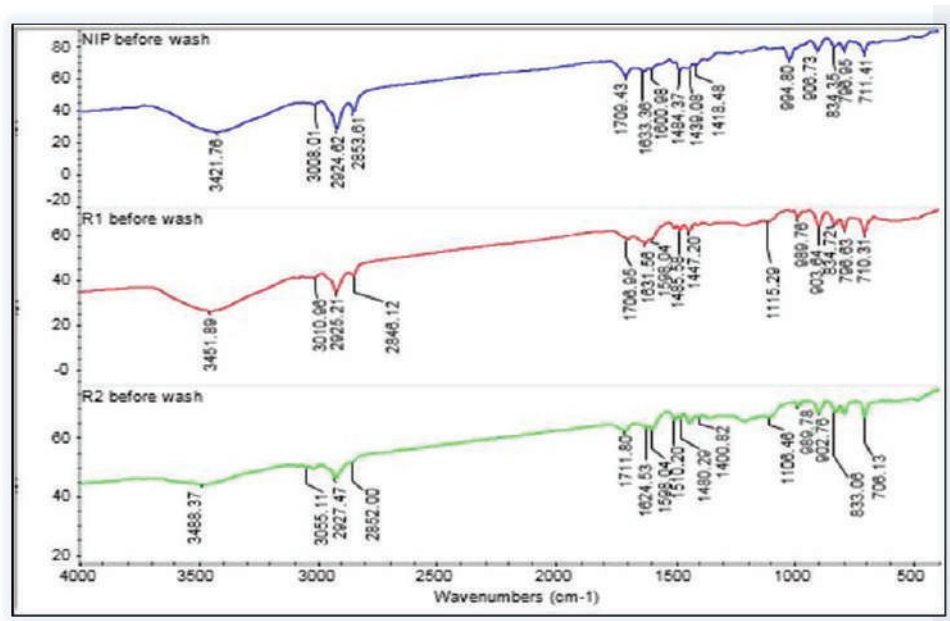

Fig. 1: FTIR spectra of MIPs (R1 and R2) and NIP.

characteristic peaks showed a similar significant backbone structure of different polymers. These spectra show a broad stretching vibrational band allocated to hydroxyl (OH) at about 3488 cm^{-1} - 3421 cm^{-1} (MIP-R1, MIP-R2 and NIP), and the vibrational band of the carboxyl group (C=O) in carboxylic acid at 1711 cm^{-1} - 1708 cm^{-1} (MIP-R1, MIP-R2 and NIP). The other absorption peaks that indicate the stretching band of vinylic C=C bonds in the range of 1620-1680 cm^{-1}, and C-O bonds (range of 1050-1150 cm^{-1}) as well as C-H bonds (range of 2850-2950 cm^{-1}) for all the three polymers. In NIP, there is no peak in the range of 1000-1250 cm^{-1} which represents the amine group of the template present in MIPs. The peaks in the range of 989-902 cm^{-1} represent the stretching vibrations of =C-H and $=CH_2$ and the peak at around 833 cm^{-1} represents the out of plane bending of =C-H and $=CH_2$. If we compare all the three polymers in terms of bonding between template and monomer it is clear from the spectra that there is a shift in the wavelength from 3421 cm^{-1} (NIP) to 3451 cm^{-1} (MIP-R1) and 3488 cm^{-1} (MIP-R2).

Morphological Study of MIP and NIP

The morphology of the molecularly imprinted polymers was done by scanning under a scanning electron microscope (SEM). From the micrograph (Fig. 2) it is clear that the synthesized polymers are spherical and in micro size. This can be concluded that the microemulsion polymerization method can be used for the synthesis of spherical polymer particles. The regular spherical shape of polymer particles widens the applicability of this method for various environmental applications. The effectiveness of using microemulsion as a solvent has been investigated (Zhang et al. 2012) and have obtained favourable characteristic of the imprinted microspheres in better molecular recognition of MIP.

Rebinding Efficiency of Polymers (MIPs and NIP)

The binding affinity of a polymer describes the binding strength between an analyte molecule (template) and the polymer. While binding capacity describes the maximum amount of analyte that can be bound with the polymer. Both binding affinity and binding capacity are determined by batch experiment (Rachkov & Minoura 2000). The batch binding process is used to observe the efficiency of a synthesized material in the way to determine the rebinding capacity of imprinted polymers. The rebinding results are used to evaluate the affinity and selectivity of the imprinted polymers for the template. In this study, two different ratios of monomer were used to achieve the best complementary sites for the template. The results revealed in Fig. 3 clearly show that the rebinding efficiency of MIP-R2 (80.50%) is highest as compared to the MIP-R1 (60.50%) and NIP (20.54%). This observable adsorption rate was due to the preferential and rapid adsorption of template molecule onto the recognition sites in the cavities of MIPs (Deilami et al. 2010). This indicates that the MIP-R2 can be used for further study, especially in the application. This means that the MIP-R2 has more complementarily binding sites for xylenol orange. The lowest rebinding efficiency of NIP is because of the lack of binding cavities

Selectivity

Based on the results reported in Table 2, it is clear that MIP-R2 has higher selectivity towards xylenol orange template compared to malachite green. The Kd of MIP-R2 towards xylenol orange is higher than malachite green, hence, MIP-R2 was favourable to extract xylenol orange. The relative selectivity coefficient is greater than 1 that favours the selectivity of MIP-R2 towards xylenol orange.

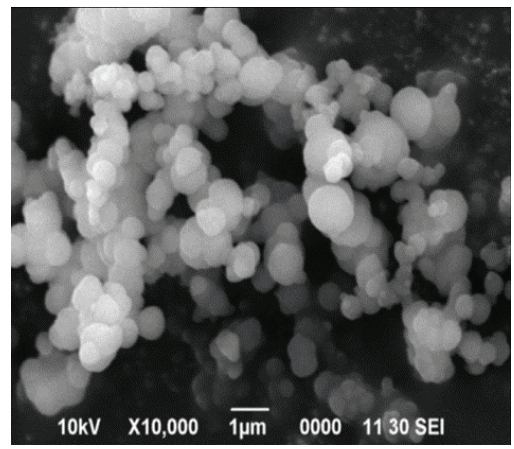

Fig. 2: SEM image of the imprinted polymer.

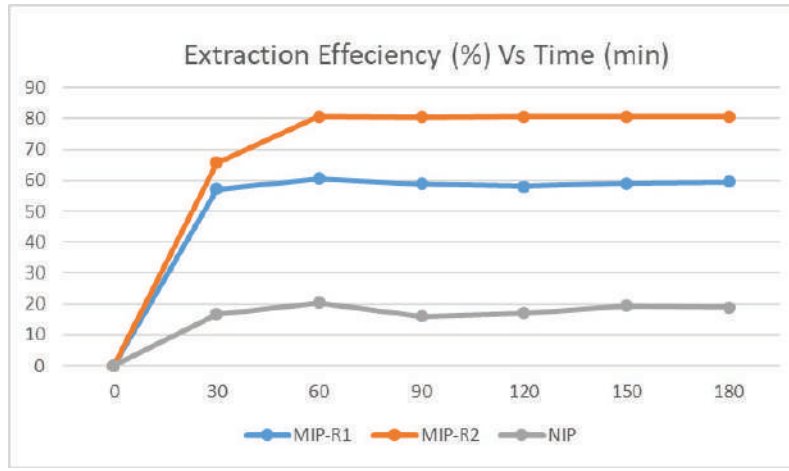

Fig. 3: Rebinding efficiency of different polymers.

Table 2: Selectivity of MIP-R2

Template	KD (MIP-R2)	KD (NIP)	*k*sel	*k*
Xylenol orange	80	20	3.2	1.6
Malachite green	25	10	2	

Removal of Xylenol Orange from Spiked Water Sample

One of the important factors is the study of the capacity of a sorbent to quantitatively remove a specific amount of dyes present in natural waters. The spiked water sample from river water was investigated for the removal of xylenol orange by using the best selected imprinted polymer. In this study, MIP-R2 and NIP were used to study the removal capacity. The results observed from the application study revealed that about 80% of xylenol orange was removed by using MIP-R2 as compared to NIP which was below 20%.

ACKNOWLEDGMENTS

Authors are thankful to the Universiti Malaysia Sarawak (UNIMAS), for providing necessary research facilities.

REFERENCES

Andersson, L., Sellergren, B. and Mosbach, K. 1984. Imprinting of amino acid derivatives in macroporous polymers. Tetrahedron Letter, 25: 5211-5214.

Arshady, R. and Mosbach, K. 1981. Synthesis of substrate-selective polymers by host-guest polymerization. Macromolecular Chemistry and Physics, 182: 687-692.

Caro, E., Marce, R.M., Borrull, F., Cormack, P.A.G. and Sherrington, D.C. 2006. Application of molecularly imprinted polymers to solid-phase extraction of compounds from environmental and biological samples. Trends Anal. Chem., 25: 143-154.

Deilami, S.A., Abdouss, M. and Seyedi, S.R. 2010. Synthesis and characterization of molecularly imprinted polymer for controlled release of tramadol. Central European Journal of Chemistry, 8(3): 687-695.

Komiyama, M., Takeuchi, T., Mukawa, T. and Asanuma, H. 2003. Molecular Imprinting from Fundamentals to Applications. Wiley-VCH, Weinheim.

Lavignac, N., Allender, C.J. and Brain, K.R. 2004. Current status of molecularly imprinted polymers as alternatives to antibodies in sorbent assays. Analytica Chimica Acta, 510: 139-145.

Lian, Z. and Wang, J. 2012. Molecularly imprinted polymer for selective extraction of malachite green from seawater and seafood coupled with high-performance liquid chromatographic determination. Marine Pollution Bulletin, 64: 2656-2662.

Lok, C. and Son, R. 2009. Application of molecularly imprinted polymers in food sample analysis - A perspective. International Food Research Journal, 16: 127-140.

Piletsky, S.A., Turner, N.W. and Laitenberger, P. 2006. Molecularly imprinted polymers in clinical diagnostics - Future potential and existing problems. Medical Engineering and Physics, 28: 971-977.

Rachkov, A. and Minoura, N. 2000. Recognition of oxytocin and oxytocin-related peptides in aqueous media using a molecularly imprinted polymer synthesized by the epitope approach. J. Chromatogr., A 889: 111.

Schreibera, T., Webera, A., Niedergalla, K., Rieglera, J., Brynioka, D., Hirtha, T. and Tovara, G.E.M. 2009. Water treatment by molecularly imprinted polymer nanoparticles. MRS Spring Meeting. Cambridge Journals Online, 11, 69.

Shinoda, K. and Lindman, B. 1987. Organised surfactant systems: Microemulsions. Langmuir, 3: 135-149.

Svenson, J. and Nicholls, I.A. 2001. On the thermal and chemical stability of molecularly imprinted polymers. Analytica Chimica Acta, 435: 19-24.

Wulff, G. and Sharhan, A. 1972. Use of polymers with enzymes-analogous structures for the resolution of racemates. Angewandte Chemie-International Edition in English, 11: 341-344.

Zhang, H., Dramou, P., He, H., Tan, S., Pham-Huy, C., & Pan, H. 2012. Molecularly Imprinted Stationary Phase Prepared by Reverse Micro-Emulsion Polymerization for Selective Recognition of Gatifloxacin in Aqueous Medi. Journal of Chromatographic Science, 250, 499-508.

Nature Environment and Pollution Technology
An International Quarterly Scientific Journal

p-ISSN: 0972-6268
(Print copies up to 2016)
e-ISSN: 2395-3454

Vol. 19 | No. 2 | pp. 831-838 | 2020

Original Research Paper

https://doi.org/10.46488/NEPT.2020.v19i02.041

Open Access Journal

Influencing Factors of Eco-Environmental Safety of Mines and Their Green Development: A Case Study of Taoshan Coal Mine in Heilongjiang Province, China

Wei Xiao Gang†, Liu Hui Li and Li Guang Hui

Department of Civil Engineering and Architecture, Zhengzhou University of Aeronautics, Zhengzhou 450046, China

†Corresponding author: Wei Xiao Gang; zzxmwxg@163.com

Nat. Env. & Poll. Tech.
Website: www.neptjournal.com

Received: 25-02-2020
Accepted: 20-04-2020

Key Words:
Mine ecology;
Eco-environment;
Ecological safety;
Influencing factors;
Green development

ABSTRACT

The demand for mineral resources is continuously increasing due to the accelerated industrialization and urbanization progress. However, most mines in China have backward mining technology, enormous destruction and waste, too low recycling proportion, unstable mineral market, and low management efficiency. Thus, the eco-environmental safety of mines has various difficulties. Identifying the influencing factors of eco-environmental safety of mines, which are typical ecologically vulnerable areas, is important. The green development of mines is a clean production mode that will not generate any harmful effect on human social and natural environments and will be important to realizing sustainable development of mines. In this study, a retrospective analysis of considerable foreign literature on eco-environmental safety management of mines in developed countries was conducted. An index system of the influencing factors of eco-environmental safety of Taoshan Coal Mine in Heilongjiang Province, China was established. ISM model (Interpretative Structural Modeling) was used to analyze the influencing factors of eco-environmental safety, and corresponding countermeasures for critical factors were proposed. Results indicate that studies on resource development and utilization and environmental protection of mines in some developed countries, such as America, Australia, and the UK, have been considerably mature. The influencing factors in ISM (Interpretative Structural Modeling) can be divided into three layers, among which the completeness of institution setting for environmental protection supervision is a factor with the most significant influence on mine eco-environmental safety. Input into eco-environmental protection and ecological protection laws and systems of mines are also important factors. The study results are important in determining the most critical influencing factors of mine eco-environmental safety, innovating the new industrial development pattern featured by conservation and intensive and comprehensive utilization of mineral resources, promoting green transformation and upgrading of the mining industry, and boosting sustainable development of the mining industry and eco-environment.

INTRODUCTION

With today's continuous and rapid development of industry-based economy, the increasingly urgent demand for mineral resources has aggravated the imbalance between supply and demand of natural resources; this situation forces enterprises to accelerate resource development. Excessive resource exploitation has caused irretrievable harms despite the enormous economic benefits it brings. Ecosystem degradation, exhaustion of natural resources, and sharp environmental deterioration have far exceeded the load, which can be carried and recovered by the environment. The triggered environmental pollution and ecological damage have hindered economic development to a certain degree. China is starting to enter a rapid development phase of industrialization, urbanization, and marketization; this situation further expands the demand and consumption of mineral resources but hastens the generation of all kinds of small-scale and private mines. The development of mineral resources has endowed enormous economic benefits and abundant material wealth improved the local economic development level and facilitated social progress. However, the unlimited exploitation has led to extreme damage. A large quantity of cultivated lands is also occupied by mining. The local original underground water balance system is destructed as well. Consequently, local people are short of drinking water and experience various geological disasters, such as surface cracking, collapse, and landslide; this situation generates a large number of chemical wastes, damages natural landscapes, and greatly impacts the surrounding environment. Moreover, the environmental quality around original mines has plummeted, and eco-environmental carrying capacity is becoming increasingly fragile.

Most mines in China, which are traditional resource-based enterprises, have facilitated national economic development. However, the continuously aggravated mine exploitation worsens the environmental situation. Unreasonable mine exploitation has resulted in environmental pollution and damage and frequent geological disasters. Although China has taken related measures and achieved good effects, the severe situation still exists in protecting the geological environment and improving the eco-environment of mines. As shown in Fig. 1, the number of people occupied in mine engineering and its operating revenue in China during 2007-2018 kept a continuous growing tendency with a certain fluctuation. Therefore, extensive exploitation of mineral resources seriously damaged the mine environment, and the surrounding environment failed to evade such impact. The exploitation of mineral resources is accompanied by many secondary disasters, some of which have endangered human living environment. Therefore, analysing the influencing factors of mine ecological safety is important to guarantee a good state of eco-environment needed by survival and development of mining areas and their surrounding ecosystems. In other words, this task does not aim to damage and threaten, mildly if ever, the mining areas as well as the life, health, and settling environment of the surrounding residents and their abilities to adapt to the environment.

PAST STUDIES

Studies on development and utilization of mineral resources and environmental protection for eco-environmental safety of mines in some developed countries, such as America, Australia, and the UK, have been quite mature through the long-term adjustment of environmental protection measures for mines. These works have opened and explored a set of paths referable by developing countries and provided many sound strategies and experience in the aspects of eco-environmental safety, green development, and environmental protection of mines. The studies involving eco-environmental safety and green development of mines are presented as follows. Lubchenco et al. deemed that eco-environmental protection should be considered an important objective of mining process and that green and sustainable mine development could be realized only when the geological environment of mines was recovered to the state before mining (Lubchenco et al. 1991). Pring et al. believed that the 21st century witnessed the industry of mineral resources entering a new era of legal regulation, discussed environmental regulation tendency in mine exploitation process, and analyzed the development status of ever-increasing international influencing laws of various phases from processing to final product in the mining industry (Pring et al. 1999). Weatherstone N. deemed that attention should be paid to the protection of wild animals and water resources in the mining process and investigated the influencing factors of sustainable development opportunity of the mining industry and the way to take these factors as the decision-making basis for sustainable development opportunity (Weatherstone 2005). Maharaj et al. comparatively analyzed the differences between original and newly generated soils in reclaimed land in the aspect of organic carbon and emphasized that organic carbon content in the land during the mining process was the basis for evaluating the quality of reclaimed land in the mining area (Maharaj et al. 2007).

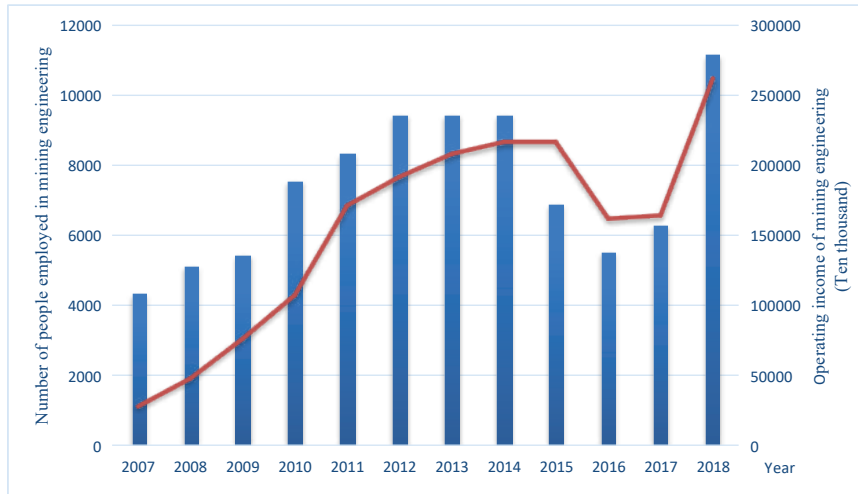

Fig. 1: Number of people occupied in mine engineering and its operation revenue in China during 2007-2018. (Data derived from National Statistic Database of China (http://data.stats.gov.cn/)).

Reddick et al. explored the potential of introducing clean production into coal mines and the processing industry in South Africa and stressed that potential clean production would remarkably mitigate the environmental pollution caused by coal mines (Reddick et al. 2008). Wu et al. believed that mine bodies had special geological conditions, backward mining technology, and imperfect management system; all these factors led to mine subsidence in a large area and generated enormous damage of mining environment and infrastructure; these authors also discussed the influence of mining subsidence on eco-environment and public infrastructure and proposed preventive measures (Wu et al. 2009). Franks et al. discussed the reactions made by the mining industry to the sustainable development in the field of waste disposal, introduced a set of sustainable development principles of disposing of mining and mineral processing-induced wastes, and highlighted urgency and necessity of taking new methods in the mining industry (Franks et al. 2011). Tripathi et al. obtained from a survey on age gradients of vegetation on 19-year wasteland in Singrauli mining area in India that soil revegetation in mines was an important management measure of relieving the negative effect of mining and improving the carbon fixation capacity of spoils in mines (Tripathi et al. 2014). Vintró et al. investigated the practice of a small and medium-sized enterprise in the open-pit mining industry in Spain. The results showed that reasonable resource exploitation was a key measure of reducing the environmental pollution. They also introduced some good examples of environmental sustainability (Vintró et al. 2014). Kopacz et al. evaluated the sustainable development level of the hard coal mining industry in Poland. The results indicated that the improvement of sustainable development of the hard coal mining industry in Poland was restricted during the period of analysis. They proved that the green mining industry considerably improved the local environmental status (Kopacz et al. 2017). Lechner et al. deemed that planning of the mining area needed to adapt to the exploitation of mineral products and energy resources and to combine the use of lands already built for agricultural development and ecological protection. They proposed a research framework regarding the development of the mining area for a case study and evaluated the scientificity of this analytical framework (Lechner et al. 2017). Stemn et al. (2019) examined the maturity level of the safety culture of Ghana mines and discussed the relationship between cultural maturity and accident rate. The results showed that the maturity score of the factor safety culture of a mine with low morbidity was always higher than those with high morbidities. The authors proposed improving and intervening fields with weak management of eco-environmental safety of mines. Zuo et al. (2019) deemed that coal mining method in China was already gradually transformed from chamber and pillar method into fully mechanized coal mining. The results showed that surface subsidence in the mining process seriously impacted the geological environment and led to seepage of underground water, decline of water level, and flow of surface water with the ground fracture. Cui et al. (2020) argued that recycling pattern of waste coal resources was the precondition and critical problem for effectively developing idle resources on abandoned mines, particularly Beijing west mining area in China. The results could provide a reference for the recycling of already closed or about to be closed underground coal mines (Cui et al. 2020). Foreign developed countries have achieved a certain performance in environmental protection of mines, which is worthy of reference by mining enterprises and governmental administrative departments in China, through multi-year research and practice. However, few comprehensive evaluation studies on eco-environmental safety of mines are available. Different regions vary in mineral resource endowment, mining technology, technical characteristics, and socio-economic background. Thus, they have greatly different main eco-environmental problems. A comprehensive discussion about their associations remains to be conducted. Meanwhile, different scholars have gaps in professional background and research perspective. Thus, they show regional and subjective features when selecting evaluation indexes and evaluation criteria for eco-environmental safety of mines. Therefore, their evaluation results cannot be compared, which restricts the popularization and application of their evaluation methods and results. Thus, the ISM model was used in the current study to calculate the influencing indexes of eco-environmental safety of a mine in China and its hierarchical structure. In the end, measures promoting green development of the mine were proposed to positively facilitate mining enterprises to take technological innovation as the internal driving force, create a sound macro-environment for reasonably guiding the release of production capacity of mining enterprises for a long time and promoting transformation and upgrading of the mining industry, and provide suggestions for gradually exploring and establishing a long-term mechanism conducive to the green development of the mining industry.

MODEL INTRODUCTION AND INDEX SYSTEM

Model Introduction (ISM)

ISM method refers to the interpretative structural modelling method. This method is developed by American Professor J N to analyze complicated problems related to the socio-economic system. This method decomposes a complicated system into several subsystems (factors) and constructs the system into a multistage hierarchical structural model using

people's practical experience and knowledge (Warfield et al. 1977). The main calculation steps of the ISM model are as follows:

Analysis of main system factors: Factor analysis is conducted, primary influencing factors of the objects are selected, and the influencing factors needed to construct the ISM model are determined. For the convenience of operation, each influencing factor can be defined as S_i.

Establishment of the adjacency matrix of influencing factors: On the basis of the overall structure of the influencing factors and their internal correlations, an adjacency matrix A is established, as shown in Formula (1).

$$A = \begin{bmatrix} a_{11}a_{12}a_{13}\cdots a_{1j} \\ a_{21}a_{22}a_{23}\cdots a_{2j} \\ a_{31}a_{32}a_{33}\cdots a_{3j} \\ \vdots \quad \vdots \quad \vdots \quad \vdots \\ a_{i1}a_{i2}a_{i3}\cdots a_{ij} \end{bmatrix} \quad \ldots(1)$$

The adjacency matrix A is obtained according to the following principles: if influencing factor S_i directly impacts S_j, then $a_{ij} = 1$; otherwise, $a_{ij} = 0$. If the influencing factor S_j directly influences S_i, then $a_{ij} = 1$; otherwise, $a_{ij} = 0$. If strong mutual influence exists between S_i and S_j, then $a_{ij} = a_{ji} = 0$.

***M* Reachable matrix *M* obtained through calculation:** After the adjacency matrix A is acquired, the sum $A+I$ of A and unit matrix $A+I$ is solved, followed by power operation of matrix $A+I$ until Formula (2) holds. Matrix M is called reachable matrix.

$$M = (A+I)^r = (A+I)^{r+1} \neq (A+I)^{r-1} \quad \ldots(2)$$

Decomposition of reachable matrix and establishment of hierarchical structure: The reachable matrix M is decomposed, and reachable set $R(S_i)$, advanced set $A(S_i)$, and the intersection set $R(S_i) \quad A(S_i)$ between the two sets are solved. According to conditions of $R(S_i) \quad A(S_i)=R(S_i)$, $R(S_i)$ is the highest factor set, and $L_1, L_2, \cdots L_K$ denote stages from the top down. $L_0 = S_\phi$ is defined, and $L(n)$ can be obtained using the iterative algorithm, that is, Formula (3).

$$L_K = \{S_i \in N - L_0 - L_1 - \cdots - L_{K-1} \,|\, R_{K-1}(S_i \cap A_{K-1}(S_i) = R_{K-1}(S_i)\} \quad \ldots(3)$$

On this basis, regional division, inter-stage division, and division of strongly connected blocks can be conducted for the reachable matrix. The row and column corresponding to the highest stage S_0 are ruled out, and the reachable and advanced sets of the next state are obtained. In the end, the hierarchy chart of the ISM model of each primary factor in the system can be obtained through the above-mentioned analysis, and the model can be further analyzed and explained.

Index System

By referring to several studies on the influencing factors of mine eco-environmental safety, 18 influencing factors of eco-environmental safety of Taoshan Coal Mine in Heilongjiang Province were concluded. An ISM research group was formed with 14 members composed of administrators of Taoshan Coal Mine, environmental experts, and local residents. The group members comprehensively analyzed the actual situation of eco-environmental safety of Taoshan coal mine. Among the 18 influencing factors, the ISM group believed that eight influencing factors were core influencing factors of Taoshan coal mine, as given in Table 1.

EMPIRICAL RESEARCH

According to basic conditions of the coal mine, the ISM group combined their own working experience in mines and studies related to the influencing factors of mine eco-environmental safety to obtain the adjacency matrix A, as given in Table 2.

According to Formula (2), the reachable matrix M, as given in Table 3, can be calculated by Matlab 2012b software.

Table 1: Influencing factors of mine eco-environmental safety.

No.	Factor	Mark
1	Input into mine eco-environmental protection	S_1
2	Institution setting of environmental regulation	S_2
3	Improvement of environmental protection methods and means	S_3
4	Mine environmental protection access mechanism	S_4
5	Environmental restoration margin mechanism	S_5
6	Governmental participation in eco-environmental protection	S_6
7	Innovation of equipment and process technology	S_7
8	Mine ecological protection laws and systems	S_8

Reachable set $R(S_i)$, advanced set $A(S_i)$, and the intersection set $R(S_i) \quad A(S_i)$ between the two are further obtained. Table 4 is obtained according to Formula (3).

Based on the above-mentioned analysis, the ISM model regarding the influencing factors of eco-environmental safety of the coal mine was established, as shown in Fig. 2.

Fig. 2 shows that the institution setting of environmental regulation (S_2) is the most significant influencing factor of eco-environmental safety of Taoshan Coal Mine. Therefore, in most grassroots mine eco-environmental safety management, environmental protection disposition of personnel at all levels of environmental protection regulators influences enterprises' environmental protection methods and means, their environmental protection culture and local participation degree in mine eco-environmental protection, and regulators' thoughts and awareness of environmental protection. This factor especially influences enterprises' cultural construction of environmental protection, shapes concepts, values, and actions in eco-environmental protection during the production and management practice of mining enterprises to a certain degree, and subconsciously influences enterprises' decision-making objectives and employees' behaviours. Input into mine eco-environmental protection (S_1) has a bearing on environmental protection methods and means, equipment renewal, use of advanced production technology, and environmental protection-related cultural construction of enterprises. Moreover, this factor facilitates enterprises to establish their own environmental protection mechanisms through local participation and law enforcement of regulators to reduce eco-environmental pollution and damage of the coal mine from source and strengthen regional eco-environmental safety. Ecological protection laws and systems (S_8) of the mine are the foundation and basis for intensifying environmental management. Environmental regulators, local participants, and responsible departments can do nothing without specific and clear environmental protection laws. Complete laws and systems can improve regulators' ideological understanding, establish complete supervision organizations, and elevate local participation degree in eco-environmental protection to achieve the results obtained through inspection and monitoring of mine eco-environmental safety. Complete laws and systems can also generate a strong promoting effect on environmental access mechanism and environmental restoration margin mechanism for mining to facilitate eco-environmental safety of the coal mine.

Table 2: Adjacency Matrix *A*.

	S_1	S_2	S_3	S_4	S_5	S_6	S_7	S_8
S_1	0	1	0	0	1	1	0	0
S_2	0	0	0	0	0	0	0	0
S_3	0	0	0	0	1	0	0	0
S_4	0	0	1	0	0	1	0	0
S_5	0	1	1	1	0	0	0	0
S_6	1	1	0	0	0	0	0	0
S_7	0	0	1	1	0	0	0	0
S_8	1	0	0	1	1	1	0	0

Table 3: Reachable matrix *M*.

	S_1	S_2	S_3	S_4	S_5	S_6	S_7	S_8
S_1	1	1	1	1	1	1	0	0
S_2	0	1	0	0	0	0	0	0
S_3	1	1	1	1	1	1	0	0
S_4	1	1	1	1	1	1	0	0
S_5	1	1	1	1	1	1	0	0
S_6	1	1	1	1	1	1	0	0
S_7	1	1	1	1	1	1	1	0
S_8	1	1	1	1	1	1	0	1

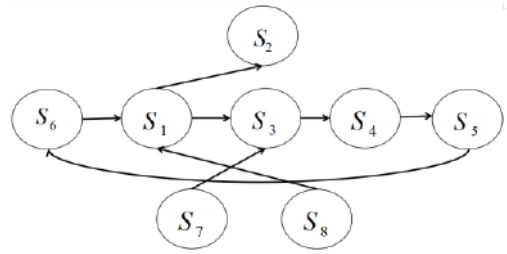

Fig. 2: Three-stage hierarchical ISM model of the influencing factors of eco-environmental safety of Taoshan coal mine.

POLICY SUGGESTIONS FOR GREEN MINE DEVELOPMENT

Establishment of Long-Term Mechanism for Green Development of the Mining Industry and Reduction in Waste of Resources

Traditional extensive management should be replaced with intensive management, and mineral resource energy structure should be optimized. Green and clean energy should be energetically developed, the proportion of non-energy sources, such as coalbed gas, natural gas, geotherm, and shale gas should be elevated, CO_2 emission should be reduced, local air quality should be improved, and occupation and damage caused by solid wastes to the mining area and surrounding lands should be decreased. Green mining industry-related supporting policies should be comprehensively studied and developed, intensive production and management should be actively encouraged, and rapid development of the mining industry with non-coal clean energy should be facilitated. A long-term mechanism for the development of green mining industry should be reasonably and scientifically constructed, and the development and development pattern coordinating high efficiency and intensiveness should be gradually formed. Special financial funds for package exploration, conservation and comprehensive utilization of mineral resources, and restoration and control of geological environment should be increased, and financing channels should be broadened to enlarge the inclination to green mining enterprises. The government should urge mining enterprises to improve their comprehensive development and utilization level of mineral resources and continuously improve their comprehensive development and utilization modes in accordance with issued construction standards for green mines. The government should also motivate enterprises to undertake social responsibilities, implement energy conservation and emission reduction, and create a good environment for the construction of green mines and the development of the green mining industry.

Broadening of Financing Channels for Mine Environmental Pollution Control and Perfecting Ecological Compensation Mechanism

The ecological compensation and restoration and environmental government work of mining enterprises should abide by the principle of "give different guidance to different enterprises," that is, different financial support policies and input modes should be implemented for different enterprises. The government should urge mining enterprises to enlarge capital investment and encourage them to construct an ecological compensation mechanism for the sake of vegetation

Table 4: Reachable and advanced sets of the influencing factors of mine ecological safety.

Factor	$R(S_i)$	$A(S_i)$	$R(S_i) \cap A(S_i)$
S_1	1,2,3,4,5,6	1,3,4,5,6,7,8	1,3,4,5,6
S_2	2	1,2,3,4,5,6,7,8	2
S_3	1,2,3,4,5,6	1,3,4,5,6,7,8	1,3,4,5,6
S_4	1,2,3,4,5,6	1,3,4,5,6,7,8	1,3,4,5,6
S_5	1,2,3,4,5,6	1,3,4,5,6,7,8	1,3,4,5,6
S_6	1,2,3,4,5,6	1,3,4,5,6,7,8	1,3,4,5,6
S_7	1,2,3,4,5,6,7	7	7
S_8	1,2,3,4,5,6,8	8	8

recovery, land reclamation, and environmental protection. In environmental governance and ecological compensation work of mining enterprises, all enterprises should raise funds for restoration and control in addition to national financial supports according to the principle of "whoever develops will be responsible for governance and control." Enterprises should be encouraged to develop and utilize associated minerals and gangues for improving the comprehensive utilization efficiency of resources. Furthermore, they should strictly implement mine eco-environmental governance margin mechanism and facilitate cooperation and coordination among iron mine enterprises, environmental protection departments, and geological department for mineral resources. By deepening integration work of mineral resources, the government can realize optimal allocation of resources. The government should practice industrialization of ecological compensation among iron mine enterprises and guide enterprises' ecological recovery and environmental governance work to a development road of the virtuous cycle.

Accelerating the Development of Green Mining Technology and Reducing Environmental Pollution to the Minimum Extent

Technological innovation is a driving force for green economic development. The application of green technology can effectively relieve the contradiction between economic development and natural resources and environment and realize the healthy and sustainable development of the mining economy. Associated and secondary resources in the development and utilization of mineral resources can be used to promote the transformation and upgrading of the traditional mining industry, hasten emerging industries, and realize the transition of consumption structure of resources and energy. The development of the green mining industry cannot be separated from a series of technical supports in the exploitation and utilization process of mineral resources, such as green exploration technology of mineral products, clean production technology, environmental monitoring technology, waste reuse technology, pollution abatement technology, and process technology used to prevent pollution. Technological innovation is conducive to the cultivation of emerging industries and improvement and upgrading of the traditional mining industry. Advanced technologies should be used to accelerate the green transformation of geological exploration, which is an advanced concept, culture, and development mode. During the field geological exploration process and under the guidance of win-win balance between green development concept and ore prospecting and environmental protection as the objective while scientific management as the precondition, advanced exploration means, methods, equipment, and processes should be used to reduce negative impacts on eco-environment and restore disturbed eco-environment to the greatest extent.

Reinforcing Law Enforcement Efforts into Mine Environmental Pollution Control and Improving Environmental Awareness

Law enforcement for mine environmental pollution and environmental protection and pollution prevention should be strengthened. The relationship between environmental law enforcement and environmental protection and environmental pollution prevention should be clearly defined. The government should define the administrative status of law enforcement, complete internal supervision and restriction mechanism in the environmental protection system, establish and perfect environmental early warming and environmental safety network covering the whole province, and realize double protection of mine environment from the angles of system and economy. The emphasis should be laid on the relationship between public and environmental protection. Various environmental protection information should be published to ensure that the public can know enterprises' consciousness of environmental protection and check, suggest, and jointly manage enterprises' environmental protection behaviours. The government should encourage public welfare organizations to unite and make joint efforts in environmental protection and hold down all kinds of ecological destruction activities from legal level. Moreover, the public should be allowed to participate in the establishment of some projects to fully utilize people's strength, protect the environment to the highest degree, and construct a cyclical and green ecosystem. Accordingly, guidance for transforming the requirement for improving the environment into practical environmental protection action can be provided.

CONCLUSION

Human production activities in the mining industry will not only promote economic development but also directly lead to land ecosystem destruction of the mines. Large-scale and high-intensity resource exploitation of Chinese mines has resulted in a contradiction between supply and demand of resources and ecological problems. The mining process shall not repeat the road of excessive consumption and low-efficiency use of mineral resources. Carrying out the evaluation research of mine ecological safety and proposing the pattern and path of constructing green mines and developing the green mining industry will be important to realizing harmony between mining and eco-environment for establishing a long-term mechanism for the development of the mining industry. A retrospective analysis of studies on mine eco-environmental management in foreign developed

countries was performed. An index system of the influencing factors of the eco-environmental safety of a mine in China was constructed, and the ISM model was used to analyze the influencing factors of mine eco-environmental safety. The results show that studies on the development and utilization of mineral resources and environmental protection in some developed countries, such as America, Australia, and the UK, have been already quite mature. The completeness of institution setting for environmental regulation is the most significant influencing factor of mine eco-environmental safety among the rest. Input into mine eco-environmental protection and mine ecological protection laws and systems are also important influencing factors. The proposed policy suggestions include establishing a long-term mechanism for the development of green mining industry, broadening the financing channels for mine environmental pollution control, accelerating the development of green mining technology, and strengthening law enforcement for mine environmental pollution. In-depth research should be conducted on exploring new patterns and paths for the development of the green mining industry, enriching the evaluation index systems for mine eco-environmental safety, using combinational evaluation method to give eco-environmental safety rating to one specific mine, and measuring and rating ecological compensation work of mining enterprises.

REFERENCES

Cui, C.Q., Wang, B., Zhao, Y.X. and Xue, L.M. 2020. Waste mine to emerging wealth: Innovative solutions for abandoned underground coal mine reutilization on a waste management level. Journal of Cleaner Production, 252: 119748.

Franks, D.M., Boger, D.V., Côte, C.M. and Mulligan, D.R. 2011. Sustainable development principles for the disposal of mining and mineral processing wastes. Resources Policy, 36(2): 114-122.

Kopacz, M., Kryzia, D. and Kryzia, K.2017. Assessment of sustainable development of hard coal mining industry in Poland with use of bootstrap sampling and copula-based Monte Carlo simulation. Journal of Cleaner Production, 159: 359-373.

Lechner, A.M., McIntyre, N., Witt, K., Raymond, C.M., Arnold, S., Scott, M. and Rifkin, W. 2017. Challenges of integrated modelling in mining regions to address social, environmental and economic impacts. Environmental Modelling & Software, 93: 268-281.

Lubchenco, J., Olson, A.M., Brubaker, L.B., Carpenter, S.R., Holland, M.M., Hubbell, S.P., Levin, S.A., Macmahon, J.A., Matson, P.A. and Melillo, J.M. 1991. The sustainable biosphere initiative: an ecological research agenda: A report from the Ecological Society of America. Ecology, 72(2): 371-412.

Maharaj, S., Barton, C.D., Karathanasis, A.D. and Rowe, H. 2007. Distinguishing" new" from" old" organic carbon in reclaimed coal mine sites using thermogravimetry: II. Field validation. Soil Science, 172(4): 302-312.

Pring, G., Otto, J. and Naito, K. 1999. Trends in international environmental law affecting the minerals industry. Journal of Energy & Natural Resources Law, 17(1): 39-55.

Reddick, J.F., Blottnitz, H.V. and Kothuis, B. 2008. Cleaner production in the South African coal mining and processing industry: a case study investigation. International Journal of Coal Preparation and Utilization, 28(4): 224-236.

Stemn, E., Bofinger, C., Cliff, D. and Hassall, M. 2019. Examining the relationship between safety culture maturity and safety performance of the mining industry. Safety Science, 113: 345-355.

Tripathi, N., Singh, R.S. and Nathanail, C.P. 2014. Mine spoil acts as a sink of carbon dioxide in Indian dry tropical environment. Science of the Total Environment, 468: 1162-1171.

Vintró, C., Sanmiquel, L. and Freijo, M. 2014. Environmental sustainability in the mining sector: Evidence from Catalan companies. Journal of Cleaner Production, 84: 155-163.

Warfield, J.N. and Fitz, R. 1977. Societal Systems: Planning Policy, Complexity. IEEE Transactions on Systems, Man, and Cybernetics, 7(10): 759-760.

Weatherstone, N. 2005. The role of the mineral reserve estimator in promoting sustainable development in the mining industry. Applied Earth Science, 114(1): 14-22.

Wu, X., Jiang, X.W., Chen, Y.F., Tian, H. and Xu, N.X. 2009. The influences of mining subsidence on the ecological environment and public infrastructure: a case study at the Haolaigou iron ore mine in Baotou, China. Environmental Earth Sciences, 59(4): 803.

Zuo, Q., Wang, Y. and Li, J. 2019. Ground Subsidence in old coal mining area and Its Geological and Ecological Environment Effect. Ekoloji, 28(108): 2429-2433.

Nature Environment and Pollution Technology
An International Quarterly Scientific Journal

p-ISSN: 0972-6268
(Print copies up to 2016)
e-ISSN: 2395-3454

Vol. 19 | No. 2 | pp. 839-844 | 2020

Original Research Paper

https://doi.org/10.46488/NEPT.2020.v19i02.042

Open Access Journal

Water Environment Carrying Capacity Evaluation by Cloud Theory in Beijing

Men Baohui† and Lina Tuoku
North China Electric Power University, Renewable Energy Institute, Beijing 102206, China
†Corresponding author: Men Baohui; menbh@ncepu.edu.cn

Nat. Env. & Poll. Tech.
Website: www.neptjournal.com

Received: 10-07-2019
Accepted: 19-09-2019

Key Words:
Water environment;
Carrying capacity;
Comprehensive evaluation;
Cloud theory

ABSTRACT

With human social and economic development, the problem of consumption and pollution of water resources greatly reduces the quality of human life. The research on the carrying capacity of the water environment can provide a theoretical basis and data support for coordinating the contradiction between man and nature and the green development of the urban economy. The driving force-pressure-state-response model evaluation index system, combined with entropy method to strike the index weight, using cloud theory calculated the level of 2004-2017 for each year of the Beijing water environmental carrying capacity. The results show that the water environment carrying capacity of Beijing has been rising in the past 14 years. It is the lowest in 2004 and tends to be stable after reaching a higher level in 2010. Despite Beijing's water environment carrying capacity has increased, but overall still in the overload state.

INTRODUCTION

Water resources interact with human life, and the quality of the water environment sustains the survival and development of mankind. With the development of human society and economy and the continuous expansion of population, the contradiction between human beings and nature has become increasingly prominent. The issue of resource and environmental carrying capacity has become an important indicator to measure the quality of development of a certain country or region and widely received by the people of the world (Wang & Li 2018). The water environment is an important environment in which humans depend. People's research on water environment carrying capacity (WECC) has been very long, although many researches have been made, there is still no consensus on the concept. However, in the existing content of the WECC, the actual content still has many similarities (Qu et al. 2017). In essence, even if the definition of WECC is different in different fields, it is a statement of the relationship between water environment and economic development and human activities. From a macro perspective, the WECC refers to the basic ability to support human production, life and social and economic development under specific preconditions. Microscopically, it refers to the ability of the water environment to effectively degrade pollutants and realize effective energy cycle based on ensuring its normality. Regardless of the type of research, we find that the water environment changes with the evolution of human society, and the actual carrying capacity has certain limits. Once this limit is exceeded, the water environment will be greatly affected, which in turn affects the normal production and life of human beings (Zhang 2018).

With the deepening of research, domestic and foreign scholars have used different methods to study the environmental carrying capacity and achieved a lot of results. Based on the analysis of Beijing wetland water resources system, Wang et al. (2017) evaluated the carrying capacity of water resources through the system dynamics model and put forward suggestions on the optimization of urban wetland management policies. Wang et al. (2018) took Zhengzhou city as the research object, used entropy weight method to allocate the weight of corresponding indexes from 2007 to 2016, and used TOPSIS model to evaluate the carrying capacity of water resources. Huang et al. (2017) took 4 subsystems coupling as the basic framework, selected 12 indicators to construct the water environment carrying capacity model, and improved the traditional catastrophe theory by using the refinement method of the ranking table to obtain the adjusted comprehensive value. Then, according to the evaluation habit, the fuzzy evaluation method is selected to determine the evaluation threshold, and the five-level evaluation method is adopted to evaluate the water environment carrying capacity, and finally, the water environment carrying capacity of Yichang City is evaluated. Zhang et al. (2015) established a comprehensive evaluation index system and compared the carrying capacity of resources and environment from 2005 to 2012 from land, water resources, transportation and the environment. Song (2016) analysed the land, water, biological environment and air pollution in the Pearl River

Delta region of China to understand the pollution situation in the region, and analysed the sustainable development of tourism resources. Based on environmental carrying capacity, they discussed the interaction mechanism between the external environment (natural, economic, social) and internal environment (tourism subject and object). Wang (2016) took Xihe River basin as the research object, constructed an index system based on Water-Ecology-Socio-Economic system, and established a System Dynamics (SD) model to deduce the carrying capacity of water resources under different circumstances, and then analysed methods to improve the carrying capacity of water resources in this basin. It can be seen that the research method of environmental carrying capacity provides better guidance for the research and practice of environmental carrying capacity improvement in different regions.

In this paper, based on the index system of comprehensive evaluation method to build the corresponding evaluation system, with Beijing as the object of evaluation, combining the entropy weight method was carried out on the related data in 2004-2017 index weight distribution, based on the cloud theory is adopted to improve the corresponding bearing capacity evaluation, to coordinate the development of social economy and the connection between the natural environment to provide the reference.

MATERIALS AND METHODS

Establishment of Evaluation Index System

The water environment not only provides the necessary material foundation for social and economic development and the ecology but also is the place which bears the pollution. To ensure the scientificity and applicability of policy suggestions, as well as the accuracy and rationality of evaluation results, it is necessary to build a reasonable and complete index system, which is also the basis of quantitative evaluation of WECC (Wang & Li 2018). Economic development and social demand will have a driving force on the water environment and human activities on water environment pressure, the driving force and pressure change the state of the water environment, according to the situation of environment and society to respond, to ease the economic, social, and human activities on water environment pressure, maintain the health and stability of the system status of water environment (Wang 2016). The above logic relations can be well reflected by the Driving Force-Pressure-State-Response evaluation model. The selection of each indicator should be based on the actual situation of the research area and should be representative and take into account the difficulty of obtaining and processing index data. Based on the above considerations, the evaluation index system of Beijing's water environment carrying capacity adopted in this paper is shown in Table 1.

According to the real situation of each index and referring to the average level of each index at home and abroad, the evaluation criteria are divided into five classes. Class I represents the extremely weak carrying capacity and serious water resources overload under this state. Class Ⅱ represents the relatively weak carrying capacity under this state, with slight water resources overload. Class III represents the matching of carrying capacity under this state with economic development. Class IV represents the state of bearing capacity is strong, has great potential for development and utilization of. Class V represents the extremely strong carrying capacity under this condition, and has great potential for development and utilization. The specific classification criteria are shown in Table 2.

Table 1: Beijing WECC evaluation index system.

Target layer	Rule layer	Index layer	Serial number	Unit	Property
Water environment capacity	Driving Force	GDP per capita	A_1	10,000 Yuan /person	+
		Urbanization rate	A_2	%	+
		Permanent population density	A_3	People/km²	-
	Pressure	Ratio of effective irrigated area to sown area	B_1	%	+
		Per capita daily domestic water consumption	B_2	L/(person·y)	-
		Forest coverage	B_3	%	+
	State	Water resources per capita	C_1	m³/person	+
		Fertilizer application per unit area	C_2	kg/hm²	-
		Chemical aerobic discharge	C_3	10,000t	-
	Response	Percentage of Sewage Disposed	D_1	%	+
		Water consumption per ten thousand Yuan GDP	D_2	m³	-
		Ecological water use rate	D_3	%	+

Survey of Research Area

Influenced by geographical and climatic conditions, the rainfall in Beijing is not evenly distributed in time and space within the year, and the per capita water resource at the end of 2017 is only 137 m^3, which is a typical mega-city with severe water resource shortage. With the rapid development of society and economy, the per capita GDP of Beijing has been increasing rapidly in recent years, and the consequent demand for water has also increased sharply. Therefore, the water resource problem is extremely urgent.

Data Information

This paper evaluated the WECC of Beijing from 2004 to 2017, and the required data come from the national bureau of statistics, Beijing water resources bulletin, Beijing statistical yearbook and other data. Through simple calculation, the final values of each indicator are shown in Fig. 1 (A_3, B_2, C_1 and C_2 data are based on the right vertical axis, while the other indicators are based on the left vertical axis). Among them, the statistical calibre and accounting method of chemical oxygen demand (COD) emission index has been adjusted since 2011.

Cloud Theory

When evaluating the bearing capacity of water environment, we can use words like strong bearing capacity, general, weak overload and other words with a certain ambiguity. There is no specific value corresponding to them, but the only vague range of value. And the range of values defined by different people is also different. It is highly random and there is no uniform standard. Cloud model (Yuan 2017) can scientifically and effectively deal with the fuzziness and randomness of such language. This method mainly uses the cloud model transformation method to quantitatively represent the qualitative language existing in people's production and life, to strengthen people's quantitative analysis of uncertain things and data operability.

Assuming the U representation domain, represented by precise numerical values, A is a qualitative concept on U, x is a qualitative language value on U. x corresponds to a degree y ($0 \le y \le 1$), is a random number with a stable trend, the distribution of y on U is called the membership cloud, referred to as the cloud, each group (x, y) becomes a cloud drop. The cloud is a map from domain U to the interval [0,1] (Ni 2018).

The cloud uses digital characteristics such as E_x (expectation), E_n (entropy), and H_e (hyper entropy) to represent its concept of uncertainty. The above three numerical features can unify fuzziness and randomness, and form a mapping relationship between qualitative concepts and quantitative values (Shao 2018).

Expectation E_x: is the value of a qualitative concept that determines the centre of gravity of the cloud. The calculation method is:

$$E_x = (B_{\min} + B_{\max})/2 \quad \ldots(1)$$

Where, B_{min} and B_{max} represent the minimum boundary and maximum boundary of an evaluation grade respectively.

Entropy E_n: the measure of the uncertainty of a qualitative concept. Because the boundary value is a kind of fuzzy boundary in the transition state and corresponds to two levels at the same time, that is, the membership degree of the two levels is equal, so there is:

$$\exp\left[-\frac{(B_{\max}-B_{\min})^2}{8E_n^{\ 2}}\right] \approx 0.5 \quad E_n = \frac{(B_{\max}-B_{\min})}{2.355} \quad \ldots(2)$$

Table 2: Beijing water environment carrying capacity evaluation grade standard.

Index	Class I	Class II	Class III	Class IV	Class V
A_1	0-1	1-3	3-5	5-7	7-13
A_2	0-60	60-70	70-80	80-90	90-100
A_3	1200-1400	800-1200	500-800	300-500	100-300
B_1	0-20	20-30	30-50	50-80	80-100
B_2	220-240	200-220	180-200	160-180	140-160
B_3	8-30	30-50	50-60	60-70	70-100
C_1	90-500	500-1000	1000-1700	1700-2600	2600-3500
C_2	550-700	490-550	420-490	360-420	0-360
C_3	45-60	30-40	20-30	15-20	0-15
D_1	0-60	60-85	85-90	90-95	95-100
D_2	300-400	250-300	150-250	50-150	10-50
D_3	0-15	15-30	30-45	45-55	55-100

Hyper entropy H_e: It is the fuzzy measure of entropy that determines the thickness of the cloud. The calculation method is:

$$H_e=k \quad \ldots(3)$$

Where, k is constant. It is determined by the fuzzy threshold of the variable itself (Qi & Zhao 2016). In this paper, k=0.1.

The cloud droplets generated by the forward cloud generator based on the digital characteristics of the cloud (E_x, E_n, H_e) are a mapping from qualitative to quantitative. This paper mainly uses forward cloud generator, and the calculation method (Zhang et al. 2017) is:

(1) First create normal random numbers E_{ni}, with E_n as the expectation and H_e^2 as the variance. Secondly, create normal random number x_i, whose expectation is E_x and variance is E_n^2.

(2) Then calculate the corresponding membership value $r_i = e^{-\frac{(x_i-E_x)^2}{2(E_{ni})^2}}$, (x_i, r_i) to form any cloud droplet in the number domain.

(3) Repeat the above process until n cloud droplets are generated.

The corresponding membership degree R is calculated by relevant steps of forward cloud generator:

$$R = \begin{pmatrix} r_{11} & r_{12} & \cdots & r_{1m} \\ r_{21} & r_{22} & \cdots & r_{2m} \\ \vdots & \vdots & \ddots & \vdots \\ r_{n1} & r_{n2} & \cdots & r_{nm} \end{pmatrix}$$

Where: n=1, 2, …, 5, m=1, 2, …,12.

The evaluation grade value $P = (p_1, p_1, \cdots, p_n)$ of water resource carrying capacity can be calculated as follows:

$$P = W \times R \quad \ldots(4)$$

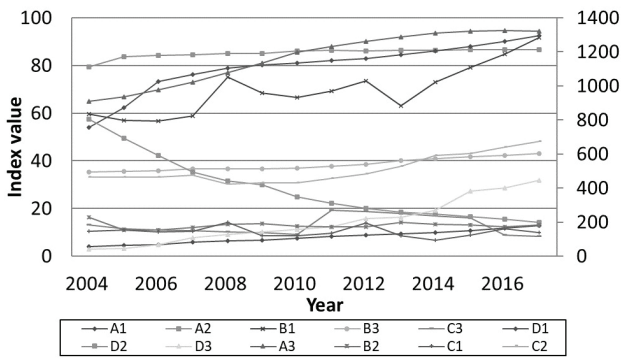

Fig. 1: Original data of each indicator.

Where, W is the weight of each index, which is determined by the entropy weight method in this paper.

Entropy Weight Method

Entropy weight method is a comprehensive and objective method to reflect the characteristics of information contained in index data by using original data. It is widely used in various fields of statistics. In this paper, the entropy weight method is adopted to allocate the weight of evaluation indicators. The specific steps are as follows.

To eliminate the dimension of each index value and unify the variation range of each index value, the following formula is adopted for normalization.

$$\begin{cases} y_{ij}=\frac{x_{ij}-x_{j\min}}{x_{j\max}-x_{j\min}} & \textit{Positive indicators} \\ y_{ij}=\frac{x_{j\max}-x_{ij}}{x_{j\max}-x_{j\min}} & \textit{Negative indicators} \end{cases} \quad \ldots(5)$$

$i = 1,2, \cdots, I. j = 1, 2, \cdots, J$

Where, x_{ij} refers to the initial value of the ith indicator to be evaluated in the jth year. y_{ij} refers to the standardized value of the jth year indicator. $x_{j\max}$, $x_{j\min}$ refers to the maximum and minimum value of the (ith) index sequence.

Each evaluation index has a different influence on the evaluation of water environment bearing capacity, so the evaluation index should have different weight. The calculation formula of information entropy w_j is as follows:

$$w_j = \frac{1-e_j}{\sum_{j=1}^{m}(1-e_j)} \quad \ldots(6)$$

Where: $e_j = -\frac{1}{\ln n}\sum_{i=1}^{n} H_{ij} \ln H_{ij}$, $H_{ij} = \frac{y_{ij}}{\sum_{i=1}^{n} y_{ij}}$., .

THE ANALYSIS AND RESULTS

To reduce the influence of human subjective factors on the weight distribution, the data in Fig. 1 are firstly normalized by equation (5), and the weights of each index are calculated by equation (6) of the entropy weight method. The final weights are 0.092, 0.030, 0.172, 0.121, 0.037, 0.137, 0.064, 0.057, 0.082, 0.040, 0.049, 0.119. Put this weight into cloud theory, and get the digital characteristics of cloud from equations (1)-(3), as given in Table 3.

According to the corresponding index values, weights and digital features, the forward generator algorithm is used to generate the membership matrix, and then the bearing capacity evaluation results are obtained, as provided in Table 4.

To further analyse the development trend of WECC of Beijing in recent years, the trend chart of water environment carrying capacity for each year from 2004 to 2017 is drawn according to the results in Table 4, as shown in Fig. 2. The

year is in the horizontal axis, and the value of water environment carrying capacity is in the vertical axis. According to the principle of entropy weight method and the evaluation grade standard established, the larger the evaluation value of the water environment carrying capacity is, the better the water environment carrying capacity is.

It can be seen from the above results that the carrying capacity of Beijing's water environment has entered a relatively stable state after rapid improvement in the past 14 years. Combining the results of other scholars' research (Qi & Zhao 2016, Liu 2018, Han et al. 2018) on the WECC in Beijing, the results are similar.

It is believed that the carrying capacity of Beijing has been on the rise in the past 14 years, with the lowest carrying capacity in 2004 and stabilizing after reaching a higher level in 2010. From 2004 to 2010, the carrying capacity level of the water environment increased rapidly year by year. This may be due to the low rate of urbanization around 2004. And affected by the technical level, the effective irrigation rate per unit area is not high, COD and sewage treatment rate have room for progress, and the public awareness of environmental protection is not strong enough. But with the development of cities, the industrial structure has changed greatly. The annual industrial output value of Beijing has been growing, while the industrial water consumption has been decreasing. The agricultural industrial structure is gradually adjusting to the direction of water-saving agriculture, which makes the ratio of effective irrigation area to sowing area increase year by year, thus slightly relieving the overload of bearing capacity.

From 2010 to 2014, there was a slight decrease, and the corresponding resident population density continued to increase, which will increase the bearing pressure to some extent. Fundamental changes have taken place in people's forms of water use, such as the rapid development of the food and lodging industry, the popularity of household shower equipment and water appliances, the adjustment of water prices and the equipment of water-saving equipment, etc. On the one hand, the pressure will be alleviated, which can be reflected by the fluctuation of per capita daily water consumption. Since 2011, the statistical calibre and accounting method of chemical oxygen demand (COD) emission index have been adjusted, so the chemical oxygen demand emissions around 2010 have obvious fluctuations, which will inevitably have a greater impact on the evaluation results, which may lead to the highest level of water environment carrying capacity in 2010, and the decline after 2010.

Table 3: Digital characteristics of clouds.

Index	A_1	A_2	A_3	B_1	B_2	B_3	C_1	C_2	C_3	D_1	D_2	D_3
	5	30	1300	10	230	19	295	625	50	30	375	7.5
	2	65	1000	25	210	40	750	520	35	72.5	300	22.5
E_x	4	75	650	40	190	55	1350	455	25	87.5	200	37.5
	6	85	400	65	170	65	2150	390	17.5	92.5	100	50
	10	95	200	90	150	85	3050	180	7.5	97.5	30	77.5
	0.4	25.4	84.9	8.5	8.5	9.3	174.1	63.7	8.5	25.5	21.2	6.4
	0.8	4.2	169.9	4.2	8.5	8.5	212.3	25.5	4.2	10.6	42.5	6.4
E_n	0.8	4.2	127.4	8.5	8.5	4.2	297.2	29.7	4.2	2.1	42.5	6.4
	0.8	4.2	84.9	12.7	8.5	4.2	382.2	25.5	2.1	2.1	42.5	4.2
	2.5	4.2	84.9	8.5	8.5	12.7	382.2	152.9	6.4	2.1	17.0	19.1

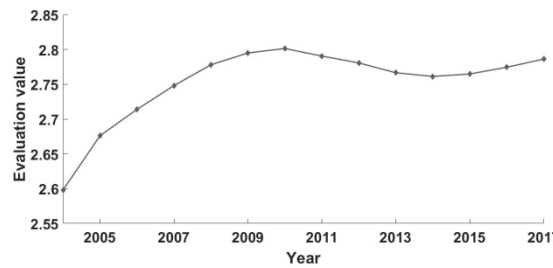

Fig. 2: Trend of water environment carrying capacity in Beijing.

Table 4: The evaluation results.

Year	2004	2005	2006	2007	2008	2009	2010
Result	2.598	2.676	2.714	2.748	2.778	2.795	2.801
Year	2011	2012	2013	2014	2015	2016	2017
Result	2.791	2.781	2.767	2.761	2.765	2.774	2.786

Compared with other years, the total amount of water resources in 2014 was relatively low. Although the technical level was improved, the carrying capacity was slightly reduced due to the great influence of climate on the water resource environment. The carrying capacity increased slowly after 2014, and the ecological water use rate showed a trend of rapid growth after that year. The forest coverage rate also increased slowly since 2013, indicating that people are more and more aware of the importance of environmental protection. Besides, the implementation of the south-to-north water diversion project can relatively alleviate the water pressure in Beijing. From 2015 to 2017, the chemical aerobic discharge has a tendency to decrease, which also alleviates the pressure on the water environment to some extent. However, due to the limitation of large population base and other factors, the carrying capacity has not been significantly improved.

CONCLUSIONS

In this paper, an evaluation index system is constructed based on the model of Driving Force-Pressure-State-Response. Entropy weight method can reduce the interference of human factors on weight distribution, and cloud theory can effectively take into account the fuzziness and randomness of concepts. Both methods have relatively objective results. Through the analysis of the evaluation model established by the organic combination of the two methods, relatively reliable evaluation results can be obtained. Although the carrying capacity level in Beijing in recent years has been improved to a certain extent, the overall state is still overloaded. The pressure on its sustainable use of water resources remains high. As a mega-city with a large population, Beijing is faced with problems such as water shortage and large population pressure. Therefore, while vigorously developing economy and urban construction, we should avoid pursuing economic growth and neglecting the negative impact of population concentration. We should give full play to the role of economic leverage, according to the needs of economic and social development "selective" to attract the population, increase the non-capital function evacuation, and reduce the mismatch of resources waste, to obtain the greatest social, economic and ecological benefits.

ACKNOWLEDGEMENTS

This work was supported by the National Key R& D Program of China (Grant No. 2016YFC0401406), and the Famous Teachers Cultivation planning for Teaching of North China Electric Power University (the Fourth Period).

REFERENCES

Han, Y., Zhang, S.F. and Lv, A.F. 2018. Study on the impact of foreign water transfer on the carrying capacity of water resources in Beijing, Tianjin and Hebei. Resource Science, 40(11): 2236-2246.

Huang, X., Chen, H.T. and Guan, Z.Y. 2017. Study on water environmental carrying capacity based on improved catastrophe theory. Nature Environment and Pollution Technology, 16(4): 1223-1228.

Liu, W. 2018. Study on the change of ecological environment carrying capacity- taking Beijing as an example. Price Theory and Practice, (09): 74-77.

Ni, X.P. 2018. Research on the navigation safety evaluation of Bayuquan harbor based on cloud theory. Dalian Maritime University.

Qi, X. and Zhao, Q. 2016. Water environment carrying capacity evaluation in Beijing. Ecological Economy, 32(02): 152-155.

Qu, H., Bao, J.L. and Zhang, W. 2017. Analysis and prospect of water environment bearing capacity. Journal of Hebei University of Geosciences, 40(5): 25-30.

Shao, N.H. 2018. Application of uncertainty reasoning model based on cloud theory in runoff prediction. Water Technology and Economy, 24(9): 62-66.

Song, D.Y. 2016. Countermeasure study on sustainable utilization of tourism resources and tourism environmental pollution in coastal areas of the Pearl River Delta, China. Nature Environment and Pollution Technology, 15(3): 873-879.

Wang, C.H., Hou, Y.L. and Xue, Y.J. 2017. Water resources carrying capacity of wetlands in Beijing: analysis of policy optimization for urban wetland water resources management. Journal of Cleaner Production, 161: 1180-1191.

Wang, H., Yu, W.X. and Jia, Y.Z. 2018. Comprehensive evaluation of water resources carrying capacity of Zhengzhou city. Water Conservancy Economy, 36(6): 57-61,74.

Wang, L.P. and Li, S.Q. 2018. Research progress on resource and environment carrying capacity. Resource Development and Market, 34(5): 644-648.

Wang, Y. 2016. Research on carrying capacity of water resources in Xihe River basin based on SD model. Hydroelectric Power, 42(6).

Yuan, L.W. 2017. Study on comprehensive evaluation of driving safety of mountain road landscape based on cloud theory. Kunming University of Science and Technology.

Zhang, A., He, J. and Chen, X.N. 2017. Research on evaluation model of regional water resource carrying capacity based on cloud theory. Water Conservancy and Hydropower Technology, 48(1): 18-22.

Zhang, J.S., Hu, X.Z., Li, Q. and Kopytov, C. 2015. Evaluation and comparison of the resource and environmental carrying capacity of the 10 main urban agglomerations in China. Nature Environment and Pollution Technology, 14(3): 573-578.

Zhang, Q. 2018. Research methods and development trend of water environment carrying capacity analysis and discussion. Chemical Management, (31): 101-102.

Nature Environment and Pollution Technology
An International Quarterly Scientific Journal

p-ISSN: 0972-6268
(Print copies up to 2016)
e-ISSN: 2395-3454

Vol. 19 | No. 2 | pp. 845-850 | 2020

Original Research Paper

https://doi.org/10.46488/NEPT.2020.v19i02.043

Open Access Journal

Biodegradation of Textile Wastewater by Naturally Attenuated *Enterobacter* sp.

N. Sharma*†, H. Bhagwani*, N.Yadav* and D. Chahar**

*Environmental Microbiology and Toxicology Lab, Department of Zoology, Poddar International College, Sector-7, Shipra Path, Mansarovar, Jaipur-302020, India

**Department of Zoology, Shri R. K. Post Graduate College, Bissau, Jhunjhunu-331027, Rajasthan, India

†Corresponding Author: N. Sharma; nehamicrobiologist@gmail.com

Nat. Env. & Poll. Tech.
Website: www.neptjournal.com

Received: 06-08-2019
Accepted: 29-08-2019

Key Words:
Anthropogenic;
Biodegradation;
Enterobacter sp.;
Natural attenuation;
Textile effluent;
RBRR

ABSTRACT

The exponential increase in anthropogenic activities has led to the accumulation of xenobiotics into the environment, synthetic dyes being one of the culprits. Noteworthy is the fact that the textile industry utilizes enormous volumes of water for dyeing and printing unit operations thereby generating wastewater proportionately. Taking into consideration, implications of toxic textile effluents, a pilot study was planned to screen for naturally attenuated bacterial isolates capable of degrading textile effluents. Requisite effluent samples were collected from Kelki Printers Co-operative Society Limited, Sanganer, Jaipur and bacterial screening was carried out by bioaccumulation of Remazol Brilliant Blue R (RBRR) (formation of halo around colonies). Of the 19 bacterial isolates obtained, the most promiscuous isolate was biochemically characterized as *Enterobacter* sp. For biodegradative investigations, it was inoculated in sterilized textile effluent and incubated at 37°C for 7 days under agitating conditions. Pre and post bacterial inoculation (1% v/v), Physico-chemical parameters were analysed following standard procedures. A significant ($p<0.05$) lowering of pollution indicators was monitored when contrasted with abiotic control. The present study was aimed to explore the role of naturally attenuated and effluent adapted *Enterobacter* sp. screened from untreated textile effluent based on its colour (RBRR) removal efficacy under *in vitro* conditions. Furthermore, it was also explored for its biodegradative properties to minimize the level of potential pollution indicators through the microcosm approach. This pilot study based on a three-tier approach encompassing bioprospecting, bio enrichment and bioaugmentation plausibly provided insights for enhanced degradation of real dye wastewaters by unlocking the biochemical pathways of adapted microbes.

INTRODUCTION

Attainment of Sustainable Development Goals (SDGs) has become questionable in the current scenario, taking into account the ever-increasing concerns of environmental pollution. Industrial practices have contributed to socio-economic development but lack of sustained industrial practices aggravates bioaccumulation and persistence of toxicants. Synthetic dyes are extensively used by textile industries leading to the generation of enormous volumes of coloured effluents post dyeing and printing process (Sharma et al. 2019). Besides synthetic dyes, effluents are composed of heavy metals, bleaching agents, surfactants and other recalcitrant compounds (Mondal et al. 2017). Mainstream investigations have focused upon evaluation of physico-chemical profile of textile effluents and their potential toxicological implications (Bhatia et al. 2018).

Catering to address toxicity hazards generated by textile effluents, biological interventions utilizing the role of indigenous microbes for biodegradation have been investigated in recent past (Chanwala et al. 2019, Vikrant et al. 2018). Majorly, bacteria have been explored for their metabolic potential to degrade synthetic dyes, heavy metals and chemical surfactants from dye house effluents. Different mechanisms have been explored for microbial mediated dye removal like biosorption (Solis et al. 2012), biodegradation by catalytic enzymes like azoreductase (Ehlfarash et al. 2017), laccase (Mirzadeh et al. 2014), peroxidase (Saroj et al. 2014).

Considering the above-cited facts, we proposed an *in situ* bioremediation study wherein, the role of microbes native to dye house effluent was explored to biodegrade textile effluent based on its dye removal efficacy in synthetic medium.

MATERIALS AND METHODS

Study Area: Sanganer town with co-ordinates (26°49′ to 26°51′N latitude and 75°46′ to 75°51′ longitude) is located within outskirts of Jaipur, famous for its ethnic hues, hand-

made paper and block prints. It houses around 700 small and medium textile units which release toxic effluents into adjoining drains (Tambi 2013).

Sampling: Kelko Printers Co-operative Society Limited, Sanganer, Jaipur (Fig. 1a) was chosen for the collection of requisite samples (Fig. 1b) which were transported and stored following standard procedures (APHA 2000).

Screening and characterisation of indigenous bacteria: Naturally attenuated bacterial strains were isolated from textile effluent and qualitatively screened by plate assay by supplementing Remazol Brilliant Blue R (RBRR) dye (1% w/v) in Nutrient Agar with following composition (Table 1) (Shah 2014). Based on the formation of halo, the most promising strain was biochemically characterized (Cappucino & Shermann 2009).

Table 1: Composition of Nutrient Agar.

S. No	Component	Quantity (g)
1	Beef extract	3
2	NaCl	5
3	Peptone	5
4	Agar	15
5	Remazol Brilliant Blue R	1
6	Distilled Water	1000 mL

Acclimatisation assay: The screened isolate was grown in Nutrient Broth (NB) (composition similar to Nutrient Agar with the exclusion of agar) comprising two sets. In the first set, RBRR was amended (1% w/v) (NBD), while another set was devoid of RBRR and was referred to as negative control (NBND). Both the sets were incubated at 37°C for 24 to 48 hours under agitated conditions (120 rpm) till a desirable ($O.D._{600}$= 0.6) was attained (Sharma et al. 2019).

Biodegradation assay: Heat killed effluent (500 mL) was inoculated with acclimatized bacterial cells (1%w/v) (TEXE). Similarly, 500 mL heat-killed effluent devoid of inoculum (TEXC) was used as abiotic control to obliterate the role of pre-existing micro-flora in a biodegradation study (Bennet et al. 2002) (Fig. 2).

Pre-sterilized textile effluent samples were analysed for the reduction in pollution indicators viz. colour, pH, biochemical oxygen demand (BOD), chemical oxygen demand (COD), chloride, nitrate and phosphate (APHA 2000). Degradation study was carried out following the protocol devised by Rajeswari et al. (2013). Briefly, aliquots of samples (50 mL) were withdrawn and centrifuged at 4,000

Fig. 1a: Sampling site.

Fig. 1b: Raw textile effluent.

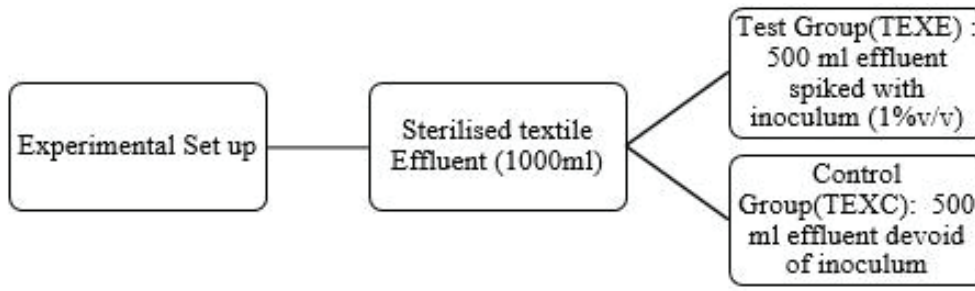

Fig. 2: Experimental set-up for biodegradation study.

rpm (REMI CM-8 Plus) for 15 minutes to remove biomass. Bio-efficacy of bacterial strains to reduce pollution indicators was analysed in Cell-Free Extract (CFE) and expressed as % pollutant removal (Sharma et al. 2014) as shown in the following equation:

$$\%\ Pollutant\ Removal = \frac{TEXC\left(\frac{mg}{L}\right) - TEXE\left(\frac{mg}{L}\right)}{TEXC\left(\frac{mg}{L}\right)} \times 100 \quad \ldots(1)$$

RESULTS AND DISCUSSION

Screening and characterisation of indigenous bacteria: Based on the halo formation, the most potential bacterial isolate was biochemically characterized as *Enterobacter* sp. (Fig. 3a). Formation of halo around bacterial colonies (Fig. 3b) is the phenomenon attributed to uptake of dye by cell membranes and/or cell walls through physical adsorption, electrostatic interaction, ion exchange, chelation and chemical precipitation and the structure remains intact (Ali 2010) concomitant with accumulation of redox-active enzymes or biochemical substances being released into medium during the growth of bacterial cells (Khalid et al. 2008). Screening of micro-organisms from dye contaminated sites has gained momentum in the recent past, the strategy being explored for biodegradation of textile effluents (Lalnunhlimi & Krishnaswamy 2016). Chaube et al. (2010) analysed soil samples collected from Nag Nadi (River) for isolation of dye degrading bacteria and found the isolates to be chromogenic mixture used for differentiation of organism found to be *Proteus* sp., *Pseudomonas* sp. and *Enterococcus* sp.

Acclimatisation assay: Bacterial growth curve was plotted as a measurement of $O.D_{600}$ versus incubation duration (in hours) (Fig. 4).

Enterobacter sp. was grown in nutrient broth amended with RBRR (1% w/v) and growth pattern was observed. Growth was found to be significantly increased ($p<0.05$) under dye induced conditions (NBD) (Sinha et al. 2009) attributing to the utilization of dye as a sole source of carbon and energy (Agarval & Singh 2012). Kuberan et al. (2011) reported a higher concentration of protein in *Listeria sp.* under (Black B) dye induced conditions. Contrary to the above-cited fact, Anjanyulu et al. (2005) have speculated the possibility that upon utilization of pollutants as a sole source of carbon and nitrogen, it is the toxicological manifestation which is apparent thus deteriorating the bacterial growth.

Biodegradation assay: A significant reduction in pollution indicators ($p<0.05$) of pre-sterilized textile effluent was adjudged as bioefficacy of *Enterobacter* sp. when contrasted with abiotic control and was expressed as per cent decrease. Table 2 elucidates the reduction in Physico-chemical properties in the effluent. The values are expressed at Mean ±S.D.

Colour: Our findings suggested, the dark blue colour of the effluent is attributed to excessive usage of anthraquinone dyes, Remazol Brilliant Blue R (RBRR) being commonly used for dyeing of cotton fabrics (Velayutham et al. 2018). Post bacterial treatment, 57.3% colour was removed owing to bacterial biosorption which is accumulation of chemicals and dyes by microbial mass (Bras et al. 2001).

pH: The pH of textile effluent was found to be 12 which is reportedly found to be associated with the use of bleaching agents and chemicals like sodium hypochlorite, sodium hydroxide, sodium phosphate and surfactants (Paul et al.

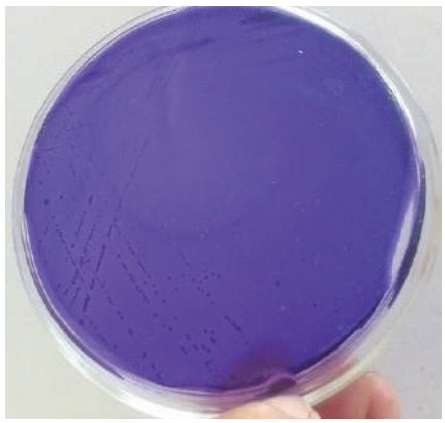

Fig. 3a: Pure culture of *Enterbacter* sp.

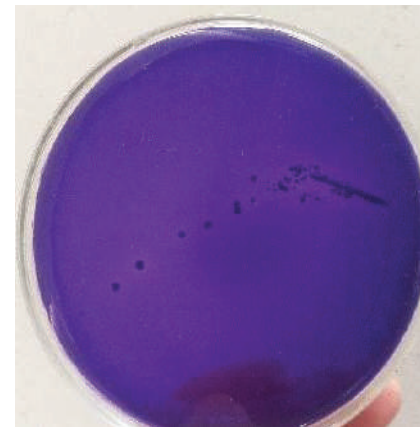

Fig. 3b: Halo around bacterial colonies.

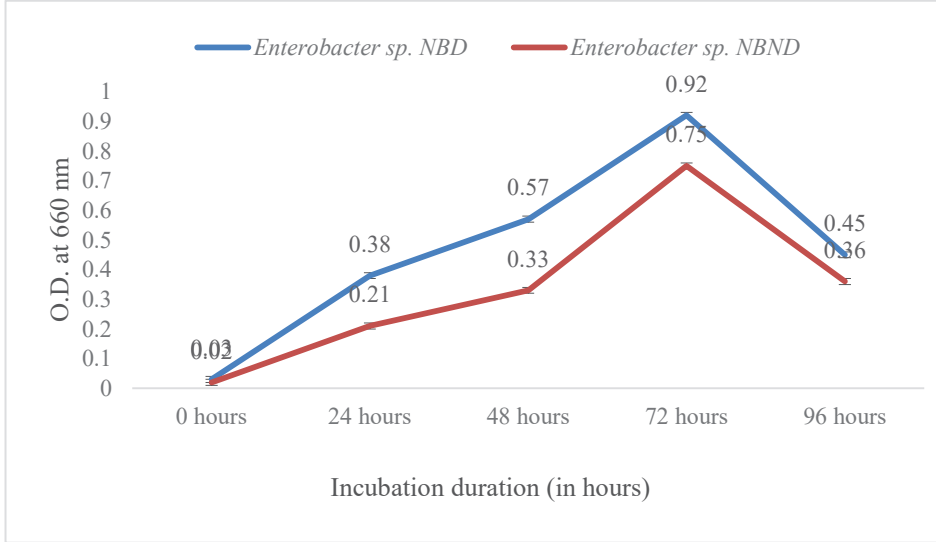

Fig. 4: Bacterial growth curve under dye induced and uninduced conditions.

2012). A similar trend (11.3±1.6) in pH of textile effluent was reported in our previous study (Sharma et al. 2013).

BOD: It is estimated as the amount of oxygen required for oxidation of organic matter by microbes. Significantly, the reduction of 54.8% (130±0.28 mg/L) was observed. High load of organic and inorganic constituents contributes to depletion in dissolved oxygen (DO) and an increase in BOD (Garg & Kaushik 2008).

COD: It determines the amount of chemically oxidizable organic matter. We observed a reduction of 61.1% (270±0.36 mg/L) in the bacterially treated effluent. Previously, we explored the effect of different inoculum concentration of monocultures and bacterial consortium for COD reduction in textile effluents (Sharma et al. 2014). Sur & Mukhopadhya (2017), have explored the potential of *Pseudomonas aureofaciens* and *Escherichia coli* using three-phase fluidized bioreactor for COD reduction in textile effluent.

Nitrate: Our findings reported a reduction of 16% (11.5±0.06 mg/L) owing to bio×efficacy of *Enterobacter* sp. Saharimoghaddam et al. (2018) explored the combinatorial effect of Gambusia fish and *Phragmites australis* in constructed wetlands for nitrate reduction in textile effluent. The biological denitrification is recommended for the removal of relatively low concentration of nitrogen components and it is operated by the so-called denitrifying bacteria in anoxic conditions, where they use nitrates as electron acceptors during their respiratory process in the place of the oxygen (Sharma & Dwivedi 2017).

Table 2: Reduction in Physico-chemical attributes of textile effluent post bacterial treatment.

Pollution indicators	Units	TEXC	TEXE	% Pollutant Removal $= \frac{TEXC\ (\frac{mg}{L}) . - TEXE(\frac{mg}{L})}{TEXC(\frac{mg}{L})} \times 100$
Colour	-	Dark blue	Light blue	57.3
pH	-	12±0.1	8±0.07	33.3
BOD	mg/L	278±0.4	130±0.28	54.8
COD	mg/L	670±0.32	270±0.36	61.1
Nitrate	mg/L	13.7±0.06	11.5±0.06	16.0
Phosphate	mg/L	13.9±0.03	9.5±0.04	10.5

Phosphate: Different types of chemicals used in unit processes and unit operations contribute to high phosphate levels (Metcalf & Eddy 2003). Post bacterial inoculation, 10.5 % (9.5±0.04 mg/L) reduction was observed. Enhanced Biological Phosphate Removal (EPBR) has been investigated in industrial wastewaters, the fact based on extrapolation of bacterial metabolism leading to biomineralization of phosphate (Sharma 2018).

CONCLUSION

Textile effluents are characterized by the presence of synthetic colourants, heavy metals, bleaching agents, chlorinated compounds and other xenobiotic compounds significantly contributing to excessive water pollution. Microbes adapted to a harsh environment have been known to degrade and mineralize toxic components of effluents. The present study was aimed to explore the role of naturally attenuated and effluent adapted *Enterobacter* sp. screened from untreated textile effluent based on its colour (RBRR) removal efficacy under *in vitro* conditions. Furthermore, it was also explored for its biodegradative properties to minimize the level of potential pollution indicators through the microcosm approach. This pilot study based on a three-tier approach encompassing bioprospecting, bioenrichment and bioaugmentation plausibly provided insights for enhanced degradation of real dye wastewaters by unlocking the biochemical pathways of *Enterobacter* sp. which led to biodegradation. Further, our lab is focused on developing fungal-bacterial consortium for *in situ* bioremediation models.

ACKNOWLEDGEMENTS

The authors thank authorities of Poddar International College, Jaipur for providing necessary infrastructural facilities, Kelko Printers Co-operative Society Limited, Sanganer, Jaipur for requisite sample collection and Department of Science and Technology, Government of Rajasthan, Jaipur for providing financial assistance under the Sanctioned Project Biotechnology Business Incubator [F 15(12) DST/EDP-SDP/2017-18/Part I/6032].

REFERENCES

Agarval, T. and Singh, R. 2012. Bioremedial potential of a moderately halophilic soil bacteria. Journal of Pharmaceutical and Biological Sciences, 19(16): 1-6.

Ali, H. 2010. Biodegradation of synthetic dyes-a review. Water, Air & Soil Pollution, 213(3): 251-273.

Anjaneyulu, Y., Sreedhara, N.C. and SumanRaj, D.S. 2005. Decolourisation of industrial effluents - available methods and emerging technologies – A Review. Reviews in Environmental Science and Biotechnology, 4: 245–273.

APHA 2000. Standard Methods for Examination of Waters and Wastewater. American Public Health Association, Washington American Water Works Association (AWWA), Water Environment Federation (WEF) Washington DC USA (20th Ed.).

Bennet, J.W., Wunch, K.G. and Faison, B.D. 2002. Use of Fungi Biodegradation. Manual of Environmental Microbiology, (2nd Ed.) ASM Press, Washington, D.C., pp. 960-971.

Bhatia, D., Sharma, N.R., Kanwar, R. and Singh, J. 2018. Physicochemical assessment of industrial textile effluents of Punjab (India). Applied Water Sciences, 8(83): 1-12.

Bras, R., Ferra, I.A., Pinheiro, H.M. and Goncalves, I.C. 2001. Batch tests for assessing decolourisation of azo dyes by methanogenic and mixed cultures. Journal of Biotechnology, 89(2-3): 155-62.

Cappucino, J.G. and Shermann, N. 2009. Microbiology: A Laboratory Manual. 6th Edition. Pearson Education. Benjamin Cummings, San Francisco.

Chanwala, J., Kaushik, G., Ashraf, D.M., Upadhyay, S. and Agrawal, A. 2019. Process optimization and enhanced decolorization of textile effluent by *Planococcus* sp. isolated from textile sludge. Environmental Technology and Innovation, 13:122-129.

Chaube, P., Indurkar, H. and Moghe, S. 2010. Biodegradation and decolorization of dye by mix consortia of bacteria and study of toxicity on *Phaseolus mungo* and *Tritium aestivum*. Asiatic Journal of Biotechnology and Research, 1: 45-56.

Ehlfarash, A., Mawaad Asma, M.M., Yousef Naeima, M.M. and Shoreit Ahmed, A.M. 2017. Azoreductase kinetics and gene expression in synthetics dyes-degrading *Pseudomonas* sp. Egyptian Journal of Basic and Applied Sciences, 4: 215-222.

Garg, V.K. and Kaushik, P. 2008. Influence of textile mill wastewater irrigation on growth of sorghum cultivars. Applied Environmental Research, 6:1-12.

Khalid, A., Arshad. M. and Crowley, D.E. 2008. Accelerated decolorization of structurally different azo dyes by newly isolated bacterial strains. Applied Microbiology and Biotechnology, 78(2): 361-369.

Kuberan, T., Anburaj, J., Sundaravadivelal, C. and Kumar, P. 2011. Biodegradation of azo dye by *Listeria* sp. International Journal of Environmental Sciences, 1: 1760-1770.

Lalnunhlimi, S. and Krishnaswamy, V. 2016. Decolorization of azo dyes (Direct Blue 151 and Direct Red 31) by moderately alkaliphilic bacterial consortium. Environmental Microbiology, 47: 39-46.

Metcalf and Eddy 2003. Wastewater Engineering: Treatment and Reuse. 4th Ed., McGraw-Hill, Boston.

Mirzadeh, S.S., Khezri, S.M., Rezaei, S., Forootanfar, H., Mahvi, A.H. and Faramarzi, M.A. 2014. Decolorization of two synthetic dyes using the purified laccase of *Paraconiothyrium variabile* immobilized on porous silica beads. Journal of Environmental Health, Science and Engineering, 12: 1-9.

Mondal, P., Baksi, S. and Bose, D. 2017. Study of environmental issues in textile industries and recent wastewater treatment technology. World Scientific News, 61: 98-109.

Paul, S.A., Chavan, S.K. and Khambe, S.D. 2012. Studies on characterization of textile industrial wastewater in Sholapur city. International Journal of Chemical Sciences, 10: 335-342.

Rajeswari, K., Subhaskumar, R. and Vijayaraman, K. 2013. Decolorization and degradation of textile dyes by *Stenotrophomonas maltophila* RSV-2. International Journal of Environmental Bioremediation and Biodegradation, 1: 60-65.

Saharimoghaddam, N., Massoudinejad, M. and Ghaderpoori, M. 2018. Removal of pollutants (COD, TSS, and NO_3^-) from textile effluent using Gambusia fish and *Phragmites australis* in constructed wetlands. Environmental Geochemistry and Health. 41(3): 1433-1444.

Saroj, S, Karunesh, K., Prasad, M. and Singh, R. 2014. Differential expression of peroxidase and ABC transporter as the key regulatory components for degradation of azo dyes by *Penicillium oxalicum* SAR-3. Functional & Integrative Genomics, 14(4): 631-642.

Shah, M.P. 2014. Microbial degradation of textile dye (Remazol Black B)

by *Bacillus* sp. ETL-2012. Journal of Applied Environmental Microbiology, 1: 6-11.

Sharma, N. 2018. Screening of phosphate accumulating bacteria (PAB) from dairy wastewater. International Journal of Pharma and Bio Sciences, 9: 102-107.

Sharma, N. and Dwivedi, A. 2017. Bioremediation of dairy wastewater for nitrate reduction. World Journal of Pharmaceutical and Life Sciences, 3: 375-384.

Sharma, N., Chatterjee, S. and Bhatnagar, P. 2019. Degradation of Direct Red 28 by *Alcaligenes* sp. TEX S6 isolated from aeration tank of common effluent treatment plant (CETP), Pali, Rajasthan. Nature Environment and Pollution Technology, 18: 9-20.

Sharma, N., Saxena, S., Fatima, M., Iram, B., Datta, A. and Gupta, S. 2014. Microcosm analysis of untreated textile effluent for cod reduction by autochthonous bacteria. International Journal of Current Research in Chemistry and Pharmaceutical Sciences, 1: 15-23.

Sharma. N., Chatterjee, S. and Bhatnagar, P. 2013. Assessment of physicochemical properties of textile wastewaters and screening of bacterial strains for dye decolourisation. Universal Journal of Environmental Research and Technology, 3: 345-355.

Sinha, S.P., Chattopadhyay, I., Pan, S., Chatterjee, P., Chanda, D., Bandyopadhyay, K.D. and Sen, S.K. 2009. Microbial transformation of xenobiotics for environmental bioremediation. African Journal of Biotechnology, 8: 6016-6027.

Solis, M., Solis, S., Perez, H.I. and Manzarezz, N. and Flores, M. 2012. Microbial decolorisation of azo dyes: a review. Process Biochemistry, 47: 1723-1748.

Sur, D.H. and Mukhopadhyay, M. 2017. COD Reduction of textile effluent in three-phase fluidized bed bioreactor using *Pseudomonas aureofaciens* and *Escherichia coli*. 3 Biotech, 7:141.

Tambi, S. 2013. The challenges faced by SMEs in the textile industry: special reference to hand printing enterprises in Jaipur. Global Journal of Management and Business Studies, 3: 741-750.

Velayutham, K., Madhava, A.K., Pushparaj, M. Thanarasu, A., Devaraj, T., Periyasamy, K. and Subramanian, S. 2018. Biodegradation of Remazol Brilliant Blue R using isolated bacterial culture (*Staphylococcus* sp. K2204). Environmental Technology, 39: 2900-2907.

Vikrant, K., Giri, B.S., Raza, N., Roy, K., Kim, K.H., Rai, B.N. and Singh, R.S. 2018. Recent advancements in bioremediation of dye: Current status and challenges. Bioresource Technology, 253: 355-367.

Nature Environment and Pollution Technology
An International Quarterly Scientific Journal

p-ISSN: 0972-6268
(Print copies up to 2016)
e-ISSN: 2395-3454

Vol. 19 | No. 2 | pp. 851-855 | 2020

Original Research Paper

https://doi.org/10.46488/NEPT.2020.v19i02.044

Open Access Journal

Experimental Study on Transport of Carboxylate Polystyrene Microspheres Using as *Cryptosporidium* Oocysts Surrogate with Runoff from the Slope Soil to the Surface Water Bodies

Tao Yuan*(***), Sen Cheng, Lai Zhou**, Qiyan Feng** and Ping Lu**†**

*Department of Architectural Intelligence, Jiangsu Vocational Institute of Architectural Technology, Xuzhou, Jiangsu 221000, China

**Department of Environmental Science and Spatial Informatics, China University of Mining and Technology, Xuzhou 221116, China

***Jiangsu Collaborative Innovation Centre for Building Energy Saving and Construct Technology, Xuzhou 221116, China

†Corresponding author: Ping Lu; lupingcumt@126.com

Nat. Env. & Poll. Tech.
Website: www.neptjournal.com

Received: 05-06-2019
Accepted: 24-07-2019

Key Words:
Cryptosporidium surrogate; Runoff factors; Transport of carboxylate polystyrene; Slope soil

ABSTRACT

Cryptosporidium can transport from the soil to the water resulting in the contamination of the surrounding water bodies. However, there are few pieces of research on the transport of *Cryptosporidium* from the slope soil to the surrounding water. The experiment simulated the transport of *Cryptosporidium* surrogate, carboxylate YG polystyrene, influenced by the rainfall intensity, rainfall pattern, soil type, and land slope, from the soil to water, to understand the transport of *Cryptosporidium* surrogate under these different conditions. The results showed that the transport of *Cryptosporidium* surrogate was affected by the surface runoff factors, that is, the high rainfall intensity, high rainfall frequency, steep slope and high sand content soil that resulted in the high transport of the *Cryptosporidium* surrogate.

INTRODUCTION

Cryptosporidium is a pathogenic microorganism that induces diarrhoea and vomiting (Yue & Ni 2014, Wang 1993), which has serious implications for the development of recreational water body activities and human health.

In recent years, an outbreak of *Cryptosporidium* caused by the medium of water has been reported in countries such as the UK and the United States. After the reported cases of human infection with *Cryptosporidium* in 1976 (Ryan et al. 2003), more than 90 countries appeared in succession with regard to report about *Cryptosporidium* infection (Wu et al. 2006). In the United States, about 2 per cent of the population was tested positive for *Cryptosporidium*. Each year, of every 150000 patients with diarrhoea, about 30000 are caused by *Cryptosporidium* infection. In 1984 and 1987, the United States experienced two outbreaks of cryptosporidia, and the total number of cases was 15,000. In 1993 at Minkwakee, Wisconsin, the largest outbreak of cryptosporidia was reported with up to 400,000 people infected and it has remained to be the highest and most serious case of *Cryptosporidium* outbreak up to date. In 1987, the first cases of *Cryptosporidium* infection in humans were diagnosed in Nanjing, China.

The main transmission channels of *Cryptosporidium* are direct contact of the skin such as swimming and diving, as well as through food and water. According to the survey, the infection rate of swimming in lakes and swimming pools is much higher than that of eating contaminated food (Zhang & Jiang 2001, Wang & Yan 2008, Wu & Li 2005). Kong et al. (2017) reported that the risk of *Cryptosporidium* infection in a certain lake in China was 18 cases/10,000 person.

Therefore, adequately understanding the transport pathway of *Cryptosporidium* in lakes is of great significance to control surface water quality and maintenance of human health. This experiment simulated the different conditions of rainfall, rainfall patterns, soil types and soil slope study on the transport of *Cryptosporidium* surrogate from slope soil to the surface water, to reveal the interface between soil and water transportation law of *Cryptosporidium* and key function parameters.

MATERIALS AND METHODS

The Carboxylate YG Polystyrene Microspheres

Cryptosporidium is detrimental to human health, so it is diffi-

cult to fully guarantee that its leakage would pose a threat to the operator and the environment. Therefore, the experiment will be carried out with the surrogate of *Cryptosporidium* oocysts, the polystyrene microspheres, which have been proved to be effective as a surrogate for *Cryptosporidium* oocysts (Lu et al. 2013, Lu et al. 2014a, Lu et al. 2014b, Lu et al. 2016). In this experiment, Fluoresbrite^{TM} Carboxylate YG polystyrene microspheres (Polysciences, Inc., Warrington, PA, USA) with a diameter of 4.869 μm were used as a model particle surrogate for *Cryptosporidium*. The microsphere has the same shape, diameter, density and surface charge as the true *Cryptosporidium*.

In this study, the microspheres were counted by fluorescence microscope. The collected experimental samples were put into a centrifugal machine, shocked and homogeneously mixed, then filtered by using a circular filter with an aperture of 2.5μm and a diameter of 20mm. The filter was placed in the slide, and after fixation of the slide, it was observed with the fluorescence microscope (Zhang et al. 2014).

The Experimental Setup

The experimental device is composed of 50cm slope organic glass tank and rainfall device, as shown in Fig. 1. The organic glass tank simulates the soil slope of the surface water body. The lowest point has the sampling port, and the surface runoff is collected to analyse the contents of the surrogate for *Cryptosporidium*. Rainfall devices include rainfall sprinkler, circulating pump, collecting bottle and catheter, etc. Note that rainfall is adjustable when using the organic glass tank.

The Experimental Method

The effects of rainfall intensity, rainfall pattern, soil type and land slope on the transport of *Cryptosporidium* were simulated. According to the rainfall situation in Xuzhou, the rainfall intensity was simulated, which can be categorized into three modes: heavy rain (21mm/12h), rainstorm (42mm/12h) and heavy rainstorm (63mm/ 12h) (Xu et al. 2008). The sand slope was 30°C. The 1 mL surrogate (the *Cryptosporidium* oocysts' content was 100/mL) was mixed into the soil. Then the rainfall intensity was adjusted by rainfall device, respectively 21mm/12h, 42mm/12h, and 63mm/12h, to determine the transport quantity of *Cryptosporidium* in 30 minutes at different rainfall intensity. The rainfall pattern was set to three modes while the total rainfall duration was 4 hours. The three modes are further elaborated below.

Rainfall was 2h, stopped 2h;

Rainfall was 1h, intermitted 1h, and repeated once;

Rainfall was 0.5 h, intermitted 0.5 h, and repeated 4 times.

Under the same rainfall intensity (21mm/12h), the soil was divided into four types of sand content, which was 100%, 80%, 60% and 40% respectively, and matched with granulated sand grains and clay. Under the same rainfall intensity (21mm/12h), the land slope was 10°, 20°, 30°.

RESULTS AND DISCUSSION

Effect of Rainfall Intensity on the Transport of Microspheres

The effects of rainfall intensity on the transport of microspheres are shown in Fig. 2. The transport of microspheres was positively correlated with rainfall intensity. The escalation of rainfall intensity increased the runoff through the sandy soil. In the case of constant soil pore size, the increase of runoff in unit time resulted in the increased number of the microspheres that were transported.

Effects of Rainfall Patterns on the Transport of Microspheres

The effects of rainfall patterns on the transport of microspheres are shown in Fig. 3. The higher the rainfall frequency was, the greater the total transport of microspheres was. In the

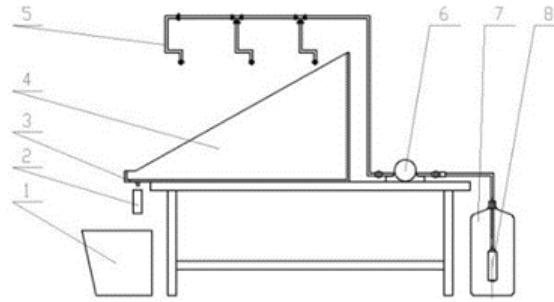

Fig. 1: Schematic diagram of the experimental model device (1. Wastewater tank, 2. Sampling pipe, 3. Sampling, 4. Soil tank, 5. Sprayer, 6. Pump, 7. Clean water tank, 8. Filter).

case of high rainfall frequency, the rainfall was stopped, but the runoff persisted, which caused the microspheres to continue to transport with the surface runoff when the short-term rainfall was suspended.

Effects of Soil Type on the Transport of Microspheres

The effects of soil type on the transport of microspheres are shown in Fig. 4. The amount of sand contained in soil was positively proportional to the transport of microspheres. The higher the sediment concentration was, the greater the transport of the microspheres was. The underlying reason is that absorption and water-retention of sandy soil is indisputably smaller than clay.

Effects of Land Slope on the Transport of Microspheres

The effects of land slope on the transport of microspheres are shown in Fig. 5. The augmentation of land slope decreases the water storage capacity of river slope, and the amount of water in the soil can be reduced. When the rain went through flat slope (e.g., 10° slope), the quantity of the trapped water was more than the steep slope, resulting from the less runoff,

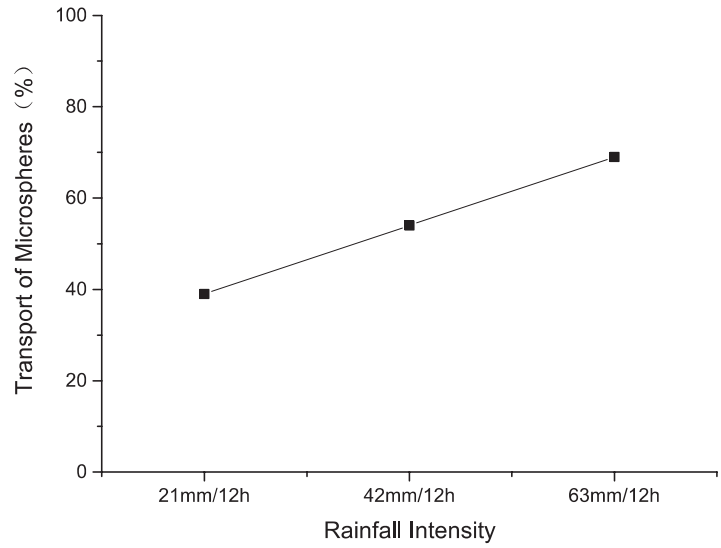

Fig. 2: Influence of rainfall intensity.

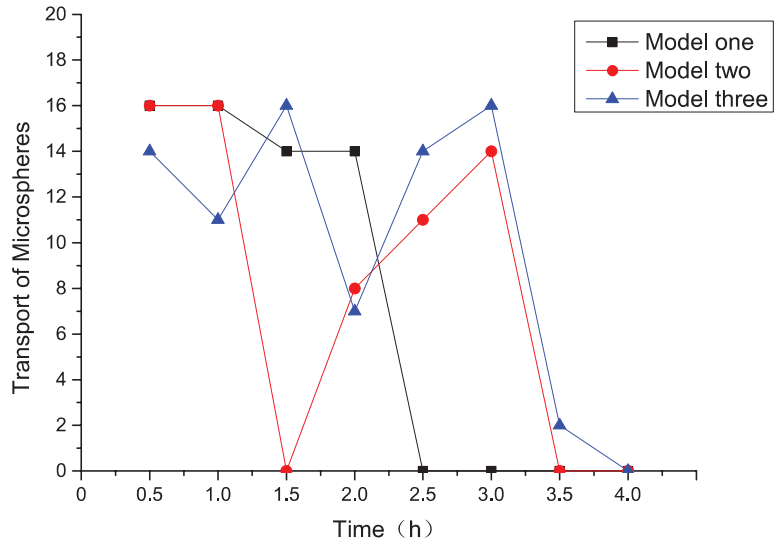

Fig. 3: The number of microspheres transported under the influence of rainfall pattern.

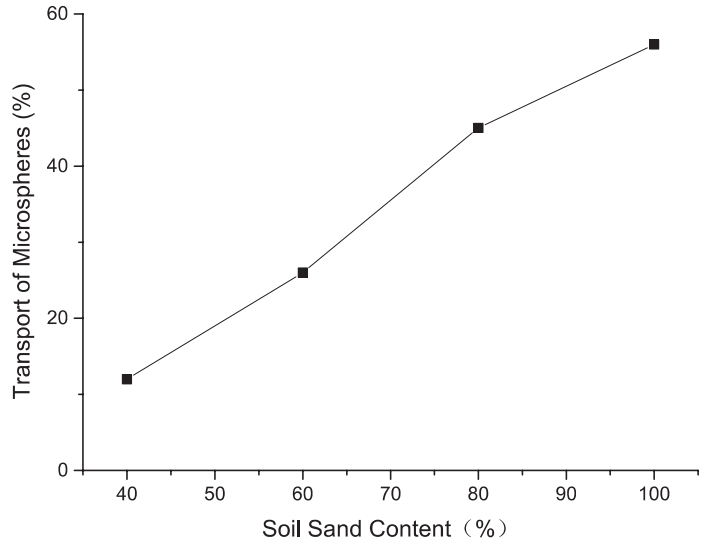

Fig. 4: Per cent of microspheres transported under the influence of soil type.

and the transport of microspheres was relatively minute. With the increase of slope, the amount of runoff increased, and the transport of microspheres was increased as well.

CONCLUSIONS

The soil is a sink of faecal pollutants such as *Cryptosporidium oocyst*. The transport of *Cryptosporidium* surrogate, which is caused by rainfall, to the overlying water of the surrounding surface rivers or lakes, is the main passway of the soil-water transport of *Cryptosporidium* surrogate. The transport of *Cryptosporidium* surrogate was more influenced by the surface runoff factors, the high rainfall intensity, frequent rainfall frequency, steep slope and high sand content of the soil. The results could serve as a significant guide to control the transport of *Cryptosporidium* from the slope to the overlying water.

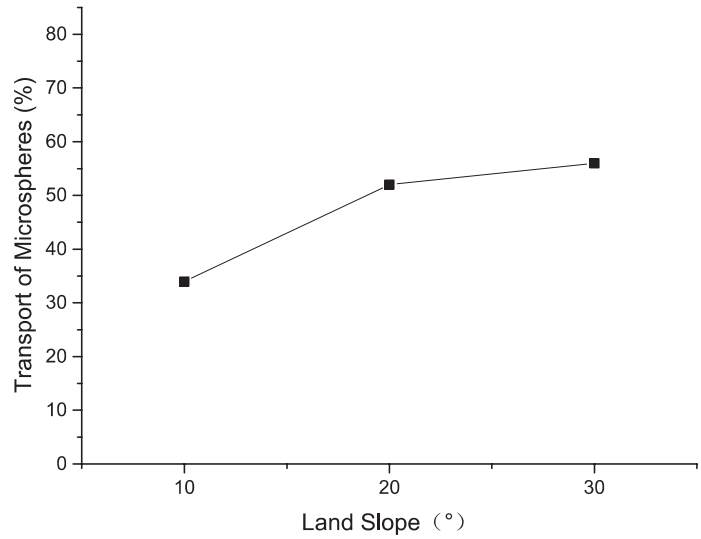

Fig. 5: Per cent of microspheres transported under the influence of land slope.

ACKNOWLEDGEMENT

This project was supported by the Foundation of Ministry of Housing and Urban-Rural Development of China (2016-K4-076) the Foundation of Jiangsu Provincial Department of Housing and Urban-Rural Development(2017ZD013) and Provincial University Natural Science Fund of Jiangsu (16KJB610016).

REFERENCES

Kong, Y., Lu, P., Tao Yuan., Niu, J., Li, Z. and Yang, B. 2017. *Cryptosporidium* contamination and attributed risks in Yunlong Lake in Xuzhou, China. Canadian Journal of Infectious of Infectious Diseases and Medical Microbiology, 1-6.

Lu, P., Yuan, T., Feng, Q., Xu, A. and Li J. 2013. Review of swimming-associated Cryptosporidiosis and *Cryptosporidium* oocysts removals from swimming pools. Water Quality Research Journal of Canada, 48(1): 30-39.

Lu, P., Yuan, T., Feng, Q., Li, J., Sun, Y. and Li, T. 2014. Pilot-scale studies on *Cryptosporidium* oocysts surrogate removal from swimming pool. Chinese Journal of Environmental Engineering, 8(7): 2822-2826.

Lu, P., Yuan, T. and Feng, Q. 2014. Using of poly diallyl dimethylammonium chloride for removal *Cryptosporidium* from the public recreational water venue. Journal of Chemical and Pharmaceutical Research, 6(6): 39-43.

Lu, P., Yuan, T. and Zhang, B. 2016. *Cryptosporidium* removal from runoff by active carbon filter with goal gangue. Journal of Chemistry, 1-3.

Ryan, U.M., Samarasinghe, B., Read, C., Buddle, J.R., Robertson, I.D. and Thompson, R.C.A. 2003. Identification of a novel *Cryptosporidium* genotype in pigs. App. Enviro. Microbiol., 69(7): 3970-3974.

Wang, G. 1993. Human Cryptosporidiosis research progress in our country. The Journal of Epidemiology, 14(1): 52.

Wang, L. and Yan, G. 2008. Human Cryptosporidiosis epidemiological and clinical studies. Chinese Journal of Pathogen Biology, 12(3): 953-956.

Wu, L., Chen, S. and Cao J. 2006. The popularity of Cryptosporidiosis and diagnosis research progress. Parasitic Disease International Medical Journal, 30(5): 277-281.

Wu, L. and Li, P. 2005. The research progress of *Cryptosporidium* pathogenesis. The Chinese Veterinary Parasitic Diseases, 13(3): 28-33.

Xu,L., Zhang, Q. Xu, J., Jiang, H. and Huang, L. 2008. Different rainfall intensity on nutrient vertical transport and leaching rate. Journal of Soil, 45(3): 437-444.

Yue, H. and Ni, C. 2014. *Cryptosporidium* and its research progress of the disease. Jiangsu Preventive Medicine, 25(5): 44-46.

Zhang, L. and Jiang, J. 2001. Research progress of *Cryptosporidium* and Cryptosporidiosis. Journal of Insect Parasites and Medicine, 8(3): 184-192.

Zhang, W., Xu, A. and Zhang, R. 2014. Soil classification research review and revision of the Chinese soil classification systems. China's Agricultural Science, 47(16): 3214-3230.

Nature Environment and Pollution Technology
An International Quarterly Scientific Journal

p-ISSN: 0972-6268
(Print copies up to 2016)
e-ISSN: 2395-3454

Vol. 19 | No. 2 | pp. 857-864 | 2020

Original Research Paper

https://doi.org/10.46488/NEPT.2020.v19i02.045

Open Access Journal

Measurement of Tourism Industry-Ecological Environment Coupling Degree and Management and Control Measures for Tourism Environment: A Case Study of Henan Province, China

Yan Fei Shen
School of Construction Engineering, Sanmenxia Polytechnic, Sanmenxia 472000, China
†Corresponding author: Yan Fei Shen; shyf213@163.com

Nat. Env. & Poll. Tech.
Website: www.neptjournal.com

Received: 24-02-2020
Accepted: 20-04-2020

Key Words:
Tourism industry;
Ecological environment;
Coupling degree;
Environmental management

ABSTRACT

The tourism industry has the largest scale of economic activities worldwide with the most powerful development momentum but has generated a negative effect on the ecological environment. The development of the tourism industry is a precondition and guarantee of eco-environmental optimization, and a harmonious ecological environment is an important dynamic support for the growth of tourism economy, making them mutually associated with evident coupling characteristic. In this study, related literature regarding the tourism industry and eco-environmental protection of developed countries in Europe and America were first reviewed, and tourism industry-ecological environment coupling model was constructed using Henan Province, China, as a case study. The coupling degrees in Henan Province during 2013-2018 were measured, and a comparative analysis of the spatial changes in tourism industry-ecological environment coupling degrees of 18 prefecture-level cities in Henan in 2013 and 2018 was conducted. Results showed that the order degree of the tourism industry in Henan Province maintained a rising trend during 2013-2018, whereas that of the ecological environment exhibited a fluctuating trend. The overall tourism industry–ecological environment coupling of 18 prefecture-level cities in Henan Province enhanced in 2013 and 2018, where the coupling degrees in Zhengzhou, Nan yang, and Luoyang presented an outward radiation trend from high to low. The study results serve as significant reference values for revealing the spatial-temporal evolution characteristics of the ecological environment and the tourism industry and completing the research regarding the coordinated development of the tourism industry and ecological environment.

INTRODUCTION

As an industry highly depending on resources and environment, the tourism industry is attached to benign eco-environmental and economic development. The tourism industry has become the main means of improving economic development in various areas. Whether the tourism industry can achieve sustainable development relies on eco-environmental quality. Various contradictions have continuously emerged with the continuous development of the tourism industry. Although the economy is uplifted, environmental contradictions are increasingly becoming prominent, thereby leading to the imbalance between the tourism industry and ecological and environmental development and harming the developmental relationships among regional economy, tourism industry, and ecological environment. The tourism industry can be well developed mainly because it exerts an enormous driving effect on economic development and has green, environmentally friendly, low-pollution, and low-carbon advantages, thereby facilitating environmental protection. However, some regions blindly transform, utilize, and conquer nature to improve the regional economy with the increasing regional tourism competition, thereby contributing to the growth of the tourism industry and economy to a certain degree but posing unrecoverable damage to the ecological environment.

Henan Province is a province with a large population and developed tourism industry in China. As shown in Fig. 1, the numbers of domestic and foreign tourists that stayed overnight in Henan Province during 2007–2018 present a fluctuating growth trend. Considering that Henan Province has invigorated the development of tourist destinations, the quantity and quality demands of demand subjects for tourist environment are and the pressure imposed by various subject demands for tourist environment is gradually elevated. The scale effect of tourist destinations has resulted in the increasing reliance of destinations for complicated infrastructures, frequent occurrence of tourism disasters, and gradually aggravating chain reaction of disasters. However, the tourism industry does not exert a destructive effect on the environment, and the blind pursuit of the benefits of tourist economy will seriously impact the eco-environmental

quality of tourist destinations, such as water pollution, air pollution, noise pollution, and damage of soil and vegetation caused by tourist activities. The eco-environmental system is extremely difficult to recover when it is destructed because of its fragility and its recovery requires a certain cycle. The tourism industry is strongly associated with the ecological environment, and the degradation of eco-environmental quality will certainly influence the sustainable development of the tourism industry. Therefore, the tourism industry and eco-environmental system are mutually promoted and contradicted, and a better understanding of the tourism industry–ecological environmental coupling degree provides important realistic values.

PAST STUDIES

With the continuous improvement of the social and material standards of living, mass tourism activities have become increasingly frequent because of the continuous expansion of tourism size, and the relationship between tourism and environment becomes increasingly close. Studies regarding the relationship between tourism and the environment in foreign developed countries can be traced back to the 1920s. The literature investigating the tourism industry and the ecological environment is provided as follows. Stankey (1981) believed that the number of received tourists within a certain time should be maintained at a moderate level to ensure the environmental quality of tourist destinations, and he divided the tourism environmental capacity into biological, cultural, psychological, and management capacities. Hunter (2002) assumed that the development of the tourism industry may generate a far-reaching influence on the local environment, combined sustainable tourism with the concept of ecological footprint, and proposed all types of concepts of "tourism ecological footprint" and some potential applications. Gössling et al. (2015) evaluated the total use amount of global resources by the tourism industry, indicated that the overall resource consumption in the tourism industry might increase by 92% (water)-189% (land use) from 2010 to 2050, and stated that the resource input should be increased to maintain the global tourism system, exerting an important effect on the ecological environment. Ying (2015) defined tourism environment, analyzed the influences of tourism development on water resources, soil, vegetations, and landscapes, and proposed the main protective measures for the tourism industry. Dann et al. (2013) surveyed the potential economic effects of climate change on the related tourism industry. The results showed that the sea level rise during windstorms will impact the tourism infrastructure construction, especially for countries with marine environment. Scott et al. (2010) discussed how global tourism industries can complete their quotas in the aspects of energy conservation and emission reduction. The results indicated that whether emission reduction can be successfully realized depends on the changes in major policies and practices of airline businesses to a great extent. Sun et al. (1988) reviewed the influences of the Australian tourism industry on the environment, especially on vegetations and soil. The results showed that tourism activities might generate adverse effects on the values of Australian natural and seminatural resources when they are improperly

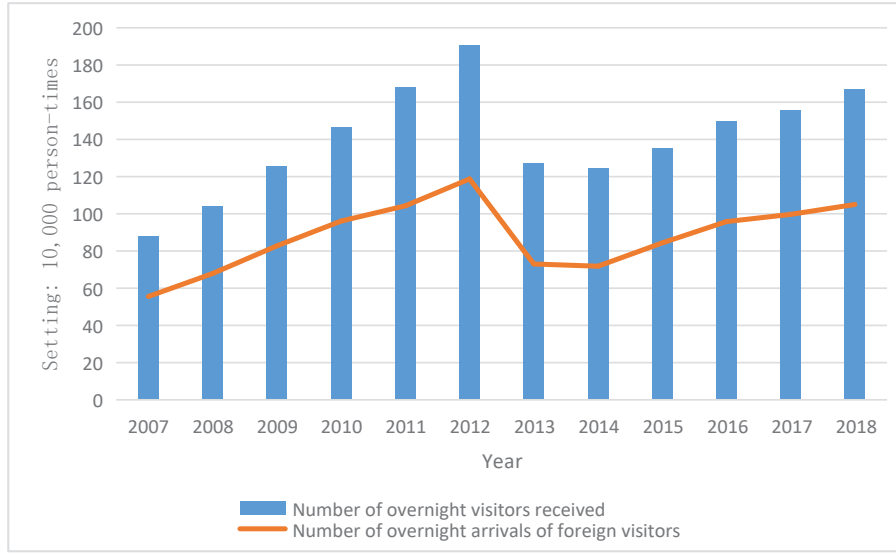

Fig. 1: Numbers of domestic and foreign tourists that stayed overnight in Henan Province during 2007-2018.

managed, and the quantitative relationship between tourism activities and environmental influence of main vegetations should be determined in subsequent studies. Kytzia et al. (2011) investigated Alps Davos tourist destination and indicated that many successful tourist destinations in highly populated areas in Central Europe experience the problem of approaching the growth potential limit. The results showed that low land utilization efficiency induced by the tourism industry can be solved by strengthening the space planning, architectural design, and facility management. Perch-Nielsen et al. (2010) studied the increasing greenhouse gas intensity caused by the added value of Swiss tourism industry. The results showed that the greenhouse gas emission in Swiss tourism industry is more than four times of the average economic level in Switzerland, and a mitigation plan under the background of preventing the dangerous climate change is proposed. Qiu et al. (2017) calculated and decomposed the CO_2 emission in China's tourism industry, discussed its evolution and distribution characteristics on the basis of tourism-ecological efficiency ratio, and used a regression model to analyze the influencing factors. The results indicated that the CO_2 emission in China's tourism industry remarkably increases, and the main factors influencing the economic benefits of the tourism industry are scale effect, structural effect, technological effect, and environmental regulation. Reilly et al. (2010) suggested that transportation consumes the maximum energy in the tourism system and proposed transferring tourists through transportation with energy-saving mode to improve the ecological efficiency of tourist traffic. Dwyer et al. (2010) estimated the greenhouse gas emissions of Australian tourism industry and its related activities. The results showed that the tourism industry accounts for 3.9%-5.3% of the total industrial greenhouse gas emissions in Australia. Surugiu et al. (2012) investigated the influences of the tourism industry on CO_2 emissions using the economic and environmental data of Romania and proposed several measures for the tourism industry to reduce CO_2 emissions. Taking Nepal as an example, Rabindra et al. (2019) evaluated the short-and long-term relationships among the number of tourists, per capita economic output, emission, energy consumption, and capital formation and indicated that energy consumption generates a negative effect on tourist arrivals and more attention should be paid to energy efficiency and energy diversity. Zhang et al. (2019) discussed the associations among the CO_2 emissions, actual GDP, unrenewable and renewable energy sources, and tourism industry in 10 Northeast and Southeast Asian countries during 1995-2014 and indicated that the development of the tourism industry will result in environmental degradation. The studies regarding the tourism industry and ecological environment conducted by domestic and foreign scholars have largely shifted from qualitative analysis to quantitative analysis with the emergence and continuous expansion of the tourism industry at global scope. Scholars have emphasized the eco-environmental pollution effect of the tourism industry, where many of them have conducted studies on tourism environmental carrying capacity, but studies on the coupling and coordinated development of the tourism industry and ecological environment are rare. In this study, the interaction and mutual influence between the tourism industry and the ecological environment and their coupling attribute were analyzed using Henan Province, China as an example. The coupling degree was explored, and pertinent policy suggestions were proposed to analyze the coordinated development laws of the tourism industry and ecological environment and predict their evolution trends. This study provides a scientific basis for the coordinated development between the tourism industry and the ecological environment in China

MODEL INTRODUCTION AND DATA DESCRIPTION

Tourism Industry-Ecological Environment Coupling Model

Order degree of systems: Considering tourism and environmental subsystems $S_j, j \in [1, k]$ investigated in this study, the order parameter during their development process is set as $e_j = (e_{j1}, e_{j2}, \cdots, e_{jn})$, where $n \geq 1, \beta_{ji} \leq e_{ji} \leq \alpha_{ji}, i \in [1, n]$. Without loss of generality, the assumption is that the greater the value of $e_{j1}, e_{j2}, \cdots, e_{jl}$, the higher the order degree of the system, otherwise, the lower the order degree; The greater the value of $e_{jl+1}, e_{jl+2}, \cdots, e_{jn}$, the lower the order degree, otherwise, the higher the order degree.

The tourism-environment coupling model includes the tourism industry subsystem and ecological environmental system. The order parameter in the development process of the tourism industry system is $e_1 = (e_{11}, e_{12}, \cdots, e_{1n})$. Based on the concept of order degree of the system, the order degree of order parameter component e_{1j} of the tourism industry subsystem is defined as follows:

$$u_1(e_{1i}) = \begin{cases} \dfrac{e_{1i} - \beta_{1i}}{\alpha_{1i} - \beta_{1i}} (i = 1, 2, \cdots l) \\ \dfrac{\alpha_{1i} - e_{1i}}{\alpha_{1i} - \beta_{1i}} (i = l+1, l+2, \cdots n) \end{cases}, \quad \ldots(1)$$

Where α_{1i} and β_{1i} denote the maximum and minimum values of the i (th) index of the tourism industry subsystem, respectively. On the basis of this definition, $u_1(e_{1i}) \in [0, 1]$ can be known through normalization, and the greater the value, the greater the contribution of e_{1i} to the order degree of the tourism industry subsystem.

The total contribution of the order parameter to the order degree of tourism industry subsystem is realized through the ensemble method of $u_1(e_{1i})$, and a method commonly used linear weighting method, as shown in Formula (2).

$$u_1(e_1) = \sum_{i=1}^{n} \omega_{u1}(e_{1i}) \ (\omega \geq 0, \sum_{i=1}^{n} \omega = 1), \qquad \ldots(2)$$

Where ω is the index weight. The order degree of the tourism industry subsystem is $u_1(e_1) \in [0, 1]$, and the greater the value of $u_1(e_1)$, the higher the contribution of the order parameter e_1 of the tourism industry subsystem to order degree of the system. Otherwise, the higher the order degree of the tourism industry subsystem, the lower the order degree.

The order parameter during the development process of the eco-environmental subsystem is set as $e_2 = (e_{21}, e_{22}, \cdots, e_{2i})$. Similar to the calculation method of the order degree of the tourism industry subsystem, the order degree of parameter component e_{2i} of the eco-environmental subsystem can be obtained as $u_2(e_{2i})$, and $u_2(e_{2i}) \in [0, 1]$.

Synergy degree of systems: The order degrees of the tourism industry and eco-environmental subsystems at the initial time t_0 are set as $u_1^0(e_1)$ and $u_2^0(e_2)$, respectively. When the systems evolve to time t_1, the order degrees of the tourism industry and eco-environmental subsystems are $u_1^1(e_1)$ and $u_2^1(e_2)$, respectively. When $u_1^1(e_1) \geq u_1^0(e_1)$, $u_2^1(e_2) \geq u_2^0(e_2)$ simultaneously hold, then the tourism industry and ecological environment systems are under synergistic development, and their synergistic degree model is expressed as:

$$c = sig(\bullet)\sqrt{\left|u_1^1(e_1) - u_1^0(e_1)\right|\left|u_2^1(e_2) - u_2^0(e_2)\right|}, \qquad \ldots(3)$$

where,

$$sig(\bullet) = \begin{cases} 1, u_1^1(e_1) \geq u_1^0(e_1) \ \ u_2^1(e_2) \geq u_2^0(e_2) \\ -1, u_1^1(e_1) < u_1^0(e_1) \ \ u_2^1(e_2) < u_2^0(e_2) \end{cases}. \qquad \ldots(4)$$

As shown in Formulas (3) and (4), a high degree of synergy can be only achieved when the tourism industry and eco-environmental subsystems are under the orderly state. The entire tourism industry and eco-environmental subsystems cannot achieve a good coordinated state or may not be synergistic at all when the order degree of one subsystem is immensely elevated and that of the other is slightly elevated or declined.

Data Description

No unified standard is used for the selection of evaluation indexes related to the coupling development of tourism industry and eco-environmental systems. Therefore, the factors influencing the coordinated development of tourism industry and eco-environmental were screened in this study, and an evaluation index system about their coupling and coordinated development was constructed following the abovementioned methods and principles and referring to related literature (Table 1). All statistical data were obtained from the Henan Statistical Bureau website, Henan Statistical Yearbook, and Yearbook of China Tourism Statistics. The investigated period ranged from 2012 to 2018, the investigated objects were Henan Province and 18 of its subordinate prefecture-level cities, and the data in the nearest year were used for individual missing data.

Table 1: Index system of coupling and coordinated development between the tourism industry and the ecological environment.

System	Index	Unit
Tourism industry subsystem	Total number of tourists	10,000 people
	Number of domestic tourists	10,000 people
	Number of inbound tourists	10,000 people
	Total tourism revenue	100 million yuan(RMB)
	Ratio of tourism output value to the tertiary industry	%
Eco-environmental subsystem	Number of parks	Number
	Park area	Hectares
	Green coverage	Hectares
	Industrial waste gas emission	100million tons/m^3
	Industrial wastewater discharge	100million tons
	Urban domestic sewage discharge	100 million tons
	Treatment rate of domestic sewage	%
	Harmless treatment rate of household waste	%
	Comprehensive utilization rate of industrial solid wastes	%

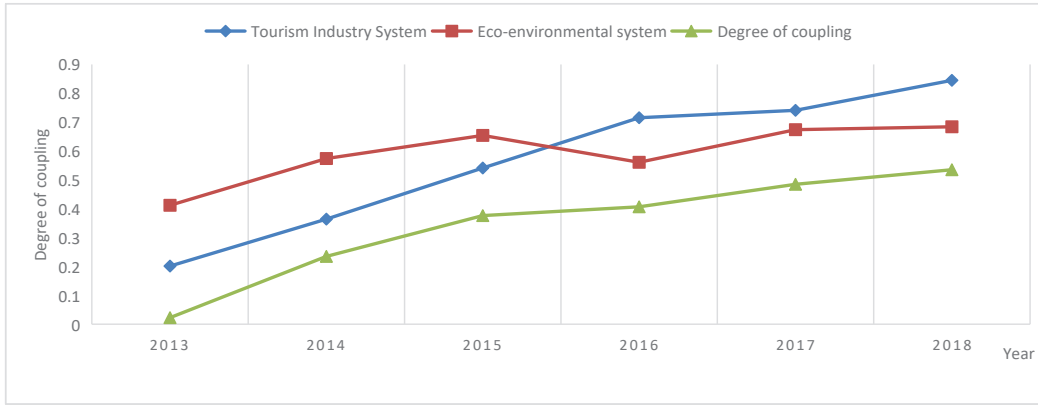

Fig. 2: Tourism industry-ecological environment coupling degree in Henan Province during 2012-2018.

RESULT ANALYSIS

Tourism Industry-Ecological Environment Coupling Results in Henan Province During 2012-2018

As shown in Fig. 2, the comprehensive development level of Henan's tourism industry during 2013-2018 maintained a rising trend, where the order degree of the tourism industry system increases every year. Since 2013, the development of the tourism economy in Henan Province changed every day. Positive fiscal policies were used by persisting government-led development strategies, including completely developing the financial sector and positively participating in tourism development planning. The tourism infrastructure construction was effectively managed under the effect of governmental investments, and positive fiscal policies were used to cultivate the tourism industry into a pillar industry. An important orientation was determined, that is, cultivating the tourism industry into a strategically important pillar industry and constructing it into a large province with prosperous tourism industry because Henan issued some positive policies, such as Action Program of Tourism Industry Transformation and Upgrading in Henan Province (2017-2020) and Henan Tourism Industry Development Planning in the 13th Five-Year Plan. Compared with the sustainable development of the tourism economy, the ecological environment presented a fluctuation tendency of "first rising, declining, and rising again," and the growth trend was slow. The eco-environmental level in Henan Province was slowly developing and its eco-environmental carrying capacity experienced great pressure under the strategic background of the "Rise of Central China" implemented in Henan Province in recent years and the social background characterized by economic rise and continuous advancement of industrialization and urbanization in addition to the fragility of the ecological environment itself and frequent occurrence of natural disasters. The tourism industry–ecological environment coupling

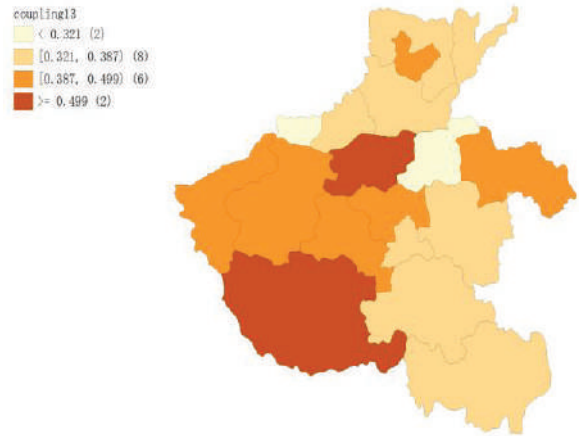

Fig. 3: Tourism industry-ecological environment coupling degree of prefecture-level cities in Henan Province in 2013.

degree in Henan Province increased from 0 to 0.535, the coupling grade gradually developed from low coupling degree to high coupling degree, and the entire system developed toward an increasingly orderly direction, suggesting that their correlation become increasingly close. However, the growth trend of coupling degree was slow, indicating that the rapid development of tourism economy in Henan Province during 2015-2018 generated a certain impact on the ecological environment, thereby relatively weakening their coupling relation.

Tourism Industry-Ecological Environment Coupling Results of Prefecture-Level Cities in Henan Province

As shown in Figs. 3 and 4, the tourism industry-ecological environment coupling of 18 prefecture-level cities in Henan Province improved in 2013 and 2018. The increasing trend of the comprehensive level of the tourism industry in the18 prefecture-level cities extremely accorded with the development status of Henan's tourism industry in recent years. The comprehensive development levels of the tourism economy in individual regions increased decreased in some years, but the fluctuation range was small. Subsequently, the levels increased again and became better, indicating that the comprehensive levels of the tourism economy in the regions maintained a continuous development tendency. The comprehensive development index of Henan's tourism industry had evident spatial differences, and development differences were found between the southern regions and northern prefecture-level cities. The coupling degree in the central region was high, regions with high development index of the tourism industry were mostly concentrated in Zhengzhou, Luoyang, and Nan yang, and the spatial shift of comprehensive tourism development was prominent, reflecting the fierce competitive development status of the tourism economy in these prefecture-level cities.

MANAGEMENT AND CONTROL MEASURES FOR TOURISM ENVIRONMENT

Adjust the Tourism Industry Structure and Realize Environmentally Friendly Development Mode

Ecological environment is a fundamental guarantee for realizing the sustainable development of the tourism economy and constitutes a hard-won tourism resource itself. Although the tourism industry is recognized as "green industry" and "smoke-free industry" with relatively minor direct pollution to the ecological environment, various eco-environmental problems will still occur when the economy is blindly pursued while the eco-environmental carrying capacity is ignored. The traditional extensive tourism development mode should be shifted into the green and low-carbon intensive direction in the future to realize the transformation and upgrade of the tourism industry. First, the support structure of tourism sectors should be optimized and ecological tourism services, such as recreational tourism, sightseeing tour, rural tourism, and life cultivation and health preservation tourism, should be vigorously developed. The tourism industry structure should be actively adjusted to promote the transition of tourist attractions from a traditional sightseeing type into complex functions and realize the integrative development of the tourism industry with other types of businesses, such as ecological agriculture and industry. A batch of tourism service enterprises with low energy consumption and minimal pollution should be introduced, cultivated, and integrated into the entire tourism activity to enhance Henan's tourism industry.

2013.

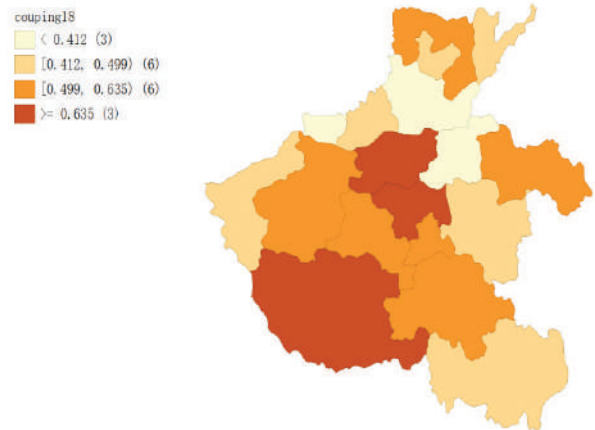

Fig. 4: Tourism industry-ecological environment coupling degree of prefecture-level cities in Henan Province in 2018.

Realize the High Matching Ratio Between Tourism Development Speed and Environmental Carrying Capacity

Henan Province owns abundant tourism resources, and unique tourism landscapes provide power for its tourism development. With the gradually elevated governmental emphasis on the tourism industry, the popularity of Henan tourism industry rapidly increases. However, the high tourist population pressure generates a certain influence on its ecological environment, and the development scale of tourism economy exceeds the speed of eco-environmental protection and construction, which is unfavourable to its overall coordinated development. The concept of sustainable development should be clarified and the tourism development should be facilitated with high-quality and strict requirements. High attention should be paid to resource protection and development. The number of tourists should be prevented from exceeding the upper limit of environmental capacity to reduce eco-environmental destruction. Tourist attractions should be reasonably planned and arranged, overdevelopment should be strictly prevented, and their development should be integrated with resource protection by strictly following the construction procedures to accelerate the steady development of Henan's tourism industry.

Strengthen the Publicity and Education of Tourism Eco-Environmental Protection

Human quality and concept are of great importance to the ecological environment, and ecological civilization construction cannot be separated from the extensive participation of the social public. The joint participation of governmental sectors, tourism enterprises, tourists, and local residents is necessary to promote the tourism of ecological civilization. The publicity and education on eco-environmental protection in tourism activities should be promoted by the social public, including tourism management staff, tour guides, hotel and restaurant service staff, tourists, and local residents. The awareness of tourism management staff and emphasis on eco-environmental protection should be enhanced, and the training of environmental management and protection skills of tourist attractions should be strengthened. Tour guides should be encouraged to convey environmental protection knowledge or ecological ethics to tourists when introducing and interpreting natural landscapes and remind tourists in practicing civilized tourism behaviours toward the ecological environment. For tourism service staff in hotels and restaurants, the common sense of eco-environmental protection should be popularized among them to create a thick tourism atmosphere of nature-loving, ecological protection, and civilized tourism.

Explore and Establish A Tourism Ecological Compensation Mechanism

Henan Province has numerous sightseeing places, such as mountains, rivers, lakes, forests, and natural heritages. The destruction of the ecological environment will certainly impact the sustainable development of the tourism industry. Henan Province should positively explore and immediately establish a tourism ecological compensation mechanism from province to cities and counties, especially for those sightseeing places with natural landscapes. The government can complete the evaluation and compensation work related to ecological compensation through various means, such as taxes, fiscal transfer, and policy support. The tourism ecological compensation is for the compensation of eco-environmental factors and should aim to realize the compensation for residents in sightseeing places, tourism eco-environmental management staff, and defenders. A comprehensive and long-term effective tourism ecological compensation mechanism can only be established when human compensation is realized to achieve the coordinated development between the tourism economy and ecological environment.

CONCLUSION

As an industry highly relying on resources and environment, the tourism industry is closely attached to the benign development of ecological environment and economy. However, environmental conflicts caused by the tourism industry are increasingly prominent, thereby leading to the imbalance between the tourism industry and economic and environmental development and harming the developmental relationships among regional economy, tourism industry, and ecological environment. In this study, the tourism industry-ecological environment coupling model was constructed using Henan Province, China as an example. The tourism industry-ecological environment coupling degrees in Henan Province during 2013-2018 were measured, and a comparative analysis of the spatial changes in the tourism industry-ecological environment coupling degrees of 18 prefecture-level cities in Henan Province in 2013 and 2018 was conducted. The results showed that the order degree of Henan's tourism industry maintained a rising trend during 2013-2018, whereas that of its ecological environment displayed a fluctuating trend, and the tourism industry-ecological environment coupling degree improved by a small margin. The comparison of tourism industry-ecological environment coupling degrees of 18 prefecture-level cities in Henan Province in 2013 and 2018 showed that the coupling degrees in Zhengzhou, Nan yang, and Luoyang presented an outward radiation trend from high to low. The policy measures proposed include adjusting the tourism industry structure, realizing the high matching ratio

between the tourism development speed and environmental carrying capacity, strengthening the publicity and education of tourism eco-environmental protection, and exploring and establishing a tourism ecological compensation mechanism. An in-depth study should be conducted to perfect the measurement index system of tourism industry-ecological environment coupling degree. A comprehensive evaluation model should be utilized to quantitatively analyze the tourism and ecological environment and the evolution of spatial coordinated development between the tourism industry and the ecological environment.

ACKNOWLEDGEMENT

This work was supported by the Henan science and technology research project (192102310524).

REFERENCES

Dwyer, L., Forsyth, P., Spurr, R. and Hoque, S. 2010. Estimating the carbon footprint of Australian tourism. Journal of Sustainable Tourism, 18(3): 355-376.

Dann, P. and Chambers, L. 2013. Ecological effects of climate change on little penguins Eudyptula minor and the potential economic impact on tourism. Climate Research, 58(1): 67-79.

Gössling, S. and Peeters, P. 2015. Assessing tourism's global environmental impact 1900-2050. Journal of Sustainable Tourism, 23(5): 639-659.

Hunter, C. 2002. Sustainable tourism and the touristic ecological footprint. Environment, Development and Sustainability, 4: 7-20.

Kytzia, S., Walz, A. and Wegmann, M. 2011. How can tourism use land more efficiently? A model-based approach to land-use efficiency for tourist destinations. Tourism Management, 32(3): 629-640.

Perch-Nielsen, S., Sesartic, A. and Stucki, M. 2010. The greenhouse gas intensity of the tourism sector: The case of Switzerland. Environmental Science & Policy, 13(2): 131-140.

Qiu, P., Fang, P., Yang, T. and Zhu, B. 2017. Tourism eco-efficiency measurement, characteristics, and its influence factors in China. Sustainability, 9(9): 1634.

Reilly, J., Williams, P. and Haider, W. 2010. Moving towards more eco-efficient tourist transportation to a resort destination: The case of Whistler, British Columbia. Research in Transportation Economics, 26(1): 66-73.

Rabindra, N., Irsyad, M. I. and Nepal, S. K. 2019. Tourist arrivals, energy consumption and pollutant emissions in a developing economy-implications for sustainable tourism. Tourism Management, 72: 145-154.

Surugiu, C., Surugiu, M. R., Zelia, B. and Dinca, A. I. 2012. An input-output approach of CO_2 emissions in tourism sector in post-communist Romania. Procedia Economics and Finance, 3: 987-992.

Scott, D., Peeters, P. and Gössling, S. 2010. Can tourism deliver its "aspirational" greenhouse gas emission reduction targets. Journal of Sustainable Tourism, 18(3): 393-408.

Sun, D. and Walsh, D. 1998. Review of studies on environmental impacts of recreation and tourism in Australia. Journal of Environmental Management, 53: 323-338.

Stankey, G.H. 1981. Integrating wildland recreation research into decision making: Pitfalls and promises. Recreation Research Review, 9(1): 31-37.

Ying, A.N. 2015. Tourism Development and Ecological Environment Protection. Journal of Landscape Research, 7(01): 43-44.

Zhang, S. and Liu, X. 2019. The roles of international tourism and renewable energy in the environment: New evidence from Asian countries. Renewable energy, 139: 385-394.

Nature Environment and Pollution Technology
An International Quarterly Scientific Journal

p-ISSN: 0972-6268
(Print copies up to 2016)
e-ISSN: 2395-3454

Vol. 19 | No. 2 | pp. 865-871 | 2020

Original Research Paper

https://doi.org/10.46488/NEPT.2020.v19i02.046

Open Access Journal

Analysis of the Spatial Patterns of Particulate Pollution in the Persistent Haze in Northeast China: A Case Study in Harbin City

Lei Wang*(***), Jiarong Deng**, Lijin Yang*****, Yunlong Yao**† and Dawei Xu*(***)**

*College of Landscape Architecture, Northeast Forestry University, Harbin 150040, China

**College of Wildlife and Protected Area, Northeast Forestry University, Harbin 150040, China

***Key Lab for Garden Plant Germplasm Development & Landscape Eco-restoration in Cold Regions of Heilongjiang Province, Harbin 150040, China

****College of Architectural Engineering, Heilongjiang University of Science and Technology, Harbin 130012, China

*****College of Mining Engineering, Heilongjiang University of Science and Technology, Harbin 130012, China

†Correspondence author: Yunlong Yao; yl.yao@163.com

Nat. Env. & Poll. Tech.
Website: www.neptjournal.com

Received: 16-07-2019
Accepted: 05-10-2019

Key Words:
Spatial Pattern;
Particulate pollution;
Persistent haze;
HYSPLIT-4;
Straw burning

ABSTRACT

With the help of $PM_{2.5}$, PM_{10}, and the Air Quality Index (AQI) and other air quality data, the posterior trajectory model of the Hybrid Single Particle Lagrangian Integrated Trajectory (HYSPLIT-4) model, having researched fire points of the straw in Harbin City, spatial pattern characteristics and genesis of the persistent haze in Harbin City from 20th October 2016 to 11th November 2016 were analysed. During the study period, the highest value of $PM_{2.5}$ reached 1880μg/m^3, the PM_{10} reached 1411μg/m^3, the daily average concentration was high, and the AQI concentration reached a maximum value on 28th October and 4th November, and the persistent haze phenomenon was the most significant. Besides, the study found that the haze incident and a large quantity of pollutants due to the concentration of burning straw around Harbin had a strong connection. The burning of particulate matter had a significant impact on the region's pollution level. The results of this study contribute to the control of particulate pollution in winter cities of developing countries.

INTRODUCTION

With the rapid industrialization and urbanization in developing countries, air pollution became an increasingly problematic issue in daily life (Seinfeld 2004). Serious environmental problems such as air quality, human health, regional climates, and global climates are influenced by particulate pollution (Wang et al.2014, Cao 2012). Haze in the country has become a multi-regional environmental disaster that cannot be ignored (Li et al. 2017, Fang et al. 2016, Liu et al. 2015, Liang et al. 2015). Harbin City has witnessed severe and persistent hazy weather from 20th October to 11th November, during this time, the heavy air pollution and air quality problems caused the visibility of the atmosphere to decrease, and had significant socio-economic impacts, especially on human health. Analysing the changing features and causes of haze weather in the Harbin area is of great significance for accurately observing and forecasting hazy weather, and reducing disaster loss, and ensuring traffic safety and environmental quality (Ou et al. 2015, Li et al. 2017).

Air quality problems are becoming increasingly prominent in many major cities around the world and reduced visibility in the cities has become a prominent phenomenon. Huang et al. (2014) found that fossil fuel combustion and biomass burning is likely to be important for controlling China's $PM_{2.5}$ levels and for reducing the environmental, economic, and health impacts resulting from particulate pollution. Appel et al. (1985) analysed the $PM_{2.5}$, PM_{10}, and NO_2 concentration changes to explain the phenomenon of reduced urban visibility. Marcazzan et al. (2001) studied the concentrations of $PM_{2.5}$ and PM_{10} in different seasons in Milan and found that $PM_{2.5}$ concentrations were higher in winter. Kassomenos et al. (2014), Shen et al. (2016), Fang et al. (2017) found that during fog and haze, changes in the concentration of each pollutant trend is similar and that the degree of change of NO_2, CO, $PM_{2.5}$, and PM_{10} were similar. Seinfeld et al. (2016) studied the impact of particulate matter on human beings in an in-depth study by focusing on the relationship between atmospheric aerosol and air pollution. Gautam (2014) used remote sensing image data to study heavy haze phenomena in a given area and studied the corresponding early warning system to reduce the impact of haze on society. Many studies exist on the characteristics and causes of haze in China, mainly focusing on the causes

of haze, the weather situation, haze control, haze detection, haze forecast, and so on (Wu 2008, Wu et al. 2008, 2010, Yue et al. 2013). Wu et al. (2016) found that the main factor affecting smog in monitoring points in 74 countries in China was industrial and that the use of motor vehicles and domestic gas was also becoming influential factors, and Pu (2017) analysed the trend of $PM_{2.5}$ in different regions of China from an economic development perspective. However, due to the different situations in different countries, there are differences in the time and causes of haze (Fan 2010, Zhang et al. 2017, Han et al. 2016).

Taking Harbin City as an example, this paper analyses the characteristics and causes of haze pollution from 20th October 2016 to 11th November 2016. This paper analyses the air quality status during the pollution period with air quality data and traces the movement of pollutants at different heights through the backward trajectory mode to trace the source of the pollutants. Furthermore, this paper also looks into the distribution of straw fire points in Harbin and discusses the main causes of haze pollution to provide a basis for controlling the impact of haze in Harbin City.

MATERIALS AND METHODS

Data Collection and Sample

Based on the data of air quality, Lagrangian hybrid single particle orbit model, and the distribution of the straw fire points, the spatial pattern and genesis of haze were studied in Harbin City.

1) The Air Quality Index (AQI) data and Particulate Matter (PM) are derived from environmental cloud work platforms and mainly analyse the air quality status during the pollution period.
2) The trajectories of pollutants are calculated using the Hybrid Single Particle Lagrangian Integrated Trajectory Model (HYSPLIT) jointly released by the National Oceanic and Atmospheric Administration (NOAA) and the Australian Bureau of Meteorology. The backward trajectory model is used to trace the source and trend of air masses during the pollution period because it can handle the meteorological transmission, diffusion, and settlement at different heights and there are various meteorological input fields and physical processes. The meteorological data were provided by the National Environmental Forecast Center (NCEP) of the United States from the simultaneous global data assimilation system (GDAS) data (Zhang et al. 2017, Ge et al. 2017).
3) The distribution data of the straw fire points in Harbin in autumn comes from the satellite environmental application centre of the Ministry of Environmental Protection, which is used to analyse the situation of straw burning in the surrounding areas of Harbin.

The downtown area of Harbin (45.64°N -45.86°N, 126.47°E -126.81°E) is used as the target of the HYSPLIT model and the GDAS data of 28th October 2016 and 4th November 2016 are analysed retrospectively. The back-push time is set at 72 hours, UTC time is 16:00. The interval time is set to six hours and air mass monitoring at three different altitudes is set at 100 m, 500 m, and 1000 m, respectively, to monitor the movement trajectories of pollutants at different heights. This draws the Harbin City HYSPLIT-4 backward trajectory model.

Air Quality Analysis of the Smog Process

Analysis of air pollution during the status of the pollution process can be reviewed and the changes and characteristics

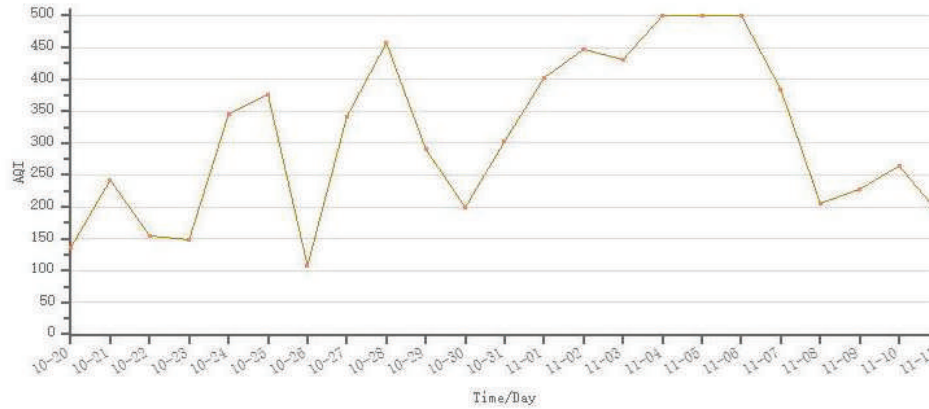

Fig. 1: The Harbin Air Quality index trend map from 20th October to 11th November.

can be understood. China issued the relevant provisions in the first half of 2012 in which the Air Quality Index (AQI) replaced the original Air Pollution Index (API) and the relevant provisions were implemented on 1st January 2016 (China Meteorological Administration 2010).

From 20th October 2016 to 11th November 2016, the air pollution in Harbin continued for 23 days. The primary pollutants were $PM_{2.5}$ and PM_{10}. Fig. 1 shows the trend of AQI during the pollution period. As shown in Fig. 1, the air quality conditions were mildly polluted on 20th, 22th, 23th, 26th, 30th October, and 11th November. On 21th and 29th October, and on 8th, 9th, and 10th November, the air quality was heavily polluted. On the 24th, 25th, 27th, 28th, and 31th of October, and on the 1st, 2nd, 3rd, 4th, 5th, 6th, and 7th of November, the air quality status showed serious pollution levels. Among these, the AQI on 4th, 5th, and 6th November, exceeded 500. This is the most long-lasting and serious haze pollution in Harbin since 20th October 2016 when the Heilongjiang Provincial Department of Environmental Protection issued a haze red warning. Fig. 2 shows that from 20th October-11th November, Harbin City's (11 monitoring sites: Lingbei Station, Songbei Shangda Station, Huining Station, Taiping Grand Park Station, Chengde outside the road, Xiangfang Hongqi Street station, He Ping Road station, Daoli Jianguo Road station, Square East Light Station, Hulan Teachers College station, Provincial Academy of Agricultural Station) daily average of $PM_{2.5}$, PM_{10}, NO_2, and SO_2 levels. The NO_2 and SO_2 trends are roughly the same, the daily concentrations of $PM_{2.5}$ and PM_{10} from 20th October to 11th November were above 100μg/m^3; on 4th November, the average daily $PM_{2.5}$ reached its maximum of 1880μg/m^3. On 5th November, PM_{10} reached its maximum of 1411μg/m^3, corresponding to an AQI of 500 and severe air quality conditions. After 6th November, the $PM_{2.5}$ and PM_{10} daily average concentrations showed a downward trend.

RESULTS AND DISCUSSION

Analysis of the Backward Trajectory of Air Mass

Using the HYSPLIT-4 model, GDAS meteorological data, and UTC time, we analysed two of the most severe smog hazes during the study period, with the AQI value reaching 458 at 3:00 AM on 28th October 2016 and 500 at 4:00 PM on 4th November 2016. Using the model, we calculated the 72-hour backward transfer trajectory, as shown in Figs. 3 and 4. The red, blue, and green trajectories in the images represent the air mass transport trajectories at the low altitude of 100 m and the high altitudes of 500 m and 1000 m in the air. As can be seen in Fig. 3, the 100-meter low air mass began at 00:00 on 25th October and moved northeastward from Inner Mongolia to the northeast at noon on the 25th. It moved southwards along the eastern boundary of Inner Mongolia and entered the provinces of Jilin and Liaoning at noon on the 26th and then the air mass moved north again and finally arrived in Harbin. The 500-meter and 1000-meter air masses showed roughly similar movement trends with the declining phenomenon. The 500-meter air mass at 0:00 on the 25th rose to 1000 m and then gradually decreased at 0:00 on the 26th down to 100 m. The height of the 1000-meter air mass at 0:00 on the 25th dropped to about 100 m and then at 12:00 on the 27th, the air mass rose to more than 500 m and moved from Southern Inner Mongolia to the Liaoning area, and then turned to the north, eventually reaching Harbin. It can be seen that part of the heavy haze on the 28th is due to the descent of the high air mass, transporting high-altitude pollutants to a low altitude and transporting low-level pollutants from other regions to Harbin. In Fig. 4, it can be seen that the 100-meter low-level air mass reaches Harbin from the south from Russia, but in the case of high pressure in Russia, the air mass rises from 0:00 on 1st November, and

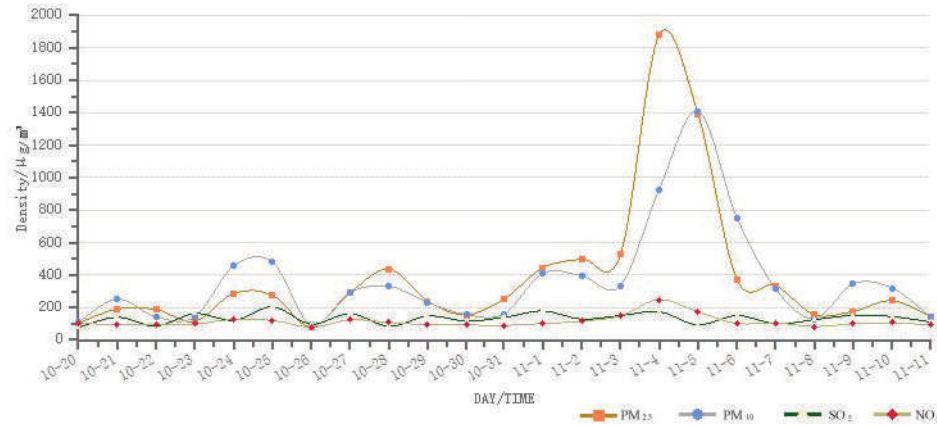

Fig. 2: The daily concentration changes of $PM_{2.5}$, PM_{10}, NO_2 and SO_2 in Harbin from 20th October to 11th November.

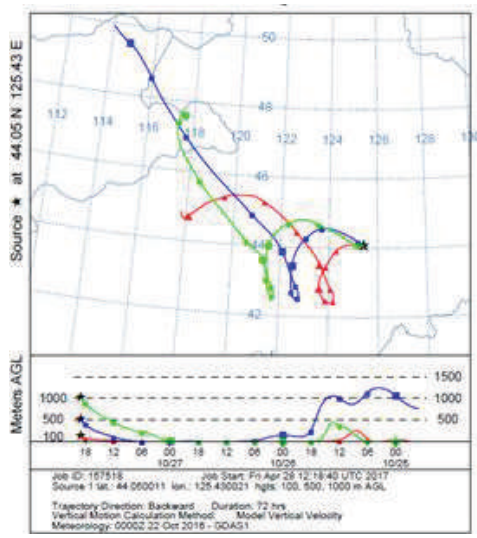

Fig. 3: The 72 hours back trajectory map on 28th October.

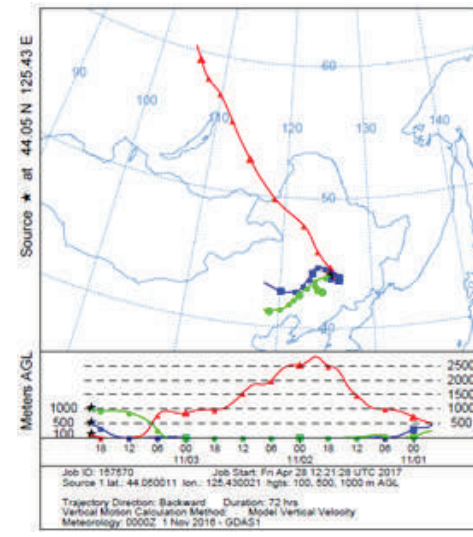

Fig. 4: The 72 hours back trajectory map on 4th November.

the air mass continues to rise to a height of about 2500 m at 20:00 on January 1, then it gradually declines. At 12:00 on the 3rd November, it drops to about 100 m. The 500-meter and 1000-meter air masses move in roughly the same direction. They move northward from Hebei and Inner Mongolia and are at a height of about 100 m from 1st November-3rd November at 6:00. The air mass carrying particulate contaminants did not rise to the original altitude when it reached Harbin. The reason for the haze on the 4th was because the high air mass had been moving at a low altitude and transported the pollutants in other areas to Harbin.

Combining the trajectories of the air masses on 28th October and 4th November, it can be found that the high-air masses are all reduced to low-level movement. The air currents transport the pollutants in the northwestern and southwestern parts of the country to Harbin and the airborne pollutants of Harbin to the lower part of the sky, indicating that part of the reason for the haze weather in Harbin was due to the regional pollution.

Monitoring and Analysis of the Straw Incineration Fire Points

Heilongjiang Province is a major grain-producing province. After harvesting, a large number of straw burning incidents continue to occur. Small particles floating in the air have caused serious air pollution in Harbin after long-term heating and burning a large amount of coal for heating. This article studies the sources and causes of smog pollution in Harbin from 20th October -11th November. As can be seen from Fig. 2, the AQI reached a peak on October 28th and reached a maximum on 4th November (AQI of 500). Table 1 shows the Ministry of Environmental Protection satellite environment application centre test data. Table 2 shows that in October and November, the number of straw burning stoves in Heilongjiang Province were 702 and 715, respectively. Fig. 5 is from 20th to 31st October, showing the distribution area of straw burning fire spots in Heilongjiang Province, which totalled 598, accounting for 85% of the total in October. Fig. 6 shows Harbin's burned fire point distribution area of Harbin from

Table 1: The environmental satellite monitoring of the fire points of straw burning in October 2016.

Sort	Province	Fire Points	Fire Intensity (A/thousand hectares of arable land area)
1	Heilongjiang	702	0.0600
2	Inner Mongolia	100	0.0177
3	Jilin	73	0.0146
4	Liaoning	58	0.0179
5	Shanxi	54	0.0164
6	Xinjiang	35	0.0155

Note: The data of arable land in each province in this statistical table comes from the China Statistical Yearbook 2014.

Table 2: The environmental satellite monitoring of the fire points of straw burning in November 2016.

Sort	Province	Fire Points	Fire Intensity (A/thousand hectares of arable land area)
1	Heilongjiang	715	0.0611
2	Shanxi	94	0.0286
3	Inner Mongolia	40	0.0071
4	Jilin	39	0.0078
5	Liaoning	25	0.0077
6	Hebei	13	0.0021

Note: The data of arable land in each province in this statistical table comes from the China Statistical Yearbook 2014.

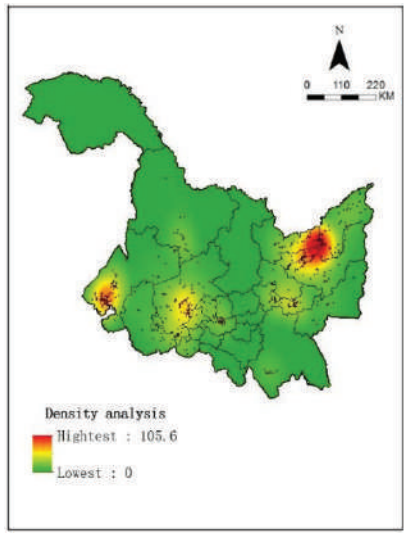

Fig. 5: 20th-31st October Heilongjiang province straw burning fire points.

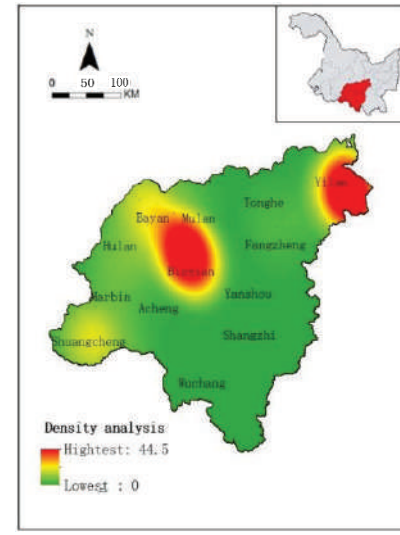

Fig. 6: 20th-31st October Harbin City straw burning fire points.

20th to 31st October, with a total of 52, mainly distributed in Binxian, Bayan County, Acheng District, Tonghe County, Yilan County, Magnolia County, Shuangcheng District, Wuchang City, Daoli District, and Hulan District, of which 18 are from the Yilan County, 12 are from the Bin County and 9 are from the Bayan County. Based on the HYSPLIT-4 model, the source of air pollutants in Harbin was analysed. Combining the distribution of fire density of straw burning in Fig. 5 and Fig. 6, the main cause of smog pollution in Harbin on 28th October is the transportation of extraneous air pollutants. From Fig. 3, it can be seen that the wind on 25th, 26th, and 27th of October was not conducive to the spread of pollutants. The straw burning from the northwest and southwest areas of Harbin (that is, Shuangcheng, Acheng, Daoli, and Hulan) causes the particles to stay in Harbin, thus exacerbating the extent of ambient air pollution.

Fig. 7 shows the 1st-11th November Heilongjiang Province Environmental Satellite Monitoring of the straw burning fire density distribution area: a total of 715. Fig. 8 shows the 1st to 11th November Harbin Environmental Satellite Monitoring straw burning fire density distribution area: a total of 50, mainly in Bayan County, Bin County, Hulan District, Mulan County, Shuangcheng District, Yilan County, Acheng District, Songbei District, Tonghe County, and Yanshou County. From these, 20 were in the Hulan District, 9 in the Lan County and Bayan County, and 4 in the Binxian County. Compared with October, the incineration points around Harbin urban area increased significantly in November. According to the backward deduction of Fig. 4, the distribution location of straw burning fire spots in Fig. 7 and Fig. 8 resulted in the AQI "explosion table" on November 4 in Harbin mainly due to the transportation of air pollutants from the northwest and southwest directions. As can be seen from Fig. 4, on 1st, 2nd, and 3rd days of November, the 500-meter altitude and the 1000-meter altitudes were windless and due to the 100-meter low air mass movement, the pollutants in

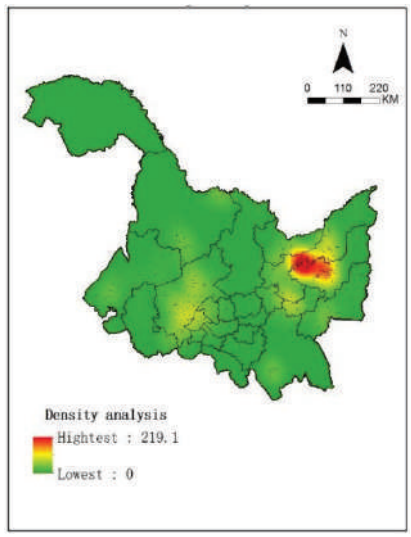

Fig. 7: 1st-11th November Heilongjiang province straw burning fire points.

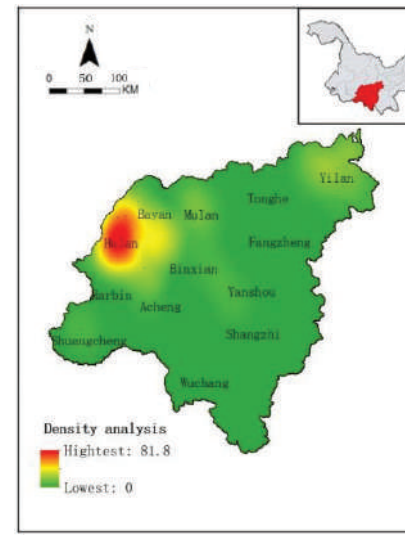

Fig. 8: 1st-11th November Harbin City straw burning fire points.

the surrounding area of Harbin were transported to Harbin. Furthermore, a large amount of incinerated particles remain in the Harbin, which further intensified the air pollution.

CONCLUSION

The Air quality in Harbin has been in a poor state since heating. Based on the air quality data provided by the environmental cloud platform, this paper analyses the air quality status of Harbin from 20th October 2016 to 11th November 2016, period (23 days). In this period, 6 days showed mild pollution and 17 days showed more serious pollution, of which 4th November to 6th November was the most serious, with AQIs exceeding 500. Through the backward trajectory simulation of the HYSPLIT-4 model, we found that the straw burning in the surrounding area of the Heilongjiang Province and Harbin continued for nearly a month, resulting in the main reason of the "explosion table" on the 28th and the 4th. The excessive combustion of straw burning in Harbin on the 28th and the high altitude windless conditions are not conducive to the spread of pollutants and cause the straw burning particles to stay in Harbin. During the winter period in Harbin, the temperature is low, and the air mass decreases, thus exacerbating Harbin's urban ambient air quality pollution levels.

This article is a preliminary study on the causes of haze smog, during winter in Harbin. There are still some factors that are not involved and will be further explored in the following research.

ACKNOWLEDGEMENTS

The authors would like to express gratitude to the research grant support provided by China Postdoctoral Science Foundation (Grant No.2017M621229), Postdoctoral Science Foundation of Heilongjiang Province (Grant No. LBH-Z17001), the National Natural Science Foundation of China for Young Scholars (Grant No. 41101177), Philosophy and Social Science Program in Heilongjiang Province (Grant No. 17GLD173, Grant No. 16GLC04), Scientific Research Foundation for the Returned Overseas Chinese Scholars, Heilongjiang Province, the University Strategic Reserve Personnel Abroad Research project funded by the Heilongjiang Province, Doctoral Fund of Ministry of Education of Heilongjiang Province, University Nursing Program for Young Scholars with Creative Talents in Heilongjiang Province.

REFERENCES

Appel, B.R., Tokiwa, Y., Hsu, J., Kothny, E.L. and Hahn, E. 1985. Visibility as related to atmospheric aerosol constituents. Atmospheric Environment, 19(9): 1525-1534.

Cao, J. J. 2012. Pollution status and control strategies of $PM_{2.5}$ in China. Journal of Earth Environment, 3: 1030-1036.

China Meteorological Administration 2010. Observation and Forecast level of Haze in China Meteorological Administration. QX/T113-2010. Beijing: Meteorological Press.

Fan, X.Q. 2010. Study on Haze Weather Characteristics and its Relationship with Atmospheric Environmental Pollution in Xiamen City. Nanjing University of Information Science and Technology.

Fang, C.S., Zhang, Z.D., Jin, M.Y., Zou, P.C. and Wang, J. 2017. Pollution characteristics of $PM_{2.5}$ aerosol during haze periods in Changchun, China. Aerosol and Air Quality Research, 17(04): 888-895.

Fang, D.Q., Wei, Y.J. and Huang, W. 2016. Characterization and source apportionment of organic carbon during a heavy haze episode in Beijing in October 2014. Research of Environmental Science, 29(1): 12-19.

Gautam, R. 2014. Challenges in early warning of the persistent and widespread winter fog over the Indo-Gangetic plains: A satellite perspective. In: Reducing Disaster: Early Warning Systems for Climate Change.

Springer, Dordrecht, pp. 51-61.

Ge, Y., Wang, M. X., Bai, X., Yao, J. B. and Zhu, Z. R. 2017. Pollution characteristics and potential sources of $PM_{2.5}$ in Su-Xi-Chang region. Acta Scientiae Circumstantiae, 37(03): 803-813.

Han, R., Wang, S.X., Shen, W.H., Wang, J.D., Wu, K., Ren, Z.H. and Feng M.N. 2016. Spatial and temporal variation of haze in China from 1961 to 2012. Journal of Environmental Science, 46: 134-146.

Huang, R.J., Zhang, Y., Bozzetti, C., Ho, K.F., Cao, J.J., Han, Y., Daellenbach, K.R., Slowik, J.G., Platt, S.M., Canonaco, F. and Zotter, P. 2014. High secondary aerosol contribution to particulate pollution during haze events in China. Nature, 514: 218-222.

Kassomenos, P.A., Vardoulakis, S., Chaloulakou, A., Paschalidou, A.K., Grivas, G., Borge, R. and Lumbreras, J. 2014. Study of PM_{10} and $PM_{2.5}$ levels in three European cities: Analysis of intra and inter urban variations. Atmospheric Environment, 87: 153-163.

Li, P. W., Haridah, A., Nasrin, A., Azadeh, G and Nik Meriam, N. S. 2017. Control measures and health effects of air pollution: A survey among public transportation commuters in Malaysia. Sustainability, 9(9): 1616.

Li, Z., Zhang, H. and Ye, H. 2017. Characteristics of air pollution during typical haze periods and HYSPLIT model analysis of its source in Hangzhou. Acta Scientiae Circumstantiae, 11: 1-16.

Liang, D., Wang, B. and Wang, Y.Q. 2015. Distribution characteristics and sources of $PM_{2.5}$ and gaseous pollutants in winter in Chongqing. Research of Environmental Science, 28(07): 1039-1046.

Liu, L.W., Li, W.C. and Shang, K.Z. 2015. Analysis of a serious haze process and its impact factors in Jing-jin-Ji region. Journal of Meteorology Environment, 31(1): 35-42.

Marcazzan, G.M., Vaccaro, S. Valli, G. and Vecchi, R. 2001. Characterisation of PM_{10} and $PM_{2.5}$ particulate matter in the ambient air of Milan (Italy). Atmospheric Environment, 35(27): 4639-4650.

Ou, N.Y., Wang, W. and Bo, J.F. 2015. An analysis of the causes and characteristics of a rare and persistent haze weather in Harbin. Heilongjiang Meteorology, 32(2): 1-4.

Pu, Z. N. 2017. Time-spatial convergence of air pollution and regional economic growth in China. Sustainability, 9(7): 1284.

Seinfeld, J. H. 2004. Air pollution: A half century of progress. American Institute of Chemical Engineers Journals, pp. 1096-1108.

Seinfeld, J. H. and Pandis, S. N. 2016. Atmospheric Chemistry and Physics: From Air Pollution to Climate Change. New York: John Wiley & Sons.

Shen, L.J., Wang, H.L. and Li, L. 2016. Observation analysis on the characteristics of meteorological elements and pollutants during a continuous fog and haze episode in spring in Jiaxing City. Environmental Science, 37(08): 2871-2880.

Wang, Y., Zhang, R.Y. and Saravanan, R. 2014. Asian pollution climatically modulates mid-latitude cyclones following hierarchical modeling and observational analysis. Nature Communications, 5: 2098.

Wu, D. 2008. Identification and data analysis of haze and fog. Environmental Chemistry, 27(3): 327-330.

Wu, D., Liao, G. L., Deng, X. J., Bi, X. Y., Tan H. P., Li F., Jiang C. L., Xia D. and Fan S. J. 2008. Study on the transport conditions of haze in the Pearl River Delta. Journal of Applied Meteorological Science, 19(1): 1-9.

Wu, D., Wu, X. J., Li, F., Tan, H. P., Chen, Cao, Z. Q., Sun, X., Chen, H. H. and Li, H. Y. 2010. Temporal and spatial changes of haze in Chinese mainland from 1951 to 2005. Journal of Meteorological, 68(5): 680-688.

Wu, J. N., Zhang, P., Yi, H. T. and Zhao, Q. 2016. What causes haze pollution? an empirical study of $PM_{2.5}$ concentrations in Chinese cities. Administrative Tribune, 8(2): 132.

Yue, Y. F., Liu, D. Y., Zhou, B., Xia, J., Wu, Y. and Hu, Y. H. 2013. Study on haze weather characteristics and influencing factors in Wuxi. Meteorological Monthly, 39(10): 1314-1324.

Zhang, J.Y., Song, S. H., Xu, R. and Wen J. H. 2017. Source analysis of regional air pollution particles based on backward air mass trajectory. Environmental Monitoring in China, (02): 42-46.

Nature Environment and Pollution Technology
An International Quarterly Scientific Journal

p-ISSN: 0972-6268
(Print copies up to 2016)
e-ISSN: 2395-3454

Vol. 19 | No. 2 | pp. 873-880 | 2020

Original Research Paper

https://doi.org/10.46488/NEPT.2020.v19i02.047

Open Access Journal

Optimization of Incubation Period, pH and Moisture Content for Vermicomposting of Biomethanation Sludge Admixed with Fruits and Vegetable Waste Collected from Gultekadi Market Yard, Pune Using *Eudrilus eugeniae*

A. I. Mulla* and G.R. Pathade**
*Department of Environmental Science, Fergusson College, Pune, Maharashtra, India
**Department of Microbiology, H.V. Desai College, Pune, Maharashtra, India
†Corresponding author: A. I. Mulla; amir.karad@gmail.com

Nat. Env. & Poll. Tech.
Website: www.neptjournal.com
Received: 20-08-2019
Accepted: 26-11-2019

Key Words:
Vermicomposting;
Biomethanation;
Sludge;
Eudrilus eugeniae

ABSTRACT

The present study had an objective to optimize important parameters viz., incubation period, pH and moisture per cent for vermicomposting of biomethanation sludge admixed with fruits and vegetable waste collected from Gultekadi Market Yard, Pune using *Eudrilus eugeniae*. The experiment was conducted on the terrace of H.V. Desai College of Arts, Commerce and Science, Pune. The sludge from biomethanation digester running on fruits and vegetable waste was collected and dewatered. The fruits and vegetable waste was collected from Gultekadi Market Yard, Pune and used for the experiment by processing it. The dewatered sludge was admixed with partially decomposed fruits and vegetable waste. The 1kg working capacity plastic trays were used for the optimization of parameters. It was found that incubation period of six weeks, pH 7.0 and moisture content of 70-80% were the optimum condition for *Eudrilus eugeniae* vermicomposting. The average growth rate mg/worm/day for the optimized incubation period, pH and moisture % was 4.4±0.14, 5.57±0.1 and 7.5±0.47, respectively and at all the three optimized conditions was 7.8±0.6.

INTRODUCTION

The vermicomposting is the use of earthworms for the treatment of organic waste to get mineralized humus like manure (Ansari & Ismail 2012). The vermicomposting is an environmentally sound technique of waste management. The technique is effective for partially decomposed organic waste such as market waste, agricultural waste, kitchen waste, industrial anaerobic treatment's sludge etc. The earthworms can consume biomass/food equivalent to their body weight in a day (Gurav & Pathade 2011). The earthworms are used to degrade waste material into economically profitable manure. India has an agricultural economy (Mathew 2006) and so organic waste generated like fruits and vegetable waste (FVW), can be managed through earthworms. India has a tropical climate and more than 500 earthworm species are reported from different parts of the nation. The vermicomposting with selected earthworm species is an effective solution for organic waste management. The vermicompost contains a higher amount of nutrients required for plant growth, especially nitrogen, phosphorus and potassium along with other micronutrients (Bansal & Kapoor 2000). Devi et al. (2012) and Hemalatha (2013) and many others have worked on fruit waste management using vermicomposting technique and produced good quality vermicompost.

The earthworms are of three types as per their preference to food and habitat (Butt & Lowe 2011). The first one is epigeic earthworms, prefer to be on the top layer of soil and get their food from decomposed organic matter of leaf litter (Gajalakshmi & Abbasi 2004). The examples of epigeic worms are *Eisenia andrei, Lumbricus rubellus, Eisenia fetida (Ef)*, *Eudrilus eugeniae* (*Ee*). The epigeic earthworms possess high metabolic activities which make them a good choice for vermicomposting (Kale & Bano 1992). The endogenic earthworms are the second category. An endogenic earthworm stays below the top layer of soil where mineralized soil is present. They make horizontal burrows to the top layer of soil and feed on the organic matter of the soil. The third category of earthworms is anecic earthworms which prefer to stay in deep burrows but come to the top surface for feeding (Kadam & Pathade 2004).

MATERIALS AND METHODS

Earthworm Used

The earthworm used was *Eudrilus eugeniae* whose taxonomical classification is given in Table 1. A photograph of the earthworm species is presented in Fig. 1.

Biomethanation Plant Sludge and FVW as Feed

The biomethanation project was undertaken with FVW. The effluent from biogas digester was subjected for the separation of solids (Biogas Digester Sludge-BDS) and the liquid portion. The liquid portion was used as fertilizer to the plants while the solid portion was mixed with Partially Decomposed Fruits and Vegetable Waste (PDFVW). This admixture was then subjected as feed to the vermicomposting. The vermicomposting in the laboratory was performed in the plastic trays of 5kg capacity with working volume 1 kg (Mane & Raskar 2012). Using same trays, the vermicomposting process parameters, e.g. incubation period, pH and moisture were optimized as per Kadam & Pathade (2004), while the ambient temperature was used as incubation temperature and was around 25-30°C**.**

Vermicompost Pots

The present experiments were carried out in 1 kg (25cm×17cm×7cm) working capacity plastic trays. All the trays of 1 kg capacity were provided with the facility for aeration and removal of vermiwash by making 1mm sized holes at the base and all sides of walls of the tray for ventilation. All the trays were covered with cotton fabric and kept in the rack. The rack was covered with wet empty jute bags during the experiment to prevent infestation of insects and rodents and to maintain dark conditions to avoid direct exposure of sunlight during the experiment.

Table 1: Classification of *Eudrilus eugeniae.*

Rank	Classification
Kingdom	Animalia
Phylum	Annelida
Class	Clitellata
Subclass	Oligochaeta
Order	Haplotaxida
Family	Eudrilidae
Genus	*Eudrilus*
Species	*eugeniae*

Source: https://en.wikipedia.org/wiki/Eudrilus_eugeniae

Optimization Studies for Vermicomposting of FVW

Acclimatization of earthworms to feed: The optimization of pH and moisture was an important part of the study. The initial pH of the feed was kept around 7.0 and moisture around 60-80%. The one set in triplicate was performed with a selected range of pH-7 and moisture (60-80%). The earthworms were acclimatized to experimental conditions for six to eight weeks. The acclimatized earthworms were then used for the optimization studies.

***Optimization of the incubation period for vermicomposting using the above substrate (feed)*:** The experiment for incubation period was conducted in triplicate using the above substrate (feed) for earthworm species *Ee*. The moisture of feed was maintained around 70 to 80% by manually spraying water regularly throughout the experiment. The pH of feed was maintained around 7.0. The ambient temperature during the experiment was around 25-30°C. The ten juveniles/tray of each *Ee* species were released in respective trays containing 1kg of feed/tray and trays were incubated as described above for 8 weeks of the incubation period. The weight gain/tray/week by earthworms and mortality if any was recorded every week for all experimental sets. For the recording of weights, earthworms were removed from trays and washed with tap water. The blotting paper was used to blot/absorb excess water. The weight of earthworms was recorded and

Fig. 1: The Adult earthworm, *Eudrilus eugeniae.*

earthworms were released back in respective trays. The incubation period (weeks) at which maximum average weight gain in case of earthworms and maximum vermicompost amount was obtained, was taken as an optimum incubation period for vermicomposting.

The average growth rate (mg/tray/day) of earthworm was calculated by the method of Manaf et al. (2009) and Suthar (2009). The formula used for the same is given in equation 1.

$$\text{Earthworm growth rate (mg/tray/day)} = \frac{\text{Maximum biomass (mg)-Initial biomass (mg)}}{\text{Total number of days in which biomass is obtained}} \quad \ldots 1$$

The average growth rate (mg/worm/day) of earthworm was calculated by the method of Manyuchi & Phir (2013). The formula used for the same is as given in equation 2.

$$\text{Earthworm growth rate (mg/worm/day)} = \frac{\text{Maximum biomass (mg)-Initial biomass (mg)}}{\text{Total number of days in which biomass is obtained} \times \text{Number of earthworms inoculated}} \quad \ldots 2$$

***Optimization of pH of feed for vermicomposting*:** The pH range selected for the experiment was pH 5.0, 6.0, 7.0, 8.0 and 9.0 for earthworms *Eudrilus eugeniae*. The experiments were run in triplicates. The ten juvenile earthworms of *Eudrilus eugeniae* species were released per tray. The entire experiment was conducted with the moisture content of up to 70-80% and an ambient temperature of 25-30°C. The pH values of feed were adjusted with 1N HCl /1N NaOH. The initial weight of earthworms was recorded before releasing in trays. The weekly readings for average weight gain and mortality if any were recorded. The pH value of feed at which maximum weight gain in the inoculated earthworms and average maximum vermicompost obtained, was considered as optimum pH of the feed. The experiment was run for six weeks (six weeks was the optimum incubation period obtained in the previous experiment (Fig. 2).

***Optimization of moisture content of feed for vermicomposting*:** The moisture range used was 50-60, 60-70, 70-80 and 80-90% for the earthworms. The experiments were run in triplicates. The entire experiments were conducted by maintaining pH 7.0 of feed (optimized condition) and at ambient temperature (25-30°C) for feed and six weeks incubation period (optimized). The 10 juvenile earthworms were released/tray. The initial weights of earthworms were recorded before releasing in the trays. The feed provided with various moisture ranges were monitored for growth of earthworms. The weekly readings were recorded for average weight gain, the final amount of vermicompost and mortality if any. The moisture value of feed at which maximum weight gain in the inoculated earthworms and average maximum vermicompost produced was taken as optimum moisture range value of the feed (Fig. 3).

Vermicomposting Using Optimized Conditions

The experiment was performed in triplicates for *Eudrilus eugeniae* earthworm species. The optimized conditions

Fig. 2: Vermicomposting trays in the racks for the experiment of optimization of pH of feed.

obtained from the above experiments for *Eudrilus eugeniae* species were used to perform in this experiment. The 1 kg feed prepared with optimized conditions was used for this experiment. The 10 juvenile earthworms were released/tray. The initial weights of earthworms were recorded before releasing in the trays. The average maximum weight gain and average maximum vermicompost produced for the experimental period (six weeks) were recorded weekly/ tray.

RESULTS AND DISCUSSION

Optimization Studies for Vermicomposting of BDS and PDFVW

Optimization of incubation period: It is evident from Table 2 and Fig. 4 that there was a gradual increase in weight gain from week one (166.83±20.42) to week six (1936.64±64.05) and average maximum weight gain by *Ee* earthworm species was recorded at 6th week. The further incubation on 7th week onwards resulted in weight loss. The average maximum weight gains for three sets of were obtained as 1936.64±64.05 mg. The weight loss in 7th and 8th week indicated nutrient deficiency, thus the optimum incubation period for *Ee* species was taken as six weeks. The average growth rate (mg/worm/day) and vermicompost obtained (g/kg of feed) for *Ee* were reported as 4.4±0.14 and 348.9±21.5 respectively. Hence, six weeks was considered as an optimum incubation period.

The previous study by Pandit & Maheshwari (2012) reported growth of *Eisenia fetida* with optimum of 6 weeks with pH 7.0, particle size 1-2mm, temperature 25°C, and moisture level of 80% and obtained 175 to 3363mg with 1999% gain in biomass. The present study also reported 6 week period as the optimum incubation period for *Ee.* Kadam & Pathade (2004) reported weight loss on 7th and 8th week of incubation for *Eudrilus eugeniae* which is similar to the present results.

Optimization of pH of feed for *Ee*: It was evident from Table 3 and Fig. 5 that pH 6.0 and below and at pH 8.0 and above of feed, average maximum weight gain for earthworm was less as compared to weight gain at pH 7.0 and hence pH 7.0 was taken as optimum for vermicomposting of BDS and PDFVW, and the experiment incubation period of six weeks was taken. The average maximum weight gain was found at pH 7 for *Ee* earthworm species. The average maximum weight gain for the three sets of *Ee* on 6th week was 2427.7±23.1. The average growth rate has the maximum value at pH 7.0 as 5.57±0.1 for *Ee*. The average growth rate (mg/worm/day) for *Ee* was reported as 3.31±0.11. The vermicompost obtained at pH 7.0 was 364.7±23.1/g/kg of feed. Hence pH 7.0 was considered as optimum.

The results of the present study are similar to previous studies by Gajlakshmi & Abbasi (2004) who reported pH 7.0 as optimum and migration of earthworms if pH value

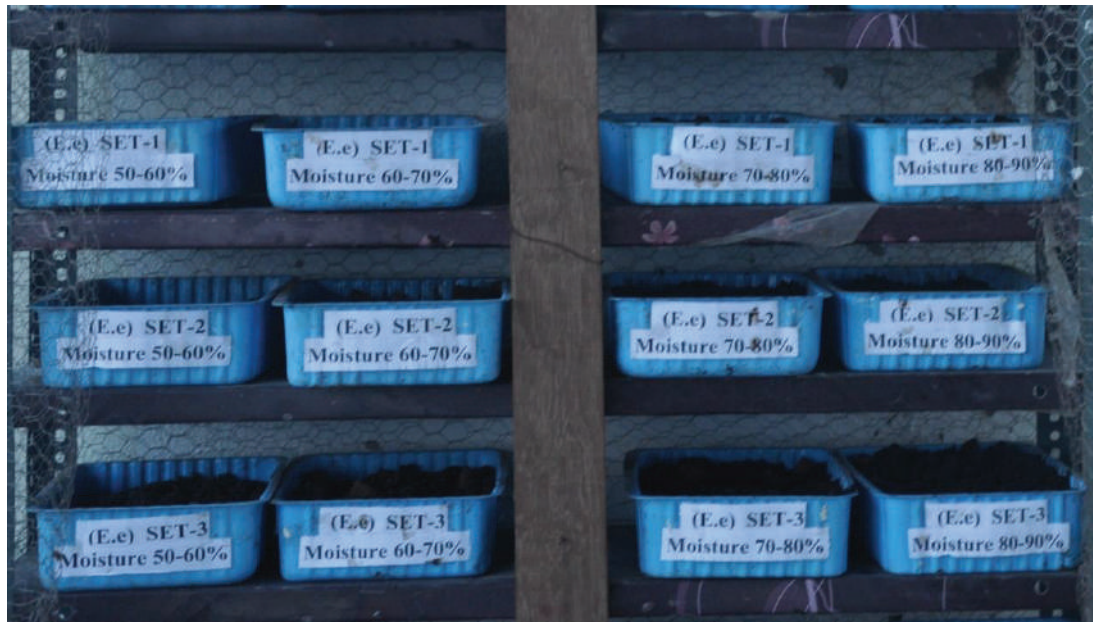

Fig. 3: Optimization of the moisture of feed for vermicomposting (trays in the rack) (Optimized conditions: incubation period 6 week, pH of feed 7.0 and moisture content of feed 70-80%).

Table 2: Optimization of the incubation period for *Ee* (mg/tray).

Incubation period : Average weight gain of *Ee* in (mg/tray)	
Week of incubation	Average weight gain
0	83.35±3.6
1	166.83±20.42
2	318.01±47.23
3	601.56±68.14
4	995.85±49.14
5	1289.05±89.15
6	1936.64±64.05
7	1823±26.10
8	1725.68±61.05
Average Total weight gain/ tray/ week	999.6±39.7
Average growth rate (mg/tray/ day)	44.1±1.4
Average growth rate (mg/worm/ day)	4.4±0.14
Vermicompost (g/kg of feed)	348.9±21.5

decreased below six. Kadam & Pathade (2004) reported that the average maximum weight gain for *Ee* at pH 7 was from 81.3mg to 3351mg. Gurav & Pathade (2012) reported that average maximum weight gain for *Ee* at pH 7 was from 159mg to 7090mg, while Utekar & Deshmukh (2016) reported average maximum weight gain for *Ee* at pH 7 from 2400mg to 28660 mg.

Optimization of moisture content of the feed for *Ee*: It is evident from Table 4 and Fig. 6 that there was a gradual increase in weight up to 70-80% moisture which then decreased. The results indicated that the maximum weight gain was at the moisture content 70-80%. The average maximum weight gain for three sets of *Ee* on 6th week at 70-80% moisture was 3263.8±201.6 (Table 4 and Fig. 6). The average maximum growth rate for *Ee* at the moisture content of 70-80% was found as 7.5±0.47 mg/worm/day. The average total vermicompost obtained at the moisture level of 70-80% and was 416.2±14.3 g/kg of feed for *Ee*.

The results of the present study seem to be almost similar to the previous reports. Kadam & Pathade (2004) reported average maximum weight gain for *Ee* at the moisture of 70-80% was from 194 mg to 3099 mg. Palsania et al. (2005) had reported faster vermicomposting rates for *Ee* at moisture % of 75±5. Gurav & Pathade (2012) reported the average maximum weight gain for *Ee* at the moisture of 80% was from 171 mg to 3585 mg. Pandit & Maheshwari (2012) reported the average maximum weight gain for *Ee* at the moisture level of 80% was from 175 mg to 3363 mg. Utekar & Deshmukh (2016) reported average maximum weight gain for *Ee* at the moisture of 80% was from 2400 mg to 19720 mg.

The average maximum weight gain for earthworm *Ee* was found at 70-80% moisture optimized conditions of six weeks incubation period, pH 7.0 and feed ambient temperature of 25-30°C.

At 50-60% and 60-70% moisture level the average weight

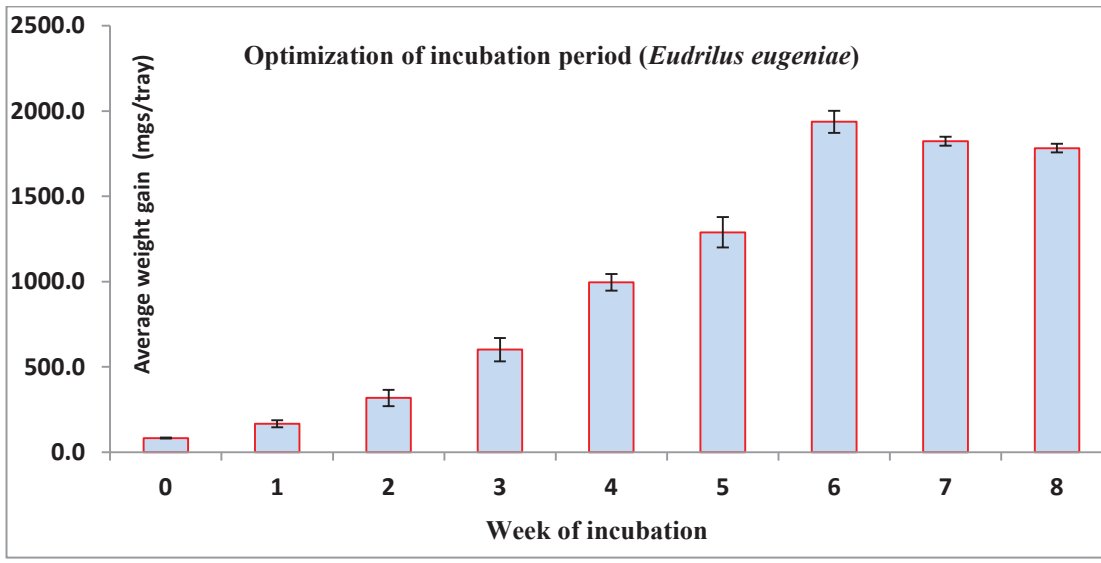

Fig. 4: Optimization of the incubation period for *Ee* and average weight gain (mg/tray).

gain and average growth rate for the earthworms were less as compared to 70-80% for *Ee* hence 70-80% moisture content was taken as optimum for *Ee*.

The optimized conditions for vermicomposting at 1 kg tray level studies: The experiments conducted for optimization of pH and % moisture of substrate/feed and optimized sets of conditions for vermicomposting of BDS and PDFVW were as below: (Table 5).

Vermicomposting using the optimized set of conditions at 1 kg tray level study: The experiment was performed in triplicate at 1 kg tray level using optimized incubation period of 6th week, feed pH 7.0 and % moisture of feed to 70-80% for *Ee.* The average maximum weight gain of *Ee* found on the 6th week was 3378.7±24.7mg and vermicompost produced was 485.7±6.7g/kg of feed. The *Ee* had a growth rate of 78.3±0.6 mg/tray/day (Table 6 and Fig. 7).

It was further found that the average weight gain and growth rates increased when all the optimized conditions were used as compared to results at the time of optimization of individual conditions.

CONCLUSIONS

- The BDS and PDFVW are amenable to vermicomposting using *Ee*.
- The earthworm *Ee* significantly produced the vermicompost from the above-mentioned substrate (feed).

Table 3: Optimization of pH of feed for *Ee* (mg/tray).

Optimization of pH of *Ee* (mg/tray)					
Week/pH of feed of incubation	pH 5	pH 6	pH 7	pH 8	pH 9
0	86.06 ±7.9	94.9 ±8.1	87.6 ±6.3	92.4 ± 4.1	83±11.0
1	184.73 ±10.71	185.77±21.39	207.57 ±6.37	177.47±33.25	173.1±24.04
2	184.33±22.96	239.73±26.48	362.03 ±15.49	241.73±46.15	168.8±18.19
3	189.53±3.84	315.3±23.51	706.3 ±16.67	340.33±44.06	184.1±20.74
4	208.67±11.8	397±13.66	1034.67 ±64.72	415.5±39.65	206.83±29.82
5	234.0 ±6.13	493±35.55	1512 ±23.82	505.57±23.53	234.57±40.11
6	228.1±16.74	619.37±21.04	2427.67 ± 23.08	611.8±12.5	274±48.37
Average Total weight gain/ tray/week	187.9± 8.2	423.9±6.3	905.4±8.9	340.7±26.3	189.2±27.6
Average growth rate (mg/tray/day)	3.5±0.02	17.3±0.02	55.7±0.6	12.4±0.04	4.5±0.9
Average growth rate (mg/worm/day)	0.35±0.02	1.73±0.02	5.57±0.1	1.24±0.04	0.45±0.1
Vermicompost (g/kg of feed)	163.1±12.7	247.3±14.8	364.7±23.1	263.4±11.2	187.4±13.6

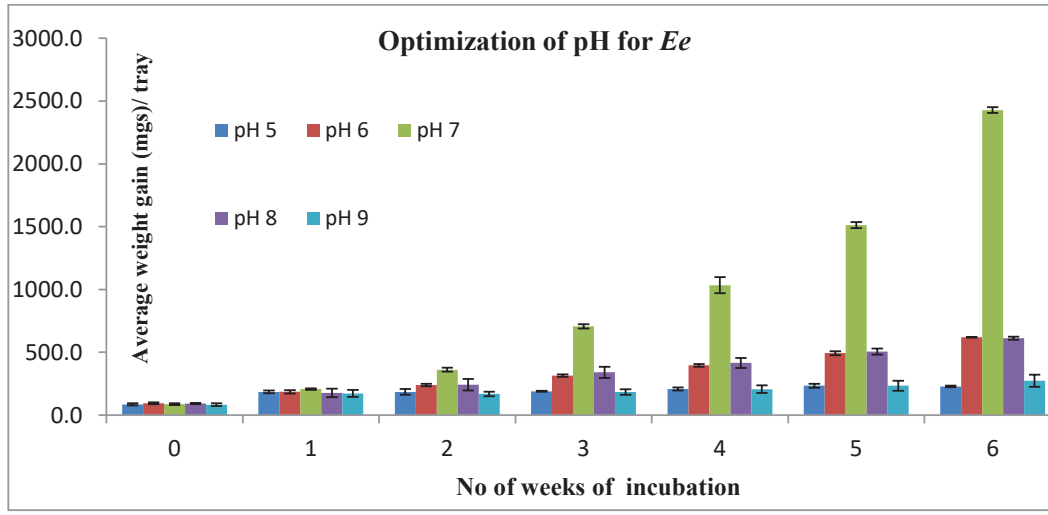

Fig. 5: Optimization of pH of feed for *Ee* (mg/tray).

- The optimized pH of feed for vermicomposting of BDS and PDFVW was pH 7.0.
- The optimized moisture range of feed was 70-80% for *Ee*.
- The average growth rate for *Ee* using at 1 kg feed with optimized conditions was found to be 7.8±0.06 mg/worm/day.
- The vermicompost obtained using all the optimized conditions was 485.7±6.7 g/kg of feed

REFERENCES

Ansari, A.A. and Ismail, S.A. 2012. Earthworms and vermiculture biotechnology. In: Sunil Kumar and Ajay Bharti (Eds.) Management of Organic Waste, pp. 87-96.

Bansal, S. and Kapoor, K.K. 2000. Vermicomposting of crop residues and cattle dung with *Eisenia fetida*. Biores. Technol., 73(2): 95-98.

Butt, K.R. and Lowe, C.N. 2011. Controlled cultivation of endogeic and anecic earthworms. In: Biology of Earthworms. Springer, Berlin, Heidelberg, pp. 107-121

Table 4: Optimization of moisture content of feed for *Ee* (mg/tray).

Optimization of moisture content for *Ee* (mg/tray)				
Week/Moisture (%) of feed of incubation	50-60	60-70	70-80	80-90
0	82.7±7.71	86.57±7.39	92.23±5.73	84.97±7.02
1	161.3±12.1	192.9±29.2	200.4±15	167.5±20.3
2	219.6±25.9	297.5±46.7	338.5±19.9	334.2±42.3
3	283.8±22.6	406±57.9	805.2±20.6	661.6±93.5
4	359.8±28.9	529.5±51.2	1340.1±77.7	1026.9±107.2
5	440.7±32.3	806.7±103.2	1756.6±209	1537.9±75.7
6	594.47±54	1231.8±180	3263.7±201.6	2241.9±111.4
Average Total weight gain/ tray/week	306.08±25.74	507.3±39.12	1113.8.0±65.59	865.01±56.14
Average growth rate (mg/tray/day)	12.18±1.1	27.27±4.1	75.5±0.4.6	51.36±2.5
Average growth rate (mg/worm/day)	1.22±0.12	2.73±0.41	7.5±0.47	5.14±0.25
Vermicompost (g/kg of feed)	362.3±16.7	374.8±17.4	416.2±14.3	386.2±12.7

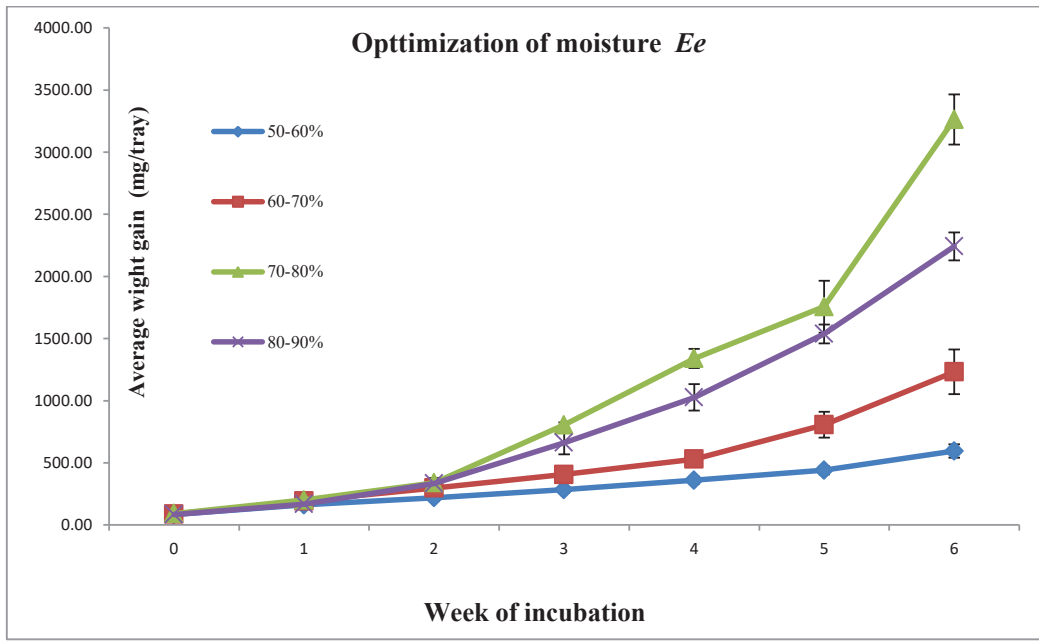

Fig. 6: Optimization of moisture content (average weight gain) for *Ee* (mg/tray).

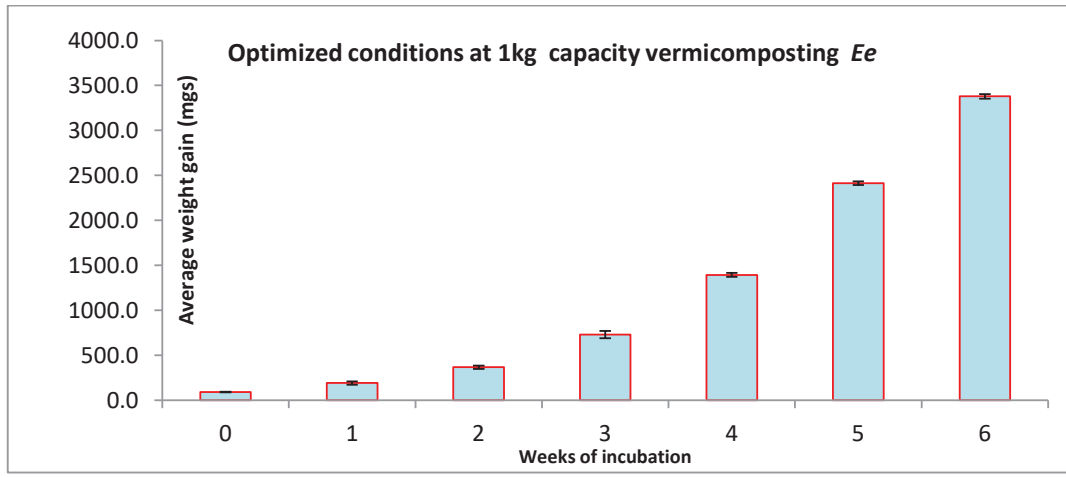

Fig. 7: Vermicomposting using the optimized set of conditions using *Ee* (1 kg tray level study).

Table 5: Optimized conditions for vermicomposting.

Parameter	*Ee*
pH	7
Moisture (%)	70-80
Temperature (ambient ^{0}C)	25-30
Incubation period (weeks)	6

Table 6: Vermicomposting results for optimized conditions for vermicomposting.

Vermicomposting using the optimized set of conditions with *Ee*	
Weeks of incubation	Average weight gain (mg/tray)
0	90.9±3.2
1	190.7± 19
2	366.23± 18.6
3	729.7± 39.4
4	1392.5± 22.1
5	2413.56±19.7
6	3378.7±24.7
Average Total weight gain/ tray/ week	1223.2±1.4
Average growth rate (mg/tray/ day)	78.3±6.1
Average growth rate (mg/worm/ day)	7.8±0.6
Vermicompost (g/kg of feed)	485.7±6.7

Devi, G.S., Karthiga, A., Susila, S. and Muthunarayanan, V. 2012. Bioconversion of fruit waste into vermicompost by employing *Eudrillus eugeniae* and *Eisenia foetida*. International Journal of Plant, Animal and Environmental Sciences, 2(4): 245-252.

Gajalakshmi, S. and Abbasi, S.A. 2004. Earthworms and vermicomposting. Indian Journal of Biotechnology, 3: 486-494.

Gurav, M.V. and Pathade, G.R. 2011. Production of vermicompost from temple waste (Nirmalya): A case study. Universal Journal of Environmental Research and Technology, 1(2): 182-192.

Hemalatha, B. 2013. Comparative evaluation of biodegradability of yard waste and fruit waste with industrial effluents by vermicomposting. Int. J. Adv. Eng. Technol., 2(2): 36-39.

Kadam, D.G. and Pathade, G.R. 2004. Studies on vermicomposting of tendu leaf *Diospyros melanoxylon* Roxb. refuse with emphasis on microbiological and biochemical aspects. Ph.D. Thesis.

Kale, R.D., Bano, K. and Krishnamoorthy, R.V. 1982. Potential of *Perionyx excavatus* for utilizing organic wastes. Pedobiologia, 23(6): 419-425.

Manaf, L.A., Jusoh, M.L.C., Yusoff, M.K., Ismail, T.H.T., Harun, R., Juahir, H. and Jusoff, K. 2009. Influences of bedding material in vermicomposting process. International Journal of Biology, 1(1): 81.

Mane, T.T. and Raskar Smita, S. 2012. Management of agriculture waste from market yard through vermicomposting. Research Journal of Recent Sciences, 1(ISC-2011): 289-296.

Manyuchi, M.M. and Phiri, A. 2013. Vermicomposting in solid waste management: A review. International Journal of Scientific Engineering and Technology, 2(12): 1234-1242.

Mathew, J. 2006. The impact of new economic policy on Indian agriculture a study of selected cash crops. Thesis. Department of Economics, Dr. John Matthai Centre, University of Calicut.

Palsania, J., Sharma, R., Srivastava, J.K. and Sharma, D. 2008. Effect of moisture content variation over kinetic reaction rate during vermicomposting process. J. Applied Ecology and Environmental Research, 6(2): 49-61.

Pandit, N.P. and Maheshwari, S.K. 2012. Optimization of vermicomposting technique for sugarcane waste management by using *Ef.* Int. J. Biosci., 10(1): 143-155.

Suthar, S. 2009. Vermicomposting of vegetable-market solid waste using *Eisenia fetida*: Impact of bulking material on earthworm growth and decomposition rate. Ecological Engineering, 35(5): 914-920.

Utekar, G. and Deshmukh, H. 2016. Optimization of parameters for preparation of vermicompost from bagasse and press mud by using *Ee*. Res J. Chem. Environ. Sci., 4(3): 67-70.

Nature Environment and Pollution Technology
An International Quarterly Scientific Journal

p-ISSN: 0972-6268
(Print copies up to 2016)
e-ISSN: 2395-3454

Vol. 19 | No. 2 | pp. 881-888 | 2020

Original Research Paper

https://doi.org/10.46488/NEPT.2020.v19i02.048

Open Access Journal

Impact of Environmental Investment on Performance of Intelligent Manufacturing Enterprises in the Yangtze River Delta of China

Wanqing Shao
*School of Economics and Management, Ningbo University of Technology, Ningbo 315211, China; swq1624@163.com

Nat. Env. & Poll. Tech.
Website: www.neptjournal.com

Received: 18-02-2020
Accepted: 07-04-2020

Key Words:
Environmental investment;
Performance appraisal;
Intelligent manufacturing;
Yangtze river delta

ABSTRACT

The rapid development of information technology has promoted the transformation of the manufacturing industry and the upgrading of Chinese intelligent manufacturing enterprises. Environmental protection and enterprise benefits have become the pursuit target. To explore the impact of environmental investment on the performance of intelligent manufacturing enterprises, an evaluation index system from the four dimensions of debt paying, operation, profitability, and growth ability was constructed. Then, factor analysis method was used to analyse the index data of 33 intelligent manufacturing enterprises in the Yangtze River Delta in 2018, and a multiple regression model was constructed to analyse the impact of environmental investment on enterprise performance. Results show a significant difference in the performance of intelligent manufacturing enterprises in the Yangtze River Delta and a positive correlation between environmental investment and enterprise performance. Finally, specific optimization measures are given to help the managers of intelligent manufacturing enterprises make scientific and reasonable decisions.

INTRODUCTION

The report of the 19th National Congress of the Communist Party of China emphasizes the implementation of the strictest ecological environment protection system. The promulgation of various laws and policies reflects the party and the state's attention to environmental protection and determination to control environmental pollution. Intelligent manufacturing enterprises inevitably pollute the environment in the process of production. Thus, they should improve the level of environmental governance and bear the responsibility for environmental protection (Xu 2020). The manner of pursuing the maximization of benefits and walking out of the win-win road of environmental protection and economic benefits is the key to the sustainable development of intelligent manufacturing enterprises (Huang 2019).

According to the intelligent manufacturing development plan (2016-2020), the proportion of R&D expenditure of the manufacturing industry above the designated size in the main business income will increase from 0.95% to 1.68% by 2025, and the number of effective invention patents per billion RMB of the main business income will increase from 0.36 to 1.10 (Wang et al. 2019). The Yangtze River Delta has a strong advantage based on industry. However, shortcomings remain evident in the intelligent manufacturing industry in the delta, especially in the cultivation of various enterprises, the layout of key nodes in the industrial chain, and the supply of core technologies (Fang et al. 2019). The 2019 Yangtze River Delta Intelligent Manufacturing Development White Paper was released in Nanjing. It aims to promote the Yangtze River Delta to explore the mechanism of intelligent manufacturing collaborative innovation, deploy and build a collaborative innovation network, and support the transformation and upgrading of small-and-medium-sized manufacturing enterprises.

PAST STUDIES AND RESEARCH HYPOTHESIS

The relationship between environmental investment and enterprise performance has always been the core issue of environmental management research. The three representative views in the academic community are negative correlation, positive correlation, and non-correlation (Zhang et al. 2019). Traditional economic theory holds that a negative correlation exists between environmental investment and enterprise performance. The implementation of environmental management increases the cost and burden of enterprises because enterprises cannot obtain profit while increasing important investment expenditure (Shan et al. 2018, Azadegan et al. 2018). Moreover, the increase of investment in environmental management squeezes the resources of other profitable projects, disperse time and manpower, and reduce the production efficiency of the enterprise, which is not conducive to the promotion of competitiveness and long-term development of the enterprise. Other scholars believed that environmental management is positively related to enterprise performance,

and investment in environmental management may increase enterprise cost in the early stage. In the long run, this cost can be made up by improving ecological efficiency and innovating environmental protection technology (Lopez et al. 2017, Xia et al. 2019). On the one hand, the excellent performance of enterprises in environmental protection meets the green demand of consumers, increases the sales volume of products, and improves the market share. On the other hand, it is conducive to the establishment of an attractive social image, the promotion of brand awareness, the enhancement of competitive advantage of enterprises, and the realization of a win-win situation between environmental management and enterprise development (Tang et al. 2019). Another view is that no correlation exists between environmental management and enterprise performance, and the improvement of environmental management does not affect the improvement of enterprise competitiveness (Gai 2019). Enterprises engage in environmental protection investment to reduce the level of environmental pollution, achieve the environmental protection indicators of the government, and gain the attention of the public and investors to environmental protection (Chen et al. 2017). Such investment minimizes the frequency of environmental supervision from the environmental protection department of the government, maintain the normal production and operation order of enterprises, and reduce the compliance cost of enterprise environmental regulations.

This study holds that, in the process of environmental investment, intelligent manufacturing enterprises need to integrate various resources, promote enterprises to innovate production processes, and improve organizational management capabilities. Thus, forming unique competitive advantage and improving the efficiency of resource allocation (Zhao 2018) and the profitability of enterprises environmental investment help enterprises establish a reputable social image, enhance brand value, increase product sales and market share, and reduce long-term risks related to the disposal costs of environmental pollution, energy price fluctuations, and product quality responsibility. Based on the above points of view, this study puts forward the following hypothesis: A positive correlation exists between environmental investment and the performance of intelligent manufacturing enterprises.

Many studies on enterprise performance evaluation exist, and the differences between evaluation indexes and evaluation methods are significant (Bravo-Macias et al. 2019). First, this study constructs the performance evaluation index system of intelligent manufacturing enterprises regarding relevant regulations of the Ministry of Finance, uses factor analysis method to analyse the index data of 33 intelligent manufacturing enterprises in 2018, and obtains the comprehensive performance score. According to the performance score, a multiple regression model is constructed to analyse the impact of environmental investment on corporate performance. Finally, according to the empirical results, the study puts forward the countermeasures to improve the performance of intelligent manufacturing enterprises.

MODELLING

Data Source

The annual financial reports of intelligent manufacturing enterprises in the Yangtze River Delta of China in 2018 are referred through Sina Finance, China Stock Market, and Accounting Research Database, and 33 sample enterprises are collected. The environmental protection input data of listed companies come from the environmental protection information disclosed by enterprises, which is included in the corporate social responsibility, environmental, and sustainable development reports. The information comes from the Shanghai Stock Exchange, the Shenzhen Stock Exchange, and official websites of enterprises. This study uses an Excel table to process the original data and SPSS19.0 software for processing and analysis.

Model

According to the above hypothesis, this study uses multiple linear regression models to examine the relationship between variables. In addition, it tests the relationship between environmental investment index and performance comprehensive score to analyse the impact of environmental investment on the performance of intelligent manufacturing enterprises in the Yangtze River Delta. The specific model is as follows:

$$Y = c + \alpha X + \beta_1 H10 + \beta_2 SIZE + \beta_3 AGE + \beta_4 RATE + \varepsilon \ldots(1)$$

Where c is the intercept; X, $H10$, $SIZE$, AGE, and $RATE$ represent environmental investment, equity concentration, enterprise scale, enterprise age, and business income growth rate, respectively; $\alpha, \beta_1, \beta_2, \beta_3$, and β_4 are the coefficients of explanatory variables; ε is the error term.

Variables

Dependent variable: Enterprise performance evaluation refers to the objective, accurate, and comprehensive evaluation of the operating efficiency, manager ability, and performance of an enterprise within a certain period by using specific methods in the financial index system based on the enterprise financial data. This kind of evaluation can truly reflect the actual business situation and predict the future development prospect of the enterprise.

According to the relevant requirements of the revised operational rules for enterprise performance evaluation issued by the Ministry of Finance and by following the principles

of feasibility, importance, relevance, and effectiveness, the performance evaluation index system of listed companies in the household appliance industry is constructed from the four dimensions of solvency, operation ability, profitability, and growth ability, as shown in Table 1.

The idea of the factor analysis method can be expressed by a mathematical model, with the p variables $x_1, x_2,\ldots, x_p$. The mean value after standardization is 0, and the standard deviation is 1. $x_1, x_2,\ldots, x_p$ are expressed in linear form by using k ($k<p$) factors, namely, $f_1, f_2, \ldots, f_k$.

$$\begin{cases} x_1 = a_{11}f_1 + a_{12}f_2 + \ldots + a_{1k}f_k + \varepsilon_1 \\ x_2 = a_{21}f_1 + a_{22}f_2 + \ldots + a_{2k}f_k + \varepsilon_2 \\ \ldots \\ x_p = a_{p1}f_1 + a_{p2}f_2 + \ldots + a_{pk}f_k + \varepsilon_p \end{cases} \quad \ldots(2)$$

Equation (1) shows the linear equations of this method. The matrix expression is

$$x = af + \varepsilon'. \quad \ldots(3)$$

In the above formula, f is the factor, and the correlation coefficient $f_j(j = 1, 2,\ldots, k)$ is 0. a is the factor load matrix and $a_{ij}(i = 1, 2,\ldots, p, j = 1, 2,\ldots, k)$ is the factor load. ε' is a special factor, which is independent of $f_j(j = 1, 2,\ldots, k)$.

Independent variable: Environmental investment is set as a virtual variable in this study. If the enterprise has environmental investment, it is recorded as 1, otherwise 0. The existence of environmental protection investment is based on the summary of all environmental protection-related investment data disclosed by the enterprise, including the summary of environmental protection expenditure disclosed in terms of environmental protection investment, environmental protection operation cost, environmental protection tax, pollution discharge fee, and greening fee. A virtual variable is taken because few companies disclose environmental investment information in the listed companies. Excluding the data of these companies that do not disclose environmental protection information causes a shortage of sample size, estimation error, and sample selectivity error.

Control variable: Equity concentration (*H10*): The relatively concentrated ownership structure can encourage shareholders to implement effective supervision. However, the further expansion of the ownership concentration may result in the phenomenon that large shareholders infringe on the interests of small shareholders, especially when large shareholders are "vacant." Scholars mostly use the first, top five, top ten shareholders ratio, and Hefndal index to measure equity concentration. This study selects the shareholding ratio of the top ten shareholders to measure the degree of equity concentration.

Enterprise scale (*SIZE*): According to the review of previous literature, large-scale enterprises engaged in production and operation activities tend to have a considerable impact on society and the environment. They pay considerable attention to environmental protection and governance issues and seek the long-term development of enterprises. Moreover, large scale enterprises are better than smaller ones in terms of management level, sales ability, and production efficiency. Therefore, large-scale enterprises perform efficiently whether in the aspect of environmental investment or enterprise performance. This study uses the natural logarithm of total assets to measure the scale of enterprises.

Enterprise age (*AGE*): The establishment time, experience,

Table 1: Performance evaluation index system construction of intelligent manufacturing enterprises.

Primary index	Secondary index	Calculation formula	Variable
Solvency	Liquidity ratio	Current assets / current liabilities	X_1
	Quick ratio	Quick assets / current liabilities	X_2
	Asset liability ratio	Total liabilities / total assets	X_3
Operational capability	Turnover rate of accounts receivable	Operating income / average balance of accounts receivable	X_4
	Inventory turnover	Operating cost / average inventory balance	X_5
	Turnover rate of total assets	Operating income / average balance of assets	X_6
Profitability	Return on equity	Net profit / average net assets	X_7
	Return on invested capital	Operating profit / invested capital before interest and after tax	X_8
	Operating profit margin	Operating profit / revenue	X_9
Growth ability	Growth rate of total assets	Total assets growth of the year / total assets at the beginning of the year	X_{10}
	Growth rate of net intangible assets	Increase in net intangible assets / net intangible assets at the end of last year	X_{11}
	rate of capital accumulation	Ending owner's equity / beginning owner's equity	X_{12}

and reputation of the company affect the performance. They also have an indirect impact on environmental investment. This study takes the number of years of the establishment of the enterprise as a regulating variable.

Operating income growth rate (*RATE*): Fast-growing enterprises can often adapt quickly to policy changes and have the corresponding strength to increase environmental investment to ensure the sustainable, healthy, and green development of enterprises. All variables are given in Table 2.

RESULT ANALYSIS

Performance Appraisal

KMO test and Bartlett's spherical test: After testing, the KMO value is 0.53, which is higher than the critical value of 0.50, thus meeting the preconditions for factor analysis. The approximate chi-square value of Bartlett's spherical test results is 411.59. The corresponding probability value is 0.00, which is less than the given significance level of 0.01, indicating that validity meets the requirements and the preconditions of factor analysis.

Factor analysis results: The variance contribution of the first common factor is 3.09, and the variance contribution rate after rotation is 25.73%. The extracted four common factors explain most of the information of the original variables, reaching 83.08%, as given in Table 3. Given the retention of two decimal places, a certain error exists but does not affect the whole.

In this study, the factor load matrix is rotated by the maximum variance method. Given that the current ratio (X_1), quick ratio (X_2), and asset-liability ratio (X_3) have a high load in common factor 1, the three indicators reflect the solvency. Thus, F_1 is named as the "solvency factor." Given that the inventory turnover rate (X_5), total asset growth rate (X_{10}), and capital value preservation and appreciation rate (X_{12}) have a high load in common factor 2, inventory turnover rate reflects

Table 2: Definition of variables.

Type	Name	Symbol	Measurement
Dependent Variable	Enterprise performance	*Y*	Comprehensive score or factor score of enterprise performance
Independent Variable	Turnover rate of account receivable	*X*	Virtual variable. If there is environmental investment, it is recorded as 1, otherwise it is recorded as 0
Control Variable	Equity concentration	*H10*	Shareholding ratio of top ten shareholders
	Enterprise scale	*SIZE*	Logarithm of total assets of enterprise
	Enterprise age	*AGE*	Age from establishment to data analysis
	Growth rate of operating revenue	*RATE*	Growth of operating revenue / total operating revenue of the previous year

Table 3: Characteristic value and variance contribution rate in 2018.

Factor	Initial eigenvalue			Extract square sum load			Rotate square sum load		
	Total	Variance%	Cumulative%	Total	Variance%	Cumulative%	Total	Variance%	Cumulative%
1	3.59	29.89	29.89	3.59	29.89	29.89	3.09	25.73	25.73
2	2.93	24.38	54.26	2.93	24.38	54.26	2.79	23.29	49.01
3	2.05	17.05	71.31	2.05	17.05	71.31	2.66	22.14	71.15
4	1.41	11.77	83.08	1.41	11.77	83.08	1.43	11.94	83.08
5	0.87	7.23	90.31						
6	0.57	4.78	95.09						
7	0.21	1.78	96.87						
8	0.21	1.72	98.59						
9	0.09	0.77	99.36						
10	0.05	0.45	99.82						
11	0.02	0.15	99.96						
12	0.00	0.04	100.00						

Note: Due to the retention of two decimal places, there is a certain error, but does not affect the whole.

operating capacity, and total asset growth rate; capital value preservation, and appreciation rate reflect growth capacity. Thus, F_2 can be named as the "growth operation factor." Given that return on equity (X_7), return on invested capital (X_8), and operating profit rate (X_9) have a high load in common factor 3, the three indicators reflect profitability indicators. Thus, F_3 can be named as the "profit factor." Given that the turnover rates of accounts receivable (X_4) and total assets (X_6) and the growth rate of net intangible assets (X_{11}) have a high load in common factor 4, the first two items reflect the operating capacity, and the growth rate of net intangible assets reflects the growth capacity. Thus, F_4 is named as the "operation growth factor." In this study, the score function of each main factor after rotation can be written as

$$F_1 = 0.96X_1 + 0.97X_2 - 0.86X_3 + 0.07X_4 + 0.11X_5 - 0.48X_6 + 0.04X_7 - 0.01X_8 + 0.47X_9 - 0.01X_{10} - 0.05X_{11} - 0.03X_{12}$$

$$F_2 = -0.05X_1 - 0.02X_2 - 0.10X_3 - 0.22X_4 + 0.94X_5 + 0.24X_6 + 0.04X_7 + 0.10X_8 + 0.01X_9 + 0.91X_{10} - 0.06X_{11} + 0.97X_{12}$$

$$F_3 = 0.10X_1 + 0.08X_2 - 0.14X_3 - 0.05X_4 + 0.03X_5 + 0.09X_6 + 0.97X_7 + 0.99X_8 + 0.83X_9 + 0.04X_{10} + 0.02X_{11} + 0.07X_{12}$$

$$F_4 = 0.12X_1 + 0.11X_2 + 0.18X_3 + 0.70X_4 + 0.02X_5 + 0.60X_6 - 0.03X_7 + 0.06X_8 - 0.10X_9 - 0.04X_{10} - 0.71X_{11} - 0.02X_{12} \quad \ldots(4)$$

According to the weight determined by the variance contribution rate, the comprehensive score function of performance can be written as

$$F = (25.73\%F_1 + 23.29\%F_2 + 22.14\%F_3 + 11.94\%F_4 / 83.08\% \quad \ldots(5)$$

According to the factor score function of Formula (4) and the comprehensive score function of Formula (5), the common factor score and the financial performance comprehensive score of intelligent manufacturing enterprises in the Yangtze River Delta of China in 2018 can be calculated, as given in Table 4.

DISCUSSION

According to the performance score table of intelligent manufacturing enterprises in the Yangtze River Delta of China

Table 4: Public factor scores and rankings of intelligent manufacturing enterprises in the Yangtze River delta of China in 2018.

Stock name	F1	F2	F3	F4	F	Rank	Stock name	F1	F2	F3	F4	F	Rank
Zhongnan Construction	-0.95	-0.55	0.01	-0.32	-0.49	30	DragonNet Technology	2.30	-0.23	-0.39	-0.48	0.47	4
Miracle Automation	-0.70	-1.19	-0.07	0.21	-0.53	31	Ningbo Cixing	0.10	-0.17	-0.32	-2.35	-0.44	27
Dun'an Artificial	-0.69	0.12	-4.06	0.73	-1.15	33	SVG	-0.12	0.18	-0.28	-0.26	-0.09	19
Good-Ark Electronics	0.81	0.13	-0.10	1.01	0.40	5	Yinbang Clad Material	-0.67	-0.24	-0.87	0.21	-0.47	29
Haisum Engineering	-1.15	0.00	0.60	2.00	0.09	13	Digiwin Software	-0.32	-0.46	-0.10	0.92	-0.12	21
Tongfu microelectronics	-0.83	-0.34	-0.40	-1.94	-0.73	32	Lead Intelligent	-0.69	0.07	1.50	-0.47	0.14	10
Sanlux	2.06	-0.48	-0.47	2.11	0.67	3	Fullhan microelectronics	1.58	-0.42	-0.38	-0.91	0.13	11
Canny Elevator	-0.41	0.02	-0.65	-1.21	-0.47	28	RoboTechnik Intelligent	-1.25	0.22	2.07	-0.32	0.18	9
Sciyon Wisdom	1.49	-0.38	0.01	-0.98	0.21	7	NARI Technology	-0.38	0.15	0.94	-0.44	0.11	12
Great Star Industrial	0.30	-0.20	0.37	0.47	0.20	8	Joyson Electronic	-1.15	0.10	0.14	1.88	-0.01	16
Great Chinasoft	-0.92	0.18	-0.33	0.71	-0.22	24	Nanjing Panda	-0.34	-0.14	-0.18	0.22	-0.16	22
Shuanghuan Driveline	-0.50	0.66	-0.24	-0.51	-0.10	20	Mechanical & Electrical	-0.68	-0.46	0.57	0.85	-0.06	17
Morningstar Network	-0.49	0.06	-0.12	-0.49	-0.24	25	Baosight Software	0.17	-0.30	0.41	-0.05	0.07	14
Hangzhou Century	-0.08	-0.38	0.04	-0.83	-0.24	26	China Wafer	1.61	-0.41	-0.34	0.38	0.34	6
HAND Enterprise	0.62	5.24	0.18	0.08	1.72	1	Yijihe Technology	1.91	-0.63	1.99	0.59	1.02	2
Tofflon Science and	0.09	0.21	-0.47	-0.34	-0.09	18	Kelai Mechatronics	-0.41	-0.20	0.67	0.34	0.05	15
CSG Smart	-0.35	-0.14	0.26	-0.79	-0.19	23	-	-	-	-	-	-	-

in 2018, the top companies in the comprehensive score f are as follows: HAND Enterprise Solutions, Yijihe Technology, Sanlux, DragonNet Technology, Good-Ark Electronics, China Wafer Level CSP, Sciyon Wisdom Technology, Great Star Industrial, RoboTechnik Intelligent Technology, and Lead Intelligent Equipment. The number of enterprises with a comprehensive score of F less than 0 reached 18, accounting for 54.55%. HAND Enterprise Solutions scored the highest (1.72), whereas Dun'an Artificial Environment scored the lowest. The range was 2.87. The number of enterprises with debt service factor F1 scores less than 0 reached 21, accounting for 63.64%. DragonNet Technology scored the highest (2.30), whereas RoboTechnik Intelligent Technology scored the lowest (−1.25). The range was 3.55. The number of enterprises with a growth operating factor F2 scores less than 0 reached 20, accounting for 60.61%. HAND Enterprise Solutions scored the highest (5.24). The lowest score was −1.19. The range was 6.43. The number of enterprises with a profit factor F3 scores less than 0 reached 18, accounting for 54.55%. RoboTechnik Intelligent Technology scored the highest (2.07). Dun'an Artificial Environment scored the lowest (−4.06). The range was 6.12. The number of enterprises with an operating growth factor F4 scores less than 0 reached 17, accounting for 51.52%. Sanlux scored the highest (2.11). Ningbo Cixing scored the lowest was −2.35. The range was 4.46. In 2018, more than half of the enterprises scored less than 0 in terms of performance, debt service factor, operation growth factor, profit factor, and operation growth factor. The main reason is that the overall economic environment in 2018 was poor, the economic situation was declining, the financial market was turbulent, and most intelligent manufacturing enterprises were unable to obtain enough capital to support innovation investment. As a result, the overall profit, growth, and operation declined. In addition, corporate performance and revenue were underperforming.

Multiple Regression Analysis

Descriptive statistics: The average value of the environmental investment is 0.42, indicating that more than half of enterprises have not invested in environmental protection. The standard deviation is 0.50, which is greater than the average and median, indicating that the distribution of enterprise environmental investment is relatively scattered. The maximum value of *H10* is 1.00, the minimum value is 0.32, and the average value is 0.59. Thus, the sample enterprises have a high concentration of equity. The average age of the company is 18.82 years, the longest time is 28 years, and the shortest time is 7 years. Therefore, the sample enterprises have a long period of continuous operation, and most of them have relatively stable development. From the perspective of the growth rate of business income, the maximum value is 1.32, the minimum value is −0.10, and the average value is 0.26, indicating that the sample enterprises have rapid overall growth and good market development, as given in Table 5.

Correlation analysis: Pearson correlation test results show that company size (*SIZE*), operating revenue growth rate (*RATE*), and debt service factor F1 scores are significant at 1% and 5% levels. The correlation coefficients are −0.47 and −0.41, showing a negative correlation. Equity concentration (*H10*), operating revenue growth rate (*RATE*), and profit factor F_3 score are significant at 5% level. The correlation coefficients are 0.43 and 0.38, which show a positive correlation. A negative correlation exists between company size (*SIZE*) and comprehensive score *F*. The correlation coefficient is −0.35, which is significant at 5% level, as given in Table 6. This value may be due to the excessive enterprise size and consumption of enterprise profits and may ultimately lead to the decline of enterprise performance.

Regression results: According to Table 7, the maximum value of *F* test is 3.35, which is significant at 1% level. The

Table 5: Descriptive statistics.

Variable		N	Range	Minimum	Maximum	Mean	Standard deviation
	F_1	33	3.55	-1.25	2.30	0.00	1.00
	F_2	33	6.43	-1.19	5.24	0.00	1.00
Y	F_3	33	6.12	-4.06	2.07	0.00	1.00
	F_4	33	4.46	-2.35	2.11	0.00	1.00
	F	33	2.87	-1.15	1.72	0.00	0.51
X		33	1.00	0.00	1.00	0.42	0.50
H10		33	0.68	0.32	1.00	0.59	0.14
SIZE		33	5.60	20.59	26.19	22.37	1.24
AGE		33	21.00	7.00	28.00	18.82	4.77
RATE		33	1.41	-0.10	1.32	0.26	0.31

minimum value is 2.07, which is significant at the 10% level. That is, a significant linear relationship exists between variables. The regression results of comprehensive score *F* show that environmental investment (*X*) has a positive correlation with enterprise performance, with a coefficient of 0.37, which is significant at 5% level, indicating that increasing environmental investment can promote the improvement of enterprise performance and the hypothesis is true. Among the control variables, enterprise size (*SIZE*) has a negative correlation with enterprise performance, with a coefficient of −0.16, which is significant at 5% level. That is, the larger the enterprise is, the more risks it faces in the process of environmental investment, the more aspects it needs to pay attention to, and the more constraints it receives, resulting in the decline of enterprise performance. Meanwhile, other variables are not significant. According to the regression results of the F_1 score of the debt service factor, environmental investment (*X*) is positively correlated with it but not significantly. Enterprise size (*SIZE*) is negatively correlated with it at 1% level. The coefficient is −0.35. The rate of business income growth is also negatively correlated with it and significant at 5% level. The correlation coefficient is −1.03. The fast-growing enterprises choose to borrow further to expand the market scale, which leads to an increase in the debts undertaken by the enterprises and the decrease of the corresponding solvency. Only equity concentration (*H10*) has a negative correlation with the regression result of F_2 score of growth operation factor, which is significant at 5% level. The correlation coefficient is −2.76, indicating that equity is highly concentrated. The development direction is affected by the factors of the decision-maker. Making mistakes is easy and blocks the growth of enterprises. Environmental investment (*X*) is positively correlated with the profit factor F_3 score but not significantly. Equity concentration (*H10*) is positively correlated with the profit factor F_3 score, with a coefficient of 2.62, which is significant at 5% level. Thus, concentrated equity can enhance the profitability of enterprises and place limited resources into high-profit products. The rate of growth of business income (*RATE*) is also positively correlated with the profit factor F_3 score, with a coefficient of 1.14, which is significant at 5% level. That is, the faster the growth of business income, the greater the profits the enterprise obtains. Environmental investment (*X*) is positively correlated with the F_4 score of operation growth, with a coefficient of 0.6, which is significant at 10% level, indicating that enterprises can increase environmental investment, optimize the operation environment, gain the support of the government and society, and contribute to the operation and growth of enterprises. The rate of growth of business income (*RATE*) is also positively correlated with the F_4 score of operation growth with a coefficient of 1.04, which is significant at the 10% level. This rate also shows that the increase of business income can increase capital investment in environmental protection, continuously optimize the business environment, and ensure the good operation of enterprises.

CONCLUSION

This study designs the performance evaluation index system of enterprises in Yangtze River Delta from four aspects: solvency, operation ability, profitability, and development ability. It selects 12 indexes, extracts four common factors by factor analysis, and calculates the comprehensive performance score. Environmental investment is taken as the independent variable. The study selects equity concentration, size, age, and rate of revenue growth as the control variables to analyse the impact of environmental investment on corporate performance. The conclusions obtained in this study as follow: there is a positive correlation between environmental investment and corporate performance. Increasing

Table 6: Correlation test between variables.

	F1	F2	F3	F4	F	X	H10	SIZE	AGE	RATE
F_1	1									
F_2	0.00	1								
F_3	0.00	0.00	1							
F_4	0.00	0.00	0	1						
F	0.60**	0.55**	0.52**	0.28	1					
X	0.09	0.16	0.15	0.21	0.27	1				
H10	-0.23	-0.29	0.43*	-0.21	-0.13	0.16	1			
SIZE	-0.47**	-0.04	-0.09	0.00	-0.35*	0.11	0.06	1		
AGE	-0.10	-0.14	-0.12	0.25	-0.13	0.02	-0.17	0.34	1	
RATE	-0.41*	0.03	0.38*	0.19	0.03	-0.12	0.18	0.10	-0.12	1

Note: ** Significant correlation at 0.01 level (bilateral), * Significant correlation at 0.05 level (bilateral).

Table 7: Multiple regression results.

	Y				
	F_1	F_2	F_3	F_4	F
c	8.70*** (3.10)	1.82 (0.56)	1.12 (0.38)	2.05 (0.66)	3.76** (2.39)
X	0.24 (0.78)	0.46 (1.27)	0.31 (0.95)	0.60* (1.74)	0.37** (2.12)
H10	-1.25 (-1.07)	-2.76** (-2.05)	2.62** (2.14)	-1.90 (-1.48)	-0.73 (-1.12)
SIZE	-0.35*** (-2.61)	0.01 (0.10)	0.15 (1.05)	-0.12 (-0.79)	-0.16** (-2.11)
AGE	0.01 (-0.14)	-0.04 (-1.05)	0.01 (0.27)	0.06 (1.56)	-0.01 (-0.11)
RATE	-1.03** (-2.03)	0.32 (0.54)	1.14** (2.15)	1.04* (1.87)	0.23 (0.81)
F_{test}	3.35***	2.07*	2.57**	2.21*	2.44*

Note: *** indicates a significant correlation at 1% level, ** indicates a significant correlation at 5% level, and * indicates a significant correlation at 10% level.

differences in the performance of intelligent manufacturing enterprises are observed, and their environmental investment status is not the same. The development should be balanced and coordinated from the aspects of profitability, solvency, operation ability, growth ability, and environmental investment. Moreover, the performance level of enterprises should be constantly improved to achieve the sustainable development of intelligent manufacturing enterprises.

ACKNOWLEDGEMENT

The study was supported by the Soft Science Foundation of Ningbo City (Grant: 2018A10017).

REFERENCES

Azadegan, A., Golara, S., Kach, A. and Mousavi, N. 2018. Corporate environmental investments: a cross-national study on managerial decision making. International Journal of Production Economics, 199: 47-64.

Bravo-Macias, C., Sarmentero-Bon, I., Rodriguez-Sanchez, Y. and Gomez-Figueroa, O. 2019. Evaluation of organizational competencies through performance indicators. DYNA, 94(5): 90.

Chen, W.H., Zhong, X. and Song, T. B. 2017. Performance expectation gap, equity concentration and enterprise environmental protection investment. Industrial Technology Economy, 36(12): 10-18.

Fang, X. and Lu, W. 2019. Research on the transformation and upgrading of traditional manufacturing to intelligent manufacturing in the Yangtze River Delta. Modern Management Science, (10): 28-30.

Gai, T.Q. 2019. Research on the correlation between enterprise environmental protection investment and financial performance: Taking the coal industry as an example. Journal of Liaoning University of Engineering and Technology (Social Science Edition), 21(2): 106-112.

Huang, Q.H. 2019. Review of Research Report on the development of China's manufacturing industry 2019: 40 years of manufacturing in China and intelligent manufacturing. Economic Trends, (11): 156-157.

Lopez, J.M.R., Sakhel, A. and Busch, T. 2017. Corporate investments and environmental regulation: the role of regulatory uncertainty, regulation-induced uncertainty, and investment history. European Management Journal, 35(1): 91-101.

Shan, C.X. and Zhong, W.Z. 2018. Study on the impact of environmental protection investment on the core competitiveness of coal enterprises. East China Economic Management, 32(1):137-144.

Tang, Y.J. and Xia, L. 2019. Environmental protection investment, environmental information disclosure quality and enterprise value. Science and Technology Management Research, 39(10): 256-264.

Wang, R.X., Yu, Z.W., Guo, Y. 2019. Made in China 2025 Ningbo practice. Beijing: China Finance and Economics Press.

Xia, T.T. and Li, M.Y. 2019. Environmental protection investment, policy support and green financial efficiency. Research on Technology Economy and Management, (7): 68-72.

Xu, Y. 2020. Executive incentive, environmental regulation and enterprise environmental protection investment. Technology and Industry, 20(1): 129-135.

Zhang, T., Chen, Y.X. and Wu, J.B. 2019. An empirical analysis of the impact of environmental management of Listed Companies in China's chemical industry on corporate performance. Business Accounting, (21): 33-38.

Zhao, P. 2018. Analysis of the development status and demand of China's intelligent manufacturing industry. Journal of Liaoning Transportation College, 20 (5):36-39.

Nature Environment and Pollution Technology
An International Quarterly Scientific Journal

p-ISSN: 0972-6268
(Print copies up to 2016)
e-ISSN: 2395-3454

Vol. 19 | No. 2 | pp. 889-895 | 2020

Original Research Paper

https://doi.org/10.46488/NEPT.2020.v19i02.049

Open Access Journal

Facile Preparation of β-Fe_2O_3/$BiOCl_{0.875}Br_{0.125}$ Composites for Enhanced Visible-light Photocatalytic Degradation of Organics from Water

Jihao Zhou*, Zhiwei Zhao, Ping Xiao***, Jie Liu*, Zhaoxia Ding*†, Yuting Han*** and Jie Shi******

*Department of Military Facilities, Army Logistics University, Chongqing, 401331, China
**College of Environment and Ecology, Chongqing University, Chongqing, 400044, China
***Green Intelligence Environmental School, Yangtze Normal University, Chongqing 408100, China
****PLA, No. 93413, Yongji, Shanxi 044500, China
†Corresponding author: Zhaoxia Ding (E-mail: Jihao Zhou; rainbowin@qq.com)

Nat. Env. & Poll. Tech.
Website: www.neptjournal.com

Received: 30-06-2019
Accepted: 30-08-2019

Key Words:
Bismuth oxyhalide;
Catalyst modification;
Organics degradation;
Visible-light photocatalysis

ABSTRACT

Visible light-driven photocatalytic oxidation technology has shown great potential for effective removal of organic pollutants from water and mitigation of energy crises at the same time. The highly effective and economic β-Fe_2O_3/$BiOCl_{0.875}Br_{0.125}$ photocatalyst was prepared by a facile hybrid compositing method with β-Fe_2O_3 and $BiOCl_{0.875}Br_{0.125}$ to overcome relatively high material cost and limited catalytic efficiency. Characterization techniques, such as XRD, SEM and XPS were used to study the purity and crystallization characteristics of the as-prepared photocatalyst. Furthermore, taking rhodamine b (RhB) as a simulated organic pollutant, the photocatalytic property of β-Fe_2O_3/$BiOCl_{0.875}Br_{0.125}$ with different Bi content was further evaluated by static catalytic degradation test under visible-light. The results indicated that the photocatalytic efficiency of the novel composites increases with the improvement of Bi content. Additionally, in comparison to equal mass of pure phase $BiOCl_{0.875}Br_{0.125}$, when the Bi content reached to 30%, a comparable and even better photocatalysis performance was achieved by the as-prepared β-Fe_2O_3/$BiOCl_{0.875}Br_{0.125}$. The hybrid β-Fe_2O_3/$BiOCl_{0.875}Br_{0.125}$ has a potential cost advantage in practical water treatment, and provide an attractive method for fabricating efficient visible-light-driven photocatalysts.

INTRODUCTION

In the past decades, with the rapid development of modern industry and agriculture, environmental and energy-related issues are increasingly becoming two major problems facing humanity (Elimelech & Phillip 2011). A wide range of pollution sources including domestic sewage, pesticides, pharmaceuticals, and chemicals, have aggressively spread around the soil, atmosphere, and the natural waters, resulting in serious damage to the ecosystem (Omenn 2006). Water safety, as one of the current high-profile topics, is seriously threatened by various Persistent Organic Pollutants (POPs) (Zhang et al. 2019). Therefore, seeking efficacious technologies for the removal of POPs is of particular importance to ensure safe production of drinking water and sustainable development of aquatic environment. At present, traditional methods for treating organic pollutants in water mainly include biological treatment, chemical oxidation, membrane filtration and adsorption (Hasan & Jhung 2015). However, there are always some inevitable defects hidden behind these conventional processes, such as the inability to completely degrade organic pollutants, high cost, and the easiness to produce secondary pollution, and so on (Amini et al. 2015). Advanced oxidation processes (AOPs)-based treatment technologies are receiving special recognition as alternatives to traditional water disposal processes and as a means of effluent polishing for water reclamation (Ribeiro et al. 2015, Deng & Zhao 2015). Since the AOPs have been continuously proven to perform a significant effect on the removal of organic pollutants with high stability and toxicity in water, exploring novel AOPs with strong degradation efficiency, low cost, high stability, mild reaction conditions and no secondary pollution, occupied the position of the hottest research field currently.

Photocatalytic oxidation technology is one of the most promising AOPs and growing popularity to be applied to water treatment due to its unique advantages like highly efficient organic mineralization, energy-saving, non-toxic, and no or fewer chemicals consume. Photocatalysis is inseparable from photocatalysts. By utilizing the energy of light to convert into the chemical energy required for chemical reactions, photocatalysts can degrade almost all harmful organic pollutants and some inorganic substances, accelerating

chemical reactions (Hoffmann et al. 1995). It recognized that once the semiconductor photocatalyst was subjected to light illumination (visible or ultraviolet light), the electrons on the valence band are excited to leap into the conduction band, resulting in leaving behind a hole in the valence band (Lee et al. 2016, Masih et al. 2017, Martin et al. 2015). Thus, the hole-electron pairs are continually generated in the presence of the electrostatic field force. During this process, part of the excited photogenerated electrons and holes migrate to the surface of the photocatalyst, producing multiple strong oxidizing species that are competent to degrade organic contaminants from the water (Jaiswal et al. 2016, Mohamed et al. 2016). Unfortunately, not all photogenerated electron-hole pairs migrate to the semiconductor surface, some of which will recombine in the form of photons. The existence time of the electron-hole pair is very short, but their recombination can still occur inside the photocatalyst, and the recombination rate is the key factor determining the performance of the photocatalyst.

As a new type of photocatalytic material, bismuth oxyhalide (BiOX, X=Cl, Br, I) performs an exceptional photocatalytic activity due to its peculiar layered structure in which X (X=Cl, Br, I) ion layer and $[Bi_2O_2]^{2+}$ layer is alternately arranged. Although BiOX has many advantages, they are still limited in practical applications. To be specific, among the three BiOX, only BiOBr and BiOI possess the narrow enough energy gap with the value of 2.6 and 1.8 eV, respectively, which can be excited by visible light, while BiOCl with an energy gap of 3.2 eV is only allowed to be excited by ultraviolet light (Ren et al. 2013). Besides, in addition to the inferior stability of pure BiOI, the recombination rate of photogenerated electron-hole pairs of three kinds of BiOX in practical applications is relatively fast, resulting in unsatisfactory photocatalytic performance (Li et al. 2014). Thus, aiming to enhance the photocatalytic activity, physical-chemistry stability, photocatalytic response to visible light, as well as to reduce the recombination rate of electron-hole pairs, many attempts such as morphological regulation, complex hybridization and crystal structure control have been carried out to modify BiOX (Ren et al. 2013, Deng et al. 2005, Xiao et al. 2012). However, these modification strategies may be constrained by problems such as complex manufacturing processes or high material costs.

In nature, nano-iron oxide exists mainly in the form of Fe_2O_3 with three crystal configurations of α, β and γ (Brázda et al. 2014). Compared with other metal oxide-based photocatalytic materials, nano-iron oxide, especially in the presence of β-Fe_2O_3, exhibits high structural stability, wide distribution, low preparation cost, and no pollution. Most notable is that the narrow enough bandgap endows β-Fe_2O_3 with excellent visible light absorption performance, which holds great promise in photocatalysis field (Christoforidis et al. 2016). Currently, Br-based blending modification has proven to be an effective way to reduce the electron-hole pair recombination rate of BiOCl (Gnayem & Sasson 2013). However, this method is limited by the large consumption of Bi, which leads to an increase in cost, and there is still room for improvement in the activity of the $BiOCl_xBr_{1-x}$ composite. To the best of our knowledge, from the perspective of composite hybridization, the modification strategy of preparing bismuth oxyhalide-based composite by further compounding β-Fe_2O_3 has not been reported.

The overall objectives of this study were: (1) to successfully synthesize and characterize the hybrid β-Fe_2O_3/$BiOCl_xBr_{1-x}$ composite photocatalyst; (2) to evaluate the photocatalytic degradation performance of β-Fe_2O_3/$BiOCl_xBr_{1-x}$ on organics removal; (3) to analyse the photocatalytic mechanism of the composite material of β-Fe_2O_3/$BiOCl_xBr_{1-x}$.

MATERIALS AND METHODS

Materials: All chemical reagents were of analytical grade and were used as received. Ferric sulphate, sodium sulphate decahydrate, sodium chloride, potassium bromide and rhodamine B (RhB) were purchased from Macklin Biochemical Co., Ltd (China). Other reagents including bismuth nitrate pentahydrate, cetyltrimethylammonium chloride (CTAC), nitric acid and absolute ethyl alcohol were obtained from Sinopharm (China).

Preparation of β-Fe_2O_3, $BiOCl_{0.875}Br_{0.125}$ and β-Fe_2O_3/$BiOCl_{0.875}Br_{0.125}$: Deionized water (15 mL), ferric sulphate (15 mmol), and sodium sulphate decahydrate (15 mmol) are placed into a 50 mL flask followed by stirring and drying at 70°C. The obtained powder products were mixed with 30 mmol of NaCl and ground, and then transferred to a tube furnace (SKGL-1200M, SIOMM, China) and calcinated at 500°C for 1 h.

For the synthesis of $BiOCl_xBr_{1-x}$, according to the method reported by Gnayem & Sasson (2013), the procedure of preparing a 3D flower-like $BiOCl_{0.875}Br_{0.125}$ with relatively high photocatalysis activity are as follows: Deionized water (50 mL) and bismuth nitrate pentahydrate (5 mmol) are mixed in a 150 mL flask and stirred at room temperature for 30 min, the obtained solution was denoted as solution A. Then CTAC (1.36 g dissolved in 25 mL of water,) and potassium bromide (0.09 g, 0.75 mmol) are added to the above solution in one batch, following, the obtained flocculent precipitate was magnetically stirred at room temperature for 2 h. The precipitate after centrifugation was washed 3 times with ethanol and deionized water, respectively. The white solid powder

was finally dried at 60 °C in an electrothermal blowing dry box (DHG-9123A, MARIT, China) and was denoted as M0.

For the preparation of β-Fe_2O_3/$BiOCl_{0.875}Br_{0.125}$, a certain amount of β-Fe_2O_3 was added to 40 mL of deionized water, which was subjected to ultrasonic dispersion for 5 min. Afterwards, a certain amount of CTAC and potassium bromide was added to above solution and stirred for 10 min followed by adding different volumes of solution A. After stirring for 2 h, the sample was centrifuged and washed three times with absolute ethanol and deionized water, respectively, and finally dried at 60°C for 6 h. For comparison, a series of β-Fe_2O_3/$BiOCl_{0.875}Br_{0.125}$ with various Bi contents ranging from 10% to 30% were synthesized and the details are presented in Table 1.

Characterization: Employing a scanning electron microscope (SEM, FEI Nova 400 Nano, Philips, Netherlands) to study the morphologies of as-prepared β-Fe_2O_3/$BiOCl_{0.875}Br_{0.125}$. X-ray diffraction (XRD, XRD-6100 Lab, SHIMADZU, Japan) was performed to determine the crystal structure of β-Fe_2O_3/$BiOCl_{0.875}Br_{0.125}$, and its patterns from 20° to 80° were recorded at room temperature following the reported conditions (Gnayem & Sasson 2013). The X-ray photoelectron spectroscopy (XPS, Escalab 250Xi, ThermoFisher Scientific, USA) was carried out to analyse the chemical composition of β-Fe_2O_3/$BiOCl_{0.875}Br_{0.125}$.

Evaluation of photocatalytic property: The RhB, a typical carcinogenic substance from the effluent of the textile industry, was selected as the target organic pollutant to evaluate the photocatalytic performance of as-prepared β-Fe_2O_3/$BiOCl_{0.875}Br_{0.125}$. A 300 W Xe lamp was employed as the visible-light source device (λ> 420 nm, KJS-300W, Kajing Intelligence, China) to simulate natural sunlight. 10 mg of the photocatalyst was added in 50 mL of RhB aqueous solution (20 mg/L). 4 mL of sample was collected at 5, 10, 15, 30 min and filtrated through a 0.22 μm aqueous filter, then was measured at 550 nm with a UV-vis spectrophotometer (DR600, HACH, USA). The degradation rate (D) of RhB was calculated by Eq. (1), and the quasi-first-order kinetic model of this photocatalytic process was shown in Eq. (2).

$$D = [(A_0 - A)/A_0] \times 100\% \quad \ldots(1)$$

$$\ln(A_0/A) = kt \quad \ldots(2)$$

Table 1: β-Fe_2O_3/$BiOCl_{0.875}Br_{0.125}$ prepared with different Bi contents.

name	Bi Content (wt%)	Chemical Addition			
		β-Fe2O3 (g)	CTAC (g)	KBr (g)	Solution A (mL)
M1	10	0.54	0.06	0.004	2
M2	20	0.48	0.12	0.008	4
M3	25	0.45	0.15	0.010	5
M4	30	0.42	0.18	0.012	6

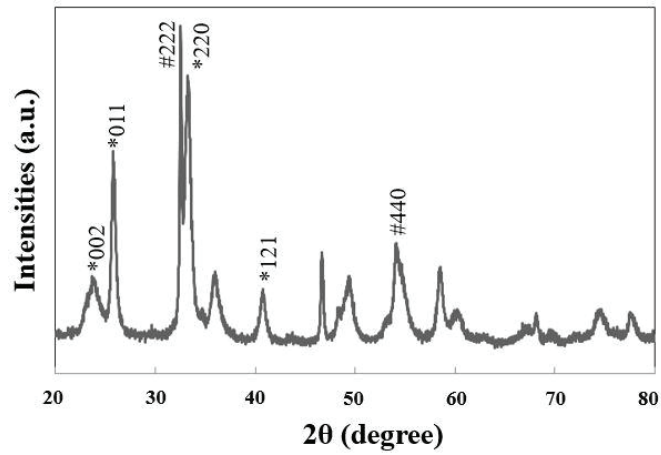

Fig. 1 XRD diffraction pattern of β-Fe_2O_3/$BiOCl_{0.875}Br_{0.125}$

Where, A_0 and A mean the absorbance of RhB solution at 0 and t min under visible-light irradiation, respectively.

RESULTS AND DISCUSSION

Characterization of β-Fe_2O_3/$BiOCl_{0.875}Br_{0.125}$: Fig. 1 displays the XRD diffraction pattern of the composite β-Fe_2O_3/$BiOCl_{0.875}Br_{0.125}$ with a Bi content of 30%. It can be seen that the characteristic diffraction peak of as-prepared β-Fe_2O_3/$BiOCl_{0.875}Br_{0.12}$ coincided with the standard card of the tetragonal BiOX catalyst. Among them, there were strong diffraction peaks at 23.98° and 26.12° corresponding to the diffraction peaks of the (002) and (011) crystal faces of BiOCl. Besides, the peaks at 40.85° and 33.6° were corresponding to the diffraction peaks of the (121) and (220) crystal faces of BiOBr, and these diffraction peaks attributed to BiOX were marked as *. Meanwhile, there are also strong diffraction peaks at 32.7° and 55.21°, which were corresponding to the diffraction peaks of the (222) and (440) crystal faces of β-Fe_2O_3, and were marked as #. As seen in Fig. 1, the intensity of these diffraction peaks were relatively high and the peak shape was sharp, indicating that the composite material synthesized under this condition possessed a superior purity and crystallinity.

Fig. 2 shows the SEM images of the as-prepared β-Fe_2O_3/$BiOCl_{0.875}Br_{0.125}$ sample with a Bi content of 30%. It can be seen from the SEM images at low magnification (a) and high magnification (b) that the synthesized photocatalyst sample had a uniform morphology and size, meanwhile, it exhibited a transparent sheet structure. Fig. 3 indicates the XPS patterns of the composite sample. It can be found from Fig. 3a that the sample had the absorption peaks corresponding to the elements of Bi, Cl, Fe, Br and O, and no absorption peaks of other elements. Besides, the binding energies of the Bi, Cl, Fe and Br elements were attributed to the absorption peaks of Bi 4f, Cl 2p, Fe 2p and Br 3d, respectively (Fig. 3b-3d). From the numerical values of the binding energy of the respective elements, it can be further concluded that the prepared sample had no obvious impurities and exhibited high purity.

Evaluation of the photocatalysis performance: To study the effect of β-Fe_2O_3 doping on the catalytic performance of BiOX, the static photodegradation of RhB over different β-Fe_2O_3/$BiOCl_{0.875}Br_{0.125}$ (10wt%, 20wt%, 25% and 30% of Bi contents) as well as the pure $BiOCl_{0.875}Br_{0.125}$ were shown in Fig. 4. The M1 and M2 present the similarly low degradation efficiency with C/Co of 0.441 and 0.092 after reacting for 30 min, respectively, suggesting that the effective active site exposed to visible light in a short time was incompetent at low Bi contents. However, when the Bi content exceeded 25%, the modified BiOX-based photocatalyst exhibited significantly enhanced degradation efficiency as that the degradation rate of RhB within 15 minutes reached 95.2% and 99.4%, respectively (Fig. 4c and 4d). In comparison to the pure phase $BiOCl_{0.875}Br_{0.125}$ (Fig. 4e), β-Fe_2O_3/$BiOCl_{0.875}Br_{0.125}$ with a Bi content of 30% achieved an excellent photodegradation performance that could be comparable or even better.

In the insets of Fig. 4, the quasi-first-order dynamic models corresponding to each process were also presented, and the coefficients of determination were 0.9629, 0.9547, 0.9939, 0.9638 and 0.9632 in turn, indicating that the model equation could fit the experimental observations well. Besides, the more intuitive comparison of the K value of each reaction is shown in Fig. 5. It can be found that $BiOCl_{0.875}Br_{0.125}$ itself exhibited excellent visible light catalytic performance as that the K value of the reaction rate reached 0.24, which was consistent with findings of Gnayem & Sasson (2013). For the β-Fe_2O_3-doped modified composites, the visible light catalytic degradation process of the RhB was significantly accelerated with the increase of Bi content in the composite. When the Bi content was gradually elevated

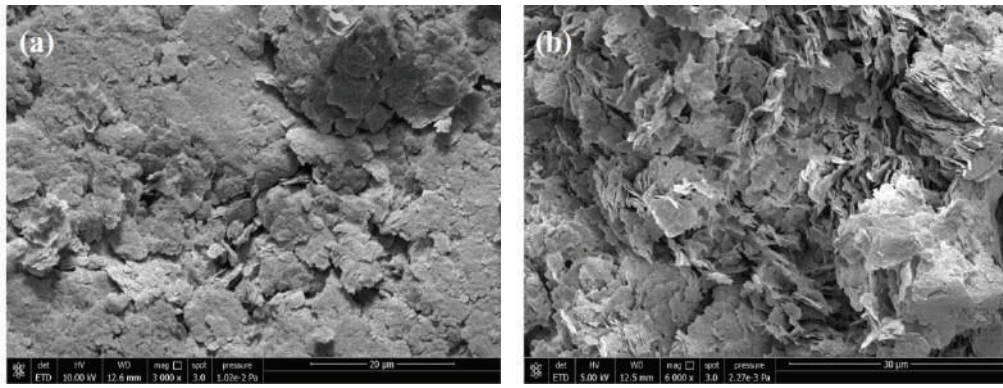

Fig. 2: SEM images of β-Fe_2O_3/$BiOCl_{0.875}Br_{0.125}$ with a magnification of (a) 3000, and (b) 6000.

to 30% (M4), the photocatalytic efficiency of the composite material had exceeded that of the pure $BiOCl_{0.875}Br_{0.125}$, with the highest K value of 0.26.

Mechanism of the enhanced photocatalytic activity: Based on the above experimental results and analysis, this experiment puts forward several interpretations about the enhanced photocatalytic performance of β-Fe_2O_3/$BiOCl_{0.875}Br_{0.125}$ on the degradation of RhB. First, semiconductor photocatalysis relies on the generation and separation of charge carriers, as well as the redox capability of semiconductors with different valence bands and conduction bands to improve the efficiency of interfacial charge transfer (Ge et al. 2011). It is known that β-Fe_2O_3 has a narrower bandgap (2.0~2.2) compared to $BiOCl_{0.875}Br_{0.125}$, and thus significantly enhances the response to visible light under light irradiation of λ>420 nm. The electrons on the β-Fe_2O_3 valence band are excited to reach a more potentially advantageous position to form a virtual conduction band, accordingly, these photogenerated electrons are more easily transferred to the conduction band of the relatively more positive $BiOCl_{0.875}Br_{0.125}$. In turn, it can effectively react with intermediates generated during the degradation process. This process can greatly reduce the recombination rate of photogenerated electrons and holes, thereby improving its photocatalytic performance. Second, photogenerated holes can react with OH^- in aqueous solution to form ·OH, while ·OH possesses strong oxidation capacity, which can oxidize organics quickly and efficiently. Third, the doping of β-Fe_2O_3 is beneficial to increase the specific surface area and pore volume of the composite catalyst, which is more favourable for the transfer of photogenerated electrons, holes and reactants to the reaction sites, thereby improving the photocatalytic performance of the catalyst (Martin et al. 2015).

CONCLUSION

BiOX-based composite photocatalyst has a good photocatalytic performance. The degradation rate of Rhodamine B solution reached 97.7% within 15 minutes under visible light irradiation, which was higher than most other photocatalysts.

The strategy of β-Fe_2O_3 doping BiOX shows great potential as that the introduction of β-Fe_2O_3 can significantly improve visible light response and reduce the recombination rate of the electron/hole pairs. Among the as-prepared β-Fe_2O_3/$BiOCl_{0.875}Br_{0.125}$ composite, the higher the content of Bi, the better the degradation effect was observed.

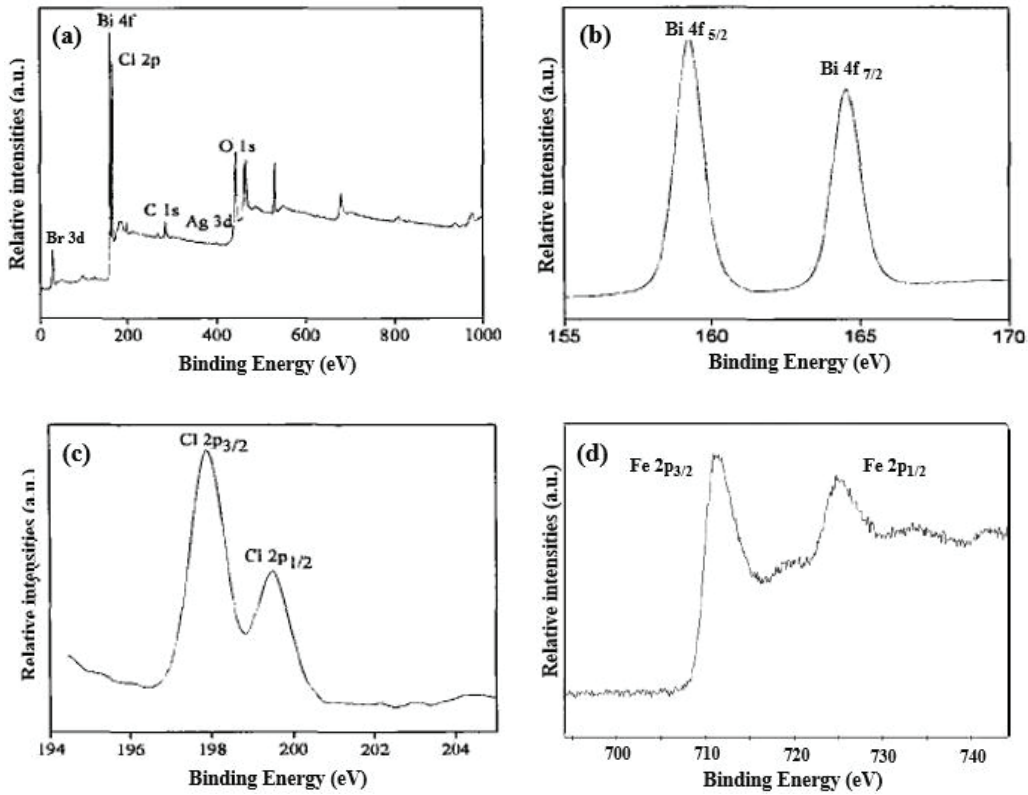

Fig. 3: XPS patterns of the composite β-Fe_2O_3/$BiOCl_{0.875}Br_{0.125}$: (a) survey, (b) Bi 4f, (c) Cl 2p, (d) Fe 2p.

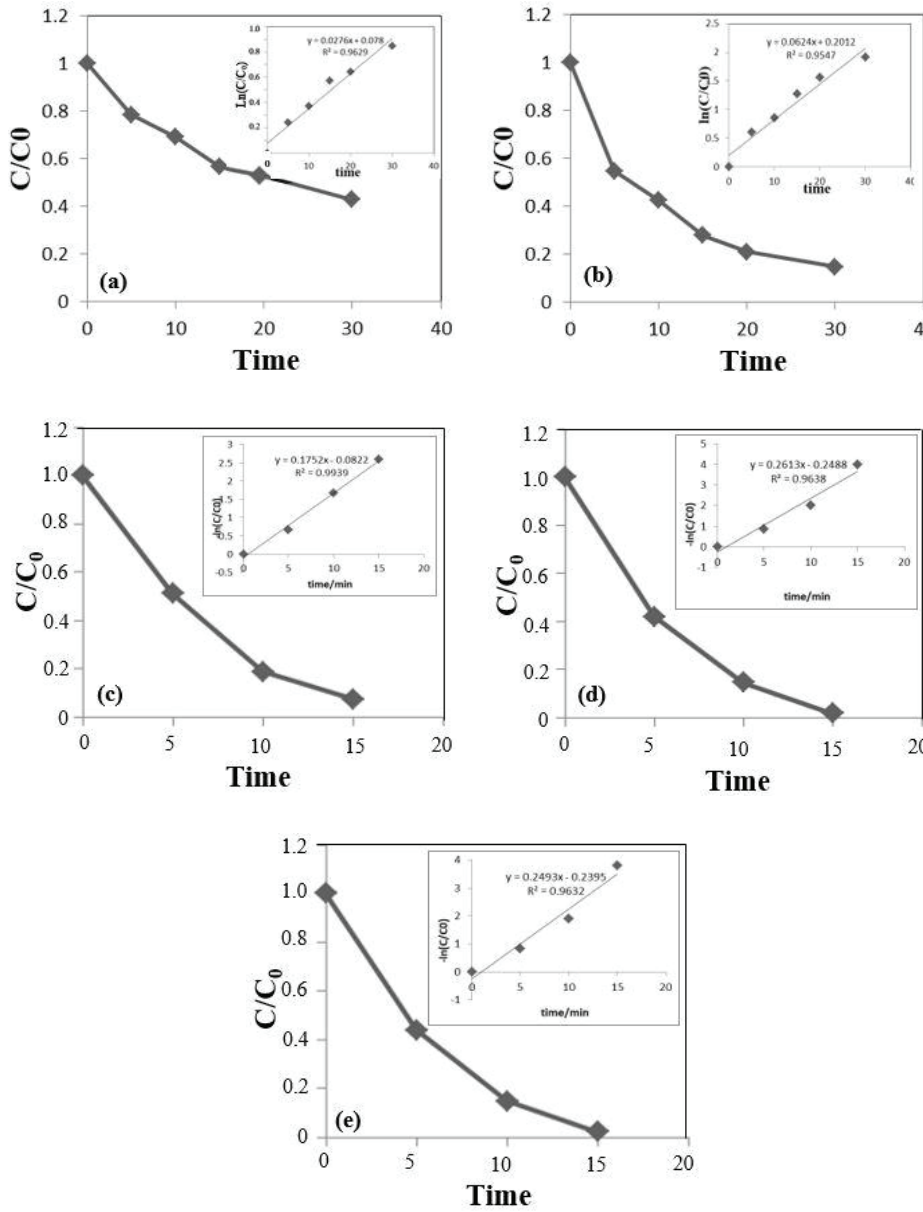

Fig. 4: Photocatalysis degradation efficiencies of RhB by various catalysts of (a) M1, (b) M2, (c) M3, (d) M4, (e) M0. The inset shows the quasi-first-order dynamic models corresponding to each process.

The modified β-Fe_2O_3/$BiOCl_{0.875}Br_{0.125}$ with Bi content of 30% can achieve a comparable and even better photocatalysis performance in comparison to an equal mass of pure phase $BiOCl_{0.875}Br_{0.125}$. Therefore, under the condition of ensuring catalytic efficiency, the material preparation cost can be greatly reduced.

ACKNOWLEDGEMENT

This work was financially supported by the Graduate Scientific Research and Innovation Foundation of Chongqing, China (Grant No. CYB18127).

REFERENCES

Amini, A., Kim, Y., Zhang, J., Boyer, T. and Zhang, Q. 2015. Environmental and economic sustainability of ion exchange drinking water treatment for organics removal. Journal of Cleaner Production, 104: 413-421.

Brázda, P., Kohout, J., Bezdička, P. and Kmječ, T. 2014. α-Fe_2O_3 versus β-Fe_2O_3: Controlling the phase of the transformation product of β-Fe_2O_3 in the Fe_2O_3/SiO_2 system. Crystal Growth & Design, 14(3): 1039-1046.

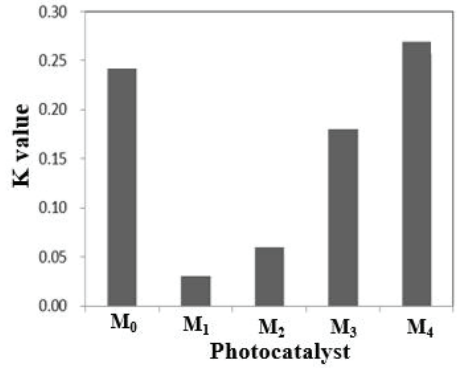

Fig. 5: Comparison of the K value of each photodegradation process.

Christoforidis, K. C., Montini, T., Bontempi, E., Zafeiratos, S., Jaén, J. J. D. and Fornasiero, P. 2016. Synthesis and photocatalytic application of visible-light active β-Fe_2O_3/g-C_3N_4 hybrid nanocomposites. Applied Catalysis B: Environmental, 187: 171-180.

Deng, H., Wang, J., Peng, Q., Wang, X. and Li, Y. 2005. Controlled hydrothermal synthesis of bismuth oxyhalide nanobelts and nanotubes. Chemistry-A European Journal, 11(22): 6519-6524.

Deng, Y. and Zhao, R. 2015. Advanced oxidation processes (AOPs) in wastewater treatment. Current Pollution Reports, 1(3): 167-176.

Elimelech, M. and Phillip, W.A. 2011. The future of seawater desalination: energy, technology, and the environment. Science, 333(6043): 712-717.

Ge, L., Han, C. and Liu, J. 2011. Novel visible light-induced g-C_3N_4/Bi_2Wo_6 composite photocatalysts for efficient degradation of methyl orange. Applied Catalysis B: Environmental, 108: 100-107.

Gnayem, H. and Sasson, Y. 2013. Hierarchical nanostructured 3D flowerlike $BiOClxBr_{1-x}$ semiconductors with exceptional visible light photocatalytic activity. ACS Catalysis, 3(2): 186-191.

Hasan, Z. and Jhung, S. H. 2015. Removal of hazardous organics from water using metal-organic frameworks (MOFs): plausible mechanisms for selective adsorptions. Journal of Hazardous Materials, 283: 329-339.

Hoffmann, M.R., Martin, S.T., Choi, W. and Bahnemann, D.W. 1995. Environmental applications of semiconductor photocatalysis. Chemical Reviews, 95(1): 69-96.

Jaiswal, R., Patel, N., Dashora, A., Fernandes, R., Yadav, M., Edla, R., Varma, R. S., Kothari, D. C., Ahuja, B. L. and Miotello, A. 2016. Efficient Co-B-co-doped TiO_2 photocatalyst for degradation of organic water pollutant under visible light. Applied Catalysis B: Environmental, 183: 242-253.

Lee, K. M., Lai, C. W., Ngai, K. S. and Juan, J. C. 2016. Recent developments of zinc oxide based photocatalyst in water treatment technology: a review. Water Research, 88: 428-448.

Li, J., Yu, Y. and Zhang, L. 2014. Bismuth oxyhalide nanomaterials: layered structures meet photocatalysis. Nanoscale, 6(15): 8473-8488.

Martin, D. J., Liu, G., Moniz, S. J., Bi, Y., Beale, A. M., Ye, J. and Tang, J. 2015. Efficient visible driven photocatalyst, silver phosphate: performance, understanding and perspective. Chemical Society Reviews, 44(21): 7808-7828.

Masih, D., Ma, Y. and Rohani, S. 2017. Graphitic C_3N_4 based noble-metal-free photocatalyst systems: A review. Applied Catalysis B: Environmental, 206: 556-588.

Mohamed, A., El-Sayed, R., Osman, T. A., Toprak, M. S., Muhammed, M. and Uheida, A. 2016. Composite nanofibers for highly efficient photocatalytic degradation of organic dyes from contaminated water. Environmental Research, 145: 18-25.

Omenn, G.S. 2006. Grand challenges and great opportunities in science, technology, and public policy. Science, 314(5806): 1696-1704.

Ren, K. X., Liu, J., Liang, J., Zhang, K., Zheng, X., Luo, H. D., Huang, Y. B., Liu, P. J. and Yu, X. 2013. Synthesis of the bismuth oxyhalide solid solutions with tunable band gap and photocatalytic activities. Dalton Transactions, 42(26): 9706-9712.

Ribeiro, A. R., Nunes, O. C., Pereira, M. F. and Silva, A. M. 2015. An overview on the advanced oxidation processes applied for the treatment of water pollutants defined in the recently launched Directive 2013/39/EU. Environment International, 75: 33-51.

Xiao, X., Liu, C., Hu, R., Zuo, X., Nan, J., Li, L. and Wang, L. 2012. Oxygen-rich bismuth oxyhalides: generalized one-pot synthesis, band structures and visible-light photocatalytic properties. Journal of Materials Chemistry, 22(43): 22840-22843.

Zhang, L. P., Liu, Z., Faraj, Y., Zhao, Y., Zhuang, R., Xie, R., Ju, X. J., Wang, W. and Chu, L. Y. 2019. High-flux efficient catalytic membranes incorporated with iron-based Fenton-like catalysts for degradation of organic pollutants. Journal of Membrane Science, 573: 493-503.

Book Review

Microbial Applications and Environment by Pawan Kumar Bharti, Narendra A. Kulkarni and Avnish Chauhan; Published by Discovery Publishing House Pvt. Ltd., 4383/4B, Ansari Road, Darya Ganj, New Delhi-110 002, India; ISBN: 978-93-5056-515-5; Pages188; Price: Rs. (INR) 1400.

This book presents a common review, particularly of the crucial themes, challenges and controversies about the environment. At some point, authors try to provide an analytical framework for highlighting an inclusive understanding of the current environmental problems worldwide. Some major discussion points about ecology and environment-related policies are also highlighted in the book. Almost all-pervading microbes in the biosphere perpetually affect the surrounding atmosphere in which they grow. Their biosynthetic capabilities are all the time showing the solution for maintaining the eminence of the environment. This book comprises of a total of 8 different chapters. They include well-defined tables, figures, charts, images and references. Each chapter is acceptably organized with just about the required amount of information; some examples, on the other hand, are cited providing an overview of the chapter. The very first chapter explains information about mangroves, a typical group of the plants which plays a key role in maintaining the quality and productivity of coastal waters, with collective information from the ground survey and remote sensing data. Theoretically, chapter 3 found similar to the first chapter considering the theme and content presented. That the threatened species indicate priorities for conservation, it is suggested, that for the conservation of mangroves there is need to implement the CRZ notification (1991) quite effectively with the active participation of people from society. According to some of the recent reports, it was noticed that agriculture activities, urbanization and different human behaviours are responsible for the rapidly declining rate of mangroves in India over the last century. There is no evident guidance available in the book to solve environmental problems or even no ideas for public awareness for the problem discussed.

Chapter 3 consists of inaccurate theoretical materials, where chapter 3 and chapter 1 represent the same printable abstract for both separate chapters in the book. This may be typing or printing error but needs to be corrected to avoid false impression and misunderstanding to a variety of readers. In between Chapter 2 was altogether different from the aspects of the book, where evaluation study of some selected kinds of toothpastes was done to find their effect on the salivary of *Streptococcus mutans*. This information is totally variable and different from the theme of the book. Similar mismatch chapter found was Chapter 4 which captures representative spectroscopic investigation of kaolinite by XRD, XRF, EPMA, DTA, FTIR only, with no further information provided with its effect on the environment. With a brief introduction Chapter 5 explains structure and function about ecosystems and their prevention from the harmful impacts of humans. Rest of the chapters show some elementary data, available from localized surveys and estimates from different regions. Some Chapters end with a conclusion which helps in understanding the overview of the topic discussed. Along with the enhancement of a long-term collaboration nationwide to solve the problems for shaping the better environmental protection in real practice. Recent advances in microbial technologies help in exploring a large proportion of microorganisms which are still undiscovered, to learn their role in maintaining ecological balance.

There is a lack of comprehensive reliable data on various aspects of microbes and their application in the environment. Furthermore, these texts have not kept major developments that have taken place in recent years. Most of the book provides a comprehensive amount of information on different topics of environment. Authors fail to grab the attention of the reader while going through the pages by way of short information presented. Besides, I found that this text does not make the reader more inquiring, to learn about microbes and the environment. The provided information is not much updated in terms of the developments that have taken place in this field, and content provided do not fulfil the demand of the title for present work in the book. A particular comprehensive evaluation of crucial environmental themes not noticed in the book. At no point controversies regarding the use of microbes in environmental governance systems focused, and also the innovative socio-economic framework for highlighting inclusive environmental problems was absent. Authors fall short to explain optimal solutions to global environmental problems, how to handle them for a better environment in reality. Expectantly, this book will help readers to bring out some information with different environmental aspects.

Dr. Ruby E Jalgaonwala
Assistant Professor in Microbiology
Department of Microbiology
SRKI, Surat, Gujarat, India
r_jalgaonwala@yahoo.co.in

... Continued from inner front cover

- The text of the manuscript should run into **Abstract, Introduction, Materials & Methods, Results, Discussion, Acknowledgement** (if any) and **References** or other suitable headings in case of reviews and theoretically oriented papers. However, short communication can be submitted in running with **Abstract and References.** The references should be in full with the title of the paper.
- The figures should preferably be made on a computer with high resolution and should be capable of withstanding a reasonable reduction with the legends provided separately outside the figures. Photographs may be black and white or colour.
- Tables should be typed separately bearing a short title, preferably in vertical form. They should be of a size, which could easily be accommodated in the page of the Journal.
- References in the text should be cited by the authors' surname and year. In case of more than one reference of the same author in the same year, add suffix a,b,c,.... to the year. For example: (Thomas 1969, Mass 1973a, 1973b, Madony et al. 1990, Abasi & Soni 1991).

List of References

The references cited in the text should be arranged alphabetically by authors' surname in the following manner: (Note: The titles of the papers should be in running 'sentence case', while the titles of the books, reports, theses, journals, etc. should be in 'title case' with all words starting with CAPITAL letter.)

Dutta, A. and Chaudhury, M. 1991. Removal of arsenic from groundwater by lime softening with powdered coal additive. J. Water Supply Res. Techno. Aqua., 40(1) : 25-29.

Hammer, D.A. (ed.) 1989. Constructed Wetlands for Wastewater Treatment-Municipal, Industrial and Agricultural. Lewis Publishers Inc., pp. 831.

Haynes, R. J. 1986. Surface mining and wetland reclamation. In: Harper, J. and Plass, B. (eds.) New Horizons for Mined Land Reclamation. Proceedings of a National Meeting of the American Society for Surface Reclamation, Princeton, W.V.

Submission of Papers

- The paper can be submitted by e-mail as an attachment in a single WORD file at **contact@neptjournal.com**
- The paper can also be submitted online in a single WORD file through the journal's website: **www.neptjournal.com**

Attention

1. Any change in the authors' affiliation may please be notified at the earliest.
2. Please make all the correspondence by e-mail, and authors should always quote the manuscript number.

Note: In order to speed up the publication, authors are requested to send the publication charges as soon as they get the 'initial acceptance' letter, and also correct the galley proof immediately after receipt. The galley proof must be checked with utmost care, as publishers owe no responsibility for mistakes. The papers will be put on priority for publication only after receiving the processing and publication charges.

Nature Environment and Pollution Technology

(Abbreviation: Nat. Env. Poll. Tech.)

(An International Quarterly Scientific Journal)

Published by

Technoscience Publications

A-504, Bliss Avenue, Opp. SKP Campus

Balewadi, Pune-411 045, Maharashtra, India

In association with

Technoscience Knowledge Communications

Mira Road, Mumbai, India

For further details of the Journal please visit the website. All the papers published on a particular subject/topic or by any particular author in the journal can be searched and accessed by typing a keyword or name of the author in the 'Search' option on the Home page of the website. All the papers containing that keyword or author will be shown on the home page from where they can be directly downloaded.

www.neptjournal.com

Published for Proprietor, Printer and Publisher: Mrs. T. P. Goel, B-34, Dev Nagar, Tonk Road, Jaipur, Rajasthan, India; Editors: Dr. P. K. Goel and Prof. K. P. Sharma